THE PHYSICAL REVIEW

VOLUME 94 NUMBER 3

MAY 1, 1954

Published by the

AMERICAN PHYSICAL SOCIETY

at

Minneapolis, Minnesota

A Journal of

Published by the American Institute
for the
AMERICAN PHYSICAL S

Officers

President

H. A. Bethe
Cornell University
Ithaca, New York

Vice-President

R. T. Birge
University of California
Berkeley, California

Secretary

K. K. Darrow
Bell Telephone Laborato
Office:
Columbia University
New York 27, New York

Treasurer

G. B. Pegram
Columbia University
New York 27, New York

Local Secretary
for the Pacific Coast

J. Kaplan
University of California
Angeles
Los Angeles, California

Managing Editor

S. A. Goudsmit
Brookhaven National Labo
Upton, Long Island
New York

The Physical
Entered as second-class
Acceptance for mailing at special

THE
PHYSICAL REVIEW

A journal of experimental and theoretical physics established by E. L. Nichols in 1893

SECOND SERIES, VOL. 94, NO. 3 MAY 1, 1954

Energy Transfer by Means of Collision in Liquid Organic Solutions under High Energy and Ultraviolet Excitations*

MILTON FURST AND HARTMUT KALLMANN
Physics Department, New York University, Washington Square, New York, New York

(Received January 18, 1954)

Experiments are described which show that energy transfer by means of "collisions" occurs when a liquid organic solution is excited by ultraviolet light as well by high-energy radiation. With light excitation the possibility of any transfer by ionization and/or by hidden radiation could be completely eliminated. It was found that energy transfer by way of collision between various molecules under excitation by light is of the same magnitude as with high-energy radiation excitation. Energy transfer by way of absorption and subsequent re-emission occurs only in complex solutions containing at least two kinds of efficient fluorescent molecules. Basically the technique of the experiments with light consisted of irradiating different solutions with various wavelengths, thereby selectively exciting various components of the solutions, and of observing the corresponding effects on the fluorescent light output. The solutions measured in this investigation used xylene and cyclohexane as solvents; anthracene, *p*-terphenyl, and 9,10-diphenylanthracene as fluorescent solutes; and additional naphthalene which in some respects behaves like a solvent when present in large concentrations. In complete agreement with results under gamma-ray excitation, energy transfer under light excitation takes place from naphthalene to anthracene and diphenylanthracene, and from xylene to terphenyl, while none occurs from naphthalene to terphenyl.

INVESTIGATIONS of the fluorescence of dilute liquid organic solutions under high-energy radiation have shown that energy is transferred from the solvent molecules to those of the solute.[1,2] The primary radiation is certainly absorbed mostly by the solvent which makes up the bulk of the solution; nevertheless, the outcoming fluorescence from "effective" solutions with a single solute is invariably associated with the spectral characteristics of the solute rather than of the solvent. With complex solutions containing more than one solute, the energy transfer has even been traced from one type of solute molecule to the other.[2,3]

In the earlier papers this energy transfer was attributed to a migration of excitation energy[4–6] from one solvent molecule to another until it is eventually trapped by a solute molecule; the emission then takes place from the solute. Another possible type of energy transfer, that by means of absorption, was also studied.[2–8] In this type of transfer, a light quantum is emitted by one type of molecule and reabsorbed by by another, and then the fluorescent emission occurs. Such transfer was observed to take place in complex solutions containing several fluorescent solutes from one kind of solute molecule to the other but not ordinarily from the solvent molecule to that of the solute. Generally a considerable decrease in emitted energy accompanies transfer via radiation because of the internal quenching of the absorbing solute. The transfer can occur only if the transferring material emits radiation; since, however, almost all of the pure solvents used in fluorescent work (e.g., xylene, *p*-dioxane, etc.) emit only small amounts of radiation, it was concluded that the energy transfer from an excited solvent occurs almost entirely by way of collision. There is also the possibility that the fluorescence of a solution excited by high-energy radiation is due to the ionization of the solvent (rather than excitation) and to the transfer

* This work was supported by the U. S. Signal Corps Engineering Laboratories, Evans Signal Laboratory, Belmar, New Jersey.

[1] H. Kallmann and M. Furst, Phys. Rev. 79, 857 (1950); M. Furst and H. Kallmann, Phys. Rev. 85, 816 (1952).

[2] H. Kallmann and M. Furst, Phys. Rev. 81, 853 (1951).

[3] M. Furst and H. Kallmann, Phys. Rev. 89, 912 (1953).

[4] S. I. Weissman, J. Chem. Phys. 10, 214 (1942).

[5] Bowen, Mikiewicz, and Smith, Proc. Phys. Soc. (London) A62, 26 (1949).

[6] E. J. Bowen and P. D. Lawley, Nature 164, 572 (1949).

[7] E. J. Bowen, Symposia Soc. Exptl. Biol. 5, 152 (1951).

[8] J. B. Birks, *Scintillation Counters* (McGraw-Hill Book Company, Inc., New York, 1953), p. 68.

of the positive charge from the solvent molecule to that of the solute. This type of transfer seems, however, also to be of only minor importance since it could not account for the high efficiency observed with some solutions and for the almost complete lack of fluorescence under high-energy radiation in many organic solutions which exhibit strong fluorescence under light excitation. A change of the solvent often results in a considerable decrease of the high-energy-induced fluorescence without any decrease of the light-induced fluorescence, which is very difficult to understand if the transfer occurs by means of ions.

Some authors, nevertheless, assume that in solutions containing only one solute the energy transfer takes place essentially by way of transfer of hidden radiation (1000A−2000A). In order to further clarify this situation and to trace more directly the energy transfer by the described migration of excitation energy and its final trapping by a solute molecule, experiments employing excitation by light were performed where excitation and transfer by means of hidden radiation is impossible. These experiments (described below) also show that collision transfer occurs with considerable probability.

The light-excitation experiments have been carried out by using ultraviolet light of various wavelengths in different kinds of solutions. For this purpose a Bausch and Lomb monochromator employing a mercury arc lamp as light source was used. The light from this instrument was directly incident on the surface of a solution placed in a glass or quartz beaker. The fluorescent light was viewed by a 1P28 photomultiplier in a direction perpendicular to the incident light.

Of particular interest in relation to the energy transfer were effects observed when naphthalene was added to various xylene solutions while excited by gamma radiation. Naphthalene solutions without additional solutes fluoresce only slightly under high energy or light excitation. The addition of large amounts of naphthalene into anthracene solutions (up to 200 g/l of naphthalene to 0.3 g/l of anthracene) produces practically no change in the fluorescent light output (see Table I). When a similar experiment is carried out, however, with *p*-terphenyl as the fluorescent solute, the addition of naphthalene results in a strong decrease in the fluorescent output. These findings were explained by assuming that the energy which is primarily absorbed in the xylene (greater than 75 percent even with 200 g/l of naphthalene) is first transferred mainly to the naphthalene because of its large excess in concentration and subsequently from it to the fluorescent solute. In the case of anthracene, the lowest excitation energy of the anthracene molecule is sufficiently below that of the naphthalene molecule that a transfer of energy from the naphthalene to the anthracene can occur rather easily. This transfer takes place almost entirely by means of collisions rather than by means of radiation since the light output of naphthalene is relatively weak. On the other hand, with *p*-terphenyl the excitation levels of both solutes are close to each other as shown by the similarities in the absorption ranges. Consequently, the energy transfer is expected to be much less probable from the naphthalene to terphenyl than to the anthracene if it occurs at all. The excitation energy of the naphthalene is therefore quenched before it has a chance to go over to the terphenyl; thus the final outcome is a decrease in the light output when the amount of naphthalene is increased. Such a difference in behavior as that found between anthracene and terphenyl solutions could perhaps also be explained by assuming that no energy transfer at all occurs to naphthalene; the decrease of the terphenyl fluorescence

TABLE I. Effects of addition of naphthalene on the fluorescence of various xylene solutions under γ-ray and uv excitations.

Solute	g/l	Additional solute	g/l	Fluorescent intensity[a] γ-ray excitation No Filter	γ-ray excitation 0-52 Filter[b]	Light (3130A) excitation No Filter	Light (3130A) excitation 0-52 Filter[b]
(a) Miscellaneous solutes							
...	...	...	...	0.025	0.005	0.03	0.003
Naphthalene	70	...	...	0.04	0.012	0.07	0.01
Terphenyl	0.5	...	...	0.29	0.10	1.0	0.30
Terphenyl	0.5	Anthracene	0.05	0.12	0.085	0.26	0.18
Terphenyl	0.5	Anthracene	0.3	0.09	0.077	0.18	0.155
(b) Anthracene as fluorescent solute							
Anthracene	0.3	Naphthalene	0	0.06	0.05	0.19	0.15
Anthracene	0.3	Naphthalene	1	0.06	0.05	0.16	0.13
Anthracene	0.3	Naphthalene	10	0.06	0.05	0.11	0.09
Anthracene	0.3	Naphthalene	40	0.06	0.05	0.11	0.09
Anthracene	0.3	Naphthalene	70	0.06	0.05	0.11	0.09
Anthracene	0.3	Naphthalene	100	...	...	0.11	0.09
Anthracene	0.3	Naphthalene	200	0.06	...	0.10	0.08
(c) Terphenyl as fluorescent solute							
Terphenyl	4	Naphthalene	0	0.5	0.16	1.0	0.28
Terphenyl	0.5	Naphthalene	0	0.29	...	0.97	0.25
Terphenyl	0.5	Naphthalene	0.5	0.20	..	0.92	0.23
Terphenyl	0.5	Naphthalene	10	0.085	...	0.35	0.08
Terphenyl	0.5	Naphthalene	70	0.046	...	0.09	0.02
(d) Diphenylanthracene as fluorescent solute							
9,10-Diphenylanthracene	0.5	Naphthalene	0	0.17	0.14	0.47	0.44
9,10-Diphenylanthracene	0.5	Naphthalene	0.5	0.15	0.13	0.33	0.30
9,10-Diphenylanthracene	0.5	Naphthalene	1	0.13	0.12	0.28	0.25
9,10-Diphenylanthracene	0.5	Naphthalene	5	0.13	0.12	0.22	0.19
9,10-Diphenylanthracene	0.5	Naphthalene	10	0.13	0.12	0.20	0.17
9,10-Diphenylanthracene	0.5	Naphthalene	20	0.14	0.13	0.21	0.18
9,10-Diphenylanthracene	0.5	Naphthalene	40	0.14	0.13	0.20	0.17
9,10-Diphenylanthracene	0.5	Naphthalene	70	0.15	0.14	0.20	0.17
9,10-Diphenylanthracene	0.5	Naphthalene	100	0.17	0.16	0.21	0.18
(e) Terphenyl as solute—3340-A exciting light							
...	...	...	...	0.025	0.005	0.17	0.01
Naphthalene	70	...	...	0.04	0.01	0.18	0.02
Terphenyl	2	Naphthalene	0	0.49	0.16	1	0.33
Terphenyl	2	Naphthalene	1	0.36	0.12	1	0.33
Terphenyl	2	Naphthalene	10	0.21	0.07	0.9	0.30
Terphenyl	2	Naphthalene	70	0.09	0.03	0.6	0.23

[a] All gamma-ray intensity values are referred to anthracene crystal of the same mass without any filters present as 1, the light excitation values for 3130A refer to the value of terphenyl (4 g/l) in xylene as 1, without filters being present; and the intensity values for 3340A refer to xylene and terphenyl 2 g/l as 1 with no filters present.

[b] Corning 0-52 filter cuts off all radiation below 3400A and has a transmission of greater than 50 percent for wavelengths above 3600A. The filter is placed in front of the photomultiplier.

would then be attributed to a special quenching of terphenyl fluorescence by the naphthalene. However, the light experiments described below reject this possibility.

A behavior somewhat similar to that of anthracene was also displayed by 9,10-diphenylanthracene,

This molecule has a fluorescent spectral range similar to that of anthracene and its state of lowest excitation energy is therefore assumed to be close to that of anthracene. Its fluorescent light output in xylene solutions is, however, considerably larger than that of anthracene and is almost as great as that of *p*-terphenyl. Under gamma rays, the addition of small amounts of naphthalene to this substance produces a small decrease in light output which is not found with anthracene; increasing the concentration of naphthalene, however, here results in an increase in light output. The initial decrease may be due to a small quenching of diphenylanthracene by naphthalene (possibly because of impurities). The later rise is attributed to the better energy transfer (by collisions) from naphthalene to diphenylanthracene than that from xylene to diphenylanthracene.

Experiments analogous to those with gamma radiation have also been performed with light. The advantage of using light consists essentially in the possibility of primarily exciting only a single constituent of the solution such as one of the solutes or the solvent by appropriate choice of the wavelength. In particular, with light as the exciting agent, the excitation may be localized in the solute molecules, thus by-passing the solvent if it is transparent to the exciting radiation. First xylene-anthracene solutions with various amounts of additional naphthalene were excited by light of 3130A. For this wavelength xylene is essentially transparent, though the solutes (anthracene, diphenylanthracene, naphthalene, and terphenyl) show considerable absorption. If the absorption coefficient of the naphthalene molecule at this wavelength is arbitrarily taken as 1, the absorptions of anthracene and *p*-terphenyl molecules are about 5 and 32, respectively;[9] with 10 g/l of additional naphthalene 90 percent of the light is absorbed by naphthalene, and with 100 g/l about 99 percent. The absorption of 9,10-diphenylanthracene is also in this range of values. The depth of the solution was such that in any event the light was "completely" absorbed either by the fluorescent solute or by the naphthalene.

Examination of Table I shows that the fluorescence of pure xylene is rather weak under light as well as under gamma radiation, and the addition of 70 g/l of naphthalene produces only a relatively small increase of light output. It reveals further that the emitted light, even with large amounts of naphthalene present, occurs mostly at wavelengths below about 3500A. The addition of naphthalene to the anthracene solution brings about a decrease in fluorescence of about 47 percent; the light output is characteristic of anthracene though almost all of the incident radiation is absorbed by the naphthalene. The light output is almost constant beyond 10 g/l of naphthalene (90 percent absorption by naphthalene).

These experiments demonstrate the energy transfer from naphthalene to the anthracene by collision. Energy transfer by ions is excluded since the exciting radiation is not energetic enough to produce ionization. Energy transfer by absorption of radiation is also excluded since, because of quenching in the anthracene molecule when in solution, the observed anthracene radiation should be five times smaller than the original naphthalene radiation if transfer occurred by way of radiation. Since the anthracene radiation is even larger than that of the naphthalene radiation, the energy transfer must take place by way of "collision." The reason that energy transfer by absorption is always connected with a decrease in light output is the fact that the quantum yield of most solutes is smaller than one (as crystals the quantum efficiency may be of the order of 1). This means that considerably less light is re-emitted than absorbed. In the case of anthracene in solution, the quantum yield is of the order of 20 percent; thus a decrease in light output by a factor of about five is to be expected. This is also demonstrated by the values in the first portion of Table I where the light output for 0.5 g/l of *p*-terphenyl in xylene without naphthalene is described for both 0.05 g/l and 0.3 g/l of additional anthracene. Small amounts of anthracene are sufficient to absorb most of the terphenyl radiation. Consequently, a clear indication that there is energy transfer by collision is given by the result that when 200 g/l of naphthalene are present, 53 percent of the anthracene light output is obtained compared to that when no naphthalene is present, and the fact that this light emission is 1.5 times larger than that of naphthalene (but in the spectral region of anthracene). The decrease in light emission of anthracene because of the addition of naphthalene is explained as follows: at the higher naphthalene concentrations all light is absorbed by the naphthalene, but only 53 percent of this energy is transferred by collisions to anthracene at anthracene concentrations of 0.3 g/l. This value is in fair agreement with the calculated energy transfer from gamma radiation (see below).

Similar types of light excitation experiments were carried out with *p*-terphenyl and 9,10-diphenylanthracene which further bear out these conclusions. With *p*-terphenyl, the addition of naphthalene produces a strong decrease in light output. Thus when the molecular ratio of naphthalene to terphenyl is 250 to 1, which

[9] R. A. Friedel and M. Orchin, *Ultraviolet Spectra of Aromatic Compounds* (John Wiley and Sons, Inc., New York, 1951).

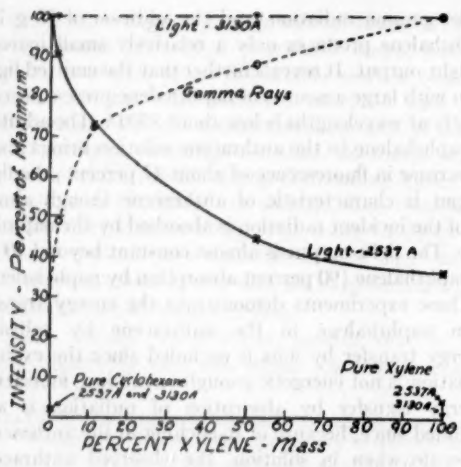

FIG. 1. Fluorescence of *p*-terphenyl in mixtures of cyclohexane and xylene.

means a light absorption ratio of 8 to 1 in favor of naphthalene, there is a decrease of intensity of about 90 percent, almost down to the value of naphthalene without terphenyl. Most of the decrease in intensity is here accounted for by the absorption of the incident energy by naphthalene and the lack of transfer to the terphenyl either by collision or otherwise.

Experiments with 9,10-diphenylanthracene yield results similar to those with anthracene, as is to be expected from the emission spectrum of this substance; its fluorescent efficiency under light excitation is about one-half that of terphenyl. Addition of naphthalene to such solutions produces (as in anthracene) a decrease of the fluorescence, here of about 55 percent. Again the results are attributed to the absorption by naphthalene of the incident radiation and an energy transfer to diphenylanthracene by collisions. The essential difference compared to anthracene is the almost three times larger emitted intensity due to smaller internal quenching. The experiments show again that no energy transfer by way of absorption occurs, since this would again result in an eventual light output smaller than that of naphthalene.

One further point to be cleared up is the strong decrease of radiation when naphthalene is added to *p*-terphenyl. This is certainly associated with the increased amount of absorption by the naphthalene; but it might be argued that this decrease is not due to a lack of energy transfer by collisions from naphthalene to terphenyl, but rather to a special quenching of the excited terphenyl molecule by naphthalene. In order to make a decision between these possibilities, experiments were performed with light of 3340A. This radiation is scarcely absorbed by naphthalene, though it is still comparitively strongly absorbed by terphenyl and excites it. The results are described in the last portion of the Table I. Additional naphthalene here produced only a small drop in fluorescent intensity compared to that observed with 3130A, very little change in intensity taking place with molecular ratios up to about 9 to 1 (10 g/l naphthalene). Thus, whereas under excitation by gamma rays or light of 3130A wavelength, a decrease in fluorescence by a factor of 2.5 or 3 is found the decrease in fluorescence under the light of 3340A wavelength amounts to only 10 percent, indicating that the quenching of the excited terphenyl molecules by naphthalene is small if present at all. This supports our earlier contention that the decrease in the terphenyl-naphthalene radiation occurs because there is no energy transfer from naphthalene to terphenyl, and only a relatively small special quenching of the terphenyl radiation by naphthalene.

These experiments show principally that there is an energy transfer from atom to atom by way of collision in liquid systems. In these light experiments, the naphthalene can be considered as playing to some extent the role of the bulk material from which the energy is transferred to other solutes. Xylene is essentially inactive in these light excitation experiments and has the purpose of making the systems liquid. Some experiments with light excitation in which xylene has the function of the bulk material for primary excitation have also been performed. First the fluorescent efficiency of *p*-terphenyl excited by a wavelength of 3130A was determined for xylene and cyclohexane as solvents; this wavelength is absorbed almost entirely by the terphenyl and not by either of these solvents. This experiment was carried out to determine the difference in quenching of terphenyl in both solvents; practically no difference was found. Then this experiment was repeated with wavelengths of about 2537A which are absorbed considerably by xylene but scarcely at all by cyclohexane, as well as with gamma rays for comparison; the results are shown in Fig. 1. For comparison, the light-induced intensities for the pure solvents without terphenyl are also indicated. In these experiments the relative amounts of xylene and cyclohexane were varied while the amount of terphenyl was kept unchanged. For 3130A, the fluorescent output is found to be practically constant for all the solvent ratios (straight line of Fig. 1). For the shorter wavelengths, the fluorescent intensity of terphenyl is greatest with pure cyclohexane and registers only 36 percent of this value for pure xylene. Under gamma radiation, in contrast, an increase by a factor of 3 was found when varying from pure cyclohexane to pure xylene. This decrease of fluorescent output with ~2537A light, and no change with 3130A light, is certainly due to the absorption of the ~2537A light by the xylene. With 2537A light in 100 percent xylene, the relative absorption ratio between xylene and 1 g/l of terphenyl is about 20 to 1 when the available data (for toluene) are used.[9] Since pure xylene without terphenyl has only a very small fluorescent emission, one would also expect a very weak fluorescent intensity for xylene and 1 g/l

terphenyl from these absorption values, since all radiation is practically absorbed by xylene. Thus the fluorescent intensity of these terphenyl solutions should drop by a factor of about 20 when cyclohexane is replaced by xylene. Instead only a drop by a factor of 2.8 is observed. This result can again be explained by assuming that the energy is transferred from xylene to terphenyl by collisions just as in the experiments with gamma radiation.

If the energy transfer calculated from these light experiments is compared with that computed from gamma-ray results, it is found that the transfer with light excitation is about half of that with gamma radiation and of the same order as that found in the alpha particles.[1] This may be associated with the large density of excitation present with the light intensities employed. Preliminary experiments indicate that with lower incident light intensities, higher efficiencies of energy transfer are obtained. The smaller efficiency under gamma rays in cyclohexane compared to that in xylene, although both solvents are found to have roughly the same quantum yield (as shown in experiments with 3130A), is due to the fact that the energy transfer in cyclohexane is considerably weaker than that in xylene.

The correlation of the gamma-ray excitation results with those obtained with ultraviolet excitation in all of the above experiments can be taken as very strong evidence in favor of transfer of excitation energy by means of collisions and against any essential contribution by ionization to any of the mechanisms for high-energy organic liquid fluorescence which are found in the literature. The energy transfer that takes place from solvent to solute or from one solute to another in these experiments under light excitation as well as under high-energy radiation has been shown to be due in large part of a "collision" mechanism† and certainly cannot be completely attributed to radiation absorption and re-emission (photon exchange) as is claimed by Birks.[4] It may be mentioned that if photon exchange did occur, it should be more pronounced for terphenyl than for anthracene because of its larger absorption coefficient. In this case the experiments described above could not be explained. Finally, it may be remarked that any energy transfer by means of absorption of radiation with wavelengths shorter than that of the absorption edge of naphthalene (~3250A) is also excluded by the fact that in this range *p*-terphenyl has a larger absorption coefficient than anthracene or diphenylanthracene. If such a transfer by absorption did occur, then terphenyl solutions should behave like anthracene or diphenylanthracene since no special quenching of terphenyl radiation by naphthalene occurs. Instead, the addition of naphthalene produced a large decrease in the light output of terphenyl solutions. Energy transfer by absorption of radiation with wavelengths greater than 3250A is excluded because such radiation, if present, would not have escaped detection in our arrangement.

The energy transfer described here for liquid systems is essentially similar to that observed by Bowen in solid solutions of organic materials.[5,6] These experiments also support the previously reported idea that energy transfer and subsequent fluorescence can occur only if the energy difference between the excited levels of the two types of molecules concerned is great enough so that the energy can be trapped and not returned to the transferring molecule. At the same time they show, as noted above, that no interaction of the self-quenching type occurs between these different types of molecules.

† *Note added in proof.*—Similar conclusions were also reached from analogous experiments by S. G. Cohen and A. Weinreb, Phys. Rev. 93, 1117 (1954).

The Reflection of Shock Waves from a Blunt Wedge*

V. H. BLACKMAN AND D. K. WEIMER†
Palmer Physical Laboratory, Princeton University, Princeton, New Jersey
(Received January 27, 1954)

The pseudostationary field resulting from the head-on reflection of a shock wave at a corner of angle $(\pi-\delta)$, where δ is small, has been investigated with the shock tube and interferometer. The wave configuration and the pressure along the wall are compared with the theory developed by Lighthill. The results are in qualitative agreement and indicate that the theory is correct for vanishingly small δ. The density field is also given.

INTRODUCTION

THE problem of a shock wave of arbitrary strength reflecting from a rigid wall has never been completely solved. The situation as it exists at the present time has been summarized in recent papers.[1,2] For several special cases asymptotic solutions have been given, solutions that depend on some assumption, such as glancing incidence, which will linearize the equations. Among these is the solution of Lighthill[3] for the reflection of a shock wave incident on a very blunt corner of included angle $(\pi-\delta)$, where δ is small. The purpose of this paper is to present the results of recent experiments in which shock waves were reflected from blunt wedges. The results are compared with the calculations of Lighthill. Since there are no characteristic dimensions the pattern is pseudostationary, that is, it can be described in terms of x/t and y/t. Lighthill assumes that there are regions behind the reflected shock where the flow is uniform and which are bounded by straight segments of the reflected shock. These two straight segments are connected by a curved segment behind which there is a region of nonuniform flow; see Figs. 2(a) and 3(a). By making the restriction of nearly head-on incidence, which allows the assumption that the pressure and density in the disturbed region are not greatly different from their values in the

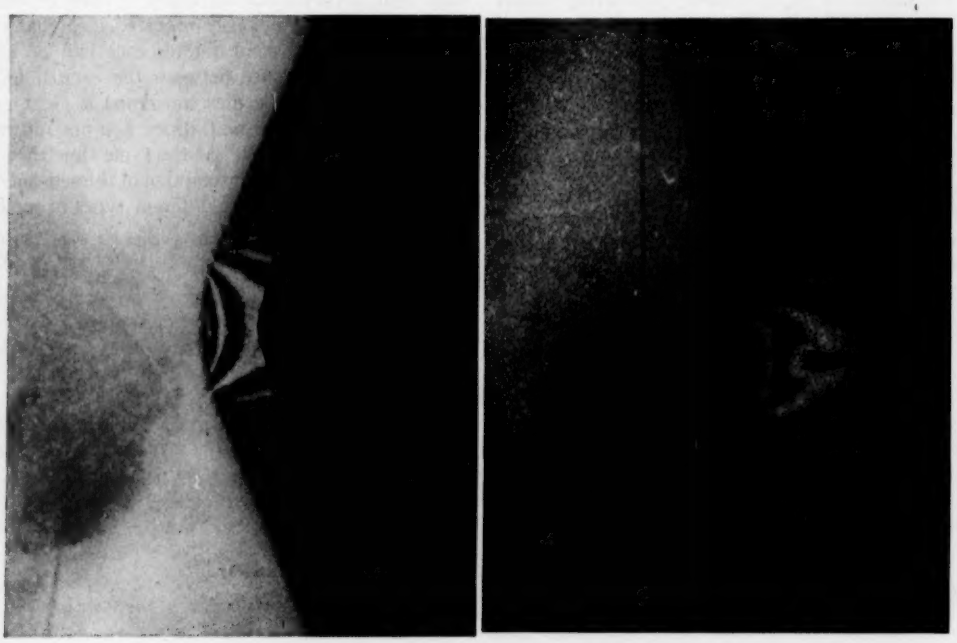

(a) (b)

FIG. 1. A single or contour fringe picture showing the nature of the disturbance for (a) a convex wedge (b) a concave wedge. The incident shock wave is moving to the right.

* This work was supported by the U. S. Office of Naval Research.
† Now at Armour Research Foundation, Chicago, Illinois.
[1] Walker, Bleakney, and Taub, Revs. Modern Phys. **21**, 584–605 (1949).
[2] Fletcher, Taub, and Bleakney, Revs. Modern Phys. **23**, 271–286 (1951).
[3] M. J. Lighthill, Proc. Roy. Soc. (London) **A200**, 554 (1950).

undisturbed region behind the reflected shock, he calculates the strength and position of the reflected wave and the pressure along the wall.

EXPERIMENTAL RESULTS

In the experiments four models were used. Each model completely spanned the four-inch width of the shock tube. Two of the models were convex wedges for which δ is positive, and the other two wedges were concave for which δ is negative. The four wedge angles used were $(\pi-\delta)$ where δ had the values $+0.5$, $+0.37$, -0.33, and -0.5 radian. The theory and operation of the shock tube have been described in a previous paper[4] and hence no detailed explanation will be given here. Pictures of the shock pattern were taken through

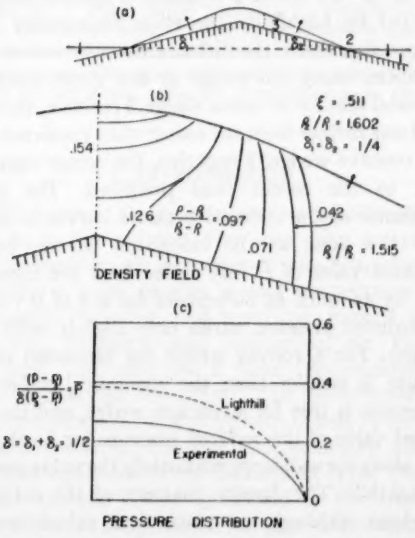

FIG. 2. (a) Shock wave pattern for a convex wedge showning the subscripts used on quantities in the various regions. (b) Density field for a convex wedge of $\delta=0.5$ radian for an incident shock strength of $\xi=0.5$. (c) Reduced pressure curve for the case shown in (b) with the Lighthill curve for comparison.

five-inch diameter windows with the aid of a Mach-Zehnder interferometer. Illumination was provided by a spark of 1-μsec duration which was triggered by an adjustable delay circuit. This made it possible to photograph the shock wave in the desired position after reflection from the wedge.

To interpret the experiments, the fringe shifts in the field were drawn up by using a method which involves superimposing a "blank" (fringe system of the undisturbed field) on a picture of the disturbed field.[5] From the fringe shift at a given point the density ratio at the same point could be calculated. Typical interferograms of the contour fringe type, shown in Fig. 1,

[4] Bleakney, Weimer, and Fletcher, Rev. Sci. Instr. **20**, 807 (1949).

[5] W. Griffith, J. Aeronaut. Sci. **19**, 252 (1952).

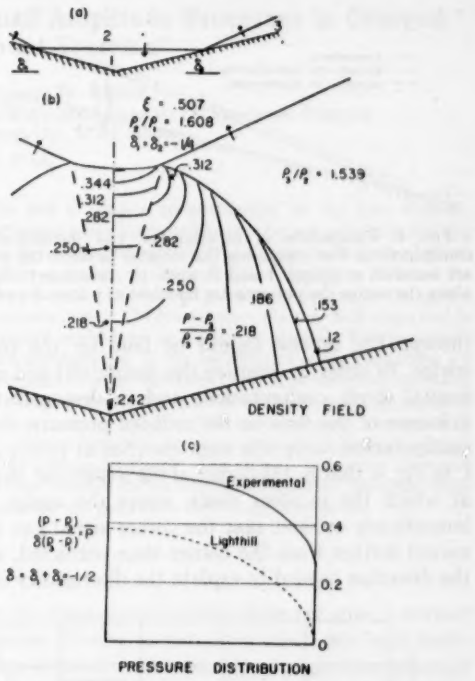

FIG. 3. (a) Shock pattern that exists before the incident wave has reached the corner showing the subscripts used in the various regions. (b) Density field for a concave wedge of $\delta=-0.5$ radian for an incident shock strength of $\xi=0.5$. (c) Reduced pressure curve for the case shown in (b) with the Lighthill curve for comparison.

illustrate the nature of the disturbance. Throughout this paper the following conventions will be used: no subscript on a quantity refers to the disturbed region around the corner, a subscript 1 refers to quantities in front of the incident shock, 2 to quantities behind the incident shock, and 3 to quantities in the uniform region behind the reflected shock. Figures 2(b) and 3(b) show typical density patterns for a convex and a concave wedge, respectively, for an incident shock strength of $\xi=0.5$ $(\xi=P_1/P_2)$. For the two cases the value of the quantity $\bar{P}=(P-P_3)/\delta(P_3-P_1)$ along the wall is plotted as a function of the distance from the corner in Figs. 2(c) and 3(c). The value of this so-called reduced pressure $\bar{P}$, as obtained from Lighthill's theory, is plotted for comparison. For the purposes of this comparison, the experimental and theoretical configurations have been matched at the corner of the wedge and at the intersection of the corner signal with the wedge. In Fig. 4 these points of matching are at A and B. It may be noted that for the convex wedge the reduced pressure along the wall is less than the predicted value, while for the concave wedge the reverse is true. This result is not surprising, since for any actual convex wedge there should be a flow away from the corner, thus lowering the pressure in this region below the value which is predicted by a linearized

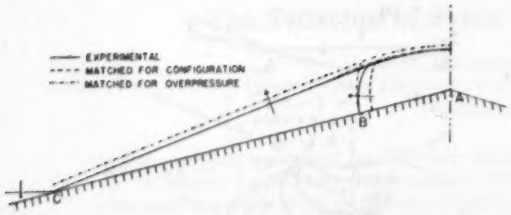

FIG. 4. Comparison of experimental and theoretical wave configurations. For comparing the reduced pressure the patterns are matched at points A and B while to demonstrate the flow along the wedge the patterns are matched at points A and C.

theory. The reverse should be true for the concave wedge. In order to compare the theoretical and experimental shock configurations and to demonstrate the influence of the flow on the reduced pressure, the two configurations have also been matched at points A and C in Fig. 4, that is, the corner of the wedge and the point at which the incident shock meets the wedge. It is immediately evident that the corner signal has indeed moved farther from the corner than predicted, and in the direction needed to explain the discrepancy in $\bar{P}$.

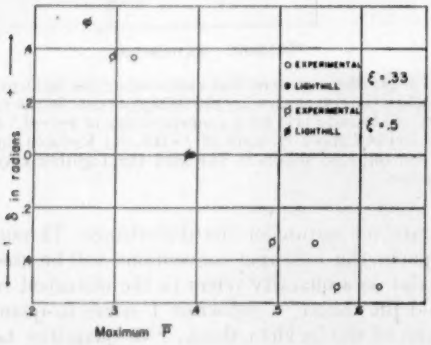

FIG. 5. The maximum value of the reduced pressure at two different shock strengths for the four wedges used, showing that $\bar{P}$ is relatively independent of shock strength. The predicted value is between the experimental values.

To compare further the experimental results with theory, the maximum value of the reduced pressure $\bar{P}$, which is the value at the corner, is plotted in Fig. 5 for the four wedge angles used. Since the reduced pressure in the Lighthill theory is independent of δ it has been assumed for the purposes of the plot that $\delta=0$ for the theoretical value. It is seen that for both $\xi=0.33$ and $\xi=0.5$ the predicted value is between the values for the convex wedge on one hand and the concave wedge on the other. In fact the value of $\bar{P}$ varies approximately linearly with the angle δ.

CONCLUSION

The configuration which results when a shock wave reflects symmetrically from a corner whose included angle is $(\pi-\delta)$, where δ is small, is qualitatively that predicted by Lighthill. The main discrepancy in the configuration lies in the distance that the corner signal has moved along the wedge at any given instant. It was found that for a convex wedge, δ positive, the corner signal was further from the corner than predicted, while for a concave wedge, δ negative, the corner signal was closer to the corner than predicted. The general appearance of the reduced pressure curves is qualitatively the same as the calculated curves, but the maximum value of $\bar{P}$ may differ from the theoretical value by as much as 50 percent for a δ of 0.5 radian. The reduced pressure varies only slightly with shock strength. For a convex wedge the measured reduced pressure is smaller than the theoretical value while the reverse is true for a concave wedge, and the interpolated value of the reduced pressure for $\delta=0$ at any point along the wall is approximately the value predicted by Lighthill. The density contours of the entire field are given although no theoretical calculations are available with which to compare them.

The authors wish to thank Professor Bleakney and Professor Griffith for their valuable suggestions.

A Model for Collision Processes in Gases. I. Small Amplitude Processes in Charged and Neutral One-Component Systems*

P. L. BHATNAGAR,† E. P. GROSS,‡ AND M. KROOK
Astronomy Department, Harvard University, Cambridge, Massachusetts and Laboratory for Insulation Research, Massachusetts Institute of Technology, Cambridge, Massachusetts

(Received November 27, 1953)

A kinetic theory approach to collision processes in ionized and neutral gases is presented. This approach is adequate for the unified treatment of the dynamic properties of gases over a continuous range of pressures from the Knudsen limit to the high-pressure limit where the aerodynamic equations are valid. It is also possible to satisfy the correct microscopic boundary conditions. The method consists in altering the collision terms in the Boltzmann equation. The modified collision terms are constructed so that each collision conserves particle number, momentum, and energy; other characteristics such as persistence of velocities and angular dependence may be included. The present article illustrates the technique for a simple model involving the assumption of a collision time independent of velocity; this model is applied to the study of small amplitude oscillations of one-component ionized and neutral gases. The initial value problem for unbounded space is solved by performing a Fourier transformation on the space variables and a Laplace transformation on the time variable. For uncharged gases there results the correct adiabatic limiting law for sound-wave propagation at high pressures and, in addition, one obtains a theory of absorption and dispersion of sound for arbitrary pressures. For ionized gases the difference in the nature of the organization in the low-pressure plasma oscillations and in high-pressure sound-type oscillations is studied. Two important cases are distinguished. If the wavelengths of the oscillations are long compared to either the Debye length or the mean free path, a small change in frequency is obtained as the collision frequency varies from zero to infinity. The accompanying absorption is small; it reaches its maximum value when the collision frequency equals the plasma frequency. The second case refers to waves shorter than both the Debye length and the mean free path; these waves are characterized by a very heavy absorption.

1. INTRODUCTION

THE dynamic theory of gases may be studied from two points of view. One may take as starting point the macroscopic equations of aerodynamics with the density ρ, mass velocity $\mathbf{q}$, and temperature T as independent variables, and involving various coefficients, e.g., viscosity, heat conduction, etc. On the other hand, one may use a more fundamental and general microscopic formalism. The most fruitful of such formalisms available at present is that in terms of one particle distribution functions satisfying integro-differential equations of the Boltzmann type. The distribution function $f(\mathbf{v},\mathbf{r},t)$ is defined by the condition that $f(\mathbf{v},\mathbf{r},t)d\mathbf{v}d\mathbf{r}$ is the number of particles at time t, in volume element $d\mathbf{r}$ about position $\mathbf{r}$, which have velocities in a range $d\mathbf{v}$ about $\mathbf{v}$.

The aerodynamic equations are adequate for treating a certain wide class of problems in gas dynamics and most of the developments of the theory have been in this domain. In this range the microscopic theory would not yield significantly different results. In fact, subject to certain conditions which delimit their range of applicability, the aerodynamic equations, together with explicit formulas for the various coefficients entering into them, are derivable from the microscopic theory. A detailed account of this derivation is presented in the book of Chapman and Cowling.[1]

There are, however many important situations in which the macroscopic theory does not give a correct description. During recent years interest in such problems has increased considerably. An extreme example of the breakdown of the aerodynamic theory, *viz.*, in the Knudsen region, has been known for some time; here the mean free path of a molecule is large compared to some linear dimension of the apparatus, and behavior at the boundaries becomes important. Other examples are provided by high-frequency sound waves in a rarefied gas and by plasma oscillations.

The solution of the Boltzmann equation is, in general, a matter of considerable difficulty even in cases corresponding to the physically simplest situations. Significant progress has been confined practically to the study of two limiting cases in which two different approximation procedures can be applied. A criterion for the range of validity of the approximate methods is provided by the comparison of some characteristic time τ (or characteristic length L) for the relevant process with the average time τ_e (or mean free path L_e) between molecular collisions.

For high density ($\tau \gg \tau_e$ or $L \gg L_e$) the Enskog-Chapman (E-C) theory may be used. The first approximation of the theory consists in assuming local thermodynamic equilibrium and a common drift velocity for all molecular species. The next approximation corrects the distribution function by terms proportional to the first derivatives of temperature, velocity, and density; this corresponds to the aerodynamic equations with coefficients of heat conduction, viscosity, and diffusion. The high-density region ($\tau \gg \tau_e$) is in fact the range in which the aerodynamic equations provide an adequate description. Higher approximations of the E-C theory lead to correction terms proportional to higher deriva-

* Sponsored by the U. S. Office of Naval Research, the U. S. Army Signal Corps, and the U. S. Air Force.

† Present address, New Delhi University, New Delhi, India.

‡ Present address, Physics Department, Syracuse University, Syracuse, New York.

[1] S. Chapman and T. G. Cowling, *The Mathematical Theory of Non-Uniform Gases* (Cambridge University Press, London, 1952), second edition.

tives of T, $\mathbf{q}$, ρ. The successive approximations of the E-C theory correspond to an expansion of the distribution function in powers of the mean free path L_c. If we consider sound waves with wavelength $L \gg L_c$, the first and second approximations are already sufficient to give all significant features of the process. However, when L becomes comparable with L_c, it is necessary to go to the third and even higher approximations to obtain adequate results; as discussed by Herzfeld[2] important dynamic contributions appear only in approximations higher than the second. The third approximation already involves formidable labor and has been used to solve only the simplest problems. Consideration of higher approximations is, in any case, of doubtful value as the entire procedure breaks down in just the range where the contributions from these higher-order terms become important. In addition, the boundary conditions in many problems cannot be specified properly within the scope of the F-C formalism. A different approach, using expansions in terms of Hermite polynomials in velocity space, has been given by Grad.[3] He uses some moments of low order in addition to the usual ones representing ρ, $\mathbf{q}$, and T. The procedure involves a gain in simplicity over the E-C theory but is still quite complicated. It is basically a high-density theory and is capable of dealing only with boundary conditions which can be specified in terms of the moments appearing in the theory. The limitations of any theory based on the use of a finite number of moments will be brought out in the discussions of this series of papers.

The opposite limiting case ($\tau \ll \tau_c$ or $L \ll L_c$) has been studied extensively by mean-free-path methods. Jaffé[4] has shown that this case can be treated from the point of view of the Boltzmann equation by expanding the distribution function in a series of inverse powers of the mean free path; the first approximation consists in neglecting collisions completely. In contrast to the high density limit, the problem can be solved subject to correct microscopic boundary conditions. The method becomes extremely complicated when one attempts to carry out higher approximations to obtain results which go much beyond those obtainable by simple mean-free-path arguments. For this reason this method has not been applied to any great extent.

The low-density case is of particular interest for ionized gases where the coupling of the material motions with the electromagnetic field plays an essential and determining role. Ionized gases occur widely in nature and in the laboratory with densities and temperatures covering a large range. In laboratory discharge tubes and similar devices pressures ranging from 10^{-3} mm up to 10^{4} mm are commonplace. In the negative glow of a discharge tube at 10^{-2} mm the material is at least singly ionized; the electron density is about 10^{11}/cc and the mean free path is of the order of a few cm. At pressures of the order of an atmosphere the ionization is only partial; the electron density is of the order of 10^{15}/cc and mean free paths are of the order of 10^{-5} cm. In nature the range covered is considerably wider.[5] The interstellar medium has a density varying from 10^{-24} g/cc up to 10^{-21} g/cc. The gas may be neutral as in the low-temperature HI regions, or completely ionized as in HII regions near very luminous stars. In the outer corona of the sun the degree of ionization is high and the electron density is of the order of 10^{8}/cc. As we proceed in towards the center of the star, the degree of ionization varies considerably. In the photospheric layers (mainly responsible for the sun's continuous spectrum), the particle density is of the order of 10^{11}/cc and the ionization is small. Near the center of the sun we of course have very much greater densities and temperatures and a very high degree of ionization.

It would be very desirable to have a theory capable of treating the whole range from low to high densities for mixtures of neutral and ionized gases. The treatment of an ionized gas involves certain new elements in addition to those for neutral gases; this will be discussed in detail in Sec. 2. The region of intermediate density ($\tau \simeq \tau_c$ or $L \simeq L_c$) has thus far been practically unexplored on account of excessive mathematical complications. The procedures discussed above for the two limiting cases of high and low density are not applicable in this region. For similar reasons, the solution of definite initial and boundary value problems with the Boltzmann equation has also not been studied to any extent. In order to make some progress in the investigation of such problems it is necessary to simplify the mathematical procedures quite considerably.

The aim of this series of papers is to propose a treatment of collision processes in gases which leads to just such a simple mathematical formalism. The main difficulty in handling the full Boltzmann equation arises from the complicated nature of the collision terms. In contrast to other procedures, ours consists in replacing these troublesome collision integrals by mathematically simpler terms; these, however, are chosen so as to conform to the conservation laws for mass, momentum, and energy and at the same time to represent certain essential features of collisions, e.g., persistence of velocity. This approach makes possible a survey of the whole range from low density to high density, including the intermediate region. It leads to the correct asymptotic behavior in the two limiting cases mentioned above. The mathematical simplification introduced with the model enables one to solve problems which are physically more complex than those soluble with the standard

[2] K. F. Herzfeld, Ann. Physik 23, 465 (1935); see also H. Primakoff, J. Acoust. Soc. Am. 14, 14 (1942); H. Tsien and R. Schamberg, J. Acoust. Soc. Am. 18, 334 (1946); C. S. W. Chang and G. Uhlenbeck, Univ. Mich. Dept. Eng. Research, Repts., February, 1948 (unpublished); M. Kohler, Abhandl. braunschweig. wiss. Ges. 2, 104 (1950).

[3] H. Grad, Commun. Pure and Appl. Math. 2, 331 (1949).

[4] H. Jaffé, Ann. Physik 6, 195 (1930).

[5] J. A. Hynek, *Astrophysics* (McGraw-Hill Book Company, Inc., New York, 1951).

Boltzmann equation; in addition, one is able to treat definite initial and boundary-value problems.

Each collision term in a Boltzmann equation consists of two parts. The one part,[1] $-\int\int f_1(\mathbf{v}_1,\mathbf{x},t)f_2(\mathbf{v},\mathbf{x},t) \times k_{12}d\mathbf{k}d\mathbf{v}_2$, represents particles removed or absorbed from a definite velocity range by collisions; the other part represents the particles emitted into that range as a result of collisions. Our absorption term, $-n(\mathbf{x},t) \times k(\mathbf{v},\mathbf{x},t)f(\mathbf{v},\mathbf{x},t)$, where $n(\mathbf{x},t)=\int f(\mathbf{v},\mathbf{x},t)d\mathbf{v}$, is substantially the same as that in the Boltzmann equation. The emission term (which is the real source of difficulty) is replaced in our crudest model by a term representing a Maxwellian distribution of the emitted particles with a density, mass velocity, and temperature satisfying mass, momentum, and energy conservation requirements. This bears some resemblance to the "local thermodynamic equilibrium" model used in discussing the formation of the continuous spectrum in stellar atmospheres. The similarity of the Boltzmann equation to that governing propagation of radiation has been discussed by Jaffé.[4] The method proposed here is quite different, however, and is capable of considerable extension and generalization to include the study of physically complex problems.

The plan of this series of papers is the following: In the first paper we study systems which are, or may be represented by, one-component systems; to illustrate the technique we avoid mathematical complications by making the simplified assumption of constant collision time. This model is applied to the study of dispersion and absorption of sound in a simple un-ionized gas and also to the oscillations of an ionized gas with the additional simplifying assumption that the positive ions may be replaced by a uniform constant distribution of positive charge. The physically most significant feature here is the transition from low-pressure plasma waves to high-pressure sound-type waves.

In the second paper we extend this treatment to a consideration of two- and three-component systems. This includes a discussion of the translational dispersion effect for sound waves in un-ionized gas mixtures. The further effect on small oscillations arising from the coupling between positive ions and neutrals will be studied over the whole range from low to high pressures; the two types of wave which occur at low pressures are found to merge into a single type of wave as the pressure increases and the collision mechanism begins to predominate.

A third paper will deal with the oscillations of ionized gases in static external magnetic fields. The range of validity of the conventional magnetohydrodynamic theory will be discussed there. An important point dealt with in that paper is the way in which gaps in the frequency spectrum, present at low densities, disappear as the density is increased.

The discussions of the first three papers are confined to initial value problems in the theory of small oscillations. The accent there is substantially on the study of the mechanism of cooperation in ionized and unionized gases. In a fourth paper we abandon the assumption of constant collision time and examine physically more realistic models. The connection of our kinetic equations with the standard Boltzmann equation is discussed in more detail. In subsequent papers we shall study particular boundary value problems and some nonlinear processes.

2. EARLIER TREATMENTS OF SYSTEMS OF CHARGED PARTICLES

The theory of oscillations in ionized gases is still in a rather tentative state. However, a number of features can be understood at least qualitatively. An essential difference from the theory for neutral gases is that approximately undamped waves can be propagated not only at high pressures ($\tau \gg \tau_c$), but also at low pressures ($\tau \ll \tau_c$).

The mechanisms responsible for the cooperative behavior of the medium are different in the extreme cases of low density and high density.[6] At low densities the collisions are only of secondary importance, and the forces acting to change the state of motion of a particle are electromagnetic in character. Energy and momentum are transferred from one group of particles to another through the intermediary of the electromagnetic field in a way now familiar from the study of microwave devices. It is important to note, however, that the transfer of energy by the high-frequency components of a pulse is a very slow process in low-pressure plasmas. If one neglects the effect of random thermal motion, the group velocity of the waves is zero and a disturbance would remain completely localized. The angular frequency ω is independent of the wave number p and is the plasma frequency $\omega_p=(4\pi n_0 e^2/m)^{\frac{1}{2}}$, where $-e$, m are the charge and mass of the electron, and n_0 is the number density. Including the effects of thermal motions, the group velocity of high-frequency waves is approximately $v_g=(3pa/\omega_p)a$, where $a=(kT/m)^{\frac{1}{2}}$, and k is Boltzmann's constant; this is much smaller than the sound velocity, $5a/3$, for waves whose wave number p is smaller than the inverse of the Debye length (a/ω_p). In addition, waves with $p \simeq a/\omega_p$ are very heavily damped.

Let us now consider some attempts which have been made to treat the oscillations of ionized gases quantitatively by the methods of kinetic theory. The long range of the Coulomb force implies that the concept of a definite binary collision will be inadequate except for very close encounters. Instead, every charge particle is continually interacting with all the particles of the assembly. An important theoretical step, making possible the approximate treatment of many properties of ionized gases, was taken by Vlasov.[7] Langmuir[8] had already pointed out that the Debye length is character-

[6] D. Bohm and E. P. Gross, Phys. Rev. **75**, 1851, 1864 (1949).
[7] A. Vlasov, J. Phys. (U.S.S.R.) **9**, 25, 130 (1945).
[8] I. Langmuir, Proc. Natl. Acad. Sci. U. S. **14**, 627 (1928).

istic of the dynamic behavior as well as of the static properties of an ionized gas. Processes involving characteristic lengths longer than the Debye length call into play the cooperative behavior of the particles of an ionized gas. Vlasov assumed that apart from close collisions, a particle moves in an average electric field arising from the other particles and proposed to describe the system by a one-particle distribution function $f(\mathbf{v},\mathbf{x},t)$. He wrote for the description of longitudinal disturbances,

$$\frac{\partial f}{\partial t}+(\mathbf{v}\cdot\nabla)f-\frac{e\mathbf{E}}{m}\cdot\frac{\partial f}{\partial v}=\left.\frac{\delta f}{\delta t}\right|_c, \tag{1}$$

$$\nabla\cdot\mathbf{E}=4\pi e\left\{n_0-\int f d\mathbf{v}\right\}, \tag{2}$$

where n_0 is the density of the uniform continuous positive background. The force $e\mathbf{E}$ arising from the charge concentrations of the particles themselves has been inserted in the kinetic equation in the position appropriate to body forces. Vlasov termed this the integral interaction term; it is designed to treat the forces on a given particle arising from other particles at distances greater than a Debye length. The term $\delta f/\delta t|_c$ represents the instantaneous change of the distribution function arising from closer collisions. The question then arises as to the explicit form to take for $\delta f/\delta t|_c$. The very close encounters at a distance less than the interparticle distance can be represented by the binary collision term of Boltzmann type. For the more distant collisions such a representation is less certain. It is important to note that in a low-pressure plasma the Debye length is, in general, many times the interparticle distance. Thus, in a collision between two particles there are, in general, many other particles between them. In spite of this, many authors[9] have treated various processes in ionized gases using the binary collision approach even for distant collisions. Such distant collisions involve small momentum transfers. Expansion of the distribution functions in the collision integral term in powers of the momentum transfers leads to terms very similar to those given by the Fokker-Planck equation. This procedure is, of course, approximate since it attempts to replace many-body collisions by a series of binary collisions. The equation neglects the "Onsager correction" and other correlation effects; these require a more refined description in terms of many particle distribution functions. However, in the present primitive state of the theory it is worth while exploring the consequences of this approach. In a later paper we shall discuss the application of this method to the plasma oscillation problem in some detail. The Fokker-Planck approach has already been used in the study of plasma oscillations by Logunov.[10] He obtains damping and dispersion of the waves, but his method is incapable of treating high-pressure plasmas because of an inadequate representation of the collision terms.

3. KINETIC MODELS OF COLLISION PROCESSES

The equations described above for neutral and ionized gases are complicated to handle in practice because of the intractable nature of the Boltzmann binary collision term. We shall now discuss some simple kinetic models which permit of exact mathematical treatment including the solution of definite boundary value problems. A more detailed discussion of the validity of our representation of collisions and its relation to the standard Boltzmann equation will be given in a subsequent paper. In this section of the present paper we introduce the simplest kinetic model; we give the underlying motivation for the form of this model from one point of view.

In many kinetic problems, for example, the effect of electron collisions on the propagation of radio waves in the ionosphere, it is convenient to avoid the complexities of the Boltzmann equation by using a mean-free-path treatment. One replaces the collision integral by a relaxation term of the form

$$\left.\frac{\delta f}{\delta t}\right|_c=\frac{f_0-f(\mathbf{v},\mathbf{x},t)}{\tau(v)}, \tag{3}$$

where $\tau(v)$ is a velocity-dependent collision time. This expresses the fact that collisions tend to relax the distribution function to an equilibrium value f_0. We illustrate our discussion of collision models by referring to oscillatory problems where a characteristic time enters in a natural way. The relaxation model then describes the destruction of phase of an ordered motion on collision and leads to a damping frequency of order $1/\tau$ in the amplitude, where τ is some suitable average collision time. This type of model has the defect[11] that charge is not conserved instantaneously but only on the average over a cycle. It is, however, easy to remedy this at least in the case of constant collision time by taking for the collision term

$$\left.\frac{\delta f}{\delta t}\right|_c=-\frac{f}{\tau}+\frac{n(\mathbf{x},t)}{\tau}f_0(\mathbf{v}), \tag{4}$$

where $n(\mathbf{x},t)=\int f d\mathbf{v}$ is the fluctuating density. Thus, particles in a range $d\mathbf{v}$ about velocity $\mathbf{v}$ are absorbed at a rate proportional to the number $f(\mathbf{v},\mathbf{x},t)$ at $(\mathbf{x},t)$, and re-emitted at a rate proportional to the density at $(\mathbf{x},t)$ and with a Maxwellian distribution of velocities.[12] We may regard this as a model representing electron-neutral collisions. (This representation will be studied in

[9] D. Gabor, Z. Physik 84, 474 (1933); L. Landau, Physik. Z. Sowjetunion 10, 154 (1936); D. Bohm and L. H. Aller, Astrophys. J. 105, 131 (1947); Cohen, Spitzer, and Routly, Phys. Rev. 80, 230 (1950).

[10] A. A. Logunov, Zhur. Eksptl. i Teoret. Fiz. 20, 458 (1950).

[11] E. P. Gross, Phys. Rev. 82, 232 (1951).

[12] For a discussion of this model from a different point of view, see reference 6, p. 1864.

more detail in Paper 2, where we treat the coupling of charged and uncharged systems more adequately.) Upon integrating over velocities we find $\int \delta f/\delta t|_c d\mathbf{v}=0$ so that the number of particles is instantaneously conserved in collisions in contrast to the earlier case where the conservation applies only for the averages over finite times. There is, however, no instantaneous conservation of momentum or energy. In fact, we have

$$\int m\mathbf{v}\left.\frac{\delta f}{\delta t}\right|_c d\mathbf{v}=-\frac{m}{\tau}\int \mathbf{v}f d\mathbf{v}, \quad \int \frac{mv^2}{2}\left.\frac{\delta f}{\delta t}\right|_c d\mathbf{v}=\frac{m}{2\tau}\left\{\frac{3kT_0}{m}-\int v^2 f d\mathbf{v}\right\},$$

T_0 being the equilibrium temperature. This represents a gain or loss of total energy and momentum by collision, depending on the phase of f.

Thus far we have discussed a model which can represent only electron-neutral or ion-neutral collisions in which the collision term is linear in the electronic distribution function. The linear feature would also be present in a more exact study of the collisions. However, in considering electron-electron or ion-ion collisions which are important in the high-pressure ionized gas, we should have collision terms quadratic in the electron and the ion distribution functions. (In the study of small amplitude disturbances such terms may, of course, be linearized, but we now seek a general formulation.) We shall construct a simple model, quadratic in f which reproduces certain essential features of the collisions without introducing the troublesome Boltzmann collision integral. However, this model will still not satisfy all conservation requirements. Let us write

$$\frac{\partial f}{\partial t}+(\mathbf{v}\cdot\nabla)f-\frac{e\mathbf{E}}{m}\cdot\frac{\partial f}{\partial \mathbf{v}}=-\frac{n(\mathbf{x},t)}{\sigma}f(\mathbf{v},\mathbf{x},t)+\frac{n^2(\mathbf{x},t)}{\sigma}\bar{F}, \quad (5)$$

$$\bar{F}=\left(\frac{m}{2\pi kT_0}\right)^{\frac{3}{2}}\exp(-mv^2/2kT_0). \quad (6)$$

Thus, $\int \bar{F}d\mathbf{v}=1$. We have taken the rate at which particles leave a particular velocity range at $(\mathbf{x},t)$ as proportional to $f(\mathbf{v},\mathbf{x},t)$, and to the density $n(\mathbf{x},t)$. The number of particles emitted at $(\mathbf{x},t)$ equals the number absorbed at $(\mathbf{x},t)$; this number is proportional to the square of the density and is emitted with a Maxwellian velocity distribution. $\lambda=n_0/\sigma$ is a collision frequency, here assumed independent of velocity. It is easily verified that the total number of particles is instantaneously conserved by the collision processes, while momentum and energy are not.

It is now worth while to examine the dispersion relation for small-amplitude oscillatory processes governed by Eq. (5). For brevity, we adopt the approach of looking for plane-wave solutions of the type $\exp[i(px-\omega t)]$. We shall show later that this procedure is valid for the treatment of certain types of initial value problems for finite collision time and for waves of large wavelength. We write

$$f=f_0(1+\phi) \quad f_0=n_0\bar{F}, \quad (7)$$

$$n(\mathbf{x},t)=n_0(1+\nu), \quad (8)$$

where ϕ and ν are dimensionless quantities small compared to unity. We assume ϕ, ν, and $E=E_x$ oscillate as $\exp[i(px-\omega t)]$ and neglect products of these variables. Then Eq. (5) becomes

$$i(pu-\omega)\phi+(eE/kT_0)u=\lambda(\nu-\phi), \quad (9)$$

where u is the x component of $\mathbf{v}$. We also have

$$\nu=\int \bar{F}\phi d\mathbf{v}, \quad (10)$$

$$E=-(4\pi en_0/ip)\nu. \quad (11)$$

Eliminating E we find the distribution function

$$\phi=\mathrm{Re}\frac{\nu}{\lambda+i(pu-\omega)}\left\{\lambda+\frac{4\pi n_0e^2}{kT_0}\frac{u}{ip}\right\}, \quad (12)$$

and the dispersion relation

$$1=\int\frac{\bar{F}d\mathbf{v}}{\lambda+i(pu-\omega)}\left\{\lambda+\frac{4\pi n_0e^2}{kT_0}\frac{u}{ip}\right\}. \quad (13)$$

If one expands the denominator of (13) in powers of $ipu/(\lambda-i\omega)$ and restricts the study to long wavelength one finds

$$\omega^2=\omega_p^2-i\omega\lambda-\frac{kT_0}{m}p^2\left\{\frac{3\omega_p^2}{(\lambda-i\omega)^2}-\frac{\lambda}{\lambda-i\omega}\right\}. \quad (14)$$

We conclude from this relation that the oscillations are strongly damped at high pressures. For the case of a plasma gas the complex frequency is approximately $\omega\simeq-\frac{1}{2}i\lambda\pm(-\frac{1}{4}\lambda^2+\omega_p^2)^{\frac{1}{2}}$; this is of the order of the collision frequency for λ small and always corresponds to damping. For a neutral gas, $\omega_p=(4\pi n_0e^2/m)^{\frac{1}{2}}=0$, and so $\omega^2\simeq-i\omega\lambda+(kT_0/m)p^2\lambda/(\lambda-i\omega)$; thus in the limit of very high collision frequency one obtains highly damped oscillations instead of undamped sound waves.

We thus see that this model is incapable of yielding correct results at the high-pressure limit. What is the origin of this failure? As discussed earlier and in reference 6, the processes of organization are very different for a plasma and for a sound wave. In particular, one must recognize the velocity organization characteristic of a sound wave. Statistically, a particle with excess velocity at a point makes collisions which slow it down to the flow velocity at the point in question. Similarly particles which are moving too slowly tend to have their speed increased to that of the flow velocity. The collision models studied thus far fail to incorporate this

feature so that it is not surprising that they do not yield sound-type collisions in the high-density limit.

We now propose a simple model which succeeds in giving an adequate description of both the high- and low-density plasma. For a one-component system, one writes

$$\partial f/\partial t+(\mathbf{v}\cdot\nabla)f-e\mathbf{E}/m\cdot\partial f/\partial\mathbf{v} = -(n(\mathbf{x},t)/\sigma)f(\mathbf{v},\mathbf{x},t)+(n^2/\sigma)\Phi, \quad (15)$$

$$\Phi=[m/2\pi kT(\mathbf{x},t)]^{\frac{1}{2}} \times\exp\{-m/2kT(\mathbf{x},t)[\mathbf{v}-\mathbf{q}(\mathbf{x},t)]^2\}, \quad (16)$$

$$\int\Phi d\mathbf{v}=1,$$

$$n(\mathbf{x},t)=\int f(\mathbf{v},\mathbf{x},t)d\mathbf{v}, \quad (17)$$

$$q(\mathbf{x},t)=1/n(\mathbf{x},t)\int\mathbf{v}f(\mathbf{v},\mathbf{x},t)d\mathbf{v}, \quad (18)$$

$$3kT(\mathbf{x},t)/m=1/n\int(\mathbf{v}-\mathbf{q})^2fd\mathbf{v}, \quad (19)$$

$$\nabla\cdot\mathbf{E}=4\pi e\left\{n_0-\int fd\mathbf{v}\right\}, \quad (20)$$

where $\mathbf{q}(\mathbf{x},t)$ and $T(\mathbf{x},t)$ define the flow velocity and temperature at $\mathbf{x}$ and t. We have assumed the re-emitted particles at $(\mathbf{x},t)$ to emerge with a Maxwellian distribution centered about the flow velocity $\mathbf{q}$ and corresponding to temperature $T(\mathbf{x},t)$. It is easily verified that, with the definitions of $\mathbf{q}$ and T given, the collision terms instantaneously conserve particle number, momentum, and energy. The kinetic equation (15) is a nonlinear integro-partial differential equation. However, it is considerably simpler than the standard Boltzmann equation since the distribution function enters into the collision terms of Eq. (15) in a simple way: as f, $\int fd\mathbf{v}$, $\int\mathbf{v}fd\mathbf{v}$, and $\int v^2fd\mathbf{v}$. Thus, one finds a solution of Eq. (15) in terms of the undetermined functions $\mathbf{q}(\mathbf{x},t)$, $n(\mathbf{x},t)$, $T(x,t)$, $E(x,t)$, and then inserts this solution into Eqs. (17) to (20). This establishes the conditions of compatibility which serve to determine the solution completely. For the particular case of small-amplitude oscillations the procedure yields a dispersion relation specifying the connection between frequency and wavelength in its dependence on collision frequency, plasma frequency, temperature, etc.

The use of conditions of compatibility bears a certain resemblance to the first step in the Enskog-Chapman technique of solving the Boltzmann equation. However, the methods are quite different. In the E-C technique one assumes a locally Maxwellian form for the distribution function in first approximation and then determines the density, velocity, and temperature entering in this choice by conditions of compatibility; here we change the collision term itself and solve for the distribution function rigorously. The solution will, in general, not have the form assumed in the Enskog-Chapman method. Our approach has the virtue that one can solve definite initial and boundary value problems wholly within the frame work of a microscopic formalism. The model we have described involves the assumption of a collision time independent of velocity. In a later paper we shall show that this is not an essential restriction and shall make, along with other generalizations, the one to velocity-dependent collision times. In the present paper we shall study the consequences of Eqs. (15) to (20) inasmuch as it appears to be the simplest model capable of yielding physically satisfactory results throughout the entire range of pressure.

There exists a number of studies of the oscillations of ionized gases using transport equations. For example, the Thomsons[13] and subsequently Bailey[14] base their discussions on Maxwell's equations of transfer. As applied to a one-component system of charged particles these are the equations of continuity, of momentum transfer, and Poisson's equation. When no static magnetic field is present one obtains the dispersion relation $\omega^2=\omega_p^2+(kT_0/m)p^2$. It is not clear from these transport treatments whether the results are meant to apply at low pressures or high pressures; in fact, they could be valid only at high pressures. Even there, however, they are inexact, as they correspond to an isothermal treatment. Thus, in terms of the model discussed above, the temperature T is treated as a constant and energy balance is not maintained instantaneously in collisions; we shall obtain Thomson's results from our model at high pressures and in the isothermal approximation. The high-pressure nature of the Thomson approach for a one-component system is brought out in an alternative treatment by Linder[15] who adds a pressure term to the equation of motion of a particle and with an isothermal assumption obtains the same result as Thomson. At low pressures the correct dispersion relation as found by an exact treatment of the kinetic equation is $\omega^2=\omega_p^2+(3kT_0/m)p^2$, differing from that at high pressures by the factor 3. We expect then that, in an isothermal treatment, there will be a change in the frequency corresponding to a given wavelength as one goes from low to high pressures. This is indeed the case, as will be shown with our collision model; in addition, we find an accompanying absorption which reaches a maximum value when the collision frequency is of the order of magnitude of the plasma frequency.

We have thus far confined discussion of the transport method to isothermal models. It is possible to generalize the transport procedure to include temperature varia-

[13] J. J. and G. P. Thomson, *Conduction of Electricity through Gases* (Cambridge University Press, Cambridge, 1933), Vol. 2, p. 353.
[14] V. A. Bailey, Phys. Rev. 78, 428 (1950).
[15] E. G. Linder, Phys. Rev. 49, 753 (1936).

tions, by applying a moment method to the Boltzmann equation.[11] One finds a dispersion relation $\omega^2=\omega_p^2+(5/3)p^2kT_0/m$. For the uncharged case this gives the correct "adiabatic" law of sound-wave propagation $\omega=(5/3)^{\frac{1}{2}}(kT_0/m)^{\frac{1}{2}}p$. We shall see that the result is also correct for an ionized gas; the transport approach owes its validity at high pressures to the fact that momentum and energy are collisional invariants. Existing transport treatments are certainly incorrect quantitatively in the low-pressure region and even fail to give a qualitatively adequate description when magnetic fields are present.[11] For the treatment of the effects of heat conduction and viscosity which depend on the mean free path a kinetic approach of the type here presented is needed.

4. ISOTHERMAL APPROXIMATION

The simplest collision model yielding both plasma waves at low temperature and also sound waves at high pressures may be obtained by taking T constant in Eqs. (15) to (20). This is not entirely realistic since it yields the Newtonian isothermal sound speed at high pressures. But the fact that the number of variables is one less, simplifies the calculations considerably. For the sake of ease of exposition we shall discuss this case in detail and shall then merely sketch the treatment of the more general case including temperature variations. The isothermal case is also of some interest in itself since the work of Thomas and Bailey is based on the isothermal approximation. The results of main physical interest are presented in Figs. 1 to 5. Figures 1 and 2 show the dispersion and absorption of a one-component charged system as a function of collision time. Figure 5 shows the absorption and the translational dispersion effect in a neutral monatomic gas.

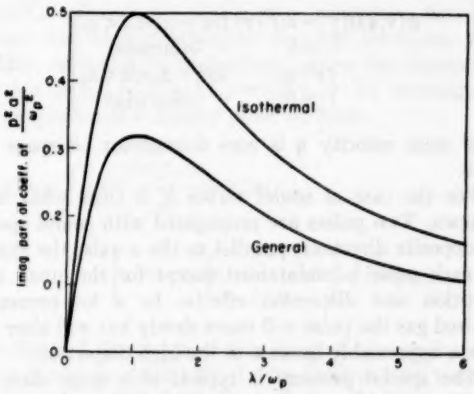

FIG. 1. Absorption of ionized gas as function of collision frequency.

The equations describing the system of particles in the approximation of this section are Eqs. (15) to (18), and (20). We do not use Eq. (19) but set the temperature equal to a constant T_0, the equilibrium temperature of the gas. As we are concerned with small amplitude oscillations we shall neglect quantities quadratic in the oscillating variables and arrive at a set of linear equations. The consistency of the linearization procedure can be checked by comparing the terms neglected (as estimated with the linear approximation) with the terms retained. For the case of low-pressure plasma oscillations a breakdown of the linear approximation is closely connected with the presence of a large number of trapped particles moving with a velocity close to the wave velocity. These particles play a role quite different from other particles and make possible types of solutions outside the scope of the linear approximation.

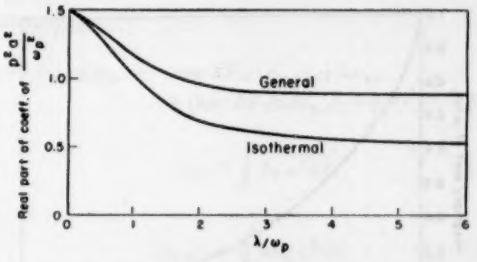

FIG. 2. Dispersion of ionized gas as function of collision frequency.

Put

$$f(\mathbf{v},\mathbf{x},t)=n_0\bar{F}\{1+\phi\}, \tag{21}$$

$$n(\mathbf{x},t)=n_0\{1+\nu\}. \tag{22}$$

Then ϕ and ν are dimensionless quantities. Equations (15) to (20) then become

$$\nu(\mathbf{x},t)=\int\phi\bar{F}d\mathbf{v}, \tag{23}$$

$$\mathbf{q}(\mathbf{x},t)=\int\mathbf{v}\phi\bar{F}d\mathbf{v}, \tag{24}$$

$$\nabla\cdot\mathbf{E}=-4\pi en_0\nu. \tag{25}$$

In the linearized theory, ϕ, ν, $\mathbf{q}$, $\mathbf{E}$ are quantities of first order of smallness. We consistently neglect all products and higher powers of these quantities. On expanding

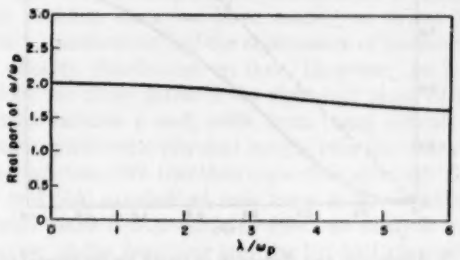

FIG. 3. Dispersion of ionized gas for wavelength equal to Debye length.

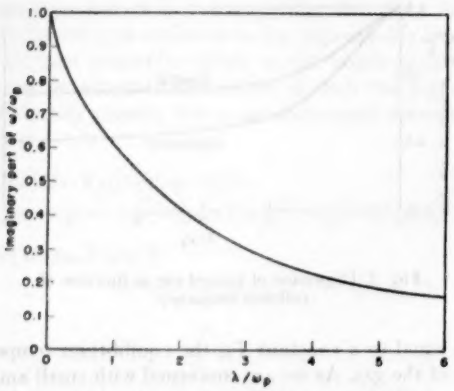

FIG. 4. Absorption of ionized gas for wavelength equal to Debye length.

the exponential in Eq. (16) (neglecting q^2 and higher powers), we find

$$\Phi=\bar{F}\left\{1+\frac{m}{kT_0}\mathbf{v}\cdot\mathbf{q}\right\}. \tag{26}$$

The linearized kinetic equation then becomes

$$\frac{\partial\phi}{\partial t}+(\mathbf{v}\cdot\nabla)\phi+\frac{e\mathbf{E}\cdot\mathbf{v}}{kT_0}=\lambda\left(\nu-\phi+\frac{m}{kT_0}\mathbf{v}\cdot\mathbf{q}\right). \tag{27}$$

Equations (21) to (27) form the basis for the further analysis of this section.

Landau[16] has emphasized the lack of rigor in the procedure of looking for solutions of Eq. (27) of the type where all quantities have a time and space variation

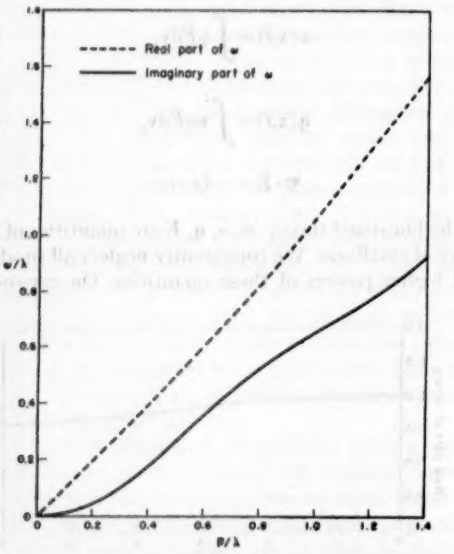

FIG. 5. Absorption and dispersion of sound for isothermal case.

[16] L. D. Landau, J. Phys. (U.S.S.R.) **10**, 25 (1946).

$e^{i(px-\omega t)}$. One must consider also the solutions of the homogeneous parts of Eqs. (20) and (27) and take the correct linear combination in order to solve a definite initial or boundary value problem. In this paper we examine a one-dimensional initial value problem, the propagation of a pulse. Suppose that at times $t<0$ the particle density is uniformly n_0 throughout unbounded space except for a small region between $-x_0$ and x_0 confined between two walls, where the density is $n_0(1+\nu_0)$. At time $t=0$ the walls are removed and we ask about the subsequent behavior of the system. To solve the problem the distribution function at $t=0$ must be specified. This initial distribution depends on the particular (macroscopic) mode of preparation of the system. If, for example, the present system has been prepared by compressing the gas in $(-x_0,+x_0)$ slowly over a time very long compared to the mean time between collisions, the initial distribution function will be very nearly Maxwellian.

We take as initial conditions at $t=0$:

$$\phi(\mathbf{v},\mathbf{x},0)\begin{cases}=\nu_0\bar{F}(\mathbf{v}) & \text{for } -x_0<x<x_0\\ =0 & \text{otherwise}\end{cases}\quad\begin{cases}\nu=\nu_0 & \text{for } -x_0<x<x_0\\ =0 & \text{otherwise}\end{cases}. \tag{28}$$

The mass velocity $\mathbf{q}$ is zero throughout all space at $t=0$.

For the case of sound waves it is clear what will happen. Two pulses are propagated with sound speed in opposite directions parallel to the x axis; the shape of each pulse is maintained except for the small absorption and dispersion effects. In a low-pressure, ionized gas the pulse will move slowly but will alter its shape appreciably because of the high dispersion.

The special problem is typical of a large class of problems which may be solved by first performing a Fourier expansion in unbounded x space. We write

$$\phi(\mathbf{v},\mathbf{x},t)=\int\phi_p(\mathbf{v},t)e^{i\mathbf{p}\cdot\mathbf{x}}d\mathbf{p}, \text{ etc.} \tag{29}$$

From Eqs. (23) to (27) we find the following equations for the Fourier transforms:

$$\frac{\partial\phi_p}{\partial t}+i\mathbf{p}\cdot\mathbf{v}\phi_p+\frac{e\mathbf{E}_p\cdot\mathbf{v}}{kT_0}=\lambda\left(\nu_p-\phi_p+\frac{m}{kT_0}\mathbf{v}\cdot\mathbf{q}_p\right), \tag{30}$$

$$\nu_p(t)=\int\phi_p(\mathbf{v},t)\bar{F}d\mathbf{v}, \tag{31}$$

$$q_p(t)=\int\mathbf{v}\phi_p\bar{F}d\mathbf{v}, \tag{32}$$

$$i\mathbf{p}\cdot\mathbf{E}_p=-4\pi en_0\nu_p(t). \tag{33}$$

These equations are a determined set if one specifies $\phi_p(\mathbf{v},t)$ at time $t=0$. Thus we must find the solutions of

Eqs. (30) to (33) for which each Fourier component satisfies the appropriate initial condition. One then superposes the ϕ_p to find $\phi(\mathbf{v},\mathbf{x},t)$.

For example, in the problem discussed above

$$\left.\begin{aligned}\phi_p(\mathbf{v},0)&=\int_{-x_0}^{+x_0}\int_{-\infty}^{+\infty}\int_{-\infty}^{+\infty}\nu_0\bar{F}e^{-ip\cdot x}d\mathbf{x}\\&=2\nu_0\frac{\sin(p_x x_0)}{p_x}\delta(p_y)\delta(p_z)\bar{F}\\ \nu_p(0)&=2\nu_0\frac{\sin(p_x x_0)}{p_x}\delta(p_y)\delta(p_z)\end{aligned}\right\},\tag{34}$$

where $\delta(x)$ is the Dirac delta function. Let us suppose that $\nu_p(t)$ has the value $\nu_p(t)=\frac{1}{2}\nu_p(0)(e^{+i\omega t}+e^{-i\omega t})$. For oscillations of a one-component plasma without thermal motions, $\omega=\omega_p$ is independent of p and the disturbance remains localized. For isothermal sound waves, $\omega=p(kT_0/m)^{\frac{1}{2}}$ and we obtain two oppositely directed pulses. For long wavelengths and low pressures, the plasma, including thermal effects, obeys the dispersion relation $\omega\simeq\omega_p+(3/2)(kT_0/m)(p^2/\omega_p)$. To investigate the properties of a density pulse we form

$$\nu(\mathbf{x},t)=\nu_0\int e^{ip\cdot x}\frac{\sin(p_x x_0)}{p_x}\delta(p_y)\delta(p_z)\times\left[e^{i\omega_p t}\exp\left(-i\frac{3}{2}\frac{kT_0}{m}p^2t\right)+\text{conj. comp.}\right].$$

The detailed discussion of this integral is complicated and will not be given here. In the limit of long times, $\nu(\mathbf{x},t)$ tends to zero throughout all space indicating the spreading of the initially sharp pulse due to dispersion. As we shall see later, the actual form of $\nu_p(t)$ is more complicated than that assumed here; for pulses with widths large compared to the Debye length the general features are unaltered.

We solve Eqs. (30) to (33), following Landau's procedure, by performing a Laplace transformation with respect to the time variable. We write

$$\phi_{p,\sigma}=\int_0^\infty\phi_p(\mathbf{v},t)e^{-\sigma t}dt,\tag{35}$$

for the image of $\phi_p(\mathbf{v},t)$. The inverse transformation is

$$\phi_p(\mathbf{v},t)=\frac{1}{2\pi i}\int_{c-i\infty}^{c+i\infty}\phi_{p,\sigma}e^{\sigma t}d\sigma,\tag{36}$$

where the integration is carried out along a line in the right-half plane of the complex variable σ. For the case of waves propagated along the x axis Eqs. (30) to (33) become

$$(\lambda+\sigma+ipu)\phi_{p,\sigma}=-(eu/kT_0)(E_{p,\sigma})_x+\lambda\nu_{p,\sigma}+(\lambda m/kT_0)u(q_{p,\sigma})_x+\phi_p(\mathbf{v},0),\tag{37}$$

$$\nu_{p,\sigma}=\int\phi_{p,\sigma}\bar{F}d\mathbf{v},\tag{38}$$

$$(q_{p,\sigma})_x=\int u\phi_{p,\sigma}\bar{F}d\mathbf{v},\tag{39}$$

$$ip(E_{p,\sigma})_x=-4\pi e n_0\nu_{p,\sigma}.\tag{40}$$

Here $\phi_p(\mathbf{v},0)$ is the Fourier transform of the initial velocity distribution. By multiplying Eq. (37) by $\bar{F}$ and integrating over all velocities one finds

$$\sigma\nu_{p,\sigma}+ip(q_{p,\sigma})_x=\nu_p(0),\tag{41}$$

where

$$\nu_p(0)=\int\phi_p(\mathbf{v},0)\bar{F}d\mathbf{v}.$$

Using this equation together with Eq. (40), we eliminate $(q_{p,\sigma})_x$ and $(E_{p,\sigma})_x$ from Eq. (37), and are left with the set of equations

$$(\lambda+\sigma+ipu)\phi_{p,\sigma}=\left(\lambda-\frac{\lambda mu}{kT_0}\frac{\sigma}{ip}+\frac{k_0^2}{ip}u\right)\nu_{p,\sigma}+\phi_p(0)+\frac{\lambda mu}{kT_0}\frac{\nu_p(0)}{ip},\tag{42}$$

$$\nu_{p,\sigma}=\int\phi_{p,\sigma}\bar{F}d\mathbf{v}.\tag{43}$$

Solving for $\nu_{p,\sigma}$ we find

$$\nu_{p,\sigma}=\frac{\int\bar{F}d\mathbf{v}\left(\frac{\lambda m}{kT_0}\frac{u\nu_p(0)}{ip}+\phi_p(0)\right)}{1-\int\frac{\bar{F}d\mathbf{v}}{\lambda+\sigma+ipu}\left\{\lambda-\frac{\lambda m}{kT_0}\frac{u\sigma}{ip}+\frac{k_0^2}{ip}u\right\}}.\tag{44}$$

Here $k_0^2=\omega_p^2/a^2$. An expression for $\phi_{p,\sigma}$ is obtained by inserting this value of $\nu_{p,\sigma}$ into Eq. (42). Equations (42) and (44) thus provide a complete solution to the initial-value problem since we have merely to invert the Laplace transform to find the dependence of the density and velocity distribution on time. However, the integrations are along paths in the right-half plane of the complex variable σ and, aside from being difficult to evaluate, yield little physical insight into the behavior of the solution. We therefore note that although Eqs. (42) and (44) are defined only for σ in the right-half complex plane it is possible to effect an analytic continuation of the functions into the left-half plane of σ by modifying the path of integration in the integrals with respect to velocity. We integrate in the complex u

plane along a path C which passes below the singularity, $u=-(\lambda+\sigma)/ip$. The two integrals entering in the numerator and denominator of Eq. (44) are then entire functions in the complex σ plane.[16]

With the path of integration C, the Laplace transform of the density $\nu_{p,\sigma}$ will have poles at values of σ given implicitly by

$$1-\int_C \frac{\bar{F}d\mathbf{v}}{\lambda+\sigma+ipu}\left\{\lambda-\frac{\lambda m}{kT_0}\frac{u\sigma}{ip}+\frac{k_0^2}{ip}u\right\}=0. \quad (45)$$

There will be an infinite number of such poles, all lying in the left-half plane of σ. If one deforms the contour into the left-half plane in Eq. (45), one finds that the density after a long time t is given very nearly in terms of the poles at the residues of $\nu_{p,\sigma}$. For shorter times the remaining parts of the contour give a significant contribution and there is in fact no advantage in deforming the contour in the above way. For t large then

$$\nu(t)=\int \bar{F}d\mathbf{v}\left(\frac{\lambda m}{kT_0}\frac{u\nu_p(0)}{ip}+\phi_p(0)\right)\sum_i e^{\sigma_i t},$$

since the numerator in Eq. (44) is independent of σ. The first term in the integrand is an odd function of u and gives no contribution. $\nu(t)$ may thus be represented approximately as a sum of damped oscillating terms. The asymptotic behavior for t large is determined by that root σ_1 of the dispersion relation Eq. (45) which has the largest real part.

The dispersion relation Eq. (45) differs from that obtained by the $e^{i(px-\omega t)}$ substitution in that the path of integration is not necessarily along the real axis. We shall see shortly, however, that the substitution analysis gives a correct account of the behavior at long times when the damping is not very great.

The behavior of the velocity distribution $\phi_p(\mathbf{v},t)$ is different from that of the density $\nu_p(t)$ since the Laplace transform of $\phi_{p,\sigma}$ has an additional pole at a value of σ given by

$$\lambda+\sigma_0+ipu=0. \quad (46)$$

In this expression the velocity u is, of course, real since we are investigating the behavior of the distribution function for particles of a given real velocity u. The asymptotic behavior of $\phi(\mathbf{v},t)$ depends essentially on the relative values of the real parts of the pole $\sigma_0=-ipu-\lambda$ and of the pole σ_1 with largest real part satisfying the dispersion relation Eq. (45). The dispersion relation will be the determining factor when the damping frequency is smaller than the collision frequency λ. For this case both the density and the distribution function (for any value of the velocity) have the same time dependence $e^{\sigma_1 t}$. We shall call this the "collision-damping" case. From our later expression Eq. (68) for the frequency as a function of wavelength and collision time, it follows that $\mathrm{Re}\sigma_1=\omega_i=-[\lambda/(\lambda^2+1)][p^2a^2/\omega_p^2]$ for waves larger than either the Debye length or the mean free path. We see that the damping frequency is indeed smaller than the collision frequency for these waves. This condition has the further consequence that the contour C may be taken along the real axis so that the $e^{i(px-\omega t)}$ substitution analysis will lead to correct results for the behavior at large values of time.

If, however, one is dealing with processes in which wavelengths less than both the Debye length and the mean free path are important, the path C cannot be deformed into the path along the real axis; this is due to the fact that the damping frequency is higher than the collision frequency. The distribution function at long times will vary as $e^{-\lambda t}e^{-iput}$, while the density will have the more rapid decay given by the root σ_1 of the Eq. (45). Thus the distribution function for long times contains, in addition to the organized component of velocity, "free-particle" components which give rise to negligible macroscopic density fluctuations.[6]

For the "collision-damping" case one can easily write explicit expressions for the asymptotic behavior of the oscillating quantities. We have

$$\nu=\nu_0\,\mathrm{Re}(e^{i(px-\omega t)})=\nu_0 e^{\omega_i t}\cos(px-\omega_r t), \quad (47)$$

$$E_x=-\frac{4\pi e n_0}{p}e^{\omega_i t}\sin(px-\omega_r t), \quad (48)$$

$$\phi=\frac{\nu_0 e^{\omega_i t}}{(\lambda+\omega_i)^2+(pu-\omega_r)^2}\Bigg[\cos(px-\omega_r t)\times\left\{(\lambda+\omega_i)\left(1+\frac{u\omega_r}{pa^2}\right)\lambda-(pu-\omega_r)\left(1-\frac{\lambda\omega_i}{\omega_p^2}\right)\frac{u\omega_p^2}{pa^2}\right\}+\sin(px-\omega_r t)\left\{\lambda(pu-\omega_r)\left(1+\frac{u\omega_r}{pa^2}\right)-(\lambda+\omega_i)\left(1-\frac{\lambda\omega_i}{\omega_p^2}\right)\frac{u\omega_p^2}{pa^2}\right\}\Bigg]. \quad (49)$$

The real and imaginary parts of ω are given by the equations obtained in our study of the dispersion relation in Secs. 5 to 7.

Using the above expressions it is now easy to verify that the approximations made in the linearization procedure are valid for all velocities in this long wavelength case. The amplitude ν_0 can be chosen arbitrarily small and, provided the collision frequency is not zero, the linearization leads to consistent results.

For the high-pressure limit we have from Eq. (68) $\omega_r\to\omega_p+\frac{1}{2}(p^2a^2)/\omega_p^2$; $\omega_i\to 0$ as $\lambda\to\infty$. The distribution function is

$$\phi\to\nu_0\cos(px-\omega_r t)[1+(u/a^2)(\omega_r/p)]. \quad (50)$$

For the low-pressure plasma $\omega_r \to \omega_p + \frac{3}{2}(p^2a^2)/\omega_p^2$; $\omega_i \to -(\lambda/\omega_p)(p^2a^2/\omega_p^2)$ as $\lambda \to 0$. Then

$$\phi \to \frac{\nu_0 e^{\omega_i t}}{\lambda^2+(pu-\omega_r)^2}\left\{-\cos(px-\omega_r t)\frac{u\omega_p^2}{pa^2}(pu-\omega_r) - \sin(px-\omega_r t)2\frac{\lambda u\omega_p^2}{pa^2}\right\}. \quad (51)$$

For sound waves in an uncharged gas we again have

$$\phi \to \nu_0 \cos(px-\omega_r t)\left(1+\frac{u}{a^2}\frac{\omega_r}{p}\right);$$

here, however, one must take $\omega_r = pa$. Thus

$$\phi \to \nu_0 \cos p(x-at)(1+u/a). \quad (52)$$

All the above distribution functions exhibit the same general feature that the magnitude is greater for those particles moving in the direction of the wave than it is for those moving in the opposite direction. This is in fact necessary for maintaining a wave. For the low-pressure plasma case we note also the opposite contributions from particles moving faster, and those moving slower than the wave.

5. DISPERSION RELATION FOR INITIAL VALUE PROBLEM

The present section is devoted to a discussion of the techniques needed for the study of the dispersion relation Eq. (45). The results for important special cases are given in the following two sections. At this stage, it is convenient to introduce dimensionless variables. We measure frequencies in units of the plasma frequency ω_p, velocities in units of the thermal velocity $a=(kT_0/m)^{\frac{1}{2}}$, and lengths in units of the Debye length $l_D=(kT/4\pi n_0 e^2)^{\frac{1}{2}}$. In these units the dispersion relation becomes

$$ip = \frac{1}{(2\pi)^{\frac{1}{2}}}\int_c \frac{d\zeta \exp(-\zeta^2/2)}{\lambda+\sigma+ip\zeta}\{\zeta+ip\lambda-\sigma\lambda\zeta\}d\zeta. \quad (53)$$

We shall at times deal with ω rather than σ; the two quantities are connected by $\sigma=-i\omega$.

Let us first study the position of the singularity of the integrand in the ζ plane. Since the oscillations are damped, σ has a negative real part and a negative imaginary part. Thus $\lambda+\sigma$ can be either positive or negative according to whether the damping frequency is less than or greater than the collision frequency. Since p is real, this means that the singularity $\zeta_0 = -(\lambda+\sigma)/ip$ is in either the first or the fourth quadrant in the ζ plane. For ζ_0 in the first quadrant, the contour appropriate to the $e^{i(px-\omega t)}$ substitution, i.e., the real axis, gives correct results. This represents the situation where the main damping arises from collisions. When ζ_0 is in the fourth quadrant, the damping frequency is larger than the collision frequency; the additional damping is of the Landau type and results from the destruction of phase by drift motion. The representation of this latter type of damping requires the use of the contour C. The damping frequency is small for long wavelengths but increases rapidly as the wavelength approaches the Debye length.

The most direct approach to the evaluation of Eq. (53) would appear to be an expansion of the term $1/(\lambda+\sigma+ip\zeta)$ in powers of $ip\zeta/(\lambda+\sigma)$ and an integration term by term. This is a development in powers of $p/(\lambda+\sigma)$ or, reverting to usual units, in powers of $pa/(\lambda-i\omega)$. Thus one requires pa to be small compared to either the collision frequency or the frequency of the waves. Alternatively, the wavelength has to be long compared to the Debye length or the mean free path. This actually applies in two important limits. The case of sound oscillations in neutral gases is one where the collision frequency is large compared to pa for all but very short waves and very low pressures. A second case occurs with electron plasma oscillations of wavelength long compared to the Debye length ($pa/\omega \simeq pa/\omega_p$ = Debye length/wavelength $\ll 1$) irrespective of the collision time, so that one can study the entire range of pressures. In fact, both of these cases can be treated by the same expansion. The expansion breaks down for heavily damped waves in both the neutral and ionized gas cases. An objection to the above procedure is that the series does not converge; it is, in fact, asymptotic so that it is useful where the first few terms are all important. In order to establish this and to give alternative developments, we express the dispersion relation in terms of the error function of complex argument.

The real axis as path of integration may be replaced by the contour C consisting of the straight line, $\mathrm{Im}\zeta = \mathrm{Im}[(\lambda+\sigma)/-ip]$, with an indentation at the singularity and below it. Resolving the integral into the contribution of the small semicircle about the singularity and that of the principal value of the integral one finds

$$\frac{1}{(2\pi)^{\frac{1}{2}}}\int_c \frac{\exp(-\zeta^2/2)d\zeta}{\zeta-\theta} = \frac{1}{(2\pi)^{\frac{1}{2}}} \times \exp(-\theta^2/2)\left\{i\pi - 2\int_0^\infty \exp(-\zeta^2/2)\frac{\sinh\theta\zeta}{\zeta}d\zeta\right\}, \quad (54)$$

where

$$\theta = (\omega+i\lambda)/p. \quad (55)$$

Making use of the identity

$$\int_0^\infty \exp(-\zeta^2/2)\frac{\sinh\theta\zeta}{\zeta}d\zeta = \left(\frac{\pi}{2}\right)^{\frac{1}{2}}\int_0^\theta d\theta' \exp(\theta'^2/2), \quad (56)$$

and introducing

$$\Omega = -i\theta\sqrt{2} = (\lambda-i\omega)/p\sqrt{2}, \quad (57)$$

we find the dispersion relation

$$-\frac{p^2}{1+i\omega\lambda} = 1+\left[\frac{ip\lambda}{1+i\omega\lambda}+\frac{\omega+i\lambda}{p}\right]i\sqrt{2}F(\Omega). \quad (58)$$

Here

$$F(\Omega)=\left\{\frac{\pi^{\frac{1}{2}}}{2}-\int_0^{\Omega}\exp(-\Omega'^2)d\Omega'\right\}\exp(\Omega^2) \quad (59)$$

is the error function of complex argument.

Examination shows that, for waves with positive real frequency, Ω lies either in the fourth or third quadrant. The function $F(\Omega)$ is treated in detail by Rosser.[17] It has the expansion

$$F(\Omega)=\exp(\Omega^2)\left\{\frac{\pi^{\frac{1}{2}}}{2}-\sum_{n=0}^{\infty}(-1)^n\frac{\Omega^{2n+1}}{(2n+1)n!}\right\}, \quad (60)$$

convergent for all values of Ω, but useful only for values of Ω with modulus less than unity. $F(\Omega)$ can also be expanded in an asymptotic series of the form

$$F(\Omega)=1/2\Omega-1/4\Omega^3+1\cdot3/8\Omega^5-1\cdot3\cdot5/16\Omega^7+\cdots. \quad (61)$$

This asymptotic series is in powers of $pa\sqrt{2}/(\lambda-i\omega)$, and yields the same result as the procedure outlined at the beginning of this section.

Finally, we note that $F(\Omega)$ can also be expanded as a continued fraction,

$$F(\Omega)=1/2\Omega+2/2\Omega+4/2\Omega+6/2\Omega\cdots, \quad (62)$$

for Ω in the first and fourth quadrants. This expansion does not correspond to a simple development in powers of the Debye length or mean free path divided by the wavelength; however, it converges rapidly over a large portion of the complex Ω plane and is more generally useful than the asymptotic development. To obtain information in the regions of moderate and strong absorption for both neutral and ionized gases, we require a knowledge of $F(\Omega)$ over portions of the complex Ω plane not covered by any of the developments given; this knowledge has been obtained by numerical computations.

We also require a knowledge of $F(\Omega)$ for Ω in the second and third quadrants. This is found by making use of the identity,

$$F(-\Omega)=\pi^{\frac{1}{2}}\exp(\Omega^2)-F(\Omega). \quad (63)$$

6. IONIZED GAS OSCILLATIONS

For an ionized gas the continued fraction and asymptotic series are useful when $|pa/(\lambda-i\omega)|<1$. Thus for waves of large wavelength where $pa/\omega_p\ll1$, one can obtain information for arbitrary values of collision frequency. If we break off the continued fraction after the third term we have

$$F(\Omega)=1/2\Omega+2/2\Omega+4/2\Omega=(\Omega^2+1)/\Omega(2\Omega^2+3). \quad (64)$$

After some algebraic manipulation the dispersion relation can be put in the form

$$i\omega\{-\omega^2+3p^2+1\}=\lambda\{1+p^2-\omega^2\}, \quad (65)$$

or, with ordinary units,

$$i\omega\{-\omega^2+3p^2a^2+\omega_p^2\}=\lambda\{\omega_p^2+p^2a^2-\omega^2\}. \quad (66)$$

The same result is obtained using the asymptotic series. This shows quite clearly the various limiting cases. If the collision frequency λ tends to zero we have

$$\omega^2=\omega_p^2+3p^2a^2,$$

the correct dispersion relation for low-pressure electron plasma oscillations of wavelength long compared to the Debye length. In the limit of high pressures the collision frequency λ tends to infinity and we find $\omega^2=\omega_p^2+p^2a^2$. This is the Thomson result.

By solving Eq. (66) for intermediate values of λ it is possible to trace the transition from the one solution to the other. From Eq. (66) we have, after grouping in powers of p^2a^2/ω_p^2,

$$\omega^2=\omega_p^2+\left(\frac{\lambda-3i\omega}{\lambda-i\omega}\right)\frac{p^2a^2}{\omega_p^2}. \quad (67)$$

We obtain results correct to order p^2a^2/ω_p^2 by substituting the value $\omega=\omega_p$ on the right-hand side. The frequency is

$$\omega=\omega_p+\frac{p^2a^2}{2\omega_p^2}\frac{1}{\lambda^2+\omega_p^2}\{\lambda^2+3\omega_p^2-i\cdot2\lambda\omega_p\}. \quad (68)$$

We see that the damping frequency is proportional to p^2, in contrast to the damping arising from the electron-neutral gas collisions, which contains a leading term independent of wavelength. The coefficient of p^2a^2/ω_p^2 is plotted in Figs. 1 and 2. The absorption reaches a maximum when $\lambda=\omega_p$, i.e., when the collision frequency equals the plasma frequency. At this point the real part of the frequency is exactly halfway between the limiting values for zero and infinite collision times. The absorption is approximately linear with λ at the low-pressure limit, varying as $(p^2a^2/\omega_p^2)(\lambda/\omega_p)$, while at high pressures it is hyperbolic, varying as $(p^2a^2/\omega_p^2)\times(\omega_p/\lambda)$. The negative frequency root of Eq. (67) yields

$$\omega=-\left[\omega_p+\frac{p^2a^2}{2\omega_p^2}\frac{1}{\lambda^2+\omega_p^2}\{\lambda^2+3\omega_p^2-i\cdot2\lambda\omega_p\}\right],$$

and gives absorption and dispersion which corresponds completely to the results for the positive frequency case. It is important to note that the absolute magnitude of the damping is very small since it is proportional to p^2a^2/ω_p^2. For example, for $pa\simeq\omega_{p/100}$ the maximum damping frequency is less than $10^{-4}\,\omega_p$.

The dispersion relation Eq. (68) gives adequate information for $pa\ll\omega_p$. We are also interested in the case where pa is approximately equal to, or greater than ω_p, i.e., waves of length comparable to the Debye length. For this case the development in powers of pa/ω_p is not appropriate; one must also have detailed numerical information concerning $F(\Omega)$. In Figs. 3 and 4 we plot the real and imaginary parts of ω for the case $pa=\omega_p$

[17] J. B. Rosser, *Theory and Application of* $\int_0^x e^{-x^2}dx$ (Mapleton House, Brooklyn, 1948).

(waves equal to the Debye length) as a function of the collision frequency. The results are the same as for the long-wavelength case when $\lambda \gg \omega_p$. However, at values of λ smaller than ω_p the very large "drift" damping discussed in Sec. 4 manifests itself.

7. OSCILLATIONS OF AN UNCHARGED GAS

The general results of Secs. 3 to 5 apply to the initial-value problem for uncharged gases; the plasma frequency ω_p is then zero. For our constant-collision time, isothermal model the general dispersion relation Eq. (58) becomes, in ordinary units,

$$-p^2a^2/i\omega\lambda = 1+[pa/\omega+\omega+i\lambda/pa]i\sqrt{2}F(\Omega), \quad (69)$$

$$\Omega = \lambda - i\omega/pa\sqrt{2}.$$

As discussed in Sec. 5 the asymptotic expansion Eq. (61) is valid provided $pa \ll \lambda$, i.e., the frequency of the sound wave is smaller than the collision frequency. The first few terms of this expansion yield the result

$$\omega^2 + p^2a^2\{-(1+4i\omega)/\lambda/(1-i\omega/\lambda)^2\} + (p^4a^4/\lambda^2)\{(3-18i\omega)/\lambda/(1-i\omega/\lambda)^4\} = 0. \quad (70)$$

In the limit of infinite collision frequency we find $\omega^2 = p^2a^2$, the correct isothermal sound speed. The correction for finite but large collision frequency, expressed in powers of pa/λ, is

$$\omega = pa\{1 - ipa/\lambda + \tfrac{1}{2}(pa/\lambda)^2\}. \quad (71)$$

This expression indicates both an absorption and dispersion of sound for finite value of the collision frequency. The physical situation is similar to the Langmuir description of the damping of plasma waves with wavelength near to the Debye length.[8] Here, because of the translational motion, fast-moving particles can occasionally move well ahead of the sound wave without undergoing a collision; they then carry ordered motion from one region to another in which the phase for ordered motion is different. The ordered energy is then dissipated into random thermal energy by collisions. This effect, of course, increases with increasing mean free path and with decreasing wavelength.

The series expansion Eq. (70) breaks down when $pa \simeq \lambda$ and one must resort to numerical methods in solving Eq. (69). The results for the real and imaginary parts are presented in Fig. 5. The accuracy of these results is, however, limited by the inadequate tables of the function $F(\Omega)$ available to us at present.

According to the discussion of Sec. 4 the asymptotic behavior of the distribution function differs according as $\sigma_0 = -i\omega_0 = -\lambda - ipu$, or $\sigma_1 = -i\omega_1$, has the larger real part, σ_1 being given by the dispersion relation Eq. (69). The second case is what we have previously called the "collision-damping" case. For this case the damping frequency is less than the collision frequency and the asymptotic behavior of the distribution function is the same as that of the density. From Fig. 5 we see that this is the situation when $pa < 1.5\lambda$. For $\mathrm{Re}\sigma_0 > \mathrm{Re}\sigma_1$ the damping frequency is greater than the collision frequency, the distribution function and density have different asymptotic behaviors, and the distribution function is directly sensitive to its initial value. The individual features of the particular initial value or boundary-value problem treated are then important.

For the "collision-damping" case, one may study the physical processes with the aid of the distribution function Eq. (49). Using the value of ω given by Eq. (71) we see that the deviation from the Maxwellian distribution is greatest for fast-moving particles and short wavelengths. From Eq. (39) we verify that the greatest contribution to the out-of-phase component of mass velocity comes from fast-moving particles and short wavelengths, in accordance with the picture discussed above.

8. GENERAL TREATMENT

In this section we shall remove the restriction made previously and allow for temperature fluctuations. The problem is now characterized by the full set of Eqs. (15) to (20). The passage to the linear approximation involves the additional fluctuating quantity $\tau(\mathbf{x},t)$, defined by

$$T(\mathbf{x},t) = T_0\{1+\tau(\mathbf{x},t)\}. \quad (72)$$

Equations (21) to (25) remain valid in the general case, but the expansion of Φ in Eq. (26) must be replaced by

$$\Phi = \bar{F}\{1+(m/kT_0)\mathbf{v}\cdot\mathbf{q}+\tau(mv^2/2kT_0-\tfrac{3}{2})\}. \quad (73)$$

Equation (19) defining the temperature leads to

$$\frac{3kT_0}{m}(\nu+\tau) = \int v^2\bar{F}\phi d\mathbf{v}. \quad (74)$$

The basic set of linear equations governing the Fourier transformed variables for a disturbance in the x direction is

$$\left.\begin{aligned} &\frac{\partial\phi_p}{\partial t} + ipu\phi_p + \frac{e(E_p)_x}{kT_0}u \\ &\quad = \lambda\left\{\nu_p - \phi_p + \frac{m}{kT_0}u(q_p)_x + \tau_p\left(\frac{mv^2}{2kT_0}-\frac{3}{2}\right)\right\}, \\ &\nu_p = \int \phi_p\bar{F}d\mathbf{v}, \\ &(q_p)_x = \int u\phi_p\bar{F}d\mathbf{v}, \\ &\frac{3kT_0}{m}(\nu_p+\tau_p) = \int v^2\phi_p\bar{F}d\mathbf{v}, \\ &ip(E_p)_x = -4\pi e n_0\nu_p \end{aligned}\right\}. \quad (75)$$

One may eliminate $(E_p)_x$ and $(q_p)_x$ in the same way as in the isothermal case. Corresponding to Eq. (44) one now finds a coupled set of equations for the Laplace transforms of ν_p and τ_p. This set is

$$\nu_{p,\sigma}\left\{1-\int\frac{\bar{F}d\mathbf{v}\left[\lambda-\frac{\lambda m}{kT_0}\frac{u\sigma}{ip}+\frac{k_0^2u}{ip}\right]}{\lambda+\sigma+ipu}\right\}$$

$$-\tau_{p,\sigma}\left\{\int\frac{\bar{F}d\mathbf{v}\left[\frac{mv^2}{2kT_0}-\frac{3}{2}\right]\lambda}{\lambda+\sigma+ipu}\right\} \tag{76}$$

$$=\int\frac{\bar{F}d\mathbf{v}\left(\frac{\lambda m}{kT_0}\frac{u\nu_p(0)}{ip}+\phi_p(0)\right)}{\lambda+\sigma+ipu},$$

$$\nu_{p,\sigma}\left\{1-\frac{m}{3kT_0}\int\frac{v^2\bar{F}d\mathbf{v}}{\lambda+\sigma+ipu}\left[\lambda-\frac{\lambda m}{kT_0}\frac{u\sigma}{ip}+\frac{k_0^2u}{ip}\right]\right\}$$

$$+\tau_{p,\sigma}\left\{1-\frac{\lambda m}{3kT_0}\int\frac{v^2\bar{F}d\mathbf{v}}{\lambda+\sigma+ipu}\left(\frac{mv^2}{2kT_0}-\frac{3}{2}\right)\right\} \tag{77}$$

$$=\frac{m}{3kT_0}\int\frac{v^2\bar{F}d\mathbf{v}}{\lambda+\sigma+ipu}\left\{\frac{\lambda m}{kT_0}\frac{u\nu_p(0)}{ip}+\phi_p(0)\right\}.$$

The dispersion relation in dimensionless units is then

$$\left\{1-\frac{1}{(2\pi)^{\frac{1}{2}}}\int\int\int\frac{\exp(-v^2/2)d\mathbf{v}}{\lambda+i(pu-\omega)}\left[\lambda+\frac{\lambda u\omega}{p}+\frac{u}{ip}\right]\right\}$$

$$\times\left\{1+\frac{\lambda}{6(2\pi)^{\frac{1}{2}}}\int\int\int\frac{\exp(-v^2/2)v^2(3-v^2)}{\lambda+i(pu-\omega)}\right\} \tag{78}$$

$$=\left\{1-\frac{1}{3(2\pi)^{\frac{1}{2}}}\int\int\int\frac{\exp(-v^2/2)v^2d\mathbf{v}}{\lambda+i(pu-\omega)}\left(\lambda+\frac{\lambda u\omega}{p}+\frac{u}{ip}\right)\right\}$$

$$\times\left\{\frac{\lambda/2}{(2\pi)^{\frac{1}{2}}}\int\int\int\frac{\exp(-v^2/2)(3-v^2)d\mathbf{v}}{\lambda+i(pu-\omega)}\right\}.$$

In order to study this dispersion relation we express all the integrals occurring in terms of the single integral

$$\frac{1}{(2\pi)^{\frac{1}{2}}}\int_c\frac{\exp(-\zeta^2/2)d\zeta}{\zeta-\theta}=i\sqrt{2}F(\Omega),$$

which was discussed in Sec. 5.

We find

$$\left.\begin{aligned}
&\frac{1}{(2\pi)^{\frac{1}{2}}}\int\int\int\frac{\exp(-v^2/2)d\mathbf{v}}{\lambda+i(pu-\omega)}=\frac{\sqrt{2}}{p}F(\Omega),\\
&\frac{1}{(2\pi)^{\frac{1}{2}}}\int\int\int\frac{\exp(-v^2/2)v^2d\mathbf{v}}{\lambda+i(pu-\omega)}=\frac{\sqrt{2}}{p}\{\Omega+2(1-\Omega^2)F(\Omega)\},\\
&\frac{1}{(2\pi)^{\frac{1}{2}}}\int\int\int\frac{\exp(-v^2/2)v^4d\mathbf{v}}{\lambda+i(pu-\omega)}=\frac{\sqrt{2}}{p}\{5\Omega-2\Omega^3+4(\Omega^4-2\Omega^2+2)F(\Omega)\},\\
&\frac{1}{(2\pi)^{\frac{1}{2}}}\int\int\int\frac{\exp(-v^2/2)uv^2d\mathbf{v}}{\lambda+i(pu-\omega)}=\frac{1}{ip}\{3-2\Omega^2-4\Omega(1-\Omega^2)F(\Omega)\},\\
&\frac{1}{(2\pi)^{\frac{1}{2}}}\int\int\int\frac{\exp(-v^2/2)(3-v^2)d\mathbf{v}}{\lambda+i(pu-\omega)}=\frac{\sqrt{2}}{p}\{-\Omega+(1+2\Omega^2)F\},\\
&\frac{1}{(2\pi)^{\frac{1}{2}}}\int\int\int\frac{\exp(-v^2/2)(3-v^2)v^2d\mathbf{v}}{\lambda+i(pu-\omega)}=\frac{\sqrt{2}}{p}\{-2\Omega+2\Omega^3+(-2+2\Omega^2-4\Omega^4)F\}
\end{aligned}\right\} \tag{79}$$

We also find

$$\left.\begin{aligned}
&\frac{1}{(2\pi)^{\frac{1}{2}}}\int\int\int\frac{\exp(-v^2/2)d\mathbf{v}}{\lambda+i(pu-\omega)}\times\left[\lambda+\frac{\lambda u\omega}{p}+\frac{u}{ip}\right]=-\frac{(1+\lambda^2-p\lambda\sqrt{2}\Omega)}{p^2}\\
&\qquad+F(\Omega)\left\{\frac{\lambda\sqrt{2}}{p}+\frac{2\Omega}{p^2}(1+\lambda^2-p\lambda\sqrt{2}\Omega)\right\},\\
&\frac{1}{(2\pi)^{\frac{1}{2}}}\int\int\int\frac{\exp(-v^2/2)v^2d\mathbf{v}}{\lambda+i(pu-\omega)}\left[\lambda+\frac{\lambda u\omega}{p}+\frac{u}{ip}\right]\\
&\qquad=\frac{\lambda\sqrt{2}}{p}\{\Omega+2(1-\Omega^2)F(\Omega)\}\\
&\qquad-\frac{1}{p^2}(1+\lambda^2-p\lambda\sqrt{2}\Omega)[3-2\Omega^2-4\Omega(1-\Omega^2)F]
\end{aligned}\right\} \tag{80}$$

Using these results we can write the dispersion relation as

$$\left\{1+\frac{(1+\lambda^2-p\lambda\sqrt{2}\Omega)}{p^2}-F(\Omega)\left[\frac{\lambda\sqrt{2}}{p}+\frac{2\Omega}{p^2}(1+\lambda^2-p\lambda\sqrt{2}\Omega)\right]\right\}$$
$$\times\left\{1+\frac{\lambda\sqrt{2}}{6}\frac{}{p}[-2\Omega+2\Omega^3+(-2+2\Omega^2-4\Omega^4)F]\right\} \quad (81)$$
$$=\left\{1-\frac{1}{3}\frac{\lambda\sqrt{2}}{p}[\Omega+2(1-\Omega^2)F]\right.$$
$$\left.+\frac{1}{3p^2}(1+\lambda^2-p\lambda\sqrt{2}\Omega)[3-2\Omega^2-4\Omega(1-\Omega^2)F]\right\}$$
$$\times\left\{\frac{\lambda\sqrt{2}}{2}\frac{}{p}[-\Omega+(1+2\Omega^2)F]\right\}.$$

The dispersion relation, Eq. (81), for the general case is considerably more involved than the corresponding relation, Eq. (58), for the isothermal case. However, as emphasized in Sec. 5, one can obtain simple results for wavelengths long compared to either the Debye length or the mean free path. For this case the asymptotic development for $F(\Omega)$ holds and one finds (in dimensionless units)

$$(1-\omega^2)(-i\omega)+\frac{\lambda p^2}{(\lambda-i\omega)^2}\left\{\frac{5}{3}-\frac{19\omega^2}{3}-\frac{5i\omega\lambda}{3}+\frac{3i\omega}{\lambda}\right\}$$
$$+\frac{p^4}{(\lambda-i\omega)^4}\left\{-5\lambda^3-\frac{20}{3}i\omega\lambda^2+\lambda(7+3\omega^2)\right.$$
$$\left.-20(1-\omega^2)-15i\omega\right\}=0. \quad (82)$$

For the study of the oscillations of an ionized gas we obtain an expression for the frequency which corresponds to Eq. (66). Retaining terms of order p^2a^2/ω_p^2 we find for the frequency,

$$\omega=\omega_p+\frac{p^2a^2}{2\omega_p}\frac{1}{(\lambda^2+\omega_p^2)}\{(\tfrac{5}{3}\lambda^2+3\omega_p^2)-i4/3\lambda\omega_p\}. \quad (83)$$

At high pressures the collision frequency λ is large compared to the plasma frequency, and one finds $\omega\to\omega_p+(p^2a^2/2\omega_p)\times5/3$. This is the value found previously by a generalization of the Thomson method[11] and verifies the high-pressure nature of the transport type of procedure. At low pressures we find $\omega\to\omega_p+(p^2a^2/2\omega_p^2)\cdot3$, the correct dispersion relation for waves of length large compared to the Debye length. The maximum damping frequency for the general case occurs again when the collision frequency is equal to the plasma frequency; this damping is $\frac{2}{3}$ that for the isothermal case. The decreased absorption accompanies the smaller dispersion for the general case. The detailed variation of frequency as a function of collision frequency is given by Eq. (83) and represented in Figs. 1 and 2. In the event that the wavelength is comparable to both the mean free path and the Debye length one must resort to numerical information concerning $F(\Omega)$. Tables of sufficient accuracy to solve the complicated Eq. (81) are not available to us at present; we leave the detailed investigation to a later time.

For a neutral gas the expression Eq. (82) reduces to

$$\omega^2+\frac{p^2a^2}{(1-i\omega/\lambda)^2}\left\{\frac{19}{3}\frac{i\omega}{\lambda}-\frac{5}{3}\right\}$$
$$+\frac{p^4a^4}{\lambda^2(1-i\omega/\lambda)^4}\left\{\frac{5i\lambda}{\omega}-\frac{20}{3}-\frac{3i\omega}{\lambda}\right\}=0. \quad (84)$$

Developing in powers of pa/λ, we have, for $pa/\lambda\ll1$,

$$\omega=(5/3)^{\frac{1}{2}}pa\left\{1-i(5/3)^{\frac{1}{2}}\frac{pa}{\lambda}\times\frac{9}{5}+11.3\frac{p^2a^2}{\lambda^2}\right\}. \quad (85)$$

Thus one finds both an absorption and a dispersion of sound waves. No attempt has been made in this paper to connect our collision frequency λ with molecular parameters; it is known, therefore, only to within a factor of the order of unity. This comparison will be undertaken in a later paper where we also discuss models more realistic than the present constant-collision-time model. For the present we note that if one fits λ by taking the absorption equal to that predicted by the Navier-Stokes equations (and also the Burnett equations), then $\lambda=(90/35)a^2/\eta$, where $\eta=\frac{1}{2}\rho_0(8kT/\pi m)^{\frac{1}{2}}l$; η is the coefficient of viscosity; l is the mean free path. The coefficient of the dispersive term in Eq. (85) is then 25 percent higher than that given by the Navier-Stokes equation; it thus lies between the predictions of the Navier-Stokes and of the Burnett equations. The interesting experimental observations of Greenspan[18] on the dispersion and absorption of helium gas reveal important discrepancies between experiment, and the predictions of both the Navier-Stokes and the Burnett equations when $pa\simeq\lambda$.[19] From the point of view of the present work the study of this region requires a numerical analysis of Eq. (81). We shall therefore later take up the study of the translational dispersion in a more detailed way.

[18] M. Greenspan, J. Acoust. Soc. Am. 22, 568 (1950).

[19] The experimental observations refer to a boundary value problem rather than an initial value problem.

Electronic Hall Effect in Diamond*

ALFRED G. REDFIELD†‡
Physics Department, University of Illinois, Urbana, Illinois
(Received January 19, 1954)

A method for measuring the Hall mobility in insulating photoconductors is described which avoids the space-charge difficulties present in previous measurements. Unconventional electrodes are used, and the method differs from the conventional one in several other ways. It is a transient method, and the electric field in the sample is rotated by the external electrodes, rather than by the electrons under study. The direction of charge flow is deduced from a current measurement, rather than by confining the current to a thin sample whose orientation gives the direction of charge flow. No attempt is made to inject or eject electrons through the surface of the sample.

Measurements using this technique have been made on a number of diamonds. Both electrons and holes are found to contribute to the photoconductivity, making interpretation of the data difficult. It is tentatively concluded that the electronic mobility varies as $T^{-\frac{1}{2}}$ and is about 1800 cm²/volt-sec at 300°K. For holes it is concluded (with far less certainty) that the mobility also varies as $T^{-\frac{1}{2}}$ and is somewhat greater than 1200 cm²/volt-sec at 300°K. These observations are consistent with the deformation potential theory of electronic mobility in nonpolar crystals.

A. INTRODUCTION

PREVIOUS attempts[1–3] to measure the Hall mobility of electrons released by light in insulating photoconductors have used continuous illumination and have been steady-state dc measurements using an electrometer to measure the Hall voltage. These measurements have suffered from uncertainties due to buildup of space charge in the crystal near the current electrodes. Although corrections for such space charge can be made,[3] these corrections are of questionable accuracy. A technique which avoids these difficulties is described in detail in this paper. This technique has been applied to the alkali halides[4] and in modified form to silver chloride.[5] In this paper some experimental results on diamond are presented. Diamond was studied because it has a high electronic mobility and high photoconductive sensitivity, and because electronic mobility theory in diamond is well developed.

MacDonald and Robinson have recently used an alternative technique[6] for making such measurements which, where applicable, is more accurate, but which requires more light and/or greater photoconductive sensitivity. Unfortunately the author was not aware of their work until research for the present paper was almost complete. It appears likely that further improvements in these measurements can be attained through the use of combinations of some of the ideas of both methods.

* Partially supported by U. S. Office of Naval Research. Part of a dissertation submitted to the University of Illinois for the degree of Doctor of Philosophy.
† U. S. Atomic Energy Commission predoctoral fellow.
‡ Present address: Division of Applied Science, Harvard University, Cambridge, Massachusetts.
[1] H. Lenz, Physik. Z. 25, 434 (1924).
[2] J. Evans, Phys. Rev. 57, 47 (1940).
[3] C. C. Klick and R. J. Maurer, Phys. Rev. 81, 124 (1951).
[4] A. G. Redfield, Phys. Rev. 91, 753 (1953); following paper, Phys. Rev. 94, 537 (1954).
[5] F. C. Brown, Phys. Rev. 92, 502 (1953).
[6] J. Ross MacDonald and John E. Robinson, Phys. Rev. (to be published). The author is indebted to Dr. MacDonald for a discussion of this work.

B. EXPERIMENTAL METHOD

The electrode arrangement first used in this work is shown in Fig. 1. The crystal is sandwiched between plates of electrically conducting glass, that is, glass coated with a very thin transparent semiconducting film. The conducting plates and the batteries across them set up a fairly uniform field in the crystal in the x direction. The potential of the entire upper plate is held constant during the experiment by the electrometer circuit, while the potential of the entire lower plate can be varied by varying the potentiometer setting. Doing this makes opposite points on the two conducting plates have different potentials, and introduces a small y component of electric field in the crystal. Adding the y component of electric field to the large x component of field gives a field at an angle to the x axis; thus, moving the potentiometer rotates the electric field inside the crystal through a small angle about the z axis.

The electrometer responds only to charge flow in the y direction. A charge flow in the x direction will produce no deflection. The situation is analogous to that in an ionization chamber; the fact that the electrodes have a built in potential gradient does not alter the situation appreciably.

To make a measurement, the magnetic field is turned on in the z direction, and the crystal is illuminated with flashes of light a few seconds long. The potentiometer is adjusted until there is no charge flow registered by the electrometer upon illumination. This means that the charge flow $\mathbf{I}$ is in the x direction, as mentioned above, but due to the Hall effect the electric field is at an angle to the x direction [Fig. 2(a)]. The magnetic field is then reversed and the potentiometer readjusted until the electrometer again gives no deflection upon illumination of the crystal. The situation in Fig. 2(b) then obtains. The current is again in the x direction but the electric field has been rotated with the potentiometer through twice the Hall angle. The

Hall angle can be approximately obtained from the voltage change ΔV_T and the geometry of the electrodes:

$$\frac{2\mu_H H}{c} \sim 2\theta \sim \frac{\Delta E_y}{E_x} \sim \frac{\Delta V_T/D}{V_L/L}, \quad (1)$$

where μ_H and θ are the Hall mobility and angle, H is the magnetic field, c is the velocity of light, D is the thickness of the crystal, L is the length of the resistance film and ΔE_y is the change in E_y due to changing the potentiometer voltage by ΔV_T. This equation holds for small θ. We will show later how it can be corrected for edge effects and other errors.

This procedure is repeated for other values of the magnetic field to see whether the Hall voltage varies linearly with the magnetic field.

To eliminate the effects of charge which would build up near the surfaces of the crystal, the potentiometer is actually adjusted during a measurement in the following way: The batteries are all turned off and a bright light is shone on the crystal, releasing charge and neutralizing any residual space charge in the crystal. The light is then turned off and the batteries turned on. The crystal is illuminated with a weak light and the *initial* deflection of the electrometer is observed. The potentiometer is adjusted accordingly, i.e., to reduce or reverse this initial deflection, and the batteries are turned off again. This cycle is repeated until the electrometer gives no deflection upon illumination. The charge observed on the electrometer is at most a few times 10^{-14} coulomb, and it can be shown that this much charge flow produces a negligible effect on the electric field inside the crystal.

If the crystal shows appreciable dark current, charge will flow as soon as the batteries are turned on. This current will make the experiment impossible because the electric field inside the crystal will be distorted and destroyed and because it will be impossible to separate the dark current from the photocurrent. Thermally delayed or secondary photocurrent may give trouble for the same reason. These difficulties can sometimes be avoided with various modifications,[5] but in this paper we will discuss only completely insulating photoconductors showing no delayed photocurrent.

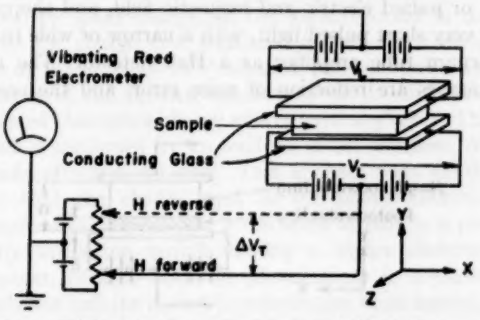

FIG. 1. Original electrode arrangement and circuit diagram.

This method differs from the conventional one in several interrelated ways. First, it is a transient method. Second, the electric field is rotated by external electrodes, rather than by the electrons under study. Third, the direction of charge flow is deduced from an electrometer measurement, rather than by confining the current to a thin sample whose orientation gives the direction of charge flow. Finally, no attempt is made to inject or eject electrons through the surface of the sample; the whole crystal takes part in the experiment. The method is similar in some respects to Freeman's method of measuring the Hall mobility of electrons released in diamond by beta particles.[7] The technique of using weak flashes of light to avoid space charge effects in photoconductivity experiments was originated many years ago by Pohl and his co-workers.[8]

The arrangement of Fig. 1 was actually used in some early measurements on diamond, but two serious difficulties arose. First, the upper plate had to be well insulated electrically from ground, and this meant that it was also well insulated thermally. This seriously limited the applied electric field because of the heat dissipated in the upper plate for high field values. Second, the upper battery had to be well insulated and shielded from ground, and the large size of the battery box resulted in unduly large noise and drift in the electrometer from ionization due to radioactive contamination.

The most important modification of the experiment is simply to remove the upper battery and connect the the electrometer directly to the upper plate (Fig. 3). The resulting electric field is highly nonuniform, but the principle of the experiment is exactly the same. The only difference is that for a given Hall angle and potential gradient on the resistance film the Hall voltage will only be about half as much, because the average x component of electric field is cut in half. The only modification of Eq. (5) is that E_x is replaced by $\bar{E}_x$, the average value of the x component of electric field in the crystal:

$$2\theta = 2\mu_H H/c = \Delta V_T/D\bar{E}_x, \quad (2)$$

where

$$\bar{E}_x = \int\int\int n\tau E_x d^3x \Big/ \int\int\int n\tau d^3x. \quad (3)$$

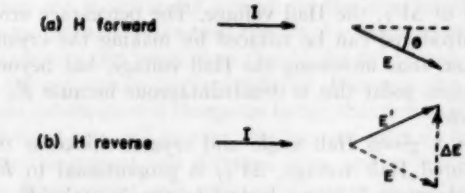

FIG. 2. Electric field and charge flow during the experiment.

[7] G. P. Freeman, thesis, Leiden, 1952 (unpublished).
[8] N. F. Mott and R. W. Gurney, *Electronic Processes in Ionic Crystals* (Oxford University Press, London, 1948), Chap. 4.

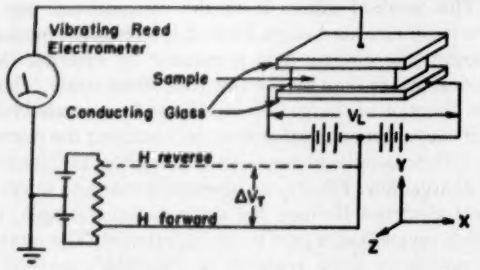

FIG. 3. Modified circuit diagram.

Here the integrations are over the volume of the crystal; n is the number of electrons per unit volume freed by the light pulse, and τ is the mean lifetime of the electrons before retrapping or annihilation. Equation (2) is proven in the appendix, and is valid for small values of θ, i.e., to first order in H. The only assumptions made in deriving Eq. (2) are that μ_H and μ_D, the Hall and drift mobilities, are constant throughout the crystal, that the area of the electrodes is much larger than the area of the sample, and that the edges of the sample are perpendicular to the electrodes.

Equation (2) applies to the arrangements of both Figs. 1 and 3. For Fig. 1, $\bar{E}_x \simeq V_L/L$ if the sample is thin; for Fig. 3, $\bar{E}_x \simeq \frac{1}{2}V_L/L$. For a thicker sample, $\bar{E}_x$ will be smaller due to the fringing field at the edge of the sample. Calculation of $\bar{E}_x$ is simply a problem in electrostatics which can be solved exactly in a few cases.

A disadvantage of the modification of Fig. 3 is that a slight amount of bleaching of the photoconductivity may make it impossible to get a reproducible setting of the potentiometer. This is because slight spatial inequalities in the amount of bleaching will cause the average position or centroid of the photoconductivity to move. With the magnetic field off, the proper potentiometer balance will be at the point where the y component of electric field is zero at the photoconductive centroid. If the centroid moves 1 percent of the length of the crystal, the proper potentiometer setting will move to change the voltage of the lower plate by 1 percent of the applied voltage V_L. This may be a large fraction of the Hall voltage. Similar arguments apply with the magnetic field turned on, and thus bleaching will give nonreproducibility and error in the measurement of ΔV_T, the Hall voltage. The percentage error so introduced can be reduced by making the crystal thicker, thus increasing the Hall voltage, but beyond a certain point this is disadvantageous because $\bar{E}_x$ is reduced.

For a given Hall angle and crystal thickness the measured Hall voltage, ΔV_T, is proportional to $\bar{E}_x$, and therefore it seems logical to try to make $\bar{E}_x$ as large as possible. E_x is obviously larger near the lower plate, a fact which suggests a further modification. If only part of the sample is photoconducting (Fig. 4), the parameter $n\tau$ is obviously zero for the upper part, and roughly constant for the lower part of the sample. If the photoconducting part is thin enough, $\bar{E}_x$ will almost equal V_L/L, rather than one-half V_L/L as in Fig. 3; if the photoconducting part is thick $\bar{E}_x$ will be somewhat less. As before, determination of $\bar{E}_x$ is simply a problem in electrostatics.

This modification has the advantage that, all other things being equal, the Hall voltage can be made as large as desired simply by increasing the thickness of the upper, nonphotoconducting part of the crystal. The required transverse field change in the photoconducting part remains constant because the Hall angle and $\bar{E}_x$ approximately do, but a larger applied voltage change ΔV_T is required to produce this given field change if the thickness is greater. This means that for samples of limited size, such as diamond, the Hall voltage can be increased several times, giving greater accuracy. Although the sensitivity of the electrometer for a given motion of charge is reduced in proportion to the thickness D, the noise due to fluctuations in the resistance film is similarly reduced, giving a constant signal-to-noise ratio. Furthermore, $\bar{E}_x$ is increased by a factor of approximately two, because the upper electrode no longer acts to reduce E_x in the photoconducting part of the sample, increasing ΔV_T by a factor of about $2D/\delta$. This modification also reduces bleaching errors by allowing the use of a thick crystal without reducing $\bar{E}_x$.

The main limitation of this method is that space charge difficulties are increased as D is made larger relative to δ, because a larger amount of charge flow is required to get a given accuracy.

Although a flat, thin sample is required for quantitative measurements, rough samples having a more or less flat shape can be used with the arrangements of either Fig. 3 or Fig. 4 if a crude measurement or a temperature dependence is all that is desired. Such measurements are useful in the case of diamond, because of the expense involved in grinding a diamond flat. Measurements can presumably also be made on polycrystalline, sintered, or powdered samples, although the possibility of space-charge difficulty is greater than with single crystals.

Further modifications of the method are the use of ac or pulsed electric and magnetic field, and chopped or very short pulsed light, with a narrow or wide band vacuum tube amplifier as a Hall detector. The advantages are reduction of noise error, and the possi-

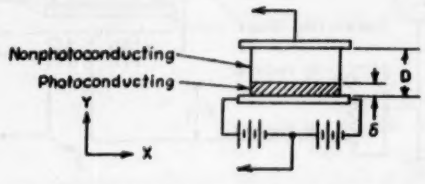

FIG. 4. Nonphotoconducting spacer modification.

bility of application to materials showing large delayed photocurrent or dark current. These variations were not used in this research, but Brown[8] has measured the Hall mobility of electrons in AgCl using a high speed pulsed light and pulsed electric field modification of the present method.

Evaluation of the parameter $\bar{E}_x$ defined in Eq. (3) is a straightforward boundary value problem if the sample is a circular cylinder or a rectangular parallelepiped with an infinite (or very large) z dimension. For a cylindrical sample in the arrangement of Fig. 4,

$$\bar{E}_x/E_0=1-b/2-\frac{2i(\epsilon-1)}{ab}\times\sum_{n=1}^{\infty}\frac{1-\cos(n\pi b)}{(n\pi)^3\left[\epsilon\dfrac{J_0(in\pi a)}{J_1(in\pi a)}-\dfrac{H_0^{(1)}(in\pi a)}{H_1^{(1)}(in\pi a)}-\dfrac{\epsilon-1}{in\pi a}\right]}, \quad (4)$$

where E_0 is the potential gradient on the lower plate, ϵ is the dielectric constant, a is the ratio of the radius of the cylinder to its thickness D, and b is the ratio of δ to D (Fig. 4). For a rectangular parallelepiped,

$$\bar{E}_x/E_0=1-\frac{b}{2}-\frac{2(\epsilon-1)}{ab}\sum_{n=1}^{\infty}\frac{1-\cos(n\pi b)}{(n\pi)^3[1+\epsilon\coth(n\pi a)]}, \quad (5)$$

where a is one-half the ratio of the thickness in the x direction to that in the y direction, and the other symbols are the same. It turns out that $\bar{E}_x$ as given in formulas (4) and (5) is almost the same for a cylinder as for a rectangular parallelepiped, if the parameters a and b are, respectively, the same, so it seems reasonable to assume that $\bar{E}_x$ for the intermediate case of an elliptical slab is also almost the same function of a and b, with a equal to one-half the ratio of the maximum thickness in the x direction to that in the y direction. Most of the samples used in this experiment were reasonably close to elliptical slabs and this approximation was used to calculate $\bar{E}_x$.

If the charge sensitivity of the electrometer is too low or if there is a large amount of noise, the charge flow required to make a measurement may be so large that the electric field in the crystal will be appreciably distorted by space charge. In the work reported in this paper the charge flow registered by the electrometer was of the order of 10^{-14} coulomb per light pulse, and because of the internal consistency of the data it is believed that space-charge effects were negligible. This belief is confirmed by an analysis of the problem, the details of which we omit. This analysis rests on the fact that the electric field in the photoconducting sample after illumination is the same as that in a perfectly insulating sample having a higher dielectric constant, because both the photocurrent in a photoconductor and the dielectric polarization in an insulator are in the direction of the electric field and proportional

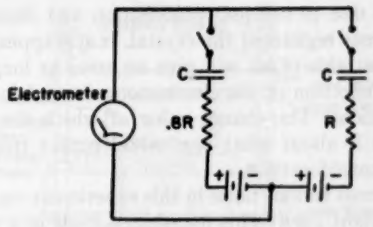

FIG. 5. Lumped circuit approximation of Fig. 4.

to it (neglecting the Hall effect, which produces only a second-order error). This assumption is valid only for relatively small charge flow.

When the crystal is illuminated the electrometer behaves in a rather unexpected way. If the potentiometer is set at one side of the "true" setting corresponding to the applied magnetic field, the electrometer needle, which registers charge (not current), will move, say, in a positive direction, with a velocity which appears to increase with time. If the potentiometer setting is now moved to the other side of the "true" setting, and the accumulated space charge in the crystal destroyed by shining in a bright light with the batteries off, the electrometer needle will initially move in the negative direction upon illumination with the batteries on. But after a deflection of about 10^{-14} coulomb (in a typical case) the electrometer needle will slow down, stop, reverse, and move in the positive direction with increasing velocity. If the potentiometer is moved farther in the same direction, the electrometer excursion will be farther but the general behavior will be the same. This effect is surprising because one generally expects an exponentially decaying current due to the buildup of space charge. The effect occurs with or without a magnetic field, and is most pronounced when only part of the sample is photoconducting.

The most likely cause for this effect can be explained with the aid of Fig. 5, which is supposed to approximate the arrangement of Fig. 4. The two resistors represent the two halves of the photoconducting part of the crystal, and the two condensers the two halves of the upper part of the crystal. Turning on the switches is equivalent to turning on the light, and the fact that the two resistors are unequal is supposed to represent the fact that the crystal may not be uniformly illuminated. When the switches are turned on, the condensers are uncharged and the current flow in the left-hand arm is opposite to and larger than that in the right-hand arm, so the net charge flow is clockwise. However, the left-hand condenser will charge up faster, the current in the left-hand arm will become smaller, and after a certain time the current will decrease, stop, and reverse, and the electrometer will eventually return to its initial reading. The latter fact is due to the equality of the condensers and the equality and opposite polarity of the batteries.

This simple analog shows that the current reverse

effect is due to unequal polarization and illumination in different regions of the crystal. It still appears, however, that this effect will give no error as long as the initial deflection of the electrometer is used in making observations. The charge value at which the current reverses is about what one would expect from space charge considerations.

The most serious noise in this experiment was caused by the light itself. This manifested itself in a swing of the electrometer needle in one direction when the light was turned on, and a swing in the reverse direction when the light was turned off. If the "sample" was not a photoconductor, the needle would return to the same reading, plus or minus a small amount due to drift. The time required for the electrometer to reach an equilibrium reading when the light was turned on or off was about 10 seconds.

This spurious signal could be divided into two parts: The first was due to photoconductivity in the resistance film, which will give a signal because the illumination and the resulting resistance change of the film may not be uniform, and a nonuniform change of resistance will result in a change in the average potential of the lower plate. This potential change will be capacitatively coupled to the electrometer. Only certain kinds of film show this photoconductivity.

The other part of the spurious signal occurred even when the batteries were turned off, so that film photoconductivity could not be responsible. It seems likely that this signal was due to the heating of some part of the crystal holder or the crystal, because it occurred most strongly at low temperatures (80°K) where the thermal contact between different parts of the system was poor; however, the signal was not due to thermal expansion of the sample, as could be proven by applying a large voltage V_T to the lower plate, with V_L off, and observing that the signal was unchanged. The exact origin of this signal is still somewhat of a mystery.

Another serious kind of noise originating in the resistance film occurred when the film was carrying current and was apparently similar to the noise which occurs in carbon resistors. This noise was serious only in certain types of film.

If the sample used is not uniformly photoconducting due to inhomogenieties in the impurity content or to absorption of light, $\bar{E}_s$ may be different from the calculated value. Since E_s varies from E_0 to zero between the bottom and top of the crystal this error may be quite important. If the error is due to inhomogeniety in the material, it can be greatly reduced by making a Hall measurement, turning the sample over, making another measurement, and averaging. A value obtained in this way is the same as that which would be obtained from the arrangement in Fig. 1, by the superposition theorem. The arrangement of Fig. 1 is not so susceptible to such errors because E_s is much more uniform throughout the crystal. If the error is due to light absorption, it may be calculable,[5] or it can be reduced by using a crystal of dimensions large compared to the light absorption length, and illuminating through the bottom plate. In this case $\bar{E}_s$ will be very nearly equal to E_0.

Other possible kinds of noise and error which were unimportant in practice are mechanical vibration, battery noise and drift, electrometer and insulator noise, surface leakage, Hall effect in the resistance film, and thermoelectric effects. The voltage applied to the resistance film, and thus $\bar{E}_s$, was limited by heating effects in the film, and the resulting noise and drift in the electrometer.

C. EXPERIMENTAL APPARATUS

The cryostat is diagramed in Fig. 6. This cryostat cools the crystal by conduction through a heavy copper bar which is in contact with an external temperature bath in a Dewar flask. The tail of the cryostat was immersed in a coolant which was ice water, dry ice and acetone, or liquid nitrogen.

The cryostat was evacuated with a mechanical pump and the pressures attained were of the order of a few microns. The vacuum served both to insulate the crystal holder and heat conductor thermally, and to reduce surface leakage current and radioactive ionization noise in the electrometer.

The copper heat conductor was in two sections, held together with a $\frac{1}{4}$-20 stud bolt and soldered with Wood's metal for effective heat conduction and ease of removal. The temperature drop between the coolant and the base

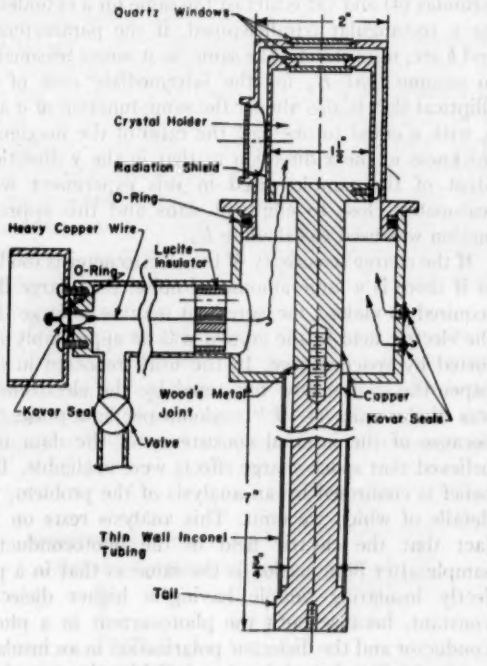

FIG. 6. Simplified cross section of the cryostat.

of the crystal holder was normally about four degrees at 80°K.

The cryostat was held below the gap of the magnet in such a way that the crystal holder and the two-inch diameter vacuum jacket around it projected up into the bottom part of the magnet gap. In this way it was possible to fit into a magnet which was already occupied with another experiment and which would otherwise have been unavailable for this work.

The lead from the crystal holder to the electrometer head consisted of a number 30 constantan wire leading to a heavy copper wire, which went down the center of a long (two-foot) tube to a Kovar seal. Constantan wire was used to minimize heat conduction. The only insulators used between the crystal holder and the electrometer were the Kovar seal and a piece of Lucite, both of which could be removed for cleaning. The Kovar seal was vacuum sealed to the end of the tube by being clamped down hard against a greased O ring. The assembly which clamped the O ring was also designed to fit the head of the vibrating reed electrometer,[9] and the sensitive lead of the electrometer made direct contact with the knob on the end of the Kovar seal. The same pipe which was used to lead out the electrometer connection was also the pumping lead, and the Lucite insulator had several holes drilled through it to reduce its pumping impedance.

Temperatures between ice, dry ice, and liquid nitrogen temperatures were obtained in one of two ways. The first was to cool the cryostat to low temperature with liquid nitrogen and keep the Dewar flask in position, but then remove enough liquid nitrogen so that the tail of the cryostat was no longer in contact with it. Doing this minimized warming of the copper rod by air convection, and the crystal holder warmed up slowly (from 100 to 200 degrees kelvin in about one hour) due to conduction up the inconel tube and radiation.

In the other method for attaining intermediate temperatures a copper appendage was screwed to the end of the tail with a spacer of brass or copper, and the appendage was placed in contact with the temperature bath. After a long time the copper bar would come to equilibrium at a temperature somewhat above that of the coolant. Although this arrangement gave a more stable temperature, it was rather unsatisfactory because the temperature attained depended strongly on the nature of the contact between the spacer and the two pieces of copper, and it was impossible to predict or prearrange the temperature at which the cryostat would reach equilibrium.

Compared to the more usual optical cryostat design, in which the crystal holder is attached to the bottom of the coolant holder of a Dewar-shaped vessel, this design has the advantages of simpler construction, ease of quick warming, and (what was most important in the present work) the possibility of being placed unobtrusively in the gap of a busy magnet. Its disadvantages are high liquid nitrogen consumption and slowness in cooling.

[9] Manufactured by the Applied Physics Corporation, Pasadena, California.

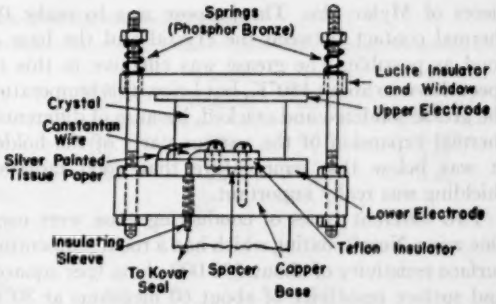

FIG. 7. The crystal holder. The radiation shield, which is omitted, fits over the whole assembly as indicated in Fig. 6. The thermocouples and two of the three electrical connections to the electrodes are also omitted.

About six different crystal holders were tried during the experiment, and the trouble with most of the early models was that the crystal was not sufficiently well shielded from thermal radiation from the outside world. The solution was to surround the crystal completely with a radiation shield held at the temperature of the crystal. A hole in the shield as small as one-quarter inch in diameter a centimeter or so from the crystal could easily raise its temperature by several degrees, which is a serious error.

A fairly satisfactory crystal holder design is shown in Figs. 6 and 7. The radiation shield, shown in Fig. 6, was screwed to the circular base with six radial screws. The two quartz windows were clamped to the top of the shield with stiff phosphor bronze springs (not shown) and the surface where they made contact with the copper shield was greased with silicone vacuum grease for better thermal contact. Silicone grease was used because of its low hardening temperature. A quartz window makes a good radiation shield because it absorbs strongly in the far infrared and thus absorbs thermal radiations from the outside, re-emitting thermal radiation characteristic of its own temperature. The outer window of the radiation shield was supposed to act as a radiation shield for the inner window, so that despite the probable poor thermal contact between the windows and the shield, the temperature of the inner window was probably very close to that of the rest of the shield.

The essential features of the crystal holder with the radiation shield removed are shown in Fig. 7. The lower electrode was insulated from the base with one or two 0.001 inch sheets of du Pont Mylar plastic film, which has great mechanical and dielectric strength. In the case of diamond, a sheet of Mylar was also placed between the crystal and the lower electrode to prevent scratching of the resistance film. Silicone grease was used liberally at all interfaces between the crystal, the electrically conducting glass, the base, and the various

pieces of Mylar film. The purpose was to make the thermal contact between the crystal and the base as good as possible. The grease was effective in this respect down to about 180°K, but below this temperature the grease solidified and cracked, because of differential thermal expansion of the various parts of the holder. It was below this temperature that good radiation shielding was really important.

Two different types of conducting glass were used. One was a Nesa[10] coating which had a room temperature surface resistivity of about 200 000 ohms (per square), and surface resistivity of about 60 megohms at 80°K.

The principle trouble with this film was that its low resistance limited the electric field because of heat dissipation problems to 400 volts per centimeter or less. At low temperature it also showed very serious photoconductivity.

The other conducting glass used was very kindly supplied by Dr. K. B. Blodgett of the General Electric Research Laboratory, and was made by heating lead glass at high temperature (about 500°C) in a stream of hydrogen.[11] This film had a room temperature surface resistivity of about 5000 megohms, and a surface resistivity at 80°K of about 100 000 megohms. This film did not show any photoconductivity, but gave serious noise whenever a voltage was applied to it. The noise was less at low temperatures, and a few measurements were made at 80°K using this film. Its higher resistance allowed the use of higher electrical fields in the crystal.

The linearity of the potential gradient on the surface of the film could be checked with a probe connected to a high-resistance potentiometer. Such measurements were made at room temperature, but it seems reasonable to assume that a film which is uniform at room temperature will also be uniform at lower temperatures.

The upper electrode was either a piece of Nesa-coated glass or a plain piece of glass painted with closely spaced stripes of silver paint.

An important use of the resistance films was to act as a check on the temperature of the crystal. If the temperature of the lower resistance film was the same as that of the base of the crystal holder, it was assumed that the radiation shielding was adequate and that the crystal was also at the same temperature. On the other hand, if the resistance film temperature was above that of the base the crystal temperature would certainly be higher also.

The temperature of the resistance film could be inferred from measurements of its resistance. The resistance was reliably known from 200 to 300°K, where the silicone grease could be relied upon to make good thermal contact. The resistance at 77°K was known from measurements made while the film was immersed in liquid nitrogen. The resistance at intermediate temperatures could not be measured directly, but the effects of inadequate radiation shielding could easily be detected because the film resistance was not a reproducible function of temperature (as measured with a thermocouple screwed to the base), and the resistance did not approach the known value at 77°K. With the crystal holder of Figs. 6 and 7 the resistance-temperature function was reasonably smooth, although there was still some scatter at the lowest temperatures. This scatter may have been due to very long time constant photoconductivity (for which there is some evidence) in the case of the Nesa film, and to inaccuracies in the resistance measurement in the case of the lead glass film.

The resistance measurements indicate that for the crystal holder of Figs. 6 and 7 the crystal temperature was probably less than four degrees below the temperature of the base. There is, however, a slim possibility that the difference was as much as 8 degrees.

In other crystal holder designs the plane of the electrodes was vertical and the illumination was horizontal through the window in the side of the vacuum jacket. Such an arrangement has the disadvantage that less space is available for the crystal; on the other hand, the crystal can be illuminated through the "bottom" electrode, i.e., the electrode connected to the batteries V_L, through a hole drilled the base of the holder. This is desirable if the crystal used absorbs light strongly, but it was not particularly advantageous in the present research.

The magnet was designed and built for nuclear resonance work by H. W. Knoebel, R. E. Norberg, and D. H. Holcomb, and was very kindly made available for this research by Professor C. P. Slichter. The magnetic field could be varied from zero to ten kilogauss. The crystal was an inch or more from the edge of the magnet gap, and flip coil measurements showed that the field at this point was 1 percent $\pm\frac{1}{2}$ percent less than the field at the center of the gap.

The optical system was exceedingly crude, and consisted of a 250-watt 110-volt sealed beam spotlight and a collection of filters. The lamp was supplied through a variac from the 110-volt ac line, and could be turned on with a pushbutton switch on the output of the variac. To eliminate electrical interference in the electrometer a Cornell-Dubilier type IF-18 interference filter was connected between the variac and the switch. A glass absorption cell containing a few percent solution of cupric chloride in distilled water was used to remove infrared radiation from the lamp. The spotlight was roughly $1\frac{1}{2}$ feet from the crystal. It was run at between 40 and 110 volts for the observational pulse of light, and usually at higher voltage for the removal of space charge.

All voltages were supplied by batteries. V_L was between 90 and 720 volts, depending on the tempera-

[10] Trade name for electrically conducting glass manufactured by the Pittsburgh Plate Glass Company. See L. B. Clark, Sr., Rev. Sci. Instr. 24, 641 (1953); R. C. Gomer, Rev. Sci. Instr. 24, 993 (1953).

[11] K. B. Blodgett, J. Am. Ceram. Soc. 34, 14 (1951).

TABLE I. Summary of the characteristics of all the diamonds studied.

Diamond	uv transmission at 2537A	Fluorescence	Mobility cm²/volt sec 300°K	Mobility cm²/volt sec 200°K	Thickness mm	½ length / thickness	½ width / thickness	$\bar{E}_s/E_0$ assumed
A	No	Yes	−720	−1300	1.2	1.45	0.9	0.435
PS	No	Very small	−1850	−3350	1.3	1.8	1.8	0.45
US1	Yes	Very small	−1700	−3150	0.35	4.5	2.7	0.48
US2	No	Very small	(−900)	(−1200)				
US3	Yes	Very small	Low photocond.					
US4	No	Very small	(−900)	(−1000)				
US5	No	Very small		(−1200)				
US6	No	Very small	Not investigated					
R1	No	Very small	(+1100)	(+1400)				
R2	No	Very small	(−800)	(−1000)				
R3	Yes	Very small	−1400	−2250	0.78	3.0	1.63	0.47
R4	No	Very small	Dark conductivity					
R5	No	Very small	Dark conductivity					
R6	No	Very small	−1200	−1700	0.66	2.6	1.8	0.465
R7	Yes	Very small	Dark conductivity					
R8	Yes	Very small	Dark conductivity					
R9	Yes	Very small	Dark conductivity					
R10	Yes	Very small	+1000	+1400	1.07	1.42	1.0	0.435
R11	Yes	Very small	+1200	+2200	0.975	1.54	1.24	0.44
R12–17	No	Very small	Not investigated					
R18–20	No	Yes	Not investigated					

ture and resistance film, and the Hall voltage ΔV_T was as much as 90 volts. At the higher temperatures it was necessary to use a lower V_L because the film resistance was lower, and therefore, the accuracy was lower.

D. EXPERIMENTAL RESULTS

The vital statistics for the diamonds studied are given in Table I, together with some rough data on the magnitude and temperature dependence of the mobility.

The samples R1 to R20 were purchased from the Rough Diamond Company, New York, New York; and samples US1 to US6 were purchased from the U. S. Industrial Diamond Company, New York, New York. Some of these were apparently whole rough diamonds and others were cleavage plates, but all were thin plates with more or less flat surfaces.

Diamond PS was the same sample studied by Pearlstein and Sutton in their measurements of the electronic drift mobility.[12] Diamond A had been previously studied by Raboy[13] and was known not to count alpha particles.

The luminescence was investigated with light from a low-pressure mercury arc filtered with a Corning No. 7–54 filter. The luminescence was blue or blue-green as reported by other investigators. The ultraviolet transmission was investigated using the same source and filter, and detecting the radiation with willemite powder. A previous crude experiment had shown that this powder was sensitive mainly to radiations below 3000A, so that this test was essentially a measure of the optical transmission of the diamond at 2537A. The results of this test were verified in the case of diamonds R3, US1, and PS with transmission spectra taken with a quartz spectrograph and a hydrogen arc.

As indicated in Table I, many of the diamonds did not photoconduct sufficiently, or showed dark conductivity. In several cases this conductivity was apparently surface leakage, and could be eliminated by cleaning the diamond in hot nitric acid, cleaning solution, or aqua regia. Another effective cleaning procedure was to heat the diamond to orange heat with a torch, burning off a microscopic surface layer. This must be done cautiously, because diamond slowly changes to graphite at high temperatures. Several diamonds were treated in this way with no apparent ill effect.

Preliminary measurements were made on a number of rough diamonds. The method of Fig. 4 was used for greater relative accuracy. Silicone grease was used to fill the spaces between the crystal and the lower electrode caused by departures from flatness of the diamond surface. The purpose was to couple the crystal to the lower electrode electrostatically so that $\bar{E}_s$ would be as close to E_0 as possible. In some cases what corresponds to the "nonphotoconducting" part of the crystal in Fig. 4 was a 3.85-mm Teflon spacer. In these cases the diamond was illuminated through the "bottom" plate, as described in the last section. In other cases this spacer was a transparent insulator and the illumination was through the top. These measurements gave an accurate idea of the temperature dependence of the mobility, though because of the irregular shape of the diamonds it was possible to get only a rough idea of the absolute magnitude.[14] These measurements were

[12] E. Pearlstein and R. B. Sutton, Phys. Rev. **79**, 907 (1950).
[13] S. Raboy, thesis, Carnegie Institute of Technology, 1950 (unpublished).

[14] To do this, the dielectric constant of diamond must be known. The value 16.5 quoted in various reference books is wrong; the correct value is 5.67. See S. Whitehead and W. Hackett, Proc. Roy. Soc. (London) **A51**, 173 (1939).

made with the tungsten lamp and the cupric chloride filter plus another blue filter with a gradual cutoff at about 5500A. In some cases a blue filter with a 4300A sharp cutoff was used. In no case did these filters make a significant difference in the measurement.

On the basis of this preliminary survey 7 interesting diamonds were chosen for further study, and their surfaces were ground and polished flat. This work was done by the Arthur A. Crafts Company, Chicago, Illinois. Only the top and bottom surfaces were ground flat; the edges were left rough. These seven diamonds were rerun after polishing using the method of Fig. 4 with a Teflon or sodium chloride spacer. As before, silicone grease was used to improve the electrostatic and thermal coupling between the crystal and the lower electrode. To get temperatures intermediate between liquid air, dry ice, and ice temperatures the cryostat was allowed to warm up slowly as described previously, and a series of measurements were made with the magnetic field alternately forward and reverse.

To get a more accurate value of the absolute magnitude of the mobility, measurements were made at dry ice and liquid air temperatures using no dielectric spacer above the crystal, as in Fig. 3. The relative measurements obtained as described in the previous paragraph were then normalized to agree with this absolute data. In Fig. 8 is plotted data for one of the most studied diamonds. The absolute measurements are denoted by the crosses, and the normalized relative data by elipses. The estimated maximum error is denoted by the size of the crosses and elipses. The measurements shown are the result of four different runs, two absolute and two relative.

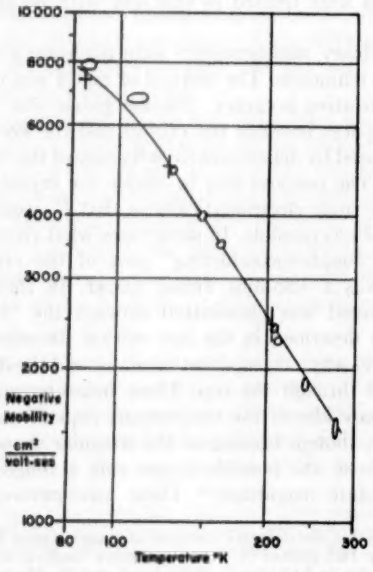

FIG. 8. Experimental data for diamond R3.

To reduce the effects of inhomogeneities in the diamonds, each absolute measurement was the average of two absolute measurements, with the diamond turned over between measurements. The ratio of the two measurements is a measure of the homogeneity of the diamond; if the ratio is one, the diamond is presumably fairly homogeneous. The observed ratios were always nearly the same at dry ice and liquid air temperatures, as expected. US1 and R3 consistently gave ratios of about 1.1:1 to 1.3:1; R6, R10, R11, and A gave ratios between 1.5:1 and 2.5:1; and PS was the least homogeneous, yielding ratios as high as 4:1. The ratio in PS was also not reproducible; a later measurement yielded a ratio of 2:1.

At temperatures near 100°K, where the Hall angle at 10 000 gauss approaches one radian in some samples, the apparent Hall mobility decreased as the magnetic field increased. That is, the ratio of ΔV_T to $\Delta H=2H$ would decrease as H was increased. This decrease is attributed to third-order terms in H (second-order Hall effect). At these temperatures the measured mobility approached a value 15 ± 5 percent larger than the 10 000 gauss value, as H approached zero. This behavior was observed unambiguously only at low temperatures in the three high-mobility samples (R3, US1, and PS). It was observed in both the absolute and relative measurements on these samples. The true Hall mobility was assumed to be the mobility as H approaches zero. The departure from this value appeared to be proportional to H^2 as expected.

An attempt was made to investigate the spectral variation of the apparent mobility in diamond R3. All that was established was that at 100°K the measured mobility was smaller by about 10 percent at 5000A, as compared to 3650A. Above 5000A the mobility was of the same order of magnitude as below.

In all the measurements described above, the Hall voltage was proportional to the electrical field. That is, for any given magnetic field, V_T was always proportional to V_L.

The Hall voltage did *not* always vary linearly with magnetic field. A survey of all the measurements made on diamond indicates that there was no clear-cut correlation between the direction of the Hall voltage asymmetry and the orientation of the crystal holder, the electric field, or the magnetic field. For any given diamond in a given run the relative asymmetry was independent of the electric field, and reversed sign with the electric field, consistent with the previous paragraph. The only cases which showed a clear-cut asymmetry above error were those where an absolute measurement was being made with no dielectric spacer between the diamond and the upper electrode; i.e., where the electric field was most nonuniform. R3 showed far and away the greatest asymmetries; in some cases the asymmetry $[V_T(+H)+V_T(-H)-2V_T(0)]/2[V_T(+H)-V_T(-H)]$ was as much as 0.1 for $H=$

$\pm 10\,000$ gauss at 80°K. At temperatures above 200°K the asymmetry was negligible.

These asymmetries probably did not affect the Hall measurements, since these measurements were made by observing the required potentiometer voltage change when the magnetic field was reversed, rather than merely turned on or off. The origin of the asymmetry is probably magnetoresistance effect; arguments which will be omitted here indicate that the anisotropic magnetoresistance effect is the most important. This explanation is, however, by no means certain.

The dark resistivity of the diamonds on which successful measurements were made was apparently 10^{16} ohm-cm or greater at room temperature and below.

The mobility data for the most thoroughly studied diamonds is summarized in Fig. 9. The accuracy for most of the data is ± 5 percent to ± 10 percent. The discrepancy between R3, US1, and PS is apparently real, but due to some scatter of the data this cannot be said with certainty.

E. DISCUSSION

The data is consistent with previous Hall mobility measurements on diamond.[1,3,7]

The fact that three of the diamonds show a Hall effect characteristic of holes is in itself interesting, and indicates that both electrons and holes can be expected simultaneously in all the diamonds studied. It should be noted that the wavelength of the light used (about 4000A) was such that the electrons and holes could be excited from energy levels roughly in the center of the energy band gap, and it is perfectly plausible that such light could yield both electrons and holes simultaneously.

It seems certain that the temperature dependence of the observed mobility is determined in part by the temperature variation of the relative number of electrons and holes produced by the light. This makes interpretation of the data difficult.

In a very thorough study of the counting properties of diamond, Freeman[6,15] has shown that the best counting diamonds tend to be the most perfect ones. For this reason it is unlikely that, as has been sometimes suggested, mosaic or grain boundary conduction is important in the conduction counting mechanism. For the same reason it is believed that such processes are unimportant in the present research.

It is assumed that the diamonds used were perfect insulators throughout their volume. It is conceivable that the diamonds contained impure semiconducting domains which would have distorted the electric field. If this were the case, however, erratic noise and drift might be expected in the electrometer. No such behavior was normally observed below room temperature.

The most striking feature of the data is that the three diamonds PS, US1, and R3, which seem to follow

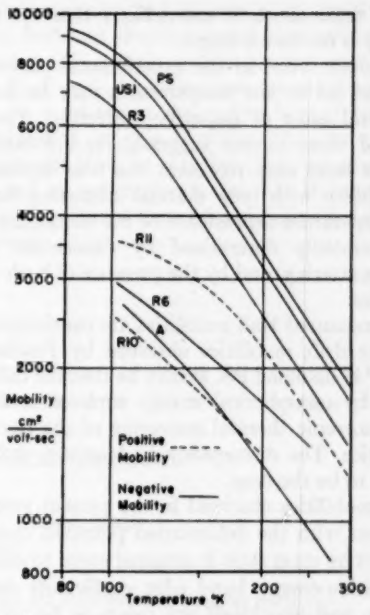

FIG. 9. Summary of the experimental data for the most thoroughly studied diamonds.

a $T^{-\frac{3}{2}}$ temperature dependence (as predicted by the deformation potential theory)[16,17] also have the highest mobility, and differ in absolute magnitude by a relatively small amount. It seems likely that these diamonds give the true order of magnitude of the intrinsic electronic mobility. If there were a large number of holes in these diamonds it seems improbable that the measured mobility would follow the $T^{-\frac{3}{2}}$ law. To do this, the electron-hole density ratio would have to remain constant with temperature (assuming that the true electron and hole mobilities follow the $T^{-\frac{3}{2}}$ law).

The difficulty with this interpretation is the 30 percent discrepancy between these three diamonds. This may conceivably be an experimental error. If the discrepancy is real it is probably due to the presence of holes in R3. If the electron-hole concentration ratio in R3 were constant to about 50 percent over the temperature range studied this would be a possible explanation.

We will tentatively assume that the electronic mobility is 1800 at 300°K. It seems certain that this is the correct order of magnitude, but on the basis of the existing data, an error of twenty to thirty percent is not inconceivable.

The measurements on R11 approach a $T^{-\frac{3}{2}}$ temperature dependence at high temperatures, and are characteristic of hole conduction. These measurements set a lower limit on the hole mobility of 1200 cm²/volt second at 300°K. Considering how close R11 approaches

[15] G. P. Freeman and H. A. van der Velden, Physica **16**, 486 (1950); **17**, 565 (1951); **18** (1952).

[16] F. Seitz, Phys. Rev. **73**, 549 (1948).

[17] J. Bardeen and W. Shockley, Phys. Rev. **80**, 72 (1950).

the $T^{-\frac{1}{2}}$ dependence, it seems likely that the true hole mobility is not much larger.

The slight bend in the experimental curves of PS, US1, and R3 at low temperatures may be due to experimental error or impurity scattering. The similar shape of these curves suggests, on the other hand, that the bend may represent the true dependence of the mobility with only thermal scattering important. The temperature dependence of the remaining samples is undoubtedly determined by dislocation and impurity scattering, and by the presence of both electrons and holes.

The measured Hall mobilities are considerably lower than the drift mobilities observed by Pearlstein and Sutton[12] in diamond PS. It may be that the difference is caused by nonspherical energy surfaces in k space,[18] or nonisotropic thermal scattering of the electrons by the lattice. The discrepancy is, however, rather large for this to be the case.

The mobilities observed in the present research are consistent with the deformation potential theory[16,17] if the effective mass ratio is assumed equal to one and the deformation-energy band edge coefficients defined by Bardeen and Shockley[17] are taken to be $|E_{1c}|=7$ ev and $|E_{1v}|=8$ ev. These values are reasonable when compared with those for silicon and germanium, although direct application of the theory to some of these cases may not be possible, owing to probable complications in the band structure or the scattering dependence on velocity.[19] On the other hand, the drift mobility measurements of Pearlstein and Sutton[12] indicate that $|E_{1c}|$ and $|E_{1v}|$ may be smaller, or that the theory may also be inapplicable to diamond. In any case, it is clear that the relatively high value of the mobility in diamond is a partial consequence of its relative inelasticity, or, equivalently, its high Debye temperature.

Further investigation of the Hall effect in a large number of diamonds might yield a better picture of the photoconductive processes in diamond and less ambiguous values of the electron and hole mobilities. Variation of the Hall mobility at high electric fields should be an interesting extension of the investigation. Finally, study of the magnetoresistance effects in diamond should be possible using similar methods, and should give information about the energy band structure.

The author wishes to thank Professor R. J. Maurer for his frequent suggestions and friendly help, Professor C. P. Slichter and his associates in the nuclear resonance group for the use of their magnet and laboratory facilities, and Mr. F. E. L. Witt for help in the design and construction of the equipment. Thanks are also due Mr. K. Teegarden and Mr. J. F. Aschner for assistance on various occasions, to Dr. A. B. Lidiard, Dr. E. Miller, Dr. E. Pearlstein, and Dr. Y. Yafet for useful ideas and information, and Professor J. Bardeen and Professor F. C. Brown for helpful criticism.

F. APPENDIX

We now derive Eq. (2) above.

If an electron is freed in the crystal at a point $\mathbf{x}$, and moves a small distance $\mathbf{d}$ before retrapping or annihilation, the resulting charge flow registered by the electrometer will be

$$Q=e\mathbf{d}\cdot\partial\mathbf{E}/\partial V_T, \tag{6}$$

where e is the electronic charge, and V_T is the potentiometer voltage, and $\mathbf{E}$ is evaluated at the point $\mathbf{x}$. This result is independent of the electrode and sample shape and of the value or presence of the batteries V_L, and was proven for the vacuum case by Shockley;[20] a more general proof applicable to the present case follows from the Carson reciprocity theorem.[21]

If $n(\mathbf{x})$ electrons per unit volume are released in the sample, Eq. (6) becomes

$$Q=\int\int\int ne\mathbf{d}\cdot(\partial\mathbf{E}/\partial V_T)d^3\mathbf{x}. \tag{7}$$

The distance $\mathbf{d}$ traveled by the electrons (*shubweg*) is given by

$$\mathbf{d}=\mathbf{v}\tau=\tau\mu_D\mathbf{E}+\tau\mu_D\mu_H\mathbf{E}\times\mathbf{H}/c, \tag{8}$$

plus higher-order terms in $\mathbf{E}$ and $\mathbf{H}$. Here $\mathbf{v}$ is the electronic velocity, and τ is the mean time before trapping or annihilation of the released electrons.

In making a measurement, V_T is adjusted until Q equals zero. Using Eqs. (7) and (8) we get

$$Q=0=\int\int\int ne\tau[\mu_D\mathbf{E}\cdot(\partial\mathbf{E}/\partial V_T)+(\mu_D\mu_H/c)(\mathbf{E}\times H)\cdot(\partial\mathbf{E}/\partial V_T)]d^3\mathbf{x}, \tag{9}$$

plus higher-order terms.

Reversing the magnetic field and readjusting V_T an amount ΔV_T until $Q=0$ once again, gives

$$Q=0=\int\int\int ne\tau[\mu_D(\mathbf{E}+\Delta V_T\partial\mathbf{E}/\partial V_T)(\partial\mathbf{E}/\partial V_T)-(\mu_D\mu_H/c)(\mathbf{E}+\Delta V_T\partial\mathbf{E}/\partial V_T)(\mathbf{H}\times\partial\mathbf{E}/\partial V_T)]d^3\mathbf{x}, \tag{10}$$

plus higher-order terms.

Subtracting Eq. (9) from (10), and using the vector identity

$$\mathbf{A}\cdot(\mathbf{B}\times\mathbf{A})\equiv 0$$

[18] W. Shockley, *Electrons and Holes in Semiconductors* (D. Van Nostrand Company, Inc., New York, 1950), p. 338.
[19] M. B. Prince, Phys. Rev. **92**, 681 (1953).
[20] W. Shockley, J. Appl. Phys. **9**, 635 (1938).
[21] J. R. Carson, Bell System Tech. J. **3**, 393 (1924); **9**, 325 (1930).

gives

$$\Delta V_T \int\int\int ne\mu_D\tau(\partial \mathbf{E}/\partial V_T)^2 d^3\mathbf{x}$$

$$= 2/c \int\int\int ne\mu_D\mu_H\tau(\mathbf{E}\times\mathbf{H})\cdot\partial\mathbf{E}/\partial V_T d^3\mathbf{x}. \quad (11)$$

This equation is exact to second order in **H**. The second-order (magnetoresistance) terms drop out because the measurement is made by reversing the magnetic field, not simply turning it on and off.

Equation (11) clearly applies to the arrangements of Figs. 1, 3, or 4. In these cases we can assume that $\partial\mathbf{E}/\partial V_T$ is a vector in the y direction of magnitude $1/D$, because Laplace's equation and the boundary conditions will then be satisfied. We can also assume that μ_D and μ_H are constant, and that **H** is uniform in the z direction. Under these assumptions Eq. (2) follows immediately.

PHYSICAL REVIEW VOLUME 94, NUMBER 3 MAY 1, 1954

Electronic Hall Effect in the Alkali Halides*

ALFRED G. REDFIELD†‡
Physics Department, University of Illinois, Urbana, Illinois
(Received January 19, 1954)

The Hall mobility of electrons in colored NaCl, KCl, KBr, and KI has been measured using an unconventional technique previously described by the author. Measurements on additively and x-ray colored NaCl yield an electronic mobility of 250±50 cm²/volt sec at 84°K, decreasing to about 25±25 at 200°K. In additively colored KCl the mobility is 100±50 at 90°K; in additively colored KBr it is about 110 at 84°K. In additively colored KI the mobility is 155±30 at 84°K, decreasing to 30±15 at 200°K. In every case the sign of the Hall effect is electronic. These observations are consistent with the mobility theory of Low and Pines assuming effective mass ratios between 0.35 and 0.6 for the unpolarizable crystal, or polaron effective mass ratios between 0.5 and 0.9. These mobility data combined with photoconductive yield data give values of the capture cross section of F centers for electrons (to form F' centers) between 0.7 and 5 times 10^{-15} cm² at about 200°K.

A. INTRODUCTION

THIS paper reports some measurements of the electronic Hall mobility in colored NaCl, KBr, and KI using techniques described in the immediately preceding paper[1] (henceforth referred to as EHED). Previous investigations[2–4] in these crystals failed to give quantitative values of the mobility, although Evans[4] established an upper limit of 20 cm²/volt sec at 300°K for the mobility in several colored alkali halides. While the present work was in progress, MacDonald and Robinson[5] succeeded in measuring the electronic mobility in KBr, obtaining a value of 12.4 cm²/volt sec at 300°K.

This work was undertaken mainly to test the theory of electronic mobility in polar substances.[6–8] Theory predicts that the mobility will vary with temperature as $\exp(\Theta/T)$, where Θ is the Debye temperature corresponding to the longitudinal optical modes of vibration of the lattice, and provided $T \ll \Theta$. Θ can be deduced[9] from the infrared absorbtion peak[10] of the crystal and its low- and high-frequency dielectric constants.[11] The values of Θ for the crystals investigated in this research are NaCl, 370°K; KCl, 300°K; KBr, 236°K; KI, 190°K. Thus the theory applies to those alkali halides only considerably below room temperature.

The electrons in this experiment are obtained by ionizing F centers with light of the proper wavelength. The F centers act only as sources of electrons, and in view of their small concentration they should not affect the experimental measurements.

* Partially supported by U. S. Office of Naval Research. Part of a dissertation submitted to the University of Illinois for the Ph.D. degree.
† U. S. Atomic Energy Commission predoctoral fellow.
‡ Present address: Division of Applied Science, Harvard University, Cambridge, Massachusetts.
[1] A. Redfield, preceding paper, Phys. Rev. **94**, 526 (1954).
[2] P. Lukirski, *Reports of the Physical-Technical Roentgenological Institute and the Leningrad Physical-Technical Laboratory 1918–26* (Leningrad, 1926), p. 185.
[3] P. Tartakowski, Z. Physik **66**, 830 (1930).
[4] J. Evans, Phys. Rev. **57**, 47 (1940).
[5] J. Ross MacDonald and John E. Robinson, Phys. Rev. (to be published).
[6] H. Frohlich and N. F. Mott, Proc. Roy. Soc. (London) **A62**, 446 (1949).
[7] Frohlich, Pelzer, and Zienau, Phil. Mag. **41**, 221 (1950).
[8] F. Low and D. Pines, Phys. Rev. **91**, 193 (1953). The expression for the parameter α given by Low and Pines is too small by a factor 2π.
[9] Lyddane, Sachs, and Teller, Phys. Rev. **59**, 673 (1941); H. B. Callen, Phys. Rev. **76**, 1394 (1949).
[10] R. B. Barnes, Z. Physik **75**, 723 (1923).
[11] N. F. Mott and R. W. Gurney, *Electronic Processes in Ionic Crystals* (Oxford University Press, London, 1948), p. 12.

B. EXPERIMENTAL RESULTS

Because of bleaching or, what is equivalent, conversion to F' and other centers, it was desirable to make ΔV_T as large as possible compared to V_L; therefore, the method of Fig. 4, EHED, was used for almost all the measurements. The upper nonphotoconducting spacer was an uncolored piece of the same crystal. The thickness D varied between 0.5 and 1.5 centimeters in different crystals; the parameter a (defined in EHED) varied between 0.3 and 0.8, and b, the ratio of the colored thickness to the total thickness, varied from 0.1 to 0.5. The z dimension of the samples (Fig. 3, EHED) was usually about 1.5 centimeters.

The samples were single crystals purchased from the Harshaw Chemical Company. 50-kev x-rays from a molybdenum target were used for x-ray coloration. In some cases a thin NaCl crystal was placed between the x-ray tube and the sample to be colored to filter out soft x-rays and achieve more uniform coloration. X-irradiation was done at room temperature, and the samples were usually x-rayed on both sides.

To color samples additively they were heated with a fraction of a cubic centimeter of sodium in a copper bomb for up to three hours at 675°C or below. Shorter times and lower temperatures were used for KBr, KCl, and KI. The copper bomb was simply a short length of 1-inch i.d. copper tubing with two wrought copper solder fitting caps slid onto each end without soldering. These caps fit the tubing snugly enough to retard the escape of the sodium vapor for several hours.

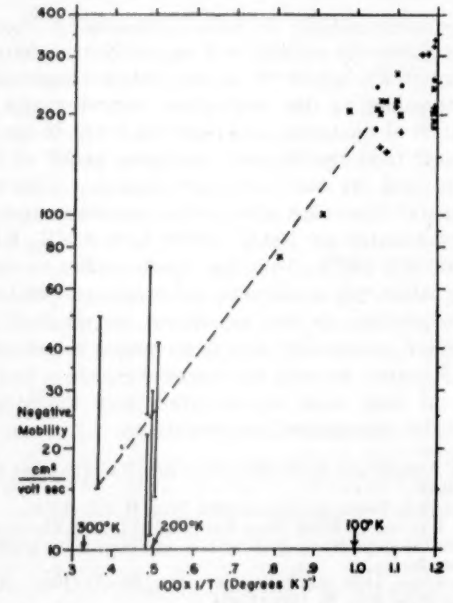

FIG. 1. Summary of mobility data on NaCl. Dots denote 10 percent probable accuracy in the mobility measurement, +'s denote 15 percent, and ×'s denote 20 percent.

After cooling slowly in the oven for several hours the bomb was forced open and the crystal was removed. The outer surfaces of the crystal were then cleaved off. KCl, KBr, and KI crystals produced in this way were deeply colored and ready for use, but in NaCl all the excess sodium was found to coagulate during cooling, imparting to the crystal a blue color for transmitted light and red for scattered light. By reheating the sample to above 500°C, where the F centers reformed, and dropping the crystal while hot into liquid air, it was possible to avoid the formation of these colloidal particles. The crystal then had the straw yellow color characteristic of F centers. Usually such a crystal contained several cracks due to thermal strains in cooling.

It was desired to anneal the samples used, because it was thought that dislocations and other imperfections in an unannealed crystal might decrease the mobility. As indicated in the last paragraph, however, colloidal particles will form if annealing is attempted. In KCl, KBr, and KI it was nevertheless possible to cool in a few hours without forming appreciable colloids. It was eventually found that this could also be done with NaCl, provided the F-center density was very small. The previously colored crystal was placed on a piece of platinum foil in an oven and kept for several hours above 600°C until almost all the coloration disappeared. The platinum made the amount of coloration visible when a flashlight was shone on the sample. The NaCl crystal was then cooled in a few hours and had a barely noticeable yellow tinge. It was found that such crystals apparently showed less tendency to form F' centers and more complex centers than NaCl crystals which were strongly colored and violently quenched.

It was not possible to make measurements on x-rayed KCl, KBr, and KI, because these crystals bleached too easily. The same was true of well-annealed x-rayed NaCl.

The data for a number of samples of NaCl is summarized in Fig. 1. To avoid confusion, the estimated maximum experimental error in mobility is indicated by the type of point used in the graph. The maximum temperature error is estimated at $\pm 2°$ for most of the points. For some of the points near 100°K the error may be as large as $\pm 4°$. The data was taken with light from the tungsten lamp filtered with a blue filter to give high intensity mainly between 4000 and 5000A. The polarity of the Hall effect was electronic in every case. Since the light used contained little energy in the V bands, it is unlikely that holes contributed to the photoconductivity.

The maximum errors for these mobility measurements were estimated from the reproducibility of the setting of V_T. The percentage errors are relatively large compared to diamond because μ_H is smaller and because higher light intensity is required because of the relatively low photoconductive sensitivity of colored alkali halides. Whereas in diamond the spurious signal due to illumination mentioned in EHED was almost negligible,

in the alkali halides it was probably the main source of error. This form of noise was more serious when the Nesa resistance plate was used, than in the lead glass plate, because of photoconductivity in the former. The spurious signal was apparently proportional to the incident light intensity, regardless of wavelength, and could be reduced relative to the desired signal by confining the light used more nearly to the center of the F band. Various procedures were used to try to separate the photoconductive signal from the spurious signals, with only partial success.

As can be seen from Fig. 1, the discrepancies between different points are in many cases larger than expected from the estimates of error based on reproducibility, even though these estimates were quite liberal. Probably the spurious signal due to light gave a larger error than was estimated, although some of the trouble might be in temperature control.

The Hall voltage was proportional to the magnetic field and the electric field, within error. This does not mean much because the error was so large. Usually the proper setting of V_T was determined for $H=0$ and $H=10\,000$ gauss. These three settings plotted as a function of H always fell on a straight line, within experimental error. The accuracy did not warrant making measurements for other values of H.

There appeared to be no clear-cut difference between the mobility in additively colored and x-rayed crystals. The mobility apparently did not depend on the degree of coloration. On the other hand, the mobility was reduced to about 150 cm²/volt sec at 84°K in two samples which had been violently quenched in liquid air as described above. However, a third crystal thus quenched showed no reduction in mobility. Apparently, slight differences in the fast quenching procedure could make a lot of difference in the mobility data. No difference in mobility was observed between crystals cooled in a few minutes and crystals cooled in a few hours, so it is assumed that further annealing would not have affected the measurement. The effect of impurities is unknown, because all the samples used came from the same source. It is unlikely that they are important, because the thermal scattering of the electrons is so strong.

$\bar{E}_z/E_0$ was determined from Eq. (5), EHED. No attempt was made to correct for the finite dimension of the sample. This is probably permissible as long as the z dimension is large compared to the thickness of the colored part of the crystal. No correction was made for the absorption of light by the sample. This correction would be only a few percent im most cases and cannot account for the scatter of the data.

Only a few measurements were made on the additively colored potassium halides. In KCl two measurements on one sample indicate a mobility of 100 ± 50 cm²/volt sec at 90 ± 10°K. In KBr three measurements on one sample indicate a mobility of 110 ± 20 cm²/volt sec at 84 ± 2°K. In KI, three measurements on two samples indicate a mobility of 155 ± 30 cm²/volt sec at 84 ± 2°K; a single measurement indicates a mobility of 30 ± 15 at 200°K.

TABLE I. Effective mass ratios obtained from the mobility data using the theory of Low and Pines.[a] m is the free electron mass, m^* is the effective mass in an unpolarizable crystal, and m_p is the effective mass of the polaron (electron plus associated lattice polarization).

	NaCl	KCl	KBr	KI
μ cm²/volt sec	250	100	110	155
T°K	84	90	84	84
m^*/m	0.55	0.6	0.35	0.35
m_p/m	0.8	0.9	0.71	0.5

[a] See reference 8.

C. DISCUSSION

In view of the large scatter in these data, extreme caution should be used in their interpretation. Little can be said about the temperature dependence of the mobility, except that it behaves qualitatively as expected. The NaCl data are barely consistent with an $\exp(\Theta/T)$ dependence with $\Theta=370$°K, the value deduced from optical absorption in the infrared (dotted line in Fig. 1). The data fit a lower Debye temperature better. The two measurements on KI are consistent with $\Theta=187$°K as predicted, and the one measurement on KBr combined with the room temperature measurement of MacDonald and Robinson ($\mu=12.4$) is consistent with a Debye temperature of 230°K as predicted. This agreement is probably fortuitous and should *not* be regarded as a confirmation of theory; the data are not good enough.

If we assume that the Debye temperature decuced from optical and dielectric constant measurements are correct, these values of mobility can be combined with the theory of Low and Pines[8] to give values of the polaron effective mass and the electron effective mass in the absence of polarization. The results of this calculation for the crystals studied are summarized in Table I, together with the assumed mobilities.

The values of the effective masses obtained in this way are reasonable, but unfortunately there are no independent experimental or theroetical values of these quantities for comparison.

The mobility data can be used to determine approximately the probability and cross section for the capture of electrons by F centers to form F' centers. To do this we use the data of Glaser and Lehfeldt,[12] who measured the charge released for a given amount of light absorbed in a colored crystal of known F-center concentration. Doing this gives the product $\eta\mu\tau$, where η is the probability that an electron excited by a light quantum to an upper level of an F center will be excited thermally to the conduction band, and τ is the mean lifetime of the

[12] G. Glaser and W. Lehfeldt, Nachr. Akad. Wiss. Göttingen, Math.-physik. Kl. (N.F.) Phys. 2, 91 (1936); see, however, H. Rogener, Nachr. Akad. Wiss. Göttingen 3, 219 (1941).

TABLE II. Mean free time and capture probability for an electron by an F center, deduced from the mobility data and the quantum yield data of Glaser and Lehfeldt.[a]

	NaCl	KCl	KBr
$T°K$	200	200	150
μ cm²/volt sec	25	15	15
$\eta\mu\tau$ cm²/volt	5×10^{-8}	10^{-8}	7×10^{-8}
N cm^{-3}	10^{16}	2×10^{17}	1.6×10^{16}
τ sec	2×10^{-9}	7×10^{-10}	5×10^{-9}
$(N\tau)^{-1}$	5×10^{-6}	7×10^{-9}	1×10^{-8}
σ cm²	5×10^{-15}	7×10^{-16}	10^{-15}

[a] See reference 12.

electrons against trapping by an F center. In a certain temperature range, η is almost certainly unity, and the electrons are captured almost entirely by F centers to form F' centers. Then the capture probability in cm²/F-center sec is given by $1/N\tau\cong\mu/N(\eta\mu\tau)$, where N is the number of F centers per cubic centimeter. The capture cross section σ, as usually defined, is the capture probability divided by the thermal velocity of the electrons.

Values of $1/N\tau$ and σ determined in this way are given in Table II. The mobilities assumed are given in the table and are interpolated or extrapolated to a suitable temperature. The thermal velocity is assumed to be $(3kT/m_p)^{\frac{1}{2}}$, the root-mean-square classical value. Not much can be said about variation of the cross section with temperature, although it does not seem to vary strongly, because $\mu\tau$ apparently varies with temperature about the same way μ does. The capture cross section is nearly the same as the area of an F center, as might be expected.

It should be possible to obtain more accurate mobility measurements on the alkali halides by using either the present method or that of MacDonald and Robinson. Measurements at lower temperatures should be interesting, although more difficult because of decreasing photoconductive sensitivity.

The author wishes to thank Professor F. Seitz, Professor D. Pines, and Dr. W. Heller for their encouragement and discussions, and Mr. B. Houston for experimental assistance.

PHYSICAL REVIEW VOLUME 94, NUMBER 3 MAY 1, 1954

Latent Heat of Transition of Superconducting Lead

R. L. DOLECEK
Naval Research Laboratory, Washington, D. C.
(Received November 16, 1953)

Utilizing magnetic heating, calorimetric measurements of the latent heat of transition of superconducting lead were made in the temperature range 2.5°K to 7.0°K. The values obtained demonstrate the inadequacy of the assumption of a parabolic or cubic critical magnetic field for lead, but are consistent with the assumption of a quartic critical field approximation. The latent heat data obtained are used to derive expressions for the normal and superconducting electronic specific heat.

INTRODUCTION

IN the presence of a magnetic field a superconductor exhibits a latent heat of transition between the superconducting and normal states. This latent heat is a direct measure of the entropy change involved and thus affords a sensitive method for determining the electronic entropies in both the normal and superconducting states. Measurements have been performed on the latent heat of transition of superconductors.[1,2] However, the results were not utilized to estimate the electronic entropies. This paper is a report of an experimental measurement of the latent heat of transition of superconducting lead utilizing eddy current heating. The measurements are in accord with previous observations of the entropy difference between the superconducting and normal states,[3] permit evaluation of the electronic specific heats, and with the assumption of a quartic critical magnetic field equation, give a consistent description of the calorimetric and magnetic properties.

EXPERIMENTAL PROCEDURE

Eddy current heating, induced by the abrupt application of a magnetic field, was balanced against the latent heat of transition from the superconducting to the normal state to yield an isothermal magnetization of a superconducting sphere. The magnetic fields were applied as step functions of time, the rise time being of order 0.01 second. Assuming an ideal isothermal magnetization curve for the superconducting sphere, the eddy current heating was calculated for that applied field yielding supression of superconductivity and zero temperature change. As the measurements were conducted under adiabatic conditions, this eddy current energy required for the transition from the superconducting to the normal state with no change in

[1] W. H. Keesom and J. A. Kok, Physica **1**, 595 (1934).
[2] W. H. Keesom and P. H. Van Laer, Physica **4**, 487 (1937).
[3] J. G. Daunt and K. Mendelssohn, Proc. Roy. Soc. (London) **A160**, 127 (1937).

temperature, measures the latent heat of the transition. Assuming that the metal behaves as a perfect conductor during the application of the magnetic field (H), one would expect the sphere to experience a change in magnetic moment per unit volume of $-3H/8\pi$. Subsequent to the change in magnetic field, the magnetic moment should then return to zero in the presence of the applied magnetic field as the superconductivity of the metal is suppressed and the eddy current decays. In Fig. 1 is shown this ideal magnetization curve for a superconducting sphere. Path ABF is the ideal isothermal magnetization path to be used with the Gorter-Casimir cycle in deriving the expression for the latent heat and path ACE is the magnetization path incurred by the abrupt application of a magnetic field to the spherical specimen. The magnetic work done

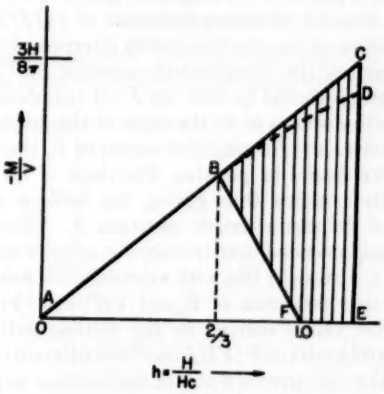

FIG. 1. Ideal magnetization curve of a superconducting sphere illustrating method for computation of eddy current heating. The ideal isothermal magnetization path for the sphere is path ABF; magnetization path for abrupt application of magnetic field is path $ABCE$; actual magnetization path corrected for resistance of specimen and finite rise time of magnetic field is path $ABDE$. Eddy current heating incurred upon magnetization of the super conducting sphere is calculated as the excess magnetic work done on the sphere during the magnetization (area $BDEF$).

on the sphere in excess of that along the isothermal magnetization path is indicated in Fig. 1 by the shaded area $BCEF$. Under the conditions outlined, ΔE, the excess magnetic work done on the specimen, (eddy current heat) would be given by

$$\Delta E = V/16\pi J[3H^2 - 2H_c^2] \text{ cal/mole}, \qquad (1)$$

where H_c is the critical magnetic field for bulk material at the temperature of observation, J is the mechanical equivalent of heat, and V is the atomic volume of the metal.

Experimental conditions of observation do not quite meet the assumption used in deriving Eq. (1) that the electrical time constant of the lead sphere ($\sim$0.5 sec) be very large compared with the rise time of the applied magnetic field ($\sim$0.01 sec). The expressions for the time dependence of currents induced in a conducting sphere upon magnetization by the sudden application of a magnetic field have been derived,[4] and from these the time dependence of the magnetic moment can be obtained. Replacing the ideal straight line BC in Fig. 1 by the function (line DB) obtained assuming the electrical resistance of the specimen during the eddy current decay to be that of the normal metal gives, under the conditions of the experiment, a correction of the order of ten percent. This correction was made in calculating the eddy current heat used in measuring the latent heat of the transition.

A carbon thermometer[5] was employed to measure temperature, the resistance of the thermometer being automatically recorded by a system having a response time of about five seconds. Temperature changes of 0.001°K could be measured, and the estimated accuracy of the latent heat values obtained is about five percent. Indicative of good thermal contact between the thermometer and the sphere was the observation that practically complete equilibrium was reached within fifteen seconds after the application of a magnetic field yielding a temperature change. Figure 2 presents a typical record obtained for the abrupt application of a magnetic field sufficient to suppress superconductivity but with insufficient eddy current heating to balance the latent heat of transition, thus resulting in a slight cooling of the specimen. The slight deflection on field application is the result of magnetic coupling between the field solenoid and the thermometer circuit. However, in preliminary experiments with the thermometer mounted at a position of largest induced current on the sphere, surface heating was observed. Measurements were taken for magnetic fields smaller than and in excess of the value required to balance the latent heat, and the magnetic field required to produce no temper-

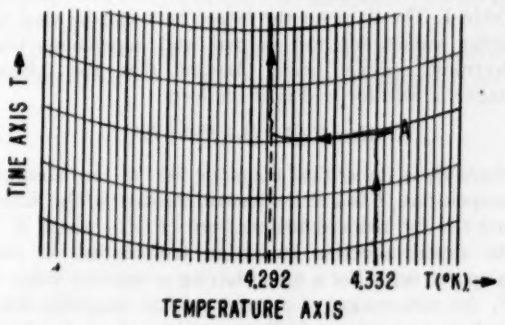

FIG. 2. Typical temperature record obtained on magnetization with a field sufficient to supress superconductivity, but too small to produce enough eddy current heating to balance the latent heat of transition. The magnetic field was turned on at A. Markers on the time axis are at 15 second intervals. Intervals along the temperature axis are only approximately equal as thermometer resistance is recorded. This record is one obtained during trial G of Table I.

[4] W. R. Smythe, *Static and Dynamic Electricity* (McGraw-Hill Book Company, Inc., New York, 1939), Chap. XI.
[5] J. R. Clement and E. H. Quinnell, Rev. Sci. Instr. **23**, 213 (1952).

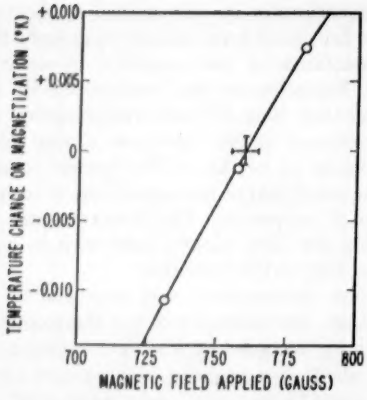

FIG. 3. Graph of temperature change on adiabatic magnetization *versus* magnitude of magnetic field applied. From such a graph was estimated the value of magnetic field required to suppress superconductivity with zero change in temperature. Indicated by the cross having dimensions 0.002°K by 10 gauss, the magnetic field required in this instance is 760 gauss. The data presented are the midrange values obtained on trial F of Table I, the initial temperatures of the observations being 5.302±0.001°K.

ature change was determined graphically. Figure 3 illustrates the graphical method used.

Using a lead sphere of one centimeter radius, observations of the latent heat were made in the temperature range 2.5°K to 7.0°K. With the magnetization method employed, measurements cannot be performed at temperatures lower than about one-third the superconducting transition temperature in zero field without encountering the intermediate state.

EXPERIMENTAL RESULTS

Measurements obtained of the latent heat of the superconducting transition for lead are presented in Table I. The data on the latent heat can be used to derive values for the normal and superconducting electronic specific heats. Assume that the critical magnetic field for lead is of the form

$$H_c = H_0[1-(1+F)t^2+Ft^4], \quad (2)$$

where H_0 is the critical magnetic field at zero absolute temperature, F is a characteristic constant of the metal, and t is the reduced temperature (T/T_c), where T_c is the superconducting transition temperature in zero magnetic field. For a metal having a negative value of F, the assumption of a cubic critical magnetic field[6] leads to expressions yielding negative values of entropy near $t=0$, and therefore is untenable. It will be shown that F is negative for lead; thus the assumption of a quartic critical field approximation is made. The assumption of an "α" model[7] critical magnetic field leads to no inconsistency. However, since the experimental data appear to be in equally good agreement with either model, for simplicity the quartic critical field approximation is used. Employing thermodynamical arguments, the latent heat, Q, should be given by

$$Q/t^2(1-t^2) = VH_0^2/2\pi J(1-Ft^2)(1+F-2Ft^2), \quad (3)$$

where V is the atomic volume of the metal, and J the mechanical equivalent of heat. If then, the latent heat data be employed to construct a plot of the left hand side of Eq. (3) against t^2, F can be estimated from values obtained by extrapolation to the intercepts at $t=0$ and $t=1$. Corresponding to this value of F, the value of t for which the right hand side of Eq. (3) reduces to $VH_0^2/2\pi J$ affords a good method for obtaining the value of $VH_0^2/2\pi J$. Having obtained $VH_0^2/2\pi J$ in this manner, estimates of F and $VH_0^2/2\pi J$ can be refined by comparison of the experimental data with the plot of Eq. (3) obtained for the values estimated.

Figure 4 presents the suggested graph of the experimental data for obtaining estimates of $VH_0^2/2\pi J$ and F. The slope of the graph is readily interpreted in terms of the sign of the characteristic constant F. The slope of the graph should be zero for $F=0$ (parabolic case). For positive values of F, the slope of the graph should be negative, and for negative values of F, the slope of the curve should be positive. The slope of the data is distinctly positive thus giving, for lead, a negative value of the characteristic constant F. Although the graph approaches linearity only for small values of F and/or t, a straight line with extrapolation was used to obtain first estimates of F and $VH^2/2\pi J$. From this graph the values derived by the method outlined are $F=-0.09\pm0.02$ and $(VH_0^2/2\pi J)=0.0460\pm0.0005$ cal/mole. The full curve is a plot of the function as given by the right hand side of Eq. (3) using the derived values of F and $VH_0^2/2\pi J$. The values $F=-0.09$ and $H_0=823$ gauss calculated from $VH_0^2/2\pi J=0.0460$ using $V=17.8$, are in good agreement with the low temperature equilibrium values of the critical field for lead observed by Daunt and Mendelssohn.[3]

From the thermodynamical arguments one obtains for the electronic specific heats:

TABLE I. Latent heat of the superconducting transition of lead.

Trial No.	Temperature of observation (°K)	Magnetic field Required for isothermal magnetization (gauss)	Indicated latent heat (cal/mole)
N	2.50	727	0.00471
A	2.63	730	0.00515
B	3.01	742	0.00627
M	3.30	755	0.00734
C	3.48	760	0.00786
L	3.80	777	0.00924
D	4.00	777	0.00952
G	4.33	788	0.01072
E	4.58	784	0.01092
F	5.30	760	0.01166
H	5.61	754	0.01196
I	6.02	695	0.01071
J	6.56	593	0.00820
K	7.03	367	0.00339

[6] E. Maxwell, Phys. Rev. **86**, 235 (1952).
[7] P. M. Marcus and E. Maxwell, Phys. Rev. **91**, 1035 (1953).

Normal electronic specific heat $=8.0\times10^{-4}T$ cal/mole deg.

Superconducting electronic specific heat $=0.329\times10^{-4}\times T^3(1+0.012T^2+2.1\times10^{-5}T^4)$ cal/mole deg.

These values have been found to be in good agreement with temperature changes resulting from suppression of superconductivity by magnetization.[8]

In Fig. 5 a comparison is made of the latent heats predicted by the quartic equation (solid curve) with $F=-0.09$ and $VH_0^2/2\pi J=0.0460$ cal/mole, and a parabolic equation (dashed curve) using $H_0=812$ gauss. Plotted in Fig. 5 are the latent heat measurements obtained in these experiments and values derived from entropy measurements of Daunt and Mendelssohn[3] obtained from critical magnetic field observations. The experimental data favor the derived quartic critical magnetic field.

CONCLUSIONS

Utilizing magnetic heating, calorimetric measurements of the latent heat of transition of superconducting lead were obtained in the temperature range 2.5°K to 7.0°K. The results are in good agreement with data obtained from critical magnetic field observations. The values obtained demonstrate the inadequacy of the assumption of a parabolic or cubic critical magnetic field for lead, but are consistent with the assumption of a quartic critical field approximation. Values were derived for the normal and electronic specific heats. The electronic specific heat functions derived are in good accord with observations on temperature changes resulting from suppression of superconductivity by magnetization.[8]

I am indebted to J. J. Madden for aid in the assembly and manipulation of the experimental equipment used.

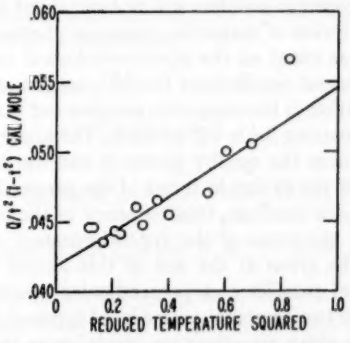

FIG. 4. Graph of the function $Q/t^2(1-t^2)$ *versus* t^2. The circled points are experimental data. The full curve is a plot of the function predicted by Eq. (3) using the values $F=-0.09$ and $VH_0^2/2\pi J=0.0460$ cal/mole.

[8] R. L. Dolecek, Phys. Rev. **91**, 490 (1953).

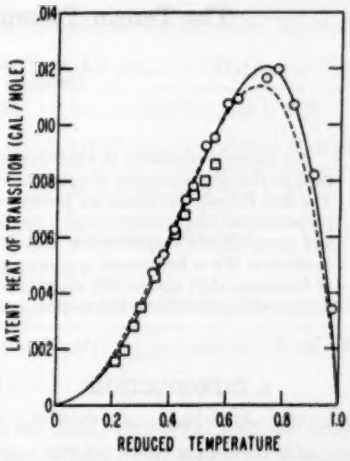

FIG. 5. Latent heat of transition of super conducting lead as a function of reduced temperature. The curves are the functions predicted by thermodynamics for two types of critical magnetic field equations. (1) A parabola using $H_0=812$ gauss, $T_c=7.22$°K (dashed curve). (2) A quartic using $F=-0.09$ and $VH_0^2/2\pi J=0.0460$ cal/mole (solid curve). The circles are values obtained in this experiment and the squares are values derived from entropy measurements of Daunt and Mendelssohn (reference 3) obtained from critical magnetic field measurements.

PHYSICAL REVIEW VOLUME 94, NUMBER 3 MAY 1, 1954

The Tensor Formulation of Ferromagnetic Resonance

J. A. YOUNG, JR.,* AND EDWIN A. UEHLING
University of Washington, Seattle, Washington
(Received December 7, 1953)

The tensor formulation of electromagnetic wave propagation in a conducting ferromagnetic medium is used to describe resonance phenomena in a test cavity under two different conditions of magnetization. The new formulation alters the prediction with respect to the shape of the resonance curve in the case of perpendicular magnetization and it predicts a different ratio of energy absorptions in the cases of parallel and perpendicular magnetization than is given by a formulation based on the concept of a permeability coefficient. When interpreted according to the new formulation the results of simultaneous measurements of frequency shift and energy absorption under different conditions of magnetization are found to be consistent with each other. Such consistency is not achieved on the basis of earlier formulations.

I. INTRODUCTION

IT has been reported previously[1] that the theory of ferromagnetic resonance based on the concept of a complex permeability coefficient is unable to explain the experimental data under all conditions of magnetization. Using a reflection type cavity with a ferromagnetic metal as one wall of that cavity we obtained results for the absorption, frequency shift, and the shape of resonance curves under two conditions of magnetization; namely, (a) the applied constant magnetic field is parallel to the surface of the ferromagnetic sample; and, (b) it is perpendicular to that surface. These conditions are frequently called the conditions of parallel and perpendicular magnetization, respectively, and we will use this terminology here. The important discrepancies observed were in the shape of the resonance curves for the case of perpendicular magnetization and in the ratio of absorptions in the two cases of parallel and perpendicular magnetization.

These discrepancies were to a large extent resolved by employing the concept of a permeability tensor first introduced by Polder.[2] A consistent application of this concept shows that only in the case of parallel magnetization is the concept of a permeability coefficient equivalent to that of a tensor. In all other cases the usual theory employing the permeability coefficient gives incorrect results.

At first sight these conclusions may appear somewhat surprising in view of the fact that Polder demonstrated the equivalence of the two formulations for the nonmetals insofar as the relation between fields and magnetization is concerned. The conditions for equivalence are that the sample dimensions be small compared with the wavelength and that the displacement currents be negligible, both of which are fulfilled in our experiments. We will again demonstrate this equivalence, but we will also show that in the parallel resonance case it is a consequence of a definite relation between the longitudinal and transverse components of the magnetic field in that part of the wave which is polarized perpendicular to the constant field, whereas, in the case of perpendicular magnetization, there is in general no such relation between magnetic field components because the two waves of opposite directions of circular polarization are essentially independent.

The theoretical problem will be formulated in Sec. II. The description of magnetic resonance phenomena will be based as usual on the phenomenological equations, and the usual restrictions to the case of saturation magnetization in ferromagnetic samples and vanishingly small alternating fields will be made. The final equations which express the quality factor Q and the frequency shift $\Delta\omega$ of the cavity in terms of the properties of the ferromagnetic medium, the frequency of the oscillating fields and the value of the applied constant magnetic field will be given at the end of this section for both the case of parallel and perpendicular magnetization and for the two commonly considered types of damping. In writing these equations we specialize to the case of metals. It is a simple matter to rewrite them for the case of semiconducting ferromagnetic media.

The remainder of the paper is devoted to a discussion of the experimental conditions under which our data on a few carefully chosen samples of nickel and supermalloy were obtained, and to a comparison of the results obtained with the theoretical predictions. The experimental conditions and the methods which we used to relate theory and experiment are described in Sec. III. Finally, in Sec. IV we discuss the experimental results. Using the theoretical formulation given in Sec. II we find that the case of perpendicular resonance is as adequately described by the theory as is the case of parallel resonance. Consequently, we have some confidence in the validity of comparisons of the results obtained under these two different experimental conditions. The principal conclusion which we are able to draw from this comparison is that the Landau-Lifshitz type of damping is not nearly as satisfactory as the Bloch type. Both of course lead to an essentially Lorentz type of resonance curve, but the Landau-Lifshitz damping introduces terms into the permeability tensor compo-

* Now at the Bell Telephone Laboratories, Holmdel, New Jersey.

[1] J. A. Young, Jr., and Edwin A. Uehling, Phys. Rev. **90**, 990 (1953).

[2] D. Polder, Phil. Mag. **40**, 99 (1949).

nents which have no Bloch counterpart and which on *a priori* grounds appear to be physically meaningless. Consequently, it is satisfying to find the data leading to the conclusion which we obtain. The conclusion appears to be unambiguous, but one would like to have an additional test at another frequency than the one of 9000 Mc/sec which we used.

Small discrepancies between theory and experiment still remain. We believe that these discrepancies lie outside of our experimental errors. These discrepancies are discussed briefly.

II. THE RESONANCE EQUATIONS

We will analyze the problem of absorption in a rectangular cavity in which one wall of the cavity consists of the ferromagnetic material under test. According to the methods first introduced by Polder[2] and subsequently applied to particular cases by Hogan[3] and Weiss and Fox[4] we begin the analysis by consideration of the propagation properties in a ferromagnetic medium of infinite extent. Magnetic phenomena in such a medium may be described by the well-known phenomenological equations[5]:

$$\dot{M}_{x,y}=\gamma[\mathbf{M}\times\mathbf{H}]_{x,y}-M_{x,y}/T_2, \tag{1}$$

for Bloch (B-type) damping, and

$$\begin{aligned}\dot{M}_{x,y}&=\gamma[\mathbf{M}\times\mathbf{H}]_{x,y}-\frac{\alpha\gamma}{|M|}[\mathbf{M}\times[\mathbf{M}\times\mathbf{H}]]_{x,y}\\&\cong\gamma[\mathbf{M}\times\mathbf{H}]_{x,y}-\alpha\gamma(H_zM_{x,y}-M_0H_{x,y}),\end{aligned} \tag{2}$$

for Landau-Lifshitz (LL-type) damping, where we have already used the fact that the applied constant magnetic field is to be taken in the z direction and that this field is sufficiently strong to produce a saturation magnetization M_0. Also, $\gamma=ge/2mc$ is the gyromagnetic ratio of the electrons which provide the magnetization, T_2 is the transverse relaxation time of Bloch, α is the damping parameter of Landau-Lifshitz, $\mathbf{M}$ is the magnetization vector, and $\mathbf{H}$ is the applied field. We now denote the constant magnetic field in the z direction by H_0. In addition we apply an oscillating magnetic field in the xy plane of components h_x and h_y of frequency ω. Then we solve (1) and (2) after introducing:

$$\begin{aligned}&H_x=h_xe^{j\omega t}, &&M_x=m_xe^{j\omega t},\\&H_y=h_ye^{j\omega t}, &&M_y=m_ye^{j\omega t},\\&H_z=H_0-N_zM_0,\end{aligned}$$

where N_z is a demagnetization factor which we must use in connection with the applied constant field. No other demagnetizing factors are used. We then obtain:

$$m_x=\frac{\gamma^2M_0(H_0-N_zM_0)h_x-\gamma M_0(j\omega+1/T_2)h_y}{\gamma^2(H_0-N_zM_0)^2+(j\omega+1/T_2)^2}, \tag{3a}$$

$$m_y=\frac{\gamma M_0(j\omega+1/T_2)h_x+\gamma^2M_0(H_0-N_zM_0)h_y}{\gamma^2(H_0-N_zM_0)^2+(j\omega+1/T_2)^2} \tag{3b}$$

for the case of B-type damping, and

$$m_x=\frac{\gamma M_0\{\gamma(H_0-N_zM_0)+\alpha[j\omega+\alpha\gamma(H_0-N_zM_0)]\}h_x-j\omega\gamma M_0h_y}{\gamma^2(H_0-N_zM_0)^2+[j\omega+\alpha\gamma(H_0-N_zM_0)]^2}, \tag{4a}$$

$$m_y=\frac{\gamma M_0\{\gamma(H_0-N_zM_0)+\alpha[j\omega+\alpha\gamma(H_0-N_zM_0)]\}h_y+j\omega\gamma M_0h_x}{\gamma^2(H_0-N_zM_0)^2+[j\omega+\alpha\gamma(H_0-N_zM_0)]^2}, \tag{4b}$$

for the case of LL-type damping.

The magnetic induction is

$$\mathbf{B}=\mathbf{b}e^{j\omega t},$$

where

$$\mathbf{b}=\mathbf{h}+4\pi\mathbf{m}.$$

Thus, we find Eqs. (3) and (4) are consistent with the relations:

$$b_x=\mu h_x-jKh_y, \quad b_y=jKh_x+\mu h_y, \quad b_z=h_z, \tag{5}$$

in which

$$\mu=1+\frac{4\pi\gamma^2M_0(H_0-N_zM_0)}{\gamma^2(H_0-N_zM_0)^2+[j\omega+(1/T_2)]^2}, \tag{6a}$$

$$K=-j\frac{4\pi\gamma M_0[j\omega+(1/T_2)]}{\gamma^2(H_0-N_zM_0)^2+[j\omega+(1/T_2)]^2}, \tag{6b}$$

for B-type damping, and

$$\mu=1+\frac{4\pi\gamma M_0\{\gamma(H_0-N_zM_0)+\alpha[j\omega+\alpha\gamma(H_0-N_zM_0)]\}}{\gamma^2(H_0-N_zM_0)^2+[j\omega+\alpha\gamma(H_0-N_zM_0)]^2}, \tag{7a}$$

$$K=\frac{4\pi\gamma\omega M_0}{\gamma^2(H_0-N_zM_0)^2+[j\omega+\alpha\gamma(H_0-N_zM_0)]^2}, \tag{7b}$$

for LL-type damping.

Our next step is to obtain plane wave solutions of the Maxwell equations:

$$\nabla\times\mathbf{e}=-(1/c)\dot{\mathbf{b}}, \quad \nabla\times\mathbf{h}=(4\pi\sigma/c)\mathbf{e}+(1/c)\dot{\mathbf{d}}, \tag{8}$$

which are of the form:

$$\begin{aligned}&\mathbf{b}=\mathbf{b}_0\exp[j\omega t-P(\mathbf{n}\cdot\mathbf{r})],\\&\mathbf{h}=\mathbf{h}_0\exp[j\omega t-P(\mathbf{n}\cdot\mathbf{r})],\\&\mathbf{e}=\mathbf{e}_0\exp[j\omega t-P(\mathbf{n}\cdot\mathbf{r})],\\&\mathbf{d}=\epsilon\mathbf{e}.\end{aligned} \tag{9}$$

[2] C. L. Hogan, Bell System Tech. J. **31**, 1 (1952).
[3] M. T. Weiss and A. G. Fox, Phys. Rev. **88**, 146 (1952).
[4] C. Kittel, Phys. Rev. **73**, 155 (1948); N. Bloembergen, Phys. Rev. **78**, 572 (1950) for applications using Bloch type damping; Yager, Galt, Merritt, and Wood, Phys. Rev. **80**, 744 (1950) for applications using Landau-Lifshitz type damping.

The substitution of Eqs. (9) into (8) leads to:

$$P[\mathbf{e}_0\times\mathbf{n}]=-j\omega\mathbf{b}_0/c, \quad P[\mathbf{h}_0\times\mathbf{n}]=(4\pi\sigma+j\omega\epsilon)\mathbf{e}_0/c.$$

We obtain a relation between $\mathbf{b}_0$ and $\mathbf{h}_0$ by eliminating $\mathbf{e}_0$ from these equations. Thus, we write the following equations connecting both $\mathbf{b}_0$ and $\mathbf{e}_0$ with $\mathbf{h}_0$

$$\lambda\mathbf{b}_0=P^2[\mathbf{n}(\mathbf{n}\cdot\mathbf{h}_0)-\mathbf{h}_0], \tag{10a}$$

$$\lambda c\mathbf{e}_0=-j\omega P[\mathbf{h}_0\times\mathbf{n}], \tag{10b}$$

where

$$\lambda=-j\omega(4\pi\sigma+j\omega\epsilon)/c^2. \tag{10c}$$

We now consider separately the two cases of propagation perpendicular to and parallel to the constant applied field H_0. From now on we drop the subscripts on $\mathbf{b}$, $\mathbf{h}$, and $\mathbf{e}$ since we will be working only with amplitudes.

(a) Propagation Perpendicular to H_0

We will take the direction of propagation as the y direction. Then,

$$n_x=n_z=0; \quad n_y=1.$$

We also use Eqs. (5). Thus, we find that Eqs. (10) have two independent solutions; namely,

$$\begin{aligned} &P^2=-\lambda,\\ &e_y=e_z=h_x=h_y=0,\\ &h_z\neq 0 \quad , \quad e_x/h_z=j\omega P/\lambda c; \end{aligned} \tag{11}$$

and

$$\begin{aligned} &P^2=-\lambda(\mu^2-K^2)/\mu,\\ &e_x=e_y=h_z=0,\\ &h_y/h_x=-jK/\mu \quad , \quad e_x/h_z=-j\omega P/\lambda c. \end{aligned} \tag{12}$$

The first case corresponds to propagation in a nonmagnetic medium. In the second case, the magnetic properties of the medium are contained in μ and K which are given by either Eqs. (6) or Eqs. (7).

(b) Propagation Parallel to H_0

Then $n_x=n_y=0$, $n_z=1$. Again using Eqs. (5) we find that Eqs. (10) have the two independent solutions:

$$\begin{aligned} &P^2=-\lambda(\mu\pm K),\\ &h_z=e_z=0,\\ &h_x/h_y=-e_y/e_x=\mp j,\\ &e_y/h_x=-e_x/h_y=j\omega P/\lambda c, \end{aligned} \tag{13}$$

where the upper and lower signs correspond to the two directions of circular polarization, each with its own propagation constant, and where the magnetic properties of the medium are again contained in μ and K given by Eqs. (6) or (7).

We will now calculate the absorption and frequency shift in a cavity in which one wall consists of a ferromagnetic metal. Thus, we specialize the equations given above to the case of $\omega\epsilon/4\pi\sigma\ll 1$ and consequently $\lambda=-4\pi j\omega\sigma/c^2$. The expressions for the quality factor Q and the frequency shift $\Delta\omega$ are conveniently determined from the equation[6]:

$$\frac{1}{Q}-2j\frac{\Delta\omega}{\omega}=\frac{c}{\omega}\frac{\int(\mathbf{n}\times\mathbf{e})\cdot\mathbf{h}_k dS}{\int\mathbf{h}\cdot\mathbf{h}_k dV}, \tag{14}$$

where $\mathbf{e}_k$ and $\mathbf{h}_k$ are the normalized unperturbed electric and magnetic fields within the cavity for the mode k in which the cavity is considered to be oscillating, $\int dS$ is the integral over the bounding surfaces of the cavity, and $\int dV$ is the integral over the cavity volume. The equation of reference 6 from which (14) is taken has been specialized here to the case of a cavity all of whose walls are conducting, and we have used in addition the relation:

$$\int\mathbf{e}\cdot\mathbf{e}_k dV=-j\int\mathbf{h}\cdot\mathbf{h}_k dV.$$

The equation is expressed in Gaussian units to agree with our other equations.

We will evaluate the integrals in Eq. (14) for each of the two cases of parallel and perpendicular magnetization.

(1) *Parallel Magnetization*

The xz plane lies in the surface of the ferromagnetic specimen with the constant magnetic field H_0 directed along the z axis. The direction of propagation is along the y axis which is normal to the surface and directed outward from the cavity. The magnetic vector $\mathbf{h}$ is linearly polarized and the direction of polarization makes an angle θ with H_0. Then from Eqs. (11) and (12) we have:

$$\begin{aligned} &P=P_0=(-\lambda)^{\frac{1}{2}}=(1+j)(2\pi\omega\sigma)^{\frac{1}{2}}/c,\\ &e_x=j\omega P_0 h_z/\lambda c=-cP_0 h\cos\theta/4\pi\sigma, \end{aligned} \tag{15}$$

for the component of $\mathbf{h}$ along the z axis, and

$$\begin{aligned} &P=(-\lambda(\mu^2-K^2)/\mu)^{\frac{1}{2}}=(1+j)(2\pi\omega\sigma)^{\frac{1}{2}}((\mu^2-K^2)/\mu)^{\frac{1}{2}}/c,\\ &e_z=-j\omega P h_x/\lambda c=cPh\sin\theta/4\pi\sigma, \end{aligned} \tag{16}$$

for the component of $\mathbf{h}$ along the x axis. Since $\mathbf{n}=\mathbf{j}$,

$$[\mathbf{n}\times\mathbf{e}]=ch(\mathbf{i}P\sin\theta+\mathbf{k}P_0\cos\theta)/4\pi\sigma.$$

We regard the unperturbed cavity oscillation as taking

[6] J. C. Slater, Revs. Modern Phys. 18, 441 (1946), especially Eq. III.53, p. 475.

place in a single mode k. Then

$$\mathbf{h}=\mathbf{h}_k\int\mathbf{h}\cdot\mathbf{h}_k dV,$$

$$[\mathbf{n}\times\mathbf{e}]\cdot\mathbf{h}_k=\frac{c}{4\pi\sigma}hh_k(P\sin^2\theta+P_0\cos^2\theta)$$

$$=\frac{c}{4\pi\sigma}h_k^2(P\sin^2\theta+P_0\cos^2\theta)\int\mathbf{h}\cdot\mathbf{h}_k dV,$$

$$\int[\mathbf{n}\times\mathbf{e}]\cdot\mathbf{h}_k dS\Big/\int\mathbf{h}\cdot\mathbf{h}_k dV$$

$$=\frac{c}{4\pi\sigma}(P\sin^2\theta+P_0\cos^2\theta)\int h_k^2 dS.$$

Then for parallel magnetization:

$$\frac{1}{Q}-2j\frac{\Delta\omega}{\omega}=\frac{c^2}{4\pi\omega\sigma}(P\sin^2\theta+P_0\cos^2\theta)\int h_k^2 dS.$$

We define $1/Q_0$ as the real part of the right member of this equation when $\mu=1$ and $K=0$. Then,

$$\frac{1}{Q}-2j\frac{\Delta\omega}{\omega}=\frac{1}{Q_0}\frac{c}{(2\pi\omega\sigma)^{\frac{1}{2}}}(P\sin^2\theta+P_0\cos^2\theta). \quad (17)$$

(2) *Perpendicular Magnetization*

The z axis is now normal to the surface of the ferromagnetic specimen and is directed outward from the cavity. It is both the direction of H_0 and the direction of wave propagation. Take the x axis as the axis of the linearly polarized unperturbed magnetic vector $\mathbf{h}$ at the surface of the cavity. The wave propagates into the medium as two independent waves of $+$ and $-$ directions of circular polarizations. From Eqs. (13) and the condition of linear polarization at the surface,

$$\begin{aligned}
&h_x=h_x^{+}+h_x^{-}, \quad \text{where} \quad h_x^{+}=h_x^{-};\\
&h_y=h_y^{+}+h_y^{-}=jh_x^{+}-jh_x^{-}=0,\\
&e_x=e_x^{+}+e_x^{-}=\omega(P^{+}-P^{-})h_z/2\lambda c,\\
&e_y=e_y^{+}+e_y^{-}=j\omega(P^{+}+P^{-})h_z/2\lambda c,\\
&P^{+}=(-\lambda(\mu+K))^{\frac{1}{2}},\\
&P^{-}=(-\lambda(\mu-K))^{\frac{1}{2}}, \quad \text{where} \quad \lambda=-4\pi j\omega\sigma/c^2.
\end{aligned} \quad (18)$$

Since $\mathbf{n}=\mathbf{k}$ and $\mathbf{h}=\mathbf{h}_k\int\mathbf{h}\cdot\mathbf{h}_k dV$, where $\mathbf{h}=\mathbf{i}h_x=\mathbf{i}h$, we have:

$$[\mathbf{n}\times\mathbf{e}]\cdot\mathbf{h}_k=-\frac{j\omega h_k^2}{2\lambda c}(P^{+}+P^{-})\int\mathbf{h}\cdot\mathbf{h}_k dV,$$

$$\int[\mathbf{n}\times\mathbf{e}]\cdot\mathbf{h}_k dS\Big/\int\mathbf{h}\cdot\mathbf{h}_k dV=-\frac{j\omega}{2\lambda c}(P^{+}+P^{-})\int h_k^2 dS$$

$$=\frac{c}{8\pi\sigma}(P^{+}+P^{-})\int h_k^2 dS.$$

Thus for perpendicular magnetization:

$$\frac{1}{Q}-2j\frac{\Delta\omega}{\omega}=\frac{c^2}{8\pi\omega\sigma}(P^{+}+P^{-})\int h_k^2 dS.$$

Defining Q_0 as before, we obtain:

$$\frac{1}{Q}-2j\frac{\Delta\omega}{\omega}=\frac{1}{Q_0}\frac{c}{(8\pi\omega\sigma)^{\frac{1}{2}}}(P^{+}+P^{-}). \quad (19)$$

We will now evaluate the propagation constants using the previously derived expressions for μ and K. Again we consider separately the two cases of parallel and perpendicular magnetization.

(3) *Parallel Magnetization*

Using Eqs. (6a), (6b), (7a), and (7b) with N_z set equal to zero we obtain:

$$\mu^2-K^2/\mu=\mu_1-j\mu_2, \quad (20)$$

where

$$\mu_1=1+\frac{4\pi\gamma^2M_0(H_0+4\pi M_0)(\omega_0^2-\omega^2)}{(\omega_0^2-\omega^2)^2+4\omega^2/T_2^2}, \quad (21a)$$

$$\mu_2=\frac{4\pi\gamma^2M_0(H_0+4\pi M_0)}{(\omega_0^2-\omega^2)^2+4\omega^2/T_2^2}\frac{2\omega}{T_2}, \quad (21b)$$

$$\omega_0^2=\gamma^2H_0(H_0+4\pi M_0)+1/T_2^2, \quad (21c)$$

for the case of B-type damping; and

$$\mu_1=1+4\pi\gamma^2M_0\frac{(H_0+4\pi M_0)(1+\alpha^2)(\omega_0^2-\omega^2)+\alpha^2\omega^2(2H_0+4\pi M_0)}{(\omega_0^2-\omega^2)^2+\omega^2\alpha^2\gamma^2(2H_0+4\pi M_0)^2}, \quad (22a)$$

$$\mu_2=4\pi\gamma M_0\alpha\omega\frac{\gamma^2(H_0+4\pi M_0)^2(1+\alpha^2)+\omega^2}{(\omega_0^2-\omega^2)^2+\omega^2\alpha^2\gamma^2(2H_0+4\pi M_0)^2}, \quad (22b)$$

$$\omega_0^2=\gamma^2H_0(H_0+4\pi M_0)(1+\alpha^2), \quad (22c)$$

for the case of LL-type damping. These results for μ_1 and μ_2 are identical with the expressions for the real and imaginary parts of the complex permeability coefficient which have been previously derived from the point of view of demagnetizing factors.[7]

Combining Eqs. (16) and (20), we have:

$$P^2=4\pi j\omega\sigma(\mu_1-j\mu_2)/c^2. \quad (23)$$

If we set $P=P_1+jP_2$, we obtain:

$$P_1=(2\pi\omega\sigma\mu_R)^{\frac{1}{2}}/c, \quad P_2(\pm)(2\pi\omega\sigma\mu_L)^{\frac{1}{2}}/c, \quad (24)$$

where

$$\mu_R=(\mu_1^2+\mu_2^2)^{\frac{1}{2}}+\mu_2, \quad \mu_L=(\mu_1^2+\mu_2^2)^{\frac{1}{2}}-\mu_2. \quad (25)$$

[7] See for example Eqs. (10) and (11) of reference 11 and Eqs. (A-2) and (A-3) in the paper of Yager *et al.* of reference 5, which are the same as our Eqs. (21a and b) and (22a and b) if in the former $N_x=N_z=0$ and $N_y=4\pi$ corresponding to the case of parallel magnetization.

We will use $(\pm)$ inclosed in parentheses to signify that the positive or negative value is to be taken according to whether the real quantity μ_1 is positive or negative. P_0 is obtained by setting $\mu_1=1$ and $\mu_2=0$. Substitution into Eq. (17) then gives us the final results for the parallel resonant case:

$$\frac{1}{Q}=\frac{1}{Q_0}[(\mu_R)^{\frac{1}{2}}\sin^2\theta+\cos^2\theta], \tag{26a}$$

$$-\frac{2\Delta\omega}{\omega}=\frac{1}{Q_0}[(\pm)(\mu_L)^{\frac{1}{2}}\sin^2\theta+\cos^2\theta]. \tag{26b}$$

(4) Perpendicular Magnetization

Using Eqs. (6a), (6b), (7a), and (7b) with N_z set equal to 4π, we obtain

$$\mu\pm K=\mu_1{}^{\pm}-j\mu_2{}^{\pm}, \tag{27}$$

where

$$\mu_1{}^{\pm}=1+\frac{4\pi\gamma M_0(\omega_0\mp\omega)}{(\omega_0\mp\omega)^2+1/T_2{}^2}, \tag{28a}$$

$$\mu_2{}^{\pm}=\pm\frac{4\pi\gamma M_0/T_2}{(\omega_0\mp\omega)^2+1/T_2{}^2}, \tag{28b}$$

$$\omega_0=\gamma(H_0-4\pi M_0), \tag{28c}$$

for the case of B-type damping; and

$$\mu_1{}^{\pm}=1+\frac{4\pi\gamma M_0(\omega_0\mp\omega+\alpha^2\omega_0)}{(\omega_0\mp\omega)^2+\alpha^2\omega_0{}^2}, \tag{29a}$$

$$\mu_2{}^{\pm}=\frac{4\pi\gamma M_0\alpha\omega}{(\omega_0\mp\omega)^2+\alpha^2\omega_0{}^2}, \tag{29b}$$

$$\omega_0=\gamma(H_0-4\pi M_0), \tag{29c}$$

for LL-type damping. In contrast with the case of parallel magnetization these expressions for $\mu_1{}^{\pm}$ and $\mu_2{}^{\pm}$ bear little resemblance to the real and imaginary parts of the permeability coefficient as previously derived on the basis of demagnetization factors.

Combining Eqs. (18) and (27), we have:

$$(P^{\pm})^2=4\pi j\omega\sigma(\mu_1{}^{\pm}-j\mu_2{}^{\pm})/c^2. \tag{30}$$

If we set $P^{\pm}=P_1{}^{\pm}+jP_2{}^{\pm}$, we obtain:

$$P_1{}^{\pm}=(2\pi\omega\sigma\mu_R{}^{\pm})^{\frac{1}{2}}/c, \quad P_2{}^{\pm}=(\pm)(2\pi\omega\sigma\mu_L{}^{\pm})^{\frac{1}{2}}/c, \tag{31}$$

where

$$\begin{aligned}\mu_R{}^{\pm}&=(\mu_1{}^{\pm 2}+\mu_2{}^{\pm 2})^{\frac{1}{2}}+\mu_2{}^{\pm},\\ \mu_L{}^{\pm}&=(\mu_1{}^{\pm 2}+\mu_2{}^{\pm 2})^{\frac{1}{2}}-\mu_2{}^{\pm},\end{aligned} \tag{32}$$

and the factor $(\pm)$ denotes that $P_2{}^{+}$ has the same sign as $\mu_1{}^{+}$. Since $\mu_1{}^{-}$ is always positive, $P_2{}^{-}$ is always positive.

Substitution into Eq. (19) gives the final results for the case of perpendicular magnetization:

$$\frac{1}{Q}=\frac{1}{2Q_0}[(\mu_R{}^{+})^{\frac{1}{2}}+(\mu_R{}^{-})^{\frac{1}{2}}], \tag{33a}$$

$$-\frac{2\Delta\omega}{\omega}=\frac{1}{2Q_0}[(\pm)(\mu_L{}^{+})^{\frac{1}{2}}+(\mu_L{}^{-})^{\frac{1}{2}}]. \tag{33b}$$

Equations (26a and b) and (33a and b), together with the immediately preceding defining equations, represent the final results of the analysis to which the experimental results presented in the next two sections will be referred.

We will conclude this section with some remarks concerning the equivalence and lack of equivalence of results based on the concept of the permeability tensor as compared with results based on the concept of a permeability coefficient.

In the parallel field case we may have, according to Eq. (12), two independent waves in which the magnetic vectors are h_x and $h_y/h_x=-jK/\mu$, respectively. Thus according to Eq. (5) the magnetic induction is:

$$\begin{aligned}b_x&=\mu h_x-jKh_y=(\mu^2-K^2)h_x/\mu,\\ b_y&=jKh_x+\mu h_y=0,\\ b_z&=h_z.\end{aligned}$$

Thus the tensor relation is reduced to diagonal form, and, in particular, the coefficient relating b_x and h_x is, as we have stated immediately after Eqs. (20) to (22), just the permeability coefficient previously derived for the case of parallel magnetization using demagnetizing factors.

The situation is different in the case of perpendicular magnetization. According to Eq. (13) the components h_x and h_y within each of the two waves of $+$ and $-$ circular polarization are related by

$$h_x/h_y=\mp i,$$

but the two waves are independent of each other. If the amplitudes of the two waves are equal at the cavity surface they will not be equal within the ferromagnetic medium since the waves are attenuated differently. But we now see why Polder obtained the same results for magnetization as are given by a theory based on a permeability coefficient. If we set the amplitudes of the two waves equal, i.e., $h_x{}^{+}=h_x{}^{-}$, it follows that $h_y=0$. Then, according to Eq. (5),

$$b_x=\mu h_x,$$

where μ is given by Eq. (6a) or (7a). These expressions for μ are precisely the permeability coefficients previously derived if in the latter we set all demagnetizing factors except N_z equal to zero and take $N_z=4\pi$ to correspond to this case of perpendicular magnetization.[8]

[8] The previously derived results are given by the equations quoted in reference 7. In order to make the comparison, the definition of ω_0 given in Eqs. (28c) or (29c) must be used.

We observe that $\mu_R^{\pm}$ and $\mu_L^{\pm}$ in Eqs. (33a and b) are different functions of the frequencies and material properties than μ_R and μ_L in Eqs. (26a and b). Consequently, the correct expressions for the perpendicular case differ from those previously used not merely in the appearance of the factor $\frac{1}{2}$, corresponding to the fact that most of the loss is in only one of the two circularly polarized waves, but also in the actual forms of the loss factors.

III. EXPERIMENTAL METHODS

The experimental techniques and the methods of reducing data are similar to those used by others and described previously. Thin metallic foils of the ferromagnetic specimen form one end or side wall of a reflection-type cavity excited in the TE_{102} mode which terminates a wave-guide system and is coupled to it by an iris of suitable dimensions. The cavity is excited at its resonant frequency of approximately 9200 Mc/sec and the wave reflected from the cavity is led through a directional coupler to a detecting system. Detection is obtained by mixing the reflected signal with the modulated signal of a local oscillator in a manner similar to that described by Yager *et al.*[8] The magnetic field is current stabilized and variable over the range of 800 to 13 000 gauss. Its intensity is measured by determining the frequency of magnetic resonance of protons and lithium nuclei. The homogeneity of the field is such that the variation of field over the volume of the cavity is never more than $\frac{1}{2}$ gauss. Frequency stabilization of the source klystron is used. This is by means of a Pound-type cavity controlled circuit[9] with some improvements in the discrimination.[10] The resulting stability was within 1000 cps at 9200 Mc/sec. With the use of this equipment frequency changes of the order 0.02 Mc/sec could be measured with accuracy.

The experimental quantities which are measured are the resonance frequency and the reflection coefficient of the cavity under prescribed conditions of cavity coupling and magnetic state of the wall material. Actually we are interested in the change of frequency and the change of Q as a function of the magnetizing field at the ferromagnetic sample in the cavity. These quantities are given by Eqs. (26a and b) and (33a and b) in Sec. II and they have the form:

$$1/Q_{fer}=A/Q_0,$$

$$-2\Delta\omega_{fer}/\omega=B/Q_0,$$

where A and B are the theoretical quantities which are to be related to the experimental measurements. The methods for doing this have been discussed previously[11] and we will mention only certain modifications in the procedure.

The quantity $\Delta\omega_{fer}$ is measured directly and the only problem is the selection of a reference point. The quantity $1/Q_{fer}$ is obtained by a measurement of reflection coefficients at two points, one corresponding to the desired magnetic state of the ferromagnetic sample and the other a reference point. Denoting the reflection coefficient by Γ and using primes to indicate the reference point we can write:

$$A-A'=\frac{2Q_0}{Q_e}\frac{\Gamma'-\Gamma}{(1+\Gamma')(1+\Gamma)},$$

where Q_e is the contribution to the Q of the cavity which is due to the radiation of power from the cavity to the microwave system.

The two problems which must be solved in order to obtain useful experimental data are the determination of Q_e and Q_0 and the determination of suitable reference points.

Q_e is determined by a measurement of the frequency response curve of the cavity.[11] Q_0 is more difficult to determine. In accordance with the definition of Q_0 given in Sec. II immediately before Eq. (17), it may be calculated using the formula given there. This value is usually larger than the correct experimental value. However, Q_0 for our case is not easily measured since it is the nonmagnetic contribution of the portion of the cavity walls which are occupied by the ferromagnetic sample and the losses due to this wall are small compared with all other losses including the iris and clamping arrangements. However, we have shown that the clamping loss in our case is nearly constant since we were able to obtain a high degree of reproducibility of data obtained after assembly, dissassembly, and reassembly of the cavity. Also the effect of the iris on Q_0 is negligible as shown by experiments on the frequency shift using different irises. In our experiments Q_0 is finally determined as that quantity which provides consistency between theoretically and experimentally determined quantities under a large variety of conditions. In particular, one obtains a relation at resonance relating A, the reference value A', the measured Γ and Γ', the measured Q_e and a theoretical expression involving the parameter $\eta=2\pi\gamma M_0/\omega_0$ and the damping constant. ω_0 is measured and γ and M_0 are determined as the solutions of simultaneous equations for ω_0 corresponding to the two cases of parallel and perpendicular magnetization. The damping parameter is determined to provide the shape of curve which most nearly fits the experimental curve. Thus, in effect an actual value of Q_0 is not required, but results consistent with a single reasonable value of Q_0 are found.

The reference points are usually chosen to correspond to some value of the applied magnetic field which is sufficiently large so that A and B are effectively equal to unity independent of the nature or approximate

[9] R. V. Pound, Rev. Sci. Instr. 17, 490 (1946) and Proc. Inst. Radio Engrs. 35, 1405 (1947).

[10] Tuller, Galloway, and Zaffarno, Proc. Inst. Radio Engrs. 36, 794 (1948).

[11] See, for example, N. Bloembergen, Phys. Rev. 78, 572 (1950); a general discussion of these and other techniques is given in C. G. Montgomery, *Technique of Microwave Measurements*, MIT Radiation Laboratory Series (McGraw-Hill Book Company, Inc., New York, 1947), Vol. 11.

magnitude of the damping constant. We performed the the following experiments to determine whether or not this procedure is correct for our maximum field.

(a) With the sample on an end wall and the constant magnetic field parallel to the surface of the sample, revolution of the cavity through 90° about the axis of the wave guide can be made to bring the system from a position corresponding to that of parallel magnetization (constant magnetic field parallel to the surface of the specimen and perpendicular to the rf field) to a position of no magnetic effects (constant magnetic field parallel to the rf field). As shown by Eqs. (26a and b) with $\theta=0$ the last case corresponds strictly to $A=B=1$. Thus, the reference points are experimentally determined for the case of parallel magnetization at the same time that the data for this case is being obtained. It is true that one also observes certain small field effects in the so-called nonmagnetic orientation which are presumably due to the fact that θ is not exactly zero, as well as other effects of greater interest which are due presumably to the failure of the small field to saturate the sample. The latter requires special study but is not relevant to our discussions of reference points.

(b) With the sample on a side wall rotation about the wave-guide axis gives the difference between the cases of parallel and perpendicular magnetization. Having the reference points for the case of parallel magnetization one now obtains them for the case of perpendicular magnetization. Thus, the reference points for both cases are measured absolutely. The results for supermalloy using $H_0=13\,000$ gauss give the experimental values:

$$(\mu_R)^{\frac{1}{2}}=1.30 \quad \text{and} \quad (\mu_L)^{\frac{1}{2}}=1.22,$$

in the parallel field case, and

$$\tfrac{1}{2}[(\mu_R{}^+)^{\frac{1}{2}}+(\mu_R{}^-)^{\frac{1}{2}}]=1.78,$$

$$\tfrac{1}{2}[(\mu_L{}^+)^{\frac{1}{2}}+(\mu_L{}^-)^{\frac{1}{2}}]=1.42,$$

in the perpendicular field case. The calculated values from Eqs. (25) and (32) are 1.27 and 1.27 in the parallel field case and 1.74 and 1.71 in the perpendicular field case. Thus, we find that A and B are not equal to unity at the highest field available and we used, consequently, these procedures for the determination of the reference points.

TABLE I. Numerical values of g and $4\pi M_0$ for nickel, supermalloy, and 399 alloy.[a]

Material	g	$4\pi M_0$
Supermalloy	2.10	7770
Nickel	2.22	6170
399 alloy	2.28	5890

[a] The supermalloy samples were furnished by Dr. S. O. Morgan of the Bell Telephone Laboratories. The nickel samples were obtained from Baker and Company and are 99.5 percent pure. The 399 alloy is a Driver-Harris alloy of nickel and 0.2 percent silicon and with no contaminant greater than 0.05 percent.

One additional remark with regard to the experimental procedure should be made. Various sizes of iris were used. It may, for example, be chosen so that at the reference point the reflection coefficient is zero corresponding to critical coupling at this point. Under these conditions small effects are most accurately measured, and in particular, one obtains an accurate determination of the cavity frequency. If one now reduces the field and thus increases the loss in the cavity which is due to the approach to resonance of the ferromagnetic sample, the cavity becomes undercoupled (negative reflection coefficient Γ). But Γ may also approach unity in magnitude and since $A-A'$ is proportional to $(1+\Gamma)^{-1}$ the errors of measurement may become fairly large. In order to reduce these errors one then chooses an iris size so that the cavity is slightly overcoupled at the resonance point and the quantity $(1+\Gamma)$ is never permitted to be very much different from unity. We believe that the over-all error in our measurement of the reflection coefficient is not greater than 10 percent.

IV. RESULTS

In principle the complete determination of an absorption or a dispersion curve is sufficient to fix the numerical values of all relevant parameters. Since we are measuring both the absorption and dispersion, and since these measurements are being made for two different conditions of magnetization, all of our parameters are overstipulated. Thus, we obtain a rather stringent test of the adequacy of the theory to describe the phenomena in question.

Two of the parameters are rather easily determined independently of the nature of the theory used and independently of the nature and numerical value of the damping constant provided that it is small.[12] These are the saturation magnetization M_0 and the gyromagnetic ratio $\gamma=ge/2mc$. The resonance frequency for the case of parallel magnetization is given by Eqs. (21c) and (22c) in the cases of B- and LL-type damping, respectively, and by Eq. (28c) or (29c) in the case of perpendicular magnetization. Thus, e.g., in the case of B-type damping M_0 and γ are determined as the solutions of the two simultaneous equations:

$$\omega^2=\gamma^2H^{\parallel}(H^{\parallel}+4\pi M_0)+1/T_2{}^2, \quad \omega=\gamma(H^{\perp}-4\pi M_0),$$

where $H^{\parallel}$ and $H^{\perp}$ are the values of the constant magnetic field intensity at resonance in the cases of parallel and perpendicular magnetization, respectively. The principal source of error is in the determination of the resonant point. An error of ± 10 gauss in $H^{\parallel}$ and $H^{\perp}$ leads to an error of 35 gauss in $4\pi M_0$ and 0.03 in g. Our errors lie within these limits. The results which we have obtained as a consequence of a number of determinations on our samples are given in Table I.

One of the original objectives of these experiments

[12] Kittel, Yager, and Merritt, Physica 15, 256 (1949).

was to distinguish between the Bloch (B) and Landau-Lifshitz (LL) types of damping. Since both types lead to a Lorentz shape of curve it was expected that within the accuracy of the experiments it would be difficult to distinguish between the two damping mechanisms on the basis of line shape alone. Thus, Healy[13] has shown that he could fit his experimental curves equally well using either type of damping. But we expected that the ratio of absorptions in the two cases of parallel and perpendicular magnetizations would permit a distinction to be made. According to the usual theory of ferromagnetic resonance this ratio is independent of the numerical value of the damping constant but its dependence on the parameter $2\pi\gamma M_0/\omega_0$ is different in the two cases. Our experimental results differed from the predicted ratio in the most favorable case by a factor of about 1.5. In addition we observed that the shape of the resonance curve was correctly predicted only in the case of parallel magnetization,[14] but that in the case of perpendicular magnetization there were marked discrepancies.

These results may be interpreted to mean that neither type of damping mechanism is appropriate. However, the agreement between theory and experiment on line shape which is obtained in the case of parallel magnetization suggested the type of analysis which we have given in Sec. II, and it is now on the basis of this analysis that we will describe the experimental results obtained.

The experimental results will be presented under three headings:

(a) The ratio of absorption at resonance in the cases of parallel and perpendicular magnetizations.
(b) The over-all shape of resonance curves.
(c) Details in the shapes of resonance curves.

(a) Ratio of Absorptions at Resonance

In the case of parallel magnetization Eq. (26a) with $\theta=0$ gives

$$1/Q=(\mu_R)^{\frac{1}{2}}/Q_0.$$

At resonance we set $\mu_1\cong 0$ and we express H_0 in terms of ω_0 and other parameters. Making the substitution into $\mu_R\cong 2\mu_2$, we obtain:

$$(Q_0/Q)^2 = 2\eta\omega_0 T_2[\eta+(1+\eta^2)^{\frac{1}{2}}] \quad \text{B-type damping}$$
$$= (2\eta/\alpha)[1+\eta(1+\eta^2)^{-\frac{1}{2}}] \quad \text{LL-type damping,} \quad (35)$$

where

$$\eta=2\pi\gamma M_0/\omega_0.$$

[13] D. W. Healy, Phys. Rev. 86, 1009 (1952).
[14] As observed also by others; e.g., N. Bloembergen, reference 11; W. A. Yager, Phys. Rev. 75, 316 (1949); W. A. Yager and F. R. Merritt, Phys. Rev. 75, 318 (1949).

TABLE II. Experimental and theoretical values of $(Q_\perp/Q_\parallel)^2$ at resonance.

Specimen	Experimental	Eq. (39) (Usual theory based on a complex permeability coefficient) LL	B	Eq. (38) (Present theory based on a permeability tensor) LL	B
Nickel	4.1±0.4	1.7	2.5	2.6	3.8
Supermalloy	5.5±0.5	1.8	2.8	2.9	4.6

In the case of perpendicular magnetization we have, from Eq. (33a):

$$(1/Q)=(1/2Q_0)[(\mu_R{}^+)^{\frac{1}{2}}+(\mu_R{}^-)^{\frac{1}{2}}].$$

At resonance we set $\mu_1{}^+\cong 0$, $\mu_2{}^-\cong 0$ and substitute $H_0=\omega_0/\gamma+4\pi M_0$ into $\mu_R{}^+\cong 2\mu_2{}^+$ and $\mu_R{}^-\cong\mu_1{}^-$. We obtain:

$$\left(\frac{Q_0}{Q}\right)^2 = \eta\omega_0 T_2\left[1+\frac{1}{2}\left(\frac{1+\eta}{\eta\omega_0 T_2}\right)^{\frac{1}{2}}\right]^2 \quad \text{B-type damping}$$
$$= \frac{\eta}{\alpha}\left[1+\frac{1}{2}\left(\alpha\frac{1+\eta}{\eta}\right)^{\frac{1}{2}}\right]^2 \quad \text{LL-type damping.} \quad (36)$$

The usual theory in the case of parallel magnetization gives Eq. (35). In the case of perpendicular magnetization it gives:

$$(Q_0/Q)^2 = 2\eta\omega_0 T_2 \quad \text{B-type damping}$$
$$= 2\eta/\alpha \quad \text{LL-type damping,} \quad (37)$$

where the values of μ_1 and μ_2 can be obtained from the equations quoted in reference 7 with N_z set equal to 4π to correspond to the case of perpendicular magnetization.

Taking the ratios of Q in the cases of parallel and perpendicular magnetization, we have:

$$\left(\frac{Q_\perp}{Q_\parallel}\right)^2 = 2[\eta+(1+\eta^2)^{\frac{1}{2}}]\left[1+\frac{1}{2}\left(\frac{1+\eta}{\eta\omega_0 T_2}\right)^{\frac{1}{2}}\right]^{-2}$$

B-type damping

$$= 2[1+\eta(1+\eta^2)^{-\frac{1}{2}}]\left[1+\frac{1}{2}\left(\alpha\frac{1+\eta}{\eta}\right)^{\frac{1}{2}}\right]^{-2}$$

LL-type damping, (38)

whereas the usual theory gives

$$\left(\frac{Q_\perp}{Q_\parallel}\right)^2 = \eta+(1+\eta^2)^{\frac{1}{2}} \quad \text{B-type damping}$$
$$= 1+\eta(1+\eta^2)^{-\frac{1}{2}} \quad \text{LL-type damping.} \quad (39)$$

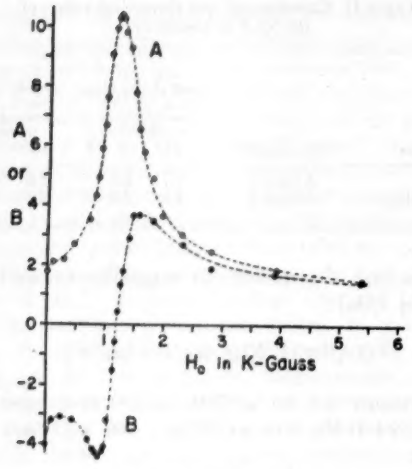

FIG. 1. Nickel parallel field case.

The parameter η is known from the experimental determinations leading to Table I. The parameters T_2 and α must be chosen to give the proper width of resonance curve. This cannot be done unambiguously to fit both the cases of parallel and perpendicular magnetization unless the type of damping used is actually the appropriate one. For our present purposes the quantities we are considering are relatively insensitive to the actual numerical value of the damping parameter. The comparisons which we now make are with $1/T_2=2.8\times10^9$ sec^{-1} and $\alpha=0.048$ for nickel and $1/T_2=1.7\times10^9$ sec^{-1} and $\alpha=0.029$ for supermalloy. Table II gives a tabulation of our experimental values of $(Q_\perp/Q_\parallel)^2$ together with the theoretical values calculated from Eqs. (38) and (39).

Thus, the theory of Sec. II gives results for the ratio of absorptions which is in fair agreement with the experimental values if Bloch damping is assumed. The remainder of the discussion will be based on only this type of damping.

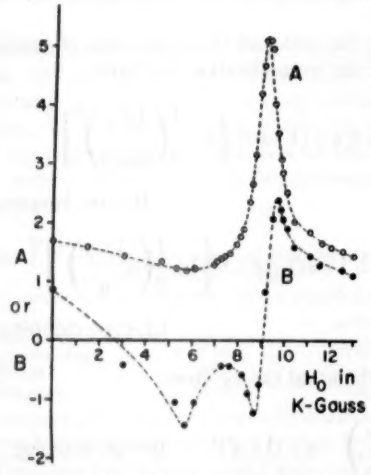

FIG. 2. Nickel perpendicular field case.

(b) Over-All Shape of Resonance Curves

Values of Q and $\Delta\omega$ are measured with respect to the appropriately chosen reference point as discussed in Sec. III. Since Q_0 enters here only as a normalization constant we will plot values of A and B as a function of the applied constant field H_0. $A=(\mu_R)^{\frac{1}{2}}$ and $B=(\pm)(\mu_L)^{\frac{1}{2}}$ for parallel magnetization, and $A=\frac{1}{2}[(\mu_R{}^+)^{\frac{1}{2}}+(\mu_R{}^-)^{\frac{1}{2}}]$ and $B=\frac{1}{2}[(\pm)(\mu_L{}^+)^{\frac{1}{2}}+(\mu_L{}^-)^{\frac{1}{2}}]$ for perpendicular magnetization. All measurements are at an rf frequency of approximately 9200 Mc/sec, the exact frequency in each case being determined by the cavity resonance.

The experimental results for nickel and supermalloy and for the cases of parallel and perpendicular magnetization are shown in Figs. 1, 2, 3, and 4.

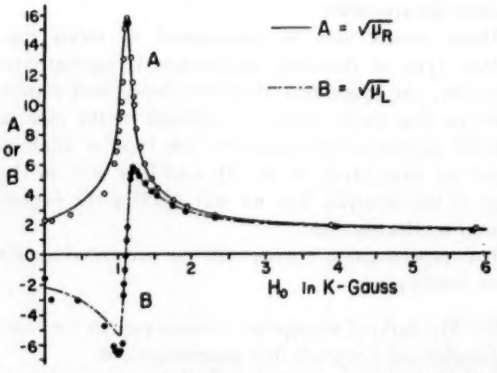

FIG. 3. Supermalloy parallel field case and comparison with theory.

We will use our measurements on supermalloy as the basis for a discussion of line shape. Exactly similar results are obtained in the case of nickel. In both cases the results depend on heat treatment and surface polishing. These effects are particularly pronounced in the case of nickel and in the measurements of frequency shift for perpendicular magnetization. They are not, however, the object of the present study and consequently we now restrict the discussion to uniformly prepared specimens of the metal supermalloy.

We consider first the case of parallel magnetization. The usual theory does not differ from the present analysis in this case, both leading to Eqs. (26a) and (26b). These equations with $\theta=0$ are plotted as continuous solid and dotted line curves in Fig. 3 for comparison with the experimental data. Bloch damping has been assumed and $1/T_2$ has been set equal to 1.7×10^9 sec^{-1}. The agreement between theory and experiment is almost as good as could be desired.

We consider next the case of perpendicular magnetization. The experimental values of A and B given in

Fig. 4 are now transferred to Figs. 5 and 6, respectively, where they are plotted against $H_0-4\pi M_0$. The dotted and solid line curves given for comparison are the theoretical curves as obtained from the usual theory in terms of demagnetization factors and the present theory leading to Eqs. (33a) and (33b). We note the following:

(1) Insofar as absorption is concerned the present theory gives results in almost perfect agreement with the experimental data. On the other hand the usual theory leads to a curve which differs from the experimental curve in two important respects. It possesses a minimum which is not observed in these X-band measurements and the curve is too wide in the neighborhood of the resonance point.

(2) Insofar as frequency shift is concerned the present theory predicts correctly the rate of frequency change near resonance together with the correct peak-

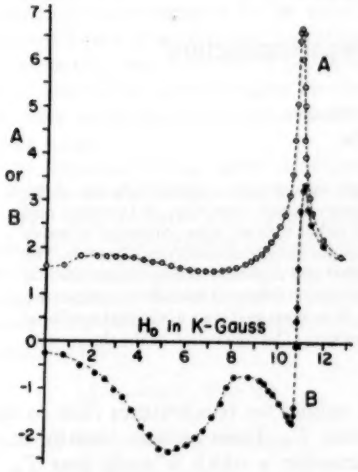

FIG. 4. Supermalloy perpendicular field case.

to-peak values. However, there are discrepancies in details of the B curve which remain to be discussed.

The minimum in the absorption which is predicted by the usual theory is a consequence of the fact that μ_1 goes through zero and remains negative over a certain portion of the range of H_0 below resonance. In the case of perpendicular magnetization it predicts that this minimum should occur at

$$(H_0-4\pi M_0)=2\pi M_0[(1+\eta^{-2})^{\frac{1}{2}}-1]\cong 1100 \text{ gauss},$$

for supermalloy at X-band frequencies. The prediction with respect to a minimum in the absorption which is made by the present theory differs in two respects. In the first place only μ_1^+ can become negative and consequently the minimum, if present, is less marked than in the usual theory. In the second place it occurs for a different value of H_0 than that given by the usual theory. According to Eq. (28) the minimum should

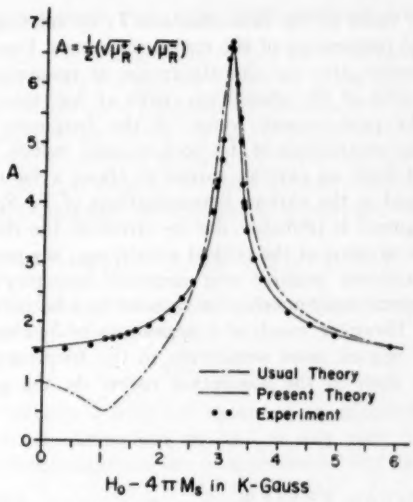

FIG. 5. Experimental and theoretical values of A in the supermalloy perpendicular field case.

occur at a value of H_0 which is approximately given by

$$(H_0-4\pi M_0)=(\omega/\gamma)-4\pi M_0.$$

Thus it will not be observed at X-band frequencies for which $\omega/\gamma\sim 4000$ gauss and $4\pi M_0\sim 7700$ gauss, but a small minimum might be detectable at K-band frequencies. This has not been observed.[12] The failure to detect a minimum in the absorption at perpendicular magnetization in our measurements at X-band frequencies as well as in previous measurements was one of the indications that the usual theory was inadequate.

(c) Details in Shape of the Resonance Curves

The data are actually of sufficient accuracy to permit a closer examination of the agreement between experimental and predicted curve shapes. We can, for example, attempt to make independent determinations

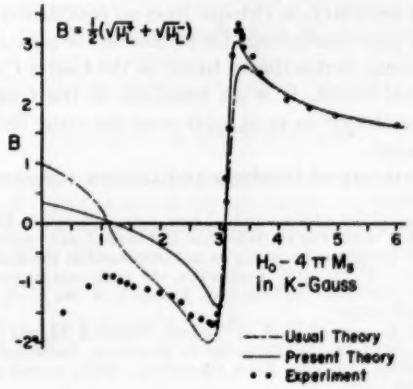

FIG. 6. Experimental and theoretical values of B in the supermalloy perpendicular field case.

of the value of the time constant T_2 by relating it to critical parameters of the resonance curves. Four such parameters are: (a) the absorption at resonance, (b) the width of the absorption curve at half-maximum, (c) the peak-to-peak value of the frequency shift, (d) the separations in the peak-to-peak values. When this is done an over-all spread of about a factor 2 is obtained in the various determinations of T_2. Some of this spread is probably due to errors in the determination of some of the critical points, e.g., the positions of maximum positive and negative frequency shift. The spread may possibly be reduced by a better choice of Q_0. However, much of it appears to be inherent and to be related more sensitively to the frequency shift curve than to the absorption curve. At the present time we are able to conclude only that the experimental methods used provide a rather stringent test of the phenomenological theory which may not be completely adequate for a precise quantitative description.

Other features of the resonance curves which remain unexplained are in the low field region. For example, in Figs. 2 and 4 we observe a second minimum in the frequency shift curve occurring at about 5700 gauss for nickel and 5500 gauss for supermalloy. Since these are perpendicular field cases, we are here in the region of unsaturated magnetization. The theory is consequently unable to explain the phenomena in question and it is for this reason that the data of Fig. 4 were replotted in Figs. 5 and 6 only for values of H_0 greater than $4\pi M_0$.

PHYSICAL REVIEW VOLUME 94, NUMBER 3 MAY 1, 1954

Theory of Boundary Effects of Superconductors*

J. BARDEEN
University of Illinois, Urbana, Illinois
(Received January 27, 1954)

An extension of the phenomenological London equations to take into account a space variation of the concentration of superconducting electrons is presented. The theory differs from that of Ginsburg and Landau in that it makes use of the Gorter-Casimir two-fluid model rather than an order parameter to derive an expression for the free energy. An effective wave function is used for the superconducting electrons. The theory is applied to calculate the boundary energy between normal and superconducting phases and the relative change $\Delta\lambda/\lambda$ of penetration depth with magnetic field. Calculated values of boundary energies are somewhat larger, and of $\Delta\lambda/\lambda$ somewhat smaller, than observed. It is suggested that additional nonlinear terms are required to account for the observed $\Delta\lambda/\lambda$ at low temperatures. The connection of the theory with Pippard's ideas on range of order is discussed briefly.

I. INTRODUCTION

TO estimate the energy of the boundary between normal and superconducting phases and for related problems, it is necessary to have a theory which takes into account a space variation in the effective concentration of superconducting electrons n_s. Across such a boundary, n_s changes from an equilibrium value on the superconducting side to zero on the normal side. We present here a theory based on the Gorter-Casimir[1] two-fluid model. It is an extension of the Ginsburg-Landau theory[2] so as to apply over the entire temperature range.

The theory of Ginsburg and Landau (denoted here by G-L) applies for temperatures close to the critical temperature T_c. These authors identify n_s with an order parameter η which is small near T_c. The free energy is expanded in a power series in η. It is assumed that n_s (and thus η) is given by the square of an effective wave function $\Psi(x)$, and that there is an energy term proportional to $|\text{grad}\Psi|^2$. The coefficient of $|\text{grad}\Psi|^2$ is evaluated in terms of the critical field H_c and the penetration depth, λ, so that there are no undetermined parameters. In addition to the calculation of the boundary energy, the theory was applied to the magnetic and thermal properties of thin films and to estimate the change in λ with magnetic field.

Using a microwave method, Pippard[3] has shown that for tin the change in λ with field is no more than 3 percent for fields up to $H=H_c$. From these results he estimated that the ordered regions must extend over distances of the order of 10^{-4} cm. Presumably the width of the normal-superconducting boundary is at least of this order.

The author[4] has pointed out that Pippard's result is

* Most of the results reported here were obtained in 1951 and 1952. The work was started while the author was employed at the Bell Telephone Laboratories and continued at the University of Illinois. At the latter institution, the work was supported in part by the Office of Ordnance Research of the U. S. Army Ordnance Corps.

[1] C. J. Gorter and H. B. G. Casimir, Physik **Z. 35**, 963 (1934); Z. tech. Phys. **15**, 539 (1934). See D. Shoenberg, *Superconductivity* (Cambridge University Press, Cambridge, 1952), second edition, Chap. VI.

[2] V. L. Ginsburg and L. D. Landau, J. Exptl. Theoret. Phys. (U.S.S.R.) **20**, 1064 (1950).

[3] A. B. Pippard, Proc. Roy. Soc. (London) **A203**, 210 (1950).

[4] J. Bardeen, Phys. Rev. **81**, 1070 (1951).

consistent with a model in which the superconducting electrons have small effective mass, $m_s \sim 10^{-4} m$. A localized electron is described approximately by a wave function $U(x)$ whose square is the probability density. We showed that the energy

$$-\frac{\hbar^2}{2m_s}\int U\nabla^2 U d\tau$$

is of the order of $k_0 T_c$ if the electron is confined to a region $<\sim 10^{-4}$ cm.

The same model was used to make some preliminary estimates of boundary energies. Before the results were published, the author learned about the G-L theory[5] and it was found that the two theories give very similar results. We shall show here the close connection between the two approaches. They both use an effective wave function for the superconducting electrons, but differ in how the free-energy difference between normal and superconducting phases depends on the wave function. Our earlier results should be better at low temperatures, $T \ll T_c$, and the G-L results should be better for $T \sim T_c$. The theory based on the Gorter-Casimir two-fluid model should be more satisfactory than either over the entire temperature range.

That the superconducting wave functions or the ordered regions should extend over large distances in space ($\sim 10^{-4}$ cm) follows from rather general considerations, as has been pointed out on a number of occasions. Superconductivity arises from some sort of interaction, involving the lattice vibrations, between electrons which lie within $\sim \Delta k$ of the Fermi surface, E_F. If it is assumed that

$$\Delta k/k_F \sim k_0 T_c/E_F \sim 10^{-4}, \tag{1.1}$$

it follows from the uncertainty relation,

$$\Delta x \Delta k \sim 1,$$

that the ordered regions must extend over distances of the order of

$$\Delta x \sim 10^4/k_F \sim 10^{-4} \text{ cm}. \tag{1.2}$$

If the degree of order, or n_s, varies in space, an additional energy is involved. It is presumed by both G-L and ourselves that the energy can be obtained from the kinetic energy term for an effective wave function.

The real significance of the "order-parameter" or "effective wave function" is uncertain, so that at this stage the theory must be regarded as a semiempirical one.

In view of the uncertain theoretical foundation for the theory, it is perhaps best regarded as an extension of the London phenomenological theory to take into account a space variation of n_s.

[5] The author is indebted to Dr. Paul Marcus for bringing to his attention a translation of the Ginsburg-Landau article made by Dr. D. Shoenberg.

II. EXPRESSION FOR THE FREE ENERGY DENSITY

Ginsburg and Landau introduce an order parameter η in accord with a general theory of phase transitions of the second kind proposed by Landau and Lifshitz. The parameter $\eta = 0$ for the normal phase, and, at least for T near T_c, where η is small, the free energy difference $f(T)$ per unit volume between superconducting and normal phases may be expressed as a quadratic function of η:

$$f(T) = F_s(T) - F_n(T) = \alpha(T)\eta + \tfrac{1}{2}\beta(T)\eta^2. \tag{2.1}$$

The equilibrium value of η in zero field is that which makes F_s or f a minimum:

$$\eta_e = -\alpha/\beta. \tag{2.2}$$

They identify η with the square of an effective wave function Ψ normalized in such a way that $|\Psi|^2$ is equal to the concentration of superconducting electrons n_s.

We shall use a different normalization, and assume that $\eta = |\Psi|^2 = 1$ at $T = 0°$K, so that

$$n_s = n_0|\Psi|^2, \tag{2.3}$$

where n_0 is the equilibrium concentration at $T = 0°$K. The free energy difference is then

$$f = \alpha|\Psi|^2 + \tfrac{1}{2}\beta|\Psi|^4. \tag{2.4}$$

The values of α and β are determined from the critical field H_c and the penetration depth λ. The equilibrium free energy difference, $-H_c^2/8\pi$ per unit volume, is obtained by inserting (2.2) into (2.1):

$$-f_e = \alpha^2/2\beta = H_c^2/8\pi. \tag{2.5}$$

The inverse relation between n_s and λ^2 follows from the London theory and is also a consequence of the equations derived by G-L. From (2.5) and (2.6), it follows that

$$\alpha = -(H_c^2/4\pi)(\lambda^2/\lambda_0^2), \tag{2.7}$$

$$\beta = (H_c^2/4\pi)(\lambda^4/\lambda_0^4). \tag{2.8}$$

In addition to (2.1), G-L introduce an energy proportional to $|\text{grad}\Psi|^2$, corresponding to the density of kinetic energy in quantum mechanics. In a magnetic field defined by a vector potential $\mathbf{A}$ the energy density becomes:

$$(n_0/2m_s)\left|-ih\,\text{grad}\Psi + (e/c)\mathbf{A}\Psi\right|^2, \tag{2.9}$$

where m_s is an effective mass for the superconducting electrons. The charge on the electron is $-e$. Taking into account the field energy $H^2/8\pi$ the total (Helmholz) free-energy difference is

$$F = \int\left\{\frac{n_0}{2m_s}\left|-ih\,\text{grad}\Psi + \frac{e}{c}\mathbf{A}\Psi\right|^2 + \frac{H^2}{8\pi} + \alpha|\Psi|^2 + \frac{\beta}{2}|\Psi|^4\right\}d\tau. \tag{2.10}$$

Here H is the local value of the magnetic field. We could equally well use the symbol B for this quantity. The magnetic properties of the medium cannot be described in terms of a permeability. Equations for Ψ and $\mathbf{A}$ such as to make F a minimum are derived by G-L. These will be discussed later, together with the boundary conditions which differ from the usual ones.

Our approach differs from G-L mainly in the way $f(T)$ is assumed to depend on Ψ. It originated from a theory of superconductivity based on interactions between electrons and lattice vibrations as proposed by the author.[6] According to this picture, electrons with energies near the Fermi surface are lowered in energy by the interactions and have a small effective mass. It is the small effective mass which presumably accounts for the superconducting properties. In this formulation, the wave function for the electrons is approximated by determinants of one-electron wave functions, each of which may depend on the coordinates of the lattice vibrations. A transition from a superconducting to a normal region may be obtained by multiplying each of the wave functions of the superconducting electrons (i.e., those with energies near the Fermi surface) by a modulating factor $U(x)$ which varies slowly from 1 to 0 across the boundary. The density of superconducting electrons is then proportional to U^2. It is assumed that the density of normal electrons varies as $1-U^2$ so as to keep the total density of electrons approximately constant.

In our original calculation it was assumed that the free-energy difference

$$f(U)=-(H_c^2/8\pi)U^2. \tag{2.11}$$

We also assumed, according to the effective mass concept, that there is an additional energy density associated with grad$U$:

$$(n_s/2m_s)|-ih\,\mathrm{grad}U+(e/c)\mathbf{A}U|^2, \tag{2.12}$$

where n_s is the equilibrium concentration. This latter expression is the same as that used by G-L since

$$n_s|U|^2=n_0|\Psi|^2. \tag{2.13}$$

Equations which we derived for U and $\mathbf{A}$ are very similar to those derived by G-L. This is to be expected since the initial assumptions differ only in the expressions used for $f(T)$.

Expression (2.11) assumes that the energy associated with a variation of U comes entirely from the superconducting electrons. The term analogous to (2.12) for the normal electrons is negligible because the effective mass is so much larger. However, the increasing density of normal electrons with decrease in U should make an appreciable contribution to the free energy. This term is to a first approximation proportional to T^2.

Probably the best way to obtain a semiempirical expression for the free energy is from the Gorter-Casimir two-fluid model. This model was used by Pippard[3] in his estimates of the size of the ordered regions from the change in penetration depth with magnetic field. A parameter ω is introduced which varies between unity at $T=0°$K and zero at $T=T_c$ and which represents the fraction of the electrons which are superconducting. The free-energy density $F_s(T)$ is given in terms of $F_n(0)$ (for $T=0°$K) as follows[1]:

$$F_s(T)=F_n(0)-(H_0^2/8\pi)[2t^2(1-\omega)^{\frac{1}{2}}+\omega]. \tag{2.14}$$

Here H_0 is the critical field at $T=0°$K and $t=T/T_c$. The term in t^2 represents the contribution of the normal electrons and $-(H_0^2/8\pi)\omega$ that of the superconducting electrons. The value of ω which makes (2.14) a minimum is

$$\omega_s=1-t^4. \tag{2.15}$$

Since $\omega\sim\lambda^{-2}$, the observed dependence of penetration depth on temperature, $\lambda^{-2}\sim(1-t^4)$ is obtained. A parabolic critical field curve also follows from the model:

$$f(T)=F_s(T)-F_n(T)=-H_c^2/8\pi, \tag{2.16}$$

with

$$H_c=H_0(1-t^2). \tag{2.17}$$

It has been pointed out to the author by P. Marcus that one can get a parabolic H_c-T curve from (2.1) by taking

$$\alpha(T)=-(H_0^2/4\pi)(1-t^2);\quad \beta=H_0^2/4\pi. \tag{2.18}$$

However, η then varies as $1-t^2$ so that it cannot be interpreted as giving the relative concentration of superconducting electrons. The temperature dependence of α and β given by (2.7) and (2.8) is more complicated. Following a suggestion of Marcus, it thus appears to be reasonable to identify ω rather than η with $|\Psi|^2$.

By setting $\omega=|\Psi|^2$ in (2.14) ,we get

$$f(T)=F_s-F_n=(H_0^2/4\pi)\{t^2[1-(1-|\Psi|^2)^{\frac{1}{2}}]-\tfrac{1}{2}|\Psi|^2\}. \tag{2.19}$$

For t small, this reduces to Eq. (2.11) which we have used, and for t near unity and Ψ small to

$$f(T)=-(H_0^2/8\pi)|\Psi|^2(1-t^2)+(H_0^2t^2/32\pi)|\Psi|^4. \tag{2.20}$$

This is in agreement with G-L, for it follows from (2.7) with $H_c=H_0(1-t^2)$ and $\lambda_0^2/\lambda^2=1-t^4$, that

$$\alpha=-(H_0^2/4\pi)(1-t^2)/(1+t^2),$$
$$\beta=(H_0^2/4\pi)(1+t^2)^{-2}. \tag{2.21}$$

As $t\to1$, α approaches the coefficient of $|\Psi|^2$ and $\beta/2$ the coefficient of $|\Psi|^4$ in (2.20). Thus the two-fluid model approaches that of Ginsburg and Landau near $T=T_c$.

III. EQUATIONS FOR Ψ AND $\mathbf{A}$

The Helmholtz free energy difference between the normal and superconducting phases may be written in

[6] J. Bardeen, Phys. Rev. **80**, 567 (1950); **81**, 829 (1951); **82**, 978 (1951); Revs. Modern Phys. **23**, 261 (1951).

the general form:

$$F=\int\left\{\frac{n_0}{2m_s}|-ih\,\mathrm{grad}\Psi+(e/c)\mathbf{A}\Psi|^2+\frac{H^2}{8\pi}+f(\Psi)\right\}d, \tag{3.1}$$

where $f(\Psi)$ is one of (2.4), (2.11), or (2.19). It is assumed that Ψ is real when the gauge in $\mathbf{A}$ is chosen appropriately ($\mathrm{div}\mathbf{A}=0$, $A_\perp=0$). It is this reality requirement which gives the Meissner effect and which leads to the London equations for field penetration.

We shall be concerned only with examples for which $\Psi(x)$ varies only in one dimension, which we take to be that of the x axis. The magnetic field is in the z direction so that the only component of $\mathbf{A}$ is $A_y(x)$:

$$H_z=dA_y/dx. \tag{3.2}$$

To simplify the notation, we shall omit the subscript y in the following. With these simplifications, (3.1) becomes

$$F=\int\left\{\frac{n_0h^2}{2m_s}\left[\left(\frac{d\Psi}{dx}\right)^2+\left(\frac{eA\Psi}{hc}\right)^2\right]+\frac{1}{8\pi}\left(\frac{dA}{dx}\right)^2+f(\Psi)\right\}dx. \tag{3.3}$$

Ginsburg and Landau derive equations for Ψ and A by requiring that F be a minimum.

Actually, it is the Gibbs free energy G which differs from (3.3) by a term $-H_aM$ in the integrand, which should be minimized. Here H_a is the applied field and $M=(H-H_a)/4\pi$ is the magnetization. The additional term makes H_a an independent variable, and the problem is to find $A(x)$ such as to make G a minimum. This added term does not in general affect the differential equations for A and Ψ but it is important in determining the boundary conditions.

The equations for Ψ and A derived from (3.3) are:

$$\frac{d^2\Psi}{dx^2}=\frac{m_s}{n_0h^2}\frac{df}{d\Psi}+\frac{e^2A^2}{h^2c^2}\Psi, \tag{3.4}$$

$$\frac{d^2A}{dx^2}=\frac{4\pi e^2n_0\Psi^2}{m_sc^2}A. \tag{3.5}$$

The boundary condition on Ψ at a free surface, as determined from the variational problem after an integration by parts, is $d\Psi/dx=0$. It is *not* required[4] that $\Psi=0$ at the boundary. It is required that $A\to0$ in the interior of a superconducting region. As in the London theory, the current density is

$$\mathbf{j}=-\frac{n_0e^2}{m_sc}\Psi^2\mathbf{A}, \tag{3.6}$$

and the effective penetration depth is given by

$$\left(\frac{m_sc^2}{4\pi e^2n_0\Psi^2}\right)^{\frac{1}{2}}. \tag{3.7}$$

Equations (3.4) and (3.5) of G-L may be regarded as a generalization of the London phenomenological equations to allow for a variation in concentration of superconducting electrons in space.

IV. CALCULATION OF THE ENERGY OF THE BOUNDARY BETWEEN NORMAL AND SUPERCONDUCTING PHASES IN THE INTERMEDIATE STATE

The intermediate state of the superconductor consists of alternate layers of normal and superconducting phases.[7] The flux is carried by the normal regions in which the field is equal to the critical values H_c. According to a theory developed by Landau,[8] the layer thickness is determined by the surface energy α_{ns} between the normal and superconducting phases. We shall derive here a value for α_{ns} in terms of H_c and the penetration depth λ, and show that the values obtained in this way are in good agreement with those estimated from analysis of experimental data on the intermediate state. Our derivation differs somewhat from that in G-L, but the result is the same when the same expression is used for the free-energy difference.

We shall calculate the energy per unit area of the actual boundary relative to an ideal boundary for which there is an abrupt transition between normal and superconducting regions and for which $H=H_c$ everywhere in the normal region and $H=0$ everywhere in the superconducting region. This is the energy which enters into the theory of Landau and others and is designated by[7]

$$\alpha_{ns}=\Delta H_c^2/8\pi. \tag{4.1}$$

The parameter Δ has the dimensions of a length.

The boundary energy is sometimes given relative to a boundary at which the field penetrates into the superconducting region with penetration depth λ as it would at a free surface. This energy is larger than (4.1) by $\lambda H_c^2/8\pi$ or is equal to

$$\alpha_{ns}^{(1)}=\Delta_1H_c^2/8\pi, \tag{4.2}$$

where

$$\Delta_1=\Delta+\lambda. \tag{4.3}$$

Desirant and Shoenberg[9] have used the symbols Δ for Δ_1 and Δ' for Δ.

The boundary is taken normal to the x direction and the magnetic field is in the z direction. As in Sec. III, the only component of $\mathbf{A}$ is $A_y=A(x)$. Let $x=x_0$ be the position of the boundary in the ideal case, so that $H=H_c$

[7] See, for example D. Shoenberg, *Superconductivity* (Cambridge University Press, Cambridge, 1952), second edition, Chap. IV.
[8] L. D. Landau, Physik. Z. Sowjetunion **11**, 129 (1937); Nature **141**, 688 (1938); J. Phys. (U.S.S.R.) **7**, 99 (1943).
[9] M. Desirant and D. Shoenberg, Proc. Roy. Soc. (London) **A194**, 63 (1948).

for $x<x_0$ and $H=0$ for $x>x_0$. The corresponding position of the actual boundary is determined by requiring the flux be the same as for the ideal boundary. If it is assumed that the transition region extends between $x=0$ and $x=a$, we have:

$$x_0H_c=\int_0^a Hdx=\int_0^a (dA/dx)dx=-A(0). \quad (4.4)$$

It is assumed that $A=0$ and $H=0$ at $x=a$, as the vector potential vanishes in the interior of the superconducting regions. The position $x=0$ is assumed to be in the normal region where $H=H_c$.

Relative to the ideal boundary, the energy difference per unit area is

$$\alpha_{ns}=\int_0^a\left\{\frac{n_0h^2}{2m_s}\left[\left(\frac{d\Psi}{dx}\right)^2+\left(\frac{eA\Psi}{hc}\right)^2\right]+f(\Psi)+\frac{1}{8\pi}\left(\frac{dA^2}{dx}\right)\right\}dx-x_0\frac{H_c^2}{8\pi}+(a-x_0)\frac{H_c^2}{8\pi}. \quad (4.5)$$

The last two terms subtract off the energy of the ideal boundary, $+H_c^2/8\pi$ in the normal and $-H_c^2/8\pi$ in the superconducting regions. Equations for A and Ψ determined by the variational method are those given in Sec. III, Eqs. (3.4) and (3.5). The variations δA and $\delta\Psi$ are required to vanish at both limits, the former by consequence of Eq. (4.4). Because the flux is the same for the ideal and actual boundaries, there is no difference between using Helmholtz or Gibbs free energies.

There is an integral of Eqs. (3.4) and (3.5) which can be used to simplify the expression for the energy:

$$\frac{n_0h^2}{2m_s}\left(\frac{d\Psi}{dx}\right)^2+\frac{1}{8\pi}\left(\frac{dA}{dx}\right)^2=f(\Psi)+\frac{e^2n_0\Psi^2A^2}{2m_sc^2}+\frac{H_c^2}{8\pi}. \quad (4.6)$$

The constant of integration $H_c^2/8\pi$ is chosen to give the proper values outside of the transition zone. In the normal region,

$$\Psi=d\Psi/dx=f(\Psi)=0, \quad (4.7)$$

$$dA/dx=H=H_c. \quad (4.8)$$

In the superconducting region,

$$A=dA/dx=d\Psi/dx=0, \quad (4.9)$$

$$f(\Psi)=-H_c^2/8\pi. \quad (4.10)$$

Equations (4.7) to (4.10) are the boundary conditions for the differential equations.

Equation (4.6) may be used to eliminate the derivatives in (4.5), and there results

$$\alpha_{ns}=2\int_0^a\left[f(\Psi)+\frac{e^2n_0\Psi^2A^2}{2m_sc^2}\right]dx+2(a-x_0)\frac{H_c^2}{8\pi}. \quad (4.11)$$

Equations (3.4) and (3.5) are nonlinear and it is not possible to get general integrals. We shall derive an expression for α_{ns} which applies when the width of the transition region is large compared with the penetration depth so that most of the energy comes from the transition region in the superconducting phase where $H\ll H_c$.

The expression for α_{ns} derived by use of the two-fluid model for $f(\Psi)$ [Eq. (2.19)] agrees with a similar limiting expression derived by Ginsburg and Landau from (2.4) in the high-temperature limit ($t=T/T_c\sim 1$) and with a result we had derived earlier from (2.11) in the low-temperature limit ($t\ll 1$). The expression for α_{ns} derived from (2.4) and (2.11) differs by less than 20 percent, so that it does not make a great deal of difference which form is taken for $f(\Psi)$.

We shall also give results obtained from a numerical integration of the equations by use of a differential analyzer at the Bell Telephone Laboratories and by the digital computor at the University of Illinois. Equation (2.11) was used for $f(\Psi)$ in this calculation, so that the results apply strictly only in the low-temperature limit. It is not believed that the two-fluid model would give results which are very different. This numerical calculation is not restricted to the limiting case of a wide transition region.

Two-Fluid Model

Equations (3.4) and (3.5) may be simplified by use of the following reduced variables:

$$U=\Psi/\Psi_s, \quad \xi=x/\lambda, \qquad V=eA\lambda/\hbar c, \quad s=eH_c\lambda^2/\hbar c, \quad (4.12)$$

in which λ is the usual penetration depth as given by

$$\lambda^2=m_sc^2/(4\pi n_s\Psi_s^2e^2), \quad (4.13)$$

and Ψ_s is the equilibrium value of Ψ in the superconducting state:

$$\Psi_s^2=1-t^4. \quad \text{[See Eq. (2.15).]}$$

With this notation, Eqs. (3.4) and (3.5) become:

$$\frac{d^2U}{d\xi^2}=s^2\frac{4\pi}{H_c^2}\frac{df}{dU}+V^2U, \quad (4.14)$$

$$\frac{d^2V}{d\xi^2}=U^2V. \quad (4.15)$$

In (2.19) we replace Ψ by $U\Psi_s$ and obtain:

$$(4\pi/H_c^2)f(U)=(H_0^2/H_c^2)t^2[1-(1-U^2\Psi_s^2)^{\frac{1}{2}}]-\tfrac{1}{2}U^2\Psi_s^2. \quad (4.16)$$

It is to be recalled that for this model, $H_c/H_0=1-t^2$ [see Eq. (2.17)]. From (4.16), it follows that

$$\frac{4\pi}{H_c^2}\frac{df}{dU}=-\frac{1+t^2}{1-t^2}\left(1-\frac{t^2}{(1-U^2\Psi_s^2)^{\frac{1}{2}}}\right)U. \quad (4.17)$$

Limiting Cases

The limiting forms of (4.14) for low and high temperatures are:

$$d^2U/d\xi^2=(V^2-s^2)U, \qquad t\to 0; \quad (4.18)$$

$$d^2U/d\xi^2=[V^2-2s^2(1-U^2)]U, \qquad t\to 1. \quad (4.19)$$

Equation (4.19) is equivalent to the one used by Ginsburg and Landau, while we have used (4.18) for the numerical integration which will be discussed later.

The width of the transition region is determined by the dimensionless parameter s. If $s\ll 1$, the width is large compared with λ and V is appreciable only where U is small. For this limiting case it is possible to derive a general expression for the boundary energy, but we shall first consider the simpler equation (4.18) which applies for $t\ll 1$. If V^2 is neglected in comparison with s^2, the approximate solution which vanishes at the boundary $x=x_0=0$ and for which $dU/d\xi\to 0$ as $U\to 1$ is

$$U=\sin s\xi. \quad (4.20)$$

This solution joins with the solution $U=1$ in the body of the superconducting region $\xi=\pi/2s$, or $x=a=\pi\lambda/2s$.

We shall use (4.11) to calculate α_{ns}. With (4.20),

$$f(U)=-(H_c^2/8\pi)U^2=-(H_c^2/8\pi)\sin^2 s\xi. \quad (4.21)$$

The term in Ψ^2A^2 gives a negligible contribution in this limiting case, so that

$$\begin{aligned}\alpha_{ns}&=(H_c^2/8\pi)\left[2a-2\int_0^a \sin^2(sx/\lambda)dx\right]\\&=(H_c^2/8\pi)a=(\pi/2)(\lambda H_c^2/8\pi s)\\&=H_c hc/16\lambda e, \quad (t\to 0).\end{aligned} \quad (4.22)$$

The corresponding expression derived by Ginsburg and Landau from (4.19) is

$$\alpha_{ns}=(4/3)(\lambda H_c^2/8\pi s)=H_c hc/6\pi\lambda e, \quad (t\to 1), \quad (4.23)$$

which is smaller by less than 20 percent.

General Expression for Small s

A general expression for α_{ns} for the limiting case of small s may be derived from the two-fluid model by use of the integral (4.6) and the expression (4.11) for the energy. We again take the boundary for $x=x_0=0$ and neglect the contributions from the magnetic field. Equation (4.11) then becomes

$$\alpha_{ns}=2\int_0^a [f(x)+(H_c^2/8\pi)]dx, \quad (4.24)$$

and (4.6) becomes, for $x>0$,

$$\frac{n_0\hbar^2}{2m_s}\frac{(d\Psi)^2}{dx}=f(\Psi)+\frac{H_c^2}{8\pi}, \quad (4.25)$$

so that

$$\alpha_{ns}=(n_0\hbar^2/m_s)\int_0^a (d\Psi/dx)^2dx. \quad (4.26)$$

The variable of integration can be changed from x to Ψ:

$$\alpha_{ns}=(n_0\hbar/m_s)\int_0^{\Psi_a}(d\Psi/dx)d\Psi. \quad (4.27)$$

Equation (4.25) may now be used to express $d\Psi/dx$ in terms of Ψ. Using (2.19) for $f(\Psi)$, we find

$$f(\Psi)+H_c^2/8\pi=(H_0^2/8\pi)[(1-\Psi^2)^{\frac{1}{2}}-t^2]^2. \quad (4.28)$$

Therefore, from (4.25),

$$\frac{d\Psi}{dx}=\left(\frac{m_s H_0^2}{4\pi n_0\hbar^2}\right)^{\frac{1}{2}}[(1-\Psi^2)^{\frac{1}{2}}-t^2]. \quad (4.29)$$

When this result is inserted into (4.27) and the integration is carried out, we find

$$\begin{aligned}\alpha_{ns}&=(hcH_0/8\pi\lambda_0 e)(\sin^{-1}\Psi_a-t^2\Psi_a),\\&=\frac{\lambda H_c^2}{8\pi}\frac{(\Psi_a^{-1}\sin^{-1}\Psi_a-t^2\Psi_a)}{s(1-t^2)},\end{aligned} \quad (4.30)$$

where $\Psi_a=(1-t^4)^{\frac{1}{2}}$. This expression reduces to (4.22) and (4.23) in the two limiting cases and changes smoothly from one limit to the other as t varies between 0 and 1. Since the over-all change in the coefficient multiplying $(\lambda H_c^2/8\pi s)$ is less than 20 percent, either limiting form of the theory will probably give reasonably satisfactory results for all t.

Numerical Integration for Small t

Equations (4.18) and (4.15), which apply for $t\ll 1$, have been integrated numerically to obtain α_{ns} as a function of s. Integration for $s>0.2$ was carried out early in 1951 with the aid of the differential analyzer of the Bell Telephone Laboratories.[10] Because of the large variation in magnitude of the functions, this method was not satisfactory for smaller values of s. A second numerical integration, carried out later with the aid of the digital computor at University of Illinois,[10] was more accurate for smaller values of s. The two integrations are in reasonable agreement for values of s larger than about 0.3.

It is convenient to express α_{ns} in the form

$$\alpha_{ns}=g(s)(\lambda H_c^2/8\pi s), \quad (4.31)$$

or

$$\Delta=(\lambda/s)g(s),$$

[10] The author is indebted to Dr. R. W. Hamming for aid with the computations on the differential analyzer at the Bell Telephone Laboratories, and to Dr. D. J. Wheeler for aid with work done with the digital computor at the University of Illinois.

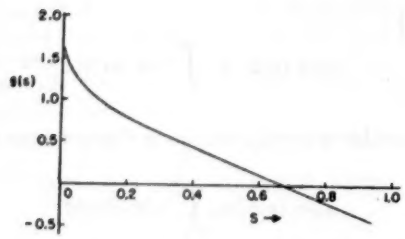

FIG. 1. Plot of $g(s)$ *versus* s [see Eqs. (4.12) and (4.31)].

where $g(s)$ is a numerical coefficient. Figure 1 is a plot of $g(s)$ as a function s. As $s\to 0$, $g(s)\to\pi/2$, in accordance with Eq. (4.22). As s increases, $g(s)$ decreases and goes through zero and becomes negative for values of s larger than about 0.68. Ginsburg and Landau find, using their value for the free energy, that α_{ns} goes through zero at $s=0.5$. A Meissner effect would not be observed if the boundary energy is negative, as it then would be favorable to form alternating lamina of normal and superconducting regions.[11] Between $s=0.1$ and 1.0, $g(s)$ varies almost linearly with s and is approximately equal to

$$g(s)\sim(1.1-1.6s). \tag{4.32}$$

It should be noted that $g(s)$ decreases rapidly from the limiting value $\pi/2$, corresponding to $s=0$, and is down by a factor of about 2 at $s=0.2$.

Comparison with Experimental Values of α_{ns}

These calculations were made with use of the free energy expression (2.11) which is valid for t small. Calculations have not been carried out using the general form of the free energy (2.19) derived from the two-fluid model. However, the errors involved in using (2.11) over the entire temperature range are probably not very large. We have seen that for s small, the various expressions for the free energy give values of α_{ns} differing by less than 20 percent.

If we assume a parabolic critical field curve, and assume that

$$\lambda^2=\lambda_0^2/(1-t^4), \tag{4.33}$$

we find that s varies as

$$s=s_0/(1+t^6). \tag{4.34}$$

Thus s changes by a factor of two between $T=0$ and $T=T_0$.

TABLE I. Values of $s_0=eH_0\lambda_0^2/\hbar c$ for various metals.

Metal	λ_0 (cm $\times 10^5$)	H_0 (gauss)	T_c (°K)	s_0
Sn	5.0	305	3.7	0.115
In	6.4	270	3.35	0.17
Pb	3.9	535	4.24	0.13
Hg	4.5	415	4.15	0.125

Table I gives values of s_0 as calculated from λ_0 and H_0 for Sn, In, Hg, and Pb. These are the only metals for which values of λ are known. Values of λ for Sn, In, and Pb are from Lock[12] and for Hg from Laurmann and Shoenberg.[13] It is to be noted that the values of s_0 are all rather small.

The width of the boundary region is of the order of λ/s. The small values of s indicate a wide transition region of the order of 10^{-4} cm. This distance is consistent with Pippard's estimate of the range of order in superconducting tin.

Our value of the boundary energy should probably be regarded as an upper limit attained only for an ideal specimen. If imperfections in the crystal limit the range of order to something less than 10^{-4} cm, the width of the boundary region and the boundary energy will both be smaller than the theoretical limit.[14]

There are as yet no reliable measurements of α_{ns}. Estimates have been made by comparing the magnetization curves obtained in the intermediate state with theory. Landau's branching model is the one most often used, but it is known that the normal lamina do not actually branch as envisaged in the theory. Further, there is evidence that the transitions in the intermediate state are not always reversible. Kuper[15] has made some estimates from a nonbranching model, but finds large differences in values of Δ estimated from different parts of the magnetization curve and there are doubts about the validity of the theory. A review of the problem is given in Shoenberg's book.[7]

We give in Table II a comparison of observed and calculated values of Δ/λ for Sn and in Table III for Hg. Other estimates of Δ/λ, both larger and smaller, can be found in Shoenberg's book. The values (L) given in Tables II and III are estimated from the slope of the falling part of the magnetization curve for transverse cylinders, as observed by Desirant and Shoenberg[9] and by Andrew,[16] and are based on Landau's branching model. Another estimate for Sn can be obtained from the measured thicknesses of the lamina in the intermediate state in a sphere. This gives[11] $\Delta\sim 5\times 10^{-5}$ cm and $\Delta/\lambda\sim 7.5$ for $T\sim 3$°K.

The calculated values are larger than most of those estimated from experiment. It is comforting that the general trend with temperature is given correctly by the theory. It would, of course, be very desirable to have more reliable measurements of boundary energies.

[11] See F. London, *Superfluids* (John Wiley and Sons, New York, 1950), p. 128.

[12] J. M. Lock, Proc. Roy. Soc. (London) **A208**, 391 (1951).

[13] E. Laurmann and D. Shoenberg, Proc. Roy. Soc. (London) **A198**, 560 (1949).

[14] A. B. Pippard, reference 3, and Proc. Roy. Soc. (London) **A216**, 547 (1953).

[15] C. G. Kuper, Phil. Mag. **42**, 961 (1951).

[16] E. R. Andrew, Proc. Roy. Soc. (London) **A194**, 98 (1948).

V. CHANGE IN SUPERCONDUCTING PENETRATION DEPTH WITH FIELD[17]

By use of a microwave method, Pippard[3] has measured the change in penetration depth with applied magnetic field. His measurements, shown by the dotted curve in Fig. 2, apply to tin and give the relative change in penetration depth between zero field and the critical field as function of temperature. The critical field itself, of course, varies with temperatures from a maximum as $T=0°K$ to zero at $T=T_c$.

It is noteworthy that the change is very small, less than 3 percent. This suggests that a linear theory should be a good approximation. The minimum near $T=3°K$ is also significant. It suggests that there are two factors affecting the penetration depth, one largest at low temperatures, becoming small near $T=T_c$ and the other large only near $T=T_c$, and dropping rapidly as the temperature is decreased.

Pippard himself accounted for the rise near $T=T_c$ as coming from a decrease in n_s near the surface. Such a

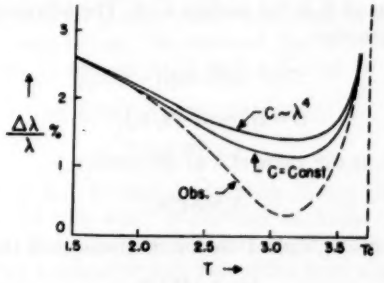

FIG. 2. Observed and calculated values of relative change in penetration depth for magnetic field $H=H_c$. Observed values from Pippard, reference 3; calculated from Eqs. (5.11) and (5.12).

decrease would allow a larger penetration of the field and a consequent decrease in free energy. The fact that the change is small suggests a rigidity or long-distance order of the superconducting electrons, and Pippard estimated that the order extends over distances of the order of 10^{-4} cm. We shall give later an estimate of this effect based on the modified Ginsburg-Landau theory.

It is believed that the increase in $\Delta\lambda/\lambda$ at low temperatures comes from essentially nonlinear terms which are left out of both the London theory and the modified theory presented here. The fact that $\Delta\lambda/\lambda$ is small indicates that the wave functions of the electrons are only slightly modified by the field. F. London suggested many years ago that superconductivity follows from such a model. He assumed that if the gauge in $\mathbf{A}$ is chosen appropriately, the wave functions are not modified at all by the field. The current density $\mathbf{j}$ is

[17] Material in this section was presented at the Washington meeting of the American Physical Society, May, 1952. See Phys. Rev. 87, 192 (1952).

TABLE II. Values of Δ for Sn, calculated and estimated from experiments on the intermediate state.

T(°K)	t	λ (cm $\times 10^5$)	s	$g(s)$	Δ/λ (calc)	Δ/λ (L)
2.1	0.56	0.53	0.0875	1.06	12	3.8
3.0	0.81	0.66	0.0695	1.14	16.5	5.6
3.5	0.94	1.06	0.061	1.17	19	6.0

then proportional to $\mathbf{A}$:

$$\mathbf{j}=-(n_s e^2/m_s c)\mathbf{A}, \tag{5.1}$$

and one is led to the London equations.

To be consistent, one should include in a linear energy terms of the first order in $\mathbf{A}$, rather than assume that Ψ is unchanged. This leads in general to an integral relation between $\mathbf{j}$ and $\mathbf{A}$:

$$\mathbf{j}(\mathbf{r})=\int g(\mathbf{r},\mathbf{r}')\mathbf{A}(\mathbf{r}')d\mathbf{r}'. \tag{5.2}$$

Pippard[14] has recently proposed a generalization of this sort for the London theory.

Terms linear in A give an energy varying quadratically with the applied field H_a. If one expands the free energy as a power series in H_a, the next higher terms will be of fourth order. These fourth-order terms come from second-order changes in the wave functions. We suggest that it is true nonlinear terms of this sort which give the change in penetration depth with field at low temperatures.

Let us then expand the free energy F in a power series in H_a and keep terms to the fourth order:

$$F=F_0+(a-\lambda)(H_a^2/8\pi)-CH_a^4, \tag{5.3}$$

where C may depend on the temperatures. We consider the penetration terms on only one plane surface of a superconducting lamina of thickness $a\gg\lambda$, and F is energy per unit area. The magnetic moment per unit area of surface is:

$$M=-F/H_a=(H_a/4\pi)(-a+\lambda+16\pi CH_a^2). \tag{5.4}$$

The effective penetration depth is

$$\lambda_{eff}=\lambda+16\pi CH_a^2. \tag{5.5}$$

The change is quadratic in the field, as observed by Pippard.[3] This effective change in λ from the fourth-order terms is in addition to changes in λ resulting from changes in n_s.

TABLE III. Values of Δ for Hg, calculated and estimated from experiments on the intermediate state.

T(°K)	t	λ (cm $\times 10^5$)	S	$g(s)$	Δ/λ (calc)	Δ/λ (L)
2.1	0.505	0.46	0.0985	1.02	10.3	2.6
3.7	0.89	0.74	0.0675	1.14	17	2.85
3.97	0.96	1.24	0.063	1.15	18	2.25

The relative change in λ at $H_a=H_c$ is

$$\Delta\lambda/\lambda=16\pi CH_c^2/\lambda. \tag{5.6}$$

If it is assumed that C is temperature independent, $\Delta\lambda/\lambda$ will vary with the reduced temperature t as

$$(\Delta\lambda/\lambda)_1\sim(1-t^2)^2(1-t^4)^{-\frac{1}{2}},\quad (H_a=H_c), \tag{5.7}$$

the first factor coming from H_c^2 and the second from λ. If it is assumed that it is the magnitude of the vector potential rather than the field which is important, C will vary as λ^4, since according to the London theory,

$$A=-\lambda H=-\lambda H_a\exp(-x/\lambda). \tag{5.8}$$

This would introduce an extra factor $(1-t^4)^{-2}$ into (5.7), so that

$$(\Delta\lambda/\lambda)_1\sim(1+t^2)^{-2}(1-t^4)^{-\frac{1}{2}},\quad (H_a=H_c). \tag{5.9}$$

Both (5.7) and (5.9) give a rapid drop in $\Delta\lambda/\lambda$ as t increases. As shown in Fig. 2, the difference between using (5.7) and (5.9) for the low-temperature contribution to $\Delta\lambda/\lambda$ is not very large.

To estimate the high-temperature contribution from the change in n_s, Pippard assumed that n_s changes uniformly in a slab of depth a adjacent to the surface. Making use of the Gorter-Casmiri two-fluid model, he found

$$\left(\frac{\Delta\lambda}{\lambda}\right)_2=\frac{\lambda}{2a}\frac{t^4}{(1-t^2)^2},\quad (H_a=H_c). \tag{5.10}$$

To get agreement with experiment, it was found necessary to take $a\sim10^{-4}$ cm.

We have attempted to fit Pippard's data by adding expressions of the form (5.10) to [(5.7) or (5.9)]. Shown in Fig. 2 are plots of the following functions:

$C=$const,

$$\frac{\Delta\lambda}{\lambda}=\frac{2.9t^4}{(1-t^2)^2(1-t^4)^2}+3.6(1-t^2)^2(1-t^4)^{-\frac{1}{2}}; \tag{5.11}$$

$C\sim\lambda^4$,

$$\frac{\Delta\lambda}{\lambda}=\frac{2.65t^4}{(1+t^2)^2(1-t^4)^{\frac{1}{2}}}+\frac{3.35(1-t^2)^{\frac{1}{2}}}{(1+t^2)^2}. \tag{5.12}$$

The only significance that can be attached to the comparison between observed and calculated values of $\Delta\lambda/\lambda$ is that the minimum occurs at about the right temperatures. Dr. Pippard has informed the author that, because of experimental uncertainties, the minimum on the observed curve may not actually be as deep as indicated.

The change in n_s near $T=T_c$ may also be estimated from the theory of Secs. II and III, but when this is done it is found that the calculated values are too small. This may indicate that because of imperfections the range of order may be less than the theoretical limit.

We shall give a brief outline of the theory. The difference between the Gibbs free energy in the superconducting and normal states is

$$G_s-G_n=\int_0^a\left\{\frac{n_0h^2}{2m_s}\left[\left(\frac{d\Psi}{dx}\right)^2+\left(\frac{eA\Psi}{hc}\right)^2\right]+f(\Psi)+\frac{1}{8\pi}\left(\frac{dA}{dx}\right)^2-\frac{H_a^2}{8\pi}-H_a\cdot M\right\}dx, \tag{5.13}$$

where the magnetization is

$$M=(H-H_a)/4\pi. \tag{5.14}$$

The boundary conditions are

$$H=H_a \text{ at } x=0, \tag{5.15}$$

$$\Psi\to\Psi_s \text{ and } A\to0 \text{ for } x \text{ large}. \tag{5.16}$$

We assume, and this will be justified by the results, that Ψ does not change much when A has an appreciable value and may be taken to be a constant Ψ_s equal to the value of Ψ at the surface $x=0$. The solutions for A and H are then

$$A=-\lambda_sH_a\exp(-x/\lambda_s), \tag{5.17}$$

$$H=H_a\exp(-x/\lambda_s), \tag{5.18}$$

where λ_s is the value of λ at the surface,

$$\lambda_s=\lambda_0/\Psi_s. \tag{5.19}$$

The terms dependent on the magnetic field then give

$$(a-\lambda_s)H_a^2/8\pi, \tag{5.20}$$

so that

$$G=\int_0^a\left[\frac{n_0h^2}{2m_s}\left(\frac{d\Psi}{dx}\right)^2+f(\Psi)\right]dx+(a-\lambda_s)\frac{H_a^2}{8\pi}. \tag{5.21}$$

The variation of G with Ψ after an integration by parts gives

$$\delta G=\delta\Psi_s\left[-\frac{n_0h^2}{2m_s}\left(\frac{d\Psi}{dx}\right)_s+\frac{\lambda_0}{\Psi_s^2}\frac{H_a^2}{8\pi}\right]+\int_0^a\delta\Psi\left[-\frac{n_0h^2}{2m_s}\frac{d^2\Psi}{dx^2}+\frac{df}{d\Psi}\right]dx. \tag{5.22}$$

Setting $\delta G=0$, we have

$$\left(\frac{d\Psi}{dx}\right)_s=\frac{\lambda_0}{\Psi_s^2}\frac{m_sH_0^2}{8\pi n_0h^2}, \tag{5.23}$$

$$\frac{d^2\Psi}{dx^2}=\frac{df}{d\Psi}\frac{m_s}{n_0h^2}. \tag{5.24}$$

The equations can be simplified by using the reduced variables U, s, ξ [see Eqs. (4.12)]. With $H_a=H_c$, we

have

$$\left(\frac{dU}{d\xi}\right)_s=\frac{s^2}{2}, \tag{5.25}$$

$$\frac{d^2U}{d\xi^2}=\frac{4\pi s^2}{H_c^2}\frac{df}{dU}. \tag{5.26}$$

A first integral of (5.26) which satisfies the boundary conditions for ξ large is

$$(dU/d\xi)^2=(8\pi s^2/H_c^2)[f(U)-f(\Psi)]. \tag{5.27}$$

Since U is nearly equal to unity, we may write

$$U_s=1-\delta U_s. \tag{5.28}$$

From (5.25) and (5.27), we have to the first order in U,

$$\delta U_s=\frac{\Delta\lambda}{\lambda}=\frac{s_0 t^2}{2(1+t^2)^2}. \tag{5.29}$$

It will be recalled (Table I) that s_0 for tin is about 0.115. At $t=1$, we then have $\delta U_s\sim 0.015$. The observed values of $\Delta\lambda/\lambda$ are at least two or three times larger, and perhaps more serious, the observed rise in $\delta\lambda/\lambda$ as T approaches T_c is more rapid than indicated by (5.29).

VI. CONCLUDING REMARKS

Thin Films

Ginsburg and Landau apply their theory to magnetization of thin films. If the film thickness is very small, n_s will not vary much across the film, but in the presence of a magnetic field may differ from the equilibrium value for bulk material. They show that in such a case the thermal transition in a magnetic field may be second order rather than first order. The value of n_s then starts at 0 as the critical temperature is reached and increases gradually as the temperature is lowered.

Our theory would yield results equivalent to those obtained by Lock by a direct application of the Gorter-Casimir two-fluid model to thin films. Lock found that allowing n_s to vary did account for some features of the observed magnetization curves, but that other nonlinear effects are probably present as well. Pippard has applied a similar analysis to small spheres and has used the results to explain some aspects of the colloid experiments of Shoenberg.

Connection with Range of Order

Pippard[14] has suggested a modification of the London equations so as to take into account a range of order of the superconducting electrons. In a pure metal, such as tin, the range is about 10^{-4} cm, but is less in an impure metal or alloy. He suggests an integral relation, such as (5.2), for the connection between current density and vector potential, and points out that such a modification of the London theory would require a corresponding modification of the Ginsburg-Landau theory. The same remarks would apply to our theory as well. Earlier,[15] Pippard discussed boundary energies in a qualitative way from the same point of view. Some of his conclusions differ from those of the Ginsburg-Landau theory.

It appears to the author that such a modification of the London equations is required, and is, in fact, suggested by quantum-mechanical approach of Sec. V. However, there do not seem to be strong reasons for taking for $g(\mathbf{r},\mathbf{r}')$ in (5.2) the particular expression chosen by Pippard. While it would not be difficult to modify our theory along similar lines, it is probably not worth while to do so until more is known about the correct form of $g(\mathbf{r},\mathbf{r}')$.

On the whole, our theory, as well as that of Ginsburg and Landau, gives values for the boundary energy which are too large and for the change in penetration depth with field which are too small. Both indicate that the "range of order" given by the theory is too large. It is possible that the theoretical results apply to ideal crystals as a result of imperfections of one sort or another. It is more likely, however, that it is the theory which is defective. It is uncertain whether or not a modification along the lines of the preceding paragraph would give better results. Pippard suggests that the "range of order" should be determined by the uncertainty relations (1.1) and (1.2), and that Δ should be roughly inversely proportional to T_c, and thus large for metals with low T_c, such as Al, and small for metals with large T_c, such as Pb. Faber[16] has proposed a test to distinguish between the Ginsburg-Landau type of theory and the suggestion of Pippard.

ACKNOWLEDGMENTS

The author is indebted to many of his colleagues for illuminating discussions. Dr. Paul Marcus made valuable contributions to the application of the two-fluid model and to the thermodynamical formulation, and Dr. R. W. Hamming and Dr. D. J. Wheeler helped with the numerical computations.

[14] A. B. Pippard, Proc. Cambridge Phil. Soc. **47**, 617 (1951).

[15] In a talk at the Third International Conference on Low-Temperature Physics and Chemistry, Rice Institute, Houston, Texas, 1953, R. Faber suggested a method for testing the phenomenological theory. From Eq. (4.31) and the expression for s in (4.12), it follows that $\Delta H_c\lambda=(\hbar c/e)g(s)$. Since the quantity $g(s)$ does not vary much when s is small, the right-hand side and thus the product $\Delta H_c\lambda$ should be nearly the same for different superconductors. He plans to compare values of the product for Al and Sn, for which H_c differs by a factor of about 3.

Resistance Anomalies in Some Rare-Earth Metals*

R. J. ELLIOTT†
Department of Physics, University of California, Berkeley, California
(Received January 27, 1954)

It is shown that the anomalies observed in the resistance of the lighter rare-earth metals can be explained in form and order of magnitude by a simple model of the interaction between the conduction electrons and the f electrons which are tightly bound to each atom. The f electrons interact with the crystal field set up by the surrounding atoms, so that there is a Stark splitting of their energy levels. The extra resistance arises because ion cores with f electrons in different states present different cross sections to the conduction electrons, and also because the conduction electrons can knock ions from one state to another. All exchange effects are neglected.

I. INTRODUCTION

WITH the advance made in the techniques of separation of the rare earths,[1] considerable quantities of the pure metals of these elements have become available and a beginning has been made in the investigation of their remarkable properties. These are so complicated, however, that the problem of finding a general theory which explains all the properties appears very difficult. It therefore seemed worth while to consider a very specific problem and to see whether an explanation of the resistance anomalies occurring in the measurements of James, Levgold, and Spedding[2] on cerium, praseodymium, and neodymium could be explained on a simple model.

Some features of a reasonable model are readily suggested by the known properties of all the rare-earth metals. Measurements of their magnetic susceptibility[3,4] over a temperature range show that, with two notable exceptions (europium and ytterbium), the metals have a paramagnetism similar to that of the corresponding trivalent rare-earth ions in ionic crystals.[5] This, together with the great similarity displayed by all the metals in general metallic properties and crystal structure,[3] has lead to the belief that a good basic approximation for these substances is to consider that all the atomic electrons are tightly bound around the nuclei at the lattice points except three per atom which form the conduction electrons. The configuration of a free rare-earth atom is often $4f^n5s^25p^65d6s^2$ outside inner closed shells, where the $5d6s^2$ electrons are loosely bound and readily lost, to form the trivalent ion in chemical compounds, and become the metallic conduction electrons. This model accounts for the fact that the metals are similar to each other in all properties depending largely on these electrons but differ widely in the properties which depend on the inner $4f$ electrons as n varies from 0 to 14 along the series. Thus ignoring the closed shells of electrons on each atom the problem is essentially that of finding the eigensolutions for the conduction electrons and the f electrons taking all the interactions into account. The four most important considerations are as follows.

(1) The energy band structure for the conduction electrons is required for an understanding of the resistivity and to find a reasonable approximation for the eigenfunctions of these electrons in order to discuss the effects of their interaction with the $4f$ electrons. Measurements[2] show an extremely high resistivity of a magnitude ($\sim 10^{-4}$ ohm-cm) similar to that shown by other metals with three conduction electrons (e.g., Sc), due possibly to overlapping bands.

(2) The interaction between the f electrons on the various atoms is important because it is the most probable cause of the ferromagnetism exhibited by gadolinium and those elements following it in the second half of the series.

(3) The f electrons will interact with the crystalline electric field set up by the lattice, and there will be a Stark splitting of the energy levels of each individual trivalent ion, similar to that observed in crystalline salts of the rare earths.[6]

(4) The interaction between the f electrons and the conduction electrons will affect the conductivity, and also possibly the ferromagnetism in the way proposed by Zener.[7]

The importance of these various interactions is indicated by other measurements on the lighter rare earths which we are considering. They are found to have a magnetic susceptibility which obeys Curie's law down to quite low temperatures, and do not appear to be ferromagnetic or antiferromagnetic. Measurements of specific heat by Parkinson *et al.*[8] have shown that in the main the quantity is very similar in all four metals (La, Ce, Pr, and Nd). This is not surprising since the lattices and conduction electrons are the same in all

* Assisted by the U. S. Office of Naval Research and the U. S. Signal Corps.
† Now at Atomic Energy Research Establishment, Harwell, Berkshire, England.
[1] F. H. Spedding *et al.* See, for example, J. Am. Chem. Soc. **72**, 2349 (1950).
[2] James, Levgold, and Spedding, Phys. Rev. **88**, 1092 (1952).
[3] W. Klemm and H. Bommer, Z. anorg. u. allgem. Chem. **231**, 138(1937).
[4] M. F. Trombe, Ann. Physik **7**, 385 (1937).
[5] J. H. VanVleck, *Theory of Electric and Magnetic Susceptibilities* (Oxford University Press, London, 1932).
[6] W. G. Penney and R. Schlapp, Phys. Rev. **41**, 194 (1932).
[7] C. Zener, Phys. Rev. **81**, 440 (1951); **83**, 299 (1951).
[8] Parkinson, Simon, and Spedding, Proc. Roy. Soc. (London) **A207**, 137 (1951).

four. However, the last three have an extra specific heat, not present in La, which displays a number of maxima (a sharp one in cerium at 12°K, two in neodymium at 7.5 and 19°K, and a broad maximum at 65°K in praseodymium). The explanation proposed by Parkinson *et al.*[8] is that this extra specific heat is from Schottky anomalies due to the Stark splitting of the f electrons mentioned in (3). They find that (except in Pr) the agreement is not particularly good and that some of the specific heat maxima are sharp and appear to come from some cooperative phenomenon. This would probably arise from (2) and just possibly (4). It is not clear, however, that these specific heat anomalies are associated with the onset of ferro- or antiferromagnetism. In particular it may be noticed that the anomalies in the resistance which occur at about the same temperatures appear to be different in form from those which occur near the known Curie temperatures of ferromagnets like gadolinium.[9]

We therefore propose to consider the effect on the resistance of a metal in which the core electrons localized on each lattice point have a number of low-lying energy levels [arising from Stark splitting (3)] but to neglect the interaction between these f electrons. It is found that an extra resistance is introduced of a form which will explain the observed anomalies. Unfortunately any calculation including the cooperative effects of (2) and (4) to try and account for the form of the specific heat anomalies seems very difficult and will not be attempted here.

2. MECHANISM FOR EXTRA RESISTANCE

The extra resistance is found to arise from two causes, each of which gives an effect of the same order and with the same temperature dependence.

(a) The conduction electrons can be inelastically scattered off an ion which is knocked from one energy state to another by giving or taking energy from the motion of the conduction electron.

(b) At finite temperatures there will be ions in these various energy states arranged at random on the lattice points and these numbers will vary, of course, with temperature according to the Boltzmann distribution. Since ions in these states will present slightly different cross sections for the elastic scattering of the conduction electrons, this scattering and thus the resistance will vary with the population and with temperature.

We start with the simplest case. Let us suppose that the metal lattice, volume V, is composed of N ions which have two energy levels separated by an energy Δ. Then in equilibrium the Boltzmann distribution gives the number of atoms in the lowest state,

$$N_l = N/(1+d), \quad \text{where} \quad d = e^{-\Delta/kT},$$

and the number in the upper state,

$$N_u = Nd/(1+d). \tag{1}$$

[8] Levgold, Spedding, Barson, and Elliott, Revs. Modern Phys. **25**, 129 (1953).

We use the wave vector $\mathbf{k}$ to describe the states of the conduction electrons, and define a distribution function $f(\mathbf{k})$ such that the number of electrons whose wave vectors lie in the interval $d\mathbf{k}$ about $\mathbf{k}$ is

$$[2V/(2\pi)^3] f(\mathbf{k}) d\mathbf{k}. \tag{2}$$

Following the usual discussion of resistivity[10] in terms of the Boltzmann equation, we require the rate of change in $f(\mathbf{k})$ with time due to interactions with the lattice denoted by $[\partial f/\partial t]_{\text{coll}}$. Now here $[\partial f/\partial t]_{\text{coll}}$ is the total change in f due to the excess of the number of electrons entering $\mathbf{k}$ over those leaving due to scattering of the ions making up the lattice, and if $W(\mathbf{k},\mathbf{k}')$ is the probability per unit time that an electron in state $|\mathbf{k}\rangle$ is scattered into state $|\mathbf{k}'\rangle$,

$$[\partial f/\partial t]_{\text{coll}} = \int \{W(\mathbf{k}',\mathbf{k}) f(\mathbf{k}')[1-f(\mathbf{k})] - W(\mathbf{k},\mathbf{k}') f(\mathbf{k})[1-f(\mathbf{k}')]\} d\mathbf{k}', \tag{3}$$

where the extra factors weight the process to ensure that there was an electron in the initial state and a vacancy in the final state. Now if $\mathcal{H}_{el}$ is the Hamiltonian of interaction between the lattice and an electron, and $|N_u,\mathbf{k}\rangle$ denotes a state of the system in which N_u ions are in the upper state and the electron has wave vector $\mathbf{k}$,

$$W(\mathbf{k},\mathbf{k}') = \sum_{N_u, N_u'} \frac{2\pi}{\hbar} |\langle N_u\mathbf{k}|\mathcal{H}_{el}|N_u',\mathbf{k}'\rangle|^2 \rho(\mathbf{k}') \times \delta[E(N_u,\mathbf{k}) - E(N_u',\mathbf{k}')], \tag{4}$$

where $\rho(\mathbf{k}')$ is the density of energy levels at $\mathbf{k}'$ and the δ function ensures energy conservation.

There are two kinds of terms which contribute to the sum in (4). The first are those terms which have $N_u = N_u'$, i.e., those which represent elastic scattering mentioned as (b) above. Of course, if $N_u = 0$, the matrix element is zero for there can be no scattering by a perfectly periodic lattice. If $N_u \neq 0$, however, the potential seen by the electron is no longer exactly periodic. The situation is exactly equivalent to that of resistivity in disordered alloys previously discussed by Nordheim[11] and Mott.[12] Since the difference between atoms as seen by the conduction electrons is entirely in the angular dependence of the charge in the f shell it will be small and can be considered by Nordheim's approximation. In this case the interaction Hamiltonian $\mathcal{H}_{el}$ is written as the sum of two terms, one representing the interaction between the conduction electrons and the f electrons, and the other between them and the rest of the charge complex of the ions. This latter term gives zero because it is periodic with the lattice. The former

[10] See, for example, A. H. Wilson, *The Theory of Metals* (Cambridge University Press, Cambridge, 1936).
[11] L. Nordheim, Ann. Physik **9**, 607 (1931).
[12] N. F. Mott, Proc. Cambridge Phil. Soc. **32**, 281 (1936).

term can be written as a screened Coulomb potential,

$$\sum_n \frac{e^2}{|\mathbf{r}_n-\mathbf{R}|}\exp(-|\mathbf{r}_n-\mathbf{R}|/q)=\sum_n h_n, \qquad (5)$$

by using the simplification of one f electron per ion, and letting the one on the ion at the nth lattice point $\mathbf{a}_n$ be at $\mathbf{r}_n$ from that point, while the conduction electron is at $\mathbf{R}$.

Then

$$\langle N_u,\mathbf{k}|\mathcal{H}_{el}|N_u,\mathbf{k}'\rangle=\sum_n\langle\psi_n,\mathbf{k}|h_n|\psi_n,\mathbf{k}'\rangle, \qquad (6)$$

where ψ_n is the wave function of the f electron near the nth lattice point, which can be the eigenfunction associated with the lower or the upper state, $\psi(l)$ or $\psi(u)$. Remembering that the expression (6) was zero if all the lattice points were alike, we can write it

$$\sum_n{}_u[\langle\psi_n(l),\mathbf{k}|h_n|\psi_n(l),\mathbf{k}'\rangle - \langle\psi_n(u),\mathbf{k}|h_n|\psi_n(u),\mathbf{k}'\rangle], \qquad (7)$$

where the summation is over those lattice points n where the electron is in the upper state. Then the square of the matrix element becomes

$$|\sum_n{}_u \exp[i(\mathbf{k}-\mathbf{k}')\cdot\mathbf{r}_n]|^2|\langle\psi_n(l),\mathbf{k}|h_n|\psi_n(l),\mathbf{k}'\rangle - \langle\psi_n(u),\mathbf{k}|h_n|\psi_n(u),\mathbf{k}'\rangle|^2, \qquad (8)$$

and since the points in the sum are randomly distributed the first factor can be written $N_u(1-N_u/N)$ a d so, calling the difference of the matrix elements A and using Eq. (1), (8) becomes

$$N|A|^2/(1+d)^2. \qquad (9)$$

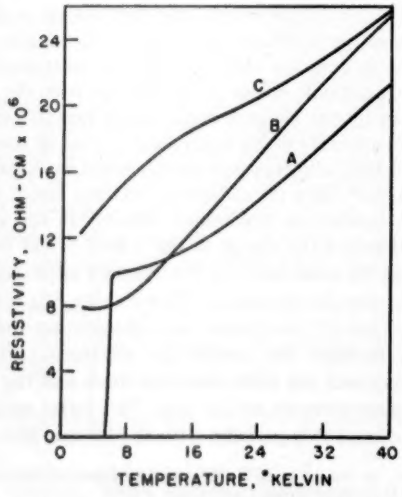

FIG. 1. Typical curves of resistivity *vs* temperature (after James *et al.*[9]). A. lanthanum, B. praseodymium, C. neodymium.

To proceed we must assume something about the conduction electron distribution function and energy. Making the simple assumption of isotropic effective mass m^* the usual treatment leads to a resistivity[10]

$$\rho=\frac{m^*}{ne^2\tau(k_0)}=\frac{NVd(2m^*)^{5/2}\epsilon^{1/2}}{(1+d)^2ne^2\hbar^4 4\pi}\int_0^\pi |A|^2(1-\cos\theta)d(\cos\theta), \qquad (10)$$

where n is the number of conduction electrons per unit volume and k_0 is the length of the wave vector of electrons having the Fermi energy ϵ. ρ depends on temperature like $\mathrm{sech}^2(\Delta/2kT)$.

Since we are assuming that there is no interaction between the f electrons on different lattice sites, the only other terms of importance in (4) are those where $N_u-N_u'=\pm1$, and the problem is simply that of inelastic scattering of the conduction electrons off a set of atoms with two energy levels and (4) becomes

$$W(\mathbf{k},\mathbf{k}')=\frac{2\pi}{\hbar}\{|\langle\psi_n(l),\mathbf{k}|h_n|\psi_n(u),\mathbf{k}'\rangle|^2N_l\delta[E(\mathbf{k}) - E(\mathbf{k}')-\Delta]+|\langle\psi_n(u),\mathbf{k}|h_n|\psi_n(l),\mathbf{k}'\rangle|^2 \times N_u\delta[E(\mathbf{k})-E(\mathbf{k}')+\Delta]\}\rho(\mathbf{k}'). \qquad (11)$$

In our approximation the matrix elements are the same [equal $B(\mathbf{k},\mathbf{k}')$, say], and substituting (11) into (3) we find

$$[\partial f/\partial t]_{\text{coll}}=\int\frac{2V|B|^2}{\hbar(2\pi)^2}\{[N_l f(\mathbf{k}')(1-f(\mathbf{k})) - N_u f(\mathbf{k})(1-f(\mathbf{k}'))]\delta(E(\mathbf{k})-E(\mathbf{k}')+\Delta) +[N_u f(\mathbf{k}')(1-f(\mathbf{k}))-N_l f(\mathbf{k})(1-f(\mathbf{k}'))] \times\delta(E(\mathbf{k}')-E(\mathbf{k})+\Delta)\}d\mathbf{k}'. \qquad (12)$$

If we take $\Delta\ll\epsilon$, this expression yields τ exactly as the above and we get an additional resistance of the form:

$$\rho=\frac{NdV(2m^*)^{5/2}\epsilon^{1/2}}{(1+d)^2ne^2\hbar^4\pi}\int_0^\pi|B|^2(1-\cos\theta)d(\cos\theta), \qquad (13)$$

which has exactly the same form as Eq. (10) except that $|A|$ has been replaced by $2|B|$. Thus the whole of the extra resistance depends on temperature like $\mathrm{sech}^2(\Delta/2kT)$.

These formulas can easily be generalized to include the case where there are an arbitrary number of energy levels for the f electrons; the energy of the ith being Δ_i and there being n_i atoms in this state at an arbitrary temperature T. If we further denote a matrix element like in Eq. (7) for elastic scattering off an ion in the ith and jth levels as in Eq. (20) by $B_{ij}(\mathbf{k},\mathbf{k}')$, the resistance arising from the first process is by analogy with Nord-

heim,[11]

$$\rho=\frac{V(2m^*)^{3/2}\epsilon^{1/2}}{ne^2\hbar^4 4\pi}\int_0^\pi\Big[\sum_i n_i|A_i(\mathbf{k},\mathbf{k}')|^2 - \frac{1}{N}|\sum_i n_i A_i(\mathbf{k},\mathbf{k}')|^2\Big](1-\cos\theta)d(\cos\theta), \quad (14)$$

and the second process gives

$$\rho=\frac{V(2m^*)^{3/2}\epsilon^{1/2}}{ne^2\hbar^4\pi}\int_0^\pi\sum_{i>j}\frac{n_i n_j}{n_i+n_j}|B_{ij}(\mathbf{k},\mathbf{k}')|^2 \times(1-\cos\theta)d(\cos\theta). \quad (15)$$

3. APPLICATION TO THE RARE EARTHS

In Fig. 1 a curve of resistivity *vs* temperature is plotted to display the temperature dependence of this extra resistivity $\rho=\rho_0\,\mathrm{sech}^2(\Delta/2kT)$. With it is also plotted a typical curve for the resistivity arising from electron scattering by the lattice waves,

$$\rho=AT\Theta^{-1}G(\Theta/T), \quad (16)$$

where A is a constant, G the Grüneisen function,[13] and Θ the Debye temperature. The total resistivity of a hypothetical rare-earth metal where each ion has two energy levels separated by Δ would, on our model, be the sum of two such effects. A particular curve representing this sum when $k\Theta=10\Delta$, and $A=5\rho_0$, is also plotted.

In Fig. 2 typical experimental curves are shown for La, Pr, and Nd, taken from Spedding's data.[2] (Actually the results always varied slightly from sample to sample, and with treatment of sample, but for these three the curves are all similar. In the case of Ce the results varied much more, probably due to phase transitions.) It will be seen that, except for the superconducting transition in La (curve *A*) and a residual resistance in Pr (curve *B*), both resistivities are very similar in form to the typical curve for lattice scattering (II), if Θ is given the Debye value $\sim 130°\mathrm{K}$ [8] and $A\sim 40\times10^{-6}$ ohm-cm. This agrees with our model since La has no *f* electrons, and in Pr the specific heat anomaly indicates that $\Delta/k\sim 150°\mathrm{K}$ and so resistivity like I would not be appreciable below 30°K. On the other hand, the specific heat anomalies indicate that in Nd there is a $\Delta/k\sim 15°\mathrm{K}$ (i.e., $\sim\Theta/10$) and we expect a curve like III in Fig. 1 (if we neglect the effect of higher levels), as is in fact observed (curve *C*). ρ_0 would have to be chosen $\sim 10^{-5}$ ohm-cm to agree with experiment. The general form of the observed curves in Ce is the same as in Nd and here it appears $\Delta/k\sim 25°\mathrm{K}$ so they can be explained in the same way. We have not considered them in detail because of the complication of the phase transition.

[13] E. Grüneisen, Ann. Physik **16**, 530 (1933).

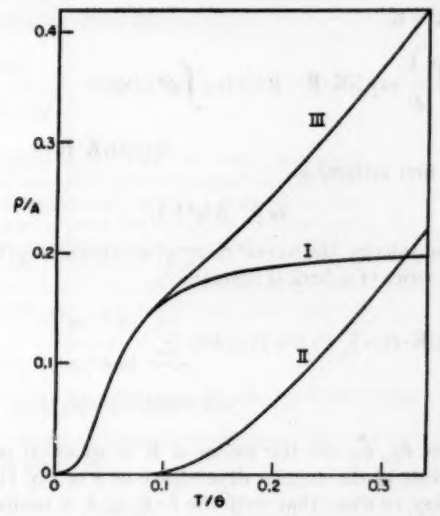

FIG. 2. Theoretical curves. I. The extra resistvity, $\rho=\frac{1}{2}A\times\mathrm{sech}^2(\Theta/20kT)$. II. Resistivity from lattice waves, $\rho=AT\Theta^{-1}\times G(T/\Theta)$. III. Sum of I and II.

It is therefore of interest to calculate the expected value of ρ_0 from our model. This reduces to evaluating the matrix elements A and B in Eqs. (10) and (13). By using the interaction Hamiltonian of Eq. (5), and assuming that the conduction electron wave functions can be written as normalized plane waves,

$$(1/\sqrt{V})\exp(i\mathbf{k}\cdot\mathbf{R}), \quad (17)$$

any A_i or B_{ij} can be written in terms of the integrals

$$\frac{1}{V}\int\int\exp[i(\mathbf{k}-\mathbf{k}')\cdot\mathbf{R}]\psi^*(j)\psi(i) \times\frac{e^2\exp(-|\mathbf{r}-\mathbf{R}|/2)}{|\mathbf{r}-\mathbf{R}|}d\tau_r d\tau_R, \quad (18)$$

where $\psi(i)$ is the wave function of the *f* electrons in the *i*th state and is a function of the positions $\mathbf{r}$ of these electrons. We assume for simplicity that each ion has one *f* electron and

$$\psi(i)=\frac{1}{(8!\rho^9)^{\frac{1}{2}}}r^3\exp(-r/\sigma)\Big[\sum_{m=-3}^{3}a_i^m Y_3^m(\theta,\phi)\Big]. \quad (19)$$

The electron wave function has, of course, the same radial dependence (here written as hydrogenic) but each state has a different angular dependence given by an appropriate linear combination of zonal harmonics of order 3. The actual values of the a_i^m are determined by the crystalline electric field, and the linear combinations for each *i* are normalized and orthogonal.

The integral in Eq. (18) can be separated by the transformation $(\mathbf{r}-\mathbf{R})\to\mathbf{R}$, $\mathbf{r}\to\mathbf{r}$ and becomes, writing

$\mathbf{k}-\mathbf{k}'=\mathbf{K}$,

$$\frac{e^2}{V}\int\frac{1}{R}\exp(i\mathbf{K}\cdot\mathbf{R}-R/q)d\tau_R\int\psi^*(j)\psi(i)\times\exp(i\mathbf{K}\cdot\mathbf{R})d\tau_r. \quad (20)$$

The first integral is

$$4\pi q^2/(K^2q^2+1). \quad (21)$$

Considering the second integral we expand $\exp(i\mathbf{K}\cdot\mathbf{r})$ in a series of spherical harmonics:

$$\exp(i\mathbf{K}\cdot\mathbf{r})=\sum_l i^l(2l+1)j_l(Kr)\sum_{m=-l}^{+l}\frac{(n-|m|)!}{(n+|m|)!}\times Y_l^m(\theta,\phi)Y_l^{-m}(\theta_K,\phi_K), \quad (22)$$

where θ_K, ϕ_K are the angles of $\mathbf{K}$ in spherical polars. Because of the angular dependence on θ of Eq. (19), it is easy to show that only the $l=0$, 2, 4, 6 terms contribute to the integrals. Further one can show that the integral arising from the $l=0$ term is zero unless $i=j$ and independent of i if $i=j$. Therefore the matrix element A which is the difference of two such integrals, and B where $i\neq j$, arise from terms $l=2$, 4, 6 only and are of the same order of magnitude. Even with these simplifications the integrals unsolved are very laborious, and it is not worth while to pursue them for an order of magnitude calculation such as this.

We therefore proceed with a rough numerical estimate. We assume $K\sigma\ll1$, which is fairly reasonable if the f electrons are deeply seated on the ion cores, and $\mathbf{k}$, $\mathbf{k}'$ are wave vectors at the top of a Fermi distribution of essentially free electrons. Further, in choosing as an example two states whose wave functions are like Eq. (19) with an angular dependence Y_3^0 and Y_3^2, respectively, we find for the $l=2$ term

$$B_{ij}=\frac{4\pi\rho^2e^2}{(K^2q^2+1)V}\cdot\frac{K^2\sigma^2}{4}(3/5)^{\frac{1}{2}}Y_2^2(\theta_K,\phi_K). \quad (23)$$

Averaging over all directions of $\mathbf{K}$ for a multiple crystal removes the angular dependence and remembering that in our processes $|\mathbf{k}|=|\mathbf{k}'|$, $K=2k\sin(\theta/2)$, we have

$$\int_0^\pi B^2(1-\cos\theta)d(\cos\theta)=\frac{48}{5}\int_0^2\frac{\pi^3\sigma^4q^4k^4e^4s^3ds}{V^2(2k^2q^2s+1)^2}, \quad (24)$$

where $2\sin^2(\theta/2)=s$. If we make a further assumption that $kq\ll1$, we have

$$\rho_0=192\pi^2(2m)^{5/2}\epsilon^{1/2}\sigma^4q^4k^4e^2/5h^4 \text{ electrostatic units}, \quad (25)$$

which for $\sigma=q\sim1$A, $1/k=(8\pi V/3N)^{\frac{1}{3}}\sim7$A, is $\sim10^{-6}$ ohm-cm. Of course the above approximations make this estimate very rough for it seems unlikely that plane waves are a good approximation for the conduction electrons. However it does demonstrate that the order of magnitude of the effects discussed here is the same as that of the observed anomalies.

It is interesting to note that the matrix element (23) has an angular dependence with respect to the crystal axes. This will remain true when the correct expression is calculated for A or B and arises because of the angular dependence of the f-electron wave functions. In a single crystal this ought to give rise to an anisotropy in the extra resistance, though this will of course always retain the same temperature dependence.

4. CONCLUSION

We have discussed a model of a metal where, besides the conduction electrons, there are other electrons not in closed shells tightly bound to each atom at a lattice point and shown the form of the extra term this introduces into the resistivity. It has also been shown that if such a term is added to the usual resistivity it will account for the curious temperature dependence of the resistivity of some rare-earth metals. A very rough calculation of the expected order of magnitude agrees with the observations. Therefore the model seems a good starting point for a general consideration of these metals, although for a complete discussion the cooperative interactions between the electrons will have to be taken into account.

Theory of the Hyperfine Structure of NO Molecule*

MASATAKA MIZUSHIMA
Department of Physics, Duke University, Durham, North Carolina
(Received November 20, 1953)

The theory of the hfs of the NO molecule due to the magnetic moment and the electric quadrupole moment of the N nucleus is worked out. Assuming that the electron which is rotating around the molecular axis is in a pure p state, some relations between coupling constants are derived and were found to agree with experimental relations. Hund's case (a) was taken as a starting point, but the actual deviation from case (a) was found to be not negligible and was also explained satisfactorily. The formula for the nuclear electric quadrupole effect was derived for Hund's case (a) and also for a general coupling case. This electric quadrupole effect was found to be different for Λ-type doublet states. The difference appears for every coupling case including Hund's case (a). The agreement between theory and experimental results is quite satisfactory.

1. INTRODUCTION

THE electronic ground state of the NO molecule is $^2\Pi_{\frac{1}{2}}$. In this state there are nonvanishing electronic orbital and spin angular momenta. Since the spin orbit coupling is strong compared to the end-over-end rotational energy, the spin is strongly coupled to the molecular axis [Hund's case (a); see Fig. 1]. In this case the molecular magnetic moment is parallel to the molecular axis and has the magnitude $\beta\Lambda+2\beta\Sigma$, where Λ and Σ are the components of the electronic orbital and spin angular momentum, respectively, along the molecular axis and β is the Bohr magneton. In our case, it so happens that since $\Lambda=1$ and $\Sigma=-\frac{1}{2}$, these contributions almost cancel each other, and no net magnetic moment is expected, while in the next excited state $^2\Pi_{\frac{1}{2}}$, where $\Lambda=1$, $\Sigma=+\frac{1}{2}$, a large magnetic moment exists. This fact was well confirmed by the susceptibility measurements.[1]

Recently Gordy and Burrus[2] and also Gallagher, Bedard, and Johnson[2] have observed the hfs of this molecule in the $^2\Pi_{\frac{1}{2}}$ state and found that the magnetic interaction is very large, while the nuclear quadrupole term is negligible. This result seems puzzling, since there is no net magnetic moment in this state except that due to the molecular rotation which is of the order of the nuclear magneton.

Recently Frosch and Foley[3] published a theory of the hfs of this kind of molecule. They derived formulas starting from Dirac's equation and discussed the various possibilities. The work done here naturally overlaps their work appreciably, but in this paper more care was taken with the physical meaning of the coupling constant, and the formulas for the electric quadrupole hfs were newly derived.

* This research was supported by the United States Air Force under a contract monitored by the Office of Scientific Research, Air Research and Development Command.

[1] J. H. Van Vleck, *The Theory of Electric and Magnetic Susceptibilities* (The Clarendon Press, Oxford, 1932), p. 269.

[2] W. Gordy and C. A. Burrus, Phys. Rev. **93**, 419 (1954); Gallagher, Bedard, and Johnson, Phys. Rev. **93**, 729 (1954).

[3] R. A. Frosch and H. M. Foley, Phys. Rev. **88**, 1337 (1952). It is called FF in this paper.

2. HAMILTONIAN AND WAVE FUNCTION

The magnetic interaction between nucleus and electrons is given by

$$H_1=\sum_k \frac{g_n\beta_n\beta}{r_k^3}(\mathbf{l}_k-\mathbf{s}_k)\cdot\mathbf{I}+3\frac{(\mathbf{s}_k\cdot\mathbf{r}_k)(\mathbf{I}\cdot\mathbf{r}_k)}{r_k^2}, \quad (1)$$

where β_n is the nuclear magneton, β is the Bohr magneton, g_n is the gyromagnetic ratio of the nucleus whose spin is I, $\mathbf{r}_k$ is the distance between this nucleus and the kth electron, and $\mathbf{l}_k$, $\mathbf{s}_k$ are the orbital and spin angular momenta of the kth electron, respectively. Although FF took a different expression for this interaction term, it can be seen that their expression is equivalent to that in Eq. (1) when there is no external field and the s-state contribution is negligible, which is our case. It is convenient to express the terms as

$$\sum_k \frac{\mathbf{l}_k}{r_k^3}=\xi\mathbf{L}, \quad (2a)$$

$$\sum_k \frac{1}{r_k^3}\left\{-\mathbf{s}_k\cdot\mathbf{I}+3\frac{(\mathbf{s}_k\cdot\mathbf{r}_k)(\mathbf{I}\cdot\mathbf{r}_k)}{r_k^2}\right\}=\eta\{\zeta(\mathbf{S}\cdot\mathbf{I})-3(\mathbf{S}\cdot\mathbf{L})(\mathbf{I}\cdot\mathbf{L})\}, \quad (2b)$$

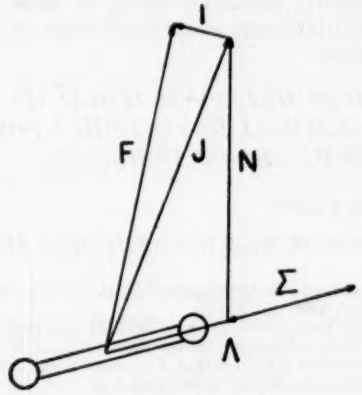

FIG. 1. Hund's case (a).

where **L**, **S** are now the total electronic orbital and spin angular momenta, ξ is an average value of r_k^{-3}, and η is $\xi/2$ in the classical case. If we assume that only one outer-shell electron is effective in the formula (1), and it is in a p state, then[4] η is $2\xi/5$ and $\zeta=2$. Inserting the formulas (2) into (1), we obtain

$$H_1=g_n\beta_n\beta\{\xi\mathbf{L}\cdot\mathbf{I}+\eta\zeta(\mathbf{S}\cdot\mathbf{I})-3\eta(\mathbf{S}\cdot\mathbf{L})(\mathbf{I}\cdot\mathbf{L})\}. \quad (3)$$

Taking z axis along the molecular axis,

$$\begin{aligned}H_1=g_n\beta_n\beta\{&\xi L_zI_z+\eta\zeta S_zI_z-3\eta S_zL_z^2I_z\\&-3\eta(S_+L_-^2I_++S_-L_+^2I_-)/4-\xi(L_+I_-+L_-I_+)/2\\&+\eta\zeta(S_+I_-+S_-I_+)/2-3\eta(S_+L_-I_-L_+\\&+S_-L_+I_+L_-+I_+L_-S_-L_++I_-L_+S_+L_-)/8\},\end{aligned} \quad (4)$$

where

$$L_+=L_x+iL_y, \quad L_-=L_x-iL_y, \quad \text{etc.}$$

The total wave function is obtained by coupling **J** and **I** into **F** by the usual procedure, where the absolute value of the component of **J** parallel to the molecular axis is $\Lambda+\Sigma$ and its perpendicular component is N, the angular momentum of the end-over-end rotation which is not well quantized in our case. There are two kinds of wave functions, in one of which $J_z=\Lambda+\Sigma=\frac{1}{2}$ and in the other $J_z=-(\Lambda+\Sigma)=-\frac{1}{2}$. Owing to the perturbation $-2B(J_xP_x+J_yP_y)$, where B is the rotational constant and P is the total electronic angular momentum, this degeneracy is removed and gives a Λ-type doublet.[5,6] If the wave function with $J_z=+\frac{1}{2}$ is denoted by $(J_+|$ and $J_z=-\frac{1}{2}$ by $(J_-|$, the proper wave functions for the nondegenerate states are $2^{-\frac{1}{2}}\{(J_+|+(J_-|\}$ and $2^{-\frac{1}{2}}\{(J_+|-(J_-|\}$. The perturbation energies due to the above operator are $-2Bf(J,\frac{1}{2})(J_+|P_x|J_-)$ and $+2Bf(J,\frac{1}{2})(J_+|P_x|J_-)$, respectively,[7] so that if we take the sign of the wave function so as to make $(J_+|P_x|J_-)$ positive, the wave function $2^{-\frac{1}{2}}\{(J_+|+(J_-|\}$ corresponds to the lower state. It is customary to denote the lower state by c and the upper state by d.[6]

3. MAGNETIC HYPERFINE STRUCTURE

The magnetic interaction energy is given by the diagonal matrix element of our Hamiltonian (4), that is, for the c state:

$$\begin{aligned}W_c&=2^{-1}\{(J_+IF|H_1|J_+IF)+(J_-IF|H_1|J_-IF)\\&\quad+(J_+IF|H_1|J_-IF)+(J_-IF|H_1|J_+IF)\}\\&=(J_+IF|H_1|J_+IF)+(J_+IF|H_1|J_-IF),\end{aligned} \quad (5a)$$

and for the d state:

$$W_d=(J_+IF|H_1|J_+IF)-(J_+IF|H_1|J_-IF). \quad (5b)$$

In Hund's case (a), we have the approximation

$$\begin{aligned}(J_+IF|H_1|J_+IF)&=g_n\beta_n\beta(\xi\Lambda+\eta\zeta\Sigma-3\eta\Sigma\Lambda^2)\\&\quad\times(J_+IF|\mathbf{z}\cdot\mathbf{I}|J_+IF),\end{aligned} \quad (6)$$

where $\mathbf{z}$ is a unit vector parallel to the molecular axis. The matrix element of $\mathbf{z}\cdot\mathbf{I}$ is shown in FF and elsewhere to be

$$\begin{aligned}(J_+IF|H_1|J_+IF)&=g_n\beta_n\beta(\xi\Lambda+\eta\zeta\Sigma-3\eta\Sigma\Lambda^2)(\Lambda+\Sigma)\\&\quad\times\{2J(J+1)\}^{-1}\{F(F+L)-J(J+1)-I(I+1)\}.\end{aligned} \quad (7)$$

In our case where $\Lambda=1$, $\Sigma=-\frac{1}{2}$, it is

$$\begin{aligned}(J_+IF|H_1|J_+IF)&=g_n\beta_n\beta(2\xi-\eta\zeta+3\eta)\{8J(J+1)\}^{-1}\\&\quad\times\{F(F+1)-J(J+1)-I(I+1)\}.\end{aligned} \quad (8)$$

As was pointed out in FF H_1 has a finite matrix element between the J_+ and J_- states. In our formula (4) this is the $S_+L_-^2I_+$ or $S_-L_+^2I_-$ term. In calculating the matrix element $(J_+IF|S_-L_+^2I_-|J_-IF)$, integrating over electronic coordinates first, S_- can be replaced by 1 and L_+ by $\{L(L+1)\}^{\frac{1}{2}}$, if the electronic angular momentum L is a good quantum number. Since because of the coupling to the molecular axis, L may not be a good quantum number, we will replace $3\eta S_-L_+^2$ by a constant, γ, which is 6η if a p-wave function is a good approximation for the electron under consideration. Thus,

$$\begin{aligned}&(J_+IF|H_1|J_-IF)\\&\quad=-g_n\beta_n\beta\gamma(J_+IF|(\mathbf{x}+i\mathbf{y})\cdot\mathbf{I}|J_-IF)/4,\end{aligned} \quad (9)$$

where $\mathbf{x}$ and $\mathbf{y}$ are unit vectors perpendicular to the molecular axis. Just as in FF, we obtain

$$\begin{aligned}(J_+IF|H_1|J_-IF)&=-g_n\beta_n\beta\gamma(2J+1)\{16J(J+1)\}^{-1}\\&\quad\times\{F(F+1)-J(J+1)-I(I+1)\}.\end{aligned} \quad (10)$$

Thus, from the formulas (5a), (5b), (8), and (10) we obtain

$$\begin{aligned}W_c&=\{a-b(2J+1)\}\{J(J+1)\}^{-1}\\&\quad\times\{F(F+1)-J(J+1)-I(I+1)\},\end{aligned} \quad (11a)$$

$$\begin{aligned}W_d&=\{a+b(2J+1)\}\{J(J+1)\}^{-1}\\&\quad\times\{F(F+1)-J(J+1)-I(I+1)\},\end{aligned} \quad (11b)$$

where

$$a=g_n\beta_n\beta(2\xi-\eta\zeta+3\eta)/8, \quad b=g_n\beta_n\beta\gamma/16. \quad (12)$$

If we take the p-electron approximation, they are

$$a=g_n\beta_n\beta(3\xi/10), \quad b=a/2. \quad (13)$$

The formulas (11a) and (11b) are already given in FF, but the sign before b was not clearly indicated there. According to our procedure there remains no ambiguity on this point. Also the relation (13) was not given in FF.

4. ELECTRIC HYPERFINE STRUCTURE

Many authors have assumed that the conventional formula can be applied in Hund's case (a) even if there

[4] See, for example, A. Abragam and M. H. L. Pryce, Proc. Roy. Soc. (London) **A205**, 135 (1951).
[5] J. H. Van Vleck, Revs. Modern Phys. **23**, 213 (1951).
[6] G. Herzberg, *Molecular Spectra and Molecular Structure, I. Diatomic Molecules* (Prentice-Hall, Inc., New York, 1939).
[7] f is the function defined in reference 5 as

$$f(J,\tfrac{1}{2})=\{J(J+1)-\tfrac{1}{4}\}^{\frac{1}{2}}.$$

exists a finite electronic spin, but it will be shown here that this is not the case.

The interaction between electrons and the nuclear electric quadrupole moment can be expressed in tensor form as

$$H_2 = \mathbf{Q}\cdot\nabla\mathbf{E}. \tag{14}$$

In Racah's formalism,[8]

$$(JIF|H_2|JIF) = (-1)^{J+I-F}(J\|\nabla E\|J)(I\|Q\|I) \times W(JIJI;F2), \tag{15}$$

where

$$(J\|\nabla E\|J) = (-1)^{-J-m}(Jm|\nabla E_0|Jm)/V(JJ2;-mm0), \tag{15a}$$

$$(I\|Q\|I) = \tfrac{1}{2}eQ\{(2I+1)(I+1)(2I+3)I(2I-1)\}^{\frac{1}{2}}, \tag{15b}$$

$$W(JIJI;F2) = (-1)^{F-J-I}6\{C(C+1) - (4/3)J(J+1)I(J+1)\}\{(2J+3)(2J+2) \times(2J+1)2J(2J-1)(2I+3)(2I+2)(2I+1) \times 2I(2I-1)\}^{-\frac{1}{2}}, \tag{15c}$$

$$C = F(F+1)-J(J+1)-I(I+1).$$

In the above formulas, V is the function defined by Racah's papers[8] and Q is the nuclear electric quadrupole moment.

In calculating the matrix element $(Jm|\nabla E_0|Jm)$, one should be careful to eliminate the electronic spin part of J. In the appendix of this paper it is shown that the wave function of the $\Pi_{\frac{1}{2}}$ state in Hund's case (a) is, if $S=\frac{1}{2}$,

$$(Jm| = (4J+2)^{-\frac{1}{2}}\{(2J-1)^{\frac{1}{2}}(KSJm| + (2J+3)^{\frac{1}{2}}(K+1SJm|\}, \tag{A6}$$

where $K=J-\frac{1}{2}$ is the sum of the angular momenta of the end-over-end rotation and the electronic orbital motion. In our case there are two possible wave functions, in one of which $K_z=1$ and in the other $K_z=-1$. If we denote them by K_+ and K_-, respectively, the Λ-type doublet can be represented by replacing $(KSJm|$ by $\{(K_+SJm|\pm(K_-SJm|\}/2^{\frac{1}{2}}$ in the formula (A6), the $+$ sign corresponds to the c state according to our definition. Thus,

$$(Jm|\nabla E_0|Jm) = (4J+2)^{-1} \times[(2J-1)(KSJm|\nabla E_0|KSJm) + (2J+3)(K+1SJm|\nabla E_0|K+1SJm) + \{(2J-1)(2J+3)\}^{\frac{1}{2}}\{(KSJm|\nabla E_0|K+1SJm) + (K+1SJm|\nabla E_0|KSJm)\}], \tag{16}$$

where

$$(KSJm|\nabla E_0|K'SJm) = \{(K_+SJm|\nabla E_0|K'_+SJm) \pm(K_+SJm|\nabla E_0|K'_-SJm)\}/2^{\frac{1}{2}},$$

and $K=J-\frac{1}{2}$, $S=\frac{1}{2}$. Using Racah's formula,[8] we have

$$(K\tfrac{1}{2}Jm|\nabla E_0|K'\tfrac{1}{2}JM) = (-1)^{-K+m+\frac{1}{2}}(2J+1)(K\|\nabla E\|K') \times W(KJK'J;\tfrac{1}{2}2)V(JJ2;-mm0), \tag{17}$$

where

$$W(KJKJ;\tfrac{1}{2}2) = (-1)^{-K-J-\frac{1}{2}} \times\{A(A+1)-(4/3)J(J+1)I(I+1)\} \times\{(2J+3)(2J+2)(2J+1)(2J)(2J-1) \times(2K+3)(2K+2)(2K+1)(2K)(2K-1)\}^{-\frac{1}{2}}, \quad A=\tfrac{3}{4}-K(K+1)-J(J+1), \tag{18}$$

and

$$W(KJK+1J;\tfrac{1}{2}2) = (-1)^{-K-J-\frac{1}{2}} \times\{(K+1)^2-1+(J+\tfrac{1}{2})(J-\tfrac{1}{2})\}\{3(K+J+5/2) \times(K-J+\tfrac{3}{2})(K+J+\tfrac{1}{2})(-K+J+\tfrac{1}{2})\}^{\frac{1}{2}} \times\{2K(K+1)(K+2)(2K+1)(2K+3)J(J+1) \times(2J-1)(2J+1)(2J+3)\}^{-\frac{1}{2}}. \tag{19}$$

It is shown by Ito *et al.*[9] that

$$(K_+\|\nabla E\|K_+) = \tfrac{1}{2}\{3\Lambda^2-K(K+1)\}(2K+1)^{\frac{1}{2}} \times\{K(K+1)(2K+1)(2K-1)\}^{-\frac{1}{2}}(\partial^2V/\partial z^2), \tag{20}$$

and using the same procedure, that is, using the formula

$$\nabla E_0 = \tfrac{1}{2}(\partial^2V/\partial Z^2) = \tfrac{1}{2}\{\Phi_x^2(\partial^2V/\partial x^2)+\Phi_y^2(\partial^2V/\partial y^2) +\Phi_z^2(\partial^2V/\partial z^2)+2\Phi_x\Phi_y(\partial^2V/\partial x\partial y) +2\Phi_y\Phi_z(\partial^2V/\partial y\partial z)+2\Phi_z\Phi_x(\partial^2V/\partial z\partial x)\}, \tag{21}$$

where z is the molecular axis and Φ_x, Φ_y, and Φ_z are the direction cosines between the Z axis and the x, y, and z axes, respectively, and a table of the matrix elements of Φ,[10] we obtain

$$(K_+\|\nabla E\|K+1_+) = -\tfrac{3}{2}\Lambda\{(K+1)^2-\Lambda^2\}^{\frac{1}{2}} \times\{3K(K+1)(K+2)\}^{-\frac{1}{2}}(\partial^2V/\partial z^2). \tag{22}$$

When $\Lambda=1$, ∇E has a finite matrix element between the K_+ and K_-' state also. Using the formula of Ito *et al.*,[9] we obtain

$$(K_+\|\nabla E\|K_-) = -\tfrac{1}{2}\{K(K+1)(2K+1)\}^{\frac{1}{2}} \times\{(2K+3)(2K-1)\}^{-\frac{1}{2}}(e_+|\partial^2V/\partial x^2-\partial^2V/\partial y^2|e_-), \tag{23}$$

where e_+ and e_- are electronic states. The last factor can be expressed by using ξ which is defined in the formula (2a) as

$$(e_+|\partial^2V/\partial x^2-\partial^2V/\partial y^2|e_-) = -\tfrac{1}{2}(2e\xi+\partial^2V'/\partial z^2), \tag{24}$$

where $-e$ is the electronic charge and V' is the potential due only to the p electron which is rotating around the molecular axis, so that $\partial^2V'/\partial z^2$ may be different from

[8] G. Racah, Phys. Rev. **62**, 438 (1942).

[9] Ito, Tanabe, and Mizushima, Phys. Rev. (to be published).

[10] See for example, Cross, Hainer, and King, J. Chem. Phys. **12**, 210 (1944).

the $\partial^2V/\partial z^2$ which appeared in the formula (22). Thus,

$$(K_+\|\nabla E\|K_-)=\tfrac{1}{4}\{K(K+1)(2K+1)\}^{\frac{1}{2}} \times\{(2K+3)(2K-1)\}^{-\frac{1}{2}}(2e\xi+\partial^2V'/\partial z^2). \quad (25)$$

It is not difficult to show that

$$(K_+\|\nabla E\|K+1_-)=-(K+1_+\|\nabla E\|K_-). \quad (26)$$

From the formulas (17), (20), and (25) we find

$$(K\tfrac{1}{2}Jm|\nabla E_0|K\tfrac{1}{2}Jm)=(-1)^{m-\frac{1}{2}J}V(JJ2;-mm0) \times[(\partial^2V/\partial z^2)12^{-1}\{3\Lambda^2-K(K+1)\}X(K)(2J+1)^{\frac{1}{2}} \times\{J(J+1)(2J-1)(2J+3)\}^{-\frac{1}{2}}\pm(2e\xi+\partial^2V'/\partial z^2)96^{-1} \times\{(2J+1)(2J+1)(2J+3)/J(J+1)\}^{\frac{1}{2}}], \quad (27)$$

and

$$(J-\tfrac{1}{2}\,\tfrac{1}{2}Jm|\nabla E_0|J+\tfrac{1}{2}\,\tfrac{1}{2}Jm)=(-1)^{m-\frac{3}{2}J+1} \times V(JJ2;-mm0)(\partial^2V/\partial z^2)3\Lambda\{(J+\tfrac{1}{2})^2-\Lambda^2\}^{\frac{1}{2}} \times\{J(J+1)(2J-1)(2J+1)(2J+3)\}^{-\frac{1}{2}}, \quad (28)$$

where

$$X(K)=2J-1, \quad \text{when} \quad K=J+\tfrac{1}{2},$$

and

$$X(K)=2J+3, \quad \text{when} \quad K=J-\tfrac{1}{2},$$

and the double sign in the formula (24) means + for the c state and − for the d state.

Inserting the formulas (27), (28), and (16) into (15a) we obtain

$$(J\|\nabla E\|J)=(\partial^2V/\partial z^2)\{2(2J+1)\}^{-1} \times\{J(J+1)(2J+1)\}^{-1} \times[6^{-1}\{(2J+3)(2J-1)\}^{\frac{1}{2}}\{3\Lambda^2-(J+\tfrac{1}{2})^2\} -6\Lambda\{(J+\tfrac{1}{2})^2-\Lambda^2\}^{\frac{1}{2}}]\pm 96^{-1}(2e\xi+\partial^2V'/\partial z^2) \times\{(2J-1)(2J+1)(2J+3)\}^{\frac{1}{2}}\{J(J+1)\}^{-\frac{1}{2}}. \quad (29)$$

Thus from the formula (15) we finally obtain the formula of the nuclear electric quadrupole moment in Hund's case (a) as

$$W_c'=eQY(F)\{A(J)(\partial^2V/\partial z^2) +B(J)(2e\xi+\partial^2V'/\partial z^2)\}, \quad (30a)$$

$$W_d'=eQY(F)\{A(J)(\partial^2V/\partial z^2) -B(J)(2e\xi+\partial^2V'/\partial z^2)\}, \quad (30b)$$

where

$$Y(F)=\{\tfrac{3}{4}C(C+1)-J(J+1)I(I+1)\} \times\{2(2J-1)(2J+3)I(2I-1)\}^{-1}, \quad (30c)$$

$$A(JF)=(2J+3)(2J-1)\{6J(J+1)\}^{-1} \times[\{3\Lambda^2(2J+1)^{-2}-\tfrac{1}{4}\}-36\Lambda\{\tfrac{1}{4}-\Lambda^2(2J+1)^{-2}\}^{\frac{1}{2}} \times(2J+1)^{-1}\{(2J+3)(2J-1)\}^{-\frac{1}{2}}], \quad (30d)$$

and

$$B(J)=48^{-1}(2J-1)(2J+3)/J(J+1). \quad (30e)$$

5. EFFECT OF $\Pi_{1/2}$ STATE

The $\Pi_{\frac{1}{2}}$ state, in which $\Lambda=1$, $\Sigma=+\frac{1}{2}$, is the first electronic excited state of this molecule. Since the excitation energy is only 121 cm^{-1}, the effect from this state on the ground state may be appreciable. The effect comes in two ways: (1) because of the end-over-end rotation, Hund's case (a) is not exactly realized and the actual wave function will be a mixture of the $\Pi_{\frac{3}{2}}$ and $\Pi_{\frac{1}{2}}$ wave functions. This will change the coupling constant of the formulas (11) slightly. (2) Nondiagonal matrix elements of the magnetic interaction between the ground state and this excited state will give the so-called pseudo-quadrupole term[5] which might change slightly the value of $A(J)$ in the formulas (30).

Due to the rotational distortion, the real wave function $(JIF|$ will be

$$(JIF|=\mu(\Pi_{\frac{1}{2}}JIF|+\nu(\Pi_{\frac{3}{2}}JIF|, \quad (31)$$

where μ and ν may be functions of J. If Hund's case (a) is a good approximation, $|\mu|\gg|\nu|$ in the ground state of the NO molecule. $(\Pi_{\frac{1}{2}}JIF|$ and $(\Pi_{\frac{3}{2}}JIF|$ are the wave functions of the pure $\Pi_{\frac{1}{2}}$ and $\Pi_{\frac{3}{2}}$ states, respectively. It is easily seen that

$$(\Pi_{\frac{1}{2}}|H_1|\Pi_{\frac{3}{2}})=g_n\beta_n\beta(\Pi_{\frac{1}{2}}|\eta\zeta S_-I_+/2-3\eta S_-L_-L_+I_+/4|\Pi_{\frac{3}{2}}). \quad (32)$$

Integrating over the electronic coordinate, S_- will be 1, while $S_-L_-L_+$ will be 2; thus we obtain

$$\tfrac{1}{2}g_n\beta_n\beta\eta(\zeta-3)(JJ_z=\tfrac{1}{2}IF|I_+|JJ_z=\tfrac{3}{2}IF). \quad (33)$$

Since

$$(JJ_z=\tfrac{1}{2}m|\mathbf{x}-i\mathbf{y}|JJ_z=\tfrac{3}{2}m) =m\{(J-\tfrac{1}{2})(J+\tfrac{3}{2})\}^{\frac{1}{2}}\{J(J+1)\}^{-1}, \quad (34)$$

we obtain

$$(JJ_z=\tfrac{1}{2}IF|I_+|JJ_z=\tfrac{3}{2}IF) =\{(2J-1)(2J+3)\}^{\frac{1}{2}}\{4J(J+1)\}^{-1} \times\{F(F+1)-J(J+1)-I(I+1)\}. \quad (35)$$

Thus, when $|\nu|\ll|\mu|$, the correction due to this mixing of states will be

$$\Delta W_{c,d}=\nu g_n\beta_n\beta\eta(\zeta-3)\{(2J-1)(2J+3)\}^{\frac{1}{2}} \times\{4J(J+1)\}^{-1}\{F(F+1)-J(J+1)-I(I+1)\}, \quad (36)$$

which is common to the Λ-doublet states.

The second-order perturbation due to the excited $\Pi_{\frac{3}{2}}$ state is

$$-(\Pi_{\frac{1}{2}}|H_1|\Pi_{\frac{3}{2}})^2/\Delta E=-(g_n\beta_n\beta)^2 \times(\Pi_{\frac{1}{2}}|-\tfrac{1}{2}\xi L_+I_-|\Pi_{\frac{3}{2}})^2/\Delta E =-(g_n\beta_n\beta)^2\xi^2(I_x^2+I_y^2)/\Delta E, \quad (37)$$

where ΔE is the energy difference of the $\Pi_{\frac{1}{2}}$ state and the $\Pi_{\frac{3}{2}}$ state. From the Van Vleck formula[5] we can easily see that it gives rise to the so-called pseudo-quadrupole term,

$$\Delta W_{c,d}'=(g_n\beta_n\beta\xi)^2(\Delta E)^{-1}\{3(\Lambda+\Sigma)^2/J(J+1)-1\} \times\{3C(C+1)-4J(J+1)I(I+1)\} \times\{(2J-1)(2J+3)\}^{-1}, \quad (38)$$

which is also common to the Λ-doublet states.

6. COMPARISON WITH EXPERIMENTAL RESULTS

Gordy and Burrus[2] observed the absorption of the $J=\frac{1}{2}\rightarrow\frac{3}{2}$ transition. In the $J=\frac{1}{2}$ state all quadrupole-type effects vanish, since $3C(C+1)-4J(J+1)I(I+1)$ is zero for all F. Also there is no effect from the $\Pi_{\frac{1}{2}}$ state since this state cannot have $J=\frac{1}{2}$. Thus the energy levels will be simply given by W_c and W_d of the formulas (11). In the $J=\frac{3}{2}$ state, on the other hand, all of these effects appear and the energy level will be given by $W_c+\Delta W_c+W_c'+\Delta W_c'$ or $W_d+\Delta W_d+W_d'+\Delta W_d'$ from the formulas (11), (36), (30), and (38). The energy can be expressed as

$$W=P\{F(F+1)-J(J+1)-I(I+1)\}+R\{\tfrac{3}{4}C(C+1)-J(J+1)I(I+1)\}, \quad (39)$$

where P and R are constants. From the experimental data one can find a set of values for these constants as shown in Table I. The calculated frequencies by using these values are compared with the experimental results in Table II. The agreement is quite satisfactory.

Using the values of P from the $J=\frac{1}{2}$ states, one obtains, from the formulas (11),

$$a=23.14 \text{ Mc/sec} \quad \text{and} \quad b=14.065 \text{ Mc/sec}. \quad (40)$$

These values are both positive, as was expected, and give the ratio $b/a=0.608$ which is not far from the value 0.5 predicted in the formula (13); this indicates that the p-electron approximation is reasonably good.

The formulas (11), with the values of a and b shown above, give the values of P for the $J=\frac{3}{2}$ states to be -8.82 Mc/sec and 21.17 Mc/sec for the c and d states, respectively. Both of these are 0.23 Mc/sec smaller than the observed values shown in Table I. Since the correction ΔW given by the formula (36) is common to the doublet states, this $+0.23$ Mc/sec may be attributed to ΔW. In the appendix of this paper ν is shown to be -0.0247 at $J=\frac{3}{2}$. If we adopt the p-electron approximation, $\eta(\zeta-3)$ would be $-2\xi/5$. Since $a=g_n\beta_n\beta(3\xi/10)$ under the same approximation, the coefficient $\nu g_n\beta_n\beta\eta(\zeta-3)$ may be not far in value from $-4a\nu/3$. If we use the value of a given in (40), the corresponding correction to the value of P will amount to $+0.18$ Mc/sec. This is a little too small but not far from the value $+0.23$ Mc/sec required above. The deviation may be attributed to the incorrectness of the p-electron approximation.

Using the value of a shown in (40) and $\Delta E=121$ cm^{-1}, we can estimate the contribution of the pseudoquadrupole effect by the formula (38). Under the p-electron approximation, this contribution to the constant R at $J=\frac{3}{2}$ states is $-(a^2/\Delta E)(20/27)$, which is -1.1×10^{-4} Mc/sec. Since this value is very small compared to the observed values shown in Table I, we may neglect this contribution and assume that the observed values of R are entirely due to the nuclear quadrupole effect.

From the formulas (30), we obtain

$$W_c'+W_d'=2eQ(\partial^2V/\partial z^2)Y(F)A(J). \quad (41)$$

TABLE I. Values of coupling constants P and R (Mc/sec).

	$J=1/2$		$J=3/2$	
	c	d	c	d
P	-6.66	68.37	-8.59	21.40
R	0	0	0.077	0.035

Comparing this formula with the observed value of R_c+R_d, we obtain

$$eQ(\partial^2V/\partial z^2)=-2.12 \text{ Mc/sec}. \quad (42)$$

In the same way, from the difference R_c-R_d we obtain

$$eQ(2e\xi+\partial^2V'/\partial z^2)=7.6 \text{ Mc/sec}. \quad (34)$$

If we estimate ξ from a by the p-electron approximation, and assume $Q=0.02\times10^{-24}$ cm^2 according to Townes and Dailey,[11] $2e^2Q\xi$ will be 38 Mc/sec, while the second term $eQ(\partial^2V'/\partial z^2)$ must be $-\frac{1}{2}$ of the pure p-electron value of the coupling constant which is given by Townes and Dailey[11] as $+24$ Mc/sec or $+10$ Mc/sec. Thus the theoretical value of the coupling constant which is to be compared with the value given in (43) is 26 Mc/sec or 33 Mc/sec. Since they are too large, a smaller value for Q may be preferred.[12] Actually if $Q=0.01\times10^{-24}$ cm^2 the theoretical value for the coupling constant (34) is 7 Mc/sec or 14 Mc/sec.

On the whole we see that the assumption that the electron which is rotating around the molecular axis is in a pure p state works very well.

7. PREDICTION OF THE HFS OF THE NO MOLECULE IN THE $\Pi_{3/2}$ STATE

Since the magnetic interaction H_1 can connect states with $\Delta J_z=0$ or 1 only, the b term in the magnetic hfs formulas (11) vanishes in the $\Pi_{\frac{1}{2}}$ state. The other coupling constant a will be $g_n\beta_n\beta(2\xi+\eta\zeta-3\eta)\frac{3}{8}$, which, under the p-electron approximation, is $g_n\beta_n\beta(21\xi/40)$ or about 40 Mc/sec.

TABLE II. Comparison between theoretical and experimental frequencies.

	F $J=1/2\rightarrow3/2$	Frequencies (Mc/sec) Observed	Calculated[a]
	3/2→5/2	150 176.54	150 176.52
	1/2→3/2	150 198.85	150 198.91
c band	3/2→3/2	150 218.89	150 218.89
	1/2→1/2	150 225.75	150 225.70
	3/2→1/2	150 245.69	150 245.68
	3/2→1/2	150 375.48	150 375.52
	3/2→3/2	150 439.22	150 439.26
d band	3/2→5/2	150 546.50	150 546.51
	1/2→1/2	150 580.70	150 580.63
	1/2→3/2	150 644.37	

[a] The frequency without hfs was taken to be 150 195.51 Mc/sec and 150 550.63 Mc/sec for the c and d bands, respectively.

[11] C. H. Townes and B. P. Dailey, J. Chem. Phys. **17**, 782 (1949).
[12] J. Sheridan and W. Gordy, Phys. Rev. **79**, 513 (1950).

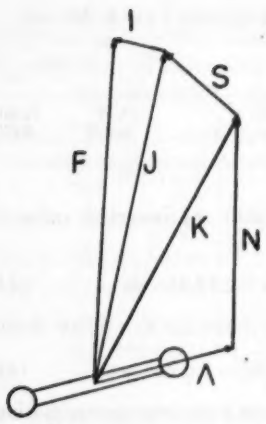

FIG. 2. Hund's case (b).

Referring to the electric hfs, we see that the $B(J)[2e\xi-(\partial^2V'/\partial z^2)]$ term will not change, so that the same difference between the Λ-doublet states will appear. Another term should be calculated using the wave equation formula (A7) of the appendix, instead of (A6). The calculation can be done as before, and the result is

$$W_e'(\Pi_{\frac{1}{2}})=eQY(F)\{A'(J)(\partial^2V/\partial z^2)+B(J)(2e\xi+\partial^2V'/\partial z^2)\}, \quad (44a)$$

$$W_d'(\Pi_{\frac{1}{2}})=eQY(F)\{A'(J)(\partial^2V/\partial z^2)-B(J)(2e\xi+\partial^2V'/\partial z^2)\}, \quad (44b)$$

where

$$A'(J)=[\{3\Lambda^2(4J^2+4J+5)/(2J+1)^2-(2J-1)(2J+3)/4\}+36\Lambda\{\tfrac{1}{4}-\Lambda^2/(2J+1)^2\}^{\frac{1}{2}}\times\{(2J+3)(2J-1)\}^{\frac{1}{2}}/(2J+1)]/\{6J(J+1)\},$$

and the coupling constants must be about the same as in the $\Pi_{\frac{1}{2}}$ state.

8. ELECTRIC HFS FORMULA FOR GENERAL COUPLING CASE

Our formulas (30) and (44) are applied for Hund's case (a). It is quite easy to extend our method to obtain the formula for the general coupling case. If the wave function is

$$(J|=a(KSJ|+b(K+1SJ|, \quad (45)$$

where $K=J-\frac{1}{2}$ and $S=\frac{1}{2}$, the corresponding formulas are

$$W_e(\text{general case})=eQY(F)\{A''(J)(\partial^2V/\partial z^2)+B(J)(2e\xi+\partial^2V'/\partial z^2)\}, \quad (46a)$$

$$W_d(\text{general case})=eQY(F)\{A''(J)(\partial^2V/\partial z^2)-B(J)(2e\xi+\partial^2V'/\partial z^2)\}, \quad (46b)$$

where

$$A''(J)=[\{3\Lambda^2-(J+\tfrac{1}{2})(J+\tfrac{3}{2})\}(2J-1)(2J+1)b^2+\{3\Lambda^2-(J-\tfrac{1}{2})(J+\tfrac{1}{2})\}(2J+3)(2J+1)a^2-72\Lambda\{\tfrac{1}{4}-\Lambda^2/(2J+1)^2\}ab]/\{6J(J+1)\},$$

and $B(J)$ and $Y(F)$ are given by the formulas (30e) and (30c), respectively. It must be remembered that the $B(J)$ term disappears when $\Lambda\neq1$.

The author wishes to thank Professor W. Gordy for his suggestions and encouragement.

APPENDIX

The Hamiltonian of the rotating molecule with electronic spin and orbital angular momentum is

$$H=D\mathbf{S}\cdot\mathbf{\Lambda}+B(\mathbf{K}-\mathbf{\Lambda})^2, \quad (A1)$$

where D and B are constants and $\mathbf{S}$ and $\mathbf{\Lambda}$ are the electronic spin and orbital angular momenta ($\mathbf{\Lambda}$ is parallel to the molecular axis), while $\mathbf{K}=\mathbf{\Lambda}+\mathbf{N}$, where N is the end-over-end rotational angular momentum. Since $\mathbf{N}\cdot\mathbf{\Lambda}=0$,

$$(KSJ|(\mathbf{K}-\mathbf{\Lambda})^2|K'SJ)=\{K(K+1)-\Lambda^2\}\delta_{K,K'}, \quad (A2)$$

and the matrix element of $\mathbf{S}\cdot\mathbf{\Lambda}$ can be obtained by the usual procedure.[8] Thus if we have a wave function

$$(J|=a(KSJ|+b(K+1SJ|, \quad (A3)$$

where $K=J-\frac{1}{2}$ and $S=\frac{1}{2}$, the corresponding secular equation is

$$\begin{vmatrix} D/(2J+1)+B\{(2J-1)(2J+1)-4\Lambda^2\}/4-E & -D\{(2J+3)(2J-1)\}^{\frac{1}{2}}/(4J+2) \\ -D\{(2J+3)(2J-1)\}^{\frac{1}{2}}/(4J+2) & -D/(2J+1)+B\{(2J+1)(2J+3)-4\Lambda^2\}/4-E \end{vmatrix}=0. \quad (A4)$$

If we neglect B, the solutions are

$$E=D/2 \text{ and } -D/2, \quad (A5)$$

where $E=D/2$ gives the $\Pi_{\frac{1}{2}}$ state, while $E=-D/2$ gives the $\Pi_{\frac{1}{2}}$ state, and they give the wave functions in Hund's case (a),

$$(\Pi_{\frac{1}{2}}J|=\{2(2J+1)\}^{-\frac{1}{2}}\{(2J-1)^{\frac{1}{2}}(KSJ|+(2J+3)^{\frac{1}{2}}(K+1SJ|\}, \quad (A6)$$

$$(\Pi_{\frac{1}{2}}J|=\{2(2J+1)\}^{-\frac{1}{2}}\{(2J+3)^{\frac{1}{2}}(KSJ|-(2J-1)^{\frac{1}{2}}(K+1SJ|\}. \quad (A7)$$

If we neglect D, on the other hand, we obtain Hund's case (b) [see Fig. 2]. In that case $(KSL|$ itself is the wave function.

In the case of the NO molecule, it is known[12] that $D=123.8$ cm^{-1}, and $B=1.720$ cm^{-1}. If we use these values and solve the secular equation (A4) for the $J=\frac{3}{2}$ state, we obtain the wave function for the lower energy state:

$$0.5213(1\ \tfrac{1}{2}\ \tfrac{3}{2}|-0.8534(2\ \tfrac{1}{2}\ \tfrac{3}{2}|=0.9998(\Pi_{\frac{1}{2}}\ \tfrac{3}{2}|-0.0247(\Pi_{\frac{1}{2}}\ \tfrac{3}{2}|; \quad (A8)$$

Margenau and Henry[12] gave the corresponding energy.

[12] H. Margenau and A. Henry, Phys. Rev. **78**, 587 (1950).

Precision Determination of the Velocity of Light Derived from a Band Spectrum Method. II*

D. H. RANK, J. N. SHEARER, AND T. A. WIGGINS
The Pennsylvania State University, State College, Pennsylvania

(Received January 22, 1954)

The rotational constant B_{000} for HCN has been measured using the method of exact orders for the 002 infrared rotation vibration absorption band. The value obtained is 1.47823_4 cm^{-1}. Combined with the microwave measurements by Nethercot and Klein of the same constant in pure frequency units, a value for the velocity of light, $c=299789.8\pm3.0$ km/sec, is found. The change in the apparent thickness of the Fabry Perot interferometer with wavelength due to the phase shift in the ZnS, MgF_2, ZnS coated plates is discussed and the experimental results compared with the calculated values. The rotational constants $\alpha_2=0.01003_4$ and $\gamma_{33}=0.00018_3$ cm^{-1} were also obtained with the aid of other interferometric results.

THE method of exact orders which we have recently described[1] makes possible the determination of molecular constants with a precision hitherto unobtainable in optical spectroscopy. In the present work we have redetermined B_{000} for HCN in order to determine the velocity of light by the band spectrum method described by Rank, Ruth, and Vander Sluis.[2]

In our preliminary work with the method of exact orders, a wavelength sensitivity in excess of 1 part in 20 million was demonstrated. However, considerable difficulty was encountered because of the change in length of the interferometer spacer with temperature. In addition, the *PV* work accomplished in changing the air pressure during the "tuning" process produced deformation of the glass plates of the etalon, which is equivalent to a change of the etalon spacer. We have largely rectified the above-mentioned difficulties by replacing the glass interferometer plates by plates of fused quartz, and also replacing the brass barrel of the etalon by a barrel constructed completely of invar.

Absorption measurements were made using a path length of HCN gas of three meters. The pressure of the gas was regulated so as to yield tuned patterns similar to those shown in Fig. 2 of our previous paper.[1] The pressure used in these measurements varied between the limits of 1 to 10 mm of Hg of HCN gas. HCN is a notorious substance with regard to pressure broadening of its spectrum lines. We have not been able to detect any wavelength shift of the HCN lines with pressure despite the sensitivity of our method. For some reason, the cause of which we are not completely certain, the fringes produced by our apparatus are slightly asymmetric. This asymmetry produces a pseudo small wavelength shift if measurements are made at widely different absorption levels. Thus it is necessary to compare "tunes" at approximately the same percentage absorption to obtain the most precise measurements of wavelength intervals.

DETERMINATION OF PHASE CHANGES

The quartz interferometer plates were coated with triple-layer dielectric films of ZnS, MgF_2, ZnS of a $\lambda/4$ thickness at 17 250A. Since no precise absolute wavelengths are known in this region of the spectrum, the method of exact orders cannot be used for determining the integral order of the interferometer. We have calibrated the integral order of the spacer by making use of second-order neon lines using the method of exact fractions as described in our former paper.[1] Phase change on reflection which occurs with the dielectric films is large and varies with wavelength. Fortunately the variation of the phase change with wavelength in these films can be calculated with considerable precision by making use of explicit formulas given by Leurgans[3] as derived from electromagnetic theory. Making use of the variation of phase with wavelength as calculated, corrections are applied to the observed fractional orders so that the integral order of the etalon can be chosen using the conventional method of exact fractions.

We can determine the phase change *versus* wavelength curve experimentally to higher precision using the method described in our previous paper.[1] This method involves obtaining the integral plus fractional orders for a number of different wavelengths using two different interferometer spacers. We have used a 13.19-mm spacer and a 5.95-mm spacer for the phase determination. The longer spacer was used for making the frequency measurement on the band lines. The ratios of these measurements made with the two spacers by using the method of exact orders can be used to derive the variation of phase with wavelength for the interferometer plates being used.[1] The ratios obtained are plotted *versus* wavelength in Fig. 1. In Fig. 2 the theoretically and experimentally determined phase shifts have been plotted *versus* wavelength. The agreement between theory and experiment is very satisfactory, since uncertainties in the film constants (thickness and indices) might well account for the slight differences observed. In any event, the correction which must be applied in the present work is small since the

* This research was assisted by support from the U. S. Office of Naval Research.

[1] Rank, Shull, Bennett, and Wiggins, J. Opt. Soc. Am. 43, 952 (1953).

[2] Rank, Ruth, and Vander Sluis, J. Opt. Soc. Am. 42, 693 (1952).

[3] P. J. Leurgans, J. Opt. Soc. Am. 41, 714 (1951).

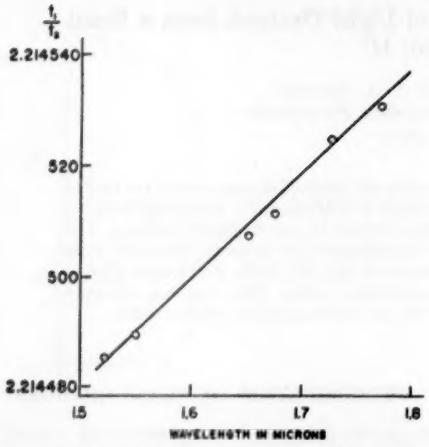

FIG. 1. Plot of the ratio I_1/I_2 *versus* wavelength λ as measured for 13.20- and 5.95-mm spacers of the Fabry Perot etalon.

interval of wavelengths covered in our measurements is only about 350A. The magnitude of the phase shift *versus* wavelength correction can be expressed as amounting to about 35 km per second in the velocity of light determination, in a direction so as to make uncorrected measurements yield a value of c too small.

DETERMINATION OF MOLECULAR CONSTANTS

In the absence of perturbations the frequencies of the lines in a rotation vibration band of a linear molecule are given by the well-known expression

$$\nu=\nu_0+(B'+B'')m+(B'-B''-D'+D'')m^2 -2(D'+D'')m^3-(D'-D'')m^4+\cdots, \quad (1)$$

where ν_0 is the band origin and B and D have their usual significance. m takes positive integral values for R branch lines and negative integral values for P branch lines. We can state as a result of our work that no perturbations in the lines of the 002 band of HCN occur which are of a magnitude greater than a few ten thousandths of a wave number, which is the limit of our precision.

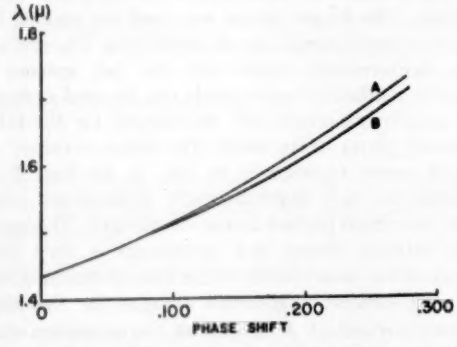

FIG. 2. Theoretically and experimentally determined phase shift in orders of interference *versus* wavelength for triple coated dielectric interferometer plates. A is the theoretical curve.

The following four equations express relationships which are useful for determining the constants of (1) above:

$$R(J-1)-P(J+1)=\Delta_2F''(J) =(4B''-6D'')(J+\tfrac{1}{2})-8D''(J+\tfrac{1}{2})^3, \quad (2)$$

$$R(J)-P(J)=\Delta_2F'(J) =(4B'-6D')(J+\tfrac{1}{2})-8D'(J+\tfrac{1}{2})^3, \quad (3)$$

$$R(J-1)+P(J)=\nabla_+(J) =2\nu_0+2(B'-B''-D'+D'')J^2-2(D'-D'')J^4, \quad (4)$$

$$R(J-1)-P(J) =\nabla_-(J)=2(B'+B'')J-4(D'+D'')J^3. \quad (5)$$

For the purpose of the determination of the velocity of light by the band spectrum method, it is only necessary to determine the constants B'' and D'' of Eq. (2). Experimentally this simply involves the determination of the frequency intervals of the line pairs designated by Eq. (2). The measurement of $R(J-1)-P(J+1)$, however, involves line pairs of considerable intensity difference especially at the large values of J which are necessary for precise evaluation of the molecular constants. When measurements of intervals are made on lines of considerably different intensity the precision is much reduced under practically all circumstances. In the present case with our method this error would be particularly vicious because of the slight fringe asymmetry.

Inspection of Eq. (3) will show that B' and D' can be obtained by the measurement of line pairs of almost identical intensity. Equation (4) shows that $B'-B''$ and $D'-D''$ can also be obtained from line pairs having nearly the same intensity. Further reflection will show that Eq. (4) yields one more decimal place for $(B'-B''-D'+D'')$ than is obtainable for B' from Eq. (3) when high values of J are used. It can be seen that $R(J-1)+P(J)-2\nu_0$ increases proportionally to J^2 while $R(J)-P(J)$ increases proportionally to $J+\frac{1}{2}$. This favorable situation with regard to the $\nabla_+(J)$ plot can be strictly taken advantage of with the interferometric method. From the preliminary measurements of Douglas and Sharma[4] and Yost[5] the band origin of the 002 band has been for the purposes of this investigation set by definition as 6519.6608 cm^{-1} *in vacuo*. Douglas and Sharma quote a value of 6519.65 cm^{-1} and Yost's value is 6519.68 cm^{-1}. The defined ν_0 yields a value of 6516.7043 cm^{-1} for $P(1)$ when combined with the known preliminary value of B''. $P(1)$ is then used for standardizing the interferometer and measurements of the band lines thus are made interferometrically with reference to the band origin. Likewise it can be seen

[4] A. E. Douglas and D. Sharma, J. Chem. Phys. **21**, 448 (1953).
[5] E. L. Yost, thesis, The Pennsylvania State College, 1953 (unpublished).

TABLE I. Summary of data obtained in measurements of the 000–002 band of HCN. Frequency intervals measured, $\nabla_+(J)-2\nu_0$ and Δ_2F' expressed in cm^{-1} *in vacuo*. Columns 3 and 7 headed L.M.S.C., least mean squares calculated values, cm^{-1} *in vacuo*. Columns headed $C-O$, calculated minus observed values. The molecular constants are given in cm^{-1} *in vacuo*.

$\nabla_+(J)-2\nu_0$	$2J^2$	L.M.S.C.	$C-O$	Δ_2F'	$4(J+1/2)$	L.M.S.C.	$C-O$
−6.0905	288	−6.0913	+0.0008	72.8078	50	72.8082	+0.0004
−8.2875	392	−8.2894	+0.0019	84.4394	58	84.4393	−0.0001
−10.8248	512	−10.8247	−0.0001	96.0616	66	96.0624	+0.0008
−13.6998	648	−13.6966	−0.0032	107.6772	74	107.6763	−0.0009
−20.4477	968	−20.4485	+0.0008	113.4802	78	113.4795	−0.0007
−22.3461	1058	−22.3461	0.0000	125.0768	86	125.0775	+0.0007
−24.3259	1152	−24.3273	+0.0014	142.4522	98	142.4518	−0.0004
−26.3932	1250	−26.3922	−0.0010	154.0175	106	154.0178	+0.0003

$B'-B''=-0.021161_7$ $\quad D'-D''=7.66\times10^{-6}$ $\quad B'=1.45707_3$ $\quad D'=2.89_8\times10^{-6}$

that a constant determined from Eq. (5) has less than half the precision of one determined from Eqs. (2) or (3). Calculations show that an absolute error in the band origin frequency will cause an absolute error in the largest Δ_2F' of 2.3×10^{-4} cm^{-1} for each 0.01 cm^{-1} absolute error in the band origin. Thus each 0.01 cm^{-1} error in band origin absolute value will cause an error in c of 0.46 km/sec. We feel reasonably certain that the absolute value of ν_0 we have chosen is correct to ±0.02 cm^{-1}.

Because of the much more favorable experimental procedure the major effort in this research was expended on the measurement of line pairs yielding $\Delta_2F'(J)$ and $\nabla_+(J)$. Measurements were also made on $\Delta_2F''(J)$ but as expected the scatter was much greater which would give them little statistical weight compared to the other measurements. The data were treated to least squares in the manner described by Rank, Ruth, and Vander Sluis.[2] The results of the least squares treatment are given in Table I.

The smallness of the residuals shows that it would serve no useful purpose to include the conventional graphic plots since the points lie so close to the straight line that on the scale usually printed the scatter would not be apparent. $\Delta_2F''(J)$ results treated to least squares yielded $B''=1.47825$ and $D''=3.01\times10^{-6}$. However, these results have little statistical weight since the scatter of the points is much greater than the results given in Table I. We shall quote as our final result the values of the constants derived from Table I in cm^{-1} *in vacuo*:

$$B'=1.45707_3, \qquad D'=2.89_8\times10^{-6},$$
$$B''=1.47823_6, \qquad D''=2.97_6\times10^{-6}.$$

DETERMINATION OF THE VELOCITY OF LIGHT

When we combine our result for B'' with the newly remeasured 0–1 transition in the microwave spectrum by Nethercot and Klein,[6] i.e., $B''-2D''=44\,315.800\pm0.010$ Mc/sec, we obtain $c=299\,789.8\pm3.0$ km/sec. The value of B'' microwave is $44\,315.978\pm0.011$ Mc/sec when the D'' correction is made by means of our newly determined D'' value.

Since our measurements are made essentially with the interferometer *in vacuo* no appreciable error is involved due to uncertainties in the index of refraction of air. $(\mu-1)$ for air is made use of only to determine the fractional order and we must use only from 1 percent to 20 percent of this quantity for our purpose depending on the fractional order. We have used our recent determination[1] at 1.65μ as the value of $(\mu-1)$ corrected by means of the dispersion formula of Barrell[7] for the proper wavelengths.

The probable error can be considered to be derived from the following sources:

Microwave $\nu=\pm0.10$ km/sec,
Absolute value of band origin $=\pm0.90$ km/sec,
Phase change *vs* $\lambda=\pm1.00$ km/sec,
Statistical $=\pm1.00$ km/sec.

We have included in Table II the frequencies of the lines of the 002 band of HCN calculated from the final values of the molecular constants. We have only tabulated lines which were used to derive the molecular constants since we are certain that no significant perturbations occur in these lines. These values are only accurate relative to $P(1)$, i.e., ±0.02 cm^{-1} in absolute value.

TABLE II. Calculated frequencies in vacuum wave numbers of lines of the 002 band of HCN.

$P(1)$	6516.7043	$R(11)$	6551.8185
$P(12)$	6481.4117	$R(12)$	6554.2198
$P(14)$	6474.4539	$R(13)$	6556.5781
$P(16)$	6467.3315	$R(14)$	6558.8932
$P(18)$	6460.0453	$R(15)$	6561.1652
$P(19)$	6456.3410	$R(16)$	6563.3939
$P(21)$	6448.8106	$R(17)$	6565.5794
$P(22)$	6444.9846	$R(18)$	6567.7216
$P(23)$	6441.1184	$R(19)$	6569.8204
$P(24)$	6437.2119	$R(21)$	6573.8880
$P(25)$	6433.2653	$R(22)$	6575.8567
$P(26)$	6429.2787	$R(23)$	6577.7819
		$R(24)$	6579.6636
		$R(26)$	6583.2965

[6] A. H. Nethercot and J. A. Klein, Quarterly Report, Columbia Radiation Laboratory, Physics Department, Columbia University, October, 1953 (unpublished).

[7] H. Barrell, J. Opt. Soc. Am. **41**, 295 (1951).

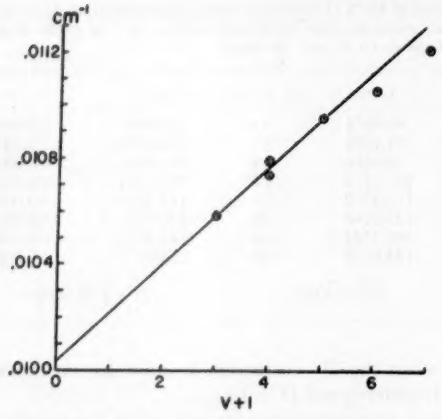

FIG. 3. $(B_0-B_v)/v$ *versus* $(v+1)$ for the progression 000–00X of HCN.

However, there is a good probability that the absolute frequency of $P(1)$ can be improved by at least an order of magnitude in the near future.

DETERMINATION OF α_3

The B_v values for a linear triatomic molecule can be expressed by the equation

$$B_v=B_e-\alpha_3(v+\tfrac{1}{2})-\gamma_{33}(v+\tfrac{1}{2})^2+f_1(\alpha_2)+f_2(\alpha_1). \quad (6)$$

Let us deal with the progression of bands 000–00X. It is easy to see that

$$\frac{B_0-B_v}{v}=\alpha_3+\gamma_{33}(v+1). \quad (7)$$

We have plotted the available data for this progression in Fig. 3. The points for the 002 band and the 004 band are the results of interferometric measurements and derived from band origin plots, i.e., $\nabla_+(J)$. The method of R. R. V.[2] is only a pseudo-interferometric method in that the major burden of the wavelength measurement falls upon the ability of the diffraction grating to locate the center of the lines. The interferometer merely furnishes closely spaced, very accurately known reference wavelengths and provides some slight additional help by means of vertical dispersion. The value plotted for the 004 band also agrees with that obtained by Douglas and Sharma.[4] The double point plotted for the 003 band refers to measurements of Douglas and Sharma.[4] The upper point is the one given by the B' value obtained by them. The lower point we have obtained from a band origin plot made from the data given in the paper of Douglas and Sharma. The points for the 005 and 006 bands were again obtained from band origin plots of the data given by Douglas and Sharma, and are much less precise than the other points due to weakness of the bands and their location in the spectrum. It should be stated that the spread of the points for the 003 band is well within the error stated by Douglas and Sharma for their determination of B'. We obtain $\alpha_3=0.01003_4$, $\gamma_{33}=0.00018_3$ expressed in cm^{-1} as the values of these constants.

It is now possible to review the situation critically with regard to the c determination made by Rank, Ruth, and Vander Sluis.[2] The discrepancy between their results and the present result involves a systematic error which it was not possible to evaluate at the time the previous work was done. No phase shift is to be expected for the aluminum interferometer coatings. Dr. Vander Sluis (private communication) has reexamined the interferometer calibrations and demonstrated no phase shift exists.

It must be remembered that the R. R. V. measurements are grating measurements. Harrison[8] has recently pointed out that the best diffraction gratings are capable of measuring wavelength to only 1 part in 10^6. It could be presumed that the "Tuxedo" grating is at least as good and probably better than those used by Harrison.[8] If we assume wavelength determination accurate to 5 parts in 10^7 for the "Tuxedo" grating in measuring the band lines which vary in intensity by a factor of 6, this would introduce a systematic error of ± 14 km/sec. The error pointed out by Harrison[8] shows the futility of using grating measurements to obtain highly precise c measurements from data obtained in the photographic infrared.

However, it can be pointed out that this same grating effect of 5 parts in 10^7 would produce a systematic error in c of only ± 3 km/sec in a band measured at 4 microns.

The value for the velocity of light obtained by the band spectrum method as reported here is the same as the value obtained by other methods of measurement.[9]

We are indebted to Dr. W. F. Koehler of the Michelson Laboratory, Inyokern, for helpful discussion concerning the calculations of phase shift in multiple layer dielectric films. We express our thanks to Jean M. Bennett for help with the least squares calculations.

[8] Harrison, Davis, and Robertson, J. Opt. Soc. Am. **43**, 853 (1953).

[9] J. W. M. DuMond and E. R. Cohen, Revs. Modern Phys. **25**, 691 (1953).

Spin Relaxation in Free Radical Solutions Exhibiting Hyperfine Structure*

J. P. Lloyd† and G. E. Pake
Department of Physics, Washington University, Saint Louis, Missouri

(Received January 15, 1954)

Experimental studies of spin-lattice relaxation in aqueous solutions of the free radical peroxylamine disulfonate ion, $ON(SO_3)_2^{--}$, have been made in fields near 30 oersteds. The continuous wave saturation technique was used to study the transition $F=\frac{1}{2}$, $m_F=-\frac{1}{2}\rightarrow F=\frac{1}{2}$, $m_F=-\frac{1}{2}$, for which the frequency was 60 Mc sec^{-1}. Because the hyperfine interaction of the unpaired electron with the N^{14} nucleus leads to six unequally spaced energy levels, a unique relaxation time cannot be defined. A general treatment of the saturation method leads to definition of the *relaxation probability*, which reduces for a system with two energy levels to the reciprocal of twice the relaxation time. The experimentally measured relaxation probability is found to be concentration independent below 0.005 molar in $ON(SO_3)_2^{--}$, approaching an asymptotic value of 2×10^6 sec^{-1}. Experiment and theory both rule out as the source for this relaxation probability the interaction of the electron moment with the nuclear moments of the H_2O solvent molecules, and theory also rules out the effect of the N^{14} electric quadrupole coupling to solvent motions; the latter can, in principle, effect electron relaxation because of the hyperfine coupling between the N^{14} nuclear spin and the electron spin. Estimates are made of the role played by spin-orbit coupling, and it appears probable that the observed relaxation involves this interaction. An interesting by-product of the analysis of the relaxation probability is the result that second order statistical processes, by which an electron spin is first carried with energy conservation to an excited Stark level before reaching the ground Stark level of opposite spin, may account for the observed relaxation. This process is somewhat similar to the Raman processes invoked by Van Vleck to explain relaxation in the alums, except that in Van Vleck's theory the intermediate excited Stark level is only virtually occupied, without energy conservation.

1. INTRODUCTION

THE paramagnetic resonance of the peroxylamine disulfonate ion, $ON(SO_3)_2^{--}$, even in crystals of the potassium salt, is not characterized by the pronounced exchange narrowing frequently observed for free radical molecules. It is perhaps attributable to this weakness of the exchange interaction that one can observe a well-resolved hyperfine splitting from the N^{14} nucleus in liquid solutions containing this ion in concentrations even larger than 0.1 molar.[1] There is, therefore, a range of concentrations over which magnetic dipole transitions of the coupled system, electronic moment plus nuclear moment, can be observed in fields near 10 gauss with adequate signal-to-noise. Measurements by Townsend[2] have shown that, in fields up to 50 gauss and at frequencies between 9 and 120 Mc/sec, the Breit-Rabi energy levels for a system with $I=1$, $J=\frac{1}{2}$ apply to the peroxylamine disulfonate ion in solution.

The present work concerns itself with the mechanism which maintains the population differential between a particular pair of levels participating in resonance absorption. This mechanism will also be shown in the system at hand to dominate in producing the observed line width. The mechanisms of interest in determining measured widths of paramagnetic resonances are, in general, the spin-spin and spin-lattice interactions, which may occasionally be markedly obscured by instrumental effects. The advantages of working in low fields (~30 gauss) are twofold. First, the individual hyperfine components become only a fraction of a gauss wide at concentrations below about 10^{-2} molar. In the magnetic fields of several thousand gauss which correspond to microwave frequencies, care must be exercised to assure that field inhomogeneities over the sample do not mask the true line width. However, if Helmholtz coils or a solenoid are used in producing the 30-gauss field, no effort at all is required to keep inhomogeneities below 10^{-2} gauss over a sample of several cubic centimeters volume. A second advantage is more compelling. To separate non-negligible spin-spin processes, if any, from the spin-lattice interactions limiting the lifetime of a spin state, one needs to know the spin-lattice relaxation time. While this can be measured with difficulty at microwave frequencies,[3,4] microwave generators with adequate power are not presently available in this laboratory, and the techniques, in any event, are not as easily applied as those using lumped parameter circuits.

The Hamiltonian function describing the interaction leading to the hyperfine structure is[5]

$$\mathcal{H}=g_J\mu_0H_0J_z+a\mathbf{I}\cdot\mathbf{J}-g_I\mu_0H_0I_z \qquad (1)$$

where g_J is the spectroscopic splitting factor for the free radical; for a free electron $g_J=g_e=2.0023$. The magnitude of the Bohr magneton is μ_0, and the antiparallellity of J and the magnetic moment of the electron is explicitly taken into account by the positive sign preceding the first term of (1). H_0 is the applied external field, and a is the hyperfine coupling constant. Since we take g_I as the nuclear g factor referred to the (positive) Bohr magneton μ_0, it is the conventional nuclear g divided by $M/m=1836$.

The Breit-Rabi energy levels[5] given by the Hamil-

* Assisted by the joint program of the U. S. Office of Naval Research and the U. S. Atomic Energy Commission.

† Now at Shell Oil Company, Houston, Texas.

[1] Pake, Townsend, and Weissman, Phys. Rev. 85, 682 (1952).

[2] Townsend, Weissman, and Pake, Phys. Rev. 89, 606 (1953).

[3] C. P. Slichter, thesis, Harvard University (unpublished); also Phys. Rev. 76, 466 (1949).

[4] E. E. Schneider and T. S. England, Physica 17, 221 (1951).

[5] G. Breit and I. I. Rabi, Phys. Rev. 38, 2082 (1931). See also J. E. Nafe and E. D. Nelson, Phys. Rev. 73, 718 (1948).

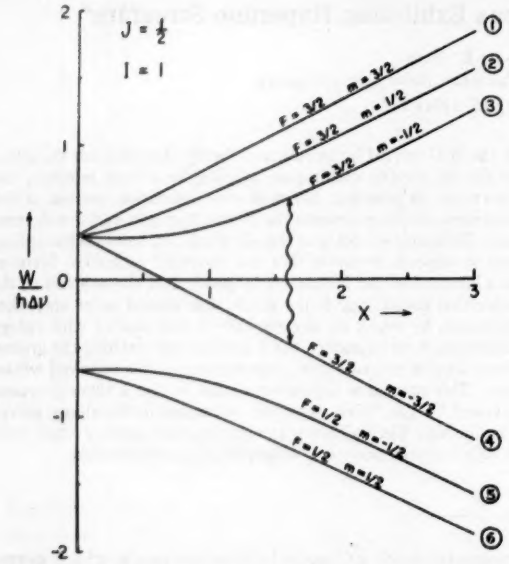

FIG. 1. Breit-Rabi levels for the $ON(SO_3)_2^{--}$ ions. The transition marked is that for which rf saturation measurements were made as a function of concentration in aqueous solution.

tonian (1) for $I=1$, $J=\frac{1}{2}$ are displayed in Fig. 1. The particular transition studied in the present work is that between the levels $F=\frac{3}{2}$, $m_F=-\frac{1}{2}$ and $F=\frac{3}{2}$, $m_F=-\frac{3}{2}$. This transition has a frequency which increases monotonically from zero. However, the ratio of frequency to field is not effectively constant until large enough fields are attained to decouple **J** from **I**. In order to treat the spin interaction processes later on, we reproduce here the wave functions and energies which apply to the levels involved in the transition marked in Fig. 1. Designating the levels by the numbers shown on the right of Fig. 1, we have

$$\begin{aligned}
&\psi(F,m)=\sum_{m_J,m_I}(Fm|m_Jm_I)\phi(m_J)\chi(m_I),\\
&\psi_1\equiv\psi(\tfrac{3}{2},\tfrac{3}{2})=\phi(\tfrac{1}{2})\chi(1),\\
&\psi_2\equiv\psi(\tfrac{3}{2},\tfrac{1}{2})=a\phi(\tfrac{1}{2})\chi(0)+b\phi(-\tfrac{1}{2})\chi(1),\\
&\psi_3\equiv\psi(\tfrac{3}{2},-\tfrac{1}{2})=c\phi(\tfrac{1}{2})\chi(-1)+d\phi(-\tfrac{1}{2})\chi(0),\\
&\psi_4\equiv\psi(\tfrac{3}{2},-\tfrac{3}{2})=\phi(-\tfrac{1}{2})\chi(-1),\\
&\psi_5\equiv\psi(\tfrac{1}{2},-\tfrac{1}{2})=c\phi(-\tfrac{1}{2})\chi(0)-d\phi(\tfrac{1}{2})\chi(-1),\\
&\psi_6\equiv\psi(\tfrac{1}{2},\tfrac{1}{2})=a\phi(-\tfrac{1}{2})\chi(1)-b\phi(\tfrac{1}{2})\chi(0).
\end{aligned}\tag{2}$$

The coefficients, as functions of $x=(g_J-g_I)\mu_0H_0/h\Delta\nu$, will be expressed in terms of $r=(1+\frac{2}{3}x+x^2)^{\frac{1}{2}}$ and $\rho=(1-\frac{2}{3}x+x^2)^{\frac{1}{2}}$:

$$\begin{aligned}
a^2&=\frac{1}{2}+\left(\frac{1}{4}-\frac{2}{9r^2}\right)^{\frac{1}{2}}, \quad c^2=\frac{1}{2}+\left(\frac{1}{4}-\frac{2}{9\rho^2}\right)^{\frac{1}{2}},\\
b^2&=\frac{1}{2}-\left(\frac{1}{4}-\frac{2}{9r^2}\right)^{\frac{1}{2}}, \quad d^2=\frac{1}{2}-\left(\frac{1}{4}-\frac{2}{9\rho^2}\right)^{\frac{1}{2}}.
\end{aligned}\tag{3}$$

The energy levels of Fig. 1 are given by

$$W_{F=1\pm\frac{1}{2}}=-\tfrac{1}{6}h\Delta\nu+g_I\mu_0H_0m \pm\tfrac{1}{2}h\Delta\nu[1+(4/3)mx+x^2]^{\frac{1}{2}}. \quad (4)$$

The experiments to be discussed in Sec. 8 involve excitation of transitions between levels 3 and 4 of Fig. 1 at a frequency,

$$\nu_{43}=\Delta\nu\{-\tfrac{1}{2}(1-x)+\tfrac{1}{2}(1-\tfrac{2}{3}x+x^2)^{\frac{1}{2}}\}+g_I\mu_0H_0/h, \quad (5)$$

of 60 Mc/sec, which corresponds to an external magnetic field of about 31.4 oersteds. Values of the coefficients of Eqs. (3) for this field are listed below:

$$a^2=0.950, \quad b^2=0.050, \quad c^2=0.903, \quad d^2=0.097,$$
$$x=g_J\mu_0H_0/h\Delta\nu=1.610.$$

For the $ON(SO_3)_2^{--}$ ion, $g_I/g_J\approx10^{-4}$ and we shall usually neglect g_I in comparison with g_J.

2. PARAMAGNETIC RELAXATION AND SPIN SATURATION

Paramagnetic relaxation is the process of energy exchange between an assembly of paramagnetic spins and its surroundings which permits the spin-state populations to adjust themselves to the equilibrium distribution corresponding to a given magnetic field and temperature. It is customary to regard the entire paramagnetic sample (solid, liquid, or gas) as a super system composed of two weakly interacting subsystems; the system of interest or spin system, having spin coordinates among its degrees of freedom, and the surroundings or lattice system having only orbital degrees of freedom.

It is the weak interaction, $\mathcal{H}_{sl}$, between spins and the lattice which is the object of relaxation studies. In practical cases, the question is one of trying to discover which of a number of possibly important spin-lattice interactions effects the experimentally observed relaxation. In certain examples relaxation has been studied experimentally through direct observation of the characteristic time required for the establishment of spin equilibrium (the *relaxation time*). In other examples, particularly if the relaxation time is short, one measures essentially the thermal conductivity between the spins and the lattice by observing the rate at which energy, absorbed by the spins from a laboratory source, is passed on to the lattice via the relaxation mechanisms; this is the saturation method.

It is of course quite feasible to cloak such measurements in thermodynamic terms, as was done by Casimir and Du Pré.[6] We shall usually confine our approach to that of quantum statistics and speak in terms of the transition probabilities per unit time induced by $\mathcal{H}_{sl}$. Either a direct relaxation time measurement or a saturation experiment will be treated in terms of the

[6] H. B. G. Casimir and F. K. Du Pré, Physica **5**, 507 (1938); H. B. G. Casimir, Physica **6**, 159 (1939).

way in which the populations of the various energy states are influenced by these probabilities.

Such an analysis of the relaxation time for an assembly of spin $\frac{1}{2}$ particles is straightforward;[7] a unique relaxation time is easily defined for the establishment of the equilibrium population difference between the two spin states accessible to each particle. However, a more complicated energy level scheme may not permit the association of a single relaxation time with each *pair* of levels between which a population difference will exist at equilibrium. An example is the coupled system consisting of the odd electron and the N^{14} nucleus of the free-radical ion $ON(SO_3)_2^{--}$. Not only are there six unevenly spaced levels, but the selection rules permit magnetic dipole transitions between all but five of the fifteen different pairs of levels. In general, one finds that the approach, from an initially disturbed state to the equilibrium level population, is described by an expression of the form

$$N_k(t)=\sum_l b_{kl}\exp(-\lambda_l t). \tag{6}$$

If, after appreciable lapse of time, several comparable terms in the sum (6) are dominant, it will be impossible to express any population difference involving level k with only one exponential term, and there will be no single relaxation time.

The saturation procedure does not suppose any specific mathematical form for the approach to equilibrium of the population difference between a pair of levels. Transitions are excited between the levels in question by means of a laboratory radiation field. (We presume throughout this discussion the existence of a constant external magnetic field which removes the orientation degeneracy of individual spins.) As we shall later verify (Sec. 4), the transition probabilities induced by the laboratory field are, for practical purposes, microscopically reversible, which means that the net energy absorption—and therefore also the detected rf absorption signal—is proportional to the population difference. In the presence of a given laboratory radiation field, then, a stationary spin population distribution will ultimately obtain in which this rf absorption is just balanced by the energy carried to the lattice through all relaxation processes. (As taken up in Sec. 5, the transition probabilities describing the relaxation processes *cannot* possess microscopic reversibility if there is to be a nonvanishing population differential at equilibrium.) It follows that a study of relative absorption intensity as a function of the rf power level must give direct information about the interaction $\mathcal{H}_{sl}$ which permits energy exchange between the spins and the lattice.

Explicit emphasis should perhaps be given to the fact that a given level of saturation is characterized by *stationarity* of spin population, but not, of course, by thermal equilibrium. Indeed, the stationarity exists only if the thermal capacity of the lattice, which is in turn normally in excellent thermal contact with its laboratory surroundings, is large. Except at very low temperatures, this condition is usually fulfilled. For this reason, although there is a steady flow of energy into the lattice, we shall speak of a lattice temperature, assumed not to change during a given measurement, which is essentially a temperature fixed by the sample's immediate laboratory surroundings.[8]

3. DEFINITION OF THE SATURATION FACTOR AND THE RELAXATION PROBABILITY

The foregoing description of the saturation procedure suggests that a useful quantity in relaxation studies is the ratio,

$$S_{jk}(H_1)=(N_k'-N_j')/(N_k-N_j), \tag{7}$$

which we shall call the saturation factor. Here N_k is the stationary population of spin state k with zero or negligible rf field present (thus the thermal equilibrium value) and N_k' is the stationary population in the presence of an rf field H_1. Evidently $S_{jk}(0)=1$ and $S_{jk}(\infty)=0$. For a given input of rf power at spin resonance, one expects S_{jk} to depend upon lattice temperature and the external field in which resonance occurs.

We now wish to obtain a relationship which expresses the saturation factor in terms of the laboratory-induced transition probability per unit time V_{jk}, and the transition probability per unit time U_{jk} which is induced by the spin-lattice interaction $\mathcal{H}_{sl}$. We shall let $W_{jk}=U_{jk}+V_{jk}$ denote the probability per unit time, due to both relaxation mechanisms and the laboratory apparatus, that a system now in spin state j will be found at a later time in state k. If there are a total number N of spin systems to be distributed over the n states accessible to an individual spin, then the following differential equations describe the shifting of the population fractions, $Q_j=N_j/N$, by expressing essentially the conservation of systems:

$$\frac{dQ_j}{dt}=\sum_{\substack{k=1\\k\neq j}}^{n}(Q_kW_{kj}-Q_jW_{jk})\quad[j=1,\cdots,n]. \tag{8}$$

Under conditions of population stationarity, Eqs. (8) become n homogeneous linear equations in the Q's which are readily seen to be consistent, since any row of their coefficient determinant is obtainable by adding the other $n-1$ rows. The Q's are of course not all independent, for if $n-1$ of them are known, the nth is determined. Thus the system of equations may be solved by replacing any one of the n homogeneous equations,

$$\sum_{\substack{k=1\\k\neq j}}^{n}(Q_kW_{kj}-Q_jW_{jk})=0\quad[j=1,\cdots n], \tag{9}$$

[7] Bloembergen, Purcell, and Pound, Phys. Rev. **73**, 679 (1948), ften referred to hereafter as BPP.

[8] In the early unsuccessful attempt of Gorter to observe nuclear paramagnetic resonance, the small change of lattice temperature during application of a strong rf field at the Larmor frequency was to be the means of detecting the nuclear spin resonance [C. J. Gorter, Physica **3**, 995 (1936)].

by

$$\sum_{k=1}^{n} Q_k = 1. \tag{10}$$

To determine the saturation factor S_{qp}, we require the difference $\Delta_{pq}=Q_p-Q_q$ under the conditions,

$$\left.\begin{aligned} W_{jk}&=U_{jk} \qquad [qp\neq jk\neq pq] \\ W_{pq}&=U_{pq}+V \\ W_{qp}&=U_{qp}+V \end{aligned}\right\}, \tag{11}$$

which express the reversibility of $V_{pq}=V_{qp}=V$ and the fact that the laboratory source induces transitions between states p and q only.

For simplicity, let us arbitrarily number the states p and q, between which the radiation field produces transitions with the probability V, by the numbers 1 and 2. Then, substituting $Q_2=\Delta_{21}+Q_1$, one obtains the following equations:

$$\begin{aligned}
&Q_1[U_{21}+V-(V+\sum_k U_{1k})]+\Delta_{21}(U_{21}+V) &&+Q_3U_{31}+\cdots+Q_nU_{n1}=0,\\
&Q_1[U_{12}+V-(V+\sum_k U_{2k})]-\Delta_{21}(V+\sum_k U_{2k})&&+Q_3U_{32}+\cdots+Q_nU_{n2}=0,\\
&\quad\vdots && \quad\vdots\\
&Q_1(U_{1m}+U_{2m}) \qquad +\Delta_{21}U_{2m} &&+Q_3U_{3m}+\cdots+Q_nU_{nm}=0,\\
&\quad\vdots && \quad\vdots\\
&Q_1(U_{1n}+U_{2n}) \qquad +\Delta_{21}U_{2n} &&+Q_3U_{3n}\cdots-Q_n\sum_k{}' U_{nk}=0.
\end{aligned} \tag{12}$$

Noting that V, by virtue of its practical microscopic reversibility, appears only in two positions in the second column, one can eliminate one V term by replacing, for example, the second equation by Eq. (10). If one then solves for Δ_{21} by expanding determinants in terms of the cofactors of the second column, he obtains

$$\Delta_{21}=C_{22}/(\sum_{k\neq 2} U_{2k}C_{2k}+V\cdot C_{21}+C_{22}), \tag{13}$$

where C_{2k} is the cofactor of the second column element in the kth row. For a spin system in thermal equilibrium at room temperature, $\Delta_{21}\sim(E_2-E_1)/kt=h\nu/kT$. For magnetic dipole transitions which would occur at radiofrequencies between 1 Mc/sec and 30 000 Mc/sec, Δ_{21} ranges between 10^{-7} and 5×10^{-3}. Then Eq. (13) indicates that $\sum_{k\neq 2} U_{2k}C_{2k}$ must exceed C_{22} by a factor at least 200 (and, for the experiments of Sec. 7, by 10^5). Hence C_{22} can be dropped from the denominator of Eq. (13), and one finds $S_{12}=\Delta_{21}(V)/\Delta_{21}(0)$ to be

$$S_{12}=\left[1+\frac{V}{U_{21}+C_{21}^{-1}\sum_{k=3}^{n} U_{2k}C_{2k}}\right]^{-1}. \tag{14}$$

This may be compared with BPP's Eqs. (13), (4), and (33) to show that our result reduces to theirs when there are just two levels. Although a system of many levels without special selection rules does not generally admit to definition of a single relaxation time for a pair of levels, the coefficient of V in Eq. (14), which for a two level system is twice the relaxation time T_1, is nevertheless the significant quantity indicating the potency of relaxation mechanisms which give rise to the U_{jk} transition probabilities. We shall define the reciprocal of the coefficient of V to be the *relaxation probability*, W_R:

$$W_R=U_{21}+\frac{1}{C_{21}}\sum_{k=3}^{n} U_{2k}C_{2k}. \tag{15}$$

We can thus speak of measuring relaxation probabilities in situations where there is no single uniquely defined relaxation time.[9]

4. THE LABORATORY-INDUCED TRANSITION PROBABILITY

Experimental measurement of W_R can be made by measuring S for a known rf field and using the result of Eqs. (14) and (15),

$$S=[1+V/W_R]^{-1}, \tag{16}$$

once we know how V depends upon the rf field.

The probability V_{jk} is often calculated from the semiclassical perturbation treatment of radiation,[10] in which event one assumes the existence of zero-order spin functions u_n, which satisfy the eigenvalue equation

$$\mathcal{H}_s u_n = E_n u_n, \tag{17}$$

and a perturbing interaction,

$$\mathcal{H}'=A[e^{i\omega t}+e^{-i\omega t}]=2A\cos\omega t. \tag{18}$$

In our case of particular interest in magnetic dipole

[9] To the extent that Bloch's phenomenological equations [Phys. Rev. **70**, 460 (1946)] adequately represent the motion of the magnetization vector associated with a particular spin system, the time T_1 describing the exponential decay of that magnetization will, of course, be a perfectly useful parameter. However, one cannot assert generally that the Bloch T_1 bears any simple relationship to the λ's of Eq. (6). Special cases in which the Bloch parameters are rigorously related to microscopic quantities are discussed by R. K. Wangsness and F. Bloch [Phys. Rev. **89**, 728 (1953)].

[10] See, for example, L. I. Schiff, *Quantum Mechanics* (McGraw-Hill Book Company, Inc., New York, 1949), Secs. 29 and 35.

transitions, A may arise from an interaction $-\boldsymbol{\mu}\cdot\mathbf{H}$ where $\mathbf{H}$ is the field of the oscillator used in the laboratory to cause spin resonance. Then the usual time-dependent perturbation calculation yields the following first-order expression for the probability that the system, initially in a state j, will be found in state k:

$$|a_k(t)|^2=\hbar^{-2}|(k|A|j)|^2\frac{4\sin^2[\frac{1}{2}(\omega_{kj}-\omega)]}{(\omega_{km}-\omega)^2}. \quad (19)$$

For times not too short,

$$\frac{4\sin^2[\frac{1}{2}(\omega_{kj}-\omega)t]}{(\omega_{kj}-\omega)^2}=t\cdot\delta(\nu_{kj}-\nu), \quad (20)$$

and the probability per unit time is

$$V_{j\to k}=\hbar^{-2}|(k|A|j)|^2\delta(\nu_{kj}-\nu). \quad (21)$$

If we take $\mathcal{H}'=-\mu_x(2H_1)\cos(\omega t)$ and suppose that the spin resonance frequencies of the individual spins of the sample are distributed over a finite frequency range according to a normalized line shape function $g(\nu)$, then

$$V_{jk}=\hbar^{-2}H_1^2|(k|\mu_x|j)|^2g(\nu). \quad (22)$$

The V_{jk} so obtained is of necessity microscopically reversible, because μ_x is Hermitian.

If, however, the quantum nature of the radiation field is taken into account, the probability of absorptive transition is proportional to the mean number of photons $n(\nu)$ per degree of freedom of the field coordinates belonging to waves of frequency ν. If $\rho(\nu)d\nu$ is the energy density of the field per unit volume in the frequency range $d\nu$, then[11]

$$n(\nu)=\frac{c^3}{8\pi h\nu^3}\rho(\nu). \quad (23)$$

The quantum treatment of emission shows it to be proportional to $n(\nu)+1$, thus including in the theory the spontaneous emission probability (when $n(\nu)=0$) arrived at by Einstein from statistical considerations of thermal equilibrium. To test the effective reversibility of emission and absorption probabilities, we evaluate $[n(\nu)+1]/n(\nu)$ for the signal generator, assuming it to produce an rf field of about 0.1 gauss in a frequency interval of at most 100 cycles/sec at 6×10^7 cycles/sec. One finds from Eq. (23) that $n(\nu)$ is at least 10^{25}. Then clearly, to the extent that $n(\nu)+1\cong n(\nu)$, we may consider that $V_{jk}=V_{kj}$ even when the quantum nature of our laboratory radiation field is taken into account. We shall use for either V_{jk} or V_{kj} the semiclassical result (22) which, since it is proportional to H_1^2 and includes no possibility of spontaneous emission, must correspond to the actual *absorption* probability.

[11] E. U. Condon and G. Shortley, *Theory of Atomic Spectra* (Cambridge University Press, Cambridge, 1935), p. 80.

5. THE TRANSITION PROBABILITIES EFFECTING RELAXATION

The application of perturbation theory to the calculation of transitions induced by $\mathcal{H}_{sl}$ is, in principle, straightforward. One treats $\mathcal{H}_{sl}$ as a perturbing interaction for the zero-order Hamiltonian,

$$\mathcal{H}_0=\mathcal{H}_s+\mathcal{H}_l, \quad (24)$$

where $\mathcal{H}_s$ and $\mathcal{H}_l$ are, respectively, the spin and lattice Hamiltonians. In practice, however, even the assembly of spins, which may often be considered as noninteracting among themselves, offers a highly degenerate system for which the orthonormal zero-order linear combinations are not known, nor are the normal modes for the lattice. The classic example of a serious effort to take into account the normal modes for a particular lattice is Van Vleck's calculation of the relaxation times for titanium and chrome alums.[12]

Our experiments deal with liquids, for which there is available almost no information on "lattice" eigenstates. Bloembergen, Purcell, and Pound[7] have, however, obtained excellent results for nuclear paramagnetic relaxation in liquids by approaching the problem from the point of view of the correlation spectrum. The procedure is effectively one of using the semiclassical perturbation treatment for the effect of an oscillatory magnetic field component which might arise through translational or rotational motions of the charges associated with molecules of the liquid; these frequency components are then taken to be distributed according to the correlation spectrum. We can illustrate this procedure by taking A of our Eq. (18) as a product (or as a sum of products), one factor containing (lattice) space coordinates and the other dependent upon particle angular momentum operators,

$$A=f(\mathbf{r})F_{op}(\mathbf{I},\mathbf{J}). \quad (25)$$

Then Eq. (19) becomes

$$U_{j\to k}=\hbar^{-2}|f(\mathbf{r})|^2|(k|F_{op}|j)|^2\delta(\nu_{kj}-\nu). \quad (26)$$

The correlation theory for liquids leads to the conclusion that $|f(\mathbf{r})|^2$ is distributed spectrally according to the intensity,[7]

$$J(\nu)=\langle|f(\mathbf{r})|^2\rangle_{\text{Av}}\frac{2\tau_c}{1+4\pi^2\nu^2\tau_c^2}, \quad (27)$$

where τ_c is the correlation time and the average is over all time or, equivalently, over all space if $f(\mathbf{r})$ is a function of coordinates which vary randomly with time. Combining Eqs. (26) and (27), one obtains

$$U_{jk}=\hbar^{-2}\langle|(k|f(\mathbf{r})F_{op}(\mathbf{I},\mathbf{J})|j)|^2\rangle_{\text{Av}}j(\nu_{kj}), \quad (28)$$

where $j(\nu)$ is the normalized spectrum

$$j(\nu)=\frac{2\tau_c}{1+4\pi^2\nu^2\tau_c^2}. \quad (29)$$

[12] J. H. Van Vleck, Phys. Rev. **57**, 426 (1940).

We now ask to what extent a proper quantum approach, analogous to Van Vleck's for the alums, would yield significant features not present in this semiclassical result.

Following the procedure of Sommerfeld and Bethe,[13] for example, we would prefer to have quantized the normal modes of the lattice. The lattice states would then be described by a set of quantum numbers n_i for the ith mode of elastic waves. The energy of the quantized mode is given by $(n_i+\frac{1}{2})\hbar\omega_i$, and energy exchange between such modes and the spins may be described as either emission or absorption of a "phonon" of energy $\hbar\omega_i$ by the spin system. The formalism is quite parallel to that for the radiation field, including the fundamental asymmetry between emission and absorption. The probability of emission (creation) of a phonon of frequency ω_i by the spin system is proportional to n_i+1, whereas that of absorption (annihilation) is simply proportional to n_i.

If the lattice temperature is T, the mean value of n_i is

$$\bar{n}_i=\frac{1}{\exp(\hbar\omega_i/kT)-1}, \tag{30}$$

so that emission and absorption probabilities are in the ratio

$$\frac{U_{\text{emission}}}{U_{\text{absorption}}}=\frac{\bar{n}_i+1}{\bar{n}_i}=\exp(\hbar\omega_i/kT). \tag{31}$$

As with the semiclassical treatment of the radiation field, Sec. 4, the semiclassical result (28) is microscopically reversible and is proportional to the intensity of the effective phonon field. We again identify the semiclassical result with the absorption probability of a full quantum treatment, and the emission probability is to be calculated from Eq. (31). Thus, if spin state k has greater energy than state j,

$$\begin{aligned} U_{j\to k}&=\hbar^{-2}\langle|(k|f(\mathbf{r})F_{op}(\mathbf{I},\mathbf{J})|j)|^2\rangle_{Av}j(\nu_{kj}) \\ U_{k\to j}&=U_{j\to k}e^{h\nu_{kj}/kT}. \end{aligned} \tag{32}$$

Note that Eq. (32) disagrees with BPP's Eq. (30) (which is for the special case of spin $\frac{1}{2}$). Although the BPP equation gives the proper ratio of emission and absorption probabilities, each depends upon the zero of the energy scale used in measuring E_p and E_q of BPP Eq. (29).

The distinction between solids and liquids, so far as application of Eq. (32) is concerned, lies in the selection of $j(\nu)$. It may be, for a solid, the normalized Debye spectrum of the familiar classical theory of the specific heat, or, for a liquid, it may be the correlation spectrum (29). The essential parameter in the first case is the Debye temperature, whereas in the second it is the correlation time.

[13] A. Sommerfeld and H. Bethe, *Handbuch der Physik* (Springer, Berlin, 1933), second edition, Vol. 24/2, p. 500 ff.

6. DETAILED BALANCE AND SPIN SATURATION

If spin state k has higher energy than state j, then at thermal equilibrium the principle of detailed balance,

$$N_kU_{kj}=N_jU_{jk}, \tag{33}$$

combines with Eq. (31) to assure a Boltzmann distribution among the spin states.

It is interesting to raise the question whether the principle of detailed balance applies to the spin system in a partially saturated state. Treatises on statistical mechanics often arrive at detailed balance by a classical argument, and none which has come to the authors' attention is clear in a quantum statistical way on whether detailed balance is applicable outside of thermal equilibrium. For our particular problem, the assumption of detailed balance outside thermal equilibrium appears to lead to a contradiction, as is perhaps most easily illustrated for three levels between any pair of which the selection rules for the interaction effecting relaxation permit transitions.

If N_1, N_2, and N_3 are the level populations, then the steady state solution of Eqs. (9) and (10) under conditions of detailed balance leads to an expression for N_1-N_2 which can be cast into the form

$$N_1-N_2=N\frac{W_{23}W_{31}-W_{13}W_{32}}{W_{13}W_{32}+W_{13}W_{23}+W_{31}W_{23}}. \tag{34}$$

Now suppose a monochromatic radiation field inducing transitions between 1 and 2 is introduced. Then $W_{12}=U_{12}+V$ and $W_{21}=U_{21}+V$ will be altered, and the other W's remain simply the corresponding U's. We know experimentally that increasing $V_{12}=V_{21}=V$ enables us to diminish N_1-N_2 as much as we please. Yet, by assuming detailed balance, we expressed N_1-N_2 independently of W_{12} and therefore of V.

Another way of making this point is to observe that detailed balance requires the condition

$$W_{12}W_{23}W_{31}=W_{21}W_{32}W_{13}, \tag{35}$$

which becomes, for no rf field,

$$U_{12}U_{23}U_{31}=U_{21}U_{32}U_{13}. \tag{36}$$

If $V_{12}=V_{21}=V$ is impressed with an external radiation field, then (35) becomes

$$(U_{12}+V)U_{23}U_{31}=(U_{21}+V)U_{32}U_{13}, \tag{37}$$

which cannot hold for all V if $U_{21}\neq U_{12}$.

Of course, the arguments of this section do not include explicit account of direct interaction between the rf field and the lattice. Although this is usually extremely weak, and is considered not to affect the lattice energy states nor their populations, the U's are in principle altered by this perturbation and a convincing demonstration would have to verify that the U's are not so altered as to keep Eq. (37) always valid. Our argument is essentially that V can be and is made

comparable to or greater than U_{12}, whereas the radiation field-lattice interaction should affect the U's only by a very small (negligible, we think) fraction.

In the analysis of Sec. 3, therefore, the simple conservation of systems, as described by Eqs. (9) and (10), and the assumption that the presence of V does not alter the U's are used to obtain the saturation factor. There is no question of applying detailed balance, since it is violated by these assumptions.

7. APPARATUS AND EXPERIMENTAL PROCEDURE

Figure 2 is a block diagram of the apparatus used to produce the transitions, detect the resonance, and measure the saturation factor S. The 60-Mc/sec rf field is produced in the tank coil of a Colpitts-type oscillator which forms part of a magnetic resonance spectrometer similar in design to that of Schuster.[14] Audio amplifiers with a total gain of about a million followed the resonance detector and fed a phase-sensitive detector.[15]

A 30-cycle signal generator produced a square wave reference signal for the phase-sensitive detector and a synchronized sinusoid which, after power amplification, modulated the Helmholtz coil field of about 30 oersteds. This generator also supplied the 30-cycle signal to the grid of the calibrator,[16] a device which essentially places the plate resistance of a triode, type 955 in this case, across the oscillator tank coil to provide dissipation which simulates a nonsaturable signal serving as a comparison standard for the paramagnetic sample.

In order to know the transition probability (22) produced by the oscillator for a given sample, one requires the half-amplitude H_1 of the rf field at the sample. For this purpose a vacuum tube voltmeter was built into the apparatus to measure the rms voltage v across the sample coil. The inductance of the coil, which was wound of small flat copper strap to minimize the capacitance between turns, was determined, and the ratio of magnetic field to current in the coil was obtained by performing an auxiliary resonance experiment for which a direct current through the coil produced the external magnetic field for a still smaller coil containing a free radical. The result so obtained is that

$$H_1 = 0.022v. \tag{38}$$

A typical measurement of the saturation factor might proceed as follows. The plate voltage of the oscillator is adjusted to provide a low level of oscillation, and the calibrator is set to give a signal equal to that obtained from the paramagnetic sample. The level of oscillation is then increased and a new comparison of calibrator and sample signals is made. In general, the power level and changes in the properties of the oscillator circuit at the new oscillation level will alter the absolute signal intensity, but these changes will affect equally the signal from a given dissipative load across the coil, whether of paramagnetic or calibrator origin, and the relative intensity is meaningful. If the calibrator and the sample still produce the same relative signal, then S is still unity and saturation has not set in. The oscillation level is then further increased until a curve of S *versus* v, the rms coil voltage, is plotted; by means of Eq. (38) such a curve can be converted to S *versus* H_1.

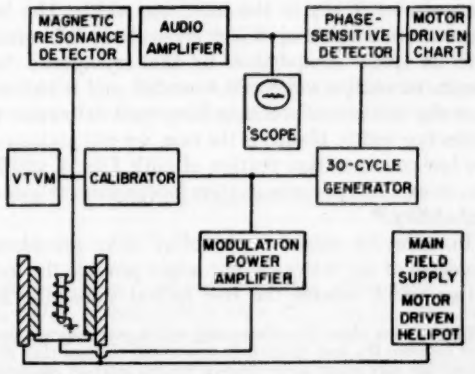

FIG. 2. Block diagram of the experimental arrangement.

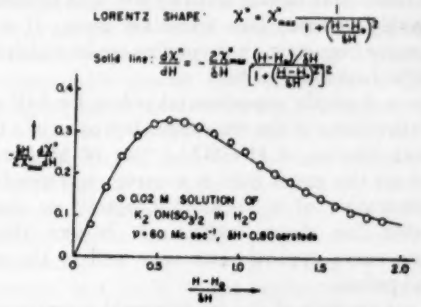

FIG. 3. Comparison of experimental absorption derivative points with the first derivative of a Lorentz shape function. To obtain the entire absorption derivative, the curve shown should be reflected in the origin.

The shape function $g(\nu)$ required to calculate V_{jk} from (22) is determined from the measured resonance curves at low power (where $S=1$). Since the modulation technique is used, the line profile actually measured is proportional to the derivative $dg/d\nu$. Of course, the calibrator triode is supplied with a 30-cycle grid signal to provide a standard signal coherent with the phase-sensitive detector reference voltage.

8. EXPERIMENTAL RESULTS

Aqueous solutions of $K_2ON(SO_3)_2$ are unstable and often become diamagnetic in a matter of several minutes, the decay products catalyzing the spin-pairing reaction. It was found that making the solution about

[14] N. A. Schuster, thesis, Washington University, 1951 (unpublished).
[15] N. A. Schuster, Rev. Sci. Instr. **22**, 254 (1951).
[16] G. D. Watkins and R. V. Pound, Phys. Rev. **82**, 343 (1951). The authors are indebted to Dr. Watkins for communicating to them further information on his work.

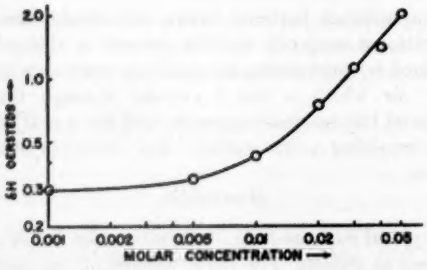

FIG. 4. Experimental line width *versus* concentration of $ON(SO_3)_2^{--}$ ion in aqueous solution. The quantity δH is defined in Fig. 3.

0.1 normal in Na_2CO_3 stabilizes the free radical solution in a *p*H range proper to prevent appreciable deterioration for several days.[17] In this way, measurements were easily made on samples containing various concentrations of $ON(SO_3)_2^{--}$ ion.

All measurements reported here were made at 60 Mc/sec for the transition $(F=\frac{3}{2},\ m_F=-\frac{3}{2})\leftrightarrow(F=\frac{3}{2},\ m_F=-\frac{1}{2})$, which is transition 4↔3 on Fig. 1. This transition was selected because its frequency *versus* field characteristic does not depart sufficiently from linearity to complicate width measurements, as may happen for those transitions having small $d\nu/dH$, and because it is reasonably intense. This transition gives, at a fixed microwave frequency, the hyperfine triplet which occurs in the highest external field.

Figure 3 graphs experimental points for half of the derivative curve of the resonance absorption of a $0.02M$ aqueous solution of $ON(SO_3)_2^{--}$ at 60 Mc/sec. Also placed on the graph field is a curve corresponding to the derivative of a so-called Lorentz[18] or damped-oscillator line shape function. It is seen that the Lorentz curve approximates very well to the experimental points.

In our analysis of the experimental saturation data, we follow BPP, whose equations[19] can be adapted to show that for our situation (BPP case I: the modulation frequency is much less than W_R) the decline in the derivative extremum under saturation is given by a saturation factor,

$$S'=\frac{d\chi''(H_1)}{d\nu}\Big/\frac{d\chi''(H_1\to 0)}{d\nu}=[1+V/W_R]^{-\frac{1}{2}}=S^{\frac{1}{2}}. \quad (39)$$

Note that S' is not a derivative of S. The value of V to be used in this expression is its maximum at the resonance center, thus corresponding to the maximum value of $g(\nu)$. For a Lorentz line, $g(\nu)_{\max}$ is $1/\pi$ times the reciprocal of the half-width $\delta\nu$ at half-maximum intensity on the unsaturated $g(\nu)$ curve. If one measures experimentally the width, in magnetic field units, between points of extreme slope, the conversion between the measured quantity ΔH and $g(\nu)_{\max}$ is, for the Lorentz shape function shown on Fig. 3,

$$g(\nu)_{\max}=(4/\sqrt{3})(\gamma\Delta H)^{-1}, \quad (40)$$

where $\gamma=d\omega/dH$ is obtained from the (angular) frequency *versus* field characteristic for the transition in question. The parameter δH of Fig. 3 is, in terms of the width between inflection points, $(\sqrt{3}/2)\Delta H$.

Figures 4 and 5 plot, respectively, the experimental values of δH and of the relaxation probability W_R *versus* the molar concentration of $ON(SO_3)_2^{--}$ ion. At concentrations above $0.05M$, the hyperfine structure begins to give way to a single broad line. The lower limit of the concentration range is determined by the decline in signal sensitivity as fewer and fewer free radicals are present in the sample.

A striking feature of Figs. 4 and 5 is that both the line width and relaxation probability appear to approach

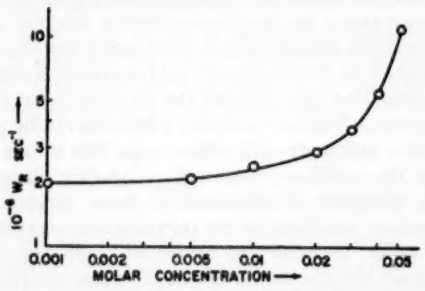

FIG. 5. Experimental relaxation probability W_R *versus* concentration of $ON(SO_3)_2^{--}$ ion in aqueous solution.

asymptotically a concentration independent value. The relaxation probability, through its limitation of the lifetime of a spin state, should contribute an amount the order of W_R/γ to the total line width. The low-concentration value of W_R/γ gives about 0.7 oersted. This is quite comparable to the asymptotic low-concentration line width of 0.3 oersted, and it indicates that the relaxation processes may well determine the entire line width. If such is the case, we will understand the low-concentration portion of both Figs. 4 and 5 if we can explain the concentration independent relaxation probability.[20]

In order to test the possibility that the nuclear moments of the water solvent might provide the interaction which relaxes the free radical spins, the low-

[17] We are indebted to Professor Weissman of the Washington University department of chemistry for this discovery.

[18] G. E. Pake and E. M. Purcell, Phys. Rev. **74**, 1184 (1948).

[19] Reference 7, Sec. IV, Eq. (17). The BPP saturation parameter s is our V/W_R.

[20] Depending upon the relationship which one assumes should exist between W_R and its contribution to δH, the fact that W_R/γ *exceeds* δH may cause some concern for the internal consistency of our measurements; the line cannot be sharper than the uncertainty principle would allow. However our procedure of calibrating the rf coil (Sec. 7) when it carries direct current is not beyond reproach, inasmuch as the current distribution throughout the cross section of the copper strap at 60 Mc/sec is certainly somewhat different from the dc distribution. Therefore a factor of perhaps 2 must be allowed in our absolute values of W_R; relative values should be good within 10 percent or better.

concentration measurements of Figs. 4 and 5 were made for solutions of $ON(SO_3)_2^{--}$ in D_2O. Although the deuteron magnetic moment is about 0.3 that of the proton, the curves for the D_2O solution were indistinguishable from those of Figs. 4 and 5. We thus have experimental indication that the nuclear moments of the solvent do *not* provide the relaxation mechanism.

9. THE SATURATION FACTOR FOR THE TRANSITION STUDIED

In order to compare postulated relaxation mechanisms with the measured value of W_R, we require the expression for W_R in terms of the U's for $ON(SO_3)_2^{--}$. There are six homogeneous equations of the form (9) for a system with the energy levels of Fig. 1. For magnetic dipole transitions in the radio-frequency range, the Boltzmann factors associated with emission [Eq. (31)] usually depart from unity by less than 10^{-4}. Furthermore, BPP finds for water at room temperature that $\tau_c = 4\times10^{-2}$ sec. In 31.4 oersteds, all transitions permitted between the levels of Fig. 1 occur at frequencies of 10^7 or 10^8 sec^{-1}. By Eq. (29), the resulting correlation spectrum $j(\nu)$ is essentially "white" with intensity $2\tau_c$ per unit frequency range.

Comparison of relative values of the coefficients in the six homogeneous equations may therefore be made from

$$U_{jk} = \hbar^{-2}\langle f(\mathbf{r})^2\rangle_{Av} |(k|\mathfrak{y}|j)|^2 2\tau_c, \tag{41}$$

in which the operator function F_{op} of Eq. (28) is

$$\mathfrak{y} = -g_J\mu_0\mathbf{J} + g_I\mu_0\mathbf{I} \cong -g_J\mu_0\mathbf{J}, \tag{42}$$

and its matrix elements are to be calculated using the spin functions (2) which apply for 31.4 oersteds. Such nonvanishing values of $|(k|J_x|j)|^2$ for the π transitions and $|(k|J_z|j)|^2$ for σ transitions are tabulated in decreasing order in Table I.

Magnetic dipole transitions between level pairs 1 and 3, 1 and 4, 1 and 5, 2 and 4, and 4 and 6 are forbidden. In addition we shall neglect the three weakest permitted transitions (3 to 6, 5 to 6, and 1 to 2) in solving for S_{43}. After so doing, one finds for S_{43} an equation of the type of Eq. (15) with W_R (43) given by

$$W_R(43) = U_{43} + U_{45} \times \frac{U_{23}U_{35} + U_{23}U_{25} + U_{25}U_{35}}{U_{23}U_{35} + U_{23}U_{45} + U_{23}U_{25} + U_{25}U_{45} + U_{25}U_{35}}. \tag{43}$$

Here we have dropped "thermal differences," i.e., $U_{jk} - U_{kj}$, in comparison with U_{ij}; this may be done as soon as the equations are placed in a form corresponding to Eq. (12) and it greatly simplifies solution.[21]

[21] It is useful to note that the form of the equations and the fact that W_R must depend upon quantities of zero order in "thermal differences" allows one to set up an analogy with a passive network of conductances. Branch points in the analog network correspond to the energy states of the system, and the conductance between j and k corresponds to U_{jk}. This is perhaps the simplest method for calculating W_R in a particular case.

TABLE I. Nonvanishing matrix elements of J_x and J_z connecting the energy states of Fig. 1 are tabulated for a value of x corresponding to 31.4 oersteds. For a "white" correlation spectrum, the respective transition probabilities (41) are proportional to the tabulated numbers.

j	k	$\lvert(k\lvert J_x\rvert j)\rvert^2$	$(k\lvert J_z\rvert j)^2$
3	5		0.350
1	6	0.237	
3	4	0.226	
2	5	0.224	
2	6		0.190
4	5	0.024	
2	3	0.023	
1	2	0.012	
5	6	0.011	
3	6	0.001	

The error in dropping the three weak transitions is evidently not serious, since the correction to U_{43} in Eq. (43) is, for an isotropic white radiation bath, easily shown from the table to be about 10 percent of U_{43}. Errors of 10 percent or so can easily creep into saturation measurements of W_R.

10. THE RELAXATION MECHANISM AT THE HIGHER CONCENTRATIONS

At the high-concentration end of the curves of Figs. 4 and 5, one expects ion-ion collisions to effect relaxation and W_R should be proportional to concentration. Experimentally the log-log plot of Fig. 4 approaches a slope measurably greater than unity, which effect, if real, is unexplained. Measurements are in general difficult to make in this region of concentration, since the hyperfine splitting is about to blur into a single broad line, and the tails of the three high-frequency transitions overlap appreciably. The true width of an individual component line is not easily arrived at under such circumstances.

However, as a check on the mechanism, one should obtain an approximately correct order of magnitude for W_R from the BPP Eq. (50), intended to be used to calculate the contribution to W_R for hydrogen nuclei through their interaction with neighboring water molecules:

$$W_R \cong (9/2)\pi^2 g^4 \mu_0^4 \hbar^{-2} \eta N_0/5kT. \tag{44}$$

Here η is the viscosity, which we take for our solution to be that of water at room temperature, about 10^{-2} cgs units. For 0.05 molar, N is 3×10^{19} cm^{-1} and Eq. (44) gives $W_R = 1.5\times10^7$ sec^{-1}.

The measured value is $W_R = 1.3\times10^7$ sec^{-1}. This is probably adequate agreement considering that we have made the approximation of free electrons by neglecting the nuclear moment coupling and that we have approximated the viscosity of the $ON(SO_3)_2^{--}$ ion.

11. INTERACTION WITH THE NUCLEAR MOMENTS OF THE SOLVENT

Although both D_2O and H_2O had the same effect as solvents, we shall estimate the contribution to W_R to

be expected for this mechanism and check the theory by noting whether the result is negligible in comparison with our measured W_R.

The dipole interaction between the ith hydrogen nucleus of the solvent and the jth ionic spin is

$$\mathcal{H}_{ij}=\boldsymbol{\mu}_i\cdot\boldsymbol{\mu}_j r_{ij}^{-3}-3(\boldsymbol{\mu}_i\cdot\mathbf{r}_{ij})(\boldsymbol{\mu}_j\cdot\mathbf{r}_{ij})r_{ij}^{-5}, \quad (45)$$

where

$$\boldsymbol{\mu}_i=g_I\mu_0\mathbf{I}_i, \quad \boldsymbol{\mu}_j=-g_J\mu_0\mathbf{J}_j. \quad (46)$$

Following BPP, we may write

$$\mathcal{H}_{ij}=-g_I g_J\mu_0^2[A+B+C+D+E+F], \quad (47)$$

where

$$\begin{aligned}
A&=J_{zj}I_{zi}(1-3\cos^2\theta_{ij})r_{ij}^{-3},\\
B&=-\tfrac{1}{4}[J_{+j}I_{-i}+J_{-j}I_{+i}](1-3\cos^2\theta_{ij})r_{ij}^{-3},\\
C&=-\tfrac{3}{2}[J_{zj}I_{+i}+J_{+j}I_{zi}]\sin\theta_{ij}\cos\theta_{ij}e^{-i\phi_{ij}}r_{ij}^{-3},\\
D&=-\tfrac{3}{2}[J_{zj}I_{-i}+J_{-j}I_{zi}]\sin\theta_{ij}\cos\theta_{ij}e^{i\phi_{ij}}r_{ij}^{-3},\\
E&=-\tfrac{3}{4}J_{+j}I_{+i}\sin^2\theta_{ij}e^{-2\phi_{ij}}r_{ij}^{-3},\\
F&=-\tfrac{3}{4}J_{-j}I_{-i}\sin^2\theta_{ij}e^{+2\phi_{ij}}r_{ij}^{-3}.
\end{aligned} \quad (48)$$

Symbols I_{+i} and J_{-j} denote the respective raising and lowering operators: $I_{+i}=I_{xi}+iI_{yi}$ and $J_{-j}=J_{xj}-iJ_{yj}$.

As an example, consider the contribution of term E from a proton at distance r:

$$U_{43}^{(E)}(r)=g_I^2g_J^2\mu_0^4\hbar^{-2}\sum_{m_i,m_i'}G_{m_i}\times\langle|(3;m_i'|E|4;m_i)|^2\rangle_{\text{av}}j\left(\frac{W'-W}{\hbar}\right), \quad (49)$$

where

$$W'=W_3-g_I\mu_0Hm_i' \quad \text{and} \quad W=W_4-g_I\mu_0Hm_i.$$

We denote by G_{m_i} the fraction of protons in state m_i, and by W_3 and W_4 the energies corresponding to the levels so numbered in Fig. 1. The nuclear contributions to W' and W are necessary to conserve energy for the transitions, but may be neglected in practice. Therefore

$$j[(W'-W)/\hbar]=2\tau_c,$$

as indicated in Sec. 9.

Apart from terms of order $g_I\mu_0H/kT$ (about 10^{-9} in 30 oersteds), $G_{m_i}=\frac{1}{2}$ for both spin states of the protons within a thin shell at distance r. In order to consider all protons of the solvent, whatever the value of r, we follow BPP by assuming that $\tau_c=r^2/12D$, D being the diffusion constant, and integrating from the distance of closest approach, r_0, throughout the solvent. If there are N_0 solvent protons per unit volume, the contribution of E is

$$U_{43}^{(E)}=g_I^2g_J\mu_0^4\hbar^{-2}\tfrac{1}{2}\sum_{m_i,m_i'}|(3;m_i'|-\tfrac{3}{4}J_{+j}I_{+i}|4;m_i)|^2\times\langle|\sin^2\theta_{ij}e^{-2i\phi_{ij}}|^2\rangle_{\text{av}}N_0\int_{r_0}^{\infty}r^{-6}(2r^2/12D)4\pi r^2dr. \quad (50)$$

Performing the indicated sums and integrations and taking the averages of the angle functions, one obtains

$$U_{43}^{(E)}=\tfrac{1}{6}\pi g_I^2g_J^2\mu_0^4\hbar^{-2}c^2N_0/Dr_0. \quad (51)$$

The diffusion constant is presumably not quite the same as for self-diffusion of pure water. However, we postulate a kind of equivalent viscosity, η, related to r_0D through Stokes law:

$$1/Dr_0=6\hbar\eta/kT. \quad (52)$$

Then

$$U_{43}^{(E)}=\pi^2g_I^2g_J^2\mu_0^4\hbar^{-2}N_0\eta c^2/kT. \quad (53)$$

For pure water, $\eta=10^{-2}$ cgs units near room temperature; lacking any other value, we use this for our solution. From Sec. 1, we find $c^2=0.903$. Finally the relaxation probability obtained from Eq. (53) is

$$W_R^{(E)}\cong 3\times10^4\ \text{sec}^{-1} \quad (54)$$

for a dilute aqueous solution of $ON(SO_3)_2^{--}$ ion. This result is indeed consistent with the conclusion from comparison of H_2O and D_2O as solvents: the interaction with solvent nuclear dipole moments is negligible in relation to the measured W_R of 2×10^6 sec^{-1}.

12. RELAXATION THROUGH THE N^{14} QUADRUPOLE MOMENT

The odd electron cannot, since it has spin $\frac{1}{2}$, possess a quadrupole moment. However, the electron is magnetically coupled to the N^{14} nucleus, and quadrupolar interactions between the N^{14} nucleus and fluctuating electric field gradients within the liquid can in principle relax the electron spins via the magnetic electron-nuclear coupling.

We deliberately overestimate this contribution to W_R by supposing for argument's sake that the entire electric quadrupole interaction of the N^{14} nucleus with fluctuating electric field gradients is effective in relaxing the electron spin. Actually such relaxation can occur only in low magnetic fields where the coefficients b and d entering into the linear combinations (2) of spin functions are appreciable. An order of magnitude upper limit to W_R from this interaction is therefore, following Eqs. (28) and (29),

$$W_R\sim\hbar^{-2}(eQ)^2\left\langle\left(\frac{\partial^2\phi}{\partial z^2}\right)^2\right\rangle_{\text{av}}2\tau_c, \quad (55)$$

in which Q is the N^{14} quadrupole moment and ϕ is the electric scalar potential at the nucleus.

Accurate theoretical evaluations of a representative component of the electric field gradient have not been made, even for a rigid lattice, and equally little is known about the average square of such a component for a liquid. However, Bloembergen[22] found that the deuteron effected nuclear relaxation in liquid D_2O, and that the electric field gradient has a magnitude essentially that

[22] N. Bloembergen, thesis, University of Lieden (Martinus Nijhoff, The Hague, 1948).

at 1A or 2A from an electronic charge. For an estimate, we take er^{-3}, with $r=1$A, as the magnitude of $\partial^2\phi/\partial z^2$. The value of Q for N^{14} is about 10^{-26} cm^2. Taking $\tau_c \cong 10^{-11}$ sec, one finds that $W_R \sim 10^{+3}$ sec^{-1}, which is again much smaller than the observed value, 2×10^6 sec^{-1}.

13. THE ROLE OF SPIN-ORBIT COUPLING

In 1936, Kronig[23] proposed that unaccountably short relaxation times in certain alums could be explained by considering the important role played by spin-orbit coupling. The modulation of the spin-spin interaction by the lattice vibrations, considered in Waller's pioneering theory[24] of spin-lattice relaxation, proved entirely inadequate to explain observed relaxation times. Another possibility, the modulation of the crystalline Stark splitting by the lattice vibrations, appears at first sight to hold no promise for relaxation in those substances which possess only Kramers degeneracy in the ground state. However, through the spin-orbit coupling, the modulation of the Stark splitting is felt by the spins.

Van Vleck[12] extended and refined Kronig's ideas in his calculation of relaxation times for titanium and chrome alums. Two processes are distinguished. One, the so-called direct process, gives a highly field-dependent relaxation time which ought to apply at a few degrees Kelvin, but was found to be still too large. The second, or Raman, process is effective in zero as well as in nonvanishing external magnetic fields. It depends upon the inelastic scattering of high-energy vibrational quanta by the spin systems, with the spin system absorbing or emitting a vibrational quantum of very low energy relative to the original vibration quantum. Although this is a second-order process compared to the direct process, it is important because the entire elastic spectrum, rather than a narrow portion at its weak end, is called into play. In fact, the Raman process probably dominates at all but the lowest temperatures.

It is a simple matter[25] to illustrate the influence of a spin-orbit term $\lambda\mathbf{L}\cdot\mathbf{S}$ on Stark orbitals which possess only spin degeneracy. The spin-orbit interaction renders incomplete the quenching of orbital angular momentum by the crystalline electric field, and, as a result, the spectroscopic splitting factor[25] departs from the free electron value, $g_e=2.0023$, by an amount the order of λ/Δ, where Δ is the Stark interaction.

It is less simple to demonstrate the existence, via the Raman process, of relaxation caused by modulation of the Stark splitting in the presence of the spin-orbit term $\lambda\mathbf{L}\cdot\mathbf{S}$. In fact, Kronig's model, as pointed out by Van Vleck,[10] yields vanishing transition probabilities even when pursued to second order in the orbit-lattice modulating interaction. The vanishing in first order is to be expected, but that in second order appears to be due to a cancellation which would not occur if the inherent quantum asymmetry between emission and absorption probabilities (see Secs. 4 and 5) were contained in the calculation. Van Vleck includes this by use of quantized normal modes for the cluster of H_2O molecules about the Ti^{++} ion, and he finds a nonvanishing result in second order (third order in reference 10, inasmuch as the zero-order functions used do not yet include the effect of the $\lambda\mathbf{L}\cdot\mathbf{S}$ coupling).

In the present problem, we have no knowledge of the normal modes of the liquid "lattice." In fact, the free radical ion presents several complications. The ion itself is not spherically symmetric. When such is the case, as pointed out by Mizushima and Koide[26] and suggested independently by H. Primakoff, the spin-orbit interaction is not simply proportional to $\mathbf{L}\cdot\mathbf{S}$. The Dirac equation, after elimination of the small component wave functions, yields two interaction terms[27] which may be included[28] in the spin-orbit interaction:

$$\mathcal{H}_{\text{spin-orbit}} = -\frac{\hbar^2}{4m^2c^2}(\text{grad}V)\cdot\text{grad} + \frac{\hbar}{4m^2c^2}\mathbf{s}\cdot[(\text{grad}V)\times\mathbf{p}]; \quad (56)$$

the potential energy function for the electron is V, $\mathbf{s}$ is the electron spin, and $\mathbf{p}$ is its linear momentum operator. A proper accounting of spin-orbit effects would thus require use of (56) instead of $\lambda\mathbf{L}\cdot\mathbf{S}$.

A second complication is that, for the $ON(SO_3)_2^{--}$ ion in aqueous solution, we may justifiably think of two sources for the orbit-lattice interaction which modulates the Stark splitting for the odd electron. One source involves the internal vibrations of the ion itself which produce fluctuating local electric fields over the orbit of the electron, and the other is the solvent as its randomly moving water dipoles also produce fluctuating local fields over the electron orbit.

Whereas a theoretical investigation of the interaction (56) presents grave difficulties for a free radical ion about which we know so little concerning the odd electron wave function, experiment may be able to distinguish which source of the orbit-lattice interaction is dominant, *provided*, of course, that spin-orbit coupling is involved in determining the W_R value measured experimentally. In order to shed some light on this important question, we brush aside our ignorance of the quantum nature of the motions and suppose that, for some fortuitous reason, the spectrum of their vibrations influences the Raman processes for $ON(SO_3)_2^{--}$ approximately as it does for Ti^{++} in titanium alum. For the latter Van Vleck obtains about 10^9 sec^{-1} as the reciprocal relaxation time (which is essentially our W_R)

[23] R. deL. Kronig, Physica **6**, 33 (1936).
[24] I. Waller, Z. Physik **79**, 370 (1932).
[25] C. Kittel, Phys. Rev. **76**, 743 (1949).
[26] M. Mizushima and S. Koide, J. Chem. Phys. **20**, 765 (1952).
[27] L. I. Schiff, *Quantum Mechanics* (McGraw-Hill Book Company, Inc., New York, 1949).
[28] Reference 9, p. 130.

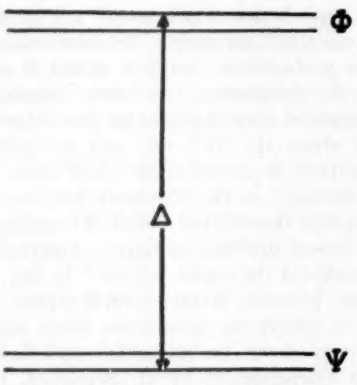

FIG. 6. The two lowest orbital levels.

due to Raman processes at normal temperatures and low fields. The matrix element in the transition probability is proportional to λ/Δ^2, where Van Vleck takes Δ, the Stark splitting, to be about 1000 cm^{-1} and λ/Δ to be about 1.5×10^{-1}. For free radicals, Δ may well be about the same as for titanium alum, but λ/Δ is much smaller; the spectroscopic splitting factor for $ON(SO_3)_2^{--}$ is 2.0055, measured in high fields,[29] indicating that $\lambda/\Delta\approx10^{-3}$. Since W_R is proportional to the square of the matrix element, our utterly crude adjustment of the titanium result simply scales it down by the square of the ratio of the respective λ's, giving $W_R\sim10^5$ sec^{-1}. In view of the high power of Δ involved and our wild approximations, this can hardly be called disagreement with the measured W_R, 2×10^6 sec^{-1}.

It is thus entirely possible that spin-orbit effects do lead to the observed W_R, and experiments are underway in this laboratory to examine whether it may be the solvent or the internal vibration of the ion which provides the orbit-lattice interaction.

14. RELAXATION THROUGH STATISTICAL PROCESSES OF SECOND ORDER

An interesting possibility for relaxation is brought out by our detailed expression (15) for the relaxation probability. In Van Vleck's calculation, discussed in the previous section, the quantity estimated corresponds only to U_{21}, and nothing has yet been said about the remaining function of U's in Eq. (15). Although this function may, as in Sec. 9, normally be small compared to U_{21}, such may not be the case if one must go to second or higher orders to obtain a nonvanishing U_{21}. Physically, this means that a relaxation mechanism which does not produce direct transitions between the levels under consideration may still effect relaxation by first carrying systems to a third level and then to the second. Such a process is second order in a *statistical* rather than a perturbation theory sense, i.e., energy is conserved for both transitions, whereas the second-order quantum perturbation transition probability does not require energy conservation for the intermediate state.

The simple model of Kronig[24] is adequate for application of this idea to a free radical ion with spin-orbit coupling. We suppose that the odd electron of $ON(SO_3)_2^{--}$ is subject to a molecular Stark field which splits the orbital states into widely separated levels. For simplicity in illustrating the point, we follow Kronig by supposing that the two lowest orbital levels (see Fig. 6) are separated by energy Δ, whereas other orbital states have much higher energies and need not be considered further. Let these two orbital states, which retain their spin degeneracy, be ψ and ϕ. Then, if α and β refer to spin states $+\frac{1}{2}$ and $-\frac{1}{2}$, respectively, the effect of a spin-orbit interaction $\lambda\mathbf{L}\cdot\mathbf{S}$ is, to first order in λ/Δ, to produce the following mixtures of the unperturbed functions $\psi\alpha$, $\psi\beta$, $\phi\alpha$, and $\phi\beta$:

$$\begin{aligned}
\Psi_1&=\psi\alpha-\frac{\lambda}{\Delta}b\phi\alpha-\frac{\lambda}{\Delta}a\phi\beta,\\
\Psi_2&=\psi\beta+\frac{\lambda}{\Delta}a^*\phi\alpha+\frac{\lambda}{\Delta}b\phi\beta,\\
\Psi_3&=\phi\alpha-\frac{\lambda}{\Delta}b\psi\alpha-\frac{\lambda}{\Delta}a\psi\beta,\\
\Psi_4&=\phi\beta+\frac{\lambda}{\Delta}a^*\psi\alpha+\frac{\lambda}{\Delta}b\psi\beta.
\end{aligned}\tag{57}$$

Here,

$$a=\tfrac{1}{2}\int\phi(L_z+iLy)\psi d\tau,\quad b=\tfrac{1}{2}\int\phi L_z\psi d\tau=-b^*.\tag{58}$$

In Eq. (58), ϕ is not denoted complex conjugate since, under the conditions of quenched orbital angular momentum, $\int\phi\mathbf{L}\phi d\tau=\int\psi\mathbf{L}\psi d\tau=0$, it is possible to express ϕ and ψ as real numbers.[17]

If one sets up Eqs. (9) and (10) and solves for the saturation factor and for W_R associated with transitions between Ψ_1 and Ψ_2, he finds the following result:

$$W_R^{(12)}\cong\tfrac{1}{2}U_{14}.\tag{59}$$

In obtaining Eq. (59), one uses $U_{12}=0=U_{34}$, as obtained from Eqs. (57). Also, in terms of absorption probabilities, the wave functions yield $U_{13}/U_{14}\approx U_{23}/U_{24}\approx(\lambda/\Delta)^2$. The relation (32) between absorption and emission holds, e.g.,

$$U_{41}=U_{14}e^{\Delta/kT}.\tag{60}$$

Here, contrary to cases previously cited, the exponential factor is far from unity if Δ corresponds to about 1000 cm^{-1} ($\Delta/kT\sim5$ at room temperature) and the result for W_R has been simplified by dropping absorption probabilities relative to emission probabilities.

[29] J. Townsend (unpublished).

We can evaluate U_{14} from Eq. (32) in which it must be recalled that we now require $j(\nu_{jk})$ at $\nu_{jk}=\Delta/h \approx 3\times10^{13}$ sec^{-1}. If we take $F_{\alpha\beta}(\mathbf{I},\mathbf{J})=1$ in Eq. (32) and denote

$$\langle(4|f(\mathbf{r})|1)|^2\rangle_{Av}$$

$$=\left|\frac{\lambda}{\Delta}a\right|^2\left\langle\left|\int\psi f(\mathbf{r})\psi d\tau-\int\phi f(\mathbf{r})\phi d\tau\right|^2\right\rangle_{Av}$$

$$=\left|\frac{\lambda}{\Delta}a\right|^2\delta^2, \tag{61}$$

where δ^2 is a measure of the mean square of the electric interaction $f(\mathbf{r})$ which modulates the Stark effect, then, by Eq. (32),

$$U_{14}=\hbar^{-2}|a|^2\left(\frac{\lambda}{\Delta}\delta\right)^2 j\left(\frac{\Delta}{h}\right). \tag{62}$$

Since $|a|^2\approx1$ and $j(\Delta/h)\approx1/(2\pi\Delta^2\tau_c/h^2)$ for $\Delta/h>1/\tau_c$, we have

$$W_R=\tfrac{1}{2}U_{14}\approx\left(\frac{\lambda}{\Delta}\right)^2\left(\frac{\delta}{\Delta}\right)^2\frac{1}{\tau_c}. \tag{63}$$

Taking $W_R=2\times10^6$ sec^{-1}, $\lambda/\Delta=10^{-3}$, and $\tau_c=10^{-11}$ for water solutions at room temperature, one finds that, if this mechanism is to be adequate, δ/Δ would have to be the order of unity. It is not unreasonable that the fluctuating Stark interaction arising from motions of the strong water dipoles or the internal vibrations of the ion might be comparable to the static Stark interaction, although the perturbation procedure would be somewhat strained in that event.

Again, the crudeness of our estimate does not lead us to very positive conclusions, but relaxation via the statistical second-order processes is not ruled out.

Whether quantum-mechanical or statistical second-order processes are involved in determining W_R, the experiments now in progress, which are aimed at distinguishing between the source of the modulating Stark field (internal vibrations in the ion or Brownian motions of the solvent), will serve a useful purpose.

15. SUMMARY

In water solutions of the free radical ion $ON(SO_3)_2^{--}$, width of the paramagnetic resonance seems to be determined by spin-lattice relaxation processes, at least for solutions sufficiently dilute to exhibit well-resolved hyperfine structure. The achievement of statistical equilibrium among the various hyperfine levels in low magnetic fields is more complex than in a simple two-level system. Where saturation methods are used, the *relaxation probability* is suggested as a more precisely defined quantity than the relaxation time.

At very low concentrations, the relaxation probability for the particular transition studied reaches a concentration-independent value of 2×10^6 sec^{-1}. Interaction between the free radical and nuclear dipoles of the solvent is demonstrated to be an inadequate mechanism both experimentally and theoretically. The interaction of the N^{14} quadrupole moment of $ON(SO_3)_2^{--}$ with the fluctuating electric field gradient due to the solvent is shown on the basis of an upper limit estimate to be an inadequate mechanism.

On the basis of very crude estimates, it is likely that spin-orbit coupling enables the spins to feel the effects of modulation of the Stark splitting which quenches electronic orbital angular momentum. However, it is not certain whether internal vibrations of the free radical ion or motions of the solvent molecules, or both, effect the modulation.

If the spin-orbit coupling is involved, an interesting possibility is that, for saturation experiments at least, *statistical* second-order processes in contrast to the quantum mechanical second-order processes of Van Vleck may be responsible for the observed relaxation.

ACKNOWLEDGMENTS

Many stimulating and informative discussions with Professor H. Primakoff, Professor S. I. Weissman, and Professor J. Townsend are gratefully acknowledged. Without the chemical skill of Professor Weissman and his research group, the samples used would never have been available for these experiments. One of us (J.P.L.) gratefully acknowledges the assistance of a Shell Fellowship during part of this work.

Determination of h/e by a New Method

F. G. DUNNINGTON, C. L. HEMENWAY,* AND J. D. ROUGH†
Physics Department, Rutgers University, New Brunswick, New Jersey
(Received January 6, 1954)

A new method for the direct determination of h/e has been developed which does not involve the short wavelength limit of the continuous x-ray spectrum. The excitation potential V_e of helium from the ground state to the $2p\ ^1P_1{}^\circ$ state is measured as the energy, in electron volts, lost by electrons causing this excitation. Experimentally, this energy is determined as the difference between two voltages. The value of h/e is calculated from the basic equation $h\bar{\nu}c=V_e e$; here $\bar{\nu}$ is the wave number of the radiation from helium in the $2p\ ^1P_1{}^\circ$ state. Four factors make possible an order-of-magnitude increase in precision over other earlier work dependent on excitation or ionization potentials: (1) the *difference* method of obtaining the excitation potential; (2) a gold evaporation technique which essentially eliminates contact potentials and makes possible a great reduction in surface charges; (3) the high precision in both the slit system and in the uniformity of the magnetic field; and (4) the fact that the absolute magnitudes of the electron beam energy, the magnetic field, and the work function of the cathode do not need to be known. A total of 156 determinations of h/e were made under varying experimental conditions. A multiple correlation analysis of these data shows no significant variation of h/e with experimental conditions. The value obtained with its standard error is $h/e=(1.3790\pm0.0002)\times10^{-17}$ erg·sec/esu. This value is in fairly good agreement with the values found from the short wavelength limit of the continuous x-ray spectrum and with the indirect value computed from all significant work on atomic constants.

I. INTRODUCTION

DURING the past fifteen years no atomic constant has received more attention than h/e, the ratio of Planck's constant to the charge of the electron. The well-known discrepancy[1] between the directly measured value and the indirect (calculated) value has led to several new precision determinations of h/e by measurement of the short wavelength limit of the continuous x-ray spectrum.[2–7] These new determinations have in general given higher values of h/e. The most recent and precise measurements by Bearden and his co-workers[5,6] and by Felt[7] have given values in close agreement with the indirect value. The current situation as to all atomic constants has been presented by DuMond and Cohen[8] and by Bearden and Watts.[9]

It was felt that it would be desirable to make a determination of h/e by an entirely different method. *All* of the experimental determinations of h/e during the last nineteen years have been by the one x-ray method mentioned above. This is probably due to the fact that this method permitted greater experimental accuracy. However, this situation is not altogether satisfactory because it may allow systematic errors characteristic of the method to go undetected. In particular, the method requires the determination of the true tail of the x-ray intensity-voltage curve, although there is no acceptable theory that accounts for the shape of this curve. Fundamentally any direct measurement of h/e involves the determination of the energy (expressed in electron volts) of photons of known wavelength. In the x-ray method the energy of the electrons which produce the photons is measured and then, in effect, the wavelength of the photons that are produced. Other possible methods involve either the photoelectric effect (the exact inverse of the x-ray method) or measurement of either the excitation or ionization potentials of atoms. These latter involve the measurement of the electron energy required to change an atom from the normal to a given excited state; the wavelength of the photon emitted on return to the normal state is assumed to be known from spectroscopic tables. No precise measurements involving the photoelectric effect have been attempted. The three[10] most accurate measurements using either ionization or excitation potentials were made during the period 1926 to 1935 by Lawrence,[11] Van Atta,[12] and Whiddington and Woodroofe[13] and had standard errors[14] averaging about 25 parts in 10^4. This is to be compared with the standard error in the most recent

* Now at Union College, Schenectady, New York.
† Now at The Johns Hopkins University, Applied Physics Laboratory, Silver Spring, Maryland.
[1] See for example R. T. Birge, Repts. Progr. in Phys. **8**, 90 (1944); J. W. M. DuMond, Phys. Rev. **56**, 153 (1939); F. G. Dunnington, Revs. Modern Phys. **11**, 65 (1939).
[2] P. Ohlin, dissertation, Uppsala, 1941 (unpublished); Nature **145**, 223 (1940); **152**, 329 (1943).
[3] J. A. Bearden and G. Schwartz, Phys. Rev. **59**, 934 (1941).
[4] Panofsky, Green, and DuMond, Phys. Rev. **62**, 214 (1942).
[5] J. A. Bearden and G. Schwartz, Phys. Rev. **79**, 674 (1950).
[6] Bearden, Johnson, and Watts, Phys. Rev. **81**, 70 (1951).
[7] G. L. Felt, thesis, California Institute of Technology, 1951 (unpublished); G. L. Felt, J. N. Harris and J. W. M. DuMond, Phys. Rev. **92**, 1160 (1953).
[8] J. W. M. DuMond and E. R. Cohen, Revs. Modern Phys. **25**, 691 (1953).
[9] J. A. Bearden and H. M. Watts, Phys. Rev. **81**, 73 (1951); **81**, 160 (1951).
[10] Summarized in Sec. F of article by Dunnington in reference 1.
[11] E. O. Lawrence, Phys. Rev. **28**, 947 (1926).
[12] L. C. Van Atta, Phys. Rev. **38**, 876 (1931); **39**, 1012 (1932).
[13] R. Whiddington and E. G. Woodroofe, Phil. Mag. **20**, 1109 (1935).
[14] The standard error is (1/0.6745) or about 1.5 times the probable error. Following the practice of DuMond and Cohen (reference 8), it will be used throughout this paper because it represents a better working estimate of the uncertainty. The probable error is expected to be *exceeded* in one out of every two successive determinations, whereas the standard error will be exceeded in only one out of three successive determinations.

x-ray work[5–7] which averages 6 parts in 10^5 and of 3.6 parts in 10^5 in the least squares adjusted value.[8]

The new method reported here involves the measurement of an excitation potential. It has not been possible to quite equal the accuracy of the recent x-ray work but the accuracy attained is an order of magnitude better than that of the earlier work mentioned above.

II. METHOD

In the method that we used,[15] we measured directly the energy (in electron volts) lost by electrons which had excited helium atoms from the ground state $1s^2\ ^1S_0$ to the lowest permitted singlet level $2p\ ^1P_1^\circ$.

The basic part of the apparatus is shown schematically in Fig. 1. From the electron gun essentially monoenergetic electrons are selected by means of the first slit system (3–4–5) and a uniform magnetic field perpendicular to the plane of the diagram. These electrons pass through a small excitation chamber (slits 6 and 7) containing helium gas. If the potential V between the first and second slit systems is zero, the electrons which do not collide with helium atoms pass on through the second slit system (8–9–10) to the collector and the resulting current i is measured by an electrometer amplifier. The electrons which collide inelastically in the excitation chamber are bent inward by the magnetic field and are stopped at slit 9. If, however, the potential V between the slit systems is made equal to that lost by the electrons which have excited helium atoms to the $2p\ ^1P_1^\circ$ level, then these latter electrons will have their original energy restored.

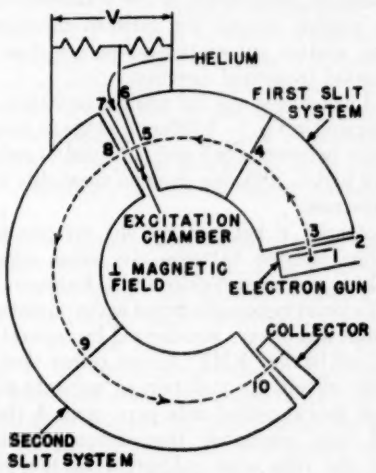

FIG. 1. Experimental arrangement of the new method. With a uniform magnetic field, the two slit systems in series each pass electrons of the same energy. Energy lost in inelastic collisions occurring between these systems can be restored by the potential V. Electron radius is 10 cm.

[15] Preliminary report: C. L. Hemenway and F. G. Dunnington, Phys. Rev. 79, 887 (1950).

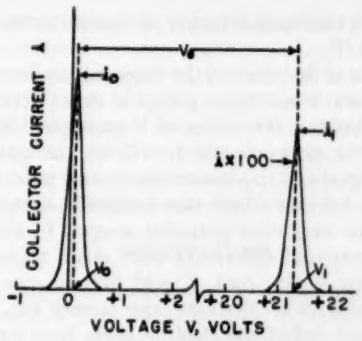

FIG. 2. Typical plot of collector current as a function of the voltage V between the slit systems. The excitation potential V_e is the difference between the voltages at the two peaks.

Those whose direction is unaltered[16] will pass on through the second slit system to the collector. On the other hand, those which have not lost energy in collisions will pass through slit 8 with their energy increased by Ve and hence will be stopped at slit 9. Likewise, electrons which have excited helium atoms to states other than $2p\ ^1P_1^\circ$ will not have the correct energy to pass through the second slit system.

The excitation potential of the transition from the ground state of helium to the $2p\ ^1P_1^\circ$ level is of the order of 21 volts. If, then, everything is held constant except the potential V between the first and second slit systems and the collector current i observed as V is varied from 0 to say 22 volts, two current peaks should be found. One peak i_0 (the "main" peak) should be found at $V=0$; a second and much smaller peak i_1 (the "excitation" peak) should be found when V is equal to the excitation potential V_e.

In practice three factors will modify the experimental results: (a) contact potentials may exist between the two slit systems and between different parts of the same system; (b) surface charges[17] will build up on the slits due to the deposition of an insulating layer during electron bombardment; (c) space charges can exist in the vicinity of the electron beam. If these factors are all made small enough, their net effect is to shift by almost exactly equal amounts the values of the voltage V at which the two current peaks i_0 and i_1 are observed; the value of the voltage for the main peak i_0 changes from zero to V_0 and for the excitation peak i_1 changes from V to V_1. The excitation potential V_e is then given by

$$V_e = V_1 - V_0. \tag{1}$$

The collector current varies with V as shown in Fig. 2. Excitation to levels other than the $2p\ ^1P_1^\circ$ is, of course, possible, but such transitions are much less probable.

[16] In inelastic scattering with 100- to 200-volt electrons, the forward direction is by far the most probable. See N. F. Mott and H. S. W. Massey, *The Theory of Atomic Collisions* (Oxford University Press, London, 1949), second edition, p. 229.

[17] F. G. Dunnington, Phys. Rev. 52, 475 (1937); in particular, pp. 494–495.

Some were observed, however, in particular the transition to $3p\,^1P_1$.

Analysis of the effect of the three factors listed above is as follows: if a contact potential exists between the two slit systems, the values of V corresponding to the two current peaks i_0 and i_1 will be changed by an amount equal and opposite to the contact potential; the difference between these two modified potentials will still be the excitation potential sought. In this work, contact potential differences were made negligible by evaporating a new coat of gold over all the interior surfaces of both slit systems prior to each run. Surface charges will deflect the electron beam from its normal path; if the deflection is small, compensation can be made by changing V. For those surface charges which remain constant with varying V, the shift in the two values of V will again be the same and will produce no error in the observed excitation potential. Surface charges which vary with V can produce an error in the observed excitation potential. All of the remarks concerning surface charges also apply to space charges. Surface charges can temporarily be reduced to negligible values by the evaporation of a fresh surface of gold. Space charges can be decreased by reducing the helium pressure in the two slit systems. Both surface and space charges can be kept small by using small electron currents.

The advantages of the new method are (1) It is not necessary to analyze the tail of a curve. (2) The work function of the cathode does not have to be measured. (3) It is not necessary to measure the energy (in volts) of the electron beam. (4) The absolute value of the magnitude field is not required. (5) To a very high degree of accuracy, the method eliminates the effect of contact potentials. (6) The *difference* between two voltages is the only quantity that has to be determined in absolute magnitude. In contrast, the measurements (1), (2), and (3) are all required in the determination of h/e by the measurement of the short wavelength limit of the continuous x-ray spectrum.

The disadvantages of this method are (1) The secondary effects of surface and space charges. (2) The fact that the observational precision (sharpness of the current peaks) cannot be improved to the desired degree because of the smallness of the collector currents when the slits are made very narrow.

A very small correction is necessary to Eq. (1). Conservation of energy and momentum causes a small amount of energy to be given to the helium nucleus in an inelastic collision. The fractional correction to the excitation potential V_e is given with sufficient accuracy by the formula

$$\frac{\Delta V_e}{V_e}=-\frac{m}{M}\left[\frac{1}{4}\left(\frac{V_e}{V_b}\right)+\frac{1}{8}\left(\frac{V_e}{V_b}\right)^2\right], \qquad (2)$$

where m is the electron mass, M is the mass of the helium nucleus, and V_b is the voltage of the electron beam. This correction amounts to 9 parts in 10^6 at an electron beam voltage V_b of 90 volts, 6 parts in 10^6 at 135 volts, and 4 parts in 10^6 at 180 volts. All data were corrected using Eq. (2).

III. APPARATUS

The measuring chamber, schematically illustrated in Fig. 1, was built with the highest mechanical precision. The general design is similar to the chamber used by one of us[18] for measuring e/m. In brief, the two slit systems were built on a central cone which both supported and aligned them without contact with the walls of the vacuum chamber. Each slit was individually adjustable as a unit to parallelism with the main axis; this adjustment was made to a precision of $\pm 0.5\times 10^{-4}$ cm in the effective axial length of 5 mm. The inner and outer slits were adjusted by a microscope system[18] to constant radii with a precision of $\pm 1\times 10^{-4}$ cm.

The excitation chamber was small so that the region between slits 5 and 8 in which an electron lost energy and regained it would be accurately localized. The distance between slits 5 and 8 was approximately 9 mm, while the total path between the electron gun and the collector was about 524 mm. The excitation chamber was connected to the midpoint of a potential divider between the slit systems. Thus, between slits 5 and 8, the average length of the path which an electron travels with an excess energy will be equal to that which it travels with a deficient energy; as a consequence, deviation from the correct path is minimized both as to radius and angle. Small angular deviations are of no importance because in inelastic collisions[16] there is a continuous angular distribution of the scattered electrons which is peaked around the forward direction; the second slit system automatically chooses those going in the forward tangential direction.

Purified helium gas was fed into the excitation chamber as indicated in Fig. 1. A differential pump, connected to the space between slits 5 and 8, helped to reduce the amount of helium diffusing through these slits into the two slit systems.

The potential V between the slit systems was obtained from isolated batteries. Its value was determined with a potential divider and a Rubicon potentiometer. To avoid systematic errors in the potentiometer, its potential was always standarized by connecting the standard cell in the "EMF" circuit rather than in the "Std. Cell" circuit. To maintain an accurate standard of voltage, five standard cells were used. A thermally insulated box prevented temperature fluctuations. Three of the cells were calibrated at the National Bureau of Standards at the beginning of the work. The correctness of the voltage as given by the group of cells was checked at the finish by comparison with three cells calibrated by the Bureau. The value of the voltage used throughout the measurements differed from the

[18] See reference 17, pp. 480–482.

mean of the three recalibrated cells by only 2 parts in 10^5. The standard error[14] in the standard cell voltage will therefore be taken as ± 1 part in 10^5.

The potential divider was calibrated at the U. S. National Bureau of Standards three separate times in a four-month interval. Two completely different sets of measuring equipment were used. The mean of the determinations gave a ratio of 19.5602 at a temperature of 27.0°C. The external standard error[14] of these three determinations was ± 2.8 parts in 10^5. To allow for systematic errors in the use of the divider this error will be taken as ± 4 parts in 10^5. Hence the value used for the ratio was 19.5602 ± 0.0008. The temperature coefficient determined by the Bureau was -0.9 part in 10^5; the data for each of the 156 values of the excitation potential were corrected by this to 27.0°C. Extensive tests both at the Bureau and at Rutgers indicated that with clean insulation there was no effect due to humidity up to a relative humidity of 70 percent. Recent ambient humidity measurements at Rutgers have indicated that no humidity corrections are necessary.

The magnetic field was supplied by a pair of precision Helmholtz coils. The axis of the chamber was accurately set parallel to the earth's field. A gradient in the earth's field was compensated; hence the total field (Helmholtz plus earth) did not vary around the electron orbit by more than about ± 3 parts in 10^5. The constancy of the Helmholtz magnetic field was monitored by a series standard resistance and a potentiometer.

The electron gun contained a special oxide coated cathode of nonmagnetic circuitry and materials. Two slits provided means for accelerating and focusing the electrons. The location of the gun relative to slit 3 could be adjusted under vacuum so that a beam could be obtained through the first slit system. The total accelerating potential between the cathode and slit 3 was monitored by a potential divider and potentiometer. It should be emphasized that both this accelerating potential and the magnetic field needed to be monitored only for constancy; neither of them needed to be measured.

The collector current i was measured by an electrometer amplifier with an FP-54 tube. With an input resistance of 2×10^{11} ohms, the sensitivity was 7×10^{-17} amp/mm. The current peaks received at the collector varied from 10^{-16} to 10^{-12} amp or larger. To avoid saturation in the electrometer tube at high currents, the input resistance could be changed to 7.8×10^9 ohms.

The system for evaporating gold over all the internal surfaces of the slit systems consisted of pairs of tungsten filaments. A pair was located in each compartment between successive slits, one filament being within and the other outside of the electron orbit and so placed that even the edges of the slits were covered with gold. To avoid electric fields from the contact potential between tungsten and gold, each filament was surrounded by a gold coated grid. To avoid peeling of the gold, the surfaces were cleaned by ion bombardment prior to each evaporation.

The measuring chamber was evacuated to a pressure of 1 to 2×10^{-6} mm of Hg by a high-speed oil diffusion pump. Oil vapors were reduced in the chamber by a large liquid air trap between the pumps and the chamber. During measurements, helium gas was admitted at a pressure between 0.3 and 2.0 microns.

IV. OBSERVATIONS

A fairly large amount of data was taken for the determination of h/e. This was done, first, to have information on the possible effect of variation in experimental conditions and, second, to improve the observational precision. Specifically, data were taken for 156 different determinations of h/e; each of these determinations will be referred to as a point. A point consists of 5 to 10 successive observations of the resonant peak voltage V_1 and a similar number of observations of the main peak voltage V_0 (see Fig. 2). To avoid systematic errors in determining a peak, the direction of misadjustment of V was alternated in each of the successive observations making up a point. Since the constancy of the magnetic field and of the electron beam voltage V_b (voltage from cathode to slit 3) were of primary importance, these were observed three times for each point: (1) before the observations on V_1, (2) between V_1 and V_0, and (3) following V_0; prior to the observations of V_0, if drift had occurred, the values were reset to the initial values for V_1. In addition, other pertinent data were recorded, including the radial slit width Δr, the elapsed time t after evaporation of a fresh coat of gold, the helium gas pressure p in the two slit systems, and the value of the excitation peak current i_1.

To determine whether the variation of any particular factor, has an effect on the observed h/e, it would be desirable to vary it while all other conditions are held constant. This is, of course, not in general possible experimentally. Thus Δr and V_b can be controlled at will; but the other variables, namely t, p, i_1, and V_0, are all interrelated to some degree and are only partially controllable. For example, changing the helium pressure p will change i_1 proportionally and will possibly affect V_0 and V_1 through space and surface changes. The magnetic field need not be considered as a separate variable since it is determined within very narrow limits by V_b.[19]

The 156 observed points were distributed with respect to these six variables as shown in Table I. For the first two controllable variables, some of the points were taken at each of the three conditions indicated. For the next two semidependent variables, the distribution was fairly continuous over the indicated ranges. The distribution of i_1 was continuous over the range

[19] Because of finite slit widths, minute variations of the magnetic field are possible with fixed V_b. The field was set at and held closely to the optimum value.

TABLE I. Distribution of the 156 observed points with respect to the six experimental variables.

Variable[a]	Conditions	No. points
Δr	0.2 mm	57
	0.3 mm	36
	0.49 mm	63
V_b	90 v	12
	135 v	133
	180 v	11
t	0.5 to 13 hours	Distributed
p	1.5 to 18×10^{-4} mm Hg	Distributed
i_1	0.4 to 3800×10^{-15} amp	Distributed
V_0	-1 to $+1$ volt	Distributed

[a] The six variables are: Δr = slit width; V_b = electron beam voltage determined by the potential between the cathode and slit 3, Fig. 1; t = time after evaporation of a new coat of gold on the slit system; p = the helium gas pressure in the two slit systems: i_1 = value of the excitation peak current; V_0 = voltage between the two slit systems when the main current peak (involving no energy loss) is being observed.

of 0.4 to 100×10^{-15} amp; there were only a few larger values. In the case of V_0, which under ideal conditions would be zero, the distribution was concentrated in the vicinity of zero with the average value equal to $+0.0047$ volt; large values occurred only occasionally with the widest slits ($\Delta r = 0.49$ mm).

V. ANALYSIS OF THE DATA

During the taking of the data, it was obvious that some of the points were more reliable than others because of better and more constant experimental conditions. In order to have an objective method of obtaining weighting factors, it was decided to base these factors on the mean deviations of the 5 to 10 potentiometer readings for V_0 and V_1 involved in each point. Specifically, the sum of the mean deviations for V_0 and for V_1 was calculated for each point; if it fell between zero and an arbitrary value L, the point was rated "excellent," if it fell between L and $2L$ the point was rated "good," between $2L$ and $3L$ "fair," and beyond $3L$ "poor." This classified the points into 20 excellent, 45 good, 47 fair, and 44 poor points. Weighting factors were then calculated in the standard way by finding numbers inversely proportional to the squares of the external standard errors[14] of each group; the weighting factors so determined (rounded to whole numbers) were respectively 12, 4, 2, and 1. It is worth mentioning that this method of classification produced groups with mean excitation voltages V_e which were in good mutual agreement; there was no trend with the weighting factor. An individual weighting factor could of course have been computed for *each* point but it was not felt that this was worth the additional statistical work which would have been required.

The reliability of the experimental results should be established to an appreciable extent by an objective analysis of the data to determine if any of the six experimental variables listed in Table I have an effect on the indicated value of the excitation potential V_e. Such a study was first attempted by finding the straight line which best fit the 156 values of V_e when they were considered a function of one of the six variables; the value of b in the equation $V_e = a + bx$, when so determined by least squares,[20] indicated the effect, if any, which that variable had on the value of V_e that was obtained.

This analysis was repeated for each of the six variables. The weakness of this method is that the values of b so obtained do not accurately represent the effect of the one variable being studied because the other five variables cannot be held constant. It was therefore felt worth the effort involved to make a multiple correlation analysis[21] with six variables; the data are then analyzed by the single equation

$$V_e = a + b_1\Delta r + b_2 V_b + b_3 t + b_4 p + b_5 i_1 + b_6 V_0, \qquad (3)$$

and each b accurately represents the effect, if any, of its associated variable on V_e. The results are given in Table II.

The significance of each b value obtained in the correlation analysis is most easily judged by multiplying it by the average value of its associated variable, because this product represents directly the effect of this variable on the excitation potential V_e; these products are listed in the second column of Table II and should be compared with the approximate value of V_e, namely 21.2 volts. Most of these products amount to only a few parts in 100 000; only one, namely that for the time t, is slightly greater than one part in 10 000. The significance to be placed in these products can be judged by the ratio of each slope to its standard error[14] σ, as listed in the third column of Table II. Thus, in the case of t, the slope b_3 is only 0.44 times as large as its standard error and hence has little significance. The significance can also be judged by assuming temporarily that b_3 actually equals zero but has the standard error calculated in the analysis. Then, if several successive sets of 156 points were obtained experimentally, two out of three such sets (see column 4 of Table II) could be expected to yield even larger values of b_3, but half of these values would be of opposite sign. Hence the value of bx for t has very little signifi-

TABLE II. Results of the multiple correlation analysis to determine the effect, if any, of each of six experimental variables on the indicated value of the helium excitation potential V_e.

Variable[a] x	(Slope) × (Mean x) $= b\bar{x}$ (volts)	Slope/std. error $= b/\sigma$	Statistically exceeded in
Δr	-0.0004	0.06	16 out of 17 obs
V_b	-0.0014	0.04	30 out of 31 obs
t	$+0.0030$	0.44	2 out of 3 obs
p	-0.0015	0.31	3 out of 4 obs
i_1	-0.0005	1.12	1 out of 4 obs
V_0	-0.0002	1.95	1 out of 19 obs

[a] See reference (a), Table I.

[20] R. T. Birge, Phys. Rev. **40**, 207 (1932); in particular, pp. 224–226.

[21] M. Ezekiel, *Methods of Correlation Analysis* (John Wiley and Sons, Inc., New York, 1941), second edition, in particular Chap. 12.

cance. This is true to an even greater extent of the values of bx for Δr, V_b, and p as can be seen from the statistics given in column 4. On the other hand, the same statistical argument indicates fair reliability in bx for i_1, and high reliability for the same product for V_0. Hence these two of the six factors can be assumed to have a small effect on the observed value of V_e. The effect of the beam current i_1 probably arises through the surface charge effects[17] which are proportional to it. The effect of the voltage V_0 between the slit systems when the main current peak is observed is possibly due to a slight change in the mean energy of the electrons which pass through the second slit system (with finite slit widths) when V_0 is not properly adjusted. Together, these two factors i_1 and V_0 produced a slight lowering of the observed V_e amounting to a total of 0.0007 volt, or that is, 3.5 parts in 100 000.

VI. RESULTS

The weighted mean value of the excitation potential V_e and its observational standard error[14] obtained from the 156 points is (21.2085±0.0031) volts absolute. This result is identical to the value obtained from Eq. (3) using mean values for the six experimental variables. Correcting this value by +0.0007 volt [that is to the value given by Eq. (3) when $i_1=V_0=0$], gives (21.2092 ±0.0031) volts. With this observational standard error, amounting to ±14.6 parts in 10^5, there must also be included the adopted uncertainty of ±4 parts in 10^5 in the ratio of the potential divider and the uncertainty of ±1 part in 10^5 in the voltage determined from the group of five standard cells.

The square root of the sum of the squares of these values amounts to ±15.2 parts in 10^5. Hence the final value of the excitation potential of helium from the ground state to the $2p\,{}^1P_1{}^\circ$ state is $V_e=(21.2091 \pm 0.0032)$ volts absolute.

The value of h/e comes from the basic equation $h\nu=V_e e$. Converting this to wave numbers and absolute volts we get

$$h/e=(V_e\times 10^8)/\tilde{\nu}c^2 \text{ erg}\cdot\text{sec/esu}. \quad (4)$$

The wave number $\tilde{\nu}$ is[22] 171 129 cm^{-1}. This number involves the uncertainty ±15 cm^{-1} of the series limit.[23] On the other hand, two direct determinations in the far ultraviolet gave an averaged value[23] only 7 cm^{-1} higher. It is therefore felt that the quantity ±15 cm^{-1} is more nearly a limit-of-error and that the standard error can be taken as ±7 cm^{-1} or ±4.1 parts in 10^5. The velocity of light with its standard error is[24] $c=(2.997929\pm 0.000008)\times 10^{10}$ cm/sec; here the uncertainty amounts to only ±0.27 part in 10^5. Substituting these values into Eq. (4) gives the value of h/e and its standard error[14] as $(1.37898\pm 0.00022)\times 10^{-17}$ erg·sec/esu. Since the fifth decimal has little significance, our final value of h/e and its standard error will be taken as

$$h/e=(1.3790\pm 0.0002)\times 10^{-17} \text{ erg}\cdot\text{sec/esu}.$$

It is of interest to compare this result with those obtained by other methods, both direct and indirect. This is done in Table III.

TABLE III. Comparison of the present determination of h/e with determinations by other methods, direct and indirect.

Method	Names	h/e erg sec/esu	Standard error
Excit. pot. of helium	Dunnington, Hemenway, and Rough[a]	1.3790×10^{-17}	±0.0002
Excit. and ion. potentials	Lawrence,[b] Van Atta,[c] Whiddington, and Woodroofe[d]	1.3743×10^{-17}	±0.0035
X-rays	Bearden and co-workers[e,f] Felt[g]	1.37926×10^{-17}	±0.00008
Least squares	DuMond and Cohen[h]	1.37943×10^{-17}	±0.00005

[a] Present paper.
[b] See reference 11.
[c] See reference 12.
[d] See reference 13.
[e] See reference 5.
[f] See reference 6.
[g] See reference 7.
[h] See reference 8.

The present result (listed on the first line of Table III) is to be compared with the weighted average from the three previous results involving excitation or ionization potentials (second line), with the weighted average from the three most recent and accurate results based on the x-ray method (third-line) and finally with the indirect result coming by least squares from all significant work on atomic constants (fourth line). All of these results have been recalculated with the new velocity of light. The standard errors listed in the second and third lines are the averages of the standard errors[25] of the three determinations involved in each case; they thus represent the typical uncertainty obtained in a single determination and are therefore directly comparable with the uncertainty of the present determination. The value of h/e from the present determination is larger by 34 parts in 10^4 (one-third of a percent) than the older excitation and ionization results and has an uncertainty smaller by a factor of over fifteen. On the other hand, the present determination is smaller than the current x-ray value by 2.1 parts in 10^4 and has an uncertainty about 2.5 times as large. Finally, it is smaller than the least squares value by 3.3 parts in 10^4 and has an uncertainty about four times as large.

VII. CONCLUSIONS

The value of h/e obtained in the present work by measurement of the first excitation potential of helium is

$$h/e=(1.3790\pm 0.0002)\times 10^{-17} \text{ erg}\cdot\text{sec/esu},$$

where the indicated uncertainty is the standard error.[14]

[22] C. E. Moore, Atomic Energy Levels, Natl. Bur. Standards (U. S.) Circ. 467 (U. S. Government Printing Office, Washington, D. C., 1948).
[23] C. E. Moore (private communication).
[24] J. W. M. DuMond and E. R. Cohen, Revs. Modern Phys. 25, 691 (1953); in particular, p. 706.
[25] The standard error of the average is $\pm 0.0020\times 10^{-17}$ erg·sec/esu for the excitation and ionization potential value and $\pm 0.00003\times 10^{-17}$ erg·sec/esu for the x-ray value.

This result is in good agreement with the values obtained in the most recent determinations by measurement of the continuous x-ray spectrum, and is in fairly good agreement with the indirect value computed by least squares from all significant work on atomic constants. It is in marked disagreement with the older "low" results obtained by other excitation and ionization methods of measurement, but in view of the large uncertainties of these older measurements these low values may have been largely due to chance.

It is a pleasure to thank F. L. Hermach of the U. S. National Bureau of Standards for his cooperation on measurements of the potential divider ratio, C. E. Moore also of the U. S. National Bureau of Standards for information on the wave numbers of the helium levels, and A. R. Crawford and F. G. Fender of Rutgers University for consultation on the multiple correlation analysis. The precision machine work of the measuring chamber was done by R. V. H. Campbell. This work was supported at various stages by the American Philosophical Society, the Rutgers Research Council and the U. S. Office of Naval Research.

PHYSICAL REVIEW VOLUME 94, NUMBER 3 MAY 1, 1954

The Collective Description of Many-Particle Systems (A Generalized Theory of Hartree Fields)

TOICHIRO KINOSHITA AND YOICHIRO NAMBU
Institute for Advanced Study, Princeton, New Jersey

(Received October 1, 1953; revised manuscript received December 29, 1953)

A systematic method of handling a system composed of a number of particles and an intermediary Bose field has been developed. The main idea consists in linearizing the interaction by taking certain average values so that it may be amalgamated to the free Hamiltonian. Only the remaining fluctuational interaction is treated by perturbation theory. The effect of the averaged interaction appears in the form of two generalized Hartree fields associated with the particle and the Bose quantum, respectively. The self-consistent equations for these Hartree fields are derived from an analysis of the S matrix, keeping close analogy to the renormalization procedure in quantum electrodynamics. The formalism includes such approximations as the Bohm-Pines, Hartree-Fock, and Thomas-Fermi theories as special cases. General criteria about the validity and plausibility of the picture involved in the present formulation are discussed from various points of view.

1. INTRODUCTION

THE purpose of the present paper is to formulate a general theory of collective description of a system which is composed of a number of particles interacting through an intermediary field. The name "collective description" was first given a specific meaning by Bohm and Pines[1] in their treatment of plasma oscillation. In order to describe the characteristic behavior of an electron gas in a convenient way, they introduce two kinds of dynamical variables. One, the plasma field, represents the coordinated, medium-like motion of the system as a whole, known as plasma oscillation, in which there is a marked correlation in the behavior of the electrons; while the other refers to the motion of individual electrons, but insofar as it concerns the fluctuations from the mean behavior which is covered by the plasma field. The new set of variables are derived from the conventional ones, namely those which describe the electromagnetic field and the electrons, by means of a canonical transformation, so that both descriptions are mathematically equivalent.

The usual theory of plasma oscillation, as has been first given by Langmuir and Tonks,[2] and recently elaborated by Bohm and Gross,[3] consists in finding out the equation of motion satisfied by a space-charge distribution. It is essentially a kind of self-consistent treatment of the Coulomb interaction since a change in the charge distribution generates a corresponding change in the accompanying Coulomb potential, which in turn is the cause of the original charge fluctuation. Thus one arrives at an oscillatory behavior of the space charge and the Coulomb field, in which the latter is employed as an auxiliary quantity associated with charge distribution.

Bohm and Pines, on the other hand, describe the system by explicitly introducing the electromagnetic field as apparently independent dynamical variables, rather than describing the system in terms of the conventional Coulomb interaction. The electromagnetic field shows a kind of dispersion due to its interaction with the charge distribution, resulting in a different propagation character from that in free space. This modified field can be interpreted as representing the plasma field, i.e., the oscillating Coulomb field accompanying the charge fluctuation. It is again a kind of

[1] D. Bohm and D. Pines, Phys. Rev. **82**, 625 (1951); **85**, 338 (1952); **92**, 609 (1953).

[2] L. Tonks and I. Langmuir, Phys. Rev. **33**, 195 (1929).

[3] D. Bohm and E. P. Gross, Phys. Rev. **75**, 1851, 1864 (1949).

self-consistent treatment since the nature of the plasma field depends on the charge distribution which is influenced by the former. The advantage of Bohm and Pines' method lies in the fact that the plasma oscillation frequency is insensitive to the minute fluctuation of the charge distribution, so that as a matter of fact we do not have to solve the equation self-consistently. Furthermore, it suggests that a wider range of many-body problems could also be attacked along the same line, namely the explicit use of field variables and introduction of (in principle) self-consistent fields, if formulated in a proper way. This is especially important since we have often to deal with problems involving radiation field or meson fields which cannot be relegated to mere interparticle potentials, and yet we have no appropriate means of handling them because of mathematical difficulty.

In the following, we shall develop a general theory of collective description along the ideas outlined above. We shall introduce two kinds of Hartree fields, one for the particle and the other for the intermediary field, which are determined by the principle that we replace the actual force acting on a particle or field quantum by its average value which should depend on the overall state of the system in a self-consistent way. The remaining interaction, that is, the fluctuation of the forces from their mean behavior, is then treated as a perturbation since it may be expected to be small. Thanks to the technical progress in handling perturbation theory, we can define and determine the Hartree fields to higher orders of approximation beyond those appearing in conventional theories, and in case the residual interaction tends to vanish it is possible to give a formal but rigorous expression for the total energy of the system in terms of these Hartree fields, that is to say, on the pure independent particle picture.

In Sec. 2 we shall give an orientating account of the formulation, taking as an example a system of particles interacting through a neutral scalar meson field. Although the ordinary plasma oscillation of electron gas may be the best suited example for physical reasons, we have avoided it because it requires a special consideration of the supplementary condition, and may deserve a separate paper. Section 3 will be devoted to a more precise mathematical formulation of the problem and derivation of various equations and formulas, which utilizes some mathematical techniques and conventions. In Sec. 4 we shall discuss the range of validity of the present description from physical as well as mathematical points of view. Its relations to some of the existing more limited theories, and the possibility of extending it to still wider areas will also be discussed. In Sec. 5 a summarizing account of what has been achieved in this paper will be given, together with a few suggestions as to actual problems which might be within the scope of the present method. In the Appendix some mathematical relations used in Sec. 3 are derived, which may themselves be of interest since they show a concise way of analysis, based on certain lemmas, of the S matrix and related quantities.

2. BASIC IDEAS OF THE FORMULATION

Let us take, as an illustrative example, a system of a number of particles (fermions) and a scalar field with mass μ interacting with each other. For the sake of convenience, we shall adopt throughout the quantized operator formalism with $\hbar$ and c taken as unity. The total Lagrangian and Hamiltonian densities can then be written as follows:

$$\begin{aligned} L&=\left\{i\psi^*\frac{\partial}{\partial t}\psi-\frac{1}{2m}\psi^*p^2\psi\right\}-\tfrac{1}{2}\left\{\frac{\partial\varphi}{\partial x_\mu}\frac{\partial\varphi}{\partial x_\mu}+\mu^2\varphi^2\right\}\\ &\qquad -g\psi^*\psi\varphi\\ &\equiv L_{\rm par}+L_{\rm mes}+L_{\rm int},\quad x_\mu\equiv(x,y,z,it),\\ H&=\frac{1}{2m}\psi^*p^2\psi+\tfrac{1}{2}\{\pi^2+(\nabla\varphi)^2+\mu^2\varphi^2\}+g\psi^*\psi\varphi\\ &\equiv H_{\rm par}+H_{\rm mes}+H_{\rm int}, \end{aligned}\tag{2.1}$$

where the particles are assumed to be nonrelativistic, while keeping for the "meson" a relativistic form. π means the canonical conjugate momentum to φ, and g is the coupling constant measured in the rational units.

The ordinary way of studying such a system is to start from a noninteracting case, and regard the interaction as a small perturbation which can be treated by standard perturbation methods. For this purpose one may, for example, go over to the so-called interaction representation, in which the Schrödinger equation is converted into

$$i\frac{\partial}{\partial t}\Psi=\bar{H}_{\rm int}\Psi,\quad \bar{H}_{\rm int}\equiv\int H_{\rm int}(dx)^3,\tag{2.2}$$

Ψ and $\bar{H}_{\rm int}$ being the state vector and the interaction Hamiltonian in this representation, respectively. The perturbation procedure then consists in the construction of the transformation function or the S matrix from the Eq. (2.2) as a power series in the interaction Hamiltonian, and its expansion into a series of normal products.

Now consider the specific case we have in mind. The above procedure would be a reasonable one in so far as the interaction is really small enough to be treated as a perturbation. In the case of the many particle system, however, this will not in general be true even if the coupling may be small. For the force acting on a particle will become larger and larger as the number of surrounding particles increases. In the same way, if a meson quantum impinges on the system of particles, it will suffer scatterings (before it is eventually absorbed or leaves the system) which becomes increasingly large with density of particles even if the elementary scattering may be small. Such defects of the ordinary treat-

ment would largely be removed, however, if it turns out that that part of the interaction which plays the dominant role in this problem can be taken into account in the starting approximation.

In the case of plasma oscillation, it was found by Bohm and Pines that this idea can be carried out by going over to a new representation by a canonical transformation which introduces the so-called plasma field. From a mathematical point of view, this is a kind of linearization of the nonlinear interaction and thus is found to be equivalent to the description of the system by the Lagrangian of the type

$$L_{\mathrm{rad}}'=L_{\mathrm{rad}}-\tfrac{1}{2}A_\mu\chi_{\mu\nu}A_\nu,$$

which is bilinear in the field variables. In the following, we shall investigate how such a kind of linearization works as an approximation method of the many-body problems.

In compliance with this consideration, we rewrite the total Lagrangian density of our system as follows:

$$\begin{aligned}
&L=L_{\mathrm{par}}'+L_{\mathrm{mes}}'+L_{\mathrm{int}}',\\
&L_{\mathrm{par}}'=L_{\mathrm{par}}-\psi^*\phi\psi,\\
&L_{\mathrm{mes}}'=L_{\mathrm{mes}}-\tfrac{1}{2}\varphi\chi\varphi,\\
&L_{\mathrm{int}}'=L_{\mathrm{int}}+\psi^*\phi\psi+\tfrac{1}{2}\varphi\chi\varphi.
\end{aligned}\tag{2.3}$$

We shall see below that ϕ and χ correspond to what may be called generalized Hartree fields for the particle and meson, respectively. They are in general c-number nonlocal functions of space-time points, so that we should write more rigorously, for example, as[4]

$$\begin{aligned}
&\psi^*\phi\psi\longrightarrow\int\psi^*(x)\phi(x,x')\psi(x')(dx')^4,\\
&\varphi\chi\varphi\longrightarrow\int\varphi(x)\chi(x,x')\varphi(x')(dx')^4.
\end{aligned}\tag{2.4}$$

Since L_{par}' and L_{mes}' are still quadratic in the field operators, it is possible, at least in principle, to pass on to a new interaction representation by regarding them as "free" Lagrangians, leaving L_{int}' as an apparent interaction Lagrangian. If the corresponding free and interaction Hamiltonians are obtained from the Lagrangians, we get, instead of Eq. (2.2), the equation[4]

$$i\frac{\partial}{\partial t}\Psi=\bar{H}_{\mathrm{int}}'\Psi.\tag{2.5}$$

[4] In the case of nonlocal Lagrangians, there is an apparent ambiguity of definition although the space-time integral of L, and hence the S matrix, is not affected by it. Thus we could also write it as $\int\psi^*(x+y/2)\phi(x+y/2,x-y/2)\psi(x-y/2)(dy)^4$, etc. There is also a question about the associated Hamiltonian since it is not well-defined in the nonlocal case. For details see Y. Nambu, Progr. Theoret. Phys. (Japan) **7**, 131 (1952).

The operators in (2.5) satisfy modified equations of motion and modified commutation relations. Sometimes the modification is so large that the propagation character of particles and mesons becomes fairly different from the ordinary one.

The transformation function $U(t,t_0)$, which solves Eq. (2.5), and the S matrix can be expressed as follows:

$$\begin{aligned}
U(t,t_0)&=1+\sum_{n=1}^{\infty}(-i)^n\int_{t_0}^{t}dt_1\int_{t_0}^{t_1}dt_2\\
&\quad\cdots\int_{t_0}^{t_{n-1}}dt_n\bar{H}_{\mathrm{int}}'(t_1)\bar{H}_{\mathrm{int}}'(t_2)\cdots\bar{H}_{\mathrm{int}}'(t_n)\\
&=\sum_{n=0}^{\infty}\frac{(-i)^n}{n!}\int_{t_0}^{t}\cdots\int_{t_0}^{t}(dx_1)^4\cdots(dx_n)^4\\
&\qquad\times P(H_{\mathrm{int}}(x_1),\cdots H_{\mathrm{int}}(x_n)),\\
S&=U(\infty,-\infty),
\end{aligned}\tag{2.6}$$

where P means Dyson's chronological ordering symbol.[5] The actual construction of the modified Hamiltonians is not straightforward since they involve nonlocal functions. Fortunately, however, necessary informations about these modified fields can be derived from their equations of motion directly, without actually constructing the Hamiltonians. Thus the S matrix can also be expressed in terms of the interaction Lagrangian L_{int}':[4]

$$\begin{aligned}
S=\sum_{n=0}^{\infty}\frac{i^n}{n!}\int_{-\infty}^{\infty}\cdots\int_{-\infty}^{\infty}&P^*(L_{\mathrm{int}}'(x_1),\cdots L_{\mathrm{int}}'(x_n))\\
&\times(dx_1)^4\cdots(dx_n)^4.
\end{aligned}\tag{2.7}$$

The symbol P^* means that we order $L_{\mathrm{int}}'(x_1),\cdots,L_{\mathrm{int}}'(x_n)$ not in the chronological order of $x_1, x_2, \cdots, x_n$, but in the natural chronological order of all their constituent operators ψ^*, ψ, and φ which occur in L_{int}' in a nonlocal way.[6] By taking first few terms of the expansion (2.6) or (2.7), we get the first few orders of the perturbation which will be sufficient if the interaction is really small.

Now, being a mere definition, Eq. (2.3) and the following discussions are valid for an arbitrary choice of ϕ and χ. It is a matter of course, that the success of a given approximation critically depends on the choice of these Hartree fields. In the following, we shall derive the principle for their determination which seems to be reasonable from the physical point of view.

Suppose we take as an approximate starting state vector of the system (at $t=-\infty$) a state vector which is a Slater determinant for the particles, corresponding to the Lagrangian L_{par}', multiplied by the vacuum state

[5] F. J. Dyson, Phys. Rev. **75**, 486 (1949).

[6] To be more rigorous, we have to take account of the anticommutativity of particle operators in defining P^*. For details see Appendix.

vector for the meson field corresponding to L_{mes}'. (We do not consider here the case of real mesons present; it would be a nonstationary problem since the mesons would eventually be absorbed. Moreover, there is another difficulty as will be discussed in Sec. 4.) It can be written as

$$\Psi=\prod_i \psi_i^*\Psi_0, \tag{2.8}$$

where Ψ_0 is the vacuum state vector defined as the lowest eigenstate of the energy operator corresponding to the free Lagrangian $L_{\text{par}}'+L_{\text{mes}}'$, and ψ_i^* stands for the creation operator of a particle occupying the state i.

Now let us consider the first few terms in the expansion of the S matrix derived from Eq. (2.6) or (2.7). Each term contains a certain product of operators ψ^*, ψ, and φ, representing some physical process. If we neglect, for the time being, the terms involving ϕ and χ, we get in the second order

$$\frac{(-i)^2}{2}\int_{-\infty}^{\infty}\int P(g\psi^*\psi\varphi(x_1),g\psi^*\psi\varphi(x_2))(dx_1)^4(dx_2)^4. \tag{2.9}$$

As usual, this can further be analyzed into various processes, namely the scattering of two particles, the scattering of a particle and a meson, and the self-energy of a particle.

Taking the vacuum expectation value of $P(\varphi(x_1),\varphi(x_2))$ in (2.9), for instance, one obtains

$$-\frac{i}{2}\int\int f_1(x_1,x_2)P(\psi^*\psi(x_1),\psi^*\psi(x_2))(dx_1)^4(dx_2)^4,$$
$$f_1(x_1,x_2)=-ig^2\langle P(\varphi(x_1),\varphi(x_2))\rangle_0, \tag{2.10}$$

which involves a term responsible for the scattering of two particles. The form of the function $f_1(x_1,x_2)$, however, is different from the ordinary one because φ now obeys the equation of motion involving χ, and consequently gives a different expectation value. In other words, the meson quantum emitted and absorbed virtually is acted on by the assumed potential χ, resulting in a modified force between particles.

The above equation (2.10) includes not only the scattering of two different particles but also the term similar to the ordinary self-energy of a particle which is bilinear in ψ and ψ^*. This is different from the ordinary self-energy because of the influence of ϕ and χ on the propagation functions and in fact involves implicitly the effect of scattering of a particle by the potentials ϕ and χ. Since these potentials are expected to represent certain characteristics of the system of particles as a whole, it is in some sense a scattering of an extra particle by the given system. Obviously the same kind of effect is to be obtained from the two-particle parts of (2.10) by leaving out a pair of operators ψ and ψ^* and summing over the given distribution of particles with respect to the remaining pair of operators. These two effects, including the self-energy in the proper sense, can be combined into a single formula as

$$-i\int\int f_2(x_1,x_2)P(\psi^*(x_1),\psi(x_2))\epsilon(x_1-x_2)(dx_1)^4(dx_2)^4,$$
$$f_2(x_1,x_2)=-ig^2\delta(x_1-x_2)\int\langle P(\varphi(x_1),\varphi(x_3))\rangle$$
$$\times\langle\psi^*\psi(x_3)\rangle\epsilon(x_1-x_2)(dx_3)^4$$
$$-ig^2\langle P(\varphi(x_1),\varphi(x_2))\rangle$$
$$\times\langle P(\psi(x_1),\psi^*(x_2))\rangle\epsilon(x_1-x_2), \tag{2.11}$$

when the expectation value is taken with respect to the state Ψ instead of Ψ_0.

As it will be seen easily, the first term represents the average potential at x_1, due to all the particles present, while the second is a nonlocal "exchange" potential including the self-energy and the effect of the Pauli principle for the particle with which we are measuring it. We shall hereafter refer to this combined effect of the proper self-energy and the average interaction potential simply as self-energy as far as no complication arises.

Now we come to the effect of the additional term $\psi^*\phi\psi$ in the interaction Lagrangian L_{int}'. It gives rise to a term

$$i\int\int\phi(x_1,x_2)\epsilon(x_1-x_2)P(\psi^*(x_1),\psi(x_2))$$
$$\times(dx_1)^4(dx_2)^4 \tag{2.12}$$

in the S matrix. Thus, if we choose ϕ just equal to the above mentioned self-energy function f_2, the matrix element for the scattering of a particle by the system of particles apparently vanishes to this order of approximation. Such a way of determining ϕ seems to be a natural one since we are now trying to minimize the effective interaction. It is almost unnecessary to say this is in close analogy to the idea of renormalization exploited in quantum electrodynamics. In other words, if we assume the particle to be moving in a potential ϕ from the beginning, it will, on the average, receive no other force from the interaction through meson field.

The above choice of ϕ is, however, not the only possibility which follows from (2.11) and (2.12). Namely, it is not necessary to put $\phi=f_2$ inasmuch as one is interested in the cancellation of (2.11) and (2.12) as integrals over all the space-time points (which would be sufficient for the present purpose). We have only to put $\int\phi\cdots=\int f_2\cdots$, and thus ϕ is determined up to an arbitrary additive function g which satisfies $\int g\cdots=0$. In the language of the momentum representation, this is the same as the statement that ϕ is identical with f_2 only on the energy shell and completely arbitrary otherwise. On the other hand, our definition of ϕ is such that it is identical with f_2 as a function of x_1 and x_2, and thus they are identical in the momentum space for all possible choices of the energy-momentum variables. We

shall adopt this definition since we have in mind such a cancellation not only in the case of the S matrix but in the case of any transformation function $U(t,t')$ or the Hamiltonian itself which gives rise to processes off the energy shell.

In the same way we can work with the scattering of a particle and a meson, which is represented by

$$-i\int\int f_3(x_1,x_2)P(\psi^*\varphi(x_1),\psi\varphi(x_2))\times\epsilon(x_1-x_2)(dx_1)^4(dx_2)^4,$$

$$f_3(x_1,x_2)=-ig^2\langle P(\psi(x_1),\psi^*(x_2))\rangle_0\epsilon(x_1-x_2), \tag{2.13}$$

where the expectation value is taken with respect to the vacuum. Now if we further take the average of this term over the occupied particles to get the scattering of a meson by the particle system, we find an expression which contains only meson operators:

$$-\frac{i}{2}\int\int f_4(x_1,x_2)P(\varphi(x_1),\varphi(x_2))(dx_1)^4(dx_2)^4,$$

$$f_4(x_1,x_2)=-ig^2\langle P(\psi^*\psi(x_1),\psi^*\psi(x_2))\rangle, \tag{2.14}$$

the expectation value now being taken with respect to the state Ψ. This is the "self-energy" of the meson field, or the average potential which a meson suffers through its scattering with the particles. Choosing χ equal to f_4, we can again make it apparently vanish.

We have thus obtained two relations which determine the unknown functions ϕ and χ. They are simultaneous nonlinear equations of a complicated form since f_3 and f_4 themselves depend on ϕ and χ. From the principle of their determination it is clear that ϕ and χ may be called the self-consistent Hartree fields for the particle and the meson, respectively. They represent the average potential exerted on a particle or a meson by the whole system. By the nature of the averaging procedure they take account of the statistics caused by the presence of the particle or meson under consideration, namely the indistinguishability and symmetry property of the particles and mesons. They do not take account completely, however, of the dynamical correlation between the acting and acted particles or mesons; this correlation is considered only in its mean behavior.

Although we kept here terms in the expansion of the S matrix only up to the second order, it is by no means a simple second-order perturbation with respect to the coupling constant g. A meson, for example, exchanged between two particles, may be scattered an arbitrary number of times by other particles in higher orders of g, and its average effect is represented through χ, resulting in an effective change of the two-particle potential. If, however, the fluctuation of the individual interaction from the average is not negligible, we shall have to consider higher order terms of the S matrix, and by separating out the self-energy effects in the same manner, we shall again obtain the Hartree fields ϕ and χ to this order of approximation, together with a residual fluctuational interaction which cannot be absorbed into ϕ and χ. If the latter turns out to be small, we can neglect it and then we may have a valid independent-particle picture.

Nevertheless, it does not follow, even in this case, that the total system can be regarded as composed of independent particles and (zero-point) mesons moving in their respective Hartree fields. For these Hartree fields are, by nature, the average potentials acting on an arbitrary test particle or meson which we put into, or pick up from the system, the reaction of the test body on the system being partially taken into account. Although any constituent particle or meson of the system may serve as a test body placed in it, the total system is not equivalent to an ensemble of such test bodies, since they cannot be brought together all at once. This situation is reflected in the fact that the expectation value of the S matrix with respect to Ψ does not reduce to unity even if the self-energy effects are completely subtracted away. Thus, in general the merit of introducing ϕ and χ is to secure a better convergence of the perturbation and an improved physical picture by taking out part of the interaction in the form of Hartree fields.

The convergence will be improved because part of the process which we would have in higher orders of conventional perturbation theory are already included as the effect of ϕ and χ; moreover, this effect is brought into a closed form, so that in certain cases our method would work even if the conventional perturbation failed due to the divergence of the series expansion of the effect represented by ϕ and χ.

As for the second-order terms of the S matrix, we get, after subtraction of the self-energy effects by means of ϕ and χ:

$$\begin{aligned}&-\frac{i}{2}\int\int f_1(x_1,x_2)\{[\psi^*\psi(x_1)-\langle\psi^*\psi(x_1)\rangle][\psi^*\psi(x_2)\\&\quad-\langle\psi^*\psi(x_2)\rangle]-[\psi^*(x_1)\psi(x_2)-\langle\psi^*(x_1)\psi(x_2)\rangle]\\&\quad\times[\psi^*(x_2)\psi(x_1)-\langle\psi^*(x_2)\psi(x_1)\rangle]\}(dx_1)^4(dx_2)^4\\&-i\int\int f_3(x_1,x_2)\epsilon(x_1-x_2)\{P(\psi^*(x_1),\psi(x_2))\\&\quad-\langle P(\psi^*(x_1),\psi(x_2))\rangle\}P(\varphi(x_1),\varphi(x_2))(dx_1)^4(dx_2)^4\\&-\frac{i}{2}\int\int f_2(x_1,x_2)\epsilon(x_1-x_2)\langle P(\psi^*(x_1),\psi(x_2))\rangle\\&\quad\times(dx_1)^4(dx_2)^4,\end{aligned} \tag{2.15}$$

where the expectation values of the first and second rows vanish, while the last is a c number. Thus we do not obtain a vanishing expectation value of the inter-

action energy of the total system in spite of our choice of ϕ and χ, which reflects the above-mentioned fact that the system is not an ensemble of test bodies. To avoid this awkward situation one might formally introduce a c-number C, which corresponds to the last term of (2.15), and modify the definition of the free and interaction Hamiltonian as

$$H_0''\equiv H_0'+C, \quad H_{\rm int}''\equiv H_{\rm int}'-C. \tag{2.16}$$

Then the total energy is, to this order of approximation, given by the eigenvalues of H_0''. The important point, however, is that both H_0' and C, and hence H_0'', can be expressed in terms of ϕ and χ only, without introducing any new functions.

In the next section we shall present a refined formulation of the ideas expounded here.

3. PRECISE MATHEMATICAL FORMULATION

We shall first mention a trick which we are going to use. Consider the state Ψ defined by Eq. (2.8), in which a number of individual states of the particle designated by i are occupied. As is easily seen, such a state has many similar features with that of the Dirac vacuum in which negative energy levels are entirely occupied while positive levels are completely unoccupied. So long as one is interested in the properties of the system in or near the state Ψ, it will be found convenient to describe this state as an apparent vacuum to which every other state shall be referred, so that removing a particle i from this state shall be regarded as creating a "hole" of state i in this vacuum. In terms of the second quantization scheme, this means that we interchange the roles of creation and annihilation operators ψ_i^* and ψ_i for the occupied states. Thus we rewrite

$$\begin{aligned}\psi(x)&=\psi^+(x)+\psi^{-*}(x),\\ \psi^*(x)&=\psi^-(x)+\psi^{+*}(x),\\ \varphi(x)&=\varphi^+(x)+\varphi^-(x),\end{aligned} \tag{3.1}$$

where $+$ and $-$ mean annihilation and creation parts, respectively; quantities with an asterisk refer to the occupied eigenstates and quantities without an asterisk to unoccupied ones. The modified vacuum Ψ is then characterized by the equations

$$\begin{aligned}&\psi^+(x)\Psi=0, \quad \psi^{+*}(x)\Psi=0,\\ &\varphi^+(x)\Psi=0, \qquad \text{for all } x.\end{aligned} \tag{3.2}$$

With this new convention, we can rearrange the Lagrangian as well as the S matrix into a "normal product," where the creation operators in the above sense stand to the left of the annihilation operators. This procedure is exactly the same as in the usual analysis of quantum electrodynamics, except for the fact that the propagation functions to be used are different:

$$\begin{aligned}&\langle P(\psi(x),\psi^*(x'))\rangle=\epsilon(x-x')S^{(\phi)}(x,x'),\\ &\langle P(\varphi(x),\varphi(x'))\rangle=\Delta^{(\chi)}(x,x'),\end{aligned} \tag{3.3}$$

where $\langle\,\rangle$ means the expectation value with respect to the new vacuum Ψ. $\Delta^{(\chi)}$ is different from Δ_F because of the presence of χ in the equation of motion. $S^{(\phi)}$ is different from the nonrelativistic analog of S_F in two respects: first, there is a ϕ in the equation of motion; second, the boundary conditions at remote past and future are defined by the state Ψ. Thus we may write

$$\begin{aligned}S^{(\phi)}(x,x')&=\sum_{\text{unocc.}} u_i(x)u_i^*(x'), \quad t>t',\\ &=-\sum_{\text{occ.}} u_i(x)u_i^*(x'), \quad t<t',\end{aligned} \tag{3.4}$$

where u_i and u_i^* are simple eigenfunctions (not operators) and the summation is over the occupied and unoccupied states, respectively. On the other hand, the $S_F^{(\phi)}$ with the ordinary boundary conditions would be given by

$$\begin{aligned}S_F^{(\phi)}(x,x')&=\sum_{\text{all}} u_i(x)u_i^*(x'), \quad t>t',\\ &=0, \qquad\qquad\qquad t<t'.\end{aligned} \tag{3.5}$$

Thus we get the relation:

$$\begin{aligned}&S^{(\phi)}(x,x')=S_F^{(\phi)}(x,x')-\rho^{(\phi)}(x,x'),\\ &\rho^{(\phi)}(x,x')=\sum_{\text{occ.}} u_i(x)u_i^*(x'), \quad \text{for all } t-t'.\end{aligned} \tag{3.6}$$

$\rho^{(\phi)}(x,x')$ is exactly what is called the density matrix corresponding to the state Ψ.

The functions $S^{(\phi)}$, $\Delta^{(\chi)}$, and $\rho^{(\phi)}$ satisfy the following differential equations and their conjugates:

$$\begin{aligned}&\left(i\frac{\partial}{\partial t}+\frac{1}{2m}\Delta\right)S^{(\phi)}(x,x')-\int\phi(x,x'')\\ &\qquad\times S^{(\phi)}(x'',x')(dx'')^4=i\delta(x-x'),\\ &(\Box-\mu^2)\Delta^{(\chi)}(x,x')-\int\chi(x,x'')\\ &\qquad\times\Delta^{(\chi)}(x'',x')(dx'')^4=i\delta(x-x'),\\ &\left(i\frac{\partial}{\partial t}+\frac{1}{2m}\Delta\right)\rho^{(\phi)}(x,x')-\int\phi(x,x'')\\ &\qquad\times\rho^{(\phi)}(x'',x')(dx'')^4=0,\end{aligned} \tag{3.7}$$

which, however, do not involve the necessary boundary conditions to be imposed on these quantities. Integral equations which are suited to treat ϕ and χ as per-

turbations and incorporate the boundary conditions are

$$S^{(\phi)}(x,x')=S^{(0)}(x,x')-i\int S^{(0)}(x-x'')\times\phi(x'',x''')S^{(\phi)}(x''',x')(dx'')^4(dx''')^4,$$

$$\Delta^{(\chi)}(x,x')=\Delta_F(x,x')-i\int \Delta_F(x-x'')\times\chi(x'',x''')\Delta^{(\chi)}(x''',x')(dx'')^4(dx''')^4,$$

$$\rho^{(\phi)}(x,x')=\rho_0(x-x')-i\int S_F(x-x'')\times\phi(x'',x''')\rho^{(\phi)}(x''',x')(dx'')^4(dx''')^4 -i\int \rho_0(x-x'')\phi(x'',x''')\times S^{(\phi)}(x''',x')(dx'')^4(dx''')^4,$$

$$S^{(0)}(x-x')=S_F(x-x')-\rho_0(x-x'), \tag{3.8}$$

where $S^{(0)}$, S_F, and ρ_0 are defined by the same equations as (3.4)–(3.6) except that u_i and u_i^* are now the eigenfunctions without ϕ, and Δ_F is the usual Feynman function without χ.

With the aid of these propagation functions, we can express the S matrix as a normal product, and obtain the "true" energy of the vacuum Ψ. By virtue of the relations (3.2), only the constant term in the normal product of the S matrix will contribute if it operates on the state Ψ, which simplifies the situation a great deal. The total energy of the state is then expressed by the following compact formula:

$$\mathcal{E}-\mathcal{E}_0=\int\int\left[\int_0^g \frac{dg'}{g'}\chi(x,x')\Delta^{(\chi)}(x',x)\right]\times(dx')^4(dx)^3-\int\left[\int_0^g\frac{dg'}{g'}\phi_1(x)S^{(\phi)}(x,x)\right](dx)^3$$
$$=-\int\int\left[\int_0^g\frac{dg'}{g'}\phi(x,x')S^{(\phi)}(x',x)\right]\times(dx')^4(dx)^3. \tag{3.9}$$

$\mathcal{E}_0$ is the energy of the state Ψ without interaction; the integration over g' means that we consider χ, $\Delta^{(\chi)}$, ϕ, and $S^{(\phi)}$ as functions of the coupling constant g, which we vary from 0 to the actual value. [See Eq. (3.11) for the definition of $\phi_1(x)$.] Since the proof of Eq. (3.9) needs some technique, we shall give it in the Appendix. The physical interpretation of Eq. (3.9) may be mentioned as follows. Expanding the integrand of the equation in powers of g, the effect of integration in g amounts to multiply the nth power of g by $1/n$; such a term would involve a chain of n interactions of particles and mesons caused by H_{int}, among which processes the resulting interaction energy must be shared, hence the factor $1/n$.

Another formula for $\mathcal{E}$, which is easier to understand than the above one, can also be derived by the following consideration. The self-energy ϕ or χ represents the extra energy carried by a particle or a quantum which is added to the vacuum Ψ. Suppose we construct the present state Ψ from Ψ_0 by adding particles one after another. At each step, the energy ϵ_i of the ith particle added is an ith eigenvalue of the equation of motion with ϕ, where ϕ depends on the $i-1$ states already occupied. Thus if we understand ϕ in this way, the total energy of the system will be put into the form

$$\mathcal{E}=\sum\epsilon_i=\sum_{\text{occ.}}\langle i|\bar{H}_{\text{par}}'|i\rangle$$
$$=\int\int\left[\int\left\{\frac{-1}{2m}\Delta\delta^3(x-x')+v(x,x')\right\}d\rho^{(\phi)}(x,x')\right], \tag{3.10}$$

where the integration over $\rho^{(\phi)}$ may be taken in the Stielties' sense, being carried out from 0 to the actual $\rho^{(\phi)}$, and $v(x,x')$ is the Hamiltonian constructed from the nonlocal potential ϕ in the Lagrangian.

The self-consistent equations to determine the self-energies ϕ and χ themselves are given by the following formulas which readily derive from the analysis of the S matrix with the aid of the Feynman diagrams:

$$\phi(x,x')=\phi_1(x)\delta^4(x-x')+\phi_2(x,x'),$$

$$\phi_1(x)=ig^2\int\Delta_F(x-x')S^{(\phi)}(x',x')(dx')^4,$$

$$\phi_2(x,x')=-ig\int\int S^{(\phi)}(x,x'')\Delta^{(\chi)}(x,x''')\times\Gamma(x'',x';x''')(dx'')^4(dx''')^4,$$

$$\chi(x,x')=ig\int\int S^{(\phi)}(x,x'')S^{(\phi)}(x''',x)\times\Gamma(x'',x''';x')(dx'')^4(dx''')^4. \tag{3.11}$$

Here Γ means the so-called vertex part, according to Dyson's terminology,[7] and can itself be expressed in terms of $S^{(\phi)}$ and $\Delta^{(\chi)}$. As was mentioned before, ϕ_1 is that part of the average field acting on a particle at x which gives rise to the so-called ordinary integral, being a sum over all source particles. ϕ_2, on the other hand, corresponds mainly to the exchange integral which represents the reduction of the average force acting on the particle because of the Pauli principle.

In these solutions are also included the ordinary self-energy of the individual particle which does not depend on the existence of other particles. Since it gives rise

[7] F. J. Dyson, Phys. Rev. 75, 1736 (1949).

to the well-known divergences, we have first to dispose of it by some conventions such as cutoff or renormalization. In the complete relativistic theory where the particles obey the Dirac equation, the renormalization works for a certain class of interactions like the present one, and Eq. (3.9) will be valid if we understand by g, ϕ, $S^{(\phi)}$, etc., the renormalized quantities. In this case, although the modified propagation functions are used, we may be able to show that after carrying out the ordinary renormalization each term in the expansion of ϕ and χ, as well as the total energy, in powers of the coupling constant is finite. This does not mean, however, the convergence of the whole expression since this expansion presupposes the convergence of the Born approximation in treating the interaction.

After thus determining the Hartree fields ϕ and χ, the general properties of the system, beside the total energy which is already given by (3.9) or (3.10), are to be described by the equation of motion (2.5), or by the general terms of the S matrix (2.7). In order to recover the ordinary picture in which Ψ_0, instead of Ψ, is the vacuum state, we have only to change the operators (3.1) back into the original ones. Instead of studying the S matrix, sometimes it may be more advisable to carry out some canonical transformation which eliminate lower order processes.

It may be said that the essence of the idea of collective description lies in writing the equations for ϕ and χ in the closed form (3.11). If we expand $S^{(\phi)}$, $\Delta^{(\chi)}$, and Γ in powers of ϕ and χ, we shall get expressions involving $S^{(0)}$ and Δ_F, which means that we treat everything in the Born approximation starting from free plane waves. When ϕ and χ really give important effects on the behavior of the individual particles and mesons, we are not allowed to use such expansion. But since these equations are nonlinear, and moreover Γ cannot be expressed in a convenient closed form, we cannot hope to get a rigorous solution, but have to resort to some kind of approximation which is appropriate for the individual case considered. The following are some of such approximations which may be of use.

(1) If the system is a large volume of uniform gas, the natural assumption will be to take $\phi(x,x')$ and $\chi(x,x')$ as uniform, i.e., functions of $x-x'$ only. Γ will have to be determined by perturbation up to a certain order of approximation. Then we get equations in which enters the density ρ of particles as a parameter, and ϕ and χ will be solved as functions of ρ. In case the density is sufficiently low, it will be legitimate to develop them in powers of ρ.

The plasma oscillation of an electron gas, as treated by Bohm and Pines' collective description, is one of the simplest examples. Since it is favored by the small coupling constant $e^2/\hbar c$ and small density, the lowest order approximation suffices, in which χ is a constant proportional to density and determines the shielding radius of an electron. This is still a better approximation than the one in which we assume a Coulomb interaction between electrons and take plane waves as their approximate eigenfunctions. For the explicit use of the modified electromagnetic field enables one to account for the average coordinated behavior of the electron gas in the form of the plasma field. In other words, the dynamical correlation of the electrons, or deformation of the plane waves, is expressed as a change in nature of the intermediary field rather than that of the particle wave functions.

(2) In order to solve the self-consistent equations it may sometimes be advantageous to start from some trial functions for ϕ, χ (and Γ), and make successive approximations. Or else we may apply the variational principle by varying some adjustable parameters in the assumed solution.

(3) In some cases it may be possible to use the classical or WKB approximation in expressing the propagation functions as functionals of ϕ and χ. This means that we solve Eq. (3.7) by putting, for example,

$$S^{(\phi)}(x,x')=\exp[i\Theta(x,x')], \tag{3.12}$$

and expand Θ in powers of $\hbar$ beginning with $1/\hbar$. As will be discussed later, the Thomas-Fermi model may be regarded as a crudest approximation of this category.

We conclude this section with a few remarks.

First, on the exact meaning of the self-energies ϕ and χ: they are the effective interaction which we would observe for a particle, a "hole" (with change of sign), or a meson added to the system of, say, N particles. Thus we would expect that the total energy of a system of $N+1$ or $N-1$ particles could be obtained from the energy $\mathcal{E}_N$ of the present system by the formulas

$$\mathcal{E}_{N+1}=\mathcal{E}_N+\epsilon_N, \tag{3.13a}$$

$$\mathcal{E}_{N-1}=\mathcal{E}_N-\epsilon_N', \tag{3.13b}$$

where ϵ_N or ϵ_N' is the energy eigenvalue of the particle added to or removed from the system, whose potential ϕ depends on the N particles originally considered. On the other hand, by simply replacing N by $N+1$ in the second equation (3.13b), we get

$$\mathcal{E}_{N+1}=\mathcal{E}_N+\epsilon_{N+1}', \tag{3.13c}$$

where now ϵ_{N+1}' depends on the $N+1$ particles. This seems rather puzzling since we would expect this expression to coincide with the first one (3.13a). The paradox will be removed if we realize that in general ϕ, and hence ϵ, is not real, but complex;[8] the total energy

[8] When ϕ or χ is complex, some caution is necessary in talking about $S^{(\phi)}$, $\Delta^{(\chi)}$, $\rho^{(\phi)}$, etc. Equations such as (3.7) and (3.11) should actually be considered by first omitting the imaginary part of the Hartree fields. Otherwise we would have to assume exponentially varying factors for these quantities, which would lose meaning since they involve space-time integrations. The imaginary part of ϕ or χ should thereafter be defined by (3.11) in terms of the Green's functions thus obtained. This procedure means that we demand the possibility of Fourier transformation for all these functions of space-time. With such a convention, Eqs. (3.9) and (3.10) will then yield meaningful, but in general complex, values.

thus obtained is not necessarily the exact eigenvalue of a stationary state. Moreover, one will get in general a solution which explicitly changes with time so that there is no eigenvalue like ϵ_N, although the total energy may remain constant.

To illustrate the first statement, let us assume that a nucleon hits a nucleus of mass number N, giving rise to a compound nucleus $N+1$. In this case the particle field and Bose field in our present formulation may be identified with the nucleon and meson field, respectively. The compound nucleus thus formed may decay subsequently by such processes as emission of one or more particles, meson production, or breaking up in a fission-like manner. (We neglect β and γ decay as well as the usual fission because we treat here only nucleon and meson fields.) The incoming nucleon is responsible for all these possible consequences. It would be impossible, however, to pack the complete information about them into the Hartree field ϕ for the incoming nucleon; ϕ would indicate the possibility of such decay processes only by being a complex potential, which says nothing about what the decayed states would be. In this case the system of $N+1$ particles has many states of nearly equal energy which are widely separated in phase space, and removing one particle from this system will not uniquely lead back to the original nucleus N. Only if the decay rate is sufficiently small it will make sense to talk about the compound nucleus and its energy, and ϵ_N and ϵ_{N+1}' will nearly coincide. Thus the magnitude of the imaginary part of ϕ and χ is a measure of validity of our present picture.

We may also conclude that our picture will not work well unless the difference between (3.13a) and (3.13c) is really small, i.e., unless the system consists of sufficiently many particles of such a nature as to make the difference of N and $N+1$ insignificant.

Next, one might raise a question about the use of the S matrix in deriving the various results of this section rather than a transformation function for a finite time interval. This is necessary to get ϕ and χ, which do not depend on the time interval arbitrarily assumed. On the other hand, it might be argued that the use of the S matrix inevitably misses some important features of interaction, such as the formation of bound states, provided they can occur at all. This could be true, however, even if we used a finite interval transformation function because we only take account of the self-energy effects in each step of the perturbation, and that is an inherent limitation of our method. But this situation is mitigated by the fact that we need not always solve the equations for ϕ and χ by perturbation methods starting from plane waves. When bound states actually occur, we could assume such ϕ and χ that will localize the particles or mesons from the beginning, so that the difference between the real interaction and the assumed Hartree fields may be successfully treated as a small perturbation.

As for the total energy expression, we have to integrate over the coupling constant or the number of the particles. There may sometimes exist, then, some points at which a kind of phase transition takes place, resulting in a sudden qualitative change in the nature of the Hartree fields and their eigenstates [as was indicated by the difference between ϵ_N and ϵ_{N+1}' in Eqs. (3.13)]. The integral may be expected to exhibit at such points some singularities or discontinuities.

4. DISCUSSIONS

A. The Validity and Limitation of the Description

The collective description developed so far may be characterized by the following features: First, we consider the system as composed of particles as well as the intermediary field, and do not explicitly describe the interaction in the form of potentials even though there is neither incoming nor outgoing field. This gives us more freedom in describing the system than does the usual case. The more important thing, however, is that the picture is essentially an independent-particle model in the sense that each particle or field quantum moves in a fixed field of force which does not explicitly depend on the coordinates of the other particles or quanta but in general changes with time. The state vector of the system is consequently represented by a product of wave functions of individual particles and quanta, with the correct symmetry properties required by statistics.

This does not mean, however, that we replace the actual wave function simply by such a product of wave functions. The situation may be explained as follows. If we start out with a state vector $\Psi(t_0)$ at $t=t_0$, it varies with time due to the interaction H_{int}', and becomes

$$\Psi(t)=U(t,t_0)\Psi(t_0),$$

$$U(t,t_0)=P\exp\left[-i\int_{t_0}^{t}H_{\text{int}}'(dx)^4\right], \tag{4.1}$$

at the time t. We can make t_0 tend to $-\infty$ under the assumption that the interaction can be turned on adiabatically. $\Psi(t)$ thus obtained represents the true eigenstate of the system (in the interaction representation) which is adiabatically connected with the initial free state $\Psi(-\infty)$. In our case $\Psi(-\infty)$ corresponds to the determinantal state vector Ψ of (2.8) in which each particle or meson moves in a Hartree field. Obviously this Ψ itself is not the representative of the true eigenstate of the total Hamiltonian

$$\bar{H}=\bar{H}_0'+\bar{H}_{\text{int}}'. \tag{4.2}$$

If we want to regard Ψ as an actual state, the Hamiltonian corresponding to such a state should be

$$\bar{H}_1=U^{-1}\bar{H}U, \quad U=U(t,-\infty), \tag{4.3}$$

and other physical quantities associated with this system should likewise be considered in the new representation.

The difference between these two pictures is concealed in our formulation since we did not explicitly deal with the Hamiltonian, but instead analyzed the structure of the S matrix (which is essentially a Lagrangian formalism) to derive necessary information about the system. If, however, we want to understand the meaning of our description, it is instructive to formulate it in terms of the Hamiltonian and the canonical transformation. Especially, it should be noticed that the true eigenstate of the system in the usual sense is $U\Psi$ rather than Ψ.

Let us now direct our attention to the transformation operator U. In general it cannot be obtained in a closed form, but has to be expanded in certain series which may not always be convergent. The problem of convergence arises in two senses (apart from the self-energy divergences which we do not discuss here). One is that, if we expand U in powers of the coupling constant, the number of terms of order n increases very rapidly with increasing n. The other is that, even if we restrict ourselves to only those higher-order processes which are iterations of lower-order ones, the resulting power series does not always converge. This means the breakdown of the Born approximation in the ordinary sense, and it will occur, for example, when a bound state is formed. Of course, the assumption of adiabatic switching-on of the interaction, which was necessary in our discussion, will then become invalid.

We have, however, a freedom in the choice of starting state vector Ψ by varying the Hartree fields to which the individual particles or mesons are subject. For each arbitrary choice of these fields there corresponds an effective interaction H_{int}' and the transformation operator U. We may then ask whether we can improve the convergence character of U with a proper choice of Hartree fields, and possibly prevent U from diverging even though it diverges when there is no Hartree field. It is unlikely that this is always possible. But we can set up, as we have seen, a formal recipe for getting the optimum functions χ and ϕ, which leads to the self-consistent equations (3.11). That this is the best choice may be understood in the light of the conventional Hartree-Fock theory, as will be discussed later.

The relation between our present description with the Hartree fields and the conventional one without them is as follows. In the latter case, the starting state vector is $\Psi^{(0)}(-\infty)$ which is defined by the plane-wave states. The actual state vector of the system will be represented formally by

$$\Psi^{(0)}(t)=U^{(0)}(t,-\infty)\Psi^{(0)}(-\infty),$$

$$U^{(0)}(t,-\infty)=P\exp\left[-i\int_{-\infty}^{t}H_{\text{int}}(dx)^4\right], \quad (4.4)$$

in the interaction representation. $\Psi(t)$ and $\Psi^{(0)}(t)$ are connected by

$$\Psi(t)=T(t)\Psi^{(0)}(t),$$

so that

$$U^{(0)}(t,-\infty)=T^{-1}(t)U(t,-\infty)T(-\infty), \quad (4.5)$$

where

$$T(t)=P\exp\left[-i\int_{-\infty}^{t}(\psi^*\pi\psi+\tfrac{1}{2}\varphi w\varphi)(dx)^4\right]. \quad (4.6)$$

The integrand in T is the Hamiltonian corresponding to the Hartree field terms $\psi^*\phi\psi$ and $\varphi\chi\varphi$ in the Lagrangian. We have thus decomposed $U^{(0)}$ into U and T hoping that an important effect of the interaction may be absorbed in the factor T, which in principle need not be treated by perturbation methods since it has a sufficiently simple structure.

In order to discuss to what extent such an idea can be justified we have to investigate more closely the nature of the Hartree fields as determined by the self-consistent equations. In the following we shall present some criteria on the validity of the Hartree field picture which follow from various points of view.

(a) What we have missed in the independent-particle picture is reflected in the fact that ϕ and χ determined by Eq (3.11) are in general complex quantities, and so is also the total energy except when the system is in its ground state. When the imaginary part of ϕ or χ is large, the individual particles (and the total system) will decay rapidly into other states which are outside of the subspace originally assumed, so that they cannot represent the major aspects of the actual system.

(b) The Hartree field ϕ or χ represents the average force exerted on a test body placed in the system. It describes, however, the reaction of the test body on the system only in its average behavior. The picture will be good, therefore, if the reaction itself or its fluctuation turns out to be small. This would mean

(1) The nature of the system is not drastically affected by the introduction of a test body in it.

(2) Each constituent particle or quantum of the system, as a potential test body, contributes only a small amount to the average field ϕ or χ. In other words the dynamical correlation among a small number of particles or quanta is not too large to outweigh the effect of the rest of the system.

The latter condition obviously breaks down, for instance, if two particles form a bound system which behaves like an inert molecule so that the system as a whole remains gaseous. In such a case, the force exerted on a single test particle placed in the gas will be essentially different from the one each "atom" of the molecule experiences. Thus the independent-particle picture of the whole system will fail when there is a tendency to form some stable subunits in the system.

By the same reasoning, it will also be easy to see that our method will not work unless there are suffi-

cient number of particles in the system, as was mentioned in Sec. 3. In particular, a simple two-body problem does not conform to our formulation since the two particles are correlated with each other by the conservation of center of gravity.

(c) From a practical point of view, we are often compelled to solve the self-consistent equations by expansion in certain power series in the coupling constant or density, and we have a further restriction if we assume a Fermi gas model, i.e., plane waves for the particles. The Hartree potentials ϕ and χ in the first approximation are the averages of the scattering amplitudes of two particles or a particle and a meson, respectively, over the plane-wave states. It is easy to see that ϕ and χ represent then the forward scattering amplitudes of the respective processes. Consequently, we may expect that the collective description provides a good picture if the scattering by the given system as a whole is predominantly forward. Such a situation would follow either from the characteristics of the elementary scattering itself or as a result of interference effects or perhaps the exclusion principle. Thus:

(1) If the coupling constant and the density of particles are sufficiently small, and particularly if the elementary scatterings are predominantly forward, we should expect that the lowest approximation of the collective description gives a good picture. The predominantly forward scattering would mean a long-range interaction between the scattering particles or mesons.

This, however, should not be confused with the statement that the collective description is especially suited for the long-range Coulomb interaction, as treated by Bohm and Pines,[1] since the photon-electron scattering is not forward at all. According to the present picture, it should be due to the small coupling between electrons and electromagnetic field which favors the gaseous behavior with small fluctuations, and that even a small effective mass χ plays an important role since originally the electromagnetic field has no mass.

On the other hand, if we apply our method to the Hamiltonian in which the electromagnetic field is eliminated in favor of the explicit Coulomb interaction (see below), the present criterion will be relevant, since then we mean by scattering the Coulomb scattering of two electrons.

(2) In case the coupling constant is not necessarily small, but the density is still small, we may treat only the scattering of two particles or mesons alone exactly. This means that we consider all powers of the coupling constant but only the lowest terms in the density expansion. ϕ and χ will then be given by the diagonal elements or the forward scattering part of the scattering matrices corresponding to these processes. If the scattering matrices again turn out to give a predominantly forward scattering, we shall again have a good picture.

(3) If both the density and the coupling constant are not small, we have to consider all the multiple scatterings and our picture will be successful only if the resulting scattering turns out to be forward.

The criterion on the validity of our picture in terms of the forward-scattering property may be related to the criterion (a) in the following way. As is well known, the imaginary part of the forward-scattering amplitude is a measure of the attenuation of the wave as it passes through a medium due to scattering out of the incident direction or real absorption. Mathematically, it is derived from the relation of the scattering matrix R:

$$2\,\mathrm{Im}R = R\cdot R^{\dagger}, \tag{4.7}$$

where $1-iR$ is the S matrix corresponding to the scattering plus absorption process, and $R^{\dagger}$ is the hermitian conjugate of R. The imaginary part of the forward scattering matrix element will be small if the total (scattering plus absorption) cross section, being proportional to the corresponding element of $R\cdot R^{\dagger}$, is small. It will be small compared to the real part if the absorption is small and the scattering is mainly forward.

When the interaction is of such a nature as to cause a large-angle scattering, we cannot expect to get a good physical picture as long as we start from the uniform-gas model. The only way to improve it in the framework of the independent-particle picture will be to assume a nonuniform distribution (spatially and/or temporally) of the particles, moving in a nonuniform Hartree field ϕ, which in turn gives rise to a nonuniform χ. The particles or quanta will then be scattered by the humps of these potentials into other directions, so that we can take account of the large-angle scattering by such potentials. Actually such a solution should follow naturally if we solve the self-consistent field equations (3.11) in the proper way. Even in that case, however, we cannot always expect to have a good result in the lower approximations of ϕ and χ. For ϕ and χ would represent only the average behavior of the scattering between various particles and quanta, while the individual fluctuations could be large. The latter will be small if the individual particles or quanta occupying different eigenstates behave more or less similarly at a fixed position in space-time, and this will be true (i) if they behave either like a uniform gas with a uniform scattering cross section; (ii) if they are rather localized in a lattice-like structure with such a strong binding as to make the scattering into much different eigenstates unimportant; (iii) or if they are under an influence of strong external fields by which their behavior is largely determined. In such cases our picture may be expected to be reasonable. On the other hand, if the system behaves more or less like a liquid, the Hartree fields being not uniform enough to allow a plane wave solution nor undulating enough to keep a particle in some limited region, the situation is more difficult, and there is no guarantee that our method should provide a reasonable picture of such a system.

B. Relation to Other Theories

We shall discuss here the relation of the present general theory to the various methods which have been devised for handling many-body problems.

(1) *Bohm and Pines' Theory*

The present formulation owes its direct origin to what Bohm and Pines[1] have named the collective description of electrons. In their theory they utilize a canonical transformation by which they go over from the original dynamical variables describing the individual motion of electrons (and electromagnetic field) to the so-called collective variables which take account of the medium-like behavior of the system as a whole. Actually it is equivalent to the statement that we use, instead of the ordinary electromagnetic field variables, the modified ones which include the effect of the presence of many particles in the form of an effective mass χ. Although the essential idea is thus the same in both theories, there are some differences in the following respects.

(a) Bohm and Pines have made an explicit use of canonical transformation in order to go over to the collective description, whereas we have defined the new variables by giving the Hartree fields in which they shall move.[9] This is due to the circumstance that we make use of the Lagrangian and the S-matrix formalism while they start from the Hamilton-Schrödinger formalism. Thus it would amount only to a matter of technique if the principle of determining the collective variables (or ϕ and χ) were exactly the same.

(b) Bohm and Pines determined χ only in the lowest approximation and did not introduce ϕ explicitly. If we understand their χ to be a Hartree field by which we can go over to the independent particle picture, our method is a systematic generalization of Bohm and Pines' since we introduce both ϕ and χ and determine them to higher orders of approximation. But ϕ and χ need not necessarily mean the rigorous self-consistent field based on the complete independent-particle picture, but can simply be some kind of average field which help us improve the picture.

As was mentioned in Sec. 2, if we determine ϕ and χ only up to a certain order of approximation, we are left with a residual interaction which represents the fluctuation from the average behavior. Since the independent-particle picture has its own limitations as we are discussing, it is sometimes more advantageous to treat the residual interaction in a different way from the independent-particle model. In this sense the successive approximation of ϕ and χ might be a kind of asymptotic expansion which should be broken off at some optimum place.

In the case of plasma oscillation, the long-range part of the Coulomb interaction is easily covered by the average field (the plasma field which is analogous to the modified meson field) as it is a sum of small contributions from a large number of particles, which comes under the criterion discussed in (A). However, when two particles approach each other (which means short wavelengths of the plasma field), the local correlation between them will become appreciable, destroying the plasma field picture based on the over-all long range correlation. On the other hand, this residual interaction, if represented as a kind of screened interaction, does not bring about so large an effect as to modify the over-all behavior of the electrons, so that it may be estimated by taking plane waves for the electrons. This is the reason why they did not consider ϕ explicitly.

In order to carry out a partial Hartree field picture, the canonical transformation is better suited since it exhibits explicitly the form of the residual interaction. Obviously the canonical transformation is generated by (4.2) or similar operators. Here the ϕ and χ used need not be the solutions of the self-consistent equations.

(2) *Hartree-Fock Equations*

Being based on the complete independent-particle picture, the Hartree-Fock method[10] is very similar to ours. Although usually it treats only particles which interact with each other by some potential, it is by no means an essential restriction of the method. Our formulation, on the other hand, can also be applied to such cases without any trouble, as we shall see below. Thus for instance, if we have a Hamiltonian,

$$\bar{H}=\int \frac{1}{2m}\psi^* p^2\psi (dx)^3-\tfrac{1}{2}\int\int \psi^*\psi^{*\prime} V\psi\psi' \times (dx)^3(dx')^3, \quad (4.8)$$

we have only to introduce ϕ. This is in the first approximation determined by

$$\phi_1(x)=\int V(x-x')\langle\psi^*(x')\psi(x')\rangle (dx')^3 = \int V(x-x')\rho^{(\phi)}(x',x')(dx')^3,$$

$$\phi_2(x,x')=-V(x-x')\langle\psi^*(x)\psi(x')\rangle = -V(x-x')\rho^{(\phi)}(x',x), \quad (4.9)$$

with

$$\rho^{(\phi)}(x,x')=\sum_{\text{occ.}} u_i^{(\phi)}(x)u_i^{*(\phi)}(x'),$$

$$(E_i-p^2/2m-\phi)u_i=0. \quad (4.10)$$

These equations are essentially the same as in the Hartree-Fock theory.

[9] The equations for the self-consistent fields obtained here are actually a refinement of those which were utilized by Bohm and Gross and by Bohm and Pines (the second paper of reference 1) for the ordinary plasma oscillation.

[10] D. R. Hartree, Proc. Cambridge Phil. Soc. **24**, 111 (1928); V. Fock, Z. Physik **61**, 126 (1930).

The Hartree-Fock method usually derives these equations on the basis of the variational principle, while we did not refer to it. The role of the variational principle becomes clear if we formulate it in the following way. Rewrite (4.8) as

$$\bar{H}=\left\{\int \frac{1}{2m}\psi^* p^2\psi (dx)^3+\int\int \psi^*\phi\psi'(dx)^3(dx')^3+C\right\}$$
$$-\left\{\tfrac{1}{2}\int\int \psi^*\psi^{*\prime}V\psi\psi'(dx)^3(dx')^3\right.$$
$$\left.+\int\int \psi^*\phi\psi'(dx)^3(dx')^3+C\right\}$$
$$\equiv \bar{H}_0'+\bar{H}_{\rm int}'. \tag{4.11}$$

The variation $\delta\langle\bar{H}\rangle$ of the expectation value of $\bar{H}$ with respect to a state vector Ψ yields

$$0=\delta\langle\bar{H}\rangle=\delta[(\Psi,\bar{H}\Psi)/(\Psi,\Psi)]$$
$$=\delta\langle\bar{H}_0'\rangle+\delta\langle\bar{H}_{\rm int}'\rangle. \tag{4.12}$$

Thus if we choose ϕ and C in such a way that

$$\delta\langle\bar{H}_{\rm int}'\rangle=\langle\bar{H}_{\rm int}'\rangle=0, \tag{4.13}$$

(4.12) reduces to

$$\delta\langle\bar{H}_0'\rangle=0, \quad \langle\bar{H}\rangle=\langle\bar{H}_0'\rangle, \tag{4.14}$$

which shows that the individual particles behave as if they were moving independently under the potential ϕ. If we assume for Ψ a single Slater determinant of one particle wave functions, (4.13) is just the condition that the effective self-energy of a particle arising from the interaction $\bar{H}_{\rm int}'$ shall vanish, since it is equivalent to differentiation with respect to the density matrix:

$$\int\int [\delta\langle\bar{H}_{\rm int}'\rangle/\delta\langle\psi(x)^*\psi(x')\rangle]\delta\langle\psi(x)^*\psi(x')\rangle$$
$$\times(dx)^3(dx')^3=0. \tag{4.15}$$

On the other hand, we get for C,

$$C=-\left\langle\tfrac{1}{2}\int\int \psi^*\psi^{*\prime}V\psi\psi'(dx)^3(dx')^3\right.$$
$$\left.+\int\int \psi^*\phi\psi'(dx)^3(dx')^3\right\rangle, \tag{4.16}$$

which is to be added to the sum of the energies of the individual particles in order to obtain the total energy [see Eq. (2.16)].

The Hartree-Fock equation, however, does not give a rigorous solution because of the special choice of Ψ; neither does it provide us with an idea how to improve the result systematically. Since our formalism overcomes these defects, it may turn out to be useful in case the Hartree-Fock method is not enough to get a satisfactory result.

(3) *Thomas-Fermi-Dirac Model*

The Thomas-Fermi model[11] is a kind of the self-consistent field theory for a degenerated system of electrons. Unlike the Bohm-Pines theory of collective description, it does not introduce the plasma field with χ, but instead considers the particle Hartree field ϕ. We shall illustrate this on our present example.

According to Eq. (3.11), ϕ obeys the equation

$$(\Box-\mu^2)\phi_1(x)=-g^2S^{(\phi)}(x,x)$$
$$\phi_2(x,x')=-ig\int\int S^{(\phi)}(x,x'')\Delta^{(\chi)}(x,x''')$$
$$\times\Gamma(x'',x';x''')(dx'')^4(dx''')^4. \tag{4.17}$$

We first neglect the so-called radiative correction for the individual particle. Next, when the source density is sufficiently high so that there are many particles coming within the force range of one particle, we can neglect the exchange part ϕ_2. If, moreover, we can consistently assume ϕ to be static in considering the ground state, we get

$$(\Delta-\mu^2)\phi_1(x)=g\rho^{(\phi)}(x,x), \tag{4.18}$$

since $S^{(\phi)}(x,x)=-\rho^{(\phi)}(x,x)$ for nonrelativistic particles.

The whole problem is reduced to that of expressing $\rho^{(\phi)}(x,x)$ in an explicit form. The Thomas-Fermi model puts it, by statistical considerations in phase space, as

$$\rho^{(\phi)}(x,x)=\int\int\int\left(\frac{dp(x)}{2\pi}\right)^3, \tag{4.19}$$

where $p(x)$ is the classical momentum at point x of a particle of energy E:

$$\frac{1}{2m}[p(x)]^2=E-\phi(x), \tag{4.20}$$

and the integration is extended from zero to the maximum value corresponding to the Fermi energy E_F.

We shall show that Eq. (4.19) can also be derived from Eq. (3.6) by the following consideration. Assume that the solution ϕ is sufficiently slow-varying compared to the wavelength of the most of the particles in various states, and apply the idea of the WKB method mentioned in Sec. 3 to express $\rho^{(\phi)}$. This method works well if the separation of variables is possible, leading to the individual eigenfunctions in one dimension of the form

$$u_i(\xi)=\frac{c_i}{(p_i(\xi))^{\frac{1}{2}}}\{\alpha_i\exp[iS_i(\xi)]$$
$$+\beta_i\exp[-iS_i(\xi)]\},$$
$$|\alpha_i|^2+|\beta_i|^2=1. \tag{4.21}$$

[11] L. H. Thomas, Proc. Cambridge Phil. Soc. **23**, 542 (1927); E. Fermi, Z. Physik **48**, 73 (1928); P. A. M. Dirac, Proc. Cambridge Phil. Soc. **26**, 376 (1930).

Here $S_i(\xi)$ is the classical action function, and $p_i(\xi)$ the classical momentum conjugate to ξ:

$$E_i = H(p_i(\xi),\xi) = \frac{1}{2m} p_i(\xi)^2 + U(\xi),$$

$$p_i(\xi) = \partial S_i/\partial \xi. \tag{4.22}$$

The quantum condition reads as

$$\frac{1}{2\pi}[S_i(\xi_1) - S_i(\xi_2)] \approx \text{integer} = n. \tag{4.23}$$

ξ_1 and ξ_2 are either the classical limits attained by the particle,

$$p(\xi_1) = p_2(\xi) = 0, \tag{4.24}$$

or else two fixed equivalent points in case of a periodic boundary condition. Next we neglect the wave-mechanical fluctuation of ρ due to the term in the bracket of Eq. (4.21), and get

$$\rho(\xi) = \sum_i \frac{|c_i|^2}{p_i(\xi)}. \tag{4.25}$$

The normalization factor c_i is determined by

$$1/|c_i|^2 = \int_{\xi_1}^{\xi_2} d\xi/p_i(\xi). \tag{4.26}$$

Now it is easy to show, under the above conditions that

$$\partial p_i/\partial E_i = m/p_i = \partial[\partial S_i/\partial E_i]/\partial \xi,$$

$$[\partial S_i/\partial E_i]_{\xi_1}^{\xi_2} = 2\pi dn_i/dE_i,$$

$$|c_i|^2/p_i(\xi) = [\partial p_i(\xi)/\partial E_i]/(2\pi dn_i/dE_i)$$

$$= (1/2\pi)(\partial p_i/\partial n_i), \tag{4.27}$$

so that

$$\rho(\xi) \approx \frac{1}{2\pi} \int_0^{P(\xi)} dp(\xi), \tag{4.28}$$

the integration being up to the local maximum $P(\xi)$. This gives the basis of the Thomas-Fermi equation under limited conditions.

In Thomas-Fermi model the linear term in ϕ is not separated out from $\rho^{(\phi)}$ to give a χ term on the left-hand side of Eq. (4.18). But when the system is not in the ground state, and ϕ is small compared to the energy of the individual particles, we can do it by using (4.25) and expanding $p(\xi) = \{2m[E - U(\xi)]\}^{\frac{1}{2}}$ in powers of $U(\xi)$. This expression for ρ, having a simple physical meaning, is essentially equivalent to what Bohm and Gross[3] found in their classical theory of plasma oscillation.

The exchange potential ϕ_2, which was neglected in the Thomas-Fermi model, can be taken into account if we approximate it by a local form:

$$\tilde{\phi}_2(x) \equiv \int \phi_2\left(x + \frac{y}{2}, x - \frac{y}{2}\right)(dy)^3,$$

$$\tilde{\phi}(x) \equiv \phi_1(x) + \tilde{\phi}_2(x), \tag{4.29}$$

while using

$$\rho^{(\phi)}(x,x') \approx \int_{|p| \le P(\frac{1}{2}x + \frac{1}{2}x')} \left(\frac{dp}{2\pi}\right)^3 e^{ip\cdot(x-x')}, \tag{4.30}$$

for the evaluation of $\phi_2(x,x')$. Dirac's improvement over the Thomas-Fermi equation then follows by substituting for $\phi_1 = \tilde{\phi} - \tilde{\phi}_2$ in (4.18):

$$(\Delta - \mu^2)[\tilde{\phi}(x) - \tilde{\phi}_2(x)] = -g\rho(\tilde{\phi}; x, x). \tag{4.31}$$

C. Possible Generalizations

(1) *Extension to an Arbitrary State Vector* Ψ

In the present investigation, we have considered only those states Ψ in which the particle wave functions can be represented by a single Slater determinant and there is no real meson present. Since the nature of Ψ is reflected in the boundary conditions of the propagation function S, it might be suggested that we could extend this result by starting from an arbitrary state with the corresponding modification in the propagation functions S and Δ.

Indeed the formulas (3.9) remain valid for any given state Ψ, provided that S and Δ are the propagation or Green's functions defined by (3.3) in which the expectation value is taken with respect to the named Ψ. However, the equations determining $S^{(\phi)}$, $\Delta^{(\chi)}$ and ϕ, χ are not so simple as the present one, as will be understood if one realizes that we cannot in general modify the definition of vacuum (and consequently that of creation and annihilation) so that Ψ may be characterized simply by

$$\psi^{+\prime}(x)\Psi = \psi^{+\prime *}(x)\Psi = \varphi^{+\prime}(x)\Psi = 0. \tag{4.32}$$

Only the propagation function without interaction can be given relatively easily. For example, we get

$$\Delta(x,x') = \Delta_P(x,x') + \sigma(x,x'),$$

$$\sigma(x,x') = \sum_{\text{occ.}} n_i v_i(x) v_i^*(x'), \tag{4.33}$$

if the meson field part of Ψ is a simple symmetrical product of eigenfunctions in which n_i particles occupy the same state i. An interesting example which might be treated with this generalized formulation would be an assembly of permanent Bose particles (or molecules) interacting through a potential with each other.

(2) *Statistical Ensemble*

Some of our results will also hold even when we take a statistical ensemble instead of a pure state. In that

case the expectation values should be interpreted as those over such a statistical ensemble. For example, the propagation functions without interaction are given by

$$S(x,x')=S_F(x,x')-\rho(x,x'),$$
$$\Delta(x,x')=\Delta_F(x,x')+\sigma(x,x'),$$
$$\rho(x,x')=\sum c_i u_i(x)u_i^*(x'),$$
$$\sigma(x,x')=\sum d_i v_i(x)v_i^*(x'), \qquad (4.34)$$

where c_i and d_i are the expectation values of the number of particles or quanta in the state i in the assumed ensemble. We could meet, however, with some intrinsic difficulties since the basic equations of quantum mechanics refer only to pure states.

(3) *Nonstationary Problems*

Although in the present paper we have exclusively considered the stationary states of the system, the idea can also be applied to nonstationary problems, i.e., transitions from one state to another. Such transition will be caused either by a small external perturbation or by the residual interaction which destroys the stability of the individual levels. In this connection we might mention that the self-energies need not necessarily be expectation values over a fixed state; we can also define their nondiagonal elements between two different states. Such off-diagonal parts will have to be considered in case the transition rate is large.

All these generalizations do not seem to be easy if we want to carry them out consistently to higher orders of approximation. But it should be borne in mind that it is not always necessary nor adequate to adopt the complete independent-particle model throughout.

5. CONCLUDING SURVEY

We have formulated here a general theory of treating many-body problems (mainly their stationary states) by a systematic application of the independent-particle (Hartree-field) picture, or the linearization procedure mathematically speaking. The Hartree fields are determined by a set of equations of generalized Hartree-Fock type, and the total energy of the system has been formally but rigorously expressed on the independent-particle picture. Also it is possible to adopt a partial independent-particle picture and reduce the effective interaction by introducing auxiliary potentials. The method includes and extends many of the less systematic approximations hitherto known, such as Bohm-Pines, Hartree-Fock, and Thomas-Fermi, whose relations to the present one have been studied.

The practical usefulness of the collective description depends essentially on the validity of the Hartree field picture, and various rather qualitative criteria about its range of applicability have been discussed in some detail. It is just the relatively flexible character of the Hartree field picture that makes it difficult to give general quantitative criteria, although in individual cases we might be able to estimate the degree of approximation quantitatively.

Among physically interesting examples which may advantageously be handled by the present formulation we might first mention the electromagnetic properties of electron gases including the plasma oscillation, property of metals, and perhaps the superconductivity. This, however, will need some additional refinements because of the supplementary condition. In the realm of nuclear physics, the method seems less promising because of the strong interaction and short-range character of the nuclear forces or meson field which makes nuclei look like liquid in some respects. Nevertheless, it would turn out helpful in investigating some important features of the nuclear forces, such as the many-body forces, saturation, and the shell structure, which have not yet been fully understood. These problems will be studied in forthcoming papers.

ACKNOWLEDGMENTS

The authors would like to express their gratitude to Professor R. Oppenheimer for the hospitality extended to them at the Institute for Advanced Study, where most part of the work was carried out, and to Professor R. F. Bacher for his hospitality at the California Institute of Technology during the last stage of the work. Thanks are also due Dr. D. Pines for his interest in our work, as well as for keeping us informed of the latest progress on his part prior to publication.

APPENDIX. FORMAL RELATIONS CONCERNING THE *S*-MATRIX AND GREEN'S FUNCTIONS

1. Lemmas on Normal Forms

We shall give here a concise derivation of the necessary formulas appearing in this paper with the aid of the following lemmas on the relation between chronological forms and corresponding normal forms. Let us begin with the consideration of a single chronological product of operators ψ, ψ^*, and φ, which we denote as $A[\psi,\psi^*,\varphi]$. The normal form with respect to the "vacuum" Ψ is obtained by decomposing ψ, ψ^*, and φ within A into creation and annihilation operators according to (3.1) and rearranging them in such a way that the creation operators stand always to the left of the annihilation operators. We shall write the resulting normal form as $N[A]$ whose structure is determined in the following way.

First watch a particular factor, say $\varphi(x)$, in the product A and write A as $A'\varphi(x)A''$. In doing so, we are encountered with commutators of $\varphi^{\pm}(x)$ with factors $\varphi^{\pm}(x')$ contained in A' and A''. As is easily seen the

result of this procedure can be expressed as

$$A'A''\varphi^+(x)+\varphi^-(x)A'A''+\int_{-\infty}^{\infty}(dx')^4\left[\Delta_{\rm ret}(x,x')\frac{\delta}{\delta\varphi^-(x')}-\Delta_{\rm adv}(x,x')\frac{\delta}{\delta\varphi^+(x')}\right]A'A''. \quad \text{(A1)}$$

Differential operators in this formula are defined by

$$[\delta/\delta\varphi^\pm(x),\ \varphi^\pm(x')]=\delta^4(x-x'), \quad \text{(A2)}$$

and the commutation functions are given by

$$\Delta_{\rm ret}(x,x')=\frac{1+\epsilon(t-t')}{2}[\varphi^+(x),\varphi^-(x')],$$

$$\Delta_{\rm adv}(x,x')=\frac{1-\epsilon(t-t')}{2}[\varphi^-(x),\varphi^+(x')], \quad \text{(A3)}$$

where $\epsilon(t)$ is a signature function assuming values 1 or -1 according as t is positive or negative. Going over to the normal form from (A1), we find that

$$N[A]=N[A'A'']\varphi^+(x)+\varphi^-(x)N[A'A'']+\int_{-\infty}^{\infty}(dx')^4\left[\Delta_{\rm ret}(x,x')\frac{\delta}{\delta\varphi^-(x')}-\Delta_{\rm adv}(x,x')\frac{\delta}{\delta\varphi^+(x')}\right]N[A'A'']. \quad \text{(A4)}$$

It is important to notice here that in the normal form every operator can be treated as a c number with respect to the commutativity of product except for the change of sign in the case of exchanging Fermi-Dirac operators. The right-hand side of (A4) can thus be regarded as identical with

$$\varphi(x)N[A'A''], \quad \text{(A5)}$$

where

$$\varphi(x)=\varphi^+(x)+\int_{-\infty}^{\infty}(dx')^4\Delta_{\rm ret}(x,x')\delta/\delta\varphi^-(x')+\varphi^-(x)-\int_{-\infty}^{\infty}(dx')^4\Delta_{\rm adv}(x,x')\delta/\delta\varphi^+(x'). \quad \text{(A6)}$$

Next let us assume that A is a chronological product with respect to the operator $\psi^*\psi(x)$. Then starting from the decomposition $A=A_1'\psi^*\psi(x)A_1''$, one obtains the formula

$$N[A]=\psi^*\psi(x)N[A_1'A_1''] \quad \text{(A7)}$$

where

$$\psi(x)=\psi^+(x)+\int_{-\infty}^{\infty}(dx')^4S_{\rm ret}(x,x')\delta/\delta\psi^-(x')+\psi^{-*}(x)-\int_{-\infty}^{\infty}(dx')^4S_{\rm adv}^*(x,x')\delta/\delta\psi^{+*}(x'),$$

$$\psi^*(x)=\psi^{+*}(x)+\int_{-\infty}^{\infty}(dx')^4S_{\rm ret}^*(x,x')\delta/\delta\psi^{-*}(x')+\psi^-(x)-\int_{-\infty}^{\infty}(dx')^4S_{\rm adv}(x,x')\delta/\delta\psi^+(x'), \quad \text{(A8)}$$

with

$$\{\delta/\delta\psi^\pm(x),\psi^\pm(x')\}=\{\delta/\delta\psi^{\pm*}(x),\psi^{\pm*}(x')\}=\delta^4(x-x'),$$
$$\{\delta/\delta\psi^\pm(x),\psi^{\pm*}(x')\}=\{\delta/\delta\psi^{\pm*}(x),\psi^\pm(x')\}=0,$$
$$\{\delta/\delta\psi^\pm(x),\delta/\delta\psi^\pm(x')\}=\{\psi^\pm(x),\psi^{\pm*}(x')\}=0,\ \text{etc.}, \quad \text{(A9)}$$

and

$$S_{\rm ret}(x,x')=\frac{1+\epsilon(t-t')}{2}\{\psi^+(x),\psi^-(x')\},$$

$$S_{\rm adv}^*(x,x')=\frac{1-\epsilon(t-t')}{2}\{\psi^{-*}(x),\psi^{+*}(x')\},$$

$$S_{\rm ret}^*(x,x')=\frac{1+\epsilon(t-t')}{2}\{\psi^{+*}(x),\psi^{-*}(x')\},$$

$$S_{\rm adv}(x,x')=\frac{1-\epsilon(t-t')}{2}\{\psi^-(x),\psi^+(x')\}. \quad \text{(A10)}$$

Here the symbol $\delta/\delta\psi^+$, etc., are not the usual functional differentiation, but are used only for the sake of convenience.

Now, operators (A6) and (A8), operating on a function of φ and $\psi^*\psi$, can be expressed as

$$\varphi(x)=R\varphi(x)R^{-1},$$
$$\psi(x)=R\psi(x)R^{-1},$$
$$\psi^*(x)=R\psi^*(x)R^{-1}, \quad \text{(A11)}$$

where

$$R=\exp\left[-\int\frac{\delta}{\delta\psi(x)}S(x,x')\frac{\delta}{\delta\psi^*(x')}(dx)^4(dx')^4\right]\times\exp\left[\tfrac{1}{2}\int\frac{\delta}{\delta\varphi(x)}\Delta(x,x')\frac{\delta}{\delta\varphi(x')}(dx)^4(dx')^4\right], \quad \text{(A12)}$$

with

$$[\delta/\delta\varphi(x),\varphi(x')]=\{\delta/\delta\psi(x),\psi(x')\}=\{\delta/\delta\psi^*(x),\psi^*(x)\}=\delta^4(x-x'),$$
$$\{\delta/\delta\psi(x),\psi^*(x')\}=\{\delta/\delta\psi^*(x),\psi(x')\}=0,$$
$$\{\delta/\delta\psi(x),\delta/\delta\psi^*(x')\}=\{\psi(x),\psi^*(x')\}=0, \quad \text{(A13)}$$

and

$$S(x,x')=S_{\rm ret}(x,x')-S_{\rm adv}{}^*(x,x')$$
$$=S_{\rm adv}(x',x)-S_{\rm ret}{}^*(x',x),$$
$$\Delta(x,x')=\Delta_{\rm ret}(x,x')-\Delta_{\rm adv}(x,x'). \quad \text{(A14)}$$

$S(x,x')$ and $\Delta(x,x')$ are the propagation functions characterizing the assumed vacuum Ψ, or the incoming and outgoing fields at remote past and future.

We have thus shown, making use of (A5), (A7), and (A11), that $N[A]$ can be expressed as one of the following forms:

$$R\varphi(x)R^{-1}N[A'A''],$$
$$R\psi^*\psi(x)R^{-1}N[A_1'A_1''], \quad \text{(A15)}$$

which have the nature of reduction formulas. The same procedure can be applied to any of the chronological products $A'A''$ and $A_1'A_1''$, and thus we can make further reductions until we are left with the final operator φ or $\psi^*\psi$ in the product A for which the obvious relation,

$$N[\varphi(x)]=\varphi(x)=R\varphi(x)R^{-1}, \text{ etc.,} \quad \text{(A16)}$$

holds. We are thus led to the following:

Lemma 1.—The normal form of the chronological product A of operators φ and $\psi^*\psi$ can be written as

$$N[A]=RAR^{-1}, \quad \text{(A17)}$$

where R is given by (A12).

This result can be extended immediately to:

Lemma 2.—The normal form of any chronological form of operators φ, and $\psi^*\psi$ which can be expressed as a sum of chronological products with numerical coefficients is given by

$$N[B]=RBR^{-1}. \quad \text{(A18)}$$

This is the fundamental expression of the normal form. Its meaning is as follows. We first consider B not as a chronological form but simply as a functional of quasi c numbers φ, ψ, and ψ^*, subject only to the commutativity or anticommutativity on which we next operate R, and then interpret the result as a symbolical expression for the normal product. It is to be noted that in these formulas $\varphi(x)$, $\psi(x)$, and $\psi^*(x)$ at different points are considered to be independent quantities so that we are not allowed to make use of the wave equations for them which would hold if they were operators in the original sense.

As a special case of the lemma 2, we find the following well-known result:

Lemma 3.—The normal form of the S matrix is given by

$$N[S]=R\exp\left[i\int_{-\infty}^{\infty}(dx)^4L_{\rm int}'(x)\right]\equiv RS_0, \quad \text{(A19)}$$

where

$$L_{\rm int}'(x)=-g\psi^*\psi\varphi(x)-\psi^*\phi\psi-\tfrac{1}{2}\varphi\chi\varphi. \quad \text{(A20)}$$

R^{-1} is omitted in this formula since it has no effect on the result.

Denoting a quantity in the mixed representation as $P[S,Q]$ which corresponds to a quantity Q in the interaction representation, we also get:

Lemma 4.—The normal form of the mixed representation of a quantity Q containing particle operators as $\psi^*\psi(x)$ is given by

$$N[P[S,Q]]=RQ\exp\left[i\int_{-\infty}^{\infty}(dx)^4L_{\rm int}'(x)\right]$$
$$=RQS_0=RS_0Q. \quad \text{(A21)}$$

Although these lemmas assume a chronological product which contains ψ and ψ^* only in pairs of the form $\psi^*\psi(x)$, it can be generalized to the case of nonlocal interaction. If the interaction Lagrangian $L_{\rm int}'$ contains a nonlocal term $\int\psi^*(x)\phi(x,x')\psi(x')(dx')^4$, the correct transformation function is obtained by

$$P^*\exp\left[i\int L_{\rm int}'(dx)^4\right], \quad \text{(A22)}$$

where P^* arranges the operators ψ and ψ^* in their chronological order, supplemented by a sign function which corresponds to the permutation necessary in bringing about the chronological form from a product composed of the operators $L_{\rm int}'$ as units. With such a definition of P^*, it can be seen that the lemmas 3 and 4 remain valid, so that there is no difficulty in applying them to the analysis of the S matrix in general cases.

2. The Green's Functions (Propagation Functions)

The various results given by Schwinger[12] on Green's functions follow immediately from these lemmas.

We shall first define the vacuum expectation value of A by

$$\bar{A}\equiv\langle A\rangle_{\rm av}=\langle P[S,A]\rangle/\langle S\rangle, \quad \text{(A23)}$$

where $\langle\ \rangle$ refers to the vacuum state Ψ. The denominator $\langle S\rangle$ is the operator-independent term in the normal form of S because of the relation (3.2).

In this section we first leave the self-energy terms inserted in the starting Lagrangian as arbitrary functions, denoted by ϕ_0 and χ_0, so that

$$L_{\rm int}'=-g\psi^*\psi\varphi-\psi^*\phi_0\psi-\tfrac{1}{2}\varphi\chi_0\varphi. \quad \text{(A24)}$$

The "free" propagation functions will consequently be denoted by $S^{(\phi_0)}$ and $\Delta^{(\chi_0)}$, respectively.

The propagation or Green's function with interaction $S^{(\phi)}$ and $\Delta^{(\chi)}$ are defined by

$$S^{(\phi)}(x,x')=\langle P(\psi(x),\psi^*(x'))\rangle_{\rm av}\epsilon(x-x'),$$
$$\Delta^{(\chi)}(x,x')=\langle P(\varphi(x)-\bar{\varphi}(x),\ \varphi(x')-\bar{\varphi}(x'))\rangle_{\rm av}, \quad \text{(A25)}$$

[12] J. Schwinger, Proc. Natl. Acad. Sci. U. S. 37, 452 (1951).

which can be rewritten by the formula (A21) as

$$S^{(\phi)}(x,x')=\langle R\psi(x)\psi^*(x')S_0\rangle/\langle RS_0\rangle,$$
$$\Delta^{(\chi)}(x,x')=\langle R(\varphi(x)-\bar{\varphi}(x))(\varphi(x')-\bar{\varphi}(x'))S_0\rangle/\langle RS_0\rangle,$$
$$\bar{\varphi}(x)\equiv\langle\varphi(x)\rangle_{Av}=\langle R\varphi(x)S_0\rangle/\langle RS_0\rangle. \quad \text{(A26)}$$

They lead to the equations:

$$\begin{aligned}
S^{(\phi)}(x,x')&=\int S^{(\phi_0)}(x,x'')(dx'')^4\\
&\quad\times\left\langle R\frac{\delta}{\delta\psi^*(x'')}\psi^*(x')S_0\right\rangle\Big/\langle RS_0\rangle\\
&=S^{(\phi_0)}(x,x')-\int S^{(\phi_0)}(x,x'')(dx'')^4\\
&\quad\times\left\langle R\psi^*(x')\frac{\delta}{\delta\psi^*(x'')}S_0\right\rangle\Big/\langle RS_0\rangle\\
&\equiv S^{(\phi_0)}(x,x')-i\int S^{(\phi_0)}(x,x'')\\
&\quad\times[(\phi-\phi_0)S^{(\phi)}](x'',x')(dx'')^4,\\
\Delta^{(\chi)}(x,x')&=\int\Delta^{(\chi_0)}(x,x')(dx'')^4\\
&\quad\times\left\langle R\frac{\delta}{\delta\varphi(x'')}\varphi(x')S_0\right\rangle\Big/\langle RS_0\rangle\\
&\quad-\bar{\varphi}(x)\bar{\varphi}(x')\\
&=\Delta^{(\chi_0)}(x,x')+i\int\Delta^{(\chi_0)}(x,x'')(dx'')^4\\
&\quad\times\left\{\left\langle\frac{\delta}{\delta\varphi}L_{\rm int}'(x'')\varphi(x')\right\rangle_{Av}\right.\\
&\quad\left.-\left\langle\frac{\delta}{\delta\varphi}L_{\rm int}'(x'')\right\rangle_{Av}\bar{\varphi}(x')\right\}\\
&\equiv\Delta^{(\chi_0)}(x,x')-i\int\Delta^{(\chi_0)}(x,x'')\\
&\quad\times[(\chi-\chi_0)\Delta^{(\chi)}](x'',x')(dx'')^4,\\
\bar{\varphi}(x)&=\int\Delta^{(\chi_0)}(x,x')\left\langle R\frac{\delta}{\delta\varphi(x')}S_0\right\rangle\Big/\langle RS_0\rangle(dx')^4\\
&=i\int\Delta^{(\chi_0)}(x,x')\langle\delta L_{\rm int}(x')/\delta\varphi\rangle_{Av}(dx')^4\\
&=-i\int\Delta^{(\chi_0)}(x,x')(g\langle\psi^*\psi(x')\rangle_{Av}\\
&\quad+[\chi_0\bar{\varphi}](x'))(dx')^4\\
&=-i\int\Delta_F(x,x')g\langle\psi^*\psi(x')\rangle_{Av}(dx')^4, \quad \text{(A27)}
\end{aligned}$$

which define the self-energy functions ϕ and χ. Further defining the "vertex part" Γ by

$$\begin{aligned}
&\langle P(\psi(x),\psi^*(x'),\varphi(x'')-\bar{\varphi}(x''))\rangle_{Av}\epsilon(x-x')\\
&\quad\equiv-i\int\int\int S^{(\phi)}(x,y)S^{(\phi)}(y',x')\Delta^{(\chi)}(y'',x'')\\
&\qquad\times\Gamma(y,y';y'')(dy)^4(dy')^4(dy'')^4, \quad \text{(A28)}
\end{aligned}$$

we get from (A27):

$$\begin{aligned}
\phi(x,x')&=\phi_1(x)\delta(x-x')+\phi_2(x,x'),\\
\phi_1(x)&=g\bar{\varphi}(x)=ig^2\int\Delta_F(x-x')(dx')^4S^{(\phi)}(x',x'),\\
\phi_2(x,x')&=-ig\int\int S^{(\phi)}(x,x'')\Delta^{(\chi)}(x,x''')\\
&\quad\times\Gamma(x'',x';x''')(dx'')^4(dx''')^4,\\
\chi(x,x')&=ig\int\int S^{(\phi)}(x,x'')S^{(\phi)}(x''',x)\\
&\quad\times\Gamma(x'',x''';x')(dx'')^4(dx''')^4. \quad \text{(A29)}
\end{aligned}$$

A closed set of equations for the unknown quantities ϕ and χ can be obtained, following Schwinger, by introducing an external source $J(x)$ in the interaction Lagrangian:

$$L_{\rm int}''(x)=L_{\rm int}'(x)-gJ(x)\varphi(x). \quad \text{(A30)}$$

Then ϕ and χ depend implicitly on J, in addition to an explicit term:

$$\begin{aligned}
\phi'&=\phi_1'+\phi_2,\\
\phi_1'(x)&=\phi_1(x)-ig^2\int\Delta_F(x,x')J(x')(dx')^4. \quad \text{(A31)}
\end{aligned}$$

In view of (A28) and (A29), and the obvious relations

$$\begin{aligned}
&\frac{\delta}{\delta J(x'')}\langle P(\psi(x),\psi^*(x'))\rangle_{Av}\\
&\quad=\frac{\delta}{\delta J(x'')}\epsilon(x-x')S^{(\phi)}(x,x')\\
&\quad=-ig\langle P(\psi(x),\psi^*(x'),\varphi(x'')-\bar{\varphi}(x''))\rangle_{Av},\\
&\frac{\delta}{\delta J(x')}g\bar{\varphi}(x)=\frac{\delta}{\delta J(x')}\phi_1'(x)=-ig^2\Delta^{(\chi)}(x,x'), \quad \text{(A32)}
\end{aligned}$$

it follows immediately that

$$\Gamma(x,x';x'')=g\delta\phi'(x,x')/\delta\phi_1'(x''),$$

and

$$\chi(x,x')=-g^2\delta S^{(\phi)}(x,x)/\delta\phi_1'(x'). \quad \text{(A33)}$$

By using (A33), the equation for ϕ_1',

$$(\Box-\mu^2)\phi_1'(x)=-g^2[S^{(\phi)}(x,x)-J(x)], \quad \text{(A34)}$$

can be rewritten as

$$(\Box-\mu^2-\chi)\phi_1'(x)=-g^2[S^{(\phi)}(x,x)-J(x)]-\chi\phi_1'(x)$$
$$=-g^2\Big[S^{(\phi)}(x,x)-\int(\delta S^{(\phi)}(x,x)/\delta\phi_1'(x'''))\times\phi_1'(x')(dx')^4-J(x)\Big],$$

or

$$\phi_1'(x)=ig^2\int\Delta^{(\chi)}(x,x')(dx')^4\Big[S^{(\phi)}(x',x')-\int(\delta S^{(\phi)}(x',x')/\delta\phi_1'(x''))\times\phi_1'(x'')(dx'')^4-J(x')\Big]. \quad \text{(A35)}$$

In the integrand of (A35) the linear term in ϕ_1' is subtracted out, and $\Delta_F(x,x')$ replaced by $\Delta^{(\chi)}(x,x')$, showing that the effective source intensity is reduced when the intermediary field with modified mass is used.

The merit of introducing the self-energy terms (beside the infinite renormalization part, which, however, is not discussed here) in the interaction representation is not clearly shown in the preceding equations. Indeed, Eqs. (A29)–(A35) do not involve ϕ_0 and χ_0 at all, being independent of the choice of the starting interaction representation. It reflects, however, our way of handling these Hartree fields. If we regard them as a small perturbation, and solve (A29) by expansion in powers of the coupling constant and density of particles, it makes no difference whether we introduce ϕ_0 and χ_0 or not. This would mean, in the first place, replacing $S^{(\phi)}$ and $\Delta^{(\chi)}$ by $S^{(0)}$ and Δ_F in (A29) to get the first approximation. This is not legitimate, however, if ϕ and χ are actually not small but seriously affect the behavior of particles and mesons; we have to leave $S^{(\phi)}$ and $\Delta^{(\chi)}$ as they are in (A29), or at least replace them by some approximate forms $S^{(\phi_0)}$ and $\Delta^{(\chi_0)}$, and treat the remainder as a perturbation, making use of (A27). This is exactly equivalent to putting the self-energy terms in the Lagrangian from the beginning. In terms of the perturbation theory, it amounts to adding up certain sets of higher-order diagrams so that they may be incorporated into the expressions $S^{(\phi)}$ and $\Delta^{(\chi)}$. In the same spirit, it would be desirable to express the vertex part Γ in a convenient closed form, but Eq. (A33) does not seem to be of very much help for that purpose.

3. Total Energy

If we take ϕ_0 and χ_0 to be zero, that is, if we start from the ordinary free Hamiltonian, the interaction energy $\mathcal{E}$ of the system is related to the S matrix by

$$\langle S\rangle=\exp\Big[-i\int_{-\infty}^{\infty}\mathcal{E}dt\Big], \quad \text{(A36)}$$

so that

$$\frac{\partial\langle S\rangle}{\partial g}=\Big(-i\int\frac{\partial\mathcal{E}}{\partial g}dt\Big)\langle S\rangle=\Big\langle i\int\frac{\partial L_{\rm int}}{\partial g}(dx)^4\Big\rangle_{hv}\langle S\rangle$$
$$=\Big\langle\frac{i}{g}\int L_{\rm int}(dx)^4\Big\rangle_{hv}\langle S\rangle,$$

or

$$\frac{\partial\mathcal{E}}{\partial g}=-\frac{1}{g}\Big\langle\int L_{\rm int}(dx)^3\Big\rangle_{hv}=-\frac{1}{g}\int\int\phi(x,x')\times S^{(\phi)}(x',x)(dx')^4(dx)^3$$
$$=\frac{1}{g}\int\int\{\chi(x,x')\Delta^{(\chi)}(x',x)-\phi_1(x)S^{(\phi)}(x,x)\delta(x-x')\}\times(dx')^4(dx)^4\Big/\int_{-\infty}^{\infty}dt. \quad \text{(A37)}$$

Integrating this, we get the formula (3.9). The relation

$$\int\int\phi_2(x,x')S^{(\phi)}(x',x)(dx)^4(dx')^4$$
$$=-\int\int\chi(x,x')\Delta^{(\chi)}(x',x)(dx)^4(dx')^4$$
$$=-ig\int\int\int\int S^{(\phi)}(x_1,x_2)\Gamma(x_2,x_3;x_4)\times S^{(\phi)}(x_3,x_1)\Delta^{(\chi)}(x_4,x_1)(dx_1)^4\cdots(dx_4)^4, \quad \text{(A38)}$$

may sometimes be useful in rewriting (3.7) or (A37) in other forms.

An alternative expression for the total energy of the system is obtained in the following way. By Eq. (A19) the vacuum expectation value of S is

$$\langle N[S]\rangle=\Big\langle R\exp\Big[i\int L_{\rm int}'(dx)^4\Big]\Big\rangle=\exp\Big[-i\int\mathcal{E}dt\Big]. \quad \text{(A39)}$$

We shall again make here a particular choice: $\phi_0=\chi_0=0$. If we change the density matrix $\rho(x-x')$ appearing in R by an infinitesimal amount, we get the formula

$$\frac{\delta\langle N[S]\rangle}{\delta\rho(x-x')}=-i\Big\langle\frac{\delta}{\delta\psi^*(x)}\frac{\delta}{\delta\psi(x')}N[S]\Big\rangle=X(x,x')\langle N[S]\rangle. \quad \text{(A40)}$$

By comparing this with

$$S^{(\phi)}(x,x') = \epsilon(x-x')\langle P(\psi(x),\psi^*(x'))\rangle_h$$
$$= \langle R\psi(x)\psi^*(x')S_0\rangle / \langle RS_0\rangle$$
$$= S^{(0)}(x-x') - \int S^{(0)}(x-x'')S^{(0)}(x'''-x')$$
$$\times \left\langle\left(\frac{\delta}{\delta\psi^*(x'')}\frac{\delta}{\delta\psi(x''')}S\right)\right\rangle_h (dx'')^4(dx''')^4$$
$$= S^{(0)}(x-x') - i\int S^{(0)}(x-x'')$$
$$\times [\phi S^{(\phi)}](x'',x')(dx'')^4,$$
$$[S^{(0)}(x-x') \text{ is defined by (3.8)}], \qquad \text{(A41)}$$

X can be written as

$$X(x,x') = -[\phi S^{(\phi)}L_0](x,x'),$$
$$L_0 \equiv i(S^{(0)})^{-1} = \left(-i\frac{\partial}{\partial t} - \frac{1}{2m}\Delta\right). \qquad \text{(A42)}$$

Now we define $\delta\rho^{(\phi)}$ by

$$[S^{(\phi)}L_0\delta\rho_0](x,x') \equiv i\delta\rho^{(\phi)}(x,x'), \qquad \text{(A43)}$$

from which follows that

$$\delta\rho^{(\phi)}(x,x') = \delta\rho_0(x,x') + i\int S^{(\phi)}(x,x'')\phi(x'',x''')$$
$$\times \delta\rho_0(x''',x')(dx'')^4(dx''')^4. \qquad \text{(A44)}$$

Hence $\delta\rho^{(\phi)}$ is the change in the density matrix $\rho^{(\phi)}$ with interaction corresponding to the change $\delta\rho_0$ in the original free density matrix. Thus we get

$$[X\delta\rho_0](x,x') = -i[\phi\delta\rho^{(\phi)}](x,x'), \qquad \text{(A45)}$$

and consequently

$$i\log\langle N[S]\rangle = \int \delta dt = \int\int (dx)^4(dx')^4$$
$$\times \left(\int \phi(x,x')\delta\rho^{(\phi)}(x',x)\right). \qquad \text{(A46)}$$

The integration over $\delta\rho^{(\phi)}$ can be interpreted that we vary the number of the occupied states from zero to the present value by adding particles one by one. Since each particle moves in the effective potential ϕ due to the other already existing particles, the expression

$$\int\int \phi(x,x')\delta\rho^{(\phi)}(x',x)(dx')^4(dx)^4 \qquad \text{(A47)}$$

is equal to the potential energy of the extra particle. Equation (A46) can then be easily understood as a summation over the potential energies of the particles corresponding to the building up process mentioned above. Equation (3.10) is essentially equivalent to (A46).

The Low Even Configurations of Hf II†

MATATIAHU GEHATIA*
Hebrew University, Jerusalem, Israel
(Received October 14, 1952)

The experimental energy levels and g values of the low even configurations ds^2, d^2s, and d^3 of Hf II, are compared with the theoretical formulas for intermediate coupling with configuration interaction. The energy levels are in good agreement, while the mean error is less than 0.7 percent of the configuration width; the agreement between calculated and observed g values is satisfactory.

1. INTRODUCTION

THE experimental data on the spectrum of Hf II show that the Landé g values depart strongly from the LS values. The comparison between theory and experiment needs, therefore, to be made in intermediate coupling.

For the electrostatic energy of the configurations d^2s and d^3 we used the formulas given by Condon and Shortley;[1] for the electrostatic interaction between configurations we used the formulas of Ufford,[2] and for the spin-orbit interaction, the matrices of Marvin.[3]

Our purpose is to fit formulas to the experimental values[4] by the method of least squares. However, as the formulas are not linear,[1] we need "starting" parameters.

2. THE ELECTROSTATIC ENERGY PARAMETERS

Since other spectra in the neighborhood of hafnium have not been theoretically investigated, we have first determined the electrostatic parameters by a least squares fitting of the center of gravity of the known terms with the Condon and Shortley formulas,[1] which are linear. In this state of the calculation we neglected $d^3\,{}^2P$, as not all levels are known.

The results are given in Table I, column A. The mean error defined by $[\sum_i \Delta_i^2/(n-m)]^{\frac{1}{2}}$ (where Δ is the difference between observed and calculated values, n is the number of equations, and m is the number of parameters) is 1072, i.e., 2.9 percent of the configuration width.

The largest deviation was caused by the term $d^2s\,{}^2P$. As this term has the largest configuration interaction ($315\,{}^1H_2$), and we have neglected this interaction in our

TABLE I. The configurations ds^2, d^2s, and d^3 of Hf II in the LS approximation.

Level			Calculated		Mean level values	Obs.-Calc.		
Conf.	Term	Obs.	A	B	C	A	B	C
$5d6s^2$	$a\,{}^2D$	1831	...	...	1865	...	...	−34
$5d^26s$	$a\,{}^4F$	6371	7123	6648	6529	−752	−277	−158
$5d^26s$	$a\,{}^4P$	13 042	12 861	13 063	13 204	+181	−21	−162
$5d^26s$	$a\,{}^2F$	13 793	12 655	13 942	14 471	+1138	−149	−678
$5d^26s$	$b\,{}^2D$	16 165	15 085	15 128	15 770	+1080	+1037	+395
$5d^26s$	$a\,{}^2P$	16 972	18 393	...	16 528	−1421	...	+444
$5d^26s$	$a\,{}^2G$	17 532	17 763	18 121	17 312	−231	−589	+220
$5d^3$	$b\,{}^4F$	21 463	21 513	21 310	21 160	−50	+153	+303
$5d^3$	$b\,{}^4P$	27 868	27 251	27 725	27 835	+617	+143	+33
$5d^3$	$b\,{}^2G$	28 262	29 351	28 885	29 445	−1089	−623	−1183
$5d^3$	$a\,{}^2H$	31 367	31 264	31 023	30 552	+103	+344	+815
$5d^3$	$c\,{}^2D$	(32 778)	...	...	32 749	...	...	+29
$5d^3$	$b\,{}^2P$	(36 883)	...	...	36 138	...	...	+745
$5d^3$	$b\,{}^2F$	37 422	37 002	37 439	38 198	+420	−17	−776
Parameters:			$F_0(ds^2)$	...	...	6748			
			$F_0(d^2s)$	16 815	17 669	18 543			
			$F_0(d^3)$	36 084	35 937	35 378			
			$F_2(d^3)$	683.430	707.285	701.570			
			$F_4(d^3)$	60.086	55.857	51.314			
			$G_2(ds)$	1844	2431	2970			
			$H_2(dd;ds)$	...	...	513			

† This work was performed by the author in 1951–1952 at the Hebrew University, Israel, in partial fulfilment of the requirements for the M.Sc. degree.

* Present address: Weizmann Institute of Science, Rehovot, Israel.

[1] E. U. Condon and G. H. Shortley, *Theory of Atomic Spectra* (Cambridge University Press, Cambridge, 1935), 5^7, pp. 203–206, and 7^9, p. 233.

[2] C. W. Ufford, Phys. Rev. **44**, 732 (1933).

[3] H. H. Marvin, Phys. Rev. **47**, 522 (1935).

[4] W. F. Meggers and B. F. Scribner, J. Research Natl. Bur. Standards, **13**, 625 (1934).

calculation, we expect to obtain more reliable values of the parameters by neglecting the $d^2s\ ^2P$ term. Repeating this calculation without $d^2s\ ^2P$, we have obtained much better agreement (see Table I, column B), the mean error being 644, i.e., 1.7 percent of the configuration width.

3. THE CONFIGURATION INTERACTION PARAMETER

From the deviations between the experimental and theoretical values we have estimated the parameter $H_2=500$; and taking this value and the values of Table I, column B, as starting values, we fitted by least squares all terms, comprising the "nonlinear" term $d^3\ ^2D$, the fundamental term $ds^2\ ^2D$, and a roughly estimated value of $d^3\ ^2P$. The results are given in Table I, column C, and the mean error is 777, i.e., 2.2 percent of the configuration width.

4. THE LEVEL VALUES CALCULATION

From the splitting of the quadruplets we have estimated the spin interaction parameter, $a=1250$, and calculated the complete matrices with this value and those of Table I, column C. With the help of Many's electrical network for diagonalization of matrices[5,6] we have found the eigenvalues and eigenvectors of these matrices. Using these eigenvectors, we calculated by the method of Racah[7] the derivatives of the eigenvalues with respect to the parameters, and were then able to adjust the parameters by least squares.

The final results are given in Table II; the mean error is 257, i.e., 0.7 percent of the configuration width. With the help of these parameters we have computed also all the remaining levels, which have not yet been found experimentally (Table II).

5. THEORETICAL CALCULATION OF THE g's

In order to obtain the splitting factors g, we have used the eigenvectors from the last calculation and applied them to the diagonal matrices for the Landé g values. The calculated g values were, however, not in satisfactory agreement with the observed values.

As the eigenvectors used for the calculation were obtained from the diagonalization of the matrices with provisional parameters, we repeated the diagonalization with the final parameters, the new g values obtained for these eigenvectors were in satisfactory agreement with the observed g values (see Table II).

TABLE II. The configurations ds^2, d^2s, and d^3 of Hf II in intermediate coupling.

Conf.	Level Term	J	Energy levels Obs.	Calc.	Diff.	g values Obs.	Calc.
$5d\ 6s^2$	$a\ ^2D$	3/2	0000	95	−95	0.80	0.79
$5d\ 6s^2$	$a\ ^2D$	5/2	3051	2928	+123	1.18	1.19
$5d^2 6s$	$a\ ^4F$	3/2	3645	3988	−343	0.45	0.43
$5d^2 6s$	$a\ ^4F$	5/2	4905	5093	−188	1.06	1.05
$5d^2 6s$	$a\ ^4F$	7/2	6344	6622	−278	1.23	1.24
$5d^2 6s$	$a\ ^4F$	9/2	8362	8590	−228	1.33	1.33
$5d^2 6s$	$a\ ^4P$	1/2	11 952	11 741	+211	2.61	2.62
$5d^2 6s$	$a\ ^4P$	3/2	12 921	12 690	+231	1.69	1.66
$5d^2 6s$	$a\ ^4P$	5/2	13 486	13 429	+57	1.42	1.34
$5d^2 6s$	$a\ ^2F$	5/2	12 071	12 154	−83	0.98	1.05
$5d^2 6s$	$a\ ^2F$	7/2	15 084	15 067	+17	1.11	1.10
$5d^2 6s$	$b\ ^2D$	3/2	14 360	14 556	−196	1.03	1.01
$5d^2 6s$	$b\ ^2D$	5/2	17 369	17 056	+313	1.29	1.26
$5d^2 6s$	$a\ ^2P$	1/2	15 254	15 558	−304	0.74	0.73
$5d^2 6s$	$a\ ^2P$	3/2	17 830	17 987	−157	1.12	1.13
$5d^2 6s$	$a\ ^2G$	9/2	17 389	17 024	+365	1.13	1.13
$5d^2 6s$	$a\ ^2G$	7/2	17 711	17 349	+362	0.92	0.94
$5d^3$	$b\ ^4F$	3/2	18 898	18 455	+443	0.46	0.46
$5d^3$	$b\ ^4F$	5/2	20 135	19 926	+209	1.01	1.04
$5d^3$	$b\ ^4F$	7/2	21 638	21 550	+88	1.23	1.23
$5d^3$	$b\ ^4F$	9/2	23 146	23 129	+17	1.29	1.29
$5d^3$	$b\ ^4P$	1/2	26 997	26 925	+72		2.62
$5d^3$	$b\ ^4P$	3/2	27 285	27 454	−169	1.76	1.63
$5d^3$	$b\ ^4P$	5/2	28 547	28 536	+11	1.51	1.57
$5d^3$	$b\ ^2G$	9/2	28 105	27 898	+207	1.05	1.01
$5d^3$	$b\ ^2G$	7/2	28 458	28 240	+218	0.92	0.90
$5d^2 6s$	$a\ ^2S$	1/2		30 295			1.91
$5d^3$	$a\ ^2H$	11/2	30 942	30 886	+56	1.10	1.09
$5d^3$	$a\ ^2H$	9/2	31 878	32 011	−133	1.05	1.04
$5d^3$	$c\ ^2D$	3/2		30 692			0.92
$5d^3$	$c\ ^2D$	5/2	32 778	33 122	−344	1.15	1.21
$5d^3$	$b\ ^2P$	1/2		35 034			0.81
$5d^3$	$b\ ^2P$	3/2	37 325	37 429	−104		1.27
$5d^3$	$b\ ^2F$	5/2	37 399	37 565	−166		0.90
$5d^3$	$b\ ^2F$	7/2	37 440	37 580	−140		1.14
$5d^3$	$d\ ^2D$	5/2		46 113			1.18
$5d^3$	$d\ ^2D$	3/2		46 250			0.81
Parameters:			$F_0(ds^2)$	6599			
			$F_0(d^2s)$	18 044			
			$F_0(d^3)$	34 663			
			$F_2(d^2)$	653.570			
			$F_4(d^2)$	43.714			
			$G_2(ds)$	2818			
			$H_2(dd;ds)$	482			
			$\zeta(d)$	1336			

The author wishes to express his gratitude to Professor G. Racah for suggesting this problem and for constant advice during the work; to Mr. Y. Lehrer for constant help, and to Dr. A. Many for his help and instruction in operating his Matrix Diagonalisation Machine.

[5] A. Many and S. Meiboom, Rev. Sci. Instr. **18**, 831 (1947).
[6] A. Many, Rev. Sci. Instr. **21**, 972 (1950).
[7] G. Racah, Phys. Rev. **63**, 367 (1943).

(p,pn) and $(p,\alpha n)$ Excitation Functions

B. L. COHEN, E. NEWMAN, R. A. CHARPIE, AND T. H. HANDLEY
Oak Ridge National Laboratory, Oak Ridge, Tennessee

(Received October 8, 1953)

Excitation functions for (p,pn) and $(p,\alpha n)$ reactions were measured with the internal, 23.5-Mev proton beam of the ORNL 86-inch cyclotron. Methods of obtaining homogeneous and known incident energy are described. The results indicate that, as found previously, emission of charged particles is much more probable than predicted by the statistical theory of nuclear reactions but that this cannot be explained, as has been proposed, by the lowering of the Coulomb barrier due to oscillations of the compound nucleus or by difficulties with the energy level density formula at low excitation energy.

INTRODUCTION AND THEORY

IT has been recognized for some time[1–4] that emission of charged particles in nuclear reactions is generally much more probable than predicted by the statistical theory of nuclear reactions.[5] It has been variously proposed that this is due (1) to difficulties with the level density formula at low excitation energy,[6] (2) to competition of a direct interaction with compound nucleus formation,[7,8] (3) to a breakdown in a fundamental assumption of the theory,[9] and (4) to a lowering of the Coulomb barriers because of oscillations of the compound nucleus. The fourth proposal has grown out of the recent calculations of Wheeler and Hill[10,11] which indicate that surface oscillations of the compound nucleus are promoted in magnitude and controlled in direction by the effect of the incident particle. Their theory, known as the "collective model," forms a very satisfying union between the "individual particle" and "liquid drop" models, and has received experimental support from angular distribution measurements.[12,13,13a] In accordance with this model, portions of the nuclear surface spend a considerable time further than their average distance from the center of the nucleus so that charged particles can be emitted without experiencing as large a Coulomb barrier as if they were emitted from an undistorted spherical nucleus. This effect would be observable as excessively large total cross sections for nuclear reactions in which charged particles are emitted, whence proposal (4) above; and as a distortion in the energy spectrum of the emitted particles in that a larger number would have energies considerably lower than the Coulomb barrier calculated for the undistorted nucleus. The experiments described in this paper were designed specifically to determine whether this second effect is observed, and thus to decide whether proposal (4) above is valid; at the same time, however, they produce new evidence for the phenomenon of excessive emission of charged particles from nuclear reactions by observing it for new types of reactions, and in a new energy region where proposal (1) above is not applicable.

It was first pointed out by Weisskopf and Ewing[14] that excitation functions for reactions of the type (x,yn) (where x and y are any nuclear particles) can be analyzed to give the approximate energy distribution with which the particle y is emitted. This is possible because, to a good approximation, the probability for neutron emission to follow emission of y is just the probability that y is emitted with energy sufficiently low to leave neutron emission energetically possible. Thus, the cross section for an (x,yn) reaction for incident energy E is

$$\sigma(x,yn)=\sigma_x\frac{1}{\sum_i f_i}\int_0^{E-B}N_y(\epsilon)d\epsilon, \qquad (1)$$

where σ_x is the cross section for capture of x to form the compound nucleus, B is the threshold for the (x,yn) reaction, $N_y(\epsilon)$ is the energy distribution with which y is emitted, $f_i=\int_0^\infty N_i(\epsilon)d\epsilon$, the total probability for the compound nucleus to decay with emission of particle i, and the sum is over all particles that can be emitted. The behavior near the threshold can best be seen by differentiating (1) with respect to E, giving

$$N_y(E-B)=\frac{d\sigma(x,yn)}{dE}\text{ plus terms in }\frac{d\sigma_x}{dE},\frac{df_i}{dE},\frac{dN_y}{dE}. \qquad (2)$$

For high-energy incident particles, $d\sigma_x/dE$ is small and relatively well known; the df_i/dE and dN_y/dE terms tend to compensate, they are much smaller than the leading term, and in any case, they can be approximately corrected for. Thus, a measurement of $\sigma(x,yn)$ as a function of E gives relatively direct information on

[1] H. Waffler, Helv. Phys. Acta. **23**, 239 (1950).
[2] B. L. Cohen, Phys. Rev. **81**, 184 (1951).
[3] E. B. Paul and R. L. Clarke, Can. J. Phys. **31**, 267 (1953).
[4] S. N. Ghoshal, Phys. Rev. **80**, 939 (1950).
[5] J. M. Blatt and V. F. Weisskopf, *Theoretical Nuclear Physics* (John Wiley and Sons, Inc., New York, 1952).
[6] B. T. Feld *et al.*, U. S. Atomic Energy Commission Report NYO-636.
[7] H. McManus and W. T. Sharp, Phys. Rev. **87**, 188 (1952).
[8] Austern, Butler, McManus, and Sharp, Phys. Rev. **91**, 453 (1953).
[9] B. L. Cohen, Phys. Rev. **92**, 1245 (1953).
[10] D. L. Hill and J. A. Wheeler, Phys. Rev. **89**, 1102 (1953).
[11] J. A. Wheeler, invited paper at Rochester Meeting of American Physical Society, June, 1953 [Phys. Rev. **92**, 843 (1953)].
[12] I. Halperin *et al.*, U. S. Atomic Energy Commission AECU-2494 (unpublished).
[13] W. L. Dickinson and J. E. Brolley, Phys. Rev. **90**, 388 (1953).
[13a] Cohen, Jones, McCormick, and Ferrell, Phys. Rev. **99**, 625 (1954).
[14] V. F. Weisskopf and D. H. Ewing, Phys. Rev. **57**, 472 (1940).

N_y. It is customary to assume N_y to be given by

$$N_y(\epsilon)=\sigma_y(\epsilon)\exp(-\epsilon/T), \quad (3)$$

where σ_y is the cross section for capture of y and T is the nuclear temperature. When y is a neutron, σ_y is approximately independent of energy so that $(x,2n)$ excitation functions give relatively sensitive determinations of T. Several measurements of this type have been reported[15–18]. In cases where y is a charged particle, σ_y is essentially the Coulomb barrier penetration factor which is strongly energy dependent, so that the measurements give good determinations of σ_y, and only rough determinations of T, being much more sensitive to the former. Thus, we see that measurements of (p,pn) and $(p,\alpha n)$ excitation functions give good determinations of the Coulomb barriers encountered by the emitted protons and alphas, and therefore provide a suitable test for the effect of the Wheeler-Hill collective model on these Colomb barriers.

If the (x,yp) threshold is considerably lower than the (x,yn), the above considerations are generally applicable to that reaction; however, the situation would be somewhat modified by the competition of γ emission with the emission of very low-energy protons.

For energies well above the threshold, it can be seen from (1) and the definition of f_i, that

$$\sigma(x,yn)=\sigma_x f_y/\sum_i f_i, \quad (4)$$

which, according to the usual definition, is $\sigma(x,y)$. Thus, the absolute cross sections at high energies can be compared with the predictions of the statistical theory of nuclear reactions in the same way as the data from references 1–3.

EXPERIMENTAL METHODS

Although measurements of excitation functions by stacked-foil techniques are among the simplest and oldest nuclear physics experiments, the extension of the method to use with an internal, circulating cyclotron beam is not simple. Two of the most difficult problems are (a) arranging the foil stack so that all incident particles which pass through any foil must pass through all foils, and (b) obtaining monoenergetic incident particles of a known energy. These requirements were met in the following manner:

Requirement (a) essentially demands that the foil stack be placed behind a thick window frame. Since the radial distance between successive orbits in a cyclotron is quite small, it is difficult to prevent almost the entire beam from striking the window frame, and in addition, since the radial width is larger for lower energies, the small fraction of the beam that does get through is likely to contain a high proportion of the low-energy components of the circulating beam. This problem was studied in detail,[19] and it was found that by detuning the magnetic field approximately 0.2 percent, the phase of the ions circulating in the cyclotron can be shifted relative to the dee voltage sufficiently to increase the radial width of the beam to about $\frac{1}{4}$ inch. A well-grounded ion source was also found to be important.

Requirement (b) was finally met by installing a thick probe in the cyclotron 180° away from the target. This limits the maximum energy of the protons entering the window. It was found that the low-energy portion of the cyclotron beam could be reduced by operating at high dee voltage. By suitably adjusting the target position and the dee voltage, the point was finally reached where the energy distribution of the protons striking the foil had a full width at half-maximum of less than $\frac{1}{2}$ Mev, and a sharp high-energy cutoff. Such a spectrum is satisfactory for measuring excitation functions which increase with increasing energy, because in these cases, the low-energy tail is not effective.

The energy distribution of the protons entering the window was obtained by measuring the excitation function for the (p,n) reaction in copper and comparing with the accurately known excitation function[20] in the region near the threshold. The maximum energy was calculated from the magnetic field and the distance between the 180° probe and the target and was found to agree with the copper excitation function measurement if the usual correction[21] of a little over 1 percent is applied to the range-energy curves.[22]

The proton current was determined by measuring the 38-minute activity induced in copper by the (p,n) reaction. The cross section for this reaction has a broad maximum of about 530 mb near 13 Mev which is ideal for calibration purposes. Absolute beta counting was carried out with thin foils mounted on cellophane about $\frac{1}{8}$ in. below a thin-window Geiger counter. Small corrections were made for beta absorption by the methods of reference 2. As a check, a few absolute cross-section determinations were made by counting the 511-kev annihilation radiation with a scintillation spectrometer and comparing with the annihilation radiation from the 38-minute copper. The decay scheme corrections are available in the literature[23] for every case except the electron capture branching ratio for Ag^{106} which was estimated theoretically. Considering these factors and the uncertainty in the copper cross section, the probable errors of the absolute calibration are about 25 percent. Samples not being used for absolute cross-section calibration were counted under convenient absorbers (to eliminate background activi-

[15] Brolley, Fowler, and Schlacks, Phys. Rev. **88**, 618 (1953).
[16] H. C. Martin and B. C. Divey, Phys. Rev. **86**, 565 (1952).
[17] D. J. Tendam and H. L. Bradt, Phys. Rev. **72**, 1118 (1947).
[18] Bleuler, Stebbins, and Tendam, Phys. Rev. **90**, 460 (1953).
[19] B. L. Cohen, Oak Ridge National Laboratory Report ORNL-1348 (unpublished).
[20] Blaser, Boehm, Marmier, and Peasleee, Helv. Phys. Acta. **24**, 3 (1951).
[21] H. Bechsel and R. F. Mozley, Phys. Rev. **90**, 354 (1953).
[22] Aron, Hoffman, and Williams, University of California Radiation Laboratory Report UCRL-121 (Rev.) (unpublished).
[23] Hollander, Perlman, and Seaborg, Revs. Modern Phys. **25**, 469 (1953).

ties) or, in the case of Cu^{60}, on a scintillation spectrometer set to count γ rays above 3 Mev.

The target is made of 2-S aluminum to avoid irradiation of personnel from long-lived impurity activities. The demountable window frames and backings are of tantalum, with the former bent in an L shape to aid in foil stacking.

RESULTS AND DISCUSSION

The excitation functions for (p,pn) reactions on Cu^{65}, Pd^{110}, Ag^{107}, and Ta^{181}, and for the $(p,\alpha n)$ reaction on Zn^{64} are shown in Figs. 1 to 5. Individual runs were normalized in the 18- to 22-Mev region since absolute calibrations were made in separate runs. The dashed lines represent calculations of the relative excitation functions from Eq. (1) using $N_y(\epsilon)$ from Eq. (3) with various values of the nuclear temperature T. The σ_y in Eq. (3), which are essentially the Coulomb barrier penetration factors for the outgoing protons or alphas, were taken from reference 5, p. 352 ff. They are calculated for spherical nuclei of radius equal to $1.4A^{\frac{1}{3}}\times10^{-13}$ cm. The dot-dash lines represent the result that would be obtained for $T=1$ Mev if the corrections discussed following Eq. (2) were not taken into account. The magnitude of these corrections—which is the most uncertain factor in the analysis of the experiments—can be seen by comparing these curves with the dashed curves labeled $T=1$ Mev.

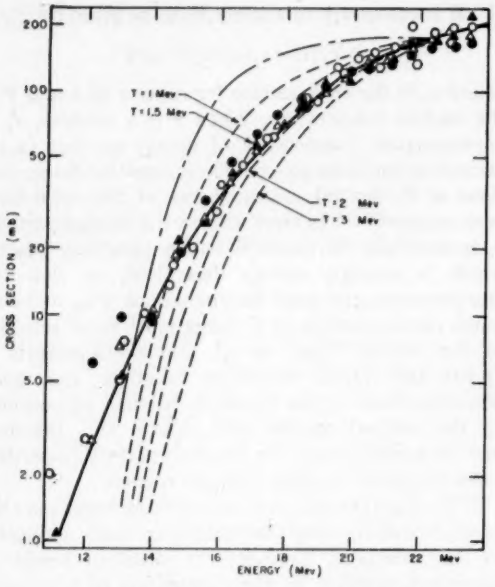

FIG. 2. Excitation function for $Pd^{110}(p,pn)Pd^{109}$. See caption for Fig. 1.

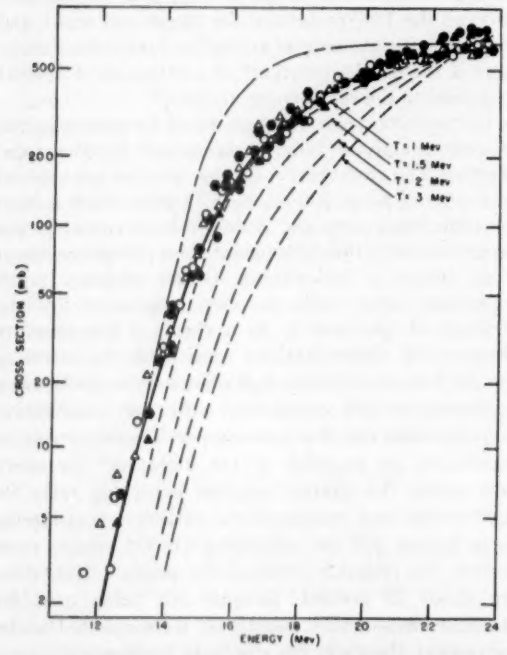

FIG. 1. Excitation function for $Cu^{65}(p,pn)Cu^{64}$. The data also include a small contribution from the (p,d) reaction as discussed in text. Dashed lines are theoretical predictions of statistical theory for various assumed nuclear temperatures, all normalized at 23 Mev. The dot-dash line is the curve for $T=1$ Mev obtained by neglecting all but first term in Eq. (2). Calculations are for nuclear radii of $1.4A^{\frac{1}{3}}\times10^{-13}$ cm. Data from various runs are normalized to superpose between 18 and 22 Mev. Absolute cross sections have probable errors of about 25 percent. Data are corrected for $(n,2n)$ reactions due to neutron background.

Figure 6 shows the excitation function for the (p,α) reaction on Zn^{64}. This excitation function decreases with increasing proton energy over a large region, so that the low-energy tail in the incident energy distribution distorts the data by a fraction of a Mev, but they can be considered at least semiquantitatively valid. The theory indicates that the dropoff in the (p,α) cross section is due to the onset of the $(p,\alpha p)$, so that the shape of the $(p,\alpha p)$ excitation function can be inferred and compared with the theory. The dashed curve in Fig. 6 labeled "$(p,\alpha p)$, $T=3$ Mev" is the theoretical $(p,\alpha p)$ excitation function calculated by the same method as that for the $(p,\alpha n)$; the fact that the experimental curve is displaced to the right of it indicates that γ emission competes favorably with emission of protons with less than about one to two Mev.

Figure 6 also shows the $(p,\alpha n)$ curve from Fig. 5. In order to calculate the $(p,\alpha n)$ threshold from mass data, it was necessary to know the threshold for the reaction $Ni^{60}(p,n)Cu^{60}$. This was measured by bombarding a stack of interleaved nickel and copper foils and comparing the two excitation functions. The $Ni^{60}(p,n)$ threshold was determined to be 6.7 ± 0.4 Mev.

Since for both the $(p,\alpha n)$ and $(p,\alpha p)$ cases, the measurements are in essential agreement with the theoretical curves or at least do not lie to the left of them, and since the theoretical curves were calculated

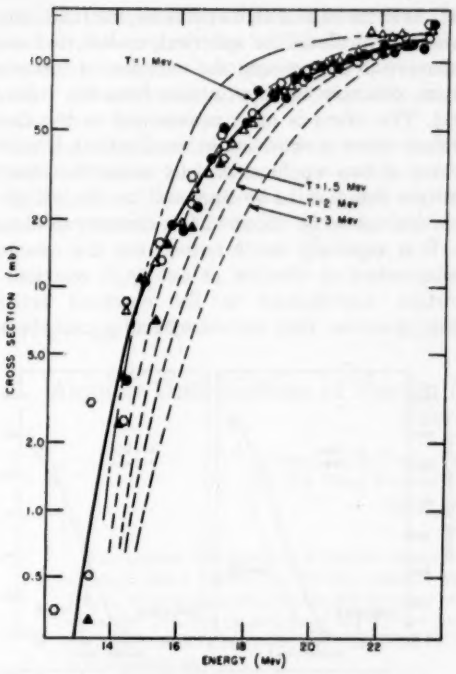

FIG. 3. Excitation function for $Ag^{107}(p,pn)Ag^{106}$. See caption for Fig. 1. Only the 24-minute isomer of Ag^{106} was observed. To correct for the other isomer, absolute values should be multiplied by about 1.6 (see reference 17). The theoretical correction for K capture has been applied.

for undistorted spherical nuclei, it is quite evident that there is no appreciable lowering of the Coulomb barriers faced by the outgoing alphas due to surface oscillations of the compound nucleus as suggested by the collective model. For example, if the Coulomb barrier were reduced by a factor of two by these oscillations as has been proposed,[11] the $(p,\alpha n)$ excitation function would rise steeply beginning at about 14 Mev, and the $(p,\alpha p)$ rise would begin between 8 and 10 Mev. Such an assumption is thus contradicted very directly by the data. This conclusion should not, of course, be construed as a contradiction of the general theory of the collective model (actually, no conclusive calculations of the expected effect have been made), but only of the proposal to extend its application to this phase of nuclear reaction theory and of the preliminary report of an experimental verification of that proposal.[11]

The absolute total (p,α) cross section at 13 Mev is in reasonable agreement with predictions of the theory. However, this is not a good case for comparison with the theory because threshold complications are extreme, the energy available for alpha emission being 12 Mev higher than for neutron emission.

The lines through the (p,pn) cross section data are shown in Fig. 7 along with the theoretical absolute values at 22 Mev. The only case where the competition between proton and neutron emission is affected by the nature of the nuclei involved is for palladium where the products of the (p,n) and (p,p) reactions are odd-odd and even-even, respectively; the theoretical (p,pn) cross section was divided by four (in Fig. 7) to correct for this.

Before drawing conclusions from Fig. 7, some account must be taken of (p,d) reactions which are known to take place by a "pick-up" process, producing the same end product as (p,pn) reactions. Attempts were made to measure absolute (p,d) cross sections by determining the outgoing deuteron flux with activation detectors.[24,25] These indicated that no more than 25 percent of the measured copper (p,pn) cross section is due to the (p,d) reaction. For the heavier elements, the method was not sufficiently sensitive.

It should be noted, however, that (p,d) reactions have thresholds 2.2 Mev lower than (p,pn) reactions, and the barrier encountered by deuterons is about 1.5 to 2.0 Mev lower than for protons.[26] Thus, if all deuterons were emitted with the maximum available energy, the excitation function would be of roughly the same shape as the theoretical (p,pn) curves but shifted 3 or 4 Mev to the left. If, on the other hand, they were emitted with a Maxwellian energy distribution, the general shape of the excitation function would be very different from the observed ones. Although the possibility cannot be

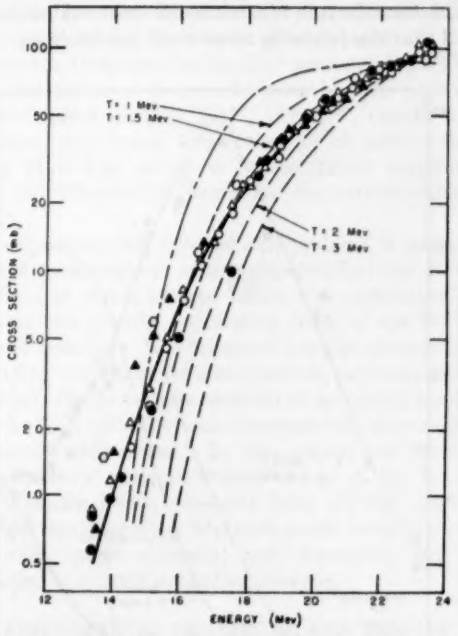

FIG. 4. Excitation function for $Ta^{181}(p,pn)Ta^{180}$. See caption for Fig. 1.

[24] B. L. Cohen and R. V. Neidigh, Rev. Sci. Instr. **25**, 255 (1954).
[25] Cohen, Newman, Handley, and Timnick, Phys. Rev. **90**, 323 (1953).
[26] M. M. Shapiro, Phys. Rev. **90**, 171 (1953).

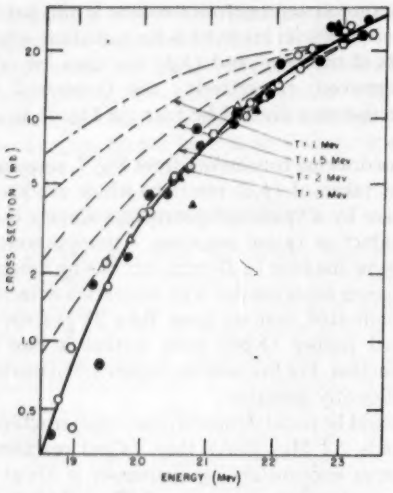

FIG. 5. Excitation function for $Zn^{64}(p,\alpha n)Cu^{60}$. See caption for Fig. 1.

logically excluded, it would require a very remarkable combination of coincidences for the spectrum of emitted deuterons to be such that the excitation functions for the (p,d) reactions reproduce so closely the theoretical excitation functions for the (p,pn) reactions.

With these facts in mind, it seems quite evident from Fig. 7 that the following conclusions can be drawn:

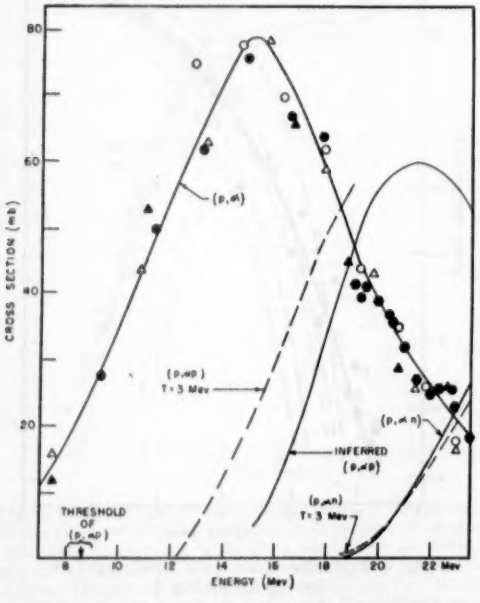

FIG. 6. Excitation functions for (p,α) and $(p,\alpha n)$ reactions on Zn^{64}. The $(p,\alpha p)$ excitation function is inferred from the dropoff in the (p,α) cross section. The $(p,\alpha n)$ curve is taken from Fig. 5. The arrow at 8.5 Mev should be captioned "Threshold for $(p,\alpha n)$."

(a) As in the case of alpha particles, the full Coulomb barrier, as calculated for spherical, undistorted nuclei, is effective in suppressing the emission of low-energy protons, contrary to expectations from the collective model. This effect is most pronounced in the case of tantalum where a reduction in the Coulomb barrier by a factor of two would essentially cause the observed excitation function to be displaced to the left of the theoretical curves by about 5 Mev, contrary to observation. It is especially worth noting that this conclusion is independent of whether or not (p,d) reactions are important contributors to the observed activities (unless, of course, they are overwhelming contributors).

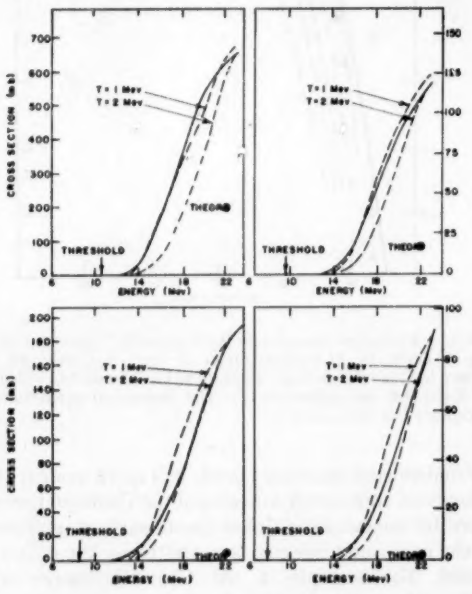

FIG. 7. (p,pn) excitation functions. The curves are lines through the data of Figs. 1–4. Solid circles are absolute cross sections at 22 Mev, calculated from the statistical theory of nuclear reactions. The upper curves are for copper (left) and silver (right); the lower curves are for palladium (left) and tantalum (right).

(b) The absolute value of the inelastic proton scattering cross sections are many times larger than the predictions of the statistical theory. This is another manifestation of the well known phenomenon of charged-particle emission being excessively probable. However, it should be noted that in previous observations of the effect,[1–3] neutron emission was energetically favored, whereas in these cases, proton emission is energetically favored. Also, the threshold complication of reference 4 is not present. The calculations are quite sensitive to these points. In addition, the calculations on these data are considerably less sensitive to the choice of nuclear temperatures. They are completely independent of the behavior of energy-level densities at low excitation energies because (p,pn) reactions are not

energetically possible unless the residual nucleus (after emission of the proton) has sufficient excitation to allow neutron emission. Actually most of the reactions leave the residual nucleus with considerably higher excitation than this minimum.

Therefore, these experiments show quite conclusively that neither the first nor the fourth proposals listed in the introduction of this paper are the correct explanations for the excessive emission of charged particles in nuclear reactions. On the other hand, they provide a new and clear-cut demonstration of that effect in an energy region where uncertainties in nuclear temperatures and in the method of correcting for thresholds cannot be important factors.

The authors would like to acknowledge the help of B. L. Ferrell and E. L. Olson in various parts of the data accumulation, and the general advice and encouragement of J. L. Fowler and R. S. Livingston.

PHYSICAL REVIEW VOLUME 94, NUMBER 3 MAY 1, 1954

Angular Distributions of Fission Fragments from 22-Mev Proton-Induced Thorium Fission

B. L. Cohen, W. H. Jones,* G. H. McCormick,† and B. L. Ferrell
Oak Ridge National Laboratory, Oak Ridge, Tennessee

(Received January 11, 1954)

The angular distributions of barium, strontium, zirconium, ruthenium, and silver fission products from thorium fission induced by 22-Mev protons were measured using the internal, circulating beam of the ORNL 86-inch cyclotron. Within the accuracy of the measurements, all angular distributions are symmetric about 90° and may be well fitted to $I(\theta)=a+b\cos^2\theta$. For Ba, Sr, Zr, Ru, and Ag fission products, for which the fission mass ratios are 1.53, 1.52, 1.37, 1.19, and 1.04, the anisotropy (b/a) is 0.26, 0.25, 0.19, 0.15, and 0.10, respectively.

INTRODUCTION

THE angular distributions of fragments from fission induced by thermal neutrons should be isotropic according to the Eisner-Sachs-Yang rule,[1] and the fact that they are, has been experimentally confirmed.[2] It has commonly been assumed that angular distributions are also isotropic for fission induced by high-energy particles, because fission proceeds by a compound-nucleus interaction in which the number of intermediate and final states is sufficiently large that the effects of individual levels, which are the usual cause of anisotropic angular distributions, would be expected to average out. This expectation, however, has not been verified by experiment.

The first reported measurements of this type was the work of Winhold, Demos, and Halpern[3] on thorium photofission; their data indicate angular distributions of the form $I=\alpha+\beta\sin^2\theta$, where β/α, which is a measure of the anisotropy, reaches values as large as 1.2. They interpret the phenomenon as due to the effects of dipole absorption. However, the recent theoretical work of Wheeler and Hill[4] has shown that compound nuclei undergo large oscillations which lower the Coulomb barrier in specified directions and thereby explain, at least qualitatively, the results of reference 3. At their suggestion, Dickinson and Brolley[2] measured the 0°/90° intensity ratios of fragments from 14-Mev neutron-induced fission of Th^{232}, Np^{237}, U^{233}, U^{235}, and U^{238}. In all cases, they found these ratios to be greater than unity (1.2–1.5), which is in qualitative agreement with the Wheeler-Hill prediction for particle-induced fission.

To throw further light on this problem, a program for the measurement of angular distributions of the products of *proton*-induced fission was undertaken by utilizing the internal, circulating beam of the ORNL 86-inch cyclotron. This approach has the advantage of providing very large incident particle currents, and is especially timely because methods of measuring angular distributions with this beam have recently been studied in considerable detail.[5] In this paper, we describe measurements of angular distributions of Ba, Sr, Zr, Ru, and Ag fission products from 22-Mev proton-induced thorium fission. The work is now being extended to other target elements, and eventually will be extended to other bombarding energies.

EXPERIMENTAL PROCEDURE AND RESULTS

The target assembly is similar to that pictured in reference 5, except that a more accurate method of

* Research participant from Chemistry Department, Emory University, Atlanta, Georgia.

† Research participant from Chemistry Department, University of Denver, Denver, Colorado.

[1] E. Eisner and R. G. Sachs, Phys. Rev. **72**, 680 (1947); C. N. Yang, Phys. Rev. **74**, 764 (1948).

[2] W. L. Dickinson and J. E. Brolley, Phys. Rev. **90**, 388 (1953).

[3] Winhold, Demos, and Halpern, Phys. Rev. **87**, 1139 (1952); I. Halpern and E. J. Winhold, U. S. Atomic Energy Commission Report AECU-2494 (unpublished).

[4] D. L. Hill and J. A. Wheeler, Phys. Rev. **89**, 1102 (1953).

[5] B. L. Cohen and R. V. Neidigh, Rev. Sci. Instr. **25**, 255 (1954).

positioning the detector foil has been incorporated. The target itself is a 0.001-inch platinum foil with a narrow strip of ½ mg/cm² thorium oxide plated on one side. The fission fragments are collected in a 7 mg/cm² aluminum detecting foil covered with a 1.3 mg/cm² aluminum wrapper to exclude thermally evaporated activities which are present in the cyclotron. Since the range of fission fragments[6] in aluminum is about 2.5 to 4.0 mg/cm², practically all fragments should be caught in the detecting foil. Independent tests indicated that about 6 percent were stopped in the wrapper, and about ½ percent went completely through the foil. Both of these quantities vary with angle because of the energy variations due to center-of-mass motion, so they require a small correction which will be discussed below.

After bombardment, the aluminum foil is cut into equal sized pieces (these are weighed and corrections are made for the small differences in their sizes) and processed chemically to isolate the various fission products. These are then counted under end-window Geiger counters to determine their activities, and later weighed to determine chemical yields. The specific activities in the various foils are thus proportional to the intensity of fission fragments emitted at the angles at which the foils were located during the bombardment. The activity measurements are corrected for variation of solid angle in the center-of-mass system and for small (~1 percent) known variations in the target-to-collector distance. For purposes of studying the experimental problems, the angular distributions thus obtained were fitted by least squares methods to a formula of the type

$$I = a + b\cos^2\theta, \tag{1}$$

and the parameter b/a, which is essentially a measure of the anisotropy of the angular distribution, was determined.

In considering the effects of various types of uncertainties in the experiment on the resulting value of b/a, it is necessary to distinguish between random and systematic errors. Random errors, which are by far the greater in any single run, are evidenced by large and uncorrelated variations in the data which are not reproduced in successive runs. The rms fractional error of this type, δ, can be determined by comparing intensity measurements at adjacent angles and correcting for the true change in intensity between these angles as determined from the final results of the experiment. (In all cases, the true change is small.) Analysis shows that the absolute error in the determination of b/a is 1.1δ to 1.4δ.

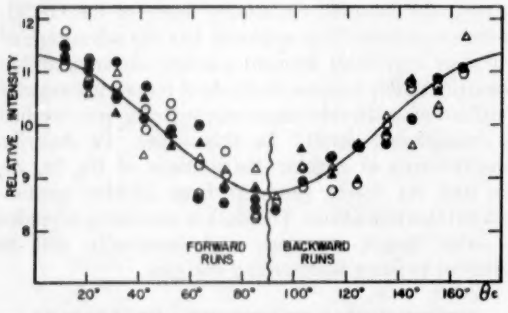

FIG. 1. Angular distribution of Ba^{139} fission fragments from the first set of runs described in text. There is no significance in the use of the same type pointers in the forward and backward direction. The internal consistency of this set is better than for any other.

[6] Katcoff, Miskel, and Stanley, Phys. Rev. 74, 631 (1948).

The principle contributor to δ is error in the chemical processing and yield determination which introduces an rms error of 6–10 percent. (Actually it varied as the chemical processes were changed in an effort to reach the best compromise between chemical purity and time requirements. For ruthenium, the process was never perfected, the average value of δ being about 0.17 percent.) Other sources of random error in the relative intensity at various angles, and their estimated magnitudes are

Counting statistics	1–3 percent,
Counter geometry	1 percent,
Beta self-absorption	1–4 percent,
Target alignment	2 percent,
Detector foil positioning	2 percent.

While the total random error in a given determination of b/a is quite large, these average out in a large number of runs, so that systematic errors are at least equally important. The estimated errors in the alignment of the thin target and the estimation of the effects of finite beam size would change b/a by about ± 0.02. The maximum uncertainties in determination of the angles and in the corrections for center-of-mass solid angle would not change it by as much as ± 0.01. None of these would cause any error in the relative values of b/a for the various fission products, or for the forward and backward directions.

One source of systematic error of the latter type is the variation with angle of the fraction of the fragments stopped in the thin wrapper covering the collector foil due to energy differences arising from center-of-mass motion. This effect, combined with any other systematic errors between the forward and backward directions, was investigated by carrying out an extensive series of runs on the angular distributions of Ba^{139} and $Sr^{91,92}$ fragments; these are emitted in the same reactions (assuming 2 or 3 neutrons per fission) and hence must be emitted in opposite directions. The values of b/a were

Barium forward	0.277 ± 0.025
Strontium backward	0.240 ± 0.030,
Barium backward	0.232 ± 0.027
Strontium forward	0.260 ± 0.026.

The systematic errors thus caused the forward values to be larger by 0.037 ± 0.040 and 0.028 ± 0.038 in the two cases; the average of these is 0.033 ± 0.027. This agrees satisfactorily with a direct determination of 2 ± 3 percent arrived at by processing the aluminum wrappers to determine the relative amounts stopped in them at various angles.

The corrected value of b/a for Ba forward (or Sr backward) can be taken as the average of the first two values, or 0.258 ± 0.019; similarly, the corrected value for Ba backward (or Sr forward) is 0.246 ± 0.019. It thus appears that the angular distributions are symmetric about 90° within the accuracy of this experiment. In the determinations of angular distributions of all other fission fragments, the difference between b/a in the forward and backward directions differed by amounts within experimental error of the difference for barium and strontium; they were thus assumed to be symmetric about 90° and the value of b/a was taken as the average of the values in the forward and backward directions, with the standard deviation taken as $\sqrt{2}/2$ times the rms deviations of the two. The values obtained in this way are shown in Table I. This procedure probably underestimates the standard deviation of the result, but was adopted as the most practical approach. If there is actually a small asymmetry about 90° so that the angular distributions are of the form

$$I(\theta)=a+a_1\cos\theta+b\cos^2\theta, \qquad (2)$$

the values of b/a given here are still correct for that formula. From the barium-strontium data, $a_1/a=0.006\pm0.013$ or, more to the point, $a_1/a<0.02$.

In the first set of runs, which were made primarily to test the feasibility of the project, the angular distributions were determined for barium only. This set included six runs for the forward direction and five for the backward, with determinations at eight angles on each run. After chemical processing, each sample was counted at least four times and the data were then plotted to determine the 85-minute activity of barium-139 in each sample. The results are shown in Fig. 1. Concurrently, tests were made to ascertain (by range considerations) that the activities actually were fission fragments and were coming from the thorium. Also, the aluminum wrappers were processed to determine their necessity (they were very necessary in most runs) and to obtain an estimate of the center-of-mass effect described previously.

Since the results seemed satisfactory, the project was enlarged to include determinations of barium, strontium, and silver, still at eight angles in each direction. To conserve time, two counters were used for each element. A single sample (No. 1) was placed in the first of the two, and each of the other seven (No. 2 –No. 8) was counted in turn in the second counter to determine the ratios of their activities to that of sample No. 1. To determine the relative efficiencies of the two counters, sample No. 2 was counted in the first counter and sample No. 1 in the second. The counting process was repeated at least twice. This method automatically corrects for decay and thus eliminates the necessity of plotting decay curves. A few samples of each element were counted exhaustively to ascertain that the half-lives were correct; this serves as a check on the adequacy of the chemical processing.

TABLE I. The values of b/a obtained by fitting the data to Eq. (1). The forward and backward data are not corrected for variation of energy with angle due to center-of-mass motion; since this correction is equal and opposite for the two cases, the average does not require this correction. The mass ratios are calculated assuming three neutrons per fission. The errors listed are standard deviations due to statistics only.

Element	Mass ratio	Measured b/a Forward	Backward	Average
Ba^{139}	1.53	0.285 ± 0.02	0.248 ± 0.02	0.264 ± 0.015
$Sr^{91,92}$	1.52	0.260 ± 0.025	0.240 ± 0.03	0.250 ± 0.020
$Ag^{112,113}$	1.04	0.105 ± 0.025	0.095 ± 0.025	0.100 ± 0.015
Zr^{97}	1.37	0.24 ± 0.025	0.15 ± 0.03	0.195 ± 0.020
Ru^{105}	1.19	0.19 ± 0.08	0.11 ± 0.08	0.15 ± 0.06

A total of twenty-eight runs, 18 forward and 11 backward, were made in this program. The values of b/a were determined for each run and plotted against time to determine whether secular variations were present. Since there was some evidence of such a variation for silver, further data on that element were taken in the next set of runs, described below. It was finally concluded, however, that the apparent secular variation was due to statistical fluctuations. No secular variations were noticeable in the barium and strontium data.

The values of b/a for barium and strontium on the same runs were plotted against each other. The resulting "scatter" diagram showed no significant correlation between the two, thus indicating that there were no major errors due to such things as target alignment, beam characteristics, etc.

The values of b/a for each element and for each direction (i.e., forward and backward) were plotted on probability paper as shown in Fig. 2. This tests how well the values can be fitted to a Gaussian error function (for a perfect fit, the points should lie on a straight line) and determines the most probable value of b/a (the abscissa for which the best line through the data crosses the ordinate "50") and the standard deviation of a single determination (the difference between the most probable value and the abscissa for which the line crosses the ordinate "16"). The fits to the Gaussian error function are generally satisfactory; the standard deviations of a single determination of b/a average about 0.09 for barium and strontium and about 0.08 for silver. The expected standard deviation, assuming that it is due only to random errors, was calculated by determining δ by the method discussed above; in this set of runs, the mean value of δ was about 0.06 to 0.07. Analysis shows that the standard deviation in b/a should be about 1.1δ for silver and about 1.2δ

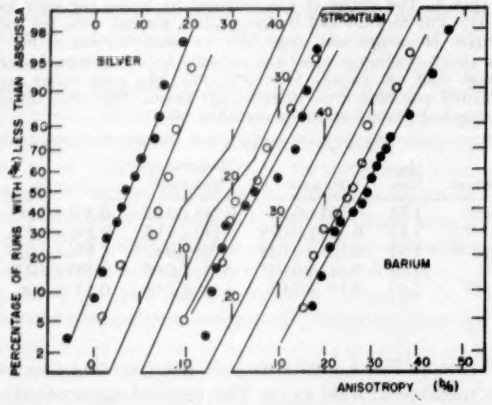

FIG. 2. Probability paper plot of anisotropies (b/a) in angular distributions of Ba, Ag, and Sr fission fragments from first and second sets of runs. The probability paper scale is such that when the percentage of runs with b/a less than each value is plotted *vs* that value, the points lie on a straight line if the data follow a Gaussian distribution. The abscissa at which the line crosses ordinate 50 is the most probable value; the difference between this and the abscissa at which the line crosses ordinate 16 is the standard deviation of a single determination, and the standard deviation of the mean is that divided by the square root of the number of runs. Solid circles represent forward direction runs and open circles represent backward direction runs. Data are not corrected for variation of fragment energy with angle due to center-of-mass effects. The correction reduces the anisotropy for the forward runs and increases it for the backward runs.

for barium and strontium. Thus the random errors account for the standard deviation in the results which supports the assumption that there are no appreciable secular variations.

The barium-strontium comparisons mentioned previously were carried out in this set of runs. The agreement between the values of b/a for barium and strontium lent confidence to the general method.

For purposes of plotting and further analysis, each run was normalized to the same total intensity and the data were grouped into series of 5 or 6 runs in chronological order. The average intensity at each angle for each group is shown plotted *vs* angle in Figs. 3, 4, and 5. One set of points in Fig. 3 (solid circles) represents the average of the data from Fig. 1. No correction was made for the center-of-mass variation of energy with angle in the plotting.

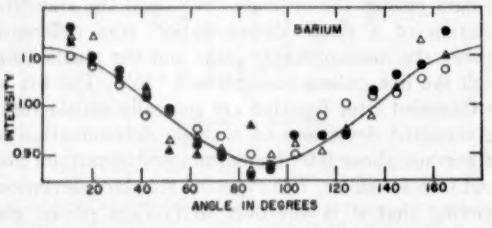

FIG. 3. Composite angular distribution of Ba^{139} fission fragments. Each set of points represents the average of a group of five or six runs. Data are not corrected for the variation in fragment energy with angle due to center-of-mass motion. The correction makes the data more nearly symmetric about 90°.

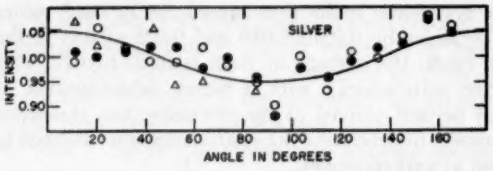

FIG. 4. Composite angular distribution of $Ag^{112,113}$ fission fragments. See caption for Fig. 3.

The average data were also fitted by least-squares methods to

$$I(\theta)=a'+b'\cos^2\theta+d'\cos^4\theta. \tag{3}$$

The values of d'/a' thus determined showed very poor reproducibility, so that it was concluded that the data is not sufficiently accurate for this type of analysis. In all cases, however, the sum of $b'/a'+d'/a'$ was nearly equal to b/a from Table I; the quantity $b/a-(b'/a'+d'/a')$ was 0.012 ± 0.007 for the forward runs and 0.000 ± 0.007 for the backward runs. Thus, if the anisotropy A is defined as

$$A=\frac{\frac{1}{2}[I(0°)+I(180°)]-I(90°)}{I(90°)}. \tag{4}$$

A is the same regardless of the method of analysis.

A third set of runs was undertaken primarily to extend the data to other fission products. The new elements chosen were zirconium and ruthenium, and due to the previously mentioned uncertainty in the silver data, further data on silver were taken concurrently. The procedure was also simplified by discontinuing intensity determinations between 25° and 65°, and between 115° and 155° since these are of little importance in determining the anisotropy; the number of foils was thus reduced to four for each run. A further simplification was achieved when it was realized that no significant information had been obtained from counting each sample several times, since, in the end, a simple average was always taken. For this set of runs, therefore, each sample was counted only once but for an extended time. A total of 19 runs, 11 backward and 8 forward, were included in this set, and least-squares fits to Eq. (1) were made to determine b/a.

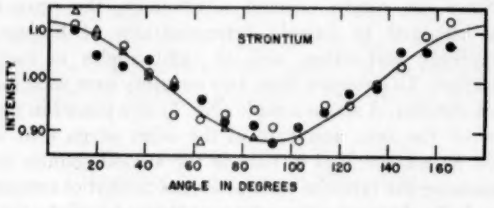

FIG. 5. Composite angular distribution of $Sr^{91,92}$ fission fragments. See caption for Fig. 3.

Before comparing these values directly with the previous data, it is necessary to determine whether the four angles omitted in this set contribute to b/a in a systematic way. An analysis of the previous data omitting these four angles was therefore carried out; it was found that b/a obtained from eight angles was greater than b/a obtained from the four by 0.026 ± 0.009 in the forward direction, and 0.000 ± 0.005 in the backward direction. The discrepancy in the forward direction is somewhat disturbing; however, the values of $(b'/a'+d'/a')$, which are probably the most accurate index of the anisotropy, lie midway between the values of b/a as calculated by the eight-angle and four-angle methods. Also, the agreement between all three methods is excellent in the backward direction. There thus seemed to be no alternative to considering the values of b/a as calculated by the eight and four angle methods as equivalent, with the realization that there may be a small systematic error introduced in the process.

The values of b/a obtained from this last set of runs are shown plotted on probability paper in Fig. 6, and their averages are listed in Table I. The entry for silver in Table I is an average over the two sets of silver runs.

CONCLUSIONS AND DISCUSSION

Two principle new quatitative conclusions can be drawn from this data. Firstly, the angular distributions are symmetric about 90° well within the experimental error, and secondly, the anisotropy is much greater for asymmetric fission than for symmetric fission. The latter point is demonstrated in Fig. 7 where the anisotropy is plotted against the mass ratio of the fission products. In considering the absolute values of the anisotropy, one should allow for possible systematic errors of about ±0.03 in the data from Table I or Fig. 7. In using the *relative* values for the various mass ratios, the systematic error is probably not much larger than ±0.01.

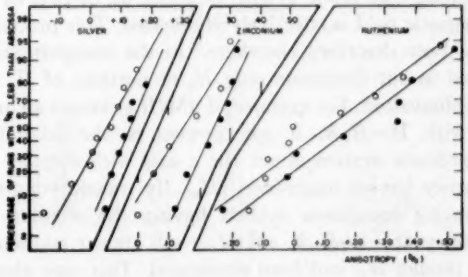

FIG. 6. Probability paper plot of anisotropies in angular distributions of Ag, Zr, and Ru fission products from third set of runs. See caption for Fig. 2. The increased slope of the forward with respect to the backward data for silver and zirconium represent an improvement in accuracy (smaller standard deviation) due to changes in the chemical processing methods. The shallow slope for ruthenium is due to difficulties in the chemical processing that were never overcome.

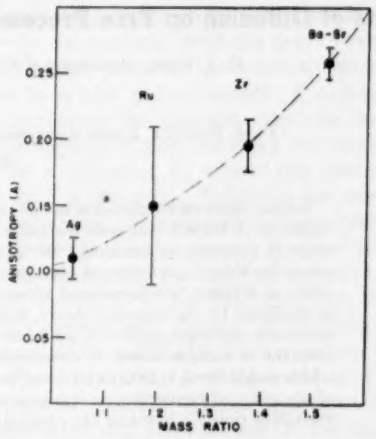

FIG. 7. Anisotropy in fission fragment angular distributions vs mass ratio (mass of heavy fragment divided by mass of light fragments). The data are taken from Table I.

The Wheeler-Hill theory, so far as is known, has not been applied to predict numerical values of the anisotropy. Also nothing is said in reference 4 about a possible dependence on mass ratio.

It is important to note that it has been demonstrated both theoretically[7] and experimentally[8] that, due to straightforward angular momentum considerations, angular distributions from compound nucleus reactions exhibit a monotonic decrease in intensity from 0° to 90° with symmetry about 90°. This is due to the fact that the angular momentum imparted to the compound nucleus by the orbital angular momentum of the incident particle is polarized in the sense that its component in the direction of incidence is zero; thus the spin of the compound nucleus is polarized in the same sense, and when it breaks up, this polarization must be shared in some fashion between the orbital angular momentum of the outgoing particles and their spins. The polarization of the outgoing orbital angular momentum causes the asymmetry in the angular distribution. The effect is sensitive to the distribution of spins in the final nuclei, so that some estimate of this would be necessary to determine the magnitude of the asymmetry. It is interesting to note, however, that this asymmetry is of about the same magnitude as the asymmetry in the angular distributions of neutrons from (α,n) reactions induced by 30-Mev alpha particles (from reference 8, $A=0.21$). The (α,n) case cannot be a Coulomb effect (such as the Wheeler-Hill effect) since neutrons are unaffected by Coulomb barriers, and the observed asymmetry is independent of atomic number.

The authors would like to acknowledge the assistance and encouragement of R. S. Livingston and J. L. Fowler in carrying out these experiments.

[7] L. Wolfenstein, Phys. Rev. **82**, 690 (1951).
[8] B. L. Cohen, Phys. Rev. **81**, 632 (1951).

Effects of Diffusion on Free Precession in Nuclear Magnetic Resonance Experiments*†

H. Y. Carr, *Department of Physics, Rutgers University, New Brunswick, New Jersey*

AND

E. M. Purcell, *Lyman Laboratory of Physics, Harvard University, Cambridge, Massachusetts*

(Received January 19, 1954)

Nuclear resonance techniques involving free precession are examined, and, in particular, a convenient variation of Hahn's spin-echo method is described. This variation employs a combination of pulses of different intensity or duration ("90-degree" and "180-degree" pulses). Measurements of the transverse relaxation time T_2 in fluids are often severely compromised by molecular diffusion. Hahn's analysis of the effect of diffusion is reformulated and extended, and a new scheme for measuring T_2 is described which, as predicted by the extended theory, largely circumvents the diffusion effect. On the other hand, the free precession technique, applied in a different way, permits a direct measurement of the molecular self-diffusion constant in suitable fluids. A measurement of the self-diffusion constant of water at 25°C is described which yields $D=2.5(\pm 0.3)\times 10^{-5}$ cm²/sec, in good agreement with previous determinations. An analysis of the effect of convection on free precession is also given. A null method for measuring the longitudinal relaxation time T_1, based on the unequal-pulse technique, is described.

I. INTRODUCTION

In order to explain the spin-echo envelopes obtained from certain samples in his nuclear magnetic resonance free precession experiments, Hahn[1] found it necessary to consider the diffusion of the molecules through the inhomogeneous external field. Recent experiments using a somewhat modified free precession technique have allowed further observation and analysis of the diffusion effects. These studies are interesting for two reasons. First, they provide a firmer basis for the use of the free precession method in measuring nuclear magnetic relaxation times. Secondly, for suitable samples a relatively direct measurement of the diffusion coefficient is possible.

In order to introduce terminology and notation, the principles of the free precession method will be briefly reviewed. Hahn[1] has described typical apparatus. The only additional equipment used in our experiments consists of two independent pulse width controls and more flexible triggering circuits.

We will denote the total magnetic moment of the nuclear sample by the vector $\mathbf{M}$. At thermal equilibrium, $\mathbf{M}$ is parallel to the strong applied field, $\mathbf{H}=H_z\mathbf{k}$, and its magnitude is given by the product of H_z and the static nuclear susceptibility. We denote this equilibrium value by M_0.

In describing the precessional motions of the nuclei of the sample it is necessary to take account of the inhomogeneity of the applied field. The fraction of the nuclei associated with a value of H_z in a small interval about a particular H_z will be denoted by $f(H_z)dH_z$. The normalized distribution function $f(H_z)$ is considered centered at $H_z=H_{z0}$. The field deviations are $\Delta H_z=H_z-H_{z0}$. The root-mean-square deviation σ may be used as a measure of the width of the distribution. With each value of H_z and with an increment dH_z, we associate an incremental magnetic moment $d\mathbf{M}(H_z)$, which is the vector sum of the moments of all nuclei within regions where the field strength is between H_z and H_z+dH_z. The motions of these incremental net magnetic moment vectors are described by the equation

$$\frac{d}{dt}d\mathbf{M}(H_z)=-\gamma\mathbf{H}\times d\mathbf{M}(H_z), \tag{1}$$

where γ the gyromagnetic ratio is the ratio of the magnetic moment to the nuclear angular momentum. Thus an incremental magnetic moment vector making a finite angle with $\mathbf{H}$ will precess in a negative sense for $\gamma>0$ with angular frequency of magnitude $\gamma|\mathbf{H}|$ about the direction of $\mathbf{H}$. In nuclear magnetic resonance studies it is customary to describe this precession in a rotating coordinate system in which all or part of the magnetic field is effectively eliminated. This procedure has been described elsewhere.[2] In the transformations used in our discussion only H_z or portions of H_z will be eliminated. For example, if $d\mathbf{M}(H_{z0})$ makes an angle θ with $\mathbf{H}=H_{z0}\mathbf{k}$, it will precess in the laboratory coordinate system about the z axis with angular frequency having magnitude γH_{z0}. By transforming to a rotating coordinate system having the angular frequency $\boldsymbol{\Omega}=-\gamma H_{z0}\mathbf{k}$, $d\mathbf{M}(H_{z0})$ will appear stationary, as though H_{z0} had been eliminated. This may also be seen from the transformation equation

$$\frac{\delta}{\delta t}d\mathbf{M}(H_{z0})=-\gamma\left(\mathbf{H}+\frac{\boldsymbol{\Omega}}{\gamma}\right)\times d\mathbf{M}(H_{z0}). \tag{2}$$

* This work was partially supported by the joint program of the U. S. Office of Naval Research and the U. S. Atomic Energy Commission, by The Radio Corporation of America, by the Rutgers University Research Council, and by the United States Air Force under a contract monitored by the Office of Scientific Research, Air Research and Development Command.

† Portions of this work have been previously described by H. Y. Carr, thesis, Harvard University, 1952 (unpublished).

[1] E. L. Hahn, Phys. Rev. **80**, 580 (1950).

[2] R. K. Wangsness, Am. J. Phys. **21**, 274 (1953).

However, for the more general incremental vector $dM(H_z)$ not all of the H_z is eliminated in the above rotating coordinate system. As a result, $d\mathbf{M}(H_z)$ precesses with the small angular frequency

$$\omega_\Delta = -\gamma(H_z - H_{z0})\mathbf{k}'.$$

This is illustrated in Fig. 1B.

In free precession experiments the radio-frequency energy is applied to the sample in short intense pulses. The rf magnetic field, as in other nuclear resonance methods, is applied to the sample at right angles to the strong static field. Its magnitude will be denoted by $2H_1$. The frequency of the rf field satisfies the resonant condition $\omega_{rf} = \gamma H_{z0}$. As is well known,[3] only one of the two circularly polarized components composing the linearly polarized rf field is effective in nutating the net magnetic moments. This component, with magnitude H_1, is the one which rotates in phase with the precessing moments. The phase of the rotating system will be so chosen that this H_1 is along the x' axis. With the rf pulse applied, the net field $\mathbf{H} = \Delta H_z\mathbf{k}' + H_1\mathbf{i}'$ will determine the precession of the incremental moment vectors. This is illustrated in Fig. 1C. However, a special approximation is possible in the present work. The magnitude of the rf field is made so large ($H_1 \gg \sigma$), and the duration of the rf pulse τ_w so short ($\tau_w \ll 1/\gamma\sigma$), that the precession about the net field is effectively equivalent to precession about $H_1\mathbf{i}'$. This precession during the time the rf pulse is applied might be referred to as pure nutation. Furthermore, in the above approximation all incremental moments will rotate together as a single total magnetic moment vector. Figure 2A illustrates the combined precession about $\mathbf{k}$ and nutation about $\mathbf{i}$ as seen from the laboratory frame of reference while Fig. 2B illustrates the pure nutation about $\mathbf{i}'$ as seen from the rotating frame of reference. In a time τ_w the angle of nutation is $\theta = \gamma H_1 \tau_w$. In the present experiments only two angles of nutation are used. These are 90° and 180°. When the rf oscillator gating circuit is so adjusted that

$$\gamma H_1 \tau_w = \tfrac{1}{2}\pi, \qquad (3)$$

the net magnetic moment vector will rotate through an angle $\theta = \frac{1}{2}\pi$, for example, from the polar z' axis down to the equatorial plane of the reference sphere. This is referred to as a 90° pulse. Similarly, if τ_w is such that the vector rotates, for example, from the positive z' axis to the negative z' axis, one has a 180° pulse.

Consider a situation in which free precession is initiated with a 90° pulse. Following the removal of the pulse the total net magnetic moment precesses in the equatorial plane and induces a rf signal in the coil surrounding the sample. For liquid and gaseous samples this signal decays, in a time long compared to the τ_w used in our experiments, because of the differences in the precessional frequencies of the incremental moment vectors. Viewed from the rotating frame of reference, the incremental moment vectors appear to fan out. This is illustrated in *C* and *D* of Fig. 3. The magnitude of the total magnetic moment vector, and hence the induced signal, is thereby reduced. The decaying nuclear signal following the 90° pulse is referred to as a "tail." For a symmetrical distribution function no x' component of the total moment vector exists. The y' component is given by

$$M_{y'} = M_0 \int f(H_z) \cos\gamma(H_z - H_{z0})t \, dH_z. \qquad (4)$$

This expression describes the time dependence of the tail. For example, if the distribution is an error function, the tail has the form

$$M_{y'} = M_0 \exp(-\sigma^2\gamma^2t^2/2), \qquad (5)$$

while if $f(H_z)$ is a rectangular function of width $2h$,

$$M_{y'} = M_0[(\sin\gamma ht)/\gamma ht]. \qquad (6)$$

Wide distributions correspond to fast decays and narrow, or more homogeneous distributions, to slow decays. This is illustrated in Fig. 4. If the distribution function consists of two or more distinct spin groups, such as those caused by different diamagnetic effects

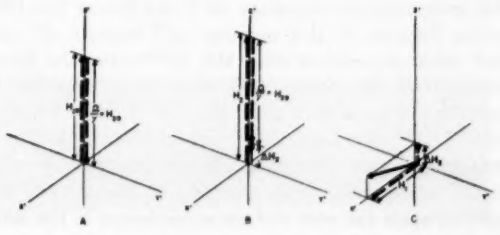

FIG. 1. The apparent elimination of H_z as viewed from a frame of reference rotating with the angular frequency $\mathbf{\Omega} = -\gamma H_{z0}\mathbf{k}$. For $H_z = H_{z0}$, there is no resultant field (*A*); but in a general case (*B*), there is a resultant field $\Delta H_z = H_z - H_{z0}$. When the rf field H_1 is applied, ΔH_z combines with H_1 to determine the direction (*C*) about which rotation occurs.

[3] G. E. Pake, Am. J. Phys. **18**, 438 (1950).

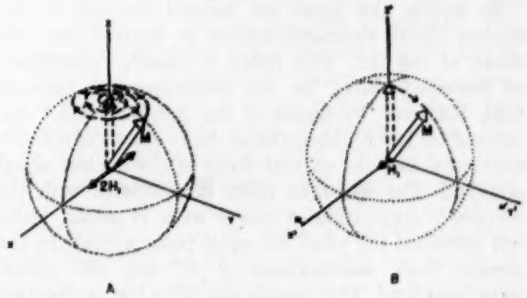

FIG. 2. (*A*) The combination of precession and nutation of the net magnetic moment as viewed from the laboratory frame of reference. (*B*) Pure nutation of the net magnetic moment as viewed from the frame of reference rotating at the precessional frequency.

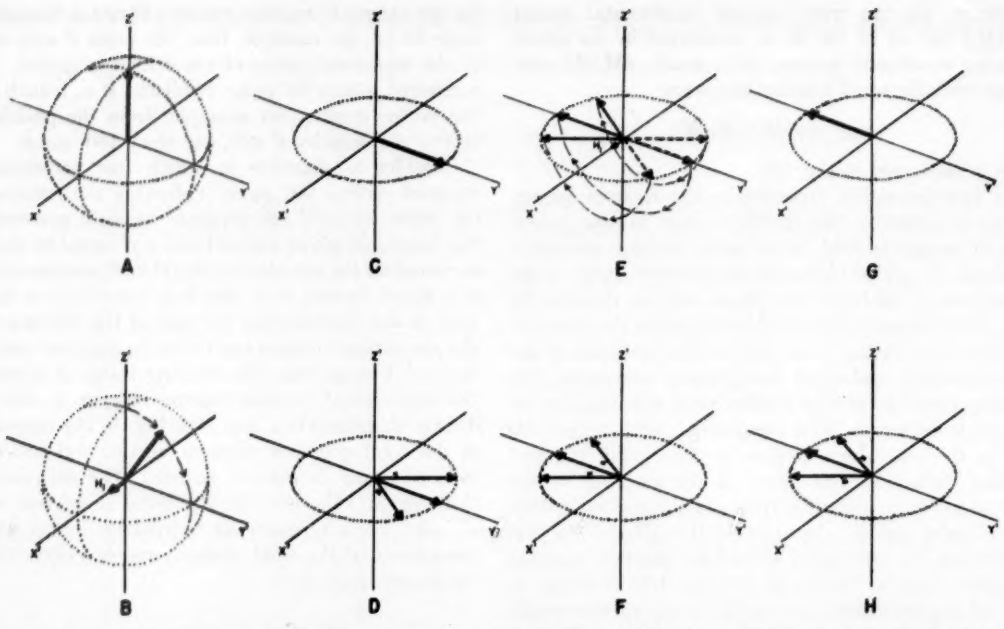

FIG. 3. The formation of an echo. Initially the net magnetic moment vector is in its equilibrium position (A) parallel to the direction of the strong external field. The rf field H_1 is then applied. As viewed from the rotating frame of reference the net magnetic moment appears (B) to rotate quickly about H_1. At the end of a 90° pulse the net magnetic moment is in the equatorial plane (C). During the relatively long period of time following the removal of H_1, the incremental moment vectors begin to fan out slowly (D). This is caused by the variations in H_z over the sample. At time $t=\tau$, the rf field H_1 is again applied. Again the moments (E) begin to rotate quickly about the direction of H_1. This time H_1 is applied just long enough to satisfy the 180° pulse condition. This implies that at the end of the pulse all the incremental vectors are again in the equatorial plane. In the relatively long period of time following the removal of the rf field, the incremental vectors begin to recluster slowly (F). Because of the inverted relative positions following the 180° pulse and because each incremental vector continues to precess with its former frequency, the incremental vectors will be perfectly reclustered (G) at $t=2\tau$. Thus maximum signal is induced in the pickup coil at $t=2\tau$. This maximum signal, or echo, then begins to decay as the incremental vectors again fan out (H).

in different parts of a molecule, the tail will be modulated by their beat pattern. The tail in Fig. 5 illustrates such a beat pattern observed with a proton sample of acetic acid CH_3COOH.

II. METHODS FOR MEASURING TRANSVERSE RELAXATION TIME

In liquids and gases the natural lifetimes of the nuclear signals ordinarily cannot be inferred from the decay of the tail. This decay is usually determined, as described above, by the inhomogeneous external field. However, by means of the spin-echo effect discovered by Hahn, this artificial decay can be effectively eliminated and the natural decay of the nuclear signal observed. The spin-echo effect is associated with the successive application of two or more rf pulses. Hahn has described the effect for equal pulse widths. In the present work combinations of 90° and 180° pulses have been used. This greatly simplifies the explanation of the effect and the interpretation of the observed data.

To obtain an echo using this technique, a 180° pulse is applied at a time τ after the 90° pulse. τ is chosen larger than the artificial decay time of the tail but smaller than the natural lifetime of the nuclear signal. As illustrated in E of Fig. 3, the incremental vectors rotate 180° about the x' axis. When the rf field is removed at the end of the pulse, all incremental vectors are again in the equatorial plane. Since it is assumed that each nucleus remains in the same H_z, each will continue to precess in the same sense and with exactly the same angular frequency as it did before the 180° pulse. Because of this memory and because of their new relative positions after the 180° pulse, the incremental moment vectors will all recluster together in exactly τ units of time after the 180° pulse. This is at time 2τ. At this time there will be a maximum total magnetic moment vector and hence maximum induced signal or an echo. Following $t=2\tau$ the incremental vectors again fan out, and the echo decays in the same manner that it formed. An echo simply appears as two tails back to back. This is vividly illustrated by the echo in Fig. 5.

In order to utilize the above effect in observing the natural lifetimes of nuclear signals, Hahn introduced a method of measurement which will be referred to as

Method A. In this method the amplitude of the echo following a single two-pulse sequence is plotted as a function of time. The data for the different points are obtained by using different values of τ.

The plot may be made photographically by taking a multiple exposure picture of the oscilloscope screen displaying the detected nuclear signals. Each exposure corresponds to a different two-pulse sequence and echo at 2τ. The envelope of the photographed echoes is the desired curve. From considerations mentioned thus far, one would expect that this plot would indicate the natural decay or lifetime of the transverse polarization $M_{y'}$.

This natural decay is expected to proceed exponentially. It is caused, if one restricts the discussion to nuclei without electric quadrupole moments, by the local magnetic field which originates in moments carried by neighboring atoms and molecules. Owing to the Brownian motion of these other dipoles as well as that of the nucleus in question, this local magnetic field varies randomly both in magnitude and in direction.[4] In liquids and gases the variation is usually so much more rapid than the Larmor precession that the local field has practically the same character whether viewed from the stationary or the rotating frame of reference. In this case it is easy to understand what happens. A moment directed originally along the y' axis, exposed to this random field, executes on the reference sphere a random walk made up of very short steps. The whole cluster of moments thus spreads by diffusion over the sphere. The exponential decay follows as a direct and general result. To illustrate with a simple if somewhat artificial model, suppose that the local field $\mathbf{h}$ at a given nucleus changes exactly once every τ_c seconds to a new magnitude and direction randomly selected. The other nuclei experience similar, but uncorrelated, variations in their local fields. It is then easy to show that

$$M_{y'}(t)=M_0\exp(-\gamma^2\langle h^2\rangle_{\mathrm{Av}}\tau_c t/3), \tag{7}$$

where

$$\langle h^2\rangle_{\mathrm{Av}}=\langle h_x^2\rangle_{\mathrm{Av}}+\langle h_y^2\rangle_{\mathrm{Av}}+\langle h_z^2\rangle_{\mathrm{Av}}. \tag{8}$$

Many other approaches lead to the same result.[5,6]

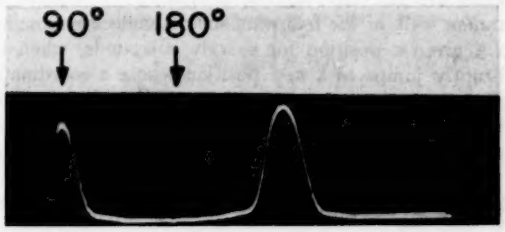

(A)

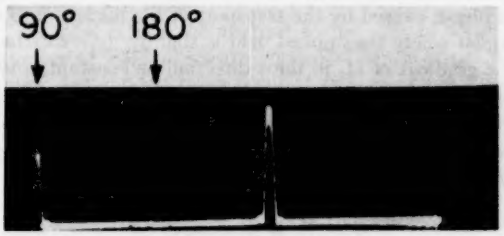

(B)

FIG. 4. Effect of the homogeneity of the field on the widths of tails and echoes. The tails and echoes associated with a sample (A) in a very homogeneous field are wide compared to those associated with a sample (B) in a less homogeneous field.

[4] Bloembergen, Purcell, and Pound, Phys. Rev. **73**, 679 (1948).

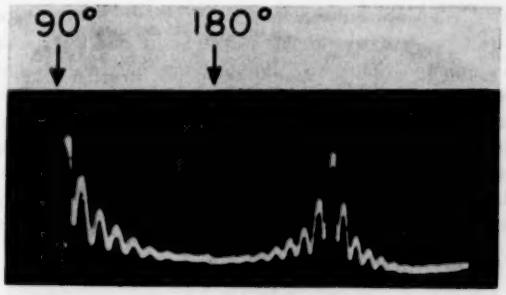

FIG. 5. A tail and echo associated with an acetic acid (CH_3COOH) sample in a very homogeneous field. The nuclear signal displays modulation typical of the beating of two signals of nearly equal frequencies, the magnitude of one being three times that of the other. The beat frequency shown, corresponding to room temperature and 7000 gauss, is approximately 220 cps.

In the cases of certain samples the echo envelopes obtained by Hahn's method, Method A, have essentially the above exponential form. However, for certain other nonviscous samples such as pure water the envelope is more nearly of the form $\exp(-kt^3)$. See Fig. 7A. Hahn was successful in showing that this is the form of the decay to be expected if the decay is caused by diffusion of the molecules through the inhomogeneous external field H_z. Therefore if diffusion is important, a decay or relaxation time measured by Method A is "artificially" determined by the external magnet.

In the present work a new method for obtaining an echo envelope which reveals the "natural" decay even in the presence of diffusion has been introduced. This method of measurement will be referred to as Method B. In Method A a number of 90° pulses must be applied to the sample in order to obtain sufficient data to plot the envelope. Each 90° pulse is followed by an 180° pulse and the accompanying echo. Between each 90°–180° sequence sufficient time must elapse to allow the sample to return to its thermal equilibrium condition. In Method B a single 90° pulse is used to obtain an entire echo envelope without requiring the sample to return to thermal equilibrium. This is accomplished by initiating the measurement with the usual 90° pulse at $t=0$. A 180° pulse is then applied at time $t=\tau$. The

[5] R. K. Wangsness and F. Bloch, Phys. Rev. **89**, 728 (1953).
[6] A. Abragam and R. V. Pound, Phys. Rev. **92**, 943 (1953).

usual echo appears at time $t=2\tau$. Next, to illustrate with a particularly simple case, an additional 180° pulse is applied at time $t=3\tau$. By reasoning identical to that previously used in connection with the first echo, it can be seen that the incremental vectors will recluster at time $t=4\tau$. Thus, a second echo is formed. If this process is continued throughout the natural lifetime of the nuclear signal, additional echoes of decreasing amplitude are formed. The envelope of these echoes indicates the decay of the polarization in the equatorial plane. In some experiments as many as 30 echoes have been formed following a single 90° pulse. Methods *A* and *B* are compared in Fig. 6.

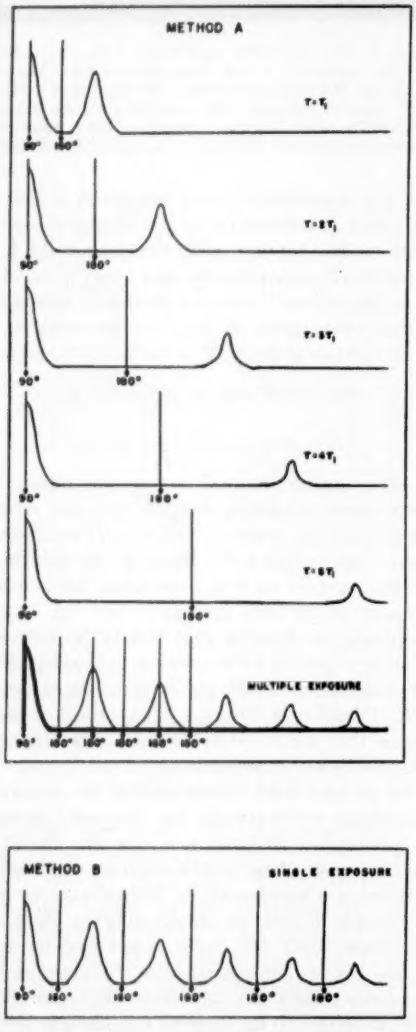

FIG. 6. Comparison of the two free precession methods for observing the decay time of the horizontal component of nuclear magnetic polarization. In "Method *A*" the sample must return to its equilibrium condition each time an additional echo is to be observed. In "Method *B*" the sample need only start from equilibrium once. The separate oscilloscope traces of "Method *A*" are usually displayed superimposed in a multiple exposure picture. Only a single trace and hence a single exposure picture is required in "Method *B*." However this latter method requires more than one 180° pulse.

In the case of viscous samples with negligible diffusion, the echo envelope obtained by Method *A* is identical to that obtained by Method *B*. This is not so if certain nonviscous samples are used. Figure 7 vividly illustrates the difference in envelopes obtained by the two methods if a water sample is used. The top photograph illustrating Method *A* is a multiple exposure picture of a series of thirteen 90°–180° pulse sequences, each with an accompanying echo at a different time 2τ. The decay is of the form $\exp(-kt^3)$. The time constant is approximately 0.2 sec. The lower photograph is a single exposure picture of a single sequence of pulses consisting of one 90° pulse followed by fifteen 180° pulses. The decay is of the form $\exp(-Kt)$. The time constant is approximately 2.0 sec!

III. THE EFFECT OF DIFFUSION

The above difference between Method *A* and Method *B* may be explained by analyzing the effect of the molecular diffusion on the distribution-in-phase of the precessing moments. One may replace the diffusion by a random walk of discrete steps. This makes it easier to formulate certain parts of the problem. As we shall pass finally to the limit of infinitesimal steps, introducing at that point the ordinary molecular self-diffusion constant D, the details of the random walk model are not critical. For simplicity we assume a random walk of the following sort: a molecule remains at a given z position for exactly τ seconds, when it abruptly jumps to a new position whose z coordinate differs from the previous one by ζa_i, where ζ is a fixed distance and a_i a random variable whose value is 1 or -1. The constant linear gradient is in the z direction. ζ might more properly be defined by $(\langle z_i^2\rangle_{Av})^{\frac{1}{2}}$, the rms z component of a three-dimensional jump of magnitude $\delta=(3\langle z_i^2\rangle_{Av})^{\frac{1}{2}}$.

The effect we are interested in is the change in the rate of nuclear precession, and the resulting discrepancy in phase, caused by the transport of the nucleus into a region where the applied field is slightly different. Let the gradient of H_z in the z direction be constant, and, in magnitude, G gauss/cm, and let $H_z(0)$ be the field in which a given nucleus finds itself at $t=0$. At some later time $t=j\tau$ the nucleus will find itself in a field $H_z(j\tau)$ given by

$$H_z(j\tau)=H_z(0)+G\zeta\sum_{i=1}^{j}a_i.$$

After N steps, that is after a time $t=N\tau$, the phase ϕ of the precessing moment of this nucleus will differ from the value ϕ_0 it would have had at this same instant if the nucleus had remained in the same place by an

angle

$$\phi_D=\phi-\phi_0=\sum_{j=1}^{N}\gamma\tau[H_z(j\tau)-H_z(0)]$$

$$=G\zeta\gamma\tau\sum_{j=1}^{N}\sum_{i=1}^{j}a_i=G\zeta\gamma\tau\sum_{j=1}^{N}(N+1-j)a_j. \quad (10)$$

As the a_j's are random variables anyway, the last sum can just as well be written

$$G\zeta\gamma\tau\sum_{j=1}^{N}ja_j. \quad (11)$$

Now it can be shown that the central limit theorem holds for this sum. Therefore, if at time $t=N\tau$ we consider the distribution in phase of an ensemble of moments, we can assert that the distribution will be Gaussian in the limit of large N. It only remains to calculate $\langle\phi_D^2\rangle_{Av}$. This is easily done:

$$\langle\phi_D^2\rangle_{Av}=G^2\zeta^2\gamma^2\tau^2\sum_{j=1}^{N}j^2$$

$$=G^2\zeta^2\gamma^2\tau^2N(N+1)(2N+1)/6. \quad (12)$$

If N is large—and in this problem it is in fact enormous—we may not only drop the lower powers of N, but we may at the same time pass over to a description in terms of a continuous diffusion rather than discrete random steps. By comparing the solution to the diffusion equation $D\nabla^2 f=\partial f/\partial t$, where $f(x,y,z)$ is the probability density, with the solution to the random walk problem of the assumed type, it is easy to show that the appropriate diffusion constant is

$$D=\delta^2/6\tau=\zeta^2/2\tau. \quad (13)$$

We thus have

$$\langle\phi_D^2\rangle_{Av}=2G^2\gamma^2Dt^3/3, \quad (14)$$

and for the distribution-in-phase after time t we have

$$P(\phi_D)=(4\pi\gamma^2G^2Dt^3/3)^{-1}\exp(-3\phi_D^2/4G^2\gamma^2Dt^3). \quad (15)$$

This is identical with the result given by Hahn,[1] and it applies directly to the behavior of the signal in the tail after a 90° pulse.

We now extend the analysis to the case in which a number of 180° pulses are applied after the initial 90° pulse. Let the 90° pulse occur at $t=0$ as before. If we return to the discrete model, the effect of a 180° pulse applied at $t=t_1$, for example, is simply to *reverse the signs* of all terms in

$$\phi_D=\sum_{j=1}^{N}\gamma\tau[H_z(j\tau)-H_z(0)] \quad (16)$$

beyond $j=t_1/\tau$. Let us specialize at once to the interesting case in which, within the whole interval $t=N\tau$, n 180° pulses are applied; the first at $t=N\tau/2n$, the second at $t=3N\tau/2n$, and so on. Echoes will then occur midway between the 180° pulses and, in particular, an

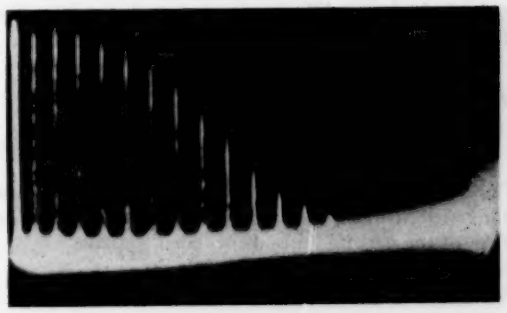

(A)

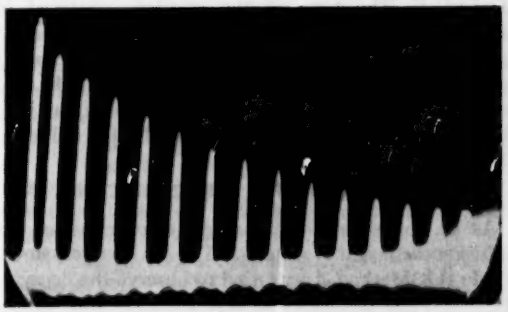

(B)

FIG. 7. (*A*) A "Method *A*" decay associated with water at 25°C. The time constant is approximately 0.2 sec. The decay is largely determined by the molecular diffusion through the 0.28 gauss/cm gradient. The decay is dominated by the factor $\exp(-kt^3)$. (*B*) A "Method *B*" decay associated with water at 25°C. The time constant of the decay is approximately 2.0 sec. The effect of diffusion has been largely circumvented.

echo will occur at $t=N\tau$. We are interested in finding the effect of diffusion on this final echo. For this case we must now rewrite ϕ_D as

$$\phi_D=\phi-\phi_0=G\zeta\gamma\tau\sum_{j=1}^{N}b_j\sum_{i=1}^{j}a_i, \quad (17)$$

where

$b_j=1$ for $0<j\leqslant N/2n$, $3N/2n<j\leqslant 5N/2n$, etc.,

$b_j=-1$ for $N/2n<j\leqslant 3N/2n$, $5N/2n<j\leqslant 7N/2n$, etc.

By writing out the terms in an array, it is easy to see that the above double sum involving the random variables can be replaced by the sum of n independent sums of the type $\sum_{k=1}^{(N/2n)-1}ka_k$, and n independent sums of the type $\sum_{k=1}^{N/2n}ka_k$. We thus find at once that

$$\langle\phi_D^2\rangle_{Av}=G^2\zeta^2\tau^2\gamma^2[(N^3/12n^2)-N/6], \quad (18)$$

or, in the limit of large N, by

$$\langle\phi_D^2\rangle_{Av}=G^2\gamma^2Dt^3/6n^2, \quad (n\neq 0). \quad (19)$$

The effect of interpolating a larger number n of 180° pulses in the interval of duration t is to reduce the mean square phase dispersion by a factor determined

by $1/n^2$. As far as diffusion is concerned, the intensity of the echo at time t is determined by

$$M_{y'}(t)=M_0\int_{-\infty}^{+\infty}\cos\phi_D P(\phi_D)d\phi_D$$
$$=M_0\exp(-\gamma^2G^2Dt^3/12n^2). \quad (20)$$

Thus decay caused by diffusion can theoretically be eliminated by simply making n large enough. If the effect of the natural decay is included we have

$$M_{y'}(t)=M_0\exp[(-t/T_2)+(-\gamma^2G^2Dt^3/12n^2)]. \quad (21)$$

This quantitative theory successfully explains the echo amplitudes obtained in both Method A and Method B. The form of the envelope obtained in Method A is given when $n=1$. There is a difference in numerical factors in the exponent of the above result and the result given by Hahn.[1] Hahn did not take into account the effectiveness of the 180° pulse in partially eliminating the artificial decay caused by the diffusion.

IV. MEASUREMENT OF A DIFFUSION CONSTANT

As an application of the above considerations, the diffusion coefficient of water at 25°C has been measured. To do this Method A was used to observe the decay of the transverse polarization. Water is a suitable sample for such an experiment. This is determined from the values of T_2 and D. For the effect to be pronounced one must require that

$$12/\gamma^2G^2D\leqslant T_2^3. \quad (22)$$

A gradient G may be obtained at the sample by placing symmetrically on either side of the sample two long current carrying wires or two circular turns of wire. The current directions should be such that the fields oppose. It is not sufficient to satisfy the above condition by simply increasing G. One must keep G small enough to insure that the condition $H_1\gg\sigma$ of Sec. I is also satisfied. This implies that our analysis in terms of simple 90° and 180° pulses is applicable. Furthermore, if one uses the value of G calculated from the current in the wires, it is necessary that this G be large compared to the average gradient of the field due to the magnet. To satisfy this condition, it is wise to search for a very homogeneous spot in the magnet.

In our measurements H_1 was the order of 10 gauss. This can be determined by measuring τ_w for a 90° pulse. The average gradient of the field due to the magnet was approximately 0.03 gauss/cm. This value can be determined either from the width of a tail following a 90° pulse, or from a Method A envelope with no current flowing in the parallel wires or the circular turns. Since a typical sample dimension is $\frac{1}{2}$ cm, it can be seen that a gradient the order of $\frac{1}{2}$ gauss/cm would satisfy both of the above conditions relating directly to G. T_2 for water at 25°C has been measured by Method B. Diffusion effects were thus eliminated. T_2 has a value of 2.4 sec. D for water at this temperature is the order of 2×10^{-5} cm²/sec. With this information available it can be seen that condition (22) is also satisfied.

The value of the diffusion constant for water at 25°C as determined by this nuclear resonance method is $2.5(\pm0.3)\times10^{-5}$ cm²/sec. The error which is indicated is the estimated maximum limit of error. This result is in good agreement with previous determinations.[7] The slope of a plot of $\ln(M_{y'}/M_0)+t/T_2$ *vs* t^3 is used to obtain D. Errors in determining this slope introduce the major portion of the uncertainty in the final value of D. For increasing values of the gradient, the experimental curve follows the straight line given by the assumed theory less well. Errors associated with the determination of the slope become greater. A gradient of 0.28 gauss/cm was used in the above determination.

The second important source of error occurs in the determination of the gradient. The gradient may be calculated from the current in the wires and the geometrical dimensions of the circuits. Corrections for the image currents in the pole faces of the magnet must be included. The estimated error in the calculation of the gradient is 2 percent. If one uses two circular turns or rings of current creating opposing fields, the gradient may be made very uniform over the volume of the sample by making the square of the diameter of the rings equal to 4/3 times the square of the ring separation. Such a uniform gradient may be measured quite directly by a second method. This involves the observation of the modulation of a tail following a 90° pulse. For a rectangular sample the tail has a form given by Eq. (6) of Sec. I. For a cylindrical sample the tail has the form

$$M_{y'}=M_0 2J_1(\tfrac{1}{2}\gamma Gdt)/\tfrac{1}{2}\gamma Gdt, \quad (23)$$

where $J_1(\frac{1}{2}\gamma Gdt)$ is the first-order Bessel function and d is the diameter of the sample. The value of G obtained by this method has an estimated maximum limit of error of 5 percent. The values obtained by the two methods agree within experimental error.

It should be noted that this method for measuring the diffusion constant is apt to fail if the echo envelope exhibits modulation.[8] Such modulation is likely to occur if the resonant nucleus interacts with another nucleus of the same species which is in a chemically nonequivalent position in the molecule. It also sometimes occurs when the resonant nucleus interacts with another nucleus of a different species.

All methods for measurement of diffusion depend on somehow "labelling" molecules. To the extent that the "label" has a negligible effect on the diffusion process itself, a method may be said to measure truly the "self-diffusion" constant. In the method here described a molecule is in effect labelled by the direction of the nuclear magnetic moment it carries; a more innocuous label would be difficult to imagine.

[7] W. J. C. Orr and J. A. V. Butler, J. Chem. Soc. **1935**, 1273.
[8] E. L. Hahn and D. E. Maxwell, Phys. Rev. **88**, 1070 (1952).

V. THE EFFECT OF CONVECTION

With any method for measuring the diffusion coefficient, it is desirable to be able to check that convection effects are not present. Fortunately we have such a check readily available here. If convection currents exist, the second echo of Method *B* may be larger than the first echo! This effect is most conspicuous when τ_2, the time between the first and second 180° pulses, is exactly equal to $2\tau_1$, where τ_1 is the time between the 90° pulse and the first 180° pulse. This is illustrated in Fig. 8.

A mathematical explanation of the effect is easily given. Consider the changing phase angle of a group of nuclei which are moving uniformly into larger values of the external field of H_z. For the short distances which the nuclei move in the time between rf pulses, one may assume that the field gradient is linear. Assume that the field increases by h units per unit time. At time τ_1 the net magnetic moment vector of these nuclei will have in the rotating coordinate system a phase angle given by

$$\phi=\int_0^{\tau_1}\gamma(\Delta H_z+ht)dt=\gamma\Delta H_z\tau_1+\tfrac{1}{2}\gamma h\tau_1^2=\phi_0+\phi_C. \quad (24)$$

ϕ_0 is the phase angle which the moment vector would have had if it had remained stationary. However, the vector is out of phase by $\frac{1}{2}\gamma h\tau_1^2$ radians more than ϕ_0. Since this portion of the phase angle is due to convection, it will be denoted by ϕ_C. After a 180° pulse is applied at $t=\tau_1$, the phase angle begins to decrease in magnitude. At time $t=2\tau_1$ the stationary component has been exactly compensated for, and ϕ_0 vanishes. However ϕ_C, being proportional to t^2, has more than compensated for the value it obtained between 0 and τ_1. It now has the value

$$\phi_C=\int_{\tau_1}^{2\tau_1}\gamma htdt-\tfrac{1}{2}\gamma h\tau_1^2=\gamma h\tau_1^2. \quad (25)$$

As time continues, both $|\phi_0|$ and $|\phi_C|$ increase. At time $\tau_1+\tau_2$ just before the second 180° pulse is applied, the value of ϕ_C is given by

$$\phi_C=\int_{\tau_1}^{\tau_1+\tau_2}\gamma htdt-\tfrac{1}{2}\gamma h\tau_1^2=\tfrac{1}{2}\gamma h(\tau_1+\tau_2)^2-\gamma h\tau_1^2. \quad (26)$$

In addition to this, the moment is out of phase by the stationary amount ϕ_0. The second 180° pulse is then applied, and again the phase angles begin to decrease in magnitude. At the time $t=2\tau_2$, ϕ_0 will have been reduced to zero, but the convection will have caused ϕ_C to change by an amount

$$\int_{\tau_1+\tau_2}^{2\tau_2}\gamma htdt=2\gamma h\tau_2^2-\tfrac{1}{2}\gamma h(\tau_1+\tau_2)^2 \quad (27)$$

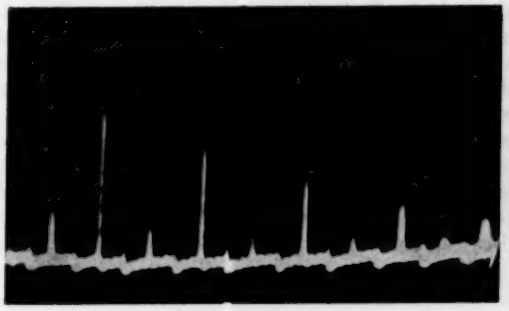

FIG. 8. The effect of molecular convection on a "Method *B*" decay. The odd-numbered echoes are much smaller than the even-numbered echoes.

radians. Thus, at time $t=2\tau_2$, when the second echo normally occurs, the phase of the net magnetic moment will be given by $\varphi=\varphi_0+\varphi_C$, where

$$\varphi_0=0, \quad \varphi_C=\gamma h\tau_2^2-2\gamma h\tau_1\tau_2. \quad (28)$$

It is clear that it is possible to have all moments perfectly reclustered or in phase, at the time of the second echo, if $\tau_2=2\tau_1$. Such perfect reclustering is not possible at the time of the first echo because of the variations in h over the sample. This implies that with $\tau_2=2\tau_1$, the second echo may have a larger amplitude than the first, in agreement with the observed effect. Thus this effect can be used as an indicator of the presence of convection.

VI. A METHOD FOR MEASURING THE LONGITUDINAL RELAXATION TIME

All discussion thus far has dealt with the equatorial or horizontal component of polarization and the associated relaxation time T_2. In conclusion, it will be mentioned that the use of 90° and 180° pulses makes possible a null method for the measurement of the longitudinal or spin-lattice relaxation time of the sample. This type of measurement is initiated by a 180° pulse. The total magnetic moment vector is inverted from the north pole to the south pole of the reference sphere. Because of the spin-lattice relaxation processes, the z component begins to return to its original value. A 90° pulse is then applied at various times τ. For very short values of τ the 90° pulse nutates the total magnetic moment vector of nearly maximum amplitude from the south pole to the equatorial plane. A tail with nearly maximum amplitude follows the 90° pulse. For very large values of τ, compared to the spin-lattice relaxation time, the 90° pulse nutates the reformed total magnetic moment vector of nearly maximum amplitude from the north pole down to the equatorial plane. Again a tail of nearly maximum value follows the 90°pulse. For intermediate values of τ the tails will have smaller amplitudes. For one value in partic-

ular, which will be designated τ_{null}, there will be no tail. Since the system relaxes or returns to equilibrium exponentially with the time constant T_1, it is easily shown that T_1 may be calculated directly from the measured value of τ_{null} by using the relation $\tau_{null} = T_1 \ln 2$. A 180° pulse at $t=\tau+\tau_2$ will cause an echo to be formed at $t=\tau+2\tau_2$. If $2\tau_2 \ll T_2$ this echo may be used as an indicator of the growth of M_z from $-M_0$ to M_0. The inhomogeneity of H_z plays no role in the decay and growth of the longitudinal component of the polarization; diffusion and convection may here be ignored. One precaution must be noted, however. It has been assumed that each sequence of pulses is initiated only after the system has returned to thermal equilibrium. Thus if the above relation is used to compute T_1, the time interval between sequences must be large compared to T_1.

One of the authors (HYC) wishes to acknowledge many beneficial discussions with H. C. Torrey and P. R. Weiss during the latter period of this research.

PHYSICAL REVIEW VOLUME 94, NUMBER 3 MAY 1, 1954

Beta-Ray Spectrum of Ag^{110}

TOSHIO AZUMA
Physics Department, Naniwa University, Mozu, Sakai, Osaka, Japan
(Received January 11, 1954)

The soft beta-ray spectrum of Ag^{110} has been measured by a double coil, magnetic lens beta-ray spectrometer, with a thin source and a thin counter window. From the analysis of the Fermi plot, three soft beta-ray groups of allowed type are found, with end points of 80 kev, 314 kev, and 530 kev. The ratio of their intensities is 10.7:3.2:15.3.

THE decay of Ag^{110} by the emission of three beta rays with end points of 87 kev, 530 kev, and 2.86 Mev, and of many groups of gamma rays, has been reported.[1-8] The difficulties involved in the analysis of these soft beta rays have also been pointed out.

In the present experiments the soft beta-ray spectrum has been measured by using a double coil, magnetic lens beta-ray spectrometer of about 2.0 percent resolving power. The detector consisted of a Geiger counter with a thin Zapon window which will detect electrons of energy 5 kev and higher. The source was prepared from radioactive solutions supplied from Oak Ridge. It has a surface density of not more than 50 $\mu g/cm^2$ on Zapon film of about 30 $\mu g/cm^2$.

The spectrum consists of two low-energy groups of beta rays and many internal conversion lines of 116, 447, 618, 655, 687, 760, 759, 883, and 932 kev gamma rays, which were designated as strong and medium groups;[1] weak groups could not be detected because of the thin sample used in the present work. Since the Fermi plot of the spectrum of the 530-kev beta ray does not fit a straight line but is convex toward the energy axis, we endeavored to fit various shape factors, as given by Konopinski and Uhlenbeck,[9] to these data. The (ft) value of this group is first forbidden. Then, in order to fit the data to a theoretically forbidden shape, it is necessary to multiply the allowed $F(z,w)$ by a certain coefficient C_1, given by Konopinski and Uhlenbeck,[9] and see if the plot $(N/C_1 \cdot F)^{\frac{1}{2}}$ against the total energy gives a straight line. The Fermi plots corrected with the correction factors of $C_{1SV}/|\int \mathbf{r}|^2$ and $C_{1TA}/|\Sigma B_{ij}|^2$ did not fit a straight line. We tried further to fit with various shape factors of second forbidden, $C_{2SV}/|\Sigma R_{ij}|^2$, $C_{2V}/|\Sigma A_{ij}|^2$, $C_{2TA}/|\Sigma S_{ijk}|^2$, $C_{2A}/|\Sigma T_{ij}|^2$, and $C_{2T}/|\Sigma A_{ij}|^2$, where certain values of ΣS_{ijk} and $\Sigma A_{ij}/\Sigma T_{ij}$ are assumed. But none of these corrected Fermi plots gave good results.

Therefore, we assume that the 530-kev beta-ray spectrum is complex, consisting of two groups. The best fit to the data for the Fermi plot is obtained in the energy range $W \geqq 1.60$ with $W_0 = 2.038$, where W is the energy in units of m_0c^2 and W_0 is the maximum energy in units of m_0c^2. The full shape of the 530-kev beta-ray group can be constructed from this straight line in the Fermi plot, which is shown in Fig. 1 as the β_3 group. The differences between the measured and constructed values at each energy give the second beta-ray group which also fit a straight line in the Fermi plot in the energy range $W \geqq 1.23$, with $W_0 = 1.615$. The full shape of this β_2 group can also be constructed from the Fermi plot, as shown in Fig. 1. The remaining soft beta-ray group can also be con-

[1] Cork, Rutledge, Branyan, Stoddard, Childs, and LeBlanc, Phys. Rev. **80**, 286 (1950).
[2] K. Siegbahn, Phys. Rev. **75**, 1277 (1949); **77**, 233 (1950).
[3] F. Maienschein and J. L. Meem, Phys. Rev. **76**, 899 (1949).
[4] W. S. Emmerich and J. D. Kurbatov, Phys. Rev. **75**, 1446 (1949).
[5] W. Rall and R. G. Wilkinson, Phys. Rev. **71**, 321 (1947).
[6] W. C. Kelly, Phys. Rev. **85**, 101 (1952).
[7] Yu, Cheng, and Kurbatov, Phys. Rev. **75**, 1278 (1949).
[8] M. Goldhaber and R. D. Hill, Revs. Modern Phys. **24**, 179 (1952).
[9] E. J. Konopinski and G. E. Uhlenbeck, Phys. Rev. **60**, 308 (1941).

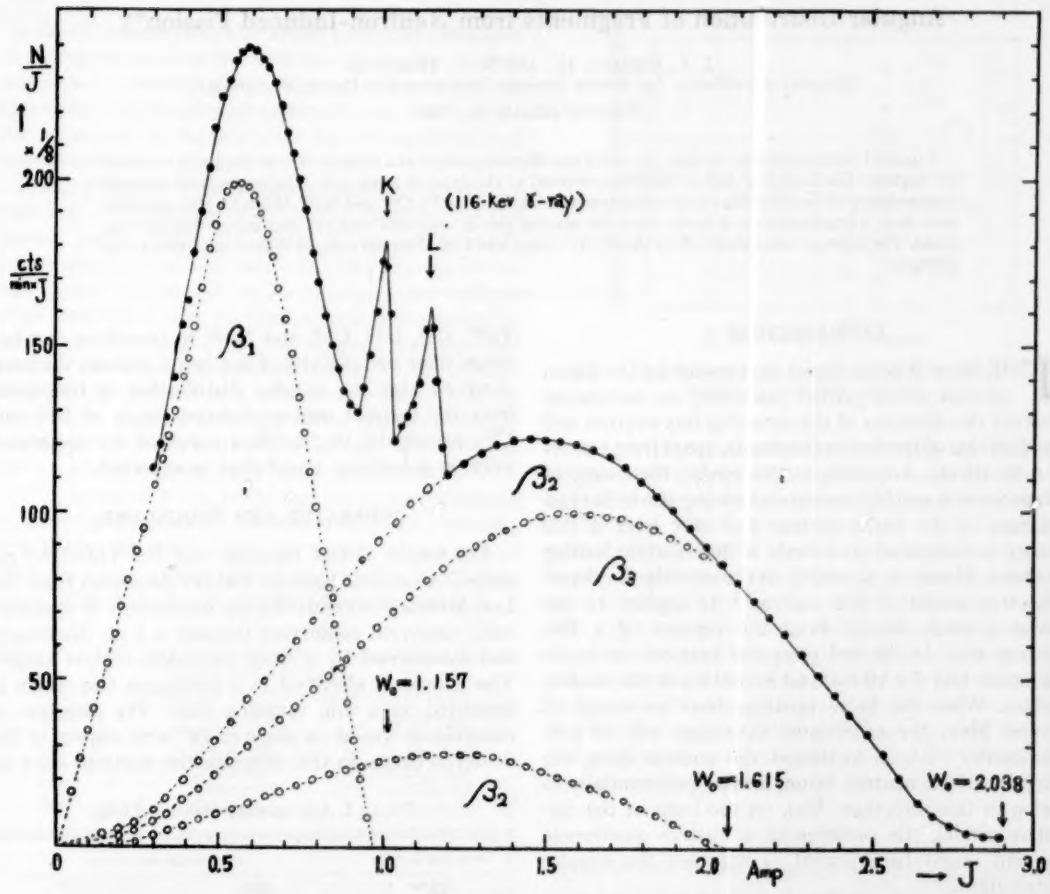

FIG. 1. Beta-ray spectrum of Ag^{110}, where β_1, β_2, and β_3 show the beta-ray groups with end points of 80 kev, 314 kev, and 530 kev, respectively. The full line shows the measured values, and the dotted lines those constructed from the Fermi plot.

structed using the above shapes of the β_2 and β_3 groups, as shown in Fig. 1, which fits a straight line in the Fermi plot with $W_0=1.157$.

In conclusion, three soft beta-ray groups of allowed type are found, with end points of 80 kev, 314 kev, and 530 kev. The ratio of their intensities is measured as 10.7:3.2:15.3. Further investigations will be necessary to determine the decay scheme of Ag^{110}.

This research was supported by the special fund of the Ministry of Education.

Angular Distribution of Fragments from Neutron-Induced Fission*†

J. E. Brolley, Jr., and W. C. Dickinson
University of California, Los Alamos Scientific Laboratory, Los Alamos, New Mexico

(Received January 18, 1954)

A parallel plate ionization chamber, in which one electrode served as a collimator, was employed to study the angular distribution of fission fragments referred to the neutron beam axis. Fragments from neutron bombardment of the following nuclei were examined: Th^{232}, U^{233}, U^{235}, U^{238}, and Np^{237}. When 14-Mev neutrons were used, a preponderance of fission along the neutron axis as compared with the orthogonal direction was noted. The average value obtained for the 0°/90° ratios was 1.26. Thermal neutron fission was found to be isotropic.

INTRODUCTION

THE Bohr-Wheeler liquid drop model[1] for the fission process would predict essentially no correlation between the direction of the incoming fast neutron and the direction of the fission fragments, apart from center-of-mass effects. According to this model, the energy of the neutron is quickly assimilated among the individual nucleons of the fissile nucleus and only later is this energy concentrated on a mode of deformation leading to fission. However, according to the recently developed collective model of the nucleus[2,3] as applied to the fission process, energy from the capture of a fast neutron may be divided promptly between nucleonic excitation and the vibrational excitation of the nuclear surface. When the beam neutrons have an energy of several Mev, the vibrational excitation will be predominantly such as to distort the nucleus along the direction of the neutron beam, leading preferentially to fission in this direction. Also, on the basis of the collective model, the presence of a nuclear quadrupole moment might be expected to influence the angular distribution.

We have measured the angular distribution of the fragments from the 14-Mev neutron-induced fission of Th^{232}, U^{233}, U^{235}, U^{238}, and Np^{237} to provide a test between these two pictures of the fission process. We have observed also the angular distribution of fragments from the thermal neutron-induced fission of U^{233} and U^{235}, principally to provide a check of our apparatus since no anisotropy would then be expected.

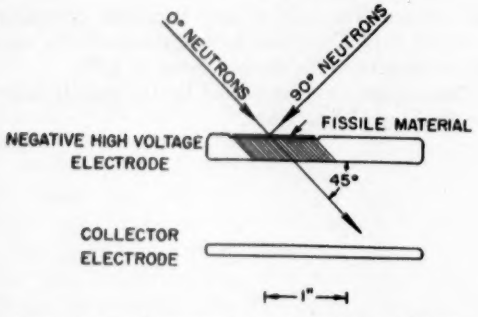

FIG. 1. Schematic representation of the fission chamber.

APPARATUS AND PROCEDURE

The source of fast neutrons was the $T(d,n)He^4$ reaction. An atomic beam of 250-kev deuterons from the Los Alamos Cockcroft-Walton accelerator is magnetically analyzed, collimated through a $\frac{1}{4}$-in. diaphragm and intercepted by a thick zirconium-tritium target. The tritium is absorbed in a zirconium film which is deposited on a thin tungsten disk.[4] The direction of observation was at an angle of 74° with respect to the deuteron beam. In this direction the neutrons have an energy of 14.3±0.1 Mev, assuming a reaction energy of 17.6 Mev for the $T(d,n)He^4$ reaction. A collimated beam of thermal neutrons was obtained from the Los Alamos homogeneous reactor.

TABLE I. Approximate analyses of foils.

Principal isotope	Percentage abundance
Th^{232}	100
U^{233}	96 (balance normal U)
U^{235}	96 ($\frac{1}{4}$% U^{234}, balance U^{238})
U^{238}	100 (16 parts/million U^{235})
Np^{237}	100

A cross section of the fission chamber is shown schematically in Fig. 1. The negative high-voltage electrode served as a collimator for the fission fragments; 0.04-in. holes were drilled on an hexagonal matrix to fill a circle 1 in. in diameter. These passages were inclined 45° with respect to the normal in order that the geometry would be in all essentials identical for the 0° and 90° angular settings. The extreme angular resolution of the collimator was ±6° and the average angle of emission of the fragments with the axis of collimation was 2½°. The foils of fissile material were 1 in. in diameter and at a distance of 6.25 in. from

* This document is based on work performed under the auspices of the U. S. Atomic Energy Commission.

† A preliminary report of these findings was presented at the meeting of the American Physical Society, New York, January, 1953 [Phys. Rev. 90, 388 (1953)].

[1] N. Bohr and J. A. Wheeler, Phys. Rev. 56, 426 (1939).

[2] A. Bohr, Kgl. Danske Videnskab. Selskab, Mat.-fys. Medd. 26, No. 14 (1952).

[3] D. L. Hill and J. A. Wheeler, Phys. Rev. 89, 1102 (1953).

[4] Graves, Rodriguez, Goldblatt, and Meyer, Rev. Sci. Instr. 20, 579 (1949).

the Zr−T target. Since the largest projected dimension of the target seen by the foils was $\frac{5}{16}$ in., the extreme angle that a neutron could make with the target-foil axis was 6° and the average angle with this axis was 3½°. No corrections to the final data due to angular spread were necessary.

A gas filling of 95 percent argon and 5 percent CO_2 was used at a pressure of 45 cm Hg in order that the fastest fission fragments would be stopped shortly before reaching the collector. A field of 118 volts per cm was applied between plates, no attempt being made to attain saturation. The rise time of the electron collection pulses was about 0.5 μsec. The chamber was mounted so that it could be rotated by means of an indexed rotary table about an axis containing a diameter of the fissile layer. Angular error of position probably did not exceed 0.5°. For the fast neutron studies with U^{233} and U^{235} a cadmium jacket surrounded the chamber.

Thin layers of ThO_2, U_3O_8, and NpO_2 were prepared by painting solutions of the nitrates on 0.01-in. Pt disks and baking at 800°C until the oxides were formed.[5] Deposits ranging from 100 μg/cm² to 5 mg/cm² were used. Table I gives approximate analyses of the foils.

TABLE II. 0°/90° fission intensity ratios (center-of-mass system) for 14-Mev neutrons.

Isotope	Type	0°/90° ratio
U^{233}	Even-odd	1.32±0.05
U^{235}	Even-odd	1.27±0.08
U^{238}	Even-even	1.31±0.05
Np^{237}	Odd-even	1.15±0.04

A preamplifier with cathode follower output was attached to the back of the fission chamber so as to form a shielded unit. Fission pulses from a linear pulse amplifier with rise time of 0.5 μsec and *RC* clipping time of 2 μsec were fed to two scalers. The discriminator setting of one scaler was such as to accept all fission pulses while that of the second scaler was such as to accept principally only pulses due to the higher energy (light) fragments. In this way it was hoped that angular distributions could also be obtained for the light fragments alone. However, later work with an 18 channel pulse-height analyzer indicated that the two fission ionization peaks were not sufficiently separated to make this feasible.

For each foil an integral bias curve was first taken to determine discriminator settings.[6] About 500 counts were then taken at each angular setting and this was repeated until adequate counts were accumulated.

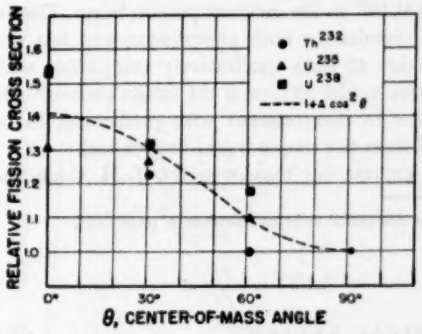

FIG. 2. Angular distribution of fragments from the 14-Mev fission of Th^{232}, U^{235}, and U^{238}.

The integrated fast neutron flux was monitored by counting a known fraction of the alpha particles generated in the d+T reaction by means of a proportional counter mounted 22 in. from the target in a geometry permitting a view of the entire target area. Also a long counter directly monitored the neutron flux. Since in some instances the ratio of the counts in these two counters fluctuated by as much as 2 percent, the alpha counter was always used as the standard monitor. The thermal neutron flux from the homogeneous reactor was maintained at a constant value within 0.5 percent throughout the measurements.

RESULTS

The 0°/90° fission intensity ratios for thermal neutrons on U^{233} and U^{235} were determined to be 1.00±0.04 and 0.99±0.05, respectively.[7] The intensity measured at 45° was no different within statistical error from that at 0°.

Table II gives the 0°/90° fission intensity ratios as measured for 14-Mev neutrons. In all cases foils of 1 mg/cm² or thinner were used.[8] Angular distributions with points at 0°, 30°, 60°, and 90° were taken for Th^{232}, U^{235}, and U^{238} using 5-mg/cm² foils. The experimental points are plotted in Fig. 2. Although these measurements are of a more qualitative nature it is seen from Fig. 2 that a curve of the form $1+A\cos^2\theta$ satisfactorily fits the points, where θ is the angle between the fragment direction and the neutron beam.

Winhold, Demos, and Halpern[9] have measured the angular distribution of fission fragments in the 16-Mev photofission of Th^{232} and found a $(1+A\sin^2\theta)$ dependence corresponding to a higher intensity of frag-

[5] We are indebted to Dr. John Povelites of this laboratory for the preparation of the foils.

[6] Because of the center-of-mass effect for 14-Mev neutrons, a fission fragment emitted at 90° has about 3½ percent less energy than if it were emitted at 0°. The rather large energy loss of the fragments in the collimator of the fission chamber results in a magnification of this effect. Thus, for a 1-mg/cm² foil, the ionization peaks were observed to shift downward about 10 percent going from the 0° to the 90° angular setting. The lower discriminator setting was always such as to count essentially all fragments at both angular settings.

[7] Errors quoted in this paper are standard deviations resulting from statistics only. Systematic errors are thought to be small by comparison.

[8] Anisotropy of about the same amount was observed for Th^{232} but because of the necessity of using a 5 mg/cm² foil to boost the counting rate we do not at present quote a 0°/90° intensity ratio for this isotope.

[9] Winhold, Demos, and Halpern, Phys. Rev. **87**, 1139 (1952).

ments at 90° to the incident photon beam. The experimental results for both photofission and fast neutron fission are at least qualitatively compatible with the collective model picture of the fission process[10] whereas they are in disagreement with predictions to be obtained from the simple liquid drop model.

We express our thanks to Dr. J. H. Coon and the Los Alamos Cockcroft-Walton group for making available to us their accelerator and necessary auxiliary equipment required to monitor the neutron beam. We also thank the Los Alamos homogeneous reactor group for the use of their reactor. We are indebted to Dr. Keith Boyer for suggesting the type of collimator used in these experiments and to Dr. D. L. Hill for several stimulating interpretative discussions on the subject of the collective model.

[10] For discussion refer to reference 3, page 1116.

PHYSICAL REVIEW VOLUME 94, NUMBER 3 MAY 1, 1954

Inner Bremsstrahlung of Cs^{131}†

BABULAL SARAF*
Bartol Research Foundation of The Franklin Institute, Swarthmore, Pennsylvania
(Received January 13, 1954)

The continuous gamma-ray spectrum (inner bremsstrahlung), accompanying orbital electron capture in Cs^{131}, has been observed by the method of scintillation spectrometry. The absolute intensity of the gamma radiation has been measured and compared with the total disintegration rate. The end point of the gamma-ray distribution was found to be 320±10 kev. The experimentally determined shape of the spectrum, as well as the intensity of the continuum, is compared with theoretical calculations. The disagreement exceeds considerably that which might be expected from a consideration of the probable errors of the observations. The growth of the 12-day isomer of Xe^{131} was not detected.

INTRODUCTION

THE continuous gamma radiation (inner bremsstrahlung) associated with the electron capture process was first investigated theoretically by Morrison and Schiff.[1] More recently, Jauch[2] has reviewed and extended the earlier studies. In addition to experimental comparisons of the spectral distributions which have been computed theoretically, this particular disintegration process can also provide information concerning the disintegration energy released in electron capture.

The gamma-ray continuum has been previously detected,[3–7] and the spectral distributions determined for the cases of Fe^{55}, A^{37}, and Ge^{71}. However, it appears that the extent of gamma-ray emission per disintegration has not been measured for any of the above-cited examples. The radioactive chain $Ba^{131} \rightarrow Cs^{131} \rightarrow Xe^{131}$ was first reported by Yu, Gideon, and Kurbatov.[8] The results of several subsequent investigations showed that neither gamma rays nor conversion electrons are emitted.[9–11] Cheng and Kurbatov[12] have reported the growth of the 12-day Xe^{131m} from Cs^{131}, whereas Canada and Mitchell[13] obtained a contrary result. To study the properties of the inner bremsstrahlung and to investigate further the possible formation of Xe^{131m}, the radiations of Cs^{131} have been reinvestigated.

CHEMICAL PROCEDURE

Eighty-eight grams of $Ba(NO_3)_2$ were exposed to neutrons in the Oak Ridge pile for a period of four weeks. From an aqueous solution of this $Ba(NO_3)_2$ with its cesium daughter element, $BaCl_2 \cdot H_2O$ was precipitated by ether and HCl, thus removing barium alone. Small portions of inactive $Ba(NO_3)_2$ were repeatedly added and precipitated as $BaCl_2 \cdot H_2O$ to extract all of the active barium from the cesium solution. The cesium solution was evaporated to small volume and again scavenged by $BaCl_2 \cdot H_2O$ precipitation. Finally, after adding approximately one milligram of cesium carrier—$CsClO_4$ was precipitated.

The first separation of cesium from the neutron irradiated barium disclosed the presence of a 660-kev gamma ray in the cesium fraction which decayed with a half-period of approximately seven days and may, therefore, be associated[14] with Cs^{132}.

† Assisted by the joint program of the U. S. Office of Naval Research and the U. S. Atomic Energy Commission.
* Research Fellow, Bartol; on leave of absence from Agra College, Agra, India.
[1] P. Morrison and L. I. Schiff, Phys. Rev. **58**, 24 (1940).
[2] J. M. Jauch, Oak Ridge National Laboratory Report ORNL-1102, 1951 (unpublished).
[3] H. Bradt *et al.*, Helv. Phys. Acta **19**, 222 (1946).
[4] Bell, Jauch, and Cassidy, Science **115**, 12 (1952).
[5] D. Maeder and P. Preiswerk, Phys. Rev. **84**, 595 (1951).
[6] C. A. Anderson and G. W. Wheeler, Phys. Rev. **90**, 606 (1953).
[7] Saraf, Varma, and Mandeville, Phys. Rev. **91**, 1216 (1953).
[8] Yu, Gideon, and Kurbatov, Phys. Rev. **71**, 382 (1947).
[9] S. Kotcoff, Phys. Rev. **72**, 1160 (1947).
[10] E. Kondaiah, Arkiv Fysik **2**, 295 (1951).
[11] R. Canada and A. C. G. Mitchell, Phys. Rev. **83**, 76 (1951).
[12] L. S. Cheng and J. D. Kurbatov, Phys. Rev. **78**, 319 (1950).
[13] R. Canada and A. C. G. Mitchell, Phys. Rev. **81**, 382 (1947).
[14] L. M. Langer and G. Ford (unpublished).

In order to remove all traces of Cs^{132}, about 20 mg of cesium was added to the barium solution and precipitated as the perchlorate. Cs^{131} was then allowed to grow from the Ba^{131}. After 10 days the barium was precipitated as $BaCl_2 \cdot H_2O$ and pure carrier-free Cs^{131} was obtained from the supernatant liquid by evaporation with H_2SO_4. The residue was heated with $(NH_4)_2CO_3$ to remove excess H_2SO_4. The source was prepared by evaporation of $CsSO_4$ solution on a thin Formvar film over a circular area of 5-mm diameter.

EXPERIMENTAL PROCEDURE

In Fig. 1 is shown the experimental arrangement for measurement of the gamma-ray spectrum. The crystal detector of NaI-Tl was cylindrical in shape, 3.5 cm in diameter and 3.5 cm in height. Because of the low intensity of the effect, it was not possible to collimate the beam of gamma rays by the introduction of a slit system or by increasing the distance between the source and the crystal. In the present investigation, the distance between the source and the top of the crystal was 1.25 cm. The scintillation spectrometer was calibrated by gamma rays of energies 70, 157, and 209 kev emitted from Au^{199}, 280 kev from Hg^{203}, 320 kev from Cr^{51}, and 662 kev from Cs^{137}. The pulse heights were found to be linear with energy over the above-indicated region of energy. The energy resolution (full width of the photopeak at half-maximum) for the 662-kev gamma ray of Cs^{137} was eight percent. The intensity of the inner bremsstrahlung is several orders of magnitude less than that of the 30-kev x-rays of Xe^{131} which are emitted after K capture in Cs^{131}. With the source in close proximity to the crystal, there was the strong possibility of "pile up" of the voltage pulses associated with the intense x-rays. This x-ray intensity was suppressed by placing copper absorbers between the source and the sodium iodide crystal. As shown in Fig. 2, the gamma-ray spectrum was recorded through several different thicknesses of the x-ray absorbing copper. A channel width of 1 volt (13.3 kev) was used. Below 150 kev counts were recorded at energy intervals of one-half volt.

To determine the probability per disintegration of emission of a gamma ray of the continuum, it was

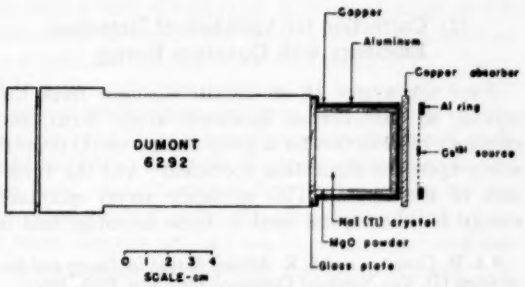

FIG. 1. Experimental arrangement for detection of the continuous gamma-ray spectrum.

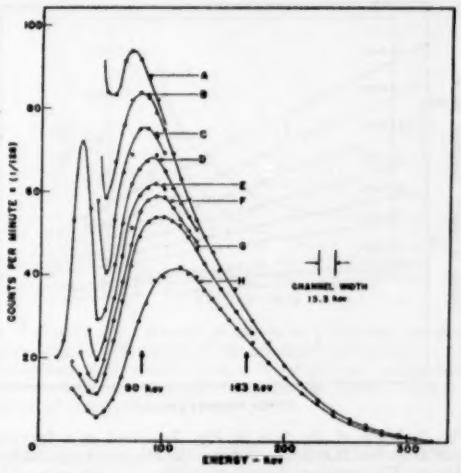

FIG. 2. Gamma-ray spectrum with various intervening amounts of copper absorber: $A = 710$ mg/cm²; $B = 840$ mg/cm²; $C = 970$ mg/cm²; $D = 1100$ mg/cm²; $E = 1230$ mg/cm²; $F = 1360$ mg/cm²; $G = 1490$ mg/cm²; $H = 2200$ mg/cm².

necessary to have an estimate of the strength of the source of Cs^{131}. To obtain an estimate of the number of disintegrations per second occurring in the source, the $CsSO_4$ previously used for observation of the quantum continuum was dissolved in 5 cc of H_2O. Of this solution, 0.1 cc was further diluted to 5-cc volume, and 0.02 cc of this amount was dried over a thin Formvar film to cover an area of 0.5 cm². This source was mounted upon a second crystal of NaI-Tl, 1.5 cm in diameter, and of thickness 0.64 cm. The amount of absorber intervening between source and crystal was 3 mg/cm² of aluminum. Pulses of such height as to correspond to a quantum energy of 30 kev were counted. In computing the absolute intensity of the x-radiation and hence the source strength, the solid angle was estimated to be fifty percent, and the intrinsic efficiency of detection in the crystal was taken to be one-hundred percent. Because the results of the measurement of the fluorescence yield of xenon have been at variance, the theoretical value,[15] calculated nonrelativistically, has been used.

The copper for absorption of the x-radiation is, of course, also effective in absorbing the continuum of gamma rays under study. In addition to this absorption, Compton scattering in the copper may result in the appearance at low energies of a contribution from regions of the spectrum of much higher energy. Similarly, Compton scattering in the crystal itself and subsequent escape of the recoil photons can also distort the spectral distribution.

In order to ascertain the extent of these several effects, the absorption curves of Fig. 3 were obtained from the data of Fig. 2. The counting rate in a channel

[15] E. H. S. Burhop, *Auger Effect* (Cambridge University Press, Cambridge, 1952), p. 45.

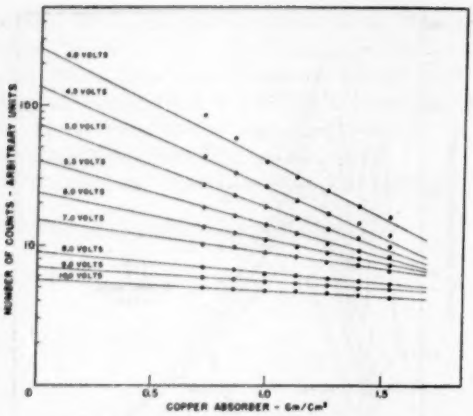

FIG. 3. Some of the data of Fig. 2 plotted as a function of copper absorber thickness at given quantum energies along the continum. The corresponding energy values are 4.0 volts—54 kev, 4.5 volts—60.5 kev, 5.0 volts—67 kev, 5.5 volts—73.5 kev, 6.0 volts—80 kev, 7.0 volts—94 kev.

width of one volt at various different pulse-height settings is plotted as a function of copper absorber thickness. From the apparent linearity of the absorption curves on the semilogarithmic plot, it is concluded that the aforementioned effects are small. Finally, extrapolation of the curves to zero absorber thickness removes any nonuniformities introduced by the variation along the spectrum of the absorption coefficient of copper.

To show further that the counting rate at each pulse height arose primarily from the total absorption in the crystal of gamma radiation of the proper corresponding energy, the half-value thickness of the counting rates at several different pulse heights of Fig. 3 are shown in Table I. It is to be noted that these comparisons are confined to the region of lower energies, where Compton scattering contributions from gamma rays of higher energy are larger than in any other part of the spectrum. The observed half-value thicknesses are compared with those for monoenergetic radiations as given by Compton and Allison.[16] The relatively good agreement between the observed and expected values of the half-thicknesses shows that any distortion of the low-energy region of the spectrum by the Compton effect at higher energies is at most a few percent.

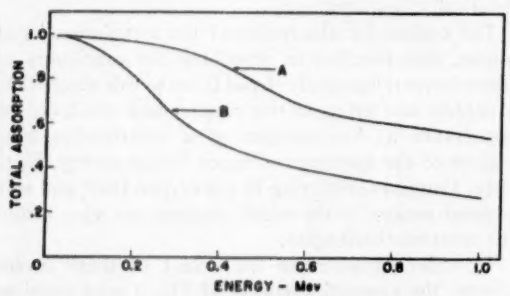

FIG. 4. Efficiency of detection as a function of energy calculated from the total absorption coefficient. Curve *A*, for gamma radiation at normal incidence relative to the face of the crystal. Curve *B*, source distance 1.25 cm from crystal surface.

In order to evaluate the counting rates at the pulse heights corresponding to low energies as shown in Fig. 3, the counting rates were extrapolated to zero absorber thickness at all points of the spectrum. The experimentally measured spectrum thus obtained is compared, after making a suitable resolution correction with the theoretically expected distribution. Before making the final comparison, however, the theoretical distribution was altered to take into account (1) variation of detection efficiency with quantum energy; (2) distortion arising from contributions to the spectrum of the Compton effect; and (3) escape, from the crystal of the x-rays of iodine.

THE CORRECTIONS

The experimental curve obtained by the extrapolation process is corrected for finite resolution by applying the following expression:[17]

$$N_c(E)=N_e(E)-KN_e'(E)-\tfrac{1}{2}KEN''(E),$$

where $N_c(E)$ is the corrected energy distribution, and $N_e(E)$ is the experimentally observed distribution. $N'(E)$ and $N''(E)$ are the first and second derivatives of $N_e(E)$; $K=[W(E)]^2/(0.693\times 2E)$, where $W(E)$ is the half-width at half-maximum of a photopeak produced by radiation of energy E.

TABLE I. Half-value thicknesses of the counting rates for several different pulse heights.

Pulse height—volts	4.0	4.5	5.0	5.5	6.0	7.0
Channel width—volts	1.0	1.0	1.0	1.0	1.0	1.0
Energy—kev	54	60.5	67	73.5	80	94
Half-thickness in Cu—mg/cm² (Compton and Allison)	325	430	540	655	900	1300
Half-thickness in Cu—mg/cm² (These measurements)	290	400	520	630	850	1200

As stated in the previous section, the theoretical distribution was subjected to three corrections before comparison with experiment. These corrections are:

(1) Correction for Variation of Detection Efficiency with Quantum Energy

Were the source at an infinite distance from the crystal, so that normal incidence would occur, the efficiency of detection for a given energy would depend solely upon the absorption coefficient[18] and the thickness of the crystal. This efficiency *versus* quantum energy for the crystal used in these investigations is

[16] A. H. Compton and S. K. Allison, *X-rays in Theory and Experiment* (D. Van Nostrand Company, Inc., New York, 1935).
[17] T. B. Novey, Phys. Rev. 89, 672 (1953).
[18] W. H. Jordon, Ann. Rev. Nuc. Sci. 2, 221 (1952).

shown in Fig. 4, curve A. This curve is to be compared with curve B where the actual source distance of 1.25 cm is taken into account. In calculating curve B, it was assumed, as is the case, that the entire face of the crystal is under irradiation.

(2) Correction for Presence of Compton Effect

When monochromatic radiation is incident upon a crystal of NaI-Tl, a peak of pulses appears which corresponds to a loss of all the quantum energy in the crystal. Because of the escape of the recoil photon, the Compton effect leads to a distribution of pulse heights, extending from zero to a certain maximum value. Figure 5 shows the percentage of all the pulses generated in the NaI-Tl crystal which falls in the peak corresponding to total absorption of the quantum energy. Curve B is a plot of the ratio of the photoelectric absorption coefficient to the total absorption coefficient. Curve A is the measured ratio of the counts in the peak corresponding to total energy loss to the total number of counts. Curve A was obtained from observations on a series of monochromatic gamma-ray sources.

(3) Correction for Escape of the X-Radiation of Iodine

Because of the rapid absorption of the softer gamma rays of the continuum in NaI(Tl), the probability of escape of the associated x-rays of iodine is greater at the lower spectral energies; that is, since the soft gamma rays of the continuum are almost totally absorbed in a thin layer of NaI(Tl) at the surface of the crystal, the chance of escape of the x-rays from the same thin layer is great. At 33.7 kev, the K-absorption edge of iodine, the escape probability is at a maximum. This escape correction has been calculated by Novey.[17]

The theoretical distribution is plotted as curve A in Fig. 6 according to the equation[1,2]

$$\frac{dP}{P_0}=\frac{\alpha}{\pi(mc^2)^2}\left(1-\frac{E}{E_0}\right)^2 EdE,$$

where P_0 is the total number of disintegrations per unit time, dP the probability of photon emission of energy between E and $E+dE$, and E_0 the end point of the gamma-ray spectrum. The electron rest mass is denoted by m, and α is the fine structure constant 1/137. Curve B is a plot of curve A corrected for variation with energy of the detection efficiency, paragraph (1) above. Curves C and D show how the counts of curve B must be redistributed between total-energy absorption on the one hand, and Compton effect and x-ray escape on the other, curve D being the sum of the contributions at lower energies arising from Compton effect and the x-ray escape process. Curve E, the sum of curves C and D, is the expected experimental curve, if the initially assumed theoretical distribution is correct.

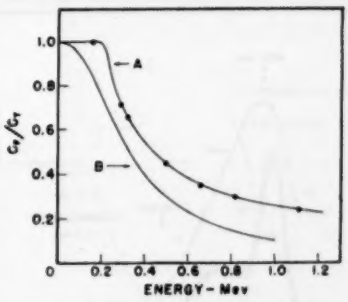

FIG. 5. Curve A—Fraction of pulses as a function of energy corresponding to absorption of the photons' full energy; C_P/C_T experimentally determined. Curve B—Ratio of photoelectric absorption coefficient to total absorption coefficient for NaI as a function of quantum energy.

SEARCH FOR MONOENERGIC GAMMA RAYS FROM Cs^{131}

It is evident that were any monoenergic nuclear gamma rays present in the decay of Cs^{131}, they would severely distort the continuous spectrum, or if having any appreciable intensity, might completely overwhelm the faint radiation of the continuum. The measured distribution of gamma rays from Cs^{131} shown in Fig. 2 gives an end point at 320±10 kev. From a consideration of the decay scheme[19] of $I^{131} \xrightarrow{\beta} Xe^{131}$, it appears that this disintegration energy is sufficient to excite levels in Xe^{131} which on deexcitation would emit gamma rays of energies 163 kev and 80 kev.

Althouth no real evidence for the presence of monochromatic radiation of energy 80 kev appears on the curves of Fig. 2, further measurements were performed to place an upper limit on its intensity. The radiation of the continuum was absorbed in platinum and gold as

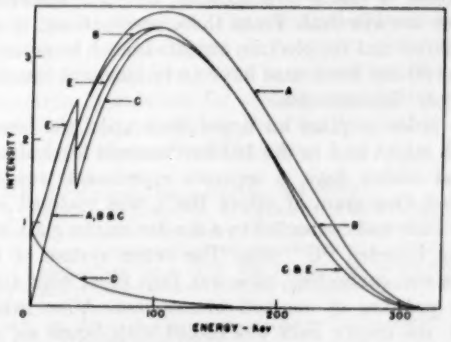

FIG. 6. Calculated energy distribution. A—Theoretical spectrum. B—Modified for detection efficiency. C—Distribution of pulses corresponding to absorption of full energy of the photon. D—Counting rate arising from escape of Compton recoil photons and iodine x-rays. E—Sum of contributions of curves C and D, the expected distribution calculated from theory and altered to take into account experimental conditions.

[19] M. Goldhaber and R. D. Hill, Revs. Modern Phys. 24, 216 (1952).

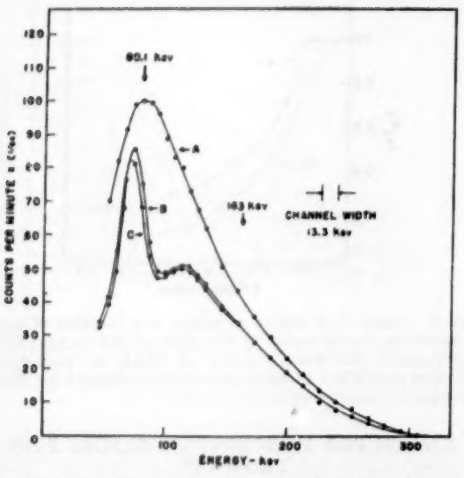

FIG. 7. Absorption of the continuous spectrum in copper, copper and gold, and copper and platinum. Curve A—860 mg/cm² Cu. Curve B—860 mg/cm² Cu+107 mg/cm² Au. Curve C—860 mg/cm² Cu+97 mg/cm² Pt. Gold and platinum foils were placed above the copper which was immediately over the canned crystal.

shown in Fig. 7. The K-absorption edge of Au occurs at 80.5 kev and that of Pt at 78.1 kev. The energy of the sought for gamma ray is accurately known by crystal spectrometer measurements[20] to be 80.133 Kev; therefore, the radiation would be more heavily absorbed in Pt than in Au. In particular, in the case of the experiments of Fig. 7, the counting rate at 80 kev would have been reduced by approximately 16 percent in the case of Au and 50 percent for Pt. Examination of the curves of Fig. 7 shows this not to be the case. The absorption in Au is slightly less than that in Pt, because the gold foil (97.5 mg/cm²) was somewhat thinner than the platinum one (107.5 mg/cm²). When this difference in thickness is taken into account, the two absorption curves are identical. From these observations, it was estimated that the electron capture branch terminating at the 80-kev level must have an incidence of less than 10^{-7} per disintegration.

In order to place an upper limit upon the branch which might lead to the 163-kev isomeric level of half-period twelve days, a separate experiment was performed. One gram of active $BaCl_2$ was enclosed in a glass bulb and connected to a similar empty glass bulb by an inverted "U" tube. The entire system of two bulbs and connecting tube was then filled with argon to a pressure of one-half atmosphere. After twenty days, the empty bulb was cooled with liquid air and the $BaCl_2$ was heated to 100°C. This process was repeated several times to insure transfer to the empty bulb of any Xe grown from Ba-Cs. The bulb containing any Xe was then sealed off and examined with the scintillation spectrometer. No evidence of a gamma ray at 163 kev was obtained. Taking into account the source-strength, the time of growth, the detection efficiency, and the conversion coefficient of the 163-kev gamma ray, the upper limit for formation of the 12-day metastable state was estimated to be 10^{-10} per disintegration.

[20] Lind, Brown, Klein, Muller, and Dumond, Phys. Rev. **75**, 1544 (1949).

DISCUSSION OF RESULTS

The end point of the continuous gamma-ray spectrum of Cs^{131} occurs at 320±10 kev; therefore, the disintegration energy of Cs^{131} or the mass difference of Cs^{131} and Xe^{131} is 353±10 kev (taking the binding energy of K electron to be 33 kev).

According to the shell model of the nucleus, the orbital of the ground state of Cs^{131} is $d_{\frac{1}{2}}$. This value has been observed in a recent experimental measurement.[21] The residual nucleus, Xe^{131}, is also the decay product of the 8-day I^{131}. From a study of the gamma rays of I^{131}, orbitals of the first two excited states of Xe^{131} have been obtained.[19] The ground state orbital of Xe^{131} has been measured.[19] The spin and parity assignments are summarized in Fig. 8.

Log ft for the electron-capture transition terminating at the ground state of Xe^{131} has been calculated from the currently reported energy measurement and is 5.3. In terms of the two measured ground-state orbitals, the transition may be described as having the selection rules $d_{\frac{1}{2}} \rightarrow d_{\frac{1}{2}}$, $\Delta I = 1$; No. These are the properties of an allowed transition if G-T selection rules are followed. If classified according to Mayer, Moszkowski, and Nordheim,[22] the measured value of log ft does indeed correspond to an allowed transition.

Transitions leading to the 80-kev and 163-kev levels would produce changes in quantum numbers given by $d_{\frac{1}{2}} \rightarrow s_{\frac{1}{2}}$, $\Delta I = 2$; No, and $d_{\frac{1}{2}} \rightarrow h_{11/2}$, $\Delta I = 3$; Yes, respectively, which transitions would, according to G-T rules, be second and third forbidden. Values of log ft calculated from upper limits of the intensities of these transitions are about 12 and 15, corresponding[21] to the respective degrees of forbiddance indicated by the selection rules.

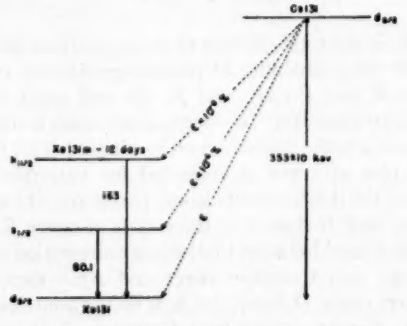

FIG. 8. Disintegration scheme of Cs^{131}.

[21] E. H. Ballamy and K. F. Smith, Phil. Mag. **44**, 33 (1953).
[22] Mayer, Moszkowski, and Nordheim, Revs. Modern Phys. **23**, 317 (1951).

The experimentally observed probability of emission of the inner bremsstrahlung is shown in Fig. 9 where it is compared with the theoretically expected result (see curve *E*, Fig. 6). The emission propability per disintegration is plotted in either case; the experimental points are determined as in Fig. 3 by extrapolation of the counting rate at each pulse-height setting to zero copper absorber thickness. Because of various experimental uncertainties in source strength determination, etc., the ordinates of the experimental curve are thought to be in error by as much as fifteen percent. Below 150 kev, because of uncertainties in extrapolation of the counting rates to zero copper absorber thickness, an additional experimental error of perhaps ten percent is thought to be present.

From Fig. 9, it is evident that below 150 kev the discrepancy between experiment and theory becomes too large to be explained by even the liberal estimates of error given above. Because of this sharp disagreement, the question of the purity of the source arises. Evidence for source purity may be cited as follows:

(1) The ratio of the intensity of gamma rays to that of x-rays remained constant over four half-periods of decay of Cs^{131}.

(2) The gamma-ray continuum followed the chemistry of cesium.

(3) The cesium sources were prepared by "milking" barium repeatedly. Each freshly prepared source of cesium exhibited the same gamma-ray continuum.

It should, perhaps, also be mentioned that when a source of cesium was mounted adjacent to a crystal with only 3 mg/cm² of aluminum intervening, no charged particles (conversion electrons or beta rays) could be detected. A similar search with a thin-walled Geiger counter likewise yielded no effect.

It is, at the moment, difficult to postulate any definite explanation for the disagreement between experiment and theory. The early theoretical considerations of Morrison and Schiff[1] did not include the effects of the *K*-shell binding energy. The calculations applied only to "low *Z*" nuclei. The effects of possible *L* capture were also neglected. In a private communication, Jauch has given the correction factor for the effect of binding energy to be

$$C=\frac{1+(1+\delta)^2}{2(1+\delta)^2},$$

where δ=binding energy/quantum energy. However, this factor is found to decrease the probability of emission at lower energies and, therefore, enhance rather than decrease the extent of disagreement between

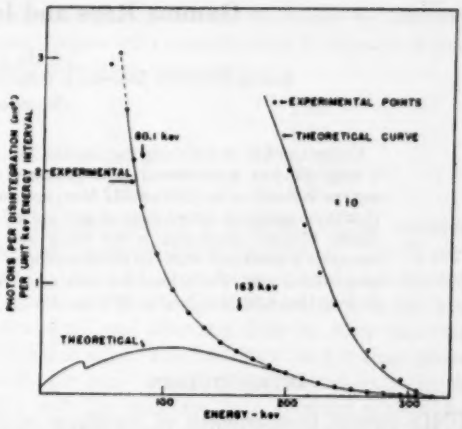

FIG. 9. Photon emission probability per disintegration per unit energy interval (1 kev). The broken portion of the experimental curve is uncertain.

experiment and theory. According to a formula given by Marshak,[23] L_I capture occurs in 13.6 percent of the disintegrations and L_{II} capture is one percent. The gamma-ray emission probability associated with *L*-electron capture has not been studied theoretically in great detail.‡

Bremsstrahlung effects relating to the magnetic moment of the emitted neutrino have recently been discussed.[24,25] However, the order of magnitude of the effect has not been accurately estimated.

ACKNOWLEDGMENT

The writer wishes to express his appreciation to Dr. C. E. Mandeville for having originally suggested this research problem and for lending encouragement. He also wishes to acknowledge the many valuable suggestions of Dr. F. R. Metzger, as well as discussions with Dr. L. Eisenbud. The chemical separations were performed by Dr. Walter B. Keighton of Swarthmore College. Finally, the writer is grateful to The Bartol Research Foundation for making possible his stay in the United States and to the Director, Dr. W. F. G. Swann, for his continued interest.

[23] R. A. Marshak, Phys. Rev. **61**, 431 (1942).

‡ *Note added in proof.*—R. E. Cutkosky (Ph.D. thesis, Carnegie Institute of Technology, May, 1953) has calculated the intensity of the inner bremsstrahlung associated with the capture of the *s* and *p* electrons of the *L* shell. The calculations indicate an intensity which is too small to account for the disagreement with theory found in the present measurements.

[24] P. M. Endt, Report of Birmingham Conference on Nuclear Physics, page 29, July, 1953.

[25] J. Weneser, Phys. Rev. **91**, 1025 (1953).

Gamma Rays and Internal Pairs from Be^9+H^1

R. J. MACKIN, JR.*
Kellogg Radiation Laboratory, California Institute of Technology, Pasadena, California
(Received January 29, 1954)

Gamma radiation following the reaction $Be^9(p,\alpha)Li^{6*}$, resonant at $E_p=2.56$ Mev, has been studied with a magnetic lens spectrometer. The gamma-ray energy, determined from photo- and Compton-electron spectra, is found to be 3.572 ± 0.012 Mev, not corrected for a possible 26-kev Doppler shift. The internal pair (positron) spectrum agrees most closely (to 4.5 percent) with the assignment of the radiation as magnetic dipole. Electric quadrupole is less likely and all other assignments are excluded. The magnetic-dipole character is consistent with the identification of the 3.57-Mev level of Li^6 as the analog of the He^6 ground state with $J=0^+$, $T=1$. Reaction data are analyzed to suggest that the resonant state of the compound nucleus (the 8.89-Mev level of B^{10}) has $J=2^+$, $T=1$.

INTRODUCTION

THE proton bombardment of beryllium exhibits resonance at 2.565 Mev for neutrons,[1,2] 3.58 $\pm$0.04-Mev gamma rays,[1,3] and gamma rays of energy greater than 6 Mev.[2] Day and Walker[3] have shown by observations of $\alpha-\gamma$ coincidences that the intense 3.58-Mev gamma rays follow the reaction $Be^9(p,\alpha)Li^{6*}$. As they point out, such a large gamma-ray yield from a level of Li^6 more than 2 Mev above the energy necessary for dissociation into He^4+H^2 implies the operation of a selection rule which inhibits that mode of disintegration. For instance, if the state is characterized by angular momentum $J=0$, even parity, or by isotopic spin $T=1$, the particle decay is forbidden. This paper presents new measurements on the gamma radiation and evidence from internal conversion pairs which supports the angular momentum assignment for the level.

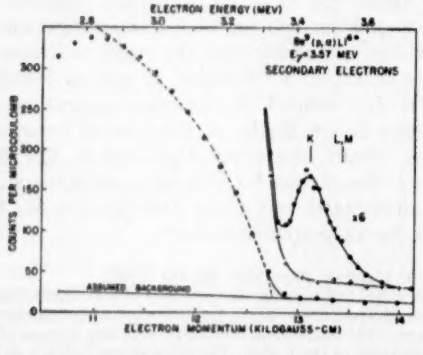

FIG. 1. Secondary Compton and photoelectric spectra from $Be^9(p,\alpha\gamma)Li^6$ at 2.72-Mev bombarding energy. Target thickness was 19 mg/cm². The Compton spectrum (dashed curve) was produced in 350 mg/cm² Al and the photopeak (ordinate multiplied by 6) in additional 23 mg/cm² Th.

EXPERIMENTAL METHOD AND RESULTS

A magnetic lens spectrometer, previously described,[4] was used with 1.9 percent resolution to study secondary electrons from gamma radiation produced by the proton bombardment of beryllium. A beam of magnetically analyzed protons from a 3-Mev electrostatic accelerator entered along the spectrometer axis to bombard a Be disk at the focal point. The beam current was measured with a current integrator accurate to about one percent, and the total gamma-ray yield at 90° was monitored with a shielded Geiger counter. The detector of focused electrons was a scintillation counter employing a *trans*-stilbene crystal. The RCA 5819 photomultiplier was shielded from the magnetic field of the spectrometer by a solenoid.[5] This detector presented the advantage of reducing background by discriminating against low-energy scattered electrons.

Figure 1 shows the Compton electron spectrum produced in a 350-mg/cm² Al converter located immediately behind the target. The dashed curve is the theoretical spectrum from an "infinitely thick" converter [reference 6, Eq. (11)] for a yield of $4.63\times10^{-6}\gamma/p$ ($E_p=2.72$ Mev). Day and Walker[3] reported $4.76\times10^{-6}\gamma/p$ at this energy. In the same figure, and on a sixfold greater scale, is the photoelectron spectrum produced in a 23-mg/cm² Th foil. Crosses indicate the background to the photospectrum. To the K-peak energy must be added the thorium K-shell binding energy and a 7-kev correction for electron energy loss in the converter.[4] There results a gamma-ray energy 3.574 $\pm$0.020 Mev.

In Fig. 2 is the spectrum of Compton electrons produced in a 23-mg/cm² Be target converter. Also shown is the Compton spectrum from the 3.097 ± 0.005-Mev gamma ray[6] from $C^{12}(d,p)C^{13*}$ produced in 39-mg/cm² graphite at $E_d=1.5$ Mev. It is normalized to the same peak height. Detailed comparison of the two curves shows the energy difference of the two gamma rays to be 473 kev, resulting in an independent (except for

* Assisted by the joint program of the U. S. Atomic Energy Commission and the U. S. Office of Naval Research.
[1] W. J. Hushley, Phys. Rev. **67**, 34 (1945).
[2] Hahn, Snyder, Willard, Bair, Klema, Kington, and Green, Phys. Rev. **85**, 934 (1952).
[3] R. B. Day and R. L. Walker, Phys. Rev. **85**, 582 (1952).
[4] Hornyak, Lauritsen, and Rasmussen, Phys. Rev. **76**, 731 (1949).
[5] C. Wong (to be published).
[6] R. G. Thomas and T. Lauritsen, Phys. Rev. **88**, 969 (1953).

calibration constant) measurement of the new line as 3.570±0.015 Mev. The average of the values is 3.572 ±0.012 Mev. It is probably necessary to subtract from this figure a 26-kev Doppler shift arising from the motion of the Li^{6*}.

The background count rate observed above the end point and with zero field was found to be nearly independent of spectrometer current but strongly dependent upon the bias setting of the scintillation-detector discriminator. To minimize this background for the internal pair measurements, the positron spectrum was covered in overlapping segments, the bias being set for each segment at the highest value consistent with complete counting of all focused particles. A 19-mg/cm² Be foil with no converter was used for this measurement. The resulting spectrum, adjusted to a common background, is shown in Fig. 3. External pairs produced less than two percent of the measured counts. The solid curves represent theoretical spectra corresponding to various multipole orders of the transition,[6] with scale

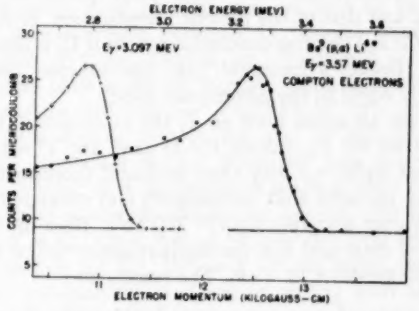

FIG. 2. Thin-converter Compton spectra from (1) $Be^9(p,\alpha)Li^{6*}$, solid circles, target converter 23 mg/cm² Be; (2) $C^{12}(d,p)C^{13*}$, crosses, E_γ=3.097, E_d=1.5 Mev, target-converter 39 mg/cm² graphite; peak height and background are matched to those of the Li^6 line.

determined by the gamma-ray yield. The Born approximation curves,[7] which drop to zero at the end point, have been adjusted to match more accurate end-point values.[8] The Compton electron spectrum was checked before and after the positron measurements to insure that any yield change resulting from carbon deposits was negligible.

Comparison of the areas under the various curves (above 3500 gauss-cm) was used to produce a quantitative measure of the agreement between the data and the respective assignments. This was regarded as a more accurate procedure than evaluation of the total internal pair coefficient, because the latter involves the area under a curve of counts/momentum (the spectrometer window is proportional to its momentum setting) thereby placing undue weight upon the statistically poorer low-momentum points. The area under the experimental curve was determined by connecting adjacent points with straight lines. If this area is taken as unity, the other areas are:

*E*1	1.66,
*E*2	1.13,
*M*1	0.955,
*E*3	0.82.

The curve representing a magnetic dipole transition gives closest agreement with experiment. The *E*2 curve is high by about 1.5 times the estimated probable error (which consists primarily of uncertainty in the yield measurement), and all others differ by more than twice the probable error. The 3.57-Mev level is thus assured of parity the same as that of the ground state (by *M*1 or *E*2) and the data are in agreement with a spin assignment of 0, 1, or 2 (the ground state has $J=1^+$).

DISCUSSION

The He^6 ground state almost certainly has spin zero, even parity. He^6 is an even-even nucleus and the beta decay to the Li^6 ground state is allowed, favored.[9] It thus seems likely that the 3.57-Mev level in Li^6 is the analog state expected on the assumption of charge independence of nuclear forces. The energy correspondence is only roughly in accord with this interpretation, but there is considerable uncertainty, for this particular case, in the Coulomb energy difference between the two isobars.[10]

Several inferences may be drawn from the $T=1$ characterization of the 3.57-Mev level. Nothing more can be said about its very small width for deuteron emission, because the strict angular momentum selection rule based on the $J=0^+$ assignment accounts for this. However, if the isotopic spin selection rules are rigid (that is, if there is little mixing of states with different T) it follows that the compound-nucleus state involved in the reaction (the 8.89-Mev level of B^{10})

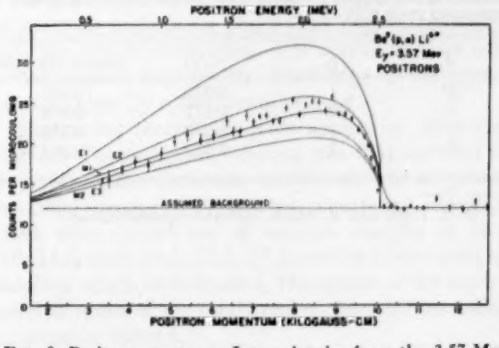

FIG. 3. Positron spectrum. Internal pairs from the 3.57-Mev gamma ray of $Be^9(p,\alpha)Li^{6*}$. E_p=2.72 Mev. Magnitude of theoretical spectra is determined by yield $4.63\times10^{-4}\gamma/p$. Curve *E*1 represents electric dipole, *E*2 electric quadrupole, etc.

[7] M. E. Rose, Phys. Rev. **76**, 678 (1949); **78**, 184 (1950).
[8] M. E. Rose and G. E. Uhlenbeck, Phys. Rev. **48**, 211 (1935).
[9] Wu, Rustad, Perez-Mendez, and Lidofsky, Phys. Rev. **87**, 1140 (1952).
[10] D. R. Inglis, Revs. Modern Phys. **25**, 390 (1953).

has $T=1$. It then follows that production by alpha emission from this B^{10} level of the ground state and 2.18-Mev level of Li^6 (both $T=0$) should be inhibited, and it has in fact been observed[11] that these alpha-particle groups do not display the 2.56-Mev resonance. Although a $J=0^+$ assignment for the 8.89-Mev level is also sufficient to explain these observations, it is shown in the appendix that the large resonant cross section for production of the 3.57-Mev level precludes this assignment. Upper limits on the partial widths for the above reactions would be of interest in establishing the purity of the T assignments involved.

The author wishes to express his appreciation for the continued advice and active assistance of T. Lauritsen and for helpful discussions with W. A. Fowler and R. G. Thomas. He is grateful to the National Science Foundation for a predoctoral fellowship during a part of the period of this work.

APPENDIX: SPIN OF THE 8.89-MEV LEVEL OF B^{10}

It is possible to infer a spin assignment for the 8.89 Mev level of B^{10}, formed by 2.56-Mev protons on beryllium. It will be noted first that the presence of the alpha group leading to the (presumed) $J=0^+$, $T=1$ state of Li^6 implies $T=1$ and parity $(-)^J$. An argument to set a lower limit on J proceeds from a comparison of the measured maximum resonant cross section for production of the 3.57-Mev gamma rays following the alpha emission with the Breit-Wigner expression for this quantity:

$$\sigma_R=4\pi\lambda^2[(2J+1)/(2i+1)(2s+1)]\Gamma_p\Gamma_a/\Gamma^2, \quad (1)$$

where λ is the wavelength ($\times 1/2\pi$) of the incident proton, J is the angular momentum of the resonant state, i and s are the spins of the incident particle and target nucleus, Γ_p is the partial width for proton emission, Γ_a is the partial width for alpha emission leading to the 3.57-Mev level of Li^6, and Γ is the total width. $\Gamma=\Gamma_a+\Gamma_p+\Gamma_n+\Gamma'$, where Γ_n is the neutron width and Γ' is a sum of several other widths (α_0,α_1,d, $n+p$) which is expected to be small in view of the $T=1$ character of the level.

TABLE I. Maximum possible values of Breit-Wigner cross section for $Be^9(p,\alpha)Li^{6*}$ reaction for various assumed values of compound state spin J.

J	l_p	Γ_n/Γ_p	σ_R(max) (10^{-24} cm^2)
0^+	1	0.270	0.031
1^-	0	0.572	0.076
2^+	1	0.270	0.156
3^-	2	0.062	0.262

[11] D. R. Inglis and R. Malm (private communication).

The charge independence of nuclear forces implies equality of the reduced widths for neutron and proton emission (γ_n^2 and γ_p^2) forming mirror levels. Γ_n/Γ_p is thus equal to the ratio of the barrier penetration factors, which may be computed from square well[12] and Coulomb[13] wave functions. Maximizing (1) with respect to Γ_p results in:

$$\sigma_R(\max)=\pi\lambda^2[(2J+1)/(2i+1)(2s+1)] \times(1-\Gamma'/\Gamma)^2/(1+\Gamma_n/\Gamma_p). \quad (2)$$

If Γ'/Γ is neglected, the value of this quantity as a function of J is given in Table I. The experimental value[2] of σ_R is 0.11×10^{-24} cm^2, a figure believed accurate to within ten percent considering the excellent agreement between the thick target yield quoted in reference 2 and that of the present investigation. It follows that $J\geqslant 2$. The same conclusion results if Γ_n is obtained from Hushley's estimate[1] that the neutron yield is roughly equal to the gamma-ray yield.

To set an upper limit on J, the expression (1) may be solved for Γ_a, taking $\Gamma=35$ kev[2] and $\Gamma'=0$. The reduced width γ_a^2 may then be found (necessarily including the level shift correction[14]) and compared with the Wigner sum-rule limit,[15] $3\hbar^2/2Ma$. Here M is the reduced mass and a is the alpha-channel radius, taken as $1.45(4^{\frac{1}{3}}+6^{\frac{1}{3}})\times10^{-13}$ cm. The results are:

J	$\gamma_a^2\cdot 2Ma/3\hbar^2$
2^+	0.19 or 0.33
3^-	2.5 or <0.

The first result found for $J=3$ is highly unlikely (the Wigner limit being only an estimate) while the latter is physically unrealizable, as are those for higher J's. It thus seems probable that the 8.89-Mev level of B^{10} has $J=2^+$. For this spin value, the proton (or neutron) reduced width is 0.0053 or 0.0016 of the Wigner limit.

[12] Feshbach, Peaslee, and Weisskopf, Phys. Rev. **71**, 145 (1947).
[13] Bloch, Hull, Broyles, Bouricius, Freeman, and Breit, Revs. Modern Phys. **23**, 147 (1951).
[14] R. G. Thomas, Phys. Rev. **81**, 148 (1951); Phys. Rev. **88**, 1109 (1952).
[15] T. Teichmann and E. P. Wigner, Phys. Rev. **87**, 123 (1952).

Scattering of Fast Neutrons in Light Nuclei*†

C. F. Cook and T. W. Bonner
The Rice Institute, Houston, Texas
(Received January 20, 1954)

The total cross section of hydrogen, deuterium, lithium, beryllium, boron 10, boron 11, carbon, oxygen, magnesium, aluminum, and sulfur have been measured for neutrons whose energies were varied from 14–18 Mev. All elements except carbon exhibit a decrease in cross section with increasing energy. Carbon exhibits a broad resonance at 16-Mev neutron energy. Nuclear radii calculated from these cross sections have the following values in units of 10^{-13} cm: Li—3.29, Be^9—3.51, B^{10}—3.56, B^{11}—3.49, C^{12}—3.41, O^{16}—3.85, Mg—4.04, Al—3.98, and S—4.33.

The $n-p$ and $n-d$ cross sections are compared with the theoretical calculations.

INTRODUCTION

MEASUREMENTS of total neutron cross sections for nuclei using fast neutrons of various energies have been previously reported.[1–6] Earlier experiments[1,2] were carried out with neutrons which were not monoenergetic. However, with the advent of neutrons from the reaction $T(d,n)He^4$, investigations have been reported giving total neutron cross sections at 14 Mev using monoenergetic neutrons in "good" geometry. The data of Coon, Graves, and Barschall[5] point to deviations from a smooth increase of nuclear radius as predicted by the relation $R=1.45\times10^{-13}A^{\frac{1}{3}}$. In fact their data showed that in the case of Be^9, B^{10}, B^{11}, and C^{12}, the cross section decreased with increasing atomic weight. It is of interest to see over what energy range these systematic deviations appear. The results of Cook *et al.*,[7] show that at 90 Mev the total neutron cross section for Li^7, Be^9, and C^{12} are much smaller, due to transparency, and are increasing with atomic weight. The purpose of the present experiments was to make measurements of total neutron cross sections for some of the light elements over the energy range 14 to 18 Mev.

In addition to checking for a systematic deviation similar to that found by Coon *et al.*,[5] considerable attention was given to determination of the neutron-proton and neutron-deuteron cross section over the above energy range.

EXPERIMENTAL PROCEDURE

Scattering cross sections were determined for the following elements: H, H^2, Li, Be, B^{10}, B^{11}, C, O, Mg, Al, and S. The scatterers were cylinders of about 1.9 cm diameter and lengths of from 2.5 to 5 cm. The lengths of the scatterers were chosen to give transmission of 60 to 70 percent. This choice of transmission kept the multiple-scattering corrections small, and at the same time permitted a sizable difference in the counting rate with the scatterer in and the scatterer out of the neutron beam. In the four cases where powders and fluids were used to hold the scatterer, ten mil aluminum cylinders were used.

Monoenergetic neutrons were produced from the $T(d,n)He^4$ reaction. Targets were tritium absorbed in a thin layer of zirconium. The neutron energy was varied from 14.1 Mev to 18.0 Mev by variation of the incident deuteron energy. The energy spread of the neutrons varied from 20 to 40 kev.

Neutrons with an energy of 14.1 Mev were observed at right angles to the incident deuteron beam of the Cockcroft-Walton accelerator when operated at 160 kev.

Higher energy neutrons were obtained by using the Rice Institute 2-Mev pressurized Van de Graaff accelerator as a source of deuterons. In order to obtain the highest energy neutrons available with this accelerator and to minimize the number of changes during the entire experiment, the neutron detector was placed at zero degrees to the incident deuteron beam.

The neutron detector was a biased anthracene scintillator, 1.8 cm in diameter and 2.5 cm long, placed 15 cm from the source of neutrons. The scatterers were supported midway between the front edge of the crystal and the target by a thin brass support.

Inscattering corrections were applied to all transmissions. The procedure followed was that outlined by Cook, McMillan, Peterson, and Sewell[7] and in general amounted to about 10 percent. Scattering measurements were carried out at neutron energies of 14.1, 15.0, 15.5, 16.0, 16.5, 17.0, 17.5, and 18.0 Mev with all materials which were studied. The results of the experiments in terms of the total cross sections for scattering are given in Table I.

In addition, scattering in carbon at 40 additional neutron energies from 15.8 to 17.0 Mev was observed. A thinner zirconium-tritium target was used in these measurements so that the energy resolution was 10 kev. The transmission varied slowly and smoothly in this

* Preliminary report given at the Physical Society Meeting (Washington, April, 1953), and at the Birmingham Conference on Nuclear Physics (July, 1953).

† Supported by the U. S. Atomic Energy Commission.

[1] Amaldi, Bocciarelli, Cacciapusti, and Trabacchi, Nuovo cimento **3**, 203 (1946).
[2] R. Sherr, Phys. Rev. **68**, 240 (1945).
[3] A. H. Lasday, Phys. Rev. **81**, 139 (1951).
[4] Poss, Salant, Snow, and Yuan, Phys. Rev. **87**, 11 (1952).
[5] Coon, Graves, and Barschall, Phys. Rev. **88**, 562 (1952).
[6] Leonard S. Goodman, Phys. Rev. **88**, 686 (1952).
[7] Cook, McMillan, Peterson, and Sewell, Phys. Rev. **75**, 7 (1949).

TABLE I. Total cross section in units of 10^{-24} cm^2.

Nucleus	Type material	Neutron energies in Mev 14.1	15.0	15.5	16.0	16.5	17.0	17.5	18.0	Nuclear radius[c] 10^{-13} cm
H	Paraffin	0.690 ±0.012	0.662 ±0.010	0.648 ±0.012	0.582 ±0.030	0.609 ±0.015	0.612 ±0.030	0.587 ±0.020	0.539 ±0.015	0.87
D	D_2O[a]	0.79 ±0.02	0.77 ±0.02	0.71 ±0.02	0.68 ±0.03	0.66 ±0.02	0.63 ±0.03	0.58 ±0.02	0.56 ±0.03	1.57
Li	Metal[b]	1.46 ±0.03	1.41 ±0.02	1.41 ±0.03	1.33 ±0.03	1.27 ±0.03	1.29 ±0.02	1.24 ±0.02	1.20 ±0.02	3.29
Be	Metal	1.49 ±0.02	1.47 ±0.02	1.42 ±0.03	1.45 ±0.02	1.46 ±0.02	1.43 ±0.03	1.39 ±0.02	1.38 ±0.03	3.51
B^{10}	Powder[a]	1.45 ±0.02	1.48 ±0.03	1.46 ±0.02	1.46 ±0.03	1.44 ±0.02	1.42 ±0.02	1.48 ±0.04	1.42 ±0.03	3.56
B^{11}	Powder[a]	1.43 ±0.02	1.42 ±0.03	1.44 ±0.02	1.45 ±0.02	1.41 ±0.03	1.41 ±0.03	1.34 ±0.03	1.30 ±0.03	3.49
C	Graphite	1.29 ±0.02	1.35 ±0.02	1.38 ±0.02	1.40 ±0.02	1.37 ±0.02	1.33 ±0.02	1.33 ±0.02	1.34 ±0.02	3.41
O	H_2O[a]	1.65 ±0.05	1.67 ±0.05	1.63 ±0.05	1.51 ±0.07	1.59 ±0.05	1.53 ±0.06	1.59 ±0.06	1.60 ±0.05	3.85
Mg	Metal	1.74 ±0.05	...	...	1.72 ±0.05	...	...	...	1.69 ±0.05	4.04
Al	Metal	1.75 ±0.05	...	...	1.67 ±0.05	...	...	...	1.58 ±0.05	3.98
S	Cast	2.00 ±0.05	...	...	1.90 ±0.05	...	...	...	1.81 ±0.05	4.33

[a] Contained in thin Al cylinder.
[b] Contained in airtight thin Al cylinder.
[c] Calculated from $\sigma = 2\pi(R+\lambda)^2$ at each energy and averaged. λ is measured in center-of-mass coordinates.

energy interval, indicating a small drop in the scattering cross section as the neutron energy is increased from 15.8 to 17.0 Mev.

Similar experiments with high resolution were carried out with a beryllium scatterer in the energy intervals 15.0 to 16.0 Mev; no rapid variations of the cross section were observed.

DISCUSSION OF RESULTS

The experiments show that the scattering cross sections become smaller as the neutron energies are increased except in the case of carbon where there appears to be a broad resonance at 16 Mev. This general decrease in the cross section can be explained in terms of the approximate relation $\sigma = 2\pi(R+\lambda)^2$, or by the more refined theory of Feshbach and Weisskopf.[8] In the case of a nuclear radius of 3.6×10^{-13} cm, a decrease in σ of 7 percent is predicted as the neutron energy varies from 14 to 18 Mev. In the case of Li a decrease of 19 percent is observed; this would indicate that there might be a broad resonance for scattering in Li at an energy lower than 14 Mev.

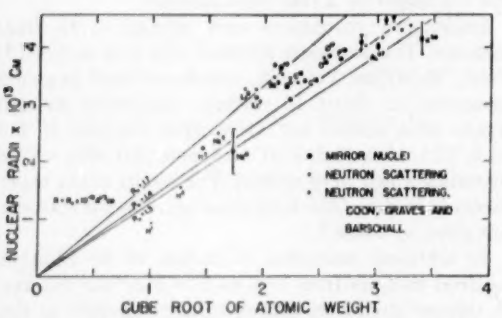

FIG. 1. Nuclear radii vs (atomic weight)$^{\frac{1}{3}}$. Solid lines represent the relations $R=1.3$, 1.4, and $1.7\times10^{-13}A^{\frac{1}{3}}$ cm. Probable errors are indicated where they are significant.

In the last column of Table I are the average values of the nuclear radii as calculated from each value of σ and λ. The method of Feshbach and Weisskopf gives nuclear radii about 5 percent larger than these. Values of the nuclear radii are compared in Fig. 1 with the theoretical relations $R=1.30\times10^{-13}A^{\frac{1}{3}}$, $R=1.40\times10^{-13}A^{\frac{1}{3}}$, and $R=1.70\times10^{-13}A^{\frac{1}{3}}$. It is apparent that there are large deviations from such a relationship in the light elements. A particularly striking effect is that the radii of Be^9 and B^{10} are greater than those of B^{11} and C^{12}. This same trend of nuclear radii has been reported by Holt[9]; his conclusions are based on fitting Butler's

[8] H. Feshbach and V. F. Weisskopf, Phys. Rev. **76**, 1550 (1949).
[9] T. J. Holt and T. N. Marsham, Proc. Phys. Soc. (London) **66**, 1032 (1953).

TABLE II. Theoretical $n-p$ cross sections compared with experiment.

E_n Mev	Yukawa $r_{0s}=2.0\ 10^{-13}$ cm $\sigma\times10^{-24}$ cm²	Yukawa $r_{0s}=2.6\ 10^{-13}$ cm $\sigma\times10^{-24}$ cm²	Shape independent $r_{0s}=2.0\ 10^{-13}$ cm $\sigma\times10^{-24}$ cm²	Shape independent $r_{0s}=2.6\ 10^{-13}$ cm $\sigma\times10^{-24}$ cm²	Experimental $\sigma\times10^{-24}$ cm²
14.5	0.675	0.666	0.673	0.658	0.676
16.0	0.616	0.608	0.613	0.599	0.616
17.5	0.563	0.557	0.560	0.547	0.579
20.0	0.496	0.490	0.490	0.478	0.504

stripping theory to experimental results in (d,p) reactions. His results indicate an even larger decrease in nuclear radii when going from Be^9 to C^{12}.

Another means of finding nuclear radii in light nuclei is from the difference in binding energies of mirror nuclei. Recent determinations[10,11] of (p,n) thresholds in the light elements give precise values of these energies. Nuclear radii calculated by assuming a uniform charge per unit volume are also shown in Fig. 1. The radii of all the nuclei obtained in this way agree rather well with those obtained by neutron scattering. This indicates that the assumption of uniform charge distribution is approximately correct in these light elements. Nuclear radii calculated by both methods cannot be explained by a single constant in the relation $R=$constant $A^{\frac{1}{3}}$; after allowing for experimental errors, values varying from 1.35 to 1.8 are required.

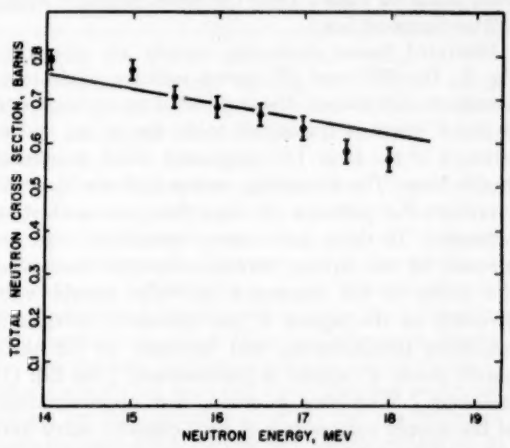

FIG. 2. $n-d$ Total cross section *vs* neutron energy in laboratory system. Solid line is theoretical prediction of Frank and Gammel.

[10] Richards, Smith, and Browne, Phys. Rev. **80**, 524 (1950).
[11] Willard, Bair, Kington, Hahn, Snyder, and Green, Phys. Rev. **85**, 849 (1952).

NEUTRON-PROTON SCATTERING

The values of the (n,p) cross sections agree well with those observed by Poss, Salant, Snow, and Yuan[4] at 14.1 Mev. The values at the higher energies can be compared to the recent results of Day and Henkel[12] at 20 Mev. Table II gives our averaged values of $n-p$ scattering cross sections at 14.5, 16.0, and 17.5 Mev together with the value of Day and Henkel at 20 Mev. The experimental cross sections are compared with the theoretical cross sections calculated from the effective range theory for S-wave neutrons.[13,14] The triplet scattering length, triplet effective range, and singlet scattering length are those given by Snow.[15] The table shows that the different theories give only small differences in $n-p$ scattering. The best agreement with experiment is the Yukawa potential with a singlet effective range of 2.0×10^{-13} cm.

NEUTRON-DEUTERON SCATTERING

The $n-d$ total scattering cross section can be compared to the theoretical calculations of Frank and Gammel.[16] Figure 2 shows our experimental results and the theoretical curve. The experimental results agree within the limits of error with the theoretical values; the experimental results indicate a somewhat more rapid variation of scattering cross section with energy but this may not be significant.

[12] R. B. Day and R. L. Henkel, Phys. Rev. **92**, 358 (1953).
[13] J. M. Blatt and J. D. Jackson, Phys. Rev. **76**, 18 (1949).
[14] H. A. Bethe, Phys. Rev. **76**, 38 (1949).
[15] G. Snow, Phys. Rev. **87**, 21 (1952).
[16] R. M. Frank and J. L. Gammel (private communication).

Shell Effects in Highly Excited Nuclei

HENRY W. NEWSON, *Duke University, Durham, North Carolina, and Oak Ridge National Laboratory, Oak Ridge, Tennessee*

AND

ROBERT H. ROHRER,* *Oak Ridge National Laboratory, Oak Ridge, Tennessee*

(Received August 17, 1953; revised manuscript received Februrary 1, 1954)

The boron absorption method has been used to obtain the following estimates of the energy of the lowest neutron resonance for each of the following target nuclides: Rb^{85}, 0.97 kev; Rb^{87}, 0.42 kev; Y^{89}, 5.0 kev; La^{139}, 0.08 kev; Pr^{141}, 0.38 kev; and Tl^{205}, 10 kev. The corrections were made in such a way that the figure found is a lower limit for the energy and consequently a lower limit for the order of magnitude of the spacing of *s*-wave resonances. These figures were added to data in the literature, and a plot of *s*-level spacing was made which included most target nuclides of odd mass and odd charge. This curve showed roughly symmetric maxima at the neutron magic numbers 50, 82, and 126. The cases where the compound nucleus contains more neutrons than the magic numbers are qualitatively understandable, since these nuclides are in a low state of excitation compared to normal nuclei in their neighborhood. An unusually close level spacing, which would be expected on the basis of excitation energy when there are slightly less than a magic number of neutrons, was not observed. It appears (at least near 126 neutrons and 82 protons) that the shell structure is not broken up to any great extent in the compound nucleus.

I. INTRODUCTION

HUGHES and his coliaborators[1] have measured the capture cross sections of many nuclides for unmoderated fission neutrons. They have shown that capture cross sections are unusually small at and near the neutron magic numbers. They attribute these anomalously low cross sections to unusually wide level spacings. An attempt is made here to determine the anomalous spacings more directly. It seemed very likely that the resonances would lie in a region inaccessible to time-of-flight methods, and it was decided to use the methods of boron and self-absorption so that a lower limit to the spacing might be obtained by estimating the position of the lowest-energy resonance. In order to approach a quantitative comparison with normal nuclei, the spacing of *s*-neutron peaks must be determined for the nuclei of odd charge.

II. EXPERIMENTAL RESULTS

A beam of pile neutrons from the graphite pile at Oak Ridge National Laboratory was used as a source. The technique does not differ appreciably from that used by Dancoff *et al.*[2] The curves (Fig. 1) have been corrected for $1/v$ absorption and boron scattering in the same way. The measurements were extended to thicknesses at which B^{10} scattering exceeds absorption, the limit of usefulness of the method. The above workers were very successful in detecting the lowest resonance of Mn, Na, and V where their results have been checked by more direct measurements.[3] However, the method is very sensitive and sometimes detects "resonances" not otherwise verifiable. The present work probably suffers from the same difficulty which will be discussed later.

Corrected boron absorption curves are shown in Fig. 1. The Tl^{205} and Y^{89} curves indicate single resonances by their shapes. The small break at the beginning of the Y curve is considered to be due to an underestimate of the large $1/v$ component which is present in this case. The remaining curves indicate by their curvature the presence of more than one activation resonance. If these are *s*-wave resonances, the expression for the capture resonance integral shows that the ratios of the resonance activities should vary inversely as the square of the resonance energies if scattering predominates, and inversely as the three halves power if capture is predominant. [See Eq. (1) following.] With this in mind, first approximations of the steeper components of each complex curve were obtained by assuming that the sum of effects of the higher-energy resonances could be approximated by a constant term. The Rb and Pr curves, when analyzed this way, were resolved into one pure exponential and a constant term. The first resonance in Cs has been reported as 5.9 ev, and no more resonances were observed as high as 20 ev.[4] A good fit of the Cs curve was obtained using the 5.9-ev value, another component near 300 ev and a constant term. The 300-ev figure is not very reliable and should be checked by time-of-flight measurements. La, like Cs, was analyzed into three components. For reference, previous boron absorption measurements on Nb are included in

* This work was carried out under the Research Participation Program while on leave of absence from Emory University. The research was performed in partial fulfillment of the requirements for the Ph.D. degree at Duke University.

[1] Hughes, Garth, and Eggler, Phys. Rev. **83**, 234 (1951); Garth, Hughes, and Levin, Phys. Rev. **87**, 222 (1952); and Hughes, Garth, and Levin, Phys. Rev. **91**, 1423 (1953).

[2] Lichtenberger, Nobles, Monk, Kubitschek, and Dancoff, Phys. Rev. **72**, 164 (1947).

[3] *Neutron Cross Sections*, Atomic Energy Commission Report AECU-2040 (U. S. Government Printing Office, Washington, D. C., 1952), plus supplements 1 and 2.

[4] H. H. Landon and V. L. Sailor, Phys. Rev. **86**, 605 (1952).

Table I. The energies were determined by a two-component analysis as above.

III. DISCUSSION OF RESULTS

The energy of the lowest resonance given in Table I is valid if the resonance is an s level and the constant term subtracted is small. If the first resonance should be due to a $p_{\frac{1}{2}}$ wave, the analysis would be invalid, but the heavy reliance placed on the initial slope would make the figure in Table I a gross underestimate of the energy of the first s resonances. These estimates for the lowest-energy s resonances are, therefore, conservative when used as lower limits to the average spacing of s resonances.

Self-absorption curves have been run on most of these materials but most of them are more difficult to interpret than the boron curves. However, self-absorption data show that in the case of Tl^{205}, if it is assumed that capture is negligible as compared to scattering, the first resonance is in the neighborhood of 10 kev or higher by a factor of 3. It is clear that Tl^{205} is not responsible for the 270-ev and the 1300-ev peaks[3] observed in natural Tl, but the Tl^{205} resonance may contribute to a 6500-ev peak[5] also seen in Tl. Attributing the 270-ev and 1300-ev peaks to Tl^{203}, one arrives at an average spacing of ~3000 ev which is in good agreement with the value ~1000 ev which may be calculated from the reduced width[6,7] of the 270-ev level.

The boron absorption method has the obvious disadvantage that, after all the corrections have been made, one is left with a very rough value of the energy of the first resonance. However, when the spacing of the resonances under study is of the order of kilovolts even qualitative information is of value since the more direct methods of time-of-flight and threshold sources have not yet been applied extensively to this region.

The method does have the advantage that separated isotopes are not necessary to study the resonances of single nuclides since radioactive properties serve to distinguish the components of an isotopic mixture. Our most interesting results were obtained on thallium and rubidium which do occur in isotopic mixtures.

A second disadvantage did us relatively little harm: the possibility that the lowest-energy resonance may be due to the p rather than s wave. In a heterogeneous neutron source varying as $1/E$, the capture resonance integral (over a single resonance)[7] is

$$R=\int\frac{\sigma(E)dE}{E}=\frac{1.3\pi g\Gamma_n\Gamma_a 10^6}{E_r^2(\Gamma_n+\Gamma_a)}, \qquad (1)$$

where E_r is the neutron energy at resonance in ev and Γ_n and Γ_a are the neutron and absorption widths,

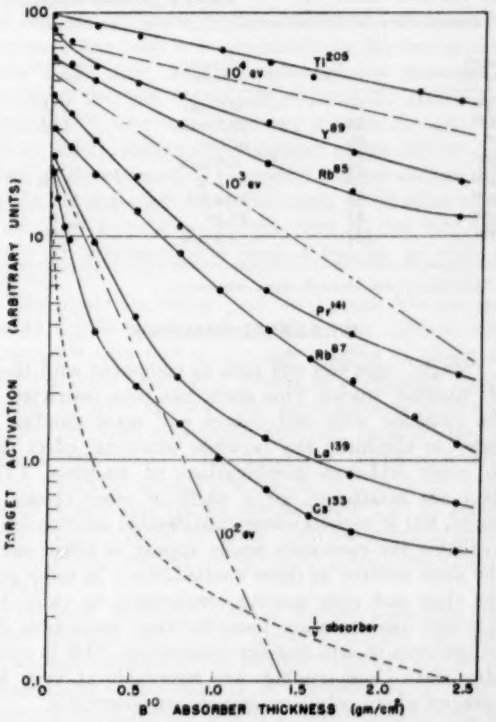

FIG. 1. Boron absorption curves corrected for scattering in the boron absorbers and for the $1/v$ activation component. The ordinates of the separate curves are not related. The broken line curves indicate the slopes associated with activation due to single resonances of various energies and pure $1/v$ activation.

respectively. If $\Gamma_n\gg\Gamma_a$, R will be independent of Γ_n, and apart from the weight factor g independent of the angular momentum of the neutron wave. Even if $\Gamma_n\approx\Gamma_a$, R will depend principally on E_r^{-2}, and a low-energy p resonance may well be activated much more than a higher-energy s resonance. For instance, if a resonance is at 2.5 kev and its spacing is 10 kev, Γ_n should be roughly[8] 50 ev for an s wave and 0.5 ev for a p wave; if $\Gamma_a\leqq 0.5$ ev, R will not depend much on the angular momentum of the resonance. (This effect will not arise in measurements of the total cross section of the resonances under study. These depend on the scattering resonance integral which is always proportional to Γ_n in the energy region considered here.) Our difficulties in interpreting the self-absorption measurements probably arose from these effects. The rather low energy found for the first resonance of La may also be due to this effect, since other evidence[3] makes it seem unlikely that there is an s resonance in the neighborhood of 76 ev.

[5] W. W. Havens (private communication).
[6] Wu, Rainwater, and Havens, Phys. Rev. **71**, 174 (1947).
[7] Harris, Muehlhouse, and Thomas, Phys. Rev. **79**, 11 (1950).
[8] J. M. Blatt and V. F. Weisskopf, *Theoretical Nuclear Physics* (John Wiley and Sons, Inc., New York, 1953), p. 463.

TABLE I. Neutron resonance energies from boron absorption data.

Target nuclide	N	Activated period	Cadmium ratio	$1/v$ fraction	High-energy fraction	Resonance energy (ev)	Chemical form
Rb^{85}	48	19.5 day	2.34	0.043	0.300	970	$RbNO_3$
Rb^{87}	50	17.5 min	2.02	0.033	0.074	420	$RbNO_3$
Y^{89}	50	62 hr	19.0	0.605	0	5000	Y_2O_3
Nb^{93}	52	6.6 min	...	0.153	0.210[a]	730[a]	Nb
Cs^{133}	78	3.2 hr	3.10	0.067	0.050	(5.9) 300	$CsNO_3$
La^{139}	82	40.4 hr	15.4	0.457	0.054	76	La_2O_3
Pr^{141}	82	19 hr	12.0	0.357	0.161	380	Pr_4O_7
Tl^{205}	124	4.2 min	2.98	0.063	0	10 000	Tl

[a] Calculated from Dancoff's data, reference 2.

IV. S-LEVEL SPACINGS

"Magic" spacings will now be compared with those of "normal" nuclei. This study has been restricted to the elements with odd charge and mass number in order to eliminate any possible structural effect due to other odd-even combinations of nucleons. (The data are insufficient for a study of other classes of nuclei, but in regions where considerable information is available the even-even nuclei appear to follow much the same pattern as those studied here.) In order that the close and wide spacing comparisons be valid, the spacings used here are those between resonances due to neutrons of zero angular momentum. This is necessary since close spacings are resolvable at very low energies where only s resonances are observable.

Figure 2 shows a plot of spacings against neutron number. Aside from a few omissions noted below, all stable odd-Z nuclei and the radioactive nuclei Rb^{87} and Re^{187} are included. The nuclide corresponding to each point may be identified from the Z scale and the numeral in the circle which is the last digit of the atomic number. Where both isotopes of the same element are plotted, the displacement in the N scale is sufficient to distinguish the lighter from the heavier. The open circles and double circles were determined by inspection of curves of cross section against energy.[8,9] The energy range over which the resolving power appeared to be reasonably adequate was estimated by inspection of the curves. It was assumed, also, that below 125 kev, all peaks shown in the published curves were s resonances. The peaks used in computing these spacings, then, were those appearing in the region below 125 kev for all the lighter elements. Other upper limits of neutron energy adopted were: for copper, 25 kev; gallium, 600 ev; bromine, 200 ev; arsenic, 150 ev; silver, 150 ev; indium, 30 ev; antimony, 27 ev; iodine, 200 ev; tantalum, 45 ev; rhenium, 30 ev; iridium, 10 ev; gold, 250 ev; thallium[203], 3 kev; and bismuth, 80 kev. One subzero resonance was counted in europium for which the energy range was taken from -1 to 13 ev. Where two or more peaks were observed on a cross-section curve, the average spacing was determined and multiplied by two to correct for the fact that two independent reactions take place depending on the relative orientation of the neutron and nuclear spins; the result was then multiplied by the number of isotopes. The reader may check these points from the curves shown in the neutron cross-section compilation, AECU 2040.[3]

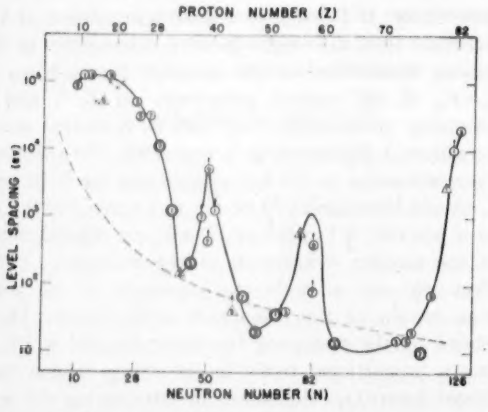

FIG. 2. The average spacing of s-wave neutron resonances of the odd elements. Circles with arrows indicate that a lower limit is plotted. (See Table I and the discussion of the interpretation of the boron absorption data.) Other circles indicate spacing estimated from resonance peaks given in reference 3; double circles signify that the spacing is the average for two isotopes of the element in question. Points plotted as crosses and triangles are explained in Table II. Numerals inside the symbols give the second digit of the atomic number, of the element. The dashed curve represents spacing calculated from the liquid drop model (reference 11).

The data from Table I appear as open circles with arrows pointing upward to indicate that the boron absorption method leads to an approximate lower limit to the level spacing. Where more direct observations are unavailable, the "nominal spacings" $D^* \simeq \Gamma_n E^{-1} \times 10^4$ ev were used.[8] D^* may be estimated with considerable uncertainty from cadmium ratios.[2,7,10] The best available estimates for a few of the nuclides were so determined, and are shown as crosses in Fig. 1. (Many of the anomalous spacings found by boron absorption were predicted from previous measurements of cadmium ratios.[10]) Table II specifies the nuclides for which the spacings have been so estimated,

[9] R. K. Adair, Revs. Modern Phys. 22, 249 (1950).

[10] H. W. Newson (unpublished). Some of the data were taken in collaboration with R. H. Rohrer and E. Rogers.

and also includes four nuclides for which the estimated spacings were not obtained directly from Table I or from AECU 2040.

The final curve is qualitatively about what one would expect from the work of Hughes *et al.*[1]; however, the direct method appears more sensitive. The largest peak-to-valley ratio of spacings is 10^3 against a capture cross-section ratio of 100. The values of the average spacings obtained by counting resonance peaks in the existing cross-section curves may be expected to be high, in general. Very few of all the resonances so far observed have been measured with sufficient resolving power to be reasonably sure that two or more levels are not combined to form a single peak in the cross-section curve. It is even more likely that apparently flat portions of a cross-section curve will be found to include resonances after being remeasured with greater resolving power. One might, therefore, expect the true values at the minima to be somewhat lower than shown in Fig. 2. These difficulties are particularly troublesome in the region between 20 and 40 neutrons. In addition, among the still lighter elements (below 20 neutrons), it is often difficult to distinguish resonances of different angular momenta. Any discussion of these lighter nuclei ($N<40$) must be postponed until more and better data are available.

The dotted curve is taken from Bethe's[11] review article; it was calculated from the liquid drop model. There is fair agreement for most of the heavy elements, but serious deviations appear for light elements and at the neutron magic numbers. The peak at 50 neutrons appears to spread at least two neutrons on either side of the magic number. The minimum at about 44 neutrons has been well established by Havens *et al.*[3,12] who found four definite resonances in bromine (2 isotopes) between 0 and 200 ev, and by Harris and Bollinger[3,13] who found resonance peaks in $_{33}As^{75}$ at 45 ev, 92 ev, and other resonances above 100 ev. The peak at 82 neutrons is somewhat less prominent than might be expected from the work of Hughes *et al.* The most interesting feature here is the fact that Cs^{133} (78 neutrons) may have a spacing as wide as 600 ev.

The most interesting peak is that at $N=126$ and $Z=82$. $_{81}Bi^{209}$ has been investigated by Gibbons and Newson[3,14] who find an average spacing of about 10 kev for both possible J values of compound nuclei formed by an s neutron. The same authors have also verified to some extent the spacings assigned to the two isotopes of Tl; the spectrum contains several small peaks at energies below 10 kev. A large peak above 10 kev may be the one found in Tl^{205} by boron absorption. Even as far away from the magic number as $_{79}Au^{197}$ the spacing is definitely anomalous (about 60 ev).[3,15]

The even elements show a similar behavior just below 126 neutrons. $_{82}Pb^{208}$ appears to have only one s resonance between 0 and 800 kev[16]; $_{82}Pb^{206}$ has many s resonances with a spacing of the order of 20 kev,[16] while an examination of the cross-section curves of even elements[3] between $_{80}Hg$ and $_{74}W$ reveals a qualitative increase of spacing for the heavier elements.

TABLE II. Level spacings plotted in Fig. 2 as triangles and crosses.

Target nuclide	N	Symbol in Fig. 2	Estimated spacing	Basis for estimate
$_{45}Rh^{103}$	58	Triangle with arrow	>40 ev	Resonances were not found between 1.4 and 1000 ev; they are very probably not present below 22 ev.[a]
$_{55}Cs^{133}$	78	Triangle	600 ev	It is assumed that the first resonance is at 5.9 ev[a] and the second at 300 ev (Table I).
$_{81}Tl^{203}$	122	Triangle	3000 ev	Resonances[a] at 270 and 1300 ev are assigned to Tl^{203}. There are apparently no additional resonances up to 3 kev in unpublished curves taken at Duke University.
$_{17}Cl^{35}$	18	Triangle	50 kev	Four resonances found at Duke University below 100 kev in natural Cl are assumed to be due to Cl^{35}. (Unpublished)
$_{15}P^{31}$	16	Cross	50 kev	Cadmium ratio[b]
$_{17}Cl^{37}$	20	Cross	100 kev	Cadmium ratio[c,d]
$_{19}K^{41}$	22	Cross	80 kev	Cadmium ratio[d]
$_{21}Sc^{45}$	24	Cross	100 kev	Cadmium ratio[b]
$_{33}As^{75}$	42	Triangle	150 ev	There are resonances at 45 and 92 ev.[e] No others are apparent up to at least 150 ev.

[a] See reference 3.
[b] See reference 7.
[c] See reference 2.
[d] See reference 10.
[e] See reference 13.

[11] H. A. Bethe, Revs. Modern Phys. **9**, 69 (1937).
[12] W. W. Havens (private communication).
[13] S. P. Harris and L. M. Bollinger, Phys. Rev. **87**, 222 (1952); also private communication.
[14] J. H. Gibbons and H. W. Newson, Phys. Rev. **91**, 209 (1953).
[15] J. Tittman and C. Sheer, Phys. Rev. **83**, 746 (1951).
[16] Barschall, Bockelman, Peterson, and Adair, Phys. Rev. **76**, 1146 (1949); Peterson, Adair, and Barschall, Phys. Rev. **79**, 935 (1950).

No points are included for Li^7, B^{11}, and N^{15}. In this region, s resonances are very rare and significant estimates of spacing cannot be made[3]; the spacings must be very large (10^5-10^6 ev). No useful cross-section curves[3] are available for the rare earths, $_{65}$Tb, $_{67}$Ho, $_{69}$Tm, and $_{71}$Lu, but their very high thermal cross sections ($\sim$100 barns)[3] make it likely that the spacings are of the order of 10 ev. This is about the same spacing as $_{63}$Eu and $_{73}$Ta, so that this wide gap is probably at a relatively flat portion of the curve.

The most interesting feature of the curve shown in Fig. 2 is the apparent symmetry of the peaks about the magic numbers. Hughes *et al.*[1] were able to account qualitatively for anomalously wide spacings when the compound nucleus has more than a magic number of neutrons by the fact that these nuclei are excited by about 2 Mev less than normal (i.e., the neutron binding energy is about 2 Mev less). This explanation cannot be used when the compound nucleus has slightly less than a magic number of neutrons. In this case the excitation is greater than normal, and an entirely different explanation is necessary.

After examining the curves of Harvey[17] which show the change of neutron binding energy near the magic numbers, we estimate that it requires all of the excitation energy of the compound nucleus to excite a few neutrons when there is just a magic number of neutrons in the nucleus, and the situation will be about the same if there are a few less neutrons. Presumably, the proton binding energies will behave similarly near the magic numbers.

The wide peak at $Z=82$ and $N=126$ is then easily understood in terms of the shell model. The extra binding energy at a closed or nearly closed shell tends to hold the nucleons in their ground states since the stable orbits, which must be postulated to account for the shells, cannot in general exist for excited states of individual nucleons.[18] Thus, few nucleons in the compound nucleus are in excited states, the life of the compound nucleus will be short, and the neutron width and level spacing, unusually large. It is not immediately clear that the same should be true when $N=50$ or 82; the above argument holds for the neutrons but the proton numbers are not at all magic, and extensive excitation of the protons might be expected. In fact, except for $_{37}$Rb^{85} and the doubtful point $_{45}$Cs^{133}, the peaks near $N=50$ and 82 may be attributed to low neutron binding energy, and more data must be obtained before the possible symmetry of the peaks around 50 and 82 is established. We note that there is no peak around 50 protons; so that, if the symmetry really exists at all three neutron magic numbers, the protons and neutrons must play a very different role in the compound nucleus.

IV. CONCLUSION

Merzbacher and Newson[19] have proposed a "semiconductor" model to account for the anomalies just below the magic number 126. This model assumes that there is a gap of about 2 Mev between the ground state of the highest-energy neutron in the nucleus and the first excited state for an individual neutron. This is obviously the approximate energy necessary to excite a neutron from a closed shell. While the model as developed, thus far, is by no means adequate to explain the details of Fig. 2, it does predict that the ratio of the spacing of Tl^{205} to Ta^{181}, a normal heavy nucleus,[3] should be about a thousand. This agrees with the data used in Fig. 2. The wide spacing of the resonances of $_{83}$Bi^{209}, due in part to excitation energy effects, is too complicated for the theory in its present state to explain.

We wish to express our indebtedness to the management and staff of Oak Ridge National Laboratory for making the facilities of the Laboratory available to us. We also wish to thank W. W. Havens, A. C. Langsdorf, and D. J. Hughes for unpublished information. The part of the work done at Duke University was supported by the U. S. Atomic Energy Commission.

[17] J. A. Harvey, Phys. Rev. **81**, 353 (1951).
[18] V. F. Weisskopf, Helv. Phys. Acta **23**, 187 (1950).
[19] H. W. Newson and E. Merzbacher, Phys. Rev. **91**, 241 (1953).

Scattering of 190-Mev Deuterons on Protons

ARNOLD L. BLOOM* AND OWEN CHAMBERLAIN
Radiation Laboratory, Department of Physics, University of California, Berkeley, California
(Received October 23, 1953)

A measurement of the total d-p scattering cross section is reported. Because of the divergence of Coulomb scattering at small angles, a small angle cutoff has been applied to the elastic scattering. The result may be stated as follows: The cross section for elastic scattering to angles greater than 10 degrees in the c.m. system, plus the total inelastic scattering cross section, is $(94_{-5}^{+7})\times10^{-27}$ cm².

Measurements are also reported of those inelastic scattering processes in which both protons suffer significant momentum changes. We have termed these events "inelastic p-p type collisions." The differential cross sections for these events appear to be smaller than would be expected in view of the theoretical considerations of others.

I. INTRODUCTION

NUCLEON-NUCLEON scattering experiments have long been considered of primary importance for the determination of the nature of nucleon-nucleon forces. We are mostly concerned at this time with high-energy scattering, in particular neutron-proton and proton-proton scattering with laboratory energies of approximately 90 Mev.[1–5] It seems most reasonable to take the view that n-p and p-p scattering are both derivable from the same interaction. If so, then the n-p and p-p scattering experiments give two approaches to this interaction. (The Pauli principle operates to explain the difference between n-p and p-p scattering measurements by excluding certain spin-angular momentum states from the p-p scattering.)

It is to be expected that in neutron-deuteron, or proton-deuteron scattering there will be interference effects between n-p and n-n (or p-p) scattering. Thus n-d or p-d scattering experiments should allow another approach to knowledge of the nucleon-nucleon interaction. It was in the hope of obtaining some measure of this interference that the present experiments on p-d scattering were undertaken.

The theory of n-d and p-d scattering has been studied in some detail by Wu and Ashkin,[6] by Chew,[7–9] and by Bethe and Gluckstern.[10] In the present paper we report measurement of the total d-p scattering cross section, and of some studies of those inelastic d-p scatterings in which both outgoing protons can be observed at significant angles from the beam direction. In the following paper[11] elastic d-p scattering will be studied.

II. METHOD

Our source of high energy deuterons was the external deuteron beam of the 184-in. Berkeley cyclotron. In this beam was placed either a hydrogenous target [polyethylene, $(CH_2)_n$], or a carbon target, and the particles scattered out of the beam were observed in scintillation counters. The counting rate due to hydrogen was determined by subtraction of carbon counts from those obtained with CH_2. The beam was monitored by means of an ionization chamber and electrometer.

Except for minor changes, the handling of the deuteron beam in this work has been the same as that given the proton beam in the p-p scattering experiments of Chamberlain, Segrè, and Wiegand.[4] The beam is obtained in the same way from the cyclotron, is collimated in the same way, and monitored with the same ionization chambers. Virtually identical precautions have been observed. The calibration of the ionization chambers has been extended to 192-Mev deuterons with the help of the range-energy relations of Aron, Hoffman, and Williams.[12]

A block diagram of one of two possible electronic arrangements is shown in Fig. 1. The crystals were used

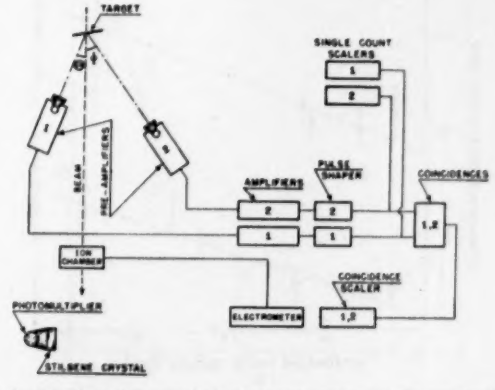

FIG. 1. Block diagram of the electronic circuits of the experiment (as used in method A of the text) together with a schematic top view of the coincidence apparatus.

* Present address: Varian Associates, Palo Alto, California.
[1] Hadley, Kelly, Leith, Segrè, Wiegand, and York, Phys. Rev. **75**, 351 (1949).
[2] Birge, Kruse, and Ramsey, Phys. Rev. **83**, 274 (1951).
[3] C. Oxley and R. Schamberger, Phys. Rev. **85**, 416 (1952).
[4] Chamberlain, Segrè, and Wiegand, Phys. Rev. **83**, 923 (1951).
[5] Cassels, Stafford, and Pickavance, Nature **168**, 468 (1951).
[6] T. Wu and J. Ashkin, Phys. Rev. **73**, 986 (1948).
[7] G. F. Chew, Phys. Rev. **74**, 809 (1948).
[8] G. F. Chew, Phys. Rev. **80**, 196 (1950).
[9] G. F. Chew, Phys. Rev. **84**, 710 (1951).
[10] R. L. Gluckstern and H. A. Bethe, Phys. Rev. **81**, 761 (1951).
[11] O. Chamberlain and M. O. Stern, following paper [Phys. Rev. **94**, 666 (1954)].
[12] Aron, Hoffman, and Williams, Atomic Energy Commission Report AECU-663 (unpublished).

in conjunction with 1P21 photomultipliers and distributed preamplifiers. The pulses were then amplified in distributed amplifiers, shaped by fast discriminators, and mixed in distributed coincidence circuits.[18] Thus it was possible to count single events in the two crystals, as well as coincidences between crystals 1 and 2. The pulses put out by the amplifiers had an approximate width of 2×10^{-8} sec; those out of the discriminator were about three times as wide, and fairly square in shape. The coincidence circuits had a dead time of about 10^{-7} sec, and the scalers a resolving time of about 10^{-6} sec.

Two methods of operation were used. In method *A*, employed in Sec. V below, two crystals were used, one on each arm of the table, and their single counts and coincidences were recorded by a scaling circuit. In method *B*, employed in Sec. IV, a single crystal was used. The hydrogeneous targets were sheets of commercial polyethylene $(CH_2)_n$. The carbon targets were of graphite machined to such a thickness that they offered about the same stopping power to 192-Mev deuterons as the CH_2 targets used in conjunction with them.

III. EXPERIMENTAL PROCEDURE

Adjustments of cyclotron parameters, the collimator, and the central axis of the scattering table were carried out in the fashion described by Chamberlain, Segrè, and Wiegand. The alignment was checked using photographic film.

In each run the final checks on alignment and tests of the counters were accomplished by a brief study of elastic *d-p* scattering at one angle. In such a coincidence measurement using two crystals *A* and *B*, and correlated angles, one crystal *A* was made "defining" by keeping its dimensions small, while the other crystal *B* was made large enough and placed close enough so that all the partners of the correlated (elastic *d-p*) events counted by *A* were sure to be received in crystal *B*. The angle between the two counters was varied, keeping Φ (angle of "defining" crystal) fixed. The hydrogen coincidence counting rate was then plotted as a function of Θ, the angle of the nondefining crystal from the beam. The location of the center of the peak in counting rate indicated the observation of the elastic *d-p* scattering, and gave a further check on alignment and the scales an which angles were measured. With the counters at the elastic *d-p* scattering angles the counter plateaus were studied. That is, the voltage of each photomultiplier was varied in turn, and the hydrogen coincidence rates were plotted as functions of each counter voltage. The plateau curves were in all cases similar to those obtained by Chamberlain, Segrè, and Wiegand, and are not shown in this paper.

Several times during the course of these experiments the energy of the deuteron beam was determined by finding its range in aluminum. This was accomplished by placing two ionization chambers in the beam with a variable aluminum absorber between them. In all cases the energy was found to be the same within experimental accuracy, namely 192 ± 2 Mev.

Before proceeding to the actual counting, the carbon subtraction factor had to be found. The coincidences CH_2 from CH_2 were counted for unit integrated beam ("integrator volt"). The carbon target was then inserted and coincidences *C* from it were recorded for one integrator volt; similarly with the coincidences *bl* (blank) when no target was in the beam. If we call *H* the number of coincidence counts per integrator volt due to hydrogen we have

$$H=CH_2-zC-(1-z)bl, \tag{1}$$

where z is the carbon subtraction factor. If we use method *B* (single crystal) the coincidence counts are replaced by single counts and clearly $z=R$, where *R* is the ratio of the surface density of carbon in the CH_2 target to the surface density of the carbon target. This equality does not hold for method *A* since in addition to the desired systematic coincidences from hydrogen we count with a CH_2 target (*a*) a background of accidental coincidences, (*b*) accidental coincidences from carbon, (*c*) systematic coincidences from carbon, (*d*) accidental "mixed" coincidences from (inelastic or elastic) hydrogen events arriving in one counter and carbon events in the other. z is now a function not only of *R*, but also of the duty cycle of the cyclotron, the photomultiplier voltages and discriminator settings, and the angles Θ and Φ.

Several methods are available for determining the carbon subtraction factor z. The method used most extensively involves repeating one counting arrangement at several different beam levels. From these data one can evaluate the effective resolving time of the

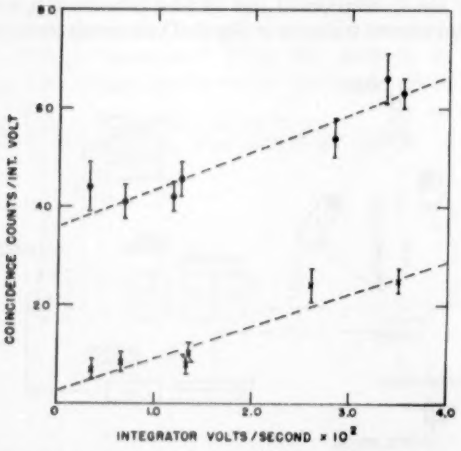

FIG. 2. Coincidence counts per unit beam charge plotted as a function of beam current for CH_2 and C targets. The ratio of CH_2 slope to C slope determines approximately the carbon subtraction factor z, here about 1.1.

[18] C. Wiegand, Rev. Sci. Instr. **21**, 975 (1950).

TABLE I. Total charged-particle scattering from d-p collisions as a function of laboratory angle Φ, obtained with method B. Errors quoted are rms counting errors.

Φ degrees	$\pi \sin\Phi\sigma(\Phi)$, 10^{-27} cm² Date 4/16/51	Date 5/28/51	Elastic scattering	Value used in integration
5		131±30		142
8	150±25	187±18		150
10		148±7		148
15	114±10	112±8		115
20		71±4		90
25	63±3	71±8		66
30		46±3		53
35	49±2			45
40		35±2		42
45	43±2	40±2		40
50		38±3		37
55	34±2			35
60		33±2		31
65	24±1	28±2	19±2	26
70		17±1	27±3	27
75	2±1	2±1	30±3	32
80		1±1		40
82	0		44±4	42
85				44

apparatus, which is essentially the electronic resolving time divided by the duty cycle of the cyclotron. When the effective resolving time has been determined, the factor z can be computed from a reasonably simple expression involving the single counting rates and coincidence counting rates from the various targets (including the "blank," meaning no target). The details will not be given here, inasmuch as they can be developed easily by standard methods. When the polyethylene and carbon targets had equal stopping power, the carbon subtraction factor z was usually between 0.7 and 1.1.

Figure 2 shows a plot of a typical set of data taken for fixed angles at various beam levels for both polyethylene and carbon targets. This type of graph lends itself well to the problem of separating the systematic coincidences from the accidental coincidences. The extrapolation to zero beam intensity gives the systematic coincidences. The slopes of the lines are due to accidental coincidences. The interpretation of the figure depends in our case on the assumptions that the cyclotron duty cycle is quite constant and the coincidence counting rates are small compared to the single crystal counting rates.

The effective resolving time was about 3×10^{-5} sec. The duty cycle corresponding to 60 pulses per second each 50×10^{-6} sec long was 3×10^{-3}. This gives an electronic resolving time of about 10^{-7} sec.

IV. TOTAL D-P SCATTERING CROSS SECTION

Deuteron-proton scattering, whether elastic or inelastic, results in two charged particles emerging from a collision. Moreover, conservation of energy and momentum require that no such particles emerge at (laboratory) angles greater than 90°. It is therefore sufficient, in finding the total cross section σ_{dp}, to count the number of hydrogen scattered charged particles at various angles Φ, integrate from 0 to $\pi/2$, and divide by two, inasmuch as we can count each scattering event twice.

$$\sigma_{dp} = \pi \int_0^{\pi/2} \sigma(\Phi) \sin\Phi d\Phi. \qquad (2)$$

Here $\sigma(\Phi)$ is the complete charged particle differential scattering cross section as can be measured using a single charged particle counter, method B. The probability of counting the neutrons associated with the inelastic scattering events is quite small.

The results of this measurement are shown in Table I. Figure 3 shows a plot of $\sigma(\Phi)\sin\Phi$, together with the curve adopted for finding σ_{dp}. It is clear that the elastic scattering cross section is infinite unless a cutoff is provided to exclude Rutherford scattering at small angles. The cutoff is made in this case by considering the elastic scattering to be zero for deflection angles of less than 10° in the c.m. system. This amounts to excluding the elastic scattering for laboratory angles smaller than 3.3° and greater than 85°. Figure 3 shows discontinuities at these angles.

Some comment is necessary concerning the methods of obtaining $\sigma(\Phi)$ in different regions of angle. Between 3.3° and 70° method B (single counter) is used as described above. In the range of angles between 70° and 85° the charged particles (all protons) are of very

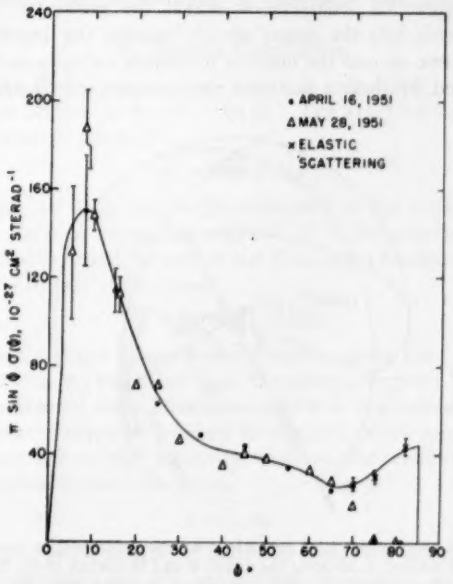

FIG. 3. Differential d-p scattering cross section for all charged particles as obtained with method B. The quantity $\pi\sin\Phi\sigma(\Phi)$ in mb sterad^{-1} is shown as a function of scattering angle Φ. The discontinuities at 3.3° and 85° are due to the cutoff of the elastic scattering. The area under this curve is proportional to the total d-p scattering cross section.

low energy and many of them do not get out of the target, hence method *B* cannot be used. Since the inelastic scattering is expected to be very small in these angles the known elastic scattering is taken as the total scattering. For angles smaller than 3.3° we take no contribution from the elastic scattering and assume that the inelastic cross section is constant, so that $\sigma(\Phi)\sin\Phi$ suffers a finite discontinuity at 3.3° and then passes linearly to the origin.

The resulting σ_{dp} is $(94_{-8}^{+7})\times10^{-27}$ cm². This is to be compared with the total *n-d* cross sections of $(117\pm5)\times10^{-27}$ cm², and $(105\pm4)\times10^{-27}$ cm² obtained by Cook *et al.*[14] for 83-Mev neutrons, and DeJuren and Knable[15] for 95-Mev neutrons, respectively. The cross section obtained in the present work is evidently of the nature of a lower limit, since there is the question of how many particles could have been omitted from the regions 0 to 3.3 degrees and 70 to 90 degrees. This fact has supposedly been taken account in the assignment of errors, which are thus slightly unsymmetrical.

V. INELASTIC PROTON-PROTON TYPE SCATTERING

1. Kinematics and Geometry

The relative de Broglie wavelength of deuteron and proton is much smaller than the average separation of the two nucleons inside the deuteron. It is therefore expected that most inelastic *d-p* collisions involve only two particles directly, the third particle going on almost undisturbed. We have looked for inelastic *p-p* type collisions, i.e., collisions in which the proton in the deuteron hits the target proton, causing the deuteron to break up and the neutron to remain virtually undisturbed. Method *A* was used. One counter, the "defining counter," was placed at angle Φ to the beam. The position of the other crystal (at angle Θ) was varied over the surface of a sphere with the target as center, and by integration of the coincidences registered over all positions of this crystal (except that corresponding to elastic scattering) it was possible to obtain $\sigma_{pp}(\Phi)$.

The kinematics can be calculated to good approximation by assuming that energy is conserved between all three particles, whereas momentum is conserved between only the two colliding ones, the momentum of the third particle remaining unchanged. Nonrelativistically, in a free *p-p* collision, the angle $(\Theta+\Phi)$ between two scattered particles must be $\pi/2$. It is not difficult to show that the effect of the 2-Mev binding energy of the deuteron is to shift $(\Theta+\Phi)$ to a slightly lower value, to about 87° at $\Phi=20°$, 88.7° at $\Phi=45°$. Relativistic corrections lower the included angle by an additional amount of the order of 1°.

Qualitatively one may say that the internal momentum of the deuteron introduces a spread in the angular distribution of one proton relative to the other. Referring to Fig. 4 we may say that the angle $(\Theta+\Phi)$ between the two out-going protons is not completely determined even if it is specified that one proton emerges at a definite angle Φ with respect to the beam. Furthermore, the two outgoing protons and the beam are not in general coplanar. The horizontal spread in $(\Theta+\Phi)$ is indicated in Fig. 4 by $\delta\Theta_1$. The vertical deviation of the second proton from the plane of the beam and the first proton is indicated by $\delta\Theta_2$. At first sight it would appear that these deviations $\delta\Theta_1$ and $\delta\Theta_2$ would both

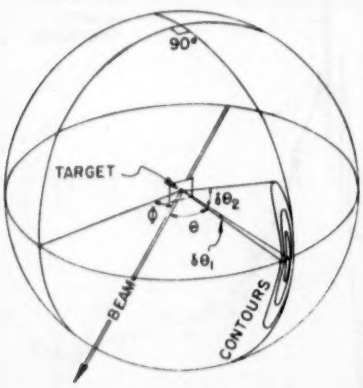

FIG. 4. Geometry of inelastic *p-p* type scattering as studied using method *A*, showing the angles Φ and Θ relative to the beam and the contours of equal coincidence counting rate. $\delta\Theta_1$ is a measure of the horizontal spread, $\delta\Theta_2$ a measure of the vertical spread.

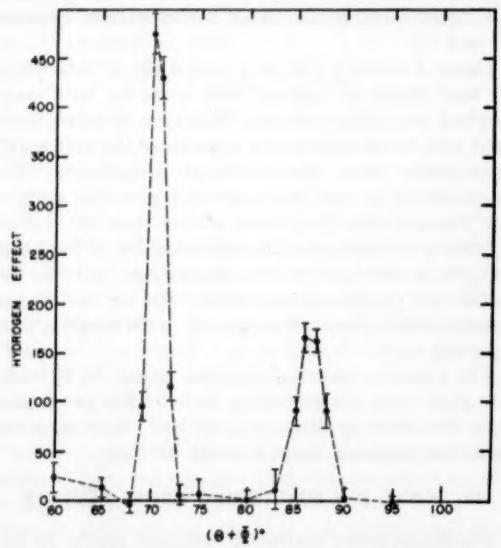

FIG. 5. Coincidence counting rate due to hydrogen plotted as a function of the angle between the counters. The large peak is from elastic scattering; the smaller one from inelastic *p-p* type scattering. The angle subtended horizontally by each crystal was approximately 4°.

[14] Cook, McMillan, Peterson, and Sewell, Phys. Rev. **75**, 7 (1949).
[15] J. DeJuren and N. Knable, Phys. Rev. **77**, 606 (1950).

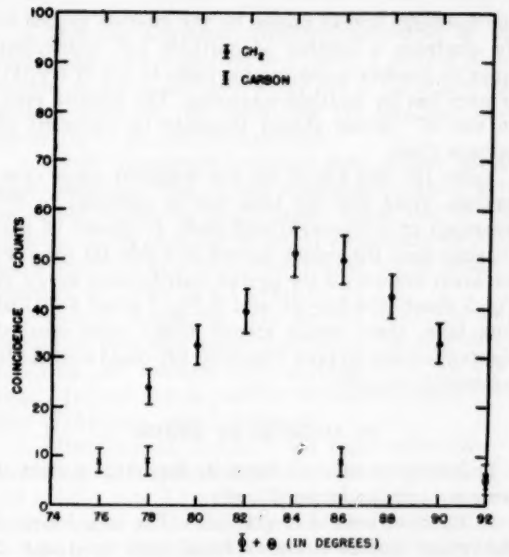

FIG. 6. Coincidence rate due to inelastic p-p type scattering as a function of the angle between crystals, at $\Phi=45°$. The angle subtended horizontally by the Θ crystal was approximately 10°.

be of the order of (p_i/p_0), where p_i is the internal momentum of the deuteron, and p_0 is the momentum of the incident particle, and indeed, this would be true if we were considering protons incident on a stationary deuteron. However, in this particular case of deuterons incident on protons, the horizontal spread $\delta\Theta_1$ is much smaller, being of the order of $(p_i/p_0)^2$. The vertical spread remains as expected of the order of p_i/p_0. These features are rather easily brought out by applying conservation of energy and momentum to the collision process, with the added provision that the momentum of the unstruck particle (neutron) is unaffected in the collision.

These considerations are in agreement with experiment. One crystal was, for example, set at $\Phi=45°$, and the other was set at a variable angle Θ in the scattering plane. Both crystals subtended approximately 4° at the target. The number of hydrogen counts per integrator volt is plotted in Fig. 5 as a function of $(\Phi+\Theta)$. The elastic scattering peak, at $(\Phi+\Theta)=70.5°$ (expected: 70.8°), is well resolved from the inelastic peak centered around 86.5°. The width of the inelastic peak is almost entirely due to the poor geometrical resolution as is evident from a comparison with the width of the elastic peak.

In practice, for purposes of finding a differential cross section, the crystal at angle Θ was made about 10° wide, and a curve of the type shown in Fig. 6 was obtained. It was then possible to operate at some point on the flat portion of the curve, say 86°, and raise and lower the Θ crystal to obtain the vertical distribution. The result of such a variation is shown in Fig. 7.

It was unnecessary to measure the height variation

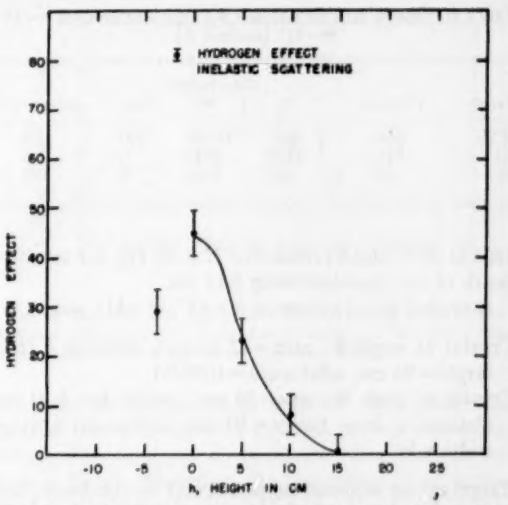

FIG. 7. p-p type inelastic scattering effect as a function of the height of the Θ crystal; $\Phi=45°$, $h_0=4.4$ cm, the Θ crystal is 50 cm from the target, and $\Phi+\Theta=86°$.

at every angle measured, for the total (integrated over height) hydrogen count H_t at some angle Θ corresponding to a defining crystal at Φ could be determined from that at another angle Θ' corresponding to a defining crystal at Φ' by the kinematic relationship,

$$(H_t/H_0)_\Theta=(H_t/H_0)_{\Theta'}(\sin\Phi'/\sin\Phi), \tag{3}$$

where H_0 is the hydrogen count at zero height. This relation was checked to be in agreement with observation.

2. Sample Calculation

We shall illustrate with a sample calculation of the cross section at $\Phi=45°$, $\Theta=41°$. The cross section is, in general, given by

$$\sigma(\Phi)=H_t/(nN\Delta\Omega), \tag{4}$$

where $\Delta\Omega$ is the solid angle subtended at the target by the defining crystal at angle Φ. N is the number of hydrogen atoms per cm² in the CH_2 target measured in the direction of the beam,

$$N=N_0\cdot 2.016/14.03t, \tag{5}$$

where t is the target surface density along the beam direction in g cm^{-2}, and N_0 is Avogadro's Number. With H measured for 1 integrator volt, n is the number of incident deuterons required to charge a capacitance C_0 connected to the collecting grid of the monitoring chamber to one volt. Thus,

$$n=C_0/e\mu, \tag{6}$$

where e is the electronic charge in coulombs, and μ the multiplication of the argon-filled chamber.[16] μ was

[16] There is no gas multiplication in these ionization chambers of the type used in proportional counters. Rather, the ratio of current in the ionization chamber to beam current is called the multiplication. Thus, one beam particle passing through the ionization chamber results in the collection of μ ion pairs.

TABLE II. Sample data for inelastic p-p type scattering at $\Phi=45°$, $\Theta=41°$ (method *A*).

Target	Time, sec	Total counts Φ	Θ	Coinc.	Integr. volts
CH_2	264	3231	18 702	100	2.0
C	142	1439	8144	9	1.0
bl	63	302	1343	2	0.5

1806 at 20°C and a pressure of 77.8 cm Hg, the sensitive depth of the chamber being 5.11 cm.

A typical set of values at $\Phi=45°$, $\Theta=41°$ was:

Crystal at angle Φ: area = 22.63 cm², distance b from target = 95 cm, solid angle = 0.00251.

Crystal at angle Θ: area = 36 cm², height $h_0=4.39$ cm, distance c from target = 50 cm, horizontal angular width = 10°.

Targets were oriented perpendicular to the beam, and had surface densities CH_2: 0.283 g cm^{-2} and C: 0.336 g cm^{-2}. $C_0=0.102\times10^{-6}$ farad, integrating condenser including capacitance of cables. Multiplication of chamber $\mu=1806$. Resolving time $\tau=1.5\times10^{-5}$ sec ±10 percent.

The counts at $h=0$ are summarized in Table II. At these low counting rates it is not necessary to correct for counting losses in the scalers. Analysis of the accidental coincidences gives the carbon subtraction factor $z=1.04\pm0.24$. Thus we obtain at $h=0$, $H=CH_2-zC-(1-z)bl=41\pm6$. Similarly we find H for other heights of the crystal at Θ. H_t is now found by integration under the curve of Fig. 7.

$$H_t=\frac{1}{h_0}\int_{-\infty}^{\infty}H\,dh=132\pm13, \tag{7}$$

where we assign a 10 percent error to H_t. Thus we obtain

$$N=2.45\times10^{22}\text{ atoms cm}^{-2},$$

$$n=3.53\times10^{8}\text{ deuterons per integrator volt,}$$

and

$$\sigma(\Phi)=(6.1\pm0.6)\times10^{-27}\text{ cm}^2.$$

3. Presentation of Data

The inelastic cross sections at various angles Φ are listed in Table III. The counting errors listed in Table III are estimates based on the possible variations in H_t within the statistical accuracies of the individual H. Systematic errors (see Sec. VI) are included under the column marked total error. Values of $\sigma(\Phi)$ marked with an asterisk are those for which the vertical distribution was calculated by means of Eq. (3) rather than measured. For $\Phi=30°$ or 25° thin targets were used. Nevertheless, at $\Phi=25°$ the particles going into the corresponding angle $\Theta=59°$ have a range of only about ½ g cm^{-2} of C, and it must therefore be assumed that due to energy spread caused by the internal motion in the deuteron a number of particles had insufficient range to produce a measurable pulse in the Θ crystal, or were lost by multiple scattering. The positive error on the 25° datum should therefore be increased to perhaps 2 mb.

Table III and Fig. 8 list the weighted mean cross sections. Note that the table can be extended to 59° inasmuch as $\sigma(\Theta)=\sigma(\Phi)\sin\Phi/\sin\Theta$. It should be emphasized that the values quoted in Table III for $\sigma(\Phi)$ are lower bounds; if the proton distributions shown in Fig. 5 about $(\Theta+\Phi)=86°$ and in Fig. 7 about $h=0$ had long tails, these would almost surely have escaped observation due to poor statistics, yet could contribute measurably to $\sigma(\Phi)$.

VI. SOURCES OF ERROR

Following are some of the more important sources of error not previously mentioned:

1. Effective area of crystal faces. The actual area of the crystal surface is known in all cases to at least 2 percent. However, the crystal faces may not have been oriented perpendicularly to the incoming particles, and the sensitivity of the crystals may not have been uniform across the surface. We believe the resulting error in the effective area of the crystal may have been as great as 3 percent.

2. Crystal position. Possibly the largest source of error in the inelastic scattering data lay in the fact that the exact zero height position for crystals at angle Θ was not known. This uncertainty alone could produce an error of 7 percent. Uncertainties in the distance of the crystals from the target were of the order of 1 percent.

3. The polyethylene targets were analyzed and shown to be of composition $(CH_2)_n$ within 1 percent. The dimensions and weight, and hence the surface densities of the targets were known to 1 percent. Since all experiments were performed with the target perpendicular to the beam, errors due to nonperpendicularity at the target were negligible.

TABLE III. Summary of inelastic p-p type differential scattering cross sections in the laboratory as a function of laboratory angle Φ. Figures of the last column include systematic errors of Sec. VI. Values marked with an asterisk were calculated with help of Eq. (3).

Θ degrees	Φ degrees	$\sigma(\Phi)$ 10^{-27} cm²/sterad	Rms counting error 10^{-27} cm²/sterad	Rms total error 10^{-27} cm²/sterad
59	25	6.3*	+2.0 −1.2	+2.1 −1.4
55	30	7.3	±0.6	±0.9
48.5	37	6.0*	±0.9	±1.1
45	41	6.1	±0.2	±0.6
41	45	5.7	±0.2	±0.6
37	48.5	4.8*	±0.7	±0.9
30	55	4.5	±0.4	±0.6
25	59	3.1*	+1.0 −0.6	+1.0 −0.7

4. Multiple scattering. Multiple scattering in the targets could have resulted in a loss of 2 percent of the events, except in the cases where one of the angles was greater than 60°, in which case the loss may have amounted to as much as 5 percent.

5. Finite coincidence resolving time. Losses due to finite resolving time of the coincidence circuit were negligible except in those cases where one of the crystals was close to the beam, in which case the high single counting rate from that crystal would produce errors of not more than 2 percent.

6. Carbon subtraction. The method of finding z by measuring the single counting rates and the coincidence resolving time resulted in an uncertainty of not more than 2 percent due to possible variations of duty cycle that might have passed unnoticed.

7. Miscellaneous. Errors in the angle calibration of scattering table and its alignment with the beam were not greater than 1 percent. The calibration of the ion chamber against the Faraday cup is believed accurate to 2 percent. The chamber was run at 1000 volts, high enough to measure better than 99 percent of the saturation current at any beam strength used.

Combining the sources of error just mentioned and those discussed in Sections IV and V, we may summarize by giving the systematic rms errors for the two experiments: 5 percent for the total cross section and 10 percent for the inelastic cross section.

VII. CONCLUSION

The total cross section for neutron-deuteron scattering has been calculated by Chew[9] and by Gluckstern and Bethe.[10] The results can be taken over to proton-deuteron scattering if we assume charge independence of the nuclear forces. In the language of proton-deuteron scattering, the total cross section calculated by Chew is:

$$\sigma' = (1-\epsilon)\sigma_{np}' + \sigma_{pp}' + I, \qquad (8)$$

where ϵ has been calculated by Chew to be 0.15 and I' the interference term, has been estimated by both Chew and Gluckstern and Bethe to be of the order of 15 mb. This calculation enables us to compare the experimentally observed total cross sections for n-p and p-p scattering, providing we take into account the small angle cutoff used to eliminate Coulomb effects. For σ_{np}' we may take the entire total cross section as measured by DeJuren and Knable[15] of 73 mb. For the total p-p cross section we will assume a constant value of $d\sigma/d\omega$ of 3.97 mb/steradian in the center-of-mass system. This figure is based on the measurements at 120 Mev of Chamberlain, Segrè, and Wiegand[4,17] and is integrated for angles greater than 10°, thus preserving a cutoff which agrees with that used in our own calculations. The total p-p cross section calculated on this basis is 25 mb. Therefore, the theoretical cross section for d-p scattering is $\sigma' = 0.85 \times 73 + 25 + 15 = 102$ mb. This figure should be compared with our experimental value of (94_{-8}^{+7}) mb.

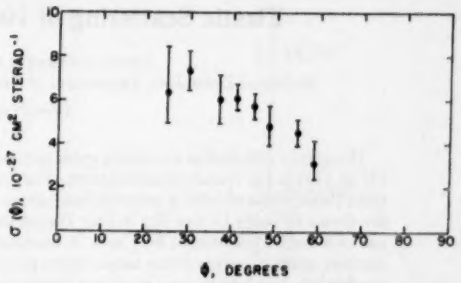

FIG. 8. Inelastic p-p type differential scattering cross section, obtained with method A, plotted as a function of the (lab.) scattering angle Φ. Errors shown are total rms errors.

The differential cross section for inelastic p-p type collisions may be compared with the free p-p cross sections at comparable energies. Comparison with the results of Chamberlain, Segrè, and Wiegand[4] taken in the laboratory frame of reference, indicates that our inelastic p-p type cross section is approximately half the free p-p cross section. This is somewhat less than has been expected theoretically. If we wish to consider the total cross section for this process, we observe that this is also the cross section for production of neutrons with little change in momentum. Transferring again to a system in which neutrons are incident on deuterons, as is employed by Chew,[9] we find that we must compare with the total cross section for production of slow protons. This cross section is given by Chew as $\sigma_{slow}' = 0.58 \times \sigma_{nn}'$. However, it must be pointed out that the inelastic p-p type cross section must deviate considerably from a fixed ratio with the free p-p cross section, at small and large angles, since small momentum transfers will favor elastic collisions. Therefore, it would appear that theoretically we should expect the inelastic collision to be perhaps 0.7 times the free cross section, rather than 0.5 as is observed. Part of this discrepancy may be explained by the fact that we could not observe low energy particles.

We wish to thank Professor E. Segrè and Dr. Martin O. Stern for their assistance and encouragement, and the crew of the 184-inch cyclotron for their cooperation during the experiment.

This work was performed under the auspices of the U. S. Atomic Energy Commission.

[17] Discrepancies in the differential proton-proton scattering cross sections obtained at Berkeley and elsewhere are believed to be due to different methods of beam integration. For this reason we prefer, at the present time, to compare our results with those of the Berkeley group, even though the comparable energies are somewhat higher, because these measurements employ the same beam integration methods as are used in our experiments and therefore allow a direct comparison.

Elastic Scattering of 190-Mev Deuterons by Protons*

OWEN CHAMBERLAIN AND MARTIN O. STERN†
Radiation Laboratory, Department of Physics, University of California, Berkeley, California
(Received October 23, 1953)

The elastic differential scattering cross section of 190-Mev deuterons by protons has been measured from 15° to 170° in the center-of-mass system. The cross sections were obtained by subtracting the carbon counts from those received with a polyethylene target. Part I presents a description of the experiments. Results are shown in Table IV and Fig. 3. Part II compares these results with those expected from theory by making use of a method developed by Chew. A summary of this comparison is given in Table VII. Some nucleon-nucleon interactions involving tensor forces give reasonable agreement between theoretical and experimental results, whereas interactions involving purely central forces appear inadequate.

INTRODUCTION

IN the preceding paper[1] it was stated that because of the interference between n-p and p-p scattering in d-p scattering the latter might provide information on nucleon-nucleon scattering that n-p and p-p experiments alone could not reveal. In this respect elastic d-p scattering, because of the single final deuteron state involved, exhibits the largest amount of interference, and, being theoretically somewhat amenable, offers, at this time at least, one of the ways to obtain more information about nuclear forces.

This paper is divided into two parts. Part I describes the experiment. Since the apparatus was almost the same as that used in the inelastic and total scattering experiments, it will not be described in detail except where different from that of BC. Part II attempts to compare experimental results with theory.

I. EXPERIMENT

A. Method and Procedure

Source of particles, targets, method of detection, and monitoring device have been described in BC.

Four methods of operation were used. In method A, the pulses from the distributed amplifiers went directly to a fast coincidence circuit[2] whose output fed into a scaler. Methods B, C, and D made use of a pulse shaper-discriminator designed by A. L. Bloom. In method B (see Fig. 1 of BC), two crystals were used, one on each arm of the scattering table, and their single counts and coincidences were recorded. Method C was of value whenever one arm had to be placed at small angles to the beam, where a large background of charged particles was to be expected. Two crystal detectors were placed telescope fashion on this arm, and one detector was placed on the other arm of the scattering table. Three single counting rates, as well as their triple coincidence rate and the double coincidence rate from the telescope, were recorded. Method D, finally, employed a single detector. All methods agreed within statistical errors in the regions in which results obtained with them overlapped. Furthermore, methods A, B, C were used interchangeably, and we shall not distinguish between them in what follows, but merely group all results under the headings "coincidence method" (A, B, or C) or "single-count method" (D).

The experimental procedure used to check circuits and geometry prior to the recording of actual data was identical to that outlined in BC.

B. Kinematics and Geometry

Let M be the rest mass of a particle incident with kinetic energy E in the laboratory system on another particle of rest mass m, initially at rest. The two particles collide; that of mass M is deflected to a direction Θ, that of mass m, to a direction Φ, with respect to the incident beam in the laboratory system. Let θ be the angle of deflection of either particle in the center-of-mass system. We have then

$$\rho=\frac{m}{M},\quad \epsilon=\frac{E}{Mc^2},\quad \beta=\frac{[(\epsilon+1)^2-1]^{\frac{1}{2}}}{\epsilon+1+\rho};$$
$$\gamma=\frac{1}{[1-\beta^2]^{\frac{1}{2}}}\quad\text{and}\quad A=\gamma\frac{\epsilon+1+1/\rho}{\epsilon+1+\rho}, \tag{1}$$

where β is the ratio of the velocity of the mass m in the center-of-mass system to that of light.

We can then derive the following relativistic relations:

$$\gamma\tan(\theta/2)=\cot\Phi, \tag{2}$$
$$\tan\Theta=[2\tan(\theta/2)]/[A+\gamma+(A-\gamma)\tan^2(\theta/2)], \tag{3}$$
$$E_m=2mc^2\beta^2\gamma^2\sin^2(\theta/2), \tag{4}$$
$$E_M=E-E_m, \tag{5}$$

where E_M, E_m are the energies of incident and struck particle in the laboratory system after collision. The

* This work was performed under the auspices of the U. S. Atomic Energy Commission.
† Now at Carnegie Institute of Technology, Pittsburgh, Pennsylvania. A part of the research on which this paper is based was undertaken while this author was Amy Bowles Johnson Memorial Fellow at the University of California, and was submitted in partial satisfaction of requirements for the degree of Doctor of Philosophy.
[1] A. L. Bloom and Owen Chamberlain, preceding paper, Phys. Rev. 94, 659 (1954); hereafter referred to as BC.
[2] C. Wiegand, Rev. Sci. Instr. 21, 975 (1950).

energy available in the center-of-mass system is

$$E_0=(E/\gamma)-c^2(m+M)(1-1/\gamma) \tag{6}$$

and the initial momentum p_i and final momentum p_f in the center-of-mass system are

$$p_i=p_{ix}=mc\beta\gamma, \quad p_{fx}=mc\beta\gamma\cos\theta, \quad p_{fy}=mc\beta\gamma\sin\theta, \tag{7}$$

where x and y are directions in the scattering plane along and perpendicular to the beam, respectively.

In our case (Fig. 1) the deuteron is to be identified with M, Θ, the proton with m, Φ; other parameters are $\rho\approx\frac{1}{2}$, $\epsilon=0.1023$, and $\beta=0.29$ so that relativistic corrections are slight, although the exact relations were used in our calculations. For purposes of discussion it is sufficient to consider these relations in their nonrelativistic limits, $\gamma=1$ and $A=1/\rho$. It is then easy to see that the center-of-mass angle θ and the laboratory angle of deflection of the proton Φ are double-valued functions of the deuteron laboratory angle Θ. Thus when Θ is 0°, θ may be 0° or 180° and Φ may be 90° or 0°. Θ is never greater than 30°; when $\Theta=30°$, $\Phi=30°$, and $\theta=120°$. The energy of the struck proton reaches its maximum of $(8/9)E$ or about 171 Mev when $\theta=180°$.

The kinematics of elastic scattering for small and large θ are summarized in Table I.

Finally, for conversion from one system to the other the relations

$$\left|\frac{d\cos\Phi}{d\cos\theta}\right|=\frac{\gamma^2}{4\cos\Phi}(1-\beta^2\cos^2\Phi)^2 \tag{8}$$

and

$$\left|\frac{d\cos\Theta}{d\cos\theta}\right|=\frac{A\cos\theta+\gamma}{\{\sin^2\theta+[A+\gamma\cos\theta]^2\}^{\frac{1}{2}}} \tag{9}$$

are useful. For example we cite the relation

$$\sigma(\theta)=\left|\frac{d\cos\Phi}{d\cos\theta}\right|\sigma(\Phi). \tag{10}$$

The targets chosen with the coincidence method were of thickness (CH_2) 0.290 g cm^{-2}, and (C) 0.338 g cm^{-2}, in the range of angles $25°\leqslant\Phi\leqslant50°$. For small and large Φ thinner targets, of surface density less than 100 mg cm^{-2}, were used to reduce multiple scattering and allow the low-energy particles to be counted in the crystals. It was found geometrically convenient to make the solid angle subtended by the proton crystal at angle Φ the defining one; this meant that the deuteron crystal at angle Θ had to be large enough and close enough to the target to count all deuterons from elastic d-p events in which the proton was counted in the other crystal. The values of distances b and c of the Φ and Θ crystals from the target (see Fig. 1) were so chosen as to satisfy this criterion, keep the angular resolution between 2° and 5°, and have the ratio of systematic to accidental coincidences as high as practicable.

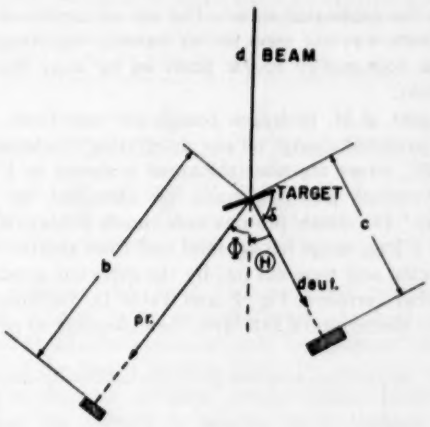

FIG. 1. Velocity diagram of a deuteron colliding with a target proton in the laboratory system; the distances b and c of the proton crystal and deuteron crystal from the target are shown, and angles Φ, Θ, and δ of the text are defined.

When $\Phi\leqslant15°$ the deuterons have too short a range to be counted reliably. However, as illustrated in Table I, in this region of angles the proton has enough energy to have a range greater than that of the deuterons from the beam and from carbon. Moreover, the beam straggling was of the order of 1 g cm^{-2} of Al. Thus it was possible to single out the forward protons by using method D: a crystal was placed at angle Φ, and variable thicknesses of Al absorber were placed immediately in front of the crystal. The area of the absorber slabs was made much larger than that of the crystal face to provide a "poor" geometry. A thin Al wedge was centered over the crystal to equalize the energy of the particles entering it. The range of the particles depended on the target used (CH_2, C, or Bl) since the targets had different stopping powers. ("Bl" indicates "blank," meaning that no target was placed in the beam.) The Al absorber was suitably adjusted to compensate for this effect. The targets were now of the order of 1 g cm^{-2}, since the hydrogen effect had to be separated from a large background coming directly

TABLE I. Angles and energies of deuterons and protons resulting from elastic scattering of 192-Mev deuterons on hydrogen. Φ and Θ are angles of deflection of proton and deuteron, respectively, in the laboratory system; θ is the angle of deflection in the center-of-mass system.

			Proton		Deuteron			
Φ degrees	Θ degrees	θ degrees	Energy Mev	Range g/cm^2 Al[a]	Energy Mev	Range g/cm^2 Al[a]	$\frac{d\cos\Phi}{d\cos\theta}$	$\frac{d\cos\Theta}{d\cos\theta}$
0	0	180	172	25.4	20	0.33	0.229	1.046
5	10.3	169.5	170	25.0	22	0.39	0.230	0.913
10	18.8	159.2	166	24.0	26	0.52	0.234	0.625
15	24.7	148.7	159	22.4	33	0.81	0.240	0.356
65.5	15	47.1	28	1.04	164	14.5	0.639	0.107
73.8	10	31.1	13	0.26	179	16.8	0.966	0.107
82.0	5	15.4	3	0.02	189	18.3	1.956	0.106
90	0	0	0	0	192	18.9	∞	0.106

[a] See reference 3.

from the collimator snout. The use of targets of this thickness was not expected to increase the straggling of the high-energy elastic particles by more than 15 per cent.

A plot of H, hydrogen counts per unit beam (one volt potential change on our integrating condenser) at $\Phi=10°$, *versus* absorber thickness is shown in Fig. 2. The various particles could be identified by their ranges.[3] The elastic protons were clearly distinguishable from a long range background and from shorter range particles, and were cut out by the expected amount of absorber (arrow *b*, Fig. 2, and Table I). Similarly, the elastic deuterons of 181 Mev, corresponding to protons

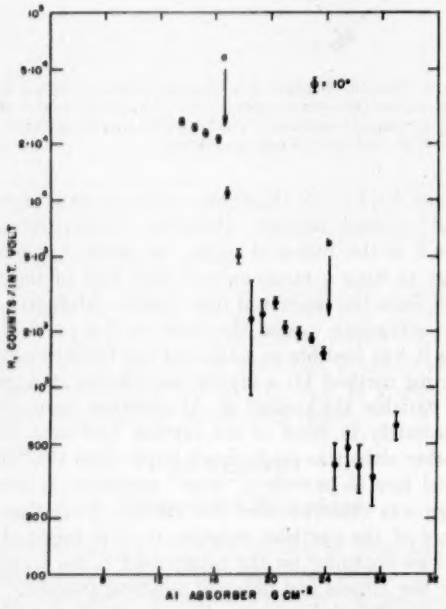

FIG. 2. Hydrogen counts per unit beam charge as a function of aluminum absorber thickness in front of the crystal (method D). Arrows *a* and *b* give the absorbers, 16.7 g cm^{-2} and 24.2 g cm^{-2}, at which, respectively, half the elastic deuterons (corresponding to $\Phi=73.8°$) and protons ($\Phi=10°$) are counted. Calculated ranges are 16.8 g cm^{-2} and 24.0 g cm^{-2}, respectively.

at $\Phi=74°$ (arrow *a*, Fig. 2) were also clearly identified. Finally, plots of C and Bl counts *versus* absorber had sharp breaks at values of absorber corresponding to the ranges of deuterons from carbon and from the beam, respectively. It was therefore possible, by this method, to obtain the elastic cross section for small and large center-of-mass angles θ for which the coincidence technique was unsuited. The relatively large background, which did not decrease appreciably with increasing absorber, was ascribed to events made by neutrons stripped[4] from high-energy deuterons in the aluminum.

[3] Aron, Hoffman, and Williams, U. S. Atomic Energy Commission Report AECU-663 (unpublished).

[4] Robert Serber, Phys. Rev. **72**, 1008 (1947).

C. Sample Calculation

1. Coincidence Method

We have chosen for illustration a set of data taken with the proton counter at the angle $\Phi=35°$ and the deuteron counter at $\Theta=29.2°$. The stilbene crystal of the proton counter had an area of 9.88 cm^2 and was located a distance *b* from the target of 92.5 cm. These figures combine to give a solid angle of $\Delta\Omega=1.155\times10^{-3}$ sterad. The deuteron crystal was of 36-cm^2 area and located at a distance $c=92.5$ cm. The polyethylene and carbon targets had surface densities of 0.290 and 0.338 g cm^{-2}, respectively. The targets were so oriented that the angle δ made by the target plane with the deuteron counter direction was 25°.

The capacity of the integrating condenser was $C_0=1.021\times10^{-7}$ f. The ionization chamber used for beam integration was filled with argon at an absolute pressure of 78.4 cm Hg when measured at the temperature 23°C. We have computed the ionization chamber multiplication[5] μ to be 1801, using the beam calibration results of Chamberlain, Segrè, and Wiegand[6] corrected by use of the range energy curves[3] to apply to the 190-Mev deuteron beam.

The effective resolving time of the counters (see BC) was $(1.5\pm0.3)\times10^{-5}$ sec.

The data from one of several cycles of counting with targets CH_2, C, and Bl are summarized in Table II. ("Bl" indicates "blank," meaning no target is placed in the target position.) The method of analysis described in BC leads in this case to the carbon subtraction factor $z=1.08\pm0.20$. Using Eq. (1) of BC, we obtain the hydrogen effect per unit beam (integrator volt) $H=26.5\pm3.5$. The target plane makes an angle of 54.2° with the beam direction. Using this angle and the target surface density given above we compute the number of hydrogen atoms per unit area normal to the beam to be $N=3.09\times10^{22}$ atoms cm^{-2}. The number of deuterons per unit beam is given by $n=C_0/e\mu$, where e is the electronic charge. We obtain $n=3.54\times10^8$ deuterons per integrator volt. Equation (4) of BC then yields $\sigma(\Phi=35°)=2.10\pm0.28$ mb sterad^{-1}. When converted to the center-of-mass system, this becomes $\sigma(\theta=107.6°)=(0.62\pm0.08)\times10^{-27}$ cm^2 sterad^{-1}.

2. Single-Count Method

Here we have taken the case of $\Phi=10°$ or $\Theta=10°$ as illustrated in Fig. 2. The crystal area was 9.55 cm^2 and the crystal was 100 cm from the target. The counting solid angle was thus $\Delta\Omega=9.55\times10^{-4}$ sterad. The

[5] In the ionization chamber there is no gas multiplication of the type used in a proportional counter. However each deuteron of the beam leaves many ion pairs in the gas of the ionization chamber, hence the ionization chamber current is much larger than the beam current. The ratio of ionization chamber current to beam current is referred to here as the ionization chamber multiplication.

[6] Chamberlain, Segrè, and Wiegand, Phys. Rev. **83**, 923 (1951).

target surface densities were 0.991 and 1.284 g cm^{-2} of polyethylene and carbon, respectively. The targets were oriented normal to the beam.

The beam integrating condenser was $C_0=0.99\times10^{-6}$ f. The ionization chamber pressure was 77.4 cm Hg at 22°C. The ionization chamber multiplication was $\mu=1784$.

Typical data are given in Table III for the most significant values of absorber thickness. The last row of the table shows the effect due to hydrogen in the polyethylene target, calculated with the appropriate value of the carbon subtraction factor $z=0.661$. A slight correction has been made for the difference in stopping power of polyethylene and carbon targets.

The number of protons counted at 10° was determined from the difference in counts with 22.9 and 24.7 g cm^{-2} absorber. For this case the hydrogen effect is $H_p=(1830\pm110)-(440\pm50)=1390\pm120$. Using the known hydrogen surface density of the target $N=8.58\times10^{22}$ atoms cm^{-2}, and the number of deuterons per unit beam $n=3.43\times10^{9}$ deuterons/integrator volt we obtain the differential cross section $\sigma(\Phi=10°)=4.95\pm0.43$ mb sterad^{-1}. In the center-of-mass system this is $\sigma(\theta=159.2)=(1.16\pm0.10)\times10^{-27}$ cm^2 sterad^{-1}.

For deuterons counted at the same angle we have taken the difference in counts with 16.1 and 20.3 g cm^{-2} absorber. The hydrogen effect is then $H_d=(21\,200\pm700)-(2800\pm200)=18\,400\pm750$. This leads to the laboratory system cross section $\sigma(\Theta=10°)=66.5\pm2.7$ mb sterad^{-1} and to the center-of-mass cross section $\sigma(\theta=31.1°)=(7.0\pm0.3)\times10^{-27}$ cm^2 sterad^{-1}.

D. Presentation of Data

It should be mentioned that the elastic cross sections obtained with method D are subject to some corrections. The protons observed at a certain angle Φ are attenuated by the nuclei in the absorber. A cross section $\sigma=\pi A^{\frac{1}{3}}r_0^2$, with $r_0=1.4\times10^{-13}$ cm, was chosen to correct for this effect, and an error of 20 percent was applied to the correction. The number of deuterons observed at a given angle Θ had to be similarly corrected; another correction of +5 percent had to be applied to compensate for stripping losses.[4] It is clear that, apart from systematic errors discussed in the next section, the elastic cross section obtained with all methods is an *upper limit*, inasmuch as some inelastic events may have been included. If one assumes a just inelastic d-p collision with one proton going forward at high energy and the other proton and neutron remaining close neighbors (say in the S state), the energetic proton would have of the order of only 3 Mev less energy than one scattered forward elastically. This effect may be sizable, especially for large θ, but no attempt has been made to correct for it.

The data, duly corrected, are summarized in Table IV. They have been averaged for a given angle over a given day's run, but results for the same angle obtained on a different day have been included separately. Values marked with asterisks were obtained with method D, all others with methods A–C. Figure 3 shows a plot of the results listed in Table IV, center-of-mass cross sections as ordinate, center-of-mass angle as abscissa. By passing a smooth curve through the weighted mean cross sections with a cutoff at $\theta=10°$ we found a total cross section from 10° to 180° in the center-of-mass system of 34±3 mb. The errors quoted in Fig. 3 are rms deviations due to counting statistics, absorber corrections and systematic uncertainties.

TABLE II. Typical set of data for elastic d-p scattering at proton angle $\Phi=35°$ (Method C). The column labeled "Integrator volts" indicates the potential to which the beam integrating condenser was charged during the counting interval.

Target	Time (sec)	♦ (Telesc. coinc.)	♥ (Total counts)	Triple coinc.	Integrator volts
CH_2	314	1989	26 988	90	3.0
C	227	1098	16 856	7	2.1
Bl	210	391	7030	2	2.0

E. Errors

The estimated errors discussed in some detail in this section refer mainly to the coincidence methods A, B, and C; however, those of the first three paragraphs apply to all four methods.

Geometry: the alignment of the scattering table with respect to the beam could be guaranteed correct to within one degree. The angles of the counters with respect to the scattering table were known to ½ degree. The distance b defined in Fig. 1 was believed measured to 5 mm in 50 to 100 cm, and so gave rise to solid angle uncertainties of about two percent. Target orientation was known to one degree, giving the effective target thickness to ½ percent or one percent. Crystal areas were all known to two percent. An error of three percent is attributed to uncertainty in interpretation of the bias curves of the counters.

Beam current measurement: the Faraday cup calibration of Chamberlain, Segrè, and Wiegand[6] was thought accurate to 2 percent. Saturation of the argon-filled ionization chamber was guaranteed to 1 percent.

TABLE III. Sample data for elastic d-p scattering at 10°, single-count method, for various thicknesses of aluminum absorber in front of the detector. All data normalized to the same integrated beam current, *viz.*, that required to give one volt on the integrating condenser. Effect due to hydrogen shown in the last row.

Target	Absorber thicknesses in g cm^{-2} of aluminum (24.7–29.1)$_{Av}$	22.9	20.3	16.1
CH_2	5590±35	7740± 70	11 740±130	81 000±500
C	6330±35	7380±100	11 860±220	83 000±700
Bl	2890±40	3040±100	3150±100	14 630±350
H	440±50	1830±110	2800±200	21 200±700

TABLE IV. Summary of elastic d-p differential scattering cross sections in the center-of-mass system as a function of center-of-mass angle θ. Figures of the last column include the systematic errors of Sec. E. Cross sections obtained with the "single-count method" are marked with an asterisk.

θ degrees	$\sigma(\theta)$ 10^{-27} cm²/sterad	Rms counting error 10^{-27} cm²/sterad	$\langle\sigma(\theta)\rangle_{Av}$ 10^{-27} cm²/sterad	Rms total error 10^{-27} cm²/sterad
15.4	31.1*	3.2	31.1	5.1
31.1	8.9*	0.5	8.9	1.3
38.4	6.6	0.4		
	4.9	0.6		
	4.8	0.3	5.3	0.5
48.1	4.4	0.3		
	4.6	0.3		
	3.65*	0.17	4.0	0.4
57.8	2.14	0.07		
	2.54	0.11	2.33	0.21
67.6	1.22	0.05	1.22	0.10
77.5	1.16	0.06	1.16	0.10
81.5	0.89	0.05	0.89	0.08
87.5	0.70	0.03		
	0.77	0.08	0.71	0.06
97.5	0.59	0.04		
	0.73	0.05	0.64	0.05
107.6	0.61	0.03	0.61	0.05
117.8	0.52	0.08	0.52	0.09
128.0	0.55	0.17		
	0.67	0.06		
	0.67	0.18		
	0.55	0.13		
	0.73	0.10		
	0.57	0.06		
	0.54	0.05		
	0.45	0.04	0.55	0.04
138.4	0.72	0.27		
	0.27	0.09		
	0.42	0.06		
	0.42	0.08	0.40	0.05
148.7	0.27	0.23		
	0.51	0.25		
	0.67	0.07		
	0.62	0.12		
	0.24	0.14		
	0.67*	0.07		
	0.61*	0.07	0.61	0.06
159.2	1.45	0.50		
	1.53*	0.13	1.52	0.20
169.5	1.75*	0.25	1.75	0.34

Targets: the hydrogen content of the polyethylene targets was known from analysis to 1 percent.

Multiple scattering: 2 percent error is estimated except where the angle Φ exceeded 60°, in which case 5 percent was estimated. No appreciable loss is attributed to multiple scattering in the telescope of method C.

Finite counter resolving time: counting rate losses amounted to no more than 2 percent at the highest counting rates allowed.

Carbon subtraction: errors were not greater than 2 percent, and were due mainly to duty cycle variations that might have escaped unnoticed.

Inelastic scattering: the possible inclusion of some inelastic d-p scattering events among those counted may have resulted in error of perhaps 3 percent.

We summarize by giving the systematic rms errors for the experiment. In the coincidence methods, when θ was greater than 60°, we have estimated 7 percent. When θ was less than 60°, the coincidence methods gave 9 percent error. Finally method D is believed accurate to 13 percent. Errors from counting statistics are to be combined with these values.

II. COMPARISON WITH THEORY

A. General Considerations

We shall try to use our experimental results on d-p scattering in order to gain additional knowledge about n-p and p-p scattering. The theory of d-p scattering has been studied by Wu and Ashkin,[7] Chew,[8–11] and Gluckstern and Bethe.[12]

In all previous work the Born or impulse approximation was used, and in some of it an attempt was made to identify certain terms in the d-p scattering amplitude with the n-p and p-p scattering amplitudes. In this connection it has usually been said that in calculating the d-p cross sections one is interested in the n-p and p-p cross sections obtained from experiments done with the same relative velocities. That is, one should be concerned with n-p and p-p differential scattering cross sections at 95 Mev when calculating the scattering of 190-Mev deuterons by stationary protons. The angles are correlated by the requirement that the magnitude of momentum transferred should be the same in all cases.

This is quite true at small angles of scattering, as is shown by both impulse approximation and Born approximation. However, it seems worth while to comment that as one examines larger angle elastic d-p scattering, one should compare with n-p and p-p scattering at a higher energy.

Our argument is based on the Born approximation and is believed to apply equally to the impulse approximation, inasmuch as one can easily construct hypothetical parameters for n-p and p-p interactions such that both Born approximation and impulse approximation are guaranteed to be valid.

We write the amplitude for elastic d-p scattering in the form used by Chew,[8] employing for the n-p interaction a potential which is partly ordinary force and partly exchange force. (The p-p interaction may be treated formally the same way.) We obtain from the ordinary force the integral Chew has called I_1, and from the exchange force the integral I_2. The factor $S^{\frac{1}{2}}$ can be taken from I_1 immediately. (S is the "sticking factor" of Chew.) The same factor can be taken from I_2 if the suitable approximation is made, that the potentials used are more singular than the deuteron wave function. The

[7] Ta-You Wu and J. Ashkin, Phys. Rev. **73**, 986 (1948).
[8] G. F. Chew, Phys. Rev. **74**, 809 (1948).
[9] G. F. Chew, Phys. Rev. **80**, 196 (1950).
[10] G. F. Chew, Phys. Rev. **84**, 710 (1951).
[11] G. F. Chew, Phys. Rev. **84**, 1057 (1951).
[12] R. L. Gluckstern and H. A. Bethe, Phys. Rev. **81**, 761 (1951).

remaining integrals are

$$I_1/S^{\frac{1}{2}}=\int d\mathbf{x}\,\exp[-i(\mathbf{k}_f-\mathbf{k}_0)\cdot\mathbf{x}]V_{\text{ord}}(x),$$
$$I_2/S^{\frac{1}{2}}\cong\int d\mathbf{x}\,\exp[-\tfrac{3}{4}i(\mathbf{k}_f+\mathbf{k}_0)\cdot\mathbf{x}]V_{\text{exch}}(x), \tag{11}$$

where $\mathbf{k}_f$ and $\mathbf{k}_0$ are final and initial momenta in the c.m. system (divided by $\hbar$). The corresponding expressions for free n-p scattering are

$$I_1'=\int d\mathbf{x}\,\exp[-i(\mathbf{k}_f'-\mathbf{k}_0')\cdot\mathbf{x}]V_{\text{ord}}(x),$$
$$I_2'=\int d\mathbf{x}\,\exp[-i(\mathbf{k}_f'+\mathbf{k}_0')\cdot\mathbf{x}]V_{\text{exch}}(x), \tag{12}$$

where $\mathbf{k}_f'$ and $\mathbf{k}_0'$ have the corresponding meanings in the c.m. system for neutron and proton. In order that $I_1/S^{\frac{1}{2}}=I_1'$ and $I_2/S^{\frac{1}{2}}=I_2'$ (so that n-p scattering amplitudes may be correctly used in the d-p expression) the following relations must hold:

$$|\mathbf{k}_f-\mathbf{k}_0|=|\mathbf{k}_f'-\mathbf{k}_0'|,\quad \tfrac{3}{4}|\mathbf{k}_f+\mathbf{k}_0|=|\mathbf{k}_f'+\mathbf{k}_0'|. \tag{13}$$

For a given energy and angle of d-p scattering these relations determine the energy and angle of the n-p scattering such that the scattering amplitudes appear directly in the d-p expressions. We include in Table V the values of energy (laboratory system) and angle (c.m. system) for n-p scattering corresponding to various angles (c.m. system) for the present case of 192-Mev deuterons scattered by protons.

B. Analysis without Tensor Forces

In this section we wish to follow the very elegant method used by Chew,[11] and to point out a few examples which may be used as guides in further work. As will perhaps be evident to some readers, we propose to take the results of Chew more seriously than he does. It is our hope that in the near future more explicit analyses of the errors in the impulse approximation, as applied to this problem, may be available.

We write Chew's result in the following form:

$$\frac{9}{16}\frac{\sigma_{dp}(\theta)}{S(K)}=|r_{np}{}^0+r_{pp}{}^0|^2+\tfrac{3}{4}|r_{np}{}^1+r_{pp}{}^1|^2, \tag{14}$$

TABLE V. Center-of-mass angle θ' and laboratory energy E' to be used in the nucleon-nucleon scattering amplitudes associated with d-p scattering at center-of-mass angle θ.

θ c.m. degrees	θ' c.m. degrees	E' lab. syst., Mev
0°	0°	96
20°	26°	98
40°	52°	103
60°	74°	115
80°	95°	127

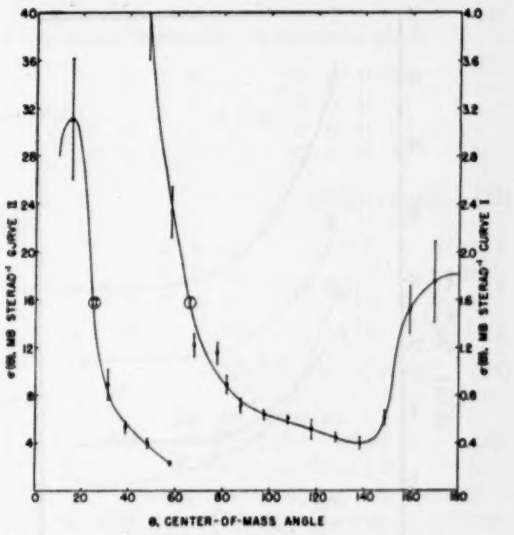

FIG. 3. Averaged differential elastic cross sections in the center-of-mass system, with their total errors. The curve was used to find the total cross section between 10° and 180°, 34±3 mb.

where $\mathbf{K}=\mathbf{k}_f-\mathbf{k}_0$, $S(K)$ is the sticking factor defined by Chew (with the Hulthèn wave function representing the bound state of the deuteron), r^0 (frequently called the "amplitude for scattering without spin flip") is defined in terms of triplet and singlet scattering amplitudes (r^t and r^s) as follows:

$$r^0=\tfrac{3}{4}r^t+\tfrac{1}{4}r^s, \tag{15}$$

and r^1 (the "amplitude for scattering with spin flip") is

$$r^1=\tfrac{1}{4}\sqrt{3}(r^t-r^s). \tag{16}$$

The complex scattering amplitudes so defined have the very convenient properties

$$\sigma_{np}(\theta)=|r_{np}{}^0|^2+|r_{np}{}^1|^2, \tag{17}$$

and an identical relation holds for p-p scattering.

If, then, the breakup of the n-p and p-p scattering into scattering with and without spin flip were known, the elastic d-p cross section could be reliably predicted, at least as fairly small angles where the approximations used are good. It is interesting that the spin-flip term enters in Eq. (14) with such a large coefficient as $\frac{3}{4}$, which corresponds to the fact that spin-flip phenomena most frequently leave the deuteron in a triplet state, owing to the large statistical weight.

We take the n-p and p-p cross sections as known,[6,13–16] even though we have to interpolate somewhat between observations to cover the energy region 95 to 130 Mev. However, the analysis into scattering amplitudes with

[13] Hadley, Kelly, Leith, Segrè, Wiegand, and York, Phys. Rev. **75**, 351 (1949).
[14] Birge, Kruse, and Ramsey, Phys. Rev. **83**, 274 (1951).
[15] Cassels, Stafford, and Pickavance, Nature **168**, 468 (1951).
[16] C. L. Oxley and R. D. Schamberger, Phys. Rev. **85**, 416 (1952).

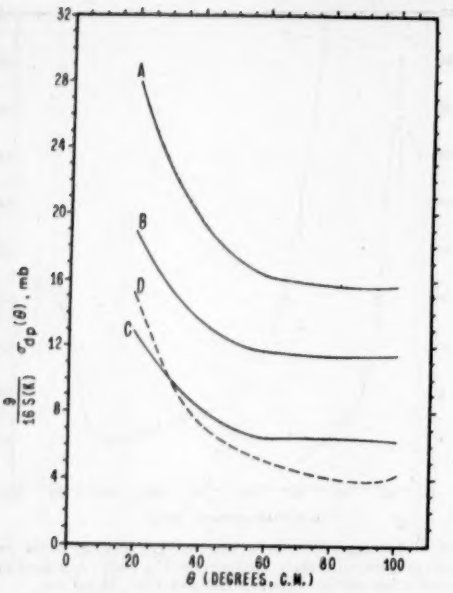

FIG. 4. Plot of $\{9/[16\,S(K)]\}$ times the elastic d-p cross section in mb as a function of center-of-mass angle θ under various assumptions, central forces only. A, n-p and p-p all nonspin flip. B, Serber potential. (see reference 17.) C, n-p nonspin flip, p-p all spin flip. D, Experimental values.

and without spin flip is not known, and we wish to test several assumptions.

The simplest assumption is that both n-p and p-p scattering are completely without spin flip and there is no great phase difference between the scattering amplitudes. This leads to the largest possible elastic d-p scattering, and the result is plotted in Fig. 4, Curve A. This cross section is much larger than that observed, Curve D, which is shown in the same figure.

The next, and more reasonable, assumption would be that n-p and p-p forces are identical (can be derived from the same potential) and that only even states are present in the scattering (Serber potential).[17] With these assumptions the Pauli principle dictates that the p-p scattering be all singlet scattering, and the p-p scattering may be used to deduce the separation of n-p scattering into singlet and triplet states. With the further assumption that the phase differences between singlet and triplet amplitudes are not large, the resulting d-p scattering is indicated also in Fig. 4, Curve B. Again the calculated result is somewhat too large.

One gets results closer to those observed by assuming that n-p scattering involves no spin flip, and that p-p scattering is all with spin flip. However, this proposal is not a reasonable one from the viewpoint of other work. It does not agree at all with any of the potentials calculated for n-p and p-p scattering, and it does not allow for charge independence of nuclear forces. Curve C shows this result quite close to that observed.

[17] R. S. Christian and E. W. Hart, Phys. Rev. **77**, 441 (1950).

We have found it helpful to visualize r^0 and r^1 as the two components of a vector in a two-dimensional space (i.e., one vector for n-p, and another for p-p scattering), and to say that this analysis is summarized by the statement that the amplitude vectors for n-p and p-p scattering must be approximately perpendicular to each other to allow agreement between theory and experiment.

C. Analysis with Tensor Forces

We must now write Chew's result in the more general form:

$$\frac{9}{16}\frac{\sigma_{dp}(\theta)}{S(K)}=|\mathbf{r}_{np}{}^0+\mathbf{r}_{pp}{}^0|^2+\tfrac{2}{3}|\mathbf{r}_{np}+\mathbf{r}_{pp}|^2, \qquad (18)$$

where $\mathbf{r}_{np}$ and $\mathbf{r}_{pp}$ have been written as vectors to indicate that there are three component amplitudes r^1 to r^3 involved. Thus four amplitudes for n-p and p-p are now needed to deduce the cross section. We shall show below how these are found. Again we have

$$\sigma_{np}(\theta)=\sum_{i=0}^{3}|r_{np}{}^i|^2, \qquad (19)$$

and a similar relation for the p-p cross section.

Once a potential has been assumed, the breakup of n-p and p-p scattering into r^0, r^1, r^2 and r^3 can be found. The d-p cross section can then be written and compared with experimental values. A suitable program would therefore be to take a great variety of potentials that lead to correct nucleon-nucleon scattering cross sections, calculate d-p scattering from them by using the nucleon-nucleon phase shifts, and compare with experiment. One would thereby hope to be able to eliminate a great number of potentials as unsuitable.

Unfortunately, the number of potentials that have so far succeeded in describing nucleon-nucleon scattering experiments adequately is small—we shall consider four—and the task of computing and using partial phase shifts is beyond our scope. We have therefore, with one exception, limited ourselves to the Born approximation in calculating the two sets of four scattering amplitudes. Instead of comparing the d-p cross section calculated from these directly with experiment, we compare it with the n-p and p-p cross sections derived from the same scattering amplitudes.

We then make the plausible postulate that the relation found to hold between experimental n-p, p-p and d-p differential scattering cross sections should exist, to good approximation, between the same cross sections as calculated from scattering amplitudes derived in Born approximation, if the potential assumed is to have validity; it is felt that this relation should be maintained to good approximation even though the Born approximation does not render the cross sections very faithfully at the energies involved here. The relation found to hold between measured cross sections was that (apart from the sticking factor) the n-p and p-p waves did not

strongly interfere in d-p scattering; i.e., the amplitude vectors for n-p and p-p scattering were roughly orthogonal. We postulate that this orthogonality must still hold when the components of the vectors (now four-vectors due to inclusion of tensor forces) are calculated in Born approximation. Accordingly we are interested in comparing the ratios $\sigma_{dp}/(\sigma_{np}+\sigma_{pp})$ for experiment and for various calculated potentials. We shall limit ourselves to scattering angles less than 90° in the center of mass, as the expression (18) breaks down at large angles.

We now write, in the usual way,

$$\psi\chi \rightarrow \exp(ik_0 z)\chi_{\text{inc}} + r^{-1}\exp(ik_0 r)S\chi_{\text{inc}}, \tag{20}$$

where ψ denotes the asymptotic form of the total wave function, χ its spin part, and k_0 is the propagation number in the center-of-mass system. S will be called the scattering matrix. When evaluated in Born approximation, it will be denoted by S_B. Our procedure will be to find the 4×4 matrix S_B for nucleon-nucleon scattering derived from a given potential and expressed in a suitably simple reference frame, to identify r^0 to r^3, and therefrom to find the nucleon-nucleon and d-p cross sections. In this process the 6×6 scattering matrix for d-p scattering can be derived and Chew's expression checked. Finally the ratios $\sigma_{dp}/(\sigma_{np}+\sigma_{pp})$ will be compared with those obtained from experimental values.

We shall derive the nucleon-nucleon cross section for identical particles labeled 1 and 2. Extension to non-identical particles is obvious. We are given a potential $U(\mathbf{r},\sigma)\hbar^2/2m$ and have, for the scattering amplitude in Born approximation,

$$f-f' = f(\theta,\phi,\chi_{12}) - f(\pi-\theta,\pi+\phi,\chi_{21}) = S_B\chi_{\text{inc}}{}^{12} - S_B'\chi_{\text{inc}}{}^{21}, \tag{21}$$

where

$$S_B = (4\pi)^{-1}\int U(\mathbf{r},\sigma)\exp[i(\mathbf{k}_0-\mathbf{k}_f)\cdot\mathbf{r}]d\mathbf{r}, \tag{22}$$

$$S_B' = (4\pi)^{-1}\int U(\mathbf{r},\sigma)\exp[-i(\mathbf{k}_0+\mathbf{k}_f)\cdot\mathbf{r}]d\mathbf{r}. \tag{23}$$

The cross section is obtained by squaring $f-f'$ and averaging over all initial spin states. We now specify

$$U^t(\mathbf{r},\sigma) = \frac{2m}{\hbar^2}[J_c(r)+J_t(r)S^{12}] \tag{24}$$

for the triplet interaction, with

$$S^{12} = 3\frac{(\boldsymbol{\sigma}_1\cdot\mathbf{r})(\boldsymbol{\sigma}_2\cdot\mathbf{r})}{r^2} - \boldsymbol{\sigma}_1\cdot\boldsymbol{\sigma}_2, \tag{25}$$

and

$$U^s(\mathbf{r},\sigma) = \frac{2m}{\hbar^2}J_c'(r) \tag{26}$$

for the singlet interaction. Substitution yields

$$S_B = F(\theta)\begin{pmatrix}1&0&0&0\\0&1&0&0\\0&0&1&0\\0&0&0&0\end{pmatrix} + F'(\theta)\begin{pmatrix}0&0&0&0\\0&0&0&0\\0&0&0&0\\0&0&0&1\end{pmatrix} + C(\theta)\|\tau(\theta,\phi)\|, \tag{27}$$

and

$$S_B' = F(\pi-\theta)\begin{pmatrix}1&0&0&0\\0&1&0&0\\0&0&1&0\\0&0&0&0\end{pmatrix} - F'(\pi-\theta)\begin{pmatrix}0&0&0&0\\0&0&0&0\\0&0&0&0\\0&0&0&1\end{pmatrix} + C(\pi-\theta)\|\tau(\pi-\theta,\pi+\phi)\|, \tag{28}$$

where

$$F(\theta) = \frac{2m}{\hbar^2}\int_0^\infty J_c(r)\frac{\sin Kr}{Kr}r^2dr, \tag{29}$$

$$F'(\theta) = \frac{2m}{\hbar^2}\int_0^\infty J_c'(r)\frac{\sin Kr}{Kr}r^2dr, \tag{30}$$

and

$$C(\theta)\|\tau(\theta,\phi)\| = \frac{m}{2\pi\hbar^2}\int J_t(r)S^{12}\exp[i(\mathbf{k}_0-\mathbf{k}_f)\cdot\mathbf{r}]d\mathbf{r}, \tag{31}$$

where

$$C(\theta) = \frac{m}{\hbar^2}\int_0^\infty J_t(r)\left[\frac{6\sin Kr}{K^3r^3} - \frac{6\cos Kr}{K^2r^2} - \frac{2\sin Kr}{Kr}\right]r^2dr. \tag{32}$$

The value of the 4×4 matrix $\|\tau\|$ depends on the polar axis chosen for the representation. As pointed out by Ashkin and Wu,[18] we can choose the polar axis along $\mathbf{K}=\mathbf{k}_0-\mathbf{k}_f$, and this procedure yields

$$\|\tau(\theta,\phi)\| = \boldsymbol{\sigma}_1\cdot\boldsymbol{\sigma}_2 - 3\sigma_{1K}\sigma_{2K}, \tag{33}$$

where the σ are the Pauli spin matrices. In particular, we can make $\mathbf{K}$ coincide with the axis of spin quantization. This will make $\|\tau(\theta,\phi)\|$ diagonal, but not $\|\tau(\pi-\theta,\pi+\phi)\|$. It is easy to see that since

$$\|\tau'\| = \|\tau(\pi-\theta,\pi+\phi)\| = \boldsymbol{\sigma}_1\cdot\boldsymbol{\sigma}_2 - 3\sigma_{1K'}\sigma_{2K'},$$

and $\mathbf{K}'\equiv-(\mathbf{k}_0+\mathbf{k}_f)$ is perpendicular to $\mathbf{K}$, $\|\tau\|$ and $\|\tau'\|$ commute, and can be diagonalized simultaneously. It will be convenient to do so. The result is

$$\|\tau\| = \begin{pmatrix}-2&0&0&0\\0&4&0&0\\0&0&-2&0\\0&0&0&0\end{pmatrix},\quad \|\tau'\| = \begin{pmatrix}-2&0&0&0\\0&-2&0&0\\0&0&4&0\\0&0&0&0\end{pmatrix}, \tag{34}$$

where the rows and columns are labelled by basis vectors

$$\xi_1 = \frac{1}{\sqrt{2}}(\alpha_1\alpha_2-\beta_1\beta_2),\quad \xi_2 = \frac{1}{\sqrt{2}}(\alpha_1\beta_2+\beta_1\alpha_2),$$
$$\xi_3 = \frac{1}{\sqrt{2}}(\alpha_1\alpha_2+\beta_1\beta_2),\quad \xi_4 = \frac{1}{\sqrt{2}}(\alpha_1\beta_2-\beta_1\alpha_2); \tag{35}$$

[18] J. Ashkin and Ta-You Wu, Phys. Rev. **73**, 973 (1948).

that is, in choosing a z axis different from the K axis we have mixed the basis vectors for spin components 1 and -1 along the K axis, leaving the components 0 in triplet and singlet unaltered.

We can now write down the result:

$$f-f'=\chi_{\text{inc}}{}^{12}\begin{bmatrix} F(\theta)-F(\pi-\theta) & 0 & 0 & 0 \\ -2[C(\theta)-C(\pi-\theta)] & & & \\ 0 & F(\theta)-F(\pi-\theta) & 0 & 0 \\ & +4C(\theta)+2C(\pi-\theta) & & \\ 0 & 0 & F(\theta)-F(\pi-\theta) & 0 \\ & & -2C(\theta)-4C(\pi-\theta) & \\ 0 & 0 & 0 & F'(\theta)+F'(\pi-\theta) \end{bmatrix} \tag{36}$$

and the p-p cross section is at once obtained by squaring and averaging over initial spins, which yields one-fourth the sum of the squares of the matrix elements. In order to derive the d-p cross section, we would like now to find r^0 to r^3. In this we are guided by our definitions for r^0 and r^1 with central forces only. Call $\phi_1\cdots\phi_4$ the four diagonal elements of the preceding matrix. We are led to write

$$r^0=(\phi_1+\phi_2+\phi_3+\phi_4)/4,$$
$$r^1=(\phi_1+\phi_2+\phi_3-3\phi_4)/4\sqrt{3}. \tag{37}$$

Note that since $\|\tau\|$ and $\|\tau'\|$ have zero trace, tensor forces do not enter r^0 and r^1. r^2, and r^3 must now be defined in such a way that condition (19) is satisfied, i.e.,

$$\sigma_{pp}=\sum_{i=0}^{3}[r_{pp}{}^i|^2=\tfrac{1}{4}\sum_{j=1}^{4}|\phi_j|^2. \tag{38}$$

This leaves two possibilities, of which we choose the one that yields the greater symmetry in $C(\theta)$ and $C(\pi-\theta)$:

$$r^2=(2\phi_1-\phi_2-\phi_3)/2\sqrt{6},$$
$$r^3=(\phi_3-\phi_2)/2\sqrt{2}. \tag{39}$$

Note that neither r^2 nor r^3 contain central force terms.

Having found the amplitude for n-p and p-p scattering in various two-particle spin states, we need merely expand the six possible total spin functions of the d-p system (four quartet and two doublet states, the latter symmetric in spins of the particles in the deuteron) $\chi_{1\cdots6}$ in terms of the two-particle functions $\xi_{1\cdots4}$ (35), multiply by each of the $\chi_{1\cdots6}$ in turn and remember that the amplitude for scattering from a state ξ_i to a state ξ_j is $\phi_i\delta_{ij}$. We thus obtain the 6×6 Born scattering matrix for deuteron-proton scattering. One-sixth the sum of squares of its elements gives the d-p cross section [apart from a factor $(16/9)S(K)$] in terms of the ϕ_i. This expression can then be expanded in terms of the r^i. Chew's expression is the result, and since we know the r^i for a given potential, $\sigma_{dp}(\theta)$ can be found in Born approximation.

It may be instructive to try to evaluate $\sigma_{dp}(\theta)$ to a somewhat higher approximation. In one of the cases (hard core, fourth potential, see below) the singlet and triplet phase shifts for definite energies were actually available. The scattering matrices for nucleon-nucleon scattering were therefore computed "exactly" in a convenient reference frame,[19] and were afterwards transformed to the reference frame in which S_B and S_B' had been found to be diagonal. In this frame it was found that all matrix elements of the exact scattering matrix

TABLE VI. Potentials used in the present calculations. CH = Christian and Hart; CN = Christian and Noyes; CNS = Christian, Noyes, and Swanson; JS = Jastrow and Swanson. IND = Charge-independent, B = Born approximation, δ = phase shift calculation. Potentials in Mev. P is the space permutation operator, and S^{12} is the tensor operator defined in Eq. (25). Parameters, in 10^{-13} cm, are: $r_0=1.35$, $r_1=2.615$, $r_2=1.6$, $r_3=0.60$, $r_4=0.40$, $r_5=0.48$, $r_6=0.24$.

Nucleon pair	Potential variety	Spin state	Potential	Method of calculation
np	CH	singlet	$-35.3(\frac{1}{2}+\frac{1}{2}P)(r_0/r)e^{-r/r_0}$	B
		triplet	$-25.3(\frac{1}{2}+\frac{1}{2}P)(r_0/r)e^{-r/r_0}-48.3(0.37+0.63P)(r_0/r)e^{-r/r_0}S^{12}$	B
pp	CN	singlet	$-13.273(\frac{1}{2}+\frac{1}{2}P)$, $r<r_1$; 0, $r>r_1$	B
		triplet	$\pm15.25(\frac{1}{2}-\frac{1}{2}P)(r_2/r)^2e^{-r/r_2}S^{12}$	B
IND	CNS	singlet	$-13.273(\frac{1}{2}+\frac{1}{2}P)$, $r<r_1$; 0, $r>r_1$	B
		triplet	$-25.3(\frac{1}{2}+\frac{1}{2}P)(r_0/r)e^{-r/r_0}-48.3(\frac{1}{2}+\frac{1}{2}P)(r_0/r)e^{-r/r_0}S^{12}\pm15.25(\frac{1}{2}-\frac{1}{2}P)(r_2/r)^2e^{-r/r_2}S^{12}$	B
IND	JS	singlet	∞, $r<r_3$; $-375(\frac{1}{2}+\frac{1}{2}P)e^{-(r-r_3)/r_4}$, $r>r_3$	δ
		triplet	$-25.3(\frac{1}{2}+\frac{1}{2}P)(r_0/r)e^{-r/r_0}-48.3(\frac{1}{2}+\frac{1}{2}P)(r_0/r)e^{-r/r_0}S^{12}+15.25(\frac{1}{2}-\frac{1}{2}P)(r_2/r)^2e^{-r/r_2}S^{12}$	B
np	JCH	singlet	∞, $r<r_3$; $-375(\frac{1}{2}+\frac{1}{2}P)e^{-(r-r_3)/r_4}$, $r>r_3$	δ
		triplet	$-25.3(\frac{1}{2}+\frac{1}{2}P)(r_0/r)e^{-r/r_0}-48.3(\frac{1}{2}+\frac{1}{2}P)(r_0/r)e^{-r/r_0}S^{12}$	δ
pp	JCN	singlet	∞, $r<r_3$; $-375(\frac{1}{2}+\frac{1}{2}P)e^{-(r-r_3)/r_4}$, $r>r_3$	δ
		triplet	∞, $r<r_6$; $15.25(\frac{1}{2}-\frac{1}{2}P)(r_2/r_5)^2e^{-r_5/r_5}S^{12}$, $r_6<r<r_5$; $15.25(\frac{1}{2}-\frac{1}{2}P)(r_2/r)^2e^{-r/r_2}S^{12}$, $r>r_5$	δ

[19] The energy dependence of the nucleon-nucleon amplitudes entering the d-p amplitude (see Table V) was here ignored: the energies available were 90 Mev for n-p, 129 Mev for p-p.

were zero except the four diagonal ones and the (23) and (32) elements, with the latter the negative of the former. Thus five parameters were now necessary to describe the nucleon-nucleon cross sections and hence the d-p cross section. The latter would have to be calculated in the same manner as before, with Chew's result no longer valid. The d-p cross section could at best be calculated in impulse approximation from exact nucleon-nucleon scattering amplitudes. It was therefore felt that inasmuch as the off-diagonal elements were rather small for the p-p case and altogether negligible for n-p, they could be omitted and the previous machinery used for calculating the d-p scattering cross section. That this method of calculating nucleon-nucleon cross sections is far superior to the Born approximation is shown by the comparisons made in Table VII.

The four different potentials used in the calculations are presented in Table VI.

The potentials proposed by Christian and Hart[17] and by Christian and Noyes[20] are denoted by CH−CN. They are charge dependent, and are characterized by Serber forces (even states only) in n-p and by a singular tensor force in odd p-p triplet states.

The potential represented by CNS was adapted by Don Swanson from the CN potential. It is charge-independent, and leads only to even states except for a singular tensor force in both n-p and p-p odd triplet states.

The JS potential was proposed by Jastrow[21] and adapted by Swanson. It is charge-independent, and its main feature is a hard repulsive core in singlet states.

The JCH−JCN potentials are charge-dependent and resemble the CH−CN potentials except that a hard core has been introduced in both singlet and triplet. They are modifications of a potential proposed by Jastrow.[21]

The Born scattering (real) amplitudes for the various potentials and the triplet (complex) exact amplitudes for the JCH−JCN potentials were provided by Don Swanson, the singlet phase shifts for the hard core potentials by R. Jastrow. Both attractive and repulsive singular tensor forces were tried in the first two potentials, only repulsive ones in the last two.

The results of the calculations are given in Table VII. It must be remembered that the n-p cross sections given are energy- and angle-dependent (see Table V), with the exception indicated.[19] A compromise value[6,14,15] of 5 mb was taken for the p-p cross section for all angles and energies.

It is clear that our conclusions derived from Table VII depend on our confidence in the impulse approximation. Deviations of the order of 10 or 20 percent from experiment certainly are not great enough to disqualify a potential.

We can say that both charge-dependent potentials, CH−CN and JCH−JCN, are admissible. The charge-independent potential CNS should perhaps be ruled out, whereas JS provides good agreement. Thus it appears that charge-independent potentials satisfying the experimental results of n-p, p-p, and d-p scattering can be found; and that Jastrow's hard core is so far compatible with experience.

TABLE VII. Summary of the calculations. Rows 1–4 give the experimental p-p and n-p cross sections, the d-p cross sections multiplied by $\{9/[16S(K)]\}$, and the ratio $\Delta=\{9/[16S(K)]\}\sigma_{dp}/(\sigma_{np}+\sigma_{pp})$, where $S(K)$ is the "sticking factor." The remaining rows list the same quantities as calculated from the indicated potentials, described in Table VI. The letters in parenthesis give the approximations to which the nucleon-nucleon amplitudes were calculated in singlet and triplet states, respectively. B = Born approximation, δ = phase shift calculation. The approximation involved in the JCH−JCN calculation consisted in omitting the off-diagonal elements in the scattering matrices. All cross sections are in 10^{-27} cm^2 sterad^{-1}.

	d-p center-of-mass scattering angle θ			
	20°	40°	60°	80°
Experimental				
σ_{pp}	5.0	5.0	5.0	5.0
σ_{np}	9.5	4.8	3.4	3.1
$\{9/[16S(K)]\}\sigma_{dp}$	15	7.2	5.4	3.9
Δ	1.03	0.73	0.64	0.48
CH−CN(BB)				
σ_{pp}	8.4	5.7	5.0	5.0
σ_{np}	4.9	3.0	2.7	3.0
With repulsive tensor forces:				
$\{9/[16S(K)]\}\sigma_{dp}$	16	7.5	6.4	7.6
Δ	1.16	0.86	0.83	0.95
With attractive tensor forces:				
$\{9/[16S(K)]\}\sigma_{dp}$	14	7.8	4.9	3.4
Δ	1.06	0.90	0.64	0.43
CNS(BB)				
σ_{pp}	8.4	5.7	5.0	5.0
With repulsive tensor forces:				
σ_{np}	5.4	3.1	3.0	3.9
$\{9/[16S(K)]\}\sigma_{dp}$	18	8.9	7.7	9.7
Δ	1.31	1.01	0.96	1.09
With attractive tensor forces:				
σ_{np}	5.6	5.8	4.6	3.4
$\{9/[16S(K)]\}\sigma_{dp}$	19	14	11	8.7
Δ	1.32	1.23	1.14	1.04
JS(δB)				
σ_{pp}	3.9	4.3	4.9	5.0
σ_{np}	3.7	3.1	2.7	2.3
$\{9/[16S(K)]\}\sigma_{dp}$	7.0	4.1	4.4	5.2
Δ	0.92	0.55	0.58	0.71
JCH−JCN($\delta\delta$)				
Exact				
σ_{pp}	4.7	5.3	5.5	5.6
σ_{np}	12	8.1	5.1	4.4
Approximate				
σ_{pp}	4.5	4.6	4.6	4.6
σ_{np}	12	8.1	5.1	4.4
$\{9/[16S(K)]\}\sigma_{dp}$	18	10	7.0	7.2
Δ	1.09	0.79	0.72	0.80

D. Conclusions

These results indicate that the effect of tensor forces must be considered if even qualitative agreement with the elastic d-p scattering experiments is to be obtained. The argument used is that the otherwise most reasonable central force models of nucleon-nucleon interaction lead to prediction of more elastic d-p scattering than is observed. Since tensor forces have been extensively

[20] R. S. Christian and H. P. Noyes, Phys. Rev. **79**, 85 (1950).
[21] Robert Jastrow, Phys. Rev. **81**, 165 (1951).

considered in nucleon-nucleon interaction, this result is perhaps not unexpected.

Unfortunately, the *d-p* scattering seems to differentiate rather poorly between the various models having significant contributions from tensor forces. In fact all of the models that have included tensor forces fit much better than any reasonable central force approximation. With some uncertainty, the CNS potential might be ruled out.

At the time this work was started there was less indication than there is at the present time of the charge independence of nuclear forces. It still seems appropriate, however, to include the results for some models which are not charge-independent, most of which explain the present results quite well. Of the charge-independent models, that of Jastrow as modified by Swanson (JS) is favored. How strongly it is favored depends to a large extent on how much confidence one has in the approximations used. The reader is referred to Table VII in which theory and experiment are compared on the basis of the quantity Δ.

Some of these conclusions have been brought out by Horie, Tamura, and Yoshida,[22] who have compared their calculations with the same experimental data presented here.

The suggestion is made that in a refined analysis of the *d-p* scattering at one energy, the data must be compared with nucleon-nucleon scattering measurements made at a variety of energies. The proposed energies and angles are indicated in Table V.

No attempt has been made in the present work to analyze the data in the region of 180 degrees in the c.m. system (the "pick-up" region).

ACKNOWLEDGMENTS

The authors wish to thank Dr. Arnold L. Bloom for great help during the experiment, Professor Emilio Segrè for advice and encouragement, Dr. Don E. Swanson for helping them to understand important parts of the theory and providing Born amplitudes and phase shifts, and Dr. Robert Jastrow for furnishing information on his hard core potentials.

[22] Horie, Tamura, and Yoshida, Progr. Theoret. Phys. Japan **8**, 341 (1952)

Decay of a Heavy Nuclear Fragment*

P. S. FREIER, G. W. ANDERSON,† AND J. E. NAUGLE
Department of Physics, University of Minnesota, Minneapolis, Minnesota
(Received September 17, 1953)

Possible explanations of a three-prong star at the end of a stopping heavy fragment are considered. The event can be tentatively explained in terms of the nonmesonic decay of a V_1^0 particle attached to the fragment.

THERE have been reported recently three cases of the disintegration of a heavy fragment ($Z \geq 2$) ejected from cosmic ray stars in emulsions.[1–3] It has been suggested in two of the events[2,3] that the disintegrations are caused by a $V_1^0(\Lambda^0)$ particle bound to the fragment, which decays and causes the star. The third case[1] has been interpreted as the mesonic decay of the V_1^0 with the resulting π meson and proton escaping from the heavy fragment rather than causing a star.

We have observed a similar disintegration which is shown in Fig. 1. It was observed in a G-5 400μ emulsion exposed for 20 hours at 90 000 feet at a geomagnetic latitude of 55°N. The parent disintegration we have classified as the type 24+10p; however, there is some uncertainty as to whether the particle marked as the incoming proton in the figure caused the disintegration. Its direction is 30° from the shower axis. The 10 shower particles are indicated by S in the figure. The incoming proton is too short to measure its energy by scattering. We estimate the energy of the primary, using the statistical results of Camerini *et al.*[4] and Daniel *et al.*,[5] as about 15 Bev. From ionization and scattering measurements on the star particles, we find the energy must be greater than 4 Bev.

Out of this star there is emitted a heavy fragment f which comes to rest in the emulsion at the center of a three-pronged star designated by B on the figure. The "thin-down" plus the existence of a sharp angle scattering near the end of f gives convincing evidence that the fragment has come to rest before making the star. Because of the short range of fragment f (30μ), it is impossible to measure its charge directly. By comparing its appearance with other stopping heavy nuclei, we conclude that the charge of f is almost certainly greater than 3 and less than 7. The star B has three particles which are coplanar to within 4°±5°, where the large measuring error of 5° is due to the short track B_1 (5.8μ).

The directions of the three tracks in star B are given below as unit vectors:

$$\mathbf{B}_1 = (-0.36\pm0.03)\mathbf{i} + (0.71\pm0.03)\mathbf{y} + (0.60\pm0.07)\mathbf{k},$$
$$\mathbf{B}_2 = (-0.032\pm0.003)\mathbf{i} - (0.45\pm0.03)\mathbf{y} - (0.89\pm0.03)\mathbf{k},$$
$$\mathbf{B}_3 = (+0.60\pm0.04)\mathbf{i} - (0.71\pm0.04)\mathbf{y} - (0.37\pm0.02)\mathbf{k}.$$

At the end of track B_1 there is an electron of 1.7±0.5 Mev. It cannot be certain whether this electron comes from the end of particle B_1 or from the center of star B since it makes a small angle with track B_1. The probability that this is a chance coincidence of an electron starting in the emulsion this close to the end of track B_1 is about 0.1 percent. Table I gives the results obtained from measurements on the tracks in star B.

Although we have made extensive scattering measurements in these emulsions, we are unable to identify the mass of particle B_3. Because of its short length and

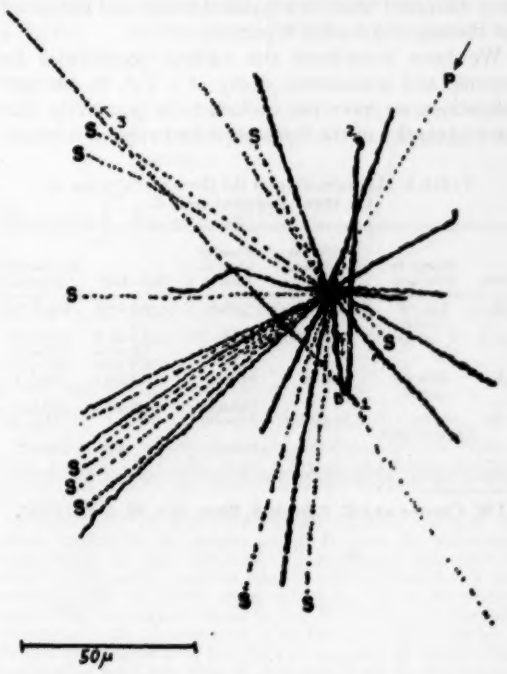

FIG. 1. A projection drawing (in the plane of the emulsion) of a star of the type 24+10p which ejects a heavy fragment, f, which, at the end of its range, is coincident with a three-pronged star, B.

* This research supported in part by the joint program of the U. S. Atomic Energy Commission and the U. S. Office of Naval Research.
† Now at Sandia Corporation, Albuquerque, New Mexico.
[1] J. Crussard and D. Morellet, Compte rend. **236**, 64 (1953).
[2] M. Danysz and J. Pniewski, Phil. Mag. **44**, 348 (1953).
[3] Tidman, Davis, Herz, and Tennent, Phil. Mag. **44**, 350 (1953).
[4] Camerini, Davies, Fowler, Franzinetti, Muirhead, Lock, Perkins, and Yekuteli, Phil. Mag. **42**, 1241 (1951).
[5] Daniel, Davies, Mulvey, and Perkins, Phil. Mag. **43**, 753 (1952).

the distortion in the emulsion, it is impossible to decide whether B_3 is a π meson or a proton.

We shall now list various possible explanations of this event, with reasons for considering the explanation plausible or not.

(1) Chance coincidence of the ending of f and a three-pronged star. The probability of finding one such event is of the order of 10^{-4}. The fact that four such similar events have been found rules out this possibility.

(2) Interaction of f with emulsion nucleus. Fragment f has an extremely small, if not zero, kinetic energy when it enters star B. It could not produce such an energetic star.

(3) The decay of an excited nucleus. The time for f to travel 30μ is about 2×10^{-12} sec, a time long compared to the mean life of an excited nucleus.

(4) Fragment f is a π-mesonic atom, with star B being a "delayed σ star." If B_3 is a π meson, this explanation is automatically ruled out. If B_3 is a proton, the energy in star B is too high for a π-meson star.

These four tentative explanations are also discarded on similar grounds for the other three heavy fragment stars found by other observers. However, all three of their stars have been explained by assuming a V_1^0 particle which is bound to the heavy fragment and either decays into a π meson and a proton which recoil against the remaining fragment, or decays "nonmesonically" with a proton being emitted and the remaining excited fragment breaking up. Cheston and Primakoff[6] have discussed these two types of decay and computed the lifetime of a bound V particle.

We have considered the various possibilities for mesonic and nonmesonic decay of a V_1^0. In our considerations we have not excluded the possibility that the coplanarity of the three particles in star B is coincidental. There is a 9 percent probability that three particles lie within $\pm5^\circ$ of a plane when all solid angle is equally available to them. We have also kept in mind that the electron from track B_1 may be coincidence, or that it could be an internal conversion electron so that B_1 need not necessarily suffer β decay.

TABLE I. Measurements on the three particles out of the heavy fragment star, B.

Track	Range in emulsion	Ionization I = plateau value	Possible identifications	KE, Mev	Momentum, Mev/c
B_1	$5.8\mu\pm1$ (ends)	Black	$_2He^6$	2.2 ± 0.3	150 ± 9
			$_3Li^6$	4.1 ± 0.3	216 ± 10
			$_4Be^9$	7.0 ± 0.6	329 ± 15
			$_5B^{10}$	10.4 ± 0.9	484 ± 22
B_2	$182\mu\pm5$ (ends)	Black	Proton	5.2 ± 0.1	94 ± 1
			Deuteron	6.8 ± 0.1	160 ± 2
B_3	759μ (goes to glass)	$2.56\pm0.15I$	π meson	19 ± 2	76 ± 3
			Proton	125 ± 10	505 ± 25

The most likely scheme for nonmesonic decay of a V_1^0 is

$$_7N^{14}\rightarrow p+p+{}_5B^{12}.$$

The $_8B^{12}$ β decays to $_6C^{12}$ with a $Q=13.4$ Mev and a lifetime of 0.022 second. This interpretation requires that B_3 be a proton of 125 ± 10 Mev, B_2 be a proton of 5.2 ± 0.1 Mev, and that B_1 be the B^{12} nucleus of 10.4 ± 0.6 Mev. (See Table I.) If this reaction takes place the visible kinetic energy of the particles and the mass difference would require an excitation of 168 ± 11 Mev for the $_7N^{14}$ which is consistent with the π mass+the Q of the free V_1^0. However, this means the charge of the fragment, f, must be 7. This is outside of our estimate of the charge; however, we consider it possible that f could have a charge that great.

If particle B_3 is a π meson resulting from the decay of a V_1^0 carried along with f, it is impossible to find any scheme to satisfy all the necessary conditions. The decay $_2He^7\rightarrow\pi+p+{}_2He^6$ does satisfy momentum conservation and $_2He^6$ decays with a 3.5-Mev electron. However, this means that fragment f would be $_2He^7$. This is unsatisfactory because the charge of f is definitely greater than 2, and it would seem difficult for such a fragment as $_2He^7$ to exist long enough to come to rest in the emulsion. No other decay scheme involving only a π meson, a proton, and the particle B_1 satisfied momentum conservation.

Although we have considered only the V_1^0 in the possible explanations of this event, we do not feel that explanations involving other heavy mesons or decay processes have been ruled out by the existing data. It is clear that more events of this type in which it is possible to carry out complete mass and momentum measurements are needed in order to establish the exact process observed in these events.

We wish to thank Mrs. Dawn Copeland for making the projection drawing and Mrs. LaDonna Wagner for helping with the scattering measurements. We wish to thank Dr. E. D. Ney and Dr. E. L. Hill for an interesting discussion regarding this event. We are grateful to Dr. Cheston for the opportunity of seeing his paper before publication.

[6] W. Cheston and H. Primakoff, Phys. Rev. **92**, 1537 (1953).

Phase Shift Analysis of High-Energy Nucleon-Nucleon Scattering Experiments*

R. M. THALER† AND J. BENGSTON‡
Yale University,§ New Haven, Connecticut

(Received January 18, 1954)

The high-energy proton-proton scattering data are analyzed in terms of s-wave and p-wave anomalies. Different phase shifts are used for the three p waves with total angular momentum $j=0, 1, 2$. It is found that the data can be fitted without violating charge independence of nuclear forces. These high energy fits vary smoothly with energy and are not in contradiction to the requirements of the intermediate energy (10–100 Mev) data. Inversion of nuclear levels suggested by the shell theory of nuclear forces can also be accounted for.

I. INTRODUCTION

SCATTERING of protons by protons at bombarding energies between 100 and 400 Mev gives[1–5] a roughly isotropic intensity distribution in the system of the center of mass of the two protons. As is well known, the large value of the cross section rules out an explanation of isotropy in terms of a pure s-wave scattering anomaly, and makes it necessary to include states of higher angular momentum in the analysis. While most of the current theories of p-p scattering use some form of phenomenologic potential energy as a starting point, their practical accomplishment is that of yielding proper combinations of phase shifts, especially those of the three p waves and of the d wave. On the other hand the most general velocity-dependent interaction, satisfying general requirements of invariance, can be described[6] through an arbitrary assignment of phase shifts. It was thought of interest therefore to make an analysis entirely on the basis of phase shifts and without any preconceived potential. The present note contains a brief account of reasonably successful fits made by employing only four phase shifts, *viz.*, one for the s wave and three for the p waves.[7]

SYMBOLS AND NOTATION

E energy of the bombarding particle.

$\mathbf{P}$ proton-proton scattering cross section per unit solid angle in the center-of-mass system.

$\mathbf{P}_{NUC}$ that part of $\mathbf{P}$ specifically due only to the nuclear interaction as distinguished from the Coulomb interaction.

$\mathbf{P}_{M}$ that part of $\mathbf{P}$ specifically due only to the Coulomb interaction.

$\mathbf{P}_{INT}$ that part of $\mathbf{P}$ due to interference between the outgoing nuclear and Coulomb waves.

$\Lambda=2\pi/k$ wavelength of relative motion.

P_L Legendere function of order L.

θ scattering angle in the center-of-mass system.

${}^1K_0, {}^1K_1$ nuclear phase shift for singlet state for $L=0, 1$.

${}^3K_0, {}^3K_2$ nuclear phase shifts for triplet state for $L=0, 2$.

L orbital angular momentum.

j total angular momentum.

$\delta_0, \delta_1, \delta_2$ nuclear phase shifts for triplet p state for $j=0, 1, 2$.

$\eta=e^2/\hbar v$.

σ^{NP} neutron-proton scattering cross section per unit solid angle in the center-of-mass system.

$$\langle \mathbf{P}_{NUC} \rangle = \tfrac{1}{2}\int_{-1}^{1} \mathbf{P}_{NUC} d(\cos\theta).$$

$\mathbf{c}=\cos\theta/2$, $\mathbf{s}=\sin\theta/2$.

$\mathbf{X}_0, \mathbf{X}_1, \mathbf{Y}_0, \mathbf{Y}_1$ quantities similar to $\mathbf{X}$, $\mathbf{Y}$ of Breit, Thaxton, and Eisenbud[8] defined by Eqs. (5–6).

$\alpha_L=\eta \log \mathbf{s}^2+2\Sigma_{n=0}^{L}\tan^{-1}(\eta/n)$.

$\beta_L=\eta \log \mathbf{c}^2+2\Sigma_{n=0}^{L}\tan^{-1}(\eta/n)$.

* Part of a dissertation submitted by J. Bengston for the degree of Doctor of Philosophy at Yale University.

† Now at Los Alamos Scientific Laboratory, Los Alamos, New Mexico.

‡ Now at the Oak Ridge National Laboratory, Oak Ridge, Tennessee.

§ Assisted by the joint program of the U. S. Office of Naval Research and the U. S. Atomic Energy Commission and by the Office of Ordnance Research.

[1] Chamberlain, Segrè, and Wiegand, Phys. Rev. **83**, 923 (1951).

[2] Birge, Kruse, and Ramsey, Phys. Rev. **83**, 274 (1951).

[3] C. L. Oxley and R. D. Schamberger, Phys. Rev. **85**, 416 (1952).

[4] O. A. Towler, Jr., Phys. Rev. **85**, 1024 (1952).

[5] Cassels, Pickavance, and Stafford, Proc. Roy. Soc. (London) **A214**, 262 (1952).

[6] G. Breit, in *University of Pennsylvania, Bicentennial Conference* (University of Pennsylvania Press, Philadelphia, 1941).

[7] Preliminary accounts of the present work were given at the 1952 Rochester Conference by G. Breit, and in Phys. Rev. **91**, 454 (1953); Phys. Rev. **93**, 643, 644 (1954). A related investigation has been published by A. Garren, Phys. Rev. **92**, 213 (1953).

[8] This has been discussed in detail in Breit, Condon, and Present, Phys. Rev. **50**, 825 (1936); Breit, Thaxton, and Eisenbud, Phys. Rev. **55**, 1018 (1939); and Breit, Kittel and Thaxton, Phys. Rev. **57**, 255 (1940).

Equation (1) of Breit, Kittel, and Thaxton contains the effects studied in the present paper. It gives the differential cross section in units $(e^2/2\mu v^2)^2$. By combining their term in $(108P_1^2/\eta^2)\Sigma\xi_i \sin^2\delta_i$, and the term in $(12/\eta^2)(3\cos^2\theta-1)$, and multiplying by $(e^2/2\mu v^2)^2$, there results Eq. (2) of the present paper. The interference terms of Eq. (4) of the text similarly correspond to the terms in $(18P_1/\eta)$ of Eq. (1) of BKT. The latter formula is arranged so as to collect in one place all effects which vanish when $\delta_0=\delta_1=\delta_2$. Since in the present work the values of the δ_i are often very different from each other the rearrangement used here proved convenient. Equation (10) of the present paper contains the terms in Eq. (15) of C. Kittel and G. Breit, Phys. Rev. **56**, 744 (1939) and in addition the effect of ${}^3K_2$.

II. *P-P* SCATTERING

The proton-proton scattering cross section in the center-of-mass system may be written as

$$\mathbf{P}=\mathbf{P}_{NUC}+\mathbf{P}_{M}+\mathbf{P}_{INT}, \tag{1}$$

where

$$\mathbf{P}_{NUC}=(\Lambda/2\pi)^2\{\sin^2{}^1K_0+\Sigma_0^2(2j+1)\sin^2\delta_j + P_2(\cos\theta)[(3/2)\sin^2\delta_1+(7/2)\sin^2\delta_2 +4\sin\delta_0\sin\delta_2\cos(\delta_0-\delta_2) +9\sin\delta_1\sin\delta_2\cos(\delta_1-\delta_2)]\}, \tag{2}$$

$$\mathbf{P}_{M}=(\Lambda/2\pi)^2\{(\eta^2/4)[\mathbf{s}^{-4}+\mathbf{c}^{-4} -\mathbf{s}^{-2}\mathbf{c}^{-2}\cos(\eta\log\mathbf{s}^2\mathbf{c}^{-2})]\}, \tag{3}$$

$$\mathbf{P}_{INT}=(\Lambda/2\pi)^2\{-(\eta/2)\mathbf{X}_0\sin{}^1K_0\cos{}^1K_0 +(\eta/2)\mathbf{Y}_0\sin^2{}^1K_0+P_1(\cos\theta) \times[-(\eta/2)\mathbf{X}_1\Sigma_0^2(2j+1)\sin\delta_j\cos\delta_j +(\eta/2)\mathbf{Y}_1\Sigma_0^2(2j+1)\sin^2\delta_j]\}, \tag{4}$$

and

$$\mathbf{X}_L=\mathbf{s}^{-2}\cos\alpha_L+(-1)^L\mathbf{c}^{-2}\cos\beta_L, \tag{5}$$

$$\mathbf{Y}_L=\mathbf{s}^{-2}\sin\alpha_L+(-1)^L\mathbf{c}^{-2}\sin\beta_L. \tag{6}$$

The choice of phase shifts is appreciably simplified by the fact that in the angular range $30°<\theta<90°$ the terms $\mathbf{P}_M$ and $\mathbf{P}_{INT}$ are practically constant. Since in the same angular range the observed $\mathbf{P}$ is practically independent of θ, the coefficient of $P_2(\cos\theta)$ in the formula for $\mathbf{P}_{NUC}$ must be approximately zero. Various combinations of the triplet p phase shifts for which the coefficient of $P_2(\cos\theta)$ in $\mathbf{P}_{NUC}$ vanishes, i.e., for which

$$(3/2)\sin^2\delta_1+(7/2)\sin^2\delta_2+4\sin\delta_0\sin\delta_2\cos(\delta_0-\delta_2) +9\sin\delta_1\sin\delta_2\cos(\delta_1-\delta_2)=0, \tag{7}$$

are plotted in Fig. 1. It is seen from Eq. (2) that as a consequence of Eq. (7) the quantity

$$\alpha\equiv\Sigma_0^2(2j+1)\sin^2\delta_j, \tag{8}$$

together with ${}^1K_0$, determine uniquely the quantity $\mathbf{P}_{NUC}/(\Lambda/2\pi)^2$. Thus the fits under consideration are such that for an assigned value of ${}^1K_0$ the observed angle independent σ_0 determines one of the contours in Fig. 1. An estimate of the s-wave phase shift ${}^1K_0$ as calculated in first Born approximation for the meson well

$$V=-\mathcal{C}'(mc^2)[r(e^2/mc^2)a']^{-1}\exp\{-[r/(e^2/mc^2)a']\},$$

with $\mathcal{C}'=89.8$, and $a'=0.42$, is used. As an example, for $E=100$ Mev and ${}^1K_0=35.0°$, numerical substitution shows that for $\langle\mathbf{P}\rangle=4.5$ mb one must have

$$\alpha=0.21,$$

defining a contour located approximately in the center of Fig. 1. It will be noted that in the same figure for $\alpha=1.30$ there appear on the edges of the diagram small subsidiary curves unconnected with the major portions of the contours. Since these subsidiary curves only occur for large values of α, they can probably be ruled out of consideration on the grounds that the solutions represented by them appear to correspond to a discontinuity with respect to energy.

Under the assumptions that the experimental value of the cross section at 90° is known to within 20 percent, and that ${}^1K_0$ is not known, there is considerable latitude in the choice of α as is illustrated numerically in Table I. Nevertheless, for the sake of definiteness, in the work that follows for $E=240$ Mev, ${}^1K_0$ is taken to be ${}^1K_0=31.3°$ (see Fig. 2), and $\langle\mathbf{P}_{NUC}\rangle$ is taken to be $\langle\mathbf{P}_{NUC}\rangle=4.5$ mb, corresponding to $\alpha=1.04$. The mathematical condition for flatness, i.e., for $\mathbf{P}_{NUC}(\theta)=$const, used in determining the plots for Fig. 1 is more stringent than the experimental data require. To fit the data it is necessary merely that $|1-\mathbf{P}_{NUC}(\theta)/\mathbf{P}(\theta=90°)|$ be small. In Fig. 2 there has been plotted the family of solutions for which $|1-\mathbf{P}_{NUC}(\theta)/\mathbf{P}(\theta=90°)|\lesssim 0.1$ at $E=240$ Mev with $\langle\mathbf{P}_{NUC}\rangle=4.5$ mb and $\alpha=1.04$. The small subsidiary regions on the edges of Fig. 2 correspond to the subsidi-

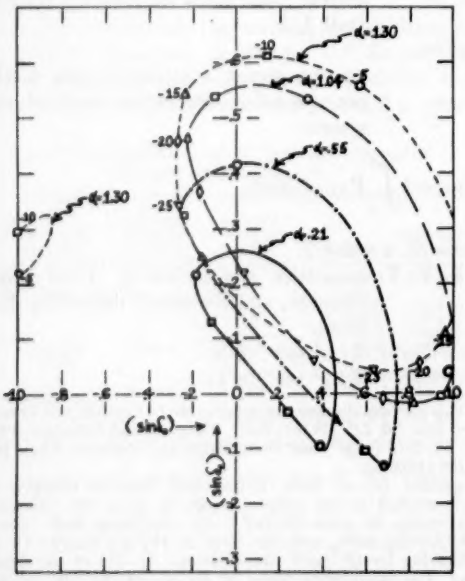

FIG. 1. Family of p-phase shift curves for which the triplet part of $\mathbf{P}_{NUC}$ is angle-independent. Each contour is labeled by a value of $\alpha=\Sigma_j\sigma^2(2j+1)\sin^2\delta_j$. Values of δ_2 in degrees are directly indicated along some of the contours. In other cases the values of $\delta_2=-5°$, $-10°$, $-15°$, $-20°$, $-25°$ are indicated by the point designations ○, □, △, ◇, ▽, respectively. A second family of contours is obtained by changing all δ_j to $-\delta_j$.

TABLE I. Values of ${}^1K_0$ and α for which $\mathbf{P}(\theta=90°)=4.5$ millibarn/sterad ±20 percent at 100 Mev and 240 Mev. Second line is for meson well with parameters $\mathcal{C}=89.8mc^2$ and $a=0.42e^2/mc^2$.

$E=100$ Mev		$E=240$ Mev	
${}^1K_0$	α	${}^1K_0$	α
47.4°±6.3°	0	90°	0.30±0.26
35.0°	0.21±0.11	31.3°	1.04±0.26
0	0.54±0.11	0	1.30±0.26

ary curve which appears in Fig. 1 for $\alpha=1.30$. There are no mathematically flat subsidiary solutions, however, for $\alpha=1.04$.

The 240-Mev Rochester[3,4] data (see Fig. 3) indicate a large increase in the cross section for small angles. At these angles, however $\mathbf{P}_{INT}$ and $\mathbf{P}_M$ are appreciable, so that some of the solutions plotted in Fig. 1 for $\alpha=1.04$ may correspond to a cross section similar to the experimentally determined cross section at all angles. The only quantity in Eqs. (1–4) which differs from one solution to another is the quantity

$$\beta\equiv\Sigma_0{}^2(2j+1)\sin\delta_j\cos\delta_j, \tag{9}$$

which appears in Eq. (4). Several typical cross sections have been plotted in Fig. 3 to indicate the dependence of the cross section on the value of the quantity β. Solutions for which β is positive correspond to a dip in the cross section in the angular region $10°<\theta<20°$ and are excluded as not fitting the data. The regions for which β is negative are indicated on Fig. 2 by cross-hatching. It may be noted that the cross-hatched region in the lower left hand corner of Fig. 2 corresponds to the well known inversion of the nuclear ^3P levels.

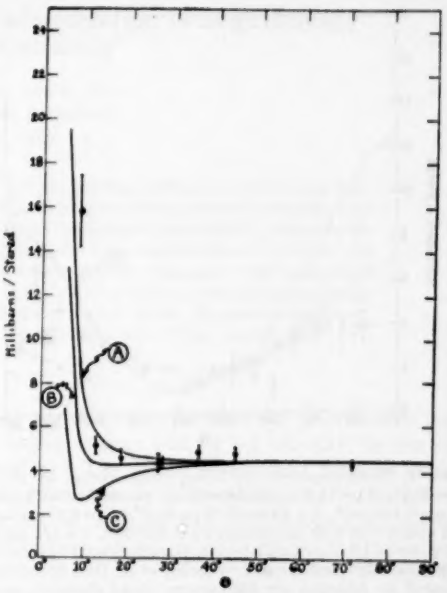

FIG. 3. Proton-proton scattering cross section at 240 Mev. For case A, $\beta=-1.0$; for case B, $\beta=0$; for case C, $\beta=+1.0$. Data due to Rochester group (see references 3 and 4).

III. *N-P* SCATTERING

In order to determine whether the results obtained are in conflict with the hypothesis of charge independence of nuclear forces, consideration was given to the possibility of obtaining a fit to the experimental neutron-proton scattering data at 260 Mev.[9] For proton-proton scattering at 260 Mev, $^1K_0$ was taken to be $^1K_0=30.9°$, as calculated from the meson well above, giving $\alpha=1.14$ for $\langle\mathbf{P}_{NUC}\rangle=4.5$ mb. From the curve for $\alpha=1.14$ in Fig. 1 may be read the values of the p-wave phase shifts, δ_j, which satisfy Eq. (7). By analogy with the result at 240 Mev, those values of the δ_j which satisfy Eq. (7), but for which $\beta>0$ are considered to be unacceptable. If after the value $^1K_0=30.9°$ and after a set of values for the triplet p phase shifts, δ_j, taken from Fig. 1 for $\alpha=1.14$, are substituted into the expression for the neutron-proton scattering cross section with all other singlet phase shifts for even L and all other triplet phase shifts for odd L being taken to be zero, it is possible to fit the 260-Mev data by adjustment of the remaining phase shifts, such a quartet of values of $^1K_0$ and δ_j will be said to represent a solution which does not violate charge independence of nuclear forces.

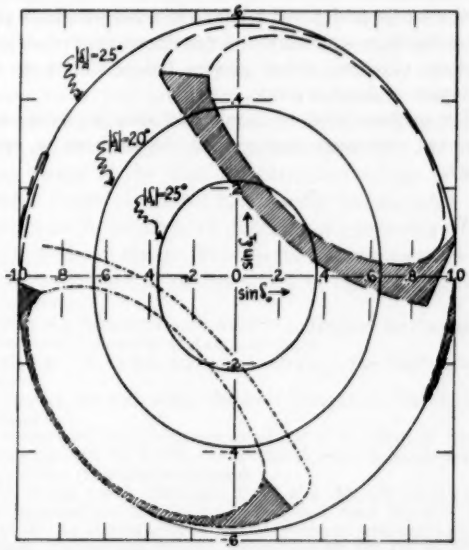

FIG. 2. Possible p-phase shifts for $E=240$ Mev. The ellipses give values of $|\delta_2|$ corresponding to $\alpha=1.04$ and to the assumed cross section. The contours in upper right-hand corner dashed lines enclose a region within which $\delta_2<0$ and $\mathbf{P}_{NUC}$ differs from its value at $\theta=90°$ by less than 10 percent, while $^1K_0=31.3°$. The region enclosed by contours in lower right-hand corner (dash-dotted lines) is for $\delta_2>0$; in other respects it satisfies conditions described for the dashed line contours. Cross hatches indicate regions for which β of Eq. (9) satisfies $\beta<0$. The cross-hatched region in the lower left-hand corner corresponds to inversion of the ^3P levels.

The neutron-proton scattering cross section may be written as

$$\begin{aligned}\sigma^{NP}=&\tfrac{1}{4}\mathbf{P}_{NUC}+\tfrac{1}{4}(\Lambda/2\pi)^2\{3\sin^2(^3K_0)\\&+[6\sin(^1K_0)\sin(^1K_1)\cos(^1K_0-{}^1K_1)\\&+2\beta\sin(^3K_0)\cos(^3K_0)+2\alpha\sin^2(^3K_0)]P_1(\cos\theta)\\&+9\sin^2(^1K_1)P_1{}^2(\cos\theta)+[10\beta\sin(^3K_2)\cos(^3K_2)\\&+10\alpha\sin^2(^3K_2)]P_1(\cos\theta)P_2(\cos\theta)\\&+75\sin^2(^3K_2)P_2{}^2(\cos\theta)\}.\end{aligned} \tag{10}$$

[9] Kelly, Leith, Segrè, and Wiegand, Phys. Rev. **79**, 96 (1950).

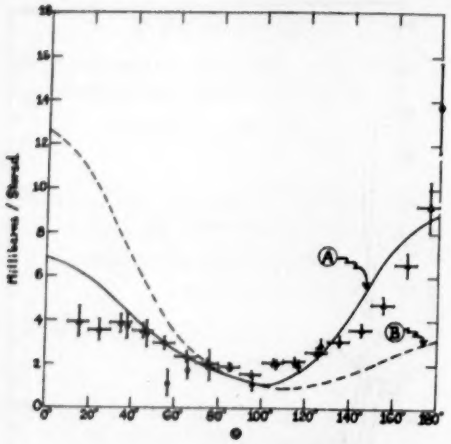

FIG. 4. Neutron-proton scattering cross section at 260 Mev ${}^1K_0=30.9°$, ${}^1K_1=13.3°$; calculated from meson well with parameters $a=0.42e^2/mc^2$, $\mathcal{C}=89.8mc^2$. ${}^3K_0=50.8°$, ${}^3K_2=9.9°$; calculated from meson well with parameters $a=0.42e^2/mc^2$, $\mathcal{C}=132.4mc^2$. For case A, $\beta=-1.4$; for case B, $\beta=1.4$. Data indicated by solid circles are for 260 Mev and are due to Kelley *et al.* (reference 9). Data indicated by triangles are high-energy cloud chamber measurements of J. De Panghen, Jr. [University of California Radiation Laboratory Report UCRL-2153, March, 1953 (unpublished)], and show the probable behavior of σ^{NP} for small angles.

All phase shifts which do not appear in the above expression have been taken to be equal to zero. The phase shifts in Eq. (10) which are now undetermined are ${}^3K_0$, ${}^3K_2$ and ${}^1K_1$.

The experimental 260-Mev neutron-proton cross section[9] (see Fig. 4) is asymmetric about $\theta=90°$, being smaller near $\theta=0$, than near $\theta=180°$. It is clear from Eq. (10) that for ${}^3K_0$, ${}^3K_2$ and ${}^1K_1$ each positive and less than 90° such an asymmetry cannot be reproduced for $\beta>0$. The condition that β cannot be positive is just the condition imposed on the δ_j by the small angle proton-proton scattering data.[4] If ${}^3K_0$, ${}^3K_2$ are calculated from the low energy triplet meson well with $\mathcal{C}'=132.4$, $a'=0.42$, and ${}^1K_0$, ${}^1K_1$ are calculated from the low energy triplet meson well with $\mathcal{C}'=89.8$, $a'=0.42$, the values obtained are

$$ {}^3K_0=50.8°;\ {}^3K_2=9.9°;\ {}^1K_0=30.9°;\ {}^1K_1=13.3°. \quad (11) $$

For Eq. (11), ${}^3K_0$ was calculated by means of a numerical integration employing Hartree's procedure, the other phase shifts were used in first Born approximation. The values of the phase shifts ${}^3K_0$, ${}^3K_2$, ${}^1K_0$, ${}^1K_1$ in Eq. (11) together with values for δ_j taken from Fig. 1 for $\alpha=1.14$ may be substituted into Eq. (10), and the resulting cross section compared with experiment. The range of β is $-1.5\lesssim\beta\lesssim1.5$. The best fit to the data occurs for β a large negative number. The large distinction between positive and negative β is illustrated in Fig. 4. It is of interest to note that the subsidiary solutions appearing on the edges of the diagram in Fig. 1 and Fig. 2, which have been ruled out on the basis of continuity with respect to energy, correspond to $-0.1\lesssim\beta\lesssim0.1$. For $|\beta|\lesssim0.1$, the condition $\sigma^{NP}(\theta=180°)/\sigma^{NP}(\theta=0)>1$ cannot be reproduced with the values of the phase shifts of Eq. (11).

CONCLUSION

It is possible to fit the high-energy proton-proton data with s waves and p waves alone in a manner such that these fits vary smoothly and continuously with energy without violating either charge independence or the inversion of nuclear levels.

The authors wish to thank Professor G. Breit, who initiated this work and guided the authors at every stage.

Intermediate State Coupling and the Interpretation of High-Energy Nucleon-Nucleon Scattering*

R. M. THALER,† J. BENGSTON,‡ AND G. BREIT
Yale University,§ New Haven, Connecticut

(Received January 18, 1954)

The effect on the scattering of protons by protons of the $^3P_2-^3F_2$ coupling due to an intermediate state of the two-nucleon system is investigated. The problem is treated in a scattering matrix formalism, with total angular momentum $j=2$, orbital angular momentum $L=j\pm1$, and partial half-width Γ_L. Only the $^1S_0$, $^1D_2$, $^3P_0$, $^3P_1$, $^3P_2-^3F_2$ scattering anomalies are considered. Fits to the experimental data at 240 Mev are studied as typical. For $^1K_0\approx31°$, $^1K_2>0$ it is found that the data may be reasonably well represented provided $(\Gamma_1+\Gamma_3)/(E_R-E)\lesssim0.3$. It has been found possible to fit data on n-p and p-p scattering employing phase shifts agreeing with the hypothesis of charge independence of nuclear forces. Reasonable agreement with experiment is obtained employing either the regular or the inverted order of $^3P_{0,1,2}$ levels.

I. INTRODUCTION

THE early work on the interpretation of nucleon-nucleon scattering was in terms of potential energies which were taken to be velocity-independent for each of the states with definite L and J. Generalizations of this description have been made through the introduction of other forms of terms in a two-particle Hamiltonian as in the case of the tensor force[1] or in the consideration of a slow variation of the magnitude of the effective potential[2] with energy for a state with definite J and L. In connection with attempts to fit data by means of meson theoretic potentials, an attempt[3] has been made more recently to estimate the approximate magnitude of the velocity dependence by ascribing it to the formation of an intermediate state. An effect of the order of 10 percent in the effective meson mass was found on the assumption that the two-nucleon system may become excited to an isobaric state at an energy equal approximately to the rest mass energy of the pion. An excitation energy in this general range of values can hardly be excluded on account of the well-known difficulty of employing weak coupling meson theory. The question arises therefore as to the possibility of modifications in the static potentials by the temporary formation of intermediate states with higher L than that of the $^1S_0$ state in the work referred to.[3] The velocity-dependent features of such coupling are difficult to ascertain since the assignment of the partial cross sections to different L is clear only at low energies. It would be premature to attempt such a test at this time. On the other hand, the question arises as to whether the experimental data admit of such coupling and as to the approximate magnitude which may be assigned to it. For these reasons it appeared desirable to investigate a case in which the intermediate state formation has other marked features than the velocity dependence. It accordingly appeared of interest to try out the possibility in the case of scattering at ~250 Mev paying attention mainly to the observed angular distributions and to the plausible requirement of charge independence of nuclear forces. This type of calculation has an additional interest also from a more general viewpoint,[4] according to which one can justify the employment of phase shifts from considerations of fundamental symmetries such as symmetry of space to rotations and independently of the applicability of special models or Hamiltonians. In this view, at sufficiently large distances the wave function may be expressed as a sum of parts, each of which has a definite real phase shift and corresponds to a definite value of the total angular momentum. There are in general, however, several states for a given J, each with a phase shift of its own. These states were distinguished from each other[4] by the subscript α.

The possibility of producing special angular effects by coupling of a state of higher L through the intermediate state to a state of lower L appeared especially intriguing because for an assumed interaction potential one expects phase shifts for sufficiently high L to become negligible and the mechanism under consideration is able to cause the appearance of effects of high L at lower energies. For p-p scattering the first possibility of this type occurs for the coupling of $^3P_2$ to $^3F_2$. The numerical work in the present paper is concerned

* Part of a dissertation submitted by J. Bengston for the degree of Doctor of Philosophy at Yale University.

† Now at Los Alamos Scientific Laboratory, Los Alamos, New Mexico.

‡ Now at the Oak Ridge National Laboratory, Oak Ridge, Tennessee.

§ Assisted by the joint program of the U. S. Office of Naval Research and the U. S. Office of Atomic Energy Commission and by the Office of Ordnance Research.

[1] W. Rarita and J. Schwinger, Phys. Rev. **59**, 436 (1941); see L. E. Eisenbud and E. P. Wigner, Proc. Natl. Acad. Sci. U. S. **27**, 281 (1941) for classification of possible forms of generalization.

[2] Breit, Condon, and Present, Phys. Rev. **50**, 825 (1936). This reference is quoted as BCP. For Eq. (3.2) of present note Eqs. (5.1) . . . (6.7) of BCP are of interest. Breit, Thaxton, and Eisenbud, Phys. Rev. **55**, 1018 (1939). This paper is referred to as BTE in the text. The velocity dependence is being discussed in connection with Table XXIII.

[3] G. Breit and M. C. Yovits, Phys. Rev. **81**, 416 (1951). Related ideas have been expressed by R. B. Raphael and J. Schwinger, Phys. Rev. **90**, 373 (1953). Preliminary publication of material in the present paper is found in: Thaler, Bengston, and Breit, Phys. Rev. **91**, 454 (1953); Phys. Rev. **93**, 644 (1954).

[4] G. Breit, in *University of Pennsylvania Bicentennial Conference* (University of Pennsylvania Press, Philadelphia, 1941).

exclusively with this possibility and makes use of values obtained for representation of the data of the preceding paper[5] by means of s and p waves alone as a starting point. In the work reported on here, it is considered that the state ${}^3P_2-{}^3F_2$ exhibits a resonance for some energy greater than the region of ~300 Mev. Such a resonance could perhaps be interpreted as due to an isobaric state of the two-proton system with an energy level approximately at the resonance energy. In preliminary publications, the state through which coupling takes place has been referred to as the isobaric state. In the present note the word "isobaric" is replaced by "intermediate" so as not to overemphasize the feature of metastability which is not directly used. The employment of resonance theory parameters is of course also not needed from a formal viewpoint, the specification of the scattering matrix sufficing for all practical purposes. It is used below mainly in order to facilitate visualization of effects by means of convenient quantities such as the resonance energy and the partial widths. The problem is formulated in terms of a one-level treatment employing a scattering matrix.[6] In addition to the contribution to the cross section caused by the coupling of ${}^3P_2$ to ${}^3F_2$, the effects of the five phase shifts for ${}^1S_0$, ${}^1D_2$, ${}^3P_{0,1,2}$ are included as non-vanishing. Since no specific nuclear interaction is assumed, the five phase shifts plus two parameters specifying the coupling give a total of seven free parameters which can be adjusted to fit experiment. Fits to data at 240 Mev[2,3] are used as typical throughout this work. It is found that the data do not exclude the possibility of intermediate state coupling, but rather indicate that such a state may prove helpful in fitting experiment. In particular they suggest that if coupling of the type investigated should be taking place, appreciable changes of values of phase shifts of states not participating in the coupling must also be made. In view of the many attempts to fit high-energy scattering data by means of phenomenologic potentials, it appears to be of interest to point out that conclusions regarding the effective potential in the ${}^1S$ state or in ${}^3P_0$, ${}^3P_1$ are not altogether independent of unknown couplings of states with different L. Only the simplest example of these has been considered below. It will be noted, however, that the effects on the phase shift without coupling are quite large.

[5] R. M. Thaler and J. Bengston, preceding paper [Phys. Rev **94**, 679 (1954)].

[6] The forms used in the calculations are related to those used in G. Breit, Phys. Rev. **58**, 1068 (1940) and especially to Eqs. (6.3), (7.7) in G. Breit, Phys. Rev. **69**, 472 (1946). While the present work was in progress, there appeared related considerations regarding the parametrization of the scattering matrix by J. M. Blatt and L. C. Biedenharn, Phys. Rev. **86**, 399 (1952). These are in part based on the use of eigenstates of the scattering matrix credited by them to J. Schwinger's 1947 unpublished lectures. The classification according to eigenstates of the scattering matrix is essentially the same as the classification according to the index α in a previously quoted reference (see reference 4). The parametrization of Blatt and Biedenharn, which employs the explicit specification of eigenstates and a total of three independent parameters, has advantages if an exhaustive enumeration is desired. On the other hand, for the purpose of qualitative consideration with unknown eigenstates the method used here is convenient.

Notation and Symbols

E = kinetic energy of incident nucleon in the laboratory system.

E_R = resonance energy as defined by Eqs. (1).

Γ_L = partial resonance width for orbital angular momentum L. In numerical applications Γ_L is used for total angular momentum $j=2$ and is expressed in terms of E.

$T=\tan^{-1}[(\Gamma_1+\Gamma_3)/(E_R-E)]$.

$y=\Gamma_3/(\Gamma_1+\Gamma_3)$.

L = orbital angular momentum about center of mass in units of $\hbar=1$.

F_L, G_L = respectively the regular and irregular solutions of the differential equation for $r\times$radial function normalized so as to be asymptotic at $r=\infty$ to $\sin\varphi$ and $\cos\varphi$ with $\varphi=\rho-\frac{1}{2}L\pi-\eta\ln 2\rho+\sigma_L$.

$\rho=kr$, $k=2\pi/$(de Broglie wavelength), $\eta=e^2/\hbar v$.

${}^1K_L, {}^3K_L$ = singlet and triplet phase shifts, respectively.

$\delta_{L,j}$ = triplet phase shifts for orbital angular momentum L in the absence of intermediate state coupling; in some cases $\delta_{J-1,J}$ is called δ_- and $\delta_{J+1,J}$ is called δ_+; in most cases the comma is omitted and the symbol is written as δ_{Lj}.

$s_{L,j}=\sin\delta_{L,j}$.

σ_L = Coulomb phase shift $=\arg\Gamma(L+1+i\eta)$.

χ_{0s}, χ_{μ} = singlet and triplet spin functions, respectively.

P_L = Legendre function, $Y_M{}^L$ = spherical harmonic $=(-1)^m(2^l l!)^{-1}[(2l+1)/4\pi]^{\frac{1}{2}}\times([l-m]!/[l+m]!)^{\frac{1}{2}}\exp(im\varphi)\sin^m\theta\times(d/d\cos\theta)^{l+m}(\cos^2\theta-1)^l$.

θ = scattering angle in the center-of-mass system.

$\psi^{L,j}{}_{\mu}$ = spin-angle factor of eigenfunction for orbital angular momentum L, total angular momentum j and projection μ.

$\begin{pmatrix} L, j \\ \mu-M, M \end{pmatrix}$ = transformation coefficient defined by Eq. (2.2).

$\mathbf{P}$ = proton-proton scattering cross section per unit solid angle in the center-of-mass system.

$\mathbf{P}_M$, $\mathbf{P}_{NUC}$, $\mathbf{P}_{INT}$ are the Mott, the specific nuclear, and the Coulomb interference parts of $\mathbf{P}$, respectively.

$\sigma^{NP}(\theta)$ = differential scattering cross section for np scattering taken per unit solid angle in the center-of-mass system at colatitude angle θ.

$\mathbf{c}$, $\mathbf{s}$ = used as in preceding paper.

II. EFFECT OF INTERMEDIATE STATE

The interaction between two levels with different values of orbital angular momentum may be represented[6] by means of the matrix

$$(C)=e^{iT}\sin T\begin{pmatrix}(1-y)\exp[2i\delta_-], & [y(1-y)]^{\frac{1}{2}}\exp[i(\delta_-+\delta_+)]\\ [y(1-y)]^{\frac{1}{2}}\exp[i(\delta_-+\delta_+)], & y\exp[2i\delta_+]\end{pmatrix}, \tag{1}$$

where the parameters are related to the resonance energy E_R and the half-widths Γ_-, Γ_+ of the disintegration channels by

$$y=\Gamma_+/(\Gamma_-+\Gamma_+),\quad \tan T=(\Gamma_-+\Gamma_+)/(E_R-E). \tag{1.1}$$

Here Γ_-, Γ_+ refer, respectively, to the levels with $L=j-1$ and $L=j+1$ and a similar convention is being used for δ_-, δ_+. The convention regarding C is that the regular functions F_-, F_+ are changed by the nuclear interaction to

$$\begin{pmatrix}F_-\\ F_+\end{pmatrix}+\left\{\begin{pmatrix}Q(\delta_-), & 0\\ 0, & Q(\delta_+)\end{pmatrix}+\begin{pmatrix}C_{--}, & C_{-+}\\ C_{+-}, & C_{++}\end{pmatrix}\right\}\begin{pmatrix}H_-\\ H_+\end{pmatrix}, \tag{1.2}$$

with

$$H=G+iF, \tag{1.3}$$

$$Q(\delta)=e^{i\delta}\sin\delta. \tag{1.4}$$

The scattering matrix in this convention has the form

$$\|S_{ij}\|=\begin{pmatrix}\tau_- & 0\\ 0 & \tau_+\end{pmatrix}\begin{pmatrix}y+(1-y)e^{2iT}, & [y(1-y)]^{\frac{1}{2}}(e^{2iT}-1)\\ [y(1-y)]^{\frac{1}{2}}(e^{2iT}-1), & 1-y+ye^{2iT}\end{pmatrix}\begin{pmatrix}\tau_- & 0\\ 0 & \tau_+\end{pmatrix}, \tag{1.5}$$

where

$$\tau=e^{i\delta}. \tag{1.6}$$

The scattering matrix contains in this form 4 parameters δ_-, δ_+, y, T. Since there are[6] only three independent parameters in the scattering matrix the results for some independently specified values of the four parameters are the same. The result of specifying two phase shifts δ_-, δ_+, which are then modified through coupling by means of an intermediate state, is not necessarily different, therefore, from the scattering obtained by means of another pair of δ_-, δ_+. It is thus not possible to distinguish uniquely between effects of phase shifts δ_-, δ_+ which would be there for $y=0$ and effects caused by the coupling through the intermediate state. In the calculations reported on below, no attempt is made to cover all possibilities systematically and the question of exhaustive and complete parametric representation is therefore not of immediate importance, the primary object being a preliminary survey of the type of effect caused by the coupling of states with different L. In the numerical work the phase shift $\delta_+=0$ and the matrix $\|S_{ij}\|$ is expressed in terms of three parameters. In this representation the diagonal element referring to the higher L is $1+y(e^{2iT}-1)$, so that there is scattering of this wave into its own channel as long as y and T do not vanish. At the same time, for such values of y and T the nondiagonal element of $\|S_{ij}\|$ is not zero. The cases covered are therefore distinct from those obtainable by employing phase shifts δ_+ and δ_- but with $y=0$.

The two nucleons are supposed to be colliding with random directions of the spins. A statistical mixture of incident plane waves with equal probabilities for each of the four mutually orthogonal spin states is used and the calculation is otherwise standard. Thus the effect of the matrix (C) and of phase shifts outside (C) is to change the part of the wave function having the smaller orbital angular momentum L, spin function χ_μ for spin projection μ, to the value

$$i^L[4\pi(2L+1)]^{\frac{1}{2}}(1/\rho)\exp(i\sigma_L)\times\left\{\sum_j\begin{pmatrix}L,j\\ 0,\mu\end{pmatrix}\psi^{L,j}{}_\mu[F_L+Q(\delta_{L,j})H_L]+\begin{pmatrix}L,J\\ 0,\mu\end{pmatrix}[\psi^{L,J}{}_\mu C_{L,L}H_L+\psi^{L+2,J}{}_\mu C_{L,L+2}H_{L+2}]\right\}, \tag{2}$$

where

$$J=L+1, \tag{2.1}$$

and the summation is taken over $j=L-1$, L, $L+1$. Here the composition of angular momenta to form a resultant function with total angular momentum J is represented by

$$\psi^{L,J}{}_\mu=\sum_M\begin{pmatrix}L,J\\ \mu-M,M\end{pmatrix}Y^L{}_{\mu-M}\chi_M. \tag{2.2}$$

Similarly, for the larger orbital angular momentum $L+2$ and incident spin function χ_μ, the effect of the phase shifts and of the matrix (C) is to change the term originally present to

$$i^{L+2}[4\pi(2L+5)]^{\frac{1}{2}}(1/\rho)\exp(i\sigma_{L+2})\times\left\{\sum_j\begin{pmatrix}L+2,j\\ 0,\mu\end{pmatrix}\psi^{L+2,j}{}_\mu[F_{L+2}+Q(\delta_{L+2,j})H_{L+2}]+\begin{pmatrix}L+2,J\\ 0,\mu\end{pmatrix}[\psi^{L+2,J}{}_\mu C_{L+2,L+2}H_{L+2}+\psi^{L,J}{}_\mu C_{L+2,L}H_L]\right\}. \tag{2.3}$$

The procedure used is closely similar to that of Kittel and Breit[7] and of Breit, Kittel, and Thaxton.[7] The formulas employed so far are valid for any L but become specialized to $L=1$ beginning with Eq. (3.3). On summing intensities for different spin orientations the cross section in the system of the center of mass is readily found. It is expressible in the form

$$\mathbf{P}=\mathbf{P}_M+\mathbf{P}_{NUC}+\mathbf{P}_{INT}, \tag{3}$$

where designations M, NUC, INT stand for "Mott," "nuclear," and "interference," respectively. The values of the three contributions to the cross section are as follows. The Mott part is

$$\mathbf{P}_M=(e^2/2\mu v^2)^2\{\mathbf{s}^{-4}+\mathbf{c}^{-4}-\mathbf{s}^{-2}\mathbf{c}^{-2}\cos[\eta\log(\mathbf{s}^2\mathbf{c}^{-2})]\}, \tag{3.1}$$

as is well known. The interference term P_{INT} may be written reasonably compactly in the notation of BCP[2] and its immediate extensions summarized by

$$\varphi_L=K_L+2(\sigma_L-\sigma_0);\quad \varphi_L{}^s=\varphi_L+\eta\ln\sigma^2,\quad (\sigma=\mathbf{c},\mathbf{s}),$$
$$\varphi_{Lj}=\delta_{Lj}+2(\sigma_L-\sigma_0),\quad \varphi_{Lj}{}^s=\varphi_{Lj}+\eta\ln\sigma^2, \tag{3.2}$$
$$\varphi_L{}^s(T)=T+\eta\ln\sigma^2+2(\sigma_L-\sigma_0),$$

and is expressible in the form

$$\begin{aligned}-(\eta/2)(2\mu v^2/e^2)^2P_{INT}&=\mathbf{s}^{-2}\cos\varphi_0{}^s+\mathbf{c}^{-2}\cos\varphi_0{}^c\\&+\{\textstyle\sum_j(2j+1)\sin\delta_{1j}[\mathbf{s}^{-2}\cos\varphi_{1j}{}^s+\mathbf{c}^{-2}\cos\varphi_{1j}{}^c]\\&+5(1-y)[\mathbf{s}^{-2}\cos(T+\delta_{12}+\varphi_{1,2}{}^s)\\&-\mathbf{c}^{-2}\cos(T+\delta_{1,2}+\varphi_{1,2}{}^c)]\sin T\}P_1\\&+5\sin K_2[\mathbf{s}^{-2}\cos\varphi_2{}^s+\mathbf{c}^{-2}\cos\varphi_2{}^c]P_2\\&+5y\sin T[\mathbf{s}^{-2}\cos\varphi_3{}^s(T)-\mathbf{c}^{-2}\cos\varphi_3{}^c(T)]P_3.\end{aligned} \tag{3.3}$$

The nuclear scattering term $\mathbf{P}_{NUC}$, is obtainable from

$$k^2\mathbf{P}_{NUC}={}^3\alpha_0P_0+{}^3\alpha_2P_2+{}^3\alpha_4P_4, \tag{4}$$

with

$${}^3\alpha_0=\sin^2K_0+\textstyle\sum_j(2j+1)(s_{1j})^2+5\sin^2T$$
$$+10(1-y)s_{12}\sin T\cos(T+\delta_{12})+5\sin^2K_2, \tag{4.1}$$

where

$$s_{Lj}=\sin\delta_{Lj}, \tag{4.2}$$

and with

$$\mathbf{C}=y^{\frac{1}{2}},\quad \mathbf{S}=(1-y)^{\frac{1}{2}}, \tag{4.3}$$

$$\begin{aligned}{}^3\alpha_2=&\tfrac{3}{2}s_{11}{}^2+(7/2)s_{12}{}^2+4s_{10}\cos(\delta_{10}-\delta_{12})\\&+9s_{11}s_{12}\cos(\delta_{12}-\delta_{11})+\sin^2T[(7/2)\mathbf{S}^4\\&+8\mathbf{C}^2\mathbf{S}^2+(32/7)\mathbf{C}^4+2(6)^{\frac{1}{2}}(1+(\mathbf{C}^2/7))\mathbf{CS}\cos B\\&+(12/7)\mathbf{C}^2\mathbf{S}^2\cos^2B]\\&+s_{10}\sin T[4\mathbf{S}^2\cos(T+2\delta_{12}-\delta_{10})\\&+4(6)^{\frac{1}{2}}\mathbf{CS}\cos(T+\sigma_3-\sigma_1+\delta_{12}-\delta_{10})\\&+6\mathbf{C}^2\cos(A+\delta_{12}-\delta_{10})]\\&+s_{11}\sin T[9\mathbf{S}^2\cos(T+2\delta_{12}-\delta_{11})\\&-6^{\frac{1}{2}}\mathbf{CS}\cos(\sigma_3-\sigma_1+T+\delta_{12}-\delta_{10})\\&+6y\cos(A+\delta_{12}-\delta_{11})]+s_{12}\sin T[7\mathbf{S}^2\cos(T+\delta_{12})\\&+2(6)^{\frac{1}{2}}\mathbf{CS}\cos(T+\sigma_3-\sigma_1)+(6/7)\mathbf{C}^2\cos A]\\&+(50/7)\sin^2K_2+10\sin K_0\sin K_2\\&\times\cos(K_2-K_0+2\sigma_2-2\sigma_0),\end{aligned} \tag{4.4}$$

where

$$A=T+2\sigma_3-2\sigma_1-\delta_{12},\quad B=\sigma_3-\sigma_1-\delta_{12}, \tag{4.5}$$

while

$${}^3\alpha_4=\{\sin^2T[10\mathbf{C}^4+(40)6^{\frac{1}{2}}\mathbf{CS}\cos B+(240)\mathbf{C}^2\mathbf{S}^2\cos^2B]$$
$$+(120)\mathbf{C}^2s_{12}\sin T\cos A+90\sin^2K_2\}/7. \tag{4.6}$$

In the above expressions the f-wave phase shifts for no coupling $\delta_{3,j}$ were taken as zero, and partial waves for $L>3$ were assumed to make no contribution to the scattering except through the Coulomb interaction.

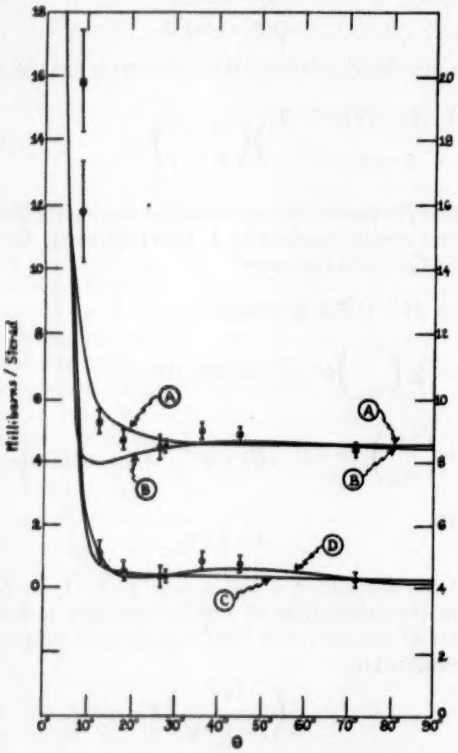

FIG. 1. Differential cross section for proton-proton scattering at $E=240$ Mev plotted against scattering angle θ in the center-of-mass system. Values of phase shifts and other parameters for the four curves are as follows (all phase shift values are in degrees):

Curve	${}^1K_0$	${}^1K_2$	δ_{10}	δ_{11}	δ_{12}	T	y
A	31.3	3.5	45.4	10.0	−20.0	5.7	0.3
B	31.3	3.5	−45.0	20.0	−10.0	5.7	0.7
C	31.3	0	−81.2	−3.0	−2.5	2.9	0.7
D	31.3	0	−50.1	10.0	−15.3	5.7	0.7

The left-hand scale is for curves *A* and *B*, the right-hand scale for *C* and *D*. Experimental points (see references 8 and 9) are indicated by circles and squares for right- and left-hand scales, respectively.

[7] C. Kittel and G. Breit, Phys. Rev. **56**, 744 (1939); Breit, Kittel, and Thaxton, Phys. Rev. **57**, 255 (1940). The four equations (unnumbered) in the middle of page 256 show the simple procedure.

III. *P-P* SCATTERING

Substitution of numerical values for the phase shifts ${}^1K_0$, ${}^1K_2$, $\delta_{1,0}$, $\delta_{1,1}$, $\delta_{1,2}$, T, and the coupling constant y into the above expression enables one to construct a good fit to the 240-Mev p-p scattering data.[2,3] In fact, it has been shown in the preceding paper[5] that the choice ${}^1K_2=T=0$ is consistent with the data. The question as to whether the data are in contradiction to the hypothesis of appreciable coupling between the ${}^3P_2$ and ${}^3F_2$ states is discussed below.

The experimental cross section[8,9] is represented in Fig. 1. The Coulomb contribution, $\mathbf{P}_M$, being negligibly small for $\theta \gtrsim 30°$, it is evident that for $\theta \gtrsim 30°$, the Coulomb and interference parts of the cross section contribute negligibly in comparison with the nuclear part $\mathbf{P}_{NUC}$. Since for $\theta \gtrsim 30°$ the cross section is approximately independent of angle, the coefficients α_2 and α_4 of Eq. (4) have been taken to be small as compared with α_0. Sets of values of the scattering parameters ${}^1K_0$, ${}^1K_2$, $\delta_{1,0}$, $\delta_{1,1}$, $\delta_{1,2}$, T, and y which satisfy, to within the experimental uncertainty, the equations

$$k^{-2}\alpha_0 = 4.5 \text{ mb}, \quad \alpha_0 = 1.30, \tag{5}$$

$$\alpha_2 = 0, \tag{5.1}$$

$$\alpha_4 = 0 \tag{5.2}$$

may be seen to fit the data for $\theta \geq 30°$. In addition, certain of these sets of values of the scattering parameters, when substituted into the complete expression for the scattering cross section, have been found to yield a reasonably good fit to the data over the entire angular range.

The s-wave phase shift ${}^1K_0$ was taken to be ${}^1K_0 = 31.3°$, as computed in first Born approximation from the meson well

$$V = -C \exp(-r/a)/(r/a), \tag{6}$$

with $C = 89.8\, mc^2$ and $a = 0.42\, e^2/mc^2$, which is consistent with the low-energy data.[10] The employment of this potential well is clearly open to serious criticism. Since the same holds for practically any other choice of ${}^1K_0$, the computation was nevertheless carried through employing the procedure just described so as to avoid unnecessary arbitrariness. The ${}^3P_2$–${}^3F_2$ anomaly is defined by the three parameters $\delta_{1,2}$, T, y, the ${}^3F_2$ contributions not arising from the coupling to ${}^3P_2$ having been taken to be zero. It is easily seen that solutions of Eqs. (5) can exist only for a limited range of these parameters. By definition $0 \leq y \leq 1$, and T is restricted by $0 < T < \pi/2$.[11] From Eqs. (5) and (5.2) there follow

TABLE I. Values of ${}^3\alpha_4$ and of γ for various T, $\delta_{1,2}$, and y. Criteria of acceptability are ${}^3\alpha_4 \leqq 0$, $\gamma \leqq 1$.

	sin$T$ = 0.1			sin$T$ = 0.2			sin$T$ = 0.3		
	$\delta_{1,2}$	γ	${}^3\alpha_4$	$\delta_{1,2}$	γ	${}^3\alpha_4$	$\delta_{1,2}$	γ	${}^3\alpha_4$
y=0.1	−40°	1.64	−0.05	−40°	1.25	−0.04	−40°	0.91	+0.04
	−30°	0.89	−0.04	−30°	0.60	−0.02	−30°	0.38	+0.07
	−20°	0.34	−0.02	−20°	0.18	−0.03	−20°	0.18	+0.14
	−10°	0.05	+0.00	−10°	0.04	+0.08			
	0	0.05	+0.04	0	0.20	+0.14			
	+10°	0.35	+0.06						
	+20°	0.91	+0.09						
y=0.3	−40°	1.74	−0.17	−40°	1.48	−0.16	−40°	1.27	+0.04
	−30°	0.98	−0.14	−30°	0.79	−0.10	−30°	0.68	+0.13
	−20°	0.40	−0.08	−20°	0.31	+0.03			
	−10°	0.32	+0.06						
	0	0.05	+0.09						
	+10°	0.32	+0.18						
y=0.5				−40°	1.70	−0.34	−40°	1.63	−0.10
	−30°	1.07	−0.25	−30°	0.98	−0.25	−30°	0.97	+0.01
	−20°	0.47	−0.15	−20°	0.45	−0.05	−20°	0.52	+0.31
	−10°	0.11	−0.02	−10°	0.18	+0.21			
	0	0.05	+0.12						
y=0.7	−30°	1.16	−0.39	−30°	1.17	−0.50	−30°	1.26	−0.32
	−20°	0.54	−0.26	−20°	0.58	−0.31	−20°	0.73	−0.04
	−10°	0.15	−0.08	−10°	0.25	+0.10	−10°	0.45	+0.54
	0	0.05	+0.12						
y=0.9	−30°	1.25	−0.56	−30°	1.36	−0.89	−30°	1.55	−0.96
	−20°	0.60	−0.40	−20°	0.72	−0.60	−20°	0.93	−0.59
	−10°	0.18	−0.18	−10°	0.32	−0.18	−10°	0.55	+0.00
	0	0.05	+0.08	0	0.20	+0.32	0	0.45	+0.72

the inequalities:

$$1.30 - \sin^2 K_0 = 1.30 - 0.27 = 1.03 \leq 5s_{12}^2 + 5\sin^2 T + 10(1-y)s_{12}\sin T\cos(T+\delta_{1,2}) \equiv \gamma(\delta_{1,2},y,T), \tag{7}$$

$${}^3\alpha_4(\delta_{1,2},y,T) \geq 0, \tag{7.1}$$

where ${}^3\alpha_4$ is as in Eq. (4.6) and its functional dependence on δ_{12}, y, and T is now indicated for emphasis. The values of $\gamma(\delta_{1,2},y,T)$ and ${}^3\alpha_4(\delta_{1,2},y,T)$ which appear in Table I illustrate the permissible range of the parameters $\delta_{1,2}$, y, T. It is seen from Table I that solutions for Eqs. (5) will probably arise only for $\delta_{1,2} < 0$ and $T < 20°$. If a set of values of $(\delta_{1,2},y,T)$ are chosen such that $\gamma(\delta_{1,2},y,T) < 1$ and ${}^3\alpha_4(\delta_{1,2},y,T) < 0$, it is usually possible to find values of $(\delta_{1,0},\delta_{1,1},{}^1K_2)$ such that Eqs. (5) are approximately satisfied. If, furthermore, these values satisfy the inequality

$$\sum_{j=0}^{2}(2j+1)\sin\delta_{1,j}\cos\delta_{1,j} + 5\sin T\cos T + 5\sin K_2\cos K_2 < 0, \tag{8}$$

then the data will be approximately represented by substituting these values into the formula for the cross section, Eq. (3); for the inequality, Eq. (8), assures that the cross section will not have a minimum in the angular region where the Coulomb interference term is important.

Several typical fits to the data, obtained by the procedure outlined above, are plotted in Fig. 1. The cross-section dependence plotted in Fig. 1B is a typical one for which Eqs. (5) are approximately obeyed, but which does not obey the inequality of Eq. (8), and so does not fit the data at small angles. If a fit to the data

[8] C. L. Oxley and R. D. Shamberger, Phys. Rev. **83**, 274 (1951).
[9] O. A. Towler, Jr., Phys. Rev. **85**, 1024 (1952).
[10] Yovits, Smith, Hull, Bengston, and Breit, Phys. Rev. **85**, 540 (1952).
[11] The quantity T is used with the restriction $|T| < \pi/2$, no resonance having been observed in the experimental region. The additional restriction $T > 0$ is being made, there being no evidence for $E_R < 0$.

also obeys the condition

$$\delta_{1,2}<\delta_{1,0},\ \delta_{1,1}, \tag{9}$$

then it will be said that such a fit corresponds to level inversion. The particular criterion used is not uniquely related to inversion of levels in nuclear spectroscopy. It is nevertheless of interest to employ a classification which has a qualitative relationship to the empirical studies of nuclear shell structure. In Fig. 1C is plotted a case which corresponds to this inversion.

It should be noted that Eqs. (5) serve as an approximate guide only. Equally good and better fits to the data can be obtained provided that $|\alpha_2/\alpha_0|\lesssim 0.2$ and $|\alpha_4/\alpha_0|\lesssim 0.2$. For example, the cross section plotted in Fig. 1D for ${}^1K_0=31.3°$, ${}^1K_2=0$, $\delta_{1,0}=-50.1°$, $\delta_{1,1}=10°$, $\delta_{1,2}=-15.3°$, $y=0.7$, $T=5.7°$ is one for which $\alpha_0=1.27$, $\alpha_2=0.00$, $\alpha_4=-0.17$.

IV. *N-P* SCATTERING

In Fig. 2 is a typical fit to the 260-Mev *n-p* data[12] which is consistent, in the sense of "charge independence," with the fit to the 240-Mev *p-p* data[8,9] plotted in Fig. 1A. The phase shifts ${}^1K_{0,1}$ and ${}^3K_{0,2}$ are calculated for 260 Mev from singlet and triplet meson wells, respectively,[13] the quantities ${}^1K_2$, $\delta_{1,0}$, $\delta_{1,1}$, $\delta_{1,2}$, y, T are as in Fig. 1A. This fit can be improved by suitable adjustment of ${}^1K_1$, ${}^3K_{0,2}$. Furthermore "inverted" fits to the 240-Mev *p-p* data, for which $\delta_{1,2}>\delta_{1,1}>\delta_{1,0}$, have been found which are likewise consistent with charge independence.

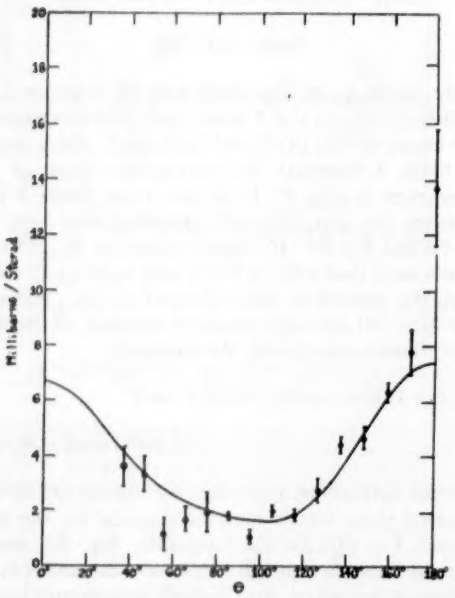

FIG. 2. Differential cross section for neutron-proton scattering at $E=260$ Mev for ${}^1K_0=30.9°$, ${}^1K_1=13.3°$, ${}^1K_2=3.5°$, ${}^3K_0=50.8°$, ${}^3K_2=9.9°$, $\delta_{10}=45.4°$, $\delta_{11}=10.0°$, $\delta_{12}=-20.0°$, $T=5.7°$, $y=0.3$. These values agree with parameters used for curve *A* of Fig. 1 in the sense of charge indepencence. Data are due to Kelly *et al.* (see reference 12).

For charge-independent nuclear forces, the neutron-proton scattering cross section corresponding to the assumption of intermediate state formation for $j=2$ in the triplet system, Eq. (7), may be written as

$$\begin{aligned}\sigma^{NP}(\theta)=(2k)^{-2}\{&k^2\mathbf{P}_{NUC}(\theta)+6P_1\sin({}^1K_0)\\
&\times\sin({}^1K_1)\cos({}^1K_0-{}^1K_1)\\
&+30P_1P_2\sin({}^1K_1)\sin({}^1K_2)\cos({}^1K_1-{}^1K_2)\\
&+9(P_1)^2\sin^2({}^1K_1)+3\sin^2({}^3K_0)\\
&+30P_2\sin({}^3K_0)\sin({}^3K_2)\cos({}^3K_0-{}^3K_2)\\
&+2P_1\sin({}^3K_0)[\textstyle\sum_{j=0}^{2}(2j+1)\sin\delta_{1,j}\\
&\times\cos(\delta_{1,j}-{}^3K_0)+5(1-y)\sin T\\
&\times\cos(2\delta_{1,2}+T-{}^3K_0)]+10P_1P_2\sin({}^3K_2)\\
&\times[\textstyle\sum_{j=0}^{2}(2j+1)\sin\delta_{1,j}\cos(\delta_{1,j}-{}^3K_2)\\
&+5(1-y)\sin T\cos(2\delta_{1,2}+T-{}^3K_2)]\\
&+10P_3\sin({}^3K_0)y\sin T\cos(T-{}^3K_0)\\
&+50P_2P_3\sin({}^3K_2)y\sin T\cos(T-{}^3K_2)\\
&+75(P_2)^2\sin^2({}^3K_2)\},\end{aligned} \tag{10}$$

where the quantities ${}^1K_{0,2}$, $\delta_{1,0}$, $\delta_{1,1}$, $\delta_{1,2}$, y, T are as in $\mathbf{P}_{NUC}(\theta)$ and where partial waves corresponding to $j>2$ have been excluded. The quantities in the above expression which may be adjusted to fit the *n-p* data are ${}^3K_{0,2}$, ${}^1K_1$.

V. CONCLUSION AND DISCUSSION

The calculations show that data on the *p-p* scattering cross section at 240 Mev admit an interpretation in which an appreciable part of the cross section is attributed to intermediate state formation resulting in the coupling of ${}^3P_2$ to ${}^3F_2$. If it is assumed on the other hand that nuclear force effects are confined to phase shifts for *s*, *p*, ${}^1D_2$ states and to ${}^3P_2-{}^3F_2$ coupling, then it is possible to exclude large values of the coupling parameters. Within these restricting assumptions regarding nuclear force effects, it proved possible to remain in agreement with the hypothesis of charge independence of nuclear forces. The *p*-wave phase shifts of the charge-independent fits may be made to correspond either to the regular or inverted level order of the two-nucleon system; there is thus no obvious difficulty in reconciling the high-energy scattering data with the shell theory of nuclear structure.

The possible influence of coupling on the determination of phase shifts not directly concerned with the intermediate state has been discussed in the introduction, and the effect on the interpretation of phase shifts participating in the coupling may be seen in

[12] Kelly, Leith, Segrè, and Wiegand, Phys. Rev. **79**, 96 (1950).
[13] Equation (11) of preceding paper.

Table I. It has a bearing on indications of the existence of semistable states in pion-nucleon scattering[14] and on attempts to use isobaric state models for the theory of the deuteron.[15] The present work was in fact begun under the influence of similar views tentatively considered at this laboratory. The continued lack of success and the possibility of omission of essential elements[14] in the development of fundamental nuclear force theory would make a claim of a connection with the isobaric state of pion-nucleon phenomena rather speculative, especially since there is serious doubt[16] regarding the justification of such an interpretation of the meson data.

[14] K. A. Brueckner, Phys. Rev. **86**, 626 (1952). The considerations of Dyson, Bethe, Salpeter, and others, are given in four abstracts from the Cambridge Meeting of the American Physical Society (July, 1953) [Phys. Rev. **90**, 372 (1953)].

[15] H. A. Bethe and N. Austern, Phys. Rev. **86**, 121 (1952); N. Austern, Phys. Rev. **87**, 208 (1952).

ACKNOWLEDGMENTS

The authors would like to express their indebtedness to Mr. A. M. Saperstein for checking many of the transformations, to Miss C. Smolen for computational assistance, and to Mr. R. L. Becker for some check calculations.

[16] Anderson, Fermi, Nagle, and Yodh, Phys. Rev. **86**, 793 (1952); H. L. Anderson and E. Fermi, Phys. Rev. **86**, 794 (1952); Anderson, Fermi, Martin, and Nagle, Phys. Rev. **91**, 155 (1953); E. Fermi and N. Metropolis, Los Alamos unclassified report LA-1492, 1952 (unpublished).

PHYSICAL REVIEW VOLUME 94, NUMBER 3 MAY 1, 1954

Interactions of Negative Pions in Carbon and Lead*

JOHN O. KESSLER† AND LEON M. LEDERMAN
Columbia University, New York, New York

(Received January 11, 1954)

A cloud chamber investigation of the nuclear interactions of 125-Mev negative pi mesons has been carried out. Carbon and lead were employed as the scattering material. The experimental arrangement was designed to observe the charge-exchange process:

$$\pi^- + C \rightarrow B^{(\pi^0)} + [\pi^0 \rightarrow 2\gamma].$$

High-energy photons, probably attributable to charge exchange, are found to arise from nuclear interaction, with a small but finite cross section. Total and differential cross sections for elastic and inelastic scattering, as well as total nuclear reaction cross sections, are presented. A square well (optical model) analysis fits the data with a potential whose real part is attractive and 30 Mev deep, and whose imaginary part corresponds to a mean free path in nuclear matter of 3×10^{-13} cm. The optical model parameters are found to be energy dependent, the well depth increasing and the mean free path decreasing as the energy is raised.

I. INTRODUCTION

A CONSIDERABLE body of experimental fact, relevant to the interaction of pions in complex nuclei, is already established. Nuclear emulsion experiments have demonstrated the principal mechanisms of the interactions,[1] and given information regarding their energy dependence.[2] More recent experiments with counters,[3] cloud chambers,[4] and emulsions,[5] have continued these studies, and have more clearly shown the dependence of these processes on nuclear size.

The following over-all picture presents itself to us: at low energies (0–40 Mev) the dominant process is mesonic absorption with subsequent nuclear excitation resulting in star formation. The star cross section is about half geometric in the 40-Mev region. Only a small elastic scattering cross section is observed. As the bombarding energy increases, both star and elastic cross sections rise. At 60-Mev inelastic scattering begins to occur with an appreciable probability which increases rapidly with energy. The total reaction cross section is nearly geometric at 80 Mev for all complex nuclei. In some cases it seems to rise slowly as higher energies of bombardment are employed.[6]

The picture is completed by consideration of the charge exchange reaction, which is found to be of great

* This research was supported by the joint program of the U. S. Office of Naval Research and the U. S. Atomic Energy Commission. A preliminary account of this research was presented at the Cambridge meeting of the American Physical Society, February, 1953 [Phys. Rev. **90**, 342 (1953)].

† Submitted in partial fulfillment of the requirements for the degree of Doctor of Philosophy. Now at RCA Laboratories, Princeton, New Jersey.

[1] Bernardini, Booth, and Lederman, Phys. Rev. **83**, 1277 (1951). This paper may also be used as a summary of references to previous emulsion work; G. Bernardini and F. Levy, Phys. Rev. **84**, 610 (1951); H. Bradner and B. Rankin, Phys. Rev. **87**, 547, 553 (1952).

[2] Bernardini, Booth, and Lederman, Phys. Rev. **83**, 1075 (1951).

[3] Chedester, Isaacs, Sachs, and Steinberger, Phys. Rev. **82**, 958 (1951); R. L. Martin, Phys. Rev. **87**, 1052 (1952); Aarons, Ashkin, Feiner, Gorman, and Smith, Phys. Rev. **90**, 342 (1953); Pevsner, Williams, and Rainwater (private communication).

[4] A. Shapiro, Phys. Rev. **84**, 1063 (1951); Byfield, Kessler, and Lederman, Phys. Rev. **86**, 17 (1952); F. Tenney and J. Tinlot, Phys. Rev. **90**, 342 (1953); Fowler, Fowler, Shutt, Thorndike, and Whittemore, Phys. Rev. **91**, 135 (1953).

[5] S. Goldhaber and G. Goldhaber (private communication); M. Schein, *1953 Rochester Conference* (Interscience Publishers, New York, 1953).

[6] R. L. Martin, Phys. Rev. **87**, 1052 (1952).

importance in high-energy pion-nucleon interactions.[7] The first experiment which sought to find this effect in complex nuclei gave negative results.[8] Relatively low-energy π's (40 Mev) were used. More recently, further experiments concerning this have been performed: in England[9] and Chicago,[10] using nuclear emulsions, at Brookhaven,[11] with cloud chamber techniques, and at Rochester[12] with counters.

The present experiment is one of a series designed to provide data on the elastic, inelastic, and absorption processes of mesons in nuclear matter. It extends the analysis of pion-carbon scattering[13] from 60 to 125 Mev. In addition, information regarding the dependence of these effects on the size of the scattering center is obtained. Lead is employed as the large comparison material. Finally, a search is made for the charge-exchange scattering in these nuclei.

II. EXPERIMENTAL

A. General

A sixteen-inch, rubber diaphragm, expansion cloud chamber, situated in a magnet having a uniform 9000-gauss field, was employed as a detector. In it were placed carbon and lead scattering plates. The disposition of scattering material was determined by the necessity of obtaining optimum observational efficiencies for all processes under simultaneous investigation. The arrangement employed is shown in Fig. 1. A 2.54 cm thick (4.3 g/cm^2) carbon plate is placed across a diameter of the cloud chamber. Parallel with, and one inch away from this plate, on each side, are located two 0.318 cm thick (3.6 g/cm^2$\simeq$0.6 radiation lengths) lead plates. These subtended $\sim$50 percent of the total solid angle at a point in the middle of the carbon plate, on the axis of the cloud chamber. The 135-Mev π^- beam of the Nevis cyclotron was incident upon this arrangement at an angle of $\sim$15° with the normal. Complete attenuation of scatterings near 90° is thereby prevented.

Both the carbon and lead plates were used to gather information concerning scattering and absorption, and to act as conversion material for γ rays produced anywhere in the cloud chamber. The lead plates, in addition, yielded an estimate of the electron contamination of the meson beam. The thickness of the lead plates was chosen as a compromise between the requirements of good conversion efficiency for π^0 gamma rays and small multiple scattering of the resulting electrons. With regard to high-energy elastic scattering, thick scattering plates mean a reduction of the observation efficiency for wide angle events. A correction for this effect may easily be made. For inelastic scattering, where range effects become important, thick scattering plates imply distortion of the differential energy spectrum in addition to reduction in the statistics. It is, however, again generally possible to calculate the correct energy for inelastically scattered tracks, providing they emerge from the plate.

B. Cloud Chamber Operation

The gas filling mixture used was 50 percent argon, 50 percent helium, saturated with 70 percent alcohol $-$30 percent water vapor. The expansion ratio was 1.08. Sweeping fields of from 400 to 900 volts were used. The two lead plates were at high potential, the carbon plate and two conducting coatings on the side wall of the cloud chamber, approximately parallel with the lead plates, were grounded.

The operating cycle of the chamber was of one-minute duration. "Cleaning" operation was secured by two slow expansions, and by an overcompression[14] immediately following the first expansion. The overcompression was made by connecting a small ballast tank under high pressure to the below-diaphragm volume. The expansion ratio was set by finely regulated com-

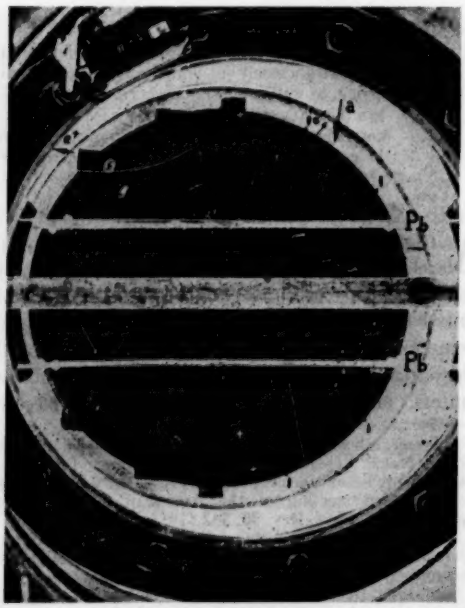

FIG. 1. The arrow (a) indicates incident meson which stops in carbon plate. A pair, marked e^+ and e^-, is observed in the backward direction. The pair axis intersects the projected meson trajectory within the carbon plate. A number of other events are marked on the picture.

[7] Anderson, Fermi, Martin, and Nagle, Phys. Rev. **91**, 155 (1953).
[8] R. Wilson and J. P. Perry, Phys. Rev. **84**, 163 (1951).
[9] W. O. Lock and G. Yekutieli, Phil. Mag. **43**, 231 (1952).
[10] M. Schein, *1953 Rochester Conference* (Interscience Publishers, New York, 1953).
[11] Fowler, Fowler, Shutt, Thorndike, and Whittemore, Phys. Rev. **91**, 135 (1953).
[12] A. Roberts and J. Tinlot, Phys. Rev. **90**, 951 (1953).
[13] Byfield, Kessler, and Lederman, Phys. Rev. **86**, 17 (1952).
[14] E. R. Gaerttner and M. L. Yeater, Rev. Sci. Instr. **20**, 588 (1949).

pressed air, fed to the underside of the rubber diaphragm through a null balance type regulator.[15]

C. Magnet

The magnet employed in this experiment is shown in Fig. 2. Helmholtz coils, 21-in. inside diameter, separated from each other by 6 in., were clad in a 2 in. thick mild steel casing around their periphery. The cloud chamber was mounted directly on the magnet. The coils were wound with copper conductor of rectangular cross section. A central hole in the conductor permitted efficient use of the circulating coolant. The magnetic field obtainable with an air-core magnet of this design is more than 30 percent higher than the field from standard Helmholtz coils of equivalent dimensions. Concurrently, no appreciable loss in field homogeneity is experienced.

The field generated in the useful region of the cloud chamber (a cylindrical volume 4 in. high and 14 in. in diameter), varied by less than 1 percent, peak to peak, from its mean value of ~9600 gauss. To obtain this field value, a current of 1100 amperes, supplied by a 300-kw motor-generator set, was used. The time necessary to reach peak field values was 10 seconds.

A Leeds and Northrup "Speedomax" potentiometer provided a record of current passing through the magnet at the time of each cloud chamber expansion with an accuracy of 0.3 percent. A marker pip, incorporated in the instrument, indicated the exact time of expansion on the current (field) graph.

Absolute and relative field magnitudes were measured with a search coil and a General Electric integrating flux meter, both of which have been calibrated in a standard 5000-gauss field at the Columbia Radiation Laboratory.

D. Optics

Events were recorded with two cameras mounted on a light-tight cylinder placed on top of the magnet (Fig. 2). The Goertz Dagor 60-mm lenses were 51¼ in. above the mid-plane of the chamber. The use of this long object-lens distance eliminates, in most cases, the need for second-order corrections to curvatures and scattering angles. This may be easily verified from the reprojection formulas derived in Appendix C. The axes were 10 in. apart, and vertical. The film planes were horizontal, the film being offset slightly from the lens axes, in order to capture the whole image of the chamber. Pictures were recorded on Kodak Linagraph-Ortho, 35-mm film, with lenses set at $f/11$. Due care to prevent emulsion distortion and to bring out maximum contrast was taken during film development.

The reprojection system consisted of two commercial projectors, fitted with lenses similar to those in the cameras. Images were viewed on a large rear-projection screen (Recordak). The projectors were adjusted for unity magnification in the median plane.

The film carriage of one projector was mounted on a rotating-translating microscope stage. It was thus possible to bring the two stereoscopic images into register. The applications of this system to the various kinds of measurements is treated below, and in the Appendix.

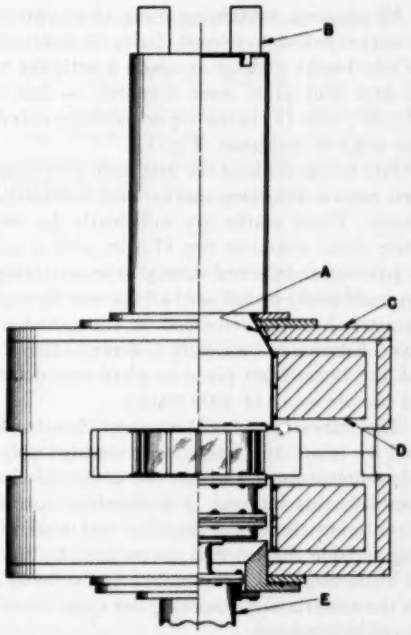

FIG. 2. Cutaway view of cloud chamber position in deflection magnet. A. Upper pole surface, B. camera, C. steel casing, D. coils, E. cloud chamber expansion mechanism. The drawing is approximately to scale. The outside diameter of the cloud chamber is 18 in.

III. ANALYSIS OF DATA

A. Criteria

Preliminary examination of the film indicated that the scanning of multiplate cloud chamber photographs, with an average of 12 tracks per picture, presents certain problems. In the present case, it was desired to obtain data yielding absolute reaction probabilities. In addition, it was hoped that clear evidence as to the existence, or nonexistence, of an unestablished reaction type would be found. The following scanning and accounting rules were therefore applied to insure impartial evaluation of the data.

(1) *Flux Counting Method*

(a) Pictures were scanned and flux counts made by at least two experienced observers, working independently. Final tallies varied by no more than 1 percent.

[15] Obtained from Moore Products, Philadelphia, Pennsylvania.

(b) All pictures containing more than twenty flux tracks were rejected, to permit clarity of observation.

(c) Only tracks making an angle δ with the normal to the first lead plate were accepted as flux, where $10° \leq \delta \leq 20°$, and 15° is the experimentally determined average angle of incidence (Fig. 1).

(d) Only tracks striking the first lead scattering plate between certain fiduciary marks were included in the flux count. These marks are sufficiently far removed from the cloud chamber rim (1.5 in. and 2 in.) that tracks passing undeflected through the scattering plate system could easily be followed all the way through, and that scattered tracks remained in the chamber for a sufficient distance to be clearly observed. The attenuation of the beam from plate to plate was determined from a sample count of 1000 tracks.

(e) The curvature of all apparent flux tracks was checked by template. Tracks were counted only if the particle momentum fell within the acceptable interval. To establish this interval, a momentum spectrum of tracks entering the cloud chamber was made. Tracks arriving outside the interval determined by the width of the histogram peak presumably had suffered energy loss in the materials surrounding the cloud chamber, or in the collimating slit.

(f) Tracks entering in fringe regions of the illumination were rejected, as only a small vertical deflection in a plate might have caused an apparent stopping. The height of the uniformly well illuminated region is 8 cm. At the boundaries the light intensity gradually decreases to zero in a space of $\sim$1.5 cm. Tracks entering in this fringe region therefore may be distinguished from more centrally located ones by their apparent faintness.

All tracks appearing faint relative to the main beam, in the opinion of the observers, were rejected. This scanning operation was the most difficult to carry out objectively. The independent records of individual observers, however, showed flux count discrepancies, per picture, of not more than 10 percent. The over-all totals showed a discrepancy of less than 1 percent. In order to account for possible errors incurred, a 5 percent error was assumed for the total flux count.

(g) The decision whether or not a given track was a "flux" or "nonflux" track was reached before the picture in question was scanned for events. It is, therefore, believed that the ratio between events observed and the number of good "flux" tracks is not subject to systematic bias.

(2) Search for, and Measurement of Events

(a) All pictures were scanned for events independently by at least two, and sometimes three observers. Each picture was scanned at least three times. The first scanning was $\sim$80 percent efficient relative to the last; the second $\sim$95 percent.

(b) Measurements of track curvature and scattering angles, as well as ionization estimates, where necessary, were performed twice, and, in the case of disagreements, three times.

(c) $\pi \rightarrow \mu$ decays in the gas of the chamber were recorded. Flux estimates from the number of $\pi \rightarrow \mu$ events observed,[16] agreed well with the actual corrected flux count.

B. Search for Charge-Exchange Scatterings

The search for charge-exchange scattering in complex nuclei was one of the objectives of the present experiment. Operationally, the reaction is characterized by the simple disappearance of a beam track. The π^0 decay time is $\cong 10^{-15}$ second. A neutral pion therefore travels only a negligible distance away from its point of origin before it decays.

The π^0 meson can be detected solely by means of the two photons arising from its decay. These photons may produce pairs in suitably located converting material. If the resulting electrons do not scatter greatly, the center line of each pair corresponds very well with the line-of-flight of its initiating γ ray. When the extrapolated pair center line coincides in space with the disappearance of a meson in a plate, the two are assumed to be associated. The kinematics of π^0 production are determined only if both resulting photons materialize.

All pictures were scanned for γ-induced electron pairs, associable with a stopped beam track. In practice, no double pairs appeared, and therefore methods of dealing with one pair only are outlined below.

The scanning adhered to certain restrictive criteria. Electron pairs corresponding to gamma rays emitted in the forward direction (within 20°) with respect to the stopped pion were rejected from the data. In this way bremsstrahlung effects due to any electron contamination of the meson beam were eliminated. Only electron pairs in which each electron had an energy ≥ 10 Mev were counted. This reduced multiple scattering effects which would increase errors in the center line extrapolation. In addition, the possibility of confusion with nuclear excitation γ rays are reduced. Events where materialization took place in the scattering plate in which the photon was produced were admitted to the total cross-section calculation. Direct decay of π^0 mesons into an electron pair cannot here be ruled out. This effect, however, is expected to be small,[17] except where it competes with conversion of photons directly in the carbon plate.

C. Scattering

Energy resolution was limited by the relatively small unobstructed areas of the cloud chamber within which curvature measurements could be made. In order to be classified into the inelastically scattered category, a meson was required to lose at least 40 Mev. In the case of short scattered tracks, due to rapid out-scattering

[16] Lederman, Booth, Byfield, and Kessler, Phys. Rev. **83**, 685 (1951).

[17] Lindenfeld, Sachs, and Steinberger, Phys. Rev. **89**, 531 (1953).

from the illuminated region, a definite change in track droplet density (at least by a factor of two) was required.

Track density determinations were based on a comparison of the track in question, with nearby tracks of beam energy.

Due to the finite angular spread of the incident beam, and the thickness of the scattering plates, it was very difficult to take systematic account of scatterings having projected angles $<15°$ in both camera views. Accordingly, no attempts were made to locate these.

The radius of curvature of tracks was measured by fitting thin plastic templates, upon which suitable radii had been inscribed, with the projected track image. Projected angles of the curved tracks were measured by fitting templates to the initial and final track projections, and measuring the angular separation of the arcs with a 360° protractor. Average error of this measurement was $\pm 1.0°$.

Projected angle and dip angle measurements were made on all scatterings (Appendix).

The depth of any point on a track below a fiduciary plane was found by bringing the images of suitable marks, inscribed previously on the top glass, into exact register, and measuring the displacement of the two images of the droplet in question. This displacement is proportional to the height of the point (droplet) below the reference plane. Inclination of a given track was measured by this method. The vertical displacement between the two droplets on the track, and the (non-orthogonal) projected distance between them, together give the dip angle of their joining chord. The derivation of relevant formulas may be found in Appendix C. All measurements of momenta on inelastically scattered and incident particles are corrected for ionization loss in traversing the scattering plate. In the case of wide angle (near 90°) scattering, this correction attains considerable importance. It was not necessary to observe the 15° cut-off criterion in the case of inelastic scatterings. The characteristic changes in curvature and ionization observed in such events are adequate for their location.

D. Stars and Stops

Stars are easily located owing to the positive curvature and generally heavy ionization of the prongs. Proton energies are usually not measurable on account of the relatively short unobstructed path length available.

Apparent "stoppings" are due to a number of effects. A phenomenological classification may be made as follows:

(a) True stoppings, due to charge-exchange scatterings, or stars in which neutrons and/or photons only are emitted.

(b) Inelastic scatterings or stars in which the emitted particle has not enough energy to escape from the scattering plate.

TABLE I. Cross sections of observed reactions.[a]

	$\sigma(1.40A^{\frac{1}{3}}\times 10^{-13})^2$	Elastic $\theta>20°$	Inelastic $\Delta E>40$	Charge[b] exchange	Stars and stops	Total reaction
Carbon	325	179±18	70± 11	20^{+20}_{-10}	220± 40	308±43
Lead	2150	700±84	530±130	100^{+80}_{-40}	1840±350	2477±385

[a] All cross sections in millibarns.
[b] Cross sections calculated under assumption of isotropic photon distribution.

(c) Scatterings or stars in which the final particle leaves the illuminated depth before emerging from the plate.

(d) Tracks which arrive in fringe regions of the illumination, and pass out of it while in the scattering plate.

(e) Beam-contamination electrons radiating a high-energy, nonconverting photon.

It was desirable to obtain a good estimate of the number of stoppings falling into categories (a) and (b), as these constitute a significant fraction of the total number of nuclear absorption events. The inclination and relative height in the cloud chamber of all tracks appearing to stop were measured. In order to minimize contributions from (c) and (d), only stoppings occurring within a central, 3.5 cm high, fraction of the illumination were accepted into categories (a) and (b). The number of stoppings seen in this region was normalized to correspond to the total flux count.

It is not possible to determine directly the relative magnitude of the contribution from (c). The efficiency for loss from observation of elastically scattered particles has, however, been calculated as a function of scattering angle, for the whole illuminated height. This correction was applied to the total and differential elastic cross sections (Appendix).

Stops falling into category (e) were eliminated before the other corrections were applied. The number of these events was determined from the percentage of electron contamination in the beam. About 5 percent of the total intensity is due to electrons. This figure has been estimated from the number of particle-induced showers, of three or more final particles, observed in the lead

TABLE II. Compilation of charge exchange events.

Scattering material	Frame No.	Angle of emission of photon	Energy of photon in Mev
Carbon	20 448 C[a]	135°	35
	20 441 C	180°	70
	20 418 Pb	153°	65
	21 426 Pb	154°	49
Lead	20 816 Pb	72°	95
	21 139 Pb	115°	150
	20 033 C	155°	80
	20 593 C	122°	135
	21 039 Pb	24°	(Event ambiguous, not counted)

[a] The letter following the frame number indicates the converter plate.

plates.[18] In lead (0.6 radiation lengths), 2_{-1}^{+2} percent of the electrons stop without further trace. The number of electrons stopping in carbon is about one-tenth of this.

IV. EXPERIMENTAL RESULTS

The experimental results are summarized in Tables I and II, and in Figs. 3–7.

A total of 1500 pictures was used to obtain these data. (One example of inelastic scattering is shown in Fig. 8.) The flux count after beam corrections corresponds to 19 900 g/cm² of carbon traversal, and 33 100 g/cm² of lead. Three-hundred-and-three events were observed in lead; 451 events make up the total carbon statistics. The further distribution of categories within these statistics is contained in Tables I and II.

To obtain the total and differential elastic cross sections, correction factors, due to the observational efficiencies, were applied. The derivation of these factors may be found in the Appendix. The total inelastic cross section is, of necessity, only a lower limit, as discussed elsewhere.

All errors, as indicated on the curves or in the table, have been calculated by taking into account uncertainties in the counting statistics $[(N+1)^{\frac{1}{2}}/N\times 100$ percent], in the flux count and beam composition (5 percent), and in the applied corrections (variable). The rms sum of standard deviations has been used throughout this experiment.

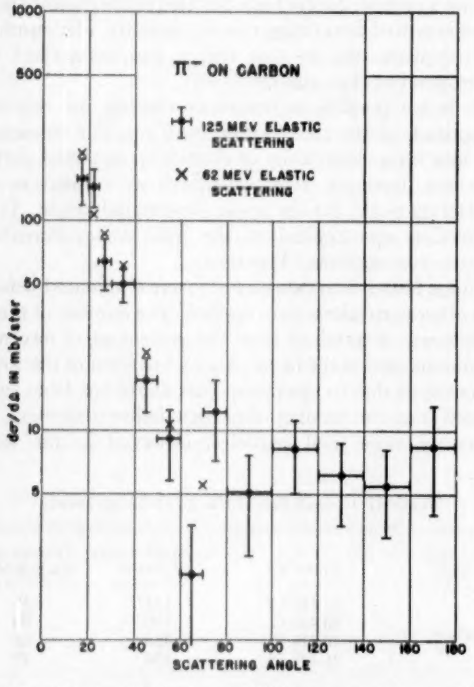

FIG. 3. Angular distribution of 125-Mev π^- elastic scattering in carbon. The crosses are points indicating the distribution for 62-Mev π mesons, and are included for comparison.

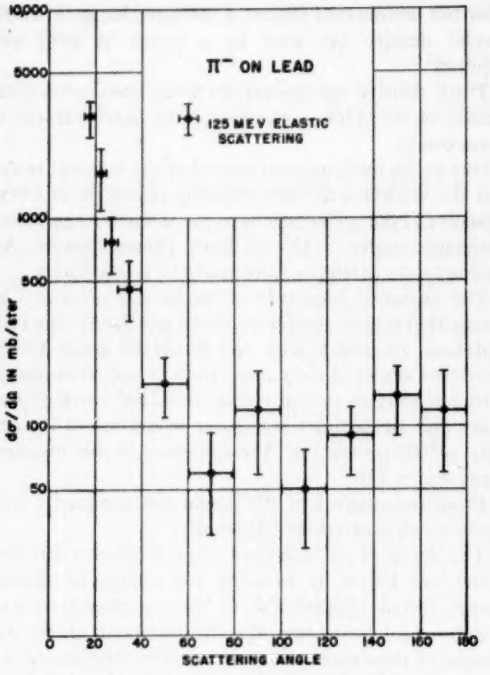

FIG. 4. Angular distribution of 125-Mev π^- elastic scattering in lead.

The correlated photon events observed are indicated in Table II. Because of the few events actually observed, and because of the statistical uncertainty in the conversion efficiency (Monte Carlo calculation—see Appendix), a very large experimental error must be quoted. The true number of charge-exchange events to be inferred from the observed number has been obtained with the aid of the Bernouilli probability distribution. If N is the true number of events, giving rise to n observed events, the a priori observation probability being p, then

$$n=Np\pm[N(1-p)p]^{\frac{1}{2}}.$$

One may solve for the desired number, N, to obtain, for $p\ll 1$,

$$N=\frac{1}{p}(n+\tfrac{1}{2})\pm\frac{1}{p}(n+\tfrac{1}{4})^{\frac{1}{2}}.$$

To obtain the total number of inferred charge-exchange events, it is necessary to sum-over all production mechanisms. In the sum, the N derived for each particular mechanism is weighted as the inverse square of its mean deviation, as given in the above equation. The carbon and lead events are of course treated separately.

[18] Results of Monte Carlo shower calculations for 200 Mev incident electrons were used. We are grateful to R. R. Wilson for the kind permission to utilize his shower graphs. See R. R. Wilson, Phys. Rev. 86, 261 (1952).

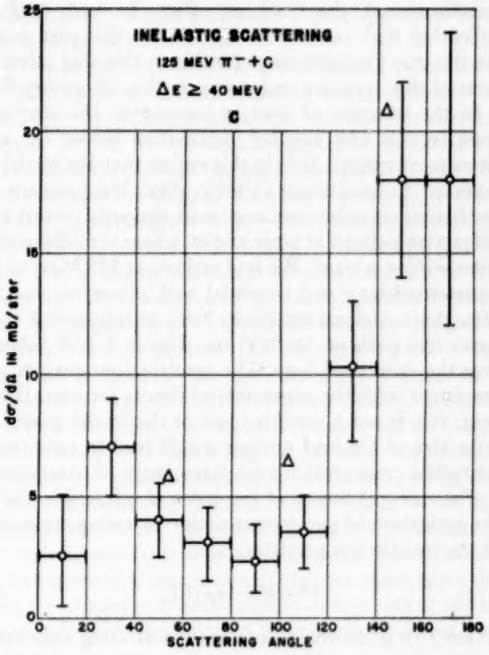

FIG. 5. Angular distribution for inelastic scattering in carbon. The triangles are comparison points describing the distribution of $\pi^+ + p \rightarrow \pi^+ + p$.

The total error is taken as the sum of the inverse squares of the partial errors, to the $-\frac{1}{2}$ power.

As the statistical probability for seeing the two direct carbon conversions is very small, in the light of the other events observed, direct "internal conversion" of the photons[17] arises as a distinct possibility in the present case.

V. DISCUSSION OF RESULTS

A. Elastic Scattering and Absorption

The "optical model," first discussed in these applications by Fernbach, Serber, and Taylor,[19] has been applied to the interpretation of high-energy neutron-[20] and pion-nucleus scattering.[13,21] The model, in its simplest form, treats the nucleus as a spherical region of uniform density, having a refractive index and absorption coefficient for the incident wave packet. The effect of the refractive index may be found[19] by considering the amplitude attenuation and change in phase of the incident wave, a procedure which neglects reflection effects. A rigorous solution of the wave equation in space, with appropriate matching to the region of complex potential, may also be made.[13] In this latter case, the approximations are inherent solely in the initial assumptions.[22]

Three parameters of the model, the radius, the real, and the imaginary part of the potential well may be used to fit the experimentally observed cross sections. The ultimate hope is that a good theory of the nucleus will naturally lead to a derivation of a model such as this, the parameters depending on the detailed properties of the nuclear constituents, and of their structure within the nuclear complex. At high bombarding energies, where binding effects presumably play minor roles, interpretation of the optical parameters in terms of elementary interaction processes, nuclear momentum distributions, and correlation effects is expected to be possible.[22] It is hoped, therefore, that interpretation of the present series of experiments in the light of the optical model may, apart from immediate conclusions, be of considerable use in the future.

Analysis of previous data[13] has yielded, for 60-Mev pions in carbon, optical parameters corresponding to a mean free path for absorption of the meson wave in nuclear matter of 8×10^{-13} cm, and a real potential well which is attractive and 20 Mev deep. The variation of these parameters with energy has been determined in the present experiment. It is found by an exact solution of the Schrödinger equation that a good fit may not be obtained here with the same parameters as in the 60-Mev case. Both the calculated angular distribution and

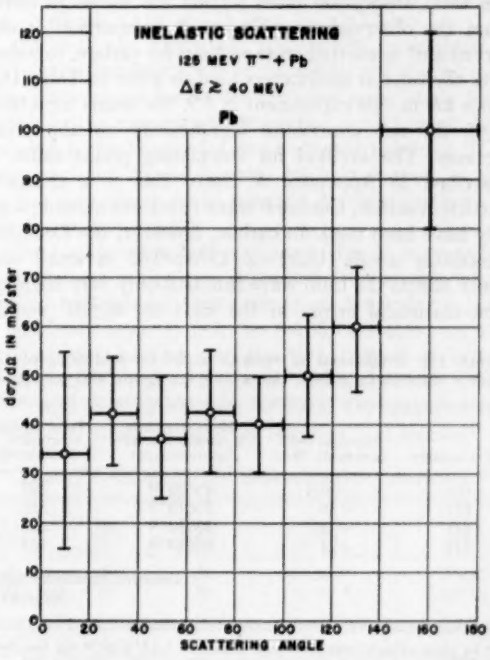

FIG. 6. Angular distribution of inelastic scattering in lead.

[17] Fernbach, Serber, and Taylor, Phys. Rev. **75**, 1352 (1949).
[20] J. DeJuren and N. Knable, Phys. Rev. **77**, 606 (1950).
[21] H. A. Bethe and R. R. Wilson, Phys. Rev. **83**, 690 (1951).
[22] K. M. Watson, Phys. Rev. **89**, 525 (1953). Also see N. C. Francis and K. M. Watson, Phys. Rev. **93**, 313 (1954).

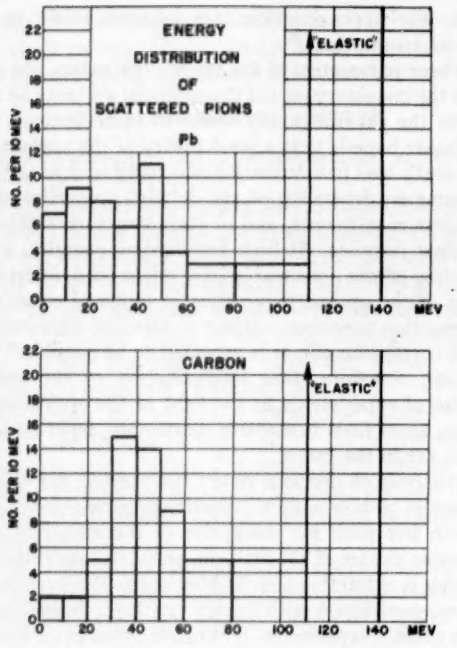

FIG. 7. Distribution of final energies of inelastically scattered mesons in lead and carbon. The data extend from 0 to ~85 Mev.

the total absorption cross section are found to differ from the observed magnitudes. A comparison of observed and calculated cross sections for carbon, together with the nuclear parameters used, is given in Table III. Since kR in this experiment is 3.9, the terms for which $L \geq 5$ do not contribute significantly to the cross sections. The method for calculating phase shifts is described in Appendix A. Since this is a charged-particle reaction, Coulomb wave functions should properly have been used. In carbon, however, the Coulomb parameter $\alpha = Ze^2/(\hbar\beta c) = Z/137\beta \simeq 0.05$ is small and hence affects the total wave function only very slightly. The statistical errors in the data for $\theta \geq 20°$ should therefore mask the Coulomb effect. In lead, $\alpha \cong 0.7$, indicating that correct calculations for this case must use the true Coulomb wave functions. Detailed calculations of this type are under way in this laboratory.[23]

TABLE III. Predictions of optical model for scattering of 125 Mev π^- mesons in carbon,[a] for a complex square well potential.

Curve number	Potential well[b] (assumed), Mev	Mean free path in nuclear matter[b] (assumed), cm	Total reaction σ(mb)[c] (calculated)
(1)	−36.6	4×10^{-13}	292
(2)	−30	3×10^{-13}	310
(3)	+32	3×10^{-13}	225
(4)	−21	9×10^{-13}	161
		observed experimentally:	308±43

[a] In these calculations, a nuclear radius of $1.4A^{\frac{1}{3}}\times10^{-13}$ cm has been assumed.
[b] A potential $V=\varphi-i\sigma$ Mev has been postulated. φ is the "potential well." This complex scattering potential leads to a complex propagation constant $k'=k+\frac{1}{2}iK$ within the nucleus. The "mean free path" is given by $(1/K)$.
[c] The angular distribution fits are best for curve (2).

In the selection of best fit parameter, the reaction cross section and angular distribution below 70° are given most weight. It is in this region that the model is expected to have more validity. Also, the presence of incoherent contributions may more seriously distort the diffraction pattern at large angles, where the differential cross section is small. We find carbon, at 125 Mev, to be represented by a real potential well, attractive and 30 Mev deep, and an imaginary well corresponding to a mean free path of 3×10^{-13} cm. Figure 3 and Table I give the data used here. The resulting parameters are consistent with the experimental results for lead. However, this is not a sensitive test of the model since the large size of the lead nucleus would lead to essentially geometric cross section for a large range of parameters.

The classical theory of the index of refraction relates the optical model parameters to the scattering properties of the constituent particles:

$$k'^2 = k^2 + 4\pi\rho f(0), \tag{1}$$

where $f(0)$ is the complex forward scattering amplitude in the elementary process and ρ is the density of scatterers. The availability of phase shifts as a function of energy in elementary pion-nucleon scattering[7,24] permits an examination of the relation of the optical parameters to the free scattering properties via the above equation. Table IV gives the result of computing $f(0)$ from the phase shift data at 80 and 155 Mev. Clearly, Eq. (1) does not allow for true absorption of the meson. The corresponding elementary process occurs in deuterium and has been observed as a function of energy.[25] Using the observed energy dependence of absorption in deuterium ($\sim p^2/v$) and the model for absorption in complex nuclei proposed by Brueckner, Serber, and Watson,[26] an estimate may be made for the mean free path for true absorption at 62 and 125 Mev. We get λ_a (62 Mev) $=8\times10^{-13}$ cm and λ_a (125 Mev) $=4.5\times10^{-13}$ cm. These values are similar in meaning to the quantities of Eq. (1) and may be added to the imaginary part in the form $R/2\lambda_a$. This has been done to obtain the calculated values given in Table IV.

It is characteristic of this model that the experimental mean free paths are much longer than those given by Eq. (1), whereas the real parts are in rough agreement. Recently, Watson[22] has examined the optical model quite generally. He finds that binding effects modify the scattering amplitude $f(0)$. These serve to reduce the imaginary part considerably. Any departure of ρ from a uniform distribution, as is possibly suggested by recent

[23] Pevsner, Williams, and Rainwater (private communication).
[24] Bodansky, Sachs, and Steinberger, Phys. Rev. **93**, 1367 (1954).
[25] Durbin, Loar, and Steinberger, Phys. Rev. **84**, 581 (1951).
[26] Brueckner, Serber, and Watson, Phys. Rev. **84**, 258 (1951).

experiments,[27] would also have a sensitive effect upon the nuclear mean free path.

The one difficulty which arises in the interpretation of the experimental data by means of the optical model is the poor fit obtained with the angular distribution beyond 70°. It has already been pointed out that the experimental points in the backward direction may be contaminated by slightly inelastic scatterings. Recent counter experiments,[28] with better energy resolution, still result in backward scattering considerably greater than that given by the model. The explanation of this effect may also be found in the strong angular dependence of the elementary nucleon scattering cross section. Although the elementary angular distribution is not expected to modify the optical model picture in a fundamental way, it may behave as a modulating form factor on the diffraction pattern. A Born approximation calculation of the scattering to be expected from a collection of nucleons has been performed, using the method described by Peaslee.[28] The result shows the expected rise in the backward direction, a reflection of the very strong backward scattering maxima observed in the elementary interaction. This data emphasizes the need for refinements in the theory of the optical model which will allow the inclusion of anisotropic elementary processes.

B. Inelastic Scattering

The energy and angular distributions of inelastically scattered mesons, presented in Figs. 5–7, appear as confirmation of earlier experiments by Bernardini *et al.*[1,2] which indicated two characteristic features of this process: strong angular dependence and large energy losses. An apparent peaking of the energy distributions of scattered mesons in carbon around 40 Mev is observed. However, the nature of the experimental arrangement is such as to favor just such distributions. The thickness of the scattering plates will certainly discriminate against the observation of very low-energy scattered mesons; the poor resolution at high energies tends to put particles suffering small energy loss into the "elastic" category. The experiment, therefore, is not to be taken as unambiguous confirmation of this effect.

Our experiment suggests that the "quasi-elastic scattering" model[29] may yield a qualitative explanation of features observed in the angular distributions. In this model, the scattering process is assumed to result from interaction solely between the incident meson and a single bound nucleon. The applicability of the model is not obvious in the present case, since the meson wavelength is 0.86×10^{-13} cm, or $\sim\frac{1}{4}$ of the nuclear radius. A many-body interaction, resulting in scattered mesons, is not to be ruled out from a priori considerations. The strong nucleon correlation inside the nucleus, found necessary to account for meson absorption, places particular emphasis on this possibility.

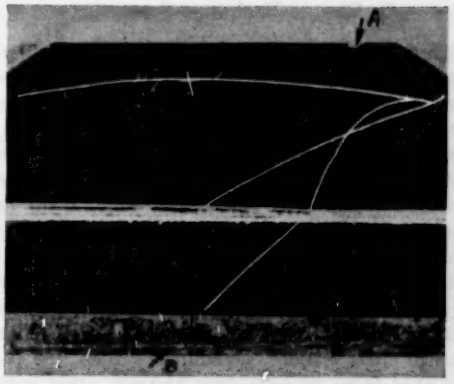

FIG. 8. Example of inelastic scattering in Pb. The incident meson A (130 ± 15 Mev) produces a single proton B and scatters through $\sim180°$ with an outgoing energy of <5 Mev. It stops in the gas, producing a sigma star of 2 protons and a recoil.

The angular distribution of mesons inelastically scattered in carbon (Fig. 3), when compared to the angular distribution for the process $\pi^+ + p \rightarrow \pi^+ + p$,[7] nevertheless strongly suggests the use of the single-scattering picture. Additional evidence favoring this hypothesis is the energy dependence of the interaction. At 40 Mev, no inelastic scatterings have been observed.[2] At 60 Mev, $\sigma_{\text{inel}} \geq 40$ mb,[13] and at 125 Mev, $\sigma_{\text{inel}} \geq 72$ mb.

The data are insufficient statistically to establish a correlation between angle of scattering and energy loss. The pronounced preference for very large angle scattering in the elementary interaction would result in a reduced mean energy for the scattered particles. In a more detailed model internal nucleon motion or potential well effects could possibly decrease further the mean scattered energy.

The angular distribution in lead (Fig. 6) is smoother than that in carbon, an indication that in this larger nucleus multiple scattering effects are beginning to play a significant part. It is to be noted here also that the angular distribution statistics are somewhat biased experimentally against angles in the interval from 60° to 120°, and that hence some artificial depression of the differential cross section may occur in that region.[30]

TABLE IV. Calculated and observed nuclear parameters.

E (Mev)	V_{obs} (Mev)	V_{calc} (Mev)	λ_{obs} (Mev)	λ_{calc} (Mev)
62	20	28	8×10^{-13}	3×10^{-13}
125	30	30	3×10^{-13}	1.2×10^{-13}

[27] V. L. Fitch and J. Rainwater, Phys. Rev. **92**, 789 (1953); Hofstadter, Fechter, and McIntyre, Phys. Rev. **91**, 439 (1953).
[28] D. C. Peaslee, Phys. Rev. **87**, 862 (1952).
[29] R. Serber, Phys. Rev. **72**, 1114 (1947); P. A. Wolff, Phys. Rev. **87**, 434 (1952).
[30] The angular distribution of inelastically scattered high-energy negative pions in nuclear emulsions, where no discrimination against this angular region occurs, agrees well with the results of the present paper. S. Goldhaber and G. Goldhaber (private communication).

C. Charge-Exchange Scattering

High-energy photons, arising from the interaction of energetic pions with nuclei have heretofore[21] not been observed. It is not possible, with the data at hand, unambiguously to specify the production mechanism for these photons. Experience with the elementary pion-nucleon interaction, however, indicates that charge-exchange scattering, $\pi^-+p\rightarrow n+(\pi^0\rightarrow 2\gamma)$, is the most probable mechanism. This view is strengthened by a detailed balancing calculation which shows that the cross section for the only possible competing process $\pi^-+p\rightarrow n+\gamma$ has, in the case of the nucleon interaction, a magnitude of only 2 percent that of the charge-exchange cross section.[7] Discounting, then, the possibility that these photons arise through other mechanisms, one may consider the charge-exchange reaction to have been established under the conditions obtaining in this experiment.

The magnitude of the observed effect, although considerably smaller than that for the comparable case of inelastic scattering, may be understood in the light of a simple assumption. Under the hypothesis that, in the first approximation, the charge-exchange and inelastic scattering cross sections for the present high bombarding energies are affected by nuclear structure in entirely similar ways, one may obtain an estimate of their relative size through use of the known[7,24] elementary cross sections. The ratio, R, obtained for the present case, is

$$R=\frac{\sigma_{\text{ch.ex.}}A(z)}{\sigma_{\text{inel.}}A(z)}=\frac{Z\sigma(\pi^-+p\rightarrow\pi^0+n)}{Z\sigma(\pi^-+p\rightarrow\pi^-+p)+N\sigma(\pi^++p\rightarrow\pi^++p)},$$

where it has been assumed that $\sigma(\pi^++p\rightarrow\pi^++p)=\sigma(\pi^-+n\rightarrow\pi^-+n)$. The calculated R, then, is 0.3 for carbon and 0.2 for lead. The experimental ratios observed were $R_C\cong 0.26$, and $R_{Pb}\cong 0.20$.

Two qualitative points may be made as to the modification of R by binding effects. The interference between neutron and proton scattering for pions incident on deuterium has been calculated by Brueckner.[22] He finds destructive (Pauli) interference for charge exchange, constructive for ordinary scattering. To the extent that such a process takes place in carbon, it may serve to reduce the calculated R.

The Pauli principle, in addition, acts to suppress the forward part of the free scattering form factor, since forward scattering implies only small momentum transfer to the struck nucleon. The ratios of backward to forward scattering in elementary collisions have been observed by the Chicago group.[7] They find, at 135 Mev,

$$r(\pi^-\rightarrow\pi^0)=2.3,\quad r(\pi^-\rightarrow\pi^-)=1.0,\quad r(\pi^+\rightarrow\pi^+)=3.9.$$

The Pauli principle, therefore, acts in this case to suppress a larger fraction of the total charge exchange than of the inelastic scattering.

It is of interest to compare these results with other workers. Lock and Yekutieli[9] deduce a large charge-exchange cross section (~30 percent geometric) for high-energy mesons (<160 Mev) in nuclear emulsion. Since the elementary cross section increases with energy up to 220 Mev, this may still be consistent with our results. Shutt[12] and co-workers obtain a charge-exchange cross section of 60 mb for 105-Mev pions in helium. This would indicate a very strong effect due to nuclear structure. Tinlot and Roberts at 40 Mev, observe a very small π^0 yield from carbon, ~ few millibarns. Schein[10] has observed high-energy electron pairs emerging from π^--induced stars in nuclear emulsion. The observed frequency (1 per 500 stars) is consistent with our results (5 percent geometric or 10 percent of star production) and the fact that one out of 80 π^0's will decay into a photon and an electron pair.[17]

We would like to express our thanks to Mr. Hugh Byfield for his contributions in the planning and execution of this experiment, and in the construction of the apparatus. We wish to acknowledge many discussions with Professor Serber, Professor Rainwater, and Professor Steinberger, concerning the various aspects of this experiment. Mr. Kenneth Rogers assisted greatly in the scanning and calculations.

One of us (JOK) would like to express appreciation to the Radio Corporation of America's Laboratories, for their support in the final phases of the research. The main body of the research was supported by the joint program of the U. S. Office of Naval Research and the U. S. Atomic Energy Commission.

APPENDIX

A. Calculation of Complex Square Well Scattering Amplitudes

The significance of complex potentials has been given by Bethe.[23] If $V=\phi+i\sigma$, the continuity equation becomes

$$\frac{\partial}{\partial t}|\psi|^2-\nabla\cdot\mathbf{S}-2\frac{|\psi|^2}{\hbar}\sigma=0,$$

where ψ is the wave function, and $\mathbf{S}$ is the usual probability current density. A potential representing attraction and absorption may, therefore, be represented by

$$V=-|\phi|-i|\sigma|.$$

Assuming that V transforms with the total energy, E, the relativistic equation determining the meson wave

[21] Recent results of Tinlot, Roberts, and Spry (private communication), indicate a cross section for charge exchange of 3–5 mb for 40-Mev negative pions, incident on Li, Be, and C.

[22] K. A. Brueckner (to be published).

[23] H. A. Bethe, Phys. Rev. 57, 1125 (1940).

propagation vector $\mathbf{k}'$, in the field of a nucleus is

$$c^2\hbar^2k'^2=E^2+V^2-m^2c^4-2EV.$$

If $E\gg V$,

$$c^2\hbar^2k'^2\cong c^2\hbar^2k_0^2-2EV,$$

where

$$k_0^2=(E^2-m^2c^4)/c^2\hbar^2.$$

With these assumptions one obtains

$$k'=\left[\left(k_0^2+\frac{2E\phi}{\hbar^2c^2}\right)^2+\left(\frac{2\sigma E}{\hbar^2c^2}\right)^2\right]^{\frac{1}{4}}\cdot\exp\left[\frac{i}{2}\tan^{-1}\left(\frac{2\sigma E}{\hbar^2c^2k_0^2+2\phi E}\right)\right].$$

One may then write a quasi-relativistic Schrödinger equation

$$\nabla^2\psi+k^2\psi=0,$$

where $k=k'$, $r<R$, and $k=k_0$, $r>R$, R being the radius of the potential well.

The scattering amplitude for a partial wave solution of the Schrödinger equation is

$$f(\theta)=\frac{1}{2ik_0}\sum_l(2l+1)[\eta_l-1]P_l(\cos\theta),$$

where η_l is determined from matching the inside and outside radial wave functions at the nuclear boundary. The radial wave may be written[34]

$$B_l^{(0)}(r)=A_l[\cos\delta_l j_l(k_0r)-\sin\delta_l n_l(k_0r)],\quad r\gtrsim R,$$
$$B_l^{(i)}(r)=C_l[j_l(k'r)],\quad r\lesssim R.$$

Defining $\eta_l=\exp(2i\delta_l)$, one may rewrite the first equation,

$$B_l^{(0)}(r)=D_l[h_l^{(2)}(k_0r)+\eta_l h_l^{(1)}(k_0r)],$$

where j_l, n_l, and $h_l^{(1),(2)}=j_l\pm in_l$, are spherical Bessel functions. Equating the logarithmic derivatives of $B^{(i)}$ and $B^{(0)}$ at R, and solving for η_l, one obtains

$$\eta_l=\frac{k_0[h_l^{(2)}(k_0R)]'j_l(k'R)-k'h_l^{(2)}(k_0R)[j_l(k'R)]'}{k'h_l^{(1)}(k_0R)[j_l(k'R)]'-k_0[h_l^{(1)}(k_0R)]'j_l(k'R)}.$$

Primed brackets denote differentiation with respect to the argument of the Bessel function. As k' is complex, calculation by means of this formula is quite involved. Considerable simplification is achieved through use of a recursion relation for complex half-order Bessel functions which has been given by Aden.[35] It may be shown that if one defines $\sigma_l(x)\equiv d/dx\log[xj_l(x)]$, that

$$x\sigma_l(x)=\frac{x^2+l[x\sigma_{l-1}(x)]-l^2}{l-x\sigma_{l-1}(x)},$$

where $x=a+ib$ and

$$\sigma_0(x)=[\sin2a-i\sinh2b][\cosh2b-\cos2a]^{-1}.$$

The expression for η_l may now be modified to permit use of the recursion relation:

$$-\eta_l=\frac{k_0R[h_l^{(2)}(k_0R)]'+h_l^{(2)}(k_0R)[1-k'R\sigma_l(k'R)]}{k_0R[h_l^{(1)}(k_0R)]'+h_l^{(1)}(k_0R)[1-k'R\sigma_l(k'R)]}.$$

In the actual calculation, tables[36] dictating a final revision of the form of the equation were used. In this final form, the calculation of a set of five η's for a given meson energy and set of nuclear parameters became a relatively minor undertaking. This form was

$$-\eta_l=\frac{\tan\delta_l(\tan\alpha_l-z_l)-i(z_l-\tan\beta_l)}{\tan\delta_l(\tan\alpha_l-z_l)+i(z_l-\tan\beta_l)},$$

where

$$\tan\alpha_l(x)=-xj_l'(x)[j_l(x)]^{-1},$$
$$\tan\beta_l(x)=-x[\eta_l(x)]'[\eta_l(x)]^{-1},$$
$$\tan\delta_l(x)=-j_l(x)[\eta_l(x)]^{-1},$$
$$z_l(kR)=1-kR\sigma_l(kR),$$
$$x=k_0R.$$

The first three of these quantities are tabulated, and the last may easily be calculated by means of the recursion relation.

B. Efficiency for Photon Conversion

Photons arising in the carbon may materialize in the carbon plate itself, or in one of the two lead plates. Photons originating in one of the lead plates may convert in it, in the other lead plate, or in carbon. It is necessary to account for all these possibilities in the derivation of the photon observation efficiency.

The calculation of these probabilities combines the solid angle efficiency factor and the elementary conversion probability. In general, it involves numerical integration and/or the averaging of efficiencies over representative photon production and materialization points.

The element of solid angle, $d\omega$ subtended at the origin by an element of area, $dxdz$, at (x,z), in a plane $y=y_0$, is given by

$$d\omega=y_0\frac{dxdy}{(x^2+y_0^2+z^2)^{\frac{3}{2}}}.$$

Defining $\theta_i=\tan^{-1}(x_i/y_0)$, one may write the total solid angle included between θ_1, θ_2 and the heights z_1 and

[34] L. I. Schiff, *Quantum Mechanics* (McGraw-Hill Book Company, Inc., New York, 1949), Chap. V.

[35] A. L. Aden, J. Appl. Phys. **22**, 601 (1951). A more general recursion relation, from which the one used in this paper was derived, is given by L. Infeld, Quart. Appl. Math. **5**, 113 (1947).

[36] *Scattering and Radiation from Circular Cylinders and Spheres* (U. S. Navy Department of Research and Inventions, July, 1946).

z_2, in the plane $y=y_0$, as

$$\Omega(\theta_1,\theta_2)=\sum_{i=1}^{2}\sum_{j=1}^{2}(-1)^{i+j}\tan^{-1}\left[\frac{x_i z_j}{y_0}(y_0^2+x_i^2+z_j^2)^{-\frac{1}{2}}\right].$$

The conversion efficiency, for cases in which a photon emerges from one of the scattering plates and converts in another, was calculated in the following way: a point of origin for the photon was chosen. The plate of destination was divided into intervals (θ_1,θ_2), the average conversion efficiency for each interval being determined from the appropriate transition curve. The solid angle and conversion efficiencies were then multiplied for each interval, and the products summed over the whole conversion plate. The calculation was repeated over a number of representative points (twelve for carbon) in the plate in question, the mean of these efficiencies then giving the final result.

The efficiencies for conversion directly in the plate of origin of the photons similarly were calculated, taking into account the available height of the illuminated region, as well as the relative magnitudes of the solid angle and conversion path. All efficiencies have been calculated under the assumption of isotropic photon angular distribution.

The transition curves needed in this experiment must give the probability, as function of converter thickness, of ~100 Mev γ-ray materialization, each resulting pair member having an energy $\geqslant 10$ Mev. To minimize secondary effects, it is required that the electrons have charge of opposite sign.

Professor R. R. Wilson has very kindly permitted us to use the data from his Monte Carlo calculations to obtain the desired transition curve. The efficiency in lead, as derived from 142 individual shower graphs,[17] rises steeply from zero to ~30 percent in the interval from zero to 1 radiation length. A relatively slow fall-off occurs beyond this thickness, the efficiency at 2 radiation lengths being ~18 percent.

The conversion efficiency for carbon was calculated under the assumption that for the thickness in question pairs once produced do not reradiate. The average ionization energy loss of pair electrons was taken into account.

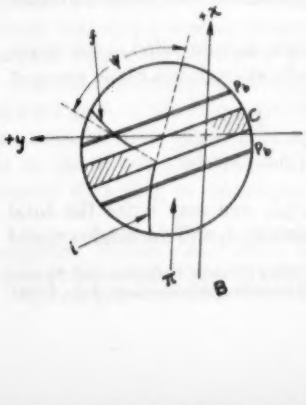

FIG. 9. Coordinate system for deriving projection formulas. $\pi\rightarrow$ indicates direction of incident beam, i—incident pion, f—scattered pion, ψ—projected scattering angle, Pb—lead plates, C—carbon plate.

If W_γ is the energy of the initial photons, ϵ the ionization loss of minimum ionizing electrons/cm of carbon, t the thickness at which the pair is produced, D the total thickness (in cm) of the carbon, λ_p the mean free path for pair production,[37] E the initial energy of the positron, and A a factor near unity, due to the pair production spectrum, then the efficiency is given by η, where

$$\eta=\frac{A}{W_\gamma}\int_0^D dt\frac{e^{-t/\lambda_p}}{\lambda_p}\int_{(D-t)\epsilon+10}^{W_\gamma-[(D-t)\epsilon+10]}dE.$$

In the region of carbon thickness of interest, and for $W_\gamma=100$ Mev, the result of the integration may be expressed by the simple formula $\eta=(1.1D+1.74)$ percent.

The per photon conversion efficiencies are:

Pb_1 or $Pb_2\rightarrow$C 1 percent (each plate),

$Pb_1\rightarrow Pb_2$ or $Pb_1\rightarrow Pb_2$ } 3.4 percent (both plates together),

$Pb_1\rightarrow Pb_1$, $Pb_2\rightarrow Pb_2$ } 12.9 percent (each plate),

C$\rightarrow$C 0.6 percent,

C$\rightarrow$(Pb_1 or Pb_2) 7.6 percent (both plates).

The element to the left of the arrow indicates the plate of origin of the photon, the element to the right, the plate of conversion. Because of the method of calculation, and the 20 percent statistical uncertainty in the lead transition curve, a possible error of ~30 percent must be allowed for in these efficiencies.

C. Measurement of Space Angles

1. Stereo Height Determination

Any point T, within the cloud chamber, is projected onto the scanning screen from two film images, through two lenses, L and Λ. The film images of a top glass fiduciary mark F are projected similarly. It is desired to measure the distance s between the planes containing F and T, respectively. If the distance between the projections of F is δ_x, and that between the projections of T is δ_0, then the value of s is determined by $\Delta=\delta_x-\delta_0$. In practice δ_x is made to vanish by suitable translations and rotations of one film relative to the other. When this is done, one measurement suffices to determine s.

Consideration of the geometry easily shows that the stereo depth calibration equation is

$$s=\frac{p\Delta}{(2lf/p)-\Delta},$$

[37] λ_p for carbon has been obtained by extrapolating the data of J. L. Lawson, Phys. Rev. 75, 433 (1949).

where $2l$ is the distance between lenses, p the distance between top glass and lens plane, and f the distance between scanning screen and lens plane.

2. *Projection Formulas*

It is necessary to account for the fact that pictures are not recorded from infinity. In many cases, depending on the location and type of the event in question, the nonorthogonality of the projection does not permit the use of standard orthogonal projection formulas. Accordingly, the relative location in the cloud chamber of all such events has been measured, and used to arrive at the correct scattering geometry.

The information needed to calculate correctly the space and dip angles of any scattered track consists of the projected angle relative to the incident track, a projected length on the scattered track, the relative heights in the cloud chamber of the ends of this length, and the position of this segment relative to the vertical projection of the recording lens onto the screen. Figure 9 shows the coordinate system used in the derivation of the formulas. The origin is located at the foot of the perpendicular from screen to lens; the x axis is chosen along the direction of the incident track, marked i. The final track, marked f, makes a projected angle ψ with the incident direction. The z direction is upward, out of the paper. Let: D_T = true length of scattered track segment, D_0 = projected length of scattered track segment, $(0,0,h)$ = projecting point (camera lens), ψ = projected scattering angle, Θ = true scattering angle, δ = true dip angle, (x_i, y_i, z_i) the space coordinates of the scattered track segment, and (x_i^0, y_i^0), $(i=1, 2)$ = the coordinated defining the projection onto the screen of the scattered track segment. Let $(x_1^h, y_1^h, z_1^h) = (0,0,h)$. Then the projection of the track onto the screen gives

$$x_1^0 = x_1 h/(h-z_1), \quad y_1^0 = y_1 h/(h-z_1)$$

$$x_1 - x_2 = x_1^0 - x_2^0 - (1/h)(z_1 x_1^0 - z_2 x_2^0)$$

$$\Delta x = \Delta x^0(1-z_2/h) - (x_1^0/h)\Delta z. \text{ (Similarly for } \Delta y.)$$

Then

$$D_T^2 = (\Delta x)^2 + (\Delta y)^2 + (\Delta z)^2$$
$$= D_0^2(1-z_2/h)^2 + (\Delta z)^2[1 + (x_1^{02} + y_1^{02})/h^2 - 2(D_0 \Delta z/h)(1-z_2/h)(x_1^0 \cos\psi + y_1^0 \sin\psi)],$$

where $D_0^2 = (\Delta x^0)^2 + (\Delta y^0)^2$. Then $\delta = \sin^{-1}(\Delta z/D_T)$ and

$$\Theta = \cos^{-1}\left[\frac{D_0}{D_T}\cos\psi\left(1-\frac{z_2}{h}\right) - \frac{x_1^0}{h}\cdot\frac{\Delta z}{D_T}\right].$$

Appropriate simplifications may be made depending on the magnitude of the parameters.

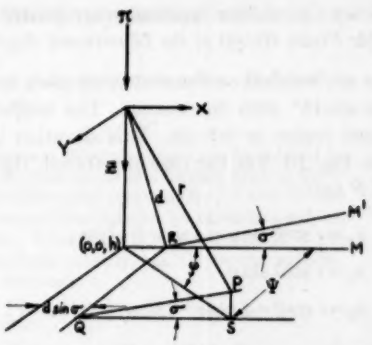

FIG. 10. Construction for calculation of number of scatterings missed due to the finite height of the illuminated region. The origin is situated at the scattering point of the incident meson. The z axis is directed along the initial horizontal flight direction, the y axis points vertically upward. The x axis is horizontal and perpendicular to both. Plane M', determined by PQR, represents the far boundary of the scattering plate. The scattering occurs at a distance d above it. Plane M is normal to the incident flight direction, and a distance $z=h$ below the scattering point. OP represents the scattered meson, and has polar angles θ, φ. P is the intersection of the rear bounding plane of the scattering plate and the scattered track.

D. Detection Efficiency for Elastic Scatterings

1. *Efficiency Calculation for 15° Projected Angle Cutoff*

During scanning, only scatterings with projected angles $\psi \geq 15°$ are recorded. This means that, in cases where the azimuth angle φ is near 0° or 180°, scatterings with space angles θ appreciably greater than 15° may be lost from observation.

To calculate the efficiency of observing an elastic scattering into θ, one must first obtain $\varphi = \varphi(\psi)_{\theta \text{ const.}}$ The efficiency of observation then becomes, in any given azimuthal quadrant,

$$E(\theta) = 1 - \frac{2}{\pi}[\varphi_\theta(\psi=15°) - \varphi_\theta(\psi=0°)].$$

Let λ be the angle between the vertical direction and a ray drawn from the observing camera lens to a point determined by the intersection of the vertical plane containing both lenses, and the scattered track. It may easily be shown that, for cases where θ is less than $\sim 70°$ (at larger θ, other corrections predominate), one has

$$\varphi(\psi) = \sin^{-1}(\tan\psi \cot\theta \cos\lambda) + \delta.$$

Averaging over-all scattering positions in the cloud chamber, and over both camera positions, one finds that for the present geometry the effect of $\cos\lambda$ in the bracket is quite negligible. The over-all efficiency, to a very good approximation, is equal to that obtaining in the case of one projection point (camera) at an infinite height above the chamber. It is given by

$$E(\theta) = 1 - \frac{2}{\pi}\sin^{-1}(\tan 15° \cot\theta).$$

2. Efficiency Calculation for Scatterings Missed because of the Finite Height of the Illuminated Region

Tracks are incident on the scattering plate system at an angle $\sigma \simeq 15°$ with the normal. The height of the illuminated region is $\simeq 8$ cm. This situation is represented in Fig. 10. For the case illustrated, the coordinates of P are

$$x_p = r \sin\theta \sin\varphi = d \sin\sigma + l \cos\sigma,$$

$$y_p = r \sin\theta \sin\varphi,$$

$$z_p = r \cos\theta = d \cos\sigma - l \sin\sigma, \quad [\langle QP \rangle_{\text{Av}} = l].$$

In the drawing, $y_p = Y$, which indicates that P is at the boundary of the illumination.

The efficiency for observing a scattering through an angle θ, taking place at a depth of d centimeters into the scattering plate, is

$$E(\theta) = \frac{1}{2\pi}[\varphi(Y,d)_+ + \varphi(Y,d)_- + \varphi(8-Y,d)_+ + \varphi(8-Y,d)_-],$$

where the subscripts refer to the two cases $\cos\varphi = \pm|\cos\varphi|$.

Solving the above coordinate equations, for the case $y_p = Y$, one obtains

$$\cos\varphi = \sin\varphi \left[\frac{\sin\sigma \tan\sigma + \cos\sigma}{\tan\sigma}\right]\frac{d}{Y} - \frac{\cot\theta}{\tan\sigma},$$

from which the explicit expression for $\varphi(Y,d)$ is easily derived. This is then inserted into $E(\theta)$. To obtain the desired efficiency, numerical averaging over representative (Y,d) is carried out.

As may be expected $E(\theta) \simeq 1$ for θ small. It is a minimum for $\theta = 75°$, and rises slowly for $75° < \theta \leqslant 90°$. In the latter case the track emerges through the front of the scattering plate. $E(\theta)$ is symmetric about $\theta = 90°$.

No correction need be applied to account for tracks passing out of the cloud chamber before emerging from the scattering plate (within the illuminated height). Owing to the track entrance criterion, and the small height of the illumination together with the narrowness of the scattering plate relative to the cloud-chamber width, the magnitude of this correction is negligible.

Green's Functions in Quantum Electrodynamics*

JAMES L. ANDERSON
Rutgers University, New Brunswick, New Jersey, and University of Maryland, College Park, Maryland†

(Received November 25, 1953)

Dyson has shown that the evaluation of the S matrix for quantum electrodynamics can be reduced to the problem of evaluating certain quantities, S'^F, D'^F, and Γ_μ. By making use of a formula relating the T product of an operator with its corresponding N product, integro-differential equations for S'^F and D'^F are obtained. These equations are identical in form with those given by Schwinger for his Green's functions, and hence it is concluded that the two formalisms are equivalent. In addition it is shown that all of the quantities introduced by Schwinger can be expressed in terms of a single quantity, S_{vac}, the vacuum expectation value of the S matrix. The renormalization problem is not discussed.

I. INTRODUCTION AND REVIEW

IN a recent work,[1] Schwinger has proposed a theory of Green's functions which appears to be applicable to many of the problems of quantum electrodynamics and similar theories. However, since his theory is based on his own formalism of quantized fields,[2] it is not immediately evident which connection exists between his results and those of conventional field theories.[3] It is with this relationship that the present paper will deal. Specifically we will show how the results of Schwinger's theory can be derived from Dyson's theory[3] of the S matrix.[4] It is hoped that such a demonstration will serve two purposes; first, to make Schwinger's results readily available in terms of an already familiar formalism, and second, to afford a set of rules whereby one may calculate directly from S-matrix theory the various Green's functions introduced by Schwinger.

In the work to follow, we shall make use of many of the results of S-matrix theory, and hence, for the sake of convenience, we will conclude this section by enumerating them. In the interaction representation, the state vector $\Psi[\sigma]$ of the system, consisting of electromagnetic and electron-positron fields in interaction, satisfies the equation

$$i\frac{\delta\Psi[\sigma]}{\delta\sigma(x)}=\mathfrak{H}(x)\Psi[\sigma],$$

where $\mathfrak{H}(x)$ is the interaction Hamiltonian density, given by[5]

$$\mathfrak{H}(x)=-A_\mu(x)\{j_\mu(x)+J_\mu(x)\}.$$

Here $j_\mu(x)$ is the field current, which for convenience we write as

$$j_\mu(x)=\tfrac{1}{2}ec\gamma_{\alpha\beta}{}^\mu[\bar{\psi}_\alpha(x)\psi_\beta(x)-\psi_\beta(x)\bar{\psi}_\alpha(x)],$$

whereas $J_\mu(x)$ is some arbitrarily given external current.[6]

In what follows, we will be mainly interested in that operator S, the "so-called" S matrix, which transforms a state of the system at $t=-\infty$, into the corresponding state at $t=+\infty$. Feynman[7] has shown that S can be written in the form

$$S=T\left[\exp\left\{-i\int_{-\infty}^{+\infty}dt\int d^3x\mathfrak{H}(x)\right\}\right]=T[\mathfrak{S}]. \quad (1)$$

The T product appearing in Eq. (1) and first introduced by Wick[8] is defined by

$$T(UV\cdots Z)=\delta_P XY\cdots W, \quad (2)$$

the factors U, V, $\cdots$ being arranged in chronological order in the ordinary product on the right. By chronological order, we mean that if two operators in the T product of Eq. (2) correspond to points separated by either a time-like or a zero interval, then in the ordinary product, that operator operates first which corresponds to the earlier time. The sign factor δ_P is the signature ±1 of the permutation [between left-hand side and right-hand side of Eq. (2) of the electron-positron operators only].

II. THE ORDERING OPERATORS

Several methods[3,7,8] have been given for actually evaluating the matrix elements of a T product such as appear in Eq. (2). All of these methods essentially involve the transformation of the T product into an N product, where the N product is defined by

$$N(UV\cdots Z)=\delta_P XY\cdots W,$$

the ordinary product on the right containing the same factors U, V, $\cdots$ ordered in such a manner that all creation operators stand to the left of all destruction operators. In this form, the matrix elements of any

* Supported in part by the U. S. Office of Naval Research.

† A portion of this paper was written while the author was at Rutgers University and the rest at the University of Maryland, which is the author's present address.

[1] J. Schwinger, Proc. Natl. Acad. Sci. **37**, 452 (1951).

[2] J. Schwinger, Phys. Rev. **82**, 914 (1951).

[3] For an excellent summary and bibliography, see F. J. Dyson, Phys. Rev. **75**, 486 and 1736 (1949).

[4] For an alternate treatment see Utiyama, Sunakawa, and Imamura, Progr. Theoret. Phys. (Japan) **8**, 77 (1952).

[5] Throughout this paper we shall employ Schwinger's notation and use units where $\hbar=1$, $c=1$.

[6] The interaction Hamiltonian employed here differs from that employed by Schwinger in that we dispense with the external spinor fields $\eta(x)$ and $\eta'(x)$. Since these quantities were introduced by Schwinger as a mathematical convenience and are eventually set equal to zero, the results obtained here will be equivalent to those obtained by Schwinger.

[7] R. P. Feynman, Phys. Rev. **84**, 108 (1951).

[8] G. C. Wick, Phys. Rev. **80**, 268 (1950).

T product can be readily calculated. In this section we will derive the fundamental expression (21), giving the relation between an arbitrary T product of electromagnetic and electron-positron field operators and its corresponding N product.

We shall treat first the case of a T product which is a functional only of the electromagnetic field operator $A_\mu(x)$. In order to introduce creation and destruction operators into the theory, we decompose $A_\mu(x)$ into two parts according to[9]

$$A_\mu(x)=A_\mu^+(x)+A_\mu^-(x),$$

where $A_\mu^+(x)$ contains only photon destruction operators, while $A_\mu^-(x)$ contains only photon creation operators. These auxiliary fields satisfy the following commutation relations

$$\begin{aligned}&[A_\mu^+(x),A_\nu(x')]=i\delta_{\mu\nu}[D_A^+(x-x')-D_R^+(x-x')],\\&[A_\mu^-(x),A_\nu(x')]=i\delta_{\mu\nu}[D_A^-(x-x')-D_R^-(x-x')],\\&[A_\mu^+(x),A_\nu^+(x')]=[A_\mu^-(x),A_\nu^-(x')]=0,\end{aligned}\tag{3}$$

where the only property of the D functions which we shall need is that

$$\begin{aligned}&D_R^\pm(x)=0, \quad \text{for} \quad x<0,\\&D_A^\pm(x)=0, \quad \text{for} \quad x>0,\end{aligned}\tag{4}$$

and

$$D^F(x)\equiv -i\{D_A^-(x)+D_R^+(x)\}\tag{5}$$

satisfies

$$\Box D^F(x)=i\delta(x).\tag{6}$$

With the help of Eqs. (3–6), we shall now prove the following statement: the N product corresponding to a given T product can be obtained by substituting for every field operator $A_\mu(x)$ the quantity $A_\mu'(x)$ given by[10]

$$A_\mu'(x)=A_\mu(x)+\int d^4x' D_F(x-x')\frac{\delta}{\delta A_\mu(x')}\tag{7}$$

in the T product, considered now as an ordinary c-number functional of the $A_\mu(x)$, and performing the indicated differentiations. The resulting expression is then to be considered as an N product, which, in fact, is equivalent to the original T product. The statement is of course trivially true when the T product to be reordered is just $A_\mu(x)$ itself. To prove it for the more general case, let us proceed by assuming that it is true for some T product, $T[\mathfrak{F}(A_\mu)]$, i.e., that

$$T[\mathfrak{F}(A_\mu)]=N[\mathfrak{F}(A_\mu')].\tag{8}$$

Then, if we can prove it for $T[A_\lambda(x)\mathfrak{F}(A_\nu)]$, we can conclude, by induction, that the above-mentioned statement is indeed valid. This last assertion follows from the fact that every operator functional can be expressed as a functional power series in the $A_\mu(x)$. To proceed with the proof, let us assume that the value of x_0 lies somewhere between the times to which the operators in $\mathfrak{F}(A)$ correspond. We express this by the equation

$$T[A_\mu(x)\mathfrak{F}(A)]=X(A)A_\mu(x)Y(A),$$

or equivalently, by

$$T[A_\mu(x)\mathfrak{F}(A)]=X\{A_\mu^-(x)+A_\mu^+(x)\}Y(A),\tag{9}$$

where

$$X(A)Y(A)=\mathfrak{F}(A).$$

In order to convert Eq. (9) into an N product we must commute $A_\mu^-(x)$ through X and $A_\mu^+(x)$ through Y. This can be done by making use of the commutation relations (3) and yields

$$\begin{aligned}T[A_\mu(x)\mathfrak{F}(A)]=&A_\mu^-(x)XY\\&+\left\{-i\int d^4x' D_A^-(x-x')\frac{\delta}{\delta A_\mu^+(x}X\right\}Y+XYA_\mu^+(x)\\&+X\left\{-i\int d^4x D_R^+(x-x')\frac{\delta}{\delta A_\mu^-(x')}Y\right\}.\end{aligned}$$

However, because of the nature of $D_A^-(x)$ and $D_R^+(x)$ and because all times in Y precede x_0 which in turn precedes all times in X, we can rewrite this equation as

$$\begin{aligned}T[A_\mu(x)F(A)]=&A_\mu^-(x)XY+XYA_\mu^+(x)\\&+\left\{-i\int d^4x' D_A^-(x-x')\frac{\delta}{\delta A_\mu^+(x')}\right.\\&\left.-i\int d^4x' D_R^+(x-x')\frac{\delta}{\delta A_\mu^-(x')}\right\}XY.\end{aligned}\tag{10}$$

When we substitute from Eq. (8) into Eq. (10) we obtain

$$\begin{aligned}T[A_\mu(x)\mathfrak{F}(A)]=&A_\mu^-(x)N[\mathfrak{F}(A')]+N[\mathfrak{F}(A')]A_\mu^+(x)\\&+\left\{-i\int d^4x' D_A^-(x-x')\frac{\delta}{\delta A_\mu^+(x'}\right.\\&\left.-i\int d^4x' D_R^+(x-x')\frac{\delta}{\delta A_\mu^-(x')}\right\}N[\mathfrak{F}(A')].\end{aligned}\tag{11}$$

Since now the quantities $A_\mu^-(x)$ and $A_\mu^+(x)$ appear in $\mathfrak{F}(A)$ only in the combination $A_\mu^+(x)+A_\mu^-(x)$, we

[9] For a detailed discussion of this method of decomposition, see J. Schwinger, Phys. Rev. 75, 651 (1949).

[10] The functional derivatives $\delta/\delta A_\mu(x)$ are defined through the equation

$$\begin{aligned}\delta\mathfrak{F}(A_\mu(x))&=\mathfrak{F}(A_\mu(x)+\delta A_\mu(x))-\mathfrak{F}(A_\mu(x))\\&=\int\frac{\delta\mathfrak{F}}{\delta A_\mu(x)}\delta A_\mu(x)d^4x.\end{aligned}$$

strictly speaking, this definition is meaningless since the quantities appearing therein are operators which do not commute with each other. We give meaning to the equation by assuming that the $\delta A_\mu(x)$ are c numbers. When so defined, the functional derivatives have the property that

$$\left[\frac{\delta}{\delta A_\mu(x)},\frac{\delta}{\delta A_\nu(x')}\right]=0.$$

note that

$$\frac{\delta}{\delta A_\mu^-(x)}N[\mathfrak{F}(A')]=N\left[\frac{\delta\mathfrak{F}(A')}{\delta A_\mu(x)}\right],$$

and

$$\frac{\delta}{\delta A_\mu^+(x)}N[\mathfrak{F}(A')]=N\left[\frac{\delta\mathfrak{F}(A')}{\delta A_\mu(x)}\right].$$

Therefore, Eq. (11) becomes

$$T[A_\mu(x)\mathfrak{F}(A)]=N[\{A_\mu^+(x)+A_\mu^-(x)\}\mathfrak{F}(A')]$$
$$-i\int d^4x'[D_R^+(x-x')+D_A^-(x-x')]N\left[\frac{\delta\mathfrak{F}(A')}{\delta A_\mu(x')}\right].$$

Finally, remembering the definition of $D^F(x)$, we have

$$T[A_\mu(x)\mathfrak{F}(A)]$$
$$=N\left[\left\{A_\mu(x)+\int d^4x'D^F(x-x')\frac{\delta}{\delta A_\mu(x')}\right\}\mathfrak{F}(A')\right]$$
$$=N[A_\mu'(x)\mathfrak{F}(A')],$$

which was to be proved.

We can reformulate this result by noting that Eq. (7) can be rewritten in the form

$$A_\mu'(x)=e^\Delta A_\mu(x)e^{-\Delta},$$

where

$$\Delta=\frac{1}{2}\int d^4xd^4x'\delta_{\mu\nu}D^F(x-x')\frac{\delta}{\delta A_\mu(x)}\frac{\delta}{\delta A_\nu(x')}, \quad (12)$$

as can readily be verified by direct calculation. Therefore, if

$$T[\mathfrak{F}(A)]=N[\mathfrak{F}(A')],$$

then it is also true that

$$T[\mathfrak{F}(A)]=N[e^\Delta\mathfrak{F}(A)e^{-\Delta}].$$

In particular, if we are interested only in the matrix elements of $T[\mathfrak{F}(A)]$ we can disregard the factor $e^{-\Delta}$, since there is nothing for it to operate on, and write finally

$$\langle T[\mathfrak{F}(A)]\rangle=\langle N[e^\Delta\mathfrak{F}(A)]\rangle. \quad (13)$$

In what follows, we shall refer to Δ as the photon ordering operator.

We can also derive an expression for an electron-positron ordering operator. In order to do so we must decompose the electron-positron operator according to

$$\psi(x)=u(x)+\bar{v}(x),$$
$$\bar{\psi}(x)=\bar{u}(x)+v(x),$$

where $u(\bar{u}=u^\dagger\beta)$ destroys (creates) electrons, and $v(\bar{v}=\beta v^\dagger)$ destroys (creates) positrons.[11] For our purposes, we shall need the following table of anti-commutators:

$$\{u_\alpha(z),\bar{u}_\beta(y)\}=-i\{S_{\alpha\beta}{}^{A+}(z-y)-S_{\alpha\beta}{}^{R+}(z-y)\},$$
$$\{\bar{v}_\beta(y),v_\alpha(z)\}=-i\{S_{\alpha\beta}{}^{A-}(z-y)-S_{\alpha\beta}{}^{R-}(z-y)\},$$

with all other possible anticommutators vanishing. The Feynman kernel function $S_{\alpha\beta}{}^F(x)$ is defined as

$$S_{\alpha\beta}{}^F(x)=-i\{S_{\alpha\beta}{}^{R+}(x)+S_{\alpha\beta}{}^{A-}(x)\}, \quad (14)$$

and satisfies

$$L_{\alpha\beta}{}^0(x)S_{\beta\gamma}{}^F(x)=i\delta_{\alpha\gamma}\delta(x), \quad (15)$$

where

$$L_{\alpha\beta}{}^0(x)\equiv(-i\gamma_{\alpha\beta}{}^\mu\partial_\mu+\delta_{\alpha\beta}m). \quad (16)$$

We can, in complete analogy with the method used to arrive at Eq. (7), derive a similar set of expressions for the electron-positron operators. We will not repeat the details of the proof, but simply assert that for any functional, $\mathfrak{H}(\psi,\bar{\psi})$,

$$T[\mathfrak{H}(\psi,\bar{\psi})]=N[\mathfrak{H}(\psi',\bar{\psi}')],$$

where

$$\psi_\alpha'(x)=\psi_\alpha(x)-\int d^4x'S_{\alpha\beta}{}^F(x-x')\frac{\delta}{\delta\bar{\psi}_\beta(x')}, \quad (17a)$$

and

$$\bar{\psi}_\beta'(x')=\bar{\psi}_\beta(x')+\int d^4x\frac{\delta}{\delta\psi_\alpha(x)}S_{\alpha\beta}{}^F(x-x'). \quad (17b)$$

Now, however, due to the fact that the electron-positron operators anticommute with each other, we must give a slightly different meaning to the functional derivative as employed in Eqs. (17a and b). A moment's consideration shows that the correct definition is given by the following:

$$\left\{\frac{\delta}{\delta\psi_\alpha(x)},\bar{\psi}_\beta(x')\right\}=0;\quad\left\{\frac{\delta}{\delta\bar{\psi}_\beta(x)},\psi_\alpha(x')\right\}=0,$$
$$\left\{\frac{\delta}{\delta\psi_\alpha(x)},\psi_\beta(x')\right\}=\delta_{\alpha\beta}\delta(x-x'),$$
$$\left\{\frac{\delta}{\delta\bar{\psi}_\alpha(x)},\bar{\psi}_\beta(x')\right\}=\delta_{\alpha\beta}\delta(x-x'),$$

from which it immediately follows that

$$\left\{\frac{\delta}{\delta\psi_\alpha(x)},\frac{\delta}{\delta\bar{\psi}_\beta(x')}\right\}=0.$$

As before, we can introduce an ordering operator Σ defined by

$$\Sigma=\int d^4xd^4x'\frac{\delta}{\delta\psi_\alpha(x)}S_{\alpha\beta}{}^F(x-x')\frac{\delta}{\delta\bar{\psi}_\beta(x')}, \quad (18)$$

and write, in place of Eqs. (17a,b),

$$\psi_\alpha'(x)=e^\Sigma\psi_\alpha(x)e^{-\Sigma}, \quad (19a)$$

[11] We represent the positrons by "negative-energy" electron wave functions and not by the charge-conjugate functions.

and

$$\bar{\psi}_\beta'(x)=e^{\Xi}\bar{\psi}_\beta(x)e^{-\Xi}. \tag{19b}$$

Hence,

$$T[\mathfrak{H}(\psi,\bar{\psi})]=N[e^{\Xi}\mathfrak{H}(\psi,\bar{\psi})e^{-\Xi}],$$

and again, if we are interested only in the matrix elements of $\mathfrak{H}(\psi,\bar{\psi})$ we can write

$$\langle T[\mathfrak{H}(\psi,\bar{\psi})]\rangle=\langle N[e^{\Xi}\mathfrak{H}(\psi,\bar{\psi})]\rangle. \tag{20}$$

Upon combining the results contained in Eqs. (13), (20), which we can do since the two fields commute, we obtain the equation linking a given T product to its corresponding N product, namely,[12]

$$\langle T[\mathfrak{G}(A,\psi,\bar{\psi})]\rangle=\langle N[e^{\Xi}e^{\Delta}\mathfrak{G}(A,\psi,\bar{\psi})]\rangle. \tag{21}$$

As we shall see later on, this result will greatly simplify our work in treating the various Green's functions to be introduced.

In passing, it is interesting to note that it is possible to derive from Eq. (21) the more conventional rules for the transformation of a T product into its corresponding N product.[3,8] For the sake of simplicity, we will carry out the demonstration only for the electromagnetic field, and leave the case of the electron-positron field to the interested reader. We shall first state the rules whereby the transformation can be effected. In any T product of the $A_\mu(x)$ we pick out a certain even number of factors, either none or all or any intermediate number, and associate them together in pairs. We replace each pair of factors $A_\mu(x)$, $A_\nu(y)$ by $\delta_{\mu\nu}D^F(x-y)$ and multiply the result by the remaining factors of the T product arranged in a normal order. For instance, in the T product $T[A_\mu(x_1),A_\nu(x_2),A_\lambda(x_3),A_\tau(x_4)]$, the possible results for such factor pairings are given below:

$$N[A_\mu(x_1)A_\nu(x_2)A_\lambda(x_3)A_\tau(x_4)],$$

$$\delta_{\mu\nu}D^F(x_1-x_2)N[A_\lambda(x_3)A_\tau(x_4)],$$

$$\delta_{\mu\lambda}D^F(x_1-x_3)N[A_\nu(x_2)A_\tau(x_4)],\ \cdots,$$

$$\delta_{\mu\nu}D^F(x_1-x_2)\delta_{\lambda\tau}D^F(x_3-x_4),$$

$$\delta_{\mu\lambda}D^F(x_1-x_3)\delta_{\nu\tau}D^F(x_2-x_4),\ \cdots.$$

Wick has then shown that a given T product is equa to the sum of the results of all such factor pairings, i.e.

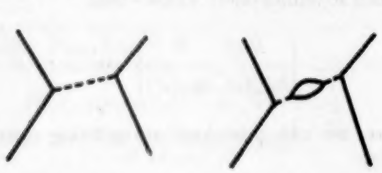

FIG. 1. Scattering of electron by electron in second and fourth orders. The photon (dotted) line is a λ line.

[12] S. Hori, Progr. Theoret. Phys. 7, 578 (1952) has obtained a similar formula but only for the special case where $\mathfrak{G}$ is the S matrix itself. We have developed Eq. (21) since we will need it to treat more general forms of $\mathfrak{G}$.

for the example given, the T product is equal to the sum of all the expressions in the above table.

In order to show that Eq. (21) is equivalent to these rules, we need merely to expand e^{Δ} in a power series. The first term in the expansion is just unity and hence we simply arrange all of the factors $A_\mu(x)$ appearing in $\mathfrak{G}$ in a normal order: for this first term we make no factor pairings. The next term in the expansion is just Δ. Because of the nature of the functional derivatives, the net effect of operating with it on $\mathfrak{G}$ is to pick out, in all possible ways, two factors $A_\mu(x)$ and $A_\nu(y)$ and insert in their place $\delta_{\mu\nu}D^F(x-y)$. Upon rearranging the remaining factors in a normal order, as the equation tells us to do, we obtain the sum of all the results of x single factor pairings mentioned above. In a similar manner we see that the third term in the expansion will give us the sum of the results obtained by making all possible pairings involving four factors $A_\mu(x)$, and so on. The factorials compensate for the fact that in the nth term of the expansion each particular pairing occurs $n!$ times.

III. THE ONE-ELECTRON GREEN'S FUNCTION

In dealing with Eq. (21), it is often convenient to employ the so-called Feynman graphs. The Feynman graph for a particular term in the expansion of the right-hand side of Eq. (21) can be drawn as follows: For every factor $D^F(x_i-x_i')$ a dotted (photon) line is drawn connecting the points x_i and x_i'; for every factor $S_{\alpha\beta}{}^F(xj-xj')$ a directed (electron, positron) line is drawn from x_j to x_j'; for the factors $\bar{\psi}_\alpha(x_k),\psi_\beta(x_k')$ directed lines are drawn leading out from x_k to the edge of the diagram, and in from the edge of the diagram to x_k'; for every factor $A_\mu(x_l)$ a line is drawn connecting the edge of the diagram with x_l. As sometimes happens, graphs corresponding to two different terms in the expansion of Eq. (21) differ from each other by only one or more self-energy parts. In Fig. 1 we have an example of such a situation. Here the single line connecting the points x and x' in one graph is replaced, in the other graph, by a subgraph which is unconnected to the rest of the diagram except by two lines running from it to x and x'. Graphs which contain self-energy portions are termed "reducible" graphs and always correspond to some particular "irreducible" or "primitive" graph. A particular line in a primitive graph, which has as its counterpart in the associated reducible graph, a self-energy subgraph, will be denoted as a λ line. Dyson has shown[3] that the sum of all of the terms in Eq. (21) which correspond to a given primitive graph, plus all of its associated reducible graphs, can be reduced to a single term to be associated with the primitive graph. This term is obtained in the following manner: In the term associated with the primitive graph we replace each factor $S_{\alpha\beta}{}^F(x-x')$ or $D^F(x-x')$ as the case may be, which corresponds to a λ line by the new factors $G_{\alpha\beta}(x,x')$, $\mathfrak{D}_{\mu\nu}(x,x')$, respectively. Substitutions

must also be made for external λ lines but for our purposes we need not consider them. These new factors are given by

$$G_{\alpha\beta}(x,x')=\langle T[\bar{\psi}_\beta(x')\psi_\alpha(x)\mathfrak{S}]\rangle_0 S_{\text{vac}}^{-1}, \quad (22)$$

and

$$\mathfrak{R}_{\mu\nu}(x,x')=\langle T[A_\mu(x)A_\nu(x')\mathfrak{S}]\rangle_0 S_{\text{vac}}^{-1}, \quad (23)$$

where the subscript 0 indicates that we are to take the vacuum expectation value of the quantity appearing between the brackets and where $\mathfrak{S}$ is defined through Eq. (1). S_{vac} is just the vacuum expectation value of the S matrix.

In this section we shall derive a closed-form expression for $G_{\alpha\beta}(x,x')$ in terms of S_{vac}, the vacuum expectation value of the S matrix and at the same time derive the differential equation satisfied by G. As we shall see, this equation will be identical with the one given by Schwinger for his one-electron Green's function, and hence we will be able to conclude that Schwinger's G is identical to the one defined in Eq. (22). With this fact in mind, we can also call our G the one-electron Green's function.

In order to investigate the properties of G, let us apply the results of Eq. (21) to Eq. (22). We have then that

$$G_{\alpha\beta}(x,x')=\langle N[e^{\Delta}e^{\Sigma}\bar{\psi}_\beta(x')\psi_\alpha(x)\mathfrak{S}]\rangle_0 S_{\text{vac}}^{-1}. \quad (24)$$

In the investigation of such quantities as appear in the right-hand side of Eq. (24) it is convenient to know the commutation properties of Σ with respect to $\psi_\alpha(x)$ and $\bar{\psi}_\beta(x')$. By combining the results of Eqs. (17a,b; 19a,b) we obtain directly that

$$[e^{\Sigma},\psi_\alpha(x)]=-\int d^4y S_{\alpha\sigma}^{F}(x-y)\frac{\delta}{\delta\bar{\psi}_\sigma(y)}e^{\Sigma}, \quad (25a)$$

and

$$[e^{\Sigma},\bar{\psi}_\beta(x')]=\int d^4y' S_{\rho\beta}^{F}(y'-x')\frac{\delta}{\delta\psi_\rho(y')}e^{\Sigma}. \quad (25b)$$

Let us now use Eq. (25b) to interchange the positions of e^{Σ} and $\bar{\psi}_\beta(x')\psi_\alpha(x)$ in Eq. (24). The net effect of this interchange is simply that

$$G_{\alpha\beta}(x-x')=S_{\alpha\beta}^{F}(x-x')-\int d^4y d^4y' S_{\alpha\sigma}^{F}(x-y)S_{\rho\beta}^{F}(y'-x')\times\left\langle N\left[\frac{\delta}{\delta\psi_\rho(y')}\frac{\delta}{\delta\bar{\psi}_\sigma(y)}e^{\Sigma}e^{\Delta}\mathfrak{S}\right]\right\rangle_0 S_{\text{vac}}^{-1}. \quad (26)$$

Because of the form of Σ, we also have that

$$\frac{\delta \ln S_{\text{vac}}}{\delta S_{\rho\sigma}^{F}(y'-y)}=\left\{\frac{\delta}{\delta S_{\rho\sigma}^{F}(y'-y)}\langle N[e^{\Delta}e^{\Sigma}\mathfrak{S}]\rangle_0\right\}S_{\text{vac}}^{-1}=\left\langle N\left[\frac{\delta}{\delta\psi_\rho(y')}\frac{\delta}{\delta\bar{\psi}_\sigma(y)}e^{\Delta}e^{\Sigma}\mathfrak{S}\right]\right\rangle_0 S_{\text{vac}}^{-1}. \quad (27)$$

Direct substitution in Eq. (27) into Eq. (26) then yields

$$G_{\alpha\beta}(x,x')=S_{\alpha\beta}^{F}(x-x')+\int\int d^4y d^4y' S_{\alpha\sigma}^{F}(x-y)\times\frac{\delta \ln S_{\text{vac}}}{\delta S_{\sigma\rho}^{F}(y-y')}S_{\rho\beta}^{F}(y'-x'). \quad (28)$$

Thus we see that the one-electron Green's function can be expressed entirely in terms of the single quantity S_{vac}.

At this point a word should be said concerning S_{vac}. In Eq. (27) we have treated S_{vac} as though it were a functional of $S^F(x)$. Actually, since S^F is a specified function of its arguments, S_{vac} is just a number. Strictly speaking then, the functional derivative of S_{vac} with respect to $S^F(x)$ has no meaning. However, we can give it meaning if we consider $S^F(x)$, and also $D^F(x)$, to be arbitrary functions of their arguments. It is only after we carry out the prescribed operations on S_{vac} that they assume their actual functional dependence.

Although we have obtained an expression for the one-electron Green's function, in terms of S_{vac}, it is sometimes convenient to know the differential equation satisfied by $G_{\alpha\beta}$. We can derive this equation by again making use of Eq. (24). It will prove convenient however, to interchange the order of $\psi_\alpha(x)$ and $\bar{\psi}_\beta(x')$ and write

$$G_{\alpha\beta}(x,x')=-\langle N[e^{\Delta}e^{\Sigma}\psi_\alpha(x)\bar{\psi}_\beta(x')\mathfrak{S}]\rangle_0 S_{\text{vac}}^{-1}.$$

Let us now commute e^{Σ} through $\psi_\alpha(x)$. If we refer to Eq. (25a), we see that the result is

$$G_{\alpha\beta}(x,x')=\left\langle N\left[\int d^4y S_{\alpha\rho}^{F}(x-y)\times\frac{\delta}{\delta\bar{\psi}_\rho(y)}e^{\Delta}e^{\Sigma}\bar{\psi}_\beta(x')\mathfrak{S}\right]\right\rangle_0 S_{\text{vac}}^{-1}. \quad (29)$$

(The term which contains the factor $\psi_\alpha(x)$ standing to the left of e^{Σ} vanishes since we are taking the vacuum expectation value of the entire expression.) Now, since the functional derivative $\delta/\delta\bar{\psi}_\rho(y)$ commutes with e^{Σ}, we can perform the indicated differentiation in Eq. (29) and so obtain

$$G_{\alpha\beta}(x,x')=S_{\alpha\beta}^{F}(x-x')-\int d^4y S_{\alpha\rho}^{F}(x-y)\langle N\{iee^{\Delta}e^{\Sigma}\times\gamma_{\rho\sigma\mu}\bar{\psi}_\beta(x')\psi_\sigma(y)A_\mu(y)\mathfrak{S}\}\rangle_0 S_{\text{vac}}^{-1}. \quad (30)$$

Let us now make use of the fact that

$$\delta\mathfrak{S}/\delta J_\mu(y)=iA_\mu(y)\mathfrak{S}$$

to rewrite Eq. (30) in the form

$$G_{\alpha\beta}(x,x')=S_{\alpha\beta}^{F}(x-x')+e\int d^4y S_{\alpha\rho}^{F}(x-y)\frac{\delta}{\delta J_\mu(y)}\times\langle N\{e^{\Delta}e^{\Sigma}\bar{\psi}_\beta(x')\psi_\sigma(y)\mathfrak{S}\}\rangle_0\gamma_{\rho\sigma\mu}S_{\text{vac}}^{-1}. \quad (31)$$

Now substitute the result of Eq. (28) into the bracketed part of Eq. (31), and obtain

$$G_{\alpha\beta}(x,x')=S_{\alpha\beta}^{F}(x-x')+e\int d^4y S_{\alpha\rho}^{F}(x-y)\gamma_{\rho\sigma}^{\mu}$$
$$\times\frac{\delta}{\delta J_\mu(y)}\Big\{S_{\beta\sigma}^{F}(x'-y)S_{\text{vac}}+\int\int d^4z d^4z' S_{\beta\lambda}^{F}(x-z)$$
$$\times\frac{\delta S_{\text{vac}}}{\delta S_{\lambda\tau}^{F}(z-z')}S_{\tau\sigma}^{F}(z'-y)\Big\}S_{\text{vac}}^{-1},$$

which becomes, after a slight rearrangement of terms,

$$G_{\alpha\beta}(x,x')=S_{\alpha\beta}^{F}(x,x')-e\int d^4y S_{\alpha\rho}^{F}(x-y)$$
$$\times\gamma_{\rho\sigma}^{\mu}S_{\sigma\beta}^{F}(y-x')\frac{\delta\ln S_{\text{vac}}}{\delta J_\mu(y)}-e\int d^4y S_{\alpha\rho}^{F}(x-y)$$
$$\times\gamma_{\rho\sigma}^{\mu}\int\int d^4z d^4z' S_{\sigma\tau}^{F}(y-z)\frac{\delta\ln S_{\text{vac}}}{\delta S_{\tau\lambda}^{F}(z-z')}$$
$$\times S_{\lambda\beta}^{F}(z'-x)\frac{\delta\ln S_{\text{vac}}}{\delta J_\mu(y)}-e\int d^4y S_{\alpha\rho}^{F}(x-y)\gamma_{\rho\sigma}^{\mu}$$
$$\times\int\int d^4z d^4z' S_{\sigma\tau}^{F}(y-z)\frac{\delta^2\ln S_{\text{vac}}}{\delta S_{\tau\lambda}^{F}(z-z')\delta J_\mu(y)}$$
$$\times S_{\lambda\beta}^{F}(z'-x).$$

This result can then be expressed in terms of $G_{\alpha\beta}$ as

$$G_{\alpha\beta}(x,x')=S_{\alpha\beta}^{F}(x-x')-e\int d^4y S_{\alpha\rho}^{F}(x-y)$$
$$\times G_{\sigma\beta}(y,x')\gamma_{\rho\sigma}^{\mu}\frac{\delta\ln S_{\text{vac}}}{\delta J_\mu(y)}-e\int d^4y S_{\alpha\rho}^{F}(x-y)$$
$$\times\gamma_{\rho\sigma}^{\mu}\frac{\delta G_{\sigma\beta}(y,x')}{\delta J_\mu(y)}. \quad (32)$$

In order to remain as close to Schwinger's notation as possible, we shall introduce at this point a quantity $\langle A_\mu(x)\rangle$ defined by

$$\langle A_\mu(x)\rangle=-i\frac{\delta\ln S_{\text{vac}}}{\delta J_\mu(x)}.$$

In terms of $\langle A_\mu\rangle$, Eq. (32) then becomes

$$G_{\alpha\beta}(x,x')=S_{\alpha\beta}^{F}(x-x')-ie\int d^4y S_{\alpha\rho}^{F}(x-y)G_{\sigma\beta}(y,x')$$
$$\times\gamma_{\rho\sigma}^{\mu}\langle A_\mu(y)\rangle-e\int d^4y S_{\alpha\rho}^{F}(x-y)\gamma_{\rho\sigma}^{\mu}\frac{\delta G_{\sigma\beta}(y,x')}{\delta J_\mu(y)}. \quad (34)$$

Finally, by applying the differential operator $L_{\alpha\beta}^{0}$ to both sides of Eq. (34) we obtain, as the differential equation satisfied by $G_{\alpha\beta}$,

$$\{L_{\alpha\beta}^{0}(x)-e\langle A_\mu(x)\rangle\gamma_{\alpha\sigma}^{\mu}\}G_{\sigma\beta}(x,x')$$
$$+ie\gamma_{\alpha\sigma}^{\mu}\frac{\delta G_{\sigma\beta}(x,x')}{\delta J_\mu(x)}=i\delta_{\alpha\beta}\delta(x-x'). \quad (35)$$

Upon comparing this equation for $G_{\alpha\beta}$ with the one given by Schwinger, we see that they are identical and hence we are justified in equating our Green's function with that introduced by Schwinger.

We shall conclude this section with a brief discussion of the so-called "mass" operator introduced by Schwinger. Schwinger has assumed that the functional derivative appearing in Eq. (35) can be represented by an integral operator, i.e., that

$$ie\gamma_{\alpha\sigma}^{\mu}\frac{\delta G_{\sigma\beta}(x,x')}{\delta J_\mu(x)}=\int d^4y\Sigma_{\alpha\sigma}(x,y)G_{\sigma\beta}(y,x'). \quad (36)$$

The mass operator $M_{\alpha\beta}(x,y)$ is then defined by the equation

$$M_{\alpha\beta}(x,y)=m\delta_{\alpha\beta}\delta(x-y)+\Sigma_{\alpha\beta}(x,y).$$

As was mentioned above, Eq. (36) is an assumption. It can be justified, however, and we shall do so by deriving an expression for $\Sigma_{\alpha\beta}(x,y)$ in terms of S_{vac}. Let us begin by rewriting Eq. (28) in Schwinger's matrix notation. We have that

$$G=S^F+S^FKS^F, \quad (37)$$

where K is an abbreviation for the functional derivative of $\ln S_{\text{vac}}$ with respect to S^F. Equation (37) can be solved for S^F, giving

$$S^F=(1+S^FK)^{-1}G.$$

Substitution of this result back into the second term in the right-hand side of Eq. (37) then yields

$$G=S^F+S^FK(1+S^FK)^{-1}G.$$

Now let us compare this equation with Eq. (34), written in matrix form and in terms of Σ, *viz.*,

$$G=S^F-ieS^F\gamma^\mu G\langle A_\mu\rangle+iS^F\Sigma G.$$

We see immediately that Σ is equivalent to

$$\Sigma=e\gamma^\mu\langle A_\mu\rangle+K(1+S^FK)^{-1}. \quad (39)$$

From this we can conclude that a Σ does exist and indeed can be expressed in terms of S_{vac}. Actually, the derivation leading to Eq. (39) rests upon the assumption that $(1+S^FK)^{-1}$ exists and is nonsingular. However, even if these conditions are not fulfilled we can still use Eq. (39), at least formally, to express Σ as a series expansion in S^F and K.

IV. PROPERTIES OF $\langle A_\mu(x)\rangle$

In Schwinger's original work on Green's functions, the idea was put forth that one might eliminate some of the difficulties inherent in the S-matrix formalism by treating Eq. (35) as a basic equation for $G_{\alpha\beta}$. In other words, one need not consider its antecedents, but attempt to solve it directly for $G_{\alpha\beta}$. In order to carry out this program consistently, one then needs an equation to determine $\langle A_\mu(x)\rangle$. In this section we shall derive such an equation, and, although we do not adhere to Schwinger's program in this paper, we shall find it useful for other purposes. From Eq. (33) we see that

$$\langle A_\mu(x)\rangle = \langle N[e^{\Delta}e^{\Xi}A_\mu(x)\mathfrak{S}]\rangle_0 S_{\text{vac}}^{-1}.$$

Upon commuting e^{Δ} through $A_\mu(x)$ we obtain

$$\langle A_\mu(x)\rangle = \left\langle N\left[e^{\Delta}e^{\Xi}\int d^4y D^F(x-y)\frac{\delta}{\delta A_\mu(y)}\mathfrak{S}\right]\right\rangle_0 S_{\text{vac}}^{-1}. \quad (40)$$

By carrying out the indicated functional differentiation, Eq. (40) runs to

$$\langle A_\mu(x)\rangle = i\int d^4y D^F(x-y)\{J_\mu(y)+\langle j_\mu(y)\rangle\}, \quad (41)$$

where

$$\langle j_\mu(y)\rangle = \langle T[j_\mu(y)\mathfrak{S}]\rangle_0 S_{\text{vac}}^{-1}. \quad (42)$$

Equation (41) can be put into the form of a differential equation by operating on it with $-i\Box$ to give

$$\Box\langle A_\mu(x)\rangle = -J_\mu(x)-\langle j_\mu(x)\rangle. \quad (43)$$

Furthermore, because of the definition of $G_{\alpha\beta}$,

$$\langle j_\mu(x)\rangle = e\gamma_{\alpha\beta}{}^\mu G_{\beta\alpha}(x,x), \quad (44)$$

Eq. (43) can be put in the form

$$\Box\langle A_\mu(x)\rangle = -J_\mu(x)-e\gamma_{\alpha\beta}{}^\mu G_{\beta\alpha}(x,x).$$

Hence we can use Eq. (45) together with Eq. (35) to determine both $\langle A_\mu(x)\rangle$ and $G_{\alpha\beta}(x,x')$.[13]

Before concluding this section, it will be of some interest to consider the particular case where $J_\mu(x)=0$. Since originally $J_\mu(x)$ was introduced into the theory as a mathematical artifice to enable us to derive Eq. (35), we see that this is the case with which we shall have to deal in all final applications of the theory. In cases where differentiation with respect to $J_\mu(x)$ is indicated we must perform the differentiation before we approach the limit of $J_\mu(x)$ going to zero. Consider now what happens to $G(x,x')$ in the limit. In general $G(x,x')$ is not an invariant function of its arguments under a translation of the coordinate axis since it depends upon $J_\mu(x)$. However, in the limit $G(x,x')$ must be an invariant function of its arguments and hence becomes a function G^0 of the coordinate difference $x-x'$. We can therefore conclude from Eq. (44) that

$$\langle j_\mu(x)\rangle_{J=0} = e\gamma^\mu G^0(0)\equiv 0,$$

since each component of $\langle j_\mu(x)\rangle$ is now a number quite independent of the coordinate system. The only vector having these properties which is invariant under Lorentz transformations is the null vector.

Upon referring to Eq. (41) we see then that

$$\langle A_\mu(x)\rangle_{J=0}=0.$$

In this case then, Eq. (38) becomes simply

$$G^0 = S^F + iS^F\Sigma^0 G^0,$$

which is just the equation given by Dyson for his Green's function S'^F [Eq. (63), Phys. Rev. **75**, 1736 (1949)].

V. THE ONE-PHOTON GREEN'S FUNCTION

In this section we shall treat some of the properties of the one-photon Green's function as given by Eq. (23). Actually, we shall follow Schwinger and define the one-photon Green's function as

$$\mathfrak{G}_{\mu\nu}(x,x') = \langle T[A_\mu(x)A_\nu(x')\mathfrak{S}]\rangle_0 S_{\text{vac}}^{-1} - \langle A_\mu(x)\rangle\langle A_\nu(x')\rangle. \quad (46)$$

From the results of the preceding section it is evident that in the limit $J_\mu\to 0$, $\mathfrak{G}_{\mu\nu}(x,x')$ is equivalent to $\mathfrak{K}_{\mu\nu}(x,x')$. If we keep in mind now the form of $\mathfrak{G}$, we see that Eq. (46) is equivalent to

$$\mathfrak{G}_{\mu\nu}(x,x') = -\frac{\delta^2 S_{\text{vac}}}{\delta J_\mu(x)\delta J_\nu(x')}S_{\text{vac}}^{-1}+\frac{\delta \ln S_{\text{vac}}}{\delta J_\mu(x)}\frac{\delta \ln S_{\text{vac}}}{\delta J_\nu(x')},$$

or

$$\mathfrak{G}_{\mu\nu}(x,x') = \frac{\delta^2 \ln S_{\text{vac}}}{\delta J_\mu(x)\delta J_\nu(x')} = \mathfrak{G}_{\nu\mu}(x',x). \quad (47)$$

If we make use of Eq. (33), we can then put Eq. (47) into the form

$$\mathfrak{G}_{\mu\nu}(x,x') = -i\frac{\delta\langle A_\mu(x)\rangle}{\delta J_\nu(x')}. \quad (48)$$

Let us now take the derivative of both sides of Eq. (41). By making use of the identity (48) we so obtain

$$\mathfrak{G}_{\mu\nu}(x,x') = \delta_{\mu\nu}D^F(x-x')+\int d^4y D^F(x-y)\frac{\delta\langle j_\mu(y)\rangle}{\delta J_\nu(x')}. \quad (49)$$

[13] For a discussion of boundary conditions to be used in connection with solving these equations, see reference 1.

Finally, by operating on Eq. (49) with $\Box$, we obtain the fundamental equation satisfied by $\mathfrak{G}_{\mu\nu}$:

$$\Box\mathfrak{G}_{\mu\nu}(x,x')=i\delta_{\mu\nu}\delta(x-x')+i\frac{\delta\langle j_\mu(x)\rangle}{\delta J_\nu(x')}. \quad (50)$$

Let us examine the last term in the right-hand side of Eq. (50). From Eq. (44) we have that

$$i\frac{\delta\langle j_\mu(x)\rangle}{\delta J_\nu(x')}=ie\gamma_{\alpha\beta}{}^\mu\frac{\delta G_{\beta\alpha}(x,x')}{\delta J_\nu(x')}. \quad (51)$$

Now Eq. (43) tells us that $J_\mu(x)$ is equal to a term linear in $\langle A_\mu(x)\rangle$ plus an additional term. Hence, by the chain rule of differentiation, we can rewrite Eq. (51) as

$$i\frac{\delta\langle j_\mu(x)\rangle}{\delta J_\nu(x')}=ie\gamma_{\alpha\beta}{}^\mu\int d^4y\frac{\delta G_{\beta\alpha}(x,x')}{\delta\langle A_\sigma(y)\rangle}\frac{\delta\langle A_\sigma(y)\rangle}{\delta J_\nu(x')}.$$

If then we define a new quantity $P_{\mu\nu}(x,x')$ by the equation

$$P_{\mu\nu}(x,x')=ie\gamma_{\alpha\beta}{}^\mu\frac{\delta G_{\beta\alpha}(x,x')}{\delta\langle A_\nu(x')\rangle},$$

we can put our fundamental Eq. (50) into a more symmetrical form, namely,

$$\Box\mathfrak{G}_{\mu\nu}(x,x')=i\delta_{\mu\nu}\delta(x-x')+i\int d^4yP_{\mu\sigma}(x,y)\mathfrak{G}_{\sigma\nu}(y,x'). \quad (53)$$

In the particular case where $J_\mu=0$, Eq. (49) becomes, in matrix notation:

$$\mathfrak{G}_{\mu\nu}{}^0=\delta_{\mu\nu}D^F-iD^FP_{\mu\sigma}{}^0\mathfrak{G}_{\sigma\nu}{}^0.$$

From this expression, we see that $\mathfrak{G}_{\mu\nu}{}^0$ corresponds to Dyson's D'^F, and iP^0 corresponds to the proper photon-self energy Π^*.

VI. DISCUSSION

In this paper we have demonstrated the equivalence between the Green's functions and associated structures such as the mass operator introduced by Schwinger and the modified propagation functions occuring in the S-matrix theory. In the course of the demonstration a curious result appeared, namely, that all of the various quantities introduced by Schwinger could be expressed in terms of a single quantity S_{vac}. This fact suggests a possible alternate approach to investigating the properties of the Green's functions. Instead of examining each one separately, as is now done, one might begin by examining the properties of S_{vac}, considered as a functional of S^F, D^F, and J_μ. Such a study would entail, in the first place, a knowledge of how S_{vac} depends upon its arguments. By making use of the results of this paper it is possible to derive certain closed-form expressions for S_{vac}. Unfortunately, these expressions all involve the Green's functions themselves, and hence are of little help at present in analyzing S_{vac}. Even if we did know the exact functional dependence of S_{vac} we would still be very far from our goal. We would need in addition a mathematical formalism somewhat akin to analysis as applied to ordinary functions since, as we have seen, the Green's functions all involve functional derivatives of S_{vac} with respect to its arguments. In this respect we can but hope that the mathematicians will become interested in the problem and develop for us a theory of functional analysis.

There also exists a second possibility which appears to be somewhat more manageable. As we have seen, the Green's functions attempt to take into account, in one fell swoop as it were, all of the virtual processes associated with a given real process. The one-electron Green's function, for example, takes into account all of the virtual processes which accompany a free electron in its flight through space. One can take the position, as Schwinger has done, that since these virtual processes are in principle not observable they ought not to appear in the theory. In other words, one should work solely with the Green's functions which are given in terms of some integro-differential equation, and not worry about their antecedents. The chief drawback to such a scheme is that some of the quantities appearing in the integro-differential equations for the Green's functions, such as the mass operator, are themselves extremely complicated objects which up to now have been expressible only as power series in the various propagation functions. An approach of this type has been attempted by Edwards with some degree of success.[14]

There does exist a third approach, however, lying intermediate between the two approaches outlined above, which we would like to outline briefly. Consider for a moment the situation in which an electron is scattered by some external field. Given its initial energy and momentum, we wish to know what will be its final energy and momentum. In attempting to answer this problem from a theoretical standpoint, one of the first questions which arises is how to describe the initial and final states of the electron. In the present form of the theory, the electron is described initially and finally by eigenstates of the free-field Hamiltonian, H_0. However, even before it interacts with the external field, the electron is in interaction with its own virtual photon field. Hence one should, in describing the initial and final states of the electron, include the effects of these virtual photons. As we have seen, our Green's functions include in their description of the electron just these virtual fields. It appears reasonable, therefore, to employ as eigenstates describing the electron, eigenstates of the operator appearing in the equation for the one-electron Green's function. Once one has done this, there exists the possibility that the matrix

[14] S. F. Edwards, Phys. Rev. 90, 284 (1953).

elements of the S matrix could then be expressed in some simple manner in terms of these eigenstates. The main problem facing the theory would then be shifted to that of calculating these eigenstates, where one would have a much better chance of separating out the infinities which arise in the present theory.

ACKNOWLEDGMENT

The author would like to express his thanks to Dr. F. Rohrlich, Dr. Y. Nambu, and Dr. P. Bergmann for their many interesting and helpful comments in connection with this work.

PHYSICAL REVIEW VOLUME 94, NUMBER 3 MAY 1, 1954

Low-Energy Limits and Renormalization in Meson Theory

S. DESER* AND W. E. THIRRING,† *Institute for Advanced Study, Princeton, New Jersey,*

AND

M. L. GOLDBERGER,‡ *Princeton University, Princeton, New Jersey*

(Received January 7, 1954)

A technique is developed for deriving rigorous expressions for zero-energy mesonic processes. Making use of the ambiguity of mesonic charge renormalization, the coupling constant is defined by zero-energy pion-nucleon scattering. The threshold photomeson production amplitude is also calculated. The experimental value of the coupling constant defined by scattering is at least an order of magnitude less than that of the coupling constant deduced from the photoproduction data. It is shown that pair suppression effects are absent in both cases. The possibility that the results obtained imply disagreement of pseudoscalar theory with experiment is discussed.

I. INTRODUCTION

IT is almost universally accepted at present that π mesons are pseudoscalar, and that to a very good approximation isotopic spin is a good quantum number in mesonic-nucleon processes. Unfortunately, it is not at all clear to what extent the conventional pseudoscalar symmetrical meson theory correctly describes such processes. Because of the difficulty of carrying out accurate calculations, it has been hard to distinguish between the predictions of the theory and the effects of the particular approximation schemes hitherto employed. In order to avoid extraneous difficulties, it seems advisable to concentrate on understanding low-energy phenomena, where both nucleons and mesons are nonrelativistic. Two such processes, which will be discussed in the present paper, are threshold photomeson production and meson-nucleon scattering at zero energy.

By the use of special techniques it has been possible to evaluate the matrix elements for these two processes rigorously in the limit of vanishing meson mass. These are, of course, purely formal results; however, as is discussed at length below, one of them, say the meson scattering, may be used to assign a precise numerical value to the coupling constant and the other then in principle serves as a check on the agreement between theory and experiment. Unfortunately we are not able to evaluate the photo-meson matrix element explicitly, and thus unambiguously settle this crucial question; nor is the present experimental data sufficiently accurate to give a reliable number for the coupling constant. We can, however, say the following: If in the computation of meson-nucleon scattering one may without serious error set the mass of the real mesons equal to zero in the portion of the scattering amplitude which is independent of isotopic spin, one deduces from the existing data the value $g^2/4\pi \sim \frac{1}{4}$. If one may assume that with such a small value of the coupling constant perturbation theory is valid (at least in an asymptotic sense), then one may conclude that the present theory does not correctly describe the behavior of π mesons. Of course, should the value of $g^2/4\pi$ turn out to be much larger or should the neglect of the meson mass mentioned above prove unwarranted, we can make no definite statement.

Before the theory can be compared with experiment, it must, of course, be renormalized. Pseudoscalar theory (with pseudoscalar coupling) is a "renormalizable" theory in the conventional sense of the term; however, in contrast to quantum electrodynamics, the renormalization program may here be carried out in a variety of nonequivalent ways. This fact is of great importance in any attempts to ascertain the physical content of mesonic calculations. Charge renormalization is uniquely defined in electrodynamics;[1] this is closely related to the existence of a charge conservation law and finds its

* Parker Fellow, Harvard University.

† On leave of absence from Physikalisches Institut, Universitat Bern, Bern, Switzerland.

‡ On leave of absence from the University of Chicago, Chicago, Illinois.

[1] G. Källén (to be published).

formal expression in the well known Ward identity.[2] One can define the charge either from the requirement that Coulomb's law should hold for large distances, or that the motion of a low-energy electron in a slowly varying field be describable classically, or that low-frequency Compton scattering be given by the Thomson formula. It turns out that all of these definitions lead to the same value for e. The underlying physical reason is that a slowly varying electromagnetic field is insensitive to the shape of the charge distribution, and radiative corrections cannot change the total charge. The above-mentioned experiments are characterized by interactions over macroscopic distances or by processes in which there is negligible energy-momentum transfer to the charged particle. In meson theory the finite meson rest mass precludes the first type of definition (as it implies a finite range of forces) and introduces a difference between processes in which the four-momentum transfer to a nucleon is zero (such as forward scattering of mesons by nucleons), or those in which the transfer is of the order of the meson rest mass (such as threshold photomeson production, or threshold production in a nucleon-nucleon collision). The ambiguity introduced by the necessity of choosing one of the two types of processes as a basis for the definition of the coupling constant g has been stressed by Thellung.[3] As we shall see, however, even in the limit of vanishing meson mass, the two alternatives lead to different definitions of the renormalized coupling constant. There is another (physically less important) ambiguity introduced by the absence of a conservation law for mesonic charge which will be discussed in Sec. II.

By analogy with electrodynamics, one would like to define the mesonic charge by one of the zero-energy phenomena discussed above, choosing the renormalized coupling constant in such a way that the rigorous matrix element becomes identical with the result of lowest-order perturbation theory. In a recent paper,[4] Kroll and Ruderman have shown how this may be done for the process of threshold photoproduction of charged mesons in the limit of vanishing meson mass. To carry out this program, they give very explicit instructions as to how the various finite functions of the theory are to be obtained, and any computations based on their coupling constant must be performed in accordance with their rules. As we have mentioned, such a procedure is only one of many possible and one of the purposes of the present paper is to discuss an alternative prescription.

A natural way to define g would appear to be (in analogy to Compton scattering) the scattering of zero-energy mesons by nucleons. This process has the virtue of involving only the nucleon and meson fields, and further is one in which the condition of zero four-momentum transfer is actually met. More specifically, we shall base our definition of g on the scattering of zero kinetic energy meson in the limit of vanishing meson mass, and insist that the rigorous matrix element in this limit be just the second order perturbation theory result with renormalized coupling constant and nucleon mass.

In order to do more than merely state this requirement on a renormalization procedure, we must develop a method for computing the exact matrix element for meson scattering in the limit of vanishing meson mass. We will then know what the consequences of our prescription are, that is what functions are absorbed into the definition of g. In Sec. II such a technique is developed. It is based on the ideas of Schwinger[5] and Feynman[6] who have shown that if the motion of a particle in external fields is known one may compute all relevant quantities by means of appropriate variational derivatives with respect to these fields.[7] In our case, since we are concerned with zero four-momentum transfer, we may specialize to a constant external field (which cannot transfer momentum) and thus replace the relevant variational derivatives by ordinary derivatives. A detailed discussion of the renormalization of the nucleon propagation function is given and a new method of renormalizing the meson vertex operator Γ_5 is presented. In Sec. III, an exact computation of meson nucleon scattering is carried out and the renormalized coupling constant is introduced. The appropriate generalization of our formalism to include electromagnetic effects is treated in Sec. IV, and is used to compute the threshold photoproduction of mesons. The well-known result[8] of the vanishing of radiative corrections to Compton scattering for zero-frequency photons is also rederived using our formalism. The various formal considerations in Secs. II, III, and IV are illustrated in detail by explicit perturbation theory computations of radiative corrections with the different renormalization prescriptions.

In Sec. V, we compare our general results with experiment. The meson scattering amplitude derived in Sec. III cannot be directly compared with experiment, since, of course, the meson mass is not zero. It has recently been pointed out,[9] however, that the general structure of the zero energy scattering amplitude is

$$R_{ji}=A\delta_{ji}+(\mu/M)[\tau_j,\tau_i]B, \tag{1.1}$$

where A and B are even functions of the meson mass which we assume are well behaved in the limit $\mu\to 0$. By our choice of mesonic charge renormalization we can compute A exactly in the limit of μ going to zero; hence, if we assume that the $(\mu/M)^2$ corrections to A

[2] J. C. Ward, Phys. Rev. **77**, 293 (1950); **78**, 182 (1950); **84**, 897 (1951).
[3] A. Thellung, Helv. Phys. Acta. **25**, 307 (1952).
[4] N. M. Kroll and M. A. Ruderman, Phys. Rev. **93**, 233 (1953).
[5] J. Schwinger, Proc. Natl. Acad. Sci. U. S. **37**, 452 (1951).
[6] R. P. Feynman, Phys. Rev. **80**, 440 (1950).
[7] The explicit formulation of the meson-nucleon problem in these terms has been given by S. Deser and P. Martin, Phys. Rev. **90**, 1075 (1953).
[8] W. Thirring, Phil. Mag. **41**, 1193 (1950); See also reference 4.
[9] M. Gell-Mann and M. L. Goldberger (to be published).

are negligible, knowing the S-wave scattering lengths, we can compute the coupling constant ($A(0)\sim g^2$). We do not assume that the masses of virtual mesons are zero. In fact, our considerations remain valid irrespective of the nature of the virtual particles, provided only that the various symmetry principles assumed are not violated by their presence. We find by this means coupling constants of at least an order of magnitude smaller than those previously considered in pseudoscalar theory. The significance of this result is discussed in relation to various suggested approximations to the theory and to its consistency with experiment. Finally, in the appendix, a technique is developed to compute μ/M corrections to the various functions in the theory and applied to obtain the form of the B in (1.1).

II. FORMAL THEORY

Consider the motion of a free nucleon in a constant symmetric pseudoscalar meson field, α_i. The Dirac equation (for a nucleon of four-momentum p) becomes

$$(i\gamma\cdot p+m+i\alpha\cdot\tau\gamma_5)\psi(p,\alpha)=0, \tag{2.1}$$

with the energy-momentum relation $p^2+m^2+\alpha^2=0$. The corresponding propagation function, $S(p,\alpha)$, is defined by

$$S^{-1}(p,\alpha)=i\gamma\cdot p+m+i\alpha\cdot\tau\gamma_5. \tag{2.2}$$

We observe that

$$\frac{1}{i}\frac{\partial}{\partial\alpha_j}S=-S\tau_j\gamma_5S, \tag{2.3}$$

and that consequently the interaction between a meson of zero four-momentum, charge index j, and a nucleon may be represented by differentiation of the propagation function with respect to α_j.

When the nucleon interacts with the quantized pseudoscalar meson field, $S(p,\alpha)$ is replaced by a modified propagation, $S'(p,\alpha)$. In view of Eq. (2.3), the effect of differentiating $S'(p,\alpha)$ with respect to α_j is equivalent to the interaction of the coupled nucleon with a zero four-momentum meson of charge j.[10] Similarly, its interaction with n such mesons may be obtained from the nth derivative of $S'(p,\alpha)$. This is a special case of the general variational derivative technique developed by Schwinger and others[5,6] in which variational derivatives may be replaced by ordinary derivatives.[11] Our method is somewhat analogous to use of the Ward trick[12] in quantum electrodynamics which has been extensively applied in connection with zero-frequency photon problems.

To proceed with our development we must exhibit the structure of the modified propagation function, $S'(p,\alpha)$, mentioned above. From invariance requirements, we conclude that the most general form may be written as

$$S'^{-1}(p,\alpha)=i\gamma\cdot pg_0+mf_0+i\alpha\cdot\tau\gamma_5d_0+i\gamma\cdot p\alpha\cdot\tau\gamma_5h_0, \tag{2.4}$$

where g_0, f_0, d_0, and h_0 are scalar functions of p^2, m^2, α^2, μ^2 and, of course, the masses of any virtual fields which may be coupled to the meson-nucleon fields. Whereas all four terms may be present from the standpoint of invariance with respect to the full Lorentz group, we may actually eliminate h_0 by utilizing another symmetry principle: an examination of the general perturbation theoretic expression for $S'^{-1}(p,\alpha)$ shows that

$$[S'^{-1}(-p,-\alpha)]^T=C^{-1}[S'^{-1}(p,\alpha)]C, \tag{2.5}$$

where C is the charge conjugation matrix augmented to act also in isotopic spin space, with the properties

$$C^{-1}\gamma_\mu C=-\gamma_\mu{}^T,\quad C^{-1}\gamma_5C=\gamma_5{}^T,\quad C^{-1}\tau C=-\tau^T. \tag{2.6}$$

(In the usual representation, $C=\gamma_4\gamma_2\tau_2$.) If we apply the requirement (2.5) to (2.4), we conclude that h_0 must be zero. Our propagation function is then[13]

$$S'^{-1}(p,\alpha)=i\gamma\cdot pg_0+mf_0+i\alpha\cdot\tau\gamma_5d_0. \tag{2.7}$$

As a result of the interaction between the nucleon and the quantized meson field we know that a free nucleon satisfying the modified Dirac equation,

$$S'^{-1}(p,\alpha)\psi'(p,\alpha)=0, \tag{2.8}$$

behaves as though it had an effective mass, different from m, and were moving in an external meson field different from α. Just as in electrodynamics it is convenient to introduce a mass renormalization so that a free, but "clothed," electron has the energy momentum relation $p^2+M^2=0$, with M the experimental mass, we shall introduce a renormalization of M and α. Our demand is that a free, but clothed, nucleon must satisfy

$$p^2+M^2+\alpha'^2=0. \tag{2.9}$$

This will be possible if M and α' are suitably defined. If one iterates the modified Dirac equation, (2.8), one obtains

$$[p^2g_0{}^2(p^2,\alpha^2)+m^2f_0{}^2(p^2,\alpha^2)+\alpha^2d_0{}^2(p^2,\alpha^2)]\psi'(p,\alpha)=0. \tag{2.10}$$

We may evidently satisfy the requirement (2.9) by choosing M and α' such that

$$\begin{aligned}g_0(-M^2-\alpha'^2,\alpha^2)&=(m/M)f_0(-M^2-\alpha'^2,\alpha^2)\\&=(\alpha/\alpha')d_0(-M^2-\alpha'^2,\alpha^2).\end{aligned} \tag{2.11}$$

We assume that these equations may be solved for M and α' in terms of m and α, or rather, as is usually done, imagine that m and α are expressed in terms of the renormalized quantities M and α'. We shall in the future

[10] This may be seen by noting that differentiation of any graph composing inserts the meson vertex in all possible ways.

[11] If we were to set the external field α equal to zero after all differentiations, our results would coincide with usual pseudoscalar theory; we are not, however, forced to put α equal to zero and for the time being will not do so.

[12] Reference 2. Its statement is that $-i\partial/\partial p_\mu\cdot S'^{-1}(p)=\Gamma_\mu{}^1(p,p)$.

[13] It might be noted that while $\{i\gamma p,\alpha\cdot\tau\gamma_5\}$ does satisfy the charge conjugation requirements, it is identically zero.

also regard M as a function of α'. It is convenient to introduce new functions in place of g_0, f_0, and d_0 according to the definitions

$$g(p^2,\alpha'^2)=g_0(p^2,m^2,\alpha^2);\quad f(p^2,\alpha'^2)=(m/M)f_0(p^2,m^2\alpha^2);$$
$$d(p^2,\alpha'^2)=(\alpha/\alpha')d_0(p^2,m^2,\alpha^2). \quad (2.12)$$

We have then

$$S'^{-1}(p,\alpha')=i\gamma\cdot pg(p^2,\alpha'^2)+Mf(p^2,\alpha'^2)+i\alpha'\cdot\tau\gamma_5 d(p^2,\alpha'^2), \quad (2.13)$$

and

$$g(-M^2-\alpha'^2,\alpha'^2)=f(-M^2-\alpha'^2,\alpha'^2)=d(-M^2-\alpha'^2,\alpha'^2)\equiv f. \quad (2.14)$$

Then for a free nucleon,

$$S'^{-1}(p,\alpha')=(i\gamma\cdot p+M+i\alpha'\cdot\tau\gamma_5)f. \quad (2.15)$$

Up to this point, we have been acting as though everything were finite in our theory. In practice, of course, the various functions g_0, f_0, and d_0 are divergent, and we must imagine a suitable cutoff to have been introduced so as to give meaning to our mass and α renormalizations. (It is worth pointing out that these particular renormalizations would be required even if the theory were completely convergent.) We wish now to extract the convergent part of our function S' just as is done in electrodynamics. We shall in fact follow the conventional procedure of Dyson[14] and Ward[2] except that we retain our α field, and state the procedure in a somewhat different manner. We remark that for a bare nucleon one may define a particle current density, χ_μ, (not to be confused with the conventional electric current density $j_\mu=ie\bar{\psi}\gamma_\mu\psi$) by

$$\chi_\mu(p,\alpha)=\bar{\psi}(p,\alpha)\gamma_\mu\psi(p,\alpha)=\bar{\psi}(p,\alpha)\left[\frac{1}{i}\frac{\partial}{\partial p_\mu}S^{-1}(p,\alpha)\right]\psi(p,\alpha). \quad (2.16)$$

The analogous quantity for a clothed nucleon is

$$\chi_\mu'(p,\alpha')=\bar{\psi}'(p,\alpha')\Gamma_\mu'(p,p,\alpha')\psi'(p,\alpha'), \quad (2.17)$$

where

$$\Gamma_\mu'(p,p,\alpha')\equiv\frac{1}{i}\frac{\partial}{\partial p_\mu}S'^{-1}(p,\alpha'). \quad (2.18)$$

In the limit as $\alpha'\to 0$, this becomes exactly the unrenormalized vertex operator of the usual theory (see Sec. IV). We now demand that after renormalization χ_μ' shall be numerically equal to the current density as computed from the renormalized spinors according to

$$\chi_\mu^{(c)}=\bar{\psi}_c(p,\alpha')\gamma_\mu\psi_c(p,\alpha'), \quad (2.19)$$

where ψ_c is a solution of

$$(i\gamma\cdot p+M+i\alpha'\cdot\tau\gamma_5)\psi_c(p,\alpha')=0, \quad (2.20)$$

and differs from ψ' by a constant factor. Physically, our requirement is that the particle current density of a one particle state is unmodified by interaction with the virtual field provided the appropriate adjustments of m and α are made. In the usual notation we write

$$\psi'(p,\alpha')=[Z_2(\alpha')]^{\frac{1}{2}}\psi_c(p,\alpha'),$$
$$\bar{\psi}'(p,\alpha')=[Z_2(\alpha')]^{\frac{1}{2}}\bar{\psi}_c(p,\alpha'), \quad (2.21)$$
$$S'(p,\alpha')=Z_2(\alpha')S_c(p,\alpha').$$

Our demand becomes

$$\bar{\psi}_c(p,\alpha')\Gamma_{\mu c}(p,p,\alpha')\psi_c(p,\alpha')=\bar{\psi}_c(p,\alpha')\gamma_\mu\psi_c(p,\alpha'), \quad (2.22)$$

where

$$\Gamma_{\mu c}=\frac{1}{i}\frac{\partial}{\partial p_\mu}S_c^{-1}(p,\alpha').$$

We have, carrying out the differentiation,

$$\Gamma_{\mu c}=Z_2(\alpha')[\gamma_\mu g-2ip_\mu(i\gamma\cdot pg'+Mf')+2\alpha'\cdot\tau\gamma_5 p_\mu d'], \quad (2.23)$$

where $g'=\partial g/\partial p^2$, etc. Using Eq. (2.20) and the elementary results deduced from it, namely,

$$\bar{\psi}_c(p,\alpha')\gamma_\mu\psi_c(p,\alpha')=(p_\mu/iM)\bar{\psi}_c(p,\alpha')\psi_c(p,\alpha'),$$
$$\bar{\psi}_c(p,\alpha')\tau_j\gamma_5\psi_c(p,\alpha')=(\alpha_j'/iM)\bar{\psi}_c(p,\alpha')\psi_c(p,\alpha'), \quad (2.24)$$

one finds

$$\bar{\psi}_c(p,\alpha')\Gamma_{\mu c}(p,p,\alpha')\psi_c(p,\alpha')=Z_2(\alpha')[f+2M^2(f'-g')+2\alpha'^2(d'-g')]\bar{\psi}_c\gamma_\mu\psi_c, \quad (2.25)$$

and all of the functions are to be evaluated at $p^2=-M^2-\alpha'^2$. Our requirement (2.22) fixes $Z_2(\alpha')$:

$$Z_2(\alpha')=[f+2M^2(f'-g')+2\alpha'^2(d'-g')]^{-1}. \quad (2.26)$$

In terms of new finite functions F, G, D, defined by

$$F=Z_2f,\quad G=Z_2g,\quad D=Z_2d, \quad (2.27)$$

our convergent propagation function $S_c(p,\alpha')$ becomes

$$S_c^{-1}(p,\alpha')=i\gamma\cdot pG(p^2,\alpha'^2)+MF(p^2,\alpha'^2)+i\alpha'\cdot\tau\gamma_5 D(p^2,\alpha'^2). \quad (2.28)$$

The unrenormalized meson vertex operator, $\Gamma_5'_j(p,p,\alpha')$, is defined by

$$\Gamma_{5j}'(p,p,\alpha')\equiv\frac{1}{i}\frac{\partial}{\partial\alpha_j}S'^{-1}(p,\alpha')=\frac{\partial\alpha_k'}{\partial\alpha_j}\{\tau_k\gamma_5 d-2i\alpha_k'\times[i\gamma\cdot p\dot{g}+M\dot{f}+\dot{M}f+i\alpha'\cdot\tau\gamma_5\dot{d}]\}, \quad (2.29)$$

where $\dot{g}=\partial g/\partial\alpha'^2$, etc. Using Eqs. (2.24) one finds immediately,

$$\bar{\psi}'(p,\alpha')\Gamma_{5j}'(p,p,\alpha')\psi'(p,\alpha')=\bar{\psi}'(p,\alpha')\tau_k\gamma_5\psi'(p,\alpha')\frac{\partial\alpha_k'}{\partial\alpha_j}\times\{d+2M\dot{M}f+2M^2(\dot{f}-\dot{g})+2\alpha'^2(\dot{d}-\dot{g})\}. \quad (2.30)$$

[14] F. J. Dyson, Phys. Rev. 75, 1736 (1949).

If we substitute for S' its expression in terms of S_c given in Eq. (2.21), we obtain

$$\Gamma_{5j}'(p,p,\alpha')=\frac{\partial\alpha_k'}{\partial\alpha_j}\frac{\Gamma_{5k_c}(p,p,\alpha')}{Z_2(\alpha')}+S_c^{-1}(p,\alpha')\frac{1}{i}\frac{\partial}{\partial\alpha_j}\frac{1}{Z_2(\alpha')}, \quad (2.31)$$

where we define the convergent vertex operator, $\Gamma_{5k_c}(p,p,\alpha')$, by

$$\Gamma_{5k_c}(p,p,\alpha')=\frac{1}{i}\frac{\partial}{\partial\alpha_k'}S_c^{-1}(p,\alpha'). \quad (2.32)$$

If we substitute (2.32) into the right-hand side of (2.31), and use Eqs. (2.21) to express the spinor amplitudes in terms of renormalized quantities and use (2.26) for $Z_2(\alpha')$, we find

$$\bar\psi_c(p,\alpha')\Gamma_{5k_c}(p,p,\alpha')\psi_c(p,\alpha')=\bar\psi_c(p,\alpha')\tau_k\gamma_5\psi_c(p,\alpha')\times\left\{\frac{f(1+2M\dot M)+2M^2(\dot f-\dot g)+2\alpha'^2(\dot d-\dot g)}{f+2M^2(f'-g')+2\alpha'^2(d'-g')}\right\}, \quad (2.33)$$

where all quantities are evaluated at $p^2=-M^2-\alpha'^2$ and we have used the fact that $d=f$ under this condition. Derivatives of the various functions $f(p^2,\alpha'^2)$, etc., with respect to p^2 and α'^2, evaluated at $p^2=-M^2-\alpha'^2$ can be related to each other using Eq. (2.14) which we rewrite very explicitly as

$$\begin{aligned}f[-M^2(\alpha'^2)-\alpha'^2,\alpha'^2]&=g[-M^2(\alpha'^2)-\alpha'^2,\alpha'^2],\\ d[-M^2(+\alpha'^2)-\alpha'^2,\alpha'^2]&=g[-M^2(\alpha'^2)-\alpha'^2,\alpha'^2].\end{aligned} \quad (2.34)$$

Differentiating with respect to α'^2, we find

$$\begin{aligned}(f'-g')(1+2M\dot M)&=\dot f-\dot g,\\ (d'-g')(1+2M\dot M)&=\dot d-\dot g.\end{aligned} \quad (2.35)$$

Thus Eq. (2.33) reduces to

$$\bar\psi_c(p,\alpha')\Gamma_{5k_c}(p,p,\alpha')\psi_c(p,\alpha')=(1+2M\dot M)\bar\psi_c(p,\alpha')\gamma_5\tau_k\psi_c(p,\alpha'). \quad (2.36)$$

The presence of the factor $\partial\alpha_k'/\partial\alpha_j$ in Eq. (2.31) and of $(1+2M\dot M)$ in Eq. (2.36) shows that even in the limit as $\alpha\to 0$, there is no analog of the Ward identity in meson theory. In terms of the finite functions F, G, and D defined in Eq. (2.27) there are two identities worth recording:

$$F+2M^2(F'-G')+2\alpha'^2(D'-G')=1, \quad (2.37)$$

$$F(1+2M\dot M)+2M^2(\dot F-\dot G)+2\alpha'^2(\dot D-\dot G)=1+2M\dot M. \quad (2.38)$$

These relations play a fundamental role in our later work.

Our renormalization procedure gives, in the limit of $\alpha\to 0$, precisely the same convergent propagation function $S_c(p)$ as would be computed by the conventional Dyson-Ward procedures. More precisely, our method can be shown to be exactly equivalent to casting S'^{-1} as given by (2.7) into the form

$$S'^{-1}(p,\alpha)=S^{-1}(p,\alpha')+AS^{-1}(p,\alpha')+S^{-1}(p,\alpha')BS^{-1}(p,\alpha'), \quad (2.39)$$

where $S^{-1}(p,\alpha')=i\gamma\cdot p+M+i\alpha'\cdot\tau\gamma_5$, A is a divergent function of M^2 and α'^2 and B is an operator involving $i\gamma\cdot p$, M, and $i\alpha'\cdot\tau\gamma_5$ which is nonsingular on the one-particle energy shell. A is related to $Z_2(\alpha')$ by the relation $Z_2^{-1}(\alpha')=1+A$. It is very important to notice that the convergent part of the vertex operator Γ_5, computed in our scheme, in general, differs from that computed by the usual procedure. As has been pointed out by Kroll and Ruderman, a precise statement of the conventional procedure is that

$$\lim_{p'\to p}\psi_c(p')\Gamma_{5j}(p',p)\psi_c(p)/\psi_c(p')\gamma_5\tau_j\psi_c(p)=1, \quad (2.40)$$

whereas our method is that detailed in Eqs. (2.31) and (2.36). The reason for the ambiguity at this point (which has nothing to do with the ambiguities of mesic charge renormalization discussed in Sec. I) is that as $\alpha\to 0$, the expectation value of γ_5 in a state of given momentum p vanishes; the usual procedure is based on the limit, as p' approaches p of $\bar\psi(p')\gamma_5\psi(p)$, whereas our method is based on considering the limit, as $\alpha'\to 0$, of $\bar\psi(p,\alpha')\gamma_5\psi(p,\alpha')$. These two limiting processes are entirely independent of each other. It is perhaps worth remarking that our procedure is well defined with a nonzero value of α', and consequently has the advantage of avoiding the ratio considerations [see Eq. (2.36)] of the usual method. In a sense, our renormalization scheme is not yet completely specified in that we have said nothing about what shall be called the renormalized coupling constant. A little consideration shows that this is a decision which can be reserved until a later time; the essential infinity to be absorbed in the coupling constant is evidently the quantity $\partial\alpha'/\partial\alpha$ (aside from the usual Z_3) and any finite multiple may be chosen at our convenience. We shall return to this point later on in Secs. III and IV.

Rather than go into detail and show how all divergences are removed in perturbation theory, which would essentially require a repetition of previous work,[15] we shall illustrate our method by a second-order perturbation calculation which will also be useful in later applications.

Using the standard Feynman techniques, the mass operator $\Sigma(p,\alpha)$ [which is related to S'^{-1} by the relation $S'^{-1}=S^{-1}-\Sigma(p,\alpha)$] is easily found to be (to order g^2,

[15] P. T. Matthews and A. Salam, Revs. Modern Phys. 23, 311 (1951).

and with the neglect of the mass of the virtual meson)

$$\Sigma(p,\alpha)=\lim_{\lambda\to\infty} ig^2\int\frac{d^4q}{(2\pi)^4}\frac{1}{q^2}\frac{\lambda^2}{q^2+\lambda^2}\gamma_5\tau_k \times[i\gamma\cdot(p-q)+m+i\alpha\cdot\tau\gamma_5]^{-1}\gamma_5\tau_k$$
$$=\lim_{\lambda\to\infty}\frac{(-g^2\lambda^2)}{(4\pi)^2}\int_0^1 dx\int_0^x dy \times\frac{3i\gamma\cdot p(1-y)+i\alpha\cdot\tau\gamma_5+3m}{\Lambda^2}, \quad (2.41)$$

where

$$\Lambda^2=(m^2+\alpha^2)y^2+\lambda^2(1-x)+(p^2+m^2+\alpha^2)y(1-y). \quad (2.42)$$

Reference to Eq. (2.7) shows that (dropping the explicit passage to the limit of the cutoff λ going to infinity)

$$f_0(p^2,\alpha^2)=1+\frac{3g^2}{(4\pi)^2}\lambda^2\int_0^1 dx\int_0^x dy\frac{1}{\Lambda^2},$$
$$g_0(p^2,\alpha^2)=1+\frac{3g^2}{(4\pi)^2}\lambda^2\int_0^1 dx\int_0^x dy\frac{1-y}{\Lambda^2}, \quad (2.43)$$
$$d_0(p^2,\alpha^2)=1+\frac{g^2}{(4\pi)^2}\lambda^2\int_0^1 dx\int_0^x dy\frac{1}{\Lambda^2}.$$

In the limit of α approaching zero, the various quantities that appear in our formalism can be calculated directly from (2.43). We summarize below some of the relevant ones:

$$M=m\left(1+\frac{3g^2\lambda^2}{(4\pi)^2}\int_0^1 dx\int_0^x dy\frac{y}{\Lambda_0^2}\right),$$
$$\frac{\partial\alpha_k'}{\partial\alpha_j}=\delta_{jk}\left(1+\frac{g^2\lambda^2}{(4\pi)^2}\int_0^1 dx\int_0^x dy\frac{3y-2}{\Lambda_0^2}\right),$$
$$Z_2(0)=1-\frac{3g^2\lambda^2}{(4\pi)^2}\int_0^1 dx\int_0^x dy\frac{1-y}{\Lambda_0^2}+\frac{3g^2}{(4\pi)^2},$$
$$1+2M\dot{M}=1-3g^2/(4\pi)^2,$$
$$F(p^2)=1+3g^2/(4\pi)^2 \quad (2.44)$$
$$+\frac{3g^2\lambda^2}{(4\pi)^2}\int_0^1 dx\int_0^x dy\left(\frac{1}{\Lambda^2}-\frac{1}{\Lambda_0^2}\right),$$
$$G(p^2)=1+3g^2/(4\pi)^2$$
$$+\frac{3g^2\lambda^2}{(4\pi)^2}\int_0^1 dx\int_0^x dy\left(\frac{1}{\Lambda^2}-\frac{1}{\Lambda_0^2}\right)(1-y),$$
$$D(p^2)=1+3g^2/(4\pi)^2$$
$$+\frac{g^2\lambda^2}{(4\pi)^2}\int_0^1 dx\int_0^x dy\left(\frac{1}{\Lambda^2}-\frac{1}{\Lambda_0^2}\right),$$

where $\Lambda_0^2=M^2y^2+\lambda^2(1-x)$ and Λ^2 is given by (2.42) with α set equal to zero and m replaced by M.

This simple procedure is to be compared with the usual[16] one in which one is required to cast the mass operator into the special form related to (2.39):

$$\Sigma(p,\alpha)=-\frac{g^2\lambda^2}{(4\pi)^2}\int_0^1 dx\int_0^x dy\left\{\frac{3my}{\Lambda_0^2}+i\alpha\cdot\tau\gamma_5\frac{3y-2}{\Lambda_0^2}\right.$$
$$+\frac{S^{-1}}{\Lambda_0^2}\left[3(1-y)-\frac{3m^2y^2(1-y)}{\Lambda_0^2}-\frac{(3y-2)y(1-y)2\alpha^2}{\Lambda_0^2}\right]$$
$$+S^{-1}\frac{y(1-y)}{\Lambda_0^2}\left[\frac{3(1-y)}{\Lambda_2}(i\gamma\cdot p+i\alpha\cdot\tau\gamma_5-m)\right.$$
$$\left.-\frac{3my+(3y-2)i\alpha\cdot\tau\gamma_5}{\Lambda^2}+\frac{6my}{\Lambda_0^2}\right]S^{-1}+\frac{S^{-1}y(1-y)^2}{\Lambda^2\Lambda_0^4}$$
$$\times[6my^2(i\gamma\cdot p+i\alpha\cdot\tau\gamma_5)-(3y-2)(2\alpha^2)]$$
$$\left.\times(i\gamma\cdot p+i\alpha\cdot\tau\gamma_5-m)S^{-1}\right\}.$$

III. APPLICATION TO MESON-NUCLEON SCATTERING

We shall now apply the techniques developed in Sec. II to the problem of meson-nucleon scattering. The first application will be a derivation of the exact scattering amplitude in the limit of zero kinetic energy and zero external meson mass. The result obtained will be compared in detail with a perturbation theoretic treatment of the same problem and the precise way in which radiative corrections disappear in our scheme will be exhibited.

The exact scattering amplitude, expressed entirely in terms of unrenormalized quantities, is given by[17]

$$T_{ji}=\phi_j'^{(-)}\phi_i'^{(+)}g_u^2\lim_{\alpha\to 0}\bar{\psi}'(p,\alpha')S'^{-1}(p,\alpha')$$
$$\times\left[\frac{1}{i^2}\frac{\partial^2}{\partial\alpha_j\partial\alpha_i}S'(p,\alpha')\right]S'^{-1}(p,\alpha')\psi'(p,\alpha'). \quad (3.1)$$

This is the scattering amplitude for the process: meson in charge state i going into meson in charge state j with the appropriate changes in the charge states of the nucleon of momentum p, in the limit of zero total energy mesons; g_u is the unrenormalized coupling constant. Carrying out the indicated differentiations and using the definition (2.29) we obtain

$$T_{ji}=\phi_j'^{(-)}\phi_i'^{(+)}g_u^2\lim_{\alpha\to 0}\bar{\psi}'(p,\alpha')\left\{\Gamma_{5j}'(p,p,\alpha')S'(p,\alpha')\right.$$
$$\times\Gamma_{5i}'(p,p,\alpha')+\Gamma_{5i}'(p,p,\alpha')S'(p,\alpha')\Gamma_{5j}'(p,p,\alpha')$$
$$\left.-\frac{1}{i}\frac{\partial}{\partial\alpha_j}\Gamma_{5i}'(p,p,\alpha')\right\}\psi'(p,\alpha'). \quad (3.2)$$

[16] See, for example, R. Karplus and N. M. Kroll, Phys. Rev. 77, 536 (1950).

[17] This is a special case of the general expression for the scattering amplitude given in reference 7 in terms of variational derivatives.

We now substitute for the unrenormalized quantities their expressions in terms of renormalized quantities. The only renormalization which has not yet been defined is that relating to the meson field.[18] This is, following the usual convention,

$$\phi' = (\sqrt{Z_3})\phi.$$

In order to avoid any possible ambiguity in the evaluation of (3.2), it is convenient to imagine that the momentum p of the internal nucleon lines is kept slightly different from the actual momentum $\dot{p}$ appearing in the spinors until α has been set equal to zero.

In carrying out the operations indicated in Eq. (3.2), the following facts should be borne in mind: (1) α', the renormalized external field, must be an odd function of α since it is a pseudoscalar; consequently in the limit as $\alpha \to 0$, $\partial\alpha_i'/\partial\alpha_j \sim \delta_{ij}$ and we shall write the coefficient of δ_{ij} as simply $\partial\alpha'/\partial\alpha$. (2) The renormalization constant $Z_2(\alpha')$ is a function of α'^2 alone and therefore $\partial Z_2/\partial\alpha'$ is zero in the limit as $\alpha \to 0$. (3) As $\alpha \to 0$, the expectation value of γ_5 approaches zero. Using Eqs. (2.29) and (2.31) to evaluate Eq. (3.2) we obtain

$$T_{ji} = \phi_j^{(-)}\phi_i^{(+)} Z_3 g_u^2 \left(\frac{\partial\alpha'}{\partial\alpha}\right)^2_{\alpha=0} \bar{\psi}_e(p)$$
$$\times\{2\delta_{ij}F^2\gamma_5 S_c(p)\gamma_5 + 2\delta_{ij}(M\dot{F}+F\dot{M}+M\dot{G})\}\psi_e(p). \quad (3.3)$$

[We have set $D(-M^2-\alpha'^2) = F(-M^2-\alpha'^2)$ since we may now go on to the energy shell.] Recalling that on the energy shell with $\alpha = 0$, $S_c(p) = F^{-1}(i\gamma\cdot p + M)^{-1}$ and that $\bar{\psi}_c\gamma_5(i\gamma\cdot p + M)^{-1}\gamma_5\psi_c = (2M)^{-1}\bar{\psi}_c\psi_c$, we have

$$T_{ji} = \phi_j^{(-)}\phi_i^{(+)} Z_3 g_u^2 \left(\frac{\partial\alpha'}{\partial\alpha}\right)^2_{\alpha=0} \frac{\delta_{ij}}{M}\bar{\psi}_e(p)$$
$$\times\{F(1+2M\dot{M}) + 2M^2(\dot{F}-\dot{G})\}\psi_e(p). \quad (3.4)$$

By using (2.38), this result may be written as

$$T_{fi} = \phi_j^{(-)}\phi_i^{(+)}(g_s\delta_{ij}/M)\bar{\psi}_e(p)\psi_e(p), \quad (3.5)$$

where we have defined the renormalized coupling constant g_s^2 to be

$$g_s^2 = g_u^2 Z_3 \left(\frac{\partial\alpha'}{\partial\alpha}\right)^2_{\alpha=0} (1+2M\dot{M}). \quad (3.6)$$

The scattering amplitude as given by Eq. (3.5) is identical with the result of second-order perturbation theory in the limit of zero meson mass with, of course, the replacement of the unrenormalized coupling constant and nucleon mass by the renormalized quantities. The significance of this result will be discussed in Sec. V.

In order to illustrate our formal procedure in detail we present in Table I a summary of the calculation of the same process in second-order perturbation theory.

[18] One may speculate that there exists a close connection between $\sqrt{Z_3}$ and $(\partial\alpha'/\partial\alpha)$ since both are meson field renormalizations.

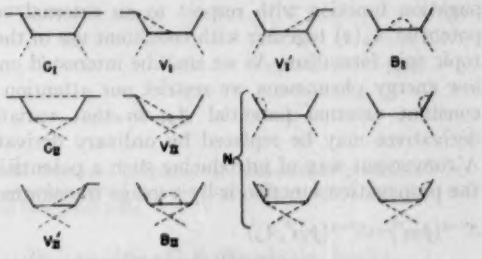

FIG. 1. Feynman diagrams for meson-nucleon scattering. Nucleons are represented by solid lines, mesons by dashed lines.

The appropriate Feynman diagrams are shown in Fig. 1. The calculation is completely standard and one need only use the values of F, G, D, M, and α' given in Sec. II to carry out the evaluation. The results of the conventional procedure of calculating the scattering are also given in Table I.

In the appendix we derive an expression for the μ/M corrections to the scattering amplitude in terms of quantities which can be computed (in principle) from the theory.

IV. THE THREE-FIELD PROBLEM

Having established a method to handle the meson-nucleon problem, and settled upon a renormalization scheme, we now turn to the more involved three-field situation.

We begin by suitably generalizing the technique developed in Sec. II in order to include interactions with the electromagnetic field. The construction of the electric current operator, $j_\mu = ie\bar{\psi}\Gamma_\mu\psi$, is complicated by the fact that charge is exchanged between the meson field and the nucleon. As will be seen in more detail below, the difficulty is not due to the virtual meson field but rather to the charge bearing external field. The direct use of the vertex operator, $\Gamma_\mu(\dot{p},\dot{p})$, as defined in Eq. (2.18) does not provide us with the desired quantity. The appropriate electric current vertex operator Γ_μ can be constructed by variational differentiation of the pro-

TABLE I. Lowest order corrections to meson-nucleon scattering.[a]

Method	Contribution	Type of graph			
		C_I+C_{II}	V_I+V_{II}	$V_I'+V_{II}'$	$B_I+B_{II}+N$
α formalism	Finite	-6	0	0	3
	Infinite	0	1	1	$6y-6$
Conventional	Finite renorm.	0	7/6	7/6	6
	Infinite renorm.	0	1	1	$6y-6$
	Finite correction	-6	2	2	-3

[a] All finite terms are multiplied by $g^6/(4\pi)^3$, all infinite ones by $[g^6/(4\pi)^3]\cdot\int_0^1 dx\int_0^x dy\lambda^2/[m^2y^2+\lambda^2(1-x)]$, both times the lowest order matrix element. Types of graph refer to Fig. 1. It will be noted that the sum of all terms in the α formalism is precisely $(\partial\alpha'/\partial\alpha)^3(1+2M\dot{M})$ to this order, as can be seen from Eq. (2.44). The infinite contributions, but not the finite ones, are the same in each column for both methods; the conventional method yields finite corrections to scattering. Effects from vacuum polarization, giving rise to an over-all Z_3 factor, have been omitted.

pagation function with respect to an external vector potential $A_\mu(x)$ together with consistent use of the isotopic spin formalism. As we shall be interested only in low energy phenomena we restrict our attention to a constant external potential A_μ, so that variational derivatives may be replaced by ordinary derivatives. A convenient way of introducing such a potential into the propagation function is by a gauge transformation:

$$S'^{-1}(p,\alpha')\to S'^{-1}(p,\alpha',A_\mu) = \exp(i\$)S'^{-1}(p,\bar\alpha')\exp(-i\$), \quad (4.1)$$

where

$$\$=\tfrac{1}{2}(1+\tau_3)x_\mu A_\mu, \quad (4.2)$$

$$\bar\alpha'\cdot\tau=\exp(-i\$)\alpha'\cdot\tau\exp(i\$),$$

and x_μ is to be interpreted as a differential operator, $i\partial/\partial p_\mu$. In the absence of the external meson potential α, the sole effect of the transformation $\$$ would have been to replace p_μ by the gauge invariant combination $p_\mu-\frac{1}{2}(1+\tau_3)A_\mu$; this must still be true in the more general case, hence the replacement of α' by $\bar\alpha'$. Since the transformation is a rotation in isotopic spin space, α'^2, a scalar, is of course equal to $\bar\alpha'^2$.

At this point we must recall that, of the terms permitted by invariance and charge conjugation considerations in $S'^{-1}(p,\alpha')$, one, having the form $\{i\gamma\cdot p, i\alpha'\cdot\tau\gamma_5\}h$ was identically zero. Such is no longer the case when α' is replaced by $\bar\alpha'$, since $\bar\alpha'$ and p no longer commute, and this term must be reinstated. Further, the term $i\bar\alpha'\cdot\tau\gamma_\mu d$ must now be properly symmetrized because $\bar\alpha'$ and d do not commute. Therefore, according to Eq. (4.1) and the above remarks, our complete propagation function becomes

$$S_c^{-1}(p,\alpha',A)=\exp(i\$)\Big[i\gamma\cdot pG(p^2,\alpha'^2)+MF(p^2,\alpha'^2) + \frac{i\gamma_5}{2}\{\bar\alpha'\cdot\tau,D(p^2,\alpha'^2)\} + \frac{1}{4}\Big\{H,\Big\{\frac{i\gamma\cdot p}{M},i\bar\alpha'\cdot\tau\gamma_5\Big\}\Big\}\Big]\exp(-i\$). \quad (4.3)$$

(None of the renormalization considerations of Sec. II are affected since $\alpha'^2=\bar\alpha'^2$, so we discuss only the convergent function.) We now define the electric current vertex operator $\Gamma_{\mu c}(p,p,\alpha',A)$ as follows:

$$\Gamma_{\mu c}(p,p,\alpha',A)=i\frac{\partial S_c^{-1}}{\partial A_\mu}=\exp(i\$)\Big[\frac{1+\tau_3}{2}\gamma_\mu G-\frac{1+\tau_3}{2}2ip_\mu \times(i\gamma\cdot pG'+MF')+\gamma_5 p_\mu D'(\bar\alpha_3'+\bar\alpha'\cdot\tau) + \frac{iH}{4M}\gamma_\mu\gamma_5[\tau_3,\bar\alpha'\cdot\tau]+\frac{1+\tau_3}{2}2ip_\mu\frac{H'}{4M} \times\{i\gamma\cdot p,i\bar\alpha'\cdot\tau\gamma_5\}\Big]\exp(-i\$). \quad (4.4)$$

In the limit as α' and A_μ approach zero, $\Gamma_{\mu c}(p,p)$ is indeed given by $\frac{1}{2}(1+\tau_3)(\partial/i\partial p_\mu)S_c^{-1}(p)$ and is thus [except for the factor $\frac{1}{2}(1+\tau_3)$] the same as the $\Gamma_\mu(p,p)$ of Sec. II. The actual vertex operator in the presence of the α field is, of course, the limit of Eq. (4.4) as $A_\mu\to0$; the complications introduced by the external field are evident.

The meson vertex operator $\Gamma^5 j_c(p,p,\alpha',A)$ is defined as before as the derivative of S_c^{-1} with respect to $i\alpha_j'$. In the limit of $A_\mu\to0$, it approaches (2.32).

We may remark at this point that the transition matrix element for the zero frequency Compton effect on a nucleon may be written as

$$T_{\lambda\lambda_0}=e_0^2A_\mu'^{(-)}(\lambda)\bar\psi'(p)\lim_{A\to0}\Big[S'^{-1}(p)\Big\{i^2\frac{\partial^2}{\partial A_\mu\partial A_\nu}S'(p)\Big\} \times S'^{-1}(p)\Big]\psi'(p)A_\nu'^{(+)}(\lambda_0), \quad (4.5)$$

where λ,λ_0 are polarization indices, e_0 is the unrenormalized electric charge, $A'^{(\pm)}$ are the unrenormalized amplitudes of the photons. The external meson field may be set equal to zero, consequently there are no isotopic spin complications. An over-all factor of $\frac{1}{2}(1+\tau_3)$ insures that in the limit of zero frequency, the light scattering from a neutron vanishes. For a proton, $\frac{1}{2}(1+\tau_3)=+1$ and the derivatives with respect to the external field A may be replaced by derivatives with respect to the momentum p, i.e., $\partial/\partial(-iA_\mu)=\partial/\partial ip_\mu$. To evaluate Eq. (4.7) we replace the unrenormalized quantities by renormalized ones, noting that all $Z_2(0)$'s cancel out and that as far as the photon amplitudes are concerned, we must take $e_0A'=e_1A$, where e_1 and A are the renormalized quantities. Using (4.4), with α' and A equal to zero, and choosing a transverse gauge to describe the photons, so that all terms proportional to p_μ vanish, we find for $T_{\lambda\lambda_0}$ the result:

$$T_{\lambda\lambda_0}=\frac{e_1^2}{M}A_\mu^{(-)}(\lambda)A_\mu^{(+)}(\lambda_0) \times[F+2M^2(F'-G')]_{p^2=M^2}\bar\psi_c(p)\psi_c(p) =\frac{e_1^2}{M}A_\mu^{(-)}(\lambda)A_\mu^{(+)}(\lambda_0)\bar\psi_c(p)\psi_c(p). \quad (4.6)$$

The last step follows from Eq. (2.37). This is not a new result and has been included simply to show precisely how it comes out in our formalism, which differs in detail from the earlier work of Thirring and of Kroll and Ruderman.

We turn now to the problem of threshold photomeson production in the limit of vanishing meson mass, the problem discussed by Kroll and Ruderman. There is

one slight complication in this process which must be considered before we can perform the explicit calculation. We must allow for the interaction between the electromagnetic field (photon) and the meson produced. We shall not go into this question exhaustively because, as will be seen, the meson current contributions vanish at threshold. If the propagation function for a meson of four-momentum q, $\Delta_{ij}'(q)$, (i and j are isotopic spin indices) is known, the effect of a constant vector potential may be introduced conveniently by a gauge transformation:

$$\Delta_{ij}'(q,A)=(e^{iTx\cdot A}\Delta'(q)e^{-iTx\cdot A})_{ij}, \tag{4.7}$$

where T is the matrix

$$T=\begin{bmatrix} 0 & 1 & 0 \\ -1 & 0 & 0 \\ 0 & 0 & 0 \end{bmatrix}, \tag{4.8}$$

and x_μ is to be interpreted as $i\partial/\partial q_\mu$. The transition matrix $T_{j\lambda}$ for the threshold photo production of a meson of isotopic spin j by a photon of polarization λ in the limit of vanishing meson mass, is given by

$$T_{j\lambda}=e_0g_u\lim_{\alpha,q_\mu,A_\mu\to 0}\bar{\psi}'(p,\alpha')\phi_k'^{(-)}(j)S'^{-1}(p,\alpha',A)\times\Delta_{kl}'^{-1}(q,A)\left\{\frac{\partial}{\partial A_\mu}\left[\frac{\partial S'(p,\alpha',A)}{\partial\alpha_n}\Delta_{ln}'(q,A)\right]\right\}\times S'^{-1}(p,\alpha',A)A_\mu'^{(+)}(\lambda)\psi'(p,\alpha'). \tag{4.9}$$

All repeated indices in Eq. (4.9) are to be summed over; in the subsequent equations our notation will be less specific, e.g., $\phi_k(j)$ will be set simply equal to ϕ_j as was done in Sec. III. We now remark that the term arising from the meson current, i.e., from the derivative of Δ_{ln}', vanishes in our limit since, by invariance, it can only be proportional to q_μ.[19] In terms of our previously defined vertex operators, we may write this as

$$T_{j\lambda}=e_0g_u\lim_{\alpha,q_\mu,A_\mu\to 0}\bar{\psi}'(p,\alpha')\phi_j'^{(-)}[\Gamma_{kj}'S'\Gamma_\mu'+\Gamma_\mu'S'\Gamma_{kj}'-\partial^2S'^{-1}/\partial\alpha_j\partial A_\mu]\psi'(p,\alpha')A_\mu'^{(+)}(\lambda). \tag{4.10}$$

The arguments of the vertex operators are all p, p, α', A and of the propagation function p, α', A [see Eqs. (4.3) and (4.4)]. The renormalized functions may now be introduced in the usual way. The third term in (4.10) makes the contribution

$$\frac{\partial^2S_c^{-1}}{\partial\alpha_j\partial A_\mu}=\left(\frac{\partial\alpha'}{\partial\alpha}\right)\frac{1}{2M}\gamma_\mu\gamma_5(\tau T)_jH, \tag{4.11}$$

where $(\tau T)_j=\tau_iT_{ij}$. The first two terms yield (aside from a factor of $\partial\alpha'/\partial\alpha$), in the limit as α, A approach zero, $(i/2)(\gamma_\mu\gamma_5/M)(\tau T)_jF$. We obtain, finally,

$$T_{j\lambda}=e_1g_u\left(\frac{\partial\alpha'}{\partial\alpha}\right)_{\alpha=0}Z_3^{\frac{1}{2}}(F+H)\phi_j^{(-)}A_\mu^{(+)}(\lambda)\bar{\psi}_c(p)\frac{i}{2M}\times\gamma_\mu\gamma_5(\tau T)_j\psi_c(p).$$

If we were to choose our renormalized coupling constant to be

$$g_{j'}=(\partial\alpha'/\partial\alpha)Z_3^{\frac{1}{2}}(F+H)g_u, \tag{4.13}$$

we would obtain no finite correction to the photoproduction amplitude. The numerical value of g_P, obtained by comparison with experiment is of course the same as that found by Kroll and Ruderman. It should be carefully borne in mind, however, that the precise structure of g_P, regarded as a theoretically calculable quantity, is dependent on the procedure followed in carrying out the meson vertex renormalizations. The form given in Eq. (4.13) is what results from using our computational schemes throughout. This point has been discussed at the end of Sec. II and is illustrated in detail in Table II where an explicit comparison between the two procedures is presented. The appropriate Feynman diagrams are shown in Fig. 2.

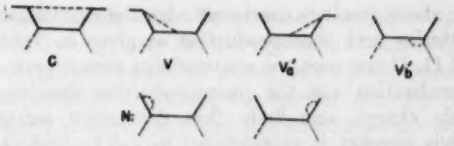

FIG. 2. Feynman diagrams for photomeson production. Nucleons are represented by solid lines, mesons by dashed lines, and photons by dotted lines.

The relation between the coupling constants g_s [defined in Eq. (3.6)] and g_P is seen to be

$$g_s^2/g_P^2=(1+2M\dot{M})(F+H)^{-2}. \tag{4.14}$$

Computing these functions in lowest order perturbation theory, we get for this ratio:

$$g_s^2/g_P^2=1-5g_s^2/16\pi^2. \tag{4.15}$$

TABLE II. Lowest-order corrections to photomeson production.[a]

Method	Contribution	Type of graph C	V	$V_a'+V_b'$	B	N
α formalism	Finite	−2	0	0	0	3
	Infinite	0	1	−3y+3	3y−3	3y−3
Conventional	Finite renorm.	0	7/6	−3	3	3
	Infinite renorm.	0	1	−3y+3	3y−3	3y−3
	Finite correction	−2	2	1+2	−3	0

[a] All finite terms are multiplied by $g^2/(4\pi)^2$; all infinite ones by $[g^2/(4\pi)^2]\cdot\int_0^1dx\int_0^xdy\lambda^2/[m^2y^2+(1-x)\lambda^2]$, both times the lowest order matrix element. Types of graph refer to Fig. 2. It can be seen that there are no net corrections in the conventional method. The infinite contributions are the same in both cases, but there is a finite correction in the α formalism, as the first two lines do not add up to $(\partial\alpha'/\partial\alpha)(1+2M\dot{M})^{\frac{1}{2}}$ but rather to $(\partial\alpha'/\partial\alpha)(F+H)$. Vacuum polarization effects have been omitted.

[19] M. Kroll and M. A. Ruderman have shown more generally that the outgoing meson current does not contribute to threshold production.

The above result is consistent with the calculations of scattering and photoproduction as given in Tables I and II. If one uses the conventional meson vertex renormalization and the photoproduction definition of mesic charge, one finds that the meson scattering matrix element is proportional to $g_P^2(1-5g_P^2/(4\pi)^2)$, which (to this order) is just equal to g_s^2. Similarly, if one calculates photomeson production with our vertex renormalization and uses the meson scattering definition of mesonic charge, one obtains a matrix element proportional to $g_s[1+5/2g_s^2(4\pi)^2]$, which is just equal to g_P by Eq. (4.15).

V. COMPARISON WITH EXPERIMENT AND DISCUSSION

We may now compare the various results obtained in the previous sections with experiment. First, we shall determine the value of our renormalized coupling constant, and second, we shall investigate, in so far as it is possible, whether or not the resultant theory is in agreement with experimental data.

The general expression for the scattering matrix describing the forward scattering of a meson of four-momentum q by a nucleon of four-momentum p is[9]

$$T_\mu=\frac{g_s^2}{2M}\left\{2\delta_{j\mu}A(q^2/M^2,\mu^2/M^2)-\frac{p\cdot q}{2M^2}[\tau_i,\tau_j]B(q^2/M^2,\mu^2/M^2)\right\}, \quad (5.1)$$

where we do not write the various field amplitudes explicitly. We have written the functions A and B with two arguments to emphasize that the external and internal meson masses need not be assumed equal. Designating temporarily the external meson mass by μ', we obtain, for zero energy, the scattering lengths corresponding to isotopic spin states 3/2 and 1/2:

$$\begin{aligned} a_{\frac{3}{2}}&=-\frac{g_s^2}{4\pi M}\left\{A\left(\frac{\mu'^2}{M^2},\frac{\mu^2}{M^2}\right)+\frac{\mu'}{2M}B\left(\frac{\mu'^2}{\mu^2},\frac{\mu^2}{M^2}\right)\right\},\\ a_{\frac{1}{2}}&=-\frac{g_s^2}{4\pi M}\left\{A\left(\frac{\mu'^2}{M^2},\frac{\mu^2}{M^2}\right)-\frac{\mu'}{2M}2B\left(\frac{\mu'^2}{M^2},\frac{\mu^2}{M^2}\right)\right\}. \end{aligned} \quad (5.2)$$

In our renormalization scheme, $A(0,\mu^2/M^2)=1$; if we assume that $A(\mu'^2/M^2,\mu^2/M^2)$ may be approximated by $A(0,\mu^2/M^2)$, we may solve Eqs. (5.2) for $g_s^2/4\pi$ and B. Little can be said as to the reliability of such an approximation. In lowest order perturbation theory A is $[1-\mu'^2/4M^2]^{-1}$, so that the approximation is very good. As far as higher terms are concerned, the numerical value of the corrections depends on the size of the coupling constant. In the appendix, a formal expression for $B(0,\mu^2/M^2)$ will be derived.

Before going on to the experimental determination of $g_s^2/4\pi$ by means of Eqs. (5.2), attention must be drawn to one point concerning the definition of g_s^2. It will be recalled that there appeared in this definition (aside from inherently positive factors) the quantity $(1+2M\dot{M})$. Its behavior as a function of M and g_s is, of course, unknown in practice. This is in contradistinction to electrodynamics where the theory is known to predict a definite sign for the Compton scattering amplitude. If it were possible to obtain the sign of $(1+2M\dot{M})$, then a severe test of the theory could be made with just the scattering data, as the signs of the scattering lengths are known. That is, a direct contradiction could exist with experiment if the predicted sign turned out to be wrong. We have not been able to determine the sign of $(1+2M\dot{M})$, however, and will therefore take it as dictated by experiment.

Unfortunately there do not exist measurements of meson-nucleon scattering cross sections at sufficiently low energies to permit an unambiguous extrapolation to zero energy. Fermi and Steinberger have each given extrapolated scattering lengths based on analyses of the data for scattering at energies greater than about 40 Mev. These sets have both been adjusted to agree with the π^- capture data.[20] This effect relates charge-exchange scattering and photoproduction at zero energy and leads to the requirement that

$$|a_{\frac{3}{2}}-a_{\frac{1}{2}}|=0.17/\mu. \quad (5.3)$$

(a) Fermi[21] gives $a_{\frac{3}{2}}=-0.11/\mu$, $a_{\frac{1}{2}}=0.06/\mu$. This implies that $g_s^2/4\pi=0.36$, taking $1+2M\dot{M}>0$.

(b) Steinberger[22] gives $a_{\frac{3}{2}}=0$, $a_{\frac{1}{2}}=+0.17/\mu$. This leads to $g_s^2/4\pi=+0.37$. Here, however, we had to take $1+2M\dot{M}<0$.

Recent preliminary observations at Columbia on π^- scattering at 7 Mev, however, imply that $g_s^2/4\pi$ may be perhaps as large as 1 or 2.[23]

It seems striking that all the above results yield far smaller $g_s^2/4\pi$ than usually employed for the pseudoscalar coupling constant, and in particular far smaller than the value of 25 one obtains for $g_P^2/4\pi$ by adjusting it to agree with the photomeson production data.[24] We obtain very small values for $g^2/4\pi$ since our renormalization scheme is based on matching the s-wave scattering amplitudes which are experimentally of the order of $1/M$, just the size of the Born approximation amplitudes if $g^2/4\pi$ is about unity.

It is frequently claimed[25] that the large values of the

[20] Panofsky, Aamodt, Hadley, and Phillips, Phys. Rev. **80**, 94 (1950).

[21] E. Fermi (private communication).

[22] J. Steinberger (private communication).

[23] Cornelius, Sargent, Rinehart, Lederman, and Rogers, Phys. Rev. **92**, 1583 (1953).

[24] It may be mentioned that with a pseudovector coupling theory (assuming that the theory exists in some sense) the renormalization to the meson scattering experiment would lead to a pseudovector coupling constant f_s equal (since this is the lowest order perturbation theory requirement) to our g_s. This is to be contrasted with the photomeson situation where one has the equivalence relation $f_P=g_P(\mu/2M)$. Thus, whereas we had previously had $g_P>g_s$, in this new situation one would have $f_s\geq f_P$.

[25] S. Drell and E. Henley, Phys. Rev. **88**, 1053 (1952); G. Wentzel, Phys. Rev. **86**, 802 (1953).

coupling constant which are presumably needed to explain the p wave meson scattering can still yield the correct s scattering at low energies, provided one computes more accurately than Born approximation. This belief is based on the observation that the scattering length obtained from an interaction of the form $g^2\phi^2/2M$ (which is supposed to represent, for low energies, the s wave interaction in pseudoscalar theory) is, for $g^2/4\pi \gg 1$, given by the cut-off radius independent of $g^2/4\pi$. It should be pointed out that the analogous procedure in electrodynamics, in the problem of low-frequency Compton scattering (where the interaction is described by $e^2A^2/2M$) would again lead for large e^2 to a scattering length which does not exceed the cut-off radius. However, as we have seen, the exact value predicted by the theory is e^2/M, regardless of the size of e^2. This seems to indicate that the use of just the ϕ^2 part of the equivalent pseudoscalar interaction may well be incorrect.

The expectation that one would find small s scattering in an accurate treatment of pseudoscalar theory due to suppression of pair effects[26] is belied by the observation that the damping introduced through the propagation function is (for low energies) precisely cancelled by the vertex operator. It is easy to show, using the results of Sec. II that the following equations[27] are true:

$$\begin{aligned} S_c(p)\Gamma^{\delta j_c}(p,p)\psi_c(p) &= S(p)\tau_j\gamma_0\psi_c(p), \\ \bar{\psi}_c(p)\Gamma^{\delta j_c}(p,p)S_c(p) &= \bar{\psi}_c(p)\tau_j\gamma_0 S(p). \end{aligned} \tag{5.4}$$

These results do not depend upon our choice of the coupling constant.

Two alternative renormalization methods exist, as we have seen, corresponding to fixing the coupling constant by two different experiments. If the theory is assumed to be consistent with both experiments, then the method of renormalization yielding the smaller coupling constant may well be of considerable practical use; it effectively re-sums the series in such a way that the expansion in powers of the renormalized coupling constant may have some significance, albeit perhaps only in an asymptotic sense. If, however, one computes in perturbation theory, using our small values of $g_s^2/4\pi$, the threshold photomeson production, one obtains disagreement with experiment by at least an order of magnitude. If one uses the value $g_s^2/4\pi \sim \frac{1}{3}$, the terms in the series are decreasing very rapidly; with $g_s^2/4\pi \sim 2$, the decrease is so slow that one cannot say much.[28]

It is evidently desirable to obtain accurate experimental data on very low energy meson scattering. If the coupling constant as determined by scattering is indeed as small or perhaps even smaller than the value of about $\frac{1}{3}$ given by the Fermi and Steinberger extrapolations, the outlook for pseudoscalar meson theory with pseudoscalar coupling seems dim.

In conclusion, it is to be emphasized that all of our numerical results have been based on the assumption that $A(0,\mu^2/M^2)$ is a good approximation to $A(\mu'^2/M^2, \mu^2/M^2)$. Very little can be said at present as to the legitimacy of the assumption. On the other hand, if such a small quantity as $(\mu/M)^2$ is not negligible, it is difficult to see what can be neglected in any given calculation within the theory. Perturbation theory calculations indicate that (with our small coupling constants) the error is small, but this point deserves further study.

ACKNOWLEDGMENTS

We are indebted to Dr. N. M. Kroll and Dr. M. A. Ruderman for sending us a preprint of their paper, and to Dr. Kroll for several enlightening discussions. We have also benefited from conversations with Dr. G. Källén and with Dr. R. Oppenheimer. Thanks are due Drs. E. Fermi and J. Steinberger for discussions of current experiments. Two of us (S.D. and W.T.) are grateful to the Institute for Advanced Study for grants-in-aid, and to Dr. Oppenheimer for the hospitality extended to us at the Institute.

APPENDIX

The evaluation of the μ/M terms, that is of $B(0,\mu^2/M)$ in the notation of Sec. V, breaks naturally into two separate parts, namely those diagrams in which there is at least one free nucleon line (aside from the external meson lines), and those for which there is never a free nucleon line. (The general structure of the scattering amplitude is of this form as can be seen from the exact expression given by Deser and Martin.[7]) Since we are still interested in the scattering amplitude at zero kinetic energy, it is sufficient to calculate the scattering amplitude in the forward direction, the scattering being entirely in s states. Let us take the two classes of terms referred to above separately.

The total contribution of the first class to the forward scattering amplitude (for a meson of initial and final four-momentum q) is given exactly by

$$\begin{aligned} T_{ji}^{(1)} = \phi_j'^{(-)}\phi_i'^{(+)} g_u^2 \lim_{\alpha\to 0} \bar{\psi}'(p,\alpha') \\ \times\{\Gamma_{sj}'(p,p+q,\alpha')S'(p+q,\alpha')\Gamma_{si}'(p+q,p,\alpha') \\ +\Gamma_{si}'(p,p-q,\alpha')S'(p-q,\alpha')\Gamma_{sj}'(p-q,p,\alpha')\} \\ \times\psi'(p,\alpha'). \end{aligned} \tag{A.1}$$

---

[26] Brueckner, Gell-Mann, and Goldberger, Phys. Rev. **90**, 476 (1953).

[27] Equations (5.4) are analogous to the results of Kroll and Ruderman for $S_c\Gamma_\mu$ and bear out their conjectures as to the behavior of products like $S_c\Gamma_s$.

[28] It is clear that a perturbation calculation of meson-nucleon scattering using $g_s^2/4\pi \approx \frac{1}{3}$ fails to reproduce the nonzero energy data. On the other hand, a similar calculation of the π^0 lifetime does agree with the observed value. With $g_s^2/4\pi \approx 2$, the apparent convergence is again too slow to enable one to reach any conclusions.

This expression is correct for any value of q; we shall, however, in the following keep only the zero and first order terms in q. The zero-order term yields, of course, the first two terms in Eq. (3.2) and essentially requires no further discussion. In order to proceed with the evaluation, we must derive expressions for the Γ_5's of unequal arguments. The S_F''s present no difficulty since we have an explicit expression for them which may be expanded in a straightforward way. It is sufficient to work with the first term in (A.1) since the second follows by interchanging i and j and replacing q by minus q. Since there are no differentiations with respect to α to be performed, we may safely pass to the limit $\alpha\to 0$ and retain only the obviously non-vanishing terms. Expressing everything in terms of the renormalized quantities we have for the portion under discussion the following:

$$t_{ji}=\phi_j^{(-)}\phi_i^{(+)}g_u^2\left(\frac{\partial\alpha'}{\partial\alpha}\right)^2_{\alpha=0}Z_3\bar{\psi}_c(p)$$
$$\times\{\Gamma_{5j}(p,p+q)S_c(p+q)\Gamma_{5i}(p+q,\,p)\}\psi_c(p). \quad \text{(A.2)}$$

(We have dropped the subscript c from the renormalized vertex operators.) We may write $S_c(p+q)$ explicitly as

$$S_c(p+q)=\frac{MF[(p+q)^2]-i\gamma\cdot(p+q)G[(p+q)^2]}{(p+q)^2G^2[(p+q)^2]+M^2F^2[(p+q)^2]}. \quad \text{(A.3)}$$

By using the facts that $p^2=-M^2$ and $q^2=-\mu^2$, $S_c(p+q)$ may easily be expanded in powers of q. It is necessary to keep only terms which are quadratic in q in both numerator and denominator; although one does not obtain in this way all of the terms linear in q, those which are omitted make no contribution to the matrix element. Designating derivatives of F and G with respect to p^2, evaluated at $P^2=-M^2$, by primes, we find for the relevant terms:

$$S_c(p+q)\simeq\frac{1}{F(2p\cdot q-\mu^2)}\Big[(-i\gamma\cdot p+M)F-i\gamma\cdot qF$$
$$+(2p\cdot q-\mu^2)(-i\gamma\cdot pG'+MF')-i\gamma\cdot q(2p\cdot q-\mu^2)G'$$
$$+\tfrac{1}{2}(2p\cdot q-\mu^2)^2(-i\gamma\cdot pG''+MF'')$$
$$-(2p\cdot q-\mu^2)\left\{2G'+M^2\left(F''-G''+\frac{F'^2-G'^2}{F}\right)\right\}$$
$$\times\{(2p\cdot q-\mu^2)(-i\gamma\cdot pG'+MF')-Fi\gamma\cdot q\}\Big]. \quad \text{(A.4)}$$

The general structure of the off-diagonal elements of Γ_5 may be inferred from invariance considerations and certain inter-relations among the coefficients may be deduced from the behavior of Γ_5 under charge conjugation. The charge conjugation requirement is

$$C^{-1}\Gamma_{5i}(p_1,p_2)C=-\Gamma_{5i}^T(-p_2,-p_1), \quad \text{(A.5)}$$

where C is the same matrix defined in Sec. II, and the transposition operation refers both to ordinary spin and isotopic spin indices. One may then show easily that to first order in ϵ_1, and ϵ_2,

$$\Gamma_{5i}(p+\epsilon_1,\,p+\epsilon_2)=\Gamma_{5i}(p,p)+(\epsilon_1+\epsilon_2)\cdot p\tau_i\gamma_5\frac{H_1(p^2)}{M^2}$$
$$+(\epsilon_1-\epsilon_2)\cdot p\tau_i\gamma_5 i\gamma\cdot p\frac{H_2(p^2)}{M^3}+i(\epsilon_1-\epsilon_2)\cdot\gamma\tau_i\gamma_5\frac{H_3(p^2)}{M}$$
$$+\tau_i\gamma_5(\epsilon_1-\epsilon_2)_\mu\sigma_{\mu\nu}p_\nu\frac{H_4(p^2)}{M^2}. \quad \text{(A.6)}$$

It is evident that the term proportional to $(\epsilon_1+\epsilon_2)$ may be expressed entirely in terms of Γ_5's of equal arguments, in fact:[29]

$$(\epsilon_1+\epsilon_2)\cdot p\tau_i\gamma_5H_1(p^2)/M=\tfrac{1}{2}\{\Gamma_{5i}(p+\epsilon_1,\,p+\epsilon_1)$$
$$+\Gamma_{5i}(p+\epsilon_2,\,p+\epsilon_2)-2\Gamma_{5i}(p,p)\}. \quad \text{(A.7)}$$

We may replace the unknown functions introduced in Eq. (A.6) by previously defined ones by means of certain identities between the off-diagonal elements of Γ_5 and the derivatives with respect to A of the diagonal part of Γ_5. These identities hold only to first order in q, and are deduced by comparing the method of Sec. IV and that used by Kroll and Ruderman for tracing the charge in the photoproduction calculation. That is, one finds (to first order in q):

$$\Gamma_{5-}(p+q,\,p)=\Gamma_{5-}(p,p)-q_\mu\frac{\partial}{\partial A_\mu}\langle P|\Gamma_{5-}(p,p)|N\rangle|_{A=0},$$
$$\Gamma_{5+}(p,\,p+q)=\Gamma_{5+}(p,p)-q_\mu\frac{\partial}{\partial A_\mu}\langle N|\Gamma_{5+}(p,p)|P\rangle|_{A=0}, \quad \text{(A.8)}$$

where $\pm$ and 0 indices on Γ_5 refer to the creation of negative, positive, and neutral mesons, respectively, and the labeling of the matrix elements refers to the charge state of the nucleon ($\tau_3=\pm 1$ for p and n, respectively). No such relation holds for Γ_{50}, but rather one involving Γ_{50} of equal arguments only. By use of Eq. (A.8) we can deduce by comparison with Eq. (A.6) that

$$H_2=H_4=0,$$
$$H_1=M^2D', \quad \text{(A.9)}$$
$$H_3=H.$$

The evaluation of $T_{ji}^{(1)}$ can now be carried out in a straightforward fashion. One obtains finally [making frequent use of the identity $F+2M^2(F'-G')=1$] for

[29] The technique outlined above was developed by M. Gell-Mann and M. L. Goldberger in another connection (unpublished).

$T_{ji}^{(1)}$ the value:

$$T_{ji}^{(1)}=\phi_j^{(-)}\phi_i^{(+)}\frac{g_u^2}{M}Z_3\left(\frac{\partial\alpha'}{\partial\alpha}\right)^2_{\alpha=0}\bar{\psi}_e(p)\psi_e(p)\Big\{F\delta_{ji}+\frac{[\tau_j,\tau_i]}{4}\frac{p\cdot q}{M^2}[1+4M^2(D'-F')-4H]\Big\}. \quad (A.10)$$

The first term in brackets is, of course, our old result. We turn now to the somewhat more difficult task of evaluating to first order in q those diagrams for which there is never a free nucleon line.

In the notation of Deser and Martin these are the terms described by $\delta\Gamma_b/\delta\phi$. Careful consideration of the various diagrams which contribute to the class under consideration enables one to conclude that, to first order in q, the entire contribution of all these terms is

$$T_{ji}^{(2)}=\phi_j^{(-)}\phi_i^{(+)}g_u^2\left(\frac{\partial\alpha'}{\partial\alpha}\right)^2_{\alpha=0}Z_3\bar{\psi}_e(p)\times\Big\{2\delta_{ji}(M\dot{F}+\dot{M}F-M\dot{G})-\frac{1}{i}\frac{\partial}{\partial\alpha_j'}[\Gamma_{bi}(p+q,\,p,\alpha')-\Gamma_{bi}(p,p,\alpha')]-\frac{1}{i}\frac{\partial}{\partial\alpha_i'}[\Gamma_{bj}(p-q,\,p,\alpha')-\Gamma_{bj}(p,p,\alpha')]\Big\}\psi_e(p). \quad (A.11)$$

We have gone directly to the renormalized quantities; the first term is just our previous one and the last two are the essentially new ones which are correct to first order in q. The identities (A.8) are unfortunately of no use in evaluating these terms, since their only non-vanishing contributions, being proportional to $[\tau_i,\tau_j]$ involve Γ_{b0}. We are, therefore, reduced to finding the off-diagonal elements of Γ_b, for $\alpha\neq0$, by the procedure outlined above, except that the charge conjugation relation now takes the form

$$C^{-1}\Gamma_{bi}(p_1,p_2,\alpha')C=-\Gamma_{bi}{}^T(-p_2,-p_1,-\alpha'). \quad (A.12)$$

One finds

$$\Gamma_{bj}(p+q,\,p,\alpha')=\Gamma_{bj}(p,p,\alpha')+\tfrac{1}{2}[\Gamma_{bj}(p+q,\,p+q,\,\alpha')-\Gamma_{bj}(p,p,\alpha')]+\frac{i\gamma\cdot q}{M}\tau_j\gamma_5H_3(p^2,\alpha'^2)+\frac{p\cdot q}{M^2}[i\tau_j,\,\alpha'\cdot\tau]\times H_5(p^2,\alpha'^2)+\frac{p\cdot q}{M^2}\frac{i\gamma\cdot p}{M}[i\tau_j,\,\alpha'\cdot\tau]H_6(p^2,\alpha'^2)+\frac{i\gamma\cdot q}{M}[i\tau_j,\,\alpha'\cdot\tau]H_7(p^2,\alpha'^2). \quad (A.13)$$

If we evaluate (3.16) we obtain

$$T_{ji}^{(2)}=\phi_j^{(-)}\phi_i^{(+)}g_u^2\left(\frac{\partial\alpha'}{\partial\alpha}\right)^2_{\alpha=0}Z_3\bar{\psi}_e(p)\times\Big\{2\delta_{ji}(M\dot{F}+\dot{M}F-M\dot{G})-\frac{2p\cdot q}{M^2}[\tau_i,\tau_j](H_5-H_6+H_7)\Big\}\psi_e(p); \quad (A.14)$$

adding the contribution from Eq. (A.10) to (A.14), we get for the total μ/M correction,

$$\Delta T_{ji}=\phi_j^{(-)}\phi_i^{(+)}\frac{g_u^2}{M}\left(\frac{\partial\alpha'}{\partial\alpha}\right)^2Z_3\bar{\psi}_e(p)[\tau_j,\tau_i]\frac{p\cdot q}{4M^2}\times\{1+4M^2(D'-F')-4H+2(H_5-H_6+H_7)\}. \quad (A.15)$$

This result is a purely formal one at present, since the unknown functions involved cannot be calculated exactly. It is, therefore, not very useful to compare it with experiment, as could be done via Eqs. (5.2). It may be possible, however, to relate some of these functions to other low energy processes, in which case such a comparison would be of interest.

Letters to the Editor

PUBLICATION of brief reports of important discoveries in physics may be secured by addressing them to this department. The closing date for this department is five weeks prior to the date of issue. No proof will be sent to the authors. The Board of Editors does not hold itself responsible for the opinions expressed by the correspondents. Communications should not exceed 600 words in length and should be submitted in duplicate.

Optical Absorption of Single-Crystal Strontium Titanate

JAMES A. NOLAND
Physics Laboratories, Sylvania Electric Products, Bayside, New York
(Received March 16, 1954)

A BRIEF investigation of the optical absorption of single-crystal strontium titanate in the spectrum range from 0.35 to 15.0 microns has been carried out in this Laboratory. The crystals measured were obtained through the courtesy of National Lead Company where they were grown by the flame fusion technique.[1] Data from 0.35 to 1.0 microns were taken with a Beckman Model DU spectrophotometer while the region from 1.0 to 15.0 microns was investigated with a Perkin-Elmer Model 12C spectrophotometer equipped with rocksalt optics.

The absorption coefficient was obtained by measuring optically polished samples of several thicknesses ranging from 0.20 mm to 17.0 mm. By applying the equation for the absorption coefficient,

$$a=\ln(T_1/T_2)/(x_2-x_1),$$

where T_1 and T_2 are transmission values for samples of thickness x_1 and x_2, respectively, a was computed as a function of wavelength throughout the range where it was possible to detect transmission in the samples measured. The results of these calculations are shown in Fig. 1.

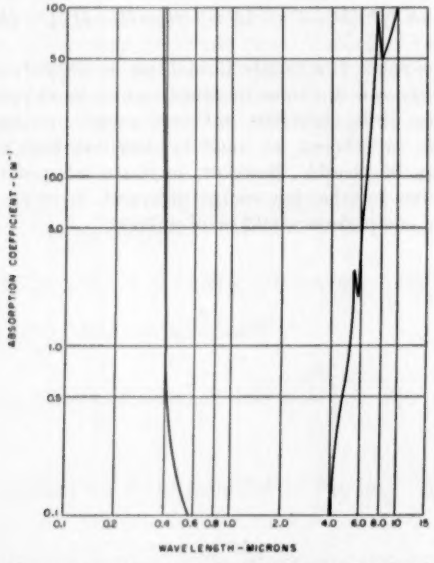

FIG. 1. Absorption coefficient of single crystal $SrTiO_3$ as a function of wavelength.

The ultraviolet cutoff for strontium titanate is found to be 0.385 micron. This edge is probably associated with the energy gap from the valence band to the conduction band, and therefore this gap is evaluated by optical methods to be 3.22 electron volts. Because of the low absorption in this material, a transmission of better than 70 percent was obtained from 0.55 to 5.0 microns for a 1.0-mm thick sample. A maximum transmission of 80 percent was found at 4.0 microns for this sample. It is possible that this high transmission in the near infrared could make strontium titanate applicable as a window material for this spectral region. The absorption bands observed at 5.5 and 7.5 microns are presumably due to vibrations of the crystal.

According to Linz,[2] an absorption is observed at about 2.0 microns for strontium titanate single crystals. However, no such absorption was observed at this laboratory. Since the crystals studied here and the ones reported on by Linz were obtained from the same source and grown in the same way, no explanation is advanced at this time for this apparent discrepancy in transmission data.

[1] L. Merker and L. E. Lynd, U. S. Patent 2,628,156, February 10, 1953 (unpublished).
[2] Arthur Linz, Jr., Phys. Rev. 91, 753 (1953).

Hall Mobility of Electrons and Holes in Silicon*

P. P. DEBYE AND T. KOHANE
Research Division, Raytheon Manufacturing Company, Waltham, Massachusetts
(Received March 16, 1954)

THE mobility of charge carriers has been investigated as a function of the resistivity in a number of silicon single crystals,[1] all of which were grown from Dupont hyperpure material. The n-type crystals ranged in resistivity from 0.01 to about 94 ohm cm and the p-type crystals from 0.025 to about 110 ohm cm.

Slices were cut from the crystals perpendicular to the direction of growth, and proper sample shape[2] was obtained by using an ultrasonic machine tool.[3] All data were taken at room temperature (295 Kelvin).

The measured values ($R\sigma$) for the mobility as a function of resistivity are given for electrons in Fig. 1 and for holes in Fig. 2.

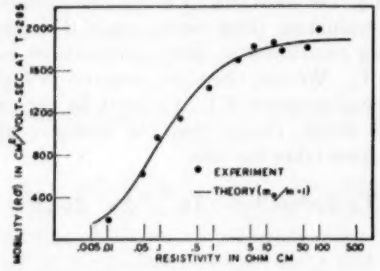

FIG. 1. Hall mobility of electrons in silicon as a function of resistivity.

The solid line represents the theoretical relationship which was calculated from the Herring[4] expression for the impurity mobility μ_I:

$$\mu_I=\frac{2^{7/2}}{\pi^{\frac{1}{2}}}\frac{\kappa^2(kT)^{\frac{3}{2}}}{m_e^{\frac{1}{2}}e^3N_I}\frac{1}{\ln(1+b)-b/(1+b)},$$

where

$$b=\frac{6}{\pi}\frac{\kappa m_e k^2T^2}{n\hbar^2e^2}.$$

In this formula the dielectric constant κ was taken as 12, the absolute temperature was $T=295$, and the effective mass m_e of the charge carriers was the electron mass. The density of the ionized impurities N_I was assumed to be equal to the density of conduction electrons n. The theoretical Hall mobility plotted in Figs. 1 and 2 was obtained by combining the lattice mobility μ_L and the im-

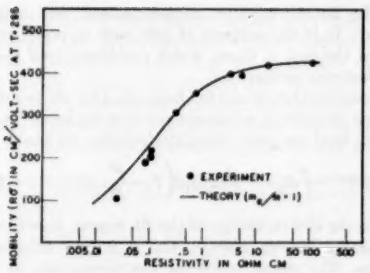

FIG. 2. Hall mobility of holes in silicon as a function of resistivity.

purity mobility μ_I. This was done by assuming a lattice drift mobility of 1600 for electrons and 360 for holes and then using the plot μ/μ_L *versus* μ_L/μ_I published by Conwell.[5] The drift mobility obtained from this was then converted into Hall mobility by using the curve published by Jones.[6]

The agreement of theory and experiment seems to be quite good, with the possible exception of the low-resistivity region in p-type silicon. In material of high purity the Hall mobility is apparently about 1900 cm²/volt-sec for electrons and 425 for holes, but it may be well to recall at this point the results on germanium, where—over a period of years—a gradual rise of the measured mobility was observed. This presumably was due to increasing perfection of the crystals and a similar development may manifest itself for the case of silicon.[7]

* This work was supported in part by the U. S. Bureau of Ships, U. S. Signal Corps, and U. S. Air Force.

[1] The crystals were grown by W. D. Straub and A. Adams, Jr., of the Research Division, Raytheon Manufacturing Company, Waltham, Massachusetts.

[2] Similarly shaped samples were used for the measurements described by P. P. Debye and E. M. Conwell, Phys. Rev. **93**, 693 (1954).

[3] J. P. Aloisio and N. Clark, Jr., A.S.T.E. annual collected papers of Industrial Exposition, April 26–30, 1954 (to be published). The sample preparation was done by Ann Cassola.

[4] C. Herring (private communication). See also H. Brooks, Phys. Rev. **83**, 879 (1951).

[5] E. M. Conwell, Proc. Inst. Radio Engrs. **40**, 1331 (1952), Fig. 3.

[6] H. Jones, Phys. Rev. **81**, 149 (1951). See also V. A. Johnson and K. Lark-Horovitz, Phys. Rev. **82**, 977 (1951).

[7] G. deMars (private communication). Preliminary result of drift mobility measurements seem to indicate good agreement for the case of electrons; however, the measured drift mobility for holes is considerably larger than the measured Hall mobility.

Atomic Hydrogen Hyperfine Structure in Irradiated Acids*

RALPH LIVINGSTON, HENRY ZELDES, AND ELLISON H. TAYLOR
Chemistry Division, Oak Ridge National Laboratory, Oak Ridge, Tennessee
(Received March 3, 1954)

PARAMAGNETIC resonance absorption lines have been observed in a variety of substances after irradiation with Co^{60} gamma rays at 77°K, and are attributed to free radicals. One of the radicals formed and trapped in $HClO_4$, H_2SO_4, and H_3PO_4 has been identified as atomic hydrogen.

Samples were frozen in Pyrex capillaries (usually to glasses), irradiated in liquid N_2 at a dose rate of about 3000/min for several days, and stored in liquid N_2 until measured.

The spectrometer operated at 23 000 Mc/sec and used a rectangular cavity excited in the TE_{102} mode. The magnetic field, of about 8000 gauss, was applied normal to the H vector of the rf field, and was modulated sinusoidally at 60 cps. The lines were displayed on an oscilloscope, and the magnetic field was measured with a proton magnetic resonance signal superimposed on the paramagnetic resonance line. The microwave frequency, held constant during each set of measurements, was measured by proton resonance superposition on the line from a sample of diphenyl picryl hydrazyl placed simultaneously in the cavity beside the tip of the Dewar vessel holding the capillary sample.

TABLE I. Hyperfine separations ν_H and electron g factors for hydrogen in irradiated acids.

Acid[a]	Mole ratio H_2O: acid	Microwave freq., Mc/sec[b]	High-field line, gauss[a]	Low-field line, gauss[a]	ν_H, Mc/sec	g
$HClO_4$	7.0	23 033.5	8462.7	7960.2	1407.1	2.0022
		23 033.7	8462.6	7960.6	1405.6	2.0022
		23 033.7	8462.9	7960.2	1407.3	2.0022
H_2SO_4	2.1	23 045.1	8467.0	7961.4	1415.7	2.0025
		23 042.7	8466.8	7961.5	1414.9	2.0023
		23 043.7	8466.6	7961.4	1414.5	2.0024
H_3PO_4	0.0	23 065.2	8475.3	7967.0	1423.5	2.0025
		23 064.7	8475.6	7967.3	1423.3	2.0024
		23 065.5	8475.8	7967.5	1423.4	2.0024

[a] The measurements on each acid were made in succession on a single sample.
[b] From measurements on hydrazyl radical; see text.
[c] From proton resonance measurements, using $\gamma_p = 2.67523 \times 10^4$ sec^{-1} gauss^{-1}; Thomas, Driscoll, and Hipple, Phys. Rev. **78**, 787 (1950).

Four lines were observed in concentrated H_2SO_4. Two of these were near the g value of the free electron, one rather sharp and one very broad and probably complex. The other two were symmetrically placed on either side of the central pair, were of about equal strength and width (about 4-gauss width at half-height), and were about 500 gauss apart. $HClO_4$ and H_3PO_4 showed the same satellites but different central lines. Irradiated mixtures of these acids with D_2O showed three additional lines, one near the g value of the free electron and two located like the sharp satellites above, but much closer together.

No changes in the strengths of the lines were observed on prolonged storage at 77°K. However, they disappeared at higher temperatures that were still well below the softening points. A marked dependence of relative line intensities on water content was observed. In the case of H_2SO_4, dilution first strengthened the satellites and weakened the sharp central line, the latter almost disappearing at a water-to-acid mole ratio of about 2:1. The satellites behaved similarly in the other two acids. Extreme dilution weakened the whole pattern.

The microwave frequency in each experiment was calculated from the observations on the diphenyl picryl hydrazyl radical using $g = 2.0037$ for this radical,[1] and was always in good agreement with that given by a cavity wave meter used simultaneously. Since the separations of the satellite lines in the samples suggested atomic hydrogen hyperfine structure, the frequencies and magnetic fields for these lines were reduced to the hyperfine separation and the electron g factor by the Breit-Rabi formula.[2,3] The transitions measured (Nafe and Nelson's[2] notation) were $(0, 0 \rightarrow 1, 1)$ and $(1, -1 \rightarrow 1, 0)$ for hydrogen. The polarization described above permits only those transitions for which $\Delta m = \pm 1$.

The data and calculated results are summarized in Table I. All of the values for the g factor are equal, within our present experimental error, to the free electron value of 2.0023. The ν_H values are strikingly close to Nafe and Nelson's[2] atomic beam value of 1420.410 Mc/sec. This indicates that the unpaired electron is represented very well by an atomic hydrogen 1s wave function, and that the hydrogen has no chemical bond in the usual sense. The spread in values between the different acids is, however, outside the experimental error, and indicates a small environmental effect on the wave function.

One set of preliminary measurements has been made on H_2SO_4 diluted with D_2O. The three lines observed for deuterium were the satellites $(\frac{1}{2}, -\frac{1}{2} \rightarrow \frac{1}{2}, -\frac{1}{2})$ and $(\frac{1}{2}, \frac{1}{2} \rightarrow \frac{1}{2}, \frac{1}{2})$ and the unresolved central doublet $(\frac{1}{2}, -\frac{1}{2} \rightarrow \frac{1}{2}, \frac{1}{2})$ and $(\frac{1}{2}, \frac{1}{2} \rightarrow \frac{1}{2}, -\frac{1}{2})$. The calculated hyperfine separation for deuterium ν_D and for hydrogen ν_H in the same sample gave a ratio $\nu_H/\nu_D = 4.342$, in good agreement with Nafe and Nelson's[2] more accurate value of 4.33867.

A more detailed study of these acids is now under way. We wish to thank J. Jauch for helpful discussion.

* This work was performed for the U. S. Atomic Energy Commission.

[1] C. A. Hutchison and R. C. Pastor, Phys. Rev. **81**, 282 (1951).
[2] J. E. Nafe and E. B. Nelson, Phys. Rev. **73**, 718 (1948).
[3] G. Breit and I. I. Rabi, Phys. Rev. **38**, 2082 (1931).

Rearrangement Collisions

B. H. Bransden
Department of Physics, Queen's University of Belfast, Belfast, Northern Ireland
(Received February 8, 1954)

THE theory of exchange and rearrangement collisions has been discussed recently, in *The Physical Review*, by several authors.[1–4] The scattering amplitude determining the cross section for a transition between stationary states i and j, wave functions ϕ_i and ϕ_j, may be written, to Born's approximation, in either of the forms $\langle\phi_i|U|\phi_j\rangle$, $\langle\phi_i|V|\phi_j\rangle$, U and V being the interaction potentials between the separated systems before and after the rearrangement, respectively. It is well known that these expressions are identical[5] provided ϕ_i, ϕ_j are the exact unperturbed wave functions, but that they may differ seriously when approximate wave functions are employed. Under these circumstances, it has been claimed[1,2] that the scattering amplitude containing the *prior* interaction U is "correct" and is to be preferred to that containing the *post* interaction V.

The Born scattering amplitude satisfies the requirement of the reciprocity theorem[6,7] that the scattering amplitudes, for the transition $i\rightarrow j$ and for the time-reversed transition $j\rightarrow i$, shall be identical. However, for the time-reversed collision V is the *prior* and U the *post* interaction, so that it is *a priori* meaningless to assert the superiority of either the post or the prior forms of interaction, when used in conjunction with approximate unperturbed wave functions.

It may be remarked, that if approximate cross sections are required that satisfy the reciprocity theorem, it has been the reasonable practice to take either the geometric[8] or the arithmetic[9] means of the post and prior amplitudes, although no theoretical justification can be given for this procedure.

[1] S. Altshuler, Phys. Rev. **91**, 1167 (1953).
[2] S. Altshuler, Phys. Rev. **92**, 1157 (1953).
[3] S. Borowitz and B. Friedman, Phys. Rev. **89**, 441 (1953).
[4] A. Dalgarno, Phys. Rev. **91**, 198 (1953).
[5] L. I. Schiff, *Quantum Mechanics* (McGraw-Hill Book Company, Inc., New York, 1949), p. 230.
[6] Bates, Fundaminsky, Leech, and Massey, Trans. Roy. Soc. (London) **243**, 93 (1950).
[7] B. A. Lippman and J. Schwinger, Phys. Rev. **79**, 469 (1950).
[8] M. H. Hebb and D. H. Menzel, Astrophys. J. **92**, 408 (1940).
[9] R. S. Christian and J. L. Gammel, Phys. Rev. **91**, 100 (1953).

Effect of Deuteron Formation on Multiple Meson Production*

K. A. Brueckner and J. S. Kovacs
Indiana University, Bloomington, Indiana
(Received March 12, 1954)

IN a statistical theory of multiple meson production such as that proposed by Fermi,[1] it is supposed that the probabilities of various competing final states are determined by statistical considerations. This is made reasonable by the argument that in a high-energy collision, the energy available for the reaction is momentarily concentrated in a small volume of very high excitation in which a thermal equilibrium is very rapidly established. Even if this situation actually exists, however, it is easy to see that an equilibrium established in this region does not simply determine the weighting of the final states. One can suppose that in the region of high temperature, very strong interactions rapidly bring about equilibrium, but as the particles leave this volume, the less strong but longer range interactions become predominant. These serve to perturb the wave functions of the outgoing particles in such a way as to enhance the transitions into a final state in which the amplitude at small distances is large relative to the asymptotic value. These "final-state interaction" effects are very familiar in low-energy phenomena where, for example,[2–4] the final state 2-nucleon interaction increases single meson production by 2 or 3 orders of magnitude. Three types of such final state interactions can be expected to be appreciable in multiple meson production, namely, the nucleon-nucleon, meson-nucleon, and meson-meson interactions. It is the purpose of this note to point out the importance of the first of these, which manifests itself most simply through deuteron formation.[5]

Let us consider the volume in phase space for the production in a two-nucleon collision of n mesons and two nucleons. Treating the mesons and final nucleons nonrelativistically, we have

$$\rho_F=(2\pi)^{-3(n+1)}\int d\mathbf{q}_1\cdots\int d\mathbf{q}_n d\mathbf{p}\,\delta\left(T_0-\frac{p^2}{M}-T_1-\cdots-T_n\right), \quad (1)$$

where T_i is the kinetic energy of the ith meson, $T_0=E_0-n\mu$ is the total available kinetic energy, and $\mathbf{p}$ is the relative nucleon momentum. The phase space for the production of the same number of mesons and a deuteron is obtained from this by the simple modification,[2,3]

$$(\rho_F)_D=(2\pi)^{-3n}\int d\mathbf{q}_1\cdots\int d\mathbf{q}_n\,\delta(T_0-T_1-\cdots-T_n)\,|\psi_D(0)|^2, \quad (2)$$

where $\psi_D(0)$ is the deuteron wave function in coordinate space evaluated at the origin. Let us for simplicity consider only the ratio of these two processes. The integrals of Eqs. (1) and (2) are easily carried out to give the simple result:

$$\sigma(n\pi+D)/\sigma(n\pi+N+P)=(\rho_F)_D/\rho_F=\frac{8\pi^{\frac{1}{2}}|\psi_D(0)|^2\Gamma(\frac{3}{2}n+\frac{3}{4})}{M^{\frac{1}{2}}(E_0-n\mu)^{\frac{1}{2}}\Gamma(\frac{3}{2}n)}, \quad (3)$$

where Γ is the gamma function. In evaluating this ratio, we shall use the Hulthén wave function. It is interesting to note that for large n this ratio takes on the simple form:

$$\sigma(n\pi+D)/\sigma(n\pi+N+P)\underset{n\gg1}{=}\frac{8\pi^{\frac{1}{2}}|\psi_D(0)|^2}{M^{\frac{1}{2}}(E_0-n\mu)^{\frac{1}{2}}}\left(\frac{3n}{2}\right)^{\frac{1}{4}}, \quad (4)$$

so that the importance of the effect increases rapidly for large multiplicities.

The result of Eq. (3) is given in Fig. 1 for various meson multiplicities and for various values of $E_0-n\mu$ (E_0 the total energy) above threshold. The very large effect near threshold is apparent, as is also the strong dependence on multiplicity.

For comparison with this result, we have also evaluated this ratio for the case in which the matrix elements depend linearly on

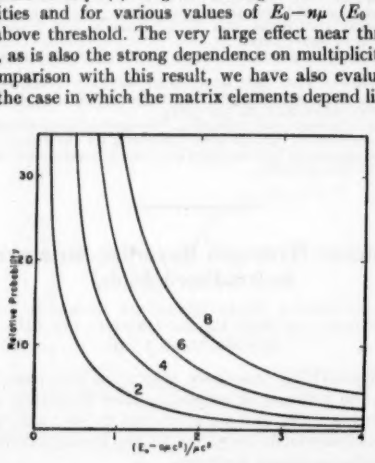

FIG. 1. Probability of multiple meson production with deuteron formation, relative to the statistical result neglecting neutron-proton interaction. The curves are labeled by multiplicity of mesons produced.

the meson momentum, as might be expected in pseudoscalar meson theory. The result is very easily evaluated as in the simple case of Eqs. (3) and (4), to give

$$\sigma(n\pi+D)/\sigma(n\pi+N+P)=\frac{8\pi^{\frac{1}{2}}|\psi_D(0)|^2\Gamma(5n/2+\frac{3}{4})}{M^{\frac{1}{2}}(E_0-n\mu)^{\frac{1}{2}}\Gamma(5n/2)}. \quad (5)$$

The effect is similar, except that the enhancement of the deuteron cross section is larger (by a factor of 2.5 to 3.0) than for the case of constant matrix elements.

These results are only valid in the nonrelativistic limit for all of the final particles involved; it is, however, easy to verify that the

effect persists into the high-energy region with only relatively small changes in the simple formulas we have derived.

It is clear from these results that the possibility of deuteron formation can be expected to increase very markedly the near-threshold production of mesons at high multiplicities. The additional effects of other "final-state interactions" cannot be expected to be small; these will be discussed in a paper now in preparation.

* Supported in part by a grant from the National Science Foundation and the joint program of the U. S. Office of Naval Research and the U. S. Atomic Energy Commission.

[1] E. Fermi, Progr. Theoret. Phys. Japan **5**, 570 (1950).
[2] K. Brueckner, Phys. Rev. **82**, 598 (1951).
[3] K. M. Watson and K. A. Brueckner, Phys. Rev. **83**, 1 (1951).
[4] Kenneth M. Watson, Phys. Rev. **88**, 1163 (1952).
[5] The development used here closely follows that of references 2 and 3.

Nuclear Reactions of Copper with 2.2-Bev Protons*

G. FRIEDLANDER, J. M. MILLER,† R. WOLFGANG, J. HUDIS, AND E. BAKER
Chemistry Department, Brookhaven National Laboratory, Upton, New York
(Received March 4, 1954)

THE circulating proton beam of the Brookhaven Cosmotron has been used to determine the cross sections for the formation of about 50 radioactive nuclides in the bombardment of copper with 2.2-Bev protons. Target foils between 40 and 1200 mg/cm² thick were irradiated in one of the straight sections of the machine for periods ranging from a few minutes to several hours. To avoid irradiation of the targets with stray protons of less than the desired energy, the foils were in a shielded position except during the final 200 milliseconds of each acceleration cycle; during that time they were propelled, by means of an air-driven ram, to a location at a slightly smaller radius than the equilibrium proton orbit. When the rf acceleration was turned off at the end of the cycle, the protons spiralled in towards the target. Activity levels were found to be practically independent of target thickness, which indicates that, for the range of thicknesses used, the number of beam traversals through a target foil is about inversely proportional to the foil thickness. With beam intensities of the order of 10^{11} protons per minute, saturation activities in the range of 10^5 to 10^7 disintegrations per minute were found for practically all the products investigated.

After each irradiation the target was dissolved, appropriate carriers were added and one or more elements were separated by fairly standard radiochemical procedures. In most runs a manganese fraction was isolated, and the Mn^{52} yield was used as a measure of the relative beam intensity. In some other cases the Na^{24} activity induced in an aluminum monitor foil[1] was used for this purpose. Activities of beta-emitting nuclides were measured with thin-window G-M or proportional counters; the x-rays from nuclides decaying mostly by K-electron capture were measured with a large proportional counter and pulse-height analyzer. Scintillation gamma-ray detectors were used for Be^7 and Cr^{51}. All counters were appropriately intercalibrated, and the measured counting rates were converted to disintegration rates by means of factors for counter geometry and efficiency and for branching decay.[2] Corrections for self-absorption, backscattering, and window absorption of beta rays were made for beta groups with $E_{max} \leq 0.4$ Mev, according to published data.[3] Conversion of the relative yield values for the various products to absolute cross sections was based on the value 9.0 mb[4] for the cross section of the reaction $Al^{27}(p,3pn)Na^{24}$.

The measured cross sections are listed in Table I. Their relative values are believed to be good to ±20 percent except where otherwise stated. To show the very striking differences between these results and the corresponding cross sections measured[5-7] with proton energies of 340 and 370 Mev, the ratio of high-energy to low-energy cross section is plotted against product mass number in Fig. 1. Only experimentally determined cross sections are included. It is evident that deposition of small amounts of excitation energy, leading to products within a few mass numbers of the target, has become relatively less important at the higher energy, while loss of 15 or more nucleons is much more probable. In fact, interpolation of cross sections for undetected product nuclides on the basis of approximate evaporation calculations leads to the conclusion that the total cross section for a given product mass number peaks

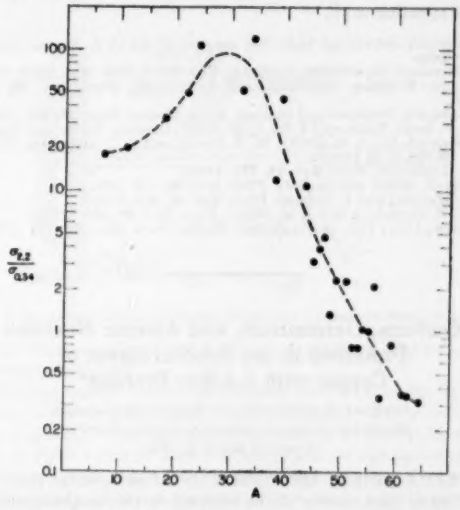

FIG. 1. Ratios of formation cross sections at 2.2-Bev proton energy to those at 340 Mev. The low-energy data are taken from references 5, 6, and 7. The points at $A = 11$, 18, and 42 were obtained at 370 rather than 340 Mev (see reference 7).

somewhere in the region of $A = 45$ to 50. This behavior may well be connected with a mechanism for energy deposition which involves production and reabsorption of mesons. Adding up all the measured and interpolated cross sections one arrives at an inelastic cross section for Cu of about 0.8 barn, in reasonable agreement with the value of 0.75 barn measured[8] with neutrons of average

TABLE I. Cross sections (in mb) for the formation of nuclides in the bombardment of copper with 2.2-Bev protons.

Zn^{65}	0.4 –0.8[a]	Mn^{56}	2.3	Sc^{48}	<0.8[b,c]	S^{35}	0.95
Zn^{62}	0.16–0.6[a]	Mn^{54}	12[c]	Sc^{46}	2.4[c,d]	P^{32}	0.9[c]
Cu^{64}	7.2[c]	Mn^{52}	5.4	Sc^{47}	3.5[c,d]	P^{32}	6.4
Cu^{62}	17[c]	Mn^{52m}	1.6[c]	Sc^{46}	6.5[c]	Mg^{28}	0.41
Cu^{61}	6.5[c]	Mn^{51}	1.4	Sc^{46m}	5.0[c,d]	Na^{24}	3.2
Cu^{60}	1.8[c]	Cr^{51}	19	Sc^{44+44}	9.7[c]	Na^{22}	1.8[c]
Ni^{57}	0.6	Cr^{49}	2.2	Ca^{47}	0.10	F^{18}	1.0[c]
Co^{61}	3.6[c]	Cr^{48}	0.5	Ca^{45}	1.1	C^{11}	≥0.65[e]
Co^{58}	1.5	V^{52}	<0.05[b]	K^{42}	1.3	Be^7	10
Fe^{59}	0.6	V^{49}	27	K^{43}	3.7		
Fe^{55}	12	V^{48}	9.6	Cl^{39}	0.40		
Fe^{52}	1.3[c]	V^{47}	2.7	Cl^{38}	0.67[d]		
Fe^{52}	0.19	Ti^{45}	2.5	Cl^{34}	0.89[d]		

[a] The Zn yields varied with target thickness, indicating that low-energy secondaries contribute to the production of these activities.
[b] These nuclides were not detected.
[c] Based on single run.
[d] Large uncertainty because of difficult decay curve analysis.
[e] $\sigma(C^{11})$ was found to be variable, depending on the chemical procedure used; the value given is the highest obtained. In this run the target was dissolved in a mixture of H_2SO_4, H_3PO_4, and CrO_3; and CO_2 was distilled out.

energy 1.4 Bev. This may be taken as evidence that the absolute cross sections reported here have probably somewhat smaller errors than the ±50 percent quoted by Turkevich[4] for the $Al(p,3pn)Na^{24}$ cross section.

It may be noted that relative yields of members of isobaric pairs are not drastically different from those observed at lower bombarding energies; however, the contribution of the neutron-richer member of any pair is found to be consistently higher in the present work than in other spallation studies. Another striking

feature is the large cross section for Be^7 formation, which almost certainly indicates a high probability for direct ejection of light nuclei.

It is a pleasure to thank the Cosmotron operating staff for its tireless cooperation, Mrs. M. Lykaas for help in some of the experiments, Dr. R. Stoenner and Miss E. Norton for performing many of the chemical yield analyses, and Miss N. Baylis for much of the counting work.

* Research carried out under the auspices of the U. S. Atomic Energy Commission.
† Chemistry Department, Columbia University, New York, New York.
[1] Hudis, Wolfgang, Sugarman, and Friedlander, Phys. Rev. 94, 775 (1954).
[2] Hollander, Perlman, and Seaborg, Revs. Modern Phys. 25, 469 (1953).
[3] B. P. Burtt, Nucleonics 5, No. 2, 28 (1949); Gleason, Taylor, and Tabern Nucleonics 8, No. 3, 12 (1951); W. E. Nervik and P. C. Stevenson, Nucleonics 10, No. 3, 18 (1952).
[4] A. Turkevich, Phys. Rev. 94, 775 (1954).
[5] Batzel, Miller, and Seaborg, Phys. Rev. 84, 671 (1951).
[6] L. Marquez and I. Perlman, Phys. Rev. 81, 953 (1951).
[7] D. H. Greenberg and J. M. Miller, Phys. Rev. 84, 845 (1951).
[8] Snow, Coor, Hill, Hornyak, and Smith, Phys. Rev. 94, 791 (1954).

Gallium, Germanium, and Arsenic Nuclides Produced in the Bombardment of Copper with 2.2-Bev Protons*

ANTHONY TURKEVICH† AND NATHAN SUGARMAN†
Brookhaven National Laboratory, Upton, New York
(Received March 4, 1954)

ALPHA particles and nuclei with charges greater than two have been shown[1] to be emitted in the bombardment of medium-weight nuclei with particles of energy greater than 100 Mev. Some of these ejected particles may be energetic enough to produce transtarget species by secondary nuclear reactions inside the bombarded target.[2,3] This communication reports on such nuclear reactions in copper bombarded with 2.2-Bev protons at the Brookhaven Cosmotron identified by the radiochemical isolation of isotopes of gallium, germanium, and arsenic.

The irradiations were carried out with a pulsed target[4] consisting of a copper foil which was usually at least 10 mil thick, with aluminum monitors in front and back. Gallium, germanium, and arsenic were isolated from an acid solution of the irradiated copper by standard procedures.[5] The radioactivity of each element was assigned to a particular isotope on the basis of the decay period. Consideration of the effect of possible impurities in the copper indicates that perhaps 10 percent of the arsenic radioactivity, but much less of the germanium or gallium, can have such an origin.

Table I summarizes the results on the nuclides found and the effective cross sections for their production in thick targets. For comparison, the yields reported in the 340-Mev bombardment of copper[2] are also given. It is seen that the gallium yields at 2.2 Bev are four times higher than those at 340 Mev, and that the germanium yields have increased by a factor of ten. Arsenic had not previously been reported as a result of such reactions. In the bombardment of tin with 350-Mev protons,[2] isotopes of iodine, of atomic number three larger than tin, were observed with cross sections of about 0.005 millibarn. These cross sections are anomalously high as compared to the analogous cross sections from copper even at the higher energy of 2.2 Bev.

One irradiation of a bare copper foil, 10.7 mg/cm² thick, gave an effective cross section for Ga^{66} 83 percent lower than that found in the thicker foil. Similarly, the cross section for Ge^{69} was 64 percent lower, but less than a 15 percent change was observed for As^{71} and As^{72}.

These gallium, germanium, and arsenic nuclides are interpreted as being formed by reactions of the type $Cu(Z,xn)$ with Z a helium, lithium, or beryllium nucleus formed by the primary interaction of the 2.2-Bev protons with copper, and x the number of emitted neutrons. The decreased production in the thin foil can be used to estimate the reaction distances of these fragments if it is assumed that they are formed isotropically in the target. The number of such reacting fragments produced per proton interacting with copper can then be calculated if some assumption is made about the cross section to give an observed product. For the $Cu(\alpha,n)$ reaction, Ghoshal's[6] cross-section curve for $Ni^{60}(\alpha,n)Zn^{63}$ was assumed. The yields of the $Cu(\alpha,xn)$ reactions were consistent with this analysis. For the lithium and beryllium reactions, cross sections to produce each observed product were assumed to be about 300 millibarns. Table I also lists the results of the calculations on the number and energy of the He, Li, and Be nuclei responsible for the reactions yielding Ga, Ge, and As nuclides, respectively. The calculated cross sections for production of the lithium and beryllium nuclei reacting are about 10 millibarns, amounting to about one percent of the proton interaction cross section. These high yields support the direct radiochemical evidence[4] of a marked increase in the production of mass numbers just above four at Cosmotron energies.

The authors gratefully acknowledge the cooperation of Dr. G. Friedlander, the other members of the nuclear chemistry group of the Brookhaven National Laboratory, and the Cosmotron operating staff.

* Research carried out under the auspices of the U. S. Atomic Energy Commission.
† Permanent address: Institute for Nuclear Studies, University of Chicago, Chicago, Illinois.
[1] S. C. Wright, Phys. Rev. 79, 838 (1950); W. H. Barkas and H. Tyren, Phys. Rev. 89, 1 (1953); R. W. Deutsch, Phys. Rev. 90, 499 (1953).
[2] Batzel, Miller, and Seaborg, Phys. Rev. 84, 671 (1951).
[3] L. Marquez and I. Perlman, Phys. Rev. 81, 953 (1951).
[4] Friedlander, Miller, Wolfgang, Hudis, and Baker, preceding letter [Phys. Rev. 94, 727 (1954)].
[5] *Radiochemical Studies: The Fission Products* (McGraw-Hill Book Company, Inc., New York, 1951; Part VI, National Nuclear Energy Series, Plutonium Project Record, Vol. 9, Div. IV; W. W. Meinke, University of California Radiation Laboratory Report UCRL-432, 1949 (unpublished).
[6] S. N. Ghoshal, Phys. Rev. 80, 939 (1950).

TABLE I. Formation of transtarget nuclides in the bombardment of copper with 2.2-bev protons.

Nuclide	Half-life	Thick-target cross sections, millibarns: 340 Mev	2.2 Bev[a]	Interaction distance in copper, mg/cm²	Secondary particle assumed	Energy of secondary particle, Mev	Yield of reacting secondaries, millibarns
Ga^{66}	9.45 hr	0.01	0.04	136	$_2He^4$	35	~300
Ga^{67}	67 hr	0.006	0.06[b]				
Ga^{68}	68 min	0.01	0.04				
Ge^{66}	2.5 hr	~0.0001	<0.000035				
Ge^{67}	21 min	~0.0001	<0.0018[c]				
Ge^{69}	40 hr	~0.0001	0.0011	41	$_3Li^7$	40	~10
As^{70}	52 min	···	<0.000063[c]				
As^{71}	60 hr	···	0.00021[c]	<6	$_4Be^9$	<30	~10
As^{72}	26 hr	···	0.00020[c]				

[a] These cross sections are based on a cross section of 6.0 millibarns for Cu^{64}, and 9.0 millibarns for Na^{24} from aluminum [Hudis, Wolfgang, Sugarman and Friedlander, Phys. Rev. 94, 775 (1954)].
[b] The counting efficiency of this K-capture nuclide is particularly hard to estimate.
[c] Decay assumed to be entirely by positron emission.

Photoproduction of π^+ Mesons from Hydrogen Near Threshold*

G. Bernardini and E. L. Goldwasser
University of Illinois, Champaign, Illinois
(Received March 15, 1954)

AN experiment has been undertaken with the purpose of investigating, in detail, the photoproduction of π^+ mesons from hydrogen near the meson threshold.

The procedure was to use Ilford G-5 nuclear emulsions as detectors of mesons produced in a liquid hydrogen target by the x-ray beam of the Illinois 300-Mev betatron. Figure 1 shows a schematic diagram of the experimental setup. The target proper was a vertical cylinder 1½ in. in diameter. In the region of the x-ray beam, the cylinder walls were 0.0005-in. brass. These walls contributed to a total meson background which was less than 5 percent. Outside the vacuum shell, plate holders constructed of light materials were distributed. Plates were mounted so that mesons from the target came through 0.017-in. aluminum windows in the vacuum shell, and entered at a glancing angle of about 5°. The low-energy limit for meson detection in the plates was taken to be 5 Mev. This corresponds to a 9–10 Mev meson produced in the target. Particles whose tracks were observed in the emulsions were identified by measuring the relative grain density and angular deviations of the tracks. The energy of each meson identified by this procedure was taken to be the mean of the two energies thus obtained. Energies of stopping mesons were calculated from their ranges. Scattering and grain counting calibrations were established for each plate from measurements made on stopping mesons.

Plates were exposed at laboratory angles ranging from 30° to 150°. Three independent types of exposures were made during the course of the experiment. Most runs were made with no absorber in front of the plates; some were made with absorbers, and finally some pellicles were exposed. These were immersed in a sea of emulsion so arranged as to constitute detectors in an infinite homogeneous medium.

In the analysis of the plates, surface scanning was employed. For the pellicles, volume scanning for $\pi-\mu$ decays was used. The three different methods were used as a check on inefficiencies inherent in the various scannings. Consistent results have been obtained for all mesons having more than twice minimum grain density on fully developed plates.

Energy measurements made on individual tracks by scattering and grain count usually differed by less than 5 Mev. Each calculated meson energy is believed to have less than 10 percent probable error.

The differential cross sections per unit solid angle in the center-of-mass system, measured at 175, 185, and 195 Mev photon energy in the laboratory system are shown in Table I listed under the center-of-mass angles at which they were obtained. The indicated errors are statistical.

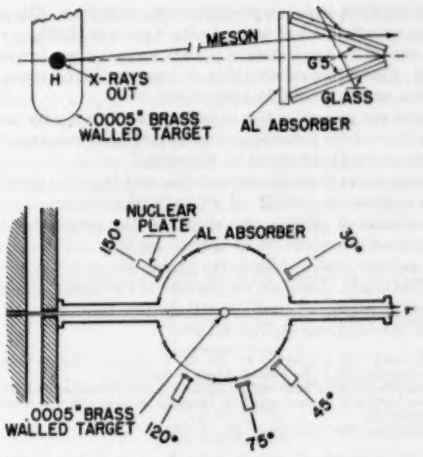

FIG. 1. Schematic diagram of liquid target and nuclear emulsion detectors.

Previous results[1–3] at higher energies, considered in the light of current theoretical proposals,[4,5] may be interpreted as a combination of S and P wave emission of the mesons. It is clear from the data in Table I that at these low energies an interpretation of the results can be given in terms of a predominant S wave. This aspect of the angular distribution is further borne out by a rough check of the momentum dependence of the cross sections at 90° as shown in Table II. It is apparent here that the momentum dependence is very closely linear and therefore is consistent with the S-wave interpretation.

A more detailed discussion of these results will soon be forthcoming.

TABLE I. Cross section as a function of lab energy and c.m. angle.

	$(d\sigma/d\Omega^*) \times 10^{29}$					
E_γ, Mev \ θ	40°	59°	93°	123°	148°	159°
175		0.61 ±0.07	0.64 ±0.04	0.64 ±0.07		
185	0.60 ±0.14	0.63 ±0.15	0.69 ±0.08	0.74 ±0.06	0.85 ±0.13	0.82 ±0.08
195	0.79 ±0.17		0.90 ±0.07	1.09 ±0.1	0.99 ±0.14	0.90 ±0.12

TABLE II. Cross section *vs* lab energy and meson c.m. momentum.

E_γ	$\frac{d\sigma}{d\Omega^*}$	$\frac{d\sigma}{d\Omega^*}\left(\frac{mc^2}{pc}\right)$	$\frac{d\sigma}{d\Omega^*}\left(\frac{mc^2}{pc}\right)^2$
165	0.48×10^{-29}	1.35×10^{-29}	10.8×10^{-29}
175	0.64×10^{-29}	1.31×10^{-29}	5.45×10^{-29}
185	0.69×10^{-29}	1.16×10^{-29}	3.24×10^{-29}

* Work supported in part by the joint program of the U. S. Office of Naval Research and the U. S. Atomic Energy Commission.
[1] J. Steinberger and A. S. Bishop, Phys. Rev. **86**, 171 (1952).
[2] Goldschmidt-Clermont, Osborne, and Winston, Phys. Rev. **91**, 468 (1953).
[3] Bacher, Kick, Peterson, Teasdale, Tollestrup, Walker and Worlock, Phys. Rev. **92**, 1090 (1953).
[4] K. A. Brueckner and K. M. Watson, Phys. Rev. **86**, 923 (1952).
[5] B. T. Feld, Phys. Rev. **89**, 330 (1952).

Nuclide V^{53}†

Raymond K. Sheline and Joseph R. Wilkinson
Department of Chemistry, Florida State University, Tallahassee, Florida
(Received March 15, 1954)

A SEARCH for the nuclide V^{53} was made by bombarding separated Cr^{53} as Cr_2O_3 with neutrons in the pile at Oak Ridge for 16 hours. The isotopic composition of the separated Cr^{53} was as follows: Cr^{54}, 1.7 percent; Cr^{52}, 92.1 percent; Cr^{53}, 5.7 percent; Cr^{50}, 0.5 percent. The nuclear reaction expected was $Cr^{53}(n,p)V^{53}$.

The sample was dissolved in concentrated HCl and 4 mg of vanadium carrier added. The solution was evaporated nearly to dryness and 10 ml of 4 percent H_2SO_4 added. This solution was then cooled in an ice bath and 5 drops of 6 percent cupferron

reagent was then added to precipitate the vanadium. The precipitate was centrifuged and washed with 4 percent H_2SO_4.

The vanadium precipitate was then mounted in planchet and counted. Absorption curves taken at two-day intervals indicate a beta with an energy of 0.56 ± 0.1 Mev.[1]

Gamma-ray spectra of the vanadium precipitate were obtained using a sweep-type differential and integral discriminator, similar to the one already described by Fairstein.[2]

Measurements from the decay curve and from the gamma-ray spectra indicate the half-life of V^{52} to be 23 ± 1 hours.

The number of gamma rays shown by the gamma-ray spectra data indicate a complex decay scheme for V^{52}.

The authors wish to thank the Stable Isotopes Division, Oak Ridge National Laboratory for the loan of the separated Cr^{53} used in this experiment.

Work is continuing on this nuclide.

† This work was supported by the U. S. Atomic Energy Commission under a contract with the Florida State University.

[1] An isotope of vanadium with a 23-hour half-life and ~0.6-Mev β^- has been observed by L. Hsiao and R. B. Duffield (private communication from R. B. Duffield).

[2] E. Fairstein, Rev. Sci. Instr. 22, 76 (1951).

Spins of the Lowest States of the K^{40}, P^{32}, and Al^{28} Nuclei

HARALD A. ENGE

Department of Physics, University of Bergen, Bergen, Norway

(Received March 16, 1954)

COMPOUND nucleus theories as well as stripping theories of nuclear reactions predict the differential cross section at a given reaction angle to vary with the spin I of the final nuclear state. Because there are as a rule other unknown parameters and because of the approximate nature of the theories, a predicted spin dependence is in general of little value for determining the spins of nuclear states. In certain special cases, however, the dependence might be useful, namely for levels that are members of closely spaced (j,j) multiplets where the only parameter differing appreciably from state to state is the resultant spin. The simplest cases are perhaps those stripping processes in which the captured particle can be assumed to go directly into a vacant "orbit" without appreciably agitating the target "core."

In stripping theories the cross section is expressed as a sum over all channels allowed by conservation rules of angular momentum and parity. In the simple cases mentioned above, however, the shell model (insofar as it is valid) requires that the captured particle brings with it the right orbital angular momentum $l\hbar$ and has the right spin direction. In that case the number of open channels are the same as the number of degeneracies of the final state or $(2I+1)$. When the energy separations between multiplet states are small, the variation in yield from state to state will be determined mainly by this factor. Because the states considered all have the same l value for the captured particle, the angular distributions are the same or very nearly so.

The compound nucleus theory of Wolfenstein[1] gives predictions about angular distributions and about the variation of the average cross section with spin of the final state, among other things. The experimental relative (d,p) yields considered in this letter have been measured at a reaction angle $\theta_{lab}=90$ degrees, with incident deuteron energies from 2 to 5 Mev and emerging proton energies above 7 Mev. From Wolfenstein's work it may be inferred that it is a fairly good approximation for these cases to assume a $(2I+1)$ dependence also for the part of the cross section that is due to compound nucleus formation.

Various experimental data concerning the lowest states of K^{40}, P^{32}, and Al^{28} have been collected in Table I. The combinations of odd-proton and odd-neutron states expected to yield the lowest levels are given in column 2. Two possible configurations are given for Al^{28}. Apparent disagreement between experimental data prevents one at the moment from deciding between the alternatives. The lowest states observed[2-4] (column 3) are tentatively assumed to be members of the (j,j) multiplets in column 2. (These assumptions are not very well founded, especially for the two higher levels in K^{40}.)

Results from the stripping analysis[5-8] of angular distribution data are quoted in column 4 for the unresolved P^{32} and Al^{28} doublets. As judged from available experimental data, small contributions from larger orbital angular momentum values (e.g., $l_n=2$) cannot be entirely excluded in the Al^{28} case. Spin values compatible with the measured l_n values are given in column 5 and other restrictions on the spins in column 6 [from β decays and (n,γ) measurements]. Suggested final spin assignments for the various levels are presented in column 7. They are based on all available data and also on relative yields. The relative yields expected when employing the $(2I+1)$ rule are given in column 8 (I_0 = ground-state spin). These figures should be compared with the experimental values in column 9.

For the $P^{31}(d,p)P^{32}$ stripping process also, $l_n=0$ is allowed for the ground state by ordinary conservation rules. The fact that only $l_n=2$ occurs is a great tribute to the shell model[7,9] and it proves that one of the basic ideas behind the $(2I+1)$ rule is correct. This rule is further based on the assumption that in stripping processes only one spin direction is allowed for the incident particle when forming a specific state. The ordinary law of conservation of angular momentum very often allows different numbers of incident spin directions (1 or 2) for different members of the same multiplet (l_n given). An approximate validity of the $(2I+1)$ rule in such cases for pure stripping would further strengthen the view that shell-model considerations should be taken into account when describing these processes. The measured (d,p) yields referred to

TABLE I. Suggested spin assignments for the lowest states of K^{40}, P^{32}, and Al^{28}, partly based on the assumption that the (d,p) yield is proportional to $(2I+1)$.

Nucl.	Assumed config. of multiplet	Exc. energy Mev	Stripping data l_n	Stripping data I	Other spin data	Final spin assign.	$\frac{(2I+1)}{(2I_0+1)}$	Exper. yield ratio
K^{40}	$(d_{3/2},f_{7/2})$	0			4	4^-	1	1
		0.032[a]			3[f]	3^-	0.78	0.8[i]
		0.800[a]			3[f]	2^-	0.56	0.6[i]
		0.893[a]			4[f]	5^-	1.22	1.1[i]
P^{32}	$(s_{1/2},d_{3/2})$	0	2[d]	1, 2, (3)	0, 1[g]	1^+	1	1
		0.077[b]	2[d]	1, 2, (3)		2^+	1.67	1.5[j]
Al^{28}	$(d_{5/2},s_{1/2})$ or $(d_{5/2},d_{3/2})$	0	0[e]	2, 3	2, 3[g]	3^+ or 2^+	1	1
		0.031[a]	0[e]?	2, 3	1[h]	2^+ or 1^+	0.71 (0.60)	0.63[k]

[a] See reference 2. [b] See reference 3. [c] See reference 4. [d] See references 6 and 7. [e] See references 5, 6, and 8. [f] From $K^{39}(n,\gamma)K^{40}$ yields. See reference 2 and G. A. Bartholomew and B. B. Kinsey, Can. J. Phys. 31, 927 (1953). [g] From β decay. Further references given in Hollander, Perlman, and Seaborg, Revs. Modern Phys. 25, 469 (1953). [h] From β decay of Mg^{28}. Also $\Delta I \gtrless 1$ between states. See A. H. Wapstra and A. L. Veenendaal, Phys. Rev. 91, 426 (1953). [i] Taken out of Fig. 1 in reference 2. $E_d=5$ Mev. [j] Average for $E_d=1.8$ and 2 Mev. See reference 3. [k] Average for $E_d=1.5$, 1.8, 2.1, and 5.2 Mev. Author's results and W. W. Buechner (private communication).

in Table I are probably in large part due to compound nucleus formation.

[1] L. Wolfenstein, Phys. Rev. **82**, 690 (1951).
[2] Buechner, Sperduto, Browne, and Bockelman, Phys. Rev. **91**, 1502 (1953).
[3] Van Patter, Endt, Sperduto, and Buechner, Phys. Rev. **86**, 502 (1952).
[4] Enge, Buechner, Sperduto, and Van Patter, Phys. Rev. **83**, 31 (1951).
[5] S. T. Butler, Proc. Roy. Soc. (London) **A208**, 559 (1951).
[6] C. F. Black, Massachusetts Institute of Technology, Laboratory of Nuclear Science and Engineering Progress Report, Aug. 31, 1952 (unpublished), p. 73.
[7] Parkinson, Beach, and King, Phys. Rev. **87**, 387 (1952).
[8] J. R. Holt and T. N. Marsham, Proc. Phys. Soc. (London) **A66**, 249 (1953).
[9] H. A. Bethe and S. T. Butler, Phys. Rev. **85**, 1045 (1952).

Bubble Tracks in a Hydrogen-Filled Glaser Chamber*

JOHN G. WOOD
Radiation Laboratory, Department of Physics, University of California, Berkeley, California
(Received March 3, 1954)

GLASER[1] first showed that the boiling of superheated ethyl ether was sensitive to ionizing radiation, and later photographed the bubble tracks in his apparatus. A liquid-hydrogen chamber would have a number of attractive features, and it is therefore not surprising that several groups have been working to produce such a device. At Chicago, Hildebrand and Nagle,[2] working in cooperation with Glaser, have produced superheated liquid hydrogen, and have shown that it boils sooner in the presence of a γ-ray source. We have taken the next step, but with somewhat different technique, and can report the photography of bubble tracks in hydrogen. (See Fig. 1.)

The bulk of the Chicago apparatus was immersed in a bath of hydrogen which was boiling at atmospheric pressure, but the bubble chamber was in the vapor space, and superheated by a coil of resistance wire. This arrangement involves problems of heat transfer and temperature measurement, in addition to some serious problems if photography were to be attempted. We have therefore immersed our bubble chamber in a bath of hydrogen which boils at high pressure; this provides a convenient heat reservoir, whose temperature is easily controlled by a pressure regulator. First, hydrogen is condensed into the bubble chamber at a pressure somewhat higher than that over the bath. After temperature equilibrium has been established, the following cycle is initiated: (1) The pressure in the bubble chamber is suddenly reduced to one atmosphere. (2) At a variable time after the pressure release, an electronic circuit triggers a stroboscopic lamp, which takes a photograph of the chamber, and (3) pressure is reapplied to the chamber to condense any bubbles that may have formed.

We have been unable to duplicate the long times of superheat reported by the Chicago group, but we have been using considerably higher degrees of superheat. We were discouraged by our inability to attain the long times of superheat, until the track photographs showed that it was not important in the succeseful operation of a large bubble chamber. Tracks have even been observed in cases where the liquid hydrogen was not completely condensed in the chamber prior to expansion.

FIG. 1. 1¼-inch chamber irradiated with a Po-Be source.

I wish to thank Dr. Luis W. Alvarez, Dr. Frank S. Crawford, Jr., and Dr. M. Lynn Stevenson for their advice and help in these experiments. I am indebted to A. J. Schwemin for help with the electronic circuits, and to H. Powell and T. Robbins for their cooperation with the glass work.

* This work has been performed under the auspices of the U. S. Atomic Energy Commission.
[1] D. A. Glaser, Phys. Rev. **87**, 665 (1952).
[2] R. H. Hildebrand and D. E. Nagle, Phys. Rev. **92**, 517 (1953).

Angular Distribution of Deuterons from $N^{14}(p,d)N^{13}$†

K. G. STANDING*
Palmer Physical Laboratory, Princeton University, Princeton, New Jersey
(Received March 15, 1954)

BUTLER'S interpretation[1] of the angular distribution of particles from (d,p) and (d,n) stripping reactions has yielded much information on the spins and parities of nuclear states.[2] By the reciprocity theorem,[3] a similar analysis should apply to the inverse processes, (p,d) and (n,d) pickup. Most pickup reactions

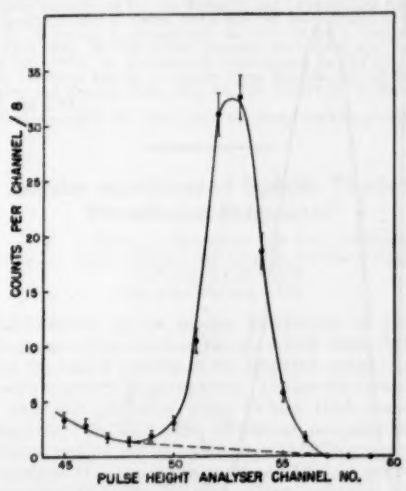

FIG. 1. Gated scintillation counter spectrum at 15° in the laboratory system. The peak consists of $N^{14}(p,d)N^{13}$ ground-state deuterons. Background was estimated from the general shape of the curve and from spectra taken with larger absorbers (which move the deuteron peak to a lower pulse height).

have Q's which are negative and several Mev in magnitude, so it is necessary to select low-energy deuteron groups in the presence of background caused by relatively high-energy protons. Because of this difficulty, angular distributions from (p,d) reactions have been examined in a few favorable cases[4,5] only.

A thin NaI crystal in a scintillation counter may be used to distinguish deuterons from proton background. The maximum possible energy loss of any deuteron passing normally through such a crystal comes from a deuteron whose range in NaI is equal to the thickness T of the crystal. This deuteron *just* stops in the crystal and loses its entire energy E_T. A higher-energy deuteron will pass through the crystal and lose energy $<E_T$ because of the smaller rate of energy loss at higher energy. A similar relation holds for protons, but, since the range of a proton is greater than the range

of a deuteron of the same energy, the maximum energy loss of a proton is $\approx\frac{1}{4}E_T$.[6] Therefore, deuterons of energy E_T will give larger pulses from the scintillation counter than will protons of any energy.

Protons of energy 18.7 Mev struck a melamine[7] target ≈0.001 in. thick, and the reaction products passed through an Al absorber into a thin NaI(Tl) crystal[8] in a scintillation counter. The Al absorber thickness was varied until the deuterons of the group being studied had energy E_T on reaching the crystal. These deuterons then appeared as a peak at maximum pulse height when the pulses from the scintillation counter were recorded on a 20-channel pulse-height analyzer.[9]

It was found that a small proportion of protons gave anomalously large pulses in the scintillation counter; presumably these were high-energy protons scattered through large angles in the crystal. A thin proportional counter[10] was introduced between the Al absorber and the scintillation counter to reduce this background. Since protons of energy $\geqslant E_T$ have a smaller mean rate of energy loss than deuterons of energy E_T, a discriminator could be set to accept all the proportional counter pulses from the deuterons and reject most of the pulses from these protons. The output of the discriminator was used as a coincidence gate for the pulse-height analyzer.

Figure 1 shows the gated scintillation counter spectrum obtained at 15° (lab) from the deuterons to the N^{13} ground state [$N^{14}(p,d)N^{13}$, $Q=-8.3$ Mev]. Figure 2 gives the angular distribution of the deuterons and indicates[1] an $l_n=1$ angular momentum transfer. This shows that the ground states of N^{13} and N^{14} have opposite parity and is consistent with the usual assignment of 1+ to the N^{14} ground state. The measurement thus agrees with the results of Bromley[11] on the $C^{13}(d,n)N^{14}$ angular distribution, and disagrees with the tentative results of Benenson[12] on the same reaction.

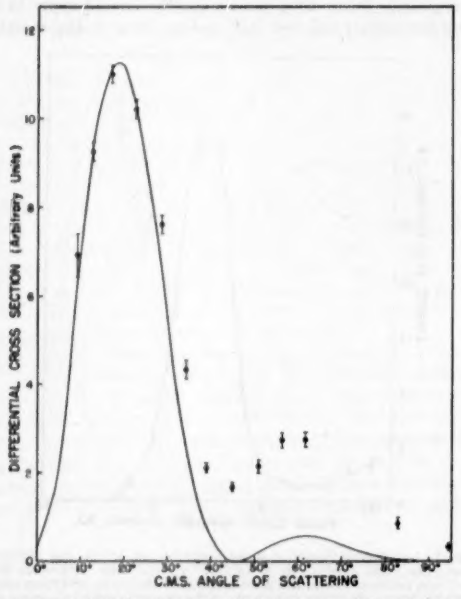

FIG. 2. Angular distribution of the $N^{14}(p,d)N^{13}$ ground-state deuterons in the center-of-mass system. Bars on the experimental points indicate standard deviations. The curve was calculated from Butler's formula (see reference 1) for $l_n=1$ and $r_0=5.4\times10^{-13}$ cm. Corresponding curves for $l_n=0$ and $l_n=2$ would peak at 0° and 30°, respectively. Experimental results greater than theoretical predictions for large angles are also a common feature of stripping reactions (see reference 1).

It has been suggested[13] that a measurement of the angular distribution of the deuterons to the first excited state of $N^{13}(\frac{1}{2}+)$ would give information about the N^{14} ground state useful in interpreting the slow C^{14} β decay. The deuterons from this reaction [$N^{14}(p,d)N^{13*}$, $Q=-10.7$ Mev] were searched for at angles of 12°, 20°, and 30° (lab), and none were found above background. The intensity of the excited state transition with $l_n=2$, $l_n=1$, and $l_n=0$ was less than 4 percent, 4 percent, and 15 percent, respectively, of the intensity of the ground-state transition ($l_n=1$). Since the N^{13} ground state is expected to be a $(p)^{-3}$ configuration and the first excited state $(p)^{-4}s$, this result indicates that the admixture of $(p)^{-4}s^2$ and $(p)^{-4}sd$ configurations[14] in the N^{14} ground state [predominately $(p)^{-2}$] must be small.

I am indebted to Professor R. Sherr and Professor M. G. White for helpful advice, to Dr. A. M. Feingold and Mr. J. B. Reynolds for informative discussions, and to Mr. Fred Elser for valuable assistance in the calculations and measurements.

† This work was supported by the U. S. Atomic Energy Commission and The Higgins Scientific Trust Fund.

[6] Now at Physics Department, University of Manitoba, Winnipeg, Canada.

[1] S. T. Butler, Proc. Roy. Soc. (London) **A208**, 559 (1951).

[2] F. Ajzenberg and T. Lauritsen, Revs. Modern Phys. **24**, 321 (1952).

[3] J. M. Blatt and V. F. Weisskopf, *Theoretical Nuclear Physics* (John Wiley and Sons, Inc., New York, 1952), p. 336.

[4] $Be^9(p,d)Be^8$, $Q=559$ kev: J. A. Harvey, Phys. Rev. **82**, 298 (1951) and Massachusetts Institute of Technology Progress Report NP-3434, October 1, 1950 (unpublished); Cohen, Newman, Handley, and Timnick, Phys. Rev. **90**, 323 (1953).

[5] $He^4(p,d)He^3$, $Q=-18.3$ Mev: J. Benveniste and B. Cork, Phys. Rev. **89**, 422 (1953).

[6] Aron, Hoffman, and Williams, U. S. Atomic Energy Commission Report AECU-663 (unpublished).

[7] Melmac 4047, American Cyanamid Company. The foil was formed between glass plates at ~5000 lb/in.^{2} and ~400°F.

[8] Cleaved crystals of thickness ≈0.015 in. and ≈0.009 in. were used in this experiment.

[9] Bell and Kelley model—described by A. B. Van Rennes, Nucleonics **10**, No. 10, 50 (1952).

[10] $\frac{1}{2}$-in. argon at a pressure of 32 cm Hg. By itself, such a counter is not very efficient in distinguishing deuterons from protons because of its large spread in pulse height—see Igo, Clark, and Elsberg, Phys. Rev. **89**, 879 (1953).

[11] D. A. Bromley, Phys. Rev. **88**, 565 (1952).

[12] R. E. Benenson, Phys. Rev. **90**, 420 (1953).

[13] A. M. L. Messiah, Phys. Rev. **88**, 151 (1952); A. M. Feingold, Phys. Rev. **89**, 318 (1953).

[14] As suggested to explain the long life of C^{14}—D. R. Inglis, Revs. Modern Phys. **25**, 390 (1953).

The Elastic Scattering of Photons*

E. G. FULLER AND EVANS HAYWARD
National Bureau of Standards, Washington, D. C.
(Received February 9, 1954)

THE absorption of high-energy photons with the subsequent emission of nuclear particles, primarily neutrons, has been studied extensively, and the cross sections as a function of energy have been shown to have maxima near 15 Mev. It can be shown by a very general dispersion argument that associated with the total absorption there will be an elastic scattering of the photons. The general features of the absorption curves (width, position of maxima) can be obtained from a measurement of the elastic scattering as a function of photon energy. This scattering has been discussed in a number of theoretical papers,[1] and several experiments[2] have been performed to detect this radiation. Stearns used a NaI(Tl) scintillation spectrometer to observe the scattering of the gamma rays from the $Li(p,\gamma)$ reaction by various nuclei. The results indicated that the total elastic scattering cross section at 17 Mev is a few millibarns for the heavy elements.

The purpose of this experiment is to measure the elastic scattering cross section as a function of photon energy and is an extension of the Stearns experiment. X-rays produced by the NBS 50-Mev betatron are scattered from targets of gold, lead, and uranium, about one mean free path thick. The detector[3] consists of a NaI(Tl) crystal five inches in diameter and four inches long viewed by a DuMont five-inch diameter photomultiplier tube. The electronic equipment consists of a linear amplifier and a series of discriminators with associated scaling units. The outputs of the discriminators are gated so that only pulses occurring in a 40-μsec gate around the 10-μsec beam pulse are registered. The bias of one of the discriminators is set so that only photons having energies above ninety percent of the maximum energy are detected; this

criterion defines "elastic scattering" for this experiment. By varying the electron energy in the betatron and at the same time the discriminator bias, it is possible to observe the scattering as a function of photon energy. Figure 1 shows the experimental

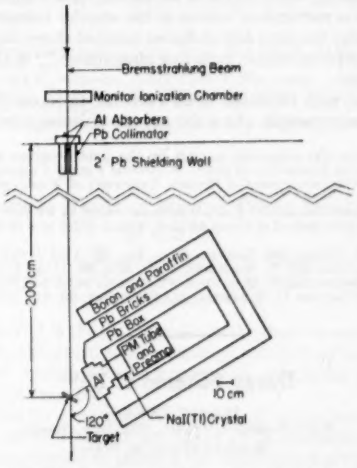

FIG. 1. Experimental arrangement. The counter and associated shielding is mounted on a table that rotates about a pivot below the target.

arrangement. The aluminum absorbers harden both the direct and scattered beams in order to decrease the number of small pulses contributing to pileup.

The experimental procedure is to observe the number of counts (N_1) produced for a charge (Q_1) collected on the ionization chamber when the crystal is in the direct beam from the betatron at the zero degree position. These counts are detected in the differential channel positioned just below the tip of the pulse-height distribution produced by the filtered bremsstrahlung spectrum. The crystal is then swung to the 120° position, and the number of counts (N_2) for a charge (Q_2) collected on the ionization chamber is determined. The differential cross section is given by:

$$\frac{d\sigma}{d\Omega_{120}} = C\frac{Q_1}{N_1}\times\frac{N_2}{Q_2}\ \text{mb/sterad},$$

where the constant C contains geometrical factors, the number of atoms of the target irradiated, and a correction for absorption in the target. The maximum counting rates in the scattered beam are about 20 per hour, $Q_1/Q_2 \sim 10^{-3}$. Cosmic-ray background in the differential channel is less than one count per hour. The data are corrected for this background and for neutron background from the uranium target.

The results are given in Table I. The energy spreads indicated are determined from the width of the discriminator channel and the errors indicated for the intensities are the standard deviations based only on the numbers of counts. Systematic errors, while not affecting the relative values, may be large enough to make the absolute cross section in error by as much as twenty-five percent.

The lead data are plotted in Fig. 2. The absolute cross section at 17 Mev agrees with the value obtained by Stearns.[3] The "resonance" scattering by Pb and Au peaks near 15 Mev and at a slightly lower energy for U. The "resonances" are about 5 Mev wide for all three elements. Further experiments are underway extending these measurements both to lighter materials and over a greater energy range.

TABLE I. Elastic scattering cross sections in mb/sterad.

E (Mev)	Au	Pb	U
9.00– 9.75	0.08 ±0.03	0.19 ±0.06	0.16 ±0.04
11.3 –12.3	0.20 ±0.04	0.24 ±0.05	0.45 ±0.08
14.0 –15.1	0.60 ±0.10	0.81 ±0.11	0.59 ±0.12
15.2 –16.3	0.58 ±0.10	0.77 ±0.13	0.49 ±0.12
17.6 –19.6	0.32 ±0.06	0.37 ±0.08	0.20 ±0.07
21.7 –24.3	0.11 ±0.04	0.23 ±0.06	0.18 ±0.06

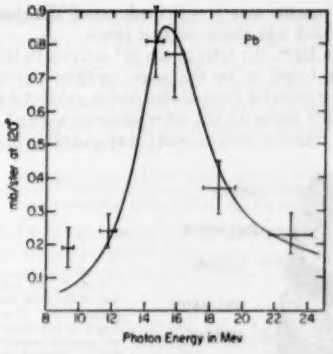

FIG. 2. The elastic scattering cross section for lead. The indicated spread in energy is the width of the differential discriminator channel, and the standard deviations are based only on the number of counts. The smooth curve is a Breit-Wigner single resonance curve normalized to give a cross section of 0.85 mb/sterad at 15 Mev ($\hbar\omega_0 = 15$ Mev, $\Gamma = 5$ Mev).

The authors would like to thank Dr. U. Fano and Dr. H. W. Koch for their interest.

* This research was supported by the U. S. Air Force, through the Office of Scientific Research of the Air Research and Development Command.

[1] M. Goldhaber and E. Teller, Phys. Rev. **74**, 1046 (1948); H. Steinwedel and J. H. D. Jensen, Z. Naturforsch. **5a**, 413 (1950); J. Levinger and H. Bethe, Phys. Rev. **78**, 115 (1950); Ferentz, Gell-Mann, and Pines, Phys. Rev. **92**, 836 (1953); A. Reifmann, Z. Naturforsch. **8a**, 505 (1953).

[2] E. R. Gaerttner and M. L. Yeater, Phys. Rev. **76**, 363 (1949); Dressel, Goldhaber, and Hanson, Phys. Rev. **77**, 754 (1950); M. B. Stearns, Phys. Rev. **87**, 706 (1952).

[3] R. S. Foote and H. W. Koch, Rev. Sci. Instr. (to be published).

Angular Anisotropy of Specific Thorium Photofission Fragments*

A. W. FAIRHALL, I. HALPERN,† AND E. J. WINHOLD
Laboratory for Nuclear Science, Massachusetts Institute of Technology, Cambridge, Massachusetts

(Received March 8, 1954)

ANISOTROPY in the angular distribution of photofission fragments from thorium has previously been observed by counting the total β activity of the fragments caught at various angles with respect to the x-ray beam.[1] The present measurements, which were also performed using 16-Mev thick-target bremsstrahlung‡ from the MIT linear accelerator, compare the number of fragments emitted per unit solid angle at 90° to the x-ray beam to the average of the numbers at 0° and 180° for seven specific fission-product elements: bromine, silver, antimony, tellurium, iodine, barium, and cerium. Over the range measured, the anisotropy appears to be a monotonically increasing function of the mass ratio of the fission fragment pairs.

The collimated fragments were caught in thin foils, specific fission elements were separated with carriers, and their respective β activities measured and corrected for chemical yield and radioactive decay. The exposure arrangement consisted of a series of thorium and catcher foils alternated and separated by aluminum collimators, as shown in Fig. 1. Two such stacks were mounted on the periphery of a turntable and were rotated alternately into the beam for five-minute intervals during each four-hour exposure. When in the beam one stack had its axis parallel, the other its axis perpendicular to the x-ray beam. Using thin aluminum catchers, the β activity of the unseparated fragments was first measured, after which barium and tellurium were radio-chemically separated and counted. To facilitate the chemical separations of the other elements, thin films of ice were substituted for the aluminum foils, and barium was separated in every run as an internal standard.

At least six measurements were made on all the elements except antimony, which was measured four times.

For 85-min Ba^{139}, the ratio of the 90° activity to the (0°+180°) activity was found to be the same (within 1 percent) as the corresponding ratio for unseparated fission product β activity. The 90°/(0°+180°) ratios for the other elements were all measured in terms of the ratio for barium, which was separated in all runs. The

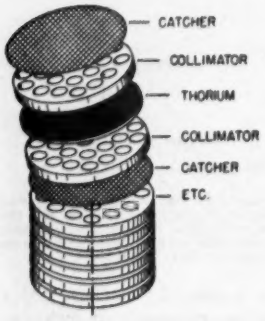

FIG. 1. An exploded view of one of the two stacks of foils and collimators. The axis of the stack is oriented either parallel or perpendicular to the x-ray beam. The half-angle of the collimator holes is 15°.

angular distribution of the unseparated fragments has been measured previously[1] using the same bremsstrahlung beam, and was found to be compatible with the form $a+b\sin^2\theta$ with respect to the x-ray beam. The experimental value of b/a was found to be 0.41 ± 0.05. The values of b/a for the other elements, taking barium

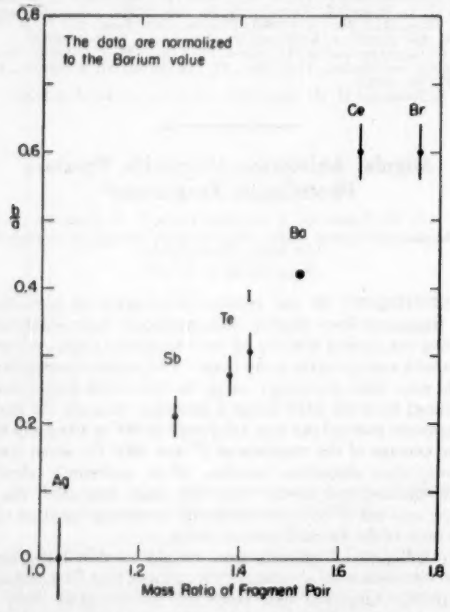

FIG. 2. Angular anisotropy of Th^{232} fission fragments as a function of the mass ratio of the fragment pair.

to be 0.41 exactly, are shown in Fig. 2, plotted as a function of the mass ratio of heavy-to-light fission fragment pair.

The errors shown on the points are probable errors based on the spread of the values obtained in the different runs. The experimental procedure was checked for systematic errors by making several runs with only one stack, dividing the catchers in two equal portions and separating several elements in each portion. The ratios of the fission yields of the several elements were the same within 5 percent in each of the two portions, indicating that the errors of chemical separation, determination of chemical yield, and counting are small.

The data of Fig. 2 imply that the mass-yield curve for the $\sin^2\theta$ component of the angular distribution is warped toward greater mass asymmetry than the curve for the isotropic component. But whatever the mechanism leading to the angular anisotropy, both curves display the same sort of double-humped shape characteristic of various types of fission, including photofission,[2-4] in this general energy region.

We hope, with increased beam currents, to repeat the experiment at lower energies where the angular anisotropy is larger.

* This work was supported in part by the joint program of the U. S. Office of Naval Research and the U. S. Atomic Energy Commission.

† Now at the Department of Physics, University of Washington, Seattle, Washington.

‡ The electron beam used had a maximum energy of 16 Mev and a broad energy spectrum peaked at about 13 Mev, with a width at half-maximum of 5 Mev.

[1] Winhold, Demos, and Halpern, Phys. Rev. **87**, 1139 (1952).
[2] R. A. Schmitt and N. Sugarman, Phys. Rev. **89**, 1155 (1953).
[3] H. G. Richter and C. D. Coryell, Phys. Rev. **90**, 389 (1953).
[4] D. M. Hiller and D. S. Martin, Jr., Phys. Rev. **90**, 581 (1953).

Decay Scheme of Xe^{135}

SIGVARD THULIN
Nobel Institute of Physics, Stockholm, Sweden
(Received March 16, 1954)

THE 9.2-hr Xe^{135} has been shown to decay by emission of 910-kev β particles to an excited level of energy 250 kev in Cs^{135}.[1,2] Moreover, a very weak γ ray of energy 610 kev has been reported.[2] This γ ray has now been studied by means of coincidence measurements on electromagnetically separated Xe^{135} samples in an intermediate image β spectrometer.[3] Behind the β source a large NaI(Tl) crystal (diameter 1 in.×1 in.) was placed. This was optically connected with an EMI 6262 photomultiplier by means of a perspex light pipe of 15-cm length. The G-M pulses and the scintillation spectrometer pulses were fed to a coincidence circuit of resolving time 2.5×10^{-7} sec.

No coincidences were found between K conversion electrons of the 250-kev γ ray and γ quanta of energy higher than 550 kev. However, coincidences were recorded between these K-conversion electrons and γ quanta of energy ~370 kev. A small bump on the high-energy tail of the very strong 250-kev γ line in the scintillation spectrum of Xe^{135} may partly be explained as due to a γ ray of energy ~370 kev.

It was also shown that the 600-kev γ ray is emitted in cascade with a β continuum. A Fermi plot of the coincidence distribution showed an upper limit of 548 kev.

The results of the coincidence measurements strongly support the decay scheme given in Fig. 1.

According to the extreme one-particle shell model,[4] the second excited level might be $s_{\frac{1}{2}}$ or $d_{\frac{1}{2}}$. The former alternative seems im-

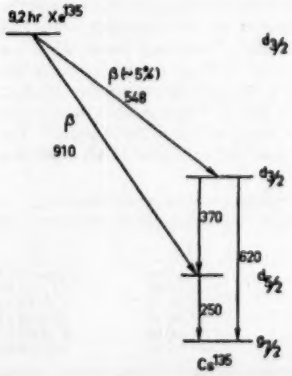

FIG. 1. Proposed decay scheme of Xe^{135}. Energy values in kev.

probable, since then the transition to the ground state would be of the $M3$ type. The half-life of the 620-kev level would then be $\sim 10^{-2}$ sec, according to the semiempirical formula of Goldhaber and Sunyar.[5] This would be in contradiction to our coincidence data. Therefore the d_1 alternative, shown in Fig. 1, seems to be the most probable.

[1] Thulin, Bergström, and Hedgran, Phys. Rev. **76**, 87 (1949).
[2] I. Bergström, Arkiv Fysik **5**, 191 (1952).
[3] H. Slätis and K. Siegbahn, Arkiv Fysik **1**, 339 (1949).
[4] M. G. Mayer, Phys. Rev. **75**, 1969 (1949); Haxel, Jensen, and Suess. Z. Physik **128**, 295 (1950).
[5] M. Goldhaber and A. W. Sunyar, Phys. Rev. **83**, 906 (1951).

Thermal Neutron Fission Cross Section of Am^{242m}

G. H. Higgins and W. W. T. Crane
Radiation Laboratory, University of California, Berkeley, California
(Received March 3, 1954)

SINCE Am^{242m} is the first member in the chain of nuclides produced by successive neutron captures on Am^{241}, its fission cross section is of considerable importance for calculating yields of masses heavier than 242.

The method for measurement consisted of irradiating a sample of Am^{241} in the high neutron flux of the MTR (Materials Testing Reactor, Arco, Idaho) to produce the Am^{242} and Am^{242m}, placing the americium on a platinum plate in one side of a double-fission counter and exposing it to a well-thermalized flux of neutrons. Since Cm^{242} has a very small fission cross section,[1] the observed counting rate decayed with the sixteen hour half-life of Am^{242m}, superimposed on a long-lived background due to the fissions of Am^{241}, Am^{242}, and small amounts of uranium. The experimental data are presented graphically in Fig. 1.

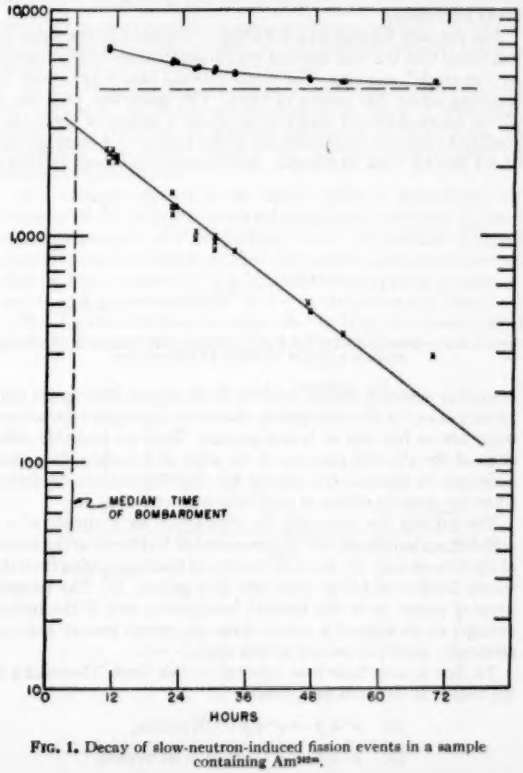

FIG. 1. Decay of slow-neutron-induced fission events in a sample containing Am^{242m}.

A weighed sample of U^{235} was irradiated in the other side of the same counter in the same flux, and the number of Am^{242m} atoms was determined by alpha pulse analyses of the Cm^{242}–Am^{241} mixture after the Am^{242m} had decayed. The fission cross section of Am^{242m} was then calculated from the number of atoms of U^{235} and Am^{242m}, the counting rate of the two samples in the same flux, and the known fission cross section of U^{235}:

$$\sigma_f(Am^{242m}) = \frac{\text{counting rate } Am^{242m} \times \text{No. atoms } U^{235} \times \sigma_f(U^{235})}{\text{counting rate } U^{235} \times \text{No. atoms } Am^{242m}}.$$

The results of this experiment lead to a value of 2950 barns for the fission cross section of Am^{242m}. This value may be in error if the transition between Am^{242m} and Am^{242} occurs in more than 5 percent of the decay events.[2–4]

[1] Hanna, Harvey, Moss, and Tunnicliffe, Phys. Rev. **81**, 893 (1951).
[2] O'Kelley, Barton, Crane, and Perlman, Phys. Rev. **80**, 293 (1950).
[3] R. Hoff, University of California Radiation Laboratory Report UCRL-2325, 1953 (unpublished).
[4] H. Jaffe (unpublished work, 1953).

Electric Excitation of Tantalum†*

J. T. Eisinger, C. F. Cook, and C. M. Class
The Rice Institute, Houston, Texas
(Received March 4, 1954)

IT is now well known that low-lying levels of heavy and intermediate nuclei can be excited by the interaction between the electric field of an incident charged particle and the nuclear protons.[1–3] This process, called electric or Coulomb excitation, occurs at energies for which the penetration of the bombarding particle into the nucleus is negligible. A particularly interesting example of this type of interaction is furnished by Ta^{181} when bombarded with protons. Gamma rays corresponding to levels at 137 kev and 303 kev are observed, and conversion electrons have been detected[4] with energies corresponding to transitions from the 137-kev level to the ground state and between the two excited states. Measurements carried out in this laboratory have also established the presence of a 166-kev gamma ray. The spectrum, shown in Fig. 1, was taken at a proton energy of 3 Mev, and the radiation was detected with a conventional NaI scintillation spectrometer having a resolution of 10 percent. The background due to target x-rays was reduced to an acceptable level by using a 1-mm thick gold absorber. The energies assigned to the observed gamma rays were 139, 167, and 309 kev, to an accuracy of 5 kev, in agreement with the more accurate measurements of 137, 166, and 303 kev.[4] The possibility that the Compton edge of the 303-kev line, which comes at 164 kev, was contributing significantly to the observed intensity of the 166-kev line was excluded by measurements with appropriate Pb absorbers.

The relative probabilities of gamma-ray transitions from the 303-kev level directly to the ground state, and through the 137-kev level, were determined from the data of Fig. 1. Corrections to the measured intensities were made for (1) background, (2) absorp-

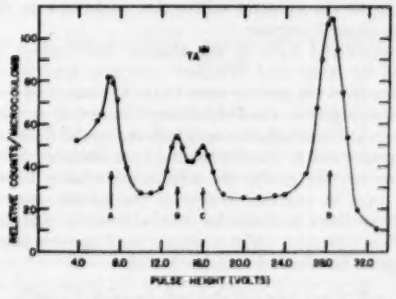

FIG. 1. The pulse-height distribution obtained for the radiation from a 5-mil tantalum target bombarded with 3-Mev protons using a 1-mm gold absorber. Peak A corresponds to the tantalum K x-ray. Peaks B, C, and D correspond to gamma rays of 139, 167, and 309 kev.

tion, and (3) the relative contribution of the photopeak to the total intensity.[5] The graphical resolution of the 137–166 kev doublet and the allowance for background were somewhat arbitrary, but the latter correction was guided by results obtained with absorbers which had a very small transmission for the 166-kev radiation while attenuating the 303-kev radiation only moderately. The ratio of the crossover to the cascade transitions was found to be 0.8. Using the result that 85 percent of the 166-kev radiation is due to $M1$ transitions,[4] the magnetic moment of the ground state of Ta was calculated[7] to be 3 nm. This is to be compared with the value of 2.8 nm obtained by Huus and Bjerregaard using a somewhat less direct method and a spectroscopic value of 2.1 nm.[6]

Further interest in the energy levels of tantalum arises from the agreement of the spacing of these levels with that predicted by the rotational model of the nucleus of Bohr and Mottelson.[7] For an even-odd nucleus with ground-state spin 7/2, (Ta^{181}) the model predicts excited states of spins 9/2 and 11/2 having energies above the ground state in the proportion of 9 to 20. This proportion agrees well with that found in experiments. Additional evidence supporting the spin assignments can be obtained from the angular distributions of the gamma radiation from these levels with respect to the beam. Figure 2 shows the experimental distribution obtained

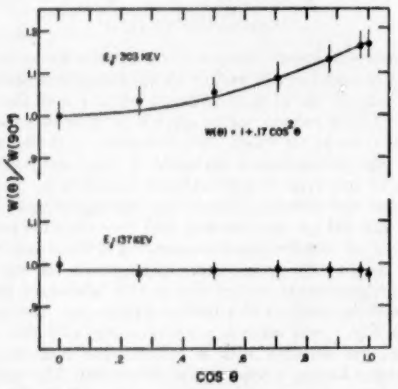

FIG. 2. The angular distributions of the 137-kev and 303-kev gamma rays from tantalum measured between 0° and 90° to the beam at $E_p = 3$ Mev. The theoretical distribution is shown for the 303-kev radiation.

for a proton energy of 3 Mev with the counter subtending a solid angle of 0.13 steradian. The data were taken with a 3 mm Cu absorber which transmitted a strong 137-kev line relative to background but did not impair the resolution of the 303-kev line. The intensity of the 166-kev line was then only about 15 percent of that of the 137-kev line so that these two lines were not resolved. The data of Fig. 2 were corrected for the absorption of the radiation in the target (5 mils of tantalum) and for background. Errors shown in the curves are statistical. A systematic error due to uncertainties in the background subtraction could change the asymmetry by about 3 percent.

The theoretical form of the angular distributions has been predicted by Alder and Winther[8] assuming electric quadruple transitions from the ground state to the excited state in question ($E2$ in keeping with the B-M theory[7] according to which such transitions are especially favored) followed by $E2$ transitions back to the ground state. The distributions are obtained in a manner analogous to that giving the angular correlation between two gamma rays in cascade. However, the special nature of the excitation process modifies the distributions through energy dependent factors $a_k(\xi)$ which multiply the Legendre polynomials. The angular distribution function is then

$$W(\theta) = 1 + a_2(\xi)B_2P_2(\cos\theta) + a_4(\xi)B_4P_4(\cos\theta),$$

where the B_k are the gamma-gamma correlation coefficients tabulated by Biedenharn and Rose.[9] Expressing the theoretical distributions in a form easily compared with experiment gives $W(\theta) = 1 + 0.171\cos^2\theta + 0.006\cos^4\theta$ for the 303-kev gamma ray, which is the curve shown in Fig. 2, and $W(\theta) = 1 - 0.032\cos^2\theta + 0.037\cos^4\theta$ for the 137-kev gamma ray, which is isotropic within the accuracy of this experiment. The $a_k(\xi)$ were calculated for 3-Mev protons[10] and the B_k were determined by assuming the spins of the 137-kev and 303-kev states to be 9/2 and 11/2, respectively.

The good agreement between the experimental and theoretical distributions lends further support to the spin assignments and the excitation process which was postulated.

† Supported in part by the U. S. Atomic Energy Commission.

* Part of this work was reported at the New York meeting of the American Physical Society, January 28–30, 1954 [Bull. Am. Phys. Soc. **29**, No. 1, (1954). This bulletin appears in this issue, Phys. Rev. **94**, 742–801 (1954)].

[4] T. Huus and Č. Zupančič, Kgl. Danske Videnskab. Selskab, Mat.-fys. Medd. **28**, No. 1 (1953).
[5] C. L. McClelland and C. Goodman, Phys. Rev. **91**, 760 (1953).
[6] G. M. Temmer and N. P. Heydenburg, Phys. Rev. **93**, 351 (1954).
[4] T. Huus and J. H. Bjerregaard, Phys. Rev. **92**, 1579 (1953).
[5] C. M. Davisson and R. D. Evans, Revs. Modern Phys. **24**, 79 (1952).
[6] B. M. Brown and D. H. Tomboulian, Phys. Rev. **88**, 1158 (1952).
[7] A. Bohr and B. Mottelson, Kgl. Danske Videnskab. Selskab, Mat.-fys. Medd. **27**, No. 16 (1953).
[8] K. Alder and A. Winther, Phys. Rev. **91**, 1578 (1953).
[9] L. C. Biedenharn and M. E. Rose, Revs. Modern Phys. **25**, 729 (1953).
[10] The error in the coefficients due to the neglect of the effect of the thick target is small because of the form of the yield curve and the slow variations of $a_k(\xi)$ with energy.

$\pi^- - p$ Interactions at 1.5 Bev*

J. CRUSSARD, W. D. WALKER, AND M. KOSHIBA
Physics Department, University of Rochester, Rochester, New York
(Received February 23, 1954)

STACKS of 400μ G-5 stripped emulsion were exposed to the 1.5-Bev π^- beam at the Brookhaven cosmotron. The plates were aligned with respect to each other by means of x-ray dots so that it was possible to trace even minimum ionizing tracks through many emulsions.

The primary interest was in finding $\pi^- -$ proton interactions. It was found that the only efficient way to detect these interactions is by "on-track" scanning. The work reported here is the result of scanning about 300 meters of track. The mean free path for a $\pi^- - p$ interaction was found to be about 4 meters of track. According to counter measurements of the total $\pi^- - p$ cross section at 1.5 Bev by Cool, Madansky, and Piccioni,[1] the mean free path

FIG. 1. A $\pi^- - p$ collision in which a π^0 is produced. The more heavily ionizing track is a proton of about 40-Mev energy.

in nuclear emulsion should be about 9–10 meters. This means that 50–60 percent of the interactions classed as hydrogen interactions occur not on free but on bound protons. They are probably collisions of the π's with protons on the edge of a nucleus. It is thus necessary to examine the criteria for classification and to decide what the possible effects of accepting edge collisions are.

The criteria for accepting an interaction as a simple $\pi^- - p$ collision are as follows: (1) No evaporation fragments at the vertex of the interaction. (2) An even number of tracks emerging from the interactions of which at most one is a proton. (3) The protons must of course be in the forward hemisphere, and if the proton emerges at an angle θ it cannot have an energy greater than an elastically scattered proton at this angle.

To date 4 cases have been rejected on this basis. The results of the search to date are as follows:

(a) $\pi^- + p \rightarrow \pi^- + p$ — 16 events,

(b) $\pi^- + p \rightarrow \pi^- + \pi^0 + p$ — 31 events,

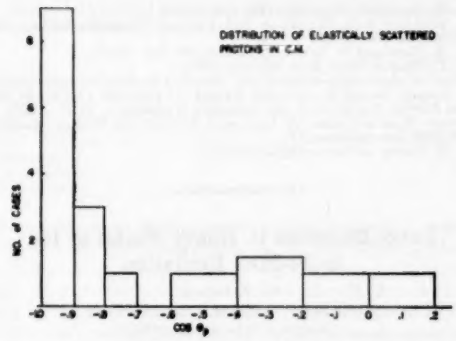

FIG. 2. Angular distribution in the c. m. system of 22 elastically scattered protons.

(c) $\pi^-+p\rightarrow\pi^++\pi^-+n$ — 20 events,

(d) $\pi^-+p\rightarrow\left.\begin{matrix}\pi^0+n\\ 2\pi^0+n\\ \Lambda^0+\theta^0\end{matrix}\right\}$ — 22 events,
etc. . . .

(e) $\pi^-+p\rightarrow\pi^++2\pi^-+p$ — 1 event.

It is possible that some of the cases which appear to be π^0 production are cases of elastic collisions in which one of the products has struck a neutron. However, it seems likely that this does not happen often for the following reasons: (1) Frequent secondary interactions would tend to scatter protons to large angles which in turn should result in many rejections by criterion (3). (The inelastic protons actually seem to come out very much in the forward direction in the lab system.) (2) In a three-particle reaction the energy of one of the particles with its angle and the angle of one other track uniquely specifies the reaction. In 12 cases good momentum measurements on both charged particles could be made, and on this basis 2 were rejected.

Some of the cases classed as single π^0 production might be double π^0 production. There are not thought to be many of these since there are so few cases of multiple production of charged π's. By momentum and energy balance one can occasionally check for multiple π^0 production.

If a collision appears to be elastic within a momentum discrepancy of 200 Mev/c it is classed as an elastic collision. Figure 1 shows an example of π^0 production in a π^-+p collision. Figure 2 shows the angular distributions of the protons in elastic scattering. Figures 3 and 4 show the angular distributions of the protons, π^- and π^0, and angles between π^- and π^0 in the production cases.

The angular distributions show that in both the elastic and π^0 production cases the protons tend to go backward and the π^- forward in the center-of-mass system. The elastic scatterings seem to break into two categories: a diffraction-type scattering which gives deflections of 10°–30° in the center-of-mass system, and a low-angular-momentum interaction which gives a big deflection and change of momentum in the center-of-mass system. The π^- and π^0 have rather different angular distributions. The π^- and π^0 seem to have a tendency to come apart with a rather large angular separation. This angular separation between mesons seems to be characteristic of the cases in which $\pi^++\pi^-+n$ are produced. In the center-of-mass system the π^0, π^-, and proton have on the average about equal momenta.

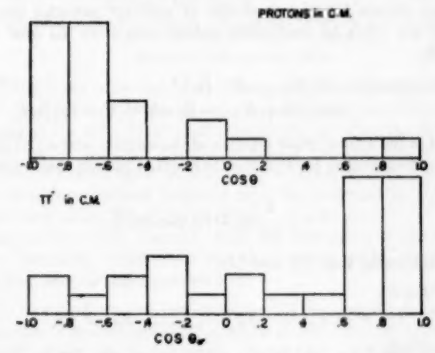

FIG. 3. Angular distribution of p and π^- from the reaction $\pi^-+p\rightarrow\pi^-+p+\pi^0$.

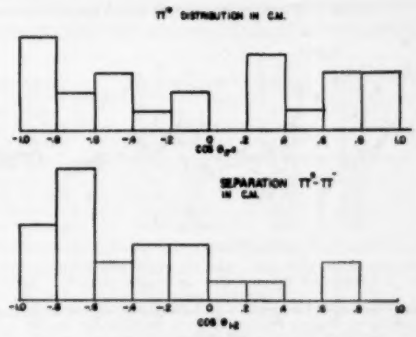

FIG. 4. Angular distribution of π^0 in the c. m. system and the distribution of π^0 with respect to the π^- in the c. m. system.

If the angular distributions of the π^0 and π^- are different, it seems to rule out the possibility of a statistical-type theory of these interactions.

The authors wish to thank Dr. Cool, Dr. Piccioni, and Dr. Madansky for their aid in making the first exposures and also Dr. Hill and Dr. Widgoff for making the later exposures. The authors wish to acknowledge the scanning aid given by Miss P. Griesbach, Mrs. E. Awschalom, H. Fisher, B. Munir, and J. Klose. It is a real pleasure to acknowledge the cooperation and hospitality of Dr. G. B. Collins and Dr. E. O. Salant.

* This research was supported in part by the U. S. Atomic Energy Commission.

[1] Cool, Madansky, and Piccioni, Phys. Rev. **93**, 249 (1954).

Nuclear Potential Well Depth*

ROBERT K. ADAIR
Brookhaven National Laboratory, Upton, New York
(Received March 11, 1954)

FESHBACH, Porter, and Weisskopf[1] have shown that the pattern[2] of variation of the total cross sections of heavy nuclei with neutron energy and nuclear size can be explained by representing the neutron-nucleus interaction as that of a square well with absorption

$$V(r)=-19\text{ Mev}(1+i0.05),\quad 0\leq r\leq R=1.45A^{\frac{1}{3}}\times10^{-13}\text{ cm};$$
$$V(r)=0,\qquad r>R.$$

Bohr and Mottelson[3] have pointed out that the value of 19 Mev used for the real part of the potential is considerably smaller than that necessary to account for the bound levels of heavy nuclei as described by the shell model. It is the purpose of this note to show that a well depth of about 40 Mev, consistent with the shell model, is indicated by the scattering data.

A most striking characteristic of the total cross-section pattern is the variation of the average low-energy neutron-nucleus cross section as the value of A, the number of nucleons in the nucleus, increases from about 100 to about 200. A characteristic well-type S-wave resonance behavior occurs at about $A=150$. Using a square-well shape, and neglecting absorptive effects for simplicity, it is clear that σ_T will at resonance be equal to $(N+\frac{1}{2})$ for $r=R$,

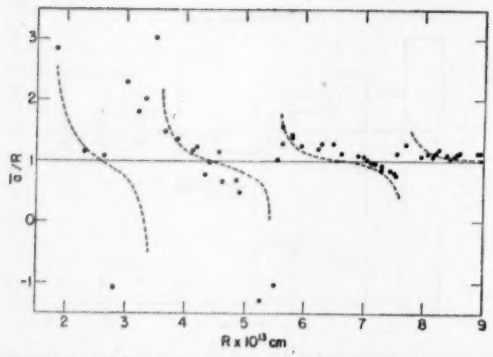

FIG. 1. The points show the variation of the average scattering length $\bar{a}$ divided by the nuclear radius R, as a function of R. The dashed curve represents the variation of a/R to be expected from a well with the parameters: $V=-42$ Mev, $0\leq r\leq R$; $V=0$, $r>R$; $R=1.45\times10^{-13}A^{\frac{1}{3}}$ cm.

where κ is the wave number associated with the potential well depth. If a well depth of 19 Mev is chosen, the resonance near $A=150$ will be the third S-wave resonance, and N will equal 2. However, the following examination of the low-energy neutron cross sections of lighter elements indicates that the resonance near $A=150$ is the fourth S-wave resonance, not the third, hence $N=3$ and the proper well depth must be about $[(3+\frac{1}{2})/(2+\frac{1}{2})]^2\times19$ Mev, or about 40 Mev.

Ford and Bohm[4] have previously discussed variations of the thermal neutron scattering length, a, with nuclear size, and concluded that a nuclear potential well of about 40-Mev depth was in agreement with the data. Since scattering lengths are strongly affected by individual, narrow, low-energy resonances, which the optical theory treats only on the average, it has not been clear that the deviations of the values of a from that expected from hard sphere scattering, for example, were significant of anything but the presence of nearby narrow energy levels.[5] Such fluctuations, which are not pertinent to the theory, can largely be eliminated by using for the value of the scattering length an average value defined as $\bar{a}=(\sigma_0/4\pi)^{\frac{1}{2}}$ where σ_0 represents the low-energy cross section averaged over narrow resonances. Values of $\bar{a}$, divided by R, are shown in Fig. 1, plotted against R, the nuclear radius. These values are taken primarily from total neutron cross-section measurements made at the University of Wisconsin by Barschall, Miller, Bockelman, and others.[6] Any estimate of this average cross section at zero energy is necessarily subjective but in only a few cases are the uncertainties in $\bar{a}$ greater than 5 percent, while the variations of interest are much larger than five percent. The sign of $\bar{a}$ is taken as negative when the measured coherent scattering lengths are negative.[7] Also plotted on Fig. 1 is the variation of a to be expected from a square well 42 Mev deep. The data show clearly that the number of resonances observed is that which one would expect from a well about 40 Mev deep, verifying the conclusions of Ford and Bohm.[4]

It seems likely that the increase of well depth from 19 Mev to about 40 Mev will not invalidate the general success of the Feshbach, Porter, and Weisskopf[1] formulation in predicting the variation of average neutron cross section with energy and nuclear radius near $A=150$, since application of the Sturm-Liouville theorem leads us to expect P- and D-wave resonances to bracket the S resonance, as a function of either neutron energy or nuclear radius, in much the same way, near $\kappa R=7\pi/2$, as near $\kappa R=5\pi/2$, independent of details of well shape. Preliminary calculations by Porter[8] seem to substantiate this view.

Conversations and correspondence with Dr. C. E. Porter, Dr. Ben Mottelson, and Dr. H. H. Barschall have contributed in an important way to this work.

* Work performed under the auspices of the U. S. Atomic Energy Commission.

[1] Feshbach, Porter, and Weisskopf, Phys. Rev. **90**, 166 (1953).
[2] H. H. Barschall, Phys. Rev. **86**, 431 (1952).
[3] A. Bohr and B. R. Mottelson, Kgl. Danske Videnskab. Selskab, Mat.-fys. Medd. **27**, 159 (1953).
[4] K. W. Ford and D. Bohm, Phys. Rev. **79**, 745 (1950).
[5] D. C. Peaslee, Phys. Rev. **85**, 554 (1952).
[6] Most of these cross sections are compiled in *Neutron Cross Sections*, U. S. Atomic Energy Commission Report AECU-2040 (Technical Information Service, Department of Commerce, Washington, D. C., 1952).
[7] These values are primarily from work of Shull and Wollan compiled in AECU-2040 (see reference 6).
[8] C. E. Porter (private communication).

Level Densities in Heavy Nuclei of 10- to 20-Mev Excitation

D. B. BEARD
University of California, Davis, California
(Received February 15, 1954)

IT is quite evident that nuclei of 8- or 10-Mev excitation or less cannot be treated as excited Fermi gases of all the nucleons present. Hughes and his co-workers[1] have shown that capture cross sections for thermal and 1-Mev neutrons are a function of eveness or oddness of the atomic number of the target nucleus and a particularly pronounced function of the magic property of the target nucleus. The difference between even and odd Z, or between magic nuclei and their neighbors is entirely a matter of how the last few nucleons are bound. And if the behavior of two or three nucleons makes a great difference in the level densities of the compound nucleus as Hughes[1] and others[2] have shown to be the case, then a statistical theory cannot be valid. Moreover, it is clear that few of the total number of nuclear particles participate in the excitation.

Further evidence is supplied by Feshbach, Porter, and Weisskopf,[3] who show that a surprisingly good fit to Barschall's[4] total neutron scattering data from 1–3 Mev is obtained by scattering in a nuclear well in which the mean free path of a neutron in a 10-Mev excited nucleus is 20 nucleons long. This means that in nuclei of 100–200 atomic mass number only 5–10 nucleons can participate in the excitation. As Feshbach, Porter, and Weisskopf[3] have further observed, however, the data of Phillips, Davis, and Graves[5] on inelastic neutron cross sections at 14 Mev, in which the target nuclei appeared totally "black," indicate that all the nucleons in the target nuclei participate in a compound nucleus excitation of around 20 Mev.

We assume a general level-density formula whose energy dependence is common to many different nuclear models:[6-9]

$$\omega(E_{\max}-E)=\text{const}\,(E_{\max}-E)^{-1}\exp[KA'(E_{\max}-E)]^{\frac{1}{2}}, \quad (1)$$

where $(E_{\max}-E)$ is the excitation energy of the nucleus, A' is the number of nucleons participating in the excitement, and K is an experimentally fitted parameter. We make a linear interpolation for A' between E_0, the excitation energy below which few nucleons are able to participate in the excitation, and E_1, the excitation energy above which all the nucleons can participate in the reaction. We then obtain for the spectrum of emitted particles from a nucleus left with an excitation energy less than E_1 and well above E_0

$$I(E)dE=\text{const}E\sigma_c(E)[E_{\max}-E-E_0]^{-1}\times\exp[KA(E_{\max}-E_0-E)^2/(E_1-E_0)]^{\frac{1}{2}}dE, \quad (2)$$

where A is the atomic mass number of the nucleus and $\sigma_c(E)$ is the capture cross section for the inverse event. Defining the temperature as

$$1/T=-\frac{d}{dE}\ln[I(E)/E\sigma_c(E)], \quad (3)$$

we obtain, using Eqs. (1) and (2),

$E_{\max}-E\leqslant E_1$:

$$1/T=[KA/(E_1-E_0)]^{\frac{1}{2}}-[E_{\max}-E_0-E]^{-1}; \quad (4)$$

$E_{\max}-E\geqslant E_1$:

$$1/T=\tfrac{1}{2}[KA/(E_{\max}-E_0-E)]^{\frac{1}{2}}-[E_{\max}-E_0-E]^{-1}. \quad (5)$$

TABLE I. Calculated and experimentally observed temperatures.

	Sn^{118}			Pt^{195} and Au^{197}		
$E_{max}-E$(Mev)	10	12	24	10	12	23
T_{calc}(Mev)	0.9	0.8	1.6	0.7	0.6	1.2
T_{obs}(Mev)	1.0[a]	0.6[b]	~1.8[c]	0.7[a]	0.7[b]	~1.7[c]

[a] Reference 11.
[b] Reference 10.
[c] Reference 12.

We would expect E_0 to decrease with A for large A, reflecting the lower binding energy of these nuclei; and following Hurwitz and Bethe[2] we might expect a very slight increase in E_0 for magic nuclei. At any rate, setting $E_0=8$ Mev, $E_1=20$ Mev (as is suggested by the experiments),[4,5] and $K=\frac{1}{4}$ (as is suggested by Bethe and Bardeen's work),[6] results for all nuclei in a considerably better fit to the experimental data[10–12] than the usual theory gives,[9,13] as is shown in Table I. The calculated temperatures are all well within the estimated error of the observed temperatures.

In the analysis of this work we used a nuclear radius of $1.2\times10^{-13}A^{\frac{1}{3}}$ cm for proton emission,[14] and we allowed for the emission of knock-on protons.[15] Temperatures in this preliminary report were computed for energies of emitted particles such that the emitted particles all had approximately the same orbital angular momentum. If this were not done, it was feared that the large nuclear spin changes possible for the highest-energy emitted particles would be forbidden for other examples of lower energy. Comparison of residual nuclei level densities was sought for those cases where approximately the same fraction of the total number of levels was observed.

An attempt is being made to estimate shell energies and to employ the statistical method[6–8] to compute $I(E)$ more precisely.

[1] Hughes, Garth, and Levin, Phys. Rev. **91**, 1423 (1953).
[2] H. Hurwitz, Jr., and H. A. Bethe, Phys. Rev. **81**, 898 (1951).
[3] Feshbach, Porter, and Weisskopf, Phys. Rev. **90**, 166 (1953) and U. S. Atomic Energy Commission Report NYO-3076 (unpublished); Nuclear Development Associates Report NDA-15B-4 (unpublished).
[4] H. H. Barschall, Phys. Rev. **86**, 431 (1952).
[5] Phillips, Davis, and Graves, Phys. Rev. **88**, 600 (1952).
[6] H. A. Bethe, Revs. Modern Phys. **9**, 69 (1937).
[7] C. Van Lier and G. E. Uhlenbeck, Physica **4**, 531 (1937).
[8] I. N. Sneddon and B. F. Touschek, Proc. Cambridge Phil. Soc. **44**, 391 (1948).
[9] J. M. Blatt and V. F. Weisskopf, *Theoretical Nuclear Physics* (John Wiley and Sons, Inc., New York, 1952), pp. 365–374.
[10] E. R. Graves and L. Rosen, Phys. Rev. **89**, 343 (1953).
[11] P. C. Gugelot, Atomic Energy Commission Report NYO-6182, 1953 (unpublished); and Phys. Rev. **81**, 51 (1951).
[12] R. M. Eisberg and G. J. Igo, Phys. Rev. **93**, 1039 (1954).
[13] B. L. Cohen, Phys. Rev. **92**, 1245 (1953).
[14] F. Bitter and H. Feshbach, Phys. Rev. **92**, 837 (1953).
[15] Austern, Butler, and McManus, Phys. Rev. **92**, 350 (1953).

Nuclear Shell Model *ft* Values for Intermediate Coupling

R. SCHULTEN AND R. A. FERRELL*
Max-Planck-Institut fuer Physik, Goettingen, Germany and University of Maryland, College Park, Maryland
(Received January 28, 1954)

USING the wave functions already calculated by one of us for various light nuclei of mass number from 6 to 15,[1] we have evaluated the beta-decay matrix elements, and thus the *ft* values, for several of the beta transitions among the light nuclei. These theoretical results agree satisfactorily with experiment,[2] and indicate that intermediate coupling is to be preferred as a nuclear model over strict *LS* or *j-j* coupling.[3]

The present work depends upon the derivation of the nuclear wave functions, which used the shell model with intermediate coupling. Specific assumptions were:

(1) Two protons and two neutrons fill the $1s$ shell, forming an inert core. The remaining nucleons lie in the $1p$ shell, whose one-particle space wave functions, $(r/r_0)\exp[-\frac{1}{2}(r/r_0)^2]\times Y_1^{1,0,-1}$ (where $r_0=1.7\times10^{-13}$ cm and $Y_1^{1,0,-1}$ are the spherical harmonics), are coupled to the Pauli spin functions to form $p_{\frac{3}{2}}$ and $p_{\frac{1}{2}}$ one-particle wave functions.

TABLE I. Log *ft* values of various beta decays.

		Log *ft*		
β transition	Experimental[a]	*LS* coupling	*j-j* coupling	Intermed. coupling
$n\rightarrow p+e^-+\nu$[b]	3.13	3.13	3.13	3.13
$He^6\rightarrow Li^6+e^-+\nu$	2.94 ±0.04	2.95	3.21	2.98
$Be^7\rightarrow Li^7+\nu$	3.37 ±0.01	3.31	3.45	3.41
$Be^7\rightarrow Li^{7*}+\nu$	3.53	3.61	4.08	3.58
$C^{10}\rightarrow B^{10*}+e^+\nu$[c]	3.77 ±0.20	3.43	3.43	3.43
$N^{13}\rightarrow C^{13}+e^++\nu$	3.67	3.61	3.61	3.69
$C^{14}\rightarrow N^{14}+e^-+\nu$[b]	8.95	2.95	3.91	5.70
$O^{15}\rightarrow N^{15*}+e^++\nu$[c]	3.52 ±0.10	3.43	3.43	3.43
$O^{15}\rightarrow N^{15}+e^++\nu$[c]	3.59 ±0.03	3.61	3.61	3.61

[a] These entries do not represent new work. The Fermi transitions are independent of nuclear structure, while the O^{15} beta-decay is completely described by *j-j* coupling. (Also see reference 4).
[b] *L* forbiddenness gives rise to a factor of ten in this matrix element, and a further partial cancellation of contributions occurs, as conjectured by Sachs [R. Sachs, *Nuclear Theory* (Addison-Wesley Publishing Company, Chicago, 1953), p. 347]. This is at variance with Inglis' finding (reference 3, p. 442), which is based on a different assumption for the nuclear interactions.

(2) The interaction between all nucleon pairs is a four-forces mixture weighted 0.35 Wigner, 0.35 Majorana, 0.15 Bartlett, and 0.15 Heisenberg force, with a well depth of 30 Mev and a common radial dependence of $\exp[-(r/1.9\times10^{-13}\text{ cm})^2]$, and an additional spin-orbit force of

$$-2.8\text{ Mev}\,[\mathbf{s}_1\cdot(\mathbf{r}_{12}\times\mathbf{p}_1)+\mathbf{s}_2\cdot(\mathbf{r}_{21}\times\mathbf{p}_2)]\frac{1}{\hbar^2}\exp\left(-\frac{r_{12}^2}{(1.9\times10^{-13}\text{ cm})^2}\right),$$

where 1 and 2 designate a pair of nucleons and the remaining symbols have their conventional significance. (The spin-other orbit terms of the usual interaction are neglected as being of secondary importance.) The tensor force is neglected.

(3) The wave functions contain no admixtures from higher shells—the energy is diagonalized wholly within the $1p$ (that is, $p_{\frac{3}{2}}$ and $p_{\frac{1}{2}}$) shell.

The above assumptions led to wave functions yielding magnetic moments in agreement with experiment to the accuracy with which (3) can be expected to hold, (~5 percent). Using the same wave functions to calculate the matrix elements in $\log ft=C-\log(|\int 1|^2+|\int\boldsymbol{\sigma}|^2)$, (where we take the Fermi and Gamow-Teller coupling constants equal, and fit the constant C to the neutron *ft* value), we find values which are presented in Table I and compared with those calculated on the basis of strict *LS* or *j-j* coupling.

We are grateful to Professor W. Heisenberg for suggesting and stimulating this work. One of us (RAF) is indebted to the Max-Planck-Institut for the hospitality extended to him, and to the U. S. Atomic Energy Commission for fellowship support.

* Present address: Physics Department, University of Maryland, College Park, Maryland. Publication assisted by the U. S. Office of Naval Research.
[1] R. Schulten, Z. Naturforsch. **12**, 759 (1953).
[2] To roughly the experimental error, except for C^{14}, for which see reference 4 and reference b of Table I.
[3] For work already carried out on intermediate coupling see D. R. Inglis, Revs. Modern Phys. **25**, 390 (1953); N. Zeldes, Phys. Rev. **90**, 416 (1953); A. M. Lane, Phys. Rev. **92**, 839 (1953); G. E. Tauber and Ta-You Wu, Phys. Rev. **91**, 443 (1953) and Phys. Rev. **94**, 762 (1954); Sharp, Gellman, and Tauber, Phys. Rev. **94**, 762 (1954).
[4] We are indebted for information on the experimental data to R. W. King, National Research Council.

Energy Spectra of Nucleons Evaporated from a Compound Nucleus*

R. M. EISBERG
Brookhaven National Laboratory, Upton, New York
(Received March 8, 1954)

SEVERAL experiments appear to disagree with the idea that a compound nucleus de-excites itself by evaporating nucleons according to a Maxwellian energy distribution. A Maxwellian distribution follows from the assumption of the compound nucleus

model and the assumption that the density of levels, ω, of the residual nucleus at excitation E is given by $\omega = b \exp[(aE)^{\frac{1}{2}}]$.[1] Some of these experiments are: the inelastic scattering of 14-Mev neutrons[2] and 18-Mev protons[3] from various elements; the inelastic scattering of 30-Mev protons from Al[4]; and the neutron spectra from nuclear reactions induced in various elements by 16-Mev protons.[5] The results of these experiments have been conveniently compiled in a recent article by Cohen.[6] All of these data indicate that there are more high-energy nucleons emitted, compared to the number of low-energy nucleons emitted, than can be explained by a Maxwellian distribution.

The following explanations of this discrepancy have been proposed: (a) at low excitation, the level density of the residual nucleus varies much more slowly than exponentially[4]; (b) the excitation energy of a nucleus should not be measured from the ground state but from a state which is above the ground state[7]; (c) there are selection rules in effect which make transition probabilities to low-lying levels in the residual nucleus very much larger than transition probabilities to highly excited levels[6]; and (d) the excess of high-energy nucleons is due to a direct interaction between the incoming particle and the nucleons forming the surface of the target nucleus.[3]

The purpose of this letter is to indicate that the last explanation is certainly adequate to account for the results obtained from the inelastic scattering of 30-Mev protons by Al, and is probably adequate to account for the results obtained from the lower energy (p,p'), (n,n'), and (p,n) experiments. The information required to prove this statement is obtained from recent experiments on the inelastic scattering of 31-Mev protons from several heavy elements.[8] In these experiments it is found that the energy distributions of the inelastically-scattered protons bear no resemblance to Maxwellian distributions, except at a scattering angle of 135°. Further, it is found that the angular distributions for inelastic scattering are strongly peaked forward, and that the total cross sections for inelastic scattering are at least an order of magnitude larger than the compound nucleus cross section for evaporating protons through the Coulomb barrier of a heavy nucleus. These data definitely disagree with what would be expected in a compound nucleus process but can be explained qualitatively by assuming that, in heavy elements at 31 Mev, the inelastic scattering occurs when the incident proton collides with the rim of the target nucleus and makes a direct interaction with one or several nucleons.

In the 30-Mev (p,p') experiment on Al, the excess of protons, compared to a Maxwellian distribution, emitted in the energy range 15–25 Mev and at an angle of 90°, corresponds to an inelastic-scattering cross section $d^2\sigma/d\Omega dE$ of about 0.5 mb/sterad-Mev. In the 31-Mev experiment on the heavy elements, the cross section for producing inelastically-scattered protons by the direct interaction effect, in the energy range 15–25 Mev and at an angle of 90°, is about 1.0 mb/sterad-Mev. Furthermore, the direct interaction cross section at 90° shows only a very slow decrease with decreasing A in the range Pb to Sn. Thus the excess of high-energy protons emitted from Al can be accounted for by the direct interaction effect.

Now, the extrapolation of the direct interaction cross sections down to the lower energies is not known. However, some comparisons can be made. In the inelastic-scattering experiments involving 18-Mev incident protons, the difference between the 60° and 150° cross sections of Sn for the emission of 15-Mev protons, $d^2\sigma/d\Omega dE(60°, 15 \text{ Mev}) - d^2\sigma/d\Omega dE(150°, 15 \text{ Mev})$, is about 2 mb/sterad-Mev. At 31-Mev incident energy, the cross section of Sn for the emission of 15-Mev protons at 60° by the direct interaction effect was measured to be 1.5 mb/sterad-Mev. Thus, the direct interaction effect appears to be capable of accounting for the excess of high-energy protons emitted in the forward direction in the 18-Mev experiment. Numerical comparisons cannot be made in the experiments involving the emission of neutrons since absolute cross sections are not quoted. However, the cross sections for neutron emission would be expected to be similar to those for proton emission at emission energies greater than the Coulomb barrier energy.

Finally it should be pointed out that, in the heavy elements at 31 Mev, the evidence indicates that even the inelastic scattering at 135° is predominantly a direct interaction effect. Although the energy distributions at this backward angle are of Maxwellian form, the differential cross sections are much larger than the predictions of compound nucleus theory and the temperatures required to fit the distributions are very high. For instance, the best fit to the Au energy distribution at 135° corresponds to a temperature of 7 Mev. If any thermodynamic significance is to be attributed to these high-temperature Maxwellian-like distributions, then the excitation of the compound nucleus must necessarily be confined to a very few nucleons (~3), since the total excitation energy is only about 40 Mev. This immediately leads back to the direct interaction picture. If the direct interaction cross sections in the backward directions extrapolate to lower energies as the forward cross sections seem to, then it would not be correct to assume that the energy distributions of evaporated nucleons, which are observed in the lower-energy experiments, are free from contamination due to the direct interactions effect, even when these energy distributions are measured in backward directions.

* Research performed under the auspices of the U. S. Atomic Energy Commission.

[1] V. F. Weisskopf, Phys. Rev. **52**, 295 (1937).
[2] E. R. Graves and L. Rosen, Phys. Rev. **89**, 343 (1953).
[3] P. C. Gugelot, Phys. Rev. **93**, 425 (1954).
[4] Levinthal, Martinelli, and Silverman, Phys. Rev. **78**, 199 (1950).
[5] P. C. Gugelot, Phys. Rev. **81**, 51 (1951).
[6] B. L. Cohen, Phys. Rev. **92**, 1245 (1953).
[7] H. Hurwitz and H. A. Bethe, Phys. Rev. **81**, 898 (1951).
[8] R. M. Eisberg, University of California Radiation Laboratory Report UCRL-2240, 1953 (unpublished); G. J. Igo, University of California Radiation Laboratory Report UCRL-2242 (1953) (unpublished); R. M. Eisberg and G. J. Igo, Phys. Rev. **93**, 1039 (1954).

Statistical Factors in Radiation Widths of Nuclear Energy Levels

D. J. HUGHES*
Cavendish Laboratory, Cambridge, England
(Received February 24, 1954)

INASMUCH as theoretical evaluations of the radiative transition probabilities of nuclear energy levels are in the nature of rough estimates, statistical factors are usually omitted.[1] At the present time, however, the number of well-measured radiation widths is being increased rapidly by the results of high-resolution neutron spectroscopy,[2] which allows measurement of the parameters of the highly excited states of compound nuclei formed by neutron capture. The extent and accuracy of the radiation width measurements (of the order of 10–20 percent) justifies the use of statistical factors in the theoretical formulas and in particular makes possible an investigation of any variations in width, for a given multipole order, that might arise from statistical factors.

In the past few years some use of statistical factors has been made in comparison of radiative widths with theory. Thus Goldhaber and Sunyar[3] multiplied measured transition probabilities of low-lying (isomeric) states by $(2J+1)$, with J the spin of the emitting state, in the comparison of these probabilities with Weisskopf's[1] theoretical single particle estimate. In this case, the transition probabilities used were those obtained from measured lifetimes. Radiation widths of highly excited states of light nuclei were compiled by Wilkinson[4] in the form $(2J+1)\,\Gamma_\gamma$, although here the reason was that the experimental data (reaction cross sections) give this quantity rather than Γ_γ itself. Kinsey and Bartholomew,[5] in comparing the measured widths of particular high-energy capture gamma transitions with theory, multiplied these widths by $(2J+1)$ in the process. The "measured width" is obtained from the total radiation width, Γ_γ, resulting from resonance analysis,[2] and measurement[5] of the fraction of neutron captures resulting in occurrence of the particular gamma transition. In the light of these applications of statistical factors and the

increasing number of experimental widths, some discussion of statistical factors seems pertinent: For example, as radiation widths[2] of slow neutron resonances are about the same for a wide range of J's, the presence of a $(2J+1)$ statistical factor for dipole transitions appears unlikely.

The radiation width Γ_γ that occurs in the Breit-Wigner formula and is measured by the methods of neutron spectroscopy, is equal to $\hbar/\tau$, where τ is the lifetime of the state toward gamma emission. This lifetime is independent of any spatial degeneracy of the state and is the same whether one considers only a single magnetic substate or all $(2J+1)$ substates of the level. It is true that the "strength" of a spectral line, as defined by Condon and Shortley,[6] contains a $(2J+1)$ weighting factor, but this factor (included to obtain symmetry for inverse transitions) is removed in calculation of the Einstein A coefficient, which is inversely proportional to the lifetime of the state. The theoretical transition probability, or reciprocal lifetime, is obtained by summing over the possible final states and averaging over the initial states (equally occupied for the levels formed by neutron capture). The $(2J+1)$ spatial degeneracy of the compound state is taken into account in the Breit-Wigner formula by the factor $g=\frac{1}{2}(2J+1)/(2I+1)$, appropriate for S resonances of a target nucleus of spin I. Because of specific experimental conditions, g can be evaluated and the radiation widths obtained in the case of slow neutron resonances, whereas for high-energy resonances in light nuclei g usually cannot be evaluated and only the product $(2J+1)\Gamma_\gamma$ is obtained. It is for this reason that the widths compiled by Wilkinson[4] appear with a $(2J+1)$ factor; it should be removed for comparison with theory but unfortunately is usually not known.

The theoretical expression for the one-particle radiative transition probability, as given by Weisskopf,[1] applies to transitions from a state of spin J to one of spin $\frac{1}{2}$, for which transition the statistical factor is taken as unity. For other initial and final J's, the statistical factor, given by Blatt and Weisskopf,[7] involves the Racah and Clebsch-Gordon coefficients. For the particular case of the inverse transition, $\frac{1}{2}\rightarrow J$, the factor will of course be $(2J+1)/2$ because of detailed balancing, and the observed transition probability should be *divided* by this factor to compare with Weisskopf's estimate. Goldhaber and Sunyar[3] instead, on the basis of empirical considerations, multiplied the $J\rightarrow\frac{1}{2}$ transition probability by $(2J+1)$, a procedure that equalizes the $J\rightarrow\frac{1}{2}$ and $\frac{1}{2}\rightarrow J$ transitions but does not reduce them to statistical factor unity for comparison with theory.[1]

For radiation widths of slow neutron resonances, the principal components are the electric dipole transitions.[5,7] Here the statistical factors, which can be evaluated from the formulas given by Blatt and Weisskopf[7] or Condon and Shortley[6] [Eq. (7[5])], reduce to simple forms. The following factors result for different J's, where, as before, we take a unit statistical factor for the $\frac{1}{2}\rightarrow\frac{1}{2}$ transition.[1]

	$J=\frac{1}{2}$	$\frac{3}{2}$	$\frac{5}{2}$	$\frac{7}{2}$	$\frac{9}{2}$	$\cdots$	J	$\cdots$	∞
$\Delta J=-1$	$\cdots$	1	$\frac{6}{5}$	$\frac{9}{7}$	$\frac{4}{3}$		$\frac{3(2J-1)}{4J}$		$\frac{3}{2}$
$\Delta J=+1$	2	$\frac{9}{5}$	$\frac{12}{7}$	$\frac{5}{3}$	$\frac{18}{11}$		$\frac{3(2J+3)}{4(J+1)}$		$\frac{3}{2}$
$\Delta J=0$	1	$\frac{1}{5}$	$\frac{3}{35}$	$\frac{1}{21}$	$\frac{1}{33}$		$\frac{3}{4J(J+1)}$		0

Measured widths for individual electric dipole transitions[5] should be divided by these factors in the comparison with theory rather than multiplied by $(2J+1)$; the net result of this change in procedure can be large for high J. If we are considering Γ_γ, the total radiation width of a level, we must add the probabilities for $\Delta J=\pm1$ and 0, and thus conclude, assuming a level density independent of J, that Γ_γ will be constant with J. The experimental finding[2] that Γ_γ does not depend on J is thus a strong indication that the level density is itself independent of J. (A J dependence of the radial overlap integral in the radiative matrix element that by chance just cancels a J dependence of level density seems extremely unlikely.)

During the course of this investigation, discussions with J. M. C. Scott have been of great value.

* Fulbright Professor on leave from Brookhaven National Laboratory, Upton, New York.

[1] V. F. Weisskopf, Phys. Rev. **83**, 1073 (1951).
[2] D. J. Hughes and J. A. Harvey, Nature (to be published).
[3] M. Goldhaber and A. W. Sunyar, Phys. Rev. **83**, 906 (1951).
[4] D. H. Wilkinson, Phil. Mag. **44**, 450 (1953).
[5] B. B. Kinsey and G. A. Bartholomew, Phys. Rev. **93**, 1260 (1954).
[6] E. U. Condon and G. H. Shortley, *The Theory of Atomic Spectra* (Cambridge University Press, Cambridge, 1951), p. 48.
[7] J. M. Blatt and V. F. Weisskopf, *Theoretical Nuclear Physics* (John Wiley and Sons, Inc., New York, 1952), p. 627. See also S. A. Moszkowski, Phys. Rev. **89**, 474 (1953).

Strange Particles and Multiple Meson Production

GIUSEPPE COCCONI
Cornell University, Ithaca, New York
(Received March 15, 1954)

THE large number of "strange" particles discovered in the last few years among the products of the interactions of high-energy cosmic rays with matter has brought confusion among physicists, since no theory is able to give a justification of their existence and of their properties.[1] On the other hand, the very facts that these particles are so many[2] and that they all disintegrate with lifetimes around 10^{-10} sec (actual limits: $\sim10^{-9}$ and $\sim10^{-11}$ sec) and mass excesses Q around 100 Mev (actual limits: ~30 and ~250 Mev) can be interpreted as an indication that these particles are not to be considered as many separate species.

What we would like to propose is that the strange particles are "compounds" of "elementary" particles, compounds which can be formed whenever the energy available is sufficiently high. "Elementary" particles denote here, besides the nucleons, the particles which can be considered as quanta of a strongly interacting field and thus can be created directly by the excitation of the field. In discussing multiple production this definition seems to be applicable only to the π mesons. The word "compound" is used instead for a particle which, to be created, requires the presence of two or more elementary particles in appropriate spatial and kinematical conditions. Of course there is no need to assume that the elementary particles required to give rise to the compound have to be the same particles into which the compound eventually disintegrates. In fact, it is likely that no weakly interacting particles, μ mesons and neutrinos, are required to build a compound, though they are sometimes present among the disintegration products.

If analogies have any meaning, the study of the properties of the strange particles could then be similar to the study of the complex nuclei. All possible combinations would eventually be found, and some rules discovered which determine the condition of their formation.

However, even at the present state of our knowledge, the mere assumption that the strange particles are a class of compounds may lead to some general conclusions which, in some cases, may be compared with experimental results.

Let us consider the problem of the multiple production of particles in high-energy collisions. The most convincing approach is probably that of Fermi,[3] and we shall develop our arguments along that line. However, our considerations are so general that any of the various models of multiple production thus far proposed could be used, and the conclusions would remain practically unchanged.

According to Fermi, the energy available in the center-of-mass system of two interacting particles stays inside a volume comparable to the volume of the particles for a time long enough to excite all the possible modes of the fields involved, so that the

number and the nature of the particles eventually emerging from this volume represent, at least in first approximation, the most probable statistical distribution of the various modes. In the original calculation of Fermi, all strongly interacting particles are considered as elementary; so, when the energy available increases, all of them can be produced with probabilities essentially proportional to their statistical weights. Therefore, all strange particles are expected to be produced with relative probabilities which become asymptotically constant at extremely high energies.

If instead the idea of compounds is introduced, the probability of emission of strange particles is determined by the probability that two or more elementary particles have such momenta as to allow the formation of the compound, and the relative probability of formation of the various particles will then depend on the available energy in a manner radically different from that described by Fermi.

A specific calculation requires quantitative knowledge that we lack; however, some general features of the solution can be tentatively predicted.

At very high energies the probability of formation of strange particles should be very small in comparison to the probability of formation of elementary particles since too much momentum space is available. A similar situation is met in the case of the emission of, e.g., deuterons and alpha particles from strongly excited nuclei.

There is some experimental evidence supporting this prediction. In interactions observed in photographic plates and produced by protons of energy 10^{12}–10^{13} ev ($\sim 10^{11}$ ev available in the c.m. system of the two nucleons), the ratio between the neutral particles decaying very rapidly (lifetime 10^{-14} sec) into two photons, hence probably π^0, and the charged particles, is close to 0.5.[4] At these energies the production of nucleon pairs is still small, and the ratio 0.5 is predicted if mostly π mesons are produced. The original Fermi theory would instead predict at these energies a substantial production of K particles.

At intermediate energies, where a few Bev are available in the c.m. system, the probability of emission of strange particles should be substantial, though never preponderant, in comparison with the probability of producing π mesons.

It is an experimental fact that most of the strange particles observed in photographic plates and in cloud chambers are produced by primaries of intermediate energies. Experimental biases could be in part responsible for this, but in the opinion of several authors this is not a sufficient explanation of the effect.

Another fact which could fit the picture is the observation that some of the strange particles are preponderantly produced with charge of one sign. This could be interpreted as due to the necessity, for the formation of the particle, of the presence of a charged nucleon. At intermediate energies only protons are available; at very high energies, where antiprotons might be present, the probability of formation is small.

The identification of a strange particle with a compound is not new. In fact it was essentially a compound model which was proposed some years ago by several authors for the only strange particle known at the time, namely the V particles (see, e.g., Pais, reference 1); according to that model these particles were isobaric states of the nucleon with high angular momentum. The last condition was introduced to explain the long lives of the particles, but it appeared so artificial that the model was not taken seriously.

Granted that the justification of the long lifetimes is still the crucial point to be explained, we feel that the recent discoveries of so many strange particles gives new strength to the compound model. Encouragement also comes from the fact that while the existence of one meson field, the π-meson field, can be now considered as proved, there is no indication that more than one meson field is required to explain the experimental facts known thus far.

We are fully aware that the present note does not offer any solution of the fundamental difficulties involved in the problem of the strange particles. It is only meant to present a point of view which does not seem to be inconsistent with the known facts and may possibly indicate a path for further discussion and for elaboration of a model.

[1] The theories presented by A. Pais, Phys. Rev. **86**, 663 (1952) and Progr. Theoret. Phys. Japan **10**, 457 (1953); M. Gell-Mann, Phys. Rev. **92**, 833 (1953); M. Goldhaber, Phys. Rev. **92**, 1279 (1953), cannot be considered thus far as more than tentative.

[2] At the date of this writing 4 varieties of hyperons and 5 or 6 varieties of K mesons are listed in the literature; all seem to be strongly interacting with nuclear matter.

[3] E. Fermi, Progr. Theoret. Phys. Japan **5**, 570 (1950).

[4] Evidence presented by M. F. Kaplon for the Rochester group and by G. D. Freier for the Minnesota group at the Durham, North Carolina, meeting (December 1953), and private communication of B. Peters to M. F. Kaplon.

PHYSICAL REVIEW VOLUME 94, NUMBER 3 MAY 1, 1954

Proceedings of the American Physical Society

Minutes of the 1954 Annual Meeting Held at Columbia University, New York City, January 28–30, 1954

THE 1954 Annual Meeting of the American Physical Society was held in the buildings of Columbia University, in New York City, on Thursday, Friday, and Saturday, January 28, 29, and 30, 1954. Like its recent predecessors, it was a huge meeting—there were twenty-one hundred registrants, and people had to be turned away from several sessions because the halls (including the very largest) were not capacious enough. The stupendous labor of preparing and administering this convention was borne by innumerable staff members and students of the University, ably headed, as for the previous five years, by W. W. Havens, Jr., who names as his principal aides A. M. Sachs and L. Lederman.

This was the latest of eleven Annual Meetings held at Columbia University during the twelve years since we broke the tradition of holding our Annual Meeting jointly with the A.A.A.S. It was also the last. Our generous host has finally admitted that it is overtaxed by the burden of these conventions, and who can wonder or protest? As a valedictory to Columbia and as a tribute made doubly fitting by the fact that 1954 is its Bicentennial Year, a session on Saturday morning was devoted to three speeches on the history of physics and to one on

the history of the Society in this glorious University. A plaque is to be affixed to a wall of Pupin Physics Laboratories: its text was shown at the session in question, and here it is:

IN GRATITUDE FOR ITS LONG
AND GENEROUS HOSPITALITY
THIS PLAQUE IS GIVEN
TO COLUMBIA UNIVERSITY
IN ITS BICENTENNIAL YEAR
BY THE AMERICAN PHYSICAL SOCIETY
WHICH WAS FOUNDED
IN FAYERWEATHER HALL
ON MAY 20, 1899

The plaque speaks of an event which happened forty-four years before the first of the eleven Annual Meetings which have just been mentioned. Add to these last not fewer than half a hundred general meetings of the Society which were held at Columbia during those forty-four years. Add also the fact that for thirty-six years the Society has been granted office space in Fayerweather Hall and later in Pupin Physics Laboratories, and that this beneficence continues.

The next Annual Meeting will be held in hotels in the neighborhood of Pennsylvania Station in New York City. We may partly console ourselves by reflecting that the dispersal of the sessions will be less than it has perforce been at Columbia. Now let us return to the meeting just concluded.

The banquet of the Society and of the American Association of Physics Teachers was held on Friday evening in the Grand Ballroom of the Hotel New Yorker, with an attendance of 317. President Grayson Kirk of Columbia University honored us with an address, and so did two members of our Society, Leon Brillouin and S. A. Korff. The 1954 Oliver E. Buckley Solid-State Physics Prize was awarded to John Bardeen.

The Business Meeting of the Society was held on Friday morning, with the normal scant attendance. The Treasurer presented a far rosier picture of the financial situation of the Society than has hitherto been possible during the last few years: the Managing Editor pointed to a continuing expansion of *The Physical Review*. The Secretary reported that the membership of the Society as of the moment is about 11 200.

The Tellers of Election reported the results of the recent election. Elected were: *President* (1954) H. A. BETHE; *Vice-President* (1954) R. T. BIRGE; *Secretary* (1954) K. K. DARROW; *Treasurer* (1954) G. B. PEGRAM; *Councillors* (1954–1957) JOHN BARDEEN and A. O. NIER; *Members of the Board of Editors allocated to The Physical Review* (1954–1956) P. BERGMANN, G. BREIT, F. J. DYSON, P. KUSCH, R. SMOLUCHOWSKI, and J. C. STREET; *Members of the Board of Editors allocated to Reviews of Modern Physics* (1954–1956) R. F. CHRISTY and H. MARGENAU. In deference to a request made at the Business Meeting the votes received by the four candidates to the two posts of Councillor are here recorded: John Bardeen 1898, L. J. Haworth 1040, A. O. Nier 1951, L. S. Taylor 977.

The Council met on Thursday afternoon. It elected to Membership 185 candidates and to Fellowship 11: the names follow. It nominated Frederick Seitz to the Governing Board of the American Institute of Physics for a three-year term. It appointed the following nine Fellows of the Society to constitute the 1954 Nominating Committee: J. B. Platt (Chairman), E. U. Condon, H. L. Dryden, S. A. Goudsmit, M. H. Hebb, T. H. Johnson, A. O. Nier, M. K. H. Panofsky, and F. Seitz. It made important revisions in the rules pertaining to members who omit to pay their dues; the new rules will be published either in the Washington or the Minneapolis Bulletin. Watch for them!

KARL K. DARROW, *Secretary*
American Physical Society
Columbia University
New York 27, New York

Elected to fellowship: F. D. Bennett, W. W. Berning, J. T. Burwell, Jr., J. H. Frazer, W. F. Fry, Peter Havas, B. L. Hicks, H. W. Lewis, W. T. Read, Jr., P. A. Wolff, and K. A. Yamakawa.

Elected to Membership: Robert C. Abbott, Gosta Carl Akerlof, D. Altman, Milton Robert Baker, Peter Anthony Barakos, Hamilton Barhydt, Cran Hardin Barrow, Mark Q. Barton, Robert P. Bauman, Wayne Machon Beasely, Charles William Beckett, Logan M. Belleville, Donald Drysdale Betts, Robert William Bickmore, David Soren Bloom, Jeffrey Jay Bowe, Ralph Carter Brainard, Philip Samuel Brody, James Harold Brown, Hans Rudolf Brugger, Robert Melvin Brugger, Glenn M. Burgwald, Edward Michael Burtsavage, Thomas William Buttery, Joseph Calloway, Herbert Lawrence Cannon, Gerald Burton Carrier, David Marion Chase, Robert Leon Chuoke, Stanley Howard Clark, Moody Lee Coffman, Paul Fenimore Cooper, Jr., Richard Henry Dalitz, Ulf Danielson, Warren E. Danielson, Jean Loup Delcroix, Donald John Denny, Charles Whitney Drake, Jr., Loyal Durand III, James Michael Early, Russell Keith Edwards, Frederick Ernest Eidman, Jr., Norman Gerald Einspruch, Herman Epstein, Robert William Estin, John Paul Evans, John Amedeo Fasolo, Gerald Feinberg, Frank Feiner, Jose F. Fernandez, George B. Finn, Jr., Harold Forstat, Hellmut Fritzsche, James Joseph Gallagher, Carl Wesley Garland, David Garvin, Phillip Herbert Geil, Jr., Gordon Gibson, Homer Holt Givin, Jr., Ben Roger Gossick, Preston Frazier Gott, Lawrence Gould, Hans Gunter Graetzer, Rita D. Gugganheim, Michael Hacskaylo, Ted Carter Harman, Carl Anthony Heller, Leah Kirstina Hendriksen, Warren Elliott Henry, Willard Geldard Henry, Wendell Gene Holladay, Chaang Huang, Raymond Hargett Hughes, Thomas Rogers Hughes, George S. Hurst, Hiroshi Ichimura, Kenzo Iwanaga, Claude Francois Jaccard, Laurence Duane Jennings, Jr., Albert David Johnson, Alan Edwin Johnsrud, Weyland Thomas Joyner, Gerard John King, George Herbert Kinsey, Jr., Manfred Kochen, Wolf Kuebler, Tom Taketo Kumagai, J. Eugene Kunzler, Constantine Peter Kutrumanes,

Raymond O. Lane, Jean Pierre Lascoux, John Laufer, Kiuck Lee, Herbert Ernest Lense, Chun Chia Lin, Ernest Laverne Lippert, Jr., Tung-Sheng Liu, Joseph John Loferski, Dan H. Lorenz, Ralph Addison Lowry, Jerry Bascervil Marion, Kenneth Stuart McAlpine, David Warren McCall, William John McDonald, Nathan T. Melamed, James Edgar Mercereau, Marvin Clark Mertz, Axel Meyer, George Patrick Millburn, Lowell Gilbert Miller, Tatsuoki Miyazima, Francis Joseph Morin, Harvey Louie Morrison, Edward Masaki Nakaji, Richard B. Neal, Robert Everest Newnham, Minoru Nishida, Richard Eyre Norton, David Charles Oakley, Samuel Wendell Obetz, Kazuo Ono, Agnes Orkin-Lecourtois, Sune Lambert Overby, Sudhir Pradyumna Pandya, Frank Rudolph Paolini, Lyle Alexander Patrick, John Henry Pingel, John S. Plaskett, Benjamin Post, Richard Swain Preston, Frederick John Radd, J. B. Rajam, S. J., Theodore Herman Rautenberg, Jr., George Warren Reed, Jr., Richard Blaine Rhody, Wesley Arthur Robinson, John W. Robson, Bill Franklin Roe, Simcha Rosendorff, Jack Rosenthal, John David Ross, Theodore Justin Rowland, Ephraim Leo Rubin, Masakatsu Sakisaka, Richard Girard Satterfield, Richard Isaac Schoen, John Robert Schrieffer, Dan William Scott III, Christopher Sherman, Woodfin Epps Shuler, Ralph E. Simon, Ferrol B. Simpson, Orval D. Simpson, William Robert Sinclair, Klaus Julius Sixtus, Richard R. Smith, Robert Karl Smither, Elias Snitzer, Russell Duty Southwick, Brian Milton Spicer, Hermann Statz, Robert Leo Stearns, Donald Keith Stevens, George Cofforth Stierhoff, Clinton Allen Stone, Edward Thomas Sullivan, Robert George Summers-Gill, Taro Tamura, Norman Taslitt, Jerome Johnson Tiemann, Dennis David Triantos, Terry Triffet, Noboru Tsuya, Herbert Jack Vale, Robert George Perceval Voss, John A. Vreeland, Roselin Seider Wagner, Robert Mowbray Walker, George Wallis, Harold Vern Watts, Robert Halley Wertheim, Bernard N. Wiener, Robert Kent Willardson, Ross E. Williams, and Wendell Sterling Williams.

Errata Pertaining to Papers C3, F5, F6, F11, G7, I7, JA7, RA9, XA10, and Y11

C3, by C. M. Class, C. F. Cook, and J. T. Eisinger. In lines 12 to 14, instead of Pt, 212, 240, and 33 kev; Au, 1.73 Mev and W, 450 kev, with errors of 5 kev, read Pt, 212, 240, 333 kev; Au 188 and 280 kev, and W, 120 kev with errors of 5 kev.

F1, by J. A. Dillon, Jr., and H. E. Farnsworth. In line 19, (110) face should read (100) face.

F5, by N. Efremov. In the first equation, $R_i(\mathrm{Si}\cdots)$ should read $R_i(\mathrm{Si}\cdots)$.

F6, by G. Wolff, P. H. Keck, and J. D. Broder. In line 1, the title should read **Preparation and Properties of III-V Compounds.**

G7, by B. Wolfe, J. W. DeWire, and A. Silverman. The table of results should read:

76°	94°	110°	130°
4.3±0.6	3.3±0.5	2.5±0.4	1.2±0.3

I7, by D. Finder and W. J. Sturm. The first author's name was misspelled in the abstract and in the index.

JA7, by J. W. Gardner. The title should read **Effect of Knock-On Electrons on Ionization Loss.**

RA9, by J. M. Luttinger and R. Karplus. Mr. Karplus' name was omitted. In line 2, *University of California* should follow Mr. Karplus' name.

XA10, by Robert N. Schwartz. In line 10, rotational should read rotionless.

Y11, by J. W. Knowles. The last sentence should read, A measurement of 2×10^{-11} sec for the lifetime of this γ ray has been reported.[2]

PROGRAMME

THURSDAY MORNING AT 10:00

McMillin Theatre

(L. J. HAWORTH presiding)

Brookhaven-Nevis Symposium

A1. The Cosmotron as a Research Tool. G. B. COLLINS, *Brookhaven National Laboratory.* (30 min.)
A2. Heavy Unstable Particles and Multiple Meson Production Observed in a Cloud Chamber at the Cosmotron. R. P. SHUTT, *Brookhaven National Laboratory.* (30 min.)
A3. Interpretation of High-Energy Experiments. R. L. SERBER, *Columbia University.* (30 min.)
A4. Meson Reactions in Hydrogen. L. M. LEDERMAN, *Columbia University.* (30 min.)

THURSDAY MORNING AT 10:00

Pupin 428

(A. PAIS presiding)

Theoretical Physics, I (Field-Theory)

B1. Renormalization Questions in Curved Spaces. M. DRESDEN AND MARTIN GUTZWILLER, *University of Kansas.*—It has been investigated whether the renormalization procedures for field theories need modifications when a space of constant curvature rather than the flat space of special relativity is used. The field equations described previously[1] may be quantized simplest by observing that the commutator for the field quantities is directly related to the "elementary solution" of Hadamard of the field equations. This commutator (the analog of the Schwinger D function) is given by $D(s^2)=(1/R^2)\delta[sh^2(s/R)]+W(s^2)$ here s is the geodesic distance between two points, R is the radius of curvature, W is a hypergeometric function. It can be shown that the field equations and the commutation rules may be obtained from an appropriate modification of the Schwinger action principle.[2] An interesting difference as compared with the flat case arises from the circumstance that the solutions of the field equations do not allow an unambiguous splitting in positive and negative frequencies for all time. This complicates the Feynman type interpretation of the theory, although some of the formal relations of Feynman may be obtained directly from the Hadamard propagation formula.

[1] M. Gutzwiller, Phys. Rev. **91**, 478 (1953).
[2] J. Schwinger, Phys. Rev. **82**, 914 (1951).

B2. Avoiding Perturbation Methods in Quantum Electrodynamics, Meson Theory, Etc. F. J. BELINFANTE, *Purdue University.*—The radial function in an H atom cannot be obtained by perturbation calculus starting from a free-electron $j_l(kr)$ function. Similarly, solution of problems on bosons surrounding a fermion may require rigorous solution of a radial problem for wave functions depending on relative position of fermion and bosons. In 1932, V. Fock developed a representation "in configuration space" for finite numbers of B.E. as well as F.D. particles. Recently I discussed how positon theory can be reformulated avoiding the hole concept by means of a somewhat generalized Fock-type theory.[1] It is simple to develop theories for photons and for mesons along these lines. This enables us to write the "radial problem" for stationary states of interacting bosons and fermions, as an infinite set of simultaneous integral equations, corresponding to an expansion in numbers of particles present. Introducing the vacuum solution, one should solve for the energy difference of actual and vacuum states, for instance by relating the actual to the vacuum state vector. In complicated problems one might possibly neglect most many-particle contributions to the state vector.

[1] F. J. Belinfante, Bull. Am. Phys. Soc. (Chicago meeting) **28**, No. 6 (1953), abstract T5.

B3. "Dressed" Particles in Quantum Field Theory.* JAMES L. ANDERSON, *University of Maryland.*—In time dependent perturbation theory there exists a certain ambiguity in the breaking up of the Hamiltonian into two parts, one of which is to be considered as the perturbation. If one breaks the Hamiltonian into the two parts H_o and H_I and calls H_I the perturbing part, then it would appear equally justified to break it into two other parts H_o' and H_I', where $H_o'=(H_o+K)$, $(H_I'=H_o-K)$, and to call H_I' the perturbation. Since now the eigenstates of H_o' are employed in the specification of initial and final conditions in the theory, one might determine H_o' (or K) by requiring that it describe properly the "dressed" particles of the theory. This means that H_o' must be so chosen that

$$\langle\Psi_o,\ T[\bar{\psi}(x)\psi(y)]\Psi_o\rangle=\langle\Phi_o,\ T[\bar{\psi}(x)\psi(y)]\Phi_o\rangle,$$

where Ψ_o is the vacuum state of the interacting system, Φ_o the lowest energy state of H_o', $\bar{\psi}(x)$ and $\psi(y)$ are Heisenberg operators, and $\bar{\psi}(x)$ and $\psi(x)$ are operators in an interaction representation defined by H_o'. The existence of an H_o' satisfying this condition and its relation to the renormalization program will be discussed.

* Supported by the U. S. Office of Naval Research.

B4. Meson Nucleon Scattering. I. R. J. RIDDELL, JR., AND BURTON D. FRIED, *University of California, Berkeley.*—The problem of meson scattering from a fixed nucleon has been investigated for intermediate values of the coupling constant g. The nonrelativistic one-body problem (i.e., one real, fixed nucleon and no real mesons) can be treated by a variational procedure due to Tomonaga which is correct in both the weak and strong coupling limits. In the same spirit, we have tried

to find a consistent method of calculating the scattering cross section which is correct in *both* limiting cases and which leads to feasible numerical calculations for intermediate values of g. To find the wave function of the scattered meson, we use the matrix equations of motion in an energy representation. This leads to an infinite system of coupled equations which can be reduced to a finite set by the approximation of neglecting all states containing more than one *real* meson. It is to be emphasized that this implies *no* restriction on the *total* number of mesons present, since we allow the nucleon to be surrounded by any number of bound, virtual mesons. This is in contrast to the Tamm-Dancoff approximation which limits the total number of mesons present and which consequently cannot give the correct strong coupling limit.

B5. Meson Nucleon Scattering. II. BURTON D. FRIED AND R. J. RIDDELL, JR., *University of California, Berkeley.*—To illustrate the method described in the preceding abstract, we apply it to the charged scalar meson field. Let $|Q, p_1 \cdots q_m)$ denote an exact energy eigenstate of charge Q in which there are asymptotically n positive mesons of momenta $p_1 \cdots p_n$ and m negative mesons of momenta $q_1 \cdots q_m$. The wave function of a positive meson incident with momentum p on a proton is then $(1|A|2p)$ where A is the annihilation operator for positive mesons. To find this matrix element from the equations of motion we need terms like $(1|A\tau_3|2p)$. These we evaluate by matrix multiplication, neglecting all intermediate states with more than one real meson and making the further approximation that $(2p'|\tau_3|2p) = (1|\tau_3|1)\delta(p-p')$, etc. Finally, one-body matrix elements like $(1|\tau_3|1)$ are evaluated by using for $|Q)$ the corresponding Tomonaga state vector. The resulting equations can be solved analytically in both the weak and strong coupling limits, giving cross sections which agree with perturbation theory and strong coupling theory, respectively. For intermediate coupling, numerical computations have been carried out and curves of cross section *vs* meson energy will be presented. It may be noted that the approach described here also gives the correct strong coupling isobar separation.

B6. Effect of Negative Energy Components in the Two-Nucleon System. R. ARNOWITT AND S. GASIOROWICZ, *University of California, Berkeley.*—A feature of the Levy-Klein solution of the Bethe-Salpeter equation for the deuteron is the elimination of ϕ_{+-}, ϕ_{-+}, and ϕ_{--} in terms of the ϕ_{++} component of the wave function via a perturbation expansion. To investigate the validity of this procedure, the coupled equations for the various components in the first nonadiabatic approximation to the Δ_+ interaction were examined. A set of first-order radial equations with multiplicative potentials (in the region $r>1/m$) was obtained, involving $\phi_{\pm\pm}(r) = \frac{1}{4}(1\pm\beta_1)(1\pm\beta_2)\phi(r)$. A rigorous elimination of ϕ_{+-} and ϕ_{-+} led to equations containing ϕ_{++} and ϕ_{--}. In addition to velocity dependent terms, potentials of the type

$$\frac{\mu^2}{2m}\frac{g^2}{4\pi}\tau_1\cdot\tau_2\frac{Y(r)}{P_0+\frac{1}{4}\frac{g^2}{4\pi}\tau_1\cdot\tau_2 Y(r)}$$

appear. Expanding the denominator yields the usual Yukawa second-order potential plus a term proportional to $g^4(\tau_1\cdot\tau_2)^2$. Such an expansion however is poor even for $r\sim 1/\mu$, a pole actually existing near $r\sim 0.7/\mu$ for the charge singlet state. Thus the perturbation expansion appears to alter radically the structure of the equations.

B7. Interaction Between Two Nucleons.* BEHRAM KURŞUNOĞLU, *Cornell University.*—A three-dimensional equation for two interacting nucleons can be obtained from the covariant Bethe-Salpeter equation which is identical with the one derived recently by Dyson[1] through the introduction of a new Tamm-Dancoff amplitude that takes correct account of the interacting vacuum state. The energy denominators for the positive-energy projected components of the wave function in G^2 order charge-symmetric $ps-ps$ theory is the same as in the old T.D. method. In the G^4 order interaction the no-pair terms agree with the T.D. method, but in the one-pair and two-pair terms the signs of the intermediate energies in the denominators appear in accordance with the particle and antiparticle description. The resulting adiabatic nuclear forces is being investigated. The renormalizations of mass and charge to any order do not present any formal difficulty.

* Supported by the Turkish Government and U. S. Office of Naval Research.

[1] F. J. Dyson, Phys. Rev. **91**, 1543 (1953).

B8. Low Energy Limits of Meson Processes. S. DESER AND W. E. THIRRING, *Institute for Advanced Study,* AND M. L. GOLDBERGER, *Princeton University.*—It is well known that the perturbation-theoretical matrix element for meson-nucleon scattering is finite at zero energy. A similar result holds for the threshold photo-production of charged mesons. It has been shown by Kroll and Ruderman,[1] on the basis of a particular renormalization scheme, that at threshold, the exact photoproduction matrix element reduces to the perturbation-theoretic result with renormalized coupling constant in the limit of zero meson mass. There is, however, some arbitrariness in mesic charge renormalization. We have developed a new computational technique which permits an exact evaluation of the meson-nucleon scattering matrix in the limit of zero energy and zero meson mass. By a suitable choice of renormalization it reduces to the perturbation-theoretic value with renormalized coupling constant and nucleon mass. In the new scheme, the photoproduction theorem no longer holds nor do the two definitions of g bear any close relation. Using the fact that the isotopic spin dependence occurs with odd powers of μ/M,[2] dropping terms higher than the first, our coupling constant may be computed from the two s-wave scattering lengths. Using Fermi's latest data (unpublished) we find $g^2/4\pi = 0.36$. The possible significance of this result will be discussed.

[1] N. Kroll and M. Ruderman, Phys. Rev. (to be published).
[2] M. Gell-Mann and M. L. Goldberger (private communication).

B9. Classical Theory of High-Energy Processes. M. A. RUDERMAN, *University of California, Berkeley,* AND H. BROWN, *University of California, Livermore.*—In the classical limit ($\hbar\to 0$) there exists a nondivergent pseudoscalar meson theory with gradient coupling. Infinities can be renormalized in terms of the experimental nucleon mass and the moment of inertia associated with changing the nucleon spin direction.[1,2] The high-energy collisions of two such nucleons have been investigated. Results will be reported for the cross section and spectrum of meson emission and their dependence upon coupling constant and moment of inertia.

[1] H. J. Bhabha, Proc. Roy. Soc. (London) **A178**, 314 (1941).
[2] H. J. Bhabha and H. C. Corben, Proc. Roy. Soc. (London) **A178**, 273 (1941).

B10. Quantized Interaction of Relativistic Fields. HANS FREISTADT, *Newark College of Engineering.*—An attempt is made to describe observed quantum effects by a classical relativistic field theory. The procedure followed by Bohm[1] for particle physics does not suggest any general method of finding classical equations which describe quantum effects (a modified Hamilton-Jacobi equation and the equation of continuity) except by recourse to the usual formulation of quantum theory. To circumvent this difficulty, it is suggested that only the interaction between fields exhibits quantum effects, the free fields remaining unquantized. A Hamilton-Jacobi equation for interacting relativistic fields is developed, a very simple extension of which yields the equations of the usual

interaction representation of quantum electrodynamics. The method is applicable to any theory of interacting fields, but it remains to be seen whether physically meaningful results are obtained in cases other than that of interacting electromagnetic and spinor fields.

[1] D. Bohm, Phys. Rev. **85**, 166, 180 (1952).

B11. Collision Matrix for Dirac Particles.* BRUNO ZUMINO, *New York University.*—The collision matrix for a quantized Dirac field in an external electromagnetic potential is calculated by a method different from the commonly used Feynman technique. Our method may supply a basis for a more rigorous mathematical justification of the results. First the collision matrix for the unquantised Dirac field is obtained from the solution of an integral equation. The collision matrix for the field quantized in the sense of the theory of positrons can be then derived in an exponential form which shows clearly that the matrix is unitary. The creation and annihilation operators are now separated by means of a method due to Friedrichs, which uses a theorem by Baker and Hausdorff on exponentials of noncommuting quantities. One obtains the collision matrix expressed as a product of exponentials, involving creation and annihilation operators in a way suitable for the calculation of matrix elements in the configuration space of the electrons. It is possible to show that the matrix-elements obtained by this method are the same as those calculated by use of Feynman graphs.

* Supported by the U. S. Office of Naval Research.

Invited Paper

B12. Survey of Quantum Electrodynamics. N. M. KROLL, *Columbia University.* (40 min.)

THURSDAY MORNING AT 10:00

Pupin 301

(W. W. BUECHNER presiding)

Reactions of Transmutation, I

C1. Energy Dependence of Coulomb Excitation of Ta and Au.* W. I. GOLDBURG AND R. M. WILLIAMSON, *Duke University.*—Low-lying levels in Ta and Au were excited by means of the Coulomb excitation process[1,2] using 2- to 4-Mev protons from the Duke Van de Graaff accelerator. Gamma yields at 90° to the incident protons were taken with a NaI scintillator and a single-channel pulse-height analyzer. Thick target yields of 135-kev and 290-kev gammas from Ta, normalized to the theoretical yields[3] at 2-Mev proton energy, were found to increase to 25 percent above the calculated yields at 4 Mev. The cascade 155-kev gamma was also partially resolved. Both thick and thin target data taken on the gold 280-kev gamma gave an experimental cross section the slope of which was 30 percent in excess of the theoretical slope between 2.5 and 4 Mev. A 550-kev gamma behaved similarly between 3.5 and 4.25 Mev.

* Work supported by the U. S. Atomic Energy Commission.

[1] T. Huus and Č. Zupančič, Kgl. Danske Videnskab. Selskab, Mat.-fys. Medd. **28**, 1 (1953).
[2] C. L. McClelland and C. Goodman, Phys. Rev. **91**, 760 (1953).
[3] K. Alder and A. Winther, Phys. Rev. **91**, 1578 (1953).

C2. Coulomb Excitation of Heavy and Medium Nuclei by Alpha Particles. G. M. TEMMER AND N. P. HEYDENBURG, *Department of Terrestrial Magnetism.*—We have investigated the Coulomb excitation of the low-lying levels of some 30 nuclei between $Z=20$ and $Z=90$ with our electrostatic generator and a NaI crystal spectrometer. Because of their higher charge and lower velocity at a given energy, alpha particles satisfy the condition $(2Z_1Z_2e^2/\hbar v)\gg 1$ down to $Z\sim 20$, hence allowing the application of the simplified theory[1] of the excitation process. We have studied Ta^{181} and Mn^{55} in detail, obtaining thick target alpha excitation curves between 1.00 and 3.80 Mev for the 137-kev γ ray and K x-ray of Ta and the 128-kev γ ray of Mn, the energy dependence being in good agreement with theory.[1] We have also measured proton excitation of Ta[2] over the same energy interval. At 3 Mev the ratio of K to gamma excitation is 2.27 for alphas and 14.8 for protons, illustrating the relative advantage of aphas for the heavy elements. Gamma background for the lighter elements under proton bombardment is prohibitive whereas it is quite negligible for alphas. In most nuclei investigated we find the low-lying excited states as known from beta and gamma spectroscopy, ranging in energy from 50 kev (Th^{232}) to 440 kev (Se^{77}). A table of the observed transitions and their approximate relative intensities will be presented. The importance of light element target impurities will be discussed.

[1] K. Alder and A. Winther, Phys. Rev. **91**, 1578 (1953).
[2] T. Huus and Č. Zupančič, Kgl. Danske Videnskab. Selskab, Mat.-fys. Medd. **27**, No. 16 (1953); C. McClelland and C. Goodman, Phys. Rev. **91**, 760 (1953).

C3. Coulomb Excitation of Heavy Nuclei. C. M. CLASS, C. F. COOK AND J. T. EISINGER, *Rice Institute* (received by wire).—Supported in part by U. S. Atomic Energy Commission stop Gamma rays believed to be due to nuclear coulomb excitation footnote one were observed when TA, W, AU, and PT targets were bombarded with three Mev protons stop The intense K x-rays were suppressed by using appropriate absorbers stop The target and accelerator background was negligible stop The radiation was detected with a sodium iodide counter having a resolution of ten percent stop Energies assigned to the well resolved gamma rays are colon TA comma 139 comma 167 and 309 kev semicolon PT comma 212 comma 240 and 33 kev semicolon AU comma 1.73 Mev and W comma 450 kev comma with errors of 5 kev stop Additional lines from PT comma AU and W are poorly resolved stop The measurement of yield curves and the use of selective absorbers for the three TA lines indicate that the 167 kev line is due to a cascade gamma ray between the 309 kevs and 139 kev leves. The relative intensities of the lines allow a better determination of the cross-over transition probability than heretofore possible. The angular distribution of the 139 kev and 309 kev radiations from tantalum has been measured. The former is isotropic while the latter distribution fits one plus .23 cosine squared theta in agreement with the theory. Footnote two.

Paragraph. Footnote one. T. Huus and C. Zupancic, Kglo Danske Videnskaboselskab, Mat.-fys. Medd. **28**, No. 1 (1953) C. McClelland and C. Goodman, Phys. Rev. **91**, 760 (1953) Footnote two. K. Alder and A. Winther, Phys. Rev. **91**, 1578 (1953).

C4. Angular Distribution of Alpha-Particles from (p,α) Reactions. E. NEWMAN AND W. L. ALFORD,* *Oak Ridge National Laboratory.*—Using the internal, 22-Mev proton beam of the Oak Ridge National Laboratories 86-inch cyclotron, the angular distribution of alpha particles resulting from (p,α) reactions on several elements have been studied. The detectors consisted of a thin layer (approximately 5 mg/cm²) of $ALPO_4$ sprayed on an aluminum backing and utilized the activation detection[1] reaction $P^{31}(\alpha,n)Cl^{34}$. The chlorine was separated chemically and counted under end-window Geiger counters. Separate runs were made to establish the adequacy of the chemistry and to prove the effect of impurities in the aluminum phosphate to be negligible. Absorption tests performed at various angles demonstrated the validity of the method for detecting the desired angular distributions. Data were obtained from 15° to 170° with respect to the incident proton beam. Since the observed angular distributions are strongly peaked in the forward direction this may indicate the process to be one of direct interaction rather than compound nucleus formation.

* Research participant from Alabama Polytechnic Institute.
[1] B. L. Cohen and R. V. Neidigh, Rev. Sci. Instr. (to be published).

C5. Gamma Rays from the Inelastic Scattering of Alpha Particles by Lithium and Fluorine. N. P. HEYDENBURG AND G. M. TEMMER, *Department of Terrestrial Magnetism.*—We have observed the 478-kev gamma ray, excited by inelastic scattering of alpha particles from lithium, with a NaI crystal spectrometer. A thin target yield curve showed resonances, corresponding to energy levels in the compound nucleus B^{11}, at the following bombarding energies: 1.91, 2.46, 2.60, 2.70, 2.81, and 3.06 Mev. A search for alpha- capture gamma-ray resonances up to 2.5 Mev revealed none above the known resonances at 820 and 960 kev. The bombardment of a thin CaF_2 target by alpha particles gave three gamma-ray lines at 108±2, 196±2, and 1280 kev. The NaI spectrometer was calibrated with the 68- and 142-kev lines of Th^{230}, the 190-kev line of In^{114} and the 1.28-Mev line of Na^{22}. The first two gamma lines are due to the inelastic excitation of the first two excited states of F^{19}. The 1.28-Mev line is due to the excitation of the 1.28 level in Ne^{22} by the reaction $F^{19}(\alpha,p\gamma)Ne^{22}$. A yield curve for the 108- and 196-kev lines gave resonances at alpha energies: 2.48, 2.55, 2.64, 2.77, 2.90, 3.02, 3.05, 3.18, and 3.34 Mev, corresponding to levels in the compound nucleus Na^{23}. There is evidence for Coulomb excitation of the 196-kev level below 2.2 Mev.

C6. Alpha-Neutron Reactions in Be^9, B^{11}, and C^{13}. R. E. TRUMBLE, JR.,* *Catholic University of America, and Department of Terrestrial Magnetism.*—The neutron yields from thin targets of Be^9, B^{11}, and C^{13} (23 percent) bombarded by alpha particles have been observed for alpha-particle energies between 1.0 and 3.5 Mev. B^{10} and C^{13} thick targets were found to give negligible neutron yield for B^{10} and no detectable yield for C^{13}. A paraffin-imbedded BF_3 "long counter" subtending a 60° cone at the target was used to detect neutrons whose mean directions made angles of 0° and 90° with the direction of the incident alpha particles. Several neutron resonances were found to have marked angle dependence. Strong resonances were found at 1.91, 2.24, 2.58, and 3.40 Mev for Be^9; at 1.54, 2.09, 2.63, 3.00, and 3.26 Mev for B^{11}; and at 2.44, 2.66, 2.76, and 3.30 Mev for C^{13}. Numerous weaker resonances were observed for each of these targets. Neutron yield curves for Be^9, B^{11}, and C^{13} and calculated energy levels in C^{13}, N^{14}, and O^{17} will be shown.

* United States Naval Academy, Annapolis, Maryland.

C7. Energies of Excited States of Be^{10}. C. K. BOCKELMAN AND J. J. JUNG,* *M.I.T.*—Thin targets of beryllium evaporated on a Formvar backing were bombarded by deuterons accelerated in the MIT–ONR electrostatic generator.† A magnetic spectrograph, calibrated with polonium alpha particles, was employed to obtain the momentum spectrum of protons emitted at 90 degrees to the incident beam. Measurements made at several deuteron energies between 5.4 and 7.6 Mev permitted identification of the target nucleus involved. The ground-state Q value for $Be^9(d,p)Be^{10}$ and the position of excited states at 3.37, 7.37, and 7.54 Mev agree with previous measurements.[1] The reported 6.2-Mev level was found to consist of states at 5.96 and 6.26 Mev. A summary of previous experimental results may be found in reference 1.

* On leave from the University of Strasbourg, Strasbourg, France.
† This work has been supported by the joint program of the U. S. Office of Naval Research and U. S. Atomic Energy Commission.
[1] F. Ajzenberg and T. Lauritsen, Revs. Modern Phys. **24**, 321 (1952).

C8. Energy Levels from the Reaction $B^{10}(\alpha,p)C^{13}$. W. J. FADER AND A. SPERDUTO, *M.I.T.*—Levels in the C^{13} nucleus have been studied by the $B^{10}(\alpha,p)C^{13}$ reaction with the MIT–ONR electrostatic generator.* The region of excitation from the ground state to 4.7 Mev was covered using singly charged helium ions with incident energies of 4.8 and 5.8 Mev. Three excited states in C^{13} were found with energies of 3.09, 3.68, and 3.85 Mev, which values are in good agreement with the $C^{13}(d,p)C^{13}$ results.[1] No evidence has been found for proton groups which would correspond to the 0.7 and 4.6 levels previously reported from $B^{10}(\alpha,p)C^{13}$.

* This work has been supported by the joint program of the U. S. Office of Naval Research and the U. S. Atomic Energy Commission.
[1] F. Ajzenberg and T. Lauritsen, Revs. Modern Phys. **24**, 321 (1952).

C9. Differential Cross Sections for the $C^{13}(d,t)C^{13}$ Reaction.* H. D. HOLMGREN, J. M. BLAIR, B. E. SIMMONS, AND R. V. STUART, *University of Minnesota.*—The differential cross sections for the $C^{13}(d,t)C^{13}$ pickup reaction[1] have been measured at laboratory energies of 2.19 Mev and 3.29 Mev for thirteen center-of-mass angles extending from 17° to 144°. The tritons were separated from the scattered deuterons and the other reaction products by a combination of magnetic analysis and range measurements in nuclear emulsions. The targets were prepared by cracking C^{13}-enriched methyl iodide onto 0.005-mil Ni foils. The center-of-mass differential cross section at 3.29 Mev decreases from 34 mb/sterad at 17° to a minimum of 3.0 mb/sterad near 60°; then increases to 4.5 mb/sterad at 80° and remains approximately constant out to 144°. At 2.19 Mev the behavior of the differential cross section is similar, decreasing from 23 mb/sterad at 17° to 4.0 mb/sterad in the neighborhood of 70°, then rising to 6.0 mb/sterad at 100°.

* Assisted by the joint program of the U. S. Office of Naval Research and the U. S. Atomic Energy Commission.
[1] Strait, Van Patter, Sperduto, and Buechner, Phys. Rev. **81**, 747 (1951).

C10. Excitation Functions for Nitrogen Induced Nuclear Reactions in Carbon. A. ZUCKER AND H. L. REYNOLDS, *Oak Ridge National Laboratory.*—Nuclear reactions produced by high-energy nitrogen ions on carbon have been observed previously.[1] With the 28-Mev deflected nitrogen beam of the Oak Ridge National Laboratory 63-inch Cyclotron the absolute cross sections for the reactions $C^{13}(N^{14})F^{18}Be^8$, $C^{12}(N^{14})Na^{24}2H^1$, and $C^{12}(N^{14})Na^{22}He^4$ have been determined as a function of incident beam energy. An eight-position target holder was rotated rapidly through the collimated external beam. In seven of its positions were located carbon disks together with suitable nickel foil absorbers, while the eighth position was used to measure beam current. The nickel absorbers varied the incident energy between 16 and 28 Mev. The cross sections were determined by β counting of the produced radioactive nuclei with a calibrated end-window Geiger counter. The total yield curves, obtained in this way, were differentiated to give excitation functions. At 24 Mev the cross section for both reactions $C^{13}(N^{14})F^{18}Be^8$ and $C^{12}(N^{14})Na^{24}2H^1$ is of the order of $2\cdot10^{-26}$ cm². Above this energy the reaction

$C^{12}(N^{14})F^{18}Be^{8}$ becomes more probable, while at lower energies the cross section for $C^{12}(N^{14})Na^{24}2H^{1}$ is the larger one. For example at 18 Mev the cross section for $C^{12}(N^{14})Na^{24}2H^{1}$ is approximately six times the cross section for $C^{12}(N^{14})F^{18}Be^{8}$.

[1] Reynolds, Scott, and Zucker, Proc. Natl. Acad. Sci. U. S. **39**, 975 (1953).

C11. Energy Levels of Al^{27}. S. F. ZIMMERMAN, JR., AND C. P. BROWNE, *M.I.T.*—The nuclear-energy levels of Al^{27} up to an excitation of 5.9 Mev have been investigated through inelastic proton scattering.* Protons accelerated to energies of 5 to 8 Mev by the MIT–ONR electrostatic generator bombarded targets of thin foil on a thin layer of aluminum evaporated onto Formvar. The energies of protons scattered at 90 degrees were measured with the annular magnetic spectrograph. Of the proton groups observed, twenty-four have been assigned to Al^{27}. The general picture of the previously published[1] spectrum is confirmed. However, in two cases, the previous groups have been resolved to show two closely spaced levels. One pair occurs at 3.0 Mev and another at 5.4 Mev. In general, the level positions disagree by amounts increasing with excitation up to as much as 70 kev.

* This work has been supported by the joint program of the U. S. Office of Naval Research and the U. S. Atomic Energy Commission.
[1] Reilley, Allen, Arthur, Bender, Ely, and Hausman, Phys. Rev. **86**, 857 (1952).

C12. Gamma-Ray Energies from Al^{27} and S^{33}.* J. A. SMITH, J. N. COOPER, AND J. C. HARRIS, *Ohio State University.*—A scintillation spectrometer has been used to measure energies of gamma rays present at nine resonances in the reaction $Mg^{24}(p, \gamma)Al^{27}$, and at five resonances in the reaction $P^{31}(p, \gamma)S^{32}$. All resonances are in the range 400-kev to 1200-kev proton energy. The gamma-ray energies observed in both reactions were consistent with the intermediate level schemes for the respective product nuclei, as determined by the Pittsburgh group[1,2] by $p-p$ scattering (although not all intermediate levels seemed to be involved in the decays).

* This research was performed under the auspices of the U. S. Atomic Energy Commission.
[1] Reilley, Allen, Arthur, Bender, Ely, and Hausman, Phys. Rev. **86**, 857 (1952).
[2] Arthur, Allen, Bender, Hausman, McDole, Diana, Rhodes, and Barjon, Phys. Rev. **87**, 237 (1952).

C13. Angular Distribution of Gamma Rays from $Al^{27}(p\gamma)Si^{28}$. H. E. GOVE, E. B. PAUL, G. A. BARTHOLOMEW, AND A. E. LITHERLAND, *Chalk River Laboratories.*—The Chalk River electrostatic generator has been used to investigate the reaction $Al^{27}(p\gamma)Si^{28}$. The high-energy proton-capture γ rays were detected in a 2-inch diameter by 2-inch long NaI crystal and a Dumont 6292 photomultiplier. Gamma rays below 2 Mev were detected in a 1-inch diameter by 1-inch long NaI crystal. The high-energy γ-ray spectrum has been studied at 48 resonances in the range of proton energies from 0.65 to 2.2 Mev. The angular distributions of the capture γ ray to the first excited state of Si^{28} have been obtained at 17 of these resonances. The angular distribution of the ground-state γ ray has been measured at one resonance, and in a few cases the angular distribution of γ rays to higher states was measured. The angular distribution obtained at the 0.65 Mev resonance for the γ ray to the first excited state agrees with the result previously obtained by Rutherglen.[1] All angular distributions measured were symmetric about 90°. In a few cases a definite spin and parity assignment can be made from the angular distributions.

[1] J. G. Rutherglen (private communication).

C14. Partial Widths for the Reactions $Al^{27}(p\gamma)Si^{28}$ and $Al^{27}(pp')Al^{27}$*. E. B. PAUL, H. E. GOVE, G. A. BARTHOLOMEW, AND A. E. LITHERLAND, *Chalk River Laboratories.*—The apparatus described in the previous abstract has been used to measure the absolute yields for the capture γ rays leading to the first excited state of Si^{28}, and for the γ rays (0.84 and 1.05 Mev) following inelastic scattering of protons in Al^{27} at 25 of the 48 resonances. In a few cases, the γ ray following the (p,α) reaction leading to the first excited state of Mg^{24} at 1.38 Mev has also been measured. Partial widths for capture γ rays leading to the first excited state of Si^{28} lie in the range from 0.2 to 2.0 ev while those for $(pp'\gamma)$ reactions, in the region of $E_p = 2.0$ Mev, are about 10 ev with a few as high as 60 ev. The $(p\alpha\gamma)$ widths are similar to the $(pp'\gamma)$ widths. In the reaction where the total radiation width has been measured[1] the ratio of the partial width for the γ ray to the first excited state to the total radiation width is about 0.2.

[1] Bostrom, Huus, and Tangen, Phys. Rev. **71**, 661 (1947).

THURSDAY MORNING AT 10:00

Horace Mann

(G. L. PEARSON presiding)

Invited Papers

D1. Theory of the Energy Distribution of Secondary Electrons. P. A. WOLFF, *Bell Telephone Laboratories.* (30 min.)

D2. Theory Concerning Secondary Electrons Ejected from Metals by Ions. H. D. HAGSTRUM, *Bell Telephone Laboratories.* (30 min.)

Semiconductors

D3. The Germanium-Oxygen System.* MICHAEL HOCH AND HERRICK L. JOHNSTON, *The Ohio State University.*—The high-temperature x-ray diffraction patterns of germanium plus germanium oxide, GeO_2, between 750° and 1400°C showed that germanium monoxide, GeO, is not a stable compound. At elevated temperatures germanium can dissolve up to 60 atom percent of oxygen. The oxygen causes a very slight expansion of the germanium lattice. At 850° and 930°C, the x-ray pattern of a germanium-oxygen compound, consisting of equimolecular quantities of germanium and oxygen, showed only the germanium pattern. At 1000° and higher (above the melting point of pure germanium, 965°C), the germanium pattern disappears, and a liquid-like structure is visible, though the sample is still solid (melting point 1430°C). When the temperature is lowered again to 930°C, the germanium pattern reappears. The electrical resistivity shows a sharp break at 970°C. Thus we have a disordering of the germanium lattice, in the germanium-oxygen compound above the melting point of pure germanium.

* Supported in part by the U. S. Office of Naval Research.

D4. Electrical Properties of Dislocations in Plastically Deformed Germanium. G. L. PEARSON, W. T. READ, JR., AND F. J. MORIN, *Bell Telephone Laboratories.*—Measurements of conductivity, Hall effect, and lifetime were made on rods of both p- and n-type germanium which had been bent plastically while heated by passing current through them.[1] Deformation had no measurable effect of either conductivity or Hall mobility in 15-ohm cm p-type germanium. Deformation reduced both mobility and carrier density in 15-ohm cm n-type germanium. Plots of mobility and carrier density *vs* temperature indicate that deformation introduces acceptor-type electronic energy levels lying in the middle or upper half of the energy gap. These levels are believed to be associated with dangling, unpaired electrons on edge dislocations, which accept other electrons to make a dangling pair as discussed by Shockley.[2] As the dislocation accepts electrons, it becomes a negatively charged line surrounded by a cylindrical region of fixed positive space charge. The energy per added electron on the dislocation is increased by the increase in potential in the space charge region. The variation of average carrier density with temperature is consistent with a single energy level about 0.2 ev below the conduction band and a density of dislocations 2 to 3 times the minimum, about 10^7 per cm^2, calculated from the radius of curvature.

[1] Pearson, Read, and Morin, Phys. Rev. (to be published).
[2] W. Shockley, Phys. Rev. **91**, 228 (1953).

D5. Mobility of Impurity Ions in Ge and Si. J. C. SEVERIENS* AND C. S. FULLER, *Bell Telephone Laboratories.*—It is of interest to investigate the mobilities of impurity elements in Ge and Si in order to secure information on their state of ionization and to provide, also, independent and more accurate measures of their diffusivities. By diffusing hemispherical n-type regions of Li into Ge and Si and applying dc fields of 1–10 volts, we have determined Li^+ mobilities in the range 150–850°C. The drift times varies from 5 min to 3 hours and the drift distances ranged from 3 to 25 mils. The diffusivities D calculated from the Einstein relation, $D=\mu kT/q$, where μ is the ion mobility in cm^2 per volt sec are given by $D=22\times10^{-4}\exp(-11600/RT)$ and $D=61\times10^{-4}\exp(-16600/RT)$, for Li in Ge and Si, respectively. These equations agree with those previously published[1] and show that Li^+ follows the Einstein relation in this concentration range. The same method applied to Cu in Ge showed a drift of 4 mils in 45 sec toward the negative electrode for a field of 1 volt/cm. The magnitude of the diffusivity of Cu in Ge calculated from these data agrees within error with that previously observed.[2]

* Present address: Johns Hopkins University.
[1] C. S. Fuller and J. A. Ditzenberger, Phys. Rev. **91**, 193 (1953).
[2] C. S. Fuller and J. D. Struthers, Phys. Rev. **87**, 526 (1952).

D6. Volume and Surface Recombination Rates in Germanium. J. P. MCKELVEY AND R. L. LONGINI, *Westinghouse Research Laboratories.*—Bulk minority carrier lifetimes and surface recombination rates have been studied using apparatus similar to that of Navon, Bray, and Fan.[1] Diffusion theory for carriers of bulk lifetime τ has been utilized, considering a definite nonrecombination probability, or reflection coefficient, to be associated with the surface, to examine the roles of bulk and surface recombination effects, and to derive a relationship between the surface reflection coefficient and the surface recombination velocity. If the surface recombination velocity is known, the effective recombination cross section per unit surface area can be calculated. Experimental methods of separating bulk and surface effects have been devised, and values of bulk lifetime and surface recombination velocity have been measured for both n- and p-type germanium, and for a variety of surface treatments. The "WAg" surface etch,[2] which etches preferentially along (111) planes, is found to produce the lowest observed values of surface recombination velocity, 30 cm/sec for n type and 160 cm/sec for p type germanium. It is shown also that by modifying the experimental technique, the experimental apparatus can be used to measure drift mobility of minority carriers.

[1] Navon, Bray, and Fan, Proc. Inst. Radio Engrs. **40**, 1342 (1952).
[2] R. H. Wynne and C. Goldberg, J. Metals **5**, 436 (1953).

D7. Interstitial Ge in Heat Treated Germanium. SUMNER MAYBURG, *Sylvania Electric Products, Inc.*—A special heat treatment consisting of joule heating in good vacuum has allowed the study of lattice defects in germanium by low-temperature (195°K) resistivity measurements. This heat treatment technique is required in order to prevent contamination of the germanium with impurities such as copper which contribute to the electrical conductivity. By heating the germanium over 850°C and by quenching by radiation cooling, we are able to introduce of the order of 10^{14} acceptors per cc. If the sample is now annealed at a temperature in the neighborhood of 600°C, the concentration of acceptors drops rapidly with annealing time. However, if the annealing temperature is lowered to below 500°C, the acceptor concentration increases before it decreases. This sort of data is compatible with the picture that the heat treatment produces vacancies which act as acceptors and, in addition, interstitials which act as donors. Furthermore, it suggests that the interstitials have a higher diffusion rate than the vacancies and that, at the density of defects present in the germanium, there is little direct recombination of vacancies with interstitials. Most likely, the defects are diffusing to dislocations and the surface of the crystal.

D8. Electrical Properties of the Interface between a Germanium Single Crystal and an Electrolyte. W. H. BRATTAIN AND C. G. B. GARRETT, *Bell Telephone Laboratories.*—It is found that the anodic current from a germanium surface in solutions of KCl, KOH, and HCl is controlled by the supply of holes. The half cell potential consists of three parts: the reversible electrode potential of germanium in the solution; an overvoltage of the usual form, $bkT/e\ln(1-I/I_0)$, where I is the total current flowing (negative in this case); and a term $(kT/e)\ln p_1/p$, where p and p_1 are the equilibrium and actual hole densities near the surface. For p-type germanium $p_1=p$, and this term drops out. For n-type germanium, anodic current tends to reduce p_1, making the latter term large. Additional holes may be added by light. In this case p_1/p is given by $1+(I+\alpha L)/\alpha I_s$ where L is the added hole current and I_s the hole saturation current in the dark. "α" is the order of 2. If one adds just enough light to keep p_1 equal to p, one gets the same overvoltage curve as for p type. For n-type germanium it follows that $(dV/dL)_I=(kT/eI_s)(p/p_1)$ which is identical with the photoresponse of a $p-n$ junction.

D9. Infrared Properties of *P*-Type Germanium. E. BURSTEIN, B. W. HENVIS, AND N. SCLAR, *Naval Research Laboratory.*—Infrared absorption and photoconductivity measurements have been carried out over a range of temperatures on germanium doped with zinc and with indium. At low temperatures where the holes are bound to the acceptor impurities, zinc doped germanium and indium doped germanium exhibit optical absorption involving the photoionization of bound charge carriers. At sufficiently low temperatures, e.g., liquid helium temperature, this absorption is accompanied by photoconductivity which extends to 38 microns, the limit of measurement. The structure in the low temperature absorption curves may be interpreted in terms of optical transitions of holes from bound acceptor levels to levels within the several branches of the degenerate valence band.[1] Differences between the absorption curves of zinc doped germanium and indium doped germanium are attributed to differences in the bound acceptor levels. In indium doped germanium the similarity of the 3.6 microns band at liquid nitrogen temperature (where the holes are free) to that at liquid helium temperature (where the holes are bound) is apparently due to the similarity in character of holes at the top of the valence band to those bound at the impurity centers.

[1] H. B. Briggs and R. C. Fletcher, Phys. Rev. **91**, 1342 (1953).

THURSDAY MORNING AT 10:00

Schermerhorn 501

(P. KUSCH presiding)

Invited Papers on Molecular-Beam Experiments

DA1. Rotational Reorientation Spectra of Molecular Hydrogen and Deuterium. N. F. RAMSEY, *Harvard University.* (30 min.)

DA2. Precision Measurements with Molecular Beams. J. R. ZACHARIAS, *M.I.T.* (30 min.)

Invited Papers on the Neutrino

DA3. Status of an Experiment to Detect the Free Neutrino. Thirty minutes to be divided between C. L. COWAN, JR., AND F. REINES, *Los Alamos Scientific Laboratory.*

DA4. The Electron-Neutrino Angular-Correlation Coefficient in the Decay of Helium 6. B. M. RUSTAD, *Columbia University.* (30 min.)

THURSDAY MORNING AT 10:00

Pupin 329

(I. FANKUCHEN presiding)

X-Rays and Spectra

Invited Paper

E1. Small-Angle Scattering. G. H. VINEYARD, *University of Missouri.* (30 min.)

Contributed Papers

E2. Diffraction of X-Rays by Lattice Imperfections. YIN-YUAN LI AND R. SMOLUCHOWSKI, *Carnegie Institute of Technology.*—We consider the scattered intensity around a reciprocal lattice point of a crystal containing a topological imperfection such that the jth atom is shifted from r_j^0 in the perfect lattice to $r_j = r_j^0 + u(r_j)$. It appears that the phase of the diffracted wave is changed by $2\pi H \cdot u(r)$, where H is the position vector of the reciprocal lattice point concerned, and that the strain affects the diffuse pattern through the Jacobian $\partial(r^0)/\partial(r)$. It is pointed out that two different imperfections produce, in the first approximation, the same small-angle scattering if $\nabla \cdot u$ is the same. Diffuse scattering near a Bragg maximum is calculated for an edge dislocation.

E3. Scattering by Lattices of Deformable Atoms. R. J. GLAUBER, *Harvard University.*—Diffuse scattering due to thermal vibration of lattices is usually discussed under the assumption that the atoms undergo displacement rigidly. To investigate effects of atomic distortion, we consider a model in which the continuous function which yields the nuclear displacements, when evaluated at the lattice sites, is taken to define the displacement of the electron cloud at intermediate points as well. The scattering calculations, which include the effects of arbitrarily many lattice-quanta, are performed by field theoretical techniques described previously.[1] As in the latter work, inelasticity of the collisions may be treated by introducing a time dependent generalization of the correlation function for displacements at two points. The results for the present model are broadly similar in form to those for the rigid case. In particular, the Debye factor modulating the intensity of Laue-Bragg scattering remains unchanged. No diffuse scattering, however, surrounds the central (forward) Laue spot. The intensity of diffuse scattering in the immediate neighborhoods of the other spots is the same as in the rigid case, but intensity differences are introduced in the regions between the spots. Effects in these directions may be observable in x-ray diffraction.

[1] R. J. Glauber, Phys. Rev. **87**, 189 (1952).

E4. Spectral Energy Distribution of 2-Mev X-Rays. JOSEPH DRESNER, *Hospital for Joint Diseases.*—The absorption of a highly collimated beam of 2-Mev x-rays in lead has been accurately measured to a transmission of 0.001 under conditions of good geometry. The amount of scattered radiation reaching the detector was estimated to be about 0.001 of the transmitted beam for an attenuation of 1000. It has been shown[1] that the attenuation curve of an x-ray beam in a given absorber is related to the intensity distribution as a function of the absorption coefficient by a pair of Laplace transforms. This information can be readily converted to give the intensity distribution of the incident beam as a function of the energy. The use of this method is limited to x-ray energies below 3 Mev because of the slow variation of the absorption coefficient μ with energy and by the fact that $d\mu/dE$ changes sign near 3 Mev for heavy elements. The difficulties encountered in obtaining useful experimental data for high-energy radiation will be pointed out. Results obtained for a highly filtered beam of 2-Mev x-rays will be presented.

[1] J. R. Greening, Proc. Phys. Soc. (London) **A63**, 1227 (1950).

E5. The Soft X-Ray Absorption of Tellurium.* ROBERT W. WOODRUFF AND M. PARKER GIVENS, *University of Rochester.*—Absorption measurements were made on thin films of tellurium using a two meter spectrograph with an aluminum grating employed at grazing incidence. The effects of the celluloid substrate, onto which pure tellurium was deposited by vacuum evaporation, were eliminated by comparison of various thicknesses of tellurium on celluloid films of identical thickness. The authors recently reported[1] an absorption band found at about 300A. The investigation has now been extended to shorter wavelengths showing another absorption band which is possibly due to transitions from the N_{II-III} level to the conduction band.

* This work was supported by the U. S. Office of Naval Research.
[1] Robert W. Woodruff and M. Parker Givins, J. Opt. Soc. Am. **43**, 817(A) (1953).

E6. *L*-Emission Spectrum of Zr (40).* N. SPIELBERG, C. H. SHAW, AND J. A. SOULES,† *Ohio State University.*—Precise measurements of the complete *L*-emission spectrum of high-purity zirconium metal have been completed in the wavelength region from 5 to 7A. Line shapes and wavelengths were determined on a vacuum two-crystal spectrometer not yet described in the literature which used etched quartz crystals[1] and a proportional counter detector. The physical resolving power was of the order of 15 000. Wavelength calibrations were made with the aid of well-known shorter wavelength lines in higher orders. Previously unreported structure in both diagram and nondiagram lines has been observed. In particular, γ_1, ($L_{II}\rightarrow N_{IV}$) shows considerable fine structure while $\beta_2(L_{III}\rightarrow N_{IV,V})$ shows no detectable fine structure.

* Supported by the U. S. Atomic Energy Commission.
† Du Pont Fellow 1952–1953.
[1] L. G. Parratt, Rev. Sci. Instr. **6**, 113 (1935).

E7. A Liquefied Gas X-Ray Target.* E. A. WHALIN AND R. A. REITZ, *University of Illinois.*—The target gas, hydrogen, deuterium, or helium is contained in a thin-walled brass cylinder in contact with a low-temperature reservoir. For hydrogen and helium targets the reservoir contains the same liquefied gas as the target, while for a deuterium target the reservoir contains hydrogen. Target cylinders of 1.25-inch diameter with 0.0005-inch walls and 2-inch and 4-inch diameter with 0.001-inch walls have been used. These make well-localized x-ray targets with proton and meson backgrounds from the cylinder walls of 5–10 percent. The target and reservoir are surrounded by a liquid nitrogen cooled radiation shield. The nitrogen shield and vacuum jacket have thin windows allowing one to observe the production of protons of energy >20 Mev and mesons of energy >7 Mev. With a reservoir capacity of 3 liters the loss rate of liquid hydrogen is 40 ml per hour and of liquid helium is 250 ml per hour.

* This work has been supported in part by the joint program of the U. S. Office of Naval Research and the U. S. Atomic Energy Commission.

E8. Radiation Flux in a Planetary Atmosphere. DANIEL I. FIVEL AND GILBERT N. PLASS, *The Johns Hopkins University.*—The radiation flux in a planetary atmosphere can be calculated neglecting scattering if the transmission function is known between any two levels. After integration over both frequency and the variable conditions along the atmospheric path between two levels, the transmission function can be written in a very simple form involving Legendre functions This is possible either for a single spectral line or for the Elsasser model of a band which allows approximately for the overlapping of the lines. It is assumed in this derivation that the atmosphere is isothermal, that the fractional concentration of the radiating gas does not vary with height, and that the spectral lines have the Lorentz line shape with its known variation with pressure. However, for several of the major gases that contribute to the infrared radiation flux, the variations of the concentration of the gas and of the absorption with temperature over a long path length are important. In this case it is possible to obtain a rapidly convergent series for the transmission function. The series coefficients are moments of a simple integral involving the distribution of the gas with height and the temperature dependence of the line intensity. Some examples will be presented.

E9. Line Shapes in the Infrared. W. S. BENEDICT,* *The Johns Hopkins University,* AND SHIRLEIGH SILVERMAN,† *Applied Physics Laboratory, The Johns Hopkins University.*—Attempts have been made to study the shape of spectral lines in the fundamental vibration-rotation bands of several diatomic and polyatomic molecules by using high resolution ($\sim$0.2 cm^{-1}) over a broad range of optical densities, so that reliable absorption coefficients may be obtained in the wings of lines far removed from the resonant frequency, as well as at the absorption minimum, or "troughs" between neighboring lines. Results have been obtained for the 4.3μ band of CO_2 and the fundamentals of HCl and CO. The Lorentz line shape appears to be valid only for frequencies close to resonance. At $|(\nu-\nu_0)|$ >0.5 cm^{-1} the pressure dependence of the absorption over the range 0–0.2 atmos, obeys the Lorentz law but the frequency dependence does not. For CO_2 and CO the absorption is less than Lorentzian, while for HCl it is greater. In all cases the deviations increase with $|\nu-\nu_0|$. No evidence for an asymmetrical (Lindholm) shape has been found.

* This portion of the work was supported by the U. S. Office of Nava Research.
† This portion of the work was supported by the U. S. Office of Naval Research and the Bureau of Ordnance, Department of the Navy.

E10. Vibration-Rotation Line Intensities of Diatomic Molecules.* R. C. HERMAN, S. SILVERMAN, AND R. F. WALLIS, *Applied Physics Laboratory, The Johns Hopkins University.*—Using wave mechanical methods, matrix elements have been calculated for the *P* and *R* branches of the 0–1, 0–2 and 1–2 transitions of a diatomic molecule taking into account the interaction of rotation and vibration as well as the mechanical and electrical anharmonicity. For the 0–1 and 1–2 transitions the intensities of corresponding absorption lines in the *P* and *R* branches are proportional in first-order approximation to $(1+4\gamma\theta_K)K$ and $[1-4\gamma\theta(K+1)](K+1)$, respectively, where K is the rotational quantum number of the initial state, $\gamma=2B_e/\omega_e$, and $\theta=M_0/M_1r_e$. The quantities M_0 and M_1 are the first two coefficients in the electric dipole moment expansion about the equilibrium internuclear distance r_e. These expressions are a generalization of those obtained for the 0–1 transition by Oppenheimer[1] using matrix mechanics for a special model having $\theta=1$. For HCl where $\theta\sim1$ the results are similar to those of Oppenheimer. For CO, however, where $\theta\sim-1/30$ the effect is negligible. For the 0–2 transition the present theory predicts an appreciable effect for both HCl and CO. New measurements have been made on these molecules which confirm the above predictions.

* This work was supported by the Bureau of Ordnance, Department of the Navy.
[1] J. R. Oppenheimer, Proc. Cambridge Phil. Soc. **23**, 327 (1926).

THURSDAY AFTERNOON AT 2:00

Pupin 329

(G. E. KIMBALL presiding)

Chemical Physics

F1. Adsorption of Carbon Dioxide on Nickel Single Crystal Faces Using a Radiotracer Technique. J. A. DILLON, JR.,* AND H. E. FARNSWORTH, *Brown University.*†—The adsorption of CO_2 (5.8 percent $C^{14}O_2$) on the (110) and (100) faces of a nickel single crystal in the pressure range 1×10^{-8} to 6×10^{-8} mm Hg has been studied using an adsorption chamber containing a thin-window Geiger counter. Maximum adsorption of CO_2 at room temperature takes place on an adsorbed residual gas layer of optimum thickness rather than on the cleanest nickel surface obtained by outgassing in a high vacuum. The CO_2-nickel combination has a rate of adsorption of about 1.5×10^{11} molecules per minute for each face. Dissociation of adsorbed CO_2 is a possible explanation for this low rate. The observed equilibrium adsorption values on the (110) and (100) faces were about equal after 54 hours of outgassing at 985°C. After 32 hours of additional heating at 1085°C, with a pressure during heating of approximately 10^{-7} mm Hg, the adsorption on the (110) face at room temperature was twice that on the (110) face. Possible thermal etching of the (110) face makes the reason for this difference uncertain. Equilibrium adsorption on the (110) face corresponds to a surface coverage of 2 percent. The equilibrium adsorption on the (100) face decreases linearly by 80 percent as the temperature is increased from 30°C to 110°C.

* Now at Geophysics Research Directorate, Air Force Cambridge Research Center.
† Assisted in part by U. S. Office of Naval Research.

F2. Mechanism of Adsorption. I. Theory. B. C. BRADSHAW AND R. A. SHUTTLEWORTH, *Signal Corps Engineering Laboratories.*—The heterogeneity of surfaces is discussed with emphasis on a quantitative relationship between the heat of adsorption of a gas and the amount of surface coverage. The total heat evolved is found to be the sum of a determinable fraction of the heat of condensation of the gas and the actual heat of adsorption. The fraction of the heat of condensation is determined by the number of nearest neighbor molecules when the gas is in the solid state and the number when it is adsorbed as a monolayer. The actual heat of adsorption varies in the ratio of small integers and is found to depend on the number of nearest molecules in the underlying crystalline solid. The adsorption data of Claude, Magnus and Kratz, Kimball and Rideal, Jean Perreau, and others are discussed and shown to be consistent with this relationship. Hysteresis loops appearing in the pressure *vs* volume adsorption-desorption curves below saturation pressures are interpreted.

F3. Mechanism of Adsorption. II. Application. R. A. SHUTTLEWORTH AND B. C. BRADSHAW, *Signal Corps Engineering Laboratories.*—The principles outlined in Part I are used to interpret such phenomena as the effects of particle size and long-range forces on solubility, the destruction of catalytic activity with polishing, and the inverse order of adsorption and desorption.

F4. Effect of Structure and Molecular Weight on the Viscosity of Higher Hydrocarbons at High Pressures.* W. WEBB, J. W. SPENCER,† AND R. W. SCHIESSLER, *The Pennsylvania State University.*—Using a rolling-ball viscometer, the viscosity of eight pure hydrocarbon liquids has been determined from 15 to 50 000 psi at 100°F, 140°F, 210°F, and 275°F. A flexible bellows piezometer was used to determine the density between the same limits of temperature and pressure as the viscosity measurements. The compounds divide themselves into essentially two molecular-weight series. One series is composed of branched paraffins with a molecular weight range of 142 to 535. The other series is composed of aromatic hydrocarbon liquids with a molecular weight range of 182 to 350. In the second series the molecular weight is changed by the addition of a saturated normal branch which is a different length for each compound. Molecular-weight increase in homologous series changes the viscosity variation with pressure in a much simpler fashion than does structure variation. The variation of viscosity (η) with pressure is described reasonably well by an equation of the form

$$\eta/d^{n-1}=\eta_0/d_0^{n-1}\exp\{K/T[(d^3/d_0)^n-d^n]\},$$

where (d) is the density at pressure (P).

* Part of the work of Research Project 42 of the American Petroleum Institute.
† Now at California Research Corporation, La Habra, California.

F5. A New Method of Approximate Calculation of Atomic Radii. N. EFREMOV, *1061 Intervale Avenue, New York, New York.*—The proposed method of calculation of effective ionic radii* may be applied to calculation of atomic radii. Periodic system of atoms may be divided into three vertical segments: (1) inert gases, (2) quadruple groups of atoms of elements with valence from 1 to 4, and (3) quadruple groups of atoms of elements with valence from 4 to 7. A generalized scheme of this periodic system is a matrix consisting of several series of simple total numbers (K) which were used for calculation of ionic radii. These matrix numbers characterizing atoms (e.g., Si−13, P−12, S−11, Cl−10) are the first coefficients used for calculation of atomic radii. The second coefficients are ($n+4$), where n is the corresponding quantum number, e.g., (1+4), (2+4), etc. The third coefficients are certain constants ($P=0.01462369$A or $P'=0.0109677$A) which may be derived from Rydberg constant. Thus the transition from calculation of ionic radii to that of atomic radii is a very simple one, e.g.:

$$R_i(\mathrm{Si}\cdots)=(K\times n)P=(13\times2)P=26P=0.38\mathrm{A},$$
$$R_a(\mathrm{Si})=/K(n+4)/P=(13\times6)P=78P=1.14\mathrm{A}.$$

* Paper given at the September, 1953, meeting of the American Physical Society in Albuquerque, New Mexico.

F6. Preparation and Properties of III–IV Compounds. G. WOLFF, P. H. KECK, AND J. D. BRODER, *Signal Corps Engineering Laboratories.*—Considerable interest has been shown in III–V compounds of the sphalerite type, i.e., phosphides, arsenides, and antimonides of gallium indium and aluminum. For the purpose of a more detailed investigation of the properties of single-crystal material, a technique was developed for growing single crystals from solution. Solutions of 10 to 20 atomic percent P, As or Sb in Ga, In, or Al were cooled slowly, after being heated to a temperature slightly above the solubility curve of the phase diagram. The cooling was carried on at such a rate that a constant crystallization occurred. After cooling, the crystals were separated from the Ga, In, or Al excess. The liquid Ga was removed mechanically and chemically from the crystals by dilute HCl at room temperature; In was separated by means of a dilute solution of HCl in glycerol heated to about 180°C; Al was dissolved in dilute HCl thus, single crystal plates of GaP, GaAs, GaSb, InP, InAs, InSb, and

AlSb were obtained. Some of the crystals are up to 12 mm long and 1.5 mm thick. In all cases (111), (1$\bar{1}$1), (001) planes appeared. The twinning plane (111), and the cleavage plane (011), and occasionally (111), were observed in the crystals. Differences between (111), and (1$\bar{1}$1) were found for GaAs, InP, InAs, and AlSb. Thermoelectric tests indicate *n*-type conduction more frequently than *p*-type. Some of these compounds also show a strong photoeffect.

F7. On Bubble Dynamics in a Superheated Liquid.* H. K. FORSTER AND N. ZUBER, *University of California.*—An integro-differential equation describing the growth of a vapor bubble in a superheated liquid was derived: $r\ddot{r}+3/2\dot{r}^2-A(r-1)/r+BJ(t)=q(t)$; r is a dimensionless radius; A, B are physical constants; $q(t)$ is a distributed heat source; and

$$J(t)=\int_0^t \frac{R(t')\dot{R}(t')}{R(t)(t-t')^{\frac{1}{2}}}\left\{\exp\left[-\frac{(R-R')^2}{4a(t-t')}\right]-\exp\left[-\frac{(R+R')^2}{4a(t-t')}\right]\right\}dt'.$$

It is shown that at ordinary superheats the hydrodynamic forces represented by the first two terms of the equation are of importance only in an extremely small time interval of order less than 100 microseconds. Therefore the growth of the bubble almost during its entire "life" is described by the remaining terms, i.e., a nonlinear integral equation. Physical considerations are presented by which the integral is greatly simplified. A solution in the neighborhood of $t=0$ and an asymptotic solution, both in closed form, are obtained. The latter takes the simple form $r=C(t)^{\frac{1}{2}}$ (where C is determined by the physical constants of the liquid and vapor) and although obtained asymptotically agrees well with published experiments down to a few milliseconds.

* This work was supported in part by funds of the U. S. Atomic Energy Commission.

F8. Faraday Effect in Gases.* L. R. INGERSOLL AND D. H. LIEBENBERG, *University of Wisconsin.*—By use of a new sensitive photoelectric method,[1] the Faraday effect has been measured for a number of common gases, at ordinary pressures (½ to 3 atmos) so as to avoid possible aggregation effects. The gas is contained in a large wire-wound brass tube and a path of 20 m is obtained with the White "folded beam" optical system. The Verdet constants for hydrogen, deuterium, helium, neon, oxygen, nitrogen, and several other gases have been measured, with a probable error averaging 1 percent over the wavelength range 3658A to 9877A, with the aid of 35 carefully calibrated interference filters. Where comparison is possible (e.g., at 5780A), agreement with the work of de Mallemann[2] is quite satisfactory. Most of the Verdet dispersion curves resemble that of water, but oxygen and some other gases show significant deviations.

* Supported by the U. S. Office of Naval Research.
[1] L. R. Ingersoll and W. L. James, Rev. Sci. Instr. **24**, 23 (1953).
[2] Mallemann, Suhner, and Grange, Compt. rend. **234**, 2247 (1952), and earlier papers.

F9. Electrolysis of Sintered Thorium Oxide.* D. L. GOLDWATER AND W. E. DANFORTH, *Bartol Research Foundation.*—Previous studies have been made of electrolytic phenomena in homogeneous crystals of thorium oxide. Experience with electron tube cathodes of sintered thorium oxide has yielded qualitative observations of disintegration of the material with passage of current. Observations of electrolytic effects in tube cathodes are, however, complicated by the possibility of disintegration phenomena resulting from ion bombardment. In the present work, specimens of sintered thorium oxide are mounted in vacuum, and the effects of passing current are studied. A fresh specimen, when heated to 1500° C, will have a high resistivity of the order of 10^4 ohm-cm. Passage of current reduces resistance according to a law $R=k/Q^n$, where n is in the region of 0.8 and k is of the order of 15 000. The law appears to hold at least as far as $Q\approx 10\,000$ coulombs, $R\approx 1$ ohm-cm. The temperature coefficient of resistance changes from a positive value for the initial (semiconductor) state to a negative value for the final, pseudometallic condition. Evidence of release of electrolytically-produced oxygen will be discussed, particularly with respect to the behavior at the contact between specimen and the metal electrode.

* Supported by U. S. Navy, Bureau of Ships.

F10. The Ion-Yield of the Tritium-Oxygen Reaction. LEON M. DORFMAN AND B. A. HEMMER, *Knolls Atomic Power Laboratory.*—The rate of reaction of tritium and oxygen, initiated by the tritium betaradiation, has been investigated at 25°C, in the absence of mercury vapor, by using a sensitive Bourdon gauge as the manometer. The rate is not linear with time but shows a small continual decrease as the reaction proceeds. The initial reaction rate was found to be directly proportional to the tritium pressure and hence proportional to the radiation intensity. It was independent of the oxygen concentration over the range investigated. The reaction rate shows a slight dependence on the isotopic composition of the hydrogen reactant, tending to rise with increase in the mole fraction of protium. The initial reaction rate may be represented by: $R_0=1.19\times 10^{-4}C_{T_2}(1+0.3m_H)$ where C_{T_2} is the tritium concentration in moles/liter or other absolute concentration units, and m_H is the mole fraction of protium in the hydrogen reactant. On the basis of a requirement of 33 ev per ion-pair in the reactant mixture, the initial ion-pair yield for tritium disappearance or water formation is $(M/N)_0=3.2_5$ for the reaction of pure tritium with oxygen. Material balance measurements indicate that little or no peroxide appears in the product. The mechanism is discussed in the light of these observations.

* Operated by the General Electric Company for the U. S. Atomic Energy Commission.

F11. Mass Spectra of the Deuteroethylenes. VERNON H. DIBELER AND FRED L. MOHLER, *National Bureau of Standards.*—Samples of the deuteroethylenes have become available to the authors in satisfactory purity, and mass spectra have been measured and corrected for isotopic impurities. As in most hydrocarbons, the probability of removing an H atom relative to the probability in C_2H_4 increases progressively with the number of D atoms whereas the probability of removing a D atom is less than that of removing H from C_2H_4 and increases with the number of H atoms. (The symmetrical and asymmetrical $C_2H_2D_2$ molecules have nearly identical spectra in the mass range 24 to 30.) The probability of removing one H atom is equal to the *a priori* probability times 1.10, $(1.10)^2$, and $(1.10)^3$ in molecules containing one, two, and three D atoms. The probability of removing a D atom is 0.90 in C_2D_4 and is nearly equal to the *a priori* probability times $(0.90)^2$, $(0.90)^3$, and $(0.90)^4$ in molecules containing one to three H atoms. The weighting factors for removing two or more hydrogenic atoms are appropriate powers or products of the individual weighting factors. As the factors, 1.10 and 0.90, are nearly reciprocals, all weighting factors can be approximately represented by positive and negative powers of one constant, 1.10.

F12. Molecular Beam Investigation of the Scattering of Molecules from Surfaces.* F. C. HURLBUT, *University of California, Berkeley.*—Polar flux distribution of air and N_2 molecules scattered from surfaces of mild steel, aluminum, and glass were obtained using molecular beam techniques. Several values of incident angle were used. Polar traverses were not

confined to the incident plane. An ionization gauge-beam detection system was devised to accomplish these measurements. Spatial polar plots of the measured flux distributions for the steel and aluminum surfaces were found to approximate the form of cosine distribution. Similar plots for the glass surfaces were found to have small, broad, bulging deviations from the cosine scattering shape. These findings are discussed in relation to the Maxwell surface interaction model. A modification of the present concepts concerning the formulation of low-density gas-flow boundary conditions is discussed.

* Work supported by the U. S. Office of Naval Research and the U. S. Office of Scientific Research.

THURSDAY AFTERNOON AT 2:00

McMillin Theatre

(G. B. COLLINS presiding)

Mesons, I

Invited Paper

G1. Production of Charged Mesons by Gamma Rays on Hydrogen and Deuterium. P. D. LUCKEY, *Cornell University.* (30 min.)

Contributed Papers

G2. Photodisintegration of Helium above the Meson Threshold.* V. O. NICOLAI AND E. L. GOLDWASSER, *University of Illinois.*—An experiment has been done to measure the contribution to the photodisintegration of the helium nucleus from photons with energies above the meson threshold. The γ-ray beam of the 300-Mev betatron traversed a helium-filled cloud chamber. Runs were made at maximum energies of 135 Mev and 300 Mev. The γ radiation was monitored by a calorimetrically calibrated ionization chamber. The longer recoil ranges associated with helium disintegrations were used to help distinguish them from similar-type reactions in carbon and oxygen which were also present in the chamber as alcohol and water. For two-prong disintegrations the ratio of yields $N(300)/N(135)=1.4$ while for one-prong disintegrations, $N(300)/N(135)=1.2$. To get these numbers the two irradiations were normalized to the same number of photons per Mev at 27.5 Mev, the peak of the giant resonance. Other experimenters, observing photostars in the heavier elements of nuclear emulsions, find a yield ratio of about 3.0, calculated in a similar manner.[1] For a betatron energy of 135 Mev, preliminary results give 0.028-Mev barns for the integrated γ, n cross-section and 0.015-Mev barns for the integrated γ, p cross-section.

* This work has been supported in part by the joint program of the U. S. Office of Naval Research and the U. S. Atomic Energy Commission.
[1] S. Kikuchi, Phys. Rev. **86**, 41 (1952).

G3. π^+/π^- Ratios at Low Energies from Complex Nuclei. RYOKICHI SAGANE AND WALTER F. DUDZIAK, *University of California, Berkeley.*—Measurements have been made of charged pion production ratios resulting from the interaction of 340-Mev protons with complex nuclei. For the experiment a 22-in. Spiral Orbit Spectrometer was used.[1] Eight hollow conical targets consisting of the following elements: Be, C, Al, Cu, Ag, Ta, Pb, and U, were bombarded by a monitored proton beam. The charged pions created at 90° to the proton beam were focused by the spiral-orbit principle and detected by Ilford C-2 emulsions. As the pion energy is lowered the effect of the nuclear Coulomb barrier on this production ratio becomes appreciable. At low energies there is a reversal of this ratio (i.e., $\pi^+/\pi^-<1$) with increasing mass number. To illustrate this, the production ratios of C and U are compared at the three measured energies.

Element	π^+/π^- Ratios $T_\pi=12.5$ Mev	$T_\pi=27$ Mev	$T_\pi=37$ Mev
Carbon	5.4	6.0	9.0
Uranium	0.2	0.9	1.2

The obtained results are in general agreement with the previous measurement.[2]

[1] R. Sagane and W. F. Dudziak, Phys. Rev. **92**, 212 (1953); W. F. Dudziak and R. Sagane, U.C.R.L. Report 2304; R. Sagane W. Dudziak, U.C.R.L. Report 2317.
[2] R. Sagane, Phys. Rev. **90**, 1003 (1953); R. Sagane, U.C.R.L. Report 2161.

G4. Photoproduction of π^+ Mesons Near Threshold.* E. L. GOLDWASSER AND G. BERNARDINI, *University of Illinois.*—The photoproduction of π^+ mesons near threshold has been investigated using the University of Illinois 300-Mev betatron, a liquid hydrogen target, and Ilford G-5 nuclear emulsions. The experiment was designed to give information on the angular distribution between 30° and 150° in the laboratory system, and on the excitation function from threshold to 230 Mev. Up to this time, analysis of data from angles $\geq 45°$ gives $d\sigma/d\Omega^*=0.7\times10^{-29}$ cm^2 per steradian at a photon energy of 180 Mev and at all angles. The statistical error is less than 10 percent. The observed variation of the cross section is compatable with a direct dependence on the meson momentum, p, and is certainly less steep than p^3. If the photon interaction with the nucleon system is subject to a multipole analysis,[1] the above combination of angle and energy dependence is found to arise uniquely from an electric dipole absorption. This type of absorption may be considered from the point of view of several different nucleon models. These will be discussed.

* This work has been supported in part by the joint program of the U. S. Office of Naval Research and the U. S. Atomic Energy Commission.
[1] B. T. Feld, Phys. Rev. **89**, 330 (1953).

G5. Photomeson Production from Hydrogen.† T. L. JENKINS, D. LUCKEY, AND R. R. WILSON, *Cornell University.*—Photoproduction of charged mesons from hydrogen has been studied using a magnetic deflection method at gamma-ray energies of 200, 235, and 265 Mev and between 39° and 180° cm. The differential cross sections were least squares fitted to $A+B\cos\theta+C\sin^2\theta$, which assumes only S and P waves, with

the following results:

E(Mev)	A (μb/sterad)	B (μb/sterad)	C (μb/sterad)
200±10	8.5±2.2	−1.9±1.3	1.8±2.9
235±15	10.0±1.0	−2.8±0.8	4.5±1.6
265±20	8.7±1.1	−6.9±0.9	10.4±2.0
(270±40)*	(1.0±1.2)	(−1.0±0.9)	(10.0±1.5)

The last row shows our fit of the same expression to the published M.I.T. and Cornell neutral meson data. Assuming that all the P-wave interaction goes through a resonance state of angular momentum $\frac{3}{2}$ and isotopic spin $\frac{3}{2}$, one would expect the C term for charged mesons to be $\frac{1}{9}$ that for neutrals. Our data indicate a ratio more nearly 1 contradicting this assumption. Had we assumed a $2+3\sin^2\theta$ distribution, C would be about 6 and the agreement worse.

† Supported by the U. S. Office of Naval Research.

G6. $\pi^{\pm}$ Production Cross Sections from Deuterium. WALTER F. DUDZIAK, *University of California, Berkeley.*—An experiment of interest is the measurement of the pion production cross section from the following reaction $p+n\rightarrow\pi^-$. For the experiment hollow conical $(CD_2)_n$ and C targets were mounted on the axis of a 22-in. spiral orbit spectrometer. Charged pions created at 90° to a 340-Mev proton beam were detected by C−2 nuclear emulsions. Preliminary data based on 414 π^- star forming mesons from the $(CD_2)_n$ target yield the following ratios for the negative pionp roduction cross section from deuterium to the negative pion cross section from carbon.

T_π(Mev)	12.5	21	27	37	56
$\frac{\sigma_d^-}{\sigma_c^-}$	0.4	0.4	0.06	−0.09	−0.05

A similar preliminary ratio for positive pions is likewise obtained.

T_π(Mev)	12.5	21	27	37	56	65	66.3	67.5	68.8	70
$\frac{\sigma_d^+}{\sigma_c^+}$	0.5	0.3	0.3	0.3	0.08	0.09	0.05	0.05	0.2	−0.05

From an accurate measure of (1) the π^+/π^- ratio from carbon and (2) the positive pion production cross section from carbon one can determine the production cross sections for deuterium. A preliminary estimate of the integrated π^+/π^- ratio from deuterium at 90° is 12:1. Likewise the preliminary value for the reaction $p+d\rightarrow\pi^++t$ which occurs at $T_\pi=69$ Mev is 5×10^{-31} cm²/Mev Sterad.

G7. Elastic Photoproduction of Neutral Mesons from Deuterium.* B. WOLFE, J. W. DEWIRE, AND A. SILVERMAN, *Cornell University.*—We have investigated the angular distribution for the reaction $\gamma+D\rightarrow\pi^0+D$. The reaction is observed by detecting a coincidence between the recoil deuteron and one of the π^0 decay γ rays. Details of the technique have been reported previously.[1] The differential cross sections are measured for an average γ-ray energy of 275 Mev with a spread of energies from approximately 260 Mev–290 Mev. The results are as follows:

θ_{π^0}(Lab)	76°	94°	110°	130°
$\left(\frac{d\sigma}{d\Omega}\right)\times10^{30}$ (cm²/ster)	6.3±1.0	3.3±0.5	2.7±0.4	1.2±0.3

The data are obtained by taking a CD_2-CH_2 difference for the various angles. To obtain the absolute cross section, independent of the γ-ray detection efficiency, a CD_2-CH_2 difference was measured at 110° for the π^0 by detecting only the recoil deuteron (deuteron angle = 28°). The errors shown apply to the relative values of the differential cross section. The absolute cross section has an additional uncertainty of 20 percent.

* Supported by the joint program of the U. S. Office of Naval Research and the U. S. Atomic Energy Commission.
[1] DeWire, Silverman, and Wolfe, Phys. Rev. **92**, 520 (1953).

G8. Elastic Photoproduction of π^0 in Helium.* G. DE-SAUSSURE AND L. S. OSBORNE, *M.I.T.*—The gamma-ray beam of the synchrotron operating at 350 Mev was passed through a chamber containing helium. The recoil alphas arising from the photoproduction of π^0 were detected in photographic plates placed inside the tank. The Ilford GO 400μ plates were developed so as to enable one to discriminate singly from doubly charged particles. That part of the He^3 background from the photodisintegration which falls in the same energy angle region as the recoil nuclei from π^0 production is the result of incoming gamma rays of energies smaller than 150 Mev. It can be subtracted by making a separate run at low energy. From the angle and range measurements, the center-of-mass energy of the incident photon and the angle θ and momentum of the meson were determined on 280 individual events. The following table shows the preliminary results:

θ (center of mass)	20–60°	60–80°	80–100°	100–120°	120–160°	
$\frac{d\sigma(\alpha)}{d\Omega}$	18.5±6	28±7	34±7	16.5±6	1±1	10^{-30} cm²/steradian equivalent photons
$\frac{d\sigma(\alpha)}{d\Omega}\Big/\frac{d\sigma(p)'}{d\Omega}$	2.3	1.6	1.7	0.9	0.1	

* This work was supported in part by the joint program of the U. S. Office of Naval Research and the U. S. Atomic Energy Commission.
[1] Goldschmidt-Clermont, Osborne, and Scott, Phys. Rev. **89**, 329 (1953), and B. T. Feld, Phys. Rev. **89**, 330 (1953). The cross section is assumed to be proportional to $2\cos^2\theta+5\sin^2\theta$ and the part proportional to $2\cos^2\theta$ corresponds to spin flip and has been subtracted.

G9. Elastic Production of π^0 Photomesons from Deuterium.* H. L. DAVIS AND D. R. CORSON, *Cornell University.*—The 310-Mev bremsstrahlung of the Cornell synchrotron was used to study the process $\gamma+D\rightarrow\pi^0+D$. The recoil deuterons were bent through 40° by a uniform magnetic field and were detected by Ilford C-2 200μ emulsions inclined with a vertical angle of 45° to the deuteron trajectory. The particle momentum was determined by observing the horizontal angle of incidence in the plate. Deuterons and protons with the same momentum were separated by observing the difference in grain densities of their tracks. In the momentum interval used protons had energy $\geqslant$50 Mev and were barely detectable; deuterons in the same interval were detectable with ~100 percent efficiency. With the system evacuated plates exposed with no target in position showed no background tracks. An independent check was made of the momentum resolution and the identity of the particles by observing the ranges of particles stopping in plates inclined at 5° to the horizontal. This additional information allows a determination of the particle mass. The resolution of the resulting mass spectrum agreed with the expected momentum resolution. A heavy paraffin-carbon difference was measured at 270 Mev and a π lab angle of 130°. Preliminary results give $d\sigma/d\Omega=3.1\pm1.0\times10^{-30}$ cm² sterad^{-1}.

* Supported by the joint program of the U. S. Office of Naval Research and the U. S. Atomic Energy Commission.

G10. Negative μ-Meson Capture in Carbon.* T. N. K. GODFREY,† *Princeton University.*—The experiment reported previously[1] has been completed. Cosmic-ray μ mesons that stop in an organic liquid scintillation counter are selected by an arrangement of coincidence and anticoincidence Geiger counters. In the scintillation counter the mesons may either decay or be captured by nuclei of the carbon in the scintillation liquid. The capture reaction produces either B^{12} or nuclear fragments. The number of electrons emitted by decaying μ mesons and the number emitted by decaying B^{12} nuclei are each counted. From the ratio of these two numbers and the known mean life of the free μ meson a value for the rate of the

μ-meson capture reaction that produces B^{12} is calculated. A comparison between this value and that predicted by applying the theory of orbital electron capture to the capture of μ mesons will be presented.

* Supported by the joint program of the U. S. Atomic Energy Commission and the U. S. Office of Naval Research.
† National Science Foundation Predoctoral Fellow.
[1] T. N. K. Godfrey, Phys. Rev. **92**, 512 (1953).

G11. Spectrum of Electrons from μ-Meson Decay.* R. W. WILLIAMS† AND J. H. VILAIN,‡ *M.I.T.*—We have measured the energy spectrum of positons from the decay of muons at rest. Positive pions from a paraffin target in the gamma-ray beam of the M.I.T. synchrotron passed through a cloud chamber in a magnetic field (9000 gauss) and stopped in the wall of the chamber. The electron from the subsequent muon decay was visible in the chamber if it started in a favorable direction; we have obtained 830 such events. In order to obtain an unbiased sample we have restricted the study to electrons of more than 20-Mev initial energy, and have applied to these a strict set of selection criteria. The final sample contained 280 tracks. Comparing this with the calculated spectrum,[1] and using $(207.0\pm0.6)m_e$ for the muon mass, we find, for Michel's parameter, $\rho=0.50\pm0.12$; that is, the spectrum very clearly does not go to zero at the end point.

* Supported in part by the joint program of the U. S. Office of Naval Research and the U. S. Atomic Energy Commission.
† Presently on leave at Princeton University.
‡ Present address: Ecole Nationale Superieure des Telecommunications, Paris.
[1] L. Michel, Phys. Rev. **86**, 814 (1952).

THURSDAY AFTERNOON AT 2:00

Horace Mann

(JAMES RAINWATER presiding)

High-Energy Electrons; Positrons; Fission

H1. Angular Distribution of Photoelectrons.* W. H. MCMASTER AND F. L. HEREFORD, *University of Virginia*.—The angular distribution of high-energy (0.4–0.7 Mev) photoelectrons produced in Pb and Au foils by linearly polarized photons has been investigated using scintillation counting and pulse-height analysis techniques. A Compton scattered photon beam from Co^{60} provided a source of partially polarized radiation. The cross section for the distribution of K-shell photoelectrons was first calculated by Sauter[1] using Dirac's relativistic wave equation. The cross section is of the form $d\sigma_k=A+B\cos^2\Phi$. In the nonrelativistic limit the second term predominates in agreement with nonrelativistic calculations. For high energies ($>\sim0.5$ Mev), the first term, containing the square of the energy, predominates;[2] resulting in photoemission predominately orthogonal to the electric vector of the incident photon. Experimental results confirm this phenomenon and are in good agreement with the distribution predicted by Suter.

* Supported by U. S. Office of Ordnance Research.
[1] F. Sauter, Ann. Physik **11**, 454 (1931).
[2] F. L. Hereford and J. P. Keuper, Phys. Rev. **90**, 1043 (1953)

H2. Energy Distribution of Secondary Electrons Produced by 1.3-Mev Primary Electrons.* R. A. SHATAS, J. F. MARSHALL, AND M. A. POMERANTZ, *Bartol Research Foundation*.—Utilizing the linear accelerator as a source of 1.3-Mev electrons, the secondary electron emission from thin targets which do not stop the primaries has been investigated. In the usual thick-target experiments, scattered primaries and high-energy secondaries are indistinguishable, whereas the former do not register in the present arrangement. Under these conditions, it has been possible to determine that energetic secondaries (delta rays) constitute about half of the total yield. With a 0.002-in. Ni target the total yield from both faces (I_{sec}/I_{prim}) is 3.6 percent, and the delta-ray yield exceeds 1.5 percent. The latter is at least qualitatively in accord with theoretical expectation. The customary procedure of designating as "true secondaries" all electrons which fail to reach a collector when some arbitrarily-assigned retarding field is applied thus introduces appreciable errors; similarly it is erroneous to regard all energetic electrons leaving a bombarded target as scattered primaries. Preliminary measurements have also indicated that the energy distribution in the low-energy region is roughly similar to that observed when the bombarding energy is low with the maximum for Ni occurring below 6 ev.

* Assisted by the U. S. Office of Naval Research and by the U. S. Office of Ordnance Research.

H3. Elastic Scattering of Electrons from Nuclei.* ROBERT T. BAYARD AND J. L. YNTEMA, *University of Pittsburgh*.—Considerable discrepancies in the scattering of electrons at large angles by heavy nuclei have been reported between 0.15 and 0.4 Mev and at 2.2 Mev.[1] We have measured the relative scattering of 1-Mev electrons by aluminum and gold at 30°, 60°, 90°, 120°, and 150°. The source of electrons was a Van de Graaff generator and the detectors were anthracene crystals viewed by photomultipliers. The scattering in aluminum is consistent with the α^4 approximation of Matt's theory, as given by McKinley and Feshbach,[2] within the experimental error of 0.4 percent. The scattering in gold was compared with cross sections obtained from those calculated for Hg by Bartlett and Watson[3] using the α^4 approximation to correct for the difference between Hg and Au. The experimental data do not differ by more than 1.5 percent from these theoretical values. Therefore there is no evidence of deviation from Mott theory at 1 Mev.

* Supported in part by joint program of the U. S. Office of Naval Research and U. S. Atomic Energy Commission.
[1] E. Kinzinger, Z. Naturforsch. **8a**, 312 (1953), E. Kinzinger and W. Bothe, Z. Naturforsch. **7a**, 390 (1952), W. Paul and H. Reich, Z. Physik **131**, 326 (1952).
[2] William A. McKinley, Jr., and Herman Feshbach, Phys. Rev. **74**, 1759 (1948).
[3] J. H. Bartlett and R. E. Watson, Proc. Am. Acad. Arts Sci. **74**, 53 (1940).

H4. Elastic Scattering of High-Energy Electrons by Nuclei. ALFRED E. GLASSGOLD, *M.I.T.*—The difference in the scattering phase shifts between a finite and a point nucleus has been calculated for two static charge distributions: The nuclear charge is distributed uniformly (1) throughout a sphere of radius R_1 or (2) on a sphere of radius R_2. This phase shift depends on the energy and nuclear radius only through the product kR of the wave number and the nuclear radius. The values of the atomic number used were $Z=13$, 29, 50 and 79, and the values of kR ranged from $\frac{1}{2}$ to 3. For $Z=79$ and $R=r_0A^{\frac{1}{3}}$ with $r_0=1.1\times10^{-13}$ cm, $kR=3$ corresponds to an energy of about 100 Mev. An interpolation formula has been

developed which gives the change in phase shift for small changes in Z. Comparison will be made with recent experiments.

H5. Čerenkov Radiation from Extended Electron Beams.* M. DANOS, *Columbia University Radiation Laboratory.*—The energy emitted by a flat electron beam having the charge density $\rho=\rho_0\{1+\alpha\cos[(\omega/v)(z-vt)]\}$ and moving with the velocity $v=c\beta$ at a distance d over the surface of a dielectric with dielectricity constant ϵ is given by

$$P=189I^2a^2\exp\left[-\frac{4\pi d}{\lambda}(1-\beta^2)^{\frac{1}{2}}\right]\frac{\epsilon}{\beta}\frac{(1-\beta^2)(\epsilon\beta^2-1)^{\frac{1}{2}}}{(\epsilon\beta^2-1)+\epsilon^2(1-\beta^2)}\times\mu\ \text{watts/cm}^2$$

if the beam current I is measured in ma; $\lambda=\omega/2\pi c$ is the free space wavelength. The dependence of the radiated energy on v is here qualitatively different than in the well known case of cylindrical geometry,[1] where the radiation reaches a maximum at $v\rightarrow c$. If in the plane case a second dielectric is added so as to sandwich the electron beam between the two dielectrica the behavior is similar to the cylindrical case.

An experiment has been performed to detect the Cerenkov radiation at microwave frequencies. The power observed is in reasonable agreement with the theoretical predictions.

* Work supported jointly by the U. S. Signal Corps, the U. S. Office of Naval Research, and the U. S. Air Research and Development Command.
[1] V. L. Ginsburg and I. M. Frank, Doklady Akad. Nauk **56**, 699 (1947).

H6. Scattering of 2.7-Mev Positrons by Au and Al Foils. L. GRODZINS, *Purdue University* (introduced by W. Y. Chang).—Positrons from radioactive sources are selected by a beta-ray spectrograph and sent into a 12-in. cloud chamber illuminated over a depth of 3 in. Helmholtz type coils produce a field within the chamber uniform to greater than 99.5 percent over 10 inches of its diameter. The tracks are photographed with a 35-mm double-lens camera placed above the chamber. Studies of positron interactions with the cloud-chamber gas and foils placed within the chamber are being carried out. Using a Ga^{66} source about 5000 tracks have been photographed of 2.7 ± 0.3 Mev positrons, which have traversed, in a field of 560 gauss, the helium gas and a 0.0001-in. Au and a 0.001-in. Al foil placed within the chamber. These particles enter the chamber through a $\frac{1}{4}$-in. slit, covered with a 0.001-in. Al foil, and have an azimuthal spread of about 3°. Only those positrons which strike the gold foil at an angle of $90\pm10°$ are measured. A more detailed description of the experimental arrangement, the accuracy of track measurement and the analysis of these tracks will be presented (see abstract LA2 by W. Wallenmeyer).

H7. Lifetime for Annihilation of Positrons in Aluminum and Lead. GEORGE H. MINTON, *National Bureau of Standards.*—A coincidence system of millimicrosecond resolution has been employed to compare the lifetimes for annihilation of positrons stopped in lead and aluminum. Na^{22}, which emits a positron of 575-kev maximum energy and a simultaneous 1.3-Mev gamma ray, was used as a source. The gamma rays were detected by scintillation counters employing terphenyltoluene scintillators and 5819 photomultipliers operated at over 2000 volts. The pulses from the anodes of the photomultipliers were fed directly into two diode coincidence circuits opersted as a differential unit. The curves obtained for coincidence rate *versus* inserted delay were compared with similar curves obtained with gamma-gamma coincidences from Co^{60}. In order to work with similar pulse-height distribution in obtaining the curves, the output of the coincidence unit was gated by differential pulse-height selectors driven from the last dynodes of the photomultiplier tubes and viewing appropriate parts of the Compton spectra produced in the scintillators by the gamma rays. The observed mean life of positrons in aluminum was $(2.9\pm0.3)\times10^{-10}$ second. The lifetime observed in lead was $(3.5\pm0.3)\times10^{-10}$ second. The difference of these two quantities is estimated to be $(6\pm3)\times10^{-11}$ second Comparisons with previous related experiments will be made.

H8. Annihilation of Positrons in Condensed Materials. T. A. POND,† *Princeton University.*—The previously described method[1] for comparing the fractions of positrons that annihilate with two photons in different materials has been extended. The ratio of the two-photon fraction in crystalline germanium of 45 ohm/cm resistivity to copper is 1.0009 ±0.0009. Fused quartz shows (0.6 ± 0.1) percent fewer two-photon annihilations than either crystalline quartz or Duraluminum. If this defect is attributed to triplet positronium annihilations, it corresponds, when combined with the data of Bell and Graham[2] to a lifetime for triplet positronium against three-photon annihilation of $(0.9\pm0.5)\times10^{-7}$ sec in fused quartz. Benzene shows 0.7 ± 0.1 percent fewer two-photon annihilations than magnesium. This difference is partially quenched by the addition of small amounts of the free radical, diphenyl picryl hydrazyl, to the benzene. Assuming thermal triplet positronium of mean life 2×10^{-9} sec[2], the observed variation of quenching with concentration of the free radical leads to an exchange cross section between positronium and the unpaired electron of 4×10^{-17} cm^2.

* Supported by the U. S. Atomic Energy Commission and the Higgins Scientific Trust Fund.
† Now at Washington University, St. Louis, Missouri.
[1] T. A. Pond, Phys. Rev. **91**, 455 (1953).
[2] R. E. Bell and R. L. Graham, Phys. Rev. **90**, 644 (1953).

H9. Fine Structure of Positronium.* ROY WEINSTEIN, MARTIN DEUTSCH, AND SANBORN BROWN, *M.I.T.*—We have extended the experiments of Deutsch and Brown[1] on the Zeeman splitting of the 1^3S state of positronium, using higher R.F. power, and improved control of the magnetic field. The reduction of the three quantum annihilation at resonance ranged from 5 to 20 percent and agreed with the theoretically expected quenching within the experimental uncertainty. The width of the resonance at half maximum, $\Delta H/H\simeq4\times10^{-3}$, agrees with the annihilation width broadened by a doppler effect due to a kinetic energy of the order of 1 ev. The position of the resonance was found to be independent of the nature and pressure of gas in the cavity. He, A, Kr, and CF_3Cl_3 were used at pressures between 1/3 and 4/3 atmospheres. The singlet-triplet splitting of the ground state, calculated to order α^5 from the Zeeman splitting is $\Delta W=2.03350\pm50$ mc, compared with a theoretical value[2] of 2.03370 mc.

* This work was assisted in part by the joint program of the U. S. Office of Naval Research and the U. S. Atomic Energy Commission, and in part by the U. S. Signal Corps and the U. S. Air Materiel Command.
[1] M. Deutsch and S. Brown, Phys. Rev. **85**, 1047 (1952).
[2] R. Karplus and A. Klein, Phys. Rev. **86**, 257 (1952).

H10. Angular Distributions of Fission Fragments from 22-Mev Proton Induced Thorium Fission. B. L. COHEN, W. H. JONES, G. H. MCCORMICK, AND B. L. FERRELL, *Oak Ridge National Laboratory.*—The angular distributions of barium, strontium, zirconium, ruthenium, and silver fission fragments from 22-Mev proton induced thorium fission were measured using the internal, circulating beam of the Oak Ridge National Laboratory 86-inch cyclotron. The target consisted of a thin strip of $\frac{1}{2}$ mg/cm^2 thickness of thorium oxide plated on a 0.001-in. platinum foil. The fission fragments were collected in aluminum foils which, after bombardment, were processed chemically to isolate the various fission products; these were then counted to determine the angular distribution. Approximately 60 bombardments were carried out. Within the accuracy of the experiment, all angular distributions are symmetric about 90° and can be well fitted to $I(\theta)=a+b\cos^2\theta$. For Ba, Sr, Zr, Ru, and Ag fission products, b/a is 0.265 ± 0.015, 0.250 ± 0.020, 0.215 ± 0.015, 0.17 ± 0.05, and 0.110 ± 0.015, respectively. (Errors are standard deviations due to statistics only; systematic errors introduce an uncertainty of about

± 0.02). Symmetric fission thus gives a more isotropic angular distribution than asymmetric fission. The data is fitted somewhat better by $I(\theta)=a'+b'\cos^2\theta+d'\cos^4\theta$ where in all cases, d'/a' is about -0.16 and $b'/a'+d'/a'$ is very nearly equal to b/a given above. Possible theoretical reasons for the anisotropic angular distributions will be discussed.

H11. Measurement of the Energy Released per Fission in the Bulk Shielding Reactor. J. L. MEEM, *Oak Ridge National Laboratory.*—The energy released per fission was measured in the Bulk Shielding Reactor using a specially constructed fuel element. The special element had a removable center fuel plate from which disks were punched to facilitate measurement of their activation by exposure in the reactor. A similar uranium-bearing disk was activated by exposure in a known neutron flux. By comparison, the actual fission rate in the special fuel element was determined. The temperature rise across the fuel element was measured at a known rate of water flow, special precautions being taken to prevent heat leakage. The power was thus determined and a comparison with the fission rate gave the heat released per fission in the special element. The net amount of radiation leaking out of the fuel element (less than 0.2 percent) was calculated as a correction to this figure. The energy per fission in the reactor was 193 ± 5 Mev. The energy associated with captures other than these in U^{235} is calculated to be 2.7 Mev. Accordingly, the energy released per fission (exclusive of neutrino energy) is 190 ± 5 Mev.

H12. Measurement of Fission Fragment Ranges in Aluminum.* D. H. TEMPLETON AND E. M. DOUTHETT, *University of California, Berkeley.*—Fission fragment ranges in aluminum can be measured by radio-chemical assay of the fission products in each of a stack of foils adjacent to the fissioning sample. If these foils have thickness of the order of half the range greater precision can be obtained for the *mean range* than if very thin foils are used, because of errors in thickness in the latter case. Measurements have been made by this "thick foil" technique for several products of the fission of U^{235} induced by 18-Mev deuterons or by 335-Mev protons. The forward-backward difference in the deuteron case confirms that a compound nucleus is formed prior to fission. The results in the proton case are explained by the evaporation of many neutrons followed by fission in which the neutron-proton ratio is nearly the same in the two fragments.

* Work performed under the auspices of the U. S. Atomic Energy Commission.

H13. Photofission Cross Sections.* JAMES GINDLER AND ROBERT B. DUFFIELD, *University of Illinois.*—The photofission cross sections of several elements have been measured for bremsstrahlung having maximum energies from 125 to 300 Mev. A scintillation counter was used to detect the fission recoils. For 275 Mev bremsstrahlung the following values were obtained (given as the number of fissions per atom for a flux of one erg/10^{-24} cm^2): 0.34 for tantalum, 0.60 for tungsten, 1.2 for gold, 1.7 for thallium, 2.9 for lead, 6.3 for bismuth, 240 for thorium, 570 for uranium. Cross sections have been calculated from these data. For bismuth and the elements of lower Z, the cross sections increase rapidly with energy above 125 Mev, reaching 8.5 mb for bismuth at 285 Mev in agreement with earlier work.[1] The cross sections of uranium and thorium appear also to increase at the higher energies but the measurements have a large probable error, since they are very sensitive to the large and uncertain cross sections below 125 Mev.

* Assisted by the joint program of the U. S. Office of Naval Research and the U. S. Atomic Energy Commission.
[1] Bernardini, Reitz, and Segrè, Phys. Rev. 90, 573 (1953).

THURSDAY AFTERNOON AT 2:00

Schermerhorn 501

(T. A. READ presiding)

Solid-State Physics, I

Invited Paper

I1. Effects of Pressure on Twelve Rare-Earth Metals. P. W. BRIDGMAN, *Harvard University.* (30 min.)

Contributed Papers

I2. Theory of the Crystal Geometry of the Cubic—Tetragonal Phase Changes.* M. S. WECHSLER, D. S. LIEBERMAN, AND T. A. READ, *Columbia University.*—A general theory of the formation of transformation products in a wide range of crystalline solids which undergo diffusionless phase changes will be presented. Crystallographic features of the transformation are predicted from a knowledge only of the lattice parameters of the initial and final structures and no adjustable constants are involved. These features include the orientation of the plane interface between the two phases, the orientation relationship between the crystal axes in the two phases, and the magnitude and direction of macroscopic distortion accompanying the transformation. The experimental observation that the transformation distortion is inhomogeneous is incorporated in this theory. It is postulated that the essential significance of this inhomogeneity is that it permits the interface plane to be one of zero average distortion. With the use of matrix algebra, explicit expressions are obtained for the direction cosines of the normal to the interface plane as a function of the lattice parameters of the two phases. The detailed formulation of the theory for the cubic to tetragonal transformation will be summarized.

* Work supported by the U. S. Atomic Energy Commission.

I3. Experimental Studies of Diffusionless Cubic—Tetragonal Phase Changes.* T. A. READ, M. S. WECHSLER, AND D. S. LIEBERMAN, *Columbia University.*—Experimental observations on specimens that have partly undergone a crystal structure transformation from cubic to tetragonal will be summarized. These include observations of the orientation relationship between the crystal axes in the transformed and untransformed parts of the specimen, the character of the

interface between the two regions, and the macroscopically observable distortion which accompanies the transformation process. Particular attention will be given to the transformations of this type that occur in barium titanate, indium-thallium alloys, and iron base alloys. It will be shown that these observations are in agreement with the predictions of the analysis given in the preceding paper.

* Work supported by the U. S. Atomic Energy Commission.

I4. Cubic to Orthorhombic Diffusionless Phase Change—Experimental and Theoregical Studies of AuCd.*† D. S. LIEBERMAN, M. S. WECHSLER, AND T. A. READ, *Columbia University.*—The basic ideas and mathematical formulation described above were applied successfully to the analysis of the cubic (β_1) to twinned orthorhombic (β') transformation in AuCd single crystals containing 47.5 atomic percent Cd. Because of the lower symmetry of the low temperature phase in this alloy, the calculations were of necessity more involved. In the mode of transformation studied, a single interface moves slowly along the specimen separating it into the β_1 and β' regions. The transformation is completely reversible with a hysteresis width of 15°C and a transformation temperature on cooling of 60°C. The interface is visible because of the dihedral angle caused by the net macroscopic transformation shear and there is no distortion at the interface. The direction of the interface plane, direction and magnitude of shear, direction of the twin plane, and the orientation relationships were determined experimentally. These same crystallographic features of the transformation were calculated theoretically. The calculated and observed values agree within experimental error. The agreement found between theoretical predictions and experimental observations in the three systems studied thus far constitutes powerful evidence in favor of the theory of diffusionless phase transformations proposed.

* Work supported in part by contract with the U. S. Atomic Energy Commission.
† To be published.

I5. Thermodynamics of Ordering Alloys, II. The Ordered and the Disordered Solid Solutions of the Gold-Copper System. R. A. ORIANI, *General Electric Research Laboratory.*—The thermodynamic activities in solid gold-copper alloys have been measured by the galvanic cell technique, exercising extreme care that equilibrium conditions are attained. Good agreement with the results of previous investigators is obtained in the high-temperature region; the results at lower temperatures clearly demonstrate the two-phase coexistence areas of the phase diagram which lie between successive single phases. The activities of the two components, the free energies, entropies, and enthalpies of solution have been obtained within the disordered field and within the superlattices. The entropy of mixing in the disordered field is somewhat larger than for an ideal solution in the low copper region, but at other compositions shows negative deviations from ideality which correspond to short-range order. The curve of the entropy of mixing at an isothermal which intersects the superlattice phase fields shows deep cusps at the stoichiometric compositions of the superlattices. Assymmetries in the curves of entropies and enthalpies of solution are related to the assymmetry in the boundary between the orthorhombic and the disordered phases.

I6. On the Disordering of Solids by Heavy Corpuscular Radiation. W. S. SNYDER AND JACOB NEUFELD, *Oak Ridge National Laboratory.*—A general method is outlined for determining the number of vacant lattice sites or interstitial atoms in a monoatomic solid exposed to neutron radiation. The colliding atoms are assumed to be within the energy range for which the orbital picture can be applied. Following the treatment of Bohr, the scattering regions of excessive and moderate screening, Rutherford distribution, and electronic collisions are considered separately. The number of vacancies or interstitial atoms as a function of the energy of the primary knocked out atom is given by the solution of certain integral equations that are different for various energy regions considered. It is found that if the velocity of a recoil atom resulting from neutron collision is less than $e^2/\hbar$ (region of elastic collisions) approximately half of its energy is used to produce vacancies or interstitials (for solids composed of atoms having atomic number ($Z>3$)). If the velocity of the recoil atom is above ($e^2/\hbar$) (region of inelastic collisions) then the energy used to produce vacancies and interstitials is approximately constant (for medium and heavy elements).

I7. On the Equivalence of X-Ray Lattice Parameter and Density Changes in Neutron Irradiated LiF. D. BINGER AND W. J. STURM, *Oak Ridge National Laboratory.*—The question of the equivalence of lattice parameter changes derived from x-ray and density measurements for a lattice containing vacancies and interstitials was investigated. X-ray lattice parameter and density measurements of LiF crystals were made before and after neutron irradiation. The neutron attenuation within the crystals was derived from a combination of calculations and "inhour" measurements. Taking the attenuation into account, the x-ray and density measurements were shown to be equivalent within 10 percent. Annealing data indicates a process of order higher than one.

I8. On the Interpretation of Recovery Phenomena in Cold-Worked Metals.* A. S. NOWICK, *Yale University.*—Low-temperature recovery of electrical resistivity of metals after cold working has been attributed to the annealing out of vacant lattice sites and other point defects created by the deformation. Resistivity measurements, however, are not as suitable for distinguishing dislocation effects as are other phenomena. Especially to be noted are the recovery of internal friction and the dynamic Young's modulus in the neighborhood of room temperature within several hours after deformation, as observed by Köster and others for various metals. It can be shown that the latter phenomena are not attributable to point defects but must be related to the gradual immobilization of originally unbound dislocations, by a process which may be regarded as an early stage of polygonization. In different phenomena where recovery is known to be due to point defects rather than dislocations (as in measurements on samples that have been quenched or bombarded by high energy particles) it is found that the temperature independent factor in the Boltzmann expression for the recovery time falls between 10^{-8} and 10^{-10} sec. This criterion implies that the defect involved makes about 10^4 to 10^6 lattice jumps before being rendered ineffective.

* Work supported by the U. S. Army Office of Ordnance Research.

I9. Methods for Determining the Energy for Fracture Propagation in Plates. J. A. KIES AND H. L. SMITH.—Studies at NRL of fracture propagation in metal sheets have established experimentally the validity of the assumption of a critical condition for fracture based on the balance of release rate of strain energy *versus* the absorption rate in fracturing. This assumption has been further put to use in measuring the energy absorption in fracture propagation for glass plates containing central notches and also for plates containing side notches. The two formulas used and the results obtained therefrom are compared. Both formulas contain the dimensions of the test piece and are therefore useful in predicting size effects.

I10. Energy to Create Fracture Surfaces in Glass. H. L. SMITH AND J. A. KIES.—Previous estimates of the single surface energy of glass have indicated values of 150 to 300 ergs/cm^2. In order to predict the theoretical tensile strength of glass, Griffith used $S=600$ ergs/cm^2 in his formula for breaking stress where S is the total work per unit area for the pair of

surfaces in fracturing. The Griffith formula has been modified by Kies so as to apply to finite specimens with internal cracks. In this way surface energies for fracture propagation have been determined which are ten to forty times the surface energy generally quoted. The excess energy is thought to be consumed in activating a multiplicity of separate fracture elements and in creating tear lines. Effects of temperature and humidity on the energy absorption have been measured for cracking in glass plates.

I11. Nucleation of Fracture Origins. E. A. McLEAN AND WALLER GEORGE, *U. S. Naval Research Laboratory.*—The nucleation of fracture origins has been studied in terms of their time rate of appearance, $R(t)$, in centrally-notched foils loaded in tension normal to the notch. The fracture was always less than the "critical" length at which extension is accelerated by the release of strain energy in excess of the specific fracture work. For these lengths fracture growth is accomplished by the interconnection of sub-elements which enlarge from the origins. Values of $R(t)$ are shown to contain substantial fluctuations from a mean trend $\bar{R}(t)$, part of which are approximately periodic in time, t, under load. The periodic component of the fluctuations can be removed from the data by suitable experimental precautions, and is related to compressional stress components parallel to the fracture near the free surfaces. An elastic model for this effect is outlined, based on a solution due to Westergaard.[1] Microscopically the average distance between the fracture origins is related to the grain size, suggesting that points of grain intersection act as nucleation sites. Finally, it is shown that the variance in the periodic-free rate, $[R(t)-\bar{R}(t)]^2$ is a monotonically increasing function of t.

[1] H. M. Westergaard, J. Appl. Mech. 6, A-49 (1939).

THURSDAY AFTERNOON AT 2:00

Pupin 301

(J. A. WHEELER presiding)

Theoretical Physics, II

IA1. A Complete Bacher and Goudsmit Method. C. W. UFFORD AND S. MESHKOV, *University of Pennsylvania.*—Bacher and Goudsmit[1] developed a theoretical method for the calculation of atomic energy states in terms of the experimentally observed energies of ions of higher ionization. Their results applied to configurations of s and p electrons only. Using fractional parentage coefficients together with equation (16) of a previous calculation,[2] we can give a direct method for obtaining Bacher and Goudsmit's results and can extend these results to configurations containing electrons of higher angular momentum than $l=1$. A term in a given configuration of n electrons is expressed as a linear combination of the terms of the configurations of the ions on which it is built. We must find the coefficients of this linear combination. In general, there are $\binom{n}{r}$ ways of choosing r electrons; the coefficient of each configuration is equal to the number of times this configuration occurs. The energy of each configuration is then expressed as a linear combination of the observed energies of its terms. In the general formulation, there is no specification of equivalence or nonequivalence.

[1] R. F. Bacher and S. Goudsmit, Phys. Rev. 46, 948 (1934).
[2] S. Meshkov, Phys. Rev. 91, 871 (1953).

IA2. The d^3 and d^4 Configurations of Vanadium. SYDNEY MESHKOV, *University of Pennsylvania.*—The term values of the d^3 configuration of V *III* are calculated in terms of the experimentally observed energies of the d^4 configuration of V *II*. The formalism used was previously developed.[1] The rms deviation of the calculated terms from experiment is reduced from ± 625 cm^{-1} to ± 244 cm^{-1}. An iterative type calculation is then made for the term values of d^4 in terms of both the experimental energies of d^3 and the calculated values of the still unidentified terms of d^3. The rms deviation is reduced from ± 986 cm^{-1} to ± 663 cm^{-1}. A scheme is devised to calculate the values of the matrix elements in terms of the observed energies, when terms of the same kind appear.

[1] S. Meshkov, Phys. Rev. 91, 871 (1953).

IA3. Spin-Other-Orbit Interaction in the Theory of Complex Spectra. FREDERICK R. INNES, *University of Pennsylvania.*—The development of this interaction, as given by Marvin,[1] is altered in order to obtain an expression in terms of two-particle irreducible tensor operators. This expansion of the interaction leads to combinations of spherical harmonic and angular momentum operators, the properties of which are discussed. The matrix elements are found using the known methods of Racah and others.

[1] H. H. Marvin, Phys. Rev. 71, 102 (1947).

IA4. Relativistic Contributions to Magnetic Shielding of Nuclei in Atoms. VERNON W. HUGHES AND WERNER B. TEUTSCH,* *University of Pennsylvania.*—The reduction of an externally applied magnetic field at the nucleus caused by the electronic motion has been calculated for one- and two-electron atoms using the Dirac and the Dirac-Breit equation, respectively.[1] The lowest order term is the usual nonrelativistic expression, as previously calculated from Larmor's theorem or, equivalently, from the Schroedinger equation.[2] Additional terms of relative order $\alpha^2 Z^2$ have also been obtained. In a hydrogen-like atom the relativistic contributions depend on the hyperfine structure state and for $m_J=+\frac{1}{2}$, $m_I=+\frac{1}{2}$ are $-3\alpha^2Z^2$ relative to the nonrelativistic term. For two-electron atoms, they are of relative size $-\alpha^2(Z-\frac{1}{16})\times(Z-0.01)$, as calculated with a first-order Hylleraas function for the $^1S_0$ ground state.[3] For both hydrogen and helium these relativistic contributions are smaller than the present experimental errors in the magnetic moment measurements, but for helium they are appreciable compared to the theoretical knowledge of the nonrelativistic term.[3] For heavy atoms they are estimated to be important compared to experimental errors and to knowledge of the nonrelativistic term.[4]

* National Science Foundation predoctoral fellow.
[1] Method similar to W. Perl and V. W. Hughes, Phys. Rev. 91, 842 (1953).
[2] W. E. Lamb, Phys. Rev. 60, 817 (1941); N. F. Ramsey, Phys. Rev. 78, 699 (1950).
[3] E. Hylleraas and S. Skavlem, Phys. Rev. 79, 117 (1950).
[4] W. C. Dickinson, Phys. Rev. 80, 563 (1950).

IA5. Interaction Current Contribution to Hyperfine Structure of Tritium. A. M. SESSLER, *Cornell University,* AND H. M. FOLEY, *Columbia University.*—The vector potential produced by the electron in the neighborhood of the nucleus has been

calculated by second-order perturbation theory, using free-particle intermediate states and hole theory. The zero-order Hamiltonian for the calculation of the magnetic hyperfine interaction corresponds to a fixed-point nucleus. Account must be taken of the fact that near the nucleus the electron motion centers on the proton ("adiabatic" motion). An evaluation of the D-state proton orbital hfs yields the same value as was obtained by Low, working from the adiabatic approximation. Our expression for the vector potential corresponds to a "slip," radius R for the adiabatic electron motion $R=1.9[mc^2e^2/(w_0)\hbar c]a_0$, in agreement with the estimate of A. Bohr. The magnitude of the D-state orbital interaction corresponds, on this simple model, to a value of R 15 times smaller than the above,[1] indicating the unique role of the proton orbital interaction. In view of this large value of R, comparison with experiment allows one to place an upper bound on the amount of interaction current which gives a hfs contribution proportional to R.

[1] E. N. Adams, Phys. Rev. 81, 1 (1951).

IA6. Internal Conversion in the L and M Sub-Shells. E. L. CHURCH* AND J. E. MONAHAN, *Argonne National Laboratory.*—Relative L and M sub-shell internal conversion coefficients have been computed at their respective thresholds in the non-relativistic limit neglecting screening. Although the expressions obtained are strictly valid only for $Z\ll137$ and vanishing electron momentum, the relative conversion in the various sub-shells may be indicative of the situation in cases of more physical interest. The results obtained for the L shell are in essential agreement with the relativistic calculations of Gellman *et al.*,[1] and the empirical classification of Mihelich.[2] Conversion electron spectra of several heavy nuclei are shown, illustrating the essential validity of the above extrapolation for both the L and M shells in the cases identified thus far.

* On leave from Frankford Arsenal, Philadelphia, Pennsylvania.
[1] Gellman, Griffith, and Stanley, Phys. Rev. 85, 944 (1952).
[2] J. W. Mihelich, Phys. Rev. 87, 646 (1952).

IA7. Intermediate Coupling in B^{10}. W. T. SHARP AND H. GELLMAN, *Chalk River Laboratories,* AND G. E. TAUBER,* *National Research Council of Canada.*—The intermediate coupling calculations of Tauber and Wu[1] have been extended to the $J=1$ and $J=3$ states of B^{10} with $T=0$. Harmonic-oscillator wave functions and a nucleon-nucleon interaction of the form $(mP+nQ)V(r_{12})$ are assumed, where P denotes the Majorana and Q the Bartlett operator. The eigenvalues of the energy matrix[2] were calculated on the Toronto Ferranti electronic computer for five different values of the spin-orbit coupling parameter ζ for exponential, Yukawa, and Gaussian potentials $V(r_{12})$, each for two ranges. For four of these six potentials ζ can be chosen to fit the ground state spin $J=3$ and the spins and energies of the two lowest $J=1$ states. Comparison with previous results[1] on Li^6, He^6, and C^{14} indicates that a consistent fit is obtained with a Gaussian potential of range 2×10^{-13} cm. For this potential the values of ζ are 0.7 for Li^6, 4.2 for B^{10}, and 5.0 for C^{14}.

* National Research Laboratories postdoctoral fellow.
[1] G. E. Tauber and Ta-You Wu, Phys. Rev. 91, 443(A) (1953); Phys. Rev. (to be published).
[2] N. Zeldes, Phys. Rev. 90, 416 (1953).

IA8. The Magnetic Moment of K^{40} in Intermediate Coupling. G. E. TAUBER AND TA-YOU WU, *National Research Council, Canada.*—The spin $J=4$ of the ground state of K^{40} forms a notable exception to Nordheim's rule and might indicate that pure $j-j$ coupling does not hold for this nucleus. On the other hand, the negative magnetic moment of K^{40} seems to favor $j-j$ coupling, as none of the $L-S$ states give rise to a negative magnetic moment, while one of the states in the $j-j$ limit does. However, by applying intermediate coupling to the configuration $d^{-1}f$ it has been found that even a small spin-orbit interaction gives rise to a negative magnetic moment. A central nucleon-nucleon interaction of the form $(mP+nQ)V(r_{12})$, where P denotes the Majorana and Q the Bartlett operator, is assumed and calculations have been carried out for the exponential, Yukawa and Gaussian types of potential $V(r_{12})$ with various "ranges." It has been found that for a suitable choice of the spin-orbit interaction parameter ζ the experimental value $\mu=-1.29\mu_N$ can be obtained, the exact value of depending on the type of potential and range used.

IA9. On the Phenomenological $N-P$ Interaction.*† M. H. KALOS, *Cornell University,* AND J. M. BLATT, *University of Sydney, Australia.*—A program dealing with the $N-P$ system at low energies has been prepared for the University of Illinois electronic computer. Given central and tensor wells of arbitrary shape, the machine computes the strength of the potentials required to fit the binding energy of the deuteron, and calculates the wave functions which correspond to these potentials. In addition, the singlet and triplet scattering problems at zero energy are solved and the scattering lengths and effective ranges computed. We have applied this program to a phenomenological study of the $N-P$ interaction, using a number of combinations of the usual well shapes with varying ranges and depths. In particular, we have considered the following points: the usefulness of the intrinsic range and well depth parameter in comparing potentials of different shapes; the restrictions imposed on the potentials by the requirement of fitting the low energy triplet data; the possibility that a spin-and-charge independent central force can be used to fit both singlet and triplet data; and the effect of the tensor force on the shape dependent parameter of the effective range theory.

* Supported in part by the joint program of the U. S. Office of Naval Research and the U. S. Atomic Energy Commission.
† Work begun at the University of Illinois.

IA10. On the Theory of Deuteron Stripping.* W. TOBOCMAN, *Cornell University.*—The deuteron-stripping amplitude, resulting from the usual Born approximation treatment, has the form of an integral over the coordinates of the captured particle (neutron for $d-p$ stripping) and the coordinates of the liberated particle (proton for $d-p$ stripping). Since the ranges of integration include the interior of the target nucleus where the wave functions appearing in the integrand are not known, evaluation of this amplitude has up to now depended on additional simplifying assumptions of questionable validity. It has been found possible to transform the expression for the Born approximation stripping amplitude into a form in which the contribution due to integrations over the interior of the target nucleus is obviously small, being zero when the $N-P$ interaction is assumed to have zero range. This transformation leads to an approximate expression for the stripping amplitude which is an integral over the coordinates of only one particle. This integral involves only well defined functions and the effects due to the nuclear interactions of the various particles are represented in terms of boundary conditions. The methods referred to above can be used to derive the well-known result for the deuteron-stripping cross section due to S. T. Butler.

* Supported by joint program U. S. Office of Naval Research and U. S. Atomic Energy Commission.

THURSDAY AFTERNOON AT 2:00

Hotel Astor, North Ballroom

(F. H. CLAUSER presiding)

Joint Session of the Division of Fluid Dynamics and the Institute of the Aeronautical Sciences

J1. Aerodynamics of Blasts: Diffraction of Blast Around Finite Corners. J. F. LUDLOFF AND M. B. FREIDMAN, *New York University.* (30 min.)

J2. Pseudo-Transonic Similtude and First-Order Wave Structure. W. D. HAYES, *Office of the U. S. Naval Attache, London.* (30 min.)

J3. Recent Galcit Hypersonic Experimental Investigations. H. T. NAGAMATSU, *California Institute of Technology.* (30 min.)

J4. Effect of Wind-Tunnel Contraction on Free Stream Turbulence. M. S. UBEROI, *University of Michigan.* (30 min.)

THURSDAY AFTERNOON AT 2:00

Pupin 428

(N. P. HEYDENBURG presiding)

Reactions of Transmutation, II; General Nuclear Physics

JA1. Energy Levels in Ca^{41} from the $Ca^{40}(d,p)Ca^{41}$ Reaction.* C. M. BRAAMS,† *M.I.T.*—Thin targets of calcium oxide, prepared by evaporation of natural calcium onto Formvar films, have been bombarded with deuterons from the MIT–ONR electrostatic generator. The protons emitted at 90 degrees to the incident beam have been analyzed with a 180-degree magnetic spectrograph. Incident deuteron energies from 2.5 to 7 Mev were used. The Q values for the ground state and the first excited state are 6.14 and 4.19 Mev, in good agreement with previous work.[1–3] Sixteen groups have been observed in the region of excitation between 2 and 4 Mev, but the assignment of some of these to Ca^{41} needs further verification, for which bombardments of calcium targets enriched in Ca^{44} and Ca^{42} are being made.

* This work has been supported by the joint program of the U. S. Office of Naval Research and U. S. Atomic Energy Commission.
† Fellow of the Elsevier Foundation, Amsterdam, The Netherlands.
[1] V. L. Sailor, Phys. Rev. **75**, 1836 (1949).
[2] Kinsey, Bartholomew, and Walker, Phys. Rev. **85**, 1012 (1952).
[3] J. R. Holt and T. N. Marsham, Proc. Phys. Soc. (London) **A66**, 565 (1953).

JA2. Electrodisintegration of Cu^{63}.* M. B. SCOTT, A. O. HANSON, AND D. W. KERST, *University of Illinois.*—The external electron beam from the 22-Mev betatron was focused upon a set of copper foils placed inside a Faraday cage. The Cu^{62} activity in 2-mil entrance and exit foils was measured as a function of energy. After correcting for the energy loss in traversing the foils and the 10 mil Cu radiator between them, the normalized ratio of photo- to electro-disintegrations,[1] $F=(A_s-A_0)/(A_0NZ^2r_0^2X)$, was found to be 8.9 at 21 Mev and 9.4 at 15 Mev. The value at 21 Mev can be compared with theoretical values of 9.92, 8.64, and 8.17, respectively, for the electric dipole, magnetic dipole, and electric quadrupole interactions assuming an excitation energy of 17 Mev.[2] The shape of the (γ,n) cross section, using the Faraday cage monitor and the calculated total bremsstrahlung radiation, agreed with that of other investigators using R-meter monitors and detectors intercepting only the forward beam. The absolute values of the cross sections are not yet settled.

* Assisted by the joint program of the U. S. Office of Naval Research and the U. S. Atomic Energy Commission.
[1] J. S. Blair, Phys. Rev. **75**, 907 (1949).
[2] Thie, Mullin, and Guth, Phys. Rev. **87**, 962 (1952).

JA3. Deuteron Induced Reaction Studies. N. S. WALL,* *M.I.T.*†—Using the M.I.T. cyclotron as a source of 15-Mev deuterons, in conjunction with a NaI scintillation spectrometer, (d,p) reactions on targets possessing magic or near-magic number of neutrons have been studied. The neutron binding energies of some 27 nuclei have been determined from the ground-state Q values. Where experimental techniques permitted the excited states of the various nuclei were also measured. The interpretation of the results, in general as well as for several particular measurements, will be given. The angular distributions of the protons from the (d,p) reaction on Pb^{207}, Bi^{209}, and Y^{89} were also measured. These distributions are compared to those expected on the basis of Butler's analysis of the deuteron stripping process,[1] even though for the first two nuclei the Coulomb field is expected to be important. The Pb^{208} ground-state proton group shows a striking similarity to the distribution expected for a neutron entering the nucleus with one unit of angular momentum, however, no such interpretation is as obvious for the Bi^{210} case. The Y^{90} ground-state proton group shows an angular distribution characteristic of an $l_n=2$ neutron, but the first excited state angular distribution is not characteristic of a single l_n angular distribution.

* Now at Indiana University, Bloomington, Indiana.
† Supported in part by U. S. Office of Naval Research and U. S. Atomic Energy Commission.

JA4. Photodisintegration of Deuterium by 60–280 Mev X-Rays.* BARBARA DWIGHT SCHRIEVER, E. A. WHALIN, AND A. O. HANSON, *University of Illinois.*—Betatron x-rays of 180 and 280 Mev were incident upon a liquid deuterium target. The protons were detected with 600μ G-5 emulsions placed at 30°, 45°, 75°, 120°, and 150°. The energies of the protons were determined by measuring the grain densities. Confusable mesons were distinguished by plural scattering measurements. Preliminary values of the center-of-mass cross sections are given below in microbarns per steradian with statistical errors of about 10 percent.

θ (cm) \ E (Mev)	70	95	115	145	175	205	235
~35°	12	6.7	7.5	6.1	5.7	7.2	6.1
~90°	15	7.2	6.7	5.5	7.1	10.2	4.6
~155°	7.9	5.3	4.3	3.0	2.8	4.2	4.0

The values at 70 Mev are consistent with angular distributions calculated by Marshall and Guth, and by Schiff, superimposed on an equal isotropic component. The measurements at higher energies are in reasonable agreement with measurements of Littauer and Keck,† and subsequent unpublished measurements by Perry, except for the high value in the 75° plate corresponding to about 200-Mev photons. The source of this discrepancy is being investigated.

* This work is supported in part by the joint program of the U. S. Office of Naval Research and the U. S. Atomic Energy Commission.
† R. Littauer and J. Keck, Phys. Rev. **86**, 1051 (1952).

JA5. Photoprotons from 300-Mev Bremsstrahlung.* P. C. MURRAY, R. I. SCACE,† R. O. HAXBY, AND T. R. PALFREY, JR., *Purdue University.*—Photoprotons of 80±4 Mev energy have been observed at 90° to the 300-Mev gamma-ray beam of the Purdue University electron synchrotron in the first of a series of experiments on photoproton emission. Targets of Be, C, Al, Cu, Cd, Sn, and Pb have been used. The relative cross sections per proton from the above materials, in units of $d^2\sigma/dEd\Omega \times 10^{32}$ cm² Mev⁻¹ sterad⁻¹ effective quanta⁻¹ Z^{-1}, to about 5 percent relative accuracy, are, respectively, 9.2, 8.8, 9.4, 9.6, 9.2, 9.5, and 8.6. The apparatus consists of a three-counter telescope in which coincidences $C_{1,2,-3}$ establish the range interval of the particles, and an oscilloscope recording the pulse heights of coincidence-causing pulses from counters 1 and 2 gives high certainty of correct particle identification. Work is continuing at higher proton energies.

* Supported in part by the U. S. Atomic Energy Commission.
† Now at General Electric Company, Syracuse, New York.

JA6. Nuclear Masses as Integral or Rational Multiples of the Electron Mass. ENOS E. WITMER, *University of Pennsylvania.*—The writer[1] has pointed out before that the masses of nuclei in both the ground and excited states appear to be integral or rational multiples of the mass of the negative electron. Recently Bainbridge[2] published a new table of nuclear masses, in which there are 63 masses with $A \leqslant 34$ and with a probable error of $\pm 0.08m$ or less. If the electron mass m is taken as 0.000 548 770 315 amu, corresponding to the nuclear mass of O^{16} being 29 148.100m, twelve of these 63 masses are integral multiples of m to within $\pm 0.05m$. Furthermore, if our attention is limited to those nuclei for which $A \leqslant 19$ and the probable error is $\pm 0.051m$ or less, there are seven masses out of a total of 28 that are integral multiples of m to within $\pm 0.0125m$. The probability of the latter situation occurring by chance is only 4.25×10^{-6}. The masses of n and p appear to be 1838.625m and 1836.09 375m, respectively. Two values computed from Bainbridge's table are $(12\,785.999 \pm 0.047)m$ and $(30\,982.999 \pm 0.020)m$ for Li^7 and F^{17}, respectively.

[1] E. E. Witmer, Phys. Rev. **87**, 237 (A), 1952.
[2] E. Segrè, *Experimental Nuclear Physics* (John Wiley and Sons, Inc., New York, 1953), Vol. I, Part V, Table 16.

JA7. Effect of Knock-on Electrons of Ionization Loss. J. W. GARDNER, *Chalk River Laboratories.*—When an ionizing particle traverses a layer of material, not all the energy it loses need remain in the layer because, even at energies where radiation and cascading are negligible, some energy will usually be carried away by knock-on electrons accompanying the primary particle out of the layer. In general, this effect is only partly canceled by the locally produced knock-ons which accompany the primary *into* the layer. An expression has been obtained for the energy spectrum $N(E, x)dE$ of the electrons accompanying the primary at depth x in the layer, and has been applied to the case of a 1-Bev primary muon traversing the burst chamber described by Carmichael and Steljes.[1] It is found that for $E > 1$ Mev the number of electrons accompanying the primary into the chamber is appreciably less (e.g. 50 percent at $E = 10$ Mev) than the number accompanying it out. Hence, the net energy deposited in the chamber is less than that lost by the primary in traversing it. This effect is particularly noticeable in measurements of comparatively rare large energy losses by the primary,[1] corresponding to the "tail" of the Landau-Symon fluctuation curve.

[1] H. Carmichael and J. F. Steljes, Bull. Am. Phys. Soc. **28**, No. 6, 9 (1953).

JA8. The Range of Protons in Be, Al, Cu, Ag, and Au.* H. BICHSEL AND R. F. MOZLEY,† *Princeton University.*—Protons with energies between 10 and 18 Mev were obtained using the previously described analyzing magnet.[1] The energy of the protons from the analyzing magnet was determined by two independent measurements. One method required a measurement of $\int Bds$ along the proton path and of the angle through which the protons were deflected. The other method determined the radius of curvature by measuring the position of 3 collimating slits in the uniform field region. The two methods gave energies which differed by 0.3 percent. Using the average of the above determinations, a preliminary determination of mean ranges gave:[2]

	Energy	Range
Be	17.35 Mev	399.2 mg cm⁻²
Al	17.85 Mev	466.7 mg cm⁻²
Cu	17.91 Mev	588.7 mg cm⁻²
Ag	17.93 Mev	692.0 mg cm⁻²
Au	17.56 Mev	849.2 mg cm⁻²

* Supported by the U. S. Atomic Energy Commission and The Higgins Scientific Trust Fund.
† Now at High Energy Physics Laboratory, Stanford University, California.
[1] R. F. Mozley and H. Bichsel, Phys. Rev. **90**, 354 (1953).
[2] H. Bichsel and R. F. Mozley, Phys. Rev. **90**, 354 (1953).

JA9. The Stopping Power of Several Elements for Protons.* D. W. GREEN, J. N. COOPER, AND J. C. HARRIS, *Ohio State University.*—Experiments on stopping power have been carried out using a modification of the general technique of Madsen and Venkateswarlu.[1] Instead of using foils, the material to be studied was evaporated directly on a LiF target and the resultant displacement of the Li and F resonances measured. Protons accelerated by a Van de Graaff generator were used in measuring stopping power for Cu, Se, Ag, Pb, and Bi. Results were obtained for stopping of protons of energies between 440 kev and 1050 kev. For the sake of comparison with theory, data have been plotted as atomic stopping power divided by $Z^{\frac{1}{2}}$.

* Supported in part by the U. S. Atomic Energy Commission through a contract with the Ohio State University Research Foundation.
[1] C. B. Madsen and P. Venkateswarlu, Phys. Rev. **74**, 648 and 1782 (1948).

JA10. Alpha-Particle Ionization in the Noble Gases and the Formation of Metastable Atoms. WILLIAM P. JESSE AND JOHN SADAUSKIS, *Argonne National Laboratory.*—In the course of experiments on the ionization produced by single alpha particles from polonium in helium, it was found that the presence of minute gaseous impurities greatly increased the ionization observed. Systematic studies of the ionization in helium, to which measured quantities of argon have been added, show an increase in ionization up to 40 percent for approximately 0.1 percent of argon. Similar results have been obtained with CO_2, Kr, and Xe as the contaminant. Preliminary experiments with mercury vapor confirm the large effect already reported by others. A similar increase in ionization in argon is given by the addition of C_2H_2. The increase in ionization seems caused by the production of ions when metastable helium atoms suffer collisions with molecules of the impurity. Such relative collision cross sections calculated from the present results are in reasonable agreement with those derived from other methods. These collision cross sections, however, may possibly be influenced by a parallel reaction involving the production of excited molecules at the relatively high pressures used in these experiments.

FRIDAY MORNING AT 9:00

McMillin Theatre

(ENRICO FERMI presiding)

Business Meeting of the American Physical Society

FRIDAY MORNING AT 10:00

Pupin 428

(WALKER BLEAKNEY presiding)

Symposium of the Division of Fluid Dynamics
Shock Waves in Liquids and Solids

K1. Metal Equation of State from Shock-Wave Studies. J. M. WALSH, *Los Alamos Scientific Laboratory.* (30 min.)

K2. Applications of High Explosives and High-Speed Photography to Physical Research Problems. F. J. WILLIG, *Los Alamos Scientific Laboratory.* (30 min.)

K3. The Characteristics of Shock Fronts in Liquids and Gases. D. F. HORNIG, *Brown University.* (40 min.)

K4. The Structure of Detonation in Some Liquid Explosives. T. P. COTTER, *Los Alamos Scientific Laboratory.* (30 min.)

FRIDAY MORNING AT 10:00

McMillin Theatre

(J. STEINBERGER presiding)

Mesons, II

KA1. Elastic Scattering of 80-Mev π Mesons on Aluminum.* AIHUD PEVSNER,† JAMES RAINWATER, ROSS WILLIAMS, AND SEYMOUR J. LINDENBAUM, *Columbia University and Brookhaven National Laboratory.*—The elastic scattering of positive and negative 80-Mev π mesons in aluminum has been measured. Angular distribution will be presented. An optical model calculation has been carried through, using a complex potential, $V+i\sigma$, inside the nucleus, and a Coulomb potential outside the nucleus up to $l=5$. Results of this calculation for sixteen different potentials for both π^- and π^+ mesons will be compared to the experimental data and to some of the (approximate) predictions of the optical model.

* This work was performed under the joint program of the U. S. Office of Naval Research and the U. S. Atomic Energy Commission.
† Now with the Department of Physics, Massachusetts Institute of Technology.

KA2. A Phase Shift Analysis of the Scattering of Negative Pions by Hydrogen.* R. L. MARTIN, *Cornell University.*—A phase shift analysis of the experimental data on the scattering of negative pions by hydrogen in the energy range 115 to 213 Mev will be presented. The analysis was carried out using the graphical method of Ashkin, and assuming the two P-wave phase shifts of isotopic spin $\frac{1}{2}$ to be zero. The analysis shows a resonance level at about 194 Mev in the state of isotopic spin $\frac{3}{2}$ and ordinary spin $\frac{3}{2}$ for the Fermi-type solution. It is not clear from the analysis whether or not there is a resonance level at a somewhat high energy than that investigated for the state of isotopic spin $\frac{3}{2}$ and ordinary spin $\frac{1}{2}$. The two S-wave phase shifts of isotopic spin $\frac{3}{2}$ and $\frac{1}{2}$ are well behaved and are reasonably proportional to the relative momentum with values of about $-10^{\circ}\eta$ and $+6^{\circ}\eta$, respectively. The Yang type solution has the same S-wave phase shifts and shows resonances in the P-wave phase shifts of isotopic spin $\frac{3}{2}$ and $\frac{1}{2}$ at about 204 Mev and 174 Mev, respectively. The cross section computed from the above phase-shift is somewhat outside the experimental error from the data.

* This research is supported by a joint program of the U. S. Office of Naval Research and the U. S. Atomic Energy Commission.

KA3. Elastic Scattering of Positive and Negative Pions in Lithium.* ROSS WILLIAMS,† AIHUD PEVSNER,‡ AND JAMES RAINWATER, *Columbia University,* AND SEYMOUR J. LINDENBAUM, *Brookhaven National Laboratory.*—Differential scattering of π^+ and π^- mesons at 80 ± 4 Mev and π^- mesons at 125 ± 8 has been observed between 15° and 170°, with angular resolutions from 4° to 12°. Statistics were good within 10 to 15 percent. Two scintillation telescopes feeding three fast-coincidence circuits, with outputs combined in triple coincidence, reduced background counts to about two per hour. At 80 Mev coulomb interference is pronounced in the π^+ and π^- curves at about 22°. Differential curves in lithium drop rapidly to a minimum of about 1 mb at 75° and then rise by a factor of 4 in the backward direction. At 125 Mev the differential cross sections are larger, but the backward rise is not pronounced.

* Supported by the joint program of the U. S. Atomic Energy Commission and U. S. Office of Naval Research.
† Now at Paul Rosenberg Associates, Mount Vernon, New York.
‡ Now at Massachusetts Institute of Technology, Cambridge, Massachusetts.

KA4. Angular Distribution of π^- Proton Charge Exchange Scattering at 40 Mev. I. Apparatus.* A. ROBERTS AND J. TINLOT, *University of Rochester.*—We have measured the yield of π^0 mesons from CH_2 and C targets by detecting coincident photons. π^- mesons entered the targets with 43-Mev energy and emerged with 34 Mev. The weighted mean energy was 40 Mev. Four photon telescopes, consisting of two counters each, were disposed so that their axes defined a regular tetrahedron centered on the target. Coincidences from the six possible pairs of telescopes were recorded, giving a measure of π^0 yield in the approximate forward, backward, and 90° directions. The counting rate from C was about one-half that from hydrogen. Assuming that the π^0 distribution has the form $a+b\cos\theta+c\cos^2\theta$, we have calculated the probability of detecting a π^0 meson in each pair of telescopes as a function of a, b, and c. A simple analog computer was used to evaluate solid angle, and the shower theory of Wilson[1] was used to estimate the photon conversion efficiency. We can then evaluate a, b, and c from the three experimental determinations.

* This work was supported in part by the U. S. Atomic Energy Commission.
[1] R. R. Wilson, Phys. Rev. 86, 261 (1952).

KA5. Angular Distribution of π^- Proton Charge Exchange Scattering at 40 Mev. II. Analysis of Results.* J. TINLOT AND A. ROBERTS, *University of Rochester.*—Using the results obtained in the experiment described in the previous paper, we find a π^0 distribution: $(0.35\pm0.08)-(0.91\pm0.15)\cos\theta+(0.50\pm0.24)\cos^2\theta$ mb/sterad. The corresponding total cross section is 6.5 ± 1.4 mb. The uncertainties are standard deviations, and include an estimate of error in the computer data and shower theory. Assuming that only the phase shifts α_1, α_3, α_{33} contribute to the scattering at this low energy, we deduce the values $\alpha_{33}=7.8°\pm1.2°$, $\alpha_1-\alpha_3=8.3°\pm1.4°$. The additional condition $\alpha_{33}+\alpha_1-\alpha_3=15.8°\pm1.1°$ is obtained. α_3 and α_1 cannot be determined individually from a measurement of charge-exchange scattering alone. The total cross section agrees well with our previous value,[1] and the phase shifts are consistent with those obtained by Barnes *et al.*[2] from 40 Mev $\pi^\pm$ elastic scattering. The latter agreement is evidence for the validity of charge independence in pion-nucleon scattering.

* This work was supported in part by the U. S. Atomic Energy Commission.
[1] A. Roberts and J. Tinlot, Phys. Rev. 90, 951 (1953).
[2] Barnes, Angell, Perry, Miller, Ring, and Nelson, Phys. Rev. (to be published).

KA6. Charge Exchange Scattering of Negative Pions at 42, 30, and 20 Mev in Hydrogen. W. SPRY, *University of Rochester.*—A measurement of the total cross section for the process $\pi^-+P\rightarrow\pi^0+N$ has been made at each energy using CH_2 and C targets in a difference experiment. The results are computed from the number of single-decay gamma rays detected and a transition curve indicates that these gamma rays have the energy spectrum expected for π^0 decay at these energies. The cross sections are: $6(42\text{ Mev})=6.9\pm0.7$ mb; $6(30\text{ Mev})=5.9\pm0.5$ mb; and $6(20\text{ Mev})=5.2\pm0.4$ mb. The quoted errors are statistical standard deviations only and represent the errors in relative cross sections. The estimated standard deviation in each cross section as an absolute measurement is ±15 percent. The computations assume an isotropic π^0 distribution. Adjustment to the observed 42-Mev distribution[1] has not been made, but will increase the total 42-Mev cross section by less than 10 percent. The estimated error in π^- energy is ±2 Mev.

[1] J. Tinlot and A. Roberts, University of Rochester, abstract KA5, this meeting.

KA7. Elastic Scattering of 160-Mev Pions in Emulsions.* R. A. GRANDEY AND A. F. CLARK, *Carnegie Institute of Technology.*—The elastic scattering of pions from hydrogen has been studied in nuclear plates exposed to the nominal 160-Mev positive and negative external pion beams of the Carnegie synchrocyclotron. Ilford G-5 plates exposed to negative 160-Mev pions were "area scanned." On the basis of 28 elastic scatterings, a cross section for nonexchange scattering of (12.5 ± 3.5) millibarns was found. The mean free path for star formation on the basis of 1000 stars is $\bar{l}=(28.4\pm1.7)$ cm. Plates exposed to the positive pion beam are being scanned alone the track. A total of 32 elastic scatterings have been found. Accidentally, the energy, (151 ± 7) Mev, is exactly one of the energies used by the Columbia plate group (1) in exposures to their internal positive pion beam. Addition of their 41 events gives a total cross section $\sigma=(142\pm25)$ millibarns and a least squares fit to the angular distribution gives $d\sigma/d\Omega=(6.5-4.2\cos\sigma+14.5\cos^2\beta)$ millibarns per steradian. The mean free path for stars on the basis of 241 stars is $\bar{l}=(31.7\pm2.0)$ cm in excellent agreement with the negative pion value corrected for the coulomb effect, (31.9 ± 1.9) cm. Work is in progress to improve the statistics.

* This work is supported by the U. S. Atomic Energy Commission.
[1] Homa, Goldhaber, and Lederman, Phys. Rev. (to be published).

KA8. Spectroscopy of π- and μ-Meson X-Rays.* S. DE BENEDETTI, M. B. STEARNS, M. STEARNS, AND H. J. RICHINGS, *Carnegie Institute of Technology.*—The x-rays from capture of negative π and μ mesons in atomic orbits have been studied analyzing the pulses produced in a NaI scintillator with a 24 channel selector. This operated simultaneously with the signal from a coincidence-anticoincidence telescope which revealed the appropriate mesons stopping in different targets. The energy range from 20 to 250 kv was studied using targets from $Z=4$ (Be) to $Z=20$ (Ca). Well-defined peaks (instrumental widths from 45 percent at low energy to 20 percent at high energy) were observed, corresponding to K lines ($2p$ to $1s$), L lines (presumably $3d$ to $2p$), and M lines (presumably $4f$ to $3d$). The L lines often exhibited a structure indicating the presence of transitions from $n\geqslant4$ levels to the $n=2$ level. The energies agree with elementary theory within the experimental error of roughly 10 percent. At low Z the intensity is small for both π and μ mesons because of competition with Auger effect; in the case of π mesons it decreases at higher Z because of nuclear capture.

* Work supported by U. S. Atomic Energy Commission contract.

KA9. Yields of π- and μ-Meson X-Rays in Low Z Materials.* M. STEARNS, M. B. STEARNS, S. DE BENEDETTI, AND L. LEIPUNER, *Carnegie Institute of Technology.*—The radiative transitions of π and μ mesons have been observed for elements $Z=4$ to $Z=20$. The radiative yields from both mesons are depressed at low Z because of competition from the Auger effect. The μ-meson yields level off at sufficiently high Z while the π-meson yields go through a maximum and then decrease because of nuclear capture which dominates at higher Z. The percentage of π mesons in the $2p$ state which radiate to $1s$ varies from approximately 30 percent to 0 percent in the range $Z=4$ to $Z=11$ and seems to fall appreciably faster than Z^{-4}. These values are obtained by comparing the π and μ $2p-1s$ radiation yields for the same Z and same geometry and by measuring the number of π's arriving in the $n=2$ level from higher transitions. For the π $3d-2p$ transition nuclear capture becomes important around $Z=13$ and completely dominates by $Z=20$, while the Auger effect enters around $Z=9$ and completely dominates at $Z=6$. For the $2p-1s$ transition we have found no appreciable difference between C and CH radiation yields.

* Work supported by U. S. Atomic Energy Commission contract.

KA10. Density Effect for Ionization Energy Losses in Gases. E. D. PALMATIER, J. T. MEERS, AND C. M. ASKEY, *The University of North Carolina.*—The ionization energy losses of relativistic mu mesons in argon gas have been studied in a proportional counter at various pressures up to 40 atmospheres. The analysis of the behavior of the Landau distributions as a function of gas pressure and meson energy will be presented. Our results indicate that the effect is readily observable at these pressures and is much stronger than has been predicted by previous theoretical work.

FRIDAY MORNING AT 10:00

Pupin 301

(E. L. HAHN presiding)

Contributed Papers on Magnetic Resonance

L1. Self-Quenching Superregenerative Radio-Frequency Spectrometers.* P. J. BRAY, *Rensselaer Polytechnic Institute.*—Empirical evidence suggests that there is little intrinsic difference in sensitivity of signal detection between the externally quenched and self-quenched superregenerative spectrometer. Since this question is of importance in the study of nuclear magnetic moment resonances and pure quadrupole spectra in solids, the factors governing the response of the self-quenched and externally quenched detectors will be reviewed with special application to the response pattern of the self-quenched oscillator. Details of several self-quenched spectrometers will be given for frequencies between roughly 15 and 300 mcps along with sensitivity data in the form of signal-to-noise ratio measurements of quadrupole resonances in standard compounds at various temperatures. Nuclear quadrupole resonance temperature dependence studies employing self-quenching spectrometers will be illustrated with application to some previously reported Cl^{35} resonances.[1] Resonances in a considerable number of previously uninvestigated compounds will be reported.

* Research supported by RPI Research Committee.
[1] P. J. Bray and P. J. Ring, J. Chem. Phys. (to be published).

L2. Nuclear Magnetic Resonance as a Criterion of Chemical Bonding. RICHARD A. OGG, JR., *Stanford University* (introduced by L. I. Schiff).—Study of high-resolution proton magnetic resonance at 30 megacycles in absolutely anhydrous liquid ammonia has shown the expected triplet character, resulting from spin-spin interaction with the N^{14} nucleus. A trace of water impurity, undetectable by ordinary analytical procedures, suffices to alter the proton resonance to a single sharp line. This is correlated with the exchange rate of protons between molecules catalyzed by the acid-base reaction with water molecules. It is apparent that the ordinary so-called "hydrogen bonding" in liquid ammonia has no effect on spin-spin interaction. It is suggested that spin-spin interaction between nuclei results only when true covalent sharing of electrons takes place and that this offers a truly operational criterion of covalent bonding.

L3. Nuclear Magnetic Resonance Spectra of Boranes and Derivatives. JOHN KELLY, JAMES RAY, AND RICHARD A. OGG, JR., *Stanford University* (introduced by L. I. Schiff).—High resolution proton magnetic resonance spectra have been studied (both at 30 and 40 megacycles) in liquid samples of $B_3N_3H_6$, B_2H_6, B_4H_{10}, and B_5H_9, as well as in some of the alkyl derivatives of these substances. Additional studies have been made on deuterium oxide solutions of $NaBH_4$. Fluorine magnetic resonance spectra have been studied in BF_3 and a number of addition compounds of this substance. The fine structure of the various spectra results in part from chemical shift and in part from spin-spin interaction. These are distinguished both by magnetic field dependence and by use of substances enriched in the respective boron isotopes. Correlations with the structures of the various substances are discussed. Among the most interesting aspects is the behavior of the so-called "bridge" protons in the boranes. The chemical shift of magnetic resonance of these as compare to terminally bonded protons is toward higher magnetic field. This effect and the spin-spin interaction details are discussed in relation to the theoretical aspects of the proton bridge bond.

(Abstract withdrawn.)

L5. The Ratios of Quadrupole Coupling Constants of Isotopes and Their Variation with Temperature.* T. C. WANG AND C. H. TOWNES, *Columbia University.*—One might expect the ratio of coupling constants for Cl^{35} and Cl^{37} in any molecule to be dependent on nuclear properties only and not on the molecular environment. Measurements on nuclear quadrupole resonances in solids show, however, that this ratio varies with temperature as well as that it is dependent on the molecular environment.[1] A decrease of temperature from 300°K to 78°K decreases the ratio $eqQ_{Cl^{35}}/eqQ_{Cl^{37}}$ by as much as 0.02 percent. Measurement of the quadrupole coupling ratio of Sb^{123} to that of Sb^{121} in several antimony halides and in stibnite shows similar effects. This ratio ranges from 1.274714 to 1.274770 depending on molecular environment. The asymmetry parameter η for the two antimony isotopes agrees to less than 0.01 percent. The change of ratio can be attributed largely to molecular vibrations. Extending Bayer's discussion[2] of thermal vibrations, the variation in coupling ratio can be calculated for the case of p-$C_6H_4Cl_2$ where the vibrational frequencies are known. The calculated change in ratio between 300°K and 78°K is 2.2×10^{-5}, whereas the measured value is $(4.7\pm1)\times10^{-5}$.

* Work supported jointly by the U. S. Signal Corps, U. S. Office of Naval Research, and U. S. Air Force Research and Development Command.
[1] Wang, Townes, Schawlow, and Holden, Phys. Rev. 86, 809 (1952).
[2] H. Bayer, Z. Physik 130, 227 (1951).

L6. Spin-Orbit Interaction in RbF and CsF.* G. BEMSKI,† W. A. NIERENBERG, AND H. B. SILSBEE, *University of California, Berkeley.*—The structure of fluorine nuclear magnetic resonance line in RbF and CsF has been investigated as a function of magnetic field between zero and 1000 gauss by the molecular beam technique. This corresponds to the range from complete Zeeman to complete Paschen-Back extremes for internal coupling. RBF results check the statistical theory[1] for the line shape considering only cosine interaction between the F^{19} nucleus and the molecule. The line shape for all field values fit the theoretical curves with just one parameter, the strength of the coupling based on half-width of the line. The coupling constant c/h is measured to be 11.1 ± 0.6 kc/sec in good agreement with 12 ± 3 kc/sec from the electric resonance measurements.[2] The CsF results, particularly at and near zero field, are in violent disagreement with the theory. Possible interpretation is marred by presence of Cs^{133} quadrupole lines but may be due to dimerization.[3]

* Supported in part by the U. S. Office of Naval Research.
† Now at Bell Telephone Laboratories, Murray Hill, New Jersey.
[1] W. A. Nierenberg, Phys. Rev. 82, 932 (1951).
[2] V. Hughes, Phys. Rev. 79, 314 (1950).
[3] Ochs, Coté, and Kusch, J. Chem. Phys. 21, 459 (1953).

Invited Papers

L7. Microwave Resonance in Color Centers. E. E. SCHNEIDER, *University of Durham, England (temporarily at Duke University).* (30 min.)

L8. Polarization of Nuclei in Metals by Magnetic Resonance. A. W. OVERHAUSER, *Cornell University.* (30 min.)

L9. The Solid-State Cyclotron. CHARLES KITTEL, *University of California, Berkeley.* (30 min.)

FRIDAY MORNING AT 10:00

Casa Italiana, 1161 Amsterdam Avenue

(R. P. SHUTT presiding)

General Nuclear Physics

LA1. Initial Performance of the Large Bartol Van de Graaff.* C. P. SWANN, *Bartol Research Foundation.*—The large Van de Graaff has been brought to a first stage of completion. Usable currents have been obtained with energies greater than 5 Mev; the generator has operated continuously, supplying several microamperes of magnetically resolved protons at 4 Mev. Voltage limitations are at the moment imposed by difficulties associated with delivering charge to the belt. The generator is housed in a tank designed for a pressure of 300 psi which is 35 ft high and 12.5 ft in diameter. The porcelain accelerating tube, 20 ft in length, has electrodes of inner diameter 8 inches. Baffles are spaced at intervals of 3.5 ft throughout the length of the tube to suppress secondary electrons. The combined advantages of the Bartol low pressure rf ion source and a high pumping speed eliminate the necessity of a second tube for differential pumping. Some characteristics of the reactions $Li^7(p,n)Be^7$, $Li^7(p,n)^*Be^7$, and $Li^7(p,p')^*Li^7$ will be discussed. The generator has also been employed as a neutron source to excite Ba^{137m} and Hg^{199m} as a function of neutron energy.

* Assisted by the joint program of the U. S. Office of Naval Research and the U. S. Atomic Energy Commission.

LA2. A Study of Cloud-Chamber Distortions. W. WALLENMEYER, *Purdue University* (introduced by W. Y. Chang).—In order to know the behavior of a newly built cloud chamber with magnetic field which is being used to study position scattering (see another abstract by L. Grodzins), an investigation was made of the various types of distortions, such as those due to (1) the optical system, (2) the turbulences during expansion, (3) the multiple scattering in the gas, and (4) the shrinkage of the film. The magnitudes of the possible errors in the curvature measurements (with and without field) were determined experimentally using internal conversion electrons from C_s^{137}, which traversed the helium gas in the cloud chamber. The experimental results have been analyzed, interpreted, and wherever possible, presented in curves. It shows that an overall probable error of 5 percent or less is to be expected, when the energy of an electron or a positron of about 3 Mev is determined from the measurements of the curvature and the magnetic field.

LA3. Microton Resonators. H. F. KAISER, *Naval Research Laboratory.*—The microtron[1] electron cyclotron depends upon a cavity resonator both for its electron source and for turn acceleration. The particular geometrical requirements such a resonator has to meet in a conventional microtron such as orbit clearance, gap length, aperture, and magnetic gap are discussed for a series of resonator types. The confocal ellipsoidal-hyperboloidal resonators due to Hansen and Richtmyer[2] seem to be best in respect to shunt resistance and associated Q. An analytical procedure for determining the parameters of such resonators for given accelerator conditions is developed. Resonators found to be practical in X and K band microtrons[3] will be illustrated and discussed.

[1] V. J. Veksler, Phys. USSR **9** (3), 153–158 (1945).
[2] W. H. Hansen and R. D. Richtmyer, J. Appl. Phys. **10**, 189–199 (1939).
[3] H. F. Kaiser, Phys. Rev. **87**, (1) 183 (1952); **91**, 456 (1953).

LA4. Longitudinal and Transverse Stability in Linear Accelerator Systems. G. BREIT, *Yale University.**—Relations between the two stabilities may be seen in terms of

$$\frac{d^2\eta}{dx^2}+\left[-\frac{3e}{2mv^2}\frac{\partial \mathcal{E}}{\partial x}-\frac{e}{2mv^3}\frac{\partial \mathcal{E}}{\partial t}+\frac{3e^2\mathcal{E}^2}{4m^2v^4}\right]\eta=0,$$

and of

$$\frac{d^2\rho}{dx^2}+\left[-\frac{e}{2mv^3}\frac{\partial \mathcal{E}}{\partial t}+\frac{3e^2\mathcal{E}^2}{4m^2v^4}\right]\rho=0,$$

$\rho=r(v)^{\frac{1}{2}}$, $\eta=(v)^{\frac{1}{2}}(x-x_0)$, x=longitudinal coordinate, x_0=equilibrium x, $v=dx/dt$, $\mathcal{E}$=longitudinal electric field. Relationship of action of a gap to strong focusing and the role of $\int d\mathcal{E}_x/dt=0$ in going across gap will be discussed in a comparison of traveling wave and separate gap accelerators.

* Assisted by joint program of the U. S. Office of Naval Research and U. S. Atomic Energy Commission and by Office of Ordnance Research, U. S. Army.

LA5. Stability of a Linear Accelerator with Independently Excited Cavities. M. H. HULL, JR., L. C. BIEDENHARN, P. B. DAITCH, AND R. L. GLUCKSTERN, *Yale University.**—Calculations have been performed for various modes of operation of a heavy-particle linear accelerator with independently excited acceleration gaps. The motivation of the calculations is to be found in the theory of such accelerators given by G. Breit and discussed in the preceding abstract. The longitudinal and transverse stability in various portions of the accelerator, as well as the initial phase acceptance range and final energy definition will be discussed both from the standpoint of the linear approximation, conveniently treated by means of matrices, and with the inclusion of nonlinear effects. Special attention will be given the so-called "rocking" mode of operation related to that suggested by Good,[1] where successive sections or groups of sections are operated so as to have alternate focusing and defocusing actions on the transverse or longitudinal oscillations of the beam. It will be shown that satisfactory stability can be obtained in this way without auxiliary equipment, at least in the higher energy portion of the accelerator.

* Assisted by joint program of the U. S. Office of Naval Research and U. S. Atomic Energy Commission and by Office of Ordnance Research, U. S. Army.
[1] M. L. Good, Phys. Rev. **92**, 538(A) (1953).

LA6. Continuous Parameter Approximation in a Linear Accelerator with Independently Excited Cavities. R. L. GLUCKSTERN, P. B. DAITCH, L. C. BIEDENHARN, AND M. H.

HULL, JR., *Yale University.**—Longitudinal and transverse stability for a linear accelerator with separately excited rf cavities was carried out by considering small deviations of velocity, phase, transverse displacement, and transverse angular divergence from some "equilibrium" particle. In this approximation the longitudinal and transverse oscillations separate, and the action of each cavity may be expressed by means of two-dimensional matrices mentioned in the preceding paper. If the design parameters on which these matrices depend vary slowly from section to section, stability will exist when the eigenvalues of the matrices are less than unity in absolute value. For oscillatory behavior the energy deviation, phase deviation, and transverse deviations of position and direction are damped due to slow variation of parameters after n sections according to

$$\delta E/E \sim E_n^{-5/8} V_n^{1/4} |\sin \varphi_i^{(n)}|^{1/4} l_n^{-1/4},$$
$$\delta \varphi \sim E_n^{-3/8} V_n^{-1/4} |\sin \varphi_i^{(n)}|^{-1/4} l_n^{1/4},$$
$$\delta r \sim E_n^{1/8} V_n^{-1/4} |\sin \varphi_i^{(n)}|^{-1/4} l_n^{1/4},$$
$$\delta r' \sim E_n^{-5/8} V_n^{1/4} |\sin \varphi_i^{(n)}|^{1/4} l_n^{-1/4},$$

where E_n = energy, V_n = gap voltage, $\varphi_i^{(n)}$ = input phase, and l_n = drift length in the nth section.

* Assisted by joint program of the U. S. Office of Naval Research and U. S. Atomic Energy Commission and by Office of Ordnance Research, U. S. Army.

LA7. Doubly Ionized Helium Ion Source. J. W. BITTNER, R. G. HERB, R. D. MOFFAT, AND J. A. WEINMAN, *University of Wisconsin* (received by wire).—Singly ionized helium ions, from a low voltage arc source, are accelerated to an energy of about 400 kev by means of a small electrostatic generator built inside the high voltage electrode of the Wisconsin 4-Mev electrostatic accelerator. Foot note 1 the ions then pass through a capillary tube $\frac{3}{16}$ in. in diameter and 8 in. long, into the center of which oxygen is introduced at the rate of approximately 10 cc/hr. apuroximately $\frac{1}{4}$ of the ions emerging from this tube and entering the accelerating tube of the 4-Mev accelerator are doubly ionized. The doubly charged particles emerging from the accelerator are seqarated from other components of the beam by means of a magnetic analyzer. The total doubly charged beam at the output of the accelerator is 0.6 micro amps and after passing through an electrostatic analyzer it is .3 micro amp 0.3 microamp. Work supported by the Wisconsin alumni research foundation and the U. S. atomic energy commission.

LA8. Elastic Scattering of Alqha Particles by Carbon. W. HABERLE, J. W. BITTNER, R. D. MOFFAT, *Universily of Wisconsin* (received by wire).—The elastic scattering of alpha particles by carbon has been observed in the bombarding energy range 4 to 6 Mev. Doubly charged alpha particles (see previous abstract) were passed through the electrostatic analyzer and into a scattering chamber containing propane gas at a pressure of 2 mm Hg. Proportional counters detected the particles scattered at 90 degrees and 171 degrees in the center of mass system. A strong resonance was observed at approximately 4.3 Mev and a broad one at about 5.8 Mev. Angular distributions at these anomalies suggest even parity and $J=4$ and 2 respectively for the associated levels in oxygen. A small, sharper resonance ojcurs at 5.3 Mev. Work at higher energy and other angles is in progress. Work supported by the Wisconsin alumnii research foundation and the U. S. atomic energy commission.

Footnote 1 Herb, Turner, Hudson, and Warren, Lhys. Rev. **58**, 579 (1940).

LA9. On the Use of Wires Embedded in Nuclear Emulsions to Investigate Reactions Induced by High-Energy Neutrons.* E. G. SILVER AND R. W. WANIEK, *Harvard University.*—Previous experiments on interactions induced by high-energy neutrons (90 Mev) in the nuclei of emulsions have suffered from the lack of unambiguous identification of the type of nucleus in which the event occurred.[1,2] To obviate this ambiguity we have resorted to the use of thin filaments embedded in Ilford G-5 electron sensitive emulsions.[3] We have, so far, used Nylon, molybdenum, and tungsten filaments, 10 to 28 microns in diameter. We have successfully overcome many of the problems encountered; in particular, we have eliminated distortion effects in the immediate vicinity of the filaments, so that angles can be measured reliably. The spatial angles of tracks emerging from the wires as well as their ranges are determined and appropriate corrections are made for the uncertainty in the energy measurement due to the unknown amount of energy dissipated during the traversal of the wire. Data from exposures to a hardened neutron beam from the Harvard 95-in. synchrocyclotron will be compared with equivalent exposures of unloaded plates.

* This work was supported by the joint program of the U. S. Atomic Energy Commission and the U. S. Office of Naval Research.
[1] R. W. Waniek and Taiichiro Ohtsuka, Phys. Rev. **91**, 1574 (1953).
[2] R. W. Waniek and Taiichiro Ohtsuka, Phys. Rev. **89**, 1307 (1953).
[3] G. P. S. Occhialini, Nuovo cimento **8**, 341 (1951).

LA10. Variable Mercury Delay Line Equipment for the Measurement of Short Half-Lives. C. SHEER, A. ZINN, AND N. HARTMANN, *Columbia University.**—An instrument has been developed featuring a variable mercury delay line which is capable of measuring continuously variable time intervals in the range 0.01 to 100 μsec with an absolute error <0.0016 μsec at any point in the range. This range of time intervals is too short for measurement with equivalent accuracy by conventional electronic gate circuits, and too long for convenient measurement by slotted line techniques. The continuous variation is accomplished by means of a mercury acoustic line using quartz crystal transducers where the length of the mercury path between crystals is controlled by an accurately machined feed screw. By the use of Invar alloy in the construction of the line, together with a bellows arrangement, the delay has been rendered virtually independent of ambient temperature. The instrument has been constructed with two channels, each with associated insertion-loss amplifiers. It is possible to measure delayed coincidences very accurately, when the delay times are $\sim$ several μsec or greater, by measuring the coincidence rate between the two channels as a function of relative delay. Application to the measurement of short half-lives will be discussed.

* This work partially supported by the U. S. Atomic Energy Commission.

FRIDAY MORNING AT 10:00

Schermerhorn 501

(HARVEY BROOKS presiding)

Solid-State Physics, II

M1. Viscoelasticity in Complex Static Stress Systems. A. A. MACLEOD, A. R. DIDONATO,* AND A. C. WEBBER, *Du Pont Experimental Station.*—A general method is developed for deriving time-dependent equations which relate stress and strain in complex viscoelastic stress systems. The method is easy to apply and practical. The Boltzmann superposition

principle forms the basis for the analysis whereby viscoelasticity in solids is characterized by two parameters plus the usual elastic constants. Experimental verification is given for a system of clamped beams, torsion of cylindrical bars, flexure of disks, buckling of a column, and pipe under hydrostatic pressure. The materials used were 66 Nylon, 610 Nylon, tetrafluoroethylene resin, polyethylene, molded acrylic resin, and a glass fiber-polyester laminate.

* Central Research Laboratory, Westinghouse Air Brake Company, Melpar Division, Alexandria, Virginia.

M2. Creep and Relaxation of Plastics. A. R. DiDONATO,* A. A. MACLEOD, AND A. C. WEBBER, *Du Pont Experimental Station.*—The Boltzmann superposition principle given in the form of B. Gross's equations is successfully employed to calculate 1000-hour tensile creep data from ten-hour experimental stress relaxation data for three partially crystalline plastics: 66 Nylon, 610 Nylon, and tetrafluoroethylene resin. A two-parameter empirical function given as $(1+t/b)^{-m}$ is used to represent experimental tensile relaxation data (normalized by the initial stress) and its extrapolation. The calculated expression for creep is asymptotic and valid for times, t, greater than one hour. A discussion of a time-temperature relationship is included in order to justify the extrapolations used. It is shown for materials for which the empirical stress relaxation expression is valid that a simple criterion exists for determining when extrapolations are justified.

* Central Research Laboratory, Westinghouse Air Brake Co., Melpar Division, Alexandria, Virginia.

M3. The Electrical Conduction and Dielectric Properties of Ice.* E. J. WORKMAN AND W. DROST-HANSEN, *New Mexico Institute of Mining and Technology.*—Ice frozen in an orderly manner from a weak solution of cesium fluoride incorporates substitutionally fluoride ions which facilitate the establishment of electrical domains in the structure. The electrical conductivity along the c-axis of such ice changes over a wide range with the sense and magnitude of an applied field parallel to the c-axis.[1] The effect of temperature is such as to indicate that the applied electric field—dependent upon its direction—further orders or produces disorder of highly coordinated domains within the crystalline matrix. The mechanism of coordination within the domains involves a step-by-step process providing for pronounced hysteresis (conductivity *vs* electric field) and polarization. The contributions to the dielectric constant by the order-disorder processes described above are large, ranging from approximately zero at 10 kc to approximately 100 times the generally accepted value for the static dielectric constant. The domain contribution to the dielectric constant increases sharply with temperature near the melting point, and it vanishes for a sufficiently large superimposed electric field in the nonconductivity direction.

* Supported in part by the U. S. Office of Naval Research.
[1] Truby, Bull. Am. Phys. Soc. 27, No. 6, p. 21 (1952).

M4. Theory of Volume Rectification in Ice.* W. DROST-HANSEN AND E. J. WORKMAN, *New Mexico Institute of Mining & Technology.*—The properties of halide-ion contaminated ice samples (approximately 10^{16} impurity centers per cc, see abstract M3) can be understood if one assumes the existence of domains of ordered structure surrounding each impurity center. The dc-rectification phenomenon (front to back ratio $\simeq 1:10^6$) occurs as the result of changes in the wave function describing a linear array of hydrogen-bonded water molecules —partly through the displacement of protons under the stress of the applied field. It is proposed that this may lead to a sudden increase in conductivity through critical variations in internuclear distances (analogous to the suggestion by Mott[1]) and rectification occurs because of the asymmetrical arrangement of the water molecules within the domains. Consistent with this mechanism, the rectifying properties disappear for ac fields of sufficiently high frequency. It is proposed that this mechanism has general application (e.g., may explain the rectifying properties of $BaTiO_3$)[2] and may serve as a guide to predict substances exhibiting volume-rectifying properties.

* Supported in part by the U. S. Office of Naval Research.
[1] Mott, Proc. Phys. Soc. **A62**, 416 (1949).
[2] E. P. Wigner and E. T. Jaynes, Phys. Rev. **79**, 213 (1950). See also D. L. Waidelich, J. Acoust. Soc. Am. **25**, 796 (1953).

M5. The Effects of Stepped Surfaces on the Motional Parameters of Piezoelectric Filter Plates.* CHARLES R. MINGINS, ROBERT W. PERRY, AND ALBERT D. FROST, *Tufts College.*—The relative positions in frequency of the members of the thickness-shear family of modes in a piezoelectric crystal plate can be changed by altering the shape of the major surfaces. Correspondingly, the width of the pass band and its frequency position are changed when the plate is used as a divided-electrode filter.[1] In particular, the pass band can be made wider by cutting steps in the surface of the plate.[2] The motional inductances, capacitances, and resistances effective in such a filter have been measured as the steps were gradually deepened. The parameters associated with the 1,2,1 mode were much more affected than those associated with the fundamental thickness-shear resonance. With this geometry, in contrast to the grooved case, the mechanical effects of elasticity and inertia were masked from the start by the stronger electromechanical effect.

* This work has been sponsored by the U. S. Signal Corps.
[1] Mingins, Perry, and MacLeod, Phys. Rev. **91**, 471 (1953).
[2] McDonough, MacLeod, and Larson, Phys. Rev. **88**, 154 (1952).

M6. X-Ray Study of Prismatic Punching in Thallium Chloride. EDWARD I. SALKOVITZ AND PAUL L. SMITH, *U. S. Naval Research Laboratory.*—Smakula and Klein[1] have investigated the strain patterns produced in thallium halide crystals under pressure of a cone perpendicular to the crystal surface. They describe a "superficial" pattern consisting of radial wings about the press point and a "transmitted" pattern consisting of a raised prism on the opposite side of the press point. With a simple pressing device, we have been able to push a prism of square cross section (about 2 mm on a side) nearly through a single crystal disk 2 mm thick. Since the load was applied normal to the (001) plane in the (100) direction, the "superficial" pattern showed fourfold symmetry when viewed between crossed polaroids. Grazing angle x-ray patterns showed a mosaic-block like structure within the radial wings. X-ray patterns from the walls of the prism showed asterism only in the direction of glide. Patterns from the cavity left by the extruded prism in the parent crystal were very similar in appearance. When the disk was annealed at 275°C for two weeks and then cooled at the rate of 1½°/hr, no recrystallization occurred. This would be in keeping with the dislocation model for prismatic punching as discussed by F. Seitz. The mosaic-structure in the radial wings, however, seemed to have been frozen in.

[1] A. Smakula and M. W. Klein, J. Opt. Soc. Am. **39**, 445 (1949).

M7. On the Electric Breakdown of Crystals in the High-Temperature Region. KURT LEHOVEC, *Sprague Electric Company.*—At fields smaller than Von Hippel's breakdown field F_0*, there exists an energy region ("energy barrier") where electrons lose energy on the average. Seitz[1] has discussed the chance of an individual electron's crossing this energy barrier by random processes. I shall discuss an alternate approach based on the diffusion in wave-vector space arising from the distribution function of electrons over energy states. My considerations suggest for the breakdown field F^* $F^{*2} \approx F_0^{*2} - 3mkT|\langle \partial\epsilon/\partial t\rangle|/(2e^2\epsilon\tau)$, where m equals electron mass; ϵ, electron energy; $\langle \partial\epsilon/\partial t\rangle$, average energy change per unit time due to collisions; τ, transport collision frequency: these values are taken for the peak of the energy barrier. Since F_0^{*2} increases with T, whereas

the following term decreases with T^3, the observed maximum of the breakdown field with temperature is explained.

[1] F. Seitz, Phys. Rev. **76**, 1376 (1949).

M8. Self Diffusion in KCl.* J. F. ASCHNER, *University of Illinois.*—The self-diffusion coefficient, D, of the potassium ion, K^+, in single crystals of KCl has been measured over the temperature range from 500°C to 700°C by the use of radioactive K^{42}. The electrical conductivity of the crystals was also measured by means of an ac bridge. The conductivity, σ_+, resulting from the potassium ion was calculated by combining the conductivity data and the transference number data of Kerkhoff.[1] Over the temperature range investigated, the Einstein relation $\sigma_+/D = Ne^2/kT$ is satisfied. N is the number of potassium ions per unit volume, and the other symbols have their usual significance. This result is in disagreement with the data of Witt,[2] who found a deviation from the Einstein relation in KCl. There appears to be no direct experimental evidence for the existence of vacancy pairs in KCl, as suggested by the theoretical work of Dienes.[3]

* Work supported in part by the U. S. Office of Naval Research.
[1] F. Kerkhoff, Z. Physik **130**, 449 (1951).
[2] H. Witt, Z. Physik **134**, 186 (1953).
[3] G. J. Dienes, J. Chem. Phys. **16**, 620 (1948).

M9. Tunneling of Electrons in Alkali Halides.* D. L. DEXTER, *University of Rochester.*—The tunneling of electrons from F centers to hole centers is calculated for the ground and excited states, and the accompanying bleaching is discussed. Tunneling ranges of 30 and 40A are found, corresponding to saturation concentrations of about 10^{19} per cm^3 if the F- and V-center distributions interpenetrate. The effect of an electric field is examined, and applications of the theory are made to experiments by Maurer and co-workers on optical and thermal bleaching in the presence of a field. Implications are discussed of tunneling phenomena on the x-ray coloration of crystals at low temperatures, and it is concluded that tunneling represents an important back-reaction for limiting local color-center concentrations.

* Research supported in part by the U. S. Air Force.

M10. Color Centers in KCl Crystals Produced by High-Energy Protons. W. LEIVO AND R. SMOLUCHOWSKI, *Carnegie Institute of Technology.*—Single crystals of potassium chloride were irradiated with 400-Mev protons from the Carnegie Institute of Technology synchrocyclotron. The absorption bands produced in the crystal were measured in the range 250 to 1000 mμ. Bands corresponding to F, M, R_1, R_2, and V centers were observed with a slight indication of other centers and a growth of the R bands upon bleaching was noted. No bands resulting from color centers that are not produced by x-rays were found. The absorption measurements were made with a Beckman Model DU spectrophotometer equipped with a photomultiplier attachment. Since the crystals are radioactive after irradiation, a quartz shield was placed between the crystals and the phototube to stop β rays. Under the conditions of the experiment the γ activity was negligible. To prevent undue heating of the crystals during irradiation, the crystals were enclosed in an aluminum capsule filled with helium. The temperatures during irradiation, however, may still be over 200°C. The absorption measurements were made at room temperature. Work is in progress to irradiate and measure the absorption bands of the crystals at liquid helium temperatures.

FRIDAY MORNING AT 10:00

Horace Mann

(M. W. ZEMANSKY presiding)

Cryogenics

Invited Papers

N1. Critical and Supercritical Flow of Liquid Helium II. J. G. DASH, *Los Alamos Scientific Laboratory.* (20 min.)

N2. Recent Studies of the Heat Capacities of the Superconducting Elements. H. A. BOORSE, *Columbia University.* (30 min.)

Contributed Papers

N3. Theory of Temperature Waves. PAUL M. MARCUS, *Carnegie Institute of Technology.*—Periodic variation of the temperature or heat flux at the boundary of a cylindrical rod produces propagating waves of temperature with well-defined but complex propagation constants. Such waves can be reflected at discontinuities and analyzed into modes; the lowest mode generally has much the lowest attenuation. A rigorous description in transmission line language is possible and useful, with voltage taken analogous to temperature and current to heat flux; lumped circuits then represent discontinuities (neglecting higher mode interactions between discontinuities). A circuit representation requires reciprocity, imposing a condition on the characteristic impedances of different rods meeting at a junction. The thermal impedance of any obstacle must be resistive and capacitative but can never be inductive, hence, resonant effects never occur, as might be expected from the diffusion origin of the waves. In fact, temperature waves carry neither energy nor momentum, in contrast to "higher" types of waves, e.g., acoustic which carry energy but not momentum, electromagnetic which carry both, hence, must be described as just propagating disturbances. Calculations on the single series impedance of the change of cross section and material in circular rods have been made by variational methods.

N4. Structure of Liquid Helium by X-Ray Scattering.* W. L. GORDON,† C. H. SHAW, AND J. G. DAUNT, *Ohio State University.*—The intensity scattered from liquid helium as a function of angle between 2° and 90° and as a function of temperature between 1.4°K and 4.2°K has been obtained

using counter registration. The liquid helium sample was contained in a thin-walled beryllium tube mounted directly over the axis about which the detector arm, with its proportional counter and slit system, rotated. A differential filter of Ni and Co foils was used for monochromatization of the Cu $K\alpha$ radiation from a Machlett diffraction tube operated at 40 kv and 15 ma. The operation of this filter was improved by use of a pulse-height analyzer adjusted to accept pulses from Cu $K\alpha$ radiation in the xenon-filled proportional counter, reducing both background and mismatch error in the filter. The angular resolving power was approximately one-half degree. A single intense diffraction peak was observed at 28° where the counting rate was 2000 cpm, of which about 1900 cpm were coherently scattered. At the time of writing, it appears that there are no other peaks with an intensity greater than three percent of the one above at either 1.4 or 4.2°K.

* Supported by a Research Corporation grant.
† General Electric Coffin Fellow, 1952–1953.

N5. Critical and Supercritical Flow in Liquid Helium II. JAY GREGORY DASH, *Los Alamos Scientific Laboratory*.—An empirical theory of superfluidity and dissipative processes peculiar to He II has been developed from the assumption of phonon excitation by large numbers of cooperating superfluid atoms in motion relative to a solid wall immersed in the liquid. Energy conservation and the independence of the velocity fields of normal and superfluid fractions lead to the energy dissipation $E_f=0$ for superfluid velocities v_s smaller than critical, and $E_f\alpha\rho_s(v_s^3-v_c^3)$ for all $v_s>v_c$. The magnitude of v_s is established by the liquid dimensions, which specify the wavelength, and, hence, the energy of the weakest phonons that may be excited: the functional dependence is given as $v_{sc}\alpha(\rho_s d)^{-\frac{1}{4}}$, where d is the characteristic dimension of the liquid. The predictions of the theory are compared with a large body of experimental data. Experiments in the dissipative velocity region appear to be more in accord with the present theory than with the theory of mutual friction of Gorter and Mellink. Correlation with critical velocity values observed over a range of d of six decades closely follows the present prediction, in contrast to the dependence arising from considerations of the uncertainty principle.

N6. The Role of Substrate and Surface Finish in Helium II Film Transport.* B. SMITH AND H. A. BOORSE, *Columbia University*.—An improved version of the high-frequency electrical technique[1] was used to investigate transport over copper, silver, nickel, aluminum, strainless steel, nickel-silver, and precision-bore Pyrex beakers of 5.8 cm internal depth. Measurements of transport over the latter four metals were made not only over the original *machined* surfaces,[2] but also after *superfinishing*[3] by the Chrysler Corporation. Transport rates were remeasured after superfinishing the *external* surfaces and again after *internal* superfinishing. Ground, as well as untreated Pyrex surfaces, were also studied. The results will be analyzed not only with respect to (*A*) the role of substrate and *measured* microfinish, but also with respect to (*B*) the variation of the functional dependence on temperature of the various transport rates with substrate, surface finish, and height, and (*C*) the variation of height dependence with temperature, substrate, and microfinish.

* Assisted by the U. S. Office of Naval Research and Linde Air Products.
[1] J. G. Dash and H. A. Boorse, Phys. Rev. **82**, 851 (1951).
[2] B. Smith and H. A. Boorse, Phys. Rev. **92**, 505 (1953).
[3] A. M. Swigert, *The Story of Superfinish* (Lynn Publishing Company, Detroit, 1940).

N7. The Low-Temperature Oscillatory Hall Effect.* J. S. LEVINGER AND E. G. GRIMSAL, *Lousiana State University*.—Oscillations in the Hall voltage for bismuth may exist[1] at 14°K, and are shown clearly in Reynold's measurements[2] at liquid helium temperatures. We shall present calculations of Hall effect oscillations at 0°K based on a crude model, and we shall compare with Reynold's results. We use an isotropic two-band model for the Hall effect, as a preliminary crude approximation. The number of ordinary conduction electrons is independent of H, while that of the "de Haas-van Alphen electrons" oscillates, as shown by Peierls, Blackman,[3] and others. This model, choosing values of the effective masses and Fermi energy of the same order of magnitude as Blackman's values, gives oscillations similar to those observed by Reynolds. We shall also present the results of calculations now in progress on the effect of temperature in smearing out the oscillations.

* Supported in part by the National Science Foundation.
[1] Gerritsen, de Haas, and van der Star, Leiden Comm. No. 2656 (1942). L. C. Brodie, Bull. Am. Phys. Soc. **28**, No. 6, 31 (1953).
[2] Reynolds, Leinhardt, and Hemstreet (letter submitted to Phys. Rev.).
[3] M. Blackman, Proc. Roy. Soc. (London) **A116**, 1 (1938).

N8. Neutron Diffraction Investigations on Superconducting Elements. M. K. WILKINSON, C. G. SHULL, L. D. ROBERTS, AND S. BERNSTEIN, *Oak Ridge National Laboratory*.—Neutron diffraction investigations have been made on several superconducting elements to determine if the electronic ordering, which presumably accompanies the formation of the superconducting state, causes changes in the neutron diffraction patterns. Data were taken at temperatures of 4.1°K and at 20.4°K for vanadium, lead, and niobium, which have superconducting transition temperatures of 4.7°K, 7.2°K, and 8.7°K, respectively. With the samples at the lower temperature, no extra coherent scattering features were observed, either at new positions or superimposed on the normal Bragg nuclear scattering reflections, and there were no measurable changes in the diffuse scattering which could be attributed to the transition to the superconducting state. A study of the lattice characteristic temperatures was also made from the nuclear Bragg reflections on the Nb patterns to see if the large changes, which have been measured in specific heat variation above and below the superconducting transition, could be accounted for by changes in lattice vibration effects. The neutron scattering data suggest that there is no pronounced change in the atomic lattice vibrations of Nb when it becomes a superconductor.

N9. Compressibilities of Solid Hydrogen and Deuterium at 4.2°K. J. W. STEWART AND C. A. SWENSON,* *Harvard University*.—The compressibilities of solid hydrogen and deuterium have been determined at 4.2°K. Preliminary extrusion experiments showed that these solids are quite plastic and, hence, themselves approximate transmitters of hydrostatic pressure. Pressure is applied directly to the samples with a stainless steel piston and the displacement observed. The apparatus can exert up to 4000 kg/cm². For hydrogen, the compressibility $[-1/V_0(\partial V/\partial P)]$ is $(5.0\pm1)\times10^{-4}$ cm²/kg at zero pressure and $(0.72\pm0.05)\times10^{-4}$ at 1800 kg/cm². For deuterium, the values range from $(4.0\pm1)\times10^{-4}$ at zero pressure to $(0.56\pm0.05)\times10^{-4}$ at 1800 kg/cm² and $(0.42\pm0.05)\times10^{-4}$ at 2800 kg/cm². As compared with other solids, the decrease of compressibility with pressure is abnormally rapid for both H_2 and D_2. The present results agree satisfactorily with previous work at zero pressure.[1] At higher pressures our solid samples suddenly collapse; hydrogen more readily than deuterium. The exact pressure at which this collapse (probably melting of the solid) occurs is not reproducible. Various possible causes for this "catastrophe" have been considered.

* Now at Cryogenic Engineering Laboratory, M. I. T.
[1] H. D. Megaw, Phil. Mag. **28**, 139 (1939).

FRIDAY MORNING AT 10:00

Harkness Academic Theatre

(H. A. BETHE presiding)

Symposium on Nuclear Size and Density Distribution

O1. Diffraction Scattering of 22-Mev Protons. B. L. COHEN, *Oak Ridge National Laboratory.* (30 min.)

O2. Nuclear Determinations from Electron Scattering. ROBERT HOFSTADTER, *Stanford University.* (30 min.)

O3. Nuclear Size from Mesonic Atoms. JAMES RAINWATER, *Columbia University.* (30 min.)

O4. Nuclear Size from X-Ray Fine Structure. C. H. TOWNES, *Columbia University.* (30 min.)

FRIDAY AFTERNOON AT 2:00

McMillin Theatre

(H. A. BETHE AND P. E. KLOPSTEG presiding)

Joint Ceremonial Session of the APS and the AAPT

Retiring Presidential Address of the American Physical Society

P1. What Can We Learn with High-Energy Accelerators? ENRICO FERMI, *University of Chicago.*

Presentation of the Oersted Medal of the AAPT

Response of the Oersted Medallist

P2. The Metaphysics of a Physics Teacher. C. N. WALL, *University of Minnesota.*

Twelfth Richtmyer Memorial Lecture of the AAPT

P3. Fields and Particles. J. A. WHEELER, *Princeton University.*

FRIDAY AFTERNOON AT 3:30

Pupin 301

(WALTER GORDY presiding)

Group of Papers from North Carolina Scheduled Together by Special Request

PA1. An Improved Apparatus for High Resolution Neutron Cross-Section Measurements.* J. H. GIBBONS, *Duke University.*—A neutron collimation-detection system,[1] designed to measure total neutron cross sections with high resolving power and reasonable counting rates (10^3 to 10^4 counts per minute) has been improved in stability, resolution, and energy calibration. A troublesome background counting rate has been identified as mainly resulting from forward-angle neutrons scattered in the tantalum target backing. Approximate correction factors have been determined. A cylindrical electrostatic analyzer is now being used for both proton energy calibration and beam resolution. Neutrons are obtained from the Li(p,n) reaction. Neutron monitoring at 0° appears to be quite satisfactory for our geometry. Resonances have been observed at neutron energies as low as 270 ev; however, background corrections are quite appreciable below 4 kev. Hence

the optimum energy region for investigation with this system begins at about 4 kev. The resolving power decreases with increasing neutron energy, amounting to about 0.5 kev at 5 kev, 1 kev at 12 kev, 2 kev at 30 kev, and 3 kev at 60 kev. Results of some of the cross-section measurements will be shown.

* Work supported by the U. S. Atomic Energy Commission.
[1] J. H. Gibbons and H. W. Newson, Phys. Rev. 91, 209(A) (1953).

PA2. Total Neutron Cross Sections in the Kilovolt Region: As, Zr, Nb, La, Ce, Pr, and Au.* R. C. Block and J. H. Gibbons, *Duke University*, E. G. Bilpuch and D. F. Herring, *University of North Carolina*.—Zr has resonances at 4.5, 7.5, 14, 20, 24, and 28 kev and many higher energy resonances which are only partially resolved; two which are particularly strong lie at 45 and 75 kev. Ce has one very strong resonance at 24 kev which must be due to Ce^{140} (88 percent) and 10 more much weaker ones between 5 and 50 kev. Some of the weaker peaks overlap the strong one and are probably attributable to Ce^{142} (11 percent). Pr and La each appear to have two distinct resonances below 1.5 kev, but none are resolved at higher energies. The average spacings must be ~1 kev per J value. The cross-section curves of As and Nb show evidence of partially resolved resonances; the average spacings must be <1 kev. Au shows few signs of resonance structure down to 0.6 kev; the average spacing must be $\ll$1 kev.

* Work supported by the U. S. Atomic Energy Commission.

PA3. Total Neutron Cross Sections in the Kilovolt Region: Cu, Cu^{63}, Cu^{65}, and Ga.* H. Marshak, *Duke University* (introduced by H. W. Lewis).—The total neutron cross sections of Cu, Cu^{63}, Cu^{65}, and Ga between 1 and 55 kev were measured with the equipment just described. The Cu^{63} and Cu^{65} samples were 99.4 percent and 98.2 percent pure, respectively.[1] The Cu sample showed resonances at 2.5, 6, 8.5, 11.5, 15, 19, 22, 26.5, 31, 35.5, and 44 kev. The 8.5- and 19-kev resonances are a result of Cu^{65} whereas the 15-, 26.5-, and 35.5-kev resonances show up about the same in both enriched samples; the remaining resonances are a result of Cu^{63}. Since, in general, resonance transmission is not exponential, experiments are being performed to measure the effect of the small isotopic contaminations in the samples. There were also weaker resonances at 3, 5, 41, 44, and 49 kev found only in Cu^{65}. The average level spacing per J value is about 12 kev in Cu^{63} and probably considerably less in Cu^{65} since the resonances in the latter are weaker and less well resolved. The 300-ev resonance in Ga was observed, but no other resonances were well resolved.

* Work supported by the U. S. Atomic Energy Commission.
[1] Loaned by the Isotopes Division, U. S. Atomic Energy Commission.

PA4. Total Neutron Cross Sections in the Kilovolt Region: Li, F, Cl, Sc, Rb, Mo, Ag, and Ta.* J. R. Patterson, H. W. Newson, and R. C. Mobley,† *Duke University*, T. E. Gilmer, *University of North Carolina*.—No new resonances were found in Li and F between 1 and 80 kev. Resonances were found in Sc at 5, 10, 13, 15(?), 22, 34, 72, and 81 kev; the average spacing per J value is 10 kev below 25 kev. There appear to be a number of partially resolved levels below 80 kev. Rb has resonances at 5 and 10 kev and a number of partially resolved levels below 25 kev. Resonances were observed in Cl at 8, 26, 120, and 160 kev; weaker resonances are also present. Separated isotopes will be used to obtain level spacing information on Cl and Rb. Weak resonances appear in the cross section curve for Mo. Ag and Ta show almost no resonance effects in their cross-section curves and evidently have level spacings $\ll$1 kev. The upper limits are in accord with low energy data.[1] Average spacings are calculated only when there appears to be a reasonable chance that a majority of the resonances have been resolved.

* This work was supported by the U. S. Atomic Energy Commission.
† Now at Louisiana State University, Baton Rouge, Louisiana.
[1] U. S. Atomic Energy Commission U-2040.

PA5. Total Neutron Cross Sections in the Kilovolt Region: Se, Br, Y, I, and Cs.* H. W. Newson, R. M. Williamson, A. L. Toller, and P. F. Nichols, *Duke University*.—Se has resonances at 3, 7, 21, 32, 35, 46, 52, and 62 kev. The first two have been shown by activation measurements to result from Se^{80} (48 percent abundant). Most of the other resolved resonances should probably be attributed to this predominant isotope. On this assumption the average spacing of Se^{81} is about 9 kev. Y has resonances at 8.5, 12.5, 18(?), 25(?), 31, 56, 58, 64, and 71 kev. There are other resonances between 36 and 50 kev, but this region must be remeasured. One or two weak resonances may be present between 3 and 6 kev, but no others are evident down to 0.75 kev. The average level spacing is about 12 kev per J value. Variations in the cross section curves of Br, I, and Cs have been observed below a few kilovolts, but we have been unable to obtain clearly resolved resonances in any of them. The average level spacings must be <1 kev. Nuclear shell effects and other factors which appear to influence nuclear levels will be discussed.

* This work was supported by the U. S. Atomic Energy Commission.

PA6. (p,γ) Coincidence Measurements Utilizing Proton Time-of-Flight.* W. T. Joyner, *Duke University* (introduced by H. W. Lewis).—For use in angular correlation measurements between charged particles and gamma rays, a fast coincidence circuit similar to that described by De Benedetti[1] has been developed to select proton groups by virtue of their time-of-flight. A thin terphenyl crystal served as the proton detector at a distance of one meter from the target; a thick stilbene crystal was used as the gamma detector. Each crystal was mounted on a DuMont 6292 photomultiplier. The reaction $Al(p,p'\gamma)$ has been observed with the apparatus. The curve of coincidence rate *vs* delay for a 2.33-Mev proton has a full width at half-height equivalent to 0.5 Mev. The ratio of the true coincidence rate to the accidental coincidence rate is about ten for a 0.1 microampere beam current onto a 55-kev aluminum foil, with coincidences involving elastic protons suppressed by an anticoincidence circuit. Slides showing coincidence rate *vs* time delay will be shown, and the apparatus will be described.

* This work was supported by the U. S. Atomic Energy Commission.
[1] S. De Benedetti and H. J. Richings, Rev. Sci. Instr. 23, 37 (1952).

PA7. Production of L-Shell X-Rays by Protons.* Eugene Bernstein, *Duke University* (introduced by H. W. Lewis).—The cross sections for L-shell x-ray production by 2- to 4-Mev protons on several heavy elements have been measured. The NaI scintillation apparatus was similar to that used earlier for K-shell measurements,[1] but improvements essential to the detection of the softer x-rays have been made. The use of thin windows, of a thin scintillator for background reduction, and of the high resolution Dumont 6292 phototube have made it possible to obtain well-resolved pulse-height peaks for the L x-rays between Ta (9 kev) and U. In contrast to the E^4 dependence on proton energy for K-shell ionization, the L-shell dependence for Ta is near $E^{1.4}$. The ratio of the cross sections for L and K ionization of Ta, corrected for the Auger effect, is between 10^3 and 10^4, depending on proton energy. The total thick target yield of L x-rays per proton from Ta at 2.40 Mev is 4×10^{-4}. The cross section at 2.4 Mev for Ta-L ionization is about 300 barns. Results on other elements will be discussed.

* Work was supported by the U. S. Atomic Energy Commission.
[1] Lewis, Simmons, and Merzbacher, Phys. Rev. 91, 943 (1953).

FRIDAY AFTERNOON AT 3:30

Schermerhorn 501

(J. B. H. KUPER presiding)

Group of Papers from Brookhaven Scheduled Together by Special Request

PB1. Estimation of Beam Intensity and Cross Sections at the Cosmotron from the Gross Radioactivity in Copper.* ANTHONY TURKEVICH,† *Brookhaven National Laboratory.*—The gross beta activity of thin copper foils bombarded with 2.2-Bev protons, varies approximately as $T^{-1.18}$ in the interval 0.8 hr$\leq T\leq$800 hr. Copper bombarded with 0.45-Bev protons shows only slightly larger deviations from this power law. This similarity pertains despite large changes in the relative contributions of some important radioactive nuclides.[1] The number of radioactive disintegrations measured in the stated time interval is assumed to be the same fraction of the total number of nuclear interactions in the targets at the two energies. At 0.45 Bev, the cross section for the production of the radioactive species in question is determined to be 50 mb via the known $Al^{27}(p,3pn)Na^{24}$ cross section of 10.8 mb[2]. At the higher energy the corresponding gross activation cross section is assumed to be 60 mb (because of decreased nuclear transparency). This method leads to typical proton intensities of 3×10^{10} per burst in the Cosmotron (summer 1953), and to cross sections of 9 mb for the $Al^{27}(p,3pn)Na^{24}$ reaction and 6 mb for the formation of Cu^{64} from copper with 2.2-Bev protons. It is felt that these numbers are good to about 50 percent.

* Research carried out under the auspices of the U. S. Atomic Energy Commission.
† Permanent address: Institute for Nuclear Studies, University of Chicago, Chicago 37, Illinois.
[1] Friedlander, Baker, Hudis, Miller, and Wolfgang, abstract PB4.
[2] L. Marquez, Phys. Rev. **88**, 225 (1952).

PB2. Reactions of Aluminum with 2.2-Bev Protons.* J. HUDIS, R. WOLFGANG, N. SUGARMAN,† AND G. FRIEDLANDER, *Brookhaven National Laboratory.*—Cross sections for the formation of radioactive products resulting from 2.2-Bev proton bombardment of aluminum have been determined. The values for Na^{24}, F^{18}, C^{11}, and N^{13} were obtained by analysis of gross decay curves. The Be^7/Na^{22} ratio was found by scintillation spectrometer measurements of the gamma-ray intensities of chemically separated sodium and beryllium fractions. Na^{22}/Na^{24} ratios were also determined on separated sodium samples. The absolute cross sections listed are based on the measurements of proton beam intensity described in the preceding

	Na^{24}	Na^{22}	F^{18}	N^{13}	C^{11}	Be^7
σ(mb)	9.0	8.3	5.4	~1.5	5.1	16

abstract by A. Turkevich and may therefore be in error by as much as ±50 percent. The relative values should be good to ±20 percent. The cross sections for C^{11} and Be^7 formation are about 2.5 and 11 times larger than the corresponding cross sections at 335-Mev proton energy[1] while the other cross sections are roughly the same at the two energies. The use of Na^{24} activity induced in aluminum foils for monitoring proton beam intensities will be discussed.

* Research carried out under the auspices of the U. S. Atomic Energy Commission.
† Permanent address: Institute for Nuclear Studies, University of Chicago, Chicago, Illinois.
[1] L. Marquez and I. Perlman, Phys. Rev. **81**, 953 (1951).

PB3. Momentum Transfer in High-Energy Nuclear Interactions in Aluminum.* R. WOLFGANG AND G. FRIEDLANDER, *Brookhaven National Laboratory.*—The recoil of Na^{24}, F^{18}, and C^{11} out of aluminum foils struck by 0.6- to 2.2-Bev protons has been studied. The experimental techniques used were essentially similar to those employed by Si-Chang Fung and Perlman[1] in a corresponding study at lower energies. The total loss of Na^{24} from a 0.25-mil foil is 16.3 percent at 0.6 Bev and this value decreases slowly to 14.0 percent at 2.2 Bev. Similarly, the recoil losses of F^{18} and C^{11}, although greater than that of Na^{24}, seem to be roughly constant between 0.6 and 2.2 Bev. A small and approximately constant recoil loss in the backward direction was observed in all cases. Relstivistic momentum considerations predict the slow, apparently asymptotic, decrease observed for Na^{24} recoils, if it is assumed that Na^{24} formation corresponds to the transfer of a constant amount of excitation independent of bombarding energy. This assumption thus appears to be valid for light nuclei up to energies of 2.2 Bev. In this connection the approximate constancy of the Na^{24} formation cross section with energy reported in the preceding paper is of interest.

* Research carried out under the auspices of the U. S. Atomic Energy Commission.
[1] Si-Chang Fung and I. Perlman, Phys. Rev. **87**, 623 (1952).

PB4. Radioactive Products from the Interaction of 2.2-Bev Protons with Copper.* G. FRIEDLANDER, E. BAKER, J. HUDIS, J. M. MILLER, AND R. WOLFGANG, *Brookhaven National Laboratory.*—Formation cross sections will be reported for approximately 40 radioactive nuclides produced in the interaction of copper with 2.2-Bev protons. Within about 10 mass units of copper the cross sections are somewhat lower than those observed with 340-Mev protons.[1] However, for lighter products the rapid drop-off in yields with decreasing mass number which is observed at 340 Mev is not found at the higher energy. In fact, the cross sections stay substantially constant over the whole mass range. The ratio of cross sections for pairs of isobars appears to be roughly constant with bombarding energy, even in cases where the cross section for forming the particular mass number is rather energy sensitive.

* Research carried out under the auspices of the U. S. Atomic Energy Commission.
[1] Batzel, Miller, and Seaborg, Phys. Rev. **84**, 671 (1951).

PB5. Production of Gallium, Germanium, and Arsenic Nuclides by 2.2-Bev Protons on Copper.* NATHAN SUGARMAN† AND ANTHONY TURKEVICH,† *Brookhaven National Laboratory.*—Radiochemical isolation of Ga, Ge, and As from copper bombarded with 2.2-Bev protons led to yield determinations (in millibarns) for the following nuclides: Ga^{66}, 0.04; Ga^{67}, ~0.06; Ga^{68}, 0.04; Ge^{69}, 0.01; As^{71}, 0.0002; As^{72}, 0.0002. Yields for 340-Mev protons on copper[1] are about one-fourth as high for Ga isotopes and about one-tenth for Ge. No As yields were reported at the lower energy. These Ga, Ge, and As nuclides are interpreted as being formed by reactions of the type $Cu(Z,xn)$ with Z being a He, Li, or Be nucleus formed in the primary interactions. The decreased production of Ga, Ge, and As in thin targets results in estimates of the cross sections for the production of these secondary reacting particles and their average energies. These values are: He, 0.3 barn, 32 Mev; Li, 0.01 barn, 40 Mev; Be, ~0.01 barn, ~30 Mev. The larger yields of Li and Be at 2.2 Bev as compared with 340 Mev are consistent with direct radiochemical observations[2] on low mass nuclides.

* Research carried out under the auspices of the U. S. Atomic Energy Commission.
† Permanent address: Institute for Nuclear Studies, University of Chicago, Chicago 37, Illinois.
[1] Batzel, Seaborg, and Miller, Phys. Rev. **84**, 671 (1951).
[2] Friedlander, Baker, Hudis, Miller, and Wolfgang, preceding abstract.

PB6. Disintegration of Heavy Elements by 2.2-Bev Protons.* ROBERT B. DUFFIELD† AND NATHAN SUGARMAN,‡ *Brookhaven National Laboratory.*—The cross sections for a number of nuclear reactions produced in heavy element targets (Bi, Au, Ta) by 2.2-Bev protons have been determined by examination of the radioactive products. The cross sections decrease as the number of nucleons ejected increases, but are still appreciable (a few millibarns) for reactions involving the loss of as many as 60 nucleons. Recoil energy measurements indicate that such reactions (product $Z>55$) probably occur by nucleon evaporation rather than fission. The radioactive nuclei found are more neutron deficient than those made by 450-Mev protons on bismuth. The known alpha-emitting isotopes of the rare earth elements are produced with good cross sections.

* Research carried out under the auspices of the U. S. Atomic Energy Commission.

† On leave from University of Illinois.

‡ Permanent address: Institute for Nuclear Studies, University of Chicago, Chicago, Illinois.

FRIDAY EVENING AT 7:00

Grand Ballroom, Hotel New Yorker

(ENRICO FERMI AND P. E. KLOPSTEG presiding)

Banquet of the American Physical Society and the AAPT

After-dinner speakers: **President Grayson Kirk** of Columbia University, **L. Brillouin,** and **S. A. Korff.**

Presentation of Buckley Prize

SATURDAY MORNING AT 10:00

McMillin Theatre

(H. A. BETHE presiding)

Physics at Columbia University: a Programme in Celebration of the Bicentennial of the University

Q1. Physics at Columbia University: the Early Years. G. B. PEGRAM, *Columbia University.* (30 min.)

Q2. Physics at Columbia University: the Genesis of the Nuclear-Energy Project. ENRICO FERMI, *University of Chicago.* (40 min.)

Q3. Physics at Columbia University: the Recent Years. I. I. RABI, *Columbia University.* (40 min.)

Q4. The American Physical Society at Columbia University. K. K. DARROW, *Bell Telephone Laboratories.* (20 min.)

Presentation of a plaque to commemorate the foundation of the American Physical Society at Columbia University on May 20, 1899

SATURDAY MORNING AT 9:45

Pupin 301

(R. L. SPROULL presiding)

Luminescence; Electron Physics

QA1. X-Ray Induced Luminescence in MgO. ALBERT S. EISENSTEIN, *University of Missouri.*—X-ray irradiation of MgO single crystals stimulates luminescent bands at 5.2, 3.6, and 3 ev, as well as an increasing intensity below 2 ev. The 5.2-ev band is increased in intensity by three orders of magnitude with Mg doping and is reduced in intensity with O doping. A photon counter (1*P*28 photomultiplier operated at 90°K) is used to study this luminescence and its subsequent decay following the irradiation. The 5.2-ev band decays rapidly, but the 3.6-ev band intensity falls slowly, approximating a power law with $n=-0.5$. Phosphorescence at 3.6 ev resulting from a dose of 1000 roentgens, delivered in 2 minutes, may be followed for six months. When approximately one-half of the total number of photons to be released are emitted, n increases, approaching -3. An electrical conductivity was found to accompany this phosphorescence but its decay was always more rapid than the luminescent decay. Thermal release of trapped holes followed by hole capture of trapped electrons may account for this long-time luminescence.

QA2. The Luminescence of Beryllium Oxide.* H. O. ALBRECHT AND C. E. MANDEVILLE, *Bartol Research Founda-*

tion.—Under cathode-ray and heavy ion bombardment, beryllium oxide was described by Sir William Crookes as having "a beautiful blue phosphorescence." A preliminary survey of western publications[1] has shown that although BeO has been used frequently as a constituent in silicates and other phosphors, no detailed studies of the luminescent properties of "pure" unactivated BeO appear to have been described. It has recently been observed by the writers that when powdered BeO is irradiated by polonium alphas, fluorescence occurs in a broad emission band, extending from ~2000A to 4000A and above. A tremendous light yield is obtained in the deep ultraviolet ($2000A < \lambda < 3000A$), rivaling and sometimes exceeding that of silver-activated sodium chloride. A faint long period phosphorescence was excited by a Tesla discharge at an air pressure of ~10 microns. This effect was enhanced many fold by heating the pure BeO to 1400°C in atmospheric air. The heat-treated material gives a very intense long-period ultraviolet phosphorescence. BeO is in general less luminescent under hydrogen-arc excitation than are the activated alkali halides.

* Assisted by the joint program of the U. S. Office of Naval Research and the U. S. Atomic Energy Commission.
[1] The literature of the Soviet Union and associated nations has not been thoroughly searched.

QA3. Electroluminescence in ZnS Single Crystals. W. R. WATSON, J. J. DROPKIN, AND A. T. HALFIN, *Sylvania Electric Products, Inc.*—Half-wave voltage excitation resolves the electroluminescent emission of some ZnS single crystals into two processes. At low peak voltages the emission was delayed with respect to the voltage as follows: voltage increasing—no emission; voltage decreasing—emission rising with maximum about voltage zero; voltage off—decay of emission. At higher peak voltage an emission in phase with the applied voltage was also present and increased with rise of peak voltage faster than the delayed emission. Both emissions appeared to originate from the same regions of the crystal but showed different spectral characteristics. Among the secondary effects observed was the quenching of the delayed emission by the increasing voltage of the subsequent half-cycle. The delayed emission, in-phase peak, and quenching are discussed in terms of a picture in which ionization occurs in a localized region of the crystal: charge separation, trapping, release from traps, and recombination under the action of a polarization field are used to discuss the delayed emission and quenching, whereas immediate recombination when higher levels of ionization density are reached account for the in-phase emission.

QA4. Theory of Electroluminescence of Zinc Sulfide Crystals. WILLIAM W. PIPER AND FERD E. WILLIAMS, *General Electric Research Laboratory.*—Data on the electroluminescence of single crystals of copper-activated zinc sulfide can be explained quantitatively by the mechanism proposed by Piper and Williams.[1] Conduction electrons with several volts of kinetic energy excite the activator system directly by inelastic collisions or indirectly by impact ionization of valence electrons to form electron-hole pairs which are captured by the activator system. The conduction electrons acquire their kinetic energy in a region of high electric field. The required field is attained in an exhaustion layer at the cathode in the *N*-type semiconductor. The electrons which are accelerated to high kinetic energies are field excited from deep donors. The electroluminescent brightness as a function of applied voltage depends on the distribution in energy of the deep donors, on the field dependence of the probability of accelerating conduction electrons to high kinetic energies, and on the field configuration in the exhaustion layer. Several specific distributions of deep donors have been analyzed. The experimental voltage dependence of brightness and the form of the instantaneous brightness during the voltage cycle are in accord with a continuous distribution in energy of the donor levels.

[1] W. W. Piper and F. E. Williams, Phys. Rev. **87**, 151 (1952).

QA5. Triboluminescence in Crystals.* G. WOLFF, *Signal Corps Engineering Laboratories.*—Triboluminescence can be expected where, upon crushing or cleaving of crystals, electrical charges are created on corresponding planes. As a consequence, a glow discharge takes place. In this effect, the presence of a polar axis or the absence of a center of symmetry is of importance. Secondary excited fluorescence, phosphorescence, and surface chemiluminescence can also cause triboluminescence. Relations between permanent triboluminescence and molecular structure, crystal structure, crystal size, and fluorescence will be discussed. In addition, the relation between temporary triboluminescence and lattice distortion will be presented.

* This work is based on experimental data obtained by the author and co-workers at Fritz Haber Inst., Berlin-Dahlem, 1951–1952.

QA6. Photoelectric Emission from BaO.* H. R. PHILIPP,† *University of Missouri.*—Photoelectric measurements were made on sprayed coatings of BaO. The yield curve showed an exciton rise at 3.8 ev and a rapid rise at 5.0 ev resulting from electrons excited from the occupied band. A magnetic velocity analyzer was used to determine the energy distribution of the emitted photoelectrons. Two peaks in the distribution were observed, one increasing in energy with increasing $h\nu$ and the second occurring at very low energy. The latter peak appeared for values of $h\nu$ above 3.5 ev and did not shift in energy with increasing $h\nu$. The thermionic emission distribution was observed to shift with temperature, and a value for the temperature dependence of the work function calculated from this shift was 3.25×10^{-4} ev/°K. The temperature dependence of the work function calculated from the apparent Richardson A constant was 3.15×10^{-4} ev/°K. Enhancement measurements were made which showed that shorter enhancing wavelengths produce greater increases in photoelectric emission, the relative increase being greater at longer observing wavelengths.

* Supported in part by the U. S. Office of Naval Research.
† Minneapolis Honeywell Research Fellow.

QA7. Effect of Strain on the Work Function of Polycrystalline Silver. G. WALLIS* AND H. E. FARNSWORTH, *Brown University.*—Contact potential difference measurements in a pressure range from one atmos to about 10^{-8} mm Hg have indicated that mechanically induced strain of the order of 1 percent (beyond elastic limit) in polycrystalline strips of silver is associated with an increase in work function of between 0.01 and 0.03 ev. Annealing at about 400°C for a period of ten min approximately restores the original value of work function. It is suggested that lattice imperfections induced by the stretching of the strip are responsible for the increase and that their removal during the heat treatment causes the subsequent decrease in work function.

* Socony-Vacuum Fellow. Now with the Electronics Division, Sylvania Electric Company, Ipswich, Massachusetts.

QA8. Energy Losses of Electrons in Passage Through Thin Films.* LEWIS B. LEDER AND L. MARTON, *National Bureau of Standards.*—The loss of energy of 30–35 kev electrons passing through thin films of several metals and insulators has been measured using a modified electrostatic electron microscope. The high chromatic aberration of an electrostatic lens with elongated central aperture is used to separate out those electrons which have lost energy.[1] An enlarged image of a 2-micron slit is projected onto a photographic plate, and multiple images are produced by those electrons which have lost energy. These measurements are in the same energy-loss range as those of Mollenstedt,[1] Ruthemann,[2] and others. The materials measured so far are Be, Na, Mg, Al, K, Si, Ti, Fe, Cu, Ge, Pd, Ag, Cd, Sn, Sb, Au, Bi, collodion, and quartz.

The results will be given and discussed in relation to the plasma oscillation theory of Pines and Bohm.[3]

* This work was supported by the U. S. Office of Naval Research.
[1] G. Mollenstedt, Optik **5**, 499 (1949); **9**, 473 (1952).
[2] G. Ruthemann, Ann. Physik **2**, 113 (1948).
[3] D. Pines and D. Bohm, Phys. Rev. **83**, 221 (1951); **85**, 338 (1952).

QA9. Penetration of Medium Fast Electrons into Photographic Emulsions.* L. MARTON AND LEWIS B. LEDER, *National Bureau of Standards.*—As part of the work being done in this laboratory on the inelastic scattering of electrons, measurements were made of the action of electrons passing through photographic emulsions. Lantern Slide medium plates were exposed to the beam of an electron microscope, and exposures at 30, 40, 50, and 60 kev were made in areas on the same plate. The plates were then processed in a conventional manner. With the use of an oil immersion microscope, "optical sectioning" was used to make photomicrographs at 2-micron intervals in depth of the emulsion. This was done for each mono-energetic electron exposure. The developed grains were then counted, and a distribution of the number of grains as a function of depth thereby obtained. The distribution is similar to that found in previous ionization density experiments using higher energies.[1] At those energies the peak of ionization was found to move to greater depths with increasing energy. In the energy range of our experiment, however, the variation of the peaks with voltage appears to be anomalous.

* This work was supported by the U. S. Office of Naval Research.
[1] J. G. Trump and R. J. Van de Graaff, J. Appl. Phys. **19**, 599 (1948); **21**, 345 (1950).

QA10. Propagation of Waves in Ionized Gases. E. P. GROSS, *M.I.T.*, AND M. KROOK, *Harvard University.*—A theoretical study is made of the small-amplitude oscillations of a completely ionized gas as a function of pressure. At low pressures there exist two types of waves. The high-frequency electronic plasma waves[1] are only slightly modified by the motion of positive ions. In addition, we find the low-frequency "plasma-ion" waves previously studied by Tonks and Langmuir.[2] The latter are, however, undamped only when the electron temperature is considerably greater than the ion temperature. To study the effects of collisions we make use of a model for collision processes proposed earlier.[3] It is found that the low frequency modes are increasingly damped as the pressure is raised. The high-frequency modes are also highly damped at intermediate pressure. However, at higher pressures this mode changes its nature continuously and becomes a sound wave with a propagation velocity characteristic of a mixture of gases.

[1] D. Bohm and E. P. Gross, Phys. Rev. **75**, 1851, 1864 (1949).
[2] L. Tonks and I. Langmuir, Phys. Rev. **33**, 195 (1929).
[3] E. P. Gross and M. Krook, Bull. Am. Phys. Soc. (Chicago meeting), **28**, No. 6, 32 (1953), abstract T19.

QA11. Nonuniform Microwave Transmission Lines and Solutions of Riccati Equations. STANLEY WINKLER, *U. S. Naval Material Laboratory.*—The characterization of transmission lines in terms of impedance by a Riccati equation was given by Pierce.[1] Although Riccati equations in general, are not soluble in finite terms,[2] it is possible to obtain such solutions in particular cases.[3] Some of these solutions may be utilized in a discussion of non-uniform transmission lines. Relationships are developed between transmission line distributed parameters and integrability criteria for Riccati equations. This technique is applicable in those cases where the transmission line parameters are continuous functions of the line length. Possible extension of this method may provide an approximation procedure for the solution of transmission lines with discontinuities.

[1] J. R. Pierce, Bell System Tech. J. **22**, 263 (1943).
[2] Joseph Liouville, J. de Math. **6**, 1 (1841); Joseph F. Ritt, Bull. Am. Math. Soc. **33**, 51 (1927).
[3] Stanley Winkler, M. S. thesis, New York University (1950).

QA12. Writing Speed and Tonal Range of Dark Trace Tubes. SEYMOUR NOZICK, *U. S. Naval Material Laboratory* (introduced by Stanley Winkler).—The writing speed of a dark trace tube is shown to be proportional to the ratio of beam current to spot size multiplied by a scotophor sensitivity factor. Experimental verification indicates the magnitude of screen sensitivity. A charge density of 4.37×10^{-4} microcoulomb per square millimeter produces minimum discernible contrast. A minimum of 10.9×10^{7} electrons is required per digit of information. About 10 digits per microsecond can be displayed on the 4AP10 tube face. A high writing speed tube is possible by the optimization of either the ratio of beam current to spot size or the screen sensitivity. The tonal range measured by the number of detectable contrast steps is proportional to the ratio of maximum contrast to spot size. The ability of the eye to discern contrast gradient* modifies this, giving a merit factor for tonal range. Thus an improved tube can be made by the optimization of this ratio. For the 4AP10, the figure of merit is 20. The amount of information which can be displayed can be computed by the raising of the number of possible spots to the tonal range power so that another useful factor is given.

* W. B. Nottingham, *Rad. Lab. Series* (McGraw-Hill Book Company, Inc., New York, 1948), Vol. 22, Chap. 18.

QA13. Errors in Power Spectra Due to Finite Sample.* L. M. SPETNER, *Johns Hopkins University.*—If one measures the power spectrum of Gaussian random noise by selecting a finite sample of this noise, splicing its tail to its head to form an endless loop, and then playing it through a spectrum analyzer, there arise questions of accuracy. Calculations show that the effect of the splice varies with frequency—it is worse for low frequencies than for high, and it also depends upon the frequency at which the spectrum begins to flatten out at the high end; the sooner it begins to flatten out, the less serious is the effect of the splice. In general it turns out that the effect of the splice is small compared with the statistical sampling effect. For the latter, results similar to Tukey's[1] have been derived. For a given sample length, the combination of accuracy and resolution is fixed, i.e., one can increase accuracy only at the expense of resolution and vice versa. Specific results of the calculations will be shown and applied to experimentally measured spectra.

* This work was supported by the U. S. Navy Bureau of Ordnance.
[1] J. W. Tukey, "Sampling theory of power spectrum estimates," Symposium on Applications of Autocorrelation Analysis to Physical Problems, Woods Hole, Massachusetts, June, 1949 (U. S. Office of Naval Research).

SATURDAY MORNING AT 9:45

Horace Mann

(M. GOLDHABER presiding)

Beta and Gamma Emitters, I

R1. Gamma-Ray Spectrum of the Bulk Shielding Reactor. FRED MAIENSCHEIN AND TEMPLE LOVE, *Oak Ridge National Laboratory.*—Spectral measurements have been made of the gamma rays emitted by the Bulk Shielding Reactor (BSR) at the Oak Ridge National Laboratory and of the gamma rays transmitted from the reactor through various thicknesses of

water. The power of the BSR, which consists of an assembly of aluminum-clad enriched uranium fuel elements with water moderator and coolant, was determined from the fission rate which had been previously measured with uranium fission foils. Gamma-ray spectral measurements were made with a multiple-crystal scintillation spectrometer employing both the Compton effect and pair production to give a unique energy response. Energy and sensitivity calibrations of the spectrometer were made using natural radioactive sources whose disintegration rates were determined with an ionization chamber. The general shapes of the spectra obtained indicated a decreasing flux intensity with increasing gamma-ray energy and a sharp drop-off at ~8 Mev. A definite "hardening" of the spectra with increasing water thickness was apparent. Peaks in the spectra due to neutron capture in the hydrogen of water and in the aluminum of the fuel elements were observed.

R2. Age-Diffusion Theory for Beta Ray Problems.* WM. C. ROESCH, *General Electric Company.*—Bethe *et al.*,[1] showed that problems of electron transport can be reduced to solution of the diffusion (or age) equation. Numerical calculation of the ages and of the integrals appearing in the solutions of typical problems has given results in good agreement with experiments for the practical range of monoenergetic electrons, the absorption coefficient of beta rays, the surface dose rate of an emitting material in contact with a backscatterer of any atomic number, the dose rate near a thin source in a large medium, and the response of ion chambers to gamma rays.

* This paper describes in part work done under contract between the General Electric Company and the U. S. Atomic Energy Commission.
[1] Bethe, Rose, and Smith, Proc. Am. Phil. Soc. **78**, 573 (1938).

R3. The Beta Spectra of O^{14}.* J. R. PENNING AND F. H. SCHMIDT, *University of Washington.*—We have studied the beta rays of 76 sec O^{14} with a scintillation spectrometer to determine more accurately the end-point energy, and to search for a possible ground-state transition. O^{14} is known[1] to decay by positron emission primarily to a 2.3-Mev level in N^{14}. The transition is believed to be $J=0\rightarrow J=0$. The activity was produced by the (p,n) reaction on nitrogen in the University of Washington 60-inch cyclotron. The active gases were conducted to a source chamber by means of a continuous flow system. The radiations were examined by NaI(Tl) and anthracene scintillation spectrometers. The spectrometers were calibrated with several other known β spectra. The principal beta component was counted in coincidence with the 2.3-Mev γ ray. Our tentative value for the end-point energy of this component is 1.830 ± 0.030 Mev. In addition, we observed higher energy β particles which exhibited the same half-life as O^{14}. If we assume that these β particles are due to an allowed-shape transition from O^{14} to the ground state of N^{14}, then we obtain a branching ratio of 3 percent. The log *ft* value is 6.7.

* Partially Supported by the U. S. Atomic Energy Commission.
[1] Sherr, Muether, and White, Phys. Rev. **75**, 282 (1949).

R4. Sargent Diagram and *ft* Values for Electron Capture Transitions. J. K. MAJOR AND L. C. BIEDENHARN, *Yale University.**—Knowledge of the disintegration constant λ and the energy W of electron capture transitions is useful in calculating branching ratios and transformation probabilities and in identifying nuclear transitions. While λ may be computed from observed half-lives and known decay schemes, W must be deduced indirectly, from closed decay cycles, mass differences from nuclear reaction or mass spectrometer measurements, positron emission between the same initial and final states, or end points of inner *bremsstrahlung* accompanying electron capture. Earlier studies[1] have been extended to lighter nuclei wherever adequate information on the half-life, branching ratios, and transition energy was available, and a Sargent diagram constructed. Known allowed transitions fall considerably below the line proposed by Feather,[1] but the scatter of the points does not permit differentiation of Sargent curves for different degrees of forbiddenness. Comparative half-lives have also been calculated for capture transitions and will be compared to those for beta emitters.[2]

* Assisted by the joint program of the U. S. Office of Naval Research and U. S. Atomic Energy Commission and by Air Research and Development Command, U. S. Air Force.
[1] S. G. Thompson, Phys. Rev. **76**, 319–320 (1949); N. Feather, Proc. Roy. Soc. Edinburgh **63**, 242–256 (1952); Physica **13**, 1023–1025 (1952).
[2] A. M. Feingold, Revs. Modern Phys. **23**, 10–20 (1951); E. Feenberg and G. Trigg, Revs. Modern Phys. **22**, 399–406 (1950).

R5. Recoil Spectrum in the β Decay of Ne^{19}.* W. PARKER ALFORD† AND DONALD R. HAMILTON, *Princeton University.*—A spectrum of recoil nuclei in coincidence with positrons at an angle of $180°\pm30°$ has been measured in the Ne^{19} β decay. The electrons are detected with a scintillation crystal and the recoils by being accelerated into an electron multiplier. Ne^{19} flows through the vacuum system containing the electron multiplier; this is separated from the β crystal by a thin foil. Electrostatic energy discrimination and time of flight discrimination applied to the recoils define the source volume. Preliminary analysis of present data on the recoil spectrum suggests the presence of scalar interaction in the decay. Further measurements of the recoil spectrum under different geometrical conditions and of the corresponding electron spectrum are in progress.

* This work was supported by the Atomic Energy Commission and by The Higgins Scientific Trust Fund.
† Socony-Vacuum Fellow 1952–1953.

R6. Radiative Electron Capture in Fe^{55}, A^{37}, and Ni^{59}. S. E. SINGER, W. S. EMMERICH, AND J. D. KURBATOV, *The Ohio State University.*—The radiative electron capture spectra of Fe^{55}, A^{37}, and Ni^{59} were investigated with a scintillation spectrometer. The detection efficiency of the NaI(Tl) crystal was determined in the energy range from 300 kev to 1300 kev by means of gamma-ray activities of known intensities. The monoenergetic gamma-ray spectra were applied to the continuous energy spectra for correction of the distortion caused by the Compton effect in the crystal. The data were further corrected for the effects of instrument resolution, and were then plotted after the method of J. M. Jauch.[1] Endpoint energies of 227 ± 10 kev, 815 ± 20 kev, and 1065 ± 30 kev were obtained for Fe^{55}, A^{37}, and Ni^{59}, respectively. The experimentally determined spectral shapes were found to be in agreement with the calculated intensity distributions. The spectrum of Ni^{59} appeared to be independent of the type of transition involved. The calculated value of the total radiative capture intensity for Ni^{59} was found to be consistent with the observed intensity of the radiation if a half-life of approximately 7×10^4 years was assumed.

[1] J. M. Jauch, Oak Ridge National Laboratory Report 1102, 1951 (unpublished).

R7. The Disintegration of Cobalt-56. M. SAKAI,* J. DICK, AND J. D. KURBATOV, *The Ohio State University.*—The energy levels of Co^{56} have been investigated using a magnetic lens spectrometer and a $\gamma-\gamma$ coincidence scintillation spectrometer. Cobalt-56 was obtained by the proton bombardment of ferric oxide enriched in Fe^{56} (99.84 percent). A carrier-free cobalt sample was separated from the target material by ether extraction of ferric chloride followed by precipitation of the remaining traces of iron. The cobalt source essentially contained Co^{56} thus permitting the study of the low-energy portion of its spectrum without interference from other radioactive species of cobalt. The beta spectrum was found to be complex consisting of two groups, the previously reported 1.50-Mev group and a new lower energy component with an end-point energy of about 0.44 Mev. The energies of five of the gamma rays, 0.835 Mev, 1.23 Mev, 1.74 Mev, 2.60 Mev, and 3.25 Mev were confirmed, but the sixth, previously re-

ported as 2.01 Mev was found to be 2.31 Mev. Using this data and that obtained by $\gamma-\gamma$ coincidence studies a decay scheme will be presented.

* On leave of absence from the University of Tokyo.

R8. Upper Limits for the Lifetimes of Ni^{60}.* Z. BAY, V. P. HENRI, AND F. MCLERNON, *George Washington University.*—Recent differential coincidence measurements gave less than 10^{-11} sec for the mean lives of the two excited states of Ni^{60} resulting from the β decay of Co^{60}. In addition, and also as a check, we have measured times of flight of γ's for a distance as short as 1 cm or less in air using them to correct other time measurements. We have also checked the simultaneity in the Compton scattering of γ's lowering thereby the upper limit of such measurements as given by others[1] by more than two orders of magnitude.

* This work supported by the joint program of the U. S. Office of Naval Research and the U. S. Atomic Energy Commission.
[1] R. Hofstadter and J. A. McIntyre Phys. Rev. **78**, 24 (1950).

R9. Disintegrstion of Arsenic-76. B. B. MURRAY AND J. D. KURBATOV, *The Ohio State University.*—Arsenic-76 decays by negatron emission to selenium-76 and by positron emission to germanium-76. The relative abundance of positron disintegration of arsenic-76 with respect to negatron emission has been studied by means of a Wilson cloud chamber. A chemical procedure was developed to obtain a highly purified source of arsenic. It has been established that the decay ratio of positrons to negatrons is approximately 1:1000. The endpoint of the positron spectrum was observed to be about 670 ± 30 kev. The disintegration of other species by positron and negatron emission will be summarized.

R10. The Radiations of 18-min Br^{80}. L. LIDOFSKY, R. GOLD, AND C. S. WU, *Columbia University.**—A reinvestigation of the radiations of 18-min Br^{80} has been made. A renewal of interest in this nuclide was prompted by conflicting reports on its complexity. Further, the level schemes suggested by these reports were in disagreement with the scheme suggested by the existence of a 620-kev gamma ray in Kr^{80}.[1] 18-min Br^{80} was produced by isomer separation from neutron irradiated bromobenzene. A gamma ray of 620 ± 10 kev was found with $N_\gamma/N_{\beta^-}=0.12\pm0.02$. No gamma ray of energy greater than 620 kev was present with an abundance greater than 1 percent. The beta spectrum was remeasured using the solenoid spectrometer with positron-negatron selecting baffles. The negatron spectrum was consistent with an analysis into two groups separated in end point by $\sim$600 kev. The positron spectrum was found to have the simple allowed shape with an endpoint of 862 ± 10 kev and $N_{\beta^+}/N_{\beta^-}=0.04\pm0.005$. A search was also made for the 49-kev gamma ray of 4.4-hour Br^{80*}. Its abundance was found to be less than 0.0025 per disintegration.

* This work partially supported by the U. S. Atomic Energy Commission.
[1] G. S. Goldhaber and M. McKeown, Bull. Am. Phys. Soc. **28**, 5 (1953).

R11. The Disintegration of Mo^{99}.† C. E. MANDEVILLE AND JAGDISH VARMA,* *Bartol Research Foundation.*—The radiations of Mo^{99} and Tc^{99m} have been re-investigated by means of scintillation spectroscopy. Employing single-channel pulse-height analyzers in coincidence, it has been established that a triple cascade of gamma rays, 741 kev→41 kev→140 kev occurs. The 741-kev radiation is also coincident with a gamma ray at 181 kev by an alternate branch of de-excitation which is equally probable. Radiation at 780 kev is present but is noncoincident with other gamma rays. From these data, a disintegration scheme can be constructed. A gamma ray of energy 372 kev was also detected, and although it appeared to have the proper half-period to be associated with Mo^{99}, was found to be not in immediate coincidence with beta rays or other gamma rays, suggesting that it might be related to an impurity.

† Assisted by the joint program of the U. S. Office of Naval Research and the U. S. Atomic Energy Commission.
* Research Fellow, permanent address, Morena (M.B.) India.

R12. Disintegration of In^{117}. C. L. MCGINNIS, *National Bureau of Standards.*—The radiations associated with In^{117} have been studied with a lens spectrometer and scintillation counters. Cadmium was bombarded with 18-Mev deuterons from the Carnegie Institute of Washington Department of Terrestrial Magnetism cyclotron and In^{117} was obtained by chemical separation from the Cd^{117} parent. The isomeric level of In^{117} decays with a half-life of 1.83 hours, and with the following radiations given with their percent transitions-1.77β (39 percent), 1.61β (16 percent), 0.159γ (16 percent), and 0.315γ (45 percent). The internal conversion coefficient for the 0.315 gamma ray is $\sim$1.3 making it *M*4. By means of a Szilard-Chalmers reaction[1] the ground state was separated from the isomeric level and found to have a 40-min half-life. It decays by an 0.76β followed by 0.56- and 0.159-Mev gamma rays. The following coincidences have been measured: $(\beta)(0.16\gamma)$, $(\beta)(0.56\gamma)$, $(0.56\gamma)(0.16\gamma)$. The 0.315γ is not in coincidence with either β or γ rays. The energies were measured with the mixed activity. In^{117} is not the parent of 14-day Sn(<1 percent).

[1] G. J. Goldsmith and E. Bleuler, J. Phys. Colloid Chem. **54**, 717 (1950).

R13. On the Disintegration of I^{130}. R. S. CAIRD AND ALLAN C. G. MITCHELL, *Indiana University.**—The disintegration of I^{130} has been re-examined with the help of a magnetic lens spectrometer and coincidence counting apparatus using scintillation counters. In addition to the lines at 0.409, 0.528, 0.660, and 0.744 Mev reported by Roberts *et al.*[1] a line at 1.15 Mev has been found. Two beta-ray groups[1] are emitted whose energies are 1.02 and 0.597 Mev. Coincidence experiments show that the line at 0.744 Mev is in coincidence with those at 0.409, 0.528, and 0.660 Mev. The line at 1.15 Mev is in coincidence with those of 0.660 and 0.528 Mev but not those at 0.744 and 0.409. These experiments fix the position of the 0.744- and the 0.409-Mev lines. The internal conversion coefficients of the lines at 0.528, 0.660, and 0.744 Mev show that they are *E*2 radiation. The line at 1.15 Mev is *E*1. The energy level scheme will be discussed in the light of the collective model.

* Supported by the joint program of the U. S. Office of Naval Research and U. S. Atomic Energy Commission.
[1] Roberts, Elliott, Downing, Peacock, and Deutsch, Phys. Rev. **64**, 263 (1943).

SATURDAY MORNING AT 9:45

Havemeyer 309

(J. E. GOLDMAN presiding)

Magnetism

RA1. Lattice of Partly Permanent Dipoles. M. LAX AND R. TOUPIN, *Syracuse University.*—In a previous paper,[1] the statistical mechanical analysis of a lattice of permanent dipoles was presented within the approximation we call the spherical model. This approximation, which renders the problem of determining the partition function tractable, replaces

the N constraints, that each dipole be of fixed length, by the single requirement that the combined lengths have the correct value. It was shown that such a model possesses a critical temperature (a discontinuity in the slope of the susceptibility *vs* temperature relation), above which the model behaves as a lattice of induced dipoles with an effective, temperature dependent, polarizability. We have extended the above analysis to include the case of a lattice of permanent dipoles having in addition an induced component. The spherical model approximation is again made in order to treat the permanent component while the induced component is handled exactly. The general features of the results remain unchanged and include the previous result as a special case. We find that, if a simple type of spectrum be assumed for the dipole interaction, the Onsager result[2] is obtained for the behavior of the spherical model above the critical temperature.

[1] M. Lax, J. Chem. Phys. **20**, 1351 (1952).
[2] L. Onsager, J. Am. Chem. Soc. **58**, 1486 (1936).

RA2. Critical Temperature and Susceptibility of Dipole Lattices. R. TOUPIN AND M. LAX, *Syracuse University.*—The determination of the critical temperature and susceptibility of a lattice of dipoles involves the mean eigenvalue $F(t)$ of the operator $(t-\mathbf{G})^{-1}$, where $\mathbf{G}_{ij}=\nabla\nabla 1/r_{ij}$. In particular, if λ_{max} denotes the maximum eigenvalue of $\mathbf{G}$, then $F(\lambda_{max})$ determines the critical temperature. The function $F(t)$ can be expanded as a series in inverse powers of t; the coefficients are the moments of the eigenvalue spectrum of $\mathbf{G}$. The moments up to, and including the third, have been determined exactly by a cluster sum method.[1] The very high moments of the spectrum are determined almost entirely by the behavior of the eigenvalue spectrum in the neighborhood of the maximum eigenvalue. A first approximation to the function $F(t)$ is obtained by using the exact values of the first three moments and the asymptotic form for all higher moments. An estimate is then made of the difference between the exact and approximating functions, by performing a numerical integration of the difference over the eigenvalue spectrum using the symmetry points of the spectrum. The transition temperature T_c for a simple cubic lattice of permanent dipoles in the spherical model approximation is given by $n\mu^2/3kT_c = F(\lambda_{max}) = 0.74$. The accuracy of the calculation is estimated to be about 3 percent.

[1] R. Rosenberg and M. Lax, J. Chem. Phys. **21**, 424 (1953).

RA3. The Magnetic Susceptibility of the Transition Elements. C. J. KRIESSMAN, *Remington Rand,* AND H. B. CALLEN,* *University of Pennsylvania.*—A theoretical treatment of the temperature dependence of the paramagnetic susceptibility of the transition elements according to the band theory of solids, is developed explicitly by means of a simple approximation to the Fermi function. The resulting formulation may be graphically interpreted in terms of the density-of-states curve, and the temperature dependence is divided into two distinct mechanisms: (1) the variation with temperature of the width of the Fermi distribution, and (2) the variation with temperature of the Fermi energy. On the basis of the approximate theoretical density-of-states curves which have been computed for the transition elements, the competition of these two mechanisms is found to lead to susceptibilities which are qualitatively in agreement with experiment. In particular, the observed alternation in sign of susceptibility from column to column of the periodic table, and the various maxima and minima in the temperature dependence of the susceptibility, follow from the simple graphical constructions of the theory.

* Supported in part by the U. S. Office of Naval Research.

RA4. High Field Non-Brillouin Moments for Cobalt Sulfate Heptahydrate. WARREN E. HENRY, *Naval Research Laboratory.*—A high-field induced paramagnetic anomaly in nickel fluosilicate hexahydrate has been previously reported.[1] Branching of the magnetic isotherms occurred at high fields when the moment was plotted against H/T. In this case, the dispersion of the isotherms increased as H/T was increased. However, the saturation range was not easily availabe for the nickel fluosilicate and it was decided to study cobalt sulfate heptahydrate, which from measurements on the low-field susceptibilities by Fritz and Giauque[2] should tend to saturation more easily. The magnetic isotherms show the same type of high-field accentuated branching but yield considerable data in the range near saturation, i.e. where $(\partial M/\partial H)_T$ is small. Analysis of the experiments shows a nonlinear dependence of energy levels on magnetic field.

[1] W. E. Henry, Bull. Am. Phys. Soc. **28**, 6, 31 (1953).
[2] J. J. Fritz and W. F. Giauque, J. Am. Chem. Soc. **71**, 2168 (1949).

RA5. Antiferromagnetism in Cupric Oxide.* B. N. BROCKHOUSE,† *Brookhaven National Laboratory.*—Neutron powder diffraction studies of CuO at low temperatures show the existence of a weak line corresponding to the $\bar{1}01$ line of a unit cell of double the normal size. This line was not observed with x-rays and has a temperature dependence of the kind shown by lines of magnetic origin, disappearing at about 230°K. This apparent Néel temperature coincides within the uncertainties to the temperature (220°K) of a specific heat anomaly. In the monoclinic structure, the copper atoms occupy $\bar{2}02$ planes of the normal cell in equal numbers. The appearance of the $\bar{1}01$ line of the doubled cell means that alternate planes of copper atoms are coupled antiferromagnetically. This fits in well with current ideas about antiferromagnetism in oxides; for each copper atom is coupled to a copper atom one plane away through a copper-oxygen-copper link in which the angle is about 145 degrees. Other Cu-O-Cu angles in the structure are smaller. The intensity of the line sets a lower limit of $0.5\mu_B$ for the magnetic moment per copper atom.

* Work partly performed at BNL under auspices of U. S. Atomic Energy Commission and partly at Chalk River Laboratories, Atomic Energy of Canada, Ltd.
† Guest of BNL Reactor Department, on leave from Atomic Energy of Canada, Ltd.

RA6. Volume Magnetostriction in Nickel and its Alloys.* K. AZUMI AND J. E. GOLDMAN, *Carnegie Institute of Technology.*—The volume magnetostriction is related to the pressure dependence of the magnetic moment through the thermodynamic identity $(\partial V/\partial H)_p = -(\partial M/\partial p)_H$ and its sign is, therefore, sensitive to the position of the element on the Bethe-Slater curve relating the exchange interaction to atomic separation. It is generally assumed that nickel lies on the decreasing portion of this curve. Recent experiments on the pressure dependence of the magnetization confirm this. On the other hand, the sign of volume magnetostriction as measured by Kornetzki and by Snoek do not support this view. We have adapted the resistance-strain gauge technique to the measurement of the volume magnetostriction and have obtained results on nickel and two nickel-copper alloys. The sample is in the form of a rectangular paralelopiped; and strain gauges, mounted in each of the three orthogonal directions, are connected in series. Good thermal contact is made with the magnet and great care is exercised to permit the sample to return to thermal equilibrium. We find the volume magnetostriction in all three cases to be negative, confirming the pressure effects but in disagreement with the previous investigations. A possible source of the discrepancy may be the difficulty of returning to thermal equilibrium in a liquid dilatometer after magnetization.

* Supported by U. S. Office of Naval Research.

RA7. A Method for Measuring Magnetization and Susceptibility at Low Temperatures.* A. ARROTT,† *Carnegie Institute of Technology* (introduced by J. E. Goldman).—An apparatus is described for the measurement of magnetization at liquid

helium temperatures. A cylindrical sample is placed in a uniform field. A current is passed through a coil wound around the cylindrical surface of the sample and adjusted to restore the uniform B field. The current then measures the magnetization. The null is detected by moving the sample from within one detector coil to another connected in series opposition. The sensitivity of the apparatus permits measurements of volume susceptibility as small as $\sim 10^{-6}$ to a reasonable degree of accuracy. The heating of the null coil limits the range of applicability of the method to values of magnetization smaller than the order 10 emu. In addition to the obvious advantage of measuring in a uniform field, it is pointed out that the magnetization will be uniform inside a cylindrical sample because of the presence of the null coil. The restoration of the uniform B field eliminates image effects.

* Supported by U. S. Office of Naval Research.
† Allis-Chalmers Research Fellow.

RA8. Magnetic Susceptibility of Nickel-Copper and Nickel-Chromium Alloys.* J. E. GOLDMAN AND A. ARROTT, *Carnegie Institute of Technology.*—Extrapolation of the magnetic properties of nickel-copper and nickel-chromium alloys measured at high nickel concentrations, suggests that the spontaneous magnetization at 0°K should disappear at 60 percent copper and ~14 percent chromium, respectively. The nature of the magnetism in the alloys with higher concentration of the nonferromagnetic constituent is not clearly understood. We have made measurements of the magnetization down to 2°K on samples of alloys in this range of composition. We find the alloys containing 58 and 63 atomic percent copper in nickel to be ferromagnetic. The temperature dependence of this ferromagnetism has been studied. In the case of nickel-chromium alloys, the behavior is paramagnetic and the possibility of a ferrimagnetism or antiferromagnetism seems to be precluded. The results will be discussed on the basis of the collective electron treatment, the parasitic paramagnetism of Néel, and the role of possible concentration fluctuations within the material.

* Supported by U. S. Office of Naval Research and a grant from the Allis-Chalmers Manufacturing Company.

RA9. Hall Effect in Ferromagnetics. J. M. LUTTINGER, *University of Michigan.*—It is well known that the Hall effect in ferromagnetics shows a very anomalous behavior. This may be summarized by saying that an "effective field" $H_{eff} = H_0 + 4\pi M\alpha$ acts (H_0 external field, M magnetization), where α instead of being of the order of unity, varies from this value at very low temperatures to as much as several hundred at higher temperatures. A theory is proposed which gives a qualitative account of the magnitude and temperature dependence of α. This theory is based on the fact that electrons with their spins oriented will have, because of spin-orbit interaction, an extra right-left asymmetry in their wave functions. This asymmetry gives rise to a current perpendicular to an applied electric field, to the spin, and proportional to the degree of polarization of the electrons or to the magnetization of the sample. The predicted temperature dependence, based on rough estimates of the quantities involved, is as the resistivity (ρ) squared of the material. This is qualitatively what is observed in Fe and Ni, though the situation seems not quite so simple in ferromagnetic alloys. Using the known spin-orbit coupling, one can estimate the coefficient of ρ^3, and this, too, can be fitted to experiment without implausible assumptions about the electronic wave functions of ferromagnetics.

SATURDAY MORNING AT 9:45

Pupin 428

(F. N. FRENKIEL presiding)

Fluid Dynamics

Business Meeting of the Division of Fluid Dynamics

S1. Structure of the Vibration Pattern of Transverse Waves in Slow Circular Jets. R. L. WEGEL* AND H. C. RORDEN, *Bell Telephone Laboratories.*—A series of measurements were made on two circular air jets of the mean steady impact pressure distribution and of the accompanying fluctuating pressure caused by a simple single frequency sound source placed beside it at the nozzle. The test frequency was varied from 100 to 20 000 cycles per second. The steady pressure decreased with distance, at first slowly and then rapidly, spreading radially according to a law resembling diffusion. A transverse wave is transmitted along the jet with amplitude increasing to a distance of about six nozzle diameters and then decreasing. The phase velocity decreases slightly with distance and increases slowly with frequency, being always somewhat less than the local jet speed. The amplitude decreases with radial distance to a minimum just outside the nominal jet radius and then passes over a second maximum. The phase lags increasingly with radius to the minimum amplitude point where it reverses suddenly.

* Retired.

S2. On the Stability of Vortex Sheet in Inviscid Compressible Fluid. SHIH I. PAI, *University of Maryland.*—The stability of vortex sheet in inviscid compressible fluid with respect to two-dimensional small disturbance is investigated. A new simple criterion for complete stability of this case is found. The significance of "supersonic," "sonic," and "subsonic" disturbances is discussed. It is found that only the supersonic neutral stable disturbance with respect to the free stream gives continuous eigenvalues. The determinantal equation for "supersonic" damped or self-excited disturbance with respect to the free stream here may be reduced to the same simple form as those for other subsonic or sonic disturbance, and the eigenvalues so obtained are discrete.

S3. Diffraction of Step Shocks Through Double Slits. GEORGE A. COULTER AND JAMES ALLEN, *Aberdeen Proving Ground.*—An experiment, using a four and one-half inch shock tube, is described, showing the results obtained when a step shock wave is allowed to be diffracted by a wall with two one-eighth by one-eighth inch slits spaced one inch apart. The effects of the wall were made two dimensional by letting the length of the slits extend across the vertical diameter of the tube. Spark shadowgraphs of the resulting phenomena, after the shock wave has been diffracted through the slits, are shown. Measurements taken from shadowgraphs are presented

in graphical form for five different peak pressures incident upon the wall. These pressure values are the calculated shock pressures before diffraction. These graphs include a space-time plot of the motion of the cylindrical diffracted front as it progresses outwardly from the slit; a space plot of the "triple point" of the Mach interaction region between the diffracted wave fronts after "reflection" has occurred; and a space plot of the extreme points of the various vortices as they move away from the slits.

S4. A New Approach to the Theory of Turbulence in Gases. M. Z. VAN KRZYWOBLOCKI, *University of Illinois* (introduced by G. Plain).—The author discusses briefly the existing theories of turbulence like mixing-length theory, isotropic homogeneous, locally isotropic, etc. He points out that the existing theories of turbulence assume as the principle the turbulent fluctuations of the macroscopic properties of a gas. When we refer to the statistical mechanics, it is clear that its purpose is to derive all the macroscopic properties of matter from the microscopic properties of molecules; the term includes, according to recent practice, nonequilibrium as well as equilibrium states. Staring from this point of view the author presents a new approach to the theory of turbulence based upon the concept of the turbulent fluctuations of some microscopic properties of the gas molecules.

S5. An Unnecessary, Restrictive Concept in Turbulent Boundary Layer Theory.* DONALD ROSS, *The Pennsylvania State College.*†—The concept of the overlap of the inner and outer velocity functions of a turbulent boundary layer is often assumed in theoretical analyses. Although this concept is thought to be proved by the confirmation of the logarithmic velocity and friction laws, actually it is only a sufficient condition and not a necessary one. In analyses of nonequilibrium flows, it is a restrictive condition that has in the past led to erroneous conclusions. Even for the equilibrium profiles for which it was originally postulated, overlap is an unnecessary restriction. When it is eliminated, the von Kármán similarity theory is found to be in better agreement with measured flat-plate, boundary-layer profiles. Similar conclusions for pipe flow lend support to the contention that this is an unnecessary, restrictive concept that should be discarded.

* Work partially supported by the U. S. Office of Naval Research.
† Now at the Bell Telephone Laboratories.

S6. Isotropic Temperature Fluctuations in Isotropic Turbulence.* ALAN KISTLER, VIVIAN O'BRIEN, AND STANLEY CORRSIN, *The Johns Hopkins University.*—Preliminary measurements have been made with hot-wire anemometer in the flow behind a "hot grid." Temperature auto-correlation shows a reasonable degree of isotropy, and the relative decay rates agree fairly well with the isotropic relative decay equation, showing that the field and the measurement technique are suitable for more detailed studies.

* Work supported by the National Advisory Committee for Aeronautics.

S7. A Measure of the Area of a Homogeneous Random Surface in Space.* STANLEY CORRSIN, *The Johns Hopkins University.*—We are given an indefinitely large space containing random surface or surfaces homogeneously located in the mean. The problem is to relate the average area of surface per unit volume of space to a simpler statistical quantity, in particular the average number of cuts per unit length made by a straight randomly directed sampling line with the surface. The plane case is studied first. After the three-dimensional case, application is made to extending to two- and three-dimensional variables a theorem of S. O. Rice on the average occurence rate of any particular value of a one-dimensional random variable.

* Supported by the U. S. Office of Naval Research.

S8. The Design of Diffusers to Avoid Turbulent Boundary Layer Separation. FRANCIS H. CLAUSER, *The Johns Hopkins University.*—A recent experimental investigation* obtained information about the behavior of turbulent boundary layers in adverse pressure gradients which were so adjusted that the layers had similar velocity profiles throughout their length. The appropriate nondimensional pressure gradient parameters were also constant throughout the length of the layers. It was found, contrary to general belief, that the layers able to withstand the highest pressure gradients were not those having velocity profiles nearest those of separation profiles, but rather intermediate profiles having shapes not too far removed from constant pressure profiles. The information obtained is sufficient to permit the design of diffusers having shapes for maximum diffusion. Such diffusers can give unlimited amounts of diffusion without separation. The diffuser shapes are particularly easy to calculate if the free-stream velocity is considered to be constant across the channel. The resulting shapes are not straight sided, but expand most rapidly at first where the boundary layers are thin and less rapidly as the boundary layers grow. The expansion rates are greatly affected by the thickness of the boundary layer at the beginning of the expansion, a fact not usually taken into account in the design of diffusers for wind tunnels and the like. This work was supported by the U.S.A.F. under contract AF 33 (038)9862.

* Francis H. Clauser, "Turbulent boundary layers in adverse pressure gradients," Francis H. Clauser, J. Aeronaut. Sci. (to be published).

S9. On Triple Correlations in Isotropic Turbulence.* R. BETCHOV, *University of Maryland.*—In a turbulent flow, the three points-three velocities correlation functions form a tensor depending on the two displacement vectors A and B. This tensor can be developed in a double power series in A and B with coefficients defined at one point only. Assuming incompressibility and isotropy relative to rotations and reflexions about one point, we found that the coefficients of the cubic terms in A^3, AB^2, etc., are all proportional to the mean cube of the local acceleration, that is to the skewness coefficient. Investigations on the stability of such a turbulent flow for perturbations of moderately high-wave numbers lead to the eigenvalues of certain kinematic determinants. The mean values of these determinants are proportional to the skewness coefficient and this parameter appears therefore as an essential quantity. Experimental measurements in a turbulent flow behind a grid agree with various consequences of isotropy and confirm the relation between the skewness and the Reynolds number of the turbulence. Furthermore, we found that the mechanism responsible for the skewness coefficient is highly intermittent.

* This work is supported by the Office of Air Research and Development Command.

S10. The Hugoniot of Gases by Shock Wave Measurements. RUSSELL H. CHRISTIAN AND ROBERT G. SHREFFLER, *Los Alamos Scientific Laboratory.*—Equation of state data are derivable from the simultaneous measurement of the velocity of a plane shock front through a gas and the velocity of the plate that generates the shock. The present experimental method employs a high explosive lens system to accelerate the plate into the gas. Velocities are recorded by a high-speed moving image camera with precisions of the order of 0.5 percent. A series of such experiments determines the experimental shock velocity *vs* particle velocity curve for a given gas. Experimental data have been obtained for air, argon, helium, and nitrogen. The method permits measurements using shocks in the pressure region of approximately 200 to 1000 atmospheres. The lower limit is defined by the failure of the gas to become luminescent on reflection. The upper limit is determined by the maximum particle velocity attainable with high explosives. The Rankine-Hugoniot shock equations are

used to convert the experimental data to pressure-compression data which define the Hugoniot curve. A comparison is made to theoretical predictions.

S11. Statistical Uncertainties in the Radiographic Determination of Gas Densities. DOUGLAS VENABLE AND LEO F. PERRY, *Los Alamos Scientific Laboratory.*—The uncertainties in the measurement of gas densities by flash radiographic techniques arise from the statistical fluctuation of the quanta absorbed in the specimen, the inherent instrumental errors, and inadequate time resolution. For small numbers of useful quanta the statistics of absorption can constitute the predominating error term. The absorption statistical uncertainty in measuring densities in nitrogen and argon have been worked out for the continuous x-ray spectrum of tungsten as a function of peak energy and path length for the charge delivered to the x-ray source and for the useful solid angle subtended by the detector at the target. For purposes of this work the intensity distributions, determined experimentally by Ulrey[1] and Kuhlenkampff,[2] were employed. An experimental setup was made using a 25-kev thin-window, tungsten target x-ray tube with an appropriate absorption cell and scintillation detector. Absorption in the tube window and cell windows was unimportant for the path lengths covered, 10^{-2} to 2×10^{-1} g/cm² of nitrogen. The experimentally determined fractional error in density appears in good agreement with prediction when using a quantum efficiency coefficient of 1.1 $\times10^{-3}$ per volt.

[1] Ulrey, Phys. Rev. 11, 401 (1918).
[2] Kuhlenkampff, Ann. Physik. 69, 548 (1922).

S12. Observations of Taylor Instability in Gases. R. E. DUFF AND H. T. KNIGHT, *Los Alamos Scientific Laboratory.*—Taylor instability has been observed in the gaseous system of SF_6 and air by means of a schlieren optical system and an Eastman high-speed movie camera. The gases were subjected to gravitational acceleration only. An interface between the two gases was produced by withdrawing a thin steel slide that separated them in a cell 8 in. high×4 in. wide×1 in. deep. A pulling velocity 30 ft/sec could be used without introducing observable turbulence in the interface. The results obtained for initial rate of growth of instability as a function of wave number were in agreement with theory.[1] The spikes of heavy gas had rounded ends and moved slower in the late stages of development than predicted by theory.[2] Their amplitude grew approximately as $t^{1.4}$ instead of t^2. Under these conditions the instability region appears symmetrical about the original interface.

[1] Pennington, Princeton University Report, "Effects of surface tension and viscosity on Taylor instability" (1952).
[2] Carrier (private communication, 1953).

S13. Precision Measurement of Detonation and Strong Shock Velocity in Gases. HERBERT T. KNIGHT AND RUSSELL E. DUFF, *Los Alamos Scientific Laboratory.*—A system is described for determining detonation and strong shock velocity in gases by using the conductivity behind the wave.[1] Wave contact is made by two 36-mil wires set 0.1 inch apart in a Teflon plug mounted in the experimental tube. When a wave passes, signals are produced across a 30K resistor in series with these wires and a 0.001 μf. capacitor charged to 300 volts. Any number of circuits may be parallel across a single signal resistor if a diode is added to each circuit to prevent signal deterioration. The arrival time of a wave at a pin can be determined with an accuracy of almost 10^{-8} second from an oscilloscope record of the signals. A check of the system was made by measuring the velocity of five presumably identical detonations in a 40–60 acetylene-oxygen mixture. The total spread in velocity was 4.0 m/sec and the standard deviation was 1.3 m/sec. The principal advantages of this system are excellent space resolution and very simple basic circuitry.

[1] A crude application of this principle was reported after the beginning of this development by Resler, Lin, and Kantrowitz, J. Appl. Phys. 23, 1390 (1952).

S14. Shock Tube Experiments on Grid Flow. LESLIE S. G. KOVÁSZNAY AND DARSHAN DOSANJH, *The Johns Hopkins University.*—A traveling plane shock wave is partly reflected and partly transmitted when arriving at a grid. Associated flow phenomena have been studied in a shock tube both by optical techniques and by the hot-wire anemometer. The pressure drop coefficient of the grid has been inferred by measuring the speeds of both transmitted and reflected shock waves. The turbulent flow emerging from the grid offers a good possibility of studying shock-wave interactions with homogeneous turbulent flow.

SATURDAY MORNING AT 9:45

Schermerhorn 501

(GREGORY BREIT presiding)

Nucleonic Scattering

Contributed Papers

T1. Attenuation of 870-Mev Protons by Various Elements.* F. F. CHEN, C. P. LEAVITT, AND A. M. SHAPIRO, *Brookhaven National Laboratory.*—The total interaction cross sections of Be, C, Al, Cu, Sn, and Pb for 870-Mev protons have been measured using an external proton beam scattered from a target in a cosmotron straight section. The incident beam was collimated, magnetically analyzed, and then defined by three 2½-in. diameter scintillation counters in fast coincidence. The meson contamination was less than 1 percent. A 6-in. diameter counter measured the transmitted beam. Preliminary results for the attenuation cross section in a geometry of 8° subtended half-angle are, in barns: Be, 0.21; C, 0.25; Al, 0.45; Cu, 0.85; Sn, 1.3; Pb, 2.1. The statistical uncertainty was in most cases less than 5 percent. These cross sections are close to $\sigma_{\text{absorption}}$ in the sense of the optical model, with small corrections to be made for (a) the diffraction scattering tail, (b) multiple and single Coulomb scattering, and (c) charged products of interactions emitted in the forward direction. In order to determine these corrections, it was necessary to repeat the measurements in several geometries and with several absorber thicknesses. The same procedure in "good" geometries may permit a determination of the diffraction cross section. Comparison with the optical model will be discussed.

* This research was performed under the auspices of the U. S. Atomic Energy Commission.

T2. Elastic Scattering of 340-Mev Protons by Deuterons.* † DAVID D. CLARK‡§ AND OWEN CHAMBERLAIN, *University of California, Berkeley.*—The differential cross section has been measured at eight angles employing a coincidence system detecting both emergent particles. Elastic events were separated from inelastic events in which two fast protons emerged by identification of the deuterons by pulse heights from a counter telescope. Observed center-of-mass cross sections were: 30° (center-of-mass), 2.2 mb/sterad; 40°, 1.0; 50°, 0.39; 70°, 0.11; 90°, 0.047; 110°, 0.042; 130°, 0.044; 150°, 0.10. The total (statistical and systematic) errors varied from 15 to 20 percent. Comparisons with theory using impulse approximation methods of Chew[1] and Chamberlain and Stern[2] show fair agreement between theory and experiment and indicate that effects of interference between scatterings from the two centers of the deuteron are small.

* Work done under auspices of the U. S. Atomic Energy Commission.
† Based on Ph.D. thesis of one of us (D.D.C.) submitted to the Graduate Division, University of California, Berkeley.
‡ For a portion of the period of this research, U. S. Atomic Energy Commission Pre-Doctoral Fellow.
§ Now at Brookhaven National Laboratory.
[1] G. F. Chew, Phys. Rev. **84**, 1057 (1951).
[2] Chamberlain and Stern, (to be published).

T3. Proton-Alpha Scattering at 17.5 Mev.* KARL W. BROCKMAN, JR., *Princeton University.*—The differential cross section for the scattering of 17.5-Mev protons by helium has been measured. Particles were detected using a potassium iodide scintillation counter. The experiment was performed in Princeton's 60-inch precision scattering chamber. This apparatus permitted measurements at center-of-mass angles ranging from 6.4 to 168 degrees. Thirty-three angles in all were used. Counting statistics of 1.5 percent or better were obtained throughout. Other errors are estimated to be no greater than 0.5 percent except at the smallest angles where it was necessary to apply corrections amounting to several percent in the reduction of the data to the cross section. Work on the analysis of the data is in progress.

* This work was supported by the U. S. Atomic Energy Commission and The Higgins Scientific Trust Fund.

T4. The Elastic Scattering of 18.5-Mev Protons by Nuclei.* I. E. DAYTON AND P. C. GUGELOT, *Princeton University.*—The absolute differential cross section for the elastic scattering of 18.5-Mev protons has been measured for aluminum at 35 angles between 15 degrees and 172 degrees. The statistical error at each point is less than 3 percent. The protons are detected by a sodium iodide crystal with about 2.3 percent energy resolution. Protons to the lowest level in Al^{27}, which is at 0.845 Mev, are clearly resolved from the elastic group. The angular width of the counter is about one-third of a degree. The cross section shows a very sharp minimum at 44 degrees, with maxima at 62 degrees, 123 degrees, and apparently at 180 degrees. Calculations using the optical model[1,2] with a potential $V=(-45-21i)$ Mev follow the general trend of the data, but they completely fail to reproduce its detailed structure. Measurements on other elements are in progress and will be reported at the meeting.

* Supported by the Higgins Scientific Trust Fund and the U. S. Atomic Energy Commission.
[1] R. E. LeLevier and D. S. Saxon, Phys. Rev. **87**, 40 (1952).
[2] D. M. Chase and F. Rohrlich, Phys. Rev. (to be published).

T5. Scattering of 96-Mev Protons from Light Nuclei.* I. Energy Distribution. F. TITUS AND K. STRAUCH, *Harvard University.*—The 96-Mev external proton beam of the Harvard cyclotron is being used to investigate the elastic and inelastic scattering from light elements. Proton energy spectra have been observed at 40° with Li, Be, B, C, NaN_3, H_2O, NaF, and Na targets, using a range telescope. The over-all energy resolution of the system including the beam is about 3 Mev. The characteristic features of the proton spectra are: (1) an elastic peak; (2) inelastic peaks decreasing in height with decreasing energy; (3) an unresolved continuum increasing in height with decreasing energy. Although in some cases no corresponding level has been reported, in general the positions of the inelastic peaks correspond to known excited levels of the target nuclei. For example, peaks are observed from C at 4.3, 10.0, and 20.9 Mev (±1 Mev) below the elastic peak. With Li, a very sharp peak is seen at 4.8 Mev and less prominent peaks seem to exist at 15.8 Mev and 20.7 Mev below the elastic peak. With Al, only the elastic peak has been resolved.

* Assisted by the joint program of the U. S. Atomic Energy Commission and the U. S. Office of Naval Research.

T6. Scattering of 96-Mev Protons from Light Nuclei.* II. Angular Distribution. K. STRAUCH AND F. TITUS, *Harvard University.*—Energy spectra of protons scattered from C and Al targets have been measured at several angles from 22.5° to 70° with an angular resolution of 3.5° or less. The scattering cross section decreases rapidly with angle and in general, the higher the energy of the scattered protons the more rapid the decrease. For Al the elastic peak height decreases in amplitude by a factor of 200 from 22.5° to 60°. A diffraction minimum appears at about 30°. At the larger angles, separation between elastic and inelastic protons becomes difficult. For C the elastic and first inelastic peak height decrease by factors of 77 and 49, respectively, from 30° to 70°, with smaller decreases for the lower-energy peaks. The complete results suggest that the inelastic peaks are produced by single nucleon-nucleon collisions in the target nucleus.

* Assisted by the joint program of the U. S. Atomic Energy Commission and the U. S. Office of Naval Research.

T7. Elastic Scattering of 14-Mev Neutrons.* J. H. COON AND R. W. DAVIS, *Los Alamos Scientific Laboratory.*—Measurements of angular distributions for elastic scattering of 14-Mev neutrons were made in the angular range from 6° to 50°. A ring scattering geometry similar to that employed by Amaldi *et al.*[1] was used. The neutrons were detected by means of a small stilbene scintillation counter, pulses from which were fed into a multi-channel pulse-height analyzer. Elements investigated were C, Al, Cu, and Sn. Strong forward scattering was observed, the angular width of the forward peak decreasing with increase in nuclear radius. Integration of the observed differential cross-section curves indicate that for the above listed elements probably not more than 20 percent of the elastic scattering is through angles greater than 50°.

* Work performed under the auspices of the U. S. Atomic Energy Commission.
[1] Amaldi, Bocciarelli, Cacciapuoti, and Trabacchi, Nuovo cimento **3**, 203 (1946).

T8. Interpretation of Measurements of the Total Cross Sections for Nuclear Scattering of High-Energy Neutrons. T. B. TAYLOR, *Cornell University and Los Alamos Scientific Laboratory.*—It has been possible to get observed total neutron cross sections for various elements[1,2] for neutron energies between 60 and 400 Mev by using the nuclear model and method of calculation described by Fernbach, Serber, and Taylor.[3] The nuclear radii, the average nuclear potential V, and the mean free path for inelastic scattering of neutrons in nuclear matter K are obtained by making a "best fit" to the experimental data. V and K are allowed to depend upon the neutron energy. The nuclear radii turn out to be a nonlinear function of $A^{\frac{1}{3}}$, and are equal to $1.55A^{\frac{1}{3}}$ for light elements (Carbon) and $1.35A^{\frac{1}{3}}$ for heavy elements (Lead). The nuclear radii obtained from this analysis will be compared with those obtained by other methods. Possible connections between K and V and the free nucleon-nucleon interactions will be discussed.

[1] A. E. Taylor and E. Wood, Phil. Mag. **44**, 95 (1953).
[2] V. Alexander Nedzel, Phys. Rev. **91**, 440 (1953).
[3] Fernbach, Serber, and Taylor, Phys. Rev. **75**, 1352 (1949).

T9. Angular Distribution of Neutrons Scattered from Cadmium, Tin, and Bismuth.* S. C. SNOWDON AND W. D. WHITEHEAD,† *Bartol Research Foundation.*—The differential cross sections for the scattering of 3.7-Mev neutrons from cadmium, tin, and bismuth have been measured over an angular range between 13 degrees and 140 degrees with an angular resolution of about ±10 degrees. The effects due to higher-order scattering have been removed at each measured angle by extrapolation of the observed differential cross section to zero thickness scatterer. A possible explanation of the results in light of the continuum theory of nuclear reactions will be given.

* Assisted by the joint program of the U. S. Office of Naval Research and the U. S. Atomic Energy Commission.
† Present address, North Carolina State College, Raleigh, North Carolina.

T10. Angular Distributions of 0.2–1.5 Mev Neutrons Elastically Scattered by Light Nuclei. H. B. WILLARD, J. K. BAIR, AND J. D. KINGTON, *Oak Ridge National Laboratory.*—Neutrons produced in the forward direction by the $Li^7(p,n)Be^7$ reaction were scattered elastically by cylindrical samples of lithium, beryllium, boron, and carbon. Samples were chosen to give a transmission of greater than 70 percent in order to keep multiple scattering to a minimum. Angular distributions were measured with a proton recoil counter shielded from the primary beam by a paraffin wedge. The bias was set to approximate a flat response from the incident neutron energy down to 0.6 this value, so that no correction was necessary for the variation of the scattered neutron energy with laboratory angle. Backgrounds were of the order of 50 percent. The resonances at 0.26 Mev in Li^7, 0.62 Mev in Be^9, and 1.28 Mev in B^{11} are of the form $B_0+B_2P_2(\cos\theta)$ in the center-of-mass system, whereas the resonance at 0.43 Mev in B^{11} is nonsymmetrical about 90° indicating interference. Nonresonant scattering at 0.5 Mev in Li^7, Be^9, B^{10}, and C^{12} is nearly isotropic. At 1.5 Mev B^{10} has strong forward scattering, while C^{12} remains nearly isotropic. Spin and parity assignments to the levels studied have been tentatively made.

T11. Attenuation of 14.1-Mev Neutrons in Water.* R. S. CASWELL, R. F. GABBARD, W. P. DOERING, AND D. W. PADGETT, *National Bureau of Standards.*—The attenuation of 14.1-Mev neutrons in water has been studied under conditions simulating an isotropic point source of monoenergetic neutrons in an infinite water medium. The neutrons were produced by the $H^3(d,n)He^4$ reaction, the deuteron beam from the accelerator striking a tritium-zirconium target located in a large water tank. Thermal neutron flux was measured as a function of distance from the target over the range 5 cm–125 cm with indium foils and a B^{10}-lined counter using the cadmium difference method. The mean square distance for slowing down of 14.1-Mev neutrons to the thermal energies was found to be 980 cm^2. Although the attenuation is not (and should not be) strictly exponential at large distances, over the range 40–125 cm the curve may be approximated by an exponential of attenuation length 14.5 cm. Resonance neutron flux (1.44 ev) was measured with indium foils covered with cadmium. Fast neutron dose measurements were made using a polyethylene-ethylene proportional counter[1] calibrated at 2.5 Mev and 14 Mev with measured fluxes of monoenergetic neutrons. Experimental results are in reasonable agreement with theoretical calculations.[2]

* This research was supported by the U. S. Atomic Energy Commission.
[1] G. S. Hurst and R. H. Ritchie, Radiology **60**, 864 (1953).
[2] H. Goldstein, (private communication).

Invited Paper

T12. Neutron-Proton Scattering Cross Sections at High Energies. W. M. POWELL, *University of California, Berkeley.* (30 min.)

SATURDAY MORNING AT 9:45

Casa Italiana, 1161 Amsterdam Avenue

(M. L. GOLDBERGER presiding)

Theoretical Physics, III

U1. Possible Angular Correlations Involving *V* Particles.* L. WOLFENSTEIN, *Carnegie Institute of Technology.*—It has been suggested by several authors that V_1 particles may have spin greater than $\frac{1}{2}$. It has also been suggested that the spin might be detected from observations on angular correlations of the decay products. In the rest system of the V_1 the decay is necessarily isotropic if the spin is $\frac{1}{2}$. Calculations have been made of the angular correlation between the direction of the decay products in the rest system of the V and the direction of the incident meson for the reaction $\pi^-+p\rightarrow V_1^0+X$ near the threshold where the V_1^0 and X may be assumed to emerge in an s state. If particle X has zero spin, the correlation is completely determined by the spin of the V_1 and is independent of the parity of either X or the V_1. For all spins greater than $\frac{1}{2}$, the direction of the decay products tends to be parallel to the incident meson direction; the correlation, for example, is $(3\cos^2\theta+1)$ for spin $\frac{3}{2}$. Other cases will be discussed.

* Aided in part by U. S. Office of Ordinance Research.

U2. On Relativistic Wave Equations.* HERMAN FESHBACH, *M.I.T.*—The Bhabha form of these equations are considered:

$$(\beta_\mu\partial_\mu+\kappa)\psi=0.$$

A method for generating possible forms for β_μ is developed which requires only knowledge of the sixteen Dirac operators γ_A. A simple procedure for reducing the resultant equations to a reducible form exists, the final equations being expressed in terms of vectors, scalars for the spin 1 equation, spinors, "spinor vectors," and "spinor tensors" for the spin $\frac{3}{2}$ equation, etc. The spin 1 and $\frac{3}{2}$ case have been studied, and the appropriate forms for β_μ, which lead to the Rarita Schwinger form of the $\frac{3}{2}$ spin equation and to a multiple mass equation similar to that developed by Bhabha, have been determined.

* This work was supported in part by the joint program of the U. S. Office on Naval Research and the U. S. Atomic Energy Commission.

U3. Two Extensions of the Foldy-Wouthuysen Transformation. K. M. CASE, *University of Michigan.*—A transformation of spin 0 and 1 wave equations, similar to that given by Foldy

and Wouthuysen[1] for spin ½ has been obtained. For the field-free equations, all the simplifications of interpretation found by these authors persist. Indeed, the Hamiltonian, velocity, and angular momentum operators all have precisely the same form for the three theories with the implicit inclusion of a unit $2S+1$ dimensional matrix. It is indicated that all wave equations of the Dirac-Pauli-Fierz form can be transformed in just this way. The nonrelativistic approximation in the presence of external fields is also readily obtained. A simple explanation of the vanishing of terms proportional to $1/m^2$ in the spin one nonrelativistic Hamiltonian can be given. It was also found that for spin ½ the F–W transformation can be carried out explicitly for an arbitrary time independent magnetic field. The transformed Hamiltonian is shown to be particularly suitable for discussing various properties of a Dirac particle in such a field.

[1] L. L. Foldy and S. A. Wouthuysen, Phys. Rev. **78**, 29 (1950).

U4. A New Approach to the Classical and Quantum Theory of Many Interacting Particles. I. GEORGE J. YEVICK,* *Stevens Institute of Technology*, AND JEROME K. PERCUS, *Columbia University*.—The fundamental idea is the following: We propose to solve the dynamical problem of many interacting particles by replacing the original system by an equivalent formulation. The motion of a collection of $3n$ bounded, one-dimensional harmonic oscillators q_k (k is an index referring to the wave number of the oscillation), whose fictitious masses f_k and frequencies ω_k are at our disposal, has an intimate bearing upon the dynamical behavior of n bodies. This intimate connection is afforded by the collective coordinates $\Sigma_i \exp(ik\cdot x_i)$ first extensively developed by Bohm and Pines for long-range forces. Their method is intrinsically incapable of describing short-range forces. Our q_k are simply the collective coordinates. If one substitutes the q_k into the Lagrangian for a set of fictitious oscillators, one immediately obtains an expression containing a term which is the kinetic energy of the real particles, another term which may be interpreted as the potential energy and finally an additional unwanted term which can be considered as a velocity dependent potential. It is this last term which must be minimized by an appropriate choice of the fictitious masses and frequencies of the oscillators.

* Supported in part by the National Research Council of Brazil during the summer of 1953, at the University of Sao Paulo, Sao Paulo, Brazil.

U5. A New Approach to the Classical and Quantum Theory of Many Interacting Particles. II. JEROME K. PERCUS, *Columbia University*, AND GEORGE J. YEVICK,* *Stevens Institute of Technology*.—We continue the discussion of the novel problems arising classically as well as quantum mechanically. Careful consideration must be given to a suitable selection of the Fourier coefficients representing the short-range potential inasmuch as only $3n$ Fourier terms are available. Moreover, one must reflect on the nature of the use of completely symmetric coordinates in dynamical theory. The collective coordinates are such that their domain of action is limited by the basic properties of the transformation. As regards the quantum-mechanical problem, new features are encountered: lack of uniqueness for the transition from the classical to the quantum-mechanical description; necessity for obtaining Fermi-Dirac or Einstein-Bose statistics using symmetric collective coordinates. The harmonic oscillators differ from those ordinarily met with in two respects; they are severely bounded in a manner depending upon f_k, ω_k, and q_k, and furthermore, both attractive and repulsive "elastic constants" prevail which appear to be essential to bring about crystallization. The only way to obtain the eigenfunctions and eigenvalues for the bounded oscillators is by means of perturbation methods. Finally, calculations are in progress for the evaluation of both the classical and quantum-mechanical partition functions.

* Supported in part by the National Research Council of Brazil during the summer of 1953, at the University of Sao Paulo, Sao Paulo, Brazil.

U6. Distortion of the Nucleus in μ-Mesic Atoms.* W. LAKIN AND W. KOHN, *Carnegie Institute of Technology*.—The ground-state energy of a mesic atom is lowered as a result of distortion of the nucleus by the meson. This energy shift, ΔE, was estimated by Cooper and Henley[1] for $Z=82$ as about 58 kev. We have calculated ΔE using in part empirical nuclear properties and find $\Delta E=16\pm 8$ kev for $Z=80$ (ΔE varies slowly with Z). The remaining uncertainty in ΔE is very small; it corresponds to an uncertainty of only 0.2 percent in the nuclear radius and presents no serious obstacle to the determination of more detailed features of the nuclear charge distribution. The contribution to ΔE arising from virtual dipole transitions was calculated using the collective model of Jensen and Steinwedel.[2] The result, 7 kev, is much smaller than an estimate of 28 kev obtained by sum rules with neglect of correlation of the protons.

* Supported in part by the U. S. Office of Ordinance Research.
[1] L. Cooper and E. Henley, Phys. Rev. (to be published).
[2] H. Steinwedel and J. Jensen, Z. Naturfarsh. **5a**, 413 (1950).

U7. The Lamb Shift in Mesic Atoms. H. C. CORBEN, *Carnegie Institute of Technology*.—Of the two radioactive corrections to the energy of a charged particle bound in an electrostatic field, the self-energy correction for a given unperturbed particle wave function is approximately inversely proportional to the square of the mass of the particle, whilst the vacuum polarization due to the field is approximately inversely proportional to the square of the mass of the electron. In contrast to the situation in ordinary atoms, the Lamb shift in mesic atoms therefore arises chiefly from vacuum polarization. The energy levels, especially those of S states, are thus depressed by this effect and if it is neglected the radius of the nuclear proton distribution, computed from the observed transitions to S states, is underestimated. Due to the smaller size of the mesic atom the effect is very much greater than in ordinary atoms. Even for a point nucleus, however, the percentage depression in the energy of an S state is approximately only $0.71\ \log_{10}(aZ/n^2)$ for $Z\gg n^2$, with $a=1$, 0.77 for π and μ mesons, respectively. With present experimental techniques the effect is therefore barely observable. In future more refined comparisons between nuclear force and electromagnetic measurements of nuclear radii it will be necessary to take it into account.

U8. Nuclear Charge Distribution. DAVID L. HILL, *Los Alamos Scientific Laboratory and Vanderbilt University* AND KENNETH W. FORD, *Los Alamos Scientific Laboratory and Indiana University*.—Mu-mesic x-rays, fast electron scattering, electronic x-rays, and electronic isotope shifts each depend on the nuclear charge distribution $\rho(\mathbf{r})$ in quite different ways. Adjoining theoretical analyses of observations on these different phenomena may therefore bracket an acceptable set of functional descriptions for $\rho(\mathbf{r})$. For several functional families representing conceivable forms for $\rho(\mathbf{r})$ we have obtained the resultant Coulomb potentials and have solved "exactly" by electronic computation the relativistic equations to yield the first four levels and transition energies for mu mesons bound in the field of the lead nucleus. These results permit adjustment of the effective nuclear radius R, for each form of $\rho(\mathbf{r})$ to agree with known x-ray measurements. Calculations completed for neighboring values of R will permit interpolation to improved values when corrections of the raw data for electrodynamic and special coupling effects are ultimately made. The second part of the program reported comprises the calculation by the exact phase-shift method of the angular dependence of fast electron scattering upon the different forms for $\rho(\mathbf{r})$, employing for each form the determined effective radius. Comparison of the model predictions with known observations, and looking apart from possibly small radiative and dynamic corrections, yields an indication of the charge distribution.

U9. Radiative Corrections to Electron Scattering. ROGER G. NEWTON,* *The Institute for Advanced Study.*—The second-order one-photon mass operator[1] has been applied to the calculation of the lowest-order radiative corrections to the second Born approximation[2] in the scattering of electrons by nuclei. The complete result, for a point source, is too complicated to be of practical value. The corrections are asymptotically (at high energies) proportional to the square of the logarithm of the energy. At about 100 Mev and for $\vartheta = 90°$, the leading term is several times larger than the uncorrected second Born approximation, but there may be cancellations with the next terms currently being calculated. Modifications (of the correction) due to the finite nuclear extension are probably small at energies of about 100 Mev, but they prevent it from diverging as the energy tends to infinity.

* Frank B. Jewett Fellow.
[1] R. G. Newton, (to be published).
[2] W. A. McKinley and H. Feshbach, Phys. Rev. **74**, 1759 (1948).

U10. High-Energy Events. JOSEPH V. LEPORE, MAURICE NEUMAN, AND RICHARD N. STUART, *University of California, Berkeley.*—The relative probabilities for alternate processes initiated by a nucleon-nucleon collision depend on the dynamics involved and on the volume in phase space accessible to each final state. According to arguments advanced by Fermi[1] the latter aspect alone may be of decisive importance when the energy of the colliding nucleons is very high. The assignment of relative *a priori* probabilities to the final states proportional to their extension in phase must be consistent with the translational, rotational, and Lorentz invariant properties of the colliding system. The latter in particular implies a conservation law for the center of energy $\Sigma(E_i r_i/C^2)$. Its effect is not only to lower the power of the configurational volume by one dimension but also to severely reduce the contributions from high momenta to the phase space integrals. The limitations on accessibility arising from the controllable constants of motion are not sufficient to insure well-defined probabilities. Some additional restriction on the configurational part of the phase space must be imposed. A cut-off factor of the form $\exp-[E_i^2 x_i^2/\hbar^2 C^2]$ for *each* particle is accordingly introduced. The configurational volume accessible to the particle thus decreases with increasing energy, a picture not inconsistent with the uncertainty principle. Some numerical results of this investigation will be presented.

[1] E. Fermi, Prog. Theoret. Phys. **5**, 4, 570 (1950).

U11. Restrictions on Invariant Transformation Groups in the Lagrangian and Hamiltonian Formalisms.* PETER G. BERGMANN, *Syracuse University.*—It is well known that quantum electrodynamics may be developed in several alternative forms, depending in part on the gauge transformation group with respect to which the theory is to be invariant. More generally, whenever a given theory is invariant with respect to a choice of representation or frame that depends on one or several arbitrary functions of space and time coordinates, such as the full gauge group, curvilinear coordinate transformations, and the like; it is possible to restrict the choice of frame by convenient conditions, known in relativity as coordinate conditions. In this paper it will be shown how under such a restriction, be it mild or be it so severe as to eliminate some of the original field variables, the conservation laws typical of invariant theories are preserved. In the Hamiltonian formalism we shall show how the constraints (the subsidiary conditions), which under the full group represent the extent of invariance, are modified and, under certain circumstances, partly eliminated.

* Supported by the U. S. Office of Naval Research.

SATURDAY AFTERNOON AT 1:45

Pupin 428

(J. H. VAN VLECK presiding)

Microwave Spectroscopy

V1. Microwave Spectrum of Methyl Amine.* DAVID R. LIDE, JR., *Harvard University.*—The absorption spectrum of methyl amine in the microwave region is complicated by the possibility of low-frequency internal motions in the molecule. In addition to hindered internal rotation about the C−N bond, such as occurs in methyl alcohol, an inversion of the type found in ammonia can take place. Thus a transition will generally involve changes in the torsional oscillation and inversion states as well as the change in over-all molecular rotation. The spectrum of methyl amine in the 15 000 to 35 000 mc region is currently being studied at Harvard[1] and at the University of Tokyo.[2] Some two hundred lines have so far been measured. Many of these lines fall into several well-defined series, which have been shown to correspond to $\Delta J = 0$ transitions in which the series members take on successive J values. In addition, several $\Delta J = \pm 1$ lines have been identified by means of the Stark effect. The assignments for these various lines will be discussed.

* Research supported by the U. S. Office of Naval Research.
[1] D. R. Lide, J. Chem. Phys. **20**, 1812 (1952); **21**, 571 (1953).
[2] Shimoda, Nishikawa, and Itoh, J. Phys. Soc. Japan **8**, 133, 425 (1953).

V2. The Microwave Spectrum of Ethyl Fluoride.* J. KRAITCHMAN† AND B. P. DAILEY, *Columbia University.*—A study of the microwave spectrum of ethyl fluoride has been undertaken because of its relevance to a number of problems of general interest. In particular, because of the possibility of hindered rotation about the C−C bond, analysis of the spectrum provides information pertaining to the magnitude of the potential barrier to such internal motions. While CH_3CH_2F is an asymmetric rotor its small asymmetry ($\kappa = -92$) and the absence of quadrupole hyperfine structure reduce the spectral complexity considerably. The spectrum was examined in the region from 17 to 38 kMc. The three rotational constants of the molecule were evaluated from analyses of the observed transition. By means of relative intensity measurements of rotational transitions in excited vibrational states the identification of a low-lying Raman frequency[1] as the torsional fundamental has been confirmed. This information plus a set of structural parameters obtained from the rotational constants of the molecule have allowed the hindering barrier height to be evaluated. The molecular dipole moment and its orientation in the molecule have also been determined.

* Work assisted by the U. S. Army Signal Corps and the Research Corporation.
† Present address: Westinghouse Research Laboratories, East Pittsburgh, Pennsylvania.
[1] Smith, Saunders, Nielsen, and Ferguson, J. Chem. Phys. **20**, 847 (1952).

V3. The Microwave Spectrum of 1,1 Difluoroethane.* N. SOLIMENE AND B. P. DAILEY, *Columbia University.*—The spectrum of 1,1 difluoroethane has been investigated over the region 18 000 Mc to 38 000 Mc with a conventional Stark-modulation spectrometer. This molecule is a moderately asymmetric rotor of the oblate type with components of its dipole moment along the A and C axes. About 30 lines have been identified with the aid of the Stark effect and an approximate model for the molecule. The analysis yields the following rotational constants: $A=9491.95$ Mc; $B=8962.65$ Mc; $C=5170.43$ Mc; $H=0.75504$. These fit the observed frequencies to better than 0.5 Mc for transitions involving $J\mp3$. For higher J's the observed frequencies are fitted to within 5 Mc in most cases. The barrier hindering internal rotation has been determined as $(1.3\pm0.2)\times10^{9}$ cm^{-1} from intensity ratio measurements of the torsional frequency. The presence of an internal rotation hindered by a barrier of this magnitude apparently introduces no observable complications into the spectrum.

* Assisted by the U. S. Army Signal Corps and the Research Corporation.

V4. Hyperfine Structure in DCC, Cl, DCN, and HCN due to Deuteron Quadrupole Coupling and Field Asymmetries.* ROBERT L. WHITE, *Columbia University.*—The spectrum arising from the $J=1\rightarrow2$ transition in deuterated chloroacetylene has been observed in a high-resolution spectrometer and hyperfine structure due to the quadrupole coupling of the deuteron detected. A value for the coupling of $(eqQ)_D=+175\pm20$ Kc/sec was obtained, to be compared with -114 ± 1 Kc in HD obtained by molecular beam methods. The deuteron quadrupole coupling was also observed in transitions between 1-type doublets in DCN where an unresolved hyperfine structure resulted in line broadening. Comparison with unbroadened lines from HCN gave the less accurate but consonant evaluation $(eqQ)_D=\pm145\pm60$ kc/sec. Since the deuteron quadrupole moment is known, $(eqQ)_D$ yields an experimental value of the field gradient. The value thus obtained was compared with the gradient calculated from a Heitler London molecular model. The calculated value was too large and of the wrong sign, indicating the inadequacy of the model for this calculation. Asymmetry in the quadrupole coupling of N^{14} in the 1-type doublet transitions of HCN and DCN also produced hyperfine structure. From this structure, variations in the C−N bond due to bending can be detected.

* Work supported jointly by U. S. Army Signal Corps, U. S. Office of Naval Research, and the U. S. Air Research and Development Command.

V5. The Spin and Quadrupole Moment of Se^{75}.* L. C. AAMODT, P. C. FLETCHER, G. SILVEY, AND C. H. TOWNES, *Columbia University.*—The spin and nuclear quadrupole moment of radioactive Se^{75} have been determined from the microwave spectrum of $OCSe^{75}$. The Se^{75} was produced by the reaction $As^{75}(d,2n)Se^{75}$ using 22-Mev deuterons from the Brookhaven National Laboratory's cyclotron. The presence and abundance of Se^{75} in OCSe was determined by observing characteristic γ rays of this nucleus. Three lines of the quadrupole hyperfine structure of the $J=2\rightarrow3$ transition of $OCSe^{75}$ were observed. Their measured frequencies, relative intensities, and Stark patterns agree with a spin of 5/2 for Se^{75} and a quadrupole coupling constant of 946 Mc. This spin is not consistent with predictions from the single particle version of the shell model. The quadrupole coupling constant indicates the large positive quadrupole moment of 0.9×10^{-24} cm^2 for Se^{75}.

* Work supported by the U. S. Atomic Energy Commission.

V6. The Microwave Spectrum of ReO_3F.† J. F. LOTSPEICH AND ALI JAVAN, *Columbia Radiation Laboratory,* AND ALFRED ENGELBRECHT, *Temple University.*—The microwave absorption spectrum of ReO_3F has been observed for the rotational transitions $2\rightarrow3$ and $3\rightarrow4$. In addition to the lines originating from the ground vibrational state, a number of degenerate and nondegenerate excited vibrational state lines were found from which were obtained the vibrational and 1-type doubling constants. The quadrupole hyperfine structure due to Re was resolved. The following quantities have been calculated: $B_0=3566.751\pm0.050$ Mc; $eqQ_{Re}=-53\pm4$ Mc. The isotopic change of B_0 and of eqQ due to the two Re isotopes 185 and 187 is within the quoted errors. The 1-type doubling constants of two of the three degenerate vibration modes were found to be 4.82 and 16.35 Mc; their corresponding α_r values are $+2.64$ and -10.5 Mc, respectively. A value of α_r for a nondegenerate mode was measured as $+12.4$ Mc.

† Work supported by the U. S. Atomic Energy Commission.

V7. Microwave Spectrum of the Free OD Radical. G. C. DOUSMANIS, *Columbia University.*—A microwave spectrum resulting from the free $O^{16}D$ radical has been found with a Zeeman spectrometer similar to the one with which the OH spectrum had been observed.[1] The lines are due to transitions between the two members of the doublet resulting from the Λ-type splitting of each J-level in the ground paramagnetic state of the radical. The observed frequencies and their assignments are as follows:

K	J	Frequency (Megacycles)
5	$5\frac{1}{2}$	8 672.36±0.10
6	$6\frac{1}{2}$	12 918.01
7	$7\frac{1}{2}$	18 009.60
8	$8\frac{1}{2}$	23 907.12

The parameters describing the Λ-type doubling have been obtained as $4\Sigma(-1)^{J}(\Pi|ALy+2BLy|\Sigma)(\Sigma|BLy|\Pi)/V_{\Pi\Sigma}=2096\pm16$ Mc and $4\Sigma(-1)^{J}|(\Pi|BLy|\Sigma)|^2/V_{\Pi\Sigma}=-149.3\pm0.4$ Mc. These are in agreement with the values found in OH. The magnetic hyperfine structure in OD, in contrast to that in OH, is too small to be resolved (<3 Mc for $K=8$). This gives some information about the source of hyperfine structure in OH and OD.

* Work supported by the U. S. Army Signal Corps, the Office of Naval Research and the U. S. Air Force Research and Development Command.
[1] Sanders, Schawlow, Dousmanis, and Townes, Phys. Rev. **89**, 1158 (1953).

V8. Theory of the hfs of NO Molecule. MASATAKA MIZUSHIMA, *Duke University.*—The recent experimental results of Gordy and Burrus[1] on the $J=\frac{1}{2}\rightarrow\frac{3}{2}$ lines of NO molecule in $^2\Pi_{\frac{1}{2}}$ state are explained satisfactorily. The formula $P[F(F+1)-J(J+1)-I(I+1)]+R[(3/4)C(C+1)-J(J+1)I(I+1)]$ was used with values of the constants as follows (in Mc):

J	1/2		3/2	
Λ doublet	c	d	c	d
P	−6.66	68.39	−8.61	21.40
R	0	0	0.77	0.035

Frosch and Foley's formula,[2] $P=a\pm b(2J+1)$, where the double sign corresponds to Λ-type doublet was found to be obeyed well. The ratio b/a is predicted by assuming a pure p state for the rotating electron to be 0.5, while the observed value gives 0.6. In $J=\frac{3}{2}$ state the $^2\Pi_{\frac{1}{2}}$ state contribute $+0.22$ Mc to P for both c and d states. The pseudo-quadrupole effect is found to be negligible. A new formula for the nuclear electric quadrupole effect was derived from which $eQ(\partial^2V/\partial z^2)$ was found to be -2.12 Mc. Another coupling constant was found from the difference of R between c and d states, and was explained by the p-electron approximation.

[1] W. Gordy and C. A. Burrus, Phys. Rev. (to be published).
[2] R. A. Frosch and H. M. Foley, Phys. Rev. **88**, 1337 (1952).

Post-Deadline Papers, If Any

SATURDAY AFTERNOON AT 1:45

Horace Mann

(D. ALPERT presiding)

Symposium of the Division of Electron Physics

Oxide-Coated Cathodes

W1. Review of Electronic Processes in BaO Crystals. R. L. SPROULL, *Cornell University.* (30 min.)

W2. The Conduction Mechanism in Oxide-Coated Cathodes. E. B. HENSLEY, *University of Missouri.* (30 min.)

W3. Review of Interface Compound Formation in Oxide Cathodes. E. S. RITTNER, *Philips Laboratories.* (30 min.)

W4. Noise Mechanisms in Oxide-Coated Cathodes. A. VAN DER ZIEL, *University of Minnesota.* (30 min.)

Business Meeting of the Division of Electron Physics

SATURDAY AFTERNOON AT 1:45

Pupin 301

(ENRICO FERMI presiding)

Neutron Physics

Invited Paper

WA1. Low-Energy Neutron Spectroscopy. W. W. HAVENS, JR., *Columbia University.* (30 min.)

Contributed Papers

WA2. Calculation of the Effect of Finite Resolution on the Neutron Transmission Near Resonance. E. MELKONIAN AND W. W. HAVENS, JR., *Columbia University.**—The effect of a triangular resolution function on the neutron transmission near resonance based on the Breit-Wigner formula with $\Gamma \ll E_0$ has been calculated analytically for the range of values of $n\sigma_0$ from 0 to 10 and resolution widths from 0 to 10 times the natural width of the level. An experimental transmission curve can be compared with this set of calculated curves to obtain approximate values of the level parameters. These calculations also give a relationship between σ_0 and Γ from the observed peak cross section, which can then be solved simultaneously with another relation between these parameters obtained by use of the area method.[1] Various relationships of interest, such as that between the maximum measured cross section and the sample thickness, with a given resolution, can also be obtained directly from these curves. These results are applicable only when the Doppler effect is small.

* This work partially supported by the U. S. Atomic Energy Commission.
[1] Melkonian, Havens, and Rainwater, Phys. Rev. 92, 702, 1953.

WA3. Tellurium Resonance Scattering.* H. L. FOOTE, JR.,† *Brookhaven National Laboratory.*—Scattering and total cross-section curves *versus* energy for the 2.33-ev resonance of tellurium have been observed. The scattering pipe technique of Borst[1] was used for the scattering measurements with a thin sample. The experimental data have been fitted to the one-level Breit-Wigner formula obtaining the following parameters: $E_0=2.33$ ev, $\sigma_p=4.61$ barns, $\sigma_0=668$ barns, $g=\frac{1}{4}(I=1)$, $\Gamma=0.114$ ev, and $\Gamma_n=0.0104$ ev. The method of analysis will be described which takes into account energy loss on scattering, Doppler broadening, instrument resolution, and the effect of sample thickness.

* Research performed under the auspices of the U. S. Atomic Energy Commission.
† Doctoral candidate from the University of Utah.
[1] L. B. Borst, Phys. Rev. 90, 859 (1953).

WA4. Neutron Scattering by Rotators. A. C. ZEMACH AND R. J. GLAUBER, *Harvard University.*—Neutrons colliding with molecules at diffraction energies may exchange noticeable portions of their energy with molecular rotational modes. The difficulty in treating this inelasticity has been that for all save the lightest gases the collisions induce transitions between large numbers of angular momentum states. In the present work operator methods have been employed to find simple approximations for the required summations. For $\lambda/2\pi$ smaller than molecular dimensions, separate treatments are given for scattering at small and at large angles. Some of the features of the problem are illustrated by a model in which the scatterer is simply a mass point constrained to move on a sphere. The angle-dependent energy spectrum of the scattered particles may be easily found and integrated over energies. The resulting differential cross section decreases with increasing scattering angle. At large angles the cross section is less than the isotropic result obtained in the elastic approximation. The relative difference is of order m/M, the ratio of neutron mass to scatterer mass. Additional effects due to interference of scattering by different centers in an actual molecule are being treated by the same methods. The results will be discussed in relation to experimental work on neutron scattering by gases.

WA5. Gamma Rays Excited by the Inelastic Scattering of Fast Neutrons in Bismuth, Nickel, and Copper.* M. A. ROTHMAN, H. S. HANS,† AND C. E. MANDEVILLE, *Bartol Research Foundation.*—Monochromatic neutrons of energy 3.8 Mev have been scattered in bismuth, nickel and copper. In NaI—Tl, gamma rays have been detected which are emitted in the inelastic scattering process. For bismuth the quantum energies are 0.91, 1.63, 2.60, and 3.35 Mev; for nickel 0.90 (?) and 1.36 Mev; for copper, ~0.9 Mev. Some additional data will be presented concerning zirconium and wolfram.

* Assisted by the joint program of the U. S. Office of Naval Research and the U. S. Atomic Energy Commission.
† Fulbright Fellow, on leave of absence from the University of Aligarh, India.

WA6. Neutron Yields from $D-D$ Reaction in Various Target Materials.* R. C. CAMPBELL, J. D. KORSMEYER, AND D. C. RALPH, *Louisiana State University.*—The use of a Mobley magnet for producing short intense deuteron pulses, requires stopping beam on a baffle during the major part of each cycle. To determine the magnitude of neutron background arising from deuterium retained in such baffles, an investigation has been made of the neutron yields resulting from 100-kev deuterons incident on a number of materials. Tantalum, molybdenum, copper, aluminum, steel and graphite if maintained at room temperature show neutron yields which increase with time and reach saturation after a bombardment of the order of one coulomb/cm² of deuterons. Observed neutron yields range from 0.03 to 0.5 of that obtained from a thick heavy ice target. Self targets formed in this manner show no observable decay in twenty-four hours. All materials except graphite showed decreased neutron yields when run at higher temperatures. Tantalum and molybdenum run at about 800°C gave neutron yields less than 0.001 of that obtained from a thick heavy ice target. These metals are being further studied to determine optimum temperatures for the purpose of reducing neutron background from such baffles.

* Assisted by a grant from the Research Corporation.

WA7. Gamma-Gamma Coincidences from Interaction of 3.1 Mev Neutrons with Various Materials. V. E. SCHERRER, B. A. ALLISON, AND W. R. FAUST, *Naval Research Laboratory.*—Experiments have been performed to observe gamma radiation produced by bombardment of various materials with 3.1-Mev neutrons from the $D(d,n)He^3$ reaction. Coincidences between two gamma-ray detectors were used to trigger a twenty-channel pulse-height analyzer. Pulses from one detector were selected such that they corresponded to a single strong line, while the other detector recorded the complete spectrum on the analyzer. Gamma-gamma coincidence data were taken for zinc, chromium, and nickel.

WA8. Stern-Gerlach Experiment on Polarized Neutrons. J. E. SHERWOOD, T. E. STEPHENSON, C. P. STANFORD, AND SEYMOUR BERNSTEIN, *Oak Ridge National Laboratory.*—A Stern-Gerlach experiment has been carried out on a polarized beam of slow neutrons. The polarization was accomplished by reflecting pile neutrons from a magnetized iron mirror. Preliminary experiments, using the mirror as polarizer and a magnetized iron transmitter as analyzer, established that the direction of the polarization relative to the applied magnetic field for a reflector-type polarizer is opposite to that for a transmitter-type polarizer. The Stern-Gerlach apparatus will be described and curves will be presented which show the variation of intensity in the deflected beam with distance across the beam. These curves exhibit the velocity distribution and spin state for all neutrons present, as well as small effects ascribed to depolarization. Present results indicate that the sign of the polarization agrees with the theoretical prediction; namely, that for a transmitter-type polarizer, the spin-state of largest population has its spin oriented antiparallel to the applied magnetic field.

WA9. Interaction with Argon and Lead of Neutrons with Energies up to 2.3 Bev.* E. C. FOWLER, H. L. KRAYBILL, R. M. WALKER, AND R. S. PRESTON, *Yale University.*—The Yale magnet cloud chamber has been operated with the Brookhaven National Laboratory's cosmotron, utilizing the forward beam from 2.3 Bev protons incident on a beryllium target. Our expansion type chamber contained a one inch thick lead plate and was filled with argon. 1446 stereoscopic photographs of interactions between beam neutrons and the material in the chamber were obtained in four days of operation. Preliminary analysis of these photographs shows 87 "stars" of three or more prongs produced in the argon by neutral radiation. Their distribution by size is: No. of prongs: 3 4 5 6 7 8 9 $\geq$ 10; No. of cases: 19 15 11 13 11 8 3 7. The decay of neutral V particles produced by beam particles has been observed.[1] Five examples appear to have been made in our lead plate. Details of their production and decay will be presented.

* Supported by the U. S. Atomic Energy Commission.
[1] Fowler, Shutt, Thorndike, and Whittemore, Phys. Rev. 90, 1126 (1953)

WA10. Experiments with Neutrons from the Cosmotron I.* D. A. HILL,† T. COOR, W. F. HORNYAK,‡ L. W SMITH, AND G. A. SNOW, *Brookhaven National Laboratory.*—Experiments have been made to determine the nature and interaction cross section of high-energy neutrons from Be targets bombarded with 2.2 Bev protons. The neutrons are detected by requiring them to traverse an anticoincidence counter and produce in an Al radiator charged particles which penetrate 6 in. of Pb. The angular distribution of the neutrons from the target, the excitation curve of the detector, the γ-ray contamination of the neutron beam, and the angular distribution of charged secondaries from several elements will be discussed. A collimated beam of neutrons from a Be target is used to measure the transmission of various samples as a function of the detector geometry. The angular distribution of diffraction scattering in Pb and Cu indicates a mean neutron energy of 1.4 ± 0.2 Bev. With this beam, the total $n-p$ and $n-n$ cross sections were measured by CH_2-C and D_2O-H_2O difference experiments and found to be 44 ± 3 and $42\pm3\times10^{-27}$ cm², respectively.

* Work performed under the auspices of the U. S. Atomic Energy Commission.
† Massachusetts Institute of Technology.
‡ Now on leave at Princeton University.

WA11. Experiments with Neutrons from the Cosmotron II.* G. A. SNOW, T. COOR, D. A. HILL, W. F. HORNYAK, AND L. W. SMITH, *Brookhaven National Laboratory.*—Using the apparatus described in I, transmission measurements have been made on Be, C, Al, Cu, Sn, and Pb as a function of the angle θ, subtended by the detector at the absorber. A rapid rise in transmission is found as θ varies from 0.22° ("good" geometry) to 6°–10° ("poor" geometry). The "poor" geometry points measure primarily the neutron absorption cross section, σa, while the "good" geometry points measure the sum of elastic diffraction scattering and σa. The cross sections measured in poor geometry after correcting for the residual diffraction scattering give the following values for σa in mb: 1610 Pb, 1220 Sn, 755 Cu, 446 Al, 231 C, 236 Be. The statistical accuracy in σa is 3–5 percent. Applying the optical model[1] for a uniform sphere and assuming that the bound and free $n-p$ and $n-n$ cross sections are equal, we determine the nuclear radius and the optical parameter (k_1/K) for each nucleus. The radii found for heavy elements are appreciably smaller than $1.40A^{\frac{1}{3}}$.

* Work performed under the auspices of the U. S. Atomic Energy Commission.
[1] Fernbach, Serber, and Taylor, Phys. Rev. 75, 1352 (1949).

SATURDAY AFTERNOON AT 1:45

Casa Italiana

(M. G. WHITE presiding)

Plans for Accelerators of the Future

X1. Particle Orbits in the Alternating Radiant Synchrotron. E. D. COURANT, *Brookhaven National Laboratory.* (40 min.)

X2. Design of the 25-Bev Proton Synchrotron for the European Organization for Nuclear Research. J. P. BLEWETT, *Brookhaven National Laboratory* (consultant to CERN). (40 min.)

X3. Design Study for a 15-Bev Accelerator by the Cambridge Design Study Group. M. S. LIVINGSTON, *M.I.T.* (30 min.)

X4. Summary of Other Accelerator Studies in Progress. M. G. WHITE, *Princeton University.* (10 min.)

SATURDAY AFTERNOON AT 1:45

Schermerhorn 501

(N. M. KROLL presiding)

Theoretical Physics, IV

XA1. A Corrected Theory of Relativity and its Classical Interpretation. R. V. L. HARTLEY, *174 Summit Avenue, Summit, New Jersey.*—The application of modern knowledge of signal transmission to the light signals involved in the theory of relativity shows that its assumptions are not self-consistent. When they are made so, precise times of transmission can be deduced from the fundamental physical equations only by a linear approximation. This invalidates those conclusions which depend on the times being precise. Hence the electromagnetic equations are not consistent with the principle of relativity, the modified concepts of space and time which were thought to make this true have no particular significance, and the Lorentz invariance of a set of equations insures that they are *not* consistent with the relativity principle. This leaves the equations of Newtonian mechanics as the only ones known to be consistent with the principle. An ether model, consisting of a turbulent classical liquid with suitable constants, has been found to support mobile "standing" waves which, as models of material particles, exhibit the behavior required by "relativistic" mechanics. Here also a linear approximation is used. The mass of a particle is $1/c^2$ times its wave energy.

XA2. On Bohr's Theory of Energy Losses of Moving Charged Particles. JACOB NEUFELD, *Oak Ridge National Laboratory.*—The stopping power of a particle having charge $Z_{eff}e$ and moving with velocity v has been determined by Bohr for $\kappa = 2Z_{eff}e^2/\hbar v > |$ and $\eta_s = 2v/u_s > 2$ where u_s is the velocity of the orbital electron that is effective in stopping the particle. Bohr's results are formulated differently for $\kappa/\eta_s < |$ and $\kappa/\eta_s > |$ and are based on an orbital picture of the processes involved. An alternative method has been developed in which the space surrounding the particle track has been subdivided into three regions: (a) the region of validity of the Rutherford formula (adjacent to the track), (b) the intermediate region involving large perturbations for which no adequate theory exists at the present time, and (c) the region of validity of the quantum perturbation theory (the most remote from the track). By extrapolating the formulas valid in regions (a) and (c) into the region (b), the contribution to the stopping power due to the region (b) has been estimated and adding to it the contribution due to the regions (a) and (c) an expression has been derived for the total stopping power that is applicable whenever $\kappa > |$ and $\eta_s > |$.

XA3. Time Reversal *vs* the Boltzmann Equation. J. S. LOMONT, *U. S. Naval Ordnance Test Station.*—The effect of time reversal on the solid state electronic Boltzmann transport equation has been investigated, and a simple formal mathematical transformation found which leaves it form invariant. The transformed variables can then be given physical significance in terms of a real reversed physical system. The reversion operator for the electron-phonon system in an external electric field can be explicitly constructed. The transformed distribution function must be interpreted as the distribution function for holes in the reversed system, and the transformed transition probability as the transition probability for holes. There is in fact a general relation between transition probabilities in forward and reversed systems (which does not hold for probabilities calculated by perturbation methods), whose fulfillment appears to depend on the vagaries of singular functions. The aforementioned formal transformation can then be interpreted as a time reversal transformation.

XA4. The Boltzmann Equation from the Statistical Mechanical Point of View.* MELVILLE S. GREEN, *University of Maryland.*—Recently Kirkwood and Green have given derivations of the Boltzmann equation from the so-called hierarchy of equations governing the distribution functions of n-uples of molecules. The present work will exhibit a derivation which is the first step of an expansion in powers of the concentration. If we call φ_n the distribution of the phases of an n-uple normalized so that the spacial distribution approaches 1 when all the molecules are far apart, it can be shown that for a spacially uniform situation the hierarchy can be written

$$\frac{d}{dt}\varphi_r = -c\sum_{i=1}^{n}\nabla_{\mathbf{p}_i}\cdot\int \mathbf{F}_{i,n+1}\varphi_{n+1}d\mathbf{p}_{n+1}d\mathbf{x}_{n+1},$$

where the right-hand side is the total time derivative along a trajectory of an isolated system of n molecules, c the concentration, $\mathbf{F}_{i,n+1}$ the force between the ith and the $n+1$th molecule, and $\mathbf{p}_i$, $\mathbf{x}_i$ the momentum and position of the ith molecule. These equations are solved by considering the left-hand side to be a small perturbation. The first step in the procedure leads to the Boltzmann equation for φ_1 as well as to expressions for φ_n which are functionals of φ_1.

* This work supported by U. S. Office of Naval Research.

XA5. An Application of Group Theory to Statistical Mechanics. JEROME ROTHSTEIN, *Signal Corps Engineering Laboratories.*—In calculating partition functions, one often combines complexions. Examples: indistinguishability of N particles coalesces $N!$ complexions into one, molecular symmetry σ (σ is the symmetry number). In every case (a) a set set of microscopic complexions corresponds to a macroscopic

state, the latter invariant under the group of all transformations of microscopic states into themselves, (b) subgroups exist with invariant subsets of complexions, (c) means for distinguishing between complexions in a subset are operationally undefined, (d) the number of complexions in the subset (its measure) is the symmetry number (generalized). The concept may be useful in crystal lattice theory.

XA6. Quantum Theory of the Radiation Resistance.* J WEBER, *University of Maryland.*—A previous paper[1] considered quantum effects in damping and noise. The vacuum fluctuations were shown to be observable in noise experiments. These results are extended to an electrical oscillator damped by a radiation resistance. First-order perturbation theory and the quantum statistics are employed. An expression is obtained, for the radiation resistance of a circuit, which is the same as the classical value. The damping and noise are the same as for other kinds of resistance.

* Supported by the U. S. Office of Naval Research.
[1] J. Weber, Phys. Rev. **90**, 977–982 (1953).

XA7. On Electromagnetic Scattering by a Paraboloid of Revolution.* CRAIGE SCHENSTED, *University of Michigan.* (introduced by K. M. Siegel).—On applying Kline's[1] asymptotic expansion to the scattering of a plane wave incident along the axis of a perfectly conducting paraboloid of revolution it was found that the series cuts off after only one term. It is readily found that the expression so obtained, namely

$$\mathbf{E}=\mathbf{i}\exp[i(kz-\omega t)]+\frac{R\exp\{i[k(r-R)-\omega t]\}}{r(1-\cos\theta)}\times(\cos\phi\theta'+\sin\phi\phi'),\dagger$$

is the *exact solution* of the above problem for the paraboloid $x^2+y^2=2Rz$. The result stated above is also precisely what would be given by geometric optics.

* Part of this paper appears in a larger report: UMM-115, "Studies in Radar Cross-Sections VIII, Theoretical Scattering Cross-Section as a Function of Angle at Small Wavelengths," K. M. Siegel, *et al.* (to be published).
† Primes were substituted for circumflex over theta and phi, since the printer does not have such symbols.
[1] Morris Kline, Commun. Pure and Appl. Math. **4**, 225 (1951).

XA8. Energy Equation for Sinusoidal Solutions of Maxwell's Equations with Electron Beams. PHILIP PARZEN, *The Johns Hopkins University.*—It is well known that the sinusoidal electromagnetic fields within a charge-free region are uniquely determined by specifying either the component of the electric field or the component of the magnetic field which is tangent to the boundary surface. The proof follows immediately from the conservation law for both real and reactive energy. A similar conservation law for both real and reactive energy is derived for the electromagnetic fields including electron beams if the sinusoidal current density is parallel to the sinusoidal beam velocity. The uniqueness theorem which follows from this conservation law states that the sinusoidal electromagnetic fields within a region are uniquely determined by specifying on the boundary surface the component of the sinusoidal electric field tangent to the surface, and either the sinusoidal electron velocity or the normal component of the sinusoidal current density.

XA9. Quantum Mechanics of the Scattering by a r^{-4} Attractive Potential. ERICH VOGT AND GREGORY H. WANNIER, *Bell Telephone Laboratories.*—The interaction potential of a charge carrier and a gaseous atom is at large distance attractive, varying as r^{-4}. This type of potential has, in classical mechanics, the simple property of yielding a constant "mean free time" between collisions—that is, a cross section varying inversely as the speed v. Among the various possible definitions of cross section, we picked the intrinsic cross section for spiralling orbits and investigated for it the modifications brought about by quantum mechanics. We find that the cross section oscillates about its classical value: $v^4(\sigma-\sigma_{\text{classs}})$ varies essentially sinusoidally as a function of v^4. This can be understood qualitatively in terms of the allowed orbits in the old quantum theory. We know of no reason why there should not be a steady deviation of the cross section in addition to this oscillation. We have looked for this deviation with both analytical and numerical procedures and have failed to find it. We conclude therefore, tentatively, that the classical cross section is maintained exactly as the mean over a velocity cycle. One can show that, for very low speeds, the cross section approaches the double of its classical value. It is not clear at this time how this limiting case fits in with the properties already enumerated for larger speed.

XA10. Three-Dimensional Calculation of Vibrational Relaxation Times in Gases.* ROBERT N. SCHWARTZ, *Naval Ordnance Laboratory.*—Despite the simplified geometry of the one-dimensional collisions between a pair of molecules considered by C. Zener,[1] the calculations of vibrational relaxation times based on this method have been fairly successful.[2] Zener treated the collision problem by quantum mechanics but restricted the molecules to motion along a line. In the present paper the molecules are considered to move in three dimensions. The molecules are considered rotational with respect to the apse line. To a reasonable approximation the centrifugal force, in a given collision, only affects the solution by modifying the velocity at which molecules enter into the range of the repulsive molecular field but does not otherwise affect the transitional probability. The probabilities calculated by treating the collision as a straight line motion and summing over a one-dimensional velocity distribution give nearly the same results as obtained by treating the collision processes in three dimensions and summing over a spacial distribution of velocities.

* Doctoral dissertation, Catholic University, 1953.
[1] C. Zener, Phys. Rev. **37**, 556 (1931).
[2] Schwartz, Slawsky, and Herzfeld, J. Chem. Phys. **20**, 1591 (1952).

SATURDAY AFTERNOON AT 1:45

Havemeyer 309

(C. S. Wu presiding)

Beta and Gamma Emitters, II

Y1. The Inner Bremsstrahlung for Cs^{131}.* BABULAL SARAF,† *Bartol Research Foundation.*—The continuous gamma-ray spectrum associated with orbital electron capture in Cs^{131} has been studied with the aid of a scintillation spectrometer. From the end point, the disintegration energy of Cs^{131} is estimated to be 300 ± 20 kev. Upper limits of 10^{-7} and 10^{-10} per disintegration are placed upon transitions leading to the excited levels of Xe^{131} of excitation energies 80 kev and 163 kev. Values of log ft calculated from the energy measurement and the estimates of intensities given above are in agreement with

orbital assignments of $d_{3/2}$ and $d_{3/2}$ for the respective ground states of Cs^{131} and Xe^{131}, $s_{1/2}$ for the excited level at 80 kev, and $h_{11/2}$ for the isomeric level of excitation energy 163 kev. The shape of the spectrum has been studied in detail and there is evidence that it is not in agreement with that predicted by the simple theory applicable to nuclei of low Z. The radiative capture probability of the decay process has been measured.

* Assisted by the joint program of the U. S. Office of Naval Research and the U. S. Atomic Energy Commission.
† Research Fellow, Bartol Research Foundation; on leave of absence from Agra College, Agra, India.

Y2. The Nuclear Spectra of Ce^{144} and Pr^{144}. W. J. AUTH, W. S. EMMERICH, AND J. D. KURBATOV, *The Ohio State University.*—The radiations of Ce^{144} and Pr^{144} have been investigated with a magnetic lens spectrometer, a photographic spectrograph, and a scintillation spectrometer. The energies of the principal beta and gamma rays were measured and their relative intensities established. A Kurie plot analysis of the beta rays yielded an intensity of 70 percent for the 304-kev transition to the ground state of Pr^{144}. From an analysis of the gamma rays, an intensity of 22 percent was obtained for the transition leading to the 134-kev level, and an intensity of about three percent for the 80-kev level. In the disintegration of Pr^{144}, the branching ratios were obtained by a comparison of the 2.98-Mev beta transition intensity with the 695-kev gamma ray. Applying the relative intensities of the gamma rays in Nd^{144} given by Alburger and Kraushaar,[1] an intensity of 0.9 percent was obtained for the 2.2-Mev beta transition.

[1] D. Alburger and J. Kraushaar, Phys. Rev. **87**, 448 (1952).

Y3. The Disintegration of Sm^{153}. R. L. GRAHAM AND J. WALKER,* *Chalk River Laboratories.*—The radiations from Sm^{153} (47.0 hr) have been studied by β-ray spectrometers, scintillation spectrometers, and millimicrosecond coincidence techniques. Fermi analysis of the β-ray spectra above 350 kev has given three main components of end points 810 ± 10 kev (about 20 percent), 710 ± 15 kev (about 50 percent), 640 ± 15 kev (about 30 percent). The second of these has been shown to be in coincidence with the conversion electrons of a 69.0×0.4-kev γ ray and the third with conversion electrons of a 102.5 ± 0.5-kev γ ray. Weak γ transitions of 170 kev and 520 kev have also been observed. The conversion coefficient of $\gamma69.1$ has been measured as 5.7 ± 1.0 and the K/L ratio as >4.6; for $\gamma102.6$ the K/L ratio is ≥6.1. Delayed coincidence measurements between conversion electrons and β rays have given $T_{\frac{1}{2}}=(4.0\pm0.2)\times10^{-9}$ sec for the state at 102.6 kev and $T_{\frac{1}{2}}=(1.4\pm0.4)\times10^{-10}$ sec for the one at 171.6 kev. The conversion coefficients and K/L ratios show that both radiations are predominantly $M1$. It is interesting to note that the higher transition probability is associated with the lower energy.

* U. S. Atomic Energy Commission Laboratory, Postdoctorate Fellow, on leave of absence from the University of Birmingham, Birmingham, England.

Y4. Activation Measurements in Europium with Monoenergetic Neutrons.* R. E. WOOD,† *Brookhaven National Laboratory.*—Europium foils were irradiated with monoenergetic neutrons, using the Brookhaven National Laboratory crystal spectrometer. The 9.3-hour activity of Eu^{153} was observed as a function of neutron energy. It was thus possible to determine the isotopic assignment for several of the eight resonances, between 0.2 ev and 5.0 ev, found by Sailor.[1] The ratio of the 9.3-hour activity to the total cross section was observed to vary from resonance to resonance, which indicates that the isomeric state of Eu^{153} is being populated differently for each resonance. The isotopic assignment of the resonances will be given, and the variations in population of the isomeric state in Eu^{152} will be discussed.

* Research performed under the auspices of the U. S. Atomic Energy Commission.
† Doctoral candidate from the University of Utah.
[1] V. L. Sailor (private communication).

Y5. Decay Scheme of the 5.5-Hr Isomer of Hf^{180m}.* J. W. MIHELICH, GERTRUDE SCHARFF-GOLDHABER, AND MICHAEL MCKEOWN, *Brookhaven National Laboratory.*—Recently,[1] theoretical considerations suggested the desirability of further study of the multipole character of the γ rays in Hf^{180m}. Previously only the 0.093-Mev transition was identified as electric quadrupole.[2] We measured the relative intensities of the unconverted γ rays of 0.442, 0.330, 0.214, and 0.093 Mev (energies quoted from Burson *et al.*)[2] by means of a NaI(Tl) scintillation spectrometer and found them to be compatible with the assumption of four $E2$ transitions. The γ rays were shown to succeed each other within less than a microsecond. The conversion electron spectrum obtained by a 180° magnetic spectrograph confirmed the above assignment and showed that the 0.0576-Mev transition is responsible for the 5.5-hr lifetime and is probably $M3$. Accurate energy determinations gave values of 93.3, 216.0, 332.4, and 443.6 kev, in good agreement with Bohr and Mottelson's formula. Angular correlation measurements are in progress.

* Work done under the auspices of the U. S. Atomic Energy Commission.
[1] A. Bohr and B. R. Mottelson, Phys. Rev. **90**, 717 (1953).
[2] See M. Goldhaber and R. D. Hill, Revs. Modern Phys. **24**, 179 (1952).

Y6. A 10.5-Day Isotope of Platinum.* R. A. NAUMANN, *Princeton University.*—Metallic iridium has been irradiated with 50-Mev protons in the Columbia and Harvard University synchrocyclotrons and a platinum fraction has been chemically isolated from the bombarded targets. The decay of the platinum fractions has been observed employing end-window Geiger counters and shows a 10.5-day period which has been followed for 60 days. An iridium fraction showing a 40-hour decay component has been isolated from the 10.5-day platinum while the latter fraction, after repurification, shows an increase in activity compatible with the growth of a 40-hour daughter. A mass assignment of 188 to the platinum activity is supported by a previous assignment of a 41-hour iridium activity as iridium 188.[1] Several conversion electron lines have been found to be associated with the decay of the platinum activity. Further studies on the decay schemes of these activities are continuing.

* This work was supported by the U. S. Atomic Energy Commission, The Higgins Scientific Trust Fund, the U. S. Office of Naval Research, and in part by a grant in aid of the E. I. Dupont de Nemours Company.
[1] T. C. Chu, Phys. Rev. **79**, 582 (1950).

Y7. Decay of Pt^{191}.† E. P. TOMLINSON AND R. A. NAUMANN, *Princeton University,* AND J. W. MIHELICH, *Brookhaven National Laboratory.*—Samples of 3-day Pt^{191} (and 4-day Pt^{193m}) have been obtained by bombarding Ir with deuterons in the Brookhaven cyclotron and studied with a gray-wedge coincidence analyzer[1] and 180° photographic spectrographs at Brookhaven and with the Princeton high-resolution Siegbahn-type spectrometer. We find the γ rays of 82, 96, 125, (135 from Pt^{193m}), 172, 179, 268, 350, 360, 409, 456, and 540 kev as reported by Swan, Portnoy, and Hill.[2] Conversion electrons which would give rise to the 62-kev transition reported by these authors, we believe to be Auger electrons. We also find evidence for γ rays of 42, 220, approximately 620, and possibly 158 kev. From the energies, the conversion electron and γ-ray intensities, and the coincidence measurements of these γ rays, a self-consistent energy-level scheme can be proposed for Ir^{191}. Work is continuing on these measurements.

* This work was supported by the U. S. Atomic Energy Commission and The Higgins Scientific Trust Fund.
[1] Bernstein, Chase, and Schandt, Rev. Sci. Instr. **24**, 437 (1953).
[2] Swan, Portnoy, and Hill, Phys. Rev. **90**, 257 (1953).

Y8. Resonance Fluorescence with Nuclei: Hg^{199}.* F. R. METZGER AND W. B. TODD, *Bartol Research Foundation.*—The decay of Au^{199} proceeds partially through a 209-kev excited state of Hg^{199}. The 209-kev transition to the ground state of Hg^{199} has been used to excite Hg^{199} nuclei contained in a

mercury absorber. The thermal motion in the Au^{199} source provided the velocities necessary to compensate through Doppler effect for the energy loss which the gamma rays suffer in the emission and absorption processes. When the source is heated, the contribution due to resonance fluorescence increases. From the observed change one calculates a lifetime of $(3.1\pm0.9)\times10^{-10}$ sec for the 209-kev transition in Hg^{199}, assuming isotropic distribution for the $M1$ transition of unknown $E2$ admixture. The observed value has to be compared with the upper limit of 3.4×10^{-10} sec found with electronics[1] and with a value of 3.6×10^{-12} sec estimated from Weisskopf's lifetime formula.[2]

* Assisted by the joint program of the U. S. Office of Naval Research and the U. S. Atomic Energy Commission.
[1] Bell, Graham, and Petch, Can. J. Phys. **30**, 35 (1952).
[2] V. F. Weisskopf, Phys. Rev. **83**, 1073 (1951).

Y9. Nuclear Energy Levels of Tl^{203}.† JAGDISH VARMA,* *Bartol Research Foundation.*—Using scintillation counting techniques, Pb^{203} is found to decay by K capture to the 683- and 280-kev excited levels in Tl^{203}. In addition to the 403- and 280-kev cascade gamma rays, the 683-kev cross-over transition is also observed. Careful energy measurements showed, in contrast with earlier results, that the same 280 ± 1 kev level of Tl^{203} is excited in decay of both Hg^{203} and Pb^{203}. Conversion coefficient measurements of the 280-kev quantum support this conclusion. The K-shell conversion coefficient of the 403-kev gamma ray is measured as 0.052 showing the transition to be a mixture of 87 percent $E2$ and 13 percent $M1$. The K/L ratio also indicates the same admixture of $E2$ in $M1$. The observed facts agree with orbital assignments of $d_{5/2}$, $d_{3/2}$, and $s_{1/2}$ for the levels of Tl^{203} in order of decreasing excitation energy, and of $f_{5/2}$ for the ground state of Pb^{203}. Angular correlation measurements give the anisotropy expected for a mixture-mixture correlation with mixing ratios as deduced from the conversion measurements.

† Assisted by the joint program of the U. S. Office of Naval Research and the U. S. Atomic Energy Commission.
* Research Fellow, Bartol Research Foundation; permanent address Morena (M.B.) India.
[1] G. D. O'Kelley, Ph.D. thesis, University of California. Unclassified Report URCL-1243 (May, 1951).

Y10. Energy Levels of Pb^{208}. L. G. ELLIOTT, R. L. GRAHAM, J. WALKER, AND J. L. WOLFSON, *Chalk River Laboratories.*—Measurements have been made of the K internal-conversion coefficients of the 2.62-, 0.583-, 0.860- and 0.511-Mev γ-ray transitions in Pb^{208} and also of the angular correlations between pairs of these γ rays selected by NaI(Tl) scintillation spectrometers. These results lead unambiguously to the spin and parity assignments of 0+ (assumed), 3-, 5-, 4- and 5- for the ground, 2.62-, 3.20-, 3.48-, and 3.71-Mev levels, respectively. The measured values of α_K are $(1.78\pm0.12)\times10^{-3}$ for $\gamma2.62$ and $(1.58\pm0.11)\times10^{-3}$ for $\gamma0.583$ which are in good agreement with the theoretical values for $E3$ and $E2$, respectively. The $\gamma2.62$–$\gamma0.583$ angular correlation has been studied in detail using liquid sources because of the reduced anisotropy found with solid sources. The results agree well with the (0–3–5) assignment and reject the previously proposed assignments of (0–1–3) or (0–2–4). Other correlation and conversion measurements indicate for $\gamma0.511$, an intensity ratio $E2/M1=1.7\pm0.3$ with 0° phase difference, and for $\gamma0.86$ $E2/M1=(6.5\pm6.5)\times10^{-4}$ with 180° phase difference. Delayed coincidence measurements yield half-lives of $(2.4\pm1.0)\times10^{-10}$ sec for the 3.20-Mev level and $<10^{-10}$ sec for the levels of 2.62 and 3.71 Mev.

Y11. New Method for Measuring Short γ-Ray Lifetimes. J. W. KNOWLES, *Chalk River Laboratories.*—A method for the measurement of short γ-ray lifetimes less than 10^{-12} sec is presented with particular reference to the 0.239-Mev γ ray of Bi^{212} following the β decay of Pb^{212}. The method consists of measuring the rms recoil displacements of active atoms following β emission. The active atoms occupy regular positions in a crystal lattice before emission. The recoil atoms if still in an excited state may emit a γ ray within the time of flight or time of oscillation of the atom. A fraction of these γ rays is internally converted producing x-rays which diffract from the crystal lattice as Kossel cones.[1] The intensity of these cones relative to their background is dependent on the position of the recoil atoms in the crystal unit cell when γ-ray emission occurs. A preliminary measurement of the half-life of the 0.239-Mev γ ray of Bi^{212} gives a value between the limits 10^{-12} to 10^{-14} sec. An estimate of about 10^{-12} sec for the life-time of this γ ray using K/L ratio data has been reported.[2]

[1] Z. Physik **94**, 139 (1935).
[2] Can. J. Phys. **31**, 377 (1953).

Y12. Gamma-Ray Spectrum of a Po–B Source. TEMPLE LOVE AND FRED MAIENSCHEIN, *Oak Ridge National Laboratory.*—Specta have been measured of the gamma rays emitted from excited levels in nitrogen as produced in the reactions $B^{10,11}(\alpha,n)N^{13*,14*}$ employing polonium alpha particles. The spectrometers used were a single-crystal (NaI) scintillation spectrometer and a 3-crystal pair spectrometer. The high-energy portions of the spectra were investigated with the source and detector suspended in air (~8 ft to the nearest wall) in order to lower the neutron capture gamma-ray background. A 6-in. lead shield was used to reduce the background in the low-energy regions. The polonium activity of the Po–B source was compared with the activity of a Po–Be source by measuring the relative strengths of the 0.803-Mev polonium gamma ray. Then the intensities of the Po–B gamma rays were determined and are reported here as percentages of the intensity of the 4.43-Mev gamma ray from a Po–Be source of the same Po activity. Energy calibrations were made using this same 4.43-Mev gamma ray. The results were: 2.27 Mev (6.8 percent), 3.03 Mev (1.5 percent), 3.59 Mev (6.8 percent), 5.95 Mev (~0.13 percent), and 7.7 Mev (~0.09 percent).

Y13. The Spin of RaE.* R. W. KING, *National Research Council,* AND D. C. PEASLEE, *Columbia University.*—The following evidence suggests $I=1^-$ for the ground state of RaE: (a) throughout the periodic table, $\Delta I=1$ (yes) transitions have ft values an order of magnitude larger than for corresponding $\Delta I=0$ (yes), indicating partial cancellation of large terms of order $(\alpha Z/2\rho)^2$, which make 1st forbidden spectra appear straight; (b) in the "favored" 1st forbidden region around $A=208$, the $\Delta I=0$ (yes) transitions (including 3 probable $0\rightarrow0$ cases) have log ft ≈ 5–6, as in RaD→RaE*; (c) the α decay[1] of RaE is most consistent with the lifetime energy relationship if its final state is Tl^{208*}, implying $I(\text{RaE})\neq I(Tl^{208})=0^-$. The evidence against $I=1^-$ and favoring $I=0^-$ for RaE is not conclusive: (a) several heavy nuclei show exceptions to Nordheim's rule forbidding 1^- ground state; (b) the state $(h_{9/2}\,g_{9/2})_1$ has $\mu_{\text{calc}}=0.08$ nm, probably below the limit of spectroscopic resolution; (iii) the RaE β-spectrum shape can be fitted with $\Delta I=1$, yes, as well as $\Delta I=0$, yes.[2]

* This work partially supported by the U. S. Atomic Energy Commission.
[1] E. Broda and N. Feather, Proc. Roy. Soc. (London) **A190**, 20 (1947).
[2] M. Yamada, Abstracts of Tokyo Conference, A 93 (1953).

Y14. Rates of Decay of the Observed Anisotropies in the Am^{241} α–γ and Cd^{111} γ–γ Angular Correlations. J. S. FRASER AND J. C. D. MILTON, *Chalk River Laboratories.*—Observations were made of the anisotropy $A=[W(\pi)]/[W(\pi/2)]-1$ as a function of delay between the first and second radiations of the cascade. The delayed coincidence circuit had a resolving time of about 1.5×10^{-8} sec which is shorter than the half-lives of the intermediate states in Np^{237} (6×10^{-8} sec) and Cd^{111} (8×10^{-8} sec). The anisotropy observed in a solid source of Am_2O_3 had an initial value $A=-0.15\times0.03$ but decayed with a half-life of about 5.5×10^{-8} sec to

$A \approx 0$ after 2×10^{-8} sec. The polarization of the 60-kev γ ray as measured at 110° from the α particle exhibited a comparable rate of decay from an initial value $N_{11}/N_{\perp}=0.81\pm0.04$. Cd^{111} was investigated in solid sources of $InCl_3$ and In_2O_3 and in a dilute aqueous solution of $InCl_3$. The anisotropy in $InCl_3$ and In_2O_3 had initial values -0.27 ± 0.04 and -0.24 ± 0.04, decay half-lives $(10.0\pm5)\pm10^{-9}$ sec and $(7.5\pm4)\pm10^{-9}$ sec, and final values -0.028 ± 0.01 and -0.082 ± 0.01, respectively. The liquid source, as expected, gave a constant anisotropy $A=-0.215\pm0.01$ over the measured range of 7×10^{-8} sec.

Saturday Afternoon at 1:45

McMillin Theatre

(G. T. Reynolds presiding)

Cosmic Rays and Diverse Particles

Invited Papers

Z1. Cosmic Radiation at Very High Altitudes Near the Geomagnetic Equator. W. A. Pomerantz, *Bartol Research Foundation.* (30 min.)

Z2. Properties of New *V* Particles. E. W. Cowan, *California Institute of Technology.* (30 min.)

Contributed Papers

Z3. The Flux of Primary Cosmic-Ray Alpha Particles.* John Lindsley, *University of Minnesota.*—A cloud chamber-Čerenkov counter apparatus was flown by Skyhook balloon for five hours at an atmospheric depth 17 g/cm². The chamber was triggered by sufficiently large pulse from a thin Čerenkov counter in coincidence with a gate from a geometry-defining G-M counter telescope. Of 157 photographs, 60 show the track of a counter age alpha particle within the proper solid angle. Twenty show the track of a fast particle with $Z>2$. The pulse-height requirement implied an energy threshold at 700 ± 100 Mev/nucleon for alpha particles (extrapolated to the top of the atmosphere). If it be assumed that all of the alphas were primary and that primary alphas are effectively absorbed in nuclear collisions with geometric cross section, the vertical flux of primary alpha particles above the threshold energy is 0.014 ± 0.002/sec cm² steradian.

* The research was supported in part by the joint program of the U. S. Atomic Energy Commission and the U. S. Office of Naval Research.

Z4. Mapping Particle Paths in Earth's Magnetic Field. Willard H. Bennett, *Naval Research Laboratory.*—In the course of an investigation of magnetically self-focusing streams as the mechanism responsible for producing auroral streams,[1] a model has been built with which to observe the paths of charged particles in the earth's magnetic field. Braun-tube type streams are produced in a tube, the inside of which has been made conductive by Clark's process.[2] The tube is transparent, permitting clear observation of the orbits. A bar magnet inside an aluminum sphere represents the earth. The system constitutes a true model of orbits in the earth's field except for one minor correction.

[1] Phys. Rev. 91, 1562 (1953).
[2] Rev. Sci. Instr. 24, 641 (1953).

Z5. The Influence of the Earth-Magnetic Field on Extensive Air Showers. Giuseppe Cocconi, *Cornell University.*—The lateral displacement from the rectilinear path, D_m, resulting from the influence of the earth-magnetic field on the electrons in an extensive air shower has been evaluated in first approximation and found of the same order of magnitude as the displacement, $(\langle D_s^2\rangle_{Av})^{\frac{1}{2}}$, produced by Coulomb scattering. For electrons above critical energy, arriving in vertical direction, $D_m/(\langle D_s^2\rangle)^{\frac{1}{2}}=0.45\cos\lambda/P$, ($\lambda$ = geomagnetic latitude, p = air pressure in atmos). It seems that this effect has been overlooked by the several authors who calculated the electron lateral distribution in extensive showers. At sea level and moderate latitudes, the distribution around the core of the electrons above critical energy is, roughly speaking, elliptical rather than circular, with the major axis in the $E-W$ direction and about two times larger than the minor axis. The deviations from circular symmetry are presumably smaller for electrons below critical energy, where the effect of large, single scatterings becomes important, and for the other components of the shower (mesons and nucleons), owing to their large angle of production. These considerations will make even more difficult the interpretation of the experiments on the distribution around the core of high-energy electrons.

Z6. Time Structure of Extensive Air Showers.* R. Sugarman and S. De Benedetti, *Carnegie Institute of Technology.*—The difference in time between the pulses of two liquid scintillation tanks (A: 0.17 m²; B: 0.11 m²; 1.3 m apart; 390-m elevation) was measured whenever their pulses were in quadruple coincidence with two unshielded Geiger tube trays (0.20 m²; 3.9 m apart) for the three following experimental conditions: (I) no shielding; (II) no shielding but 85 percent of tank A-area made inoperative with opaque paper cover; (III) paper removed, tank A shielded with 8-in. Pb. Root mean square deviations, including instrumental errors, were never larger than $6\cdot10^{-9}$ sec. A significant increase (from 3 to $6\cdot10^{-9}$ sec) was observed in the order (I), (II), (III). This result is attributed at least in part to variations in the detected particle density of the tanks, as will be discussed. Increase with shielding of mean delay time of tank A relative to B was $1\pm1\cdot10^{-9}$ sec, indicating that no delays between soft and hard particles were resolved by this experiment.

* Supported in part by the U. S. Atomic Energy Commission.

Z7. Distribution of Specific Ionization of Primary Cosmic Rays at $\lambda=10°$N.* G. W. McClure, *Bartol Research Foundation.*—A balloon-borne instrument comprising a G-M counter train with an interposed fast-ionization chamber has been flown at $\lambda=10°$N for the purpose of determining the distribu-

tion of specific ionization of relativistic primary cosmic rays. The ion-chamber pulse coincident with each counter telescope traversal was recorded on a continuously moving film and was specially labeled if accompanied by the discharge of 2 or more counters in a 7-counter horizontal shower tray directly under the chamber. Sea-level calibrations indicated that monoenergetic primary protons should yield a peaked differential pulse-height distribution with a 20 percent width at half-maximum, and that monoenergetic primary α particles should yield a peak of similar shape with a most-probable pulse height approximately 4 times that for protons. Data obtained in a 5-hour level flight at 12 mm Hg indicated a large peak corresponding to relativistic singly-charged particles but no pronounced peak attributable to α's. Of those pulses greater than 3 times minimum ionization—which comprised 40 percent of the total number of events and presumably include the entire α component at this altitude—nearly 70 percent were accompanied by shower indications.

* Assisted by the joint program of the U. S. Office of Naval Research and the U. S. Atomic Energy Commission.

Z8. The Energy Distribution of Neutral Mesons Produced in Cosmic-Ray Stars.* Y. B. KIM,† *Princeton University.*—The final result of a cloud-chamber experiment to study the energy distribution of π^0 mesons produced in cosmic-ray stars will be reported.[1] In estimating the energy of a photon from its shower, the maximum number of electrons observable, n_{max}, was used. An investigation shows that n_{max} is a good index in spite of fluctuations. The fluctuation at the cascade maximum $\bar{n}_{(t\ max)}$ comes from: (a) the fluctuation in the absolute maximum, and (b) uncertainty as to where this maximum occurs. To study these two kinds of fluctuations separately, R. R. Wilson's shower sheets were used. The distribution in n_{max} is much narrower than that in $\bar{n}_{(t\ max)}$, as seen in Table I.

TABLE I. Numbers of electrons of energy $\geqslant 8$ Mev. $\delta = \{\langle (n-\bar{n})^2 \rangle_{Av}\}^{\frac{1}{2}}/\bar{n}$.

Photon energy	$\bar{n}_{(t\ max)}$	δ	$\bar{n}_{max}$	δ
50 Mev	0.49	1.59	1.34	0.451
100 Mev	0.88	1.12	1.92	0.282
300 Mev	2.13	0.701	3.66	0.342

* Supported by the joint program of the U. S. Office of Naval Research and the U. S. Atomic Energy Commission.
† Now at Department of Physics, Indiana University.
[1] Y. B. Kim, Phys. Rev. 91, 445 (1953), gives preliminary results.

Z9. Gamma Rays Associated with *S*-Particle Decay.* H. COURANT.—Two additional cases of electron cascades associated with *S*-particle decays have been observed in the M.I.T. cloud chamber at Echo Lake, Colorado. In the four cases previously reported,[1] the direction of propagation of the cascades appeared as opposite to that of the charged decay product. The two new events are of special interest because in each case the electron cascade is not co-linear with the direction of the charged decay product. The probability that these events are a result of chance coincidence between an *S* particle and an electron cascade is small. Individual cases will be discussed.

* Assisted by the joint program of the U. S. Office of Naval Research and the U. S. Atomic Energy Commission.
[1] Bridge, Courant, DeStaebler, and Rossi, Phys. Rev. 91, 1024 (1953).

Z10. Unstable Heavy Particles from the Cosmotron.* R. D. HILL, E. O. SALANT, AND M. WIDGOFF, *Brookhaven National Laboratory;* L. S. OSBORNE, A. PEVSNER, AND D. M. RITSON, *M.I.T.;* J. CRUSSARD AND W. D. WALKER, *University of Rochester.*—Ilford G5 emulsions were bombarded by 1.5-Bev negative pions, magnetically analyzed after emerging from the Brookhaven cosmotron. In the scanning of 3.5 cm³ of emulsion, two heavy decaying particles were observed, both emerging from stars with a minimum track in the collimated beam. One large star shows a backward heavily-ionizing particle of range 9 mm, which stops and emits a fast particle giving a steep, light track, roughly minimum. From preliminary measurements of range and scattering, the heavy particle has a mass of $850\pm200\ m_e$, typical of a K meson. One heavy prong of a 6-pronged star has a 260μ range and is probably the result of an alpha particle (but possibly to Li^{++}), which stops and decays into 3 coplanar tracks: (a) a gray, which grain count and scattering show is due to a 25-Mev pion; (b) a 5.3-Mev proton of 196μ range; (c) a 13μ track consistent with a 3.5-Mev He^3. With these masses and energies, co-planar momenta balance. Assuming the event is a decay of a V_0^1 of 37-Mev Q bound in an alpha particle, the binding energy of the V_0^1 is 4 Mev, compared with 20-Mev neutron binding.

* This work was supported in part by the joint program of the U. S. Office of Naval Research and the U. S. Atomic Energy Commission.

Z11. Kinematics of Λ^0 Production.* GEORGE T. REYNOLDS AND S. B. TREIMAN, *Princeton University.*—Cloud-chamber observations indicate that an appreciable fraction of Λ^0 particles resulting from cosmic-ray interactions in heavy elements (lead and copper) are produced at low energies in the laboratory frame.[1] At least 10 percent of the observed Λ^0 particles are produced at energies below 70 Mev. The cloud-chamber bias against observing high-energy Λ^0 particles, however, is probably not serious up to at least several Bev. We have considered the kinematics of a variety of fundamental reactions which might lead to Λ^0 production, taking into account the internal motion of the target nucleons in the nucleus. For the reactions considered, the above observations would imply that, in the center-of-mass system of the collision, Λ^0 production is peaked in the backward direction. In particular, if the bulk of the Λ^0 particles are produced in the reaction observed at Brookhaven:[2] $\pi+n\rightarrow\Lambda+K$ (where n is a nucleon and K is a particle of intermediate mass), the peaking in the backward direction must be extremely marked.

* Supported by the U. S. Office of Naval Research and the U. S. Atomic Energy Commission.
[1] Ballam, Harris, Hodson, Rau, Reynolds, Treiman, and Vidale, Phys. Rev. 91, 1019 (1953).
[2] Fowler, Shutt, Thorndike, and Whittemore, Phys. Rev. 91, 1287 (1953)

Z12. A Search for *K* Particles Using Čerenkov Counters.* J. W. KEUFFEL† AND L. MEZZETTI,‡ *Princeton University.*—Two directional Čerenkov counters (C)[1] are mounted below a large liquid scintillator (S). The counters are surrounded by a Pb house with Al lining. The Čerenkov radiator is water in Lucite containers, painted black below and viewed from above by C-7157 photomultipliers. The measured efficiency for detecting downward relativistic particles is 2 percent; for upward particles, it is 90 percent; nonrelativistic particles ($E<\frac{1}{2}MC^2$) are not detected. This arrangement should permit precise time-measurements on the upward-going relativistic secondaries of K-particles unobscured by time-zero pulses from downward-going particles produced in the same event. The distribution of delays between S and C consists of a peak at time zero and a $\sim$5.0-mμsec exponential extending over four mean lives. The measured timing error distribution of the counters and chronotron timing circuit is approximately Gaussian with s.d. 2 mμsec. The 5-mμsec component disappears when C is displaced 70 cm laterally (but still under 20 cm of Pb). Further tests to verify the identify of the 5-mμsec lags are proceeding.

* Assisted by the joint program of the U. S. Office of Naval Research and the U. S. Atomic Energy Commission.
† Now at University of Utah.
‡ On leave from University of Rome.
[1] J. Winckler and K. Anderson, Rev. Sci. Instr. 23, 765 (1952).

SUPPLEMENTARY PROGRAMME

SP1. Virtual States of Two Meson Systems. R. ARNOWITT, *University of California, Berkeley,* AND S. DESER, *Institute for Advanced Study.**—Bound and metastable states of two mesons have been studied with an approximate equation derived from the relativistic one satisfied by the two meson Green's function,

$$\mathcal{G} = -\langle(\phi_i(\xi)\phi_j(\eta)\phi_{i'}(\xi')\phi_{j'}(\eta'))_+\rangle + \langle(\phi_i(\xi)\phi_j(\eta))_+\rangle\langle(\phi_{i'}(\xi')\phi_{j'}(\eta'))_+\rangle.$$

The equation for $\mathcal{G}$ may be written in the form

$$[(k_1^2+\mu^2)(k_2^2+\mu^2) - I_{12}]\mathcal{G} = \delta_{ij'}\delta_{jj'} + \delta_{ij}\delta_{ji'},$$

I_{12} being the interaction kernel. To lowest (g^4) order, I_{12} has a contribution only from the four-sided "box" diagrams (scattering of mesons by mesons). For the corresponding homogenous equation, which yields the energy eigenstates of the system, the adiabatic limit of the lowest order interaction was used to derive a three-dimensional Schroedinger equation in relative coordinates. For the isotopic spin 1 state, there are no renormalizations of the $\lambda\phi^4$ type. Considering angular momentum $l \geq 1$, the resulting potential was treated approximately, use being made of the great strength and short range ($\sim \frac{1}{4}$ m) of one of its factors. A search is being made for metastable and bound solutions of the simplified equation, with particular reference to the possibility of representing the V_3^0 particle in this fashion, and results will be reported.

* To be called for at the end of Session B if the Chairman rules that time permits.

Author Index to Papers Presented at the 1954 Annual Meeting

Aamodt, L. C., P. C. Fletcher, G. Silvey, and C. H. Townes—V5
Albrecht, H. O. and C. E. Mandeville—QA2
Alford, W. Parker and Donald R. Hamilton—R5
Anderson, James L.—B3
Arnowitt, R. and S. Deser—SP1
—— and S. Gasiorowicz—B6
Arrott, A.—RA7
Aschner, J. F.—M8
Auth, W. J., W. S. Emmerich, and J. D. Kurbatov—Y2
Azumi, K. and J. E. Goldman—RA6
Bay, Z., V. P. Henri, and F. McLernon—R8
Bayard, Robert T. and J. L. Yntema—H3
Belinfante, F. J.—B2
Bemski, G., W. A. Nierenberg, and H. B. Silsbee—L6
Benedict, W. S. and Shirleigh Silverman—E9
Bennett, Willard H.—Z4
Bergmann, Peter G.—U11
Bernstein, Eugene—PA7
Betchov, R.—S9
Bichsel, H. and R. F. Mozley—JA8
Binger, D. and W. J. Sturm—I7
Bittner, J. W., R. G. Herb, R. D. Moffat, and J. A. Weinman—LA7
Blewett, J. P.—X2
Block, R. C., J. H. Gibbons, E. G. Bilpuch, and D. F. Herring—PA2
Bockelman, C. K. and J. J. Jung—C7
Boorse, H. A.—N2
Braams, C. M.—JA1
Bradshaw, B. C. and R. A. Shuttleworth—F2
Brattain, W. H. and C. G. B. Garrett—D8
Bray, P. J.—L1
Breit, G.—LA4
Bridgman, P. W.—I1
Brockhouse, B. N.—RA5
Brockman, Karl W., Jr.—T3
Burstein, E., B. W. Henvis, and N. Sclar—D9
Caird, R. S. and Allan C. G. Mitchell—R13
Campbell, R. C., J. D. Korsmeyer, and D. C. Ralph—WA6
Case, K. M.—U3
Caswell, R. S., R. F. Gabbard, W. P. Doering, and D. W. Padgett—T11
Chen, F. F., C. P. Leavitt, and A. M. Shapiro—T1
Christian, R. H. and Robert G. Schreffler—S10
Church, E. L. and J. E. Monahan—IA6
Clark, David D. and Owen Chamberlain—T2
Class, C. M., C. F. Cook, and J. T. Eisinger—C3
Clauser, Francis H.—S8
Cocconi, Giuseppe—Z5
Cohen, B. L.—O1
——, W. H. Jones, G. H. McCormick, and B. L. Ferrell—H10
Collins, G. B.—A1
Coon, J. H. and R. W. Davis—T7
Corben, H. C.—U7
Corrsin, Stanley—S7
Cotter, T. P.—K4
Coulter, George A. and James Allen—S3
Courant, E. D.—X1
Courant, H.—Z9
Cowan, C. L., Jr., and F. Reines—DA3
Cowan, E. W.—Z2
Danos, M.—H5
Darrow, K. K.—Q4
Dash, J. G.—N1, N5
Davis, H. L. and D. R. Corson—G9
Dayton, I. E. and P. C. Gugelot—T4
De Benedetti, S., M. B. Stearns, M. Stearns, and H. J. Richings—KA8
DeSaussure, G. and L. S. Osborne—G8
Deser, S., W. E. Thirring, and M. L. Goldberger—B8
Dexter, D. L.—M9
Dibeler, Vernon H. and Fred L. Mohler—F11
DiDonato, A. A. MacLeod, and A. C. Webber—M2
Dillon, J. A., Jr., and H. E. Farnsworth—F1
Dorfman, Leon M. and B. A. Hemmer—F10
Dousmanis, G. C.—V7
Dresden, M. and Martin Gutzwiller—B1
Dresner, Joseph—E4
Drost-Hansen, W. and E. J. Workman—M4
Dudziak, Walter F.—G6
Duff, R. E. and H. T. Knight—S12
Duffield, Robert B. and Nathan Sugarman—PB6
Efremov, N.—F5
Eisenstein, Albert S.—QA1
Elliott, L. G., R. L. Graham, J. Walker, and J. L. Wolfson—Y10
Fader, W. J. and A. Sperduto—C8
Fermi, Enrico—P1, Q2
Feshbach, Herman—U2
Fivel, Daniel I. and Gilbert N. Plass—E8
Foote, H. L., Jr.—WA3
Forster, H. K. and N. Zuber—F7
Fowler, E. C., H. L. Kraybill, R. M. Walker, and R. S. Preston—WA9
Fraser, J. S. and J. C. D. Milton—V14
Freistadt, Hans—B10
Fried, Burton D. and R. J. Riddell, Jr.—B5
Friedlander, G., E. Baker, J. Hudis, J. M. Miller, and R. Wolfgang—PB4
Gardner, J. W.—JA7
Gibbons, J. H.—PA1
Gindler, James and Robert B. Duffield—H13
Glassgold, Alfred E.—H4
Glauber, R. J.—E3
Gluckstern, R. L., P. B. Daitch, L. C. Biedenharn and M. M. Hull, Jr.—LA6
Godfrey, T. N. K.—G10
Goldburg, W. I. and R. M. Williamson—C1
Goldman, J. E. and A. Arrott—RA8
Goldwasser and G. Bernardini—G4
Goldwater, D. L. and W. E. Danforth—F9
Gordon, W. L., C. H. Shaw, and J. G. Daunt—N4
Gove, H. E., E. B. Paul, G. A. Bartholomew, and A. E. Litherland—C13
Graham, R. L. and J. Walker—Y3
Grandy, R. A. and A. F. Clark—KA7
Green, D. W., J. N. Cooper, and J. C. Harris—JA9
Green, Melville S.—XA4
Grodzins, L.—H6
Gross, E. P. and M. Krook—QA10
Haberle, W., J. W. Bittner, and R. D. Moffat—LA8
Hagstrum, H. D.—D2
Hartley, R. V. L.—XA1
Havens, W. W., Jr.—WA1
Hayes, W. D.—J2
Henry, Warren E.—RA4
Hensley, E. B.—W2
Herman, R. C., S. Silverman, and R. F. Wallis—E10
Heydenburg, N. P. and G. M. Temmer—C5
Hill, D. A., T. Coor, W. F. Hornyak, L. W. Smith, and G. A. Snow—WA10
Hill, David L. and Kenneth W. Ford—U8
Hill, R. D., E. O. Salant, M. Widgoff, L. S. Osborne, A. Pevsner, D. M. Ritson, J. Crussard, and W. D. Walker—Z10
Hoch, Michael and Herrick L. Johnston—D3
Hofstadter, Robert—O2
Holmgren, H. D., J. M. Blair, B. E. Simmons, and R. V. Stuart—C9
Hornig, D. F.—K3
Hudis, J., R. Wolfgang, N. Sugarman, and G. Friedlander—PB2
Hughes, Vernon W. and Werner B. Teutsch—IA4
Hull, M. H., Jr., L. C. Biedenharn, P. B. Daitch, and R. L. Gluckstern—LA5
Hurlbut, F. C.—F12
Ingersoll, L. R. and D. H. Liebenberg—F8
Innes, Frederick R.—IA3
Jenkins, T. L., D. Luckey, and R. R. Wilson—G5
Jesse, William P. and John Sadauskis—JA10
Joyner, W. T.—PA6
Kaiser, H. F.—LA3
Kalos, M. H. and J. M. Blatt—IA9
Kelly, John, James Ray, and Richard A. Ogg, Jr.—L3
Keuffel, J. W. and L. Mezzetti—Z12
Kies, J. A. and H. L. Smith—I9
Kim, Y. B.—Z8
King, R. W. and D. C. Peaslee—V13
Kistler, Alan, Vivian O'Brien, and Stanley Corrsin—S6
Kittel, Charles—L9
Knight, Herbert E. and Russell E. Duff—S13
Knowles, J. W.—Y11
Kovásznay, Leslie S. G. and Darshan Dosanjh—S14
Kraitchman, J. and B. P. Dailey—V2
Kriessman, C. J. and H. B. Callen—RA3
Kroll, N. M.—B12
Kurşunoğlu, Behram—B7
Lakin, W. and W. Kohn—U6

Lax, M. and R. Toupin—RA1
Leder, Lewis B. and L. Marton—QA8
Lederman, L. M.—A4
Lehovec, Kurt—M7
Leivo, W. and R. Smoluchowski—M10
Lepore, Joseph V., Maurice Neuman, and Richard N. Stuart—U10
Levinger, J. S. and E. G. Grimsai—N7
Li, Yin-Yuan and R. Smoluchowski—E2
Lide, David R., Jr.—V1
Lidofsky, L., R. Gold, and C. S. Wu—R10
Lieberman, D. S., M. S. Wechsler, and T. A. Read—I4
Linsley, John—Z3
Livingston, M. S.—X3
Lomont, J. S.—XA3
Lotspeich, J. F., Ali Javan, and Alfred Engelbrecht—V6
Love, Temple and Fred Maienschein—Y12
Luckey, P. D.—G1
Ludloff, J. F. and M. B. Freidman—J1
Luttinger, J. M.—RA9
MacLeod, A. A., A. R. DiDonato, and A. C. Webber—M1
Maienschein, Fred and Temple Love—R1
Major, J. K. and L. C. Biedenharn—R4
Mandeville, C. E. and Jagdish Varma—R11
Marcus, Paul M.—N3
Marshak, H.—PA3
Martin, R. L.—KA2
Marton, L. and Lewis B. Leder—QA9
Mayburg, Summer—D7
McClure, G. W.—Z7
McGinnis, C. L.—R12
McKelvey, J. P. and R. L. Longini—D6
McLean, E. A. and Waller George—I11
McMaster, W. H. and F. L. Hereford—H1
Meem, J. L.—H11
Melkonian, E. and W. W. Havens, Jr.—WA2
Meshkov, Sydney—IA2
Metzger, F. R. and W. B. Todd—Y8
Mihelich, J. W., Gertrude Scharff-Goldhaber, and Michael McKeown—Y5
Mingins, Charles R., Robert W. Perry, and Albert D. Frost—M5
Minton, George H.—H7
Mizushima, Masataka—V8
Murray, B. B. and J. D. Kurbatov—R9
Murray, P. C., R. I. Scace, R. O. Haxby, and T. R. Palfrey, Jr.—JA5
Nagamatsu, H. T.—J3
Naumann, R. A.—Y6
Neufeld, Jacob—XA2
Newman, E. and W. L. Alford—C4
Newson, H. W., R. M. Williamson, A. L. Toller, and P. F. Nichols—PA5
Newton, Roger G.—U9
Nicolai, V. O. and E. L. Goldwasser—G2
Nowick, A. S.—I8
Nozick, Seymour—QA12
Ogg, Richard A., Jr.—L2
Oriani, R. A.—I5
Overhauser, A. W.—L8
Pai, Shih I.—S2
Palmatier, E. D., J. T. Meers, and C. M. Askey—KA10
Parzen, Philip—XA8
Patterson, J. R., H. W. Newsom, R. C. Mobley, and T. E. Gilmer——PA4
Paul, E. B., H. E. Gove, G. A. Bartholomew, and A. E. Litherland—C14
Pearson, G. L., W. T. Read, Jr., and F. J. Morin—D4
Pegram, G. B.—Q1
Penning, J. R. and F. H. Schmidt—R3
Percus, Jerome J. and George J. Yevick—U5
Pevsner, Alhud, James Rainwater, Ross Williams, and Seymour J. Lindenbaum—KA1
Philipp, H. R.—QA6
Piper, William W. and Ferd E. Williams—QA4
Powell, W. M.—T12
Pomerantz, W. A.—Z1
Pond, T. A.—H8
Rabi, I. I.—Q3
Rainwater, James—O3
Ramsey, N. F.—DA1
Read, T. A., M. S. Wechsler, and D. S. Lieberman—I3
Reynolds, George T. and S. B. Treiman—Z11
Riddell, R. J., Jr., and Burton D. Fried—B4
Rittner, E. S.—W3
Roberts, A. and J. Tinlot—KA4
Roesch, William C.—R2
Ross, Donald—S5
Rothman, M. A., H. S. Hans, and C. E. Mandeville—WA5
Rothstein, Jerome—XA5
Ruderman, M. A. and H. Brown—B9
Rustad, B. M.—DA4
Sagane, Ryokichi and Walter F. Dudziak—G3
Sakai, M., J. Dick, and J. D. Kurbatov—R7
Salkovitz, Edward I. and Paul L. Smith—M6
Saraf, Babulal—V1
Schensted, Craige—XA7
Scherrer, V. E., B. A. Allison, and W. R. Faust—WA7
Schneider, E. E.—L7
Schriever, Barbara Dwight, E. A. Whalin, and A. O. Hanson—JA4
Schwartz, Robert N.—XA10
Scott, M. B., A. O. Hanson, and D. W. Kerst—JA2
Serber, R. L.—A3
Sessler, A. M. and H. M. Foley—IA5
Severiens, J. C. and C. S. Fuller—D5
Sharp, W. T., H. Gellman, and G. E. Tauber—IA7
Shatas, R. A., J. F. Marshall, and M. A. Pomerantz—H2
Sheer, C., A. Zinn and N. Hartmann—LA10
Sherwood, J. E., T. E. Stephenson, C. P. Stanford, and Seymour Bernstein—WA8
Shutt, R. P.—A2
Shuttleworth, R. A. and B. C. Bradshaw—F3
Silver, E. G. and R. W. Waniek—LA9
Singer, S. E., W. S. Emmerich, and J. D. Kurbatov—R6
Smith, B. and H. A. Boorse—N6
Smith, H. L. and J. A. Kies—I10
Smith, J. A., J. N. Cooper, and J. C. Harris—C12
Snow, G. A., T. Coor, D. A. Hill, W. F. Hornyak, and L. W. Smith—WA11
Snowdon, S. C. and W. D. Whitehead—T9
Snyder, W. S. and Jacob Neufeld—I6
Solimene, N. and B. P. Dailey—V3
Spetner, L. M.—QA13
Spielberg, N., C. H. Shaw, and J. A. Soules—E6
Sproull, R. L.—W1
Spry, W.—KA6
Stearns, M., M. B. Stearns, S. De Benedetti, and L. Leipuner—KA9
Stewart, J. W. and C. A. Swenson—N9
Strauch, K. and F. Titus—T6
Sugarman, Nathan and Anthony Turkevich—PB5
Sugarman, R. and S. De Benedetti—Z6
Swann, C. P.—LA1
Tauber, G. E. and Ta-You Wu—IA8
Taylor, T. B.—T8
Temmer, G. M. and N. P. Heydenburg—C2
Templeton, D. H. and E. M. Douthett—H12
Tinlot, J. and A. Roberts—KA5
Titus, F. and K. Strauch—T5
Tobocman, W.—IA10
Tomlinson, E. P., R. A. Naumann, and J. W. Mihelich—Y7
Toupin, R. and M. Lax—RA2
Townes, C. H.—O4
Trumble, R. E., Jr.—C6
Turkevich, Anthony—PB1
Uberoi, M. S.—J4
Ufford, C. W. and S. Meshkov—IA1
Van der Ziel, A.—W4
Varma, Jagdish—Y9
Venable, Douglas and Leo F. Perry—S11
Vineyard, G. H.—E1
Vogt, Erich and Gregory H. Wannier—XA9
von Krzywoblocki, M. Z.—S4
Wall, N. S.—JA3
Wall, C. N.—P2
Wallenmeyer, W.—LA2
Wallis, G. and H. E. Farnsworth—QA7
Walsh, J. M.—K1
Wang, T. C. and C. H. Townes—L5
Watson, W. R., J. J. Dropkin, and A. T. Halpin—QA3
Webb, W., J. W. Spencer, and R. W. Schiessler—F4
Weber, J.—XA6
Wechsler, M. S., D. S. Lieberman, and T. A. Read—I2
Wegel, R. L. and H. C. Rorden—S1
Weinstein, Roy, Martin Deutsch, and Sanborn Brown—H9
Whalin, E. A. and R. A. Reitz—E7
Wheeler, J. A.—P3
White, M. G.—X4
White, Robert L.—V4

Wilkinson, M. K., C. G. Shull, L. D. Roberts, and S. Bernstein—N8
Willard, H. B., J. K. Bair, and J. D. Kington—T10
Williams, R. W. and J. H. Vilain—G11
Williams, Ross, Aihud Pebsner, James Rainwater, and Seymour J. Lindenbaum—KA3
Willig, F. J.—K2
Winkler, Stanley—QA11
Witmer, Enos E.—JA6
Wolfe, B., J. W. DeWire, and A. Silverman—G7
Wolfenstein, L.—U1
Wolff, G.—QA5
——, P. H. Keck, and J. D. Broder—F6
Wolff, P. A.—D1
Wolfgang, R. and G. Friedlander—PB3
Wood, R. E.—Y4
Woodruff, Robert W. and M. Parker Givens—E5
Workman, E. J. and W. Drost-Hansen—M3
Yevick, George J. and Jerome J. Percus—U4
Zacharias, J. R.—DA2
Zemach, A. C. and R. J. Glauber—WA4
Zimmerman, S. F., Jr., and C. P. Browne—C11
Zucker, A. and H. L. Reynolds—C10
Zumino, Bruno—B11

Proceedings of the American Physical Society

Minutes of the Meeting of 26–27 February, 1954, at Austin, Texas

THE American Physical Society met at Austin, Texas, on Friday and Saturday, February 26 and 27, 1954. This was our third meeting in Texas and our first in Austin. The University of Texas was an excellent host, and the Chairman of the Local Committee, Professor E. L. Hudspeth, arranged everything very well. The weather was memorable: 93° on the first day of the meeting, and a dust-storm on the second. There were 228 registrants, 59 ten-minute papers and 17 invited papers. The range of subjects was vast; the proportion of contributed papers in molecular spectroscopy was unusually high.

The banquet of the Society was held on Friday evening in the Driskill Hotel with attendance of 143. (We should indeed be pleased if at our bigger meetings there were even half so large a proportional attendance at the banquet!) R. T. Birge, Vice-President, presided in the absence of the President. The after-dinner speech was given by the distinguished historian Walter P. Webb of the University of Texas. Before the banquet we enjoyed the unusual privilege of a cocktail-party offered by the *Austin American-Statesman*.

The Council was not convoked at this meeting.

Karl K. Darrow, *Secretary*
American Physical Society
Columbia University
New York 27, New York

(There were no Errata for the Austin Bulletin.)

PROGRAMME

FRIDAY MORNING AT 10:00

Batts Auditorium

(E. L. HUDSPETH presiding)

Invited Papers

A1. Thermodynamic Properties of Solids Deduced from High-Pressure Measurements. D. S. HUGHES, *University of Texas.* (30 min.)

A2. Recent Advances in Nuclear Spectroscopy. A. C. G. MITCHELL, *Indiana University.* (30 min.)

A3. Recent Developments in Radio-Frequency Spectroscopy. DUDLEY WILLIAMS, *Ohio State University.* (30 min.)

A4. Millimeter and Submillimeter Wave Spectroscopy. WALTER GORDY, *Duke University.* (30 min.)

FRIDAY AFTERNOON AT 2:00

Room 203, Physics Building

(W. V. HOUSTON presiding)

Invited Papers in Solid-State Physics

B1. Nucleon Bombardment of Semiconductors. J. H. CRAWFORD, *Oak Ridge National Laboratory* (30 min.)

B2. Chemical Observations on Nonstoichiometric Zinc Oxide and Interpretation of Its Conductivity. J. J. LANDER, *Bell Telephone Laboratories.* (30 min.)

B3. The Effect of Pressure on Superconductivity. C. F. SQUIRE, *Rice Institute.* (30 min.)

B4. The Periodic Hall Effect at Low Temperatures. J. M. REYNOLDS, *Louisiana State University.* (30 min.)

FRIDAY AFTERNOON AT 2:00

Batts Auditorium

(J. G. POTTER presiding)

Invited Papers in Nuclear Physics

C1. Nuclear Spectroscopic States Deduced from Alpha Decay. I. PERLMAN, *University of California, Berkeley.* (30 min.)

C2. Recent Scintillation—Spectrometer Measurements at Louisiana State University. MAX GOODRICH, *Louisiana State University.* (30 min.)

C3. Angular Distribution of Products from 22-Mev Proton Reactions. B. L. COHEN, *Oak Ridge National Laboratory.* (30 min.)

Nuclear Physics, I

C4. Angular Correlation Apparatus for the $Li^7(p,\gamma,\alpha)He^4$ Reaction.* PAT M. WINDHAM AND G. C. PHILLIPS, *The Rice Institute.*—Angular correlation studies are being attempted in the reaction $Li^7(p,\gamma,\alpha)He^4$. This information would permit assignment of the angular momentum of the states involved. The alpha particles that are emitted from the 3-Mev excited state in Be^8 are analyzed at 90° to the beam by means of a magnetic spectrometer of about 4 percent resolution. The alpha particles are deflected through 30° and then are detected by means of a KI(Tl) scintillation counter that subtends a solid angle of 1/675 steradian at the end of a tube some 150 cm from the center of the magnet. The γ rays are detected by means of a NaI(Tl) scintillation counter that can be rotated in space about the target assembly. The γ-ray and alpha-particle pulses are fed into a coincidence circuit with a resolving time of about 10^{-8} second. The operation of the analyzer and coincidence apparatus will be discussed in addition to a brief presentation of theoretically expected correlation for various reasonable assignments of angular momenta.

* Supported by the U. S. Atomic Energy Commission.

C5. A Large Volume Scattering Chamber for Angular Distribution Experiments.* J. RUSSELL, JR., C. W. REICH, AND G. C. PHILLIPS, *The Rice Institute.*—A large volume scattering chamber made of aluminum has been designed and constructed at The Rice Institute. It has an inside diameter of 30 inches and is 13 inches in height. To avoid alignment errors due to distortion of the evacuated chamber the detector slit system turntable and the beam defining slit assembly are rigidly supported independently of the chamber. The azimuth circle, complete with vernier, from a K and E transit, is used to measure angles accurate to one half minute of arc. The present particle detector is a potassium iodide crystal. The preamplifier and phototube are inside the chamber in a vacuum-tight cylinder which is open to atmospheric pressure. Provisions are made for both gas and solid targets. Details of construction and operation will be presented.

* Supported by U. S. Atomic Energy Commission.

C6. A Differential Pumping System for Gas Targets.* C. W. REICH, J. RUSSELL, AND G. C. PHILLIPS, *The Rice Institute.*—A differential pumping system to be used in connection with the large volume scattering chamber has been designed and built. Its construction and operation will be described. The pumping system has the form of a nozzle 36 in. long and 2½ in. in diameter. Inside the tube there are 72 slits arranged in three groups which give the required pressure drops. The slits are made of brass sheet 10 mils thick. They are ¾ in. in diameter and have a circular hole 2 mm in diameter. The pressures in the various regions, with 2 cm of air in the chamber are of the following magnitude: 550 microns after the first stage, 45 microns after the second stage, and 0.10 micron after the third stage. Pumping on the first stage is a roughing pump with a speed of 5 liters per second. Pumping on the second stage is a booster pump with a speed of 100 liters per second, backed by a mechanical fore pump with a speed of 1 liter per second. Pumping on the third stage which leads into the accelerator tube is the diffusion pump of the Van de Graaff. At either end of the system there are defining slits of Tantalum sheet, 10 mils thick. In each of these is drilled a hole 1.5 mm in diameter. With this system it is possible to admit the beam into the scattering chamber without its having to pass through a foil.

* Supported by the U. S. Atomic Energy Commission.

C7. Gamma-Rays from Ne^{22}.* B. P. FOSTER,† G. S. STANFORD, AND L. L. LEE, *Yale University.*—The decay scheme of the low-lying states of Ne^{22} has been investigated by means of a proton gamma-ray coincidence study of the $F^{19}(\alpha,p)Ne^{22}$ reaction using a NaI (Tl) scintillation spectrometer to measure the gamma-ray energies. The experimental arrangement was similar to that used in the previously reported investigation of Mg^{26}.[1] The energy of excitation of the second and third excited states were rechecked and found to be 3.3 and 4.9 Mev, respectively. The results of the study cast considerable doubt on the existence of the level at about 0.6-Mev excitation which had been previously reported. For the 1.28-Mev excited state a single transition direct to ground was identified. The second excited state was found to decay principally by the cascade transition through the first excited state with a weaker cross-over transition to ground. Transitions from the third excited state to the first excited state and to ground were established.

* Assisted by the joint program of the U. S. Office of Naval Research and U. S. Atomic Energy Commission.
† Now at North Texas State College, Denton, Texas.
[1] J. E. May and B. P. Foster, Phys. Rev. **90**, 243 (1953).

C8. Disintegration of La 140. C. L. PEACOCK, A. W. OSER, AND J. F. QUIN, *Tulane University.*—The radiations of La 140 have been investigated with a conventional magnetic spectrometer of 20-cm radius. The complex beta spectrum can be resolved into at least five groups whose maximum energies are: 0.83 Mev, 1.10 Mev, 1.34 Mev, 1.67 Mev, and 2.15 Mev. Most of the reported[1,2] gamma rays were verified. Those with energies of 0.110 Mev, 0.130 Mev, 0.240 Mev, 0.270 Mev, 0.328 Mev, 0.485 Mev, 0.815 Mev, and 1.60 Mev were found by photoelectric and internal conversion methods. A disintegration scheme will be proposed.

[1] Beach, Peacock, and Wilkinson, Phys. Rev. **76**, 1624 (1949).
[2] Cork, Stoddard, LeBlanc, Branyan, Martin, and Childs, Phys. Rev. **83**, 856 (1951).

FRIDAY AFTERNOON AT 2:00

Physics Building, Room 201

(F. A. MATSEN presiding)

Molecular Spectroscopy; Atomic Physics

D1. The Infrared Spectra of Deuterated Ethylene Oxide. CHARLES W. ARNOLD AND F. A. MATSEN, *The University of Texas.*—Fully deuterated ethylene oxide has been prepared and its infrared spectra studied over the range from 3 to 20 microns. The spectra have been carefully examined to allow for the presence of possible impurities. As far as possible, the bands have been assigned from their contours and relative intensities. The Teller-Redlich Product Rule has been used as an aid in locating weak bands and in confirming all final assignments. A normal coordinate treatment has been made for the molecule. By use of certain assigned bands from C_2H_4O and C_2D_4O, a set of force constants has been calculated and reasonable values predicted for some of the doubtful band frequencies. The calculated specific heat of the light molecule at 307.18°K based on this assignment is 11.817, which is to be compared with the experimental value of 11.80. The assignment of the infrared active bands of C_2D_4O is as follows: A_1—2211, 1311, 1015, 969, 753; B_1—2176, 1163(?), 905(?), 811; B_2—2316, 896, 578.

D2. Molecular Wavefunctions in the *e*-Notation. J. M. MILLER AND F. A. MATSEN, *University of Texas.*—The *e*-notation for determinants and the summation convention, both described by Craig,[1] are useful for writing electronic wavefunctions. For example a general N-electron molecular wavefunction may be written as follows:

$$\Psi = (1/N!^{\frac{1}{2}})e^{rstu\cdots xy\cdots}A_{ij,kl,\ldots}\phi_r{}^i\bar{\phi}_s{}^j\phi_t{}^k\bar{\phi}_u{}^l\cdots\phi_x{}^p\bar{\phi}_y{}^q\cdots.$$

The sets $rstu\cdots xy\cdots$ index the N electrons. The sets $ij, kl, \cdots$ index atomic orbitals. The number of pairs of different indexes on A gives the number of bonds in the molecule. The range of indexes on A is determined as follows. Counting numbers are assigned to the atomic orbitals. The summations extend over the whole range of these numbers, except that A vanishes

when the same number is assigned to members of different pairs or if the interchanging of two or more pairs produces a previously obtained arrangement. Specific valence structures, ionic terms, or hybridization can be eliminated by suitable restrictions on the indexes. This notation reduces somewhat the amount of analytical work required to write down matrix elements.

[1] H. V. Craig, *Vector and Tensor Analysis* (McGraw-Hill Book Company, Inc., New York, 1943).

D3. The United Atom-Separated Atom Treatment of H_2^+. J. R. STREETMAN AND F. A. MATSEN, *University of Texas.*—Since H_2^+ at $r=0$ becomes He^+ and at $r=\infty$ becomes $H+H^+$, it might be expected that a linear combination of wavefunctions for each of these limiting forms would provide an improved description of the molecule ion. A trial wavefunction consisting of a linear combination of 1*S* orbitals centered on the nuclei and on a point halfway between them was used in a variational treatment. A one-electron three-center integral with nonequal charges which arises in this treatment was evaluated. The effective nuclear charges for minimum energy were found approximately by calculating energies for a range of values of the separated atom charge and of the united atom charge. The lowest energy calculated, −0.5969A, occurred where both effective nuclear charges are equal at 1.25. The energy value should be compared with −0.6031A, the exact value, and with −0.6001A obtained by hybridizing 1*S* and 2*Pz* orbitals on the separated nuclei. The mixing coefficient of the united atom was found to be 0.3501.

D4. Application of the Franck-Condon Principle to the Bent XY_2 Molecule.* J. B. COON AND J. K. WARD, *A and M College of Texas.*—A method is described for comparing the experimental intensities of vibronic bands of an XY_2 molecule with Condon overlap integrals calculated to the harmonic approximation. Using the vibrational frequencies and the apex angle for a given electronic state, normal coordinates Q_i may be calculated by known methods. Three independent Cartesian coordinates x_i of the nuclei for the ground electronic state are related to similar coordinates x_i' for the excited state by $x'=x+C$, where C is a three-element column matrix determined by the equilibrium bond distances and angles of both states. This leads to the relation $Q'=\zeta Q+K$, where ζ is a 3×3 matrix in which the elements ζ_{13}, $\zeta_{23}\neq0$ unless $\theta'=\theta$. The Condon overlap integral takes the form

$$I=N'(v_1'v_2'v_3')N(v_1v_2v_3)\int\int\int\Pi_i H_{v_i'}(\alpha_i'Q_i')\times\exp(-\tfrac{1}{2}\alpha_i'^2Q_i'^2)\Pi_j H_{v_j}(\alpha_jQ_j)\exp(-\tfrac{1}{2}\alpha_j^2Q_j^2)dQ_1dQ_2dQ_3,$$

where $\alpha_i^2=(4\pi^2/h)c\omega_i$, and $H_{v_i}(\alpha_iQ_i)$ are Hermite polynomials. This is easily evaluated for any special case. The ratio of the overlap integrals for two vibronic bands is known to be related to the integrated molecular extinction coefficients ϵ_i for these two bands by $(I_1/I_2)^2=\exp[hc(G_1-G_2)/kT](\nu_2/\nu_1)\times(\int\epsilon_1\delta\nu/\int\epsilon_2\delta\nu)$, where G_i is the ground state vibrational level associated with band i. Sufficient data are available for ClO_2 to evaluate these integrals.

* This research was supported by the U. S. Air Force through the Office of Scientific Research of the Air Research and Development Command.

D5. Vibrational Analysis of the 3400–4000A Absorption Spectrum of SO_2.* R. K. RUSSELL, *A and M College of Texas* (introduced by J. B. Coon).—The SO_2 spectrum is being investigated in the 3400–4000 A region. Wave numbers have been measured on spectrograms obtained with absorbing paths up to 18 meter-atmospheres. These wave numbers have been used in a preliminary analysis. Within an average deviation of about 2 cm^{-1}, 23 bands fit the formula $\nu=\nu_0+(G_0'-G_0'')$, where $\nu_0=25{,}776.0$ cm^{-1} and $G_0'(v_1',v_2',v_3')=938.3v_1'+362.8v_2'+1119.65v_3'-34.60v_1'^2-1.95v_2'^2-25.77v_3'^2+1.82v_1'^2-5.9v_1'v_2'-21.55v_1'v_3'-9.1v_2'v_3'$. Ground-state levels G_0'' given by Nielsen[1] were used. Previously, in a brief report, Metropolis and Beutler[2] assigned the $(0,0,0)'\leftarrow(0,0,0)''$ band and gave approximate values of ν_1' and ν_2' that are essentially in agreement with the above formula. The $G_0'(2,1,0)$ and the $G_0'(0,0,2)$ excited state vibrational levels appear to perturb each other, the shift being about 33 cm^{-1}. It is expected that spectrograms to be made with still longer absorbing paths will reveal more bands, thus providing additional data needed to confirm or improve the analysis.

* This research was supported by the U. S. Air Force, through the Office of Scientific Research of the Air Research and Development Command.
[1] Shelton, Nielsen, and Fletcher, Phys. Rev. **91**, 235 (1953).
[2] N. Metropolis and H. Beutler, Phys. Rev. **57**, 1078 (1940).

D6. Vibrational Spectra of Methyltrifluorosilane. R. L. COLLINS AND J. RUD NIELSEN, *University of Oklahoma.*—The infrared spectrum of gaseous H_3C-SiF_3 has been obtained in the region from 2.5–36μ with the aid of NaCl, KBr, and KRS-5 prisms. The Raman spectrum of liquid H_3C-SiF_3 has been photographed with a three-prism glass spectrograph of linear dispersion 15 A/mm at 4358 A, and qualitative polarization observations have been made. The eleven active fundamentals have been assigned, and a tentative value has been assigned to the inactive fundamental. A normal coordinate analysis has been made, and thermodynamic functions have been calculated for several temperatures.

D7. Vibrational Spectra of Cyclobutforene.* M. Z. EL-SABBAN AND J. RUD NIELSEN, *University of Oklahoma.*—The infrared spectrum of gaseous cyclobutforene has been obtained in the region from 2 to 38μ with the aid of LiF, NaCl, KBr, and KRS-5 prisms. The Raman spectrum of the liquid phase has been photographed with a three-prism glass spectrograph of linear dispersion 15 A/mm at 4358 A. With some uncertainties as to symmetry species, twenty-two of the twenty-four fundamental vibration frequencies have been assigned, and the spectra have been interpreted in detail.

* This work has been supported by the U. S. Atomic Energy Commission.

D8. Infrared and Raman Spectra of Fluorinated Ethanes. VIII. Pentafluoroethane.* J. RUD NIELSEN, H. H. CLAASSEN, AND NORMA B. MORAN, *University of Oklahoma and U. S. Naval Research Laboratory.*—The infrared absorption spectrum of gaseous CF_3CF_2H has been observed in the region from 2 to 38μ, and the spectrum of the liquid from 2 to 22μ, with the aid of LiF, NaCl, KBr, and KRS-5 prisms. The Raman spectrum of gaseous CF_3CF_2H has been photographed with a three-prism glass spectrograph of linear dispersion 15 A/mm at 4358 A. All but two of the fundamental vibration frequencies have been assigned, and the spectra have been interpreted in detail.

* This work has been supported by the U. S. Atomic Energy Commission.

D9. Density Effects in the Raman Spectrum of Ammonia.* C. A. PLINT, R. M. B. SMALL, AND H. L. WELSH, *University of Toronto.*—The Raman spectrum of ammonia as a high-pressure gas, liquid, solid, and aqueous solution are compared in the higher frequency region with the spectrum of the low-pressure gas. At gas pressures up to 80 atmos, no appreciable hindering of rotation is present; however, a weak satellite of the ν_1 band is an unexplained feature of the spectrum at high pressures. The spectrum of the liquid, solid, and aqueous solution can be explained without postulating dimerization: the three higher frequency maxima can be assigned unambiguously to the $2\nu_4$, ν_1, and ν_3 vibrations if it is assumed that the hindering of rotation is almost complete. The half-width of the ν_1 band increases and that of the ν_3 band decreases with decreasing temperature and increasing density. The behavior of the ν_1 band is probably due to coupling of the vibrating dipoles in pairs of molecules, and the behavior of the ν_3 band to increasing hindering of molecular rotation. The rotational fine

structure found by earlier workers for the aqueous solution could not be observed even at high dispersion.

* Supported in part by a grant from the National Research Council of Canada.

D10. Variational Wave Function for Sodium.* D. M. SMITH† AND E. L. SECREST,‡ *North Texas State College.*—A determinantal combination of one-electron wave functions[1,2] with variable parameters has been used to construct a variational wave function for the ground state of the neutral sodium atom. The resulting wave function gives a calculated ground-state energy of 325.84 atomic units compared to the experimental value of 324.63 atomic units.[3]

* This work was submitted by D. M. Smith in partial fulfillment of the requirements for the M.S. degree at North Texas State College and was supported financially by a Faculty Research Grant.
† Now at the U. S. Army Chemical Center.
‡ Now at Consolidated Vultee Aircraft Corporation, Fort Worth, Texas.
[1] Morse, Young, and Haurwitz, Physical Review **48**, 1948 (1935).
[2] W. E. Duncanson and C. A. Coulson, Proc. Roy. Soc. Edinburgh **62**, 37 (1944).
[3] R. F. Bacher and S. Goudsmit, *Atomic Energy States* (McGraw-Hill Book Company, Inc., New York, 1932).

FRIDAY EVENING AT 7:00

Driskill Hotel

(R. T. BIRGE presiding)

Banquet of the American Physical Society

After-dinner speaker: W. P. WEBB, *University of Texas.*

SATURDAY MORNING AT 9:30

Batts Auditorium

(T. W. BONNER presiding)

Invited Papers in Nuclear Physics

E1. Photoelectron Production by Polarized Gamma Rays. F. L. HEREFORD, *University of Virginia.* (30 min.)

E2. Equilibrium Charge-Exchange Ratios for Low-Energy Protons. J. A. PHILLIPS, *Los Alamos Scientific Laboratories.* (30 min.)

E3. Energy Loss of Protons and Deuterons in Gases. WARD WHALING, *California Institute of Technology.* (30 min.)

E4. Survey of Average Total Neutron Cross-Sections in the 3–12 Mev Region. NORRIS NERESON, *Los Alamos Scientific Laboratories.* (30 min.)

E5. The Diurnal Variation of Cosmic Radiation. M. S. VALLARTA, *University of Mexico.* (20 min.)

SATURDAY MORNING AT 9:30

Physics Building, Room 203

(C. M. CLASS presiding)

Nuclear Physics, II

F1. Excitation Function and Q-value for $C^{14}(d,p)C^{15}$.* JAMES A. RICKARD AND EMMETT L. HUDSPETH, *University of Texas.*—The excitation function for $C^{14}(d,p)C^{15}$ has been studied with deuterons of energy 0.6 to 3.0 Mev. The $BaCO_3$ target was enriched 18.6 percent in C^{14} and had a thickness of 124 $\mu g/cm^2$. A previously suspected resonance[1] was definitely established at 2.15 Mev, with a width of nearly 400 kev. Analysis of the excitation curve in the low-energy region (0.7 to 1.3 Mev) shows that its shape may be explained on the basis of elementary penetrability theory if one assumes a Q-value of approximately 0.15 Mev. A sudden rise in the excitation curve, beginning in the region near 1.6 Mev (excluding the resonance), may be ascribed to the increasing effectiveness of deuterons of orbital momentum unity; a spin value of C^{15} of 5/2 is suggested on this basis, in agreement with theortical predictions.[2]

* Assisted by the U. S. Atomic Energy Commission.
[1] Hudspeth, Swann, and Heydenburg, Phys. Rev. **80**, 643 (1950).
[2] D. R. Inglis, Revs. Modern Phys. **25**, 425 (1953).

F2. γ-ray Spectrum of C^{15} and γ rays from Proton Bombardment of C^{14}.* K. R. SPEARMAN, E. L. HUDSPETH, AND I. L. MORGAN, *University of Texas.*—The delayed γ radiation resulting from bombardment of C^{14} with 2-Mev deuterons has

been studied with a single crystal scintillation spectrometer. The 2.4-second activity is identical with the β decay of C^{15}. Pulse height analysis reveals a strong γ ray of energy approximately 5.3 Mev,[1] with evidence for very weak components of higher energies. A decay scheme for C^{15} will be proposed. We have also bombarded a target of $BaCO_3$ (18.6 percent enrichment in C^{14}) with protons and have observed γ-rays which apparently are formed by proton capture. A relatively strong γ-ray component of energy about 5 Mev was observed, with energies up to approximately 10 Mev also recorded but not well resolved in our present crystal. Evidence for resonances in a 44-kev target have been obtained in the bombarding region from 1 to 2 Mev.

* Assisted by the U. S. Air Force.
[1] Hudspeth, Rose, and Heydenburg, Phys. Rev. 85, 742 (1952).

F3. Angular Distribution of D(d,n) Neutrons Scattered from C, Al, S, Fe, Cd, Cu, W, and Pb. R. N. LITTLE, JR., C. P. CADENHEAD, B. P. LEONARD, JR., J. T. PRUD'HOMME, L. D. VINCENT, AND J. E. WILLS, *The University of Texas.*—The D(d,n) neutrons from a 100-kilovolt accelerator were scattered by ring scatterers of carbon, aluminum, sulfur, iron, cadmium, copper, tungsten (wolfram), and lead in a geometry similar to that described by Whitehead and Snowdon.[1] The detector used was a 2-in. right circular cylinder of terphenyl xylene scintillating solution on a 5819 photomultiplier tube. A pulse-height analysis using a single-channel analyzer was taken for some of the angular distributions to separate the elastically scattered neutrons from the inelastically scattered neutrons and accompanying decay gamma photons. For the diameter of the rings and the bombarding energy of 100 kilovolts the neutron energy is 2.8 Mev.

[1] W. D. Whitehead and S. C. Snowdon, Phys. Rev. 92, 114–119 (1953).

F4. Search for the $Li^7(n,t)$ Reaction. H. E. BANTA AND R. L. MACKLIN, *Oak Ridge National Laboratory.*—The reaction $Li^7(n,t)\alpha+n$ (or He^5) has been detected using fission neutrons and polonium-beryllium neutrons, by measuring the tritium produced upon neutron activation. The fission-neutron activation was made inside a uranium sleeve in the ORNL graphite pile, using cadmium and boron for additional shielding. Samples of natural and enriched Li^7F were used to allow for the tritium produced from Li^6. The computed threshold for the reaction $Li^7(n,t)\alpha+n$ is 2.8 Mev. The neutron population decreases exponentially above this energy; thus the measured cross section of 72 ± 18 mb is essentially that near 3 Mev. The polonium-beryllium neutron activation was carried out with source and samples suspended on a steel wire, 5 meters from possible neutron moderating structures. The cross section for the total flux (broad maximum near 4.5 Mev) was 30 ± 20 mb. The tritium was recovered by fusing the samples in 1-percent hydrogen-argon and its activity observed in a proportional counter. The tritium recovery and counting technique is to be described in a forthcoming paper on the $Li^7(d,t)Li^6$ reaction. This investigation is to be reported in a forthcoming article in Science.

F5. Neutron Thresholds from $Cu^{65}(p,n)Zn^{65}$, $Cu^{63}(p,n)Zn^{63}$, and $Li^7(p,n)Be^7$.* C. F. COOK AND T. W. BONNER, *The Rice Institute.*—A new technique for detecting neutron thresholds using a slow neutron counter and a conventional long counter is discussed. This method has been applied to the bombardment of copper by protons. Many resonances in neutron emission were observed and neutron thresholds were found at 2.15, 3.03, and 4.28 Mev. The first two thresholds are due to Cu^{65} and indicate an excited state in Zn^{65} at 0.86 Mev. The 4.28-Mev threshold is due to Cu^{63}.

* Assisted by the U. S. Atomic Energy Commission.

F6. Neutron Thresholds in the Reactions $Li^7(d,n)^8Be^8$ and $Be^9(d,n)^{10}B^{10}$. T. W. BONNER AND C. F. COOK, *The Rice Institute.*—Neutron thresholds from the deuteron bombardment of Li^7 have been studied at energies from 0.4 Mev to 4.7 Mev. Thresholds were observed at energies of 2.18 Mev, 2.55 Mev, 3.37 Mev, and 4.07 Mev. These thresholds indicate a level in Be^8 at 16.70 Mev with a half-width of 195 kev, a level at 16.99 Mev with a width of 350 kev, a narrow level at 17.63 Mev, and a wide level at 18.14 Mev. By the same method, excited states in B^{10} from the $Be^9(d,n)B^{10}$ reaction were found at 4.78, 5.11, 5.17, 5.93, 6.04, 6.16, and 6.61 Mev.

* Assisted by the U. S. Atomic Energy Commission.

F7. Neutrons from Proton Bombardment of Be^9 and H^3.* J. B. MARION, C. F. COOK, AND T. W. BONNER, *The Rice Institute.*—The two-counter technique, described in the two preceding papers, has been applied to a study of the neutrons from the proton bombardment of Be^9 and H^3. A narrow excited state of B^9 has been observed at 2.36 Mev by neutron threshold measurements ($Q=-4.21$ Mev). This state corresponds to the 2.43-Mev level in the mirror nucleus, Be^9. In addition, threshold neutrons have been observed which may be due to a broad (~1 Mev) level in B^9 at ~1.4 Mev. The $H^3(pn)He^3$ reaction shows only the single well-known threshold at $E_p=1020$ kev.

* Assisted by the U. S. Atomic Energy Commission.

F8. $N^{14}(n,2n)N^{13}$ Cross-Section Measurement with 14 Mev Neutrons.* J. D. DUDLEY AND C. M. CLASS, *The Rice Institute.*—The $N^{14}(n,2n)N^{13}$ cross section was measured for 14-Mev neutrons obtained from the $T(d,n)He^4$ reaction. A liquid nitrogen sample was contained in a hemispherical Lucite vessel half enclosing a tritium-zirconium target. This arrangement maximizes the effectiveness of the neutron flux and simplifies the calculations for the cross section. For the purpose of preventing evaporation of the sample, the assembly was surrounded by a bath of liquid nitrogen. After irradiation, the sample was transferred to a Dewar flask of dimensions appropriate for efficient coincidence counting of the annihilation radiation from the 10 minutes positron activity of the N^{13}. The counting system was calibrated with a standardized solution of Na^{22}. The neutron monitor was calibrated by counting the α particles from the $T^3(d,n)He^4$ reaction. Preliminary measurements yield a cross section for nitrogen of 3.4 mb$\pm$30 percent. The method was also applied to other elements which were available in suitable liquid form.

* Supported in part by the U. S. Atomic Energy Commission.

F9. Nuclear Energy Levels by Absolute Magnetic Analysis of Inelastically Scattered Protons.* C. R. GOSSETT, G. C. PHILLIPS, AND J. T. EISINGER, *The Rice Institute.*—The Rice Institute annular magnet has been used to measure the energies of protons scattered at 180° from thin targets. Energies of the elastic and inelastic scattered protons are determined from their $B\rho$ as measured in terms of standardized length and frequency. The energy measurements are sufficiently accurate to permit calculation of the mass number of the scattering nuclei when two different bombarding energies are used. This method offers the advantages of absolute measurement, high resolution, high accuracy, and positive identification of the scattering nuclei. The apparatus and techniques will be described and the results of experiments on F^{19} given.

* Supported by the U. S. Atomic Energy Commission.

F10. Nonelastic Scattering of Fast Neutrons.* H. L. TAYLOR, O. LÖNSJÖ, AND T. W. BONNER, *The Rice Institute.*—Nonelastic scattering cross sections have been obtained using the spherical shell method. The neutron detectors were made of small anthracene spheres embedded in CF_2 liquid. These

give good energy discrimination and do not count γ radiation. Results have been obtained with monoenergetic neutrons with energies of 4.5, 7.0, and 14.1 Mev, in Ti, Cr, Fe, Ni, Cu, Ag, Sn, Pb, and Bi. At these energies the nonelastic cross sections is geometrical and can be explained by the relation $\sigma=\pi(R+\lambda)^2$.

* Assisted by the U. S. Atomic Energy Commission.

F11. A Fast Neutron Counter with Energy Resolution.* J. H. McCrary, H. L. Taylor, and T. W. Bonner, *The Rice Institute.*—Fast neutron counters have been made of small spheres of anthracene separated from each other by either CF_2 liquid or glass. Recoil proton pulses from 3–20 Mev neutrons can be made larger than γ-ray pulses by using spheres with diameters of from 3 to 8 mm. Several millimeters of glass between the spheres prevent electrons from going through two or more anthracene crystals. Neutron energies can be obtained from the maximum pulse size.

* Assisted by the U. S. Atomic Energy Commission.

F12. LiI(Eu) Crystals as Neutron Detectors.* J. B. Marion, *The Rice Institute.*—Distributions of pulse heights produced by monoenergetic neutrons in europium-activated LiI crystals have been taken, using neutrons from the reactions $H^3(p,n)He^3$ and $Be^9(d,n)B^{10}$. In the former case, with 1200-kev neutrons, a pulse height four times that of Cs^{137} gamma rays was observed, with a resolution of 20 percent. However, with neutrons from $Be^9(d,n)B^{10}$, the peak could not be resolved because of the strong gamma-ray background present. It appears that LiI crystals will be useful for detecting neutrons only under conditions of low gamma-ray background.

* Assisted by the U. S. Atomic Energy Commission.

Saturday Morning at 9.30

Physics Building, Room 201

(J. H. Crawford presiding)

Solid-state Physics; Cryogenics

G1. The Variation Method Applied to Wave Functions in Crystals. W. V. Houston, *The Rice Institute.*—Although the variation method has been widely applied to wave functions for atoms and molecules, it has been used only recently for crystals. The wave function in a periodic potential consists of a plane wave modulated by a function with the period of the lattice. The variation method can be applied to the modulation function by expanding it in a Fourier series with the vectors of the reciprocal lattice. The coefficients of the expansion can then be determined to give the energy a stationary value. The process can be carried as far as desired, but it seems probable that a relatively small number of terms will give good indications of the dependence of the energy on the propagation vector. It is also probable, however, that a small number of terms will not give good values for the wave function in the neighborhood of the atomic core.

G2. Electron Interactions in Metals. Robert L. Chuoke, *The Rice Institute** (introduced by C. H. Fay).—A modification of Macke's variational calculation of correlation energy[1] for conduction electrons in metals yields a correlation energy still in essential agreement with Wigner's early result while providing a screening function $\beta=\beta(g)$, depending only on the magnitude g of momentum change, which is also applicable to screened Coulomb perturbation matrix elements associated with energy conservative transitions such as occur in Landsberg's calculation of the L_{III} soft x-ray emission spectrum of sodium.[2] For small g, which is the important range with regard to divergences, $\beta^2(g)=\kappa k_F^2+O(g)$ where k_F is the Fermi level and $\kappa=(2/\pi)(4/9\pi)^{\frac{1}{3}}(\rho_s/a_H)$, a_H=Bohr radius, and $4\pi\rho_s^3/3=V/N$, volume per conduction electron. For sodium, neglecting terms of order g, $\beta=10^8$ cm^{-1} which agrees with the empirical value.[3] The result predicts increasing tail lengths of soft x-ray emission spectra for increasing density of conduction electrons. It should be noted that in this approach to electron interactions the insertion of a screened potential into the exchange integral, as was done by Wohlfarth,[3] does not seem to be justified.

* Now with Shell Development Company, Houston, Texas.
[1] W. Macke, Z. Naturforsch. **5A**, 192 (1950).
[2] P. T. Landsberg, Proc. Phys. Soc. (London) **62**, 806 (1949); H. W. B. Skinner, Phil. Trans. Roy. Soc. **A239**, 95 (1946).
[3] E. P. Wohlfarth, Phil. Mag. **41**, 534 (1950). See also D. Bohm and D. Pines, Phys. Rev. **80**, 903 (1950) as well as their more recent work.

G3. Field Dependent Magnetic Susceptibility of MnSe. Robert Lindsay, *Southern Methodist University.*—A further analysis has been made of the data originally reported by the writer.[1] Comparison is made with the results obtained by other investigators. A theory is advanced to explain the observed field dependent susceptibility effects in terms of a feeble parasitic ferromagnetism. When the data are interpreted on this basis, magnetization curves can be drawn which show the parasitic ferromagnetism starting at about 10°C, increasing to a maximum at about −120°C, and decreasing to a small but finite value at −190°C. The magnitude of the ferromagnetism appears to depend on the thermal history of the sample and follows a hysteresis pattern similar to that for the susceptibility. The results are discussed in terms of the three phase model for MnSe proposed by the writer.[1]

[1] R. Lindsay, Phys. Rev. **84**, 569 (1951).

G4. Some Electrical Characteristics of Polycrystalline Boron.* L. J. Badar and V. P. Jacobsmeyer, *Saint Louis University.*—The properties of high purity boron samples deposited at 1000°C, 1300°C, and 1500°C by the pyrolytic decomposition of diborane gas were compared with results obtained by Friedrich.[1] Sample micrographs and x-ray diffraction patterns revealed large size crystallites in samples deposited at 1000°C and 1500°C, while 1300°C samples exhibited a fine grain structure. From a room-temperature value of 2700 ohm-cm, the resistivity dropped to less than 10 ohm-cm at 640°K in the 1300°C samples. A decrease in resistivity by a factor of 20 in the 1000°C samples was noted over the same temperature range. A small but definite increase in slope of the $\log\rho$ *vs* $1/T$ curves was observed for all samples at about 450°K. For the 1000°C samples the activation energy measured 0.30 ev, while a value of 0.86 ev was obtained from data on the 1300°C samples. X-rays were found to have little effect on the resistivity at high temperatures, indicating that the low-temperature resistivity change induced by the x-ray bombardment was caused by the impurities present. Activation energy values were not altered by the irradiation.

* Research carried out under contract with U. S. Office of Ordnance Research.
[1] L. W. Friedrich and V. P. Jacobsmeyer, Phys. Rev. **91**, 492(A) (1953).

G5. The Electrical Properties of Molybdenite. C. W. HEAPS, *Rice Institute.*—The resistance, magnetoresistance, and Hall effect have been measured for natural crystals of molybdenite at different temperatures. The material was an *n*-type semiconductor. The resistivity is 1.6 ohm-cm at 26°C and about 30 000 times larger at −190°C. The Hall constant is independent of magnetic field strength up to 7000 gauss. It is equal to 1260 (in e.m.u.) at room temperature and 27 000 at −76°C. Magnetoresistance is small—a resistance increase of about 0.015 percent for a magnetic field of 20 000 gauss at room temperature. There is evidence of an internal barrier layer effect which is associated with the foliated character of the crystal structure.

G6. The Time Rate of Change for the Transformation of Monoclinic Selenium into Hexagonal ALVIN E. COWAN* AND ARTHUR E. LOCKENVITZ, *University of Texas.*—Finely divided monoclinic crystals of selenium were placed in a constant temperature over x-ray diffraction apparatus. A Geiger counter feeding into a recording rate meter was set at the angle to receive a prominent line diffracted from any hexagonal selenium present. The intensity of this line was used as a measure of the amount of hexagonal selenium present and of the disappearance of the monoclinic modification. The temperature region from 70°C to 120°C was explored.

* At present at Pentagon, U. S. Army.

G7. Flow of Helium II Under a Hydrostatic Pressure Head.* R. T. SWIM† AND H. E. RORSCHACH, JR., *The Rice Institute.*—The pressure induced isothermal flow properties of HeII have been studied with an arrangement similar to that of Bowers and Mendelssohn.[1] Measurements of the flow rate have been made with hydrostatic pressures up to 2.3×10^3 dynes/cm^2 at temperatures between 1.39 and 2.10°K. Slit widths of 4.3 and 2.4 microns were used. At low pressures, the flow rate is proportional to approximately the $\frac{1}{4}$ power of the pressure head, although this power depends on the slit width. At higher pressures, the flow rate is independent of the pressure head. This saturation rate corresponds to a maximum velocity for the superfluid component of approximately 22 cm/sec. The flow rates at constant pressure head have the same temperature dependence as the superfluid concentration in liquid helium II. The significance of these flow measurements in interpreting the hydrodynamic properties of helium II will be discussed.

* This work supported in part by the U. S. Office of Naval Research.
† Magnolia Petroleum Company Fellow at Rice Institute (1952–1953). Now at the Bell Telephone Laboratories, Murray Hill, New Jersey.
[1] R. Bowers and K. Mendelssohn, Proc. Roy. Soc. (London) **A218**, 158 (1952).

G8. The Decay of Positrons in Superconducting Lead.* WALTER E. MILLETT, *University of Texas.*—The decay of positrons in superconducting lead has been studied by the method of delayed coincidences. A block of lead of questionable purity containing a sodium-22 source of positrons was fastened to a metal flask containing liquid helium at atmospheric pressure. The lead was then well below its transition temperature. A delay coincidence curve was measured with liquid helium in the flask and then measured again with liquid nitrogen in the flask. The measurements indicate that the mean life of some of the positrons in superconducting lead is increased to (3.5±0.5) millimicroseconds. The measurements of Bell and Graham[1] show that all positrons decay in lead at room temperature with a mean life (0.15±0.06) millimicrosecond. This work is being continued at the University of Texas with improved resolution and with different superconductors.

* This work was carried out during the past summer at the Cyclotron Laboratory of Harvard University. The liquid helium was supplied by both Harvard University and Massachusetts Institute of Technology.
[1] R. E. Bell and R. L. Graham, Phys. Rev. **90**, 644 (1953).

G9. Lifetime of Positrons in Superconductors. HARRY TALLEY AND ROBERT STUMP, *University of Kansas.*—The lifetime of positrons in solids is considerably different for metals and insulators. Since a metal in the transition to the superconducting state undergoes marked changes in electrical conductivity as well as other properties depending on the electron interactions, it was thought that the lifetime of positrons in superconductors might indicate something of the nature of the superconducting state. Using the method of delayed coincidence, we have measured the lifetime of positrons from Na^{22} enclosed in a lead cylinder at a temperature of 4.2°K. The experiment indicates that the lifetime of the positrons in the superconducting lead is longer than the lifetime of positrons in the same sample in the normal state. The results are in qualitative agreement with theoretical estimates of the expected change in lifetime based on the Frohlich theory of superconductivity.

SATURDAY AFTERNOON AT 1:30

Batts Auditorium

(R. T. BIRGE presiding)

Invited Paper

H1. Coulomb Excitation of Nuclei. C. M. CLASS, *Rice Institute.* (30 min.)

Nuclear Physics, III

H2. Coulomb Excitation of Heavy Nuclei.* C. M. CLASS, C. F. COOK, AND J. T. EISINGER, *The Rice Institute.*—A gold target of the highest purity available commercially has been bombarded with 3-Mev protons. Gamma radiation was observed with a NaI crystal spectrometer of good resolution which fits the known low-energy level scheme of Au^{197}. While these gamma rays are believed to be due to the Coulomb excitation[1] of the gold, the possibility that they were due to target contaminants is not excluded and is being investigated. The magic nuclei bismuth and lead were studied similarly and no radiation ascribable to nuclear excitation was observed. The spectra of various other heavy elements will be shown. Yield curves and angular distributions will be presented where obtained and compared to existing theory.

* Assisted by the U. S. Atomic Energy Commission.
[1] T. Huus and Č. Zupančič, Kgl. Danske Videnskab. Selskab, Mat.-fys. Medd. **28**, No. 1 (1953); C. McClelland and C. Goodman, Phys. Rev. **91**, 760 (1953).

H3. Sea-Level Zenith-Angle Dependence of High-Energy Mu-Mesons. N. M. DULLER,* W. D. WALKER,† J. W. GRAHAM,‡ AND J. R. RISSER, *Rice Institute.*—Preliminary experiments with counter telescopes, lead absorber, and soft shower detectors will be described. Results appear to indicate a broad maximum near 20° zenith angle in the intensity of high-energy mu-mesons. In one experiment a six-fold coincidence was required between two counter telescope elements and four individual counters below four inches of Pb. The four Pb-shielded counters were used to detect soft showers caused by bremsstrahlung and knock-on electrons from mu-meson interactions in the Pb. This shower detector was also shielded below by four inches of Pb. Counters placed beneath the lower shield were used to rule out penetrating showers. In another experiment a large proportional counter was used in place of the four Geiger counters. Counting rates were recorded as a function of zenith angle and integral pulse height. The zenith-angle variation measured for large pulses agrees qualitatively with results of the Geiger counter experiment. Some of the data are difficult to interpret in terms of decay-absorption competition of pi-mesons.

* Now at Texas A. & M. College, College Station, Texas.
† Now at University of Rochester, Rochester, New York.
‡ Now with Humble Oil & Refining Company, Houston, Texas.

H4. An Improved Spark Counter for Detecting Alpha Radiation. CHARLES E. WELLER, *University of Texas* (introduced by R. N. Little, Jr.).—A multiple-wire counter which utilizes spark discharges for the detection of heavily ionizing nuclear radiations was designed and a careful study of its properties was made. Although the counter was tested for alpha particles emitted by Po^{210} nuclei, there is a possibility that with some modifications the spark counter could be adapted for the detection of fission fragments also. The counter is definitely insensitive to all electromagnetic radiations, including high-energy gamma rays. The apparatus works in ordinary air, and it distinguishes itself by its large output pulse, low background counting rate, and high efficiency. About 56 percent counting efficiency was attained by a novel arrangement of the electrodes. This corresponds to a counting of approximately 96 percent of all the particles which pass between the electrodes. The long plateau of the counting characteristic, extending over a thousand volts, eliminates the need for a regulated power supply.

H5. Coincidences in the Scintillation Counter. A. L. ORVIS AND M. M. D. WILLIAMS, *Mayo Clinic and Mayo Foundation.*—Certain applications of the scintillation counter, such as its use for measuring high levels of activity or the simultaneous counting of two different gamma emitters, may require counting with high discriminator bias. Coincident events cause a release of energy in the scintillator which is the sum of the energies released by the individual events. Thus some pulses which would fall below the discriminator level may be augmented by coincident pulses and counted. The contribution of these augmented pulses to the counting rate is a function of the form of the pulse height spectrum and of the discriminator setting, and is not linearly related to the source strength. An expression relating the count due to coincident pulses to the appropriate variables will be presented and applied to the problem of counting only the 0.637- and 0.722-Mev photons from I^{131}.

H6. Range and Charge of Energetic Nitrogen Ions in Nickel. D. W. SCOTT, H. L. REYNOLDS, AND A. ZUCKER, *Oak Ridge National Laboratory.*—Thin nickel foils, varying from 0.5 to 8 mg/cm² thickness, were bombarded with the deflected beam of N^{3+} ions accelerated by the ORNL 63-inch cyclotron. After passing through the foils the nitrogen ions entered a shallow gas chamber filled with hydrogen at approximately 3-cm Hg pressure. Elastically scattered protons emerged from the chamber through a thin window at zero degrees and were counted with a proportional counter. The energy of the recoil protons was measured by absorption in aluminum foils, which in turn gave the energy of nitrogen ions entering the gas chamber. In another experiment energetic nitrogen ions were passed through thin nickel absorbers and collected in a Faraday cup. Making sure that cyclotron conditions do not vary during a run, the average charge of nitrogen ions as a function of absorber thickness was measured relative to the three-times-charged unattenuated beam. The experimental arrangement will be described, and comparison with theory will be made for range-energy relations and charge-velocity relations of nitrogen ions in nickel.

H7. Analyzing Magnet for a 100Kv Modified Cockcroft-Walton Accelerator. JAMES E. WILLS AND HENRY R. DVORAK,* *The University of Texas.*—Grid-controlled thyratrons were used to provide constant current to the coil of a magnet that will deflect a 100 kv beam of ionized deuterium or tritium 90 degrees in a 20-centimeter radius. The control circuit is similar to a simple error system used in servomechanism systems.

* Now at Convair, Fort Worth, Texas.

H8. NaI Gamma-Ray Spectrometry Techniques Applied to the Outlining of Brain Tumors. J. R. RISSER, *The Rice Institute,* AND H. C. ALLEN, JR., *V. A. Hospital Radioisotope Unit, Houston.*—Iodinated human serum albumen with tracer I^{131} is injected in the patient in the usual manner. The detector consists of a sodium iodide crystal, photomultiplier tube, pulse amplifier, and single channel differential pulse-height analyzer as in the standard NaI gamma-ray spectrometer. The combination is set to respond only to the 364-kev component of the I^{131} radiation. This selective response allows the elimination of gamma rays diffusely scattered by the Compton process and increases by at least a factor two the ratio to background of the significant count due to the tumor. By retracting the NaI crystal well back into a lead shield with a small opening, the counter is made to respond to the activity of a small conical section of tissue. The scan is automatic in a plane tangent to the head. Successful outlines of radioactive concentrations in phantoms and of tumors in living patients have been obtained.

SATURDAY AFTERNOON AT 1:30

Physics Building, Room 201

(A. W. NOLLE presiding)

Magnetic Resonance

I1. Analysis of Phase Detectors for the Display of Nuclear Magnetic Resonance Signals.* WILLIAM L. ROLLWITZ, *Southwest Research Institute.*—This paper presents a mathematical and experimental analysis of 4 phase detectors for the display of nuclear magnetic resonance signals. The circuits are analyzed as to their stability, linearity, sensitivity to phase and

amplitude changes of the reference, and "carrier leak balance." Several graphs and pictures are displayed to show the results and conclusions of the analysis.

* Supported by the Corn Industries Research Foundation.

I2. Nuclear Resonance Absorption in Weak, Homogeneous Fields.* R. W. MITCHELL AND MELVIN EISNER, *Texas A and M College.*—Very stable homogeneous magnetic fields have been obtained using a compensated solenoid powered by lead storage cells. The homogeneity, as indicated by the line width of distilled water, is 0.1 milligauss at 40 gauss field strength, for a sample size of 50 cc. To obtain this homogeneity permanent magnet shims have been used to reduce the effect of the inhomogeneity in the Earth's magnetic field. Slow sweep techniques are used to obtain the steady state resonance conditions and to prevent the occurrence of transients. The over-all stability of the equipment is sufficient to allow sweep rates as slow as 0.05 milligauss per second to be used. Some results obtained with this equipment will be discussed.

* Supported in part by the U. S. Office of Ordnance Research.

I3. A Narrow Gap Electromagnet for High Resolution Nuclear Resonance Spectrometry.* ALVIN F. HILDEBRANDT, *Texas A and M College.*—The homogeneity of the magnetic field produced by a narrow gap electromagnet has been studied using the nuclear resonance fine structure pattern of ethyl alcohol. Five-inch diameter pole faces were used to produce a 5000-gauss field in a $\frac{3}{4}$-inch gap. The pole caps were annealed and then polished to an optical flat. The signal strength and resolution were measured for different positions in the field for various sample sizes. While the fine structure could be resolved in samples as large as 125 mm³, the improvement in resolution for sample sizes down to 6 mm³ was not as good as would be expected for a uniform gradient inhomogeneity. The magnetic structure of the pole cap material introduces a randomly distributed inhomogeneity although isolated regions can be found which have a favorable homogeneity.

* Supported in part by the Texas Petroleum Research Committee.

I4. Paramagnetic Resonance Absorption in Diphenyl Picryl Hydrazyl at Low Values of Splitting Field. STEWART BECKER* AND MELVIN EISNER, *Texas A and M College.*—Paramagnetic resonance absorption has been observed in diphenyl picryl hydrazyl at fields of 10, 2.5, and 0.7 gauss. The line width as measured by the change in field between maximum slope points of the absorption signal was 1.25 and 1.12 gauss at fields of 10 and 2.5 gauss, respectively. Below 3 megacycles the situation is complicated since the splitting field is less than the line width. The spectral line in this region consists of contributions from both circularly polarized components of the rf field. At 2 megacycles the line width as measured by contributions from a single direction of circular polarization is 1.16 gauss and as measured by contributions from both is 0.78 gauss.

* On leave from the University of Arizona.

Post-Deadline Papers, if Any

SATURDAY AFTERNOON AT 1:30

Physics Building, Room 203

(N. D. SMITH presiding)

General Physics

J1. A Mechanical Electric Computer for Solving Polynomial Equations. HARRY J. AUVERMAN AND ARTHUR E. LOCKENVITZ, *University of Texas.*—A computer using rotating slider type variable autotransformers and sine and cosine resolvers along with a cathode-ray oscilloscope is used for obtaining the real and complex roots of a polynomial equation with real coefficients. The equation of the form

$$A+ax+bx^2+\cdots=0$$

is first transformed into

$$A+aM\cos\theta+bM^2\cos 2\theta+\cdots aM\sin\theta+bM^2\sin 2\theta+\cdots=0.$$

The M's are obtained from the autotransformers mounted on a common shaft, the coefficients A, a, b, etc., from individual autotransformers. The cosine and sine terms are generated by ac-type sine and cosine resolvers. The output of the cosine series is applied to one set of oscilloscope plates and the sum of the sine series to the other set of plates. The θ's and M's are then adjusted until zero deflection is indicated on the oscilloscope.

J2. Accurate Determination of The Tidal Variations of Gravity. HENRY NEAL CLARKSON AND ARTHUR E. LOCKENVITZ, *University of Texas.*—Using a modified La Coste-Romberg Gravity meter, continuous readings of the gravitational fields at Austin, Texas were made over a period of two months. These readings were compared with calculated gravitational field variations due to the positions of the sun and moon on the assumption that the earth is a rigid body. The differences between the observed values and the calculated values were compared to the calculated values as peak to peak amplitude ratios. An average value of 0.295 for the ratio of major peaks and 0.33 for the minor peaks ratio was found. There was no appreciable shift in phase between the difference curve and the calculated curve. The accuracy of the readings and calculations was better than one microgal. A detailed discussion of the results will be made.

J3. Shock Hugoniot of Air. W. E. DEAL, JR., *Los Alamos Scientific Laboratory.*—Gaseous shocks are created by the use of explosive-driven metal plates. An optical technique using the Schlieren principle in conjunction with a high-speed framing camera is employed for the simultaneous measurement of shock velocity and the difference between plate and shock velocities. A series of experiments with varying plate velocities yield data which allow derivation of the pressure-compression curve by use of the mass and momentum conservation equations. Since the difference between particle and shock velocities appears in the compression expression and is also small compared to either velocity, direct measurement of the difference is an advantage of this method. The velocities are measured with precisions of the order of 2 percent. The method

permits measurements for shocks in the pressure region from 10 to 500 atmospheres. Specific data are reported for air and compared to theoretical predictions.

J4. The Effect of Hydrostatic Pressure in the Two-State Model of Compressional Relaxation in Liquids. A. W. NOLLE, *The University of Texas.*—It was shown by Hall[1] that compressional energy losses in water, as determined from ultrasonic absorption data, can be related to a model in which rearrangement occurs at a finite rate between two states of local order characterized by different specific volumes. The higher free energy was attributed to the more condensed state, but it was recognized that a revised interpretation might be required for nonassociated liquids. It is shown in the present analysis that this interpretation of the two-state model predicts that the compressional losses will always increase with hydrostatic pressure. On the other hand, if the higher free energy is attributed to the less condensed state (which is consistent with the view that this is a "hole"), it is then possible for compressional losses to decrease with increasing hydrostatic pressure. Thus, experimental information concerning the pressure dependence of compressional losses can aid in distinguishing between these versions of the two-state model.

[1] L. Hall, Phys. Rev. 73, 775 (1948).

J5. Absorption of Ultrasonic Waves in Liquids under Pressure. J. F. MIFSUD, *The University of Texas.*—A pulse-reflection technique is employed to measure the absorption of ultrasonic waves in liquids under pressure in the range up to 1400 atmospheres. The absorption, and also the wave velocity, are obtained through a comparison of the amplitudes and arrival times of two reflected signals, initiated by the same source, but traversing paths of different length. The work is intended to provide further information regarding the absorption process in those liquids in which there is evidence of large compressional relaxation effects. Results are presented for carbon tetrachloride at a frequency of 5 mc. The absorption per wavelength decreases continuously with increasing pressure. This result is consistent with a picture of the compressional absorption process based on the hole theory of liquids.

J6. The Compressibility of Liquid Cholesterol Benzoate at the Isotropic-Anisotropic Transition. W. A. HOYER, *The University of Texas.*—On heating, cholesterol benzoate melts to form an anisotropic liquid, sometimes referred to as a "liquid crystal" phase. At a higher temperature there is a sharp transition to an isotropic liquid state. This transition is investigated in terms of the velocity and absorption of ultrasonic waves. The measurements are performed with a pulse-reflection technique. From the velocity measurements and from available density data, it is found that the compressibility has a sharp maximum at the transition. Also, there is a strong maximum in the absorption of ultrasonic waves near the transition. A portion of the apparent absorption actually represents scattering, which substantially restricts measurements to frequencies of the order of 1000 kc and less.

J7. Transmission of Pulses through an Elastic Plate. ARTHUR S. GINZBARG AND WILLIAM L. ROEVER, *Shell Development Company.*—It will be shown that if an elastic plate is submerged in an elastic liquid and both the pulsed point source of pressure and the point pressure detector are on the same normal to the plate, then the pressure at the detector will contain arrivals corresponding to multiply-reflected rotational as well as compressional waves in the plate.

J8. Thickness of Films Left on Capillary Wall During Displacement of One Fluid by Another. CHARLES C. TEMPLETON, *Shell Development Company* (introduced by C. H. Fay).—Techniques were devised to observe displacement of one fluid by another immiscible fluid in uniform microscopic capillaries.[1] From interfacial velocity for a constant pressure difference across the capillary, one can calculate an effective viscosity for each phase assuming that Poiseuille flow prevails, that displacement is perfect, and that static and dynamic capillary pressures are equal. Measurements were made for oil-water displacements (interfacial velocities = 1 cm/min) in capillaries initially filled with water, in which case the assumed absence of capillary pressure hysteresis appears adequate. When the oil viscosity is about one poise or more, the effective oil viscosity becomes about one-half the normal value. Assuming the absence of perfect displacement and the existence of an annular water film around the oil, film thicknesses between 20 and 100A can be calculated. By other methods it was shown that an oil film about 100A thick is left when air displaces oil.

[1] C. C. Templeton, Paper 307-G, Petroleum Branch, Am. Inst. Mining Met. Engrs. (October, 1953).

J9. Diffraction Measurements at 1.25 Centimeters. C. W. HORTON AND W. W. GRANNEMANN,* *The University of Texas.*—A series of measurements were made of the diffraction of essentially plane electromagnetic waves by conducting metallic objects. The objects studied were circular disks, circular rods, and parallel semi-infinite plates, and the dimensions were chosen to be neither large nor small compared to a wave length. The experimental techniques used were very similar to those described by Horton and Watson[1] except that in the present instance the wavelength was 1.25 centimeters. An attempt was made to select configurations of scattering objects which would be suitable for checking the formulas developed in the past few years by Bouwkamp, Clemmow, Copson, Heins, Twersky, and others. A representative set of diffraction patterns will be shown and discussed. Comparison with theory will be given for several examples.

* Now at the California Research Corporation, La Habra, California.
[1] C. W. Horton and R. B. Watson, J. Appl. Phys. 21, 16 (1950).

J10. Diffraction of Electromagnetic Waves by a Metallic Wedge of Acute Dihedral Angle. W. W. GRANNEMANN,* C. W. HORTON, AND R. B. WATSON, *The University of Texas.*—In the rigorous theory of diffraction by a conducting wedge as developed by Sommerfeld and extended by Pauli,[1] the total field is represented by the terms given by geometrical optics plus a contour integral which represents the diffracted waves. If the faces of the wedge form a dihedral angle of π/n, $n = 1, 2, 3, \cdots$, the contour integral vanishes identically and the solution given by geometrical optics is exact. This prediction has been tested and checked by measurements of the diffraction patterns of wedges whose dihedral angles were 90°, 60°, and 30°. The measurements were made at a wavelength of 1.25 centimeters and the source was far enough so that the incident wave was essentially plane.

* Now at the California Research Corporation, La Habra, California.
[1] W. Pauli, Phys. Rev. 54, 924 (1938).

J11. The Study of Electrokinetic Relations Using Sinusoidal Pressure and Voltage.* CLAUDE E. COOKE, *The University of Texas.*—The method previously described by Packard[1] for measuring streaming potentials across porous diaphragms for sinusoidal flow has been used to study the general electrokinetic relations derived from the equations[2]

$$I = C_{11}E + C_{12}P,$$
$$V = C_{21}E + C_{22}P.$$

I and V are electric current and volume flow rate, and E and P are the electric potential difference and pressure difference across a porous medium. Fritted glass diaphragms saturated

with distilled water have been used. The range of pressures is from 0 to 10 000 dynes per cm^2 (rms) and the range of voltage is from 0 to 250 volts (rms). Experimental results and curves will be given. The relations have been studied previously only for steady unidirectional flow and constant applied potential.

* Partially supported by a grant from Research Corporation.
[1] R. G. Packard, Phys. Rev. **89**, 906(A) (1953).
[2] P. B. Lorenz, J. Phys. Chem. **56**, 775 (1952).

J12. The Role of the Rydberg Constant in the Calculation of Ionic Radii. N. EFREMOV, *1061 Intervale Avenue, New York, New York.*—In the periodic system of ions[1] we discern 10 rows of positive and negative ions. The ions belong either to the inert gases rows, e.g., Ne-row,

$$C^{4-}-N^{3-}-O^{2-}-F^{1-}-(Ne)-Na^{1+}-Mg^{2+}-Al^{3+}-Si^{4+}-P^{5+}-S^{6+}-Cl^{7+},$$

or to the triplets rows, e.g.,

$$(Fe-Co-Ni)-Cu^{1+}-Zn^{2+}-Ga^{3+}-Ge^{4+}-As^{5+}-Se^{6+}-Br^{7+}.$$

Calculating the effective ionic radii [for crystalline lattices of NaCl type) by means of the quantization method[2]] worked out by us we use two constants P and P'. $P'=0.01096777$A, while $P=0.01462369$A. We use P for calculation of the radii of ions belonging to the rows of inert gases (e.g., Ne, Ar), while P' is used for calculation of the radii of ions belonging to the rows of triplets elements (e.g., Fe–Co–Ni). Constant P' may be obtained by the multiplication from the Rydberg constant for the atomic hydrogen (109677.7) expressed in reciprocal angstrom units by the factor 10, i.e., $P'=0.01096777$A. And $P=4/3\ P'$ or $P=(0.01096777\text{A}\times 4):3$, *or* $P=0.01462369$A.

[1] N. Efremov, Phys. Rev. **92**, 1031(A) (1953).
[2] N. Efremov, Bull. Am. Phys. Soc. **28**, 30 (1953).

Author Index to Papers Presented at the 1954 Austin Meeting

Arnold, Charles W. and F. A. Masten—D1
Auverman, Harry J. and Arthur E. Lockenvitz—J1
Badar, L. J. and V. P. Jacobsmeyer—G4
Banta, H. E. and R. L. Macklin—F4
Becker, Stewart and Melvin Eisner—I4
Bonner, T. W. and C. F. Cook—F6
Chuoke, Robert L.—G2
Clarkson, Henry Neal and Arthur E. Lockenvitz—J2
Class, C. M.—H1
Class, C. M., C. F. Cook, and J. T. Eisinger—H2
Cohen, B. L.—C3
Collins, R. L. and J. Rud Nielsen—D6
Cook, C. F. and T. W. Bonner—F5
Cooke, Claude E.—J11
Coon, J. B. and J. K. Ward—D4
Cowan, Alvin E. and Arthur E. Lockenvitz—G6
Crawford, J. H.—B1
Deal, W. E., Jr.—J3
Dudley, J. D. and C. M. Class—F8
Duller, N. M., W. D. Walker, J. W. Graham, and J. R. Risser—H3
Efremov, N.—J12
El-Sabban, M. Z. and J. Rud Nielsen—D7
Foster, B. P., G. S. Stanford, and L. L. Lee—C7
Ginzbarg, Arthur S. and William L. Roever—J7
Goodrich, Max—C2
Gordy, Walter—A4
Gossett, C. R., G. C. Phillips, and J. T. Eisinger—F9
Grannemann, W. W., C. W. Horton, and R. B. Watson—J10
Heaps, C. W.—G5
Hereford, F. L.—E1
Hildebrandt, Alvin F.—I3
Horton, C. W. and W. W. Grannemann—J9
Houston, W. V.—G1
Hoyer, W. A.—J6
Hughes, D. S.—A1
Lander, J. J.—B2
Lindsay, Robert—G3
Little, R. N., Jr., C. P. Cadenhead, B. P. Leonard, Jr., J. T. Prud'homme, L. D. Vincent, and J. E. Wills—F3
Marion, J. B.—F12
Marion, J. B., C. F. Cook, and T. W. Bonner—F7
McCrary, J. H., H. L. Taylor, and T. W. Bonner—F11
Mifsud, J. F.—J5
Miller, J. M. and F. A. Matsen—D2
Millett, Walter E.—G8
Mitchell, A. C. G.—A2
Mitchell, R. W. and Melvin Eisner—I2
Nereson, Norris—E4
Nielsen, J. Rud, H. H. Claassen, and Norma B. Moran—D8
Nolle, A. W.—J4
Orvis, A. L. and M. M. D. Williams—H5
Peacock, C. L., A. W. Oser, and J. F. Quin—C8
Perlman, I.—C1
Phillips, J. A.—E2
Plint, C. A., R. M. B. Small, and H. L. Welsh—D9
Reich, C. W., J. Russell, and G. C. Phillips—C6
Reynolds, J. M.—B4
Rickard, James A. and Emmett L. Hudspeth—F1
Risser, J. R. and H. C. Allen, Jr.—H8
Rollwitz, William L.—I1
Russell, J. Jr., C. W. Reich, and G. C. Phillips—C5
Russell, R. K.—D5
Scott, D. W., H. L. Reynolds, and A. Zucker—H6
Smith, D. M. and E. L. Secrest—D10
Spearman, K. R., E. L. Hudspeth, and I. L. Morgan—F2
Squire, C. F.—B3
Streetman, J. R. and F. A. Matsen—D3
Swim, R. T. and H. E. Rorschach, Jr.—G7
Talley, Harry and Robert Stump—G9
Taylor, H. L., O. Lönsjö, and T. W. Bonner—F10
Templeton, Charles C.—J8
Vallarta, M. S.—E5
Weller, Charles E.—H4
Whaling, Ward—E3
Williams, Dudley—A3
Wills, James E. and Henry R. Dvorak—H7
Windham, Pat M. and G. C. Phillips—C4